Synthesis of macrocyclic kinase inhibitors

Dissertation

zur Erlangung des Doktorgrades

der Naturwissenschaften

vorgelegt beim Fachbereich 14

Biochemie, Chemie und Pharmazie

der Johann Wolfgang Goethe – Universität

in Frankfurt am Main

von

Jennifer Alisa Amrhein

(geb. Breitenbach)

geboren in Aschaffenburg

Frankfurt am Main, 2023

(D30)

vom Fachbereich Biochemie, Chemie und Pharmazie der

Johann Wolfgang Goethe – Universität als Dissertation angenommen.

Dekan:	Prof. Dr. Clemens Glaubitz
Gutachter:	Prof. Dr. Stefan Knapp
	Prof. Dr. Eugen Proschak

Datum der Disputation: 25.04.2023

Table of content

Table of content 1

1. Introduction 4

  1.1. Protein kinases 4

  1.1.1. General information 4

  1.1.2. Structural overview of protein kinases 6

  1.2. Protein kinase inhibitors 8

  1.3. Macrocyclic protein kinase inhibitors 12

  1.4. Kinases of interest for this work 15

  1.4.1. Epidermal growth factor receptor 15

  1.4.2. Cyclin-dependent kinase 16 18

  1.4.3. Bone morphogenetic protein receptor type II 21

  1.4.4. Mammalian STE20-like protein kinases 23

2. Objective 27

3. Results and Discussion 29

  3.1. Synthesis of the quinazoline-based macrocycles 29

  3.2. Synthesis of 3-aminopyrazole-based kinase inhibitors 32

  3.3. Synthesis of 3-aminopyrazole-based macrocycles 35

  3.4. Macrocyclization of quinazoline-based EGFR inhibitors lead to exclusive mutant selectivity for EGFR L858R and Del19 36

  3.4.1. *In-vitro* characterization 36

  3.4.2. Selectivity profile 39

  3.4.3. Crystal structure 43

  3.4.4. Cell-based activity 44

  3.4.5. Pharmacochemical properties 47

3.5. Discovery of 3-amino-1*H*-pyrazole-based kinase inhibitors to illuminate the understudied PCTAIRE family 48

3.5.1. Selectivity profile 48

3.5.2. CETSA revealed CDK16 stabilization in cells 54

3.5.3. Cell-based activity 56

3.5.4. Metabolic stability 58

3.5.5. FUCCI cell cycle assay 59

3.6. Design and synthesis of pyrazole-based macrocyclic kinase inhibitors targeting BMPR2 . 61

3.6.1. *In-house* selectivity profile 61

3.6.2. *In-vitro* characterization and cell-based activity 63

3.6.3. Kinome wide selectivity 64

3.6.4. Binding mode 65

3.7. Optimization of pyrazole-based macrocycles lead to a highly selective MST3 inhibitor 66

3.7.1. *In-house* selectivity profile 66

3.7.2. *In-vitro* characterization and cell-based activity 69

3.7.3. Crystal structure 71

3.7.4. Metabolic stability 73

4. Summary 74

4.1. Macrocyclization of quinazoline-based EGFR inhibitors lead to exclusive mutant selectivity for EGFR L858R and Del19 74

4.2. Discovery of 3-amino-1*H*-pyrazole-based kinase inhibitors to illuminate the understudied PCTAIRE family 75

4.3. Design and synthesis of pyrazole-based macrocyclic kinase inhibitors targeting BMPR2 . 76

4.4. Optimization of pyrazole-based macrocycles lead to a highly selective MST3 inhibitor 77

5. Conclusion and Outlook 79

6. Zusammenfassung und Ausblick 83

7. Experimental procedure 90

7.1. General 90

7.2. Chemicals and solvents 90

7.3. Thin-layer chromatography (TLC) 90

7.4. Column chromatography 90

7.5. High performance liquid chromatography (HPLC) 91

7.6. Nuclear magnetic resonance (NMR) spectroscopy 91

7.7. Mass spectrometry 92

7.8. DSF 92

7.9. Selectivity screen 92

7.10. Experimental part of Chapter 3 93

7.10.1. Synthesis of quinazoline-based macrocycles 93

7.10.2. Synthesis of 3-aminopyrazole-based molecules 123

7.10.3. Synthesis of 3-aminopyrazole-based macrocycles 158

8. Abbreviations 182

9. References 186

10. List of Figures 199

11. List of Schemes 205

12. List of Tables 206

13. Acknowledgements 208

14. Publications 210

15. Curriculum Vitae 211

16. Appendix 212

17. Eidesstattliche Erklärung 404

1. Introduction

1.1. Protein kinases

1.1.1. General information

Since the discovery of the tyrosine kinase Scr as an oncogene in 1978, protein kinases have moved to the front of pharmaceutical research and development.[1,2] Subsequently, the first ATP-competitive kinase inhibitor based on isoquinoline sulfonamides was developed in the early 1980s and it was demonstrated that compounds of this class strongly inhibit protein kinase C (PKC) and cAMP-dependend kinases.[3] In recent years there has been an increasing scientific interest in the use of protein kinase inhibitors for the treatment of cancer. To date, cancer is worldwide one of the most frequent diseases leading to death before the age of 70 years.[4] Also the steadily rising number of FDA-approved small molecule kinase inhibitors underlines the importance of research in this area. Since the first protein kinase inhibitor sirolimus has been approved in 1999, a total of 72 therapeutic agents have been approved by 2023, whereby 62 of them are used for the treatment of neoplasms.[5,6] About 1.7% of the human genes and in total 518 protein kinases encode the human kinome.[7] They are divided into 478 eukaryotic kinases, which have a highly conserved catalytic domain and 40 atypical protein kinases, which share only a weak similarity with the others. The classification is mainly based on structural characteristics and their structural similarity within the catalytic domain. There are in total seven main groups (TK (tyrosine kinases), TKL (tyrosine kinase-like), STE (homologues of yeast sterile 7, 11, 20), CK1 (casein kinase 1), AGC (protein kinase A, G, C), CAMK (calcium/ calmodulin-dependent kinases) and CMGC (cyclin-dependent kinases, MAP kinases, glycogen synthase kinases, casein kinase 2)), 134 families and 196 subgroups, which are illustrated in a so-called kinome tree (Figure 1).[8,9] Furthermore, approximately 60 protein kinases are part of the catalytically inactive pseudokinases. They lack one or more amino acids, which are necessary for the alignment of ATP and metal ions. Although this leads to a lack of catalytic activity, they are highly important for signal transmissions by regulating the activity of other kinases.[10,11]

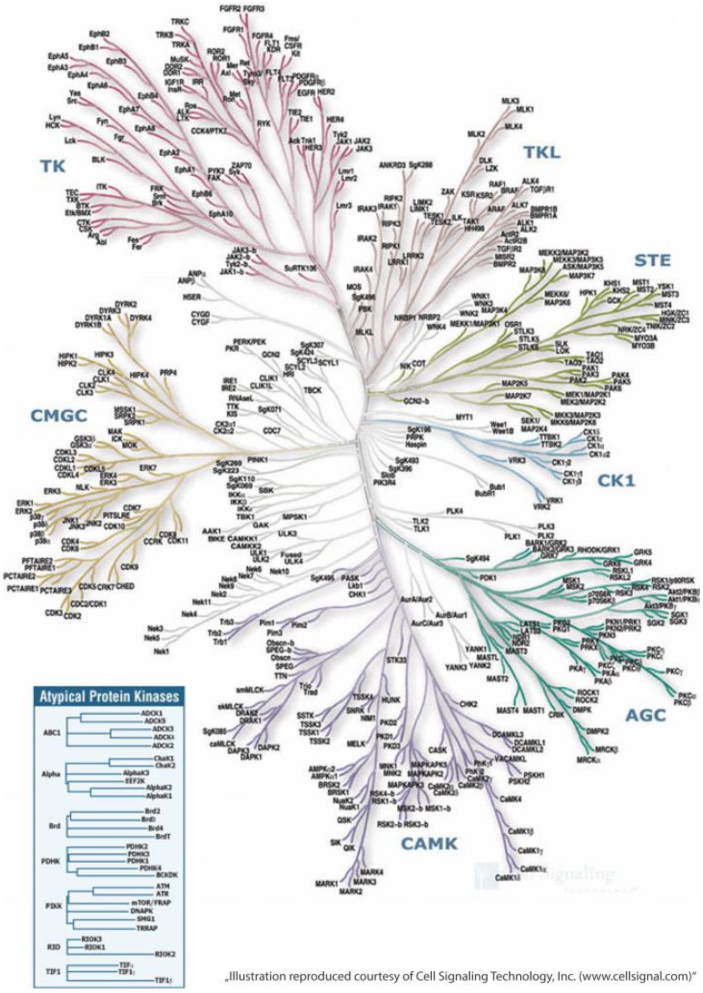

„Illustration reproduced courtesy of Cell Signaling Technology, Inc. (www.cellsignal.com)“

Figure 1. Graphic representation of the human kinome in a so-called kinome tree. The six classes of serine/ threonine-specific protein kinases (TKL, STE, CK1, AGC, CAMK, and CMGC) and tyrosine kinases (TK) are assigned by their structural similarity.

Eukaryotic protein kinases catalyze the reversible transfer of the ɣ-phosphate from adenosine triphosphate (ATP) to specific amino acid residues of different substrates (Figure 2).[12] In general, kinases are divided in serine/ threonine- (STPKs) or tyrosine- (TPKs) specific kinases, depending on the type of the hydroxyl function of the amino acid residues, which are phosphorylated. Nevertheless, there are also bispecific kinases that modify both, the serine/ threonine as well as tyrosine residues.[13] Phosphorylation is an important post-translational control mechanism of cell signaling. It is involved in the regulation of the metabolism, transcription, cell viability, differentiation, and survival of cells.[14] Dysfunction of the signal transmission can lead to uncontrolled growth and apoptosis, which results in diseases such as diabetes, Alzheimer's disease, inflammatory diseases, cardiovascular diseases, or even cancer.[15,16,17]

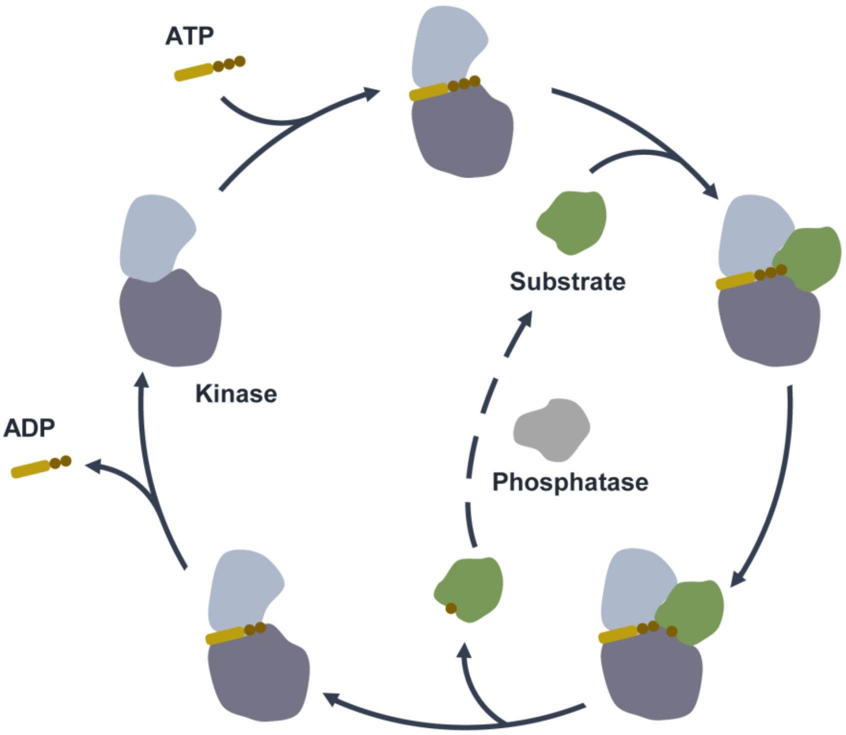

Figure 2. Graphical representation of the reversible transfer of the ɣ-phosphate from ATP to a substrate, catalyzed by a protein kinase. (Adapted from Ubersax *et. al.*)[12]

1.1.2. Structural overview of protein kinases

First insights into the structure of protein kinases were revealed by the crystal structure of protein kinase A (PKA), determined by Knighton *et. al.* in 1991.[18] The tertiary structure within the eukaryotic protein kinase family is highly conserved, whereas the kinases harbor two major subdomains, the N-terminal and C-terminal lobe. These two domains are connected through a flexible linker, called hinge region. The hydrophobic cleft in-between the lobes forms the active site and provides a space for ATP binding (Figure 3A, B). Here, the heteroaromatic adenine moiety of the ATP forms two hydrogen bonds with the backbone of the hinge region and enables the transfer of the ɣ-phosphate of ATP to the respective substrate. The gatekeeper, a single amino acid, represents the transition between the hinge region and the N-lobe. It provides access to another pocket within the active side, the so-called hydrophobic back pocket. Depending on the size of this gatekeeper, the ligand can have access to this pocket or either can be obstructed if the gatekeeper harbors a large amino acid side chain (e.g. phenylalanine or leucine). Due to the interaction with the ligand, the gatekeeper represents an addressable element in the development of kinase inhibitors.[19] The smaller N-lobe is necessary for ATP binding and consists of a five-stranded antiparallel beta-sheet (β1-β5) and an additional alpha helix (αC-helix). The conserved glutamate from the αC-helix can form a salt bridge with the lysine of the AXK motif, which is located in the β3 sheet. This interaction is required for the active state and in most cases leads to the αC-in conformation of the kinase. Additionally, the P-loop, a highly flexible and glycine-rich region, is part of the N-lobe. It is crucial for the transfer of the ɣ-phosphate as well as for the exchange of ATP/ ADP during the catalytic cycle by coordinating the β- and ɣ-phosphate of ATP through ionic interactions.[20,21] The larger C-lobe is primarily α-helical (αD-αI) with four additional beta sheets (β6-β9) and is responsible for the catalytic activity. The activation segment represents the most important regulatory element in kinases. It starts with a magnesium binding site, followed by the activation loop (A-loop), which is regulating the kinase activity. The highly conserved DFG-motif (Asp-Gly-Phe) is part of the A-loop and coordinates an Mg^{2+} ion which again interacts with the α-, β- and ɣ-phosphate of ATP. The phenylalanine of the DFG-motif can either point outwards the ATP-binding pocket which enables a substrate binding (DFG-in conformation) or it can be in an inactive form where the phenylalanine is pointing inside the ATP binding pocket (DFG-out conformation). Furthermore, the DFG-motif can interact with the Y/HRD-motif (His-Arg-Asp) of the catalytic loop through a network of hydrogen bonds. The aspartic acid of the Y/HRD-motif is highly conserved and is responsible for a proper orientation of the P-site hydroxyl acceptor moiety and acts as a base, deprotonating the respective hydroxy group of the substrate.[22,17,23]

In summary, the ATP-binding pocket can be divided into different regions: The hydrophobic back pocket, which is not involved in ATP binding but is involved in the binding of a ligand. The adenine region, which coordinates the adenine ring of ATP through two hydrogen bonds. The phosphate region, which binds the triphosphate of ATP through forming different interactions with the N-lobe or C-lobe of the kinase and the solvent-exposed region, which also does not interact with ATP however, opens the ATP binding pocket to the environment (Figure 3C).[13,19]

The regulatory spine (R-spine) and catalytic spine (C-spine) are further conserved spatial motifs, which can be found in the active state of the kinase however, they are completely missing in the inactive conformation. The R-spine consists of four hydrophobic residues, two of each lobe. A leucine from the β4 strand, a leucine from the αC-helix, a phenylalanine from the A-loop, and a tyrosine from the catalytic loop. The R-spine can impact the kinase activity due to the flexibility of some components. The C-spine also comprises residues from both lobes and the adenine ring of ATP is part of this spatial motif as well. A valine of the β2 strand and alanine of the β3 strand form the components of the N-lobe, which are connected to the adenine ring of the ATP, then followed by a leucine of the β7 strand and five further amino acids from the C-lobe. Due to the rigid core of the C-lobe, the C-spine contributes to the correct positioning of ATP in the binding pocket.[24,25]

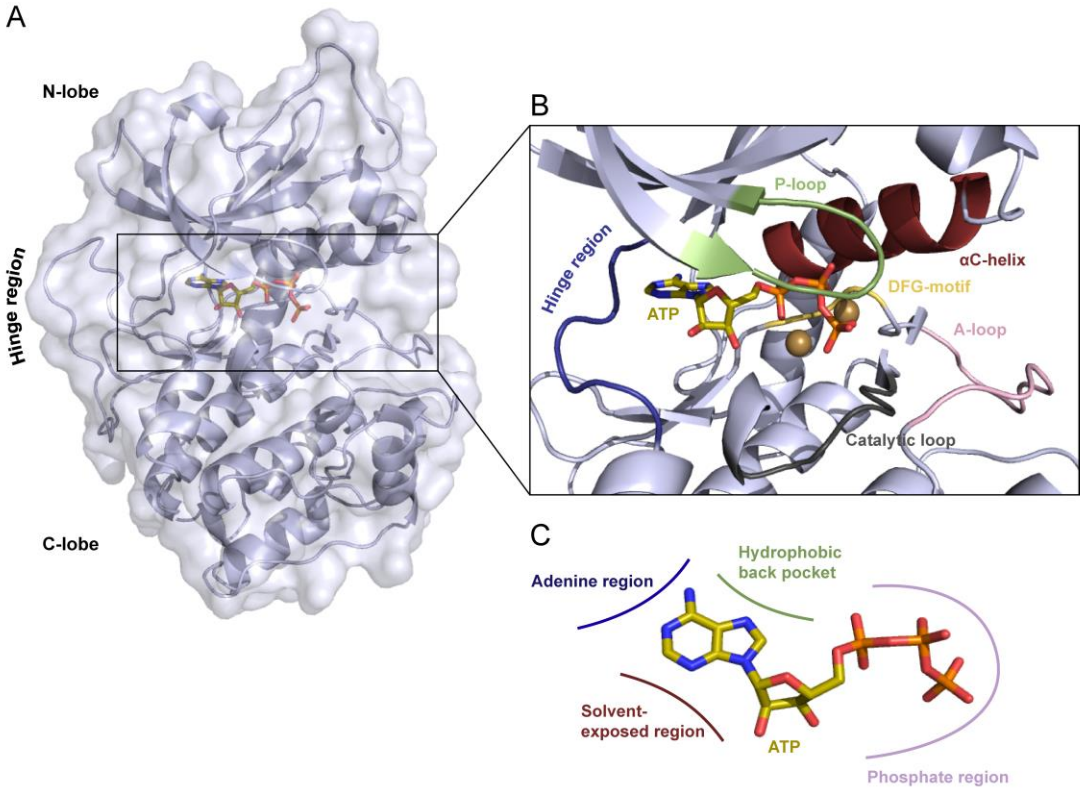

Figure 3. A. The tertiary structure of protein kinase A in complex with ATP is shown with its surface (PDB: 1ATP). **B.** Detailed structure of the ATP binding pocket (PDB: 1ATP) with a stick and ball representation. ATP is colored by elements in gold, the coordinated Mg^{2+} ions are shown as spheres in brown, and important sections are highlighted. The hinge region is shown in blue, the P-loop in green, the αC-helix in dark red, the DFG-motif in yellow, the A-loop in light pink, and the catalytic loop in dark grey. **C.** Simplified illustration of the different regions in the ATP binding pocket. The adenine region is colored in blue, the solvent-exposed region in dark red, the phosphate region in light pink, and the hydrophobic back pocket in green.

1.2. Protein kinase inhibitors

At first, the development of protein kinase inhibitors seemed to be an insurmountable challenge due to the highly conserved ATP binding pocket, as well as the high ATP concentration in cells. The potent inhibition of PKC by staurosporine, a natural product produced by streptomyces staurosporeus, was found in 1986 and laid the foundation for the development of kinase inhibitors despite its poor selectivity.[26] In 1995, the ROCK 1 and 2 inhibitor fasudil was approved in Japan for the treatment of cerebral vasospasm.[27,28] Sirolimus, a natural product, which targets mTOR was approved 1999 in the United States for the prevention of organ rejection and represents the first allosteric kinase inhibitor.[29,30] Since then, the scientific interest in the development of new kinase inhibitors has continued unabated. A variety of new inhibitors have been approved by the FDA for the treatment of different diseases. Depending on the binding mode, the kinase inhibitors can be divided into different classes: covalent and non-covalent inhibitors. The non-covalent inhibitors can be further categorized into four subgroups (type I – IV), depending on the type of binding to the kinase.[31]

Type I inhibitors address the active state of the kinase with the DFG-motif pointing inwards the ATP binding pocket and adopting the active DFG-in conformation. The compounds of this class are ATP mimetic and directly compete with ATP. They interact with the backbone of the hinge region by forming up to three hydrogen bonds through hydrogen bond donor and acceptor moieties (Figure 4). The rigid and highly conserved conformation of the active kinase makes it difficult to develop selective type I kinase inhibitors.[32,33] Kinase-specific characteristics like a small gatekeeper beside the hinge region can be taken into account when designing new inhibitors. The consequently accessible hydrophobic back pocket can be addressed by the compounds and the combination of such opportunities can lead to a selective inhibition of the kinase of interest.[34] An example of a type I inhibitor is dasatinib (Figure 4B), which is used for the treatment of chronic myelogenous leukemia (CML) and acute lymphoblastic leukemia (ALL).[35,36]

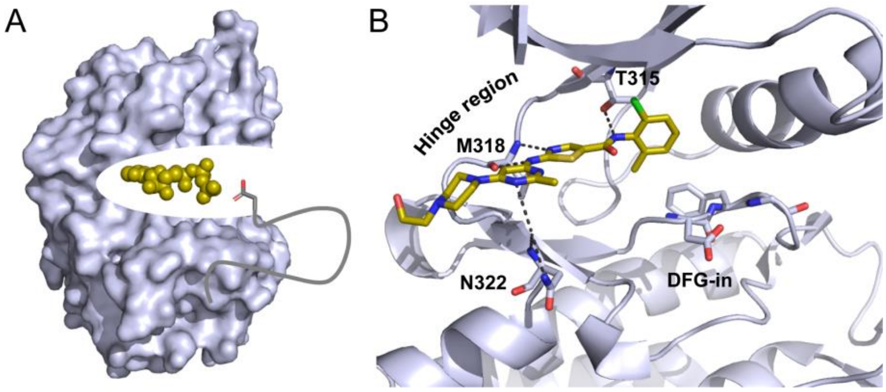

Figure 4. A. Schematic representation of a canonical type I binding mode. The inhibitor (gold) binds to the active conformation of the kinase (light blue), whereby the DFG-motif (grey) is pointing into the binding pocket. (Adapted from Wu *et. al.*)[37] **B.** Crystal structure of the type I kinase inhibitor dasatinib (gold) in complex with ABL (PDB: 2GQG). Hydrogen bonds are shown as dashed lines (black) and important sections are highlighted.

Type II inhibitors are also ATP competitive and bind to the inactive state of the kinase. This can be generated through the rotation into the αC-helix-out state or due to the aspartate residue of the DFG-motif pointing outwards the ATP binding pocket, resulting in the DFG-out conformation (Figure 5).[38,31] This state creates an extended and dynamic hydrophobic binding pocket which can be targeted by type II inhibitors. Initial assumptions suggested that this more dynamic state of the kinase would result in a more selective inhibition. However, studies have shown that many inhibitors can bind to the DFG-out conformation and are therefore not necessarily more selective than type I inhibitors.[39,40] Ponatinib, an FDA-approved type II inhibitor for the treatment of ALL and CML, in complex with ABL is shown in Figure 5B.[41]

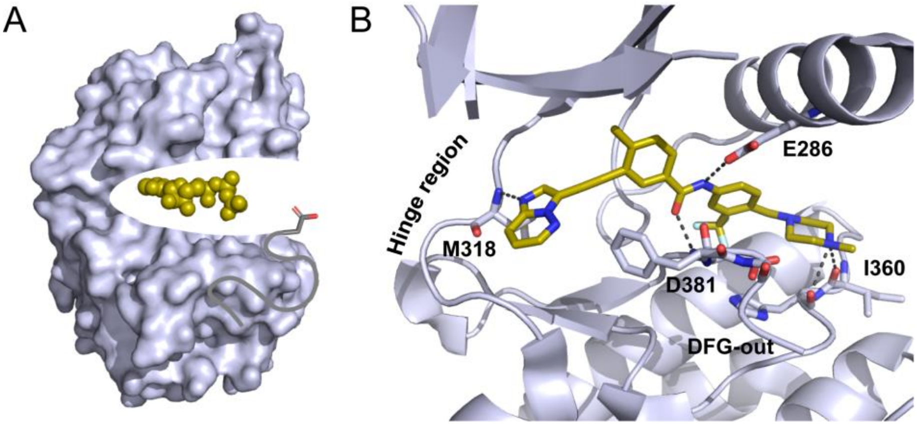

Figure 5. A. Schematic representation of a canonical type II binding mode. The inhibitor (gold) binds to the inactive conformation of the kinase (light blue), whereby the DFG-motif (grey) is pointing outwards the binding pocket. (Adapted from Wu *et. al.*)[37] **B.** Crystal structure of the type II kinase inhibitor ponatinib (gold) in complex with ABL (PDB: 3OXZ). Hydrogen bonds are shown as dashed lines (black) and important sections are highlighted.

In contrast to the previously mentioned subgroups, type III inhibitors are non-ATP competitive and bind simultaneously with ATP. They target a less conserved allosteric binding pocket beside the ATP-binding region, which may offer the advantage of a more selective inhibition (Figure 6). It has been reported that type III inhibitors can either bind to the DFG-in or DFG-out conformation, influencing the catalytic function of the kinase.[32,42,43] As mentioned before, retrospectively sirolimus represents the first allosteric kinase inhibitor.[44] Another prominent example is trametinib, a selective MEK 1 and 2 inhibitor for the treatment of mutated metastatic melanoma.[45] A further FDA-approved MEK inhibitor is binimetinib, which is shown in Figure 6B in complex with MEK1.[46]

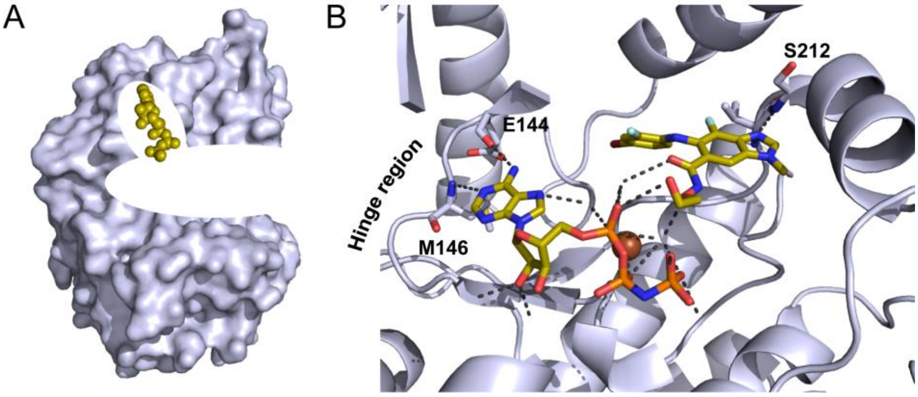

Figure 6. A. Schematic representation of a type III binding mode. The inhibitor (gold) binds to an allosteric pocket beside the ATP binding pocket of the kinase (light blue). (Adapted from Wu *et. al.*)[37] **B.** Crystal structure of the type III kinase inhibitor binimetinib and AMP-PNP (gold) in complex with MEK1 (PDB: 7M0U). Hydrogen bonds are shown as dashed lines (black), Mg^{2+} ion is shown as a brown sphere and important sections are highlighted.

Type IV inhibitors also bind to an allosteric binding pocket however, this one is located outside of the ATP-binding site. As well as the type III inhibitors, the members of this class enable a selective inhibition of the kinase due to the specific composition of the allosteric pocket. Allosteric inhibitors represent a great alternative to the most common ATP-mimetic inhibitors. However, the identification of such allosteric binding sites is quite challenging.[32,47] GNF-2 is a type IV inhibitor, which targets an allosteric pocket at the C-terminal lobe of ABL, called myristate pocket (Figure 7A). GNF-2 binds simultaneously with the ATP-mimetic inhibitor imatinib, which facilitates a combined drug therapy and may evade drug resistance.[48,49]

Covalent inhibitors represent the second class of kinase inhibitors. They typically consist of a non-covalent inhibitor moiety and a flexible linker which is connected to an electrophilic warhead (Figure 7C). The warhead enables the formation of a covalent bond with a cysteine or lysine within the ATP-binding site through either a Michael reaction, nucleophilic addition, or a nucleophilic substitution. The irreversible binding to the kinase leads to a longer occupation of the ATP binding pocket and thus results in a longer persistency until new protein is expressed.[50,51,52] Afatinib is an FDA-approved covalent inhibitor for the treatment of non-small cell lung carcinoma (NSCLC). The quinazoline moiety interacts with the hinge region of epidermal growth factor receptor (EGFR) via a hydrogen bond, whereby the warhead forms a covalent bond with C797 (Figure 7B).[53]

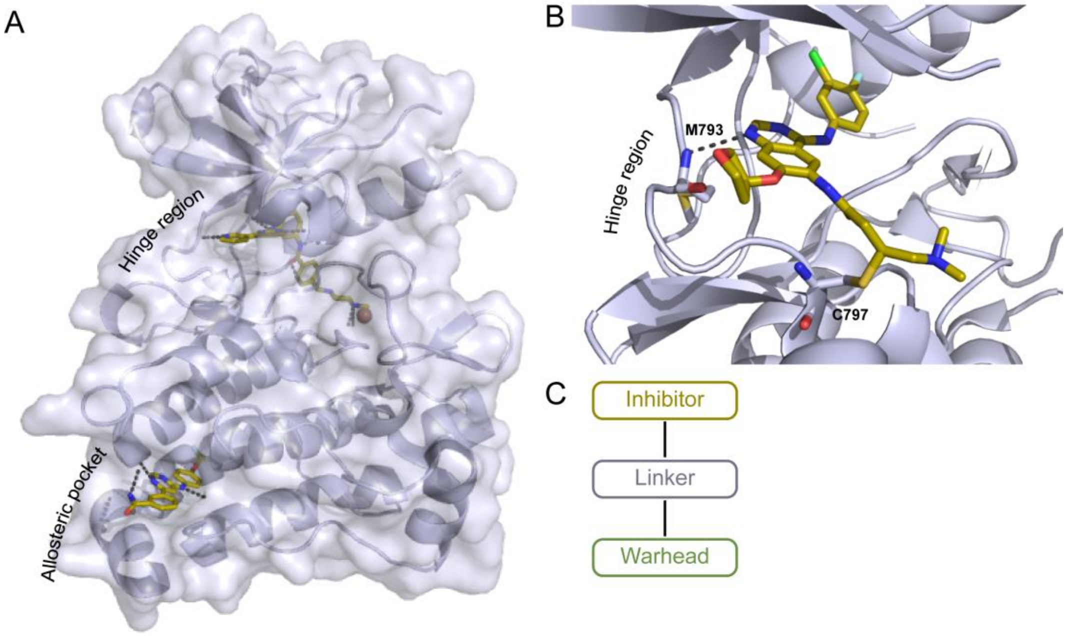

Figure 7. A. Crystal structure of the type IV kinase inhibitor GNF-2 (gold) in complex with ABL (PDB: 3K5V). Imatinib binds to the ATP binding pocket and GNF-2 (gold) to an allosteric binding pocket distant from the ATP binding pocket of the kinase (light blue). **B.** Crystal structure of the covalent kinase inhibitor afatinib (gold) in complex with EGFR (PDB: 4G5J). Hydrogen bonds are shown as dashed lines (black) and important sections are highlighted. Afatinib interacts with Met793 through a hydrogen bond and with C797 through a covalent bond. **C.** Schematic representation of the composition of covalent kinase inhibitors. The non-covalent inhibitor (gold) is attached to a linker motif (light blue) with connects it with an electrophilic warhead (green).

1.3. Macrocyclic protein kinase inhibitors

The design of selective inhibitors is still a challenging task due to the highly conserved ATP binding pocket, addressed by the ATP-mimetic compounds. Also, the majority of the FDA-approved drugs addresses the rigid and active state of the kinase,[44] leading to multi-kinase inhibitors which exhibit undesirable side effects. Macrocyclization is providing a new chemical space for designing novel ATP-mimetic compounds and gaining selectivity through rigidity. First, the usage of bioactive macrocycles was limited to natural products like rapamycin and their derivatives.[54,55] These molecules are usually very big and include stereocenters, making the synthesis and development of new macrocycles based on this scaffold quite difficult.[56] Furthermore, they often violate the Lipinski rule of five, a rule of thumb giving an indication of the oral bioavailability of the compound. The molecule of interest should not comprise more than 5 hydrogen bond donors, 10 hydrogen bond acceptors, a molecular weight higher than 500, and a calculated logP value higher than 5 to exhibit a good cell permeability or solubility.[57] Nowadays, simpler macrocycles are the focus of medicinal chemistry because they are synthetically more accessible, show favorable pharmacological properties and fulfill the Lipinski rule of five. In general, macrocycles consist of twelve or more atoms with a size of up to 2000 daltons.[58] The linear pharmacophore, typically an ATP mimetic scaffold, is connected through a linker motif at two positions (Figure 8A and B). The cyclization leads to a structural preorganization, thus minimizing the conformational freedom and improving the potency by reducing the entropic costs upon binding.[59] Furthermore, the molecule is locked in the bioactive conformation for the kinase of interest, leading to an improved selectivity against closely related off-targets.[60] The variation and optimization of the linker moiety and the length can lead to a favorable orientation in the desired binding pocket, whereby the macrocyclization can result in changed biological properties in comparison to the acyclic precursor. Furthermore, other pharmacokinetic and physiochemical properties, like the metabolic stability, solubility, bioactivity, or the ability to cross the blood-brain barrier can be optimized.[61,60]

The cyclization, in most cases the last step of the synthesis of a macrocycle, harbors some challenges as well. Side reactions like dimerization or polymerization are possible and can be avoided by high dilution even if this is an impractical strategy for drug development. Collins *et. al.* established the Emac value, which describes the feasibility of a ring-closing reaction even on a large scale. Therefore, the concentration and yield of the reaction are emphasized, whereby an Emac value between 8 and 9 is in an optimal range, with the average of currently published macrocyclization reactions being 5.8.[62] Furthermore, the ring-closing reaction can be challenging due to the necessity of a conformational preorganization of the precursor and yields depending on the size and geometry of the linker.[63,64] Various reaction types are reported in the literature, requiring different functional groups for the attachment of the linker as well as providing different structural motifs in the macrocycle. Over the last 15 years over 500 macrocyclization reactions have been reported, whereby most of them used the ring-closing metathesis (RCM) to produce a carbon-carbon double bond with an overall quite good yield.[65,66] Also, nucleophilic substitutions and palladium-catalyzed reactions, like heck- or suzuki-coupling, are often used with a yield of 13% and 10%, respectively.[67,68] Another common reaction type is the amide coupling which uses a coupling reagent like *O*-(7-Azabenzotriazol-1-yl)-*N,N,N′,N′*-tetramethyluronium-hexafluorophosphate (HATU) to gain a lactam moiety, which can be found in many macrocycles of natural products.[69] Only a minor proportion of 3.8% represents the C-O and C-N bond formation. For instance, the Mitsunobu reaction offers the possibility to form macrocyclic ethers and can be used for macrolactonization as well, depending on the used precursors (Figure 8C).[70,65]

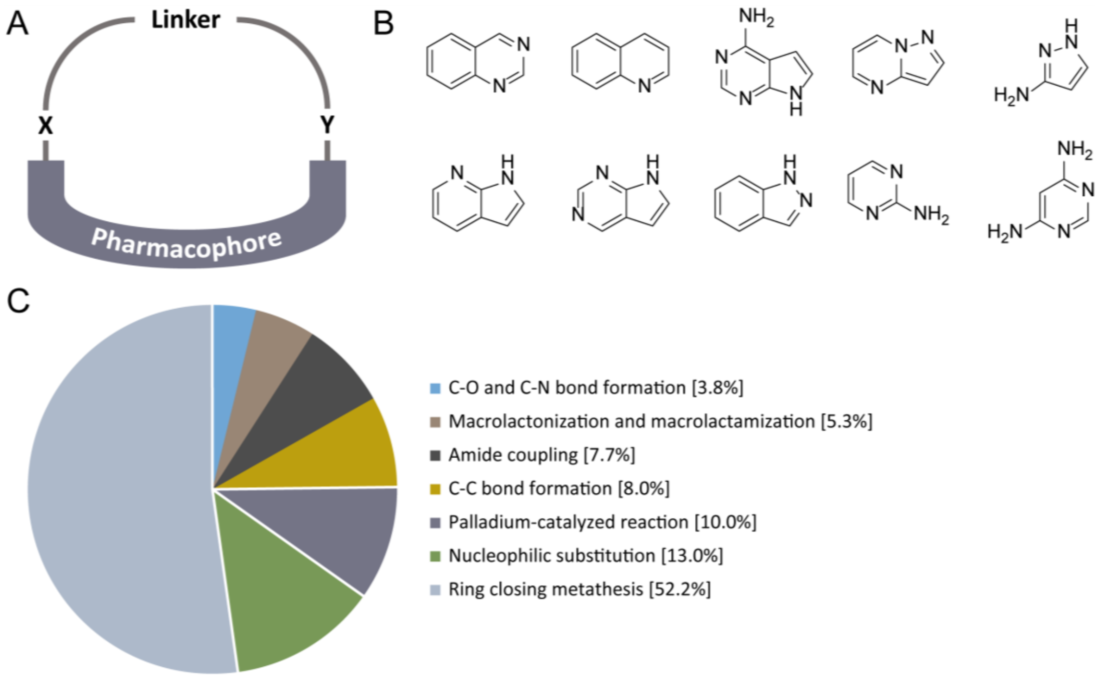

Figure 8. A. Schematic representation of a macrocyclic scaffold. The linear pharmacophore is connected through a linker motif. (Adapted from Mallinson *et. al.*).[61] **B.** Common hinge-binding moieties which can be used for macrocyclization: quinazoline, quinoline, 7*H*-pyrrolo[2,3-*d*]pyrimidin-4-amine, pyrazolo[1,5-*a*]pyrimidine, 1*H*-pyrazole-3-amine, 1*H*-pyrrolo[2,3-*b*]pyridine, 1*H*-indazole, 2-aminopyridine, pyrimidin-4,6-diamine (top left to bottom right).[71,72] **C.** Overview of different reaction types, used for macrocyclization reactions. (Adapted from Amrhein *et. al.*).[65]

Lorlatinib (**2**) represents the first type I FDA-approved macrocycle, which is an excellent example of the advance in drug discovery. It was approved in 2018 for the treatment of NSCLC, targeting ALK and ROS. The optimization of the starting point *R*-crizotinib (**1**) was done stepwise via a structure-based design resulting in a second generation ALK inhibitor and finally leading to lorlatinib

(**2**), an inhibitor of the third generation. **2** exhibits an increased potency against the main target ALK, while the kinome-wide selectivity against off-targets was improved. Additionally, **2** shows an effect on diverse known resistance mutants of the first and second generation ALK inhibitors, such as ALK^{L1152R} or ALK^{L1196M}. Furthermore, **2** has improved pharmacokinetic and physiochemical properties, due to a great central nervous system (CNS) and cell penetration as a result of a low efflux MDR BA/AB ratio of only 1.5. In comparison, *R*-crizotinib has a significant higher value of 44.5 (Figure 9A).[73–75]

Another example is the development of BI-4020 (**4**) for the treatment of the tertiary mutations EGFR$^{Del19\ T790M\ C797S}$ and EGFR$^{L858R\ T790M\ C797S}$ which occur in 12% – 47% of the NSCLC tumors. Engelhardt *et. al.* modified the starting point **3** in several steps through a QM-torsion angle scan optimization. First, different functional groups were varied, a cyclization was performed whereby the linker length was changed and lastly a solubilizing group was introduced to improve solubility as well as cell permeability. This results in **4**, a potent inhibitor for the tertiary EGFR mutations while being wild-type sparing with improved pharmacological properties (Figure 9B).[76] Both examples demonstrate the big advantage which is provided by the macrocyclization strategy. These are just two of many examples from the literature where the potency, selectivity, or even the pharmacological properties could be improved in contrast to the acyclic counterpart.[77–80]

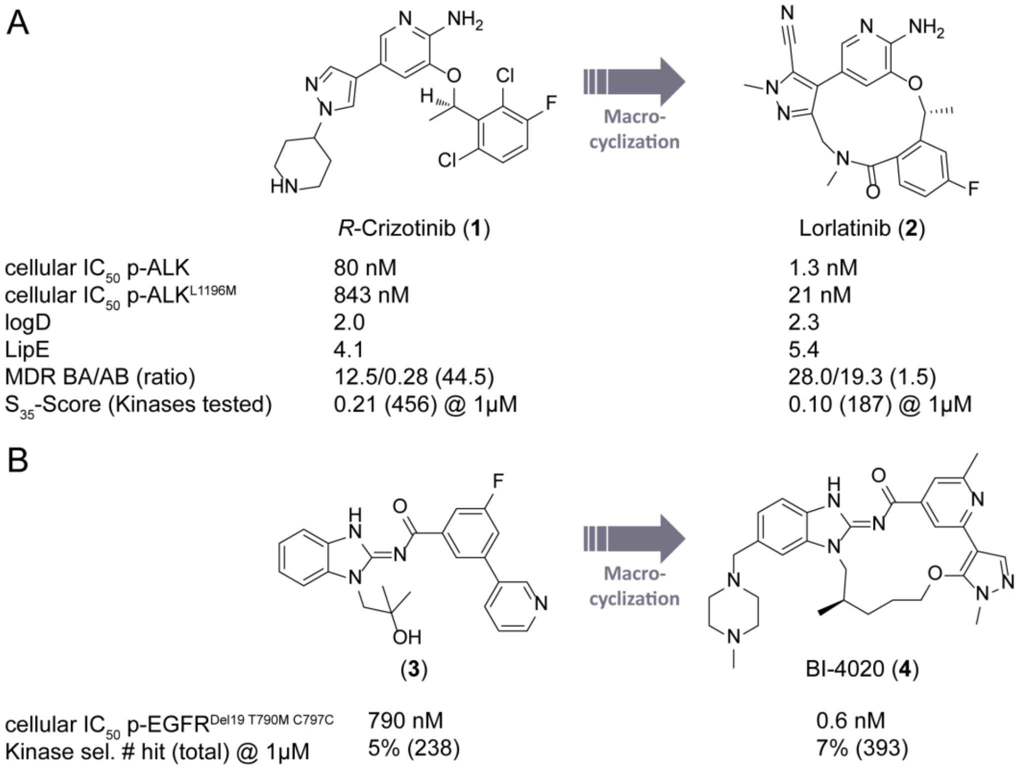

	R-Crizotinib (**1**)	Lorlatinib (**2**)
cellular IC$_{50}$ p-ALK	80 nM	1.3 nM
cellular IC$_{50}$ p-ALK^{L1196M}	843 nM	21 nM
logD	2.0	2.3
LipE	4.1	5.4
MDR BA/AB (ratio)	12.5/0.28 (44.5)	28.0/19.3 (1.5)
S$_{35}$-Score (Kinases tested)	0.21 (456) @ 1µM	0.10 (187) @ 1µM

	(**3**)	BI-4020 (**4**)
cellular IC$_{50}$ p-EGFR$^{Del19\ T790M\ C797C}$	790 nM	0.6 nM
Kinase sel. # hit (total) @ 1µM	5% (238)	7% (393)

Figure 9. A. Overview of the optimization of the potency and pharmacokinetic properties from the first (**1**) to the third generation ALK/ ROS inhibitor lorlatinib (**2**).[75,81] **B.** Overview of the optimization steps from aminobenzimidazole (**3**) to the macrocycle BI-4020 (**4**).[76]

1.4. Kinases of interest for this work

1.4.1. Epidermal growth factor receptor

The epidermal growth factor receptor (EGFR) is a transmembrane tyrosine kinase that belongs to the erbB family, a subfamily of the EGF receptors that comprises four related kinases: EGFR (also called ErbB1), HER2 (ErbB2), HER3 (ErbB3), and HER4 (ErbB4). EGFR was discovered in 1978 by Carpenter *et. al.* and it plays a central role in the embryonic development and adult homeostasis.[82,83] It comprises an extracellular domain which includes the domains I – IV, a transmembrane domain, and an intracellular domain, that involves the juxtamembrane domain, the tyrosine kinase domain, and the regulatory C-terminal domain (Figure 10A).[84] Monomeric EGFR is catalytically inactive and it is activated through the binding of different growth factors, such as the epidermal growth factor (EGF), transforming growth factor-α (TGFα), amphiregulin (AREG), betacellulin (BTC), epiregulin (EREG), epigen (EPGN), or heparin-binding EGF-like growth factor (HBEGF).[85] The extracellular domains I and III constitute the ligand binding pocket, whereby a rearrangement of the subdomains is initiated, exposing the so-called dimerization arm of the domain II and allowing the domains II and IV to be involved in the receptor homo- or heterodimerization with other HER family members. These rearrangements are conveyed to the cytoplasmic domain, leading to the formation of asymmetric dimers of the kinase domains and consequently the autophosphorylation of tyrosine residues in the C-terminal domain (Figure 10B).[86–88] The phosphorylated residues serve as docking sites for phosphotyrosine binding (PTB) domains or Src homology 2 (SH2), leading to the activation of diverse downstream signaling pathways,[89] including the Ras-Raf-MEK-MAPK pathway,[90] PI3K-Akt-mTOR pathway,[91] and the JAK-STAT pathway (Figure 10C).[92,93]

The canonical signaling pathways of EGFR are crucial for diverse biological functions, like the cell proliferation, survival, differentiation, or motility. A dysregulation can occur through autocrine activation, the overexpression of EGFR, activation mutations or a disrupted internalization, or degradation of the kinase. It can be found in various human tumors, like lung, colon, pancreas, breast, bladder, kidney cancer, or glioblastomas.[94] For instance, mutations of the extracellular domain are common oncogenic drivers in glioblastoma. The EGFR vIII mutation occurs in 30% – 50% of glioblastomas and lacks the amino acids 30 – 279 (domain I and II). It leads to an overexpression due to the constitutive activation without ligand binding, implicating an uncontrolled cell proliferation.[95,94] However, the mutations in the tyrosine kinase domain occur mainly in NSCLC patients, which build the majority with 85% of all lung cancer patients.[96] Approximately 40% – 60%

of the Asian and 10% – 20% of the Caucasian NSCLC patients exhibit mutations in the EGFR kinase domain whereby, they are divided into single-base point mutations, in-frame insertion- or deletion mutations.[97] The point mutation L858R (exon 21) and the deletion mutation Del19, which lacks the amino acids 746 – 750 (exon 19), represent the most common EGFR mutations. They occur in 41% and 47% of all cases, respectively. The remaining share represents less common mutations, like insertion mutations of exon 19 and 20, or other single-point mutations (Figure 10D).[98,99] After the successful treatment of these mutations, 50% – 70% of the patients suffer a relapse to the gatekeeper mutation T790M on exon 20.[100] This represents the secondary mutation, which is however followed by the tertiary mutation C797S in 20% – 40% of the already successfully treated patients.[101,102]

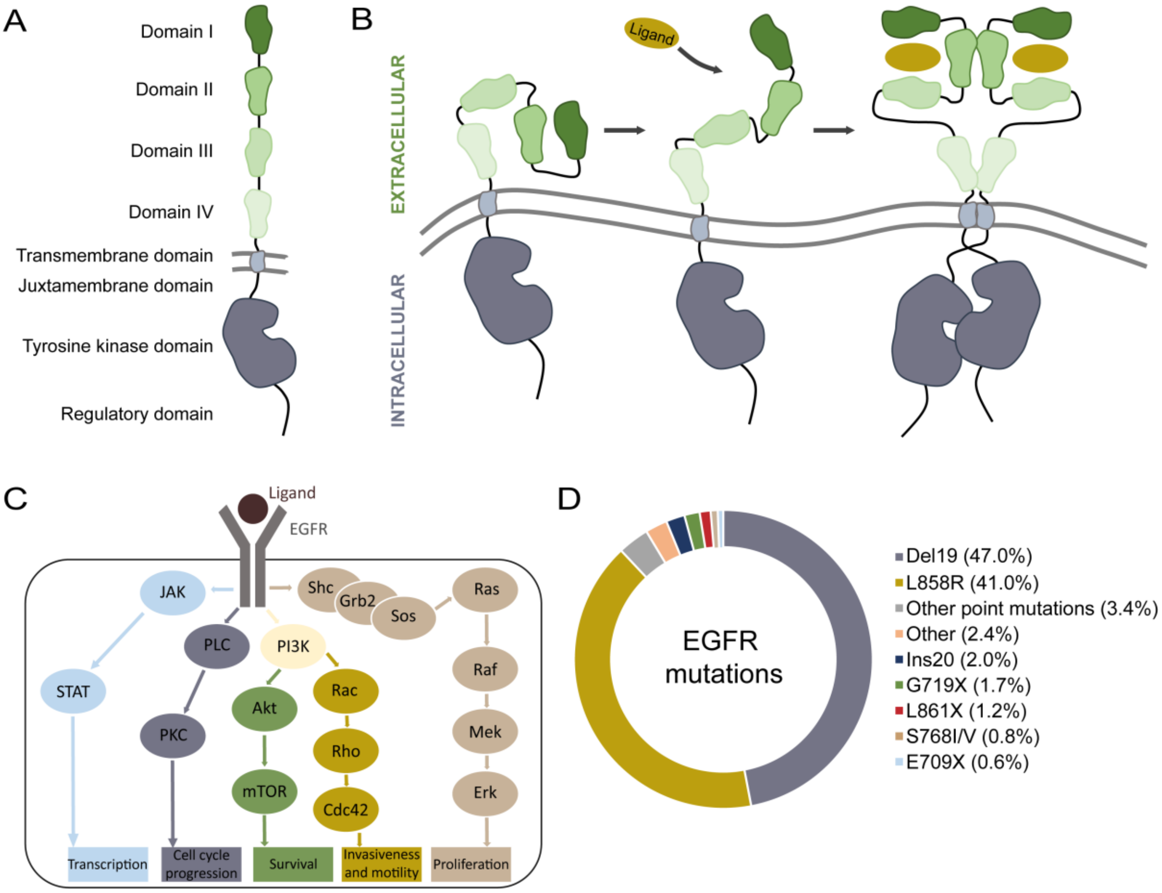
A
Domain I
Domain II
Domain III
Domain IV
Transmembrane domain
Juxtamembrane domain
Tyrosine kinase domain
Regulatory domain
B
Ligand
EXTRACELLULAR
INTRACELLULAR
C
Ligand
EGFR
JAK
Shc
Grb2
Sos
Ras
PLC
PI3K
STAT
Raf
Rac
Akt
PKC
Mek
Rho
mTOR
Erk
Cdc42
Transcription
Cell cycle progression
Survival
Invasiveness and motility
Proliferation
D
EGFR mutations
■ Del19 (47.0%)
■ L858R (41.0%)
■ Other point mutations (3.4%)
■ Other (2.4%)
■ Ins20 (2.0%)
■ G719X (1.7%)
■ L861X (1.2%)
■ S768I/V (0.8%)
■ E709X (0.6%)

Figure 10. A. Schematic representation of EGFR. The extracellular domain (green) includes the domains I, II, III, and IV, followed by the transmembrane domain (light blue). The intracellular domain (dark blue) consists of the juxtamembrane domain, the tyrosine kinase domain, and the C-terminal regulatory domain. **B.** Schematic representation of the EGFR activation. The binding of a ligand (gold) induces a structural rearrangement, followed by a formation of a dimer (Adapted from Sigismund *et. al.*).[88] **C.** The activation of EGFR is induced through ligand binding, followed by the autophosphorylation at the C-terminus. This causes the stimulation of different pathways, highlighted in different colors (Adapted from Amrhein *et. al.*).[103] **D.** Pie chart of the proportions of EGFR mutations in adenocarcinoma, whereby the resistance mutants T790M and C797S were filtered out (Adapted from Amrhein *et. al.*).[103]

Small molecule inhibitors targeting EGFR are partitioned into different generations of tyrosine kinase inhibitors (TKIs). Gefitinib (**5**) and erlotinib (**6**) are members of the first generation of EGFR inhibitors, which have a quinazoline-based hinge-binding moiety.[104,105] They are used for the treatment of EGFR mutated NSCLC, leading to survival benefits in comparison to monotherapies with for instance docetaxel.[106] In particular, the most common L858R and Del19 mutations are highly sensitive against gefitinib and erlotinib but they exhibit undesirable side effects due to multiple off-targets. The second generation of TKIs, like afatinib (**7**), show an improved kinome-wide selectivity compared to the first generation inhibitors but have a similar potency against EGFR wild type (WT). They also consist of a quinazoline-based hinge-binding moiety and additionally harbor a warhead that binds covalently to EGFR.[107] The previously mentioned gatekeeper mutation T790M weakens the potency of the quinazoline-based inhibitors of the first and second generation TKIs and dramatically increases the affinity for ATP. The gatekeeper mutation can be addressed by the third generation of EGFR inhibitors like mobocetinib (**8**) and osimertinib (**9**). Osimertinib (**9**) is an FDA-approved drug to target the T790M variant however, 20% – 40% of the successfully treated patients develop a resistance due to the tertiary mutation C797S.[108,109] This leads to the fact, that the third generation TKIs are no longer able to bind covalently to the kinase and patients harboring these mutations cannot be effectively treated through the currently approved kinase inhibitors. To address this problem, Engelhardt *et. al.* published the macrocyclic inhibitor BI-4020 (**4**), which also targets EGFR Del19/T790M/C797S with a low IC_{50} value of 0.6 nM (Figure 11).[76]

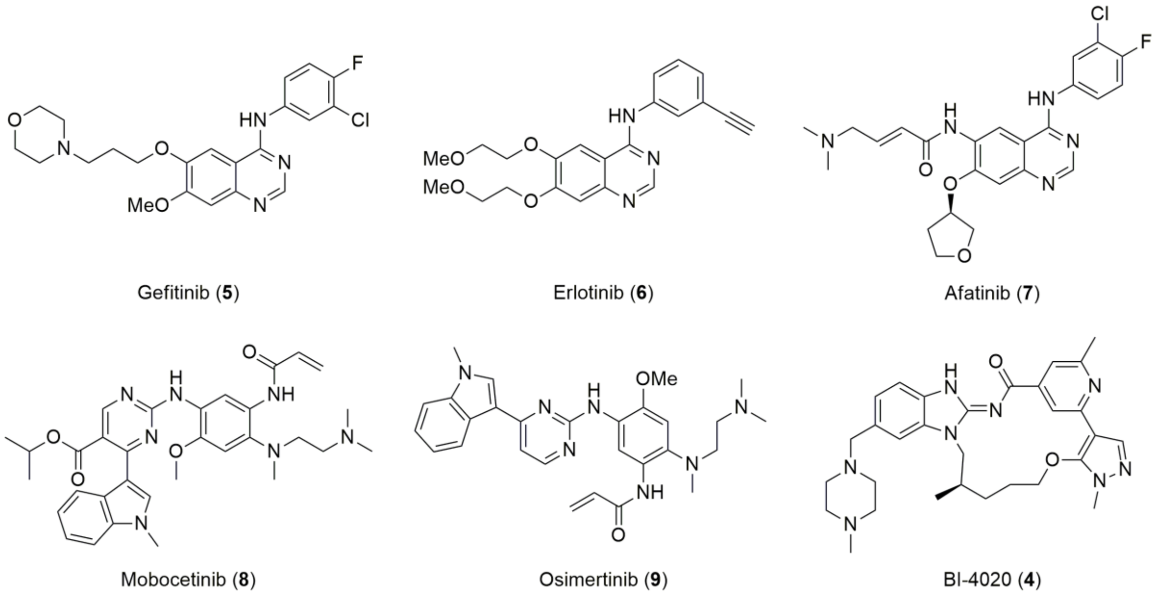

Gefitinib (**5**)

Erlotinib (**6**)

Afatinib (**7**)

Mobocetinib (**8**)

Osimertinib (**9**)

BI-4020 (**4**)

Figure 11. Chemical structures of approved first, second, and third generation EGFR inhibitors and published inhibitors, targeting EGFR.

1.4.2. Cyclin-dependent kinase 16

Cyclin-dependent kinases (CDKs) are serine-threonine kinases, which are activated through the binding of different cyclin partners. The CDK family comprises 21 members (CDK1 – 20), which are assigned by their structural similarity in a phylogenetic tree (Figure 12A).[110] All CDKs exhibit diverse cellular functions, like cell cycle regulation (CDK1 – 4, CDK6), regulation of transcription (CDK7 – 10), mRNA processing (CDK10 – 13), neuronal migration, or the release of neurotransmitters (CDK5).[111,112] The CDKs are characterized by a conserved catalytic domain that harbors the ATP binding pocket, a PSTAIRE-like cyclin binding domain, and a T-loop motif. The kinases are activated through the cyclin binding to the PSTAIRE-like binding domain, whereby the T-loop is shifted and expose the substrate-binding site, followed by the realigning of specific residues within the active site to prime the phospho-transfer reaction.[113] They are grouped in subfamilies, whereby CDK14 and 15 form the PFTAIRE subgroup and CDK16 – 18 the PCTAIRE subgroup based on their unique structural cyclin-binding sequence (Figure 12D). Despite their biological importance, the function as well as the regulation of CDK14 – 20 is poorly understood and all of them still belong to the so-called dark kinome.[114,115]

The PFTAIRE subfamily exhibits high expression levels in the human brain, whereby CDK14 is also highly expressed in the testis.[116] CDK17 is mainly expressed in the hippocampal and olfactory bulb regions of the brain, while CDK16 and 18 show the highest expression levels in the brain and the testis.[117,118] In particular, CDK16 is involved in various physiological processes, like neuronal development,[119] spermatogenesis,[120] vesicular trafficking,[121] glucose homeostasis,[122] and myogenesis.[123] CDK16 is localized in the cytoplasm and the nucleus of neurons but through forming a complex with its activator cyclin Y, CDK16 is relocalizing and is targeted to the plasma membrane. In contrast to other CDKs binding of cyclin Y to CDK16 requires a portion of the N-terminal extension in addition to the kinase domain. This prevents a further regulatory motif, whereby the phosphorylation of S153 enhances the formation of the CDK16/ cyclin Y complex, providing a mechanism to regulate the activity of this complex. Another crucial domain for the complex formation are the amino acids 112 – 121.[120] A dysregulation of the kinase activity can lead to various cancer types, like prostate, breast, cervical cancer, or melanomas.[124–127] The tumor suppressor p27 is involved in the cell cycle regulation by inhibiting the CDK4 and CDK6/ cyclin complexes, as well as the motility and apoptosis of cells.[128] CDK16 can phosphorylate p27 at S10, thus leading to the degradation of p27 through ubiquitination (Figure 12B). A downregulation is linked to high-grade tumors and a poor survival prognosis for the patients.[129,130] Yanagi *et. al.* demonstrated that CDK16 knockout induces G2/M cell cycle arrest, apoptosis, and accumulation of p27 in cutaneous squamous cell carcinoma (SCC) cells.[131] In 2018, Wang *et. al.* reported an upregulation of CDK16 in NSCLC tissues, leading to p27 degradation, thus consequently promoting NSCLC cell proliferation and inhibiting tumor cell apoptosis.[132] Furthermore, Xie *et. al.* reported that the phosphorylation of the tumor suppressor p53 at S315 by CDK16 in lung cancer results in p53 degradation via ubiquitination.[133] In 2020, Dohmen *et. al.* identified the involvement of the CDK16/ cyclin Y complex in macroautophagy. 5' AMP-activated protein kinase (AMPK) phosphorylates cyclin Y at S326, which is followed by the formation of the CDK16/ cyclin Y complex. This induces the autophosphorylation of the complex at S336 and leads to autophagy (Figure 12C). Autophagy is linked to inflammatory or neurodegenerative processes and as their data suggest, CDK16 promotes tumor growth by increasing tumor-supportive autophagy.[134–136]

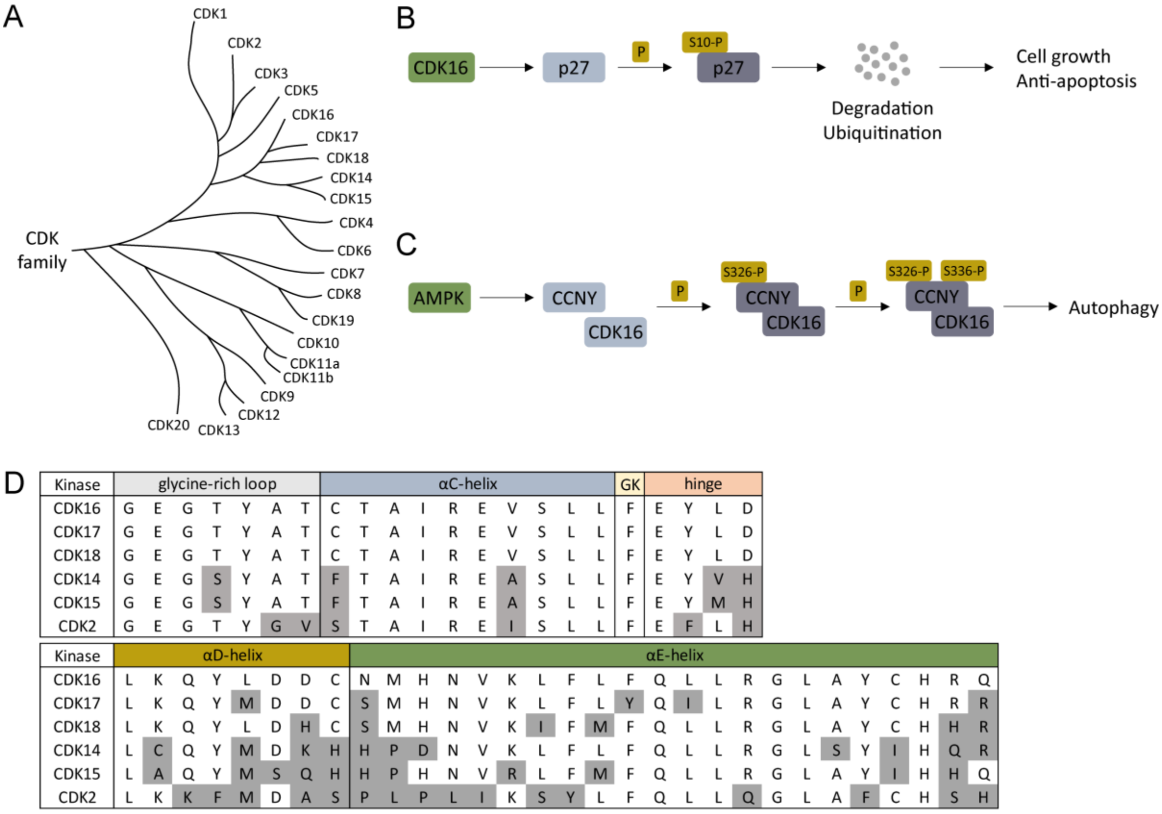
A
CDK1
CDK2
CDK3
CDK5
CDK16
CDK17
CDK18
CDK14
CDK15
CDK4
CDK6
CDK7
CDK8
CDK19
CDK10
CDK11a
CDK11b
CDK9
CDK12
CDK13
CDK20
CDK family
B
CDK16
p27
P
S10-P
p27
Degradation
Ubiquitination
Cell growth
Anti-apoptosis
C
AMPK
CCNY
CDK16
P
S326-P
CCNY
CDK16
P
S326-P
S336-P
CCNY
CDK16
Autophagy
D

Kinase	glycine-rich loop							αC-helix										GK	hinge			
CDK16	G	E	G	T	Y	A	T	C	T	A	I	R	E	V	S	L	L	F	E	Y	L	D
CDK17	G	E	G	T	Y	A	T	C	T	A	I	R	E	V	S	L	L	F	E	Y	L	D
CDK18	G	E	G	T	Y	A	T	C	T	A	I	R	E	V	S	L	L	F	E	Y	L	D
CDK14	G	E	G	S	Y	A	T	F	T	A	I	R	E	A	S	L	L	F	E	Y	V	H
CDK15	G	E	G	S	Y	A	T	F	T	A	I	R	E	A	S	L	L	F	E	Y	M	H
CDK2	G	E	G	T	Y	G	V	S	T	A	I	R	E	I	S	L	L	F	E	F	L	H

Kinase	αD-helix								αE-helix																					
CDK16	L	K	Q	Y	L	D	D	C	N	M	H	N	V	K	L	F	L	F	Q	L	L	R	G	L	A	Y	C	H	R	Q
CDK17	L	K	Q	Y	M	D	D	C	S	M	H	N	V	K	L	F	L	Y	Q	I	L	R	G	L	A	Y	C	H	R	R
CDK18	L	K	Q	Y	L	D	H	C	S	M	H	N	V	K	I	F	M	F	Q	L	L	R	G	L	A	Y	C	H	H	R
CDK14	L	C	Q	Y	M	D	K	H	H	P	D	N	V	K	L	F	L	F	Q	L	L	R	G	L	S	Y	I	H	Q	R
CDK15	L	A	Q	Y	M	S	Q	H	H	P	H	N	V	R	L	F	M	F	Q	L	L	R	G	L	A	Y	I	H	H	Q
CDK2	L	K	K	F	M	D	A	S	P	L	P	L	I	K	S	Y	L	F	Q	L	L	Q	G	L	A	F	C	H	S	H

Figure 12. A. Phylogenetic tree of the CDK family. **B.** CDK16 phosphorylates p27 at S10, thus initiating the degradation of p27 via ubiquitination. This leads to cell growth and anti-apoptosis (Adapted from Yanagi *et. al.*). [129] **C.** Schematic representation of the autophagy pathway. AMPK phosphorylates cyclin Y (CCNY) at S326 inducing the formation of the CDK16/ cyclin Y complex. The complex is autophosphorylating itself at S336, promoting autophagy (Adapted from Dohmen *et. al.*).[136] **D.** Alignment of key residues of the ATP binding pocket of CDK14 – 18 and CDK2. Differences in comparison to CDK16 are highlighted in grey.

The development of selective CDK16 inhibitors is still in the early stages and to date, no selective CDK16 inhibitors are published. The high similarity inside the kinase domain within the PCTAIRE subfamily with 73% identity (alignment of key residues of the kinase domain of CDK2 and

CDK14 – 18 are shown in Figure 12D) and the consensus homology over the whole CDK family with 59% makes it challenging to develop selective kinase inhibitors.[125] Dixon-Clarke *et. al.* screened several inhibitors, including those who are already been published or are in clinical trials to identify potential inhibitors, which target CDK16 and serve as starting points for further optimizations.[137] Most of the published inhibitors are non-selective or pan-CDK inhibitors. For instance, R547 (**10**) has a K_D value of 0.5 nM for CDK16 but it potently binds other CDK family members (e.g. CDK2 with K_D = 0.5 nM, CDK7 with K_D = 0.6 nM) and other kinases across the kinome like ICK (K_D = 2.2 nM) or CLK3 (K_D = 13 nM) as well.[34] SNS-032 (**11**) was developed for the inhibition of CDK2 (IC_{50} = 46 nM). However, it turned out to be a pan-CDK inhibitor with a potent inhibition of the PCTAIRE subfamily (CDK16 with K_D = 7.1 nM, CDK17 with K_D = 13 nM, and CDK18 with K_D = 44 nM).[138,34] AT-7519 (**12**) represents another pan-CDK inhibitor that potently binds to CDK16 (K_D = 1.1 nM)[115] but also to others of the family (e.g. CDK7 with K_D = 2.8 nM).[34] Furthermore, Dixon-Clarke *et. al.* revealed that CDK16 binds to type I and type II kinase inhibitors. Rebastinib (**13**) is a type II inhibitor, which is actually in phase 2 clinical trials for the treatment of advanced or metastatic myeloid leukemia. They showed that it inhibits CDK16 potently with IC_{50} = 32 nM. Dabrafenib (**14**), a type I kinase inhibitor for the treatment of advanced melanoma, is also inhibiting CDK16 in a similar range with IC_{50} = 35 nM.[137]

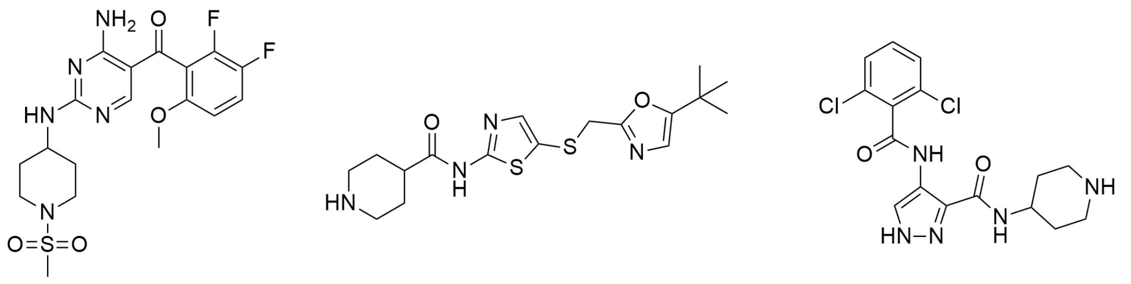

R547 (**10**) SNS-032 (**11**) AT-7519 (**12**)

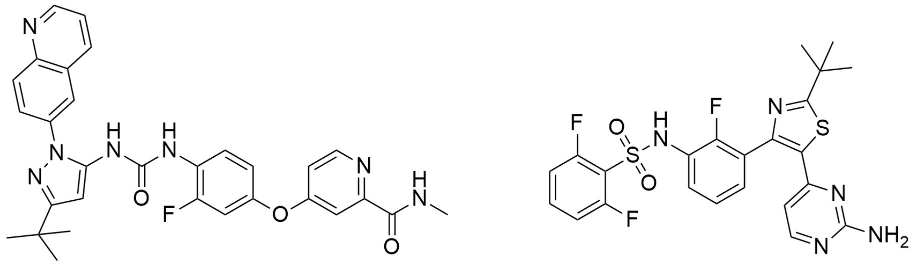

Rebastinib (**13**) Dabrafenib (**14**)

Figure 13. Chemical structures of published kinase inhibitors which target CDK16 however, no selective CDK16 inhibitor is known.

1.4.3. Bone morphogenetic protein receptor type II

The bone morphogenetic protein receptor type II (BMPR2) is a transmembrane serine-threonine receptor kinase and is a member of the STKR family.[139] It is involved in the canonical bone morphogenetic protein (BMP) signaling pathway through forming complexes with type I receptors. ALK1, ALK2, ALK3, and ALK6 are members of the type I BMP receptors and the type II receptors comprise BMPR2, ActRIIA, and ActRIIB. BMPR2 consists of an extracellular ligand-binding domain, a transmembrane helix, a short juxtamembrane domain, and an intracellular kinase domain (Figure 14A).[140] The binding of BMPs, members of the TGF-β superfamily, induces a cascade of signaling processes. Upon binding of BMPs to the extracellular domain of a type II receptor, a heterotetrameric complex is formed consisting of a type II and a type I homodimer. Crystallographic studies emphasize a symmetric complex where the type I receptors are diagonally opposite each other and a mirror-image arrangement of the type II receptors. The short juxtamembrane domain limits the reorientation, revealing a similar orientation of the intracellular domains.[141] The type I dimer is then activated through the constitutive phosphorylation of its so-called GS-box by BMPR2.[142] The GS-box is a glycine and serine-rich region which adjoins the N-lobe of the kinase domain. This motif is only present in the type I receptors (Figure 14A) and is autoinhibited, thus locking the αC-helix in the inactive conformation. The phosphorylation of the GS-box leads to the activation and loosening of the kinase domain.[143] R-Smad proteins (Smad1, 5, and 8) are then phosphorylated through the type I receptors, thus activating them and leading to a heterotrimer complex formation with Co-Smad (Smad4). The trimeric complex translocates into the nucleus and activates target genes like the DNA binding/ differentiation family (Id1, Id2, Id3, and Id4), regulating the cell proliferation, migration, or apoptosis (Figure 14B).[144,145]

BMPR2 is furthermore part of noncanonical pathways, such as the ERK, MAPK, NOTCH, LIMK, or Wnt pathway.[146] mRNA of BMPR2 is distributed in a broad range of different tissues, like lung, liver, kidney, brain, heart, skeletal muscle, or bone marrow.[147] BMPR2 is essential for the embryogenesis, neurogenesis, ossification, vascular homeostasis, and adult tissue homeostasis.[148,149,146] A dysregulated BMP signaling is linked to various diseases like vascular pathogenesis,[150] pulmonary arterial hypertension (PAH),[151] Alzheimer´s disease,[152] or different types of cancer.[145] In total there are over 400 different mutations of BMPR2 which are associated with PAH. However, the mutations are distributed throughout the entire gene and affect the extracellular domain, kinase domain, as well as the C-terminal trail. It includes frameshift, nonsense, and missense mutations.[153,154] PAH is classified as idiopathic PAH (IPAH) or heritable PAH (HPAH), whereby HPAH occurs in approximately 80% of patients. Mutations of BMPR2 account for about 75% – 80% of the cases of

HPAH and only a minor proportion of cases is attributed to mutations of other TGF-β family members.[144]

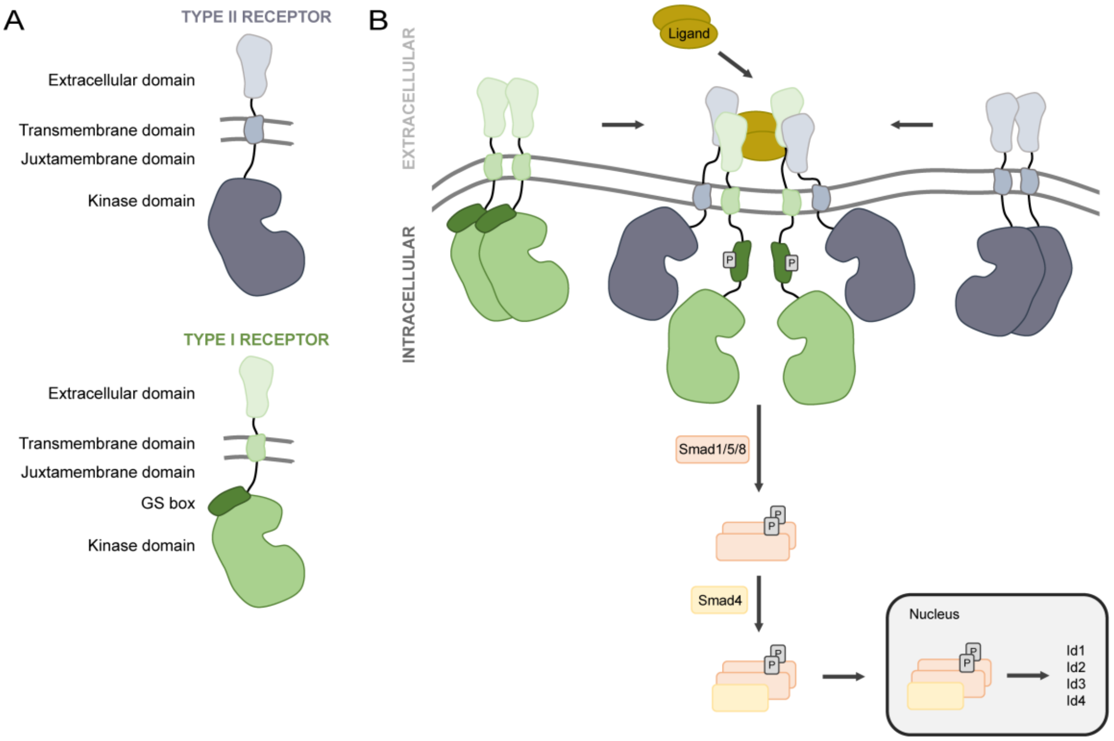
A
TYPE II RECEPTOR
Extracellular domain
Transmembrane domain
Juxtamembrane domain
Kinase domain
TYPE I RECEPTOR
Extracellular domain
Transmembrane domain
Juxtamembrane domain
GS box
Kinase domain
B
EXTRACELLULAR
INTRACELLULAR
Ligand
P
P
Smad1/5/8
P
P
Smad4
P
P
Nucleus
P
P
Id1
Id2
Id3
Id4

Figure 14. A. Schematic representation of type I and II receptor kinases. Type II receptors (blue) consist of an extracellular domain (light blue), a transmembrane domain (blue), an intracellular juxtamembrane domain, and a kinase domain (dark blue). Type I receptors (green) consist of an extracellular domain (light green), a transmembrane domain (green), an intracellular juxtamembrane domain, a kinase domain (middle green), and an additional GS-box (dark green). The GS-box locks the αC-helix of the kinase domain in the inactive conformation. **B.** Schematic representation of the canonical BMP pathway. A type I and type II homodimer form a tetrameric complex. The type I receptors are phosphorylated at the GS-box through the type II receptor, inducing the phosphorylation of Smad1, 5, 8. A heterotrimer complex is formed with Smad4, which translocates into the nucleus and activates target responsive genes (Adapted from Agnew *et. al.* and Andruska *et. al.*).[141,146]

To date, no selective BMPR2 kinase inhibitors have been reported and the number of published inhibitors is negligible. Most of them are promiscuous inhibitors like nintedanib (**15**) (K_D = 56 nM),[34] or exhibit only an off-target activity on BMPR2. Dorsomorphin (**16**) is an AMPK inhibitor that potently targets ALK2, ALK3, and ALK6 with IC_{50} values of 68 nM, 95 nM, and 235 nM, respectively. It also addresses BMPR2 in a low nanomolar range (IC_{50} = 74 nM) however, it has further off-targets and accordingly exhibits undesirable side effects.[145] In 2013, Engers *et. al.* published a SAR of kinase inhibitors based on the pyrazolo[1.5-*a*]pyrimidine scaffold of dorsomorphin. **17** is potently inhibiting BMPR2 with IC_{50} = 24 nM, but it is also targeting ALK1, ALK2, ALK2, TGFBR2, or VEGFR2 in a low nanomolar range.[155]

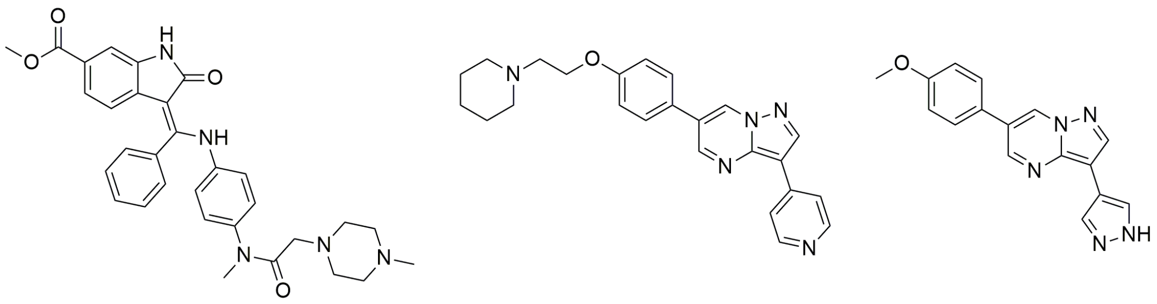

Nintedanib (**15**) Dorsomorphin (**16**) **17**

Figure 15. Chemical structures of kinase inhibitors, targeting BMPR2.

1.4.4. Mammalian STE20-like protein kinases

The Mammalian STE20-like protein kinases (MSTs) are members of the mammalian STE20 family and comprise five related proteins. The STE family consists of two subfamilies, called the P21-activated kinase (PAK) family and the germinal center kinase (Gck) family (Figure 16B).[156] These are further divided into the following subgroups: PAKI – II and GckI – VIII, whereby MST1 (also called STK4) and MST2 (STK3) are members of the GckII subgroup. They are mainly involved in the Hippo signaling pathway and are associated with tissue growth and the regulation of migration. MST3 (STK24), MST4 (STK26), and YSK1 (STK25) are responsible for the regulation of the Golgi apparatus and the cytoskeleton and are members of the GckIII subgroup. The kinase domains of the Gck subfamily are localized at the N-terminus however, they lack the GTPase binding domain, which is present in the PAK subfamily. The GckIII subgroup shares about 90% identity within their kinase domain and 20% in the C-terminal domain.[157] A sequence alignment is shown in Figure 16A.

MST3 is mainly localized in the cytoplasm and is highly expressed in the brain however, it can be found in various tissues. Autophosphorylation at T178 of the activation loop leads to the activation of the kinase. The cleavage of the C-terminal domain by caspases during apoptosis cause a nuclear accumulation of the MST3 kinase domain, leading to an increased kinase activity and promoting apoptosis (Figure 16C).[158] MST3 is involved in diverse physiological processes, such as cell morphology and cell cycle progression. Dysregulation is linked to diseases like epilepsy[159] and to a broad range of cancer types like NSCLC,[160] gastric cancer,[161] breast cancer,[162] and CNS tumorigenesis.[163] Oxidative stress promotes an upregulation of MST3 in trophoblasts, resulting in spontaneous miscarriages or the disruption of the fetal membrane tissue during the parturition.[164] The nuclear Dbf2-related (NDR) kinases are part of the NDR family, regulating the cell proliferation, cell spreading, and cytoskeleton organization. MST3 activates NDR kinases by phosphorylation of T442/ T444, thus promoting the G1 progression by stabilizing c-MYC and preventing the accumulation of p21 (Figure 16C).[165] Furthermore, MST3 as well as MST4 and YSK1 are members of the striatin-interacting phosphatases and kinases (STRIPAK) complex, which is involved in various diseases like heart diseases, autism, cancer, and cerebral cavernous malformation. It comprises the members of the striatin family, protein phosphatase 2A (PP2A), the GckIII subfamily, and other novel components. Thereby, PP2A negatively regulates the kinase activity of MST3, bound to the STRIPAK complex, through dephosphorylation at the activation loop.[166,167] Madsen *et. al.* reported FAM40A, FAM40B, and STRN3 as further STRIPAK components, whereby FAM40A negatively regulates the MST3 and MST4 kinase activity through enabling the PP2A complex to dephosphorylate them. FAM40B mutations were identified as oncogenes in breast cancer, leading to a high MST3 and MST4 activity and therefore high intracellular hydrostatic pressure by coupling contractile cytoskeleton to the plasma membrane, thus enhancing the migration through confined spaces.[168]

MST4 can be found in a broad range of tissues and is highly expressed in the placenta, thymus, brain, and peripheral blood leukocytes.[169,170] It is responsible for many diverse physiological functions, depending on the cell type. It plays a role in the Golgi reorientation, the inflammatory response, and the epithelial cell brush border formation.[171] The autophosphorylation of MST4 at T178 activates the kinase and provides the binding to GM130, a cis-Golgi protein, limiting MST4 to the Golgi matrix and enabling the control of the cell migration (Figure 16D).[158] Various cancer types, like pancreatic,[172] prostate,[167] breast cancer,[168] and hepatocellular carcinoma cells (HCC) are attributed to a dysfunction of MST4. In 2020, Hao *et. al.* reported the suppression of cell proliferation in HCC by inhibiting the GSK3β and AKT phosphorylation through MST4. This results in an inactivation of the PI3K/ AKT pathway, leading to a G1 cell cycle arrest and thereby MST4 indirectly affects the cell cycle. MST4 is downregulated in HCC, which is linked to an invasive and metastatic progression and therefore to a poor prognosis for the patients.[173] Furthermore, MST4 phosphorylates ATG4B at S383 which increases the ATG4B activity, thus promoting autophagosome formation and enhancing autophagy in glioblastoma (Figure 16D).[174] In recent studies, An *et. al.* reported the suppression of gastric tumorigenesis by MST4. Yes-associated protein 1 (YAP) is phosphorylated by MST4 at T83, which blocks the binding of importin α and leads to an inactivation and cytoplasmic retention of YAP. This represents a noncanonical Hippo signaling pathway, whereby the inactivation of this pathway is linked to a poor prognosis for the patients harboring gastric cancer.[175]

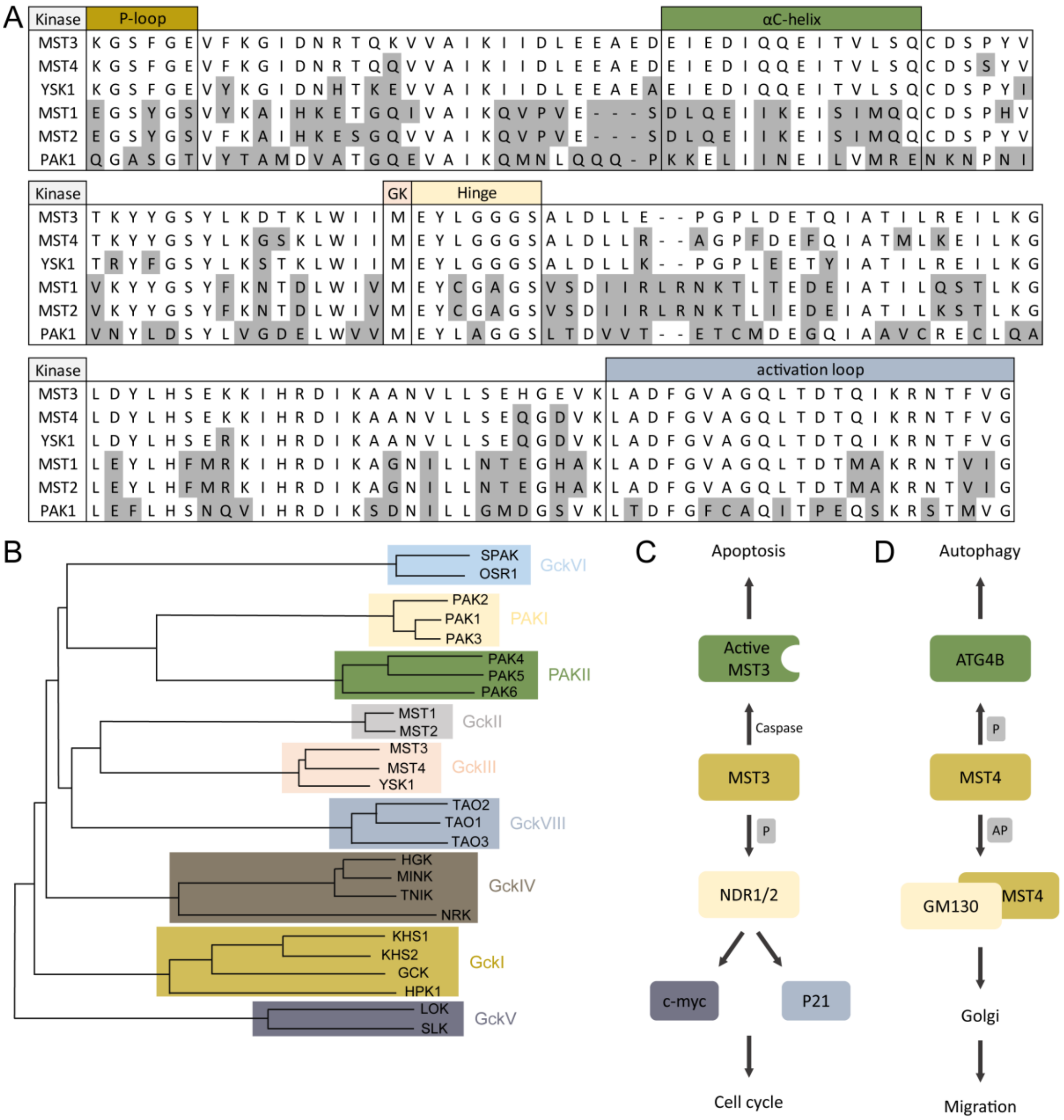
A
Kinase
P-loop
αC-helix
MST3 K G S F G E V F K G I D N R T Q K V V A I K I I D L E E A E D E I E D I Q Q E I T V L S Q C D S P Y V
MST4 K G S F G E V F K G I D N R T Q Q V V A I K I I D L E E A E D E I E D I Q Q E I T V L S Q C D S S Y V
YSK1 K G S F G E V Y K G I D N H T K E V V A I K I I D L E E A E A E I E D I Q Q E I T V L S Q C D S P Y I
MST1 E G S Y G S V Y K A I H K E T G Q I V A I K Q V P V E - - - S D L Q E I I K E I S I M Q Q C D S P H V
MST2 E G S Y G S V F K A I H K E S G Q V V A I K Q V P V E - - - S D L Q E I I K E I S I M Q Q C D S P Y V
PAK1 Q G A S G T V Y T A M D V A T G Q E V A I K Q M N L Q Q Q - P K K E L I I N E I L V M R E N K N P N I
Kinase
GK
Hinge
MST3 T K Y Y G S Y L K D T K L W I I M E Y L G G G S A L D L L E - - P G P L D E T Q I A T I L R E I L K G
MST4 T K Y Y G S Y L K G S K L W I I M E Y L G G G S A L D L L R - - A G P F D E F Q I A T M L K E I L K G
YSK1 T R Y F G S Y L K S T K L W I I M E Y L G G G S A L D L L K - - P G P L E E T Y I A T I L R E I L K G
MST1 V K Y Y G S Y F K N T D L W I V M E Y C G A G S V S D I I R L R N K T L T E D E I A T I L Q S T L K G
MST2 V K Y Y G S Y F K N T D L W I V M E Y C G A G S V S D I I R L R N K T L I E D E I A T I L K S T L K G
PAK1 V N Y L D S Y L V G D E L W V V M E Y L A G G S L T D V V T - - E T C M D E G Q I A A V C R E C L Q A
Kinase
activation loop
MST3 L D Y L H S E K K I H R D I K A A N V L L S E H G E V K L A D F G V A G Q L T D T Q I K R N T F V G
MST4 L D Y L H S E K K I H R D I K A A N V L L S E Q G D V K L A D F G V A G Q L T D T Q I K R N T F V G
YSK1 L D Y L H S E R K I H R D I K A A N V L L S E Q G D V K L A D F G V A G Q L T D T Q I K R N T F V G
MST1 L E Y L H F M R K I H R D I K A G N I L L N T E G H A K L A D F G V A G Q L T D T M A K R N T V I G
MST2 L E Y L H F M R K I H R D I K A G N I L L N T E G H A K L A D F G V A G Q L T D T M A K R N T V I G
PAK1 L E F L H S N Q V I H R D I K S D N I L L G M D G S V K L T D F G F C A Q I T P E Q S K R S T M V G
B
SPAK
OSR1
GckVI
PAK2
PAK1
PAK3
PAKI
PAK4
PAK5
PAK6
PAKII
MST1
MST2
GckII
MST3
MST4
YSK1
GckIII
TAO2
TAO1
TAO3
GckVIII
HGK
MINK
TNIK
NRK
GckIV
KHS1
KHS2
GCK
HPK1
GckI
LOK
SLK
GckV
C
Apoptosis
Active MST3
Caspase
MST3
P
NDR1/2
c-myc
P21
Cell cycle
D
Autophagy
ATG4B
P
MST4
AP
GM130
MST4
Golgi
Migration

Figure 16. A. Alignment of MST1 – 4, YSK1, and PAK1. Differences in comparison to MST3 are highlighted in grey. **B.** Phylogenetic tree of the STE family, containing the subfamilies PAKI – II and GckI – VIII. **C.** Schematic representation of MST3 signaling. MST3 can be activated through caspases, thus promoting apoptosis. MST3 can phosphorylate (P) NDR kinases, leading to cell cycle regulation via c-MYC and p21. **D.** Schematic representation of MST4 signaling. MST4 can phosphorylate ATG4B to promote autophagy. Furthermore, MST4 can autophosphorylate (AP) itself, leading to a complex formation with GM130, enabling the control of cell migration.

No selective MST3 or MST4 inhibitors are published to date. All of them are either nonselective inhibitors or were identified to show an off-target activity on MST3 or MST4. In 2014, Henderson *et. al.* published the LRRK2 inhibitor PF-06447475 (**18**) which exhibits a low IC$_{50}$ value of 178 nM against MST4.[176] G-5555 (**19**) is a potent PAK1 inhibitor with K$_i$ = 3.7 nM. Furthermore, it shows off-target activity on MST3 and MST4 with IC$_{50}$ values of 20 nM and 43 nM, respectively.[177] In 2016, Olesen *et. al.* investigated several previously published kinase inhibitors through differential scanning fluorimetry (DSF) screening and X-ray crystallography and identified nine chemical scaffolds targeting MST3. Danusertib (**20**) is a pyrazole-based aurora A, B, and C kinase inhibitor which targets MST3 with IC_{50} = 160 nM. Hesperadin (**21**) was identified to target MST3 and MST4 with IC_{50} values of 10 nM and 7 nM, respectively.[157,178] Neratinib (**22**) is an FDA-approved drug for the treatment of breast cancer targeting HER2 and EGFR in a low nanomolar range. However, MST3 and MST4 are off-targets, which are potently inhibited with IC_{50} values of 6.5 nM and 7.4 nM, respectively.[34]

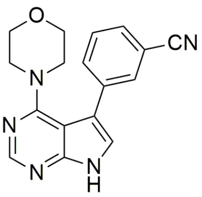
PF-06447475 (**18**)

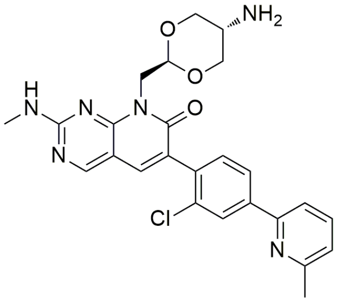
G-5555 (**19**)

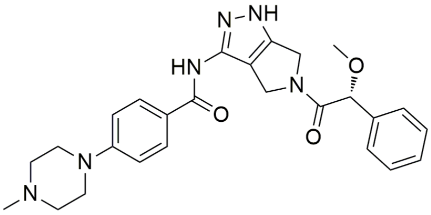
Danusertib (**20**)

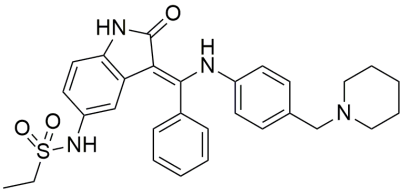
Hesperadin (**21**)

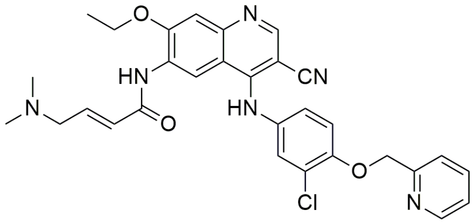
Neratinib (**22**)

Figure 17. Chemical structures of kinase inhibitors, targeting MST3 or MST4.

2. Objective

Protein kinases catalyze the reversible transfer of a ɣ-phosphate of ATP to amino acid residues of specific substrates. The phosphorylation represents a post-translational control mechanism of cell signaling within eukaryotic cells, thus influencing a variety of physiological and pathophysiological processes. The dysregulation of kinase activity is associated with various malfunctions such as inflammation, immune diseases, and cancer. The development of kinase inhibitors is the focus of scientific interest, which is emphasized by the constantly rising number of published and approved inhibitors. Due to the highly conserved ATP-binding pocket, the development of new selective ATP-mimetic inhibitors is challenging. The macrocyclization strategy provides new chemical space for ATP-mimetic compounds by locking the bioactive conformation of an acyclic inhibitor. Therefore, a linear pharmacophore is connected through a linker motif to obtain a macrocycle, composed of twelve or more atoms. Through cyclization of an acyclic conventional ATP-mimetic inhibitor, the number of possible conformations will be limited and the inherent shape of the macrocycle offers a conformationally constrained inhibitor that may adopt the bioactive conformation for binding to a certain kinase of interest. The cyclization is expected to reduce the entropic costs upon binding which results in an increased potency against the kinase of interest, as well as an improved selectivity across the kinome compared to the acyclic counterpart.

This thesis describes the structure-activity relationship (SAR)-based design and synthesis of macrocyclic kinase inhibitors, based on published inhibitors or already approved drugs which exhibit a broad range of off-targets. For this approach, gefitinib (**5**) was chosen as a starting point for the first project. It is an FDA-approved drug for the treatment of NSCLC targeting the most common EGFR mutations L858R and Del19 however, harboring various off-targets which lead to undesirable side effects. Based on this quinazoline scaffold, new selective macrocycles ought to be synthesized and subsequently, the selectivity profile and their biological activity should be evaluated. Furthermore, the multi-target kinase inhibitor **23**, published by Statsuk *et. al.* was chosen to gain macrocyclic kinase inhibitors based on the 3-aminopyrazole hinge-binding moiety.[179] A kinome-wide screen of **23** against 359 wild-type kinases emphasizes its promiscuous behavior. By targeting 337 kinases, **23** proves to be a suitable starting point for the usage of the macrocyclization strategy. The aim of the second project was the synthesis of new macrocyclic kinase inhibitors based on the 3-aminopyrazole scaffold, the identification of the potential targets, as well as the characterization of their selectivity profile and biological activity. Figure 18 shows a schematic representation of the two main projects of this thesis and it graphically summarizes the aims of this work.

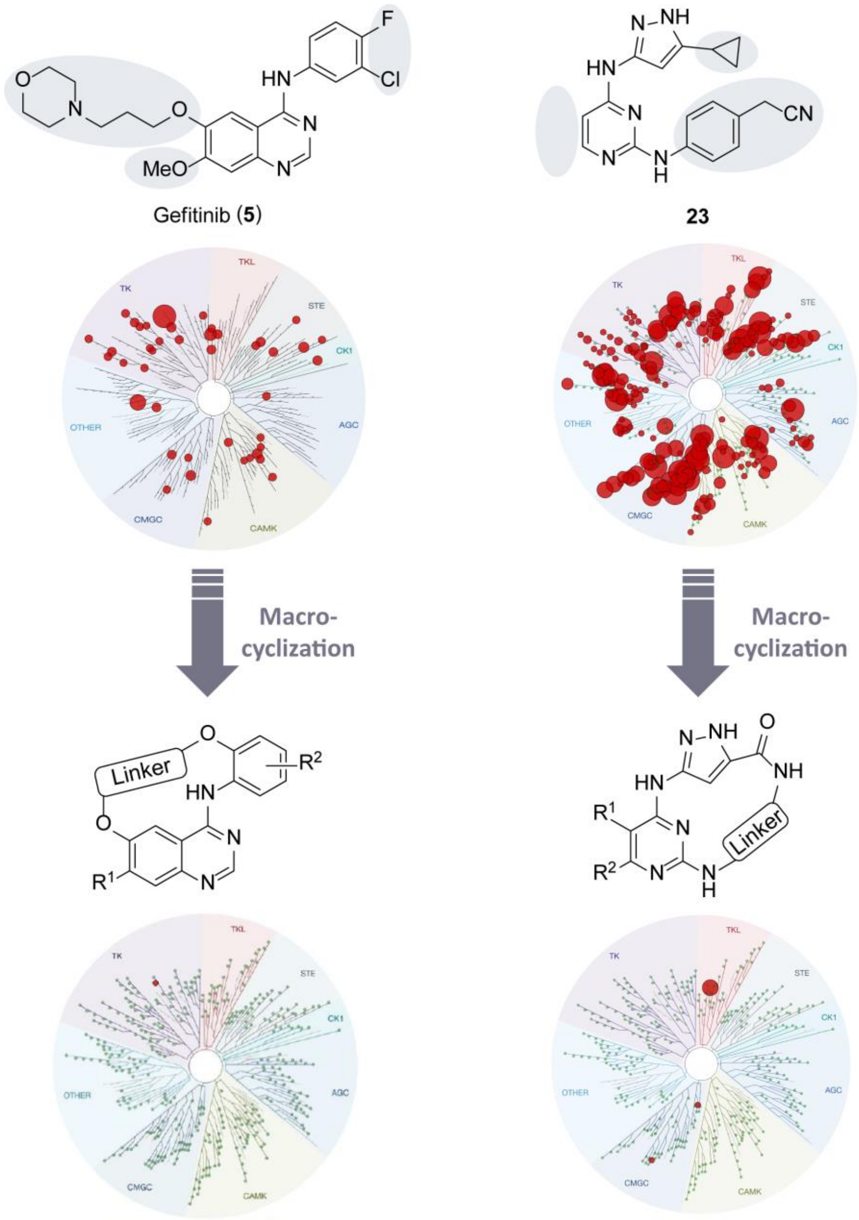
HN
F
Cl
O
N
O
MeO
N
N
Gefitinib (5)
N–NH
HN
N
N
N
H
CN
23
TK
TKL
STE
CK1
AGC
CAMK
CMGC
OTHER
Macro-cyclization
Macro-cyclization
O
Linker
O
HN
R2
R1
N
N
N–NH
O
HN
NH
R1
N
Linker
R2
N
N
H

Figure 18. Schematic representation of the aim of this thesis. Gefitinib (**5**) and **23** serve as starting points for the two projects. The modified structural motifs are highlighted in light blue and the desired kinome-wide selectivity is illustrated in a kinome tree, shown below the chemical structure. Through a SAR-based design, several macrocycles ought to be synthesized, optimized, and subsequently characterized for their biological activity.

3. Results and Discussion

3.1. Synthesis of the quinazoline-based macrocycles

The macrocycles **26a**–**f** were synthesized in a two-step synthesis route, which is shown in Scheme 1. In the initial step, the commercially available 4-chloro-7-methoxyquiazolin-6-ol (**24**) reacted with different 2-aminophenol derivatives in a nucleophilic substitution. The yields of this reaction were in a good range of 52% – 100% for all derivatives. The cyclization was done in the next step through a double Mitsunobu reaction, using diethylene glycol as a linker. Therefore, triphenylphosphine (TPP) and diisopropyl azodicarboxylate (DIAD) were used as coupling reagents to obtain the macrocycles **26a**–**f** in yields between 4% to 18%. A dimerization or polymerization could be avoided through high dilution of the reaction mixture. The poor yields of the macrocyclization can be attributed, among other things, to an incomplete reaction. It could be observed, that the diethylene glycol linker was attached to the precursor **25** once, however the second *in situ* Mitsunobu reaction failed. A second side product was the precursor **25** with two attached linker moieties.

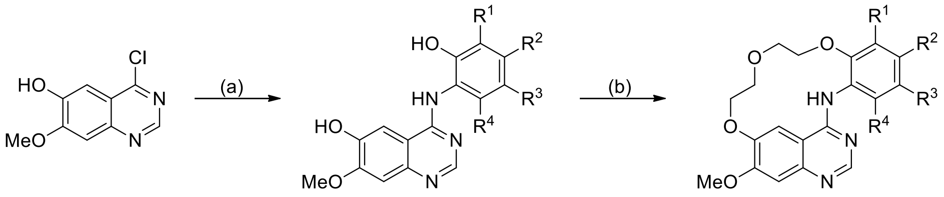

24 **25a-f** **26a-f**

a: R^1 = H R^2 = H R^3 = H R^4 = H
b: R^1 = Cl R^2 = H R^3 = H R^4 = H
c: R^1 = H R^2 = Cl R^3 = H R^4 = H
d: R^1 = H R^2 = H R^3 = Cl R^4 = H
e: R^1 = H R^2 = H R^3 = H R^4 = Cl
f: R^1 = H R^2 = F R^3 = Cl R^4 = H

Scheme 1. Synthesis of the macrocycles **26a**–**f**. Reagents and conditions: (a) 2-aminophenol derivatives and ethanol, 17 h, 70 °C; (b) diethylene glycol, TPP, DIAD, THF, and toluene, 20 h, rt – 40 °C.

A general mechanism of the Mitsunobu reaction is shown in Scheme 2. First, the azo group of DIAD (**27**) is attacked by the TPP nucleophile, resulting in the betaine **28**. This intermediate deprotonates the alcohol, yielding in **29**. In the next step, the second alcohol binds to **29** to form an alcohol-TPP-ion (**30**) whereupon, the phosphor is oxidized and the DIAD is reduced to the hydrazine derivative **31**. The deprotonated first alcohol then acts as a nucleophile and attacks **32**, whereby triphenylphosphine oxide is cleaved and the desired ether (**33**) is formed. Depending on the used educts, an ether or an ester bond can be formed, by using either two alcohols or a carboxylic acid and an alcohol. The premise for this reaction is a sufficient acidity of the desired nucleophile.[180]

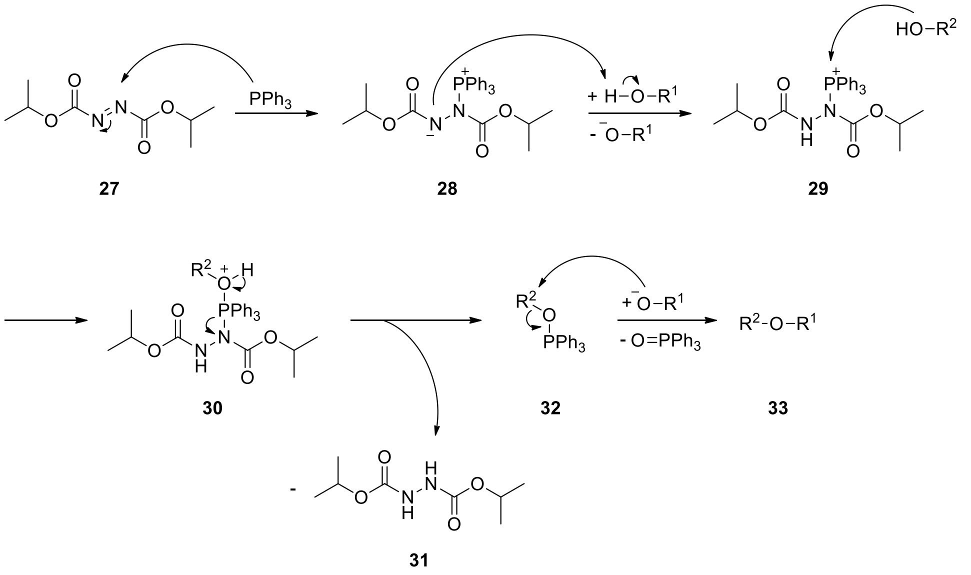

Scheme 2. General mechanism of a Mitsunobu reaction, using TPP and DIAD as coupling reagents.

In order to improve the yields of the macrocyclization step and to avoid the various side reactions of the double Mitsunobu reaction, an alternative synthetic route was established for the following compounds (Scheme 3). To determine the influence of the linker length and moiety, macrocycles **38a**–**f** and **39a**–**f** were synthesized. Therefore, the linker moieties 6-chlorohexan-1-ol (L^1) and 2-(2-(2-chloroethoxy)ethoxy)ethanol (L^2) were attached to 4-chloro-7-methoxyquiazolin-6-ol (**24**) by a Mitsunobu reaction, using TPP and DIAD as coupling reagents. The yields were in a good range of 76% to 78%. This was followed by a nucleophilic substitution, using diverse 2-aminophenol derivatives to obtain the compounds **36a**–**f** and **37a**–**f** with yields between 50% – 98% and 28% – 80%, respectively. In the last step, the macrocyclization was done by an intramolecular nucleophilic substitution, using sodium hydride. The final compounds **38a**–**f** and **39a**–**f** could be synthesized with yields between 21% – 73% and 6% – 100%, respectively. The overall yields for the synthesis of the macrocycles could be doubled on average in comparison to the previous synthetic route and the purification of the final compounds could be improved.

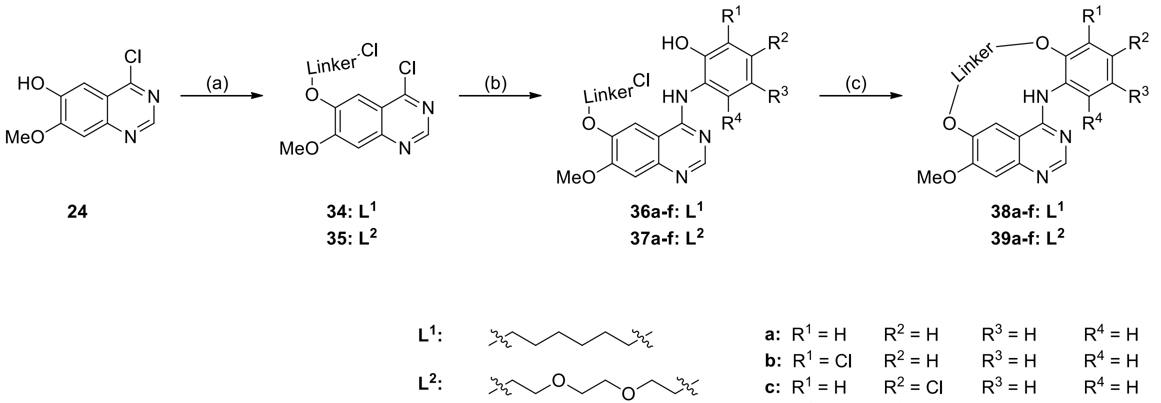

24 **34: L^1** **35: L^2** **36a-f: L^1** **37a-f: L^2** **38a-f: L^1** **39a-f: L^2**

a: R^1 = H R^2 = H R^3 = H R^4 = H
b: R^1 = Cl R^2 = H R^3 = H R^4 = H
c: R^1 = H R^2 = Cl R^3 = H R^4 = H
d: R^1 = H R^2 = H R^3 = Cl R^4 = H
e: R^1 = H R^2 = H R^3 = H R^4 = Cl
f: R^1 = H R^2 = F R^3 = Cl R^4 = H

Scheme 3. Synthesis of the macrocycles **38a**–**f** and **39a**–**f**. Reagents and conditions: (a) 6-chloro-1-hexanol or 2-[2-(2-chloroethoxy)ethoxy]ethanol, TPP, DIAD, and toluene, 2 – 5 h, rt – 80 °C; (b) 2-aminophenols and ethanol, 18 h, 70 °C; (c) NaH and DMF, 24 h, 0 – 60 °C.

The macrocycles **42a**–**d** were synthesized via the three-step synthesis route, which was described above. Therefore, the 2-(2-chloroethoxy)ethanol linker was attached to 4-chloro-7-methoxyquiazolin-6-ol (**24**) with a yield of 42%. In the next step, different 3-aminophenol derivatives were coupled to **40** with a turnover rate of 31% – 80% to introduce an alternative attachment point for the linker. The ring-closing reaction was again done via an intramolecular nucleophilic substitution to obtain the macrocycles **42a**–**d** in yields between 8% to 30%. The decreased average yields for the final step could be attributed to the ring tension due to the different attachment point.

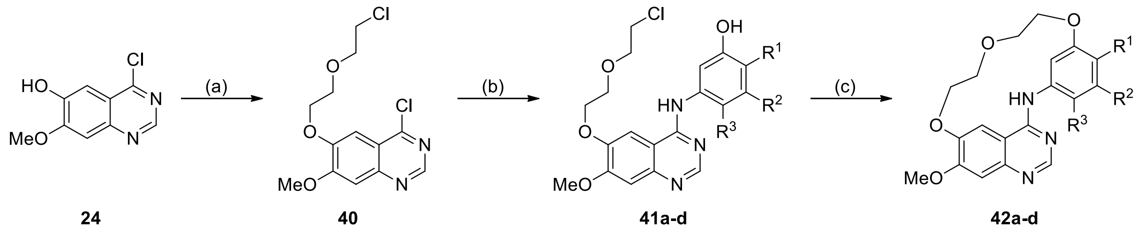

24 **40** **41a-d** **42a-d**

a: R^1 = H R^2 = H R^3 = H
b: R^1 = Cl R^2 = H R^3 = H
c: R^1 = H R^2 = Cl R^3 = H
d: R^1 = H R^2 = H R^3 = Cl

Scheme 4. Synthesis of the macrocycles **42a**–**d**. Reagents and conditions: (a) 2-(2-chloroethoxy)ethanol, TPP, DIAD, and toluene, 2 h, rt – 80 °C; (b) 3-aminophenols and ethanol, 18 h, 70 °C; (c) NaH and DMF, 24 h, 0 – 60 °C.

To evaluate the effect of the solvent-exposed residue at the C7 position of the quinazoline, macrocycle **48** was synthesized in a five-step synthetic route. In the initial step the commercially available 6-hydroxyquinazolin-4(3*H*)-one (**43**) was acetylated with a good yield of 85%. **44** was then chlorinated with thionyl chloride and was deprotected as a crude product with ammonia in methanol to obtain **46** in an overall yield of 16%. Therefore, the synthetic route published by Lyssikatos *et. al.* was adapted and slightly modified to improve the yields.[181] In the next step, 2-amino-4-chloro-5-fluorophenol was used in a nucleophilic substitution to synthesize **47** with a turnover rate of 75%. The macrocyclization was done via a double Mitsunobu reaction, using TPP and DIAD as coupling reagents. **48** could be obtained in the final step with a low yield of 5%.

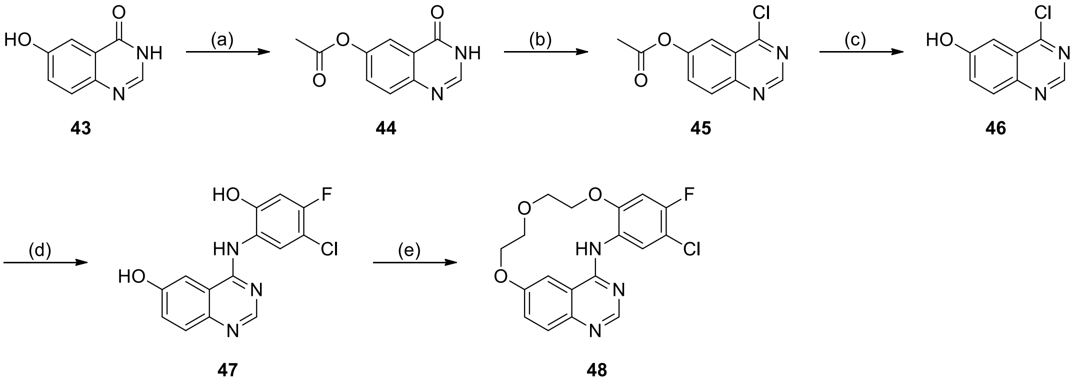

Scheme 5. Synthesis of the macrocycle **48**. Reagents and conditions: (a) acetic anhydride and pyridine, 1 h, 50 °C; (b) thionyl chloride and DMF, 3 h, 70 °C; (c) NH_3 and methanol, 1 h, rt; (d) 2-amino-4-chloro-5-fluorophenol and ethanol, 18 h, 70 °C; (e) diethylene glycol, TPP, DIAD, THF, and toluene, 20 h, rt - 40 °C.

3.2. Synthesis of 3-aminopyrazole-based kinase inhibitors

The synthetic route for the compounds **56** – **58**, and **60** is shown in Scheme 6. 5-cyclopropyl-1*H*-pyrazole-3-amine (**49**) reacted with a 2,4-dichloropyrimidine derivative (**50** – **52**) in a nucleophilic substitution under basic conditions, yielding in the intermediates **53** – **55** with a turnover rate of 32% – 89%. Different substituents like a hydrogen, a methyl, and a chlorine residue at position C5 of the pyrimidine were used. In the next step, different linker moieties were attached by a second nucleophilic substitution, whereby the reaction conditions differed depending on the desired moiety. The aniline derivatives were introduced with a catalytic amount of 1M HCl to gain the final compounds **56a**–**b**, **57a**–**b**, and **58a** with yields in a range from 16% – 90%. The aliphatic linkers and benzylamine derivatives were attached under basic conditions and microwave irradiation with yields between 5% to 60%. To determine the influence of the Boc protecting group in comparison to a smaller residue, the protecting group of **56e** was cleaved under acidic conditions, using trifluoroacetic acid (TFA) in dichloromethane (DCM). The smaller residue was introduced via an amide coupling under basic conditions, using 1-[bis(dimethylamino)methylene]-1H-1,2,3-triazolo[4,5-b]pyridinium 3-oxide hexafluorophosphate (HATU) as a coupling reagent to obtain the final compound **60** with a 30% yield.

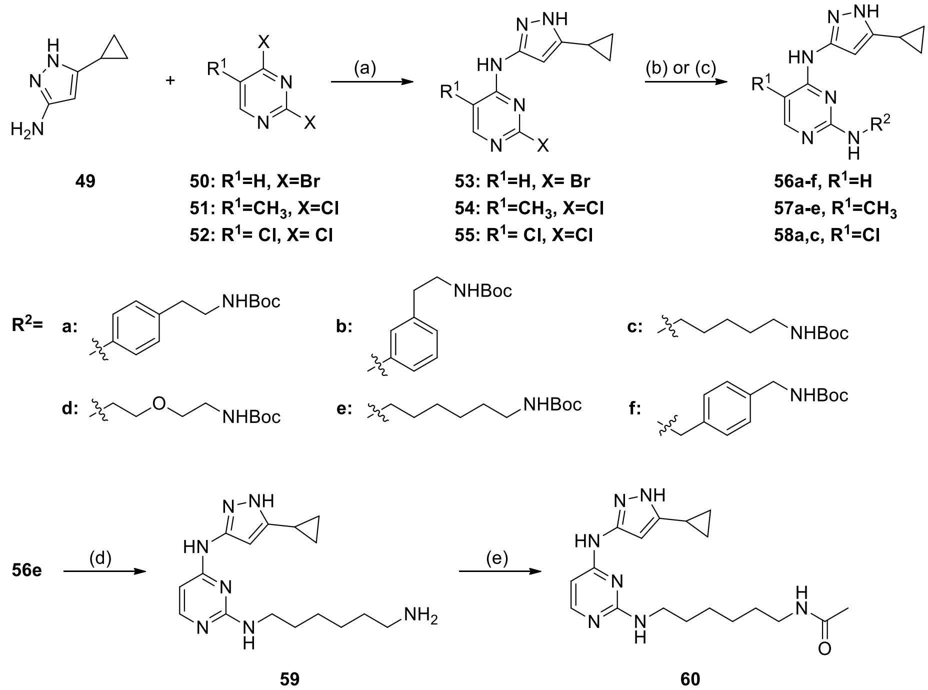
(a)
(b) or (c)
49
50: R1=H, X=Br
51: R1=CH3, X=Cl
52: R1= Cl, X= Cl
53: R1=H, X= Br
54: R1=CH3, X=Cl
55: R1= Cl, X=Cl
56a-f, R1=H
57a-e, R1=CH3
58a,c, R1=Cl
R2= a:
b:
c:
d:
e:
f:
NHBoc
56e
(d)
(e)
59
60

Scheme 6. Synthesis of **56a**–**f**, **57a**–**e**, **58a**,**c** and **60**. Reagents and conditions: (a) TEA and isopropanol, 48 h, 55 – 80 °C; (b) TEA and ethanol, microwave, 5 – 10 h, 80 – 90 °C; (c) HCl and ethanol, reflux, 4 – 18h; (d) TFA and DCM, 0 °C – rt, oN; (e) Acetic acid, HATU, DIPEA, and DMF, rt, oN.

A general mechanism of an amide coupling is shown in Scheme 7. In the initial step, the deprotonated carboxylic acid (**61**) acts as a nucleophile and attacks HATU (**62**), yielding in 1-hydroxy-7-azabenzotriazole (**63**) and the unstable O-acyl(tetramethyl)isouronium salt (**64**). **63** then attacks **64**, whereby the tetramethylurea (**65**) is cleaved and the active ester (**66**) is formed. The amine attacks the active ester (**66**), forming the intermediate **67** which decomposes to obtain 1-Hydroxy-7-azabenzotriazol (**68**) and the desired amide (**69**).[182]

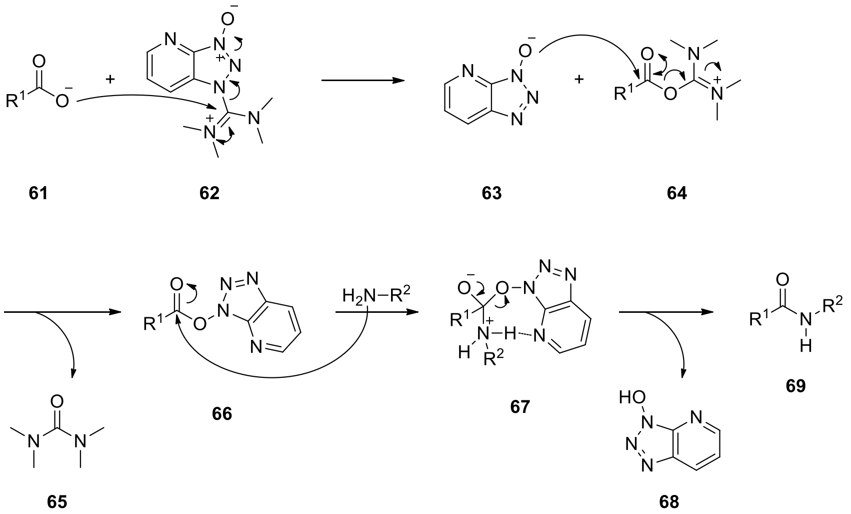
61
62
63
64
H2N−R2
65
66
67
68
69

Scheme 7. General mechanism of an amide coupling, using HATU as a coupling reagent.

The synthesis of a further series was done in the two-step synthetic route as described above and is shown in Scheme 8. Here, the commercially available 3-amino-1*H*-pyrazole-5-carboxylate (**70**) was coupled with a 2,4-dichloropyrimidine derivative (**71**, **52**, or **72**) via a nucleophilic substitution. The compounds **73** – **75** could be obtained with yields between 16% to 84%, whereby different residues at the positions C5 and C6 of the pyrimidine were used. The final compounds **76** – **78** were synthesized via a second nucleophilic substitution, using different linker moieties with a turnover rate in a range between 5% – 72%. In order to determine the influence of the Boc protecting group in comparison to a free amine, the protecting group was cleaved, using TFA in DCM. The final compounds **79** and **80** could be synthesized with a yield of 54% and 36%, respectively.

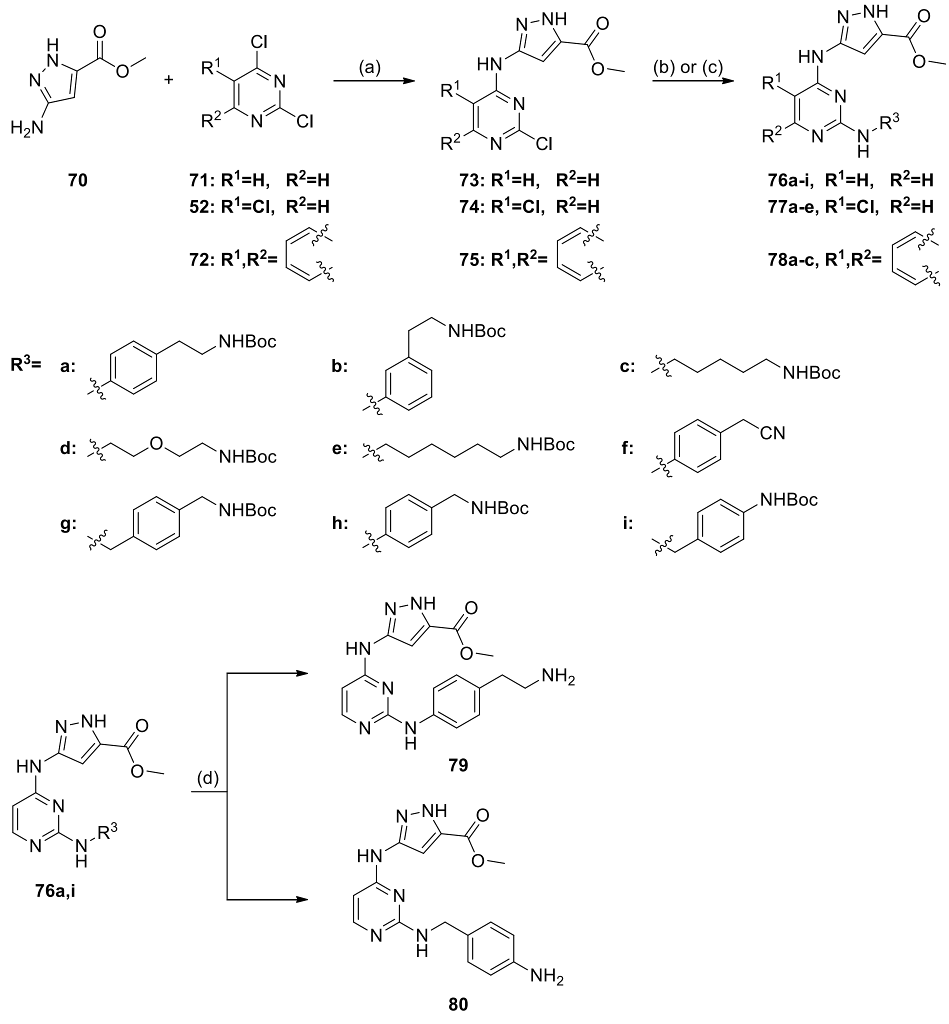

Scheme 8. Synthesis of compounds **76a**–**i**, **77a**–**e**, **78a**–**c**, **79**, and **80**. Reagents and conditions: (a) TEA and isopropanol, 24 – 72 h, 50 – 60 °C; (b) TEA and ethanol, microwave, 3 – 8 h, 80 – 120 °C; (c) HCl and ethanol, 70 °C – reflux, 18 h; (d) TFA and DCM, 0 °C – rt, oN.

A further variation of the residue at the pyrazole was done in a third series and is shown in Scheme 9. Commercially available 3-amino-1*H*-pyrazole derivatives (**81** – **86**) harboring a methyl, *iso*-propyl, *tert*-butyl, methyl amide, *iso*-propyl ester, or *tert*-butyl ester group were used. They reacted with 2,4-dichloropyrimidine (**71**) in a first nucleophilic substitution under basic conditions, yielding in the intermediates **87** – **92** with a turnover rate of 14% – 84%. The final compounds **93** – **98** could be obtained via a second nucleophilic substitution under either acidic conditions using a catalytic amount of 1M HCl or under basic conditions and microwave irradiation. The yields for the synthesis of the final products were in a range between 4% to 79%.

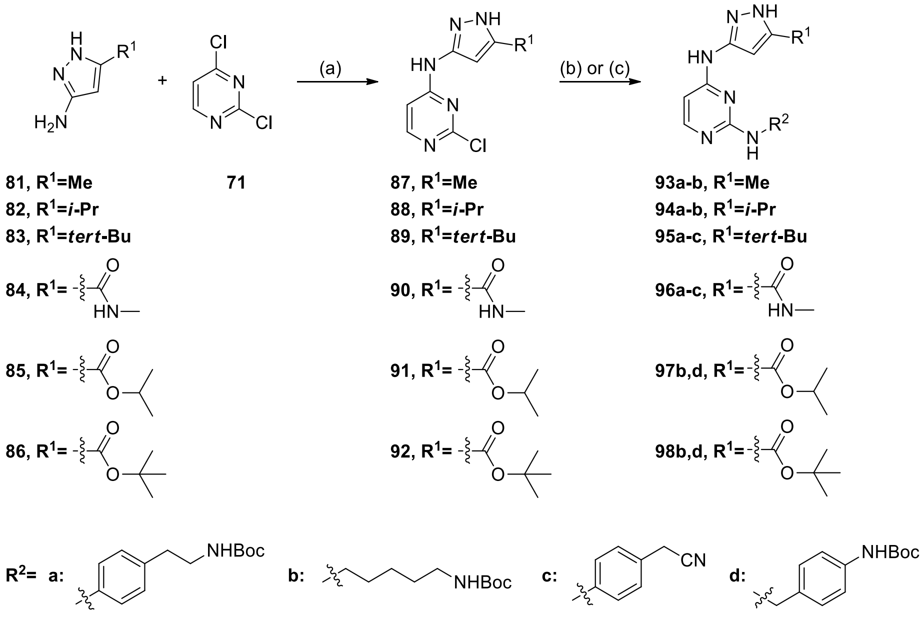

Scheme 9. Synthesis of compounds **93a**–**b**, **94a**–**b**, **95a**–**c**, **96a**–**c**, **97b,d**, and **98b,d**. Reagents and conditions: (a) TEA and isopropanol, 18 – 120 h, 60 °C; (b) TEA and ethanol, microwave, 8 h, 90 °C; (c) HCl and ethanol, 70 °C – reflux, 18h.

3.3. Synthesis of 3-aminopyrazole-based macrocycles

The macrocycles **110** – **113** were synthesized in a five-step synthetic route, which is shown in Scheme 10. The commercially available methyl 3-amino-1*H*-pyrazole-5-carboxylate (**70**) and a 2,4-dichloropyrimidine derivative (**71**, **52**, **99**, or **72**) reacted via a nucleophilic substitution under basic conditions to obtain the compounds **73**, **74**, **100**, and **75** with yields in a range from 7% to 84%. The different residues in position C5 and C6 of the pyrimidine were used to evaluate their influence by targeting the solvent-exposed region. In the next step, different linker moieties were attached via a second nucleophilic substitution. The aniline derivatives were introduced with a catalytic amount of 1M HCl and the aliphatic linkers were attached under basic conditions and microwave irradiation. The yields variate from 5% to 72%. The Boc protecting groups were cleaved under acidic conditions, using TFA in DCM. This was followed by a saponification with lithium hydroxide to enable the ring closing reaction. The cyclization was done via an amide coupling, using HATU as a coupling reagent to obtain the final compounds with low yields between 2% to 42%.

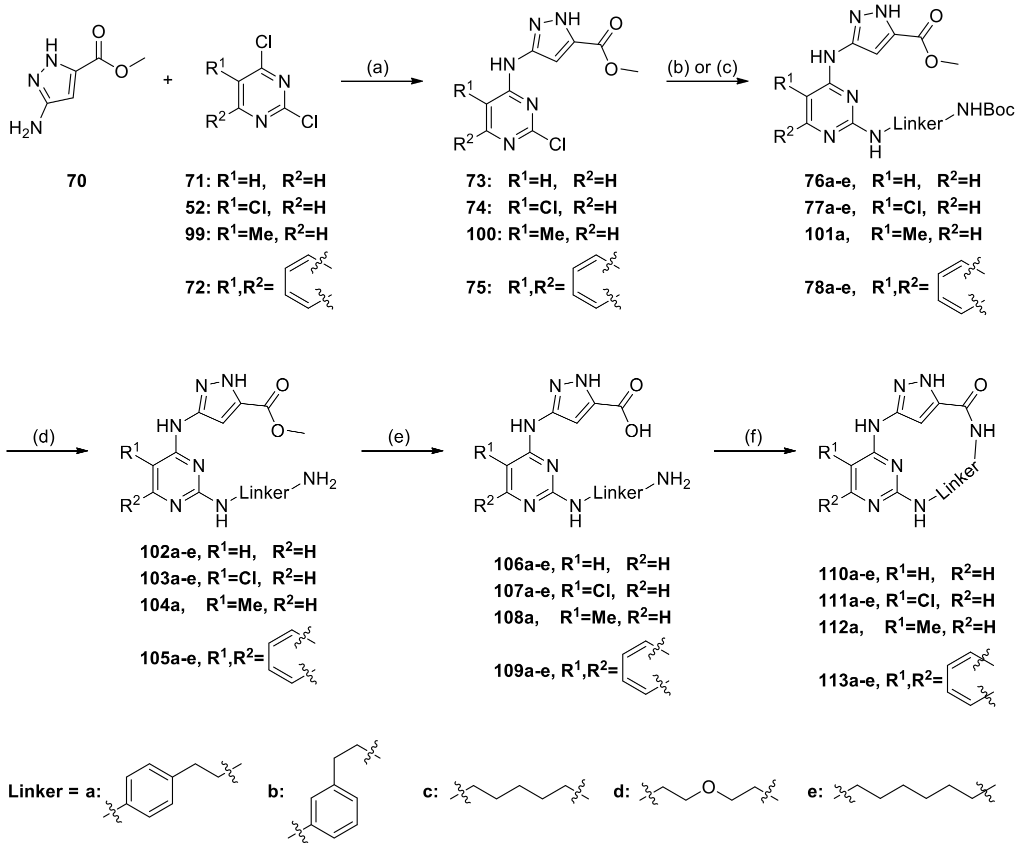
70
71: R¹=H, R²=H
52: R¹=Cl, R²=H
99: R¹=Me, R²=H
72: R¹,R²=
(a)
73: R¹=H, R²=H
74: R¹=Cl, R²=H
100: R¹=Me, R²=H
75: R¹,R²=
(b) or (c)
76a-e, R¹=H, R²=H
77a-e, R¹=Cl, R²=H
101a, R¹=Me, R²=H
78a-e, R¹,R²=
(d)
102a-e, R¹=H, R²=H
103a-e, R¹=Cl, R²=H
104a, R¹=Me, R²=H
105a-e, R¹,R²=
(e)
106a-e, R¹=H, R²=H
107a-e, R¹=Cl, R²=H
108a, R¹=Me, R²=H
109a-e, R¹,R²=
(f)
110a-e, R¹=H, R²=H
111a-e, R¹=Cl, R²=H
112a, R¹=Me, R²=H
113a-e, R¹,R²=
Linker = a:
b:
c:
d:
e:

Scheme 10. Synthesis of the macrocycles **110a**–**e**, **111a**–**e**, **112a**, and **113a**–**e**. Reagents and conditions: (a) TEA and isopropanol, 24 – 72 h, 50 – 60 °C; (b) TEA and ethanol, microwave, 3 – 8 h, 80 – 120 °C; (c) HCl and ethanol, 70 °C – reflux, 18 h; (d) TFA and DCM, 0 °C – rt, oN; (e) LiOH*H_2O, THF, and H_2O, 18 h, 55 °C; (f) HATU, DIPEA, and DMF, 18 h, rt – 60 °C.

3.4. Macrocyclization of quinazoline-based EGFR inhibitors lead to exclusive mutant selectivity for EGFR L858R and Del19

3.4.1. *In-vitro* characterization

As a first *in-vitro* characterization, the activity of the synthesized macrocycles **26a**–**f**, **38a**–**f**, **39a**–**f**, **42a**–**d**, and **48** were tested against EGFR WT, EGFR Del19, and EGFR d747–752/P753S in a radiometric protein kinase assay, provided by Reaction Biology (Table 1). The acyclic compound **25f** was also characterized and served as a control compound. **25f** was highly potent against all tested mutants and EGFR WT. The most interesting profiles could be seen for **26b** and **26f**, by potently inhibiting EGFR Del19 with 15% and 12% remaining activity, respectively. The effect on EGFR WT was quite low with 49% and 45%. **26d** inhibited all tested kinases however, the macrocycles **26c** and **26e** showed a negligible activity for all of them. The derivatives **38a**–**f**, harboring the 6-chlorohexan-1-ol linker (L^1), were also either inactive (**38b**, **38c**) or showed an effect on all kinases (**38d** – **38f**). The macrocycles **39a**–**f** with the longest 2-(2-(2-chloroethoxy)-ethoxy)ethanol (L^2) linker moiety seemed to be highly potent for all tested kinases and showed no preferred inhibition of mutant EGFR. The changed attachment point for the linker (**42a**–**d**) seemed to be not tolerated by showing no activity against the tested mutants or EGFR WT. Surprisingly, macrocycle **48** also seemed to be inactive however, it only lacked the methoxy group at the C7 position of the quinazoline moiety which constituted a relatively small change in the solvent-exposed region.

Next, the IC_{50} values of the newly synthesized compounds were determined against EGFR WT, EGFR Del19, EGFR L858R, and EGFR L858R/T790M using a homogeneous time-resolved fluorescence (HTRF) assay (Table 1). Gefitinib, BI-4020, and osimertinib were used as further control compounds. The acyclic counterpart **25f** exhibited low IC_{50} values for all tested mutants. The macrocycles **26a**–**f** showed a preferred activity on EGFR Del19, especially with low IC_{50} values of 154.6 nM, 24.9 nM, and 119.1 nM for **26a**, **26d**, and **26f**, respectively. EGFR L858R was targeted with a lower activity between 127.5 nM – 820.8 nM and an inactivity against EGFR WT (IC_{50} > 10 µM). The same tendency could be seen for the macrocycles **38d** – **38f** with IC_{50} values of 19.6 nM – 235.5 nM for EGFR Del19 and 275.1 nM – 738.6 nM for L858R. **39a** seemed to be selective for L858R (IC_{50} = 87.6 nM) against Del19 (IC_{50} = 1874.3 nM) however, the other macrocycles with the longer linker **39b** – **39f** were potent on both mutants in a low nanomolar range. The 3-aminophenol derivatives **42a**–**d**, as well as **48**, were again inactive. As expected, the double mutation L858R/T790M led to a weaker potency against the macrocycles due to the gatekeeper mutation T790M which weakens the potency of the quinazoline-based compounds by a resistance mechanism.

Table 1. Potency of the quinazoline-based macrocycles **26a**–**f**, **38a**–**f**, **39a**–**f**, **42a**–**f**, and **48** against EGFR WT and its mutants.

	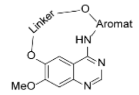		Percent of control activity [%][a]			IC_{50} [nM][b]			
ID	Linker	Aromat	WT	Del19	d747-752/ P753S	WT	Del19	L858R	L858R/ T790M
25f			1.9 ± 0.2	0.9 ± 0.1	0.4 ± 0.1	1795.3 ± 859.1	11.5 ± 2.5	18.8 ± 2.2	609.0 ± 631.5
26a	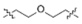		n.d.	n.d.	n.d.	> 100000	154.6 ± 58.8	685.2 ± 59.2	1681.0 ± 235.5
26b	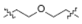	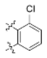	49.1 ± 3.9	14.6 ± 1.7	39.8 ± 0.3	> 100000	509.3 ± 195.2	3991.3 ± 30003.4	> 100000
26c	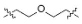	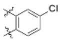	80.4 ± 3.2	52.0 ± 0.9	76.2 ± 2.1	> 100000	> 100000	> 100000	> 100000
26d	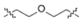	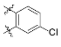	13.7 ± 2.9	1.1 ± 0.6	8.1 ± 1.7	> 100000	24.9 ± 23.7	127.5 ± 30.1	3358.0 ± 706.4
26e	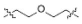	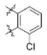	81.7 ± 8.1	64.9 ± 2.6	77.4 ± 1.4	n.d.	n.d.	n.d.	n.d.
26f	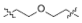	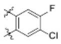	44.5 ± 6.0	12.2 ± 0.2	40.5 ± 1.9	> 100000	119.1 ± 53.8	820.8 ± 282.0	> 100000
38a	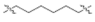		n.d.	n.d.	n.d.	> 100000	490.6 ± 516.7	>100000	> 100000
38b	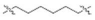	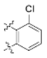	62.2 ± 2.9	29.0 ± 2.3	53.8 ± 0.9	> 100000	3034.0 ± 964.1	> 100000	> 100000
38c	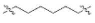	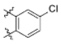	84.8 ± 0.6	93.1 ± 0.3	91.5 ± 6.4	> 100000	63506.7 ± 38404.9	> 100000	> 100000
38d	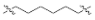	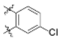	14.9 ± 2.5	3.7 ± 0.9	10.6 ± 1.7	> 100000	19.6 ± 29.9	738.6 ± 337.2	> 100000
38e	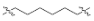	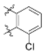	26.9 ± 3.3	7.2 ± 1.0	13.6 ± 0.9	> 100000	56.8 ± 29.4	275.1 ± 22.7	698.3 ± 114.2
38f	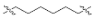	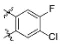	15.3 ± 2.3	9.9 ± 5.2	16.2 ± 3.6	> 100000	235.5 ± 71.8	655.1 ± 294.6	18066.7 ± 5521.3
39a	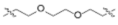		n.d.	n.d.	n.d.	> 100000	1874.3 ± 3153.8	87.6 ± 10.3	1121.0 ± 209.9
39b	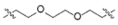	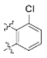	48.0 ± 13.1	17.6 ± 1.1	29.1 ± 2.4	> 100000	114.0 ± 21.6	448.5 ± 40.3	5450.0 ± 842.1
39c	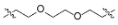	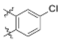	11.9 ± 0.6	5.2 ± 0.4	6.9 ± 0.4	> 100000	16.2 ± 4.1	38.3 ± 5.5	326.0 ± 41.5
39d	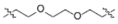	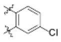	0.5 ± 0.5	0.0 ± 0.0	-0.2 ± 0.3	> 100000	0.3 ± 0.1	0.7 ± 0.5	102.8 ± 8.6
39e	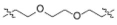	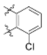	12.9 ± 0.5	4.6 ± 0.4	3.2 ± 0.8	> 100000	42.9 ± 34.3	32.6 ± 2.8	126.4 ± 34.3
39f	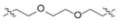	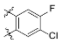	2.9 ± 0.0	0.3 ± 0.5	0.4 ± 0.9	> 100000	1.3 ± 0.4	2.8 ± 1.6	361.1 ± 365.8
42a	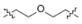	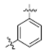	n.d.	n.d.	n.d.	> 100000	33860.0 ± 13398.0	> 100000	> 100000
42b	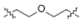	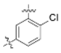	44.5 ± 3.3	29.0 ± 0.8	33.8 ± 0.1	> 100000	492.9 ± 97.5	1119.0 ± 238.8	> 100000
42c	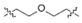	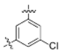	74.0 ± 1.9	70.9 ± 0.1	78.0 ± 1.5	> 100000	6302.0 ± 2057.0	9680.0 ± 5258.9	> 100000
42d	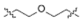	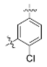	95.1 ± 9.6	133.7 ± 40.9	92.2 ± 2.7	> 100000	70396.7 ± 20988.9	19880.0 ± 3622.3	> 100000
48			55.2 ± 3.6	23.5 ± 0.7	60.4 ± 0.5	> 100000	1026.7 ± 615.2	> 100000	676.7 ± 507.5
Gefitinib			n.d.	n.d.	n.d.	> 100	0.9 ± 0.3	3.8 ± 1.8	> 100
BI-4020			n.d.	n.d.	n.d.	> 100	0.3 ±0.1	5.0 ± 2.6	0.02 ±0.01
Osimertinib			n.d.	n.d.	n.d.	34.5 ± 6.7	0.5 ±0.01	1.8 ± 0.3	0.8 ±0.4

[a] Values were determined at a screening concentration of 1 µM by Reaction Biology, using a radiometric protein kinase assay (mean ± SD, in duplicates). [b] IC_{50} values were determined using a HTRF assay in a 12-point dose response curve (mean ± SD, n = 3 in triplicates).

3.4.2. Selectivity profile

To obtain insights into the selectivity profile of the newly synthesized compounds **25f**, **26a**–**f**, **38a**–**f**, **39a**–**f**, **42a**–**d**, and **48**, a differential scanning fluorimetry (DSF) assay was performed using more than a hundred kinases distributed throughout the kinome (Table 2 – Table 3). Staurosporine was used as a positive control and the assay panel comprised known off-targets of the lead structure gefitinib (**5**), such as the kinases ABL1 or GAK. **25f** exhibited a stabilization of several kinases, like GAK, BMP2K, or STK17B, indicating a similar non-selective selectivity profile as gefitinib (**5**). The macrocycles **26a** and **38a** also revealed various hits by stabilizing 12 and 9 kinases, respectively. The introduction of chlorine residues at different positions at the aromatic ring (**26b**–**e**, **38b**–**e**) or the chlorine-fluorine residues (**26f**, **38f**) were lowering the number of stabilized kinases (Figure 19A and B). It resulted in macrocycles with a clean DSF profile by targeting 0 – 6 kinases with a ΔT_m shift > 5 °C. The macrocycles **39a**–**f** also exhibited a great selectivity profile by stabilizing 0 – 5 kinases. The different attachment points for the linker (**42a**–**d**) or the missing methoxy group at C7 of the quinazoline (**48**) seemed to be not tolerated by EGFR or other kinases. **42a**–**d** and **48** stabilized no kinases in the DSF panel with a ΔT_m shift > 5 °C.

Based on the great selectivity profile in the *in-house* DSF panel, the weak activity for EGFR WT, and the preferred inhibition for mutant EGFR, **26f** was chosen for a further kinome-wide selectivity screen, using the KINOMEscan® assay platform provided by Eurofins Scientific. Therefore, **26f** was screened against 468 human protein kinases and their mutants at a screening concentration of 1 µM (Figure 19C – E). In this extended panel, **26f** showed an excellent selectivity profile with a selectivity score (S_{35}) of 0.026. The EGFR mutants Del19 (d746–750), d747–752/ P753S, L858R, or d752–759 were potently targeted by **26f**, whereby EGFR WT, other EGFR mutants, or oncogenic FLT mutants (FLT3 D835Y, FLT3 ITD/ D835V) were only affected weakly.

Table 2. DSF data of **25f**, **26a**–**f**, and **38a**–**f**. Staurosporine was used as a positive control. The newly synthesized compounds were screened in an *in-house* panel of 103 kinases. No stabilization of the kinase is indicated in pale green, while a high stabilization is indicated in dark green.

Kinase	ΔTm [°C]													
	25f	**26a**	**26b**	**26c**	**26d**	**26e**	**26f**	**38a**	**38b**	**38c**	**38d**	**38e**	**38f**	**Staurosporine**
AAK1	3.22	9.61	9.23	2.25	7.09	0.79	3.11	5.40	3.70	0.80	1.70	0.30	0.60	15.64
ABL1	4.85	4.19	3.73	0.29	4.36	0.00	2.24	4.10	2.40	1.00	2.30	3.40	1.30	10.29
AKT3	-0.27	-0.19	0.08	-0.30	-0.14	0.30	0.03	-0.20	-0.10	-0.30	-0.30	-0.40	-0.20	6.56
AURKB	n.d.	n.d.	n.d.	n.d.	n.d.	n.d.	n.d.	-0.50	-0.80	-1.30	-0.40	-1.50	-0.90	8.30
BMP2K	5.40	9.59	3.39	0.74	1.62	0.00	1.02	8.60	1.10	0.70	2.10	1.30	1.00	19.10
BMPR2	0.80	1.47	0.41	0.24	0.22	0.24	0.19	1.50	0.20	-0.30	-0.70	1.70	-0.10	2.63
BMX	-0.28	0.09	0.15	-0.18	0.20	0.13	0.12	0.60	0.20	-0.20	0.10	0.30	0.00	7.11
BRAF	0.46	1.36	0.56	0.40	0.63	0.53	0.51	1.10	0.40	0.40	0.60	0.40	0.40	0.83
BRD4	3.66	-1.65	-0.64	-1.03	-0.10	-0.72	-0.11	0.30	0.50	0.10	0.20	0.30	0.20	1.10
BRPF1B	n.d.	n.d.	n.d.	n.d.	n.d.	n.d.	n.d.	-1.20	-1.00	-1.00	-0.70	-1.10	-1.10	-0.10
CAMK1D	0.48	-1.21	-1.93	0.48	-0.13	1.00	1.35	-0.40	0.30	0.00	-0.20	-0.20	-0.30	9.99
CAMK1G	2.47	-0.98	1.51	0.41	1.57	0.54	0.34	-0.10	0.10	-0.40	-0.10	0.20	-0.40	10.91
CAMK2B	-0.22	0.55	0.36	0.35	0.20	-0.03	0.63	0.10	0.00	-0.20	-0.10	-0.10	0.00	13.32
CAMK2D	2.62	1.27	0.75	1.20	0.21	0.64	1.13	0.90	0.30	-0.10	-0.10	0.20	0.00	16.20
CAMK4	0.13	-0.07	-0.11	-0.10	-0.03	-0.17	-0.15	0.10	0.20	0.10	0.00	-0.10	0.10	8.56
CAMKK2B	2.59	9.58	5.84	0.85	1.14	0.05	0.30	8.40	3.80	2.10	0.70	5.30	0.30	24.59
CASK	0.87	0.11	0.05	0.11	0.23	0.24	0.13	-0.40	-0.20	-0.50	-0.40	-0.20	-0.10	4.79
CDC42BPA	1.17	-0.70	-0.03	0.13	-0.36	-0.15	0.01	-0.30	-0.10	0.30	-0.10	-0.50	0.00	2.81
CDK2	1.02	2.91	0.91	-0.22	-0.23	-0.12	-0.33	2.50	0.20	0.00	-0.10	1.20	0.00	15.46
CDKL1	-0.26	0.79	0.23	-0.01	-0.16	-0.07	-0.09	1.20	0.00	-0.20	0.00	-0.20	0.00	3.12
CHEK2	3.72	1.29	1.14	0.61	1.27	1.08	0.83	0.90	0.00	-0.20	0.00	0.10	0.00	17.07
CLK1	1.93	5.89	2.53	1.08	1.08	0.95	1.41	4.90	0.00	0.10	-0.10	3.30	0.70	5.62
CLK3	1.19	1.57	0.44	-0.09	0.84	0.83	1.13	0.10	-0.10	0.00	0.00	0.10	0.00	11.86
CSNK1D	0.96	1.46	0.31	0.05	0.27	0.09	0.20	2.30	0.10	-0.20	0.60	1.90	0.20	5.58
CSNK2A1	n.d.	n.d.	n.d.	n.d.	n.d.	n.d.	n.d.	3.20	0.70	0.10	0.10	-0.20	0.20	1.77
CK2A2	1.11	4.92	3.96	0.01	4.38	0.19	2.34	5.70	2.20	0.60	1.30	-0.20	1.20	2.10
DAPK1	1.11	1.06	0.16	0.10	0.54	0.58	0.67	1.20	0.30	0.10	0.40	0.20	0.20	9.82
DAPK3	2.50	1.14	-0.54	0.40	4.56	1.73	1.13	1.20	-0.20	-0.50	1.40	-0.50	0.90	15.78
DCAMKL1	2.25	0.24	-0.48	-0.34	0.58	0.64	0.61	0.60	0.20	0.30	0.60	0.50	0.50	12.39
DMPK1	1.43	0.93	-0.31	-0.32	0.01	0.25	-0.34	0.70	0.20	-0.10	-0.10	1.80	-0.10	8.67
DYRK1A	7.76	-0.26	0.75	1.17	0.21	1.56	-0.45	0.10	-0.20	-0.70	-1.00	-0.30	-0.60	8.71
DYRK2	5.15	6.75	3.08	0.79	1.89	0.60	0.96	6.00	1.00	0.70	1.00	0.70	0.60	7.05
EPHA2	2.29	3.02	1.74	0.19	2.42	0.07	0.41	1.00	0.20	0.20	0.20	2.50	0.30	8.32
EPHA4	n.d.	n.d.	n.d.	n.d.	n.d.	n.d.	n.d.	0.60	0.40	-0.10	0.20	1.60	0.30	6.20
EPHA5	2.01	1.64	0.43	0.39	0.34	0.87	0.79	0.60	-0.10	-0.70	-0.20	1.70	-0.30	7.93
EPHA7	3.94	0.37	-1.37	0.20	1.42	1.54	-0.53	-0.80	-0.50	-0.60	-0.70	-0.80	-0.70	10.33
EPHB1	n.d.	n.d.	n.d.	n.d.	n.d.	n.d.	n.d.	0.70	0.40	-0.30	0.00	1.40	0.10	6.40
EPHB3	1.43	1.42	1.42	0.48	0.55	1.00	0.66	1.00	0.40	-0.40	0.00	1.30	0.00	4.98
FES	4.88	0.22	0.02	1.05	0.50	0.57	1.11	-0.10	-0.20	-0.40	-0.30	0.00	-0.20	6.17
FGFR1B	1.05	-0.14	-0.56	-0.28	0.32	0.01	-0.30	0.20	0.20	-0.10	-0.10	0.00	0.00	5.95
FGFR2	3.29	1.03	0.71	0.34	2.81	0.58	0.62	0.70	0.20	0.00	0.10	0.30	0.10	9.04
FGFR3	0.69	2.80	1.17	0.25	3.53	0.20	0.55	1.00	0.20	0.20	0.50	0.80	0.40	13.29
FLT1	4.45	4.18	1.40	0.82	2.26	0.93	1.16	5.90	0.70	0.40	2.20	2.50	1.40	13.56
GAK	6.51	4.90	1.29	0.45	1.61	0.31	1.11	4.40	0.50	0.20	0.80	3.70	0.70	9.01
GPRK5	0.68	0.75	-0.65	0.59	0.58	0.12	0.73	0.10	0.00	0.10	0.10	0.60	0.10	7.73
GSG2	0.45	2.08	0.06	0.02	0.06	-0.05	0.17	2.20	0.10	0.10	0.00	-0.20	-0.20	7.15
GSK3B	0.48	7.25	3.95	0.89	2.75	0.33	1.14	3.50	0.50	0.50	0.80	1.60	0.70	11.76
HIPK2	n.d.	n.d.	n.d.	n.d.	n.d.	n.d.	n.d.	1.20	0.30	0.30	0.20	0.30	0.20	4.40
MAP2K1	0.11	-0.43	-0.38	-0.29	-0.47	-0.35	-0.48	0.10	0.10	0.00	0.00	-0.10	0.00	1.33
MAP2K4	1.35	2.07	1.01	0.52	2.05	1.04	0.47	0.90	-0.10	0.20	0.20	0.30	0.30	12.01
MAP2K6	0.24	0.64	0.29	0.10	0.14	0.11	0.07	0.30	0.10	0.10	0.10	0.40	0.10	12.35
MAP2K7	2.12	-0.19	-0.35	0.47	-0.08	0.08	-0.07	0.20	0.20	0.00	0.10	0.00	-0.10	8.40
MAP3K5	0.35	4.54	0.83	0.71	1.23	0.26	0.77	0.30	0.00	0.10	0.10	0.40	0.20	18.54
MAPK10	1.62	1.44	0.05	0.89	0.33	0.43	-0.72	0.80	-0.20	-0.70	-0.70	0.60	-0.30	7.38
MAPK13A	-0.36	0.40	0.20	0.12	0.04	0.20	0.22	0.20	0.20	0.10	0.10	0.10	-0.10	7.46
MAPK14	1.68	-0.49	-0.43	-0.34	-0.17	-0.13	-0.14	0.20	0.30	0.10	0.40	0.40	0.30	0.26
MAPK15	0.82	4.02	1.56	0.55	0.24	0.16	0.21	3.00	0.30	-0.10	-0.20	1.10	-0.10	14.74
MAPK1	0.15	0.18	0.22	0.16	0.02	0.03	0.11	0.50	0.30	-0.10	-0.20	0.40	-0.20	1.42
MAPK8B	n.d.	n.d.	n.d.	n.d.	n.d.	n.d.	n.d.	0.30	-0.40	-0.40	-0.60	0.80	-0.40	7.80
MAPK9	3.36	1.23	0.86	0.29	0.28	0.27	0.58	0.50	0.40	0.30	0.10	0.20	0.10	3.75
MAPKAPK2	n.d.	n.d.	n.d.	n.d.	n.d.	n.d.	n.d.	-0.10	-0.20	-0.10	-0.30	-0.50	-0.20	3.20
MARK3	1.10	0.07	-0.95	-0.12	-0.37	-0.03	-0.01	-1.10	-0.90	-0.50	-0.60	-0.20	-0.30	19.04
MARK4	0.87	0.94	-0.35	0.30	0.10	0.66	1.30	-0.50	-0.40	-0.50	-0.40	-0.50	-0.50	16.44
MELK	1.49	3.02	1.06	0.36	0.97	-0.04	0.44	0.50	0.10	0.20	0.20	1.20	0.20	13.85
MERTK	0.17	3.13	3.21	0.11	3.58	0.60	1.78	3.20	0.30	0.10	1.40	0.60	0.40	6.59
MST3	0.55	-0.30	0.26	-0.04	-0.34	-0.13	-0.25	-0.20	-0.10	0.00	0.00	-0.10	0.00	7.29
MST4	-1.07	-0.89	-0.91	-0.31	-0.86	-0.27	-0.27	-1.00	-0.70	-0.60	-0.70	-0.60	-0.50	6.14
NEK1	0.04	0.03	0.14	0.34	0.28	0.09	0.24	0.20	0.30	0.10	0.30	0.10	0.20	-0.60
NEK2	n.d.	n.d.	n.d.	n.d.	n.d.	n.d.	n.d.	-0.30	n.d.	n.d.	n.d.	n.d.	-0.10	3.30
NEK7	n.d.	n.d.	n.d.	n.d.	n.d.	n.d.	n.d.	0.00	0.40	0.10	0.00	-0.20	0.20	1.00
OSR1	0.95	0.34	-1.14	0.09	0.17	0.03	0.04	0.00	-0.10	0.00	-0.10	-0.10	-0.10	7.71
PAK1	0.18	-0.29	-0.02	0.49	0.22	0.95	0.47	0.30	0.00	0.90	-0.10	-0.10	-0.30	6.60
PAK4	0.40	0.85	0.35	0.26	-0.53	0.44	0.41	1.50	0.00	-0.20	-0.10	0.10	-0.20	12.18
PCTK1	-0.09	1.45	1.20	0.23	0.11	0.17	0.17	0.40	0.20	-0.20	-0.10	0.30	-0.10	9.13
PDK4	0.54	0.77	0.45	0.92	1.66	0.93	1.04	0.00	0.10	0.00	-0.10	-0.20	0.00	0.25
PHKG2	3.37	1.61	0.78	0.38	0.76	0.77	1.10	0.40	-0.20	-0.20	-0.40	-0.40	-0.30	21.18
PIM1	2.84	3.48	6.05	0.87	3.25	-0.38	3.75	1.40	0.50	0.30	-0.10	-0.50	0.70	12.50
PIM3	3.10	3.49	2.90	-0.56	1.50	-0.23	1.08	1.80	0.30	0.40	0.50	0.20	0.90	19.74
PKMYT1	0.92	1.70	0.71	0.54	0.62	0.68	0.39	0.20	-0.10	-0.30	0.00	-0.40	-0.30	0.19
PLK4	2.62	8.95	5.08	1.14	3.76	0.21	1.80	6.10	0.50	0.40	1.40	3.80	0.90	16.05
RIOK1	1.32	-0.68	-1.01	-0.14	-0.70	-0.42	0.12	-0.70	-0.80	-1.20	-1.30	-1.40	-1.10	-0.01
RPS6KA1	0.74	0.60	-0.02	0.52	0.61	0.33	0.33	0.40	0.30	0.00	0.10	0.30	0.20	3.90
RPS6KA6	-0.68	-0.23	-0.19	0.17	0.11	-0.17	0.05	-0.70	-0.50	-1.10	-0.60	0.20	-0.30	-0.53
SLK	3.86	5.44	1.50	0.06	3.35	0.22	1.22	2.20	-0.50	-0.40	0.10	1.50	-0.20	17.99
SPRK1	4.72	0.10	1.32	0.62	0.57	-0.14	-0.16	0.00	0.00	-0.20	-0.20	-0.20	-0.20	6.94
SRC	0.62	0.97	0.25	0.20	0.35	0.15	0.32	0.60	0.20	-0.10	0.10	1.60	0.00	5.86
STK10	2.99	9.71	6.35	0.52	9.33	-0.40	5.09	8.40	1.00	0.40	4.80	3.70	2.10	23.29
STK17A	6.76	3.23	1.01	0.14	0.36	0.47	0.93	0.60	0.10	-0.20	-0.20	-0.60	-0.20	11.85
STK17B	8.94	1.96	1.15	2.34	1.72	1.64	1.49	0.50	0.50	-0.80	-0.90	-0.50	-0.60	11.51
STK38L	2.92	0.86	0.51	0.17	0.43	0.66	-0.02	1.70	0.10	0.10	0.00	0.50	0.00	16.61
STK39	2.59	2.01	0.36	1.03	0.93	0.99	1.19	0.10	-0.20	-0.30	-0.30	-0.10	0.00	12.55
STK3	0.11	7.10	5.89	2.24	5.65	0.41	1.88	2.00	0.10	0.10	0.20	2.10	0.20	9.64
STK4	-0.97	3.90	0.22	0.36	0.96	0.70	0.62	0.50	-0.70	-0.70	-0.70	1.20	-0.60	14.93
STK6	5.06	8.73	2.25	0.49	1.67	0.15	0.87	6.40	0.30	0.20	1.10	6.50	0.80	17.12
TAF1	1.11	0.01	-0.15	0.19	0.15	0.25	0.07	0.50	0.70	0.00	0.30	0.20	0.40	0.15
TIF1	n.d.	n.d.	n.d.	n.d.	n.d.	n.d.	n.d.	0.20	0.40	0.50	0.20	0.30	0.00	0.80
TLK1	n.d.	n.d.	n.d.	n.d.	n.d.	n.d.	n.d.	0.80	0.50	0.40	0.30	0.30	0.30	9.40
TTK	1.65	0.67	0.39	-0.26	-0.17	0.43	0.01	-0.30	-1.10	-0.80	-0.30	-0.50	0.30	11.20
ULK1	2.92	-0.10	-0.08	0.02	-0.01	0.00	0.07	0.00	0.00	0.10	0.10	3.40	0.20	19.59
ULK3	0.01	6.61	2.34	0.62	1.02	0.33	0.57	2.30	0.20	0.10	0.10	3.70	0.10	11.28
VRK1	0.89	-0.03	0.57	0.39	0.23	0.48	0.16	0.00	0.10	0.10	0.00	0.30	0.10	2.77
WNK1	-0.38	0.72	0.48	0.36	0.41	1.42	0.62	0.40	0.20	0.10	0.10	0.20	-0.10	0.87
No. kinases >5°C	7	12	6	0	3	0	1	9	0	0	0	2	0	74

Table 3. DSF data of **39a**–**f**, **42a**–**d**, and **48**. Staurosporine was used as a positive control. The newly synthesized compounds were screened in an *in-house* panel of 103 kinases. No stabilization of the kinase is indicated in pale green, while a high stabilization is indicated in dark green.

Kinase	ΔTm [°C]											
	39a	39b	39c	39d	39e	39f	42a	42b	42c	42d	48	Staurosporine
AAK1	1.90	0.80	0.60	2.50	-0.20	0.50	0.90	0.10	0.50	2.20	2.09	15.64
ABL1	4.30	5.10	5.80	6.50	3.70	4.51	0.80	0.90	0.60	1.00	0.07	10.29
AKT3	-0.20	-0.20	-0.10	-0.20	-0.20	0.30	-0.30	0.00	-0.30	-0.10	-0.04	6.56
AURKB	-1.40	-1.80	-0.80	-1.10	-2.60	-2.94	-1.40	-0.80	-0.10	-0.60	n.d.	8.30
BMP2K	3.00	2.30	1.70	4.10	0.20	0.71	1.10	0.50	0.40	3.60	1.57	19.10
BMPR2	0.40	0.00	0.20	0.20	0.20	0.34	-0.30	-0.30	-0.40	-0.20	0.34	2.63
BMX	0.40	1.40	2.10	1.10	0.60	0.71	0.00	-0.20	-0.10	0.10	-0.23	7.11
BRAF	0.90	0.40	1.60	2.70	0.50	1.68	0.60	0.60	0.30	0.70	0.98	0.83
BRD4	0.10	0.50	0.10	0.60	0.90	0.21	1.00	0.70	0.60	1.00	0.01	1.10
BRPF1B	-0.70	-1.10	-1.30	-1.20	-0.50	-0.87	-0.50	-0.70	-0.30	-1.10	n.d.	-0.10
CAMK1D	-2.20	-2.60	-1.80	-2.00	-2.50	1.31	-2.40	-2.00	-1.90	-2.10	-0.09	9.99
CAMK1G	-1.40	-1.30	-1.00	-1.00	-1.70	0.85	-1.40	-0.80	-0.80	-0.70	1.43	10.91
CAMK2B	-0.40	-0.50	-0.60	-0.20	-0.50	-0.10	-0.50	-0.80	-0.30	-0.20	0.29	13.32
CAMK2D	0.00	-0.30	-0.20	-0.30	-0.10	0.36	-0.10	-0.30	-0.20	0.20	0.72	16.20
CAMK4	-0.20	-0.30	-0.20	0.00	-0.30	0.28	-0.20	-0.50	-0.30	-0.20	-0.26	8.56
CAMKK2B	4.30	3.20	5.70	2.40	4.60	1.42	1.50	0.30	0.10	2.70	0.58	24.59
CASK	-0.30	-0.30	-0.20	0.10	-0.40	0.16	-0.10	-0.10	0.10	-0.10	0.06	4.79
CDC42BPA	-0.60	-0.70	-0.30	-0.30	-0.50	0.40	-0.20	-0.20	-0.20	-0.30	-0.45	2.81
CDK2	0.40	0.10	0.60	0.10	0.00	0.32	0.00	0.00	-0.10	0.10	-0.20	15.46
CDKL1	0.10	0.00	0.20	0.40	0.20	0.15	0.10	0.10	0.00	0.00	-0.10	3.12
CHEK2	0.20	-0.10	0.00	0.00	0.00	0.48	0.10	0.00	-0.10	0.10	1.00	17.07
CLK1	2.20	1.20	0.90	1.60	-0.10	0.95	0.40	0.20	-0.10	0.20	1.60	5.62
CLK3	2.70	3.40	2.00	1.30	1.10	1.77	0.60	0.50	-0.30	2.30	1.65	11.86
CSNK1D	0.20	0.60	0.50	0.20	0.10	0.24	0.50	0.70	0.30	2.90	0.33	5.58
CSNK2A1	0.20	0.00	0.40	2.00	-0.20	0.11	-0.20	-0.30	-0.40	0.00	0.16	1.77
CK2A2	0.60	0.00	0.00	0.70	-0.20	0.63	0.10	0.00	-0.20	0.20	n.d.	2.10
DAPK1	0.40	0.10	0.30	1.60	0.10	0.62	0.40	0.00	-0.20	0.10	0.48	9.82
DAPK3	-0.30	-0.40	-0.70	2.00	-0.60	1.55	-0.50	-1.10	-0.30	0.00	-0.27	15.78
DCAMKL1	0.40	0.20	0.30	2.00	0.20	0.70	0.00	0.10	-0.20	0.20	0.13	12.39
DMPK1	1.00	0.80	1.30	2.10	1.40	1.32	-0.30	0.00	0.10	0.20	0.04	8.67
DYRK1A	0.20	0.80	-0.90	-0.10	-1.20	1.45	0.40	-1.60	-0.50	0.50	-0.39	8.71
DYRK2	3.20	2.30	2.40	3.20	0.20	1.15	0.30	0.50	0.10	0.60	1.30	7.05
EPHA2	4.10	3.40	5.70	5.30	5.90	4.21	0.40	0.30	0.00	0.50	0.08	8.32
EPHA4	2.10	1.30	3.20	4.10	3.20	4.17	0.10	0.10	-0.10	0.30	n.d.	6.20
EPHA5	2.30	1.60	2.90	2.90	3.60	3.65	-0.60	-0.50	-0.50	-0.20	0.40	7.93
EPHA7	-0.30	-0.90	-1.00	-0.80	-0.60	-0.01	-0.20	0.10	0.10	-0.30	0.87	10.33
EPHB1	1.90	1.00	3.20	3.40	2.90	3.52	-0.30	-0.40	-0.60	-0.30	n.d.	6.40
EPHB3	1.70	0.80	n.d.	n.d.	n.d.	2.56	-0.30	-0.50	-0.50	0.10	0.35	4.98
FES	0.50	0.10	0.20	0.30	1.20	1.07	0.30	0.30	-0.30	0.10	-0.04	6.17
FGFR1B	0.20	-0.20	0.20	0.90	-0.20	0.65	-0.20	-0.20	-0.20	-0.10	-0.29	5.95
FGFR2	1.10	0.20	1.80	2.50	0.40	1.10	0.10	0.00	-0.10	0.10	0.67	9.04
FGFR3	2.00	1.00	2.40	3.90	0.90	1.13	0.50	0.40	0.30	0.50	0.24	13.29
FLT1	4.20	2.80	3.60	7.30	0.70	4.69	0.70	0.70	0.30	0.50	0.87	13.56
GAK	3.90	3.20	3.90	5.90	2.00	5.08	-0.10	-0.20	-0.10	0.20	1.39	9.01
GPRK5	0.00	0.00	0.20	0.40	0.10	0.03	0.40	-0.60	0.40	0.80	0.42	7.73
GSG2	0.20	-0.20	0.40	0.20	-0.20	0.02	0.10	-0.40	-0.30	0.20	0.90	7.15
GSK3B	1.90	2.20	0.90	2.00	0.50	-0.17	0.50	0.40	-0.20	1.10	0.99	11.76
HIPK2	0.60	0.40	0.80	0.60	0.40	0.41	0.30	0.50	0.20	0.10	n.d.	4.40
MAP2K1	0.10	0.30	0.20	0.10	0.30	n.d.	0.10	0.10	0.00	0.00	-0.36	1.33
MAP2K4	-0.10	-0.10	0.10	0.30	0.00	0.21	0.00	-0.10	0.30	0.30	0.51	12.01
MAP2K6	0.20	0.50	0.10	0.20	0.60	0.15	0.20	0.10	0.10	0.40	0.18	12.35
MAP2K7	0.20	-0.10	0.10	0.00	0.20	0.19	0.20	0.10	0.00	0.40	0.60	8.40
MAP3K5	0.40	0.40	0.80	1.20	0.30	0.33	0.30	0.40	0.20	0.40	0.55	18.54
MAPK10	-1.00	-1.50	-1.10	-0.10	-1.60	3.92	-1.50	-1.90	-2.00	-1.30	0.45	7.38
MAPK13A	0.30	0.10	0.20	0.20	0.20	-0.25	0.20	0.00	0.00	0.20	0.18	7.46
MAPK14	0.60	1.90	0.80	3.40	0.80	1.38	0.70	0.50	0.40	1.10	-0.27	0.26
MAPK15	1.20	1.30	2.90	0.50	-0.20	0.19	0.00	0.10	-0.20	0.60	0.49	14.74
MAPK1	0.20	-0.10	0.10	-0.10	0.00	0.04	0.10	0.00	0.00	0.00	0.10	1.42
MAPK8B	0.30	0.20	0.20	1.00	-0.10	1.31	0.50	0.00	0.40	1.10	n.d.	7.80
MAPK9	0.40	0.10	0.40	1.00	0.30	2.16	0.40	0.30	0.30	0.30	0.58	3.75
MAPKAPK2	-0.30	-0.40	-0.40	-0.20	-0.20	0.00	0.10	-0.60	-0.10	0.00	n.d.	3.20
MARK3	-1.20	-0.40	0.40	-0.40	0.00	0.32	-0.70	-0.20	-0.40	-0.20	0.14	19.04
MARK4	0.10	0.50	0.10	0.10	0.10	0.62	0.20	0.20	0.40	0.40	0.30	16.44
MELK	1.00	0.60	1.10	1.80	0.30	0.62	0.40	0.40	0.00	1.70	0.33	13.85
MERTK	0.90	2.10	2.20	1.60	1.10	0.89	0.10	-0.10	-0.10	0.10	0.33	6.59
MST3	-0.20	-0.20	-0.20	0.20	-0.20	-0.09	0.50	0.70	0.90	0.50	0.48	7.29
MST4	-0.60	-0.40	-0.60	-0.40	-0.40	1.98	-0.50	-0.10	-0.30	-0.40	-0.19	6.14
NEK1	0.10	0.10	0.40	0.50	0.30	0.03	0.20	-0.10	0.20	0.20	0.15	-0.60
NEK2	n.d.	0.50	n.d.	-0.20	n.d.	0.56	0.10	0.30	0.10	-0.30	n.d.	3.30
NEK7	-0.30	0.00	-0.10	0.10	-0.40	0.45	0.10	0.00	-0.10	0.20	n.d.	1.00
OSR1	-0.20	0.00	0.00	0.20	0.00	1.66	0.10	0.00	0.10	0.10	0.29	7.71
PAK1	-0.20	-0.30	-0.20	-0.20	-0.30	-0.33	-0.20	-0.60	-0.30	-0.30	0.59	6.60
PAK4	-0.10	-0.20	-0.30	0.20	0.00	-0.14	-0.30	-0.20	-0.50	-0.30	0.32	12.18
PCTK1	0.10	0.00	0.30	0.10	0.00	0.11	0.10	-0.20	-0.20	0.10	0.16	9.13
PDK4	-0.10	-0.20	-0.20	-0.30	-0.10	-0.36	0.00	0.10	-0.10	0.00	0.89	0.25
PHKG2	0.00	-0.10	0.50	-0.20	0.00	0.49	-0.10	-0.10	-0.10	-0.10	0.62	21.18
PIM1	1.50	2.60	1.90	2.50	0.70	1.69	0.50	0.20	0.20	0.60	2.43	12.50
PIM3	1.20	1.50	0.50	2.80	0.00	3.33	0.30	-1.40	0.30	0.30	2.26	19.74
PKMYT1	0.30	0.00	0.00	-0.60	0.00	1.08	-0.50	-0.40	-0.30	-0.20	0.81	0.19
PLK4	4.90	1.70	6.50	3.70	4.10	2.36	0.20	0.40	0.10	0.90	0.62	16.05
RIOK1	-1.60	-0.60	-1.40	0.50	-1.80	2.15	-1.30	-1.10	-0.80	-1.20	-0.38	-0.01
RPS6KA1	0.10	0.00	0.20	0.30	0.10	-0.02	0.30	0.30	0.20	0.40	0.53	3.90
RPS6KA6	-1.60	-1.70	-1.40	-1.80	-1.50	0.23	0.80	-1.90	-0.20	-1.00	0.32	-0.53
SLK	0.50	0.60	2.50	3.80	-0.30	n.d.	-1.20	-1.00	-1.50	-0.50	0.69	17.99
SPRK1	-0.10	-0.30	-0.40	-0.30	0.00	-0.07	-0.10	-0.40	-0.20	0.00	0.01	6.94
SRC	1.70	2.30	4.10	2.60	2.20	2.40	0.50	0.20	0.00	0.40	0.22	5.86
STK10	2.80	2.40	5.50	6.30	1.40	5.70	0.30	0.30	0.10	1.10	0.49	23.29
STK17A	0.10	-0.50	-0.30	-0.20	-0.30	1.81	-0.30	-0.50	-0.40	-0.40	0.57	11.85
STK17B	-2.10	-3.20	-2.20	-2.30	-2.40	0.06	-2.20	-3.10	-2.70	-2.60	0.82	11.51
STK38L	1.10	1.70	1.80	2.00	1.20	0.56	0.40	0.00	-0.10	0.50	0.12	16.61
STK39	0.30	0.00	0.60	-0.10	0.00	-0.01	0.00	-0.20	-0.20	0.00	0.58	12.55
STK3	-0.40	-0.10	0.10	0.70	-0.40	0.25	0.10	-0.60	-0.40	-0.20	1.09	9.64
STK4	0.20	1.00	0.80	0.70	0.40	1.22	-0.40	-0.60	-0.70	-0.40	0.07	14.93
STK6	4.30	2.50	4.80	4.20	2.60	1.95	0.40	0.10	0.20	0.40	1.21	17.12
TAF1	-0.20	-0.60	-0.60	-0.70	-0.70	0.04	-0.10	-0.80	-0.70	-0.90	0.10	0.15
TIF1	0.00	-0.10	-0.10	0.50	0.20	0.45	0.70	0.00	0.30	0.30	n.d.	0.80
TLK1	0.10	-0.20	0.00	0.20	0.10	0.95	0.60	0.10	0.10	0.60	n.d.	9.40
TTK	1.60	0.50	0.30	1.00	1.50	0.89	0.20	0.40	0.60	0.60	0.04	11.20
ULK1	1.50	0.80	2.70	1.00	2.10	0.19	0.10	0.40	-0.10	0.30	0.36	19.59
ULK3	0.10	0.20	0.30	0.50	0.00	0.20	0.20	0.30	0.20	0.40	-0.03	11.28
VRK1	0.30	0.10	0.10	0.30	0.20	0.34	0.00	-0.10	0.10	0.40	0.19	2.77
WNK1	0.50	0.60	0.70	0.10	0.40	-0.11	0.50	0.10	0.60	0.90	0.47	0.87
No. kinases >5°C	0	1	5	5	1	2	0	0	0	0	0	74

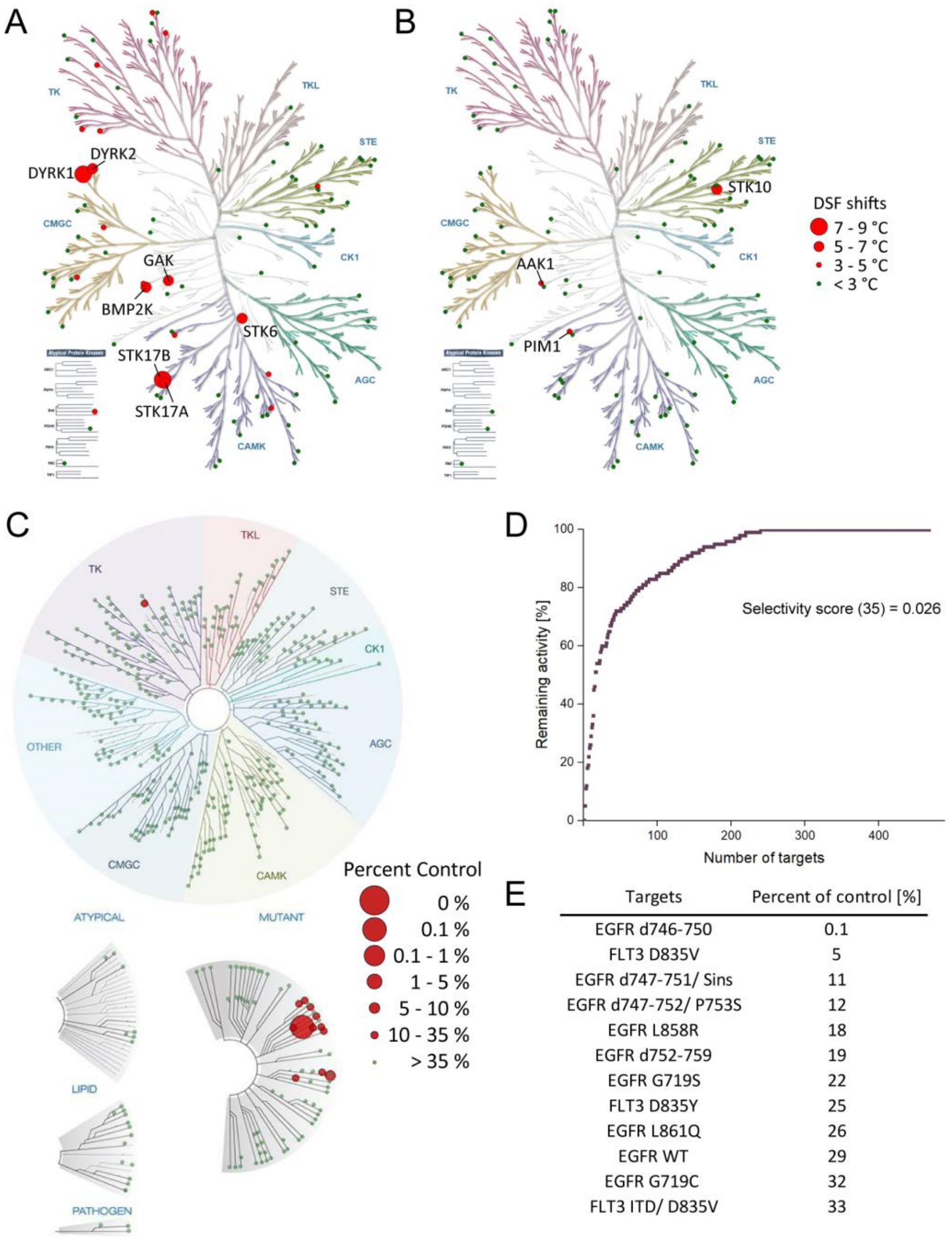

Targets	Percent of control [%]
EGFR d746-750	0.1
FLT3 D835V	5
EGFR d747-751/ Sins	11
EGFR d747-752/ P753S	12
EGFR L858R	18
EGFR d752-759	19
EGFR G719S	22
FLT3 D835Y	25
EGFR L861Q	26
EGFR WT	29
EGFR G719C	32
FLT3 ITD/ D835V	33

Figure 19. A. Graphical representation of the selectivity data of **25f** assessed by DSF. **B.** Graphical representation of the selectivity data of **26f** assessed by DSF. A phylogenetic tree (Cell Signaling Technology) was used to highlight ΔTm data that was depicted as red circles as indicated in the figure capture. **C.** Selectivity profile of **26f** assessed by the KinomeScan® panel at a screening concentration of 1 µM. Mutants and atypical kinases are depicted in the lower panel. **D.** Waterfall plot of the selectivity data of **26f**. The remaining activity (%) was plotted against the number of tested kinases. The selectivity score of **26f** was determined with a cut off value of 35% remaining activity. **E.** Table showing the top hits of the KINOMEscan® profiling of **26f** with a remaining activity < 35% at 1 µM.

3.4.3. Crystal structure

The crystal structures of **25f** and the macrocycle **39d** bound to EGFR WT (PDB: 7U99, 7U9A) as well as **39f** bound to EGFR T790M/V948R (PDB: 7U98) provided insights into the binding mode of the quinazoline-based molecules (Figure 20A – D). A superimposition of **25f** with gefitinib (**5**) is shown in Figure 20B and revealed a similar binding mode of the quinazoline moiety. The additional alcohol group at the aromatic ring of **25f** interacted with the D855 of the DFG-motif and led to a slightly rotated aromatic ring in comparison to gefitinib (**5**). The similar binding orientation of both molecules is reflected in the assay data as well, whereby they exhibited a similar activity profile towards EGFR WT and its mutants.

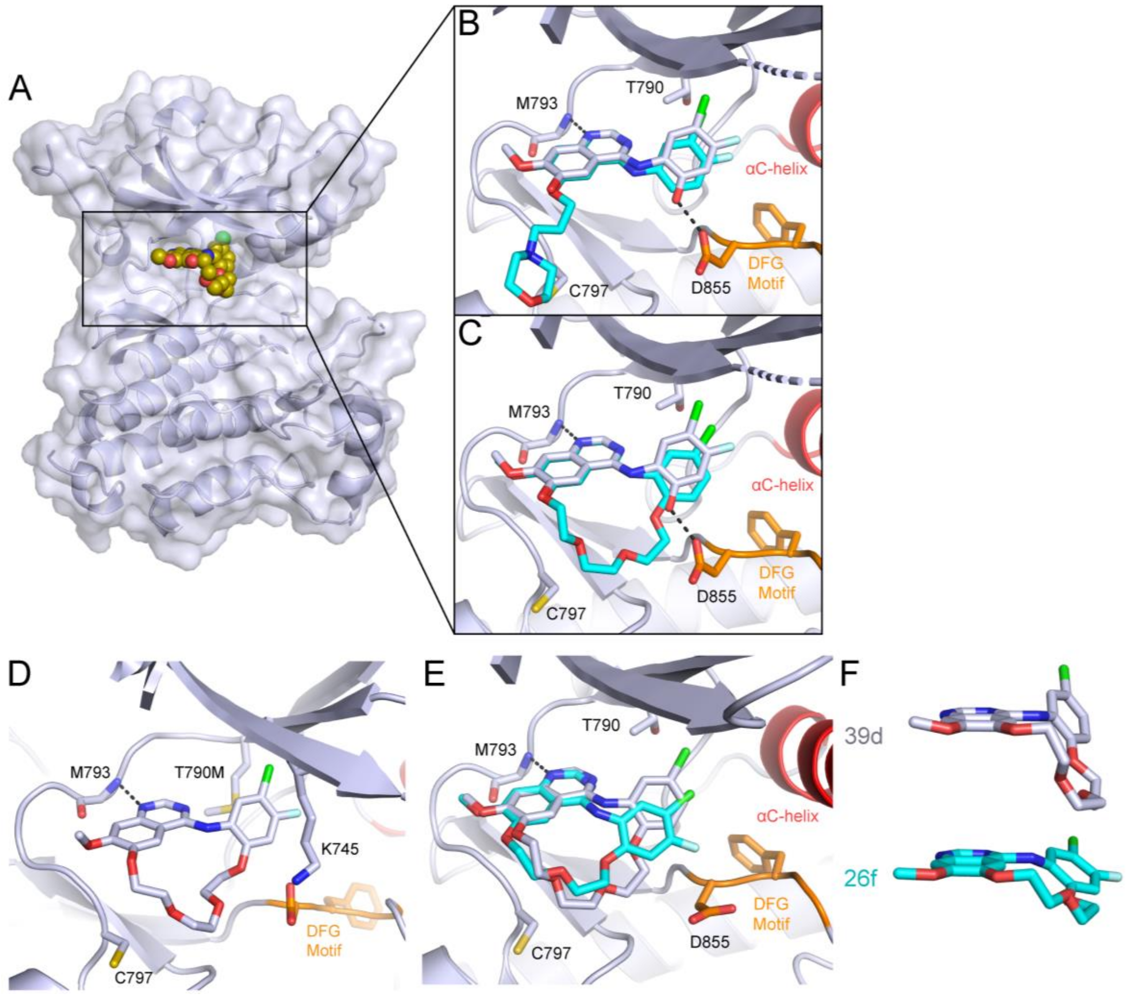
A
B
M793
T790
αC-helix
DFG Motif
C797
D855
C
M793
T790
αC-helix
DFG Motif
D855
C797
D
M793
T790M
K745
DFG Motif
C797
E
T790
M793
αC-helix
DFG Motif
D855
C797
F
39d
26f

Figure 20. A. Crystal structure of EGFR WT in complex with **39d** (PDB: 7U99). **B.** Superimposition of the structure of **25f** (PDB: 7U9A, grey carbon atoms) and gefitinib (PDB: 2ITZ, cyan carbon atoms). **C.** Superimposition of the structure of the macrocycle **39d** (PDB: 7U99, cyan carbon atoms) and **25f** (PDB: 7U9A, grey carbon atoms). **D.** Crystal structure of EGFR T790M/V948R in complex with **39f** (PDB: 7U98). **E.** Superimposition of the catalytic domain structure in complex with **39d** (PDB: 7U99, grey carbon atoms) and **26f** (cyan carbon atoms) which was docked into EGFR WT (Glide, Schrodinger). **F.** Comparison of the different binding modes of the two macrocycles **39d** (grey) and **26f** (blue).

An overlay of the macrocycle **39d** with **25f** revealed the canonical binding mode of the quinazoline hinge-binding moiety (Figure 20C) which can be seen for gefitinib (**5**). The aromatic ring of **39d** is slightly rotated and shifted in comparison to **25f** and the linker of **39d** was facing toward the C-terminal lobe. Macrocycle **39f** exhibited the same binding mode as **39d** (Figure 20D). The Del19 mutation introduces flexibility into the EGFR catalytic domains, which have precluded structure determination of this mutant so far. To gain insight into the binding mode of **26f**, harboring the shortest diethylene glycol linker, the inhibitor was docked into the active conformation of EGFR WT. A superimposition of **26f** and **39d** is shown in Figure 20E and Figure 20F. The shortening of the linker led to a less flexible macrocycle, which resulted in a different predicted ring orientation. **26f** could no longer adapt the bioactive conformation which can be seen for gefitinib (**5**) or the macrocycle **39d** with a longer linker moiety. Consequently, the truncation of the linker led to an optimally positioned molecule in the binding pocket of the Del19 mutant however, weakened the binding affinity towards EGFR WT.

3.4.4. Cell-based activity

Next, the antiproliferative activity of the selected compounds **25f**, **26f**, **39d**, **39f**, and **48** was determined, using gefitinib, BI-4020, mobocertinib, and osimertinib as positive controls. Therefore, a Ba/F3 cell model was used by transducing these cells with EGFR WT, L858R, L858R/C797S, L858R/T790M, L858R/T790M/C797S, Del19, Del19/C797S, Del19/T790M, Del19/T790M/C797S, and Ex20 insertion mutants (Table 4). The acyclic precursor **25f** exhibited once more a similar activity profile as gefitinib (**5**) for the tested mutants. It had a strong effect on EGFR WT, as well as the mutants L858R, Del19, and the corresponding double mutant including C797S. The gatekeeper mutation T790M led to an inactivity of **25f**, which is already known in the literature for quinazoline-based EGFR inhibitors like gefitinib (**5**). **48** had no impact on the cell proliferation below 10 µM for most of the tested kinases. Only a minor effect was observed for L858R, Del19, and Del19/C797S. These results underlined the statement that the methoxy group in position C7 of the quinazoline is mandatory for activity on EGFR WT and its mutants. **26f** did not affect EGFR WT however, it inhibited both L858R and L858R/C979S mutants in the submicromolar range, with IC_{50} values of 385.6 nM and 749.6 nM, respectively. It was even more potent on the Del19 and Del19/C797S mutations with IC_{50} values of 197.5 nM and 147.9 nM, respectively, and showed no significant inhibition of the other tested mutants. **39d** and **39f** exhibited a strong inhibition with IC_{50} values in the low one- to two-digit nanomolar range for EGFR WT, L858R, Del19, and the respective double mutation including C797S. **39d** showed the most potent efficacy of the tested compounds with a superior profile compared to gefitinib (**5**). None of the quinazoline-based macrocycles inhibited the gatekeeper mutation T790M or the Ex20 insertion mutations. These results demonstrated that macrocyclization can be used to improve the potency of an acyclic analog in the case of **39d** and even generate a mutant selectivity with respect to EGFR WT in the case of **26f**.

Table 4. Cell based activity data (Ba/F3 cell model) of **25f**, **26f**, **39d**, **39f**, and **48** tested against cells expressing EGFR WT and its mutants. Gefitinib, BI-4020, osimertinib, and mobocertinib were used as a reference. IC$_{50}$ values for cell proliferation were assessed by a cell titer-glo assay in triplicates ± SD. Dark green indicates a high and pale green a low potency against the desired kinase.

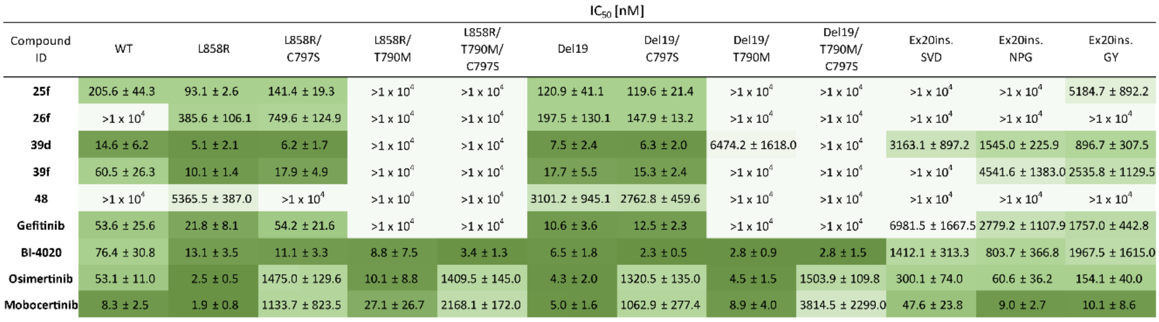

	IC$_{50}$ [nM]											
Compound ID	WT	L858R	L858R/ C797S	L858R/ T790M	L858R/ T790M/ C797S	Del19	Del19/ C797S	Del19/ T790M	Del19/ T790M/ C797S	Ex20ins. SVD	Ex20ins. NPG	Ex20ins. GY
25f	205.6 ± 44.3	93.1 ± 2.6	141.4 ± 19.3	$>1 \times 10^4$	$>1 \times 10^4$	120.9 ± 41.1	119.6 ± 21.4	$>1 \times 10^4$	$>1 \times 10^4$	$>1 \times 10^4$	$>1 \times 10^4$	5184.7 ± 892.2
26f	$>1 \times 10^4$	385.6 ± 106.1	749.6 ± 124.9	$>1 \times 10^4$	$>1 \times 10^4$	197.5 ± 130.1	147.9 ± 13.2	$>1 \times 10^4$	$>1 \times 10^4$	$>1 \times 10^4$	$>1 \times 10^4$	$>1 \times 10^4$
39d	14.6 ± 6.2	5.1 ± 2.1	6.2 ± 1.7	$>1 \times 10^4$	$>1 \times 10^4$	7.5 ± 2.4	6.3 ± 2.0	6474.2 ± 1618.0	$>1 \times 10^4$	3163.1 ± 897.2	1545.0 ± 225.9	896.7 ± 307.5
39f	60.5 ± 26.3	10.1 ± 1.4	17.9 ± 4.9	$>1 \times 10^4$	$>1 \times 10^4$	17.7 ± 5.5	15.3 ± 2.4	$>1 \times 10^4$	$>1 \times 10^4$	$>1 \times 10^4$	4541.6 ± 1383.0	2535.8 ± 1129.5
48	$>1 \times 10^4$	5365.5 ± 387.0	$>1 \times 10^4$	$>1 \times 10^4$	$>1 \times 10^4$	3101.2 ± 945.1	2762.8 ± 459.6	$>1 \times 10^4$	$>1 \times 10^4$	$>1 \times 10^4$	$>1 \times 10^4$	$>1 \times 10^4$
Gefitinib	53.6 ± 25.6	21.8 ± 8.1	54.2 ± 21.6	$>1 \times 10^4$	$>1 \times 10^4$	10.6 ± 3.6	12.5 ± 2.3	$>1 \times 10^4$	$>1 \times 10^4$	6981.5 ± 1667.5	2779.2 ± 1107.9	1757.0 ± 442.8
BI-4020	76.4 ± 30.8	13.1 ± 3.5	11.1 ± 3.3	8.8 ± 7.5	3.4 ± 1.3	6.5 ± 1.8	2.3 ± 0.5	2.8 ± 0.9	2.8 ± 1.5	1412.1 ± 313.3	803.7 ± 366.8	1967.5 ± 1615.0
Osimertinib	53.1 ± 11.0	2.5 ± 0.5	1475.0 ± 129.6	10.1 ± 8.8	1409.5 ± 145.0	4.3 ± 2.0	1320.5 ± 135.0	4.5 ± 1.5	1503.9 ± 109.8	300.1 ± 74.0	60.6 ± 36.2	154.1 ± 40.0
Mobocertinib	8.3 ± 2.5	1.9 ± 0.8	1133.7 ± 823.5	27.1 ± 26.7	2168.1 ± 172.0	5.0 ± 1.6	1062.9 ± 277.4	8.9 ± 4.0	3814.5 ± 2299.0	47.6 ± 23.8	9.0 ± 2.7	10.1 ± 8.6

Western blotting of the same set of selected compounds (**25f**, **26f**, **39d**, **39f**, and **48**) confirmed the activity profiles. Therefore, the phosphorylation/activation of EGFR was used as a marker (Figure 21). **25f** showed an effect on EGFR WT and the mutants L858R, L858R/ C797S, Del19, Del19/C797S, whereas the mutations containing the gatekeeper mutation or the Ex20 insertion were unaffected. Once more, **48** demonstrated the necessity of the methoxy group by showing no activity on all mutants tested as well as the wild-type receptor. **26f** showed significant activity at L858R and excellent activity at the EGFR mutations Del19 and Del19/C797S. The gatekeeper mutant T790M and wild-type EGFR were unaffected by **26f**. **39d** and **39f** exhibited an inhibitory activity on L858R, Del19, and the respective double mutation including C979S and a weak activity on EGFR WT, whereas **39d** had the most potent inhibitory effect on EGFR phosphorylation. The known EGFR inhibitors, used as a reference, reproduced the already published results.[183]

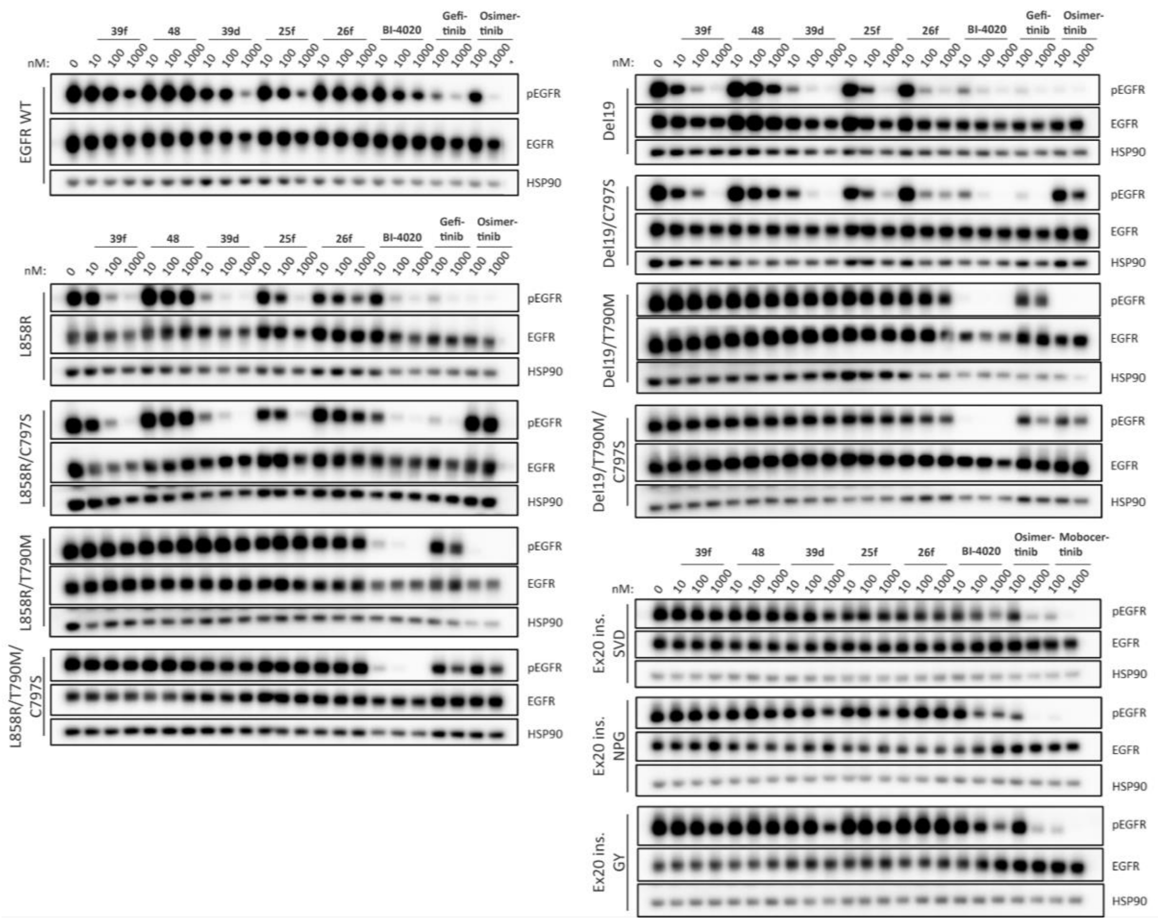
39f
48
39d
25f
26f
BI-4020
Gefi-
tinib
Osimer-
tinib
Mobocer-
tinib
nM:
0
10
100
1000
EGFR WT
L858R
L858R/C797S
L858R/T790M
L858R/T790M/
C797S
Del19
Del19/C797S
Del19/T790M
Del19/T790M/
C797S
Ex20 ins.
SVD
Ex20 ins.
NPG
Ex20 ins.
GY
pEGFR
EGFR
HSP90

Figure 21. Results of Western blot assays using compounds **39f**, **48**, **39d**, **25f**, and **26f** against EGFR WT and the most important EGFR mutants. BI-4020, gefitinib, osimertinib, and mobocertinib were used as a reference. EGFR phosphorylation (pEGFR) was used for the detection of pathway activation. Additionally, total protein levels of EGFR and HSP90 were monitored as loading and expression controls.

Additionally, the inhibitory activity of the selected compounds was determined on the downstream signaling pathways including the PI3K/AKT/mTOR and RAS/MAPK signaling. The inhibition of AKT, ERK1, and ERK2 was determined for EGFR WT, L858R, L858R/ C797S, Del19, and Del19/ C797S (Figure 22). The results showed a good concordance between the inactivation of EGFR and its downstream targets. **25f**, **39d**, and **39f** exhibited a significant inhibition of the AKT and ERK phosphorylation in the EGFR mutants L858R, L858R/C797S, Del19, and Del19/C797S, while the effect on EGFR WT was only weak. **48** showed a negligible effect on all tested variants. **26f** revealed a mutant selectivity by showing no effect EGFR WT however, showing inhibition of the downstream targets in the tested EGFR mutants L858R, L858R/ C797S, Del19, and Del19/ C797S.

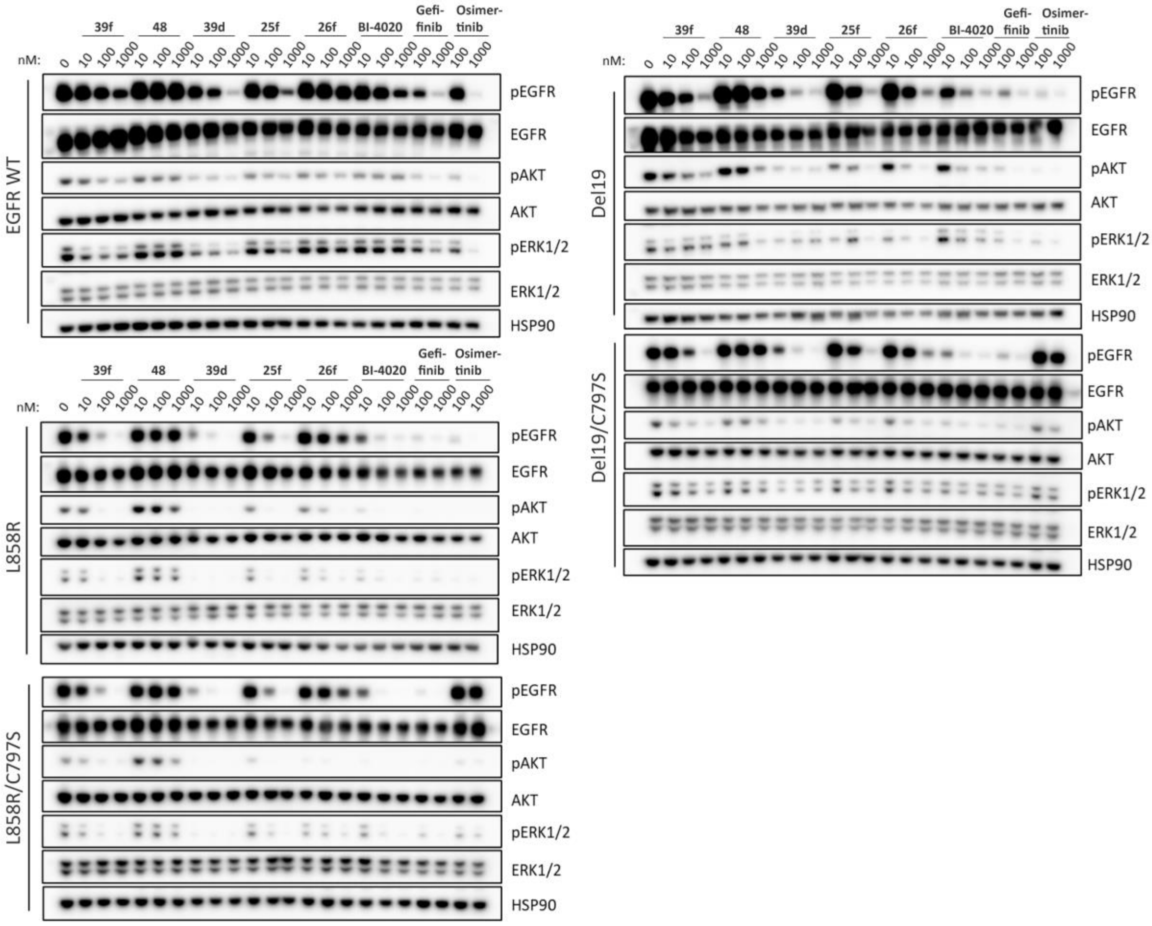

Figure 22. Results of Western blot assays using compounds **39f**, **48**, **39d**, **25f**, and **26f** against EGFR WT and the most interesting EGFR mutants L858R, L858R/C797S, Del19, and Del19/C797S. BI-4020, gefitinib, and osimertinib were used as a reference. AKT and ERK1/2 phosphorylation (pAKT, pERK1/2) was used for the detection of signaling pathway inactivation. Additionally, total protein levels of AKT, ERK1/2, and HSP90 were monitored as loading and expression controls.

3.4.5. Pharmacochemical properties

To gain first insights into the pharmacochemical properties of **26f**, the chemical stability was determined using a PBS buffer (pH 7.4) and 0.1 M HCl (pH 1.2). Therefore, **26f** was incubated at rt for 184 minutes, and the amount of the residual compound was determined by high-performance liquid chromatography (HPLC) every 23 minutes. **26f** exhibited a good chemical stability at pH 7.4 with more than 80% of residual compound after 3 hours and even an excellent stability under acid conditions with more than 95% (Figure 23A). Furthermore, the solubility of **26f** was tested in different solvents by incubating the compound at 37 °C for 24 hours. The amount of solubilized compound was then determined by HPLC. The solubility in neutral aqueous solutions is rather poor with 0.131 – 0.174 µg/mL however, it could be improved by adding 5% or 10% DMSO (0.283 –

0.294 µg/mL). By using a simulated gastric fluid (SGF) buffer,[184] the solubility could be further increased to 42.802 µg/mL and even to 2.592 mg/mL by using 100% DMSO (Figure 23B).

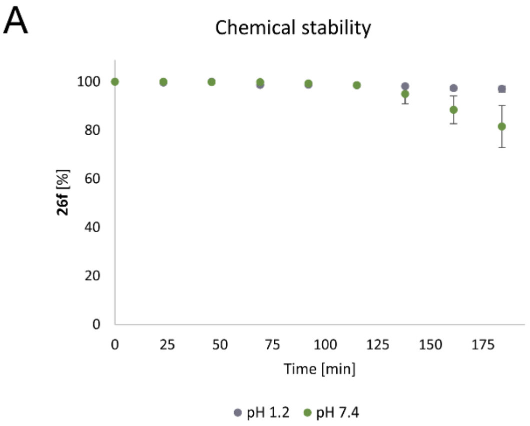

B

Solvent	Solubility per mililiter
Water	0.131 ± 0.004 µg/mL
SGF	42.802 ± 0.218 µg/mL
SIF	0.174 ± 0.009 µg/mL
PBS	0.163 ± 0.004 µg/mL
PBS + 5% DMSO	0.294 ± 0.001 µg/mL
PBS + 10% DMSO	0.283 ± 0.001 µg/mL
DMSO	2.592 ± 0.065 mg/mL

Figure 23. A. Chemical stability of **26f** under acid conditions using 0.1M HCl and neutral conditions using a PBS buffer. The compound was incubated at rt for 184 minutes and measured by HPLC in triplicates. **B.** Solubility of **26f** using different solvents. The compound was incubated at 37 °C for 24 hours and measured by HPLC in triplicates.

3.5. Discovery of 3-amino-1*H*-pyrazole-based kinase inhibitors to illuminate the understudied PCTAIRE family

3.5.1. Selectivity profile

To examine the selectivity profile of the three series of newly synthesized 3-aminopyrazole-based kinase inhibitors, a DSF assay was performed. The lead structure **23** was resynthesized, based on the synthetic route of Statsuk *et. al.*[179] Various molecules were identified by DSF, which exhibited a strong stabilization of CDK16 (Table 5 – Table 7). The compounds **56a**–**f** of the first series, which had no residue in position C5 of the pyrimidine, showed a high stabilization of CDK16. They caused on average a stabilization of 8.0 °C, whereas **56c** showed the highest ΔTm shift with 9.4 °C, which is comparable with the lead structure **23** (10.3 °C). Also, the stabilization of the related family member CDK2 was quite high for **56a**–**f**. The introduction of a methyl or chlorine residue at position C5 of the pyrimidine was in general not tolerated. The methyl group (**57a**–**e**) reduced the ΔTm shifts by 2.3 °C on average in comparison to the corresponding molecule without the methyl group. An even stronger reduction of the DSF shifts was observed by the introduction of a bulkier chlorine residue (**58a**, **58c**), showing ΔTm shifts of only 3.2 °C. The introduction of the different residues also led to a decreased stabilization of CDK2. The replacement of the Boc group to a smaller amide (**60**) did not influence the stabilization of CDK16 or CDK2, respectively.

The lead structure **23** has been published as a highly promiscuous kinase inhibitor, which was also indicated in the *in-house* DSF panel by stabilizing 60 kinases with ΔTm shifts > 5 °C. The compounds **56a**–**f** and **60** with the same precursor but an exchanged linker moiety showed also a promiscuous behavior by stabilizing 12 – 32 kinases. The introduction of an additional methyl or chlorine residue at the pyrimidine (**57a**–**e**, **58a**, and **58c**) or the replacement of the Boc group with a smaller amide (**60**) also did not affect the selectivity with 16 – 28 shifts > 5 °C.

In the second series, the cyclopropyl residue at the pyrazole was replaced through a methyl ester moiety (**76a**–**i**) (Table 6). The methyl ester led to an overall lower stabilization of CDK16 in comparison to the lead structure **23** however, **76a** and **76c** exhibited still similar ΔTm shifts with 8.5 °C compared to staurosporine (9.1 °C), which has a reported K_D value of 24 nM.[40] **76i** showed also a significant stabilization with a ΔTm shift of 6.5 °C. The introduction of a residue at R^1 or R^2 was, as in the first series, not tolerated by CDK16. An additional chlorine residue (**77a**–**e**) or the exchange of the pyrimidine to a quinazoline moiety (**78a**–**c**) reduced the stabilization on average from 5.9 °C to 1.2 °C. The influence of the Boc group was examined by cleaving it to gain the compounds **79** and **80** with the primary amine. The modification led in both cases to a decreased stabilization of CDK16.

The second series caused in general a better selectivity profile and the compounds of this series stabilized only between 0 – 9 kinases with a ΔTm shift > 5 °C. The modifications at R^1 or R^2 (**77a**–**e**, **78a**–**c**) led to no influence of the selectivity compared to compounds **76a**–**i**. The *tert*-butyl (2-(aminomethoxy)ethyl)-carbamate linker improved selectivity for **76d** however, led also to a completely inactive compound **77d**. The 4-aminobenzonitrile linker (**76f**) showed with 27 kinases an increased amount of stabilized kinases, which indicated that not only the cyclopropyl but also the 4-aminobenzonitrile linker increased inhibitor promiscuity. The free amine did not significantly influence the selectivity. **79** exhibited the same amount of potential targets and the amount was even slightly increased for **80**.

Table 5. DSF data of the first series of derivatives **23**, **56a**–**f**, **57a**–**e**, **58a**,**c**, and **60**. Staurosporine was used as a positive control. The newly synthesized compounds were screened in an *in-house* panel of 104 kinases. No stabilization of the kinase is indicated in pale green and a high stabilization in dark green.

Kinase	ΔTm [°C]															
	23	**56a**	**56b**	**56c**	**56d**	**56e**	**56f**	**57a**	**57b**	**57c**	**57d**	**57e**	**58a**	**58c**	**60**	**Staurosporine**
AAK1	13.8	14.3	8.5	13.0	9.3	11.8	9.1	12.6	8.9	11.4	9.7	10.6	11.2	13.1	10.3	15.6
ABL1	8.7	6.9	4.9	4.7	2.5	4.3	5.0	5.9	4.7	4.0	3.5	3.4	1.9	4.2	4.6	10.3
AKT3	1.4	-0.2	0.2	0.0	-0.1	0.1	-0.2	-0.2	-0.2	-0.1	0.0	-0.3	-0.6	0.0	0.2	6.6
AURKB	n.d.	0.8	1.0	1.0	0.2	1.2	0.5	0.2	0.0	0.6	0.3	0.3	-0.7	0.8	1.3	8.3
BMP2K	18.8	18.5	12.3	16.8	13.0	16.2	13.3	16.9	12.6	15.2	13.7	14.6	15.8	17.0	15.5	19.1
BMPR2	9.2	4.8	3.0	3.1	2.1	3.5	2.9	3.3	4.5	3.9	3.8	4.2	6.3	4.7	4.3	2.6
BMX	4.4	2.8	2.1	1.7	0.8	2.3	2.3	1.0	2.6	1.7	1.1	1.8	-3.5	0.0	2.0	7.1
BRAF	4.6	2.2	1.1	1.3	0.5	1.6	1.1	1.3	0.8	0.9	0.7	1.1	0.6	0.8	1.2	0.8
BRD4	1.3	2.1	0.5	0.7	1.0	0.6	0.2	3.5	2.9	0.6	0.8	1.2	1.5	1.8	1.2	1.1
BRPF1B	n.d.	-0.2	0.4	0.2	0.5	0.7	-0.5	-1.2	-1.2	-0.4	-0.8	-0.1	-1.0	-1.0	-0.2	-0.1
CAMK1D	5.4	1.6	0.1	0.3	-1.0	-0.6	-0.7	0.4	0.0	0.2	-0.7	-0.1	4.8	5.0	-0.2	10.0
CAMK1G	5.5	1.3	0.1	0.5	0.5	0.3	-0.5	0.6	0.1	0.4	-0.4	0.5	3.0	3.3	0.1	10.9
CAMK2B	4.4	1.5	0.5	0.9	0.1	0.9	0.7	1.4	0.9	1.2	1.1	1.5	1.1	3.2	1.3	13.3
CAMK2D	4.5	1.9	0.7	1.0	0.3	1.0	0.7	2.0	0.6	1.5	1.5	1.4	2.0	3.5	1.3	16.2
CAMK4A	5.4	2.8	1.6	1.5	0.8	1.5	1.4	4.4	2.6	2.7	3.4	2.6	3.6	4.9	2.0	8.6
CAMKK2B	12.0	5.8	5.0	4.9	3.1	4.1	4.2	8.3	6.8	6.5	5.7	6.2	7.4	8.8	5.6	24.6
CASK	2.0	1.3	0.2	0.5	-0.1	0.3	0.4	1.3	0.6	0.4	0.1	0.3	0.8	0.6	0.8	4.8
CDC42BPA	-0.1	-0.7	0.3	0.3	0.0	-0.4	-1.0	-1.1	-0.9	-0.2	-0.6	-0.6	0.5	0.2	-0.5	2.8
CDK2	15.2	12.3	8.2	10.4	6.3	11.2	8.4	8.7	4.7	7.2	5.3	8.1	5.9	5.1	11.3	15.5
CDK16	10.3	8.7	6.3	9.4	7.3	8.9	7.6	6.2	3.7	6.5	5.8	6.3	3.2	3.2	8.8	9.1
CDKL1	6.8	2.3	1.8	2.0	1.5	1.2	0.9	-0.1	0.8	0.9	0.9	0.5	-0.4	0.6	2.5	3.1
CHEK2	8.6	5.9	2.2	2.3	1.5	3.7	3.1	6.9	3.6	3.6	3.7	5.0	3.8	4.3	2.5	17.1
CLK1	12.2	7.0	5.4	5.5	4.5	5.8	4.8	7.9	5.2	6.3	5.6	6.5	6.7	5.8	7.8	11.9
CLK3	11.3	2.4	1.7	1.6	1.0	2.2	1.5	2.3	1.4	1.7	1.8	2.2	2.1	1.4	3.6	5.6
CSNK1D	3.1	0.8	0.9	0.2	0.2	0.4	0.2	0.7	0.8	0.7	1.0	0.6	3.6	3.1	0.4	1.8
CSNK2A1	n.d.	2.5	2.0	1.0	0.7	1.1	1.4	3.5	2.3	1.3	1.6	1.2	0.7	2.5	1.8	2.1
CK2A2	8.5	4.3	4.1	3.1	2.2	2.5	2.8	3.8	3.8	2.3	2.8	2.1	5.6	4.3	4.5	5.6
DAPK1	4.9	1.9	1.2	1.5	0.5	1.8	1.7	3.0	2.1	2.3	2.5	2.7	1.9	3.8	2.1	9.8
DAPK3	9.7	4.6	3.0	4.5	3.2	4.8	3.6	4.7	3.3	4.7	4.9	5.1	6.4	8.0	5.2	15.8
DCAMKL1	8.9	4.7	4.8	6.9	4.2	6.8	3.9	5.3	4.1	6.4	5.0	6.4	4.2	7.6	5.4	12.4
DMPK1	3.2	3.7	2.6	2.8	1.7	2.4	1.5	2.9	1.8	2.5	1.6	1.7	1.5	2.0	2.1	8.7
DYRK1A	8.2	n.d.	1.9	0.5	1.4	0.5	-0.6	2.7	0.0	-0.3	-0.4	-0.4	3.9	2.3	2.7	8.7
DYRK2	11.0	3.3	2.5	3.2	2.3	3.6	3.6	1.4	1.5	1.6	2.1	1.8	4.2	5.0	6.1	7.0
EPHA2	8.4	3.9	3.3	1.7	0.8	1.8	2.1	2.6	3.7	1.7	1.6	1.8	0.4	2.0	2.8	8.3
EPHA4	n.d.	2.4	2.4	0.8	0.4	1.0	1.0	2.1	2.8	1.3	1.1	1.2	1.7	2.7	1.3	6.2
EPHA5	6.3	3.7	3.2	1.1	1.0	1.9	0.5	2.2	3.0	1.7	0.9	1.7	1.4	2.4	2.1	7.9
EPHA7	4.9	3.3	3.0	2.1	2.2	2.0	1.0	2.9	1.6	1.9	0.9	2.4	1.4	3.2	1.6	10.3
EPHB1	n.d.	3.1	1.9	0.8	0.2	1.2	1.2	2.5	2.9	1.2	1.3	1.5	1.6	2.0	1.7	6.4
EPHB3	5.1	n.d.	n.d.	0.5	0.0	0.8	0.8	1.7	n.d.	0.9	1.0	1.0	0.3	1.4	1.1	5.0
FES	4.5	1.4	1.5	0.7	0.7	0.8	0.9	1.8	1.7	1.2	1.2	1.4	1.0	2.6	1.8	6.2
FGFR1B	4.5	3.2	3.0	1.8	1.5	2.7	2.2	3.0	2.8	2.0	1.9	3.0	2.9	2.7	2.8	5.9
FGFR2	5.9	4.0	3.8	2.7	2.0	3.5	3.4	4.5	4.3	3.4	3.2	4.1	3.9	4.0	3.3	9.0
FGFR3	9.8	6.4	5.7	4.1	2.7	5.7	5.2	6.1	5.8	5.1	4.6	6.1	4.3	6.0	5.0	13.3
FLT1	10.6	7.0	6.8	4.8	3.7	5.4	5.9	6.4	5.9	4.9	5.2	6.0	5.6	5.5	4.7	13.6
GAK	8.0	6.0	4.6	4.7	2.8	4.6	1.8	5.7	4.7	4.3	3.5	4.1	3.8	4.8	3.1	9.0
GPRK5	5.2	2.6	0.7	0.8	0.6	0.7	0.7	3.8	1.1	1.1	0.8	1.1	3.4	1.5	1.0	7.7
GSG2	2.9	-0.1	0.8	0.2	0.3	0.2	-0.2	-0.3	0.1	0.0	0.2	0.0	-0.2	1.2	0.7	7.2
GSK3B	14.0	8.2	7.2	7.1	5.9	6.8	6.3	5.7	5.1	6.1	6.6	5.8	4.6	5.9	7.9	11.8
HIPK2	n.d.	3.0	1.9	1.6	0.8	2.1	2.2	2.2	1.2	1.1	1.2	1.5	1.9	1.9	2.7	4.4
MAP2K1	1.4	0.9	0.5	0.6	0.4	0.6	0.6	1.2	0.7	0.6	0.6	0.7	n.d.	n.d.	0.6	1.3
MAP2K4	10.0	8.7	5.1	4.9	3.6	6.8	5.3	4.9	3.3	3.1	2.0	5.3	3.8	3.7	4.4	12.0
MAP2K6	10.4	8.0	5.6	7.3	5.6	6.8	6.7	4.4	2.5	3.1	2.6	3.0	3.3	3.6	6.2	12.3
MAP2K7	12.0	6.0	1.5	2.4	1.5	3.7	2.0	3.0	0.5	0.9	0.7	2.1	1.5	0.9	2.0	8.4
MAP3K5	n.d.	3.7	2.0	2.2	1.2	3.2	2.4	2.4	1.5	2.3	3.1	3.0	2.4	5.1	2.8	18.5
MAPK10	7.2	3.0	3.6	1.0	1.0	3.0	0.8	3.4	3.6	0.4	1.7	1.3	4.9	7.0	3.2	7.4
MAPK13	8.0	5.4	3.9	3.9	1.7	4.8	4.2	2.3	2.0	2.0	1.7	2.6	1.3	1.4	4.8	7.5
MAPK14	2.5	1.3	0.7	1.1	0.9	1.2	0.8	0.2	0.2	0.6	0.4	0.6	-0.7	-0.6	1.1	0.3
MAPK15	17.4	13.4	9.3	12.3	9.9	12.3	11.0	8.0	4.5	8.5	7.6	8.2	6.8	5.6	13.4	14.7
MAPK1	8.5	4.6	2.2	3.7	2.2	3.6	4.6	4.0	1.5	2.5	2.2	2.9	2.3	2.2	3.1	1.4
MAPK8	n.d.	6.8	5.7	5.1	3.8	5.4	4.4	5.5	5.1	4.1	3.6	4.6	6.5	5.6	5.5	7.8
MAPK9	6.5	4.4	2.9	3.1	2.1	3.3	3.2	4.3	3.5	2.4	2.3	2.6	6.1	5.3	3.6	3.7
MAPKAPK2	n.d.	-0.5	0.5	0.2	0.3	-0.3	-0.5	-0.3	-0.1	-0.4	-0.2	-0.1	-0.1	-0.2	-0.3	3.2
MARK3	8.1	7.0	5.4	7.1	5.0	5.7	3.9	6.0	4.3	6.3	3.5	6.0	6.7	6.5	3.8	19.0
MARK4	8.2	0.0	2.0	0.8	1.7	1.7	1.1	6.8	5.1	0.5	2.1	1.1	6.7	6.4	0.0	16.4
MELK	9.8	6.6	4.5	5.0	3.5	5.2	5.4	7.0	6.0	6.7	5.8	7.4	5.9	7.7	6.5	13.8
MERTK	4.4	3.2	1.9	2.0	1.4	2.5	1.1	3.5	2.6	2.7	2.7	2.8	2.0	2.9	2.6	6.6
MST3	9.3	4.3	1.8	3.0	1.4	2.9	1.5	2.9	1.6	4.2	2.2	5.0	3.2	1.9	3.9	7.3
MST4	7.1	4.3	2.1	2.6	1.6	2.9	1.9	3.2	1.6	3.7	2.2	4.1	3.1	2.5	3.7	6.1
NEK1	1.1	0.2	0.5	0.2	0.2	-0.1	0.3	0.9	1.6	0.3	0.4	0.3	1.2	0.5	0.4	-0.6
NEK2	n.d.	3.1	2.3	1.7	1.4	2.5	0.1	2.8	1.1	2.1	0.6	3.4	2.2	3.4	1.2	3.3
NEK7	n.d.	0.1	1.3	0.0	0.9	0.2	-0.3	0.1	0.6	0.0	-0.1	0.1	-0.6	-0.1	0.2	1.0
OSR1	5.6	5.9	3.5	5.2	3.8	4.4	2.2	4.9	3.0	4.6	4.0	3.4	4.5	5.4	2.9	7.7
PAK1	3.3	1.3	0.9	0.9	0.8	1.0	0.9	0.2	0.2	0.2	0.1	0.7	-0.3	-0.2	1.1	6.6
PAK4	7.7	5.7	3.5	4.6	3.3	4.0	3.0	3.8	4.1	2.3	2.2	2.2	2.6	2.9	3.7	12.2
PDK4	1.2	-0.8	-1.0	-0.4	-0.2	-0.8	-0.7	-0.8	-1.0	-0.4	-0.3	-0.5	-0.3	-0.9	-0.1	0.2
PHKG2	8.8	3.8	3.3	3.8	3.3	3.3	2.3	4.8	4.7	4.5	4.1	4.2	3.2	5.6	4.6	21.2
PIM1	3.3	0.2	0.2	0.0	-0.2	0.4	0.4	-0.7	-0.5	0.0	0.3	-0.4	0.2	0.0	2.2	12.5
PIM3	3.8	1.3	0.4	0.7	0.4	0.7	-0.1	0.1	0.5	0.3	0.2	0.3	1.6	1.8	1.7	19.7
PKMYT1	1.0	-0.7	-0.3	-0.4	0.4	-0.1	-0.5	-1.1	-1.4	-0.3	-1.1	-0.5	0.0	-0.2	0.1	0.2
PLK4	11.1	10.7	8.1	8.7	6.3	8.9	7.6	12.1	10.0	10.1	9.2	10.3	11.4	12.2	8.3	16.0
RIOK1	4.9	4.5	0.6	1.8	2.7	0.6	0.2	-1.1	-1.5	-0.2	-0.6	1.1	2.0	5.7	0.4	0.0
RIOK2	n.d.	n.d.	n.d.	n.d.	n.d.	n.d.	n.d.	n.d.	n.d.	n.d.	n.d.	n.d.	3.1	5.1	n.d.	1.8
RPS6KA1	5.1	0.9	0.3	0.4	0.2	0.3	0.2	0.9	0.5	0.3	0.3	0.2	0.0	0.4	0.8	3.9
RPS6KA5	n.d.	n.d.	n.d.	n.d.	n.d.	n.d.	n.d.	n.d.	n.d.	n.d.	n.d.	n.d.	4.8	7.5	n.d.	13.7
RPS6KA6	0.4	4.7	6.3	7.4	5.0	6.5	3.0	2.4	5.0	7.4	5.7	7.5	0.0	-0.2	9.1	-0.5
SLK	8.8	3.9	3.3	1.8	0.8	1.8	2.1	4.0	3.6	2.0	1.1	1.7	n.d.	n.d.	2.3	18.0
SPRK1	n.d.	0.8	1.0	0.7	0.2	0.5	0.5	1.3	2.0	1.3	1.3	0.7	1.4	2.3	0.7	6.8
SRC	4.4	3.4	2.2	2.0	1.0	2.7	1.9	2.7	3.2	2.5	2.2	2.9	2.4	2.4	3.2	5.9
STK10	10.1	4.9	3.9	3.0	1.6	3.7	2.7	5.4	4.1	3.7	2.0	4.4	4.7	4.4	4.1	23.3
STK17A	9.6	3.5	1.2	2.5	0.7	1.8	0.8	3.7	1.3	2.3	1.7	1.4	5.3	6.5	2.8	11.8
STK17B	9.7	4.0	n.d.	2.0	0.3	1.6	2.3	1.3	3.4	0.0	1.3	1.2	2.6	3.0	2.3	11.5
STK38L	8.7	12.1	7.7	10.3	6.1	10.7	8.4	8.2	4.7	7.1	5.0	8.0	4.4	5.1	11.1	12.6
STK39	7.6	7.4	4.7	6.6	5.6	5.7	3.0	5.7	3.9	6.2	4.9	5.7	4.3	5.6	4.5	9.6
STK3	11.6	8.4	5.7	7.2	4.5	7.2	8.6	8.9	7.2	8.0	7.2	7.9	6.5	7.7	9.8	16.6
STK4	9.6	6.7	4.9	6.1	4.2	6.7	6.0	6.6	5.2	6.3	5.8	6.4	7.1	7.3	8.1	14.9
STK6	14.3	15.2	12.8	13.3	11.0	13.3	13.8	12.7	13.3	13.2	12.1	13.3	13.5	14.2	13.6	17.1
TAF1	0.1	-2.0	-0.8	-1.2	-1.4	-1.8	-1.0	-0.1	0.3	0.3	-0.6	-0.4	-0.6	-0.4	0.0	0.2
TIF1	n.d.	1.4	1.1	1.0	1.1	0.4	-0.1	-0.1	0.1	0.5	0.2	0.6	0.2	-0.1	0.5	0.8
TLK1	n.d.	5.5	2.6	4.8	3.1	4.3	2.8	4.7	2.2	4.0	3.2	4.0	4.0	4.0	4.7	9.4
TTK	8.8	6.2	5.8	5.2	4.1	5.3	5.2	5.8	5.1	4.4	4.1	3.9	-0.3	6.4	5.2	11.2
ULK1	15.5	5.8	3.3	5.1	3.2	5.1	3.6	5.7	4.7	5.9	3.7	7.6	4.4	6.2	5.0	11.3
ULK3	8.3	12.1	7.4	10.9	8.4	10.3	8.3	12.3	8.8	10.9	10.2	11.1	10.3	11.4	9.9	19.6
VRK1	5.9	2.6	0.9	2.2	1.1	2.0	2.4	0.1	0.1	0.2	0.1	0.1	0.6	0.7	2.7	2.8
WNK1	1.1	0.2	1.5	0.3	0.5	0.4	0.1	0.6	0.9	0.1	0.1	0.6	0.4	0.7	0.4	0.9
No. kinases >5°C	59	32	20	22	12	25	18	28	16	21	16	24	21	34	22	75

Table 6. DSF data of the second series of derivatives **76a**–**i**, **77a**–**e**, **78a**–**c**, **79**, and **80**. Staurosporine was used as a positive control. The newly synthesized compounds were screened in an *in-house* panel of 104 kinases. No stabilization of the kinase is indicated in pale green and a high stabilization in dark green.

Kinase	ΔTm [°C]																			
	76a	76b	76c	76d	76e	76f	76g	76h	76i	77a	77b	77c	77d	77e	78a	78b	78c	79	80	Staurosporine
AAK1	6.7	5.8	8.2	4.1	7.8	7.1	3.7	7.2	2.0	4.4	5.1	6.8	2.2	4.0	5.8	3.0	9.0	6.4	4.0	15.6
ABL1	2.0	3.4	1.9	1.2	2.3	4.1	1.0	2.2	0.7	1.7	2.5	1.4	0.3	0.7	1.4	1.2	1.8	2.8	2.1	10.3
AKT3	-0.1	0.4	0.0	0.3	0.2	0.8	-0.2	0.0	-0.3	-0.4	-0.1	-0.1	-0.3	-0.5	-0.3	-0.1	-0.2	0.0	0.3	6.6
AURKB	n.d.	n.d.	n.d.	n.d.	n.d.	-0.6	n.d.	n.d.	n.d.	-1.2	-0.7	-0.6	-1.9	-0.6	-1.5	-0.9	-0.8	n.d.	n.d.	8.3
BMP2K	10.2	9.1	12.3	5.7	12.6	11.8	6.2	10.7	2.8	9.1	11.2	10.3	4.2	7.9	7.4	4.8	10.9	10.0	7.5	19.1
BMPR2	2.3	2.1	1.8	0.7	2.0	5.8	0.8	1.2	1.1	1.7	2.7	1.5	0.1	0.4	0.0	0.1	1.1	1.3	2.2	2.6
BMX	0.7	1.3	0.4	0.2	0.9	2.1	0.2	0.8	-0.1	-0.1	0.7	0.7	0.0	0.3	-1.8	-0.3	1.2	1.0	1.3	7.1
BRAF	1.3	1.8	1.6	0.9	1.5	1.8	0.9	0.8	1.0	1.1	1.2	1.0	0.7	0.6	0.2	0.6	0.8	0.9	1.1	0.8
BRD4	0.5	3.3	-0.4	0.7	2.3	1.2	0.8	1.6	1.0	4.1	6.5	1.9	0.8	2.3	1.7	3.6	1.4	0.5	-0.6	1.1
BRPF1B	n.d.	n.d.	n.d.	n.d.	n.d.	0.8	n.d.	n.d.	n.d.	-0.5	-0.4	-0.7	0.3	0.1	0.4	1.2	-1.1	n.d.	n.d.	-0.1
CAMK1D	0.2	3.2	0.3	1.4	0.1	3.5	0.0	2.1	-0.5	-0.7	0.0	-0.8	-1.6	-1.3	1.4	1.7	2.3	-0.1	1.2	10.0
CAMK1G	0.9	2.6	0.5	0.4	-0.3	2.1	-0.5	1.8	0.4	-0.3	0.1	-0.4	-1.3	-1.0	2.6	3.1	2.1	1.0	0.6	10.9
CAMK2B	0.6	0.8	0.6	0.2	1.9	1.8	0.8	1.1	0.6	-0.1	0.0	0.4	-0.3	-0.7	0.6	1.0	1.7	0.8	0.4	13.3
CAMK2D	0.5	1.2	1.4	0.8	1.2	1.4	1.1	0.5	0.6	0.0	0.2	1.2	0.1	0.7	0.5	0.7	1.2	0.6	1.3	16.2
CAMK4A	0.5	0.5	0.2	-0.2	0.5	1.8	0.0	0.3	-0.4	0.2	0.6	0.5	0.0	-0.1	0.6	0.7	1.1	0.1	0.1	8.6
CAMKK2B	0.9	2.3	1.8	0.5	1.2	5.6	0.5	1.0	1.1	4.1	5.0	3.4	1.0	3.0	1.1	1.7	1.6	1.6	2.1	24.6
CASK	0.5	0.4	0.2	0.4	0.8	1.0	0.2	0.7	0.2	0.5	-0.1	0.4	-0.1	0.6	-2.9	-6.1	0.6	0.4	0.3	4.8
CDC42BPA	-0.5	0.5	-0.8	0.5	-0.9	0.4	-0.9	0.4	-0.5	0.0	-0.2	-1.1	-0.5	-0.7	0.8	0.5	-1.2	-0.1	-0.4	2.8
CDK2	3.1	4.6	5.6	1.9	6.5	7.8	3.3	2.5	3.3	2.0	2.1	1.5	0.2	0.7	-0.1	0.6	1.3	3.0	5.1	15.5
CDK16	4.3	4.9	8.5	4.3	8.5	5.3	5.3	5.1	6.5	0.3	0.8	1.0	0.2	0.2	-0.5	0.2	3.4	2.4	5.6	9.1
CDKL1	0.3	0.4	0.3	0.1	0.6	3.8	-0.3	0.6	0.5	-1.3	0.5	0.8	0.0	0.1	0.0	-0.2	0.2	2.3	0.5	3.1
CHEK2	0.8	5.1	2.1	2.5	1.1	2.5	0.7	1.9	0.6	0.8	3.1	4.4	0.6	2.2	0.6	0.4	0.9	1.6	2.1	17.1
CLK1	2.5	3.1	2.9	1.8	2.9	6.6	1.9	2.2	1.3	1.9	2.8	2.7	2.0	1.8	3.2	2.7	3.9	2.9	4.2	11.9
CLK3	0.3	1.7	0.3	1.1	0.4	3.0	0.3	1.4	0.4	0.5	0.9	0.0	0.6	0.5	0.6	0.7	0.4	1.0	1.6	5.6
CSNK1D	0.6	1.0	0.5	0.2	0.8	3.4	0.5	0.5	0.4	0.1	1.1	1.5	0.3	0.6	0.6	1.0	0.9	1.0	0.6	1.8
CSNK2A1	n.d.	n.d.	n.d.	n.d.	n.d.	1.6	n.d.	n.d.	n.d.	3.5	2.9	1.9	1.1	1.1	0.1	0.4	1.1	n.d.	n.d.	2.1
CK2A2	3.2	4.0	3.0	1.8	3.0	6.0	1.9	2.4	1.3	5.4	5.0	2.8	2.3	2.1	1.9	2.7	2.9	4.7	3.5	5.6
DAPK1	0.9	1.9	1.3	-2.4	1.4	3.3	1.0	1.7	0.6	0.1	0.9	1.7	0.5	0.8	0.4	0.6	2.4	1.3	1.2	9.8
DAPK3	0.2	2.5	2.6	3.3	2.9	7.7	1.4	3.0	-0.6	1.0	2.4	3.0	1.2	2.0	2.3	3.3	5.5	2.4	3.2	15.8
DCAMKL1	1.0	2.1	1.7	1.5	2.3	4.3	0.8	1.5	-0.6	1.2	1.7	0.9	1.6	1.6	1.6	4.4	3.2	1.3	1.5	12.4
DMPK1	0.8	0.8	0.5	0.5	0.5	0.9	0.0	0.7	0.1	1.2	1.4	0.7	0.3	0.6	0.7	0.7	1.4	0.5	0.1	8.7
DYRK1A	2.5	0.9	1.7	1.2	0.8	7.1	1.4	2.3	3.4	-0.5	-0.1	-0.7	-0.6	0.5	0.8	0.6	-2.4	0.9	2.4	8.7
DYRK2	1.9	3.1	2.5	2.1	1.8	7.9	1.9	1.5	1.1	2.4	2.4	3.3	2.8	2.0	-0.2	0.0	0.6	2.8	4.6	7.0
EPHA2	1.0	2.4	0.4	0.2	0.9	2.0	0.5	0.6	0.4	-0.2	0.8	0.3	0.1	0.0	-0.1	0.4	0.1	1.0	1.3	8.3
EPHA4	n.d.	n.d.	n.d.	n.d.	n.d.	2.7	n.d.	n.d.	n.d.	0.0	0.6	0.3	-0.1	0.1	0.9	0.8	1.2	n.d.	n.d.	6.2
EPHA5	0.2	1.6	0.2	0.2	0.8	1.8	-0.1	0.9	0.2	0.1	1.0	-0.2	-0.8	-0.2	0.0	1.5	0.6	0.7	1.1	7.9
EPHA7	1.2	2.2	2.1	1.3	-0.9	3.0	-0.4	1.1	0.6	1.1	1.1	1.6	0.7	1.3	0.8	0.8	1.0	0.5	2.2	10.3
EPHB1	n.d.	n.d.	n.d.	n.d.	n.d.	2.3	n.d.	n.d.	n.d.	-0.2	0.6	0.5	-0.4	-0.4	0.8	0.9	1.5	n.d.	n.d.	6.4
EPHB3	0.8	2.2	0.8	0.8	0.8	1.9	0.5	1.9	0.4	-0.6	0.0	0.9	-0.4	-0.4	-1.0	-0.8	0.6	0.7	1.2	5.0
FES	0.6	1.9	0.4	1.5	0.9	1.1	0.7	0.7	0.0	0.7	1.4	0.2	0.2	-0.3	0.4	0.5	0.3	0.6	1.0	6.2
FGFR1B	1.1	2.3	0.5	0.5	0.8	2.4	0.2	1.0	0.0	0.1	1.6	0.7	0.3	0.2	1.2	2.3	1.4	1.0	2.8	5.9
FGFR2	1.8	3.4	1.4	1.5	2.0	3.4	0.9	1.4	0.2	0.5	2.3	1.4	0.4	0.8	2.3	3.6	2.5	1.2	3.7	9.0
FGFR3	2.2	3.5	1.8	0.6	2.2	4.0	1.4	1.6	1.2	1.3	3.0	1.4	1.0	0.9	0.9	2.4	2.4	2.3	4.7	13.3
FLT1	3.3	5.2	2.8	2.0	3.0	6.0	2.4	3.2	2.2	2.5	4.1	1.0	0.8	1.3	1.9	4.0	2.7	5.0	4.9	13.6
GAK	4.1	4.8	4.1	2.1	4.7	5.3	1.5	5.5	1.3	1.8	2.7	2.8	0.2	1.8	1.8	1.5	2.3	2.7	1.8	9.0
GPRK5	0.7	0.4	0.3	0.2	0.8	0.9	0.7	0.8	0.7	0.2	0.5	0.2	0.3	0.4	0.4	0.6	0.4	0.8	1.2	7.7
GSG2	-0.1	0.6	0.1	0.2	0.1	1.1	0.0	0.2	-0.2	-0.1	0.5	1.1	0.4	0.5	0.0	-0.2	0.2	0.5	0.3	7.2
GSK3B	7.8	8.6	8.6	6.2	8.6	12.3	7.7	6.0	7.2	3.3	3.9	4.8	2.1	2.9	1.0	1.4	4.2	9.5	10.3	11.8
HIPK2	n.d.	n.d.	n.d.	n.d.	n.d.	4.7	n.d.	n.d.	n.d.	1.1	1.0	0.7	0.1	0.3	0.2	0.2	0.5	n.d.	n.d.	4.4
MAP2K1	-0.2	0.3	-0.1	0.7	-0.3	n.d.	-0.5	0.2	-0.5	0.3	0.1	0.1	0.0	0.1	n.d.	n.d.	n.d.	0.1	0.2	1.3
MAP2K4	2.8	3.4	2.5	0.9	2.5	4.7	1.7	4.0	2.4	3.2	3.8	1.4	0.6	0.9	0.4	0.4	0.5	1.4	2.1	12.0
MAP2K6	2.1	1.9	4.2	1.4	3.5	3.8	2.7	1.7	5.4	1.4	1.8	0.8	0.4	0.3	0.2	0.4	0.2	1.5	2.7	12.3
MAP2K7	0.8	0.9	0.9	0.7	1.1	1.7	0.4	0.8	0.5	0.3	0.2	0.7	0.0	-0.6	0.8	1.4	0.2	n.d.	n.d.	8.4
MAP3K5	n.d.	n.d.	n.d.	n.d.	n.d.	1.9	n.d.	n.d.	n.d.	0.8	0.9	2.7	2.3	0.0	0.7	0.8	0.7	0.5	1.1	18.5
MAPK10	3.2	3.1	3.3	2.9	4.4	10.1	2.4	2.8	1.8	0.2	n.d.	2.8	0.4	1.7	3.2	3.8	5.1	1.2	4.0	7.4
MAPK13	1.0	2.8	1.4	0.5	1.4	2.5	0.7	0.7	1.0	0.8	1.5	0.9	0.3	0.3	-0.5	-0.3	0.0	0.9	1.1	7.5
MAPK14	-0.4	-0.8	-0.3	-0.3	-0.3	0.7	-0.7	-0.2	-0.6	-0.2	0.2	0.0	0.4	-0.2	0.0	0.0	-0.4	0.0	-0.4	0.3
MAPK15	6.1	5.3	7.9	4.1	7.9	11.5	4.7	6.3	5.9	4.4	2.9	0.9	0.4	0.8	-0.2	0.2	2.6	7.4	6.6	14.7
MAPK1	0.6	0.6	0.6	0.3	0.8	1.8	1.0	0.7	0.7	0.4	0.7	0.8	0.6	0.4	-0.5	-0.3	0.0	0.6	0.3	1.4
MAPK8	n.d.	n.d.	n.d.	n.d.	n.d.	5.9	n.d.	n.d.	n.d.	5.2	5.8	5.0	2.8	4.3	1.4	1.4	1.4	n.d.	n.d.	7.8
MAPK9	2.5	3.2	2.2	1.1	2.9	5.8	1.8	3.0	1.7	2.9	3.2	3.0	1.2	2.0	1.0	1.3	1.7	1.2	2.1	3.7
MAPKAPK2	n.d.	n.d.	n.d.	n.d.	n.d.	-0.3	n.d.	n.d.	n.d.	-0.3	-0.2	-0.1	0.1	-0.2	0.1	0.2	0.0	n.d.	n.d.	3.2
MARK3	0.8	3.6	1.8	2.5	1.3	3.7	0.1	1.8	1.5	1.9	2.5	0.5	-0.3	0.7	1.4	2.0	3.6	2.0	3.3	19.0
MARK4	2.2	4.2	3.4	1.7	2.4	4.5	1.4	3.0	3.3	2.2	0.2	0.2	2.2	2.0	1.5	2.5	3.4	2.3	4.5	16.4
MELK	1.2	2.7	2.1	0.8	2.7	4.0	1.2	0.9	0.9	2.3	3.1	2.5	0.8	2.4	0.7	1.0	2.6	2.1	2.3	13.8
MERTK	1.3	3.4	1.7	1.9	0.8	2.0	0.1	2.9	-0.1	1.8	2.4	1.8	0.7	0.7	0.5	0.4	0.9	1.7	1.2	6.6
MST3	0.2	0.0	1.2	-0.3	0.2	4.2	-0.6	0.6	0.1	1.3	1.1	0.7	0.1	0.3	0.7	0.7	1.9	1.2	1.0	7.3
MST4	-0.3	0.0	0.3	0.7	0.1	4.1	-0.3	0.2	-0.7	0.8	1.2	-0.1	0.0	0.4	0.9	1.7	2.7	0.5	0.7	6.1
NEK1	0.6	1.2	0.3	0.1	0.2	0.9	0.5	0.5	0.4	1.0	1.9	0.6	0.3	0.2	0.0	0.4	0.5	0.5	0.5	-0.6
NEK2	n.d.	n.d.	n.d.	n.d.	n.d.	1.2	n.d.	n.d.	n.d.	3.5	2.5	1.3	0.7	1.6	0.7	0.9	-2.6	n.d.	n.d.	3.3
NEK7	n.d.	n.d.	n.d.	n.d.	n.d.	0.7	n.d.	n.d.	n.d.	1.8	0.7	0.4	0.7	0.8	1.1	1.7	0.1	n.d.	n.d.	1.0
OSR1	1.5	1.6	2.5	0.3	1.1	1.4	0.0	1.3	0.6	1.3	1.4	1.1	0.5	0.7	1.9	1.4	3.2	1.0	0.9	7.7
PAK1	-0.4	1.6	0.9	1.1	0.2	0.9	0.6	0.3	-0.4	0.2	0.2	-0.1	0.0	0.4	0.7	1.0	0.0	0.4	0.9	6.6
PAK4	0.9	1.9	0.6	1.0	0.9	3.2	-0.3	0.9	0.2	3.0	4.5	1.6	0.4	1.2	-0.3	0.3	0.8	2.3	1.2	12.2
PDK4	0.9	1.2	0.7	1.8	-1.0	-0.2	0.9	1.2	0.9	-0.9	-0.4	-0.1	-0.2	-0.3	-0.5	-0.5	-0.6	0.8	1.1	0.2
PHKG2	0.2	1.2	1.1	0.5	1.1	2.5	0.0	0.5	-0.3	0.7	2.5	1.3	0.2	0.7	0.5	1.0	0.6	1.0	1.8	21.2
PIM1	-0.3	2.4	-0.3	2.1	-0.5	2.6	-0.9	1.1	-0.6	-0.1	0.1	0.3	0.7	1.3	0.3	0.7	-0.5	0.9	0.5	12.5
PIM3	-0.2	0.7	0.3	0.0	0.4	4.3	-0.7	0.6	-0.4	0.2	1.0	0.6	0.4	0.8	2.0	2.2	0.6	1.2	1.0	19.7
PKMYT1	0.6	1.3	0.5	1.0	0.4	0.5	0.5	1.0	0.2	0.0	-0.2	-0.3	0.2	0.0	0.7	0.5	0.3	0.9	0.6	0.2
PLK4	6.3	6.1	6.9	3.0	7.2	7.7	5.1	6.0	4.1	5.5	6.8	7.6	4.7	7.3	5.1	6.4	9.1	3.8	6.8	16.0
RIOK1	0.3	0.3	-0.1	0.1	0.0	5.7	0.4	1.0	0.8	-0.5	-0.6	0.4	1.0	2.2	1.7	2.1	-0.4	0.0	0.7	0.0
RIOK2	n.d.	n.d.	n.d.	n.d.	n.d.	6.1	n.d.	n.d.	n.d.	n.d.	n.d.	n.d.	n.d.	n.d.	-0.4	-0.5	0.0	n.d.	n.d.	1.8
RPS6KA1	0.6	0.8	0.6	0.5	0.5	1.3	0.7	0.5	1.0	0.0	0.3	1.0	0.3	0.2	-0.5	-0.1	0.3	0.8	0.8	3.9
RPS6KA5	n.d.	n.d.	n.d.	n.d.	n.d.	11.0	n.d.	n.d.	n.d.	n.d.	n.d.	n.d.	n.d.	n.d.	2.1	2.8	2.5	n.d.	n.d.	13.7
RPS6KA6	-0.6	0.3	-0.7	-0.3	-0.6	0.0	-0.8	-0.4	-0.3	0.6	3.4	1.5	-0.1	0.2	0.6	1.0	0.1	-0.2	0.2	-0.5
SLK	1.9	3.5	1.5	1.0	1.2	n.d.	0.6	2.6	0.2	1.0	3.9	-0.2	-0.1	0.8	n.d.	n.d.	n.d.	3.9	2.7	18.0
SPRK1	n.d.	n.d.	n.d.	n.d.	n.d.	0.8	n.d.	n.d.	n.d.	-0.4	0.6	0.3	-0.1	-0.2	-0.3	0.1	0.7	-0.1	0.7	6.8
SRC	2.1	2.1	1.6	0.5	2.6	2.6	0.8	2.0	0.6	-0.8	1.4	0.7	-0.1	0.3	1.1	1.1	1.8	1.9	2.1	5.9
STK10	0.8	3.3	0.3	-0.7	1.2	4.7	-0.4	1.7	-0.7	1.6	4.3	2.2	-0.3	1.0	0.9	1.3	0.4	2.9	2.6	23.3
STK17A	1.2	2.5	3.0	2.2	1.9	3.5	0.5	3.3	-0.1	0.0	0.5	0.3	0.0	0.3	2.8	2.8	0.6	1.9	1.3	11.8
STK17B	3.5	3.6	1.4	1.6	2.1	5.6	2.7	3.0	3.4	-0.8	0.4	0.3	-2.3	-2.0	1.3	1.5	3.0	1.6	3.0	11.5
STK38L	2.5	2.8	1.8	1.2	2.5	8.1	1.1	1.5	0.9	1.7	1.9	0.7	0.2	0.3	0.5	0.9	1.7	1.6	1.3	12.6
STK39	2.6	3.0	4.0	1.8	2.4	2.0	1.5	2.5	2.1	1.2	1.6	0.9	1.3	1.6	1.5	1.4	4.2	2.5	1.6	9.6
STK3	2.4	2.8	3.1	1.6	4.3	5.4	2.7	2.8	1.2	2.4	2.6	1.4	0.5	1.6	1.7	1.8	1.5	4.5	5.3	16.6
STK4	1.7	2.4	1.9	1.6	2.8	5.0	2.0	2.3	2.2	1.1	2.7	0.6	1.1	2.3	1.6	1.8	2.2	2.1	3.7	14.9
STK6	6.3	7.9	8.1	3.2	9.2	10.3	7.0	7.2	4.6	7.5	10.5	5.5	3.7	6.7	5.4	7.7	10.9	3.0	7.5	17.1
TAF1	0.3	0.2	0.1	0.0	-0.2	1.0	0.1	0.5	0.2	-1.7	-1.1	0.6	-0.7	-0.5	-2.1	-2.5	-0.3	0.2	0.2	0.2
TIF1	n.d.	n.d.	n.d.	n.d.	n.d.	0.3	n.d.	n.d.	n.d.	0.8	1.3	0.5	0.3	0.2	1.1	1.0	-0.5	n.d.	n.d.	0.8
TLK1	n.d.	n.d.	n.d.	n.d.	n.d.	4.9	n.d.	n.d.	n.d.	0.4	0.8	1.1	0.3	0.5	1.2	1.1	2.9	n.d.	n.d.	9.4
TTK	2.0	3.4	0.8	1.6	1.0	4.8	0.4	2.3	0.0	3.1	2.7	2.6	2.2	2.1	1.4	2.1	1.1	0.5	0.3	11.2
ULK1	4.3	4.5	6.5	2.3	5.9	2.8	2.0	4.6	2.7	2.0	2.8	2.5	1.2	0.4	0.7	1.3	2.2	0.8	0.4	11.3
ULK3	0.6	1.2	2.8	0.9	1.5	8.2	0.7	1.6	0.3	5.8	6.9	3.3	1.7	3.1	3.4	2.3	9.3	2.6	3.5	19.6
VRK1	0.5	1.5	1.6	1.0	1.9	2.0	1.1	0.6	1.1	-0.1	0.2	-0.1	0.1	0.2	0.2	0.3	0.4	1.0	3.1	2.8
WNK1	0.6	1.5	0.7	0.9	0.6	0.8	0.6	1.2	0.6	0.2	1.3	0.6	0.7	0.3	-0.4	0.1	0.4	0.6	0.5	0.9
No. kinases >5°C	6	8	9	2	9	27	5	8	4	6	7	4	0	3	4	2	7	5	8	75

In the third series, the residue at the pyrazole was varied and a methyl, *iso*-propyl, *tert*-butyl, methyl amide, *iso*-propyl ester, or *tert*-butyl ester group was introduced. A methyl (**93a**–**b**) or *tert*-butyl (**95a**–**c**) group led to moderate stabilization of CDK16 in a range from 4.4 °C – 5.8 °C. The *iso*-propyl (**94a**–**b**) group increased the ΔTm shifts to 7.9 °C and 8.6 °C, respectively. Additionally, these modifications exhibited also high ΔTm shifts for CDK2. The replacement to a methyl amide (**96a**–**c**) moiety seemed to be not tolerated and led to inactive compounds with a stabilization of 0.9 °C – 1.5 °C for CDK16. Next, an *iso*-propyl (**97b**,**d**) and *tert*-butyl (**98b**,**d**) ester were introduced at the pyrazole. Both moieties can be found in various already approved drugs or those that are in clinical trials, suggesting that these groups might have valuable pharmacokinetic properties.[185,186] These modifications improved the ΔTm shifts on average to 9.0 °C for CDK16, while the stabilization for CDK2 was in a moderate range of 3.0 °C – 6.5 °C.

The methyl, *iso*-propyl, or *tert*-butyl group (**93** – **96**) caused a high number of stabilized kinases with 6 – 48 kinases harboring ΔTm shifts > 5 °C. Thereby, the bulkier *tert*-butyl group (**96a**–**c**) was more selective than the smaller methyl- or *iso*-propyl groups (**93a**–**b**, **94a**–**b**). The methyl amide moiety (**96a**–**c**) was in general not tolerated in this position. **96a** and **96b** were not accepted from any kinase, only the promiscuous 4-aminobenzonitrile linker (**96c**) resulted in six stabilized kinases with ΔTm shifts > 5 °C. The replacement of the methyl ester (**76**) to an *iso*-propyl (**97**) or *tert*-butyl (**98**) ester decreased the number of potential off-targets. **97b** and **98b** exhibited 10 and 7 ΔTm shifts > 5 °C, respectively, which is in the same range as the corresponding compound **76c** with a methyl ester. The compounds **97d** and **98d** exhibited only 1 – 2 stabilized kinases besides CDK16, whereas these shifts were comparatively small compared to the staurosporine reference, thus suggesting no strong binding to these off-target kinases.

Table 7. DSF data of the third series of derivatives **93a**–**b**, **94a**–**b**, **95a**–**c**, **96a**–**c**, **97b**,**d**, and **98b**,**d**. Staurosporine was used as a positive control. The newly synthesized compounds were screened in an *in-house* panel of 104 kinases. No stabilization of the kinase is indicated in pale green and a high stabilization in dark green.

Kinase	ΔTm [°C]														
	93a	93b	94a	94b	95a	95b	95c	96a	96b	96c	97b	97d	98b	98d	Staurosporine
AAK1	9.0	9.3	11.2	10.2	8.0	6.5	9.0	4.6	3.1	5.2	5.3	0.5	3.4	1.0	15.6
ABL1	5.8	4.2	6.2	4.3	4.1	1.6	5.8	1.0	0.8	2.5	2.6	1.0	2.6	1.6	10.3
AKT3	0.7	0.1	-0.5	-0.1	-0.4	-0.2	0.7	0.5	0.4	0.6	0.4	0.6	0.3	0.5	6.6
AURKB	0.1	-0.2	-0.9	-1.0	-1.6	-2.0	0.1	-2.2	-3.7	-2.4	n.d.	n.d.	n.d.	n.d.	8.3
BMP2K	14.0	12.9	16.5	15.0	12.8	11.3	14.0	3.8	2.6	5.4	10.1	1.4	7.3	1.7	19.1
BMPR2	7.4	1.8	5.0	4.0	4.8	2.5	7.4	1.0	0.3	1.7	2.2	0.9	1.8	1.4	2.6
BMX	3.4	1.6	-0.5	1.4	0.1	0.1	3.4	0.7	0.3	0.5	0.3	-0.1	0.3	-0.4	7.1
BRAF	3.4	1.0	1.6	0.7	1.4	0.7	3.4	0.4	1.0	1.2	0.7	0.4	0.9	0.7	0.8
BRD4	0.3	-0.4	0.0	-0.1	0.4	-0.9	0.3	2.0	2.3	2.5	-1.6	-2.1	-1.4	-1.5	1.1
BRPF1B	0.3	-0.6	-0.7	-0.2	-0.9	-0.9	0.3	0.8	2.5	0.5	-1.8	-1.4	-0.5	-0.9	-0.1
CAMK1D	4.7	2.3	4.0	2.8	2.9	1.8	4.7	1.9	2.6	1.6	-2.5	-2.4	-2.0	-2.9	10.0
CAMK1G	3.4	1.4	2.6	0.9	1.6	0.6	3.4	1.3	0.1	1.1	0.1	-0.2	0.0	-0.7	10.9
CAMK2B	2.7	1.2	2.5	1.5	1.4	0.8	2.7	0.3	0.4	0.4	-0.8	-1.2	-0.3	-0.5	13.3
CAMK2D	3.9	0.6	2.7	1.5	2.6	1.2	3.9	1.2	1.0	1.3	0.3	-0.4	0.5	-0.1	16.2
CAMK4A	6.0	0.8	4.0	2.5	3.1	1.3	6.0	1.0	0.4	0.8	0.1	0.4	0.0	1.2	8.6
CAMKK2B	8.8	1.1	6.9	6.1	4.3	2.3	8.8	1.8	1.4	2.5	2.0	-0.6	2.2	0.1	24.6
CASK	1.5	0.2	1.5	0.7	0.8	0.2	1.5	1.7	0.4	0.6	0.6	0.4	1.0	0.4	4.8
CDC42BPA	0.7	0.1	-0.9	0.0	-0.8	-0.7	0.7	0.7	0.2	0.5	-1.3	-0.7	-1.9	-0.8	2.8
CDK2	10.7	4.7	9.8	9.5	5.8	4.3	10.7	1.2	1.2	2.7	6.5	3.0	6.5	3.2	15.5
CDK16	5.7	5.8	7.9	8.6	4.4	5.1	5.7	0.9	1.5	1.4	9.1	8.4	9.3	9.2	9.1
CDKL1	3.2	0.4	2.0	1.5	0.8	0.2	3.2	0.4	0.3	0.8	1.0	1.7	1.3	2.1	3.1
CHEK2	5.1	2.0	3.2	1.9	1.7	1.1	5.1	0.9	1.7	1.1	1.0	0.6	0.6	1.3	17.1
CLK1	9.3	2.0	7.4	6.8	4.6	4.2	9.3	1.9	1.2	3.1	1.8	0.0	1.7	-0.5	11.9
CLK3	8.3	0.2	2.6	2.4	1.6	1.3	8.3	0.9	1.0	0.9	-0.2	-0.4	0.9	0.0	5.6
CSNK1D	3.1	0.6	2.5	1.0	1.7	0.2	3.1	0.7	0.2	1.4	0.7	0.8	0.8	1.0	1.8
CSNK2A1	3.2	0.3	1.6	1.0	1.2	0.8	3.2	0.9	0.5	0.6	n.d.	n.d.	n.d.	n.d.	2.1
CK2A2	4.6	1.6	3.6	2.4	2.3	0.7	4.6	1.6	0.6	3.1	1.5	1.1	0.1	1.1	5.6
DAPK1	3.4	2.3	2.7	1.6	1.8	0.8	3.4	0.8	0.3	1.1	-0.3	-0.3	-0.5	-0.4	9.8
DAPK3	7.8	6.6	5.3	5.7	2.8	2.9	7.8	1.2	1.2	3.0	1.0	0.1	0.7	0.3	15.8
DCAMKL1	5.3	4.0	4.9	7.1	2.4	2.6	5.3	1.0	0.3	1.0	-1.6	-2.4	-1.8	-2.1	12.4
DMPK1	2.2	1.0	3.2	2.2	2.3	0.9	2.2	0.6	-0.2	-0.2	0.3	-0.1	0.1	-0.1	8.7
DYRK1A	7.2	-0.1	2.8	-0.3	0.6	-0.5	7.2	0.9	0.2	1.8	1.1	0.0	2.9	1.8	8.7
DYRK2	6.5	1.3	3.8	2.5	3.6	1.3	6.5	0.4	0.6	3.2	1.6	0.5	1.5	0.8	7.0
EPHA2	5.3	0.9	3.2	1.2	2.0	0.4	5.3	0.2	0.1	1.1	1.1	0.6	1.7	1.3	8.3
EPHA4	3.9	1.3	2.6	1.3	2.6	1.3	3.9	1.0	0.9	1.3	-0.1	-0.1	0.5	0.0	6.2
EPHA5	4.5	0.9	2.5	0.7	1.9	0.4	4.5	0.6	0.1	1.0	0.2	-0.6	0.8	-2.7	7.9
EPHA7	4.2	0.7	2.4	1.2	0.9	0.0	4.2	1.1	1.1	0.9	-3.5	-3.1	-2.8	-3.4	10.3
EPHB1	4.1	0.8	2.5	1.0	2.3	0.4	4.1	1.6	0.9	1.4	0.7	0.9	1.3	1.0	6.4
EPHB3	3.0	0.2	2.1	0.6	1.5	0.2	3.0	0.6	0.1	0.4	0.6	1.3	1.0	1.7	5.0
FES	3.3	0.9	1.4	1.5	1.3	0.7	3.3	0.5	1.0	1.0	0.1	0.1	0.3	1.1	6.2
FGFR1B	3.6	2.3	2.8	1.6	2.6	1.2	3.6	0.8	0.7	0.7	0.8	0.4	1.2	0.6	5.9
FGFR2	3.5	2.8	3.9	2.6	2.9	1.1	3.5	0.7	0.3	0.9	0.9	0.1	1.3	0.3	9.0
FGFR3	5.3	3.8	6.1	3.6	3.7	1.4	5.3	0.6	0.3	1.0	n.d.	n.d.	n.d.	n.d.	13.3
FLT1	5.1	3.9	5.6	3.2	3.3	1.6	5.1	1.8	-1.8	2.8	1.5	0.6	2.3	0.9	13.6
GAK	8.3	2.2	5.9	4.4	5.9	4.0	8.3	3.0	1.8	3.8	3.3	-0.9	3.1	-4.1	9.0
GPRK5	4.6	0.3	3.7	1.0	3.2	0.8	4.6	0.3	0.2	0.5	-1.4	-1.3	-1.2	-1.4	7.7
GSG2	2.2	0.2	0.6	0.4	0.5	0.3	2.2	0.3	0.3	0.5	0.3	0.5	0.0	-0.3	7.2
GSK3B	10.4	4.6	7.0	6.2	5.7	4.9	10.4	2.9	1.3	9.3	7.8	4.7	6.6	2.9	11.8
HIPK2	6.4	1.0	4.1	2.6	2.3	1.4	6.4	0.7	0.9	0.9	0.2	-0.2	0.3	0.1	4.4
MAP2K1	n.d.	n.d.	n.d.	n.d.	n.d.	n.d.	n.d.	n.d.	n.d.	n.d.	n.d.	n.d.	n.d.	n.d.	1.3
MAP2K4	6.5	3.0	6.5	4.8	4.6	2.9	6.5	1.9	0.5	2.7	1.8	0.4	1.1	1.0	12.0
MAP2K6	6.7	4.3	6.7	5.8	4.6	3.0	6.7	0.4	0.3	1.0	5.9	5.0	4.4	3.0	12.3
MAP2K7	4.0	1.3	4.6	1.8	1.7	0.6	4.0	1.5	0.7	1.2	-0.2	-0.3	-0.3	-3.0	8.4
MAP3K5	4.2	1.3	3.2	1.6	2.8	1.3	4.2	0.6	0.7	0.5	0.1	0.1	0.3	0.1	18.5
MAPK10	8.6	5.7	8.6	5.6	5.6	5.0	8.6	3.0	2.8	4.8	-1.9	-3.0	-1.0	-1.6	7.4
MAPK13	5.7	1.1	3.3	1.8	2.7	1.0	5.7	0.1	-0.4	0.7	1.4	1.0	1.3	1.3	7.5
MAPK14	2.9	0.2	0.1	-0.2	0.0	-0.1	2.9	0.5	0.6	1.3	-0.6	-0.5	-0.6	-0.3	0.3
MAPK15	11.0	6.8	12.6	11.8	7.0	5.2	11.0	1.9	0.7	3.9	8.6	7.0	7.4	5.8	14.7
MAPK1	5.1	1.7	3.2	2.6	2.8	1.8	5.1	0.5	0.2	0.7	0.1	-0.1	0.0	0.0	1.4
MAPK8	9.8	4.1	6.0	3.2	6.7	3.4	9.8	4.8	3.9	5.6	1.9	-0.8	2.9	-0.1	7.8
MAPK9	7.0	3.1	4.7	2.8	5.4	3.1	7.0	2.7	2.1	3.4	0.0	-0.7	0.3	-1.4	3.7
MAPKAPK2	0.3	-0.1	0.0	-0.1	-0.1	-0.1	0.3	0.3	0.3	0.4	-0.4	-0.3	-0.3	0.2	3.2
MARK3	5.7	3.2	5.4	4.9	3.2	3.0	5.7	1.3	-0.1	0.9	0.5	-0.4	0.4	-0.5	19.0
MARK4	6.7	2.1	5.1	4.6	3.8	3.2	6.7	2.1	1.6	1.4	1.2	0.3	1.8	-0.5	16.4
MELK	8.3	2.7	6.6	5.1	4.8	3.8	8.3	0.6	0.8	1.8	0.4	-0.8	0.8	0.2	13.8
MERTK	2.8	1.0	2.4	1.7	1.4	0.6	2.8	1.4	1.0	2.1	0.6	-0.8	0.4	-0.8	6.6
MST3	5.9	0.6	3.0	2.3	2.3	1.0	5.9	1.0	0.4	1.1	1.4	0.8	2.0	-0.3	7.3
MST4	6.2	1.0	2.4	2.5	3.0	2.3	6.2	2.7	1.9	2.0	0.8	0.1	1.6	-0.1	6.1
NEK1	0.3	0.2	0.1	0.1	0.4	0.1	0.3	0.2	0.4	0.6	0.0	0.2	0.2	0.1	-0.6
NEK2	2.4	0.7	2.0	0.9	1.9	1.3	2.4	1.9	1.6	1.1	0.7	-1.4	0.8	2.0	3.3
NEK7	2.8	-0.5	0.0	-0.3	0.3	-0.5	2.8	2.4	2.2	2.3	-2.4	-1.7	-2.1	-1.0	1.0
OSR1	4.9	2.3	5.0	4.1	3.5	2.5	4.9	1.7	3.5	2.7	0.1	-0.8	0.0	-0.4	7.7
PAK1	2.4	-0.2	0.5	0.1	-0.2	-0.4	2.4	1.0	0.4	0.7	-0.9	-1.1	-0.4	-0.6	6.6
PAK4	5.0	1.2	3.9	2.8	2.8	1.2	5.0	1.0	0.8	1.1	0.8	-0.2	0.5	-0.9	12.2
PDK4	-0.1	-0.1	-0.4	-0.5	-0.3	-0.3	-0.1	-0.3	-0.2	-0.2	n.d.	n.d.	n.d.	n.d.	0.2
PHKG2	4.8	1.0	3.1	3.4	1.1	0.8	4.8	0.9	0.6	1.4	0.7	-0.2	1.1	0.5	21.2
PIM1	2.7	-0.2	-0.5	-0.3	-0.1	-0.9	2.7	1.5	0.7	1.6	0.1	0.2	-0.4	-0.7	12.5
PIM3	3.0	1.1	1.4	1.4	0.9	0.8	3.0	2.1	1.8	2.7	-1.2	-1.1	-1.2	-1.6	19.7
PKMYT1	0.1	0.5	-0.4	-0.2	0.0	0.2	0.1	0.6	0.6	0.5	-2.8	-3.2	-3.0	-2.0	0.2
PLK4	6.5	7.9	7.1	5.4	4.6	1.8	6.5	2.3	1.2	3.5	7.2	3.7	7.2	5.5	16.0
RIOK1	5.0	1.8	3.8	0.6	2.6	1.1	5.0	2.4	3.0	4.2	n.d.	n.d.	n.d.	n.d.	0.0
RIOK2	9.1	4.4	8.2	3.2	8.1	3.4	9.1	1.8	1.2	1.8	n.d.	n.d.	n.d.	n.d.	1.8
RPS6KA1	1.6	0.1	0.4	0.3	0.1	0.0	1.6	0.5	0.6	1.4	-0.2	-0.3	-0.2	0.2	3.9
RPS6KA5	12.8	6.5	6.0	7.0	4.5	4.5	12.8	2.6	1.8	7.2	-0.1	0.8	0.5	1.7	13.7
RPS6KA6	1.1	0.1	-0.2	0.0	0.0	-0.2	1.1	0.3	1.2	1.7	n.d.	n.d.	n.d.	n.d.	-0.5
SLK	n.d.	n.d.	n.d.	n.d.	n.d.	n.d.	n.d.	n.d.	n.d.	n.d.	0.1	-0.6	1.5	0.1	18.0
SPRK1	3.2	0.2	1.7	1.3	1.5	0.7	3.2	0.2	0.4	0.5	-0.1	-0.2	0.0	0.4	6.8
SRC	3.4	1.9	2.8	1.7	2.3	0.4	3.4	0.5	0.3	1.1	0.1	0.4	0.4	0.6	5.9
STK10	5.1	1.3	3.7	2.5	1.8	-0.3	5.1	1.2	0.2	0.6	0.6	-0.7	0.8	-0.8	23.3
STK17A	10.6	1.9	5.7	4.6	6.0	5.2	10.6	3.5	3.7	3.8	0.1	-0.4	-0.2	-0.6	11.8
STK17B	4.0	1.9	2.6	1.9	0.8	0.8	4.0	1.0	0.8	2.7	-3.2	-2.8	-2.4	-2.5	11.5
STK38L	10.3	4.7	10.8	9.3	5.3	4.3	10.3	0.6	0.7	1.9	0.0	0.0	-0.3	0.0	12.6
STK39	4.7	3.4	5.6	6.0	3.1	2.9	4.7	1.3	0.7	0.3	0.1	-0.6	-0.1	-0.9	9.6
STK3	9.0	3.8	7.3	6.0	5.7	3.8	9.0	0.7	0.5	1.3	0.1	-1.0	2.9	0.3	16.6
STK4	8.7	4.4	6.2	5.8	5.1	4.2	8.7	2.0	1.1	1.7	0.9	-0.5	2.1	-0.2	14.9
STK6	10.6	12.4	12.7	10.2	9.0	5.3	10.6	4.0	2.3	6.3	7.5	3.4	7.3	4.0	17.1
TAF1	0.6	-0.1	0.0	-0.1	0.3	-0.3	0.6	0.0	-0.2	0.6	0.2	0.5	0.2	0.0	0.2
TIF1	0.9	0.1	-0.7	-1.6	0.5	-0.5	0.9	2.4	2.4	1.6	n.d.	n.d.	n.d.	n.d.	0.8
TLK1	4.5	4.0	4.1	3.4	2.6	1.9	4.5	2.0	1.8	2.4	1.2	-1.2	-1.3	-1.4	9.4
TTK	8.4	1.2	6.6	6.0	6.0	4.9	8.4	4.4	1.5	2.6	0.1	-0.1	-0.3	-0.2	11.2
ULK1	6.3	2.1	4.6	3.7	3.2	2.4	6.3	1.8	2.2	1.7	n.d.	n.d.	n.d.	n.d.	11.3
ULK3	10.3	6.0	9.6	8.1	6.9	3.9	10.3	1.7	2.0	3.0	6.0	2.3	5.0	3.3	19.6
VRK1	5.0	1.6	3.0	2.6	2.4	2.8	5.0	0.8	1.0	1.2	2.1	0.5	2.8	0.9	2.8
WNK1	1.1	0.1	0.8	0.4	0.9	0.4	1.1	0.3	0.6	0.7	-0.4	0.1	-0.3	-0.1	0.9
No. kinases >5°C	48	10	33	22	17	6	48	0	0	6	10	2	7	3	75

In conclusion, the introduction of the cyclopropyl group achieved the highest ΔTm shifts for CDK16 in the DSF assay however, these compounds exhibited a high number of other potential off-targets. Also, the replacement to other alkyl groups led to a high amount of stabilized kinases. The introduction of a substituent at the pyrimidine, as well as a methyl amide group at the pyrazole, was not tolerated by CDK16. A favorable combination of CDK16 stabilization and potential off-targets was observed for an ester moiety at the pyrazole. **76i**, harboring a methyl ester, showed a moderate stabilization of CDK16 (ΔTm = 6.5 °C) and targeted only three other kinases (Figure 24B). Through the replacement to a *tert*-butyl ester (**98d**), the stabilization of CDK16 could be even increased to 9.2 °C while decreasing the amount of stabilized kinases (Figure 24C).

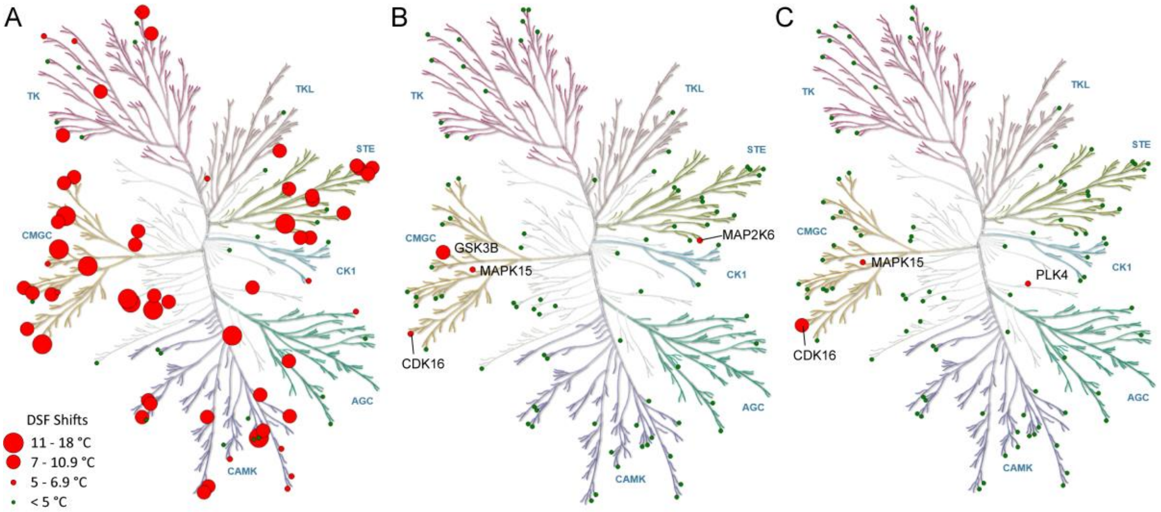

Figure 24. A. Graphic representation of the selectivity data of **23** preserved from the DSF assay, illustrated with Cell Signaling Technology. **B**. Graphic representation of the selectivity data of **76i** preserved from the DSF assay, illustrated with Cell Signaling Technology. **C.** Graphic representation of the selectivity data of **97d** preserved from the DSF assay, illustrated with Cell Signaling Technology.

3.5.2. CETSA revealed CDK16 stabilization in cells

Proteome-wide CETSA experiments were performed to verify whether the substances also lead to stabilization of proteins in the cellular system. Therefore, lead structure **23** and some compounds from the second series (**76b**, **76d**, **76e**, **76h**, and **76i**) were selected for this study. While the statistical significance is plotted on the Y-axis, the relative protein amount is shown on the X-axis. All selected compounds exhibited a stabilization of CDK16 in the CETSA experiment, whereby GSK3B was also significantly stabilized. **76b**, **76e**, and **76h** revealed a broader range of kinase off-targets, which correlated with the DSF assay data. Based on the CETSA data, CDK16 and GSK3 were the most prominently stabilized kinases for **76d** and **76i**, whereas in particular **76i** exhibited excellent selectivity and potency in CETSA MS (Figure 25). We hypothesized the same stabilization of CDK16 in the cellular system for the structurally highly related compounds **97d** and **98d**, as the DSF assay indicated more selective and potent compounds. However, for characterization of all newly synthesized compounds in a cellular system, a NanoBRET^{TM} assay was performed for CDK16.

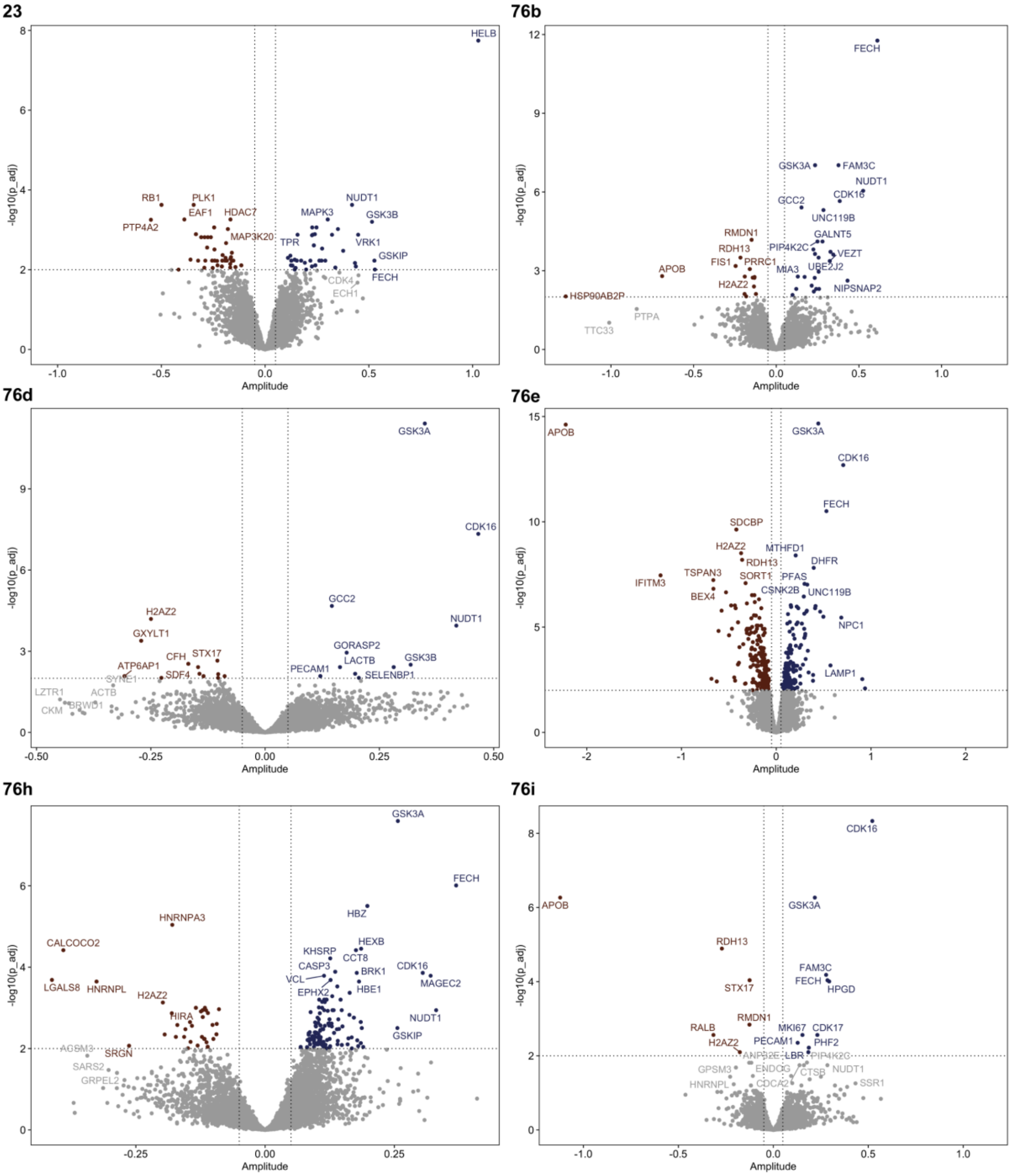

Figure 25. Volcano plots of stabilized (positive amplitude) and destabilized (negative amplitude) proteins of **23**, **76b**, **76d**, **76e**, **76h**, and **76i**.

3.5.3. Cell-based activity

The cellular potency of the newly synthesized inhibitors was determined, using the NanoBRET^{TM} cellular target engagement assay. The cellular potency on CDK16 correlated well with the corresponding DSF assay data. The lead structure (**23**) showed the highest DSF shift with 10.3 °C and a corresponding IC_{50} value of 18.0 nM. The inhibitors with the cyclopropyl residue at the pyrazole (**56a**–**f**) had a high cellular potency with IC_{50} values in a range from 33.0 nM – 124.0 nM. The introduction of a residue at position C5 of the pyrimidine (**57a**–**e**, **58a**, and **58c**) caused less potent compounds (IC_{50} = 172.0 nM – 1099.0 nM). However, all molecules from the first series showed a promiscuous behavior by targeting a high number of kinases. The introduction of a methyl ester moiety at the pyrazole (**76a**–**e**, **76g**–**i**) led to more selective compounds with only 2 – 9 identified kinases with ΔTm shifts > 5 °C, even if they are slightly less potent than the lead structure and the derivatives from the first series. Especially **76c**, **76e** **76h**, and **76i** showed a favored combination of selectivity and potency with IC_{50} values of 107.0 nM, 152.0 nM, 391.0 nM, and 380.2 nM, respectively. The introduction of an additional chlorine residue (**77a**–**e**) or the exchange of the pyrimidine to a quinazoline (**78a**–**c**) moiety caused inactive molecules with IC_{50} values > 1 µM on CDK16. A methyl, *iso*-propyl, or *tert*-butyl group at the pyrazole (**93** – **95**) led to a high stabilization of CDK16 in the DSF assay, as well as to a high cellular potency in the NanoBRET^{TM} assay with IC_{50} values between 47.0 nM – 1134.0 nM. The methyl amide moiety (**96a**–**c**) caused an inactivation against CDK16 with IC_{50} values > 1 µM. The introduction of an *iso*-propyl or *tert*-butyl ester led to a higher stabilization of the kinase in the DSF assay in comparison to the corresponding methyl ester, as well as to an improved cellular potency. **97b** and **98b** exhibited high cellular activity with IC_{50} values of 54.0 nM and 76.0 nM, respectively. An even higher ΔTm shift could be seen for **97d** and **98d** with DSF shifts comparable to the lead structure (**23**) and excellent IC_{50} values of 44.0 nM and 33.4 nM, respectively. The number of stabilized kinases with ΔTm shifts > 5 °C was favorably low for both molecules with 2 and 3 kinases. Both inhibitors exhibited a great profile, investigating them in a comprehensive selectivity study within the CDK family in the next step.

Table 8. Table of the binding affinities of the *N*-(1*H*-pyrazole-3-yl)pyrimidine-4-amine-based inhibitors against CDK16.

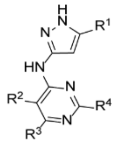
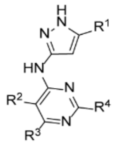

	Residues				NanoBRET
	R^1	R^2	R^3	R^4	IC_{50} [nM]^a ± SEM
23		H	H	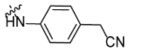	18.0 ± 0.7
56a		H	H	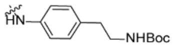	35.0 ± 0.0
56b		H	H	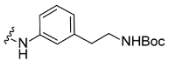	124.0 ± 10.4
56c		H	H	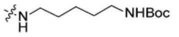	33.0 ± 0.1
56d		H	H	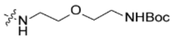	67.0 ± 1.3
56e		H	H	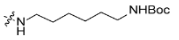	36.0 ± 1.2
56f		H	H	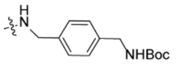	110.0 ± 9.7
57a		Me	H	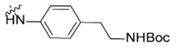	172.0 ± 20.9
57b		Me	H	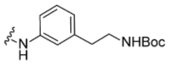	1099.0 ± 44.5
57c		Me	H	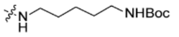	176.0 ± 3.0
57d		Me	H	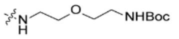	619.0 ± 32.0
57e		Me	H	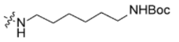	191.0 ± 5.9
58a		Cl	H	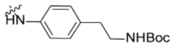	354.0 ± 60.5
58c		Cl	H	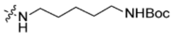	914.0 ± 11.0
60		H	H	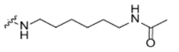	100.0 ± 7.0
76a	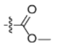	H	H	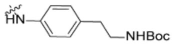	652.0 ± 15.6
76b	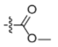	H	H	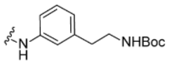	688.0 ± 22.5
76c	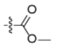	H	H	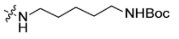	107.0 ± 3.0
76d	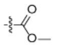	H	H	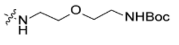	1374.0 ± 306.0
76e	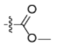	H	H	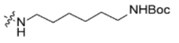	152.0 ± 2.9
76f	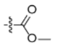	H	H	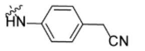	112.0 ± 8.6
76g	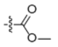	H	H	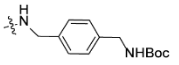	879.0 ± 5.5
76h	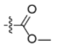	H	H	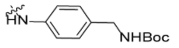	391.0 ± 46.4
76i	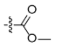	H	H	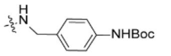	380.2 ± 230.2
77a	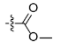	Cl	H	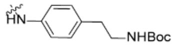	1861.0 ± 276.0
77b	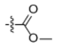	Cl	H	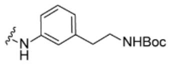	3188.0 ± 589.0
77c	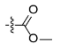	Cl	H	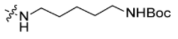	8319.0 ± 227.5
77d	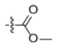	Cl	H	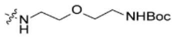	24980.0 ± 4220.0
77e	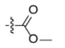	Cl	H	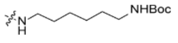	12085.0 ± 65.0
78a	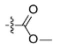	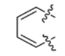		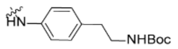	9358.0 ± 1022.5
78b	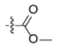	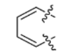		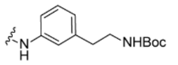	6822.0 ± 279.5
78c	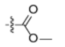	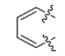		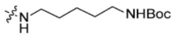	4603.0 ± 385.0
79	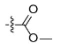	H	H	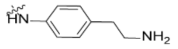	2831.0 ± 544.5
80	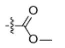	H	H	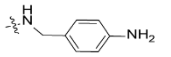	400.0 ± 30.6
93a		H	H	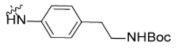	388.0 ± 32.0
93b		H	H	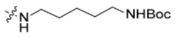	253.0 ± 19.2
94a		H	H	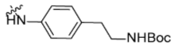	70.0 ± 4.9
94b	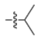	H	H	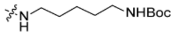	47.0 ± 4.1
95a	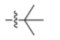	H	H	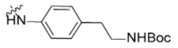	1134.0 ± 20.5
95b	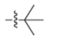	H	H	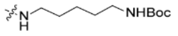	504.0 ± 9.3
95c	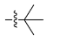	H	H	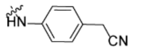	351.0 ± 34.1
96a	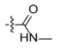	H	H	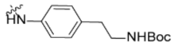	4165.0 ± 274.0
96b	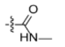	H	H	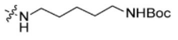	2467.0 ± 247.5
96c	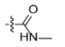	H	H	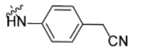	5548.0 ± 636.0
97b	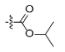	H	H	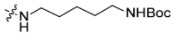	54.0 ± 1.8
97d	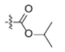	H	H	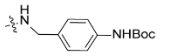	44.0 ± 7.5
98b	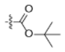	H	H	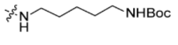	76.0 ± 0.9
98d	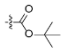	H	H	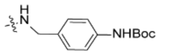	33.4 ± 5.8

$^a IC_{50}$ values were determined using the NanoBRET™ assay in a 11-point dose−response curve in duplicates.

The most promising compounds **76i**, **97d**, and **98d** were profiled against the CDK family including the corresponding co-expressed cyclins, using the NanoBRET™ technology. The lead structure (**23**) was used as a control and showed, as expected, no selectivity within the CDK family and was potent on all tested kinases. **76i** targeted only CDK16 and CDK17 in the nanomolar range with IC_{50} values of 380.2 nM and 673.1 nM, respectively. A much higher potency was observed for **97d** and **98d**, whereas **98d** exhibited the best selectivity profile within the kinase family. It targeted the PCTAIRE subfamily with 33.4 nM, 21.2 nM, and 120.6 nM for CDK16/ cyclin Y, CDK17/ cyclin Y, and CDK18/ cyclin Y, respectively. CDK14/ cyclin Y and CDK15/ cyclin Y, members of the structurally highly related PFTAIRE subfamily, were also hit by **98d** with IC_{50} values of 72.1 nM and 301.6 nM. CDK1, CDK9, and CDK10 were also addressed however, with weaker IC_{50} values of 581.9 nM, 993.4 nM, and 651.2 nM, respectively. **97d** exhibited a similar profile and showed an additional nanomolar potency for CDK6, CDK7, and CDK20 (Figure 26).

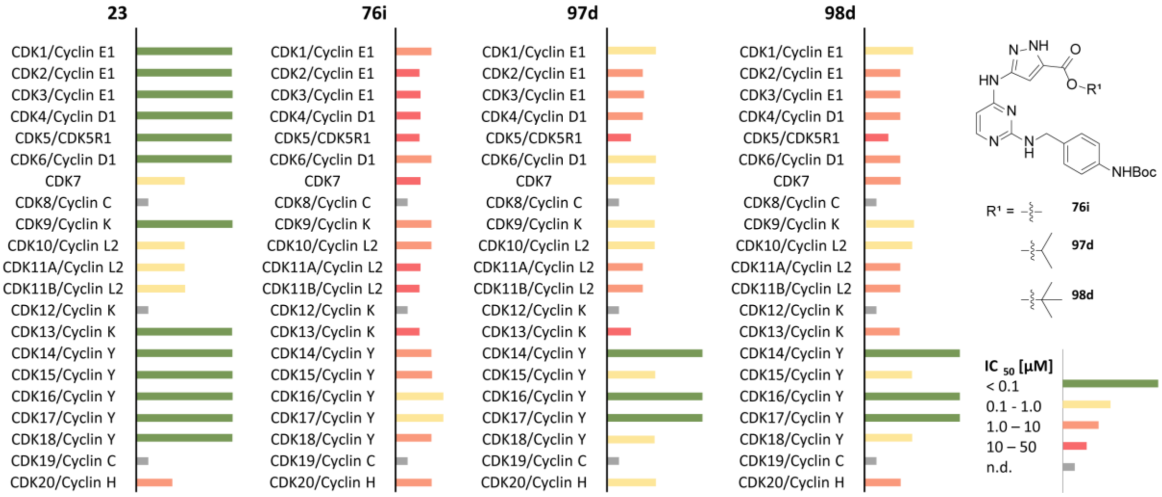

Figure 26. Cellular IC_{50} values of **76i**, **97d**, and **98d** against the CDK family were determined using NanoBRET^{TM} technology in a 11-dose-response curve in duplicates.

3.5.4. Metabolic stability

Due to the most potent and selective CDK16 inhibitors harboring an ester moiety, a metabolic stability assay was performed using liver microsomes. The compounds were tested against an activated microsome mix derived from the liver of Sprague-Dawley rats, as previously reported.[187] **76i** and **98d** were incubated at 37 °C for 60 minutes and the amount of unmetabolized compound was determined every 15 minutes, using HPLC. The metabolic stability could be increased by replacing the methyl ester in **76i** with a *tert*-butyl ester (**98d**). After an incubation time of 60 minutes, only 16% of **76i** were detected however, the microsomal stability was substantially increased to 79% for **98d** (Figure 27A).

3.5.5. FUCCI cell cycle assay

A cell-based assay in liver cells was performed, using the fluorescent ubiquitination-based cell cycle reporter (FUCCI) system to detect the cell cycle states (G1, G2/M, or S phase) on a single cell level.[188,189] Furthermore, a viability assessment was performed using Hoechst33342 as a nuclear marker.[190] Therefore, the compounds **76i**, **97d**, and **98d** were tested using the lead structure (**23**) as a reference compound and milciclib, a published CDK2 inhibitor,[191] as a positive control. **76i** and **98d** decreased the cell count at all tested concentrations (1 µM, 5 µM, 10 µM) in a dose-dependent manner in comparison to cells treated with DMSO (0.1%) with an increasing effect over the time (Figure 27B). Both compounds showed less than 50% cells after 72 h compared to the control suggesting an attenuated cell growth. Cells treated with 1 µM of **98d** showed on average 10% of pyknosed nuclei, an irreversible condensation of chromatin undergoing necrosis or apoptosis. At 10 µM of **98d**, the pyknosed nuclei rate was even higher with 45% on average (Figure 27C). These data were revealed by a machine learning algorithm, which allocated cells in healthy, pyknosed, and fragmented nuclei. The increased amount of pyknosed nuclei indicates apoptotic cell death due to typical morphological changes like DNA condensation or nuclear fragmentation. The results are in concordance with the hypothesis of Yanagi *et*. *al*. that CDK16 inhibition led to an up-regulation of p27 and consequently induced apoptosis.[131] **76i**, **97d**, and **98d** led to a G2/M phase arrest at all three tested concentrations (1 µM, 5 µM, 10 µM) (Figure 27D, E). The most significant impact on the cell cycle could be seen for **98d**. While milciclib caused a G1 cell cycle arrest, the lead structure (**23**) showed no effect on the cell cycle at all tested concentrations. At later time points, the G2/M phase arrest was no longer detectable, which can be explained by the higher amount of apoptotic cells. Also, these results were in good concordance with CDK16 knockout data, which showed a G2/M phase arrest, followed by apoptotic cell death.

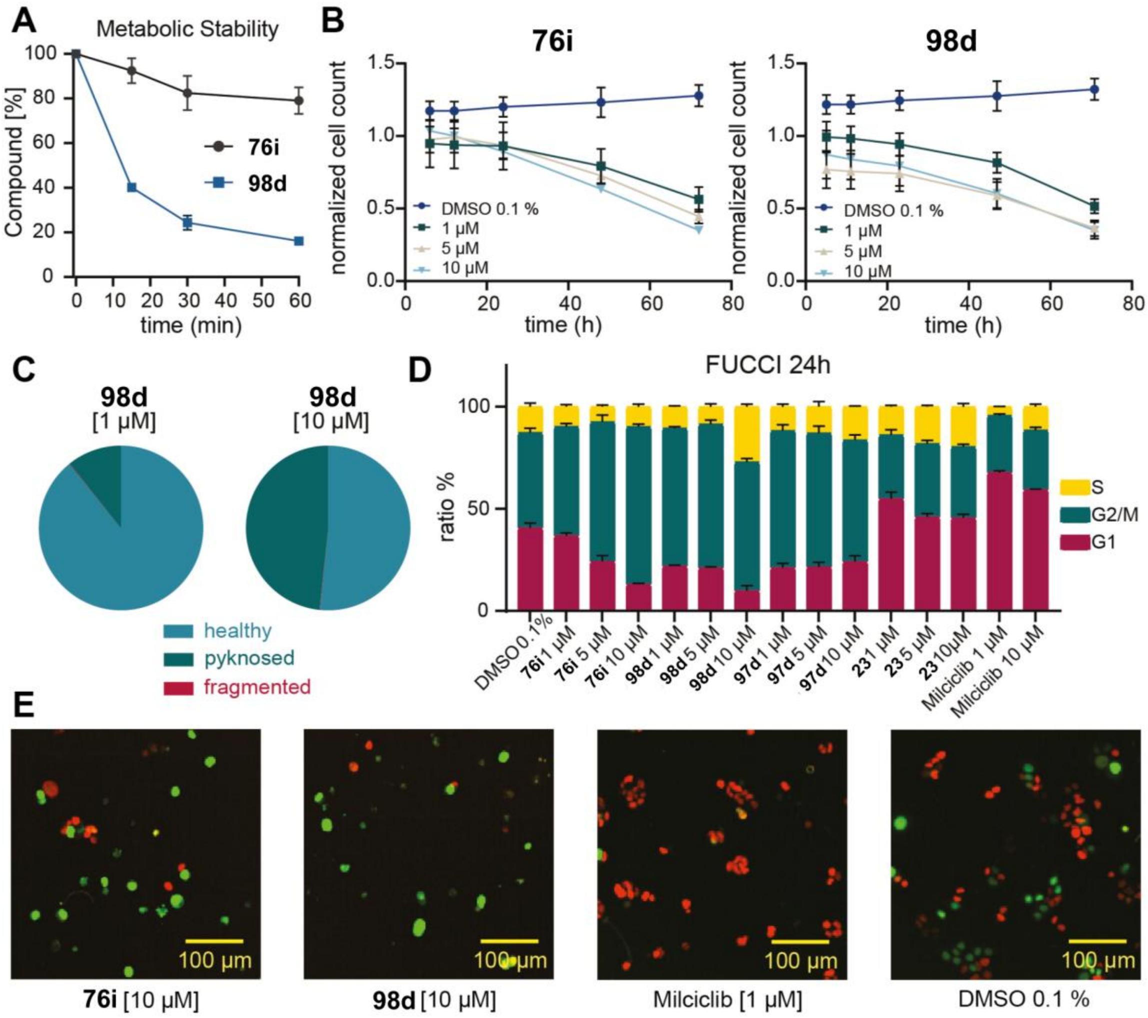

Figure 27. A. Metabolic stability of **76i** [10 µM] and **98d** [10 µM] after treatment of activated microsomes. The residual amount of compound was determined after 0, 15, 30, and 60 minutes and was plotted in percent against the time in minutes. The data is given as a mean ± SEM, measured in triplicates. **B.** Normalized cell count of HCT116-FUCCI cells after 0h, 6h, 12h, 24h, 48h and 72h of compound exposure (**76i** [1 µM, 5 µM, 10 µM], **98d** [1 µM, 5 µM, 10 µM]) in comparison to cells exposed to 0.1% DMSO. Error bars show SEM of two biological replicates. **C.** Fraction of healthy, fragmented and pyknosed nuclei after 24 h of 1µM and 10 µM compound exposure (**98d**) in HCT116 cells. Average data of two biological duplicates are shown. **D.** Fractions of red (G1), green (G2/M) or yellow (S) cells after 24 h of compound exposure (**76i** [1 µM, 5 µM, 10 µM], **98d** [1 µM, 5 µM, 10 µM], **97d** [1 µM, 5 µM, 10 µM], 1 [1 µM, 5 µM, 10 µM], Milciclib [1 µM, 10 µM]) in comparison to cells exposed to 0.1% DMSO. Error bars show SEM of two biological replicates. **E.** Fluorescence Image of HCT116-FUCCI cells after 48h of compounds exposure (**76i** [10 µM], **98d** [10 µM]) in comparison to cells exposed to Milciclib [1 µM] and cells exposed to 0.1% DMSO.

3.6. Design and synthesis of pyrazole-based macrocyclic kinase inhibitors targeting BMPR2

3.6.1. *In-house* selectivity profile

To examine the selectivity profile of the new series of 3-aminopyrazole-based macrocyclic kinase inhibitors, an *in-house* DSF assay was performed (Table 9). The lead structure **23** and staurosporine were used as a reference. **110a** showed an interesting profile in the DSF panel, by targeting only three kinases with a ΔTm shift > 5 °C. BMP2K exhibited a DSF shift of 5.8 °C however, this shift was negligible in comparison to staurosporine (19.1 °C). BMPR2 and GSK3B needed to be pursued further with ΔTm shifts of 5.3 °C and 8.4 °C, respectively. The variation of the attachment point of the phenyl ring in the linker led to an unselective macrocycle **110b**. It targeted 15 kinases with a ΔTm shift higher than 5 °C. Also, the aliphatic C5 linker (**110c**) stabilized 10 kinases > 5 °C and showed an unselective profile. Both compounds stabilized BMPR2 with slightly lower shifts than **110a** with 5.0 °C and 4.6 °C, respectively. The small exchange from a pentyl to an ethoxyethyl linker led to an inactive compound **110d**. Only BMP2K was targeted with 5.7 °C however, this value was negligible in comparison to the reference. Through the extension by one carbon, **110e** regained selectivity in comparison to **110c**. **110e** stabilized 3 kinases with a ΔTm shift > 5 °C (BMP2K, GSK3B, and STK3) however, they were low in comparison to staurosporine. **110d** and **110e** showed no notable stabilization of BMPR2 in the DSF assay with ΔTm shifts of 2.0 °C and 2.8 °C, respectively.

Table 9. DSF data of the pyrazole-based macrocyclic kinase inhibitors **110a**–**e**. **23** and staurosporine were used as a positive control. The newly synthesized compounds were screened in an *in-house* panel of 104 kinases. No stabilization of the kinase is indicated in pale green, a high stabilization is indicated in dark green.

Kinase	ΔTm [°C]						
	23	**110a**	**110b**	**110c**	**110d**	**110e**	Staurosporine
AAK1	13.8	2.2	6.6	4.9	2.2	3.2	15.6
ABL1	8.7	0.5	3.2	1.6	0.2	0.5	10.3
AKT3	1.4	0.3	0.4	-0.1	0.0	0.5	6.6
AURKB	n.d.	n.d.	n.d.	n.d.	n.d.	n.d.	8.3
BMP2K	18.8	5.8	11.2	10.4	5.7	7.9	19.1
BMPR2	9.2	5.3	5.0	4.6	2.0	2.8	2.6
BMX	4.4	0.4	2.1	0.7	0.1	0.8	7.1
BRAF	4.6	1.1	2.1	3.2	1.7	0.7	0.8
BRD4	1.3	1.0	0.9	1.0	0.2	0.1	1.1
BRPF1B	n.d.	n.d.	n.d.	n.d.	n.d.	n.d.	-0.1
CAMK1D	5.4	2.7	3.0	-0.6	-1.6	0.9	10.0
CAMK1G	5.5	2.0	1.9	0.1	-0.3	-0.6	10.9
CAMK2B	4.4	1.1	1.3	1.1	0.7	0.4	13.3
CAMK2D	4.5	1.6	1.2	1.4	0.6	1.1	16.2
CAMK4	5.4	0.2	1.1	0.3	0.0	0.1	8.6
CAMKK2B	12.0	1.9	3.7	1.6	0.1	0.8	24.6
CASK	2.0	0.0	0.4	0.2	0.1	0.2	4.8
CDC42BPA	-0.1	0.5	0.3	-0.2	-0.4	0.3	2.8
CDK2	15.2	3.8	5.3	4.4	1.7	3.7	15.5
CDKL1	10.3	0.1	0.2	0.2	-0.3	0.2	3.1
CHEK2	6.8	2.2	3.5	2.6	0.9	2.4	17.1
CLK1	8.6	1.6	5.3	5.2	3.0	2.2	11.9
CLK3	12.2	1.5	3.0	2.8	1.6	1.6	5.6
CSNK1D	11.3	1.5	1.8	2.1	1.7	0.5	1.8
CSNK2A1	3.1	n.d.	n.d.	n.d.	n.d.	n.d.	2.1
CK2A2	n.d.	0.7	4.8	2.7	1.5	1.0	5.6
DAPK1	8.5	0.5	2.3	1.2	0.5	0.6	9.8
DAPK3	4.9	0.5	4.4	0.7	0.5	0.9	15.8
DCAMKL1	9.7	0.1	2.6	1.1	-0.3	0.7	12.4
DMPK1	8.9	0.5	1.4	0.7	0.0	0.8	8.7
DYRK1A	3.2	1.7	2.6	0.7	0.6	1.5	8.7
DYRK2	8.2	1.6	4.0	3.6	2.1	1.1	7.0
EPHA2	11.0	0.2	3.1	1.1	0.2	0.7	8.3
EPHA4	8.4	n.d.	n.d.	n.d.	n.d.	n.d.	6.2
EPHA5	n.d.	0.2	3.2	0.1	-0.3	0.5	7.9
EPHA7	6.3	1.7	1.4	-0.5	0.7	0.7	10.3
EPHB1	4.9	n.d.	n.d.	n.d.	n.d.	n.d.	6.4
EPHB3	n.d.	0.9	1.7	0.7	0.4	0.8	5.0
FES	5.1	1.2	2.5	1.6	0.5	1.5	6.2
FGFR1B	4.5	1.4	1.8	1.6	0.9	0.6	5.9
FGFR2	4.5	2.2	2.5	2.3	1.1	1.1	9.0
FGFR3	5.9	2.1	3.8	3.5	2.2	1.1	13.3
FLT1	9.8	4.8	5.0	3.7	2.6	2.2	13.6
GAK	10.6	2.0	6.3	3.6	1.0	2.2	9.0
GPRK5	8.0	-0.2	1.5	1.4	1.0	1.1	7.7
GSG2	5.2	0.9	4.4	2.9	1.9	1.4	7.2
GSK3B	2.9	8.4	7.2	4.9	4.9	6.8	11.8
HIPK2	14.0	n.d.	n.d.	n.d.	n.d.	n.d.	4.4
MAP2K1	n.d.	0.9	0.0	0.1	-0.4	0.4	1.3
MAP2K4	1.4	2.6	4.1	2.9	1.1	1.9	12.0
MAP2K6	10.0	0.7	2.3	1.3	0.5	1.1	12.3
MAP2K7	10.4	n.d.	n.d.	n.d.	n.d.	n.d.	8.4
MAP3K5	12.0	0.9	2.1	3.1	1.6	1.3	18.5
MAPK10	n.d.	2.6	3.0	1.9	-0.8	2.5	7.4
MAPK13	7.2	0.3	2.2	1.1	0.4	0.4	7.5
MAPK14	8.0	-0.1	0.0	-0.2	-0.3	-0.1	0.3
MAPK15	2.5	3.8	5.4	5.3	2.5	2.8	14.7
MAPK1	17.4	0.3	0.7	0.5	0.2	0.3	1.4
MAPK8B	8.5	n.d.	n.d.	n.d.	n.d.	n.d.	7.8
MAPK9	n.d.	1.5	2.3	1.0	0.3	1.1	3.7
MAPKAPK2	6.5	n.d.	n.d.	n.d.	n.d.	n.d.	3.2
MARK3	n.d.	4.2	4.9	5.4	2.4	0.9	19.0
MARK4	8.1	3.9	5.4	5.1	2.9	3.2	16.4
MELK	8.2	2.0	6.6	6.2	3.9	2.1	13.8
MERTK	9.8	3.2	2.5	1.8	1.0	1.2	6.6
MST3	4.4	3.2	3.7	4.3	0.9	4.9	7.3
MST4	9.3	1.1	2.3	3.0	0.6	2.7	6.1
NEK1	7.1	0.1	0.7	0.6	0.4	0.0	-0.6
NEK2	1.1	n.d.	n.d.	n.d.	n.d.	n.d.	3.3
NEK7	n.d.	n.d.	n.d.	n.d.	n.d.	n.d.	1.0
OSR1	n.d.	0.1	2.3	1.2	0.4	1.2	7.7
PAK1	5.6	0.9	0.7	0.4	0.0	0.7	6.6
PAK4	3.3	0.0	1.9	0.9	0.1	0.1	12.2
PCTK1	7.7	2.6	3.0	2.6	1.1	3.1	9.1
PDK4	1.2	0.8	1.2	1.1	0.8	1.5	0.2
PHKG2	8.8	1.5	2.1	1.8	0.1	0.1	21.2
PIM1	3.3	2.3	2.4	2.1	-0.3	3.4	12.5
PIM3	3.8	0.1	2.5	2.3	0.3	1.1	19.7
PKMYT1	1.0	0.7	1.6	0.5	0.3	1.1	0.2
PLK4	11.1	0.7	3.8	1.9	0.6	0.8	16.0
RIOK1	4.9	2.0	6.8	5.9	2.1	3.7	0.0
RIOK2	n.d.	0.7	3.9	3.2	0.4	1.3	1.5
RPS6KA1	5.1	0.3	1.7	2.2	0.9	0.1	3.9
RPS6KA5	n.d.	n.d.	n.d.	n.d.	n.d.	n.d.	13.7
RPS6KA6	0.4	-0.3	0.3	-0.4	0.1	0.1	-0.5
SLK	8.8	1.8	5.2	3.5	1.9	0.7	18.0
SPRK1	n.d.	0.8	0.8	0.6	0.0	0.9	6.9
SRC	4.4	0.1	2.9	1.2	0.4	0.6	5.9
STK10	10.1	0.2	2.6	1.1	-0.1	1.1	23.3
STK17A	9.6	1.4	4.9	2.9	1.0	1.4	11.8
STK17B	9.7	1.5	2.8	3.7	1.1	2.9	11.5
STK38L	8.7	1.3	2.4	1.6	0.5	0.8	12.6
STK39	7.6	1.2	4.1	3.7	1.7	2.7	9.6
STK3	11.6	1.8	7.2	8.4	4.0	5.8	16.6
STK4	9.6	3.3	5.0	6.5	1.9	4.8	14.9
STK6	14.3	1.3	6.3	2.7	0.7	1.3	17.1
TAF1	0.1	0.3	0.3	0.3	0.0	0.1	0.2
TIF1	n.d.	n.d.	n.d.	n.d.	n.d.	n.d.	0.8
TLK1	n.d.	n.d.	n.d.	n.d.	n.d.	n.d.	9.4
TTK	8.8	1.4	2.0	0.9	-0.1	1.3	11.2
ULK1	15.5	1.1	2.8	3.6	1.4	1.3	11.3
ULK3	8.3	2.9	5.9	5.1	1.7	3.3	19.6
VRK1	5.9	2.0	1.8	3.0	0.8	0.9	2.8
WNK1	1.1	1.2	0.7	0.4	0.5	0.7	0.9
No. kinases >5°C	59	3	15	10	1	3	75

3.6.2. *In-vitro* characterization and cell-based activity

In order to determine the binding affinity of **110a** against the target BMPR2, an isothermal titration calorimetry (ITC) measurement was performed (Figure 28A). Therefore, a small volume of a highly concentrated compound solution was titrated into a protein solution (sample cell). During this process, the absorbed or released heat during the binding of the molecule to the protein was detected and compared with a reference cell. The dissociation constant K_D, the reaction stoichiometry n, the enthalpy ΔH, the entropy ΔS, and the free binding energy ΔG could be determined.[192] The measurement of **110a** revealed a strong binding affinity for BMPR2 with a K_D value of 205 nM. The binding of **110a** to the protein was driven by favorable entropic changes (-TΔS) with unfavorable changes in the binding enthalpy (ΔH), indicating conformational changes during the binding (Figure 28A). Further profiling of this kinase was done, using an ADP-Glo^{TM} assay to elucidate the potency against BMPR2. The IC_{50} values of **23**, **110a**, **110b**, and **110c** were determined, whereby the lead structure **23** exhibited the most potent inhibition with a low IC_{50} value of 36.2 nM and a corresponding ΔTm shift of 9.2 °C. The IC_{50} values of the macrocycles **110a** – **110c** were ranging from 461 nM to 630 nM with corresponding ΔTm shifts of 4.6 °C – 5.3 °C. **110a** revealed a good potency for BMPR2 with an IC_{50} value of 506 nM (Figure 28B).

The activity of **23**, **110a**, and **110c** against GSK3A and GSK3B was determined, using the NanoBRET^{TM} technology. The lead structure **23** exhibited a high cellular potency for both kinases with 4.0 nM (ΔTm shift GSK3B 14.0 °C). The DSF assay indicated also a high stabilization of GSK3B with 8.4 °C for **110a**. However, the NanoBRET^{TM} assay revealed a low cellular activity with 10.9 µM and 33.6 µM for GSK3A and GSK3B, respectively. The lysed mode of GSK3B was additionally measured to determine the *in vitro* activity against the kinase and to ascertain potential cell penetration problems. **110a** exhibited an IC_{50} value of 2.3 µM for GSK3B in the lysed mode, indicating cell penetration problems. **110c** seemed to be inactive in intact cells with IC_{50} values above 45 µM for both kinases and showed a potency in the low micromolar range in the lysed mode with an IC_{50} value of 3.5 µM for GSK3B (Figure 28B).

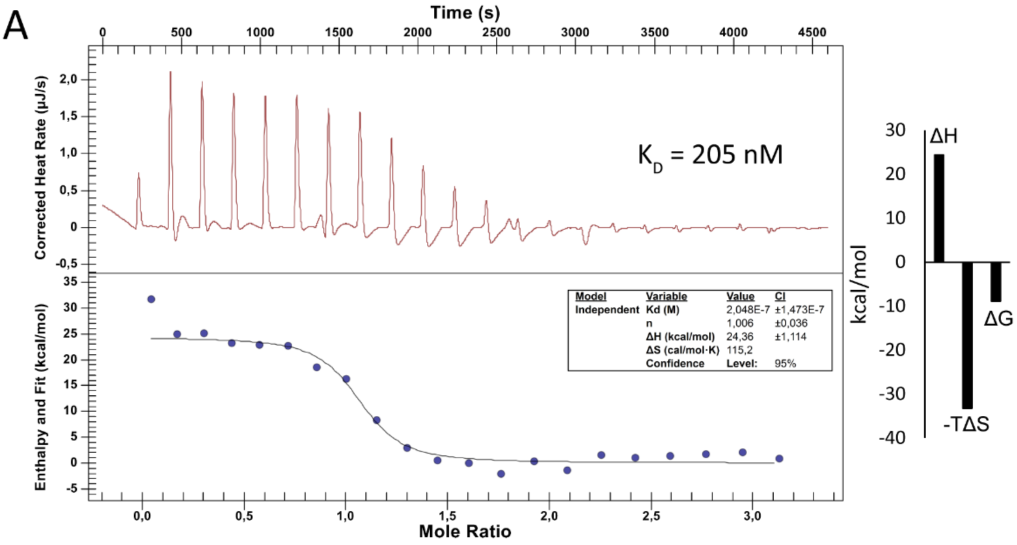

B

Compound	DSF Shift [°C]		ADP Glo^{TM} IC$_{50}$ [nM]	NanoBRET IC$_{50}$ [nM]		
	BMPR2	GSK3B	BMPR2	GSK3A	GSK3B (intact)	GSK3B (lysed)
1	9.20 ± 0.06	14.0 ± 0.14	36.2 ± 1.07	4.00 ± 1.00	4.00 ± 0.00	1.00 ± 0.04
110a	5.30 ± 0.03	8.40 ± 0.21	506 ± 70.4	10957 ± 2338	33640 ± 1245	2267 ± 235
110b	5.00 ± 0.02	7.20 ± 0.06	461 ± 17.8	-	-	-
110c	4.60 ± 0.05	4.90 ± 0.39	630 ± 162	> 45000	> 45000	3546 ± 1305

Figure 28. A. Isothermal titration calorimetry (ITC) measurement of **110a** against BMPR2 revealed a low three-digit nanomolar binding affinity. **B.** IC$_{50}$ values of **23**, **110a**, **110b**, and **110c** against BMPR2. The values were determined by an ADP-Glo^{TM} assay in a duplicate measurement. IC$_{50}$ values against GSK3A and GSK3B were determined using the NanoBRET^{TM} assay platform in a duplicate measurement. The corresponding DSF assay data is shown for each compound.

3.6.3. Kinome wide selectivity

Based on the great selectivity profile in the *in-house* DSF panel (Figure 29A) and the good binding affinity and potency against BMPR2 in a nanomolar range, **110a** was chosen for a further kinome-wide selectivity screen, using the KINOMEscan® assay platform provided by Eurofins Scientific (Figure 29B – D). Therefore, **110a** was screened against 468 human protein kinases and their mutants at a screening concentration of 1 µM. Also in this extended panel, **110a** showed an excellent selectivity profile with a selectivity score (S_{35}) of 0.01. BMPR2 was potently targeted together with the mutant kinase FLT D835V. GSK3A, JNK1, and RIOK2 were only weakly affected from **110a**.

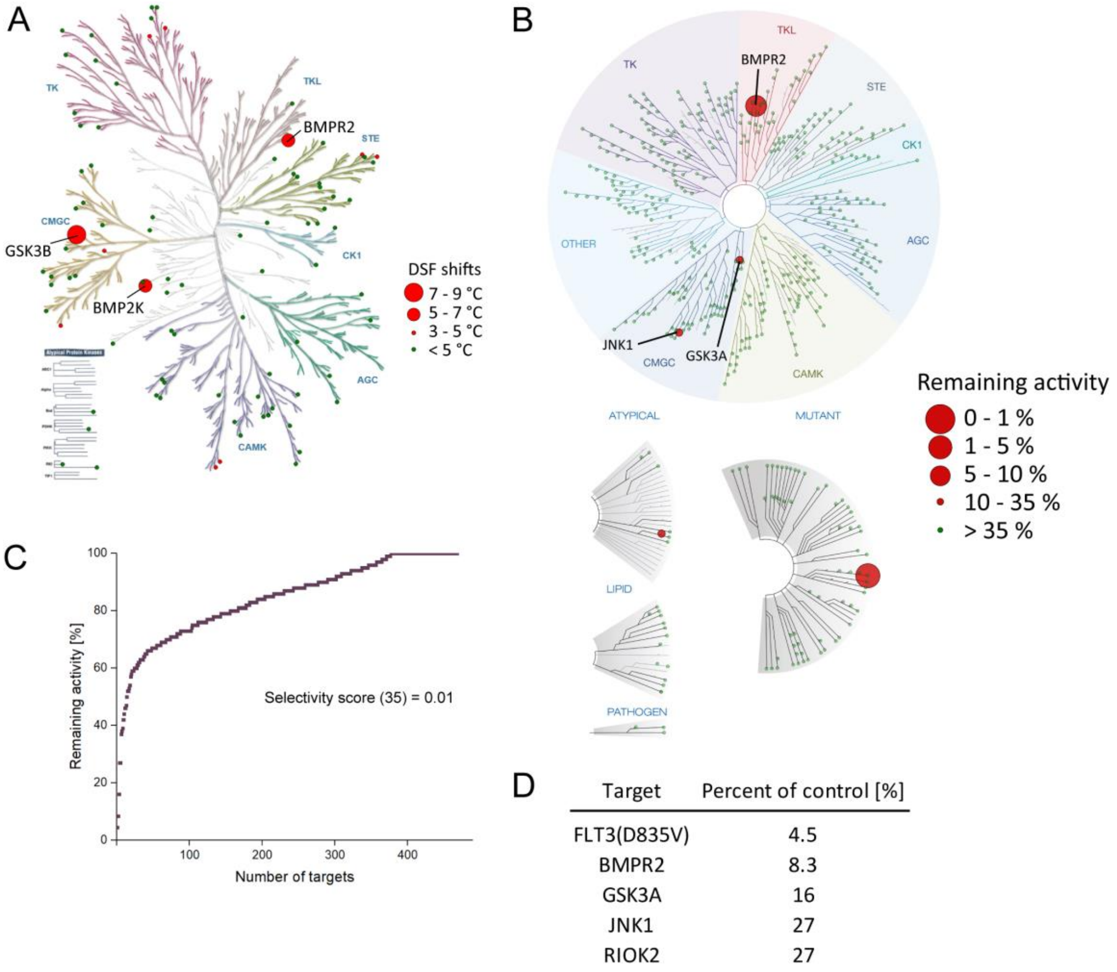

Target	Percent of control [%]
FLT3(D835V)	4.5
BMPR2	8.3
GSK3A	16
JNK1	27
RIOK2	27

Figure 29. A. Graphical representation of the selectivity data of **110a** assessed by DSF. A phylogenetic tree (Cell Signaling Technology) was used to highlight ΔTm data that was depicted as red circles as indicated in the figure capture. **B.** Selectivity profile of **110a** assessed by the KinomeScan® panel at a screening concentration of 1 µM. Mutants and atypical kinases are depicted in the lower panel. **C.** Waterfall plot of the selectivity data of **110a**. The remaining activity (%) was plotted against the number of tested kinases. The selectivity score of **110a** was determined with a cut off value of 35% remaining activity. **D.** Table showing the top hits of the KINOMEscan® profiling of **110a** with a remaining activity < 35% at 1 µM.

3.6.4. Binding mode

To gain insight into the binding mode of **110a**, the inhibitor was docked into the active conformation of BMPR2. The crystal structure of BMPR2 in complex with ATP (PDB: 3G2F) was used for this approach. The 3-aminopyrazole moiety of the macrocycle formed three hydrogen bonds with the kinase however, showed no canonical interactions with the hinge region. The pyrazole interacted with the side chain oxygen and the backbone nitrogen of the residue S286 at the transition of the hinge region to the C-lobe and the amine between the pyrazole and the pyrimidine moiety interacted with the backbone oxygen of the residue I209 of the β1 sheet. Furthermore, four hydrophobic interactions were formed. The pyrimidine interacted with the I209 side chain of the β1 sheet and the aromatic ring of the linker formed three interactions with the side chains of V217 of the β2 sheet, K230 of the β3 sheet, and V340 of the β7 sheet. The docking result emphasized the ITC data of an entropic-driven binding. The *para*-substituted phenyl ring in the linker led to a constrained and less flexible macrocycle, resulting in a twisted aromatic ring orientation. The lead structure showed a similar orientation in the binding pocket. The pyrazole formed a hydrogen bond with S286 at the transition of the hinge region to the C-lobe. The nitril interacted with the side chain nitrogen of K230, backbone nitrogen of G215, and backbone nitrogen of G212. The C5 carbon of the pyrimidine moiety interacted with I209 of the β1 sheet through a hydrophobic interaction and further interactions were formed between the linker moiety and V217, K230, D351, and V340 (Figure 30).

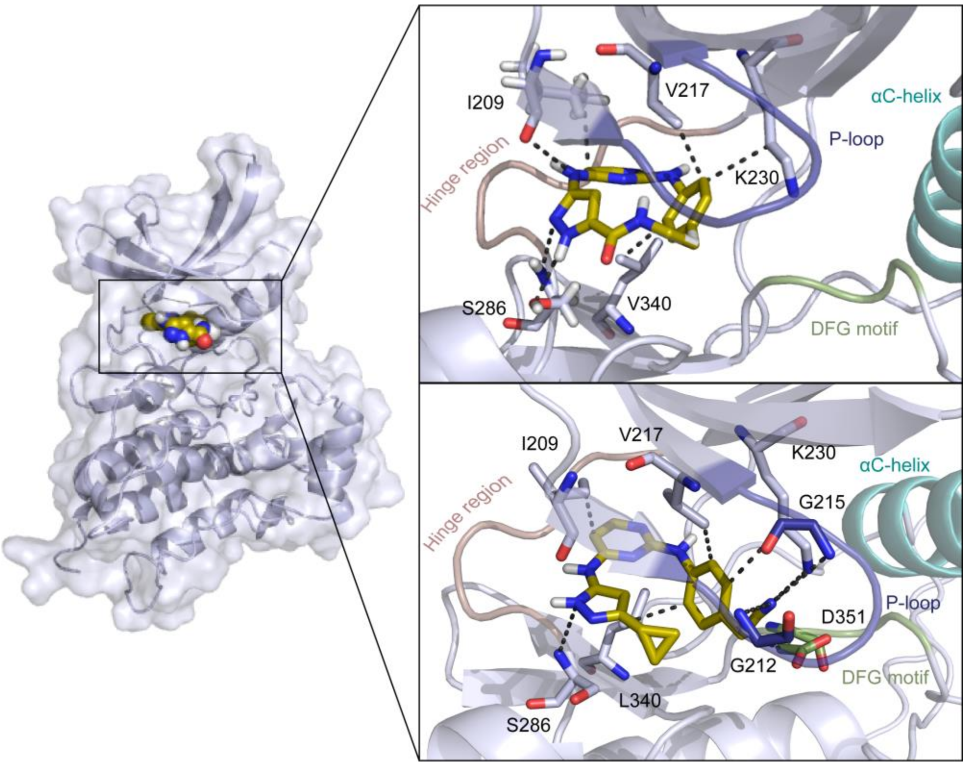

Figure 30. Binding mode of **110a** and **23** in complex with the kinase domain of the type II receptor BMPR2. The molecules were docked into the active conformation of BMPR2. The compounds are illustrated in gold, the hinge region of the kinase is shown in pale red, the P-loop in dark blue, the αC-helix in cyan, and the DFG-motif in green. The interactions were predicted, using PLIP.[193]

3.7. Optimization of pyrazole-based macrocycles lead to a highly selective MST3 inhibitor

3.7.1. *In-house* selectivity profile

Further optimization of the pyrazole-based macrocyclic kinase inhibitors **110a**–**e** led to the introduction of residues at the pyrimidine core. To gain first insights into the selectivity profile of the newly synthesized macrocycles, a DSF assay was performed, using an *in-house* panel of 104 kinases (Table 10). First, an additional chlorine residue was introduced at position C5 of the pyrimidine (**111a**–**e**). **111a** with a *para*-substituted aromatic ring in the linker showed no stabilization with a ΔTm shift higher than 5 °C. The exchange of the attachment point of the aromatic moiety (**111b**) caused a stabilization of four kinases. The introduction of an aliphatic C5 linker (**111c**) led to a more unselective macrocycle by stabilizing 15 kinases with a DSF shift > 5 °C. The variation from a pentyl to an ethoxyethyl linker (**111d**) led to a nearly inactive compound. Only RIOK1 was stabilized with a not notable ΔTm shift of 5.3 °C. The introduction of a hexyl linker (**111e**) caused a stabilization of three kinases with shifts in a range of 5.4 °C – 6.0 °C however, all of them are negligible in comparison to the reference. All of these macrocycles (**111a**–**e**) exhibited only a minor stabilization on MST3 and MST4 with ΔTm shifts of 0.3 °C – 2.9 °C and 0.6 °C – 2.8 °C, respectively.

The replacement of the chlorine residue through a methyl group (**112a**) caused also an inactive compound. No kinases were stabilized by **112a** and also MST3 and MST4 were not affected with ΔTm shifts of 0.5 °C and 2.3 °C, respectively.

For the macrocycles **113a**–**e**, the pyrimidine was replaced through a quinazoline moiety. This led to an inactive macrocycle **113a**. It stabilized PIM3 with a ΔTm shift of 6.1 °C however, this shift was negligible in comparison to staurosporine (19.7 °C). **113b** targeted four kinases with a DSF shift higher than 5 °C. All of these shifts were comparably low in relation to staurosporine. Both macrocycles exhibited only a minor DSF shift on MST3 and MST4 in a range of 3.3 °C – 4.7 °C. **113c** caused a high stabilization of MST3 and MST4 with ΔTm shifts of 7.5 °C and 7.4 °C, respectively. Both values are in the same range or even higher than the reference staurosporine with 7.3 °C and 6.1 °C and reported K_D values of 120 nM and 140 nM, respectively.[40] The related subfamily members MST1 (STK4) and MST2 (STK3) were not affected from **113c** with shifts of 1.1 °C and 1.4 °C. Overall, **113c** stabilized seven kinases with a DSF shift higher than 5 °C. STK6, CLK1, GSK3B, RIOK1, and MELK exhibited shifts between 5.1 °C – 6.5 °C however, they were comparably low in relation to the reference (Figure 31). Astonishingly, the replacement of the pentyl linker with an ethoxyethyl (**113d**) or hexyl (**113e**) linker was not tolerated by MST3 and MST4. Both macrocycles showed low DSF shifts for these kinases in a range of 2.5 °C – 3.7 °C and 2.5 °C – 4.0 °C, respectively. **113d** was completely inactive and **113e** stabilized only GSK3B with a comparably low DSF shift of 5.5 °C.

Table 10. DSF data of the pyrazole-based macrocyclic kinase inhibitors **111a**–**e**, **112a**, and **113a**–**e**. **23** and staurosporine were used as a positive control. The newly synthesized compounds were screened in an *in-house* panel of 104 kinases. No stabilization of the kinase is indicated in pale green, while a high stabilization is indicated in dark green.

Kinase	ΔTm [°C]												
	23	**111a**	**111b**	**111c**	**111d**	**111e**	**112a**	**113a**	**113b**	**113c**	**113d**	**113e**	Staurosporine
AAK1	13.8	1.5	4.8	4.5	3.2	3.8	1.1	4.1	3.4	4.0	2.3	2.2	15.6
ABL1	8.7	0.5	2.2	2.7	0.6	0.7	0.4	1.5	4.0	4.0	1.6	1.3	10.3
AKT3	1.4	-0.1	-0.1	-0.1	0.5	0.2	0.4	0.5	0.0	0.2	0.1	0.2	6.6
AURKB	n.d.	-1.3	0.7	1.7	-1.1	-2.3	-1.6	-1.7	-0.5	-1.4	-2.7	-0.9	8.3
BMP2K	18.8	4.4	11.1	8.8	4.6	5.0	1.0	3.6	4.9	4.4	2.4	1.5	19.1
BMPR2	9.2	4.8	4.3	2.5	1.2	1.6	2.4	1.5	1.1	1.7	0.9	0.8	2.6
BMX	4.4	0.2	1.0	1.0	0.1	0.3	-0.2	0.5	1.3	1.8	0.6	0.6	7.1
BRAF	4.6	1.3	1.3	4.6	1.9	1.2	0.2	0.0	0.7	0.8	0.7	0.2	0.8
BRD4	1.3	1.1	2.0	3.3	1.6	1.0	1.9	3.2	3.9	3.3	3.1	1.9	1.1
BRPF1B	n.d.	-0.2	-0.6	0.4	-1.2	-1.0	-0.3	1.0	-0.7	-0.8	0.6	0.1	-0.1
CAMK1D	5.4	-0.8	1.0	-0.4	1.5	2.7	0.7	1.4	1.8	1.8	1.3	1.8	10.0
CAMK1G	5.5	-0.2	0.8	0.5	0.5	0.4	0.4	0.9	2.2	2.2	-0.2	0.5	10.9
CAMK2B	4.4	1.0	0.1	1.5	0.6	0.7	0.1	1.4	1.0	1.2	0.7	0.6	13.3
CAMK2D	4.5	1.0	0.1	1.3	1.0	1.4	0.9	1.6	0.7	1.2	0.9	0.6	16.2
CAMK4	5.4	0.2	1.0	1.1	0.6	0.6	0.4	0.7	1.3	1.2	0.7	0.6	8.6
CAMKK2B	12.0	2.6	6.0	4.4	1.1	2.7	1.3	2.9	5.9	3.5	2.0	3.2	24.6
CASK	2.0	0.2	0.0	0.8	0.6	0.7	0.4	0.6	0.5	0.5	0.3	0.4	4.8
CDC42BPA	-0.1	0.2	-0.2	-0.6	0.6	0.7	0.2	0.0	-0.2	-0.4	0.0	0.0	2.8
CDK2	15.2	2.0	3.7	4.3	1.7	1.9	1.1	2.0	2.7	2.2	0.9	2.4	15.5
CDKL1	10.3	-0.1	0.2	0.0	0.3	0.3	0.2	0.7	-0.1	0.8	0.7	0.6	3.1
CHEK2	6.8	2.0	3.6	6.5	1.5	1.4	0.8	0.9	0.9	1.4	1.6	1.0	17.1
CLK1	8.6	2.8	4.8	6.6	4.0	3.3	1.3	2.0	3.7	5.1	3.1	2.0	11.9
CLK3	12.2	0.7	2.1	3.8	1.0	0.4	1.0	1.3	2.2	3.1	1.6	1.0	5.6
CSNK1D	11.3	1.6	1.0	3.6	1.9	1.8	0.2	2.8	2.7	3.3	1.8	2.6	1.8
CSNK2A1	3.1	0.9	3.9	3.2	2.3	1.2	0.3	1.0	1.0	1.5	1.2	0.2	2.1
CK2A2	n.d.	2.1	6.5	4.6	3.0	3.0	0.6	3.3	3.6	4.2	3.0	3.5	5.6
DAPK1	8.5	0.1	0.3	0.6	0.6	0.6	0.3	0.9	0.6	0.6	-0.2	0.5	9.8
DAPK3	4.9	0.4	1.9	2.9	2.0	1.3	0.9	2.3	1.8	2.9	2.3	1.2	15.8
DCAMKL1	9.7	0.5	0.7	2.9	1.0	0.9	0.5	0.8	0.7	1.2	0.6	0.3	12.4
DMPK1	8.9	1.0	2.6	2.3	0.8	0.6	-0.1	0.4	3.2	2.7	1.2	1.3	8.7
DYRK1A	3.2	1.3	0.2	3.3	1.1	1.4	1.0	4.2	-1.8	1.2	0.6	-1.6	8.7
DYRK2	8.2	2.5	3.2	4.8	3.1	3.0	0.2	0.4	2.0	1.5	0.9	0.5	7.0
EPHA2	11.0	0.2	1.1	1.2	0.2	0.3	0.1	0.5	1.6	1.7	0.7	0.2	8.3
EPHA4	8.4	0.2	0.7	0.4	0.7	0.6	0.7	-1.8	1.5	1.8	1.3	1.2	6.2
EPHA5	n.d.	0.2	1.1	0.4	-0.1	-0.5	-0.1	0.8	0.8	1.5	0.8	0.5	7.9
EPHA7	6.3	0.5	1.7	2.3	-0.2	0.2	0.1	0.8	1.0	0.9	0.2	0.1	10.3
EPHB1	4.9	-0.5	-0.2	0.4	0.8	0.7	1.2	1.1	1.8	2.1	0.8	1.0	6.4
EPHB3	n.d.	-0.5	0.2	0.2	0.1	-0.7	-0.1	-0.3	0.8	0.7	0.2	0.2	5.0
FES	5.1	0.9	2.5	2.5	1.6	1.3	1.1	1.1	1.0	0.9	0.7	0.5	6.2
FGFR1B	4.5	0.6	1.4	2.8	2.2	1.4	0.8	2.2	2.9	1.8	1.6	0.6	5.9
FGFR2	4.5	0.8	2.0	3.9	2.2	1.3	0.4	3.0	3.8	1.5	1.6	0.9	9.0
FGFR3	5.9	1.9	3.4	5.7	3.2	1.8	0.8	3.6	5.1	2.6	3.2	0.9	13.3
FLT1	9.8	2.3	2.5	3.6	1.8	1.7	1.9	3.5	5.7	2.8	4.2	1.8	13.6
GAK	10.6	0.2	3.9	3.5	1.3	2.5	0.8	1.2	2.7	2.4	1.2	1.0	9.0
GPRK5	8.0	0.9	1.1	2.0	0.4	0.4	0.3	0.4	2.4	2.4	1.3	1.0	7.7
GSG2	5.2	0.8	2.0	4.3	2.7	1.6	0.5	1.5	1.6	1.1	0.8	0.4	7.2
GSK3B	2.9	2.3	4.7	5.4	2.4	3.6	0.7	4.9	4.8	5.5	4.8	5.5	11.8
HIPK2	14.0	0.2	1.7	1.6	0.7	1.1	0.6	0.4	1.6	1.2	0.8	0.7	4.4
MAP2K1	n.d.	0.2	0.2	0.1	n.d.	n.d.	n.d.	n.d.	n.d.	n.d.	n.d.	n.d.	1.3
MAP2K4	1.4	3.5	3.1	3.4	1.0	1.9	0.7	0.6	0.7	0.7	1.0	1.0	12.0
MAP2K6	10.0	0.7	1.9	2.1	0.5	0.7	0.2	0.2	0.2	0.1	0.2	0.0	12.3
MAP2K7	10.4	1.1	0.4	0.4	1.1	1.0	0.9	0.3	0.1	0.3	0.5	0.2	8.4
MAP3K5	12.0	1.5	2.1	6.5	3.1	3.4	0.4	0.0	0.5	0.5	0.4	0.4	18.5
MAPK10	n.d.	1.2	0.9	1.9	1.9	3.7	1.8	2.1	2.7	2.3	1.7	0.6	7.4
MAPK13	7.2	0.7	1.0	2.0	0.4	0.7	0.2	-0.4	-0.2	-0.1	-0.1	0.0	7.5
MAPK14	8.0	0.2	0.6	0.3	0.5	0.4	1.3	0.9	0.0	0.7	1.1	0.7	0.3
MAPK15	2.5	2.3	2.8	6.2	2.6	3.5	0.2	0.6	0.6	0.9	0.4	1.0	14.7
MAPK1	17.4	0.9	0.3	1.5	0.5	0.5	0.2	0.4	0.5	0.1	0.1	-0.1	1.4
MAPK8B	8.5	3.3	4.7	5.8	2.2	4.1	2.2	3.7	3.0	3.1	2.2	1.5	7.8
MAPK9	n.d.	2.1	1.7	3.9	2.4	3.6	1.8	2.3	1.9	1.9	0.8	1.6	3.7
MAPKAPK2	6.5	0.0	-0.3	-0.2	0.2	-0.1	0.5	0.3	0.1	0.3	0.2	0.1	3.2
MARK3	n.d.	1.4	1.7	4.4	1.0	1.1	-0.4	1.0	2.2	1.0	0.6	0.5	19.0
MARK4	8.1	1.5	3.0	0.6	1.7	1.5	0.4	2.7	3.7	1.7	0.7	1.2	16.4
MELK	8.2	1.7	2.9	7.2	3.2	3.2	0.5	1.1	4.1	6.5	4.0	2.4	13.8
MERTK	9.8	3.7	2.8	3.5	2.0	2.0	2.0	2.4	1.7	2.0	1.5	0.7	6.6
MST3	4.4	1.2	2.9	2.7	0.6	0.3	0.5	3.3	3.9	7.5	2.5	3.7	7.3
MST4	9.3	0.7	0.6	1.6	2.8	2.1	2.3	4.7	4.0	7.4	2.5	4.0	6.1
NEK1	7.1	0.3	0.7	1.1	0.6	0.4	0.2	-0.2	0.4	0.5	0.1	0.0	-0.6
NEK2	1.1	1.4	2.2	4.9	1.0	0.5	1.5	1.1	-0.1	0.8	0.9	0.6	3.3
NEK7	n.d.	0.4	0.9	1.2	0.2	0.0	2.2	1.9	1.8	2.3	2.1	0.7	1.0
OSR1	n.d.	0.6	0.9	2.0	1.8	1.6	0.2	2.0	2.9	3.1	2.5	1.6	7.7
PAK1	5.6	-0.1	0.0	0.0	-0.3	-0.4	0.5	1.4	0.3	0.6	0.4	0.3	6.6
PAK4	3.3	1.6	4.0	2.1	0.5	0.4	0.8	2.4	0.8	0.6	0.5	0.9	12.2
PCTK1	7.7	1.2	1.2	2.8	1.0	1.4	0.4	1.2	1.2	1.4	0.6	1.6	9.1
PDK4	1.2	-0.1	-0.2	-0.2	-0.2	-0.2	-0.1	0.0	0.1	-0.1	-0.1	0.0	0.2
PHKG2	8.8	3.7	2.7	4.8	2.0	3.0	1.3	1.4	1.0	1.7	0.5	0.7	21.2
PIM1	3.3	3.7	1.9	5.1	1.7	2.7	1.2	3.9	2.1	2.6	1.8	1.8	12.5
PIM3	3.8	1.8	1.7	5.1	2.2	3.5	1.5	6.1	4.0	5.0	4.4	3.4	19.7
PKMYT1	1.0	0.2	-0.2	0.2	0.8	0.6	1.5	1.2	-0.1	0.8	0.8	0.7	0.2
PLK4	11.1	1.3	3.4	4.0	2.4	3.3	1.0	2.7	3.1	4.4	2.7	2.7	16.0
RIOK1	4.9	2.0	2.0	10.7	5.3	6.0	2.8	1.8	5.3	5.9	3.5	1.6	0.0
RIOK2	n.d.	0.4	1.5	4.5	1.1	2.5	0.0	-0.3	-0.1	0.3	0.0	-0.1	1.5
RPS6KA1	5.1	0.2	0.5	2.8	0.5	0.6	0.2	0.8	0.3	1.1	0.1	0.1	3.9
RPS6KA5	n.d.	n.d.	n.d.	n.d.	4.4	5.4	2.6	1.4	1.5	3.0	1.5	2.4	13.7
RPS6KA6	0.4	-0.8	1.4	5.6	1.3	0.7	0.5	0.6	0.6	0.5	0.5	0.8	-0.5
SLK	8.8	-0.1	1.7	1.8	n.d.	n.d.	n.d.	n.d.	n.d.	n.d.	n.d.	n.d.	18.0
SPRK1	n.d.	0.0	0.1	1.0	0.3	0.4	0.3	1.2	1.6	1.8	0.6	0.6	6.9
SRC	4.4	0.2	0.9	0.2	0.2	0.4	-0.7	0.4	1.9	1.5	0.7	0.4	5.9
STK10	10.1	1.1	2.0	1.3	0.8	0.3	-0.2	1.3	3.2	1.0	0.7	0.3	23.3
STK17A	9.6	-0.4	0.3	3.8	1.6	2.4	1.5	2.6	3.6	2.9	0.8	1.3	11.8
STK17B	9.7	-1.0	-0.9	0.4	1.3	0.6	0.3	0.3	1.2	1.1	0.7	0.3	11.5
STK38L	8.7	1.1	1.9	4.1	1.3	1.6	0.5	1.7	2.4	2.1	0.6	2.2	12.6
STK39	7.6	0.6	1.4	3.1	-0.9	0.4	0.1	0.4	2.2	3.5	0.9	1.5	9.6
STK3	11.6	0.7	1.7	2.8	0.6	1.0	0.2	2.3	1.3	1.1	0.5	0.4	16.6
STK4	9.6	-0.3	0.8	2.5	1.1	1.5	1.0	1.0	1.7	1.4	0.6	0.7	14.9
STK6	14.3	4.2	8.1	7.0	3.4	5.5	1.7	4.3	4.4	5.1	3.8	2.7	17.1
TAF1	0.1	-1.8	0.1	-0.3	0.3	-0.1	-0.3	-0.2	-0.4	-0.2	-0.3	0.2	0.2
TIF1	n.d.	0.3	0.6	0.2	0.7	0.6	-0.2	1.3	0.5	0.5	0.4	1.1	0.8
TLK1	n.d.	0.5	0.3	1.7	2.2	1.8	1.8	2.2	2.3	3.7	2.0	1.4	9.4
TTK	8.8	3.3	1.8	4.4	0.7	2.1	1.2	3.9	2.5	1.4	1.2	1.7	11.2
ULK1	15.5	0.9	1.5	4.5	1.9	0.3	0.6	0.6	1.2	1.2	0.8	0.5	11.3
ULK3	8.3	1.3	3.9	6.3	2.7	2.3	0.3	2.6	3.2	3.4	2.1	1.6	19.6
VRK1	5.9	0.1	0.1	0.3	0.4	0.4	0.8	1.3	0.4	0.7	0.3	0.4	2.8
WNK1	1.1	0.3	0.7	0.9	0.3	0.3	0.5	0.7	0.6	0.4	0.4	0.2	0.9
No. kinases >5°C	59	0	4	15	1	3	0	1	4	7	0	1	75

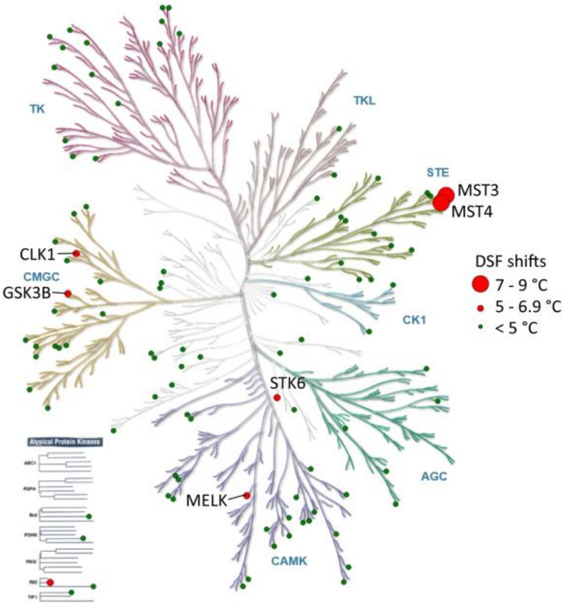

Figure 31. Graphical representation of the selectivity data of **113c** assessed by DSF. A phylogenetic tree (Cell Signaling Technology) was used to highlight ΔTm data that was depicted as red circles as indicated in the figure capture.

3.7.2. *In-vitro* characterization and cell-based activity

Representatively for the high stabilization of MST3 and MST4 in the DSF assay (7.5 °C and 7.4 °C), an ITC measurement of **113c** against MST4 was performed. **113c** revealed a strong binding affinity with a low K_D value of 116 nM for MST4 (Figure 32). Thereby, the binding of the molecule to the protein was driven by a favorable change in the binding enthalpy (ΔH), which was attenuated by the entropy (-TΔS). Due to the high stabilization of MST3 and MST4 in the DSF assay and the good *in vitro* potency of **113c** in the ITC measurement, the cellular potency of the whole macrocycles was measured against the MST family.

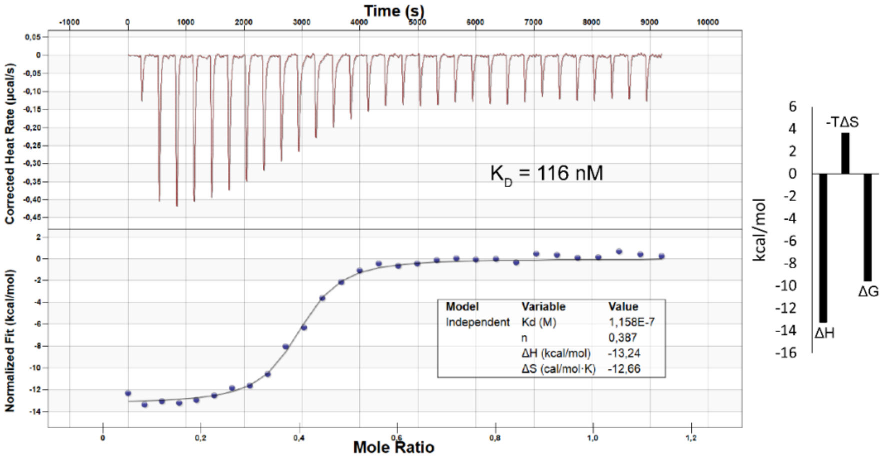

Figure 32. ITC measurement of **113c** against MST4 revealed a low three-digit nanomolar binding affinity.

The cellular potency of the newly synthesized macrocyclic kinase inhibitors was determined, using the NanoBRET^{TM} cellular target engagement assay. Furthermore, the lysed mode of MST3 and MST4 was measured, whereby the cell membrane was lysed to determine the potency regardless of possible cell penetration problems. The lead structure **23** showed a high stabilization in the DSF assay on all MSTs with shifts in a range from 4.4 °C to 11.6 °C. Astonishingly, **23** exhibited a preferred inhibition of MST1 and MST2 with IC_{50} values of 200 nM and 110 nM, respectively. MST3 and MST4 were only targeted in a micromolar range however, the lysed mode revealed IC_{50} values of 280 nM and 230 nM. The macrocycles **111a** – **111e**, harboring a chlorine residue at position C5 of the pyrimidine, as well as **112a** with a methyl residue showed no inhibition of MST1 – MST4. They showed either a weak potency for the measured kinases in a micromolar range or they were even completely inactive with IC_{50} values higher than 50 µM. These results correlated well with the DSF assay data, whereby **111a** – **111e** and **112a** caused only a minor stabilization of the corresponding kinase with shifts in a range from zero to 2.9 °C. The exchange from the pyrimidine to the quinazoline moiety led to better potency for MST3 and MST4, while MST1 and MST2 were still unaffected. The macrocycles harboring an aromatic linker moiety (**113a** and **113b**) exhibited IC_{50} values in a micromolar range for MST3 and MST4 (4.5 µM – 17.5 µM) however, were slightly better for the lysed mode with IC_{50} values of 0.9 µM – 2.8 µM. The aliphatic pentyl linker (**113c**) caused an inhibition of MST3 and MST4. **113c** exhibited a great cellular potency for MST3 with an IC_{50} value of 210 nM and a weaker activity for MST4 with 1.8 µM. In the lysed mode, both kinases were targeted in a nanomolar range with IC_{50} values of 30 nM and 510 nM, respectively. **113c** caused a selectivity within the subfamily, whereby MST1 and MST2 were not inhibited with IC_{50} values higher than 50 µM. The exchange from the pentyl linker to an ethoxyethyl linker (**113d**) caused a dramatic weakening of the potency for MST3 and MST4. Both kinases were only targeted in a micromolar range for the intact and lysed mode. Also, the extension by one carbon (**113e**) led to an unfavorable modification and caused a weakening of the potency. **113e** exhibited cellular IC_{50} values of 1.8 µM and 2.4 µM and values of 450 nM and 1.3 µM for MST3 and MST4 in the lysed mode, respectively.

Table 11. DSF data and the corresponding NanoBRET^{TM} data for the macrocyclic kinase inhibitors **111a**–**e**, **112a**, and **113a**–**e**. Lead structure **23** was used as a reference. IC$_{50}$ values were determined using the NanoBRET^{TM} assay in a 11-point dose−response curve in duplicates.

		DSF-Shifts [°C]				NanoBRET IC$_{50}$ [μM]					
Compound	Structure	MST1	MST2	MST3	MST4	MST1	MST2	MST3		MST4	
						intact	intact	intact	lysed	intact	lysed
23	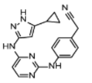	9.6 ± 0.6	11.6 ± 0.0	9.3 ± 0.3	7.1 ± 0.2	0.20 ± 0.15	0.11 ± 0.08	6.54 ± 1.08	0.28 ± 0.11	4.84 ± 0.44	0.23 ± 0.01
111a	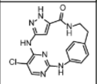	-0.3 ± 0.7	0.7 ± 0.1	1.2 ± 0.1	0.7 ± 0.0	11.82 ± 0.91	9.96 ± 1.23	4.97 ± 0.89	5.17 ± 0.01	6.71 ± 0.04	7.61 ± 0.22
111b	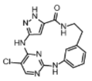	0.8 ± 0.4	1.7 ± 0.0	2.9 ± 0.0	0.6 ± 0.0	7.84 ± 0.09	7.54 ± 0.17	14.14 ± 3.24	8.53 ± 0.17	10.18 ± 1.13	10.27 ± 1.62
111c	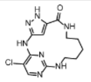	2.5 ± 0.2	2.8 ± 0.2	2.7 ± 0.1	1.6 ± 0.2	9.74 ± 0.39	10.12 ± 0.77	40.33 ± 13.68	2.67 ± 0.08	> 50.00	7.76 ± 0.32
111d	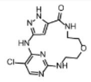	1.1 ± 0.7	0.6 ± 0.0	0.6 ± 0.2	2.8 ± 0.6	> 50.00	> 50.00	> 50.00	17.66 ± 1.17	> 50.00	41.76 ± 0.25
111e	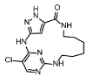	1.5 ± 0.6	1.0 ± 0.1	0.3 ± 0.3	2.1 ± 0.5	> 50.00	> 50.00	> 50.00	21.87 ± 2.33	> 50.00	45.02 ± 4.90
112a	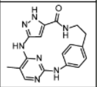	1.0 ± 0.0	0.2 ± 0.1	0.5 ± 0.6	2.3 ± 0.6	> 50.00	> 50.00	36.97 ± 15.55	38.33 ± 9.87	38.81 ± 12.13	> 50.00
113a	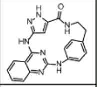	1.0 ± 0.4	2.3 ± 0.1	3.3 ± 0.7	4.7 ± 0.5	28.63 ± 4.14	28.32 ± 3.83	4.45 ± 1.16	1.46 ± 0.01	17.47 ± 5.94	2.75 ± 0.22
113b	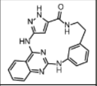	1.7 ± 0.1	1.3 ± 0.2	3.9 ± 0.4	4.0 ± 0.9	13.68 ± 1.04	13.01 ± 0.20	6.51 ± 0.04	0.92 ± 0.06	11.83 ± 3.68	2.44 ± 0.02
113c	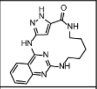	1.4 ± 0.0	1.1 ± 0.2	7.5 ± 0.6	7.4 ± 1.0	> 50.00	> 50.00	0.21 ± 0.01	0.03 ± 0.01	1.82 ± 0.49	0.51 ± 0.38
113d	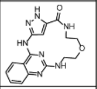	0.6 ± 0.2	0.5 ± 0.2	2.5 ± 0.4	2.5 ± 0.4	> 50.00	> 50.00	4.49 ± 0.81	1.23 ± 0.13	37.53 ± 17.64	4.30 ± 0.07
113e	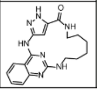	0.7 ± 0.0	0.4 ± 0.0	3.7 ± 0.6	4.0 ± 0.3	> 50.00	40.08 ± 0.68	1.75 ± 0.10	0.45 ± 0.04	2.40 ± 1.22	1.26 ± 0.12

3.7.3. Crystal structure

The crystal structure of **113c** bound to MST3 provided insights into the binding mode of the 3-aminopyrazole-based macrocycles (Figure 33A – B) and revealed a canonical ATP competitive type I binding mode for **113c**. The 3-aminopyrazole moiety formed three hydrogen bonds with the hinge region of the kinase. Thereby, the pyrazole interacted with the backbone oxygen of the residue E112 and the backbone nitrogen of L114. The amine between the pyrazole and the quinazoline moiety formed an additional hydrogen bond with the backbone oxygen of the residue L114. Further networks of polar interactions were formed between the macrocycle and the C-lobe of the kinase. The quinazoline and the following amine formed two water-mediated hydrogen bonds to the side chain oxygens of the residue D121. The nitrogen of the amide moiety interacted with a side chain oxygen of the residue D174 of the DFG-motif and another water-mediated network was formed by the oxygen of the amide moiety with the backbone nitrogen of D174 (Figure 33A). The high amount of polar interactions between the kinase inhibitor and the protein is in good concordance with the ITC results, indicating an enthalpic driven binding. A rotated presentation of the hinge region is shown beside. It could be seen that the P-loop was tilted towards the C-lobe. A superimposition of **113c** (pale blue) with AMP-PNP (pale orange) in complex with MST3 is shown in Figure 33B to elucidate the substantial tilting of the N-lobe. F47 of the P-loop was shifted by 6.2Å and packed against the activation loop, thus led to an associated stabilization of the activation loop.

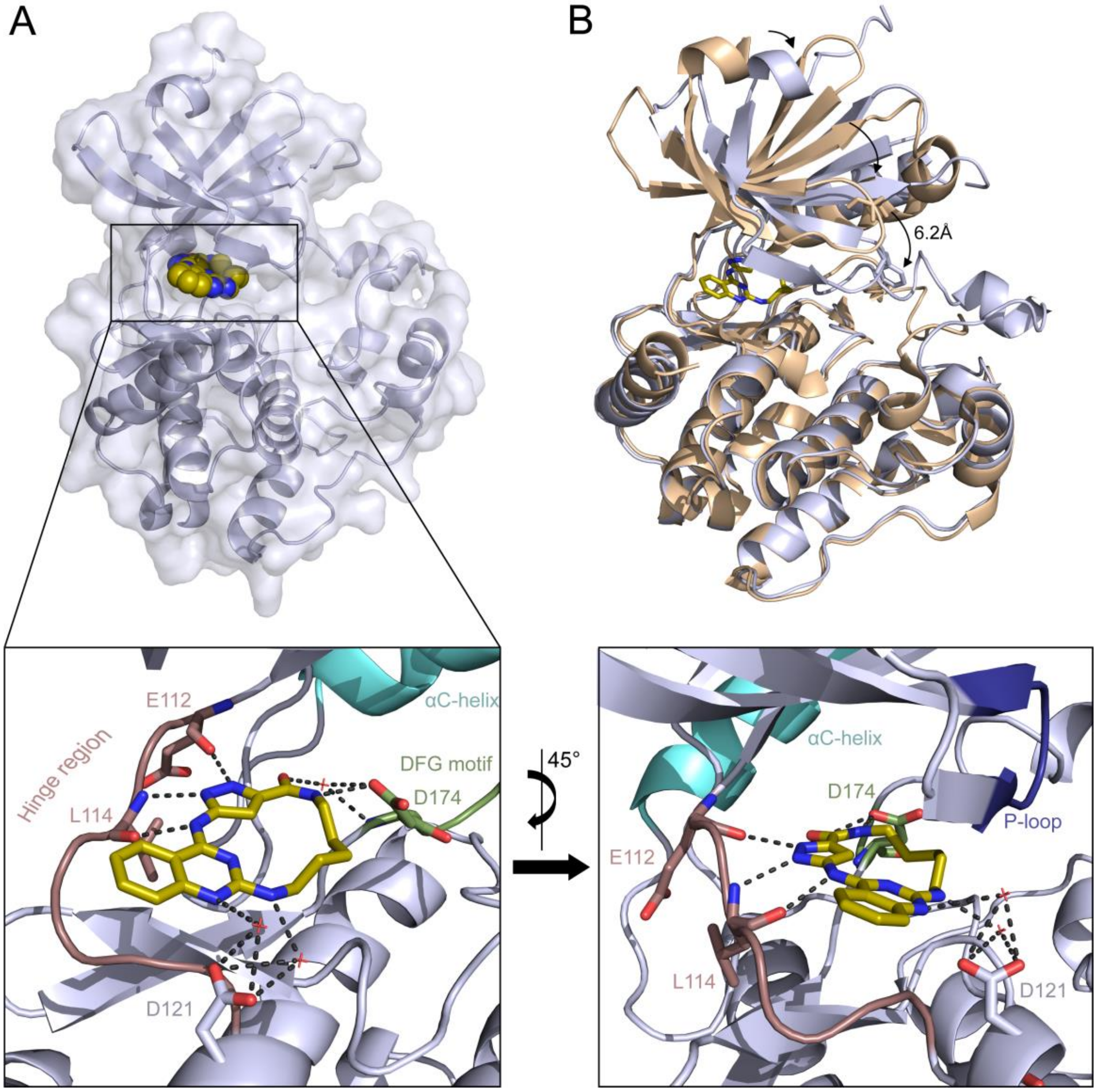

Figure 33. A. Crystal structure of MST3 in complex with **113c**. Macrocycle **113c** was identified as an ATP competitive type I inhibitor. Rotated representation of the ATP-binding pocket in complex with **113c** is shown beside. The hydrogen bonds are illustrated in dashed lines. The P-loop is tilted towards the C-terminal lobe. The compound is illustrated in gold, the hinge region of the kinase is shown in pale red, the P-loop in dark blue, the αC-helix in cyan, and the DFG-motif in green. **B.** Superimposition of the crystal structure of **113c** (pale blue) with a crystal structure of AMP-PNP in complex with MST3 (PDB: 4QML, pale orange). F47 is shifted 6.2Å towards the C-terminal lobe and packs against the activation loop.

3.7.4. Metabolic stability

The metabolic stability of **113c** was determined, using an activated liver microsome mix derived from the liver of Sprague-Dawley rats. **113c** was incubated at 37 °C for 60 minutes and the amount of unmetabolized compound was determined every 15 minutes, using HPLC (Figure 34). After an incubation time of 60 minutes, **113c** showed an excellent metabolic stability, with 88% of unmetabolized compound.

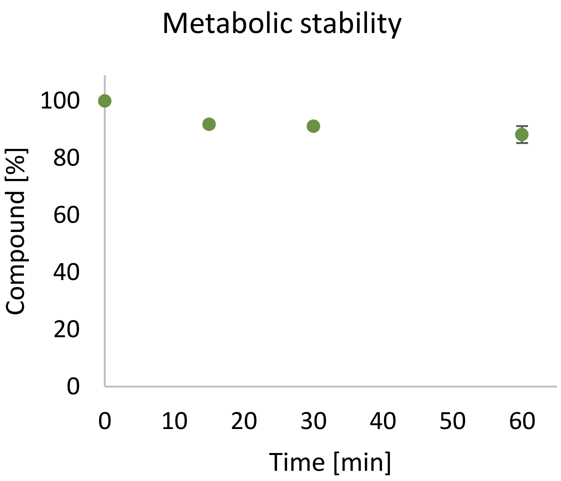

Figure 34. Metabolic stability of **113c** [10 µM] after treatment of activated microsomes. The residual amount of compound was determined after 0, 15, 30, and 60 minutes and was plotted in percent against the time in minutes. The data is given as a mean ± SEM, measured in triplicates.

4. Summary

4.1. Macrocyclization of quinazoline-based EGFR inhibitors lead to exclusive mutant selectivity for EGFR L858R and Del19

The transmembrane tyrosine kinase EGFR plays a central role in the adult homeostasis and embryonic development.[82,83] Canonical signaling pathways are responsible for diverse biological functions, like cell proliferation, survival, differentiation, or motility of cells. The dysregulation of EGFR is linked to various tumor types like glioblastomas, breast, or lung cancer.[94] NSCLC forms with 85% of all patients the majority of lung cancer, whereby EGFR is frequently overexpressed or mutated.[96] The point mutation L858R and the deletion mutant Del19 represent the most common mutations. The first generation of EGFR inhibitors comprises quinazoline-based inhibitors such as gefitinib (**5**) or erlotinib (**6**). Both are still first-line options for the treatment of mutated NSCLC however, they exhibit various off-targets and lead to adverse side effects.[194] Thus, making them a great starting point for macrocyclization strategy to gain kinome-wide selectivity.

During this work, several highly potent, macrocyclic EGFR inhibitors were developed. It could be shown that macrocyclization of the commonly used quinazoline scaffold had significant effects on the selectivity and potency. Through the introduction of halogen substituents at different positions of the aromatic ring, targeting the hydrophobic back pocket, the potency against EGFR WT and its mutants could be influenced. The variation of the linker length affected the selectivity within the kinome and even led to a mutant selective compound.

The macrocycles **39d** and **39f** were cyclized, using a 2-(2-(2-chloroethoxy)ethoxy)ethanol linker in order to improve the pharmacological profile in comparison to the acyclic counterpart gefitinib (**5**). Both compounds exhibited great cellular potencies for EGFR WT, L858R, L858R/C797S, Del19, and Del19/C797S with IC_{50} values in a low one- to two-digit nanomolar range. The gatekeeper mutation T790M was not affected by the macrocycles, presumably due to the quinazoline moiety. The DSF assay, containing 101 kinases distributed over the entire kinome, revealed a great selectivity profile for **39d** and **39f** with five and two stabilized kinases > 5 °C, respectively. The shortening of the linker for compound **26f** even increased the selectivity within the DSF panel by stabilizing only one kinase higher than 5 °C. The truncation was also sufficient to weaken the binding affinity to EGFR WT (IC_{50} > 10 µM) and introduced a mutant selectivity with cellular IC_{50} values of 385.6 nM, 197.5 nM, 749.6 nM, and 147.9 nM for EGFR L858R, Del19, and the corresponding double mutants with C797S. The minor modification of removing the methoxy group, which targets the solvent-exposed region, surprisingly led to an inactive compound **48**. The selectivity of **26f** was further validated by a kinome-wide selectivity screening using the KINOMEscan® platform. Also in this expanded panel, **26f** exhibited high selectivity with a selectivity score of S_{35} = 0.026 at a screening concentration of 1 µM. Western blotting confirmed the activity of **26f** against the mutants (L858R, L858R/C797S, Del19, and Del19/C797S) while EGFR WT was unaffected. Additionally, the influence on the downstream signaling pathways including the PI3K/AKT/mTOR and RAS/MAPK signaling were evaluated. **26f** again showed a mutant selectivity by affecting the downstream targets AKT and ERK1/2 on the tested EGFR mutants, whereas **26f** caused no effect on EGFR WT. This compound represents a valuable tool compound for the most common EGFR mutants L858R, Del19, and the double mutations L858R/C797S and Del19/C797S. The usage of mutant selective kinase inhibitors would potentially prevent adverse side effects caused by EGFR WT inhibition. Further work could additionally determine the influence of the most potent and selective macrocycles **26f**, **39d**, and **39f** in lung cancer cell lines. Additionally, further optimization of **26f** could be done by improving the solubility of the macrocycle. A starting point could be the introduction of diverse solubilizing groups, such as morpholine or methyl piperazine, targeting the solvent-exposed region, but not affecting the mutant selective profile of **26f**.

4.2. Discovery of 3-amino-1*H*-pyrazole-based kinase inhibitors to illuminate the understudied PCTAIRE family

The serine-threonine kinase CDK16 belongs to the understudied PCTAIRE subfamily of the CDK family. The CDKs are activated by the binding of specific cyclin partners. CDK16 is involved in different physiological processes, such as neuronal development or glucose homeostasis.[119,122] Binding of cyclin Y to CDK16 activates the kinase, which allows the translocation from the cytoplasm or the nucleus of neurons to the plasma membrane, forming the CDK16/ cyclin Y complex. A dysregulation of CDK16 is linked to different cancer types like cervical, breast, or prostate cancer.[124,126] Moreover, CDK16 induces a G2/M phase cell cycle arrest, followed by apoptosis in SCC cells.[131] CDK16 and the highly related family members CDK14, CDK15, CDK17, and CDK18 still belong to the dark kinome and are poorly understood.[114,115] Several highly potent kinase inhibitors targeting CDK16 have been published. However, all of them show either a promiscuous behavior or target the CDK family. Further research would benefit from selective CDK16 inhibitors as they allow further investigation of its involvement in pathophysiological processes.

Starting from the promiscuous kinase inhibitor **23**, several modifications were done to develop the potent kinase inhibitor **98d**. To evaluate the selectivity of the newly synthesized compounds, a DSF assay was used in which a panel of over one hundred kinases was tested. Besides the stabilization of CDK16 in the DSF panel, the cellular potency of all inhibitors was determined, using the NanoBRET^{TM} technology. In the initial steps, the potency against CDK16 was improved by removing additional substituents at position C5 of the pyrimidine. Through the exchange from the cyclopropyl group at the pyrazole, the selectivity profile of the compounds could be influenced. Alkyl residues generally led to an unselective profile, whereas a methyl amide moiety was not tolerated and led to inactive compounds. A methyl ester at the pyrazole caused a moderate stabilization of CDK16 and moreover a good selectivity within the tested kinases. The linker moieties at the pyrimidine were varied to find the best combination. This resulted in compound **76i** with a DSF shift of 6.5 °C for CDK16 and a corresponding IC_{50} value of 380.2 nM. Besides CDK16, only three other kinases were stabilized with shifts higher than 5 °C. Further optimization yielded in **97d** and **98d** harboring an *iso*-propyl and *tert*-butyl ester moiety. Both showed an improved selectivity profile in the DSF assay by stabilizing one and two kinases besides CDK16. Also, the potency for CDK16 was increased with DSF shifts of 9.1 °C and 9.2 °C and corresponding IC_{50} values of 44.0 nM and 33.4 nM, respectively. Follow-up determination of the selectivity within the CDK family was done for the most promising compounds **76i**, **97d**, **98d**, and the lead structure **23** by the NanoBRET^{TM} technology. Therefore, the different CDKs were activated by their specific cyclin partners. As expected, the lead structure **23** showed no selectivity within the CDK family which could be dramatically improved for **98d**. It only targeted the PCTAIRE and PFTAIRE subfamily with low nanomolar activity in cells (IC_{50} 20 nM – 120 nM and 50 nM – 180 nM). Additionally, a viability assessment and cell cycle assay were performed. **98d** induced a G2/M phase cell cycle arrest at all tested concentrations followed by apoptosis in agreement with genetic knockout studies of CDK16, reported by Yanagi *et. al*.[131] The development of **98d** provides the opportunity for further cell-based mechanistic studies on the PCTAIRE subfamily and enables an insight into this understudied class of kinases.

4.3. Design and synthesis of pyrazole-based macrocyclic kinase inhibitors targeting BMPR2

The transmembrane serine-threonine receptor kinase BMPR2 is involved in the canonical BMP signaling pathway. BMP binding to the extracellular domain of BMPR2 induces the formation of heterotetrameric complexes of type I and type II receptor kinases. Phosphorylation of this complex leads to the formation of heterotrimer SMAD complexes, which translocate to the nucleus and influence the cell migration, proliferation, or apoptosis.[144,145] A dysfunction is linked to Alzheimer´s disease, PAH, or various cancer types.[145,151,152] To date, no selective BMPR2 inhibitors have been published, making it an interesting target in drug discovery.

The development of the macrocyclic BMPR2 inhibitor **110a** was based on the scaffold of the promiscuous kinase inhibitor **23**, which was also used for the CDK16 project. First, a methyl ester moiety was introduced at the pyrazole, enabling the macrocyclization reaction. In the next step, different linker moieties were varied to improve the selectivity of the desired macrocycles and to focus on BMPR2. The introduction of a *para*-substituted aromatic linker resulted in a great selectivity profile in the DSF assay, measuring a panel of 90 kinases across the kinome. Only GSK3B was notably affected besides BMPR2. An excellent selectivity profile was also observed in a comprehensive selectivity panel, testing 468 human protein kinases and their mutants at a screening concentration of 1 µM, with a selectivity score of $S_{35} = 0.01$. The binding affinity of **110a** towards BMPR2 was determined in an ITC measurement, which revealed entropically driven binding with a low K_D value of 205 nM. Further assessment of the potency was performed by an ADP-Glo^{TM} assay. It revealed a good potency of **110a** towards BMPR2 with an IC_{50} value of 506 nM. Despite the off-target activity of GSK3B with an IC_{50} value of 2.3 µM, **110a** represents a valuable tool compound for further functional studies of BMPR2 and represents the most selective BMPR2 inhibitor published to date.

4.4. Optimization of pyrazole-based macrocycles lead to a highly selective MST3 inhibitor

MST3 and MST4 are members of the STE family and form together with YSK1 the GckIII subgroup.[157] MST3 is mainly localized in the cytoplasm and influences the cell morphology and cell cycle progression. Dysregulation is associated with diseases like epilepsy, autism, or different cancer types such as gastric or breast cancer.[159,161,162] MST4 regulates the inflammatory response or the Golgi reorientation. Malfunctions are linked to various cancer types like prostate or breast cancer.[167,168] Several nonselective inhibitors have been published that involve MST3 or MST4 as an off-target, but no selective MST3 or MST4 inhibitors have yet been described.

Minor modifications of the macrocyclic scaffold of **110a**, which was developed for the inhibition of BMPR2, shifted the selectivity towards MST3 and MST4. Additional residues such as a chlorine residue or a methyl group at position C5 of the pyrimidine were introduced or the pyrimidine was replaced by a quinazoline moiety. Different aromatic and aliphatic linkers were used analogue to the BMPR2 project. Initial screening results by DSF revealed the preferred inhibition of MST3 and MST4 for the macrocycles **113a** – **113e**, harboring a quinazoline moiety that targets the solvent-exposed region. They showed a stabilization of MST3 and MST4 up to 7.5 °C, whereby the chlorine residue and the methyl group led to stabilizations below 3.0 °C. Impressively, the related family members MST1 and MST2 were not affected by them. Further assessment of the synthesized macrocycles was done by NanoBRET^{TM} and was in a good concordance to the results of the DSF measurement. The pentyl linker in **113c** resulted in a highly potent MST3 inhibitor with IC_{50} values of 210 nM *in cellulo* and 30 nM in the lysed mode. A weaker potency was obtained for MST4 with IC_{50} values of 1.8 µM *in cellulo* and 510 nM in the lysed mode. MST1 and MST2 were not inhibited with IC_{50} values higher than 50 µM. ITC measurement of **113c** against MST4 emphasized an enthalpic-driven binding and was in agreement with the NanoBRET^{TM} data with a K_D value of 116 nM. **113c** showed a good selectivity within the DSF panel, screening 104 kinases distributed over the entire kinome. In addition to MST3 and MST4, only five kinases were stabilized however, those DSF shifts were low in comparison to the reference compound. The co-crystal structure of MST3 in complex with **113c** confirmed a type I inhibitor binding mode. The molecule led to a substantial tilting of the N-terminal lobe towards the C-lobe. Several polar interactions and water-mediated networks were formed, whereby the 3-aminopyrazole moiety interacted with the hinge region and the quinazoline moiety targeted the solvent-exposed region. To date, no selective MST3 inhibitors have been published. This highlights the importance of the newly synthesized macrocycle **113c**, which is emerging as a new tool compound for further functional studies.

5. Conclusion and Outlook

This thesis comprises the usage of two commonly known hinge-binding moieties in drug discovery. First, the quinazoline scaffold of gefitinib (**5**) was utilized in a macrocyclization strategy to introduce selectivity. In general, the quinazoline hinge-binding moiety is a commonly used scaffold which can be found in 14% of approved kinase inhibitors. The most familiar applications are EGFR inhibitors such as gefitinib (**5**), erlotinib (**6**), afatinib, or dacomitinib for the treatment of NSCLC.[44] But other kinases like CDK2, CDK4, or p38 are reported targets as well.[195,196]

The *N*-phenylquinazolin-4-amine moiety of gefitinib (**5**) was conserved however, the residues at the aromatic ring in the linker were modified, the residue targeting the solvent-exposed region was varied, and the linker at the C6 position of the quinazoline was adjusted to enable the macrocyclization. An overview of the structural modifications is shown in Figure 35A.

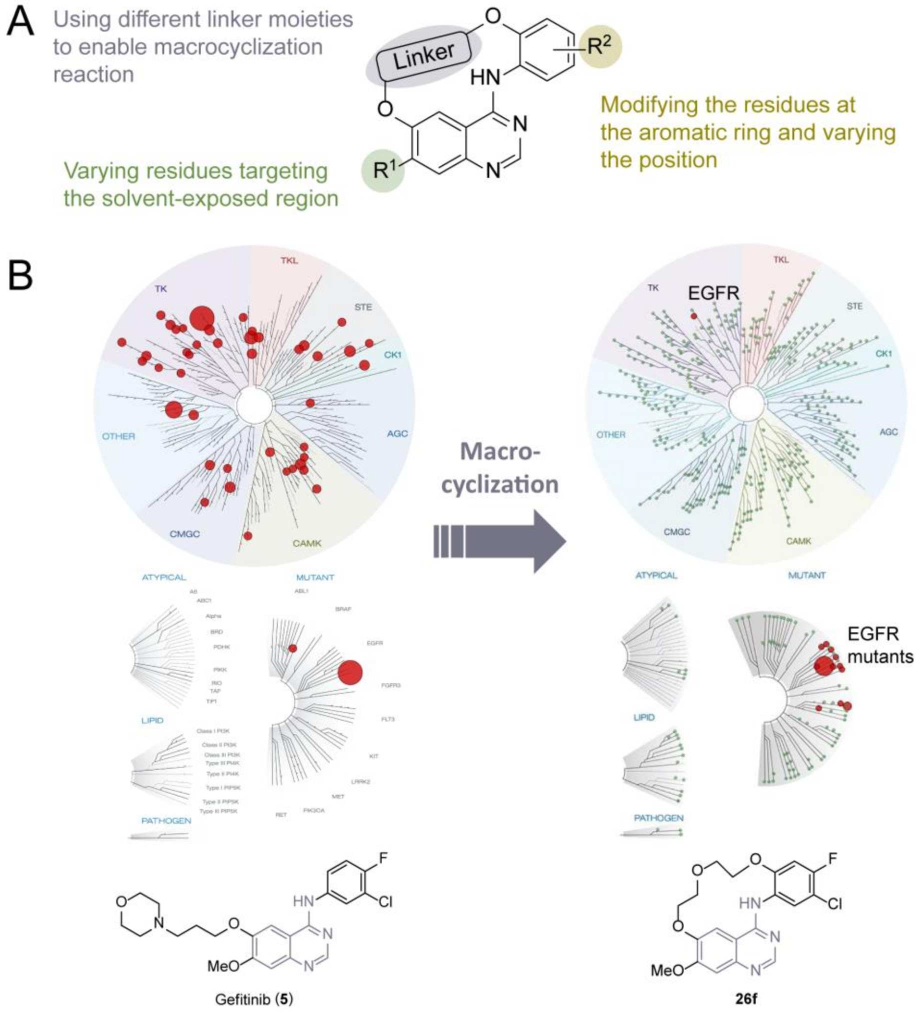
A
Using different linker moieties to enable macrocyclization reaction
Linker
O
HN
N
O
R1
N
R2
Modifying the residues at the aromatic ring and varying the position
Varying residues targeting the solvent-exposed region
B
TK
TKL
STE
CK1
AGC
CAMK
CMGC
OTHER
Macro-cyclization
EGFR
ATYPICAL
MUTANT
LIPID
PATHOGEN
EGFR mutants
HN
F
Cl
O
N
O
MeO
N
N
Gefitinib (5)
26f

Figure 35. A. Graphical representation of the structural modifications of the quinazoline-based macrocycles. **B.** Optimization of the selectivity profile of gefitinib (**5**) was achieved through the macrocyclic kinase inhibitor **26f**. The conserved quinazoline hinge-binding moiety is highlighted in purple.

Kinome-wide screening of gefitinib (**5**) revealed several off-targets besides EGFR (Figure 35B), making it an excellent starting point for a macrocyclization strategy. Introducing a linker to the *N*-phenylquinazoline-4-amine scaffold and retaining the residues on the aromatic ring as well as the methoxy group targeting the solvent-exposed region improved the selectivity profile and the efficacy towards EGFR WT and its mutants. Truncation of the linker moiety led to the mutant selective macrocycle **26f** with an excellent kinome-wide selectivity profile (Figure 35B). An inhibitor that is effective on EGFR mutations while ineffective on the EGFR WT could represent an enhancement of patient treatment, as it potentially causes less side effects. Further studies could determine the effect of the most promising macrocycles in lung cancer cell lines. Additionally, the pharmacokinetic properties could be optimized, e.g. by introducing solubilizing groups, targeting the solvent-exposed region.

The second scaffold comprises the 3-aminopyrazole-based hinge-binding moiety. It is a privileged scaffold in medicinal chemistry for the development of kinase inhibitors. Previous publications report the anti-proliferative and anti-cancer potential of pyrazole-based molecules. They play a crucial role in the treatment of various diseases and cancer types like inflammation disorders, lymphoma, or breast cancer.[197,198] This scaffold can be found e.g. in the aurora kinase inhibitor tozasertib or in the promiscuous kinase inhibitor **23**, published by Statsuk *et. al*.[179,199] Rescreening compound **23** in a comprehensive kinase panel against 468 human protein kinases confirmed the unselective behavior with a selectivity score of $S_{35} = 0.56$ (Figure 36B), making it a great starting point for further optimizations. The *N*-(1*H*-pyrazol-3-yl)pyrimidin-4-amine scaffold was conserved however, the residues targeting the solvent-exposed region were varied and different linkers were attached.

The introduction of different residues at the pyrazole dramatically influenced the selectivity profile of the desired kinases. Ester moieties caused to a favorable combination of selectivity and potency towards the kinase of interest CDK16. The removal of additional residues at the pyrimidine, targeting the solvent-exposed region, increased the efficiency towards CDK16. Further optimization led to the highly potent and selective CDK16 inhibitor **98d** (IC_{50} = 33 nM). NanoBRET^{TM} screening against the complete CDK family revealed a preferred inhibition of the PCTAIRE and PFTAIRE subfamily with cellular IC_{50} values of 20 nM – 120 nM and 50 nM – 180 nM, respectively. A FUCCI cell cycle assay and viability assessment of **98d** confirmed previously published results, reporting a G2/M cell cycle arrest followed by apoptosis and accumulation of p27 through knockout of CDK16 in SCC cells.[131] Consequently, further studies could evaluate the anti-tumor activity of **98d** in SCC and NSCLC or elucidate the effect of **98d** in AMPK-related macroautophagy.[131–133,135]

98d represents a novel tool compound to investigate the understudied kinases of the PCTAIRE family and enable to enlighten the biological role of those kinases.

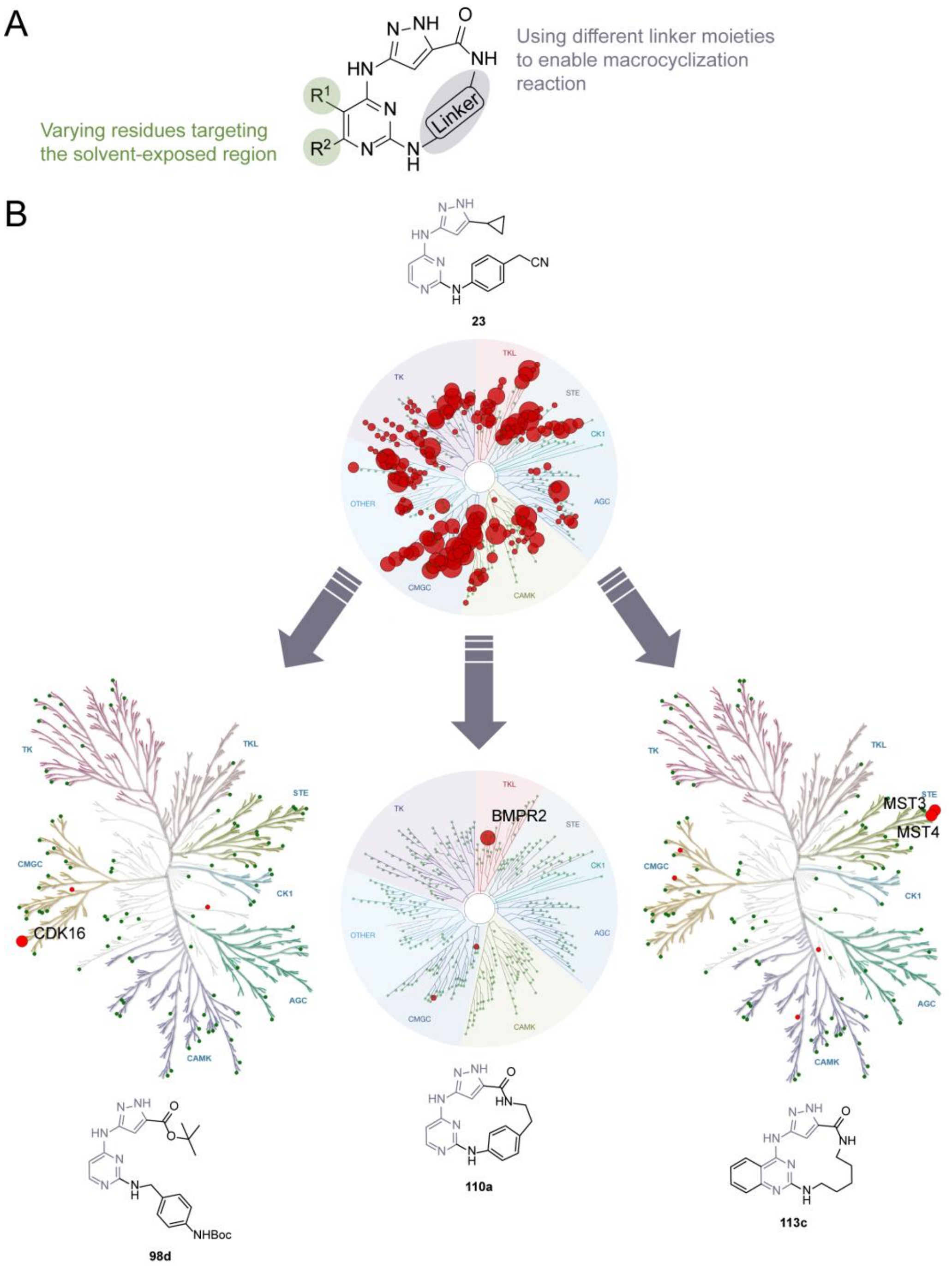
A
Using different linker moieties to enable macrocyclization reaction
Varying residues targeting the solvent-exposed region
R1
R2
Linker
B
23
TK
TKL
STE
CK1
AGC
CAMK
CMGC
OTHER
CDK16
BMPR2
MST3
MST4
98d
110a
113c

Figure 36. A. Graphical representation of the structural modifications of the 3-aminopyrazole-based macrocycles. **B.** Optimization of the selectivity profile of the promiscuous kinase inhibitor **23** was achieved through various SAR studies. The CDK16 inhibitor **98d**, the BMPR2 inhibitor **110a**, and the MST3/ MST4 inhibitor **113c** were achieved. The conserved *N*-(1*H*-pyrazol-3-yl)pyrimidin-4-amine scaffold is highlighted in purple.

Macrocyclization of the *N*-(1*H*-pyrazol-3-yl)pyrimidin-4-amine core resulted in the selective BMPR2 inhibitor **110a**. It showed a good binding affinity towards BMPR2 with a K_D value of 205 nM as well as a good potency with an IC_{50} value of 506 nM. A comprehensive selectivity screen against 468 kinases revealed an excellent selectivity profile with $S_{35} = 0.01$. As no BMPR2 inhibitors have been published so far, **110a** represents a novel compound that may provide further insights into the canonical BMP pathway, noncanonical signaling, or its impact on BMPR2-associated diseases like PAH.[140,146,151]

The introduction of additional residues targeting the solvent-exposed region shifted the selectivity towards the MST kinases. The exchange from the pyrimidine to a quinazoline moiety resulted in the highly potent and selective macrocyclic MST3 inhibitor **113c**. NanoBRET^{TM} measurements demonstrated the preferred inhibition of MST3 with IC_{50} values of 210 nM and 30 nM for intact and lysed cells, respectively. A weaker activity could be seen for MST4 with 1.8 µM and 510 nM, while MST1 and MST2 were not affected. To date, no selective MST3 inhibitors have been published, making **113c** a valuable tool compound for further functional studies. As MST3 is influencing the cell cycle progression, **113c** could be tested in a further cell cycle assay to elucidate the inhibitory effect of **113c** on MST3 and consequently on the cell cycle. Furthermore, the anti-tumor activity of **113c** in breast cancer could be determined, as Madsen *et. al.* reported a high MST3 and MST4 activity triggered by FAM40B mutations.[168]

In conclusion, this thesis yielded in the development and characterization of potent and highly selective kinase inhibitors for EGFR, CDK16, BMPR2, and MST3. Macrocyclization of the gefitinib (**5**) scaffold resulted in a mutant selective kinase inhibitor for EGFR, confirming the hypothesis to gain selectivity through macrocyclization. Structure-activity relationship studies of the promiscuous kinase inhibitor **23** demonstrated the possibility to affect the kinome-wide selectivity and the potency for the kinase of interest by minor structural modifications. This thesis has succeeded in synthesizing various new macrocyclic kinase inhibitors. Furthermore, it provides several new tool compounds to illuminate the biological functions of their target kinases and enable the specific inhibition of the partially unexplored kinases.

6. Zusammenfassung und Ausblick

Kinaseinhibitoren spielen in der Erforschung neuer Medikamente eine zentrale Schlüsselrolle, welche sich in der Zahl der klinisch zugelassenen Arzneistoffe widerspiegelt. Seit der Zulassung des ersten Kinaseinhibitors Fasudil im Jahr 1995 in Japan wurden bislang insgesamt 72 niedermolekulare Inhibitoren von der FDA zugelassen.[6] Allein in den letzten fünf Jahren hat sich deren Zahl verdoppelt. Verschiedene Krankheiten, wie Entzündungsreaktionen oder Autoimmunerkrankungen werden dadurch adressiert, wobei mit 89% die Mehrzahl der zugelassenen Kinaseinhibitoren für onkologische Indikationen eingesetzt wird.[44] Die hoch konservierte ATP-Bindetasche stellt für die Entwicklung neuer und selektiver ATP-mimetischer Inhibitoren jedoch eine große Herausforderung dar. Die Makrozyklisierung bietet eine Möglichkeit zur Erzeugung von Selektivität durch die Einschränkung der Flexibilität des Moleküls. Solche Makrozyklen bestehen aus einem linearen Pharmakophor, der durch einen Linker verbunden ist. Diese konformationelle Einschränkung kann durch Minimierung der entropischen Kosten während des Bindens an die Kinase zudem zu einer gesteigerten Affinität gegenüber der Zielkinase führen. Des Weiteren können durch diesen Ansatz die pharmakokinetischen Eigenschaften, wie die metabolische Stabilität oder Löslichkeit des Moleküls optimiert werden.[65]

Diese Arbeit umfasst die Verwendung von zwei allgemein bekannten Scharnier (englisch *hinge*) Bindemotiven in der Arzneimittelforschung. Im Rahmen des ersten Projekts wurde das Chinazolin Grundgerüst verwendet, welches in 14 % der zugelassenen Kinaseinhibitoren zu finden ist. Die bekanntesten Anwendungen sind EGFR Inhibitoren wie Gefitinib (**5**), Erlotinib (**6**), Afatinib und Dacomitinib, die für die Behandlung von nicht-kleinzelligen Bronchialkarzinomen zugelassen sind.[44]

Die transmembrane Tyrosinkinase EGFR spielt eine zentrale Rolle in der Homöostase von Erwachsenen und in der embryonalen Entwicklung.[82,83] Kanonische Signalwege sind für verschiedene biologische Funktionen, wie die Zellproliferation, das Überleben, die Differenzierung oder die Motilität von Zellen verantwortlich. Eine Dysregulation von EGFR wird mit verschiedenen Tumorarten wie Glioblastomen, Brust- oder Lungenkrebs in Verbindung gebracht.[94] Nicht-kleinzellige Bronchialkarzinome bilden mit 85% der Patienten die Mehrheit aller Fälle von Lungenkrebs, wobei EGFR häufig überexprimiert oder mutiert vorliegt.[96] Die Punktmutation L858R und die Deletionsmutante Del19 stellen die am häufigsten vorkommenden Mutationen dar. Die erste Generation der EGFR Inhibitoren besteht aus Molekülen mit einem Chinazolin Grundgerüst wie Gefitinib (**5**) oder Erlotinib (**6**). Beide sind nach wie vor die erste Wahl für die Behandlung von mutierten nicht-kleinzelligen Bronchialkarzinomen, adressieren jedoch auch weitere Kinasen und können somit zu unerwünschten Nebenwirkungen führen.[194] Dieses Bindemotiv stellt daher einen hervorragenden Ausgangspunkt dar, um eine Selektivität innerhalb des gesamten Kinoms durch Makrozyklisierung zu verbessern.

Die Makrozyklen **39d** und **39f** wurden durch einen 2-(2-(2-Chlorethoxy)ethoxy)ethanol-Linker zyklisiert, um die pharmakologischen Eigenschaften, ausgehend von Gefitinib (**5**), zu verbessern. Beide Verbindungen zeigten eine hohe zelluläre Potenz für EGFR WT, L858R, L858R/C797S, Del19 und Del19/C797S mit IC_{50} Werten im niedrigen ein- bis zweistelligen nanomolaren Bereich. Die Gatekeeper Mutation T790M wurde von den Makrozyklen nicht adressiert, was analog zu den bereits publizierten EGFR Inhibitoren der ersten und zweiten Generation auf das Chinazolin Bindemotiv zurückzuführen ist. Ein DSF Assay, der 101 Kinasen beinhaltet, die über das gesamte Kinom verteilt sind, zeigte eine sehr gute Selektivität für **39d** und **39f** mit fünf bzw. zwei stabilisierten Kinasen > 5 °C. Die Verkürzung des Linkers erhöhte die Selektivität und **26f** stabilisierte lediglich eine Kinase über 5 °C. Zusätzlich wurde dadurch die Bindungsaffinität gegenüber EGFR WT geschwächt (IC_{50} > 10 µM) und führte zu einer Mutantenselektivität mit IC_{50} Werten von 385.6 nM, 197.5 nM, 749.6 nM und 147.9 nM für EGFR L858R, Del19 und die entsprechenden Doppelmutanten mit C797S. Das Entfernen der Methoxygruppe, die die lösungsmittelzugewandte Region adressiert, führte überraschenderweise zu der inaktiven Verbindung **48**. Die Selektivität von **26f** wurde durch ein kinomweites Selektivitätsscreening unter Verwendung der KINOMEscan® Plattform validiert. Auch in diesem erweiterten Assayformat zeigte **26f** eine hohe Selektivität von S_{35} = 0.026 bei einer Screening Konzentration von 1 µM. Western Blotting bestätigte die Aktivität von **26f** gegenüber den Mutanten (L858R, L858R/C797S, Del19 und Del19/C797S), während EGFR WT nicht inhibiert wurde. Darüber hinaus wurde der Einfluss auf die PI3K/AKT/mTOR und RAS/MAPK Signalwege untersucht. **26f** zeigte erneut eine Mutantenselektivität, indem es die nachgeschalteten (englisch *downstream*) Kinasen AKT und ERK1/2 bei den getesteten EGFR Mutanten hemmte, während **26f** auf EGFR WT keine Wirkung zeigte. Verbindung **26f** stellt somit einen wichtigen Inhibitor für die häufigsten EGFR Mutanten L858R, Del19 und die Doppelmutationen L858R/C797S und Del19/C797S dar. Die Verwendung von solch mutantenselektiven Kinaseinhibitoren zur Behandlung von Krankheiten könnte die Therapie von Patienten verbessern, da unerwünschte Nebenwirkungen, die durch die Inhibition von EGFR WT verursacht werden, verhindert werden könnten. Zukünftige Studien könnten zusätzlich den Einfluss der wirksamsten und selektivsten Makrozyklen **26f**, **39d** und **39f** auf Lungenkrebszelllinien bestimmen. Darüber hinaus könnte **26f** durch eine Verbesserung der Löslichkeit weiter optimiert werden. Ein Ausgangspunkt könnte die Einführung verschiedener löslichkeitsfördernder Gruppen, wie Morpholin oder Methylpiperazin, sein, die die lösungsmittelzugewandte Region adressieren.

Das zweite Projekt basiert auf dem 3-Aminopyrazol *hinge* Bindemotiv. Es ist ebenfalls ein gebräuchliches Grundgerüst in der medizinischen Chemie für die Entwicklung von Kinaseinhibitoren. In früheren Publikationen wurde über das antiproliferative und krebshemmende Potenzial von Molekülen auf Pyrazolbasis berichtet. Sie spielen eine entscheidende Rolle bei der Behandlung verschiedener Krankheiten und Krebsarten wie Entzündungen, Lymphome oder Brustkrebs.[197,198] Dieses Bindemotiv findet sich beispielsweise im Aurora Kinaseinhibitor Tozasertib oder im promiskuitiven Kinaseinhibitor **23** wider.[179,199] Verbindung **23** wurde im Rahmen dieser Arbeit erneut in einem umfassenden Selektivitätsassay gegen 468 Proteinkinasen und deren Mutanten getestet, wobei das unselektive Verhalten ($S_{35} = 0.56$) bei einer Screening Konzentration von 1 µM bestätigt wurde.

Die Serin-Threonin Kinase CDK16 gehört zur bisher wenig erforschten PCTAIRE Gruppe der CDK Familie. CDK16 ist an verschiedenen physiologischen Prozessen beteiligt, wie beispielsweise an der neuronalen Entwicklung oder der Glukosehomöostase.[119,122] Die Bindung von Cyclin Y an CDK16 aktiviert die Kinase, wodurch die Translokalisation aus dem Zytoplasma oder dem Kern von Neuronen zur Plasmamembran induziert und der CDK16/ Cyclin Y Komplex gebildet wird. Eine Dysregulation von CDK16 wird mit verschiedenen Krebsarten wie Gebärmutterhals-, Brust- oder Prostatakrebs in Verbindung gebracht.[124,126] Darüber hinaus induziert CDK16 einen Zellzyklus Arrest in der G2/M-Phase, was in Plattenepithelkarzinomzellen zur Akkumulierung von p27 und Apoptose führt.[131] CDK16 und dessen strukturell verwandte Familienmitglieder CDK14, CDK15, CDK17 und CDK18 gehören nach wie vor zur Klasse der unerforschten Kinasen, welche bisher nur unzureichend verstanden werden.[114,115] Es wurden bislang mehrere hochwirksame Kinaseinhibitoren veröffentlicht, die CDK16 potent inhibieren. Allerdings zeigen alle von ihnen entweder ein promiskuitives Verhalten oder besitzen keine Selektivität innerhalb der CDK Familie. Die Forschung würde von selektiven CDK16 Inhibitoren profitieren, da sie weitere Untersuchungen zur Beteiligung von CDK16 an pathophysiologischen Prozessen ermöglichen würde.

Ausgehend von dem promiskuitiven Kinaseinhibitor **23** wurden verschiedene Modifikationen vorgenommen, um den potenten Inhibitor **98d** zu entwickeln. Die Selektivität wurde durch ein DSF Assay evaluiert, indem die neu synthetisierten Verbindungen gegen ein Set von über hundert Kinasen getestet wurden. Zusätzlich zur Stabilisierung von CDK16 im DSF Assay wurde die zelluläre Potenz aller Inhibitoren mit Hilfe der NanoBRET^{TM} Technologie bestimmt. Zunächst konnte die Potenz gegenüber CDK16 durch die Entfernung zusätzlicher Substituenten an der C5-

Position des Pyrimidins erhöht werden. Durch den Austausch der Cyclopropylgruppe am Pyrazol konnte anschließend das Selektivitätsprofil der Verbindungen beeinflusst werden. Alkylreste wiesen im Allgemeinen keine Selektivität auf, während ein Methylamid nicht toleriert wurde und zu inaktiven Verbindungen führte. Ein Methylester am Pyrazol führte zu einer moderaten Stabilisierung von CDK16 und darüber hinaus zu einer guten Selektivität innerhalb der getesteten Kinasen. Die Linkergruppen am Pyrimidin wurden variiert, um eine bestmögliche Kombination zu ermöglichen. Verbindung **76i** erzielte im DSF Assay eine Stabilisierung von 6.5 °C für CDK16 mit einem entsprechenden IC_{50} Wert von 380.2 nM. Neben CDK16 wurden nur drei weitere Kinasen mit mehr als 5 °C stabilisiert. Weitere Optimierungen führten im nächsten Schritt zu **97d** und **98d**, die einen *iso*-Propyl- und *tert*-Butylester enthielten. Beide zeigten ein verbessertes Selektivitätsprofil im DSF Assay, bei dem sie zusätzlich zu CDK16 nur eine bzw. zwei Kinasen stabilisierten. Auch die Potenz für CDK16 wurde mit DSF Verschiebungen von 9.1 °C und 9.2 °C und entsprechenden IC_{50} Werten von 44.0 nM bzw. 33.4 nM erhöht. Als nächstes sollte die Selektivität der vielversprechendsten Inhibitoren **76i**, **97d**, **98d** und der Leitstruktur **23** gegenüber den anderen Mitgliedern der CDK Familie mit Hilfe der NanoBRET^{TM} Technologie bestimmt werden. Die Leitstruktur **23** zeigte dabei erwartungsgemäß keine Selektivität innerhalb der CDK Familie, was jedoch durch die Modifikationen in **98d** deutlich verbessert werden konnte. **98d** inhibierte ausschließlich die PCTAIRE und PFTAIRE Familie im niedrigen nanomolaren Bereich mit IC_{50} Werten von 20 nM – 120 nM und 50 nM – 180 nM. Zusätzlich wurde ein FUCCI Zellzyklus Assay durchgeführt. **98d** führte zu einem Zellzyklus Arrest in der G2/M-Phase und anschließender Apoptose, was mit genetischen Knockout-Studien von CDK16 korreliert, die zuvor von Yanagi *et. al.* publiziert wurden.[131] Künftige Studien könnten die Anti-Tumor-Aktivität von **98d** in Plattenepithelkarzinomen und nicht-kleinzelligen Bronchialkarzinomen bestimmen oder die Wirkung von **98d** auf die AMPK-bezogene Makroautophagie aufklären.[131–133,135] Die Entwicklung von **98d** bietet die Möglichkeit für weitere zellbasierte Studien über die PCTAIRE Familie und ermöglicht einen Einblick in diese bisher wenig untersuchte Klasse von Kinasen.

Die transmembrane Serin-Threonin Rezeptorkinase BMPR2 ist an dem kanonischen BMP-Signalweg beteiligt. Die Bindung von BMP an die extrazelluläre Domäne von BMPR2 induziert die Bildung von heterotetrameren Komplexen aus Typ I- und Typ II-Rezeptorkinasen. Die Phosphorylierung des Komplexes führt anschließend zur Bildung heterotrimerer SMAD-Komplexe, die in den Zellkern wandern und die Zellmigration, -proliferation oder -apoptose beeinflussen.[144,145] Eine Dysregulation von BMPR2 wird mit Alzheimer, pulmonaler Hypertonie und verschiedenen

Krebsarten in Verbindung gebracht.[145,151,152] Da bisher noch keine selektiven BMPR2 Inhibitoren publiziert wurden stellt es ein interessantes Ziel für die Arzneimittelforschung dar.

Die Entwicklung des makrozyklischen BMPR2 Inhibitors **110a** basierte auf dem Gerüst des promiskuitiven Kinaseinhibitors **23**, der auch für das CDK16 Projekt verwendet wurde. Zunächst wurde ein Methylester am Pyrazol eingeführt, um die Makrozyklisierung zu ermöglichen. Im nächsten Schritt wurden die Linkereinheiten variiert, um die Selektivität der Makrozyklen zu verbessern und die Potenz gegenüber BMPR2 zu steigern. Die Einführung eines *para*-substituierten aromatischen Linkers führte zu einer guten Selektivität innerhalb des DSF Assay, bei dem insgesamt 90 Kinasen untersucht wurden. Neben BMPR2 wurde lediglich GSK3B mit einem nennenswerten Shift > 5 °C stabilisiert. Ein hervorragendes Selektivitätsprofil von $S_{35} = 0.01$ wurde anschließend auch in einem umfassenden Selektivitätsassay beobachtet, in dem **110a** gegen 468 Proteinkinasen und deren Mutanten bei einer Screening Konzentration von 1 µM getestet wurde. Die Bindungsaffinität von **110a** gegenüber BMPR2 wurde mittels einer ITC Messung bestimmt, die eine entropisch getriebene Bindung mit einem niedrigen K_D Wert von 205 nM ergab. Eine Validierung der Potenz wurde mittels eines ADP-Glo^{TM} Assays durchgeführt. Dabei zeigte **110a** eine gute Potenz gegenüber BMPR2 mit einem IC_{50} Wert von 506 nM. Da bisher keine selektiven BMPR2 Inhibitoren publiziert wurden stellt **110a** eine wichtige Verbindung dar, die weitere Einblicke in den kanonischen BMP-Signalweg oder die nicht-kanonische Signalübertragung liefern könnte. Zudem können die Auswirkungen einer selektiven Inhibition von BMPR2 und der assoziierten Krankheiten, wie beispielsweise pulmonale Hypertonie, näher beleuchtet werden.[140,146,151]

MST3 und MST4 sind Mitglieder der STE Familie und bilden zusammen mit YSK1 die GckIII-Gruppe.[157] MST3 ist hauptsächlich im Zytoplasma lokalisiert und beeinflusst die Zellmorphologie und die Zellzyklusprogression. Eine Dysregulation wird mit Krankheiten wie Epilepsie, Autismus und verschiedenen Krebsarten wie Magen- oder Brustkrebs in Verbindung gebracht.[159,161,162] MST4 reguliert Entzündungsreaktionen und ist für die Golgi Neuausrichtung verantwortlich. Fehlfunktionen können verschiedenen Krebsarten wie Prostata- oder Brustkrebs zur Folge haben.[167,168] Es wurden bisher diverse unselektive Inhibitoren publiziert, die MST3 bzw. MST4 neben anderen Kinasen adressieren, jedoch gelang es bisher noch nicht selektive MST3 oder MST4 Inhibitoren zu entwickeln.

Geringfügige Modifikationen des makrozyklischen Gerüsts, welches für die Inhibition von BMPR2 entwickelt wurde, verschoben die Selektivität zu MST3 und MST4. Es wurden zusätzliche Reste wie ein Chloratom oder eine Methylgruppe an der C5-Position des Pyrimidins eingeführt und das Pyrimidin wurde durch ein Chinazolin ersetzt. Analog zum BMPR2 Projekt wurden verschiedene aromatische und aliphatische Linker verwendet. Erste DSF Ergebnisse zeigten eine bevorzugte Stabilisierung von MST3 und MST4 durch die Makrozyklen **113a** – **113e**, die ein Chinazolin statt Pyrimidin enthielten. Sie zeigten eine Stabilisierung für MST3 und MST4 von bis zu 7.5 °C, wobei die Einführung eines Chlorrests oder einer Methylgruppe nur zu Stabilisierungen unter 3.0 °C führten. Die Familienmitglieder MST1 und MST2 wurden nicht beeinflusst. Die weitere Bewertung der synthetisierten Makrozyklen erfolgte mittels eines NanoBRET^{TM} Assays und bestätigte die Ergebnisse der DSF Messungen. Der Pentyl Linker in **113c** führte zu einem hochpotenten MST3 Inhibitor mit IC_{50} Werten von 210 nM in intakten Zellen und 30 nM im lysierten Modus. Eine schwächere Potenz wurde für MST4 mit IC_{50} Werten von 1.8 µM in intakten Zellen und 510 nM im lysierten Modus erzielt. MST1 und MST2 wurden mit IC_{50} Werten von mehr als 50 µM nicht inhibiert. Die ITC Messung von **113c** gegen MST4 zeigte eine enthalpische Bindung mit einem K_D Wert von 116 nM und war somit in Übereinstimmung zu den NanoBRET^{TM} Daten des lysierten Modus. **113c** wies eine gute Selektivität innerhalb des DSF Assays auf, in dem 104 Kinasen getestet wurden, die über das gesamte Kinom verteilt waren. Neben MST3 und MST4 wurden nur fünf weitere Kinasen > 5 °C stabilisiert, deren Stabilisierung im Vergleich zur Referenzverbindung gering war. Die Co-Kristallstruktur von MST3 im Komplex mit **113c** bestätigte die Hypothese eines Typ I-Inhibitors. Dabei wurden mehrere polare Wechselwirkungen und wasservermittelte Netzwerke gebildet, wobei das 3-Aminopyrazol basierte Bindemotiv mit der *hinge* Region wechselwirkte und die Chinazolin Einheit zur lösungsmittelzugewandten Region ragte. Das Binden von **113c** an MST3 führte zu einer erheblichen Verschiebung des N-terminalen Bereichs in Richtung des C-terminalen Bereichs. Bisher sind keine selektiven MST3 Inhibitoren publiziert worden, so dass **113c** eine wichtige Verbindung für zukünftige Studien darstellt. Da MST3 den Zellzyklus beeinflusst, könnte **113c** in einem Zellzyklus Assay getestet werden, um den inhibitorischen Effekt von **113c** auf MST3 und demzufolge auf den Zellzyklus zu klären. Des Weiteren berichteten Madsen *et. al.* über eine hohe MST3 und MST4 Aktivität in Brustkrebs, welche durch FAM40B-Mutationen ausgelöst wird.[168] **113c** könnte somit in Brustkrebszelllinien auf dessen Anti-Tumor Aktivität getestet werden.

Zusammenfassend lässt sich sagen, dass diese Arbeit zur Entwicklung und Charakterisierung von potenten und hochselektiven Kinaseinhibitoren für EGFR, CDK16, BMPR2 und MST3 geführt hat. Die Makrozyklisierung des Gefitinib (**5**) Grundgerüsts führte zu einem mutantenselektiven Kinaseinhibitor für EGFR und bestätigte die Hypothese durch Makrozyklisierung Selektivität gewinnen zu können. Studien zur Struktur-Wirkungsbeziehung des promiskuitiven Kinaseinhibitors **23** zeigten, dass es möglich ist Selektivität innerhalb des gesamten Kinoms zu erlangen und die Potenz für die gewünschte Kinase durch geringfügige strukturelle Veränderungen zu beeinflussen.

Im Rahmen dieser Arbeit ist es gelungen, neue makrozyklische Kinaseinhibitoren zu synthetisieren und darüber hinaus mehrere neue Verbindungen zu entwickeln, die die biologischen Funktionen ihrer Zielkinasen näher beleuchten und die spezifische Hemmung von teilweise unerforschten Kinasen ermöglichen.

7. Experimental procedure

7.1. General

All reactions in this work were carried out under an argon atmosphere at 25 °C. Distillations which were described as „removed under reduced pressure“ were carried out with a rotary evaporator with a membrane pump at 50 °C. Solids were dried in a vacuum drying oven at 40 °C. The molecular weights in brackets () refer to the natural isotope distribution.

7.2. Chemicals and solvents

All used chemicals and solvents were purchased from commercial suppliers like Abcr, Activate Scientific, Acros Organics, Alfa Aesar, BLD Pharm, Carl Roth, Enamine, Fischer Scientific, Fluorochem, Merck, Sigma Aldrich, TCI Europe and VWR. They were used without further purification. Deuterated solvents for NMR measurements were purchased from Eurisotop.

7.3. Thin-layer chromatography (TLC)

For the thin-layer chromatography, silica gel coated aluminium plates from Macherey-Nagel (TLC silica gel 60 F254 plates) were used. Ultraviolet light with 2 different wavelength λ= 254 nm and λ = 365 nm was used for the detection. In addition, ninhydrin solution (1.5 g Ninhydrin, 15 mL glacial acetic acid, 500 mL MeOH) was used as staining reagent for the detections of amines.

7.4. Column chromatography

Column purification of the compounds was done by flash chromatography. A puriFlash XS 420 device with a UV-VIS multiwave detector (200−400 nm) from Interchim was used with pre-packed normal-phase PF-SIHP silica columns with particle sizes of 15, 30 and 50 µm and RP C18 columns (Interchim).

Preparative purification by HPLC was carried out on an Agilent 1260 Infinity II device using an Eclipse XDB-C18 (Agilent, 21.2 x 250mm, 7µm) reversed phase column. A suitable gradient (98:2-5:95 over 31 min, flow rate 21 ml/min.) was used, with 0.1% TFA in water (A) and 0.1% TFA in acetonitrile (B), as a mobile phase.

7.5. High performance liquid chromatography (HPLC)

The purity of the final compounds was determined by HPLC using an Agilent 1260 Infinity II device with a 1260 DAD HS detector (G7117C; 254 nm, 280 nm, 310 nm) and a LC/MSD device (G6125B, ESI pos. 100–1000). The compounds were analyzed on a Poroshell 120 EC–C18 (Agilent, 3 x 150 mm, 2.7 µm) reversed phase column using 0.1% formic acid in water (A) and 0.1% formic acid in acetonitrile (B) as a mobile phase. The following gradient was used: 0 min 5% B – 2 min 5% B – 8 min 98% B – 10 min 98% B (flow rate of 0.5 mL/min). Also an Agilent 1260 Infinity II device, with a 1260 MWD detector (G7165A; 254 nm, 280 nm) and a LC/MSD device (G6125B, ESI pos. 100–1000) was used. The compounds were analyzed on an Eclipse XDB-C18 (Agilent, 4.6 x 250mm, 5µm) reversed phase column using 0.1% TFA in water (A) and 0.1% TFA in acetonitrile (B) as a mobile phase. The following gradient was used: 0 min. 2% B – 2 min. 2% B – 10 min. 98% B – 15 min. 98% B – 17 min. 2% B – 19 min. 2% B (flow rate of 1 mL/min.). UV-detection was performed at 254, 280 and 310 nm and all compounds used for further biological characterizations showed a purity ≥95%.

7.6. Nuclear magnetic resonance (NMR) spectroscopy

The NMR spectroscopy was performed with DPX250, AV300, AV400, AV500 or DRX600 MHz spectrometers from Bruker. Chemical shifts (δ) are reported in parts per million (ppm). DMSO-d6, chloroform-d and methylene chloride-d2 were used as a solvent, and the spectra were calibrated to the solvent signal: 2.50 ppm (1H NMR) or 39.52 ppm (13C NMR) for DMSO-d6, 7.26 ppm (1H NMR) or 77.16 ppm (13C NMR) for chloroform-d and 5.32 ppm (1H NMR) or 54.00 ppm (13C NMR) for methylene chloride-d2. Coupling constants (J) were reported in hertz (Hz) and multiplicities were designated as followed: s (singlet), d (doublet), dd (doublet of doublet), t (triplet), dt (doublet of triplets), td (triplet of doublets), q (quartet), m (multiplet). The spectra were evaluated with MestReNova from Mestrelab Research SL.

7.7. Mass spectrometry

Mass spectra were measured on a Surveyor MSQ device from ThermoFisher measuring in the positive- or negative-ion mode or directly from TLC using TLC-MS interface 2 from Camag. Final compounds were additionally characterized by HRMS using a MALDI LTQ Orbitrap XL from ThermoScientific.

7.8. DSF

Recombinant protein kinase domains with a concentration of 2 µM were mixed with a 10 µM compound solution in DMSO, 20 mM HEPES, pH 7.5, and 500 mM NaCl. SYPRO Orange (5000×, Invitrogen) was used as a fluorescence probe (1 µL per mL). Subsequently, temperature-dependent protein unfolding profiles were measured, using the QuantStudio™ 5 realtime PCR machine (Thermo Fisher). Excitation and emission filters were set to 465 nm and 590 nm. The temperature was raised with 3 °C steps per minute. Data points were analyzed with the internal software (Thermal Shift Software^{TM} Version 1.4, Thermo Fisher) using the Boltzmann equation to determine the inflection point of the transition curve. Differences in melting temperature are given as ΔTm values in °C. Measurements were performed in duplicates and were done by L. Elson, B.T. Berger and A. Krämer from the SGC, Buchmann Institute for Life Science, Max-von-Laue-Straße 15, D-60438 Frankfurt am Main.

7.9. Selectivity screen

The kinome wide selectivity was determined, using the KINOMEscan® kinase assay panel from Eurofins, Fremont, CA 94538, United States. The compounds were screened against 468 recombinant human protein kinases including the mutants. Selectivity scores (S) were calculated according to the following equation: $S(x)= \frac{\text{number of values} \leq x}{\text{total number of values}}$, x represents the activity/%ctrl. threshold.

7.10. Experimental part of Chapter 3

7.10.1. Synthesis of quinazoline-based macrocycles

Synthesis of 4-((2-hydroxyphenyl)amino)-7-methoxyquinazolin-6-ol (25a)

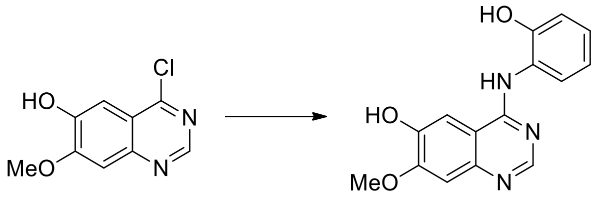

4-chloro-7methoxyquinazolin-6-ol (100 mg, 0.47 mmol, 1.0 eq) and 2-aminophenol (57 mg, 0.52 mmol, 1.1 eq) were dissolved in 7 mL anhydrous ethanol. The mixture was stirred at 70 °C for 17 h. A solid precipitated, which was filtered, washed with ethanol and dried under removed pressure to obtain the product (80 mg, 60%) as a white solid.

^{1}H NMR (400 MHz, DMSO-d6) δ 10.75 (s, 1H), 10.47 (s, 1H), 9.88 (s, 1H), 8.67 (s, 1H), 7.95 (s, 1H), 7.39 (d, J = 2.1 Hz, 1H), 7.32 (dd, J = 7.9, 1.6 Hz, 1H), 7.26 – 7.17 (m, 1H), 7.03 (dd, J = 8.2, 1.5 Hz, 1H), 6.89 (t, J = 7.6 Hz, 1H), 4.01 (s, 3H).

^{13}C NMR (75 MHz, DMSO) δ 155.88, 152.55, 148.33, 128.45, 128.18, 123.90, 118.97, 116.52, 107.44, 107.05, 56.42.

MS-ESI m/z [M + H]$^+$: calcd 284.3, found 284.2.

HRMS m/z [M + H]$^+$: calcd 284.1030, found 284.1035.

HPLC: t_R = 6.27, purity ≥ 95% (UV: 254/ 280 nm).

Synthesis of 4-((3-chloro-2-hydroxyphenyl)amino)-7-methoxyquinazolin-6-ol (25b)

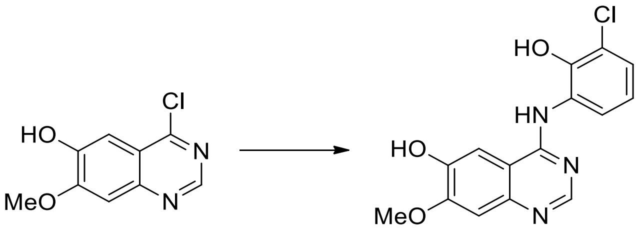

The title compound was prepared according to the procedure of **25a** using 2-amino-6-chlorophenol (75 mg, 0.52 mmol) to obtain the product (137 mg, 91%) as a beige solid.

^{1}H NMR (400 MHz, DMSO-d6) δ 10.94 (s, 1H), 10.52 (s, 1H), 9.90 (s, 1H), 8.70 (s, 1H), 7.97 (s, 1H), 7.40 (dt, J = 6.8, 1.5 Hz, 2H), 7.34 – 7.22 (m, 1H), 6.93 (td, J = 8.0, 1.5 Hz, 1H), 4.02 (s, 3H).

^{13}C NMR (101 MHz, DMSO) δ 156.01, 149.03, 148.32, 148.10, 128.95, 127.42, 125.97, 121.52, 119.71, 107.85, 107.39, 99.73, 56.45.

MS-ESI m/z [M + H]$^+$: calcd 318.7, found 318.1.

HRMS m/z [M + H]$^+$: calcd 318.0640, found 318.0648.

HPLC: t_R = 6.63, purity ≥ 95% (UV: 254/ 280 nm).

Synthesis of 4-((4-chloro-2-hydroxyphenyl)amino)-7-methoxyquinazolin-6-ol (25c)

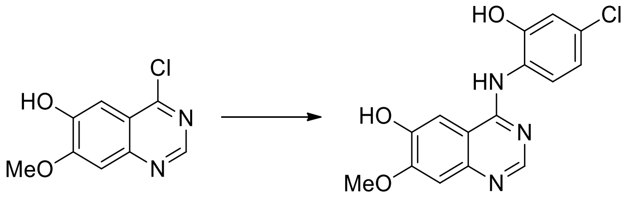

The title compound was prepared according to the procedure of **25a** using 2-amino-5-chlorophenol (75 mg, 0.52 mmol) to obtain the product (100 mg, 66%) as a beige solid.

^{1}H NMR (400 MHz, DMSO-d6) δ 10.78 (s, 1H), 10.52 (s, 2H), 8.69 (s, 1H), 7.93 (s, 1H), 7.56 – 7.26 (m, 2H), 7.09 (d, J = 2.3 Hz, 1H), 6.95 (dd, J = 8.4, 2.3 Hz, 1H), 4.01 (s, 3H).

^{13}C NMR (101 MHz, DMSO) δ 156.04, 153.66, 148.43, 132.03, 129.58, 123.19, 118.82, 116.21, 107.43, 106.96, 56.44.

MS-ESI m/z [M + H]$^+$: calcd 318.7, found 318.1.

HRMS m/z [M + H]$^+$: calcd 318.0640, found 318.0647.

HPLC: t_R = 6.74, purity ≥ 95% (UV: 254/ 280 nm).

Synthesis of 4-((5-chloro-2-hydroxyphenyl)amino)-7-methoxyquinazolin-6-ol (25d)

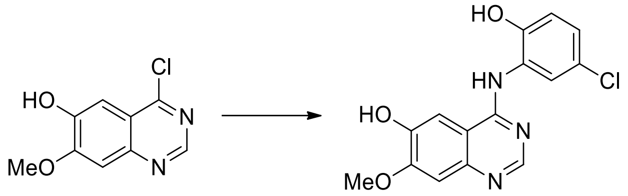

The title compound was prepared according to the procedure of **25a** using 2-amino-4-chlorophenol (75 mg, 0.52 mmol) to obtain the product (128 mg, 85%) as a beige solid.

^{1}H NMR (400 MHz, DMSO-d6) δ 10.78 (s, 1H), 10.54 (s, 1H), 10.26 (s, 1H), 8.73 (s, 1H), 7.93 (s, 1H), 7.47 (d, J = 2.6 Hz, 1H), 7.38 (d, J = 3.0 Hz, 1H), 7.25 (dd, J = 8.7, 2.6 Hz, 1H), 7.05 (d, J = 8.7 Hz, 1H), 4.02 (s, 3H).

^{13}C NMR (101 MHz, DMSO) δ 156.08, 152.36, 151.59, 148.48, 128.01, 127.68, 121.84, 117.77, 107.49, 106.91, 56.45.

MS-ESI m/z $[M + H]^+$: calcd 318.7, found 318.1.

HRMS m/z $[M + H]^+$: calcd 318.0640, found 318.0644.

HPLC: t_R = 6.76, purity ≥ 95% (UV: 254/ 280 nm).

Synthesis of 4-((2-chloro-6-hydroxyphenyl)amino)-7-methoxyquinazolin-6-ol (25e)

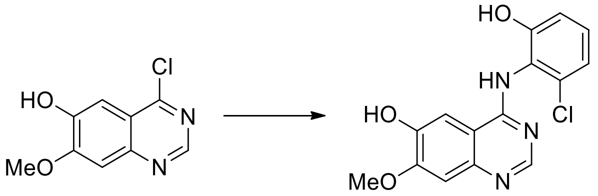

4-chloro-7methoxyquinazolin-6-ol (100 mg, 0.47 mmol, 1.0 eq) and 2-amino-3-chlorophenol (75 mg, 0.52 mmol, 1.1 eq) were dissolved in 7 mL anhydrous ethanol. The mixture was stirred at 70 °C for 17 h. The solvent was evaporated under reduced pressure and the crude product was purified by flash chromatography using DCM/ methanol as an eluent to obtain the product (79 mg, 52%) as a brown solid.

^{1}H NMR (400 MHz, DMSO-d6) δ 9.76 (s, 1H), 9.55 (s, 1H), 8.99 (s, 1H), 8.19 (s, 1H), 7.71 (s, 1H), 7.28 – 7.08 (m, 2H), 6.97 (d, J = 8.0 Hz, 1H), 6.89 (d, J = 8.2 Hz, 1H), 3.96 (s, 3H).

^{13}C NMR (101 MHz, DMSO) δ 157.92, 155.72, 153.68, 152.61, 146.20, 145.88, 133.53, 128.01, 124.32, 119.56, 114.98, 109.34, 106.91, 105.90, 55.81.

MS-ESI m/z $[M + H]^+$: calcd 318.7, found 318.1.

HRMS m/z $[M + H]^+$: calcd 318.0640, found 318.0640.

HPLC: t_R = 6.51, purity ≥ 95% (UV: 254/ 280 nm).

Synthesis of 4-((5-chloro-4-fluoro-2-hydroxyphenyl)amino)-7-methoxyquinazolin-6-ol (25f)

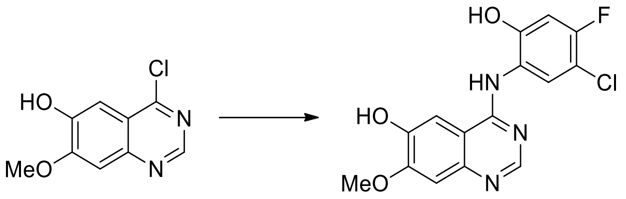

The title compound was prepared according to the procedure of **25a** using 2-amino-4-chloro-5-fluorophenol (127 mg, 0.78 mmol) to obtain the product (239 mg, 100%) as a beige solid.

^{1}H NMR (250 MHz, DMSO-d6) δ 10.79 (s, 2H), 10.55 (s, 1H), 8.73 (s, 1H), 7.92 (s, 1H), 7.60 (d, J = 8.2 Hz, 1H), 7.38 (s, 1H), 7.06 (dd, J = 10.8, 3.6 Hz, 1H), 4.02 (s, 3H).

^{13}C NMR (101 MHz, DMSO) δ 159.23, 156.32 (d, J = 246.3 Hz), 156.11, 153.27 (d, J = 10.5 Hz), 148.48, 148.09, 134.26, 129.41, 121.48 (d, J = 2.9 Hz), 108.12 (d, J = 18.9 Hz), 107.45, 106.95, 104.67 (d, J = 24.0 Hz).99.79, 56.46.

MS-ESI m/z [M + H]$^+$: calcd 335.7, found 336.0.

HRMS m/z [M + H]$^+$: calcd 335.0546, found 335.0546.

HPLC: t_R = 6.97, purity ≥ 95% (UV: 254/ 280 nm).

Synthesis of 1^7-methoxy-4,7,10-trioxa-2-aza-1(4,6)-quinazolina-3(1,2)-benzenacyclodecaphane (26a)

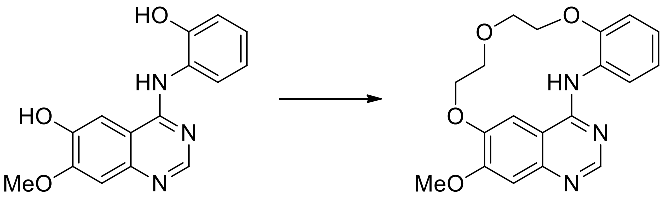

TPP (222 mg, 0.85 mmol, 3.0 eq) and DIAD (171 mg, 0.85 mmol, 3.0 eq) were dissolved in 67 mL anhydrous toluene. After 10 minutes at rt **25a** (80 mg, 0.28 mmol, 1.0 eq) in 6 mL anhydrous THF was added. After additional 20 minutes 2,2'-oxydiethanol (30 mg, 0.28 mmol, 1.0 eq) was added and the mixture was stirred at 40 °C for 20 h. The solvent was evaporated under reduced pressure and the crude product was purified by flash chromatography using DCM/ methanol and *n*-hexane/ ethyl acetate as an eluent to obtain the product (17 mg, 17%) as a white solid.

^{1}H NMR (300 MHz, DMSO-d6) δ 8.87 (s, 1H), 8.61 (s, 1H), 8.50 (dd, J = 8.0, 1.7 Hz, 1H), 8.44 (s, 1H), 7.25 (dd, J = 7.9, 1.5 Hz, 1H), 7.19 (s, 1H), 7.12 (td, J = 7.8, 1.5 Hz, 1H), 7.02 (td, J = 7.7, 1.7 Hz, 1H), 4.59 – 4.53 (m, 2H), 4.26 – 4.20 (m, 2H), 3.98 – 3.92 (m, 5H), 3.90 – 3.85 (m, 2H).

^{13}C NMR (75 MHz, DMSO) δ 155.79, 154.68, 153.30, 148.40, 147.77, 146.30, 131.68, 123.24, 122.41, 118.32, 117.16, 109.38, 106.96, 104.90, 71.92, 71.49, 70.67, 69.36, 55.92.

MS-ESI m/z [M + H]$^+$: calcd 354.4, found 354.2.

HRMS m/z [M + H]$^+$: calcd 354.1448, found 354.1453.

HPLC: t_R = 7.36, purity ≥ 95% (UV: 254/ 280 nm).

Synthesis of 3^3-chloro-1^7-methoxy-4,7,10-trioxa-2-aza-1(4,6)-quinazolina-3(1,2)-benzenacyclodecaphane (26b)

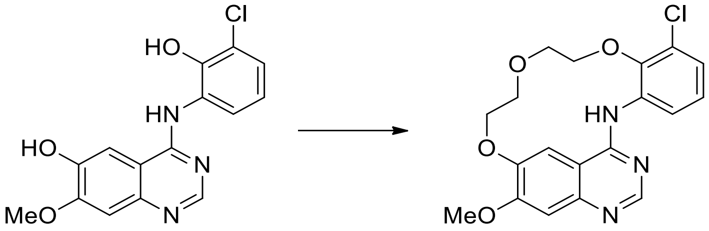

The title compound was prepared according to the procedure of **26a** using **25b** (120 mg, 0.38 mmol) to obtain the product (20 mg, 14%) as a white solid.

^{1}H NMR (250 MHz, DMSO-d6) δ 8.77 – 8.69 (m, 2H), 8.65 – 8.60 (m, 2H), 7.30 – 7.09 (m, 3H), 4.64 – 4.57 (m, 2H), 4.27 – 4.20 (m, 2H), 4.00 – 3.92 (m, 5H), 3.92 – 3.87 (m, 2H).

^{13}C NMR (75 MHz, DMSO) δ 155.81, 155.13, 153.54, 148.69, 146.69, 143.55, 135.17, 126.90, 126.27, 123.31, 118.46, 109.37, 107.38, 105.56, 73.47, 72.18, 70.86, 69.67, 56.47.

MS-ESI m/z [M + H]$^+$: calcd 388.8, found 388.2.

HRMS m/z [M + H]$^+$: calcd 388.1059, found 388.1058.

HPLC: t_R = 7.97, purity ≥ 95% (UV: 254/ 280 nm).

Synthesis of 3^4-chloro-1^7-methoxy-4,7,10-trioxa-2-aza-1(4,6)-quinazolina-3(1,2)-benzenacyclodecaphane (26c)

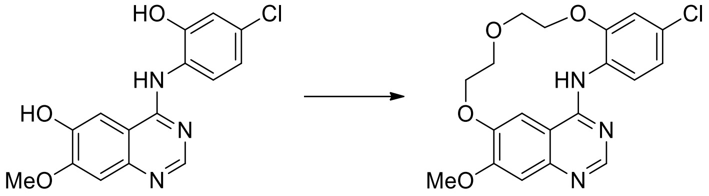

The title compound was prepared according to the procedure of **26a** using **25c** (100 mg, 0.31 mmol) to obtain the product (10 mg, 8%) as a white solid.

^{1}H NMR (300 MHz, DMSO-d6) δ 8.86 (s, 1H), 8.63 (s, 1H), 8.46 (d, J = 8.7 Hz, 1H), 8.43 (s, 1H), 7.41 (d, J = 2.4 Hz, 1H), 7.24 – 7.16 (m, 2H), 4.61 – 4.55 (m, 2H), 4.34 – 4.27 (m, 2H), 3.98 – 3.92 (m, 5H), 3.91 – 3.86 (m, 2H).

^{13}C NMR (75 MHz, DMSO) δ 155.90, 154.92, 153.14, 148.67, 148.50, 130.69, 125.90, 122.90, 119.40, 117.32, 109.45, 106.78, 105.05, 72.02, 71.52, 70.57, 69.20, 55.99.

MS-ESI m/z [M + H]$^+$: calcd 388.8, found 388.2.

HRMS m/z [M + H]$^+$: calcd 388.1059, found 388.1059.

HPLC: t_R = 7.81, purity ≥ 95% (UV: 254/ 280 nm).

Synthesis of 3^5-chloro-1^7-methoxy-4,7,10-trioxa-2-aza-1(4,6)-quinazolina-3(1,2)-benzenacyclodecaphane (26d)

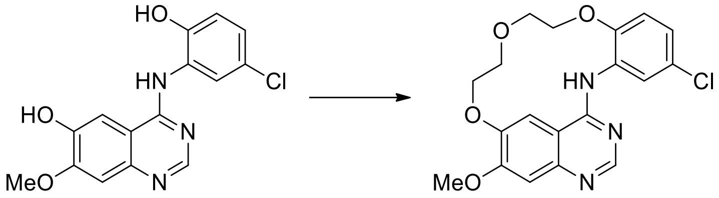

The title compound was prepared according to the procedure of **26a** using **25d** (110 mg, 0.35 mmol) to obtain the product (15 mg, 11%) as a white solid.

^{1}H NMR (300 MHz, DMSO-d6) δ 8.88 (s, 1H), 8.67 (s, 1H), 8.56 (d, J = 2.6 Hz, 1H), 8.45 (s, 1H), 7.29 (d, J = 8.6 Hz, 1H), 7.22 (s, 1H), 7.07 (dd, J = 8.6, 2.6 Hz, 1H), 4.63 – 4.54 (m, 2H), 4.30 – 4.19 (m, 2H), 4.00 – 3.92 (m, 5H), 3.92 – 3.85 (m, 2H).

^{13}C NMR (75 MHz, DMSO) δ 155.55, 154.89, 153.16, 148.54, 146.56, 146.46, 132.93, 126.96, 121.68, 118.70, 117.54, 109.39, 106.97, 104.89, 72.39, 71.46, 70.73, 69.24, 55.98.

MS-ESI m/z [M + H]$^+$: calcd 388.8, found 388.2.

HRMS m/z [M + H]$^+$: calcd 388.1059, found 388.1059.

HPLC: t_R = 7.94, purity ≥ 95% (UV: 254/ 280 nm).

Synthesis of 3^6-chloro-1^7-methoxy-4,7,10-trioxa-2-aza-1(4,6)-quinazolina-3(1,2)-benzenacyclodecaphane (26e)

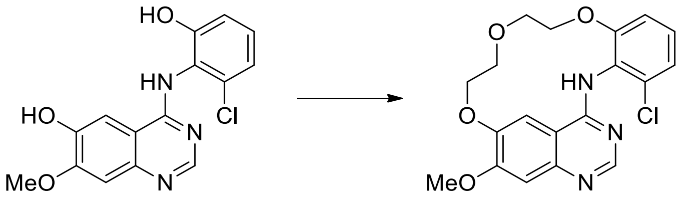

The title compound was prepared according to the procedure of **26a** using **25e** (55 mg, 0.17 mmol) to obtain the product (3 mg, 4%) as a white solid.

^{1}H NMR (500 MHz, DMSO-d6) δ 9.22 (s, 1H), 8.27 (s, 1H), 7.82 (s, 1H), 7.35 (d, J = 8.6 Hz, 1H), 7.22 – 7.06 (m, 3H), 4.19 – 3.74 (m, 9H), 3.53 – 3.45 (m, 2H).

^{13}C NMR (126 MHz, DMSO) δ 158.19, 156.21, 153.88, 153.10, 147.84, 146.35, 133.74, 121.93, 121.30, 120.93, 111.48, 108.50, 106.96, 102.30, 69.41, 69.30, 68.86, 68.54, 55.72.

MS-ESI m/z $[M + H]^+$: calcd 388.8, found 388.3.

HRMS m/z $[M + H]^+$: calcd 388.1059, found 388.1054.

HPLC: t_R = 7.37, purity ≥ 95% (UV: 254/ 280 nm).

Synthesis of 3^5-chloro-3^4-fluoro-1^7-methoxy-4,7,10-trioxa-2-aza-1(4,6)-quinazolina-3(1,2)-benzenacyclodecaphane (26f)

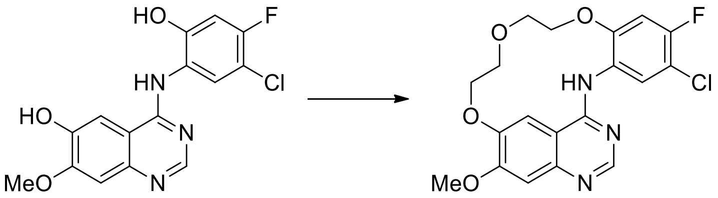

The title compound was prepared according to the procedure of **26a** using **25f** (150 mg, 0.45 mmol) to obtain the product (33 mg, 18%) as a white solid.

^{1}H NMR (250 MHz, DMSO-d6) δ 8.77 (s, 1H), 8.67 (s, 1H), 8.57 (d, J = 8.1 Hz, 1H), 8.41 (s, 1H), 7.50 (d, J = 10.2 Hz, 1H), 7.23 (s, 1H), 4.67 – 4.50 (m, 2H), 4.38 – 4.23 (m, 2H), 3.98 – 3.92 (m, 5H), 3.92 – 3.85 (m, 2H).

^{13}C NMR (126 MHz, DMSO) δ 158.73, 155.98, 154.96, 153.09, 148.47, 129.18, 118.95, 112.23, 109.49, 106.89, 106.64, 106.44, 105.14, 105.12, 72.13, 71.54, 70.41, 69.06, 55.99.

MS-ESI m/z $[M + H]^+$: calcd 405.8, found 406.0.

HRMS m/z $[M + H]^+$: calcd 406.0964, found 406.0946.

HPLC: t_R = 8.28, purity ≥ 95% (UV: 254/ 280 nm).

Synthesis of 4-chloro-6-((6-chlorohexyl)oxy)-7-methoxyquinazoline (34)

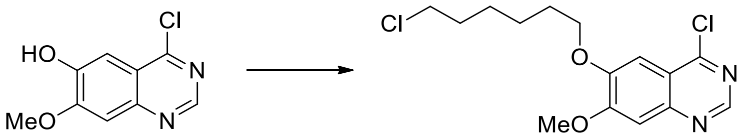

TPP (1.25 g, 4.75 mmol, 2.5 eq) and DIAD (960 mg, 4.75 mmol, 2.5 eq) were dissolved in 80 mL anhydrous toluene. After 15 minutes at rt 6-chloro-1-hexanol (324 mg, 2.37 mmol, 1.25 eq) was added. After additional 20 minutes 4-chloro-7methoxyquinazolin-6-ol (400 mg, 1.90 mmol, 1.0 eq) was added and the mixture was stirred at 80 °C for 3 h. The solvent was evaporated under reduced pressure and the crude product was purified by flash chromatography using DCM/ methanol and *n*-hexane/ ethyl acetate as an eluent to obtain the product (487 mg, 78%) as a white solid with impurities.

1H NMR (300 MHz, DMSO-d6) δ 8.86 (s, 1H), 7.43 (s, 1H), 7.36 (s, 1H), 4.18 (t, J = 6.5 Hz, 2H), 4.01 (s, 3H), 3.65 (t, J = 6.6 Hz, 2H), 1.90 – 1.69 (m, 4H), 1.53 – 1.43 (m, 4H).

MS-ESI m/z [M + H]+: calcd 330.2, found 329.1.

Synthesis of 4-chloro-6-(2-(2-(2-chloroethoxy)ethoxy)ethoxy)-7-methoxyquinazoline (35)

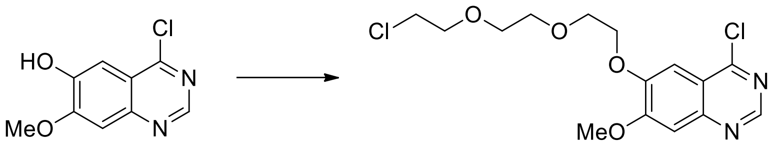

TPP (1.25 g, 4.75 mmol, 2.5 eq) and DIAD (960 mg, 4.75 mmol, 2.5 eq) were dissolved in 80 mL anhydrous toluene. After 15 minutes at rt 2-[2-(2-chloroethoxy)ethoxy]ethanol (400 mg, 2.37 mmol, 1.25 eq) was added. After additional 20 minutes 4-chloro-7methoxyquinazolin-6-ol (400 mg, 1.90 mmol, 1.0 eq) was added and the mixture was stirred at 80 °C for 5 h. The solvent was evaporated under reduced pressure and the crude product was purified by flash chromatography using DCM/ methanol and *n*-hexane/ ethyl acetate as an eluent to obtain the product (520 mg, 76%) as a yellow solid with impurities.

MS-ESI m/z [M + Na]+: calcd 383.1, found 383.2.

Synthesis of 2-((6-((6-chlorohexyl)oxy)-7-methoxyquinazolin-4-yl)amino)phenol (36a)

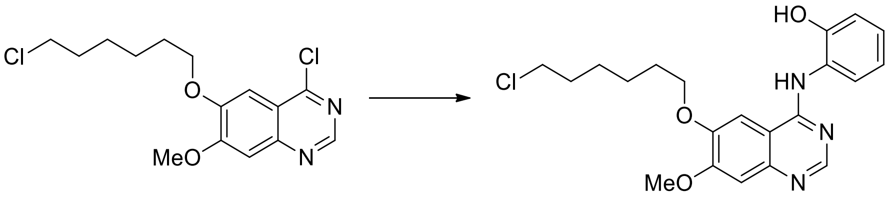

34 (124 mg, 0.38 mmol, 1.0 eq) and 2-aminophenol (41 mg, 0.38 mmol, 1.0 eq) were dissolved in 10 mL anhydrous ethanol. The mixture was stirred at 70 °C for 18 h. The solvent was evaporated under reduced pressure and the crude product was purified by flash chromatography using DCM/ methanol as an eluent to obtain the product (105 mg, 70%) as a brown oil.

^{1}H NMR (300 MHz, DMSO-d6) δ 10.81 (s, 1H), 8.65 (s, 1H), 8.17 (s, 1H), 7.38 – 7.28 (m, 2H), 7.20 (t, J = 7.7 Hz, 1H), 7.03 (d, J = 8.0 Hz, 1H), 6.89 (t, J = 7.5 Hz, 1H), 4.17 (t, J = 6.5 Hz, 2H), 3.98 (s, 3H), 3.65 (t, J = 6.5 Hz, 2H), 1.91 – 1.69 (m, 4H), 1.57 – 1.42 (m, 4H).

^{13}C NMR (75 MHz, DMSO) δ 158.83, 155.96, 152.44, 149.21, 149.06, 136.70, 128.27, 128.15, 124.07, 119.00, 116.69, 107.17, 104.28, 100.82, 69.12, 56.34, 45.35, 31.95, 28.26, 26.00, 24.80.

MS-ESI m/z [M + H]$^+$: calcd 402.9, found 402.1.

HRMS m/z [M + H]$^+$: calcd 402.1579, found 402.1693.

HPLC: t_R = 8.00, purity ≥ 95% (UV: 254/ 280 nm).

Synthesis of 2-chloro-6-((6-((6-chlorohexyl)oxy)-7-methoxyquinazolin-4-yl)amino)phenol (36b)

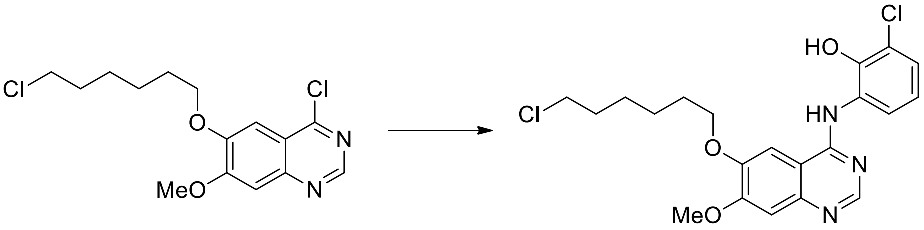

34 (124 mg, 0.38 mmol, 1.0 eq) and 2-amino-6-chlorophenol (54 mg, 0.38 mmol, 1.0 eq) were dissolved in 10 mL anhydrous ethanol. The mixture was stirred at 70 °C for 18 h. A solid precipitated, which was filtered, washed with ethanol and dried under reduced pressure to obtain the product (107 mg, 65%) as a beige solid.

^{1}H NMR (300 MHz, DMSO-d6) δ 11.30 (s, 1H), 9.90 (s, 1H), 8.75 (s, 1H), 8.28 (s, 1H), 7.48 – 7.37 (m, 2H), 7.30 (dd, J = 7.9, 1.6 Hz, 1H), 6.95 (t, J = 8.0 Hz, 1H), 4.21 (t, J = 6.5 Hz, 2H), 4.00 (s, 3H), 3.65 (t, J = 6.6 Hz, 2H), 1.97 – 1.69 (m, 4H), 1.56 – 1.42 (m, 4H).

^{13}C NMR (75 MHz, DMSO) δ 159.63, 156.38, 149.41, 148.92, 148.62, 129.00, 127.38, 125.86, 121.69, 119.79, 107.36, 104.88, 99.66, 69.30, 56.48, 45.36, 31.95, 28.22, 26.00, 24.80.

MS-ESI m/z $[M + H]^+$: calcd 437.3, found 437.1.

HRMS m/z $[M + H]^+$: calcd 436.1189, found 436.1187.

HPLC: t_R = 8.34, purity ≥ 95% (UV: 254/ 280 nm).

Synthesis of 5-chloro-2-((6-((6-chlorohexyl)oxy)-7-methoxyquinazolin-4-yl)amino)phenol (36c)

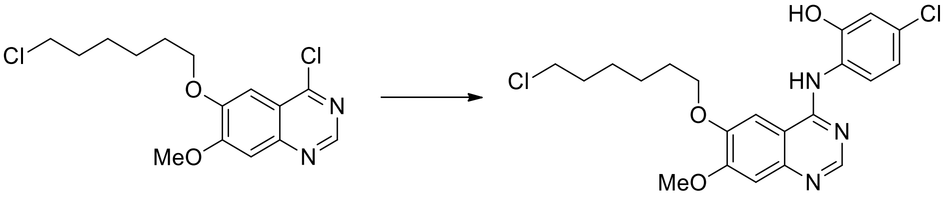

The title compound was prepared according to the procedure of **36a** using **34** (132 mg, 0.40 mmol) and 2-amino-5-chlorophenol (58 mg, 0.40 mmol) to obtain the product (156 mg, 89%) as a beige solid.

^{1}H NMR (300 MHz, DMSO-d6) δ 11.00 (s, 1H), 10.52 (s, 1H), 8.71 (s, 1H), 8.19 (s, 1H), 7.41 – 7.32 (m, 2H), 7.11 (d, J = 2.2 Hz, 1H), 6.96 (dd, J = 8.4, 2.3 Hz, 1H), 4.18 (t, J = 6.5 Hz, 2H), 3.99 (s, 3H), 3.65 (t, J = 6.5 Hz, 2H), 1.90 – 1.69 (m, 4H), 1.61 – 1.42 (m, 4H).

^{13}C NMR (75 MHz, DMSO) δ 159.08, 156.27, 153.64, 149.41, 148.64, 131.99, 129.63, 123.10, 118.87, 116.32, 107.02, 104.36, 100.08, 69.20, 56.43, 45.34, 31.94, 28.23, 25.99, 24.79.

MS-ESI m/z $[M + H]^+$: calcd 437.3, found 436.3.

HRMS m/z $[M + H]^+$: calcd 436.1189, found 436.1190.

HPLC: t_R = 8.28, purity ≥ 95% (UV: 254/ 280 nm).

Synthesis of 4-chloro-2-((6-((6-chlorohexyl)oxy)-7-methoxyquinazolin-4-yl)amino)phenol (36d)

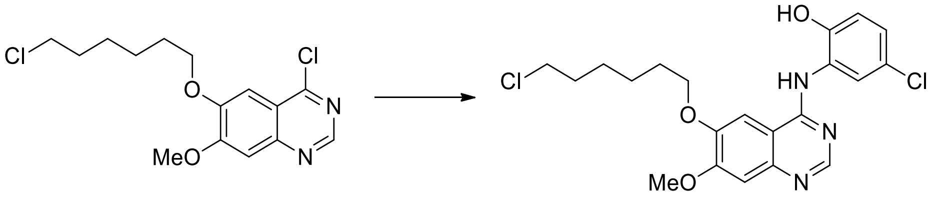

The title compound was prepared according to the procedure of **36a** using **34** (132 mg, 0.40 mmol) and 2-amino-4-chlorophenol (58 mg, 0.40 mmol) to obtain the product (172 mg, 98%) as a yellow solid.

^{1}H NMR (300 MHz, DMSO-d6) δ 11.01 (s, 1H), 10.30 (s, 1H), 8.73 (s, 1H), 8.20 (s, 1H), 7.45 (d, J = 2.6 Hz, 1H), 7.37 (s, 1H), 7.25 (dd, J = 8.7, 2.7 Hz, 1H), 7.06 (d, J = 8.7 Hz, 1H), 4.18 (t, J = 6.5 Hz, 2H), 3.99 (s, 3H), 3.65 (t, J = 6.6 Hz, 2H), 1.91 – 1.73 (m, 4H), 1.57 – 1.41 (m, 4H).

^{13}C NMR (75 MHz, DMSO) δ 158.96, 156.26, 151.58, 149.40, 148.84, 136.04, 127.97, 127.79, 125.19, 121.87, 117.93, 107.13, 104.35, 100.27, 69.21, 56.42, 45.35, 31.95, 28.25, 26.00, 24.81.

MS-ESI m/z [M + H]$^+$: calcd 437.3, found 436.3.

HRMS m/z [M + H]$^+$: calcd 436.1189, found 436.1188.

HPLC: t_R = 8.35, purity ≥ 95% (UV: 254/ 280 nm).

Synthesis of 3-chloro-2-((6-((6-chlorohexyl)oxy)-7-methoxyquinazolin-4-yl)amino)phenol (36e)

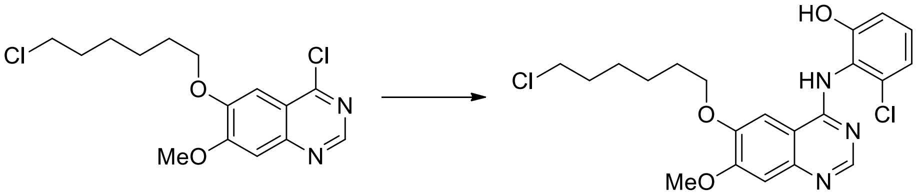

The title compound was prepared according to the procedure of **36a** using **34** (132 mg, 0.40 mmol) and 2-amino-3-chlorophenol (58 mg, 0.40 mmol) to obtain the product (87 mg, 50%) as a brown solid.

^{1}H NMR (300 MHz, DMSO-d6) δ 11.06 (s, 1H), 10.41 (s, 1H), 8.73 (s, 1H), 8.22 (s, 1H), 7.43 (s, 1H), 7.26 (t, J = 8.1 Hz, 1H), 7.06 (s, 1H), 7.04 (s, 1H), 4.19 (t, J = 6.5 Hz, 2H), 4.00 (s, 3H), 3.65 (t, J = 6.5 Hz, 2H), 1.87 – 1.72 (m, 4H), 1.57 – 1.42 (m, 4H).

^{13}C NMR (75 MHz, DMSO) δ 159.67, 156.48, 155.19, 149.59, 148.76, 135.43, 132.44, 129.50, 121.75, 119.62, 115.33, 106.73, 104.22, 99.91, 69.22, 56.49, 45.33, 31.94, 28.22, 25.98, 24.76.

MS-ESI m/z $[M + H]^+$: calcd 437.3, found 436.3.

HRMS m/z $[M + H]^+$: calcd 436.1189, found 436.1187.

HPLC: t_R = 8.14, purity ≥ 95% (UV: 254/ 280 nm).

Synthesis of 4-chloro-2-((6-((6-chlorohexyl)oxy)-7-methoxyquinazolin-4-yl)amino)-5-fluorophenol (36f)

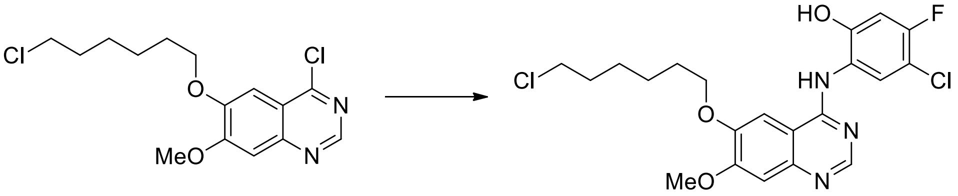

The title compound was prepared according to the procedure **36a** using **34** (123 mg, 0.37 mmol) and 2-amino-4-chloro-5-fluorophenol (60 mg, 0.37 mmol) to obtain the product (155 mg, 92%) as a brown solid.

^{1}H NMR (300 MHz, DMSO-d6) δ 11.02 (s, 2H), 8.72 (s, 1H), 8.20 (s, 1H), 7.57 (d, J = 8.0 Hz, 1H), 7.36 (s, 1H), 7.07 (d, J = 10.8 Hz, 1H), 4.17 (t, J = 6.3 Hz, 2H), 3.98 (s, 3H), 3.65 (t, J = 6.4 Hz, 2H), 1.92 – 1.69 (m, 4H), 1.57 – 1.40 (m, 4H).

^{13}C NMR (75 MHz, DMSO) δ 159.13, 156.19, 156.18 (d, J = 246.0 Hz), 153.13 (d, J = 10.5 Hz), 149.33, 148.82, 136.05, 129.33, 121.45 (d, J = 2.9 Hz), 108.10 (d, J = 19.0 Hz), 107.05, 104.69 (d, J = 24.0 Hz), 104.31, 100.24, 69.21, 56.38, 45.32, 31.93, 28.22, 25.98, 24.77.

MS-ESI m/z $[M + H]^+$: calcd 455.3, found 454.3.

HRMS m/z $[M + H]^+$: calcd 454.1095, found 454.1094.

HPLC: t_R = 8.42, purity ≥ 95% (UV: 254/ 280 nm).

Synthesis of 2-((6-(2-(2-(2-chloroethoxy)ethoxy)ethoxy)-7-methoxyquinazolin-4-yl)amino)phenol (37a)

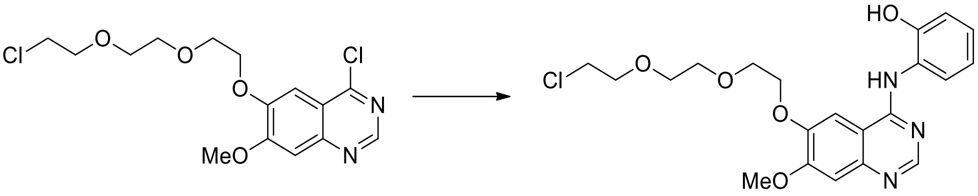

The title compound was prepared according to the procedure of **36b** using **35** (200 mg, 0.55 mmol) and 2-aminophenol (60 mg, 0.55 mmol) to obtain the product (105 mg, 44%) as a yellow solid.

^{1}H NMR (250 MHz, DMSO-d6) δ 11.09 (s, 1H), 9.90 (s, 1H), 8.71 (s, 1H), 8.28 (s, 1H), 7.44 – 7.26 (m, 2H), 7.22 (t, J = 7.7 Hz, 1H), 7.04 (d, J = 7.9 Hz, 1H), 6.90 (t, J = 7.5 Hz, 1H), 4.32 (t, J = 4.7 Hz, 2H), 3.99 (s, 3H), 3.88 (t, J = 4.6 Hz, 2H), 3.75 – 3.56 (m, 8H).

^{13}C NMR (75 MHz, DMSO) δ 156.23, 152.56, 149.20, 147.79, 145.57, 128.61, 128.27, 123.63, 119.04, 116.64, 107.67, 106.90, 70.56, 69.95, 69.69, 68.74, 68.45, 56.44, 43.57.

MS-ESI m/z $[M + H]^+$: calcd 434.2, found 434.2.

HRMS m/z $[M + H]^+$: calcd 434.1477, found 434.1476.

HPLC: t_R = 7.19, purity ≥ 95% (UV: 254/ 280 nm).

Synthesis of 2-chloro-6-((6-(2-(2-(2-chloroethoxy)ethoxy)ethoxy)-7-methoxyquinazolin-4-yl)amino)phenol (37b)

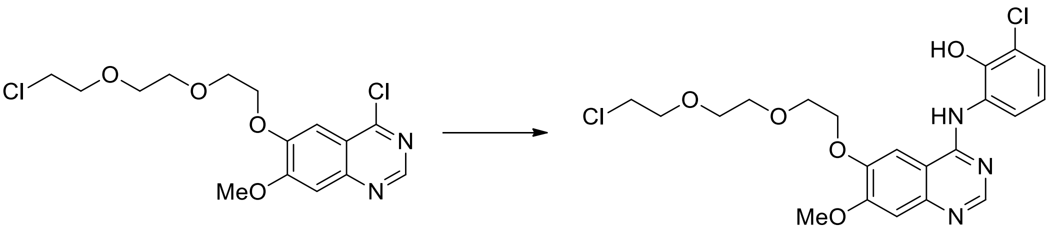

The title compound was prepared according to the procedure of **36b** using **35** (246 mg, 0.68 mmol) and 2-amino-6-chlorophenol (98 mg, 0.68 mmol) to obtain the product (88 mg, 28%) as a pale green solid.

^{1}H NMR (300 MHz, DMSO-d6) δ 11.37 (s, 1H), 9.90 (s, 1H), 8.75 (s, 1H), 8.36 (s, 1H), 7.48 – 7.39 (m, 2H), 7.30 (dd, J = 7.9, 1.6 Hz, 1H), 6.94 (t, J = 8.0 Hz, 1H), 4.35 (t, J = 4.5 Hz, 2H), 4.00 (s, 3H), 3.88 (t, J = 4.7 Hz, 2H), 3.75 – 3.59 (m, 8H).

^{13}C NMR (75 MHz, DMSO) δ 159.64, 156.31, 149.17, 148.87, 148.68, 135.21, 128.97, 127.33, 125.86, 121.70, 119.79, 107.33, 105.11, 99.71, 70.56, 69.95, 69.67, 68.91, 68.45, 56.47, 43.58.

MS-ESI m/z $[M + H]^+$: calcd 468.1, found 468.1.

HRMS m/z $[M + H]^+$: calcd 468.1088, found 468.1092.

HPLC: t_R = 7.50, purity ≥ 95% (UV: 254/ 280 nm).

Synthesis of 5-chloro-2-((6-(2-(2-(2-chloroethoxy)ethoxy)ethoxy)-7-methoxyquinazolin-4-yl)amino)phenol (37c)

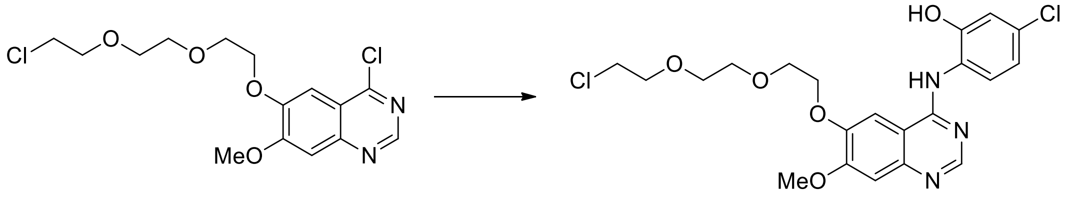

The title compound was prepared according to the procedure of **36a** using **35** (246 mg, 0.68 mmol) and 2-amino-5-chlorophenol (98 mg, 0.68 mmol) to obtain the product (130 mg, 41%) as a pale yellow solid.

^{1}H NMR (300 MHz, DMSO-d6) δ 11.10 (s, 1H), 10.54 (s, 1H), 8.73 (s, 1H), 8.26 (s, 1H), 7.42 – 7.31 (m, 2H), 7.11 (d, J = 2.3 Hz, 1H), 6.95 (dd, J = 8.4, 2.3 Hz, 1H), 4.32 (t, J = 4.5 Hz, 2H), 4.00 (s, 3H), 3.88 (d, J = 4.7 Hz, 2H), 3.77 – 3.58 (m, 8H).

^{13}C NMR (75 MHz, DMSO) δ 159.36, 156.28, 153.66, 149.24, 148.79, 132.07, 129.63, 123.02, 118.86, 116.32, 106.94, 104.63, 99.92, 70.56, 69.95, 69.68, 68.80, 68.45, 56.45, 43.57.

MS-ESI m/z $[M + H]^+$: calcd 468.1, found 468.2.

HRMS m/z $[M + H]^+$: calcd 468.1088, found 468.1102.

HPLC: t_R = 7.54, purity ≥ 95% (UV: 254/ 280 nm).

Synthesis of 4-chloro-2-((6-(2-(2-(2-chloroethoxy)ethoxy)ethoxy)-7-methoxyquinazolin-4-yl)amino)phenol (37d)

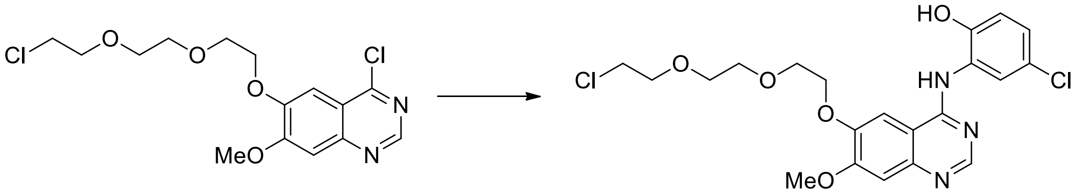

The title compound was prepared according to the procedure of **36b** using **35** (246 mg, 0.68 mmol) and 2-amino-4-chlorophenol (98 mg, 0.68 mmol) to obtain the product (104 mg, 33%) as a yellow solid.

^{1}H NMR (300 MHz, DMSO-d6) δ 11.18 (s, 1H), 10.27 (s, 1H), 8.77 (s, 1H), 8.29 (s, 1H), 7.48 – 7.35 (m, 2H), 7.26 (dt, J = 8.8, 2.2 Hz, 1H), 7.11 – 7.02 (m, 1H), 4.32 (t, J = 4.9 Hz, 2H), 4.00 (s, 3H), 3.88 (t, J = 4.6 Hz, 2H), 3.74 – 3.57 (m, 8H).

^{13}C NMR (75 MHz, DMSO) δ 159.21, 156.37, 151.68, 149.28, 148.82, 129.03, 128.18, 127.87, 124.96, 121.87, 117.94, 106.98, 104.68, 70.56, 69.95, 69.68, 68.83, 68.45, 56.47, 43.57.

MS-ESI m/z $[M + H]^+$: calcd 468.1, found 468.2.

HRMS m/z $[M + H]^+$: calcd 468.1088, found 468.1105.

HPLC: t_R = 7.58, purity ≥ 95% (UV: 254/ 280 nm).

Synthesis of 3-chloro-2-((6-(2-(2-(2-chloroethoxy)ethoxy)ethoxy)-7-methoxyquinazolin-4-yl)amino)phenol (37e)

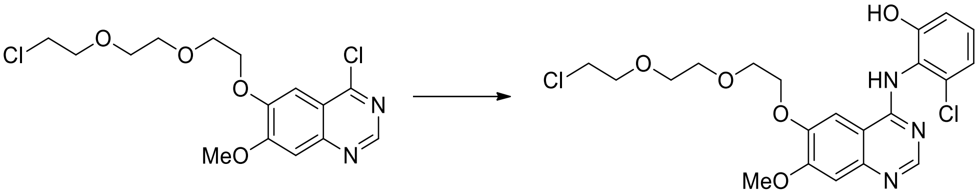

The title compound was prepared according to the procedure of **36a** using **35** (200 mg, 0.55 mmol) and 2-amino-3-chlorophenol (82 mg, 0.55 mmol) to obtain the product (119 mg, 46%) as a yellow solid.

^{1}H NMR (300 MHz, DMSO-d6) δ 11.12 (s, 1H), 10.41 (s, 1H), 8.76 (s, 1H), 8.27 (s, 1H), 7.45 – 7.39 (m, 1H), 7.27 (t, J = 8.0 Hz, 1H), 7.10 – 7.00 (m, 2H), 4.33 (t, J = 4.3 Hz, 2H), 4.01 (s, 3H), 3.89 (t, J = 4.8 Hz, 2H), 3.74 – 3.58 (m, 8H).

^{13}C NMR (75 MHz, DMSO) δ 159.80, 156.52, 155.15, 149.43, 148.80, 135.18, 132.38, 129.58, 121.65, 119.66, 115.35, 106.62, 104.45, 99.83, 70.55, 69.94, 69.68, 68.77, 68.43, 56.52, 43.56.

MS-ESI m/z $[M + H]^+$: calcd 468.1, found 468.2.

HRMS m/z $[M + H]^+$: calcd 468.1088, found 468.1089.

HPLC: t_R = 7.36, purity ≥ 95% (UV: 254/ 280 nm).

Synthesis of 4-chloro-2-((6-(2-(2-(2-chloroethoxy)ethoxy)ethoxy)-7-methoxyquinazolin-4-yl)amino)-5-fluorophenol (37f)

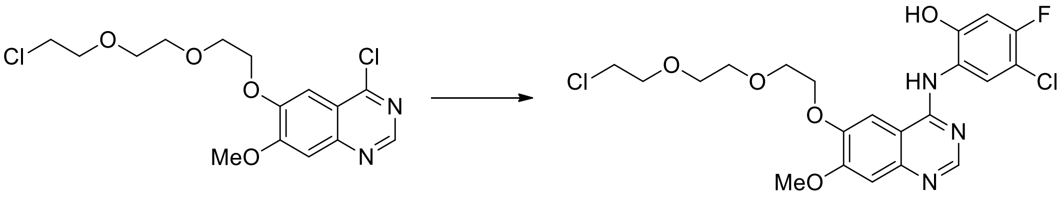

The title compound was prepared according to the procedure of **36a** using **35** (109 mg, 0.30 mmol) and 2-amino-4-chloro-5-fluorophenol (49 mg, 0.30 mmol) to obtain the product (117 mg, 80%) as a brown solid with impurities. It was used without further purification.

MS-ESI m/z [M + H]+: calcd 487.3, found 486.3.

Synthesis of ^{1}7-methoxy-4,11-dioxa-2-aza-1(4,6)-quinazolina-3(1,2)-benzenacycloundecaphane (38a)

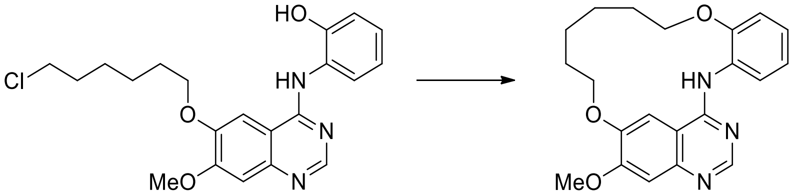

To a stirred solution of **36a** (93 mg, 0.23 mmol, 1.0 eq) in 93 mL anhydrous DMF, NaH (28 mg, 0.69 mmol, 3.0 eq, 60% dispersion in oil) was added at 0 °C. The mixture was stirred for 10 minutes at 0 °C and another 24 h at 60 °C. The reaction was quenched with methanol and H_2O and was neutralized with a 4 M HCl solution. The crude product was purified by flash chromatography using DCM/ methanol as an eluent to obtain the product (62 mg, 73%) as a orange solid.

^{1}H NMR (300 MHz, DMSO-d6) δ 8.72 (s, 1H), 8.56 (s, 1H), 8.54 – 8.49 (m, 1H), 7.49 (s, 1H), 7.21 (s, 1H), 7.08 – 6.99 (m, 3H), 4.46 – 4.35 (m, 2H), 4.14 – 4.06 (m, 2H), 3.93 (s, 3H), 1.97 – 1.73 (m, 6H), 1.52 – 1.37 (m, 2H).

^{13}C NMR (75 MHz, DMSO) δ 155.34, 154.68, 152.96, 148.77, 147.66, 145.74, 128.66, 123.20, 120.56, 120.39, 111.60, 108.87, 107.24, 100.96, 68.46, 67.30, 55.88, 29.59, 24.41, 24.24, 22.86.

MS-ESI m/z [M + H]$^+$: calcd 366.4, found 366.3.

HRMS m/z [M + H]$^+$: calcd 366.1812, found 366.1814.

HPLC: t_R = 8.17, purity ≥ 95% (UV: 254/ 280 nm).

Synthesis of 3^3-chloro-1^7-methoxy-4,11-dioxa-2-aza-1(4,6)-quinazolina-3(1,2)-benzenacycloundecaphane (38b)

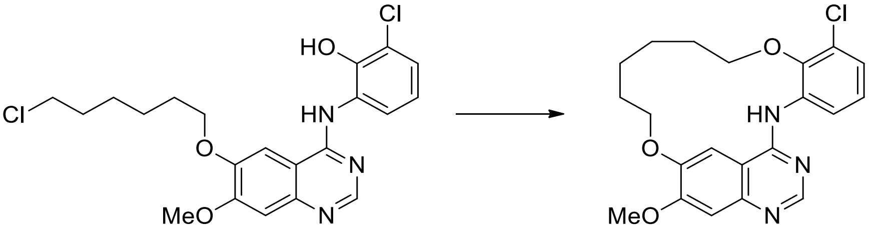

The title compound was prepared according to the procedure of **38a** using **36b** (97 mg, 0.22 mmol) to obtain the product (54 mg, 61%) as a white solid.

^{1}H NMR (300 MHz, CD2Cl2) δ 9.03 (dd, J = 8.1, 1.7 Hz, 1H), 8.66 (s, 1H), 8.42 (s, 1H), 7.23 (s, 1H), 7.16 – 6.99 (m, 3H), 4.48 – 4.38 (m, 2H), 4.34 (t, J = 5.0 Hz, 2H), 3.99 (s, 3H), 2.07 – 1.83 (m, 6H), 1.72 – 1.58 (m, 2H).

^{13}C NMR (75 MHz, CD2Cl2) δ 155.64, 155.56, 153.66, 149.20, 147.49, 145.94, 134.85, 126.44, 125.22, 123.70, 118.28, 109.76, 108.78, 99.43, 76.38, 67.56, 56.71, 31.98, 25.71, 25.58, 24.74.

MS-ESI m/z [M + H]$^+$: calcd 400.9, found 400.3.

HRMS m/z [M + H]$^+$: calcd 400.1423, found 400.1422.

HPLC: t_R = 8.90, purity ≥ 95% (UV: 254/ 280 nm).

Synthesis of 3^4-chloro-1^7-methoxy-4,11-dioxa-2-aza-1(4,6)-quinazolina-3(1,2)-benzenacycloundecaphane (38c)

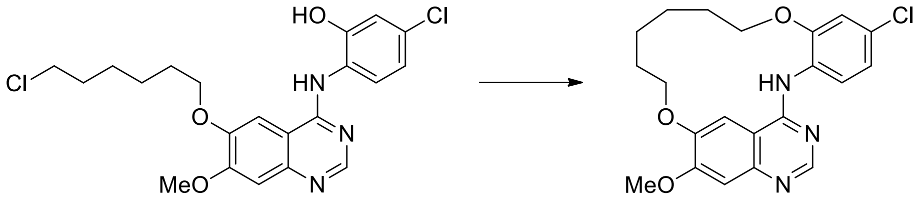

The title compound was prepared according to the procedure of **38a** using **36c** (146 mg, 0.33 mmol) to obtain the product (63 mg, 47%) as an orange solid.

^{1}H NMR (300 MHz, CD2Cl2) δ 8.74 (d, J = 8.7 Hz, 1H), 8.63 (s, 1H), 8.41 (s, 1H), 7.20 (s, 1H), 7.16 (s, 1H), 7.03 (dd, J = 8.6, 2.3 Hz, 1H), 6.91 (d, J = 2.3 Hz, 1H), 4.40 – 4.29 (m, 2H), 4.14 (t, J = 4.5 Hz, 2H), 3.98 (s, 3H), 2.08 – 1.82 (m, 6H), 1.69 – 1.49 (m, 2H).

^{13}C NMR (75 MHz, CD2Cl2) δ 155.59, 155.46, 154.05, 149.53, 148.77, 147.19, 128.84, 127.14, 121.52, 119.44, 112.18, 109.95, 108.62, 99.86, 69.70, 69.56, 56.71, 30.70, 25.65, 25.48, 23.77.

MS-ESI m/z [M + H]$^+$: calcd 400.9, found 400.4.

HRMS m/z [M + H]$^+$: calcd 400.1423, found 400.1423.

HPLC: t_R = 8.80, purity ≥ 95% (UV: 254/ 280 nm).

Synthesis of 3^5-chloro-1^7-methoxy-4,11-dioxa-2-aza-1(4,6)-quinazolina-3(1,2)-benzenacycloundecaphane (38d)

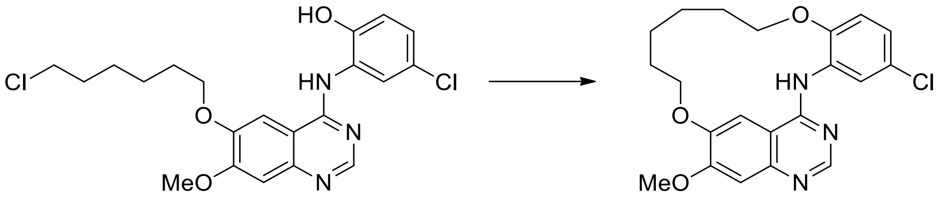

The title compound was prepared according to the procedure of **38a** using **36d** (162 mg, 0.37 mmol) to obtain the product (52 mg, 35%) as a brown solid.

^{1}H NMR (300 MHz, DMSO-d6) δ 8.83 (s, 1H), 8.66 (s, 1H), 8.61 (d, J = 2.0 Hz, 1H), 7.48 (s, 1H), 7.23 (s, 1H), 7.12 – 7.07 (m, 2H), 4.40 (t, J = 8.4 Hz, 2H), 4.12 (t, 2H), 3.95 (s, 3H), 1.98 – 1.68 (m, 6H), 1.52 – 1.37 (m, 2H).

^{13}C NMR (75 MHz, DMSO) δ 155.13, 155.03, 152.57, 147.93, 147.64, 129.72, 124.21, 122.50, 119.57, 113.03, 108.78, 106.74, 101.06, 69.10, 67.47, 55.99, 29.51, 24.39, 24.20, 22.85.

MS-ESI m/z $[M + H]^+$: calcd 400.9, found 400.4.

HRMS m/z $[M + H]^+$: calcd 400.1423, found 400.1423.

HPLC: t_R = 8.91, purity ≥ 95% (UV: 254/ 280 nm).

Synthesis of 3^6-chloro-1^7-methoxy-4,11-dioxa-2-aza-1(4,6)-quinazolina-3(1,2)-benzenacycloundecaphane (38e)

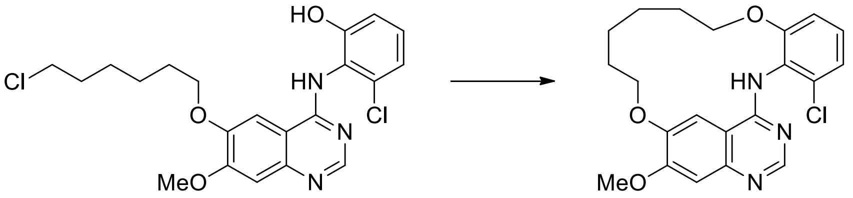

The title compound was prepared according to the procedure of **38a** using **36e** (77 mg, 0.18 mmol) to obtain the product (15 mg, 21%) as a beige solid.

^{1}H NMR (300 MHz, CD2Cl2) δ 8.53 (s, 1H), 7.37 (s, 1H), 7.25 – 7.10 (m, 4H), 6.84 (dd, J = 8.0, 1.5 Hz, 1H), 4.50 – 4.36 (m, 2H), 4.02 – 3.95 (m, 5H), 1.79 – 1.67 (m, 6H), 1.49 – 1.37 (m, 2H).

^{13}C NMR (75 MHz, CD2Cl2) δ 158.55, 156.19, 154.72, 154.10, 148.19, 147.80, 133.84, 127.85, 127.74, 122.49, 109.99, 109.96, 108.52, 101.04, 68.89, 66.91, 56.68, 29.69, 25.58, 25.54, 23.66.

MS-ESI m/z $[M + H]^+$: calcd 400.9, found 400.3.

HRMS m/z $[M + H]^+$: calcd 400.1423, found 400.1421.

HPLC: t_R = 7.67, purity ≥ 95% (UV: 254/ 280 nm).

Synthesis of 3^5-chloro-3^4-fluoro-1^7-methoxy-4,11-dioxa-2-aza-1(4,6)-quinazolina-3(1,2)-benzenacycloundecaphane (38f)

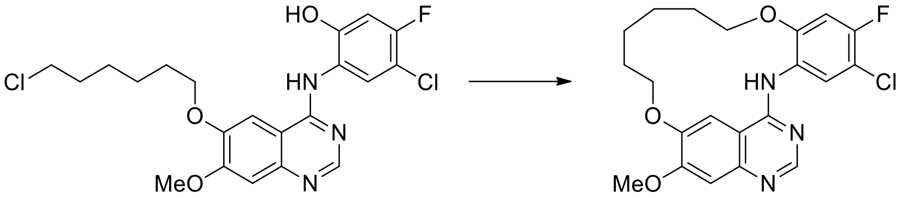

The title compound was prepared according to the procedure of **38a** using **36f** (132 mg, 0.29 mmol) to obtain the product (52 mg, 43%) as a purple solid.

^{1}H NMR (250 MHz, methylene chloride-d2) δ 8.88 (d, J = 8.1 Hz, 1H), 8.64 (s, 1H), 8.23 (s, 1H), 7.18 (s, 1H), 7.07 (s, 1H), 6.73 (d, J = 10.0 Hz, 1H), 4.38 – 4.26 (m, 2H), 4.13 – 4.07 (m, 2H), 3.98 (s, 3H), 2.03 – 1.79 (m, 6H), 1.65 – 1.48 (m, 2H).

^{13}C NMR (75 MHz, methylene chloride-d2) δ 155.63, 155.20, 153.95, 153.47 (d, J = 242.7 Hz), 149.58, 147.55 (d, J = 8.8 Hz), 147.16, 126.92 (d, J = 3.2 Hz), 119.45, 112.11 (d, J = 18.0 Hz), 109.73, 108.60, 101.12 (d, J = 26.3 Hz), 99.65, 70.02, 69.57, 56.71, 30.58, 25.63, 25.47, 23.76.

MS-ESI m/z $[M + H]^+$: calcd 418.9, found 418.4.

HRMS m/z $[M + H]^+$: calcd 418.1328, found 418.1327.

HPLC: t_R = 5.79, purity ≥ 95% (UV: 254/ 280 nm).

Synthesis of 1^7-methoxy-4,7,10,13-tetraoxa-2-aza-1(4,6)-quinazolina-3(1,2)-benzenacyclotridecaphane (39a)

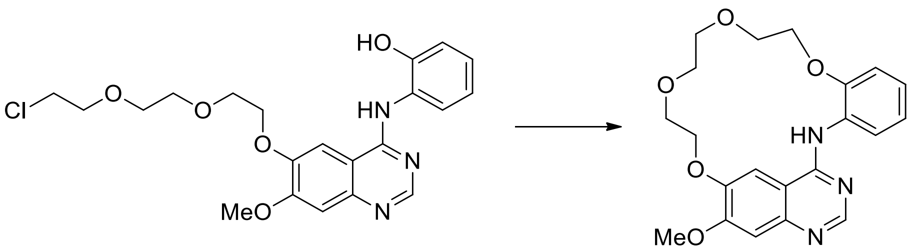

The title compound was prepared according to the procedure of **38a** using **37a** (95 mg, 0.22 mmol) to obtain the product (84 mg, 100%) as a pale yellow solid.

^{1}H NMR (300 MHz, DMSO-d6) δ 10.52 (s, 1H), 8.73 (s, 1H), 8.31 (s, 1H), 7.64 (d, J = 7.6 Hz, 1H), 7.41 – 7.32 (m, 2H), 7.18 (d, J = 8.0 Hz, 1H), 7.09 (t, J = 7.5 Hz, 1H), 4.66 – 4.58 (m, 2H), 4.16 – 4.08 (m, 2H), 3.99 (s, 3H), 3.79 – 3.72 (m, 2H), 3.66 – 3.59 (m, 2H), 3.56 – 3.49 (m, 2H), 3.48 – 3.43 (m, 2H).

^{13}C NMR (75 MHz, DMSO) δ 162.72, 158.83, 156.57, 152.70, 149.72, 148.88, 128.42, 127.70, 125.43, 120.61, 113.15, 106.68, 106.47, 99.65, 70.62, 70.01, 69.62, 68.68, 68.29, 67.78, 56.38.

MS-ESI m/z $[M + H]^+$: calcd 398.2, found 398.3.

HRMS m/z $[M + H]^+$: calcd 398.1711, found 398.1705.

HPLC: t_R = 7.03, purity ≥ 95% (UV: 254/ 280 nm).

Synthesis of 3^3-chloro-1^7-methoxy-4,7,10,13-tetraoxa-2-aza-1(4,6)-quinazolina-3(1,2)-benzenacyclotridecaphane (39b)

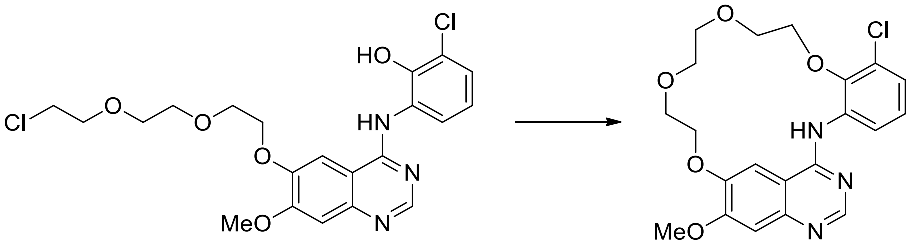

The title compound was prepared according to the procedure of **38a** using **37b** (78 mg, 0.17 mmol) to obtain the product (49 mg, 68%) as a white solid.

^{1}H NMR (300 MHz, DMSO-d6) δ 10.77 (s, 1H), 8.76 (s, 1H), 8.40 (s, 1H), 7.70 (d, J = 7.8 Hz, 1H), 7.49 (d, J = 7.9 Hz, 1H), 7.43 (s, 1H), 7.27 (t, J = 8.0 Hz, 1H), 4.64 – 4.55 (m, 2H), 4.02 – 3.94 (m, 5H), 3.84 – 3.76 (m, 2H), 3.64 – 3.56 (m, 2H), 3.53 – 3.45 (m, 2H), 3.45 – 3.37 (m, 2H).

^{13}C NMR (75 MHz, DMSO) δ 158.63, 156.80, 149.38, 149.10, 149.03, 136.30, 132.11, 128.36, 127.17, 127.04, 124.90, 107.57, 106.88, 100.21, 72.82, 71.18, 70.13, 70.02, 69.23, 68.40, 56.37.

MS-ESI m/z $[M + H]^+$: calcd 432.1, found 432.3.

HRMS m/z $[M + H]^+$: calcd 432.1321, found 432.1319.

HPLC: t_R = 7.49, purity ≥ 95% (UV: 254/ 280 nm).

Synthesis of 3^4-chloro-1^7-methoxy-4,7,10,13-tetraoxa-2-aza-1(4,6)-quinazolina-3(1,2)-benzenacyclotridecaphane (39c)

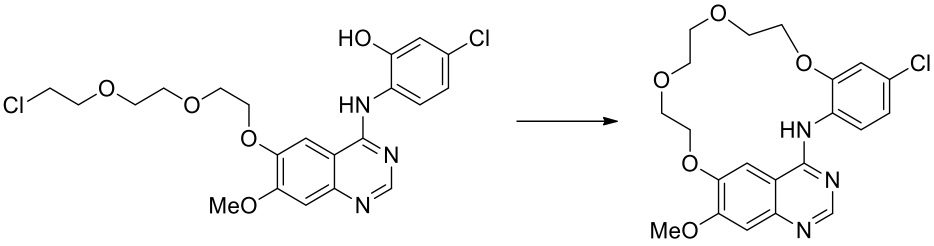

The title compound was prepared according to the procedure of **38a** using **37c** (120 mg, 0.26 mmol) to obtain the product (86 mg, 72%) as a yellow solid.

^{1}H NMR (300 MHz, DMSO-d6) δ 10.49 (s, 1H), 8.75 (s, 1H), 8.30 (s, 1H), 7.69 (d, J = 8.4 Hz, 1H), 7.43 (s, 1H), 7.29 (d, J = 2.1 Hz, 1H), 7.16 (dd, J = 8.5, 2.1 Hz, 1H), 4.67 – 4.58 (m, 2H), 4.20 – 4.12 (m, 2H), 3.98 (s, 3H), 3.80 – 3.72 (m, 2H), 3.65 – 3.58 (m, 2H), 3.56 – 3.49 (m, 2H), 3.47 – 3.40 (m, 2H).

^{13}C NMR (75 MHz, DMSO) δ 158.77, 156.60, 153.35, 149.74, 148.87, 135.39, 132.02, 128.69, 124.65, 120.45, 113.53, 106.61, 106.57, 99.84, 70.55, 69.97, 69.57, 68.77, 68.47, 67.81, 56.37.

MS-ESI m/z [M + H]$^+$: calcd 432.1, found 432.3.

HRMS m/z [M + H]$^+$: calcd 432.1321, found 432.1319.

HPLC: t_R = 7.48, purity ≥ 95% (UV: 254/ 280 nm).

Synthesis of 3^5-chloro-1^7-methoxy-4,7,10,13-tetraoxa-2-aza-1(4,6)-quinazolina-3(1,2)-benzenacyclotridecaphane (39d)

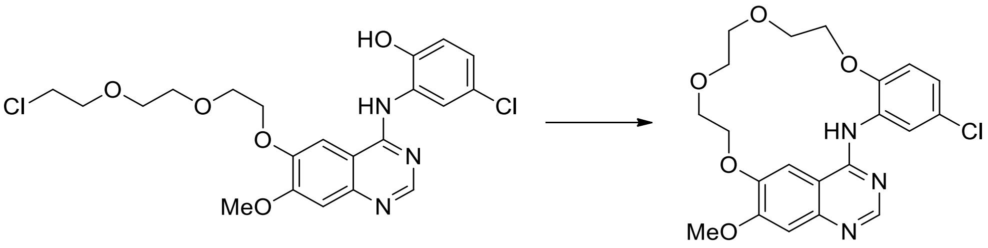

The title compound was prepared according to the procedure of **38a** using **37d** (94 mg, 0.20 mmol) to obtain the product (68 mg, 79%) as a pale yellow solid.

^{1}H NMR (300 MHz, DMSO-d6) δ 10.27 (s, 1H), 8.79 (s, 1H), 8.21 (s, 1H), 7.91 (d, J = 2.5 Hz, 1H), 7.38 (dd, J = 8.7, 2.5 Hz, 1H), 7.33 (s, 1H), 7.21 (d, J = 8.8 Hz, 1H), 4.59 (t, J = 4.6 Hz, 2H), 4.20 –

4.12 (m, 2H), 3.99 (s, 3H), 3.76 (t, J = 4.3 Hz, 2H), 3.71 – 3.64 (m, 2H), 3.59 – 3.52 (m, 2H), 3.53 – 3.46 (m, 2H).

^{13}C NMR (75 MHz, DMSO) δ 158.20, 156.67, 155.74, 151.04, 149.74, 149.52, 135.88, 127.17, 124.47, 123.98, 119.13, 114.52, 106.86, 106.44, 70.37, 69.84, 69.68, 68.76, 68.53, 68.22, 56.38.

MS-ESI m/z $[M + H]^+$: calcd 432.1, found 432.3.

HRMS m/z $[M + H]^+$: calcd 432.1321, found 432.1319.

HPLC: t_R = 7.44, purity ≥ 95% (UV: 254/ 280 nm).

Synthesis of 3^6-chloro-1^7-methoxy-4,7,10,13-tetraoxa-2-aza-1(4,6)-quinazolina-3(1,2)-benzenacyclotridecaphane (39e)

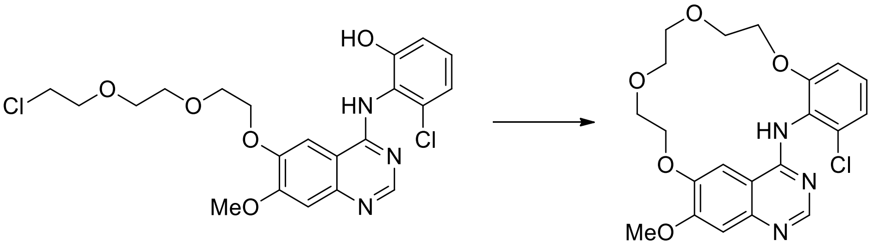

The title compound was prepared according to the procedure of **38a** using **37e** (109 mg, 0.23 mmol) to obtain the product (61 mg, 60%) as a yellow solid.

^{1}H NMR (300 MHz, DMSO-d6) δ 10.87 (s, 1H), 8.72 (s, 1H), 8.41 (s, 1H), 7.55 – 7.32 (m, 2H), 7.25 (d, J = 8.0 Hz, 1H), 7.17 (d, J = 8.1 Hz, 1H), 5.01 – 4.85 (m, 1H), 4.35 (d, J = 13.0 Hz, 1H), 4.20 (d, J = 10.2 Hz, 1H), 4.00 (s, 3H), 3.96 – 3.89 (m, 1H), 3.84 – 3.70 (m, 2H), 3.63 (t, J = 11.8 Hz, 2H), 3.50 – 3.38 (m, 2H), 3.28 – 3.17 (m, 2H).

^{13}C NMR (75 MHz, DMSO) δ 160.93, 160.01, 156.70, 155.57, 149.86, 148.84, 133.07, 130.01, 123.75, 121.44, 112.05, 106.68, 106.16, 99.41, 71.20, 70.46, 69.56, 68.67, 68.59, 67.06, 56.41.

MS-ESI m/z $[M + H]^+$: calcd 432.1, found 432.3.

HRMS m/z $[M + H]^+$: calcd 432.1321, found 432.1319.

HPLC: t_R = 7.12, purity ≥ 95% (UV: 254/ 280 nm).

Synthesis of 3^5-chloro-3^4-fluoro-1^7-methoxy-4,7,10,13-tetraoxa-2-aza-1(4,6)-quinazolina-3(1,2)-benzenacyclotridecaphane (39f)

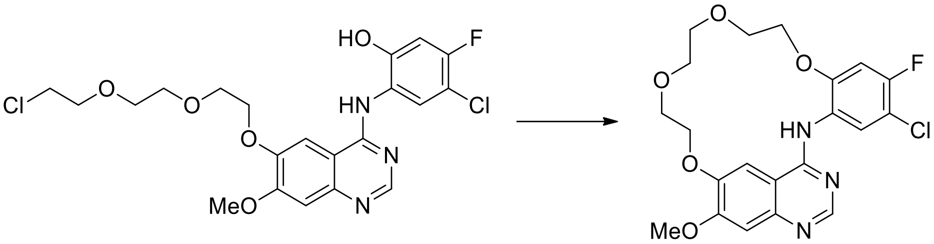

The title compound was prepared according to the procedure of **38a** using **37f** (117 mg, 0.24 mmol) to obtain the product (6 mg, 6%) as a white solid.

^{1}H NMR (250 MHz, DMSO-d6) δ 10.05 (s, 1H), 8.75 (s, 1H), 8.15 (s, 1H), 8.07 (d, J = 8.1 Hz, 1H), 7.39 (d, J = 11.0 Hz, 1H), 7.25 (s, 1H), 4.62 – 4.54 (m, 2H), 4.23 – 4.15 (m, 2H), 3.99 (s, 3H), 3.75 (t, J = 4.4 Hz, 2H), 3.71 – 3.63 (m, 2H), 3.55 – 3.52 (m, 4H).

^{13}C NMR (75 MHz, DMSO) δ 158.20, 157.36 (d, J = 122.8 Hz), 154.22 (d, J = 16.3 Hz), 152.16, 152.02, 150.06, 149.64, 127.35 (d, J = 1.6 Hz), 123.24 (d, J = 3.6 Hz), 109.89 (d, J = 19.1 Hz), 106.96, 106.20, 102.67 (d, J = 25.9 Hz), 101.57, 70.34, 69.88, 69.67, 69.16, 68.34, 68.20, 56.35.

MS-ESI m/z $[M + H]^+$: calcd 450.9, found 450.3.

HRMS m/z $[M + H]^+$: calcd 450.1227, found 450.1224.

HPLC: t_R = 7.52, purity ≥ 95% (UV: 254/ 280 nm).

Synthesis of 4-chloro-6-(2-(2-chloroethoxy)ethoxy)-7-methoxyquinazoline (40)

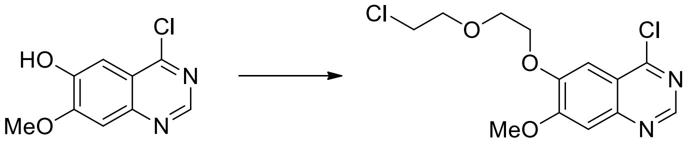

TPP (782 mg, 2.98 mmol, 2.5 eq) and DIAD (600 mg, 2.98 mmol, 2.5 eq) were dissolved in 50 mL anhydrous toluene. After 15 minutes at rt 2-(2-chloroethoxy)ethanol (185 mg, 1.48 mmol, 1.25 eq) was added. After additional 20 minutes 4-chloro-7methoxyquinazolin-6-ol (250 mg, 1.19 mmol, 1.0 eq) was added and the mixture was stirred at 80 °C for 2 h. The solvent was evaporated under reduced pressure and the crude product was purified by flash chromatography using DCM/ methanol and *n*-hexane/ ethyl acetate as an eluent to obtain the product (159 mg, 42%) as a yellow solid.

^{1}H NMR (300 MHz, DMSO-d6) δ 8.87 (s, 1H), 7.45 (s, 1H), 7.43 (s, 1H), 4.45 – 4.29 (m, 2H), 4.02 (s, 3H), 3.94 – 3.87 (m, 2H), 3.82 – 3.73 (m, 4H).

^{13}C NMR (75 MHz, DMSO) δ 157.95, 156.79, 152.22, 150.55, 148.57, 118.54, 106.97, 103.31, 70.68, 68.55, 68.48, 56.54, 43.51.

MS-ESI m/z $[M + H]^+$: calcd 317.1, found 317.1.

Synthesis of 3-((6-(2-(2-chloroethoxy)ethoxy)-7-methoxyquinazolin-4-yl)amino)phenol (41a)

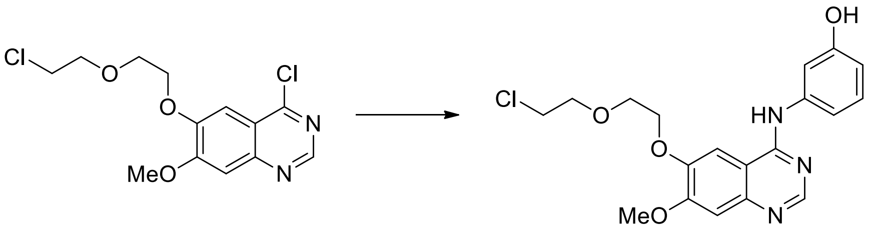

The title compound was prepared according to the procedure of **36b** using **40** (157 mg, 0.50 mmol) and 3-aminophenol (55 mg, 0.50 mmol) to obtain the product (155 mg, 80%) as a pale yellow solid.

^{1}H NMR (300 MHz, DMSO-d6) δ 11.29 (s, 1H), 9.74 (s, 1H), 8.80 (s, 1H), 8.37 (s, 1H), 7.40 (s, 1H), 7.25 (t, J = 8.0 Hz, 1H), 7.17 – 7.05 (m, 2H), 6.86 – 6.68 (m, 1H), 4.48 – 4.29 (m, 2H), 3.99 (s, 3H), 3.94 – 3.87 (m, 2H), 3.86 – 3.71 (m, 4H).

^{13}C NMR (75 MHz, DMSO) δ 158.11, 157.66, 156.25, 149.21, 148.59, 137.73, 135.41, 129.32, 115.43, 113.50, 111.91, 107.16, 104.89, 99.82, 70.71, 68.99, 68.36, 56.45, 43.56.

MS-ESI m/z $[M + H]^+$: calcd 390.1, found 390.1.

HRMS m/z $[M + H]^+$: calcd 390.1215, found 390.1211.

HPLC: t_R = 7.12, purity ≥ 95% (UV: 254/ 280 nm).

Synthesis of 2-chloro-5-((6-(2-(2-chloroethoxy)ethoxy)-7-methoxyquinazolin-4-yl)amino)phenol (41b)

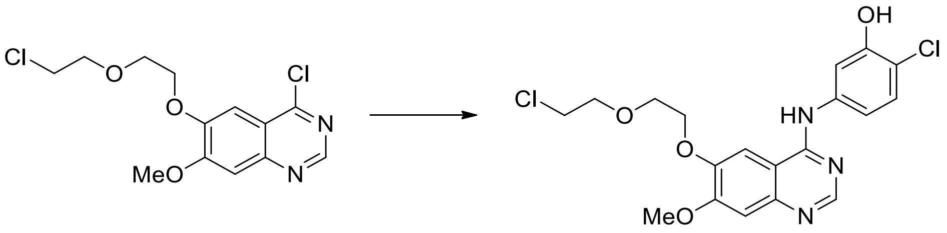

The title compound was prepared according to the procedure of **36b** using **40** (200 mg, 0.63 mmol) and 5-amino-2-chlorophenol (91 mg, 0.63 mmol) to obtain the product (84 mg, 31%) as a pale green solid.

^{1}H NMR (300 MHz, DMSO-d6) δ 11.23 (s, 1H), 10.53 (s, 1H), 8.80 (s, 1H), 8.34 (s, 1H), 7.64 – 7.35 (m, 3H), 7.17 (d, J = 8.5 Hz, 1H), 4.45 – 4.29 (m, 2H), 3.99 (s, 3H), 3.95 – 3.88 (m, 2H), 3.83 – 3.73 (m, 4H).

^{13}C NMR (75 MHz, DMSO) δ 157.94, 156.17, 153.05, 149.14, 148.90, 136.60, 129.47, 117.01, 116.34, 112.76, 107.35, 104.74, 100.38, 70.69, 68.96, 68.35, 56.42, 43.54.

MS-ESI m/z $[M + H]^+$: calcd 424.1, found 424.0.

HRMS m/z $[M + H]^+$: calcd 424.0825, found 424.0826.

HPLC: t_R = 7.48, purity ≥ 95% (UV: 254/ 280 nm).

Synthesis of 3-chloro-5-((6-(2-(2-chloroethoxy)ethoxy)-7-methoxyquinazolin-4-yl)amino)phenol (41c)

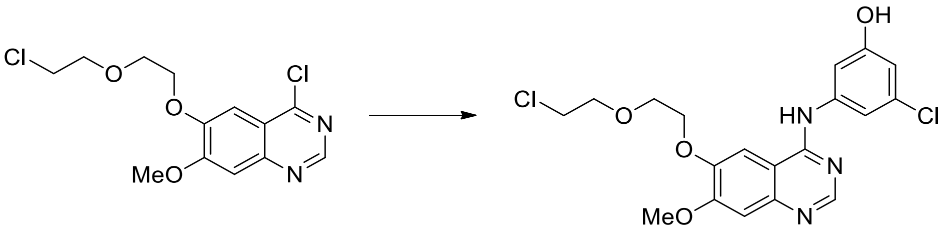

The title compound was prepared according to the procedure of **36b** using **40** (200 mg, 0.63 mmol) and 3-amino-5-chlorophenol (91 mg, 0.63 mmol) to obtain the product (89 mg, 33%) as a pale yellow solid.

^{1}H NMR (300 MHz, DMSO-d6) δ 11.31 (s, 1H), 10.28 (s, 1H), 8.88 (s, 1H), 8.37 (s, 1H), 7.38 (s, 1H), 7.31 (t, J = 1.9 Hz, 1H), 7.19 (t, J = 2.0 Hz, 1H), 6.77 (t, J = 2.0 Hz, 1H), 4.38 (t, J = 4.5 Hz, 2H), 4.00 (s, 3H), 3.96 – 3.88 (m, 2H), 3.86 – 3.73 (m, 4H).

^{13}C NMR (75 MHz, DMSO) δ 158.57, 158.15, 156.46, 149.33, 148.71, 138.99, 135.72, 133.06, 115.01, 113.07, 110.43, 107.36, 104.84, 99.90, 70.72, 69.05, 68.36, 56.51, 43.55.

MS-ESI m/z $[M + H]^+$: calcd 424.1, found 424.0.

HRMS m/z $[M + H]^+$: calcd 424.0825, found 424.0827.

HPLC: t_R = 7.52, purity ≥ 95% (UV: 254/ 280 nm).

Synthesis of 4-chloro-3-((6-(2-(2-chloroethoxy)ethoxy)-7-methoxyquinazolin-4-yl)amino)phenol (41d)

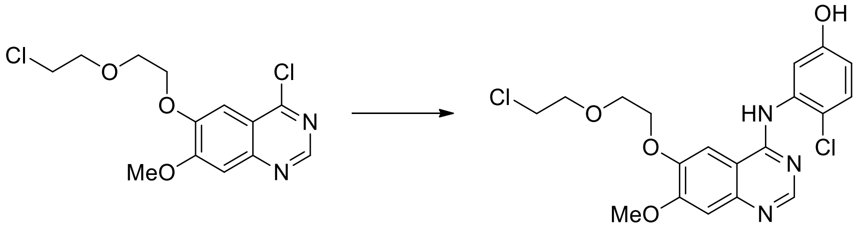

The title compound was prepared according to the procedure of **36a** using **40** (157 mg, 0.50 mmol) and 3-amino-4-chlorophenol (71 mg, 0.50 mmol) to obtain the product (70 mg, 33%) as a pale green solid.

^{1}H NMR (300 MHz, DMSO-d6) δ 11.44 (s, 1H), 10.12 (s, 1H), 8.76 (s, 1H), 8.31 (s, 1H), 7.52 – 7.32 (m, 2H), 6.96 (d, J = 2.6 Hz, 1H), 6.86 (dd, J = 8.7, 2.7 Hz, 1H), 4.40 – 4.31 (m, 2H), 4.00 (s, 3H), 3.95 – 3.86 (m, 2H), 3.86 – 3.72 (m, 4H).

^{13}C NMR (75 MHz, DMSO) δ 159.10, 156.98, 156.43, 149.30, 148.97, 136.03, 134.62, 130.24, 120.24, 116.30, 116.19, 106.71, 104.56, 100.18, 70.68, 68.84, 68.32, 56.49, 43.54.

MS-ESI m/z $[M + H]^+$: calcd 424.1, found 424.1.

HRMS m/z $[M + H]^+$: calcd 424.0825, found 424.0827.

HPLC: t_R = 7.34, purity ≥ 95% (UV: 254/ 280 nm).

Synthesis of 1^7-methoxy-4,7,10-trioxa-2-aza-1(4,6)-quinazolina-3(1,3)-benzenacyclodecaphane (42a)

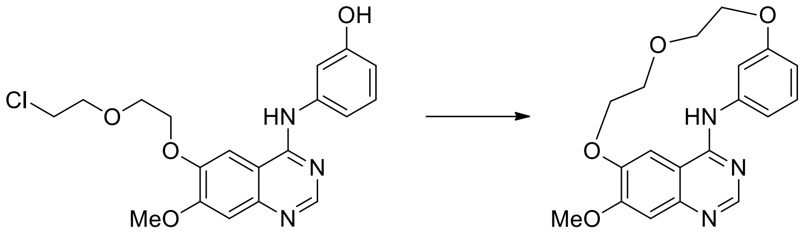

The title compound was prepared according to the procedure of **38a** using **41a** (135 mg, 0.35 mmol) to obtain the product (22 mg, 18%) as a yellow solid.

^{1}H NMR (300 MHz, DMSO-d6) δ 9.53 (s, 1H), 8.50 (s, 1H), 7.25 (t, J = 7.8 Hz, 1H), 7.16 (s, 1H), 7.03 (s, 1H), 6.86 – 6.70 (m, 3H), 4.22 – 4.12 (m, 2H), 4.04 – 3.94 (m, 2H), 3.90 (s, 3H), 3.60 – 3.46 (m, 4H).

^{13}C NMR (75 MHz, DMSO) δ 159.92, 154.74, 153.11, 148.79, 146.67, 141.77, 129.75, 115.74, 113.62, 109.81, 109.15, 107.02, 106.95, 71.75, 70.89, 66.83, 66.60, 55.70, 29.24.

MS-ESI m/z $[M + H]^+$: calcd 354.1, found 354.3.

HRMS m/z $[M + H]^+$: calcd 354.1448, found 354.1449.

HPLC: t_R = 8.86, purity ≥ 95% (UV: 254/ 280 nm).

Synthesis of 3^4-chloro-1^7-methoxy-4,7,10-trioxa-2-aza-1(4,6)-quinazolina-3(1,3)-benzenacyclodecaphane (42b)

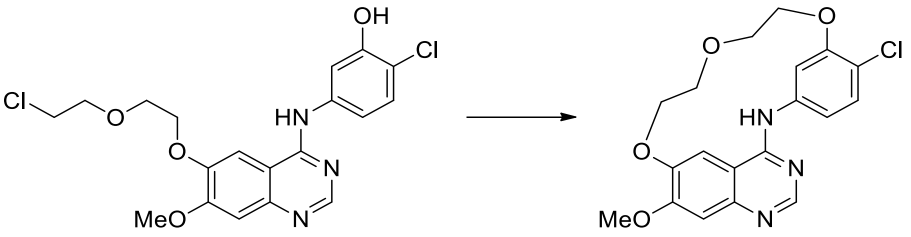

The title compound was prepared according to the procedure of **38a** using **41b** (74 mg, 0.17 mmol) to obtain the product (20 mg, 30%) as a yellow solid.

^{1}H NMR (250 MHz, DMSO-d6) δ 11.32 (s, 1H), 8.82 (s, 1H), 7.75 – 7.29 (m, 3H), 7.00 (s, 1H), 6.85 (s, 1H), 4.68 – 4.19 (m, 2H), 3.92 (s, 3H), 3.64 – 3.42 (m, 6H).

^{13}C NMR (75 MHz, DMSO) δ 158.73, 155.84, 155.74, 147.68, 147.35, 137.06, 136.55, 130.09, 121.97, 119.01, 115.63, 106.22, 105.47, 99.47, 72.17, 71.06, 68.77, 66.74, 56.02.

MS-ESI m/z $[M + H]^+$: calcd 388.1, found 388.1.

HRMS m/z $[M + H]^+$: calcd 388.1059, found 388.1059.

HPLC: t_R = 7.24, purity ≥ 95% (UV: 254/ 280 nm).

Synthesis of 3^5-chloro-1^7-methoxy-4,7,10-trioxa-2-aza-1(4,6)-quinazolina-3(1,3)-benzenacyclodecaphane (42c)

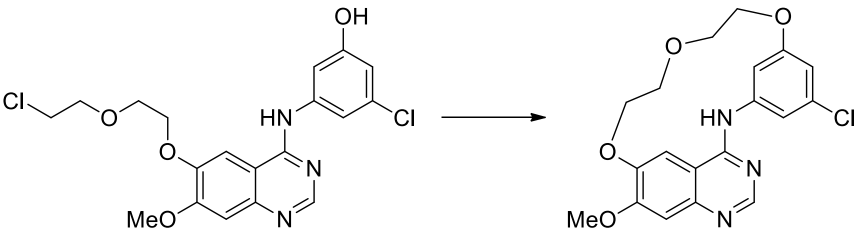

The title compound was prepared according to the procedure of **38a** using **41c** (79 mg, 0.19 mmol) to obtain the product (6 mg, 8%) as a white solid.

^{1}H NMR (300 MHz, DMSO-d6) δ 9.66 (s, 1H), 8.59 (s, 1H), 7.22 (s, 1H), 7.12 (s, 1H), 6.83 (t, J = 1.8 Hz, 1H), 6.76 – 6.63 (m, 2H), 4.20 – 4.09 (m, 4H), 3.93 (s, 3H), 3.62 – 3.51 (m, 4H).

^{13}C NMR (75 MHz, DMSO) δ 160.54, 155.12, 155.09, 152.68, 148.32, 147.39, 147.31, 133.41, 113.61, 112.28, 110.74, 109.82, 106.71, 106.24, 71.69, 66.74, 66.37, 55.82, 54.90.

MS-ESI m/z $[M + H]^+$: calcd 388.1, found 388.1.

HRMS m/z $[M + H]^+$: calcd 388.1059, found 388.1059.

HPLC: t_R = 7.35, purity ≥ 95% (UV: 254/ 280 nm).

Synthesis of 3^6-chloro-1^7-methoxy-4,7,10-trioxa-2-aza-1(4,6)-quinazolina-3(1,3)-benzenacyclodecaphane (42d)

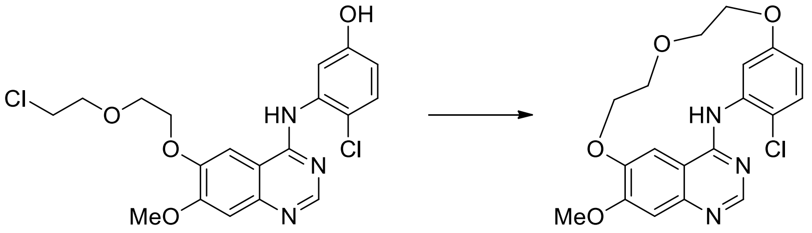

The title compound was prepared according to the procedure of **38a** using **41d** (60 mg, 0.14 mmol) to obtain the product (15 mg, 27%) as a pale yellow solid.

^{1}H NMR (300 MHz, DMSO-d6) δ 9.51 (s, 1H), 8.44 (s, 1H), 7.45 (d, J = 8.8 Hz, 1H), 7.18 – 7.12 (m, 2H), 6.95 (dd, J = 8.8, 2.8 Hz, 1H), 6.74 (s, 1H), 4.30 – 4.21 (m, 2H), 3.91 – 3.84 (m, 5H), 3.63 – 3.55 (m, 2H), 3.45 (t, J = 4.8 Hz, 2H).

^{13}C NMR (75 MHz, DMSO) δ 159.53, 157.11, 154.48, 152.57, 148.50, 146.82, 138.79, 130.01, 121.33, 117.29, 116.10, 108.75, 107.31, 106.44, 71.94, 70.05, 68.19, 67.20, 55.68.

MS-ESI m/z $[M + H]^+$: calcd 388.1, found 388.1.

HRMS m/z $[M + H]^+$: calcd 388.1059, found 388.1059.

HPLC: t_R = 7.09, purity ≥ 95% (UV: 254/ 280 nm).

Synthesis of 4-oxo-3,4-dihydroquinazolin-6-yl acetate (44)

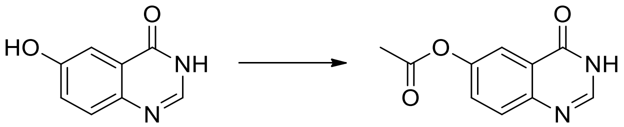

A mixture of 6-hydroxyquinazolin-4(3H)-one (5.58 g, 34.4 mmol, 1.0 eq) and pyridine (33.3 mL, 0.41 mol, 12.0 eq) in 33 mL acetic anhydride was stirred at 50 °C for 1 h. Ice was added to the reaction mixture after cooling it down to rt, leading to the precipitation of **44**. It was filtered and washed with ice water to obtain the product (7.02 g, 85%) as a beige solid.

^{1}H NMR (250 MHz, DMSO-d6) δ 12.31 (s, 1H), 8.09 (s, 1H), 7.83 (d, J = 2.7 Hz, 1H), 7.72 (d, J = 8.8 Hz, 1H), 7.58 (ddd, J = 8.8, 2.7, 0.6 Hz, 1H), 2.31 (s, 3H).

MS-ESI m/z [M + H]$^-$: calcd 203.2, found 203.2.

Synthesis of 4-chloroquinazolin-6-yl acetate (45)

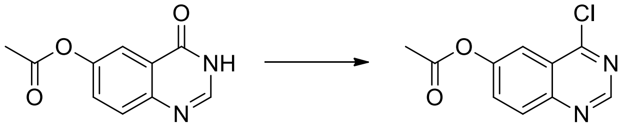

A mixture of **44** (5.97 g, 29.2 mmol, 1.0 eq) and thionyl chloride (45.0 mL, 0.62 mol, 21.0 eq) in 0.4 mL anhydrous DMF was stirred at 70 °C for 3 h. The solvent was evaporated under reduced pressure and the crude product was used without further purification as a beige solid.

^{1}H NMR (250 MHz, chloroform-d) δ 9.05 (s, 1H), 8.11 (d, J = 9.1 Hz, 1H), 8.02 (d, J = 2.5 Hz, 1H), 7.73 (dd, J = 9.1, 2.5 Hz, 1H), 2.40 (s, 3H).

MS-ESI m/z [M + H]$^+$: calcd 245.0, found 245.0.

Synthesis of 4-chloroquinazolin-6-ol (46)

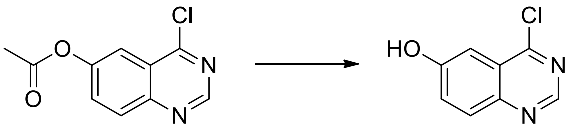

A mixture of **45** (6.51 g, 29.2 mmol, 1.0 eq) in 132 mL ammonia in methanol (2 M) was stirred at rt for 1 h. The solvent was evaporated under reduced pressure and the crude product was purified by flash chromatography using *n*-hexane/ ethyl acetate as an eluent to obtain the product (1.00 g, 19%) as a beige solid.

^{1}H NMR (250 MHz, DMSO-d6) δ 10.84 (s, 1H), 8.89 (s, 1H), 7.98 (d, J = 9.1 Hz, 1H), 7.64 (dd, J = 9.1, 2.7 Hz, 1H), 7.42 (d, J = 2.7 Hz, 1H).

MS-ESI m/z $[M + H]^+$: calcd 181.6, found 181.1.

Synthesis of 4-((5-chloro-4-fluoro-2-hydroxyphenyl)amino)quinazolin-6-ol (47)

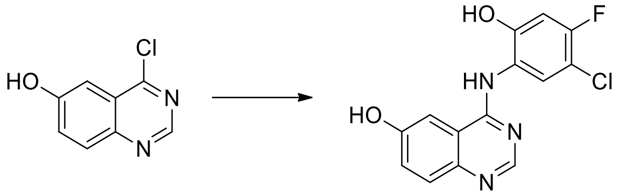

46 (154 mg, 0.83 mmol, 1.0 eq) and 2-amino-4-chloro-5-fluorophenol (148 mg, 0.91 mmol, 1.1 eq) were dissolved in 11 mL anhydrous ethanol. The mixture was stirred at 70 °C for 18 h. A solid precipitated, which was filtered, washed with ethanol and dried under reduced pressure to obtain the product (190 mg, 75%) as a yellow solid.

^{1}H NMR (500 MHz, DMSO-d6) δ 11.11 (s, 1H), 10.95 (s, 1H), 10.84 (s, 1H), 8.76 (s, 1H), 7.95 (d, J = 2.5 Hz, 1H), 7.89 (d, J = 9.1 Hz, 1H), 7.71 (dd, J = 9.1, 2.5 Hz, 1H), 7.61 (d, J = 8.2 Hz, 1H), 7.09 (d, J = 10.9 Hz, 1H).

^{13}C NMR (126 MHz, DMSO) δ 158.89 (d, J = 358.2 Hz), 157.83, 155.51, 153.28 (d, J = 10.6 Hz), 148.22, 131.65, 129.43, 126.94, 121.29, 121.22 (d, J = 3.0 Hz), 114.69, 108.22 (d, J = 18.9 Hz), 107.06, 104.76 (d, J = 23.8 Hz).

MS-ESI m/z $[M + H]^+$: calcd 306.7, found 306.4.

HRMS m/z $[M + H]^+$: calcd 306.0440, found 306.0441.

HPLC: t_R = 6.91, purity ≥ 95% (UV: 254/ 280 nm).

Synthesis of 3^5-chloro-3^4-fluoro-4,7,10-trioxa-2-aza-1(4,6)-quinazolina-3(1,2)-benzenacyclodecaphane (48)

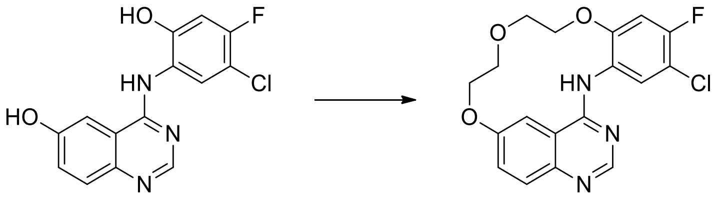

TPP (129 mg, 0.49 mmol, 3.0 eq) and DIAD (99 mg, 0.49 mmol, 3.0 eq) were dissolved in 41 mL anhydrous toluene. After 15 minutes at rt **47** (50 mg, 0.16 mmol, 1.0 eq) in 4 mL anhydrous THF was added. Another 15 minutes later 2,2'-oxydiethanol (17 mg, 0.16 mmol, 1.0 eq) was added and the mixture was stirred at 40 °C for 20 h. The solvent was evaporated under reduced pressure and the crude product was purified by flash chromatography using DCM/ methanol and *n*-hexane/ ethyl acetate as an eluent to obtain the product (3 mg, 5%) as a white solid.

^{1}H NMR (500 MHz, DMSO-d6) δ 8.99 (s, 1H), 8.72 (s, 1H), 8.59 (d, J = 8.1 Hz, 1H), 8.45 (d, J = 2.8 Hz, 1H), 7.76 (d, J = 9.0 Hz, 1H), 7.55 – 7.47 (m, 2H), 4.61 – 4.56 (m, 2H), 4.33 – 4.29 (m, 2H), 3.97 – 3.92 (m, 2H), 3.92 – 3.87 (m, 2H).

^{13}C NMR (126 MHz, DMSO) δ 157.07, 156.57, 152.66 (d, J = 243.4 Hz), 152.46, 147.99, 144.20 (d, J = 10.2 Hz), 128.84 (d, J = 6.1 Hz), 125.62, 121.90 (d, J = 17.7 Hz), 119.24, 112.39 (d, J = 18.6 Hz), 116.02, 106.66 (d, J = 24.8 Hz), 104.47, 72.16, 71.56, 70.17, 69.06.

MS-ESI m/z $[M + H]^+$: calcd 376.8, found 376.0.

HRMS m/z $[M + H]^+$: calcd 376.0859, found 376.0867.

HPLC: t_R = 8.64, purity ≥ 95% (UV: 254/ 280 nm).

7.10.2. Synthesis of 3-aminopyrazole-based molecules

Synthesis of 2-bromo-N-(3-cyclopropyl-1*H*-pyrazol-5-yl)pyrimidin-4-amine (53)

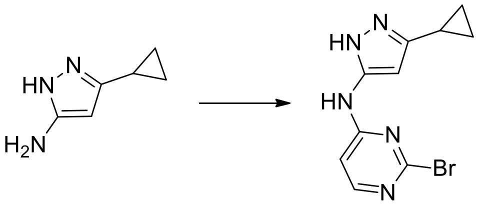

5-cyclopropyl-1H-pyrazol-3-amine (200 mg, 1.62 mmol, 1.1 eq) and 2,4-dibromopyrimidine (351 mg, 1.48 mmol, 1.0 eq) were dissolved in 5 mL anhydrous isopropanol. TEA (448 mg, 4.43 mmol, 3.0 eq) was added and the mixture was stirred at 55 °C for 48 h. The solvent was evaporated under reduced pressure and the crude product was purified by flash chromatography using *n*-hexane/ ethyl acetate as an eluent to obtain the product (133 mg, 32%) as a white solid.

^{1}H NMR (250 MHz, DMSO-d6) δ 12.17 (s, 1H), 10.26 (s, 1H), 8.08 (d, J = 5.9 Hz, 1H), 7.26 (s, 1H), 5.96 (s, 1H), 1.95 – 1.81 (m, 1H), 0.98 – 0.88 (m, 2H), 0.73 – 0.62 (m, 2H).

^{13}C NMR (126 MHz, DMSO) δ 160.36, 158.81, 151.52, 151.40, 147.27, 105.57, 92.64, 7.75, 6.69.

MS-ESI m/z $[M + H]^+$: calcd 281.1, found 280.0.

Synthesis of 2-chloro-N-(3-cyclopropyl-1*H*-pyrazol-5-yl)-5-methylpyrimidin-4-amine (54)

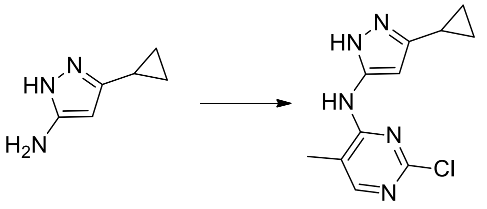

The title compound was prepared according to the procedure of **53**, using 2,4-dichloro-5-methylpyrimidine (602 mg, 3.69 mmol). The mixture was stirred at 80 °C for 48 h to obtain the product (366 mg, 40%) as a beige solid.

^{1}H NMR (300 MHz, DMSO-d6) δ 12.17 (s, 1H), 9.27 (s, 1H), 7.97 (d, J = 1.0 Hz, 1H), 6.26 (s, 1H), 2.11 (d, J = 1.0 Hz, 3H), 1.97 – 1.85 (m, 1H), 0.98 – 0.89 (m, 2H), 0.74 – 0.66 (m, 2H).

^{13}C NMR (75 MHz, DMSO) δ 159.78, 156.99, 155.86, 113.90, 94.84, 13.37, 7.66, 6.97.

MS-ESI m/z [M - H]$^-$: calcd 248.7, found 248.0.

Synthesis of 2,5-dichloro-N-(3-cyclopropyl-1*H*-pyrazol-5-yl)pyrimidin-4-amine (55)

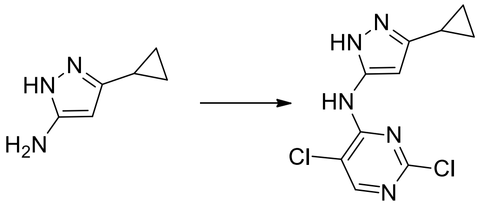

The title compound was prepared according to the procedure of **53**, using 2,4,5-trichloropyrimidine (677 mg, 3.69 mmol). The mixture was stirred at 60 °C for 48 h to obtain the product (866 mg, 89%) as a white solid.

^{1}H NMR (300 MHz, DMSO-d6) δ 12.33 (s, 1H), 9.65 (s, 1H), 8.32 (s, 1H), 6.19 (s, 1H), 1.99 – 1.82 (m, 1H), 0.99 – 0.89 (m, 2H), 0.74 – 0.66 (m, 2H).

^{13}C NMR (75 MHz, DMSO) δ 157.05, 156.86, 155.14, 145.81, 145.55, 113.13, 95.57, 7.72, 6.79.

MS-ESI m/z [M - H]$^-$: calcd 269.1, found 268.1.

Synthesis of *tert*-butyl 4-((4-((3-cyclopropyl-1*H*-pyrazol-5-yl)amino)pyrimidin-2-yl)amino)phenethyl-carbamate (56a)

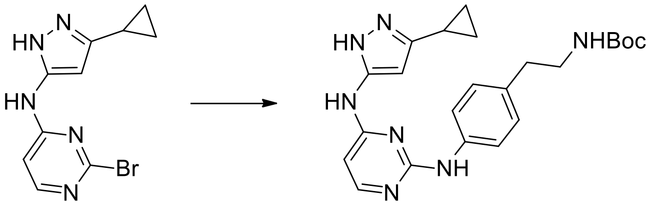

53 (150 mg, 0.54 mmol, 1.0 eq) and *tert*-butyl 4-aminophenethylcarbamate (127 mg, 0.54 mmol, 1.0 eq) were dissolved in 8 mL anhydrous ethanol. An catalytic amount of 1 M HCl was added and the mixture was stirred under reflux for 4 h. A solid precipitated, which was filtered, washed with ethanol and dried under reduced pressure to obtain the product (155 mg, 67%) as a white solid.

^{1}H NMR (300 MHz, DMSO-d6) δ 12.42 (s, 1H), 11.18 (s, 1H), 10.39 (s, 1H), 7.91 (d, J = 5.8 Hz, 1H), 7.40 (d, J = 7.8 Hz, 2H), 7.27 (d, J = 8.2 Hz, 2H), 6.91 (t, J = 5.4 Hz, 1H), 6.43 (s, 1H), 6.06 (s, 1H), 3.17 (q, J = 6.9 Hz, 2H), 2.74 (t, J = 7.5 Hz, 2H), 1.90 – 1.74 (m, 1H), 1.37 (s, 9H), 0.99 – 0.87 (m, 2H), 0.54 (s, 2H).

^{13}C NMR (75 MHz, DMSO) δ 159.54, 155.52, 152.68, 152.56, 149.03, 145.91, 137.11, 134.25, 129.20, 123.96, 99.20, 93.29, 77.53, 41.44, 35.06, 28.24, 7.88, 6.70.

MS-ESI m/z $[M + H]^+$: calcd 436.5, found 436.4.

HRMS m/z $[M + H]^+$: calcd 436.2456, found 436.2446.

HPLC: t_R = 7.57, purity ≥ 95% (UV: 254/ 280 nm).

Synthesis of *tert*-butyl 3-((4-((3-cyclopropyl-1*H*-pyrazol-5-yl)amino)pyrimidin-2-yl)amino)phenethyl-carbamate (56b)

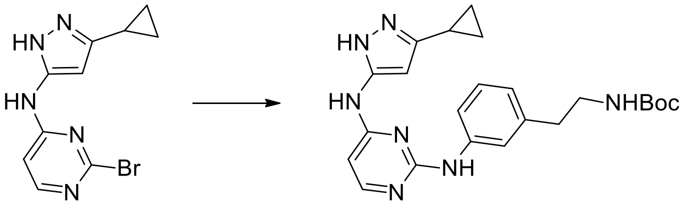

53 (100 mg, 0.36 mmol, 1.0 eq) and *tert*-butyl 3-aminophenethylcarbamate (84 mg, 0.36 mmol, 1.0 eq) were dissolved in 6 mL anhydrous ethanol. An catalytic amount of 1 M HCl was added and the mixture was stirred under reflux for 18 h. The solvent was evaporated under reduced pressure and the crude product was purified by flash chromatography using DCM/ methanol as an eluent to obtain the product (29 mg, 19%) as a colorless oil.

^{1}H NMR (300 MHz, DMSO-d6) δ 11.97 (s, 1H), 9.48 (s, 1H), 8.97 (s, 1H), 7.98 (d, J = 5.8 Hz, 1H), 7.66 (d, J = 8.2 Hz, 1H), 7.50 (s, 1H), 7.16 (t, J = 7.8 Hz, 1H), 6.86 (t, J = 5.6 Hz, 1H), 6.75 (d, J = 7.5 Hz, 1H), 6.58 – 6.09 (m, 2H), 3.21 – 3.07 (m, 2H), 2.66 (t, J = 7.6 Hz, 2H), 1.93 – 1.78 (m, 1H), 1.37 (s, 9H), 0.89 (d, J = 8.2 Hz, 2H), 0.74 – 0.62 (m, 2H).

^{13}C NMR (75 MHz, DMSO) δ 159.61, 155.90, 155.54, 140.98, 139.54, 128.28, 121.20, 119.14, 116.81, 98.14, 92.99, 77.51, 48.61, 41.66, 35.89, 28.27, 7.66.

MS-ESI m/z $[M + H]^+$: calcd 436.5, found 436.4.

HRMS m/z $[M + H]^+$: calcd 436.2456, found 436.2452.

HPLC: t_R = 7.58, purity ≥ 95% (UV: 254/ 280 nm).

Synthesis of *tert*-butyl (5-((4-((3-cyclopropyl-1*H*-pyrazol-5-yl)amino)pyrimidin-2-yl)amino)pentyl) carbamate (56c)

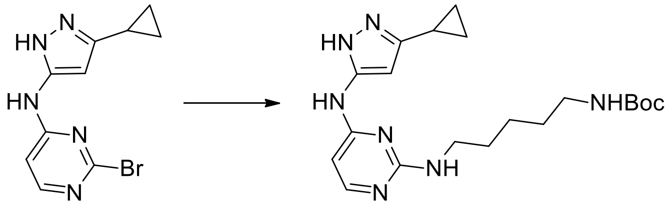

53 (60 mg, 0.21 mmol, 1.0 eq) and *tert*-butyl (5-aminopentyl)carbamate (43 mg, 0.21 mmol, 1.0 eq) were dissolved in 4 mL anhydrous ethanol. TEA (65 mg, 0.64 mmol, 3.0 eq) was added and the mixture was stirred at 90 °C for 5 h under microwave irradiation. The solvent was evaporated under reduced pressure and the crude product was purified by flash chromatography using DCM/ methanol as an eluent to obtain the product (37 mg, 42%) as a colorless oil.

^{1}H NMR (300 MHz, DMSO-d6) δ 11.92 (s, 1H), 9.31 (s, 1H), 7.77 (d, J = 5.7 Hz, 1H), 6.74 (t, J = 5.9 Hz, 1H), 6.65 (s, 1H), 6.30 – 5.97 (m, 2H), 3.21 (q, J = 6.7 Hz, 2H), 2.98 – 2.84 (m, 2H), 1.91 – 1.76 (m, 1H), 1.61 – 1.43 (m, 2H), 1.43 – 1.33 (m, 11H), 1.33 – 1.20 (m, 2H), 0.99 – 0.82 (m, 2H), 0.76 – 0.60 (m, 2H).

^{13}C NMR (75 MHz, DMSO) δ 162.30, 162.02, 155.99, 155.57, 123.51, 95.71, 77.29, 40.66, 35.77, 30.76, 29.33, 28.98, 28.26, 23.93, 7.65.

MS-ESI m/z $[M + H]^+$: calcd 402.4, found 402.2.

HRMS m/z $[M + H]^+$: calcd 402.2612, found 402.2622.

HPLC: t_R = 7.37, purity ≥ 95% (UV: 254/ 280 nm).

Synthesis of *tert*-butyl (2-(2-((4-((3-cyclopropyl-1*H*-pyrazol-5-yl)amino)pyrimidin-2-yl)amino)ethoxy)-ethyl)carbamate (56d)

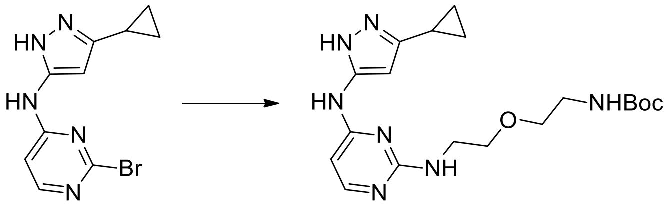

The title compound was prepared according to the procedure of **56c**, using **53** (100 mg, 0.36 mmol) and *tert*-butyl (2-(2-aminoethoxy)ethyl)carbamate (73 mg, 0.36 mmol). The mixture was stirred for 7 h at 90 °C to obtain the product (43 mg, 30%) as a colorless oil.

^{1}H NMR (300 MHz, DMSO-d6) δ 11.92 (s, 1H), 9.34 (s, 1H), 7.79 (d, J = 5.7 Hz, 1H), 6.92 – 6.50 (m, 2H), 6.30 – 6.00 (m, 2H), 3.56 – 3.46 (m, 2H), 3.45 – 3.36 (m, 4H), 3.09 (q, J = 5.9 Hz, 2H), 1.91 – 1.76 (m, 1H), 1.37 (s, 9H), 0.95 – 0.83 (m, 2H), 0.72 – 0.63 (m, 2H).

^{13}C NMR (75 MHz, DMSO) δ 161.92, 159.58, 156.01, 155.61, 95.89, 92.13, 77.61, 69.12, 40.47, 28.23, 7.84, 7.68.

MS-ESI m/z $[M + H]^+$: calcd 404.5, found 404.4.

HRMS m/z $[M + H]^+$: calcd 404.2405, found 404.2405.

HPLC: t_R = 5.46, purity ≥ 95% (UV: 254/ 280 nm).

Synthesis of *tert*-butyl (6-((4-((3-cyclopropyl-1*H*-pyrazol-5-yl)amino)pyrimidin-2-yl)amino)hexyl)-carbamate (56e)

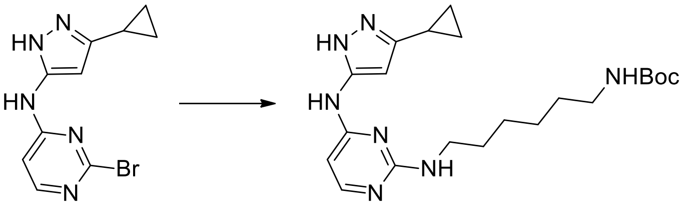

The title compound was prepared according to the procedure of **56c**, using **53** (100 mg, 0.36 mmol) and *tert*-butyl (6-aminohexyl)carbamate (77 mg, 0.36 mmol). The mixture was stirred for 7 h at 90 °C to obtain the product (66 mg, 45%) as a colorless oil.

^{1}H NMR (300 MHz, DMSO-d6) δ 11.87 (s, 1H), 9.29 (s, 1H), 7.77 (d, J = 5.6 Hz, 1H), 6.73 (t, J = 5.7 Hz, 1H), 6.62 (s, 1H), 6.35 – 6.00 (m, 2H), 3.44 – 3.28 (m, 2H), 3.28 – 3.14 (m, 2H), 2.89 (q, J = 6.5 Hz, 2H), 1.89 – 1.77 (m, 1H), 1.56 – 1.44 (m, 2H), 1.36 (s, 9H), 1.33 – 1.22 (m, 4H), 0.97 – 0.83 (m, 2H), 0.73 – 0.60 (m, 2H).

^{13}C NMR (75 MHz, DMSO) δ 162.06, 159.61, 156.03, 155.59, 95.62, 77.28, 69.07, 41.18, 40.67, 29.57, 29.33, 28.26, 26.39, 26.20, 7.66.

MS-ESI m/z $[M + H]^+$: calcd 416.5, found 416.5.

HRMS m/z $[M + H]^+$: calcd 416.2769, found 416.2768.

HPLC: t_R = 7.557, purity ≥ 95% (UV: 254/ 280 nm).

Synthesis of *tert*-butyl 4-(((4-((3-cyclopropyl-1*H*-pyrazol-5-yl)amino)pyrimidin-2-yl)amino)methyl)-benzylcarbamate (56f)

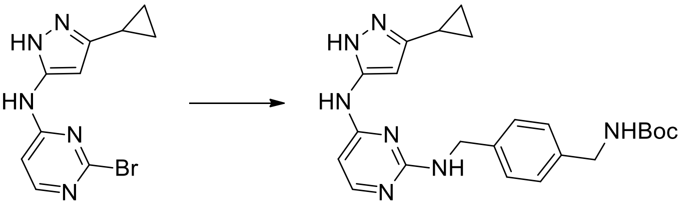

The title compound was prepared according to the procedure of **56c**, using **53** (60 mg, 0.21 mmol) and *tert*-butyl 4-(aminomethyl)benzylcarbamate (51 mg, 0.21 mmol). The mixture was stirred for 6 h at 90 °C to obtain the product (22 mg, 24%) as a colorless oil.

^{1}H NMR (300 MHz, DMSO-d6) δ 11.97 (s, 1H), 9.35 (s, 1H), 7.79 (d, J = 5.7 Hz, 1H), 7.38 – 7.10 (m, 6H), 6.26 – 5.92 (m, 2H), 4.46 (d, J = 6.2 Hz, 2H), 4.08 (d, J = 6.2 Hz, 2H), 1.88 – 1.73 (m, 1H), 1.38 (s, 9H), 0.93 – 0.79 (m, 2H), 0.71 – 0.53 (m, 2H).

^{13}C NMR (75 MHz, DMSO) δ 161.99, 159.65, 156.01, 155.77, 139.25, 138.28, 126.81, 96.08, 77.69, 43.72, 43.15, 28.24, 7.65.

MS-ESI m/z $[M + H]^+$: calcd 436.5, found 436.4.

HRMS m/z $[M + H]^+$: calcd 436.2456, found 436.2448.

HPLC: t_R = 7.45, purity ≥ 95% (UV: 254/ 280 nm).

Synthesis of *tert*-butyl 4-((4-((3-cyclopropyl-1*H*-pyrazol-5-yl)amino)-5-methylpyrimidin-2-yl)amino)-phenethylcarbamate (57a)

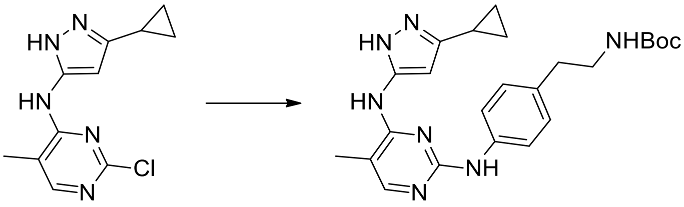

The title compound was prepared according to the procedure of **56b**, using **54** (52 mg, 0.21 mmol) and *tert*-butyl 4-aminophenethylcarbamate (49 mg, 0.21 mmol). The mixture was stirred for 18 h under reflux to obtain the product (85 mg, 90%) as a colorless oil.

^{1}H NMR (300 MHz, DMSO-d6) δ 12.56 (s, 1H), 10.61 (s, 1H), 10.16 (s, 1H), 7.88 (s, 1H), 7.38 (d, J = 7.2 Hz, 2H), 7.19 (d, J = 7.3 Hz, 2H), 6.90 (s, 1H), 6.07 (s, 1H), 3.21 – 3.07 (m, 2H), 2.77 – 2.63 (m, 2H), 2.11 (s, 3H), 1.94 – 1.81 (m, 1H), 0.99 – 0.87 (m, 2H), 0.64 – 0.51 (m, 2H).

^{13}C NMR (75 MHz, DMSO) δ 160.12, 155.41, 151.27, 146.40, 145.12, 140.12, 136.01, 134.68, 128.98, 122.29, 107.06, 95.10, 77.40, 41.38, 34.96, 28.16, 13.26, 7.84, 6.78.

MS-ESI m/z $[M + H]^+$: calcd 450.6, found 450.4.

HRMS m/z $[M + H]^+$: calcd 450.2612, found 450.2603.

HPLC: t_R = 7.54, purity ≥ 95% (UV: 254/ 280 nm).

Synthesis of *tert*-butyl 3-((4-((3-cyclopropyl-1*H*-pyrazol-5-yl)amino)-5-methylpyrimidin-2-yl)amino)-phenethylcarbamate (57b)

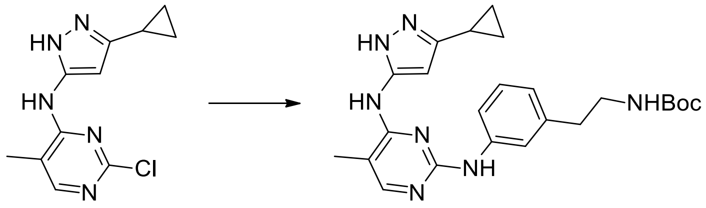

The title compound was prepared according to the procedure of **56b**, using **54** (52 mg, 0.21 mmol) *tert*-butyl 3-aminophenethylcarbamate (49 mg, 0.21 mmol). The mixture was stirred for 18 h under reflux to obtain the product (34 mg, 36%) as a colorless oil.

^{1}H NMR (300 MHz, DMSO-d6) δ 12.09 (s, 1H), 9.12 (s, 2H), 7.86 (s, 1H), 7.62 (d, J = 8.2 Hz, 1H), 7.45 (s, 1H), 7.14 (t, J = 7.8 Hz, 1H), 6.86 (t, J = 5.7 Hz, 1H), 6.72 (d, J = 7.5 Hz, 1H), 5.83 (s, 1H), 3.33 (s, 3H), 3.21 – 3.05 (m, 2H), 2.72 – 2.59 (m, 2H), 1.93 – 1.79 (m, 1H), 1.37 (s, 9H), 0.96 – 0.81 (m, 2H), 0.72 – 0.61 (m, 2H).

^{13}C NMR (75 MHz, DMSO) δ 158.12, 155.52, 155.14, 141.21, 139.56, 128.35, 120.81, 118.44, 116.14, 105.46, 77.49, 41.65, 35.91, 28.26, 13.33, 7.68.

MS-ESI m/z $[M + H]^+$: calcd 450.6, found 450.4.

HRMS m/z $[M + H]^+$: calcd 450.2612, found 450.2607.

HPLC: t_R = 7.63, purity ≥ 95% (UV: 254/ 280 nm).

Synthesis of *tert*-butyl (5-((4-((3-cyclopropyl-1*H*-pyrazol-5-yl)amino)-5-methylpyrimidin-2-yl)amino)-pentyl)carbamate (57c)

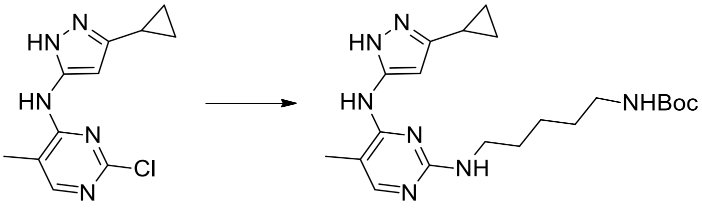

The title compound was prepared according to the procedure of **56c**, using **54** (60 mg, 0.24 mmol) and *tert*-butyl (5-aminopentyl)carbamate (49 mg, 0.24 mmol). The mixture was stirred for 6 h at 90 °C to obtain the product (5 mg, 5%) as a colorless oil.

^{1}H NMR (300 MHz, DMSO-d6) δ 12.06 (s, 1H), 8.58 (s, 1H), 7.65 (s, 1H), 6.75 (t, J = 5.5 Hz, 1H), 6.32 (s, 1H), 3.18 (q, J = 6.7 Hz, 2H), 2.90 (q, J = 6.5 Hz, 2H), 1.96 (s, 3H), 1.90 – 1.78 (m, 1H), 1.55 – 1.45 (m, 2H), 1.36 (s, 9H), 1.32 – 1.21 (m, 4H), 0.97 – 0.81 (m, 2H), 0.69 – 0.61 (m, 2H).

MS-ESI m/z $[M + H]^+$: calcd 416.5, found 416.2.

HRMS m/z $[M + H]^+$: calcd 416.2769, found 416.2769.

HPLC: t_R = 7.43, purity ≥ 95% (UV: 254/ 280 nm).

Synthesis of *tert*-butyl (2-(2-((4-((3-cyclopropyl-1*H*-pyrazol-5-yl)amino)-5-methylpyrimidin-2-yl)amino)ethoxy)ethyl)carbamate (57d)

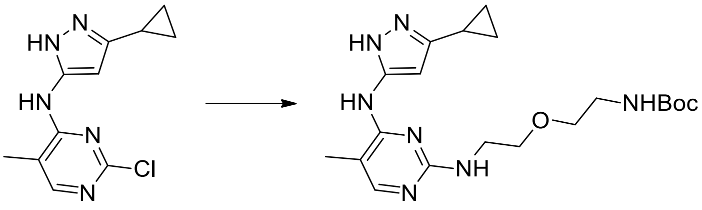

The title compound was prepared according to the procedure of **56c**, using **54** (60 mg, 0.24 mmol) and *tert*-butyl (2-(2-aminoethoxy)ethyl)carbamate (49 mg, 0.24 mmol). The mixture was stirred for 10 h at 90 °C to obtain the product (7 mg, 7%) as a colorless oil.

^{1}H NMR (300 MHz, DMSO-d6) δ 8.66 (s, 1H), 7.66 (s, 1H), 6.92 – 6.70 (m, 2H), 6.15 (s, 1H), 3.49 (t, J = 5.8 Hz, 2H), 3.44 – 3.37 (m, 2H), 3.08 (q, J = 5.9 Hz, 2H), 2.94 – 2.84 (m, 2H), 1.97 (s, 3H), 1.90 – 1.78 (m, 1H), 1.37 (s, 9H), 0.96 – 0.79 (m, 2H), 0.71 – 0.62 (m, 2H).

^{13}C NMR (75 MHz, DMSO) δ 160.77, 155.55, 116.98, 102.86, 77.61, 69.28, 69.12, 41.33, 40.57, 28.22, 23.63, 13.19, 7.70.

MS-ESI m/z $[M + H]^+$: calcd 418.5, found 418.4.

HRMS m/z $[M + H]^+$: calcd 418.2561, found 418.2559.

HPLC: t_R = 7.18, purity ≥ 95% (UV: 254/ 280 nm).

Synthesis of *tert*-butyl (6-((4-((3-cyclopropyl-1*H*-pyrazol-5-yl)amino)-5-methylpyrimidin-2-yl)amino)hexyl)carbamate (57e)

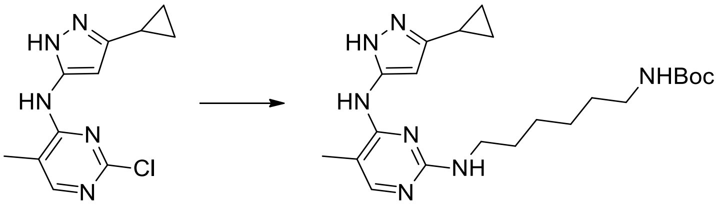

The title compound was prepared according to the procedure of **56c**, using **54** (60 mg, 0.24 mmol) and *tert*-butyl (6-aminohexyl)carbamate (52 mg, 0.24 mmol). The mixture was stirred for 6 h at 90 °C to obtain the product (5 mg, 5%) as a colorless oil.

^{1}H NMR (300 MHz, DMSO-d6) δ 12.17 (s, 1H), 8.57 (s, 1H), 7.67 (s, 1H), 6.78 (t, J = 5.0 Hz, 1H), 6.44 (s, 1H), 3.21 (q, J = 6.7 Hz, 2H), 2.91 (q, J = 6.5 Hz, 2H), 1.98 (s, 3H), 1.92 – 1.80 (m, 1H), 1.60 – 1.47 (m, 2H), 1.38 (s, 9H), 1.33 – 1.24 (m, 4H), 0.96 – 0.82 (m, 2H), 0.71 – 0.60 (m, 2H).

MS-ESI m/z $[M + H]^+$: calcd 430.6, found 430.3.

HRMS m/z $[M + H]^+$: calcd 430.2925, found 430.2924.

HPLC: t_R = 7.69, purity ≥ 95% (UV: 254/ 280 nm).

Synthesis of *tert*-butyl 4-((5-chloro-4-((3-cyclopropyl-1*H*-pyrazol-5-yl)amino)pyrimidin-2-yl)amino)phenethylcarbamate (58a)

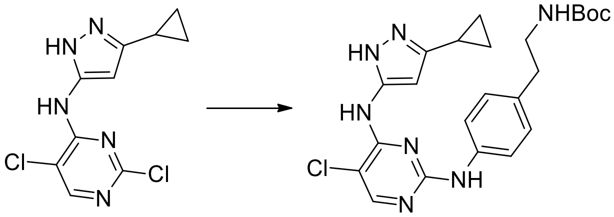

The title compound was prepared according to the procedure of **56b**, using **55** (72 mg, 0.27 mmol) and *tert*-butyl 4-aminophenethylcarbamate (63 mg, 0.27 mmol). The mixture was stirred for 18 h under reflux to obtain the product (20 mg, 16%) as a yellow oil.

^{1}H NMR (300 MHz, DMSO-d6) δ 12.25 (s, 1H), 9.31 (s, 1H), 8.58 (s, 1H), 8.09 (s, 1H), 7.54 (d, J = 8.4 Hz, 2H), 7.07 (d, J = 8.1 Hz, 2H), 6.85 (t, J = 5.6 Hz, 1H), 6.16 (s, 1H), 3.11 (q, J = 6.9 Hz, 2H), 2.63 (t, J = 7.6 Hz, 2H), 2.00 – 1.80 (m, 1H), 1.37 (s, 9H), 0.98 – 0.86 (m, 2H), 0.74 – 0.62 (m, 2H).

^{13}C NMR (75 MHz, DMSO) δ 157.86, 155.52, 155.10, 154.26, 138.41, 132.39, 128.52, 119.32, 103.36, 77.46, 41.73, 34.99, 28.26, 7.73.

MS-ESI m/z $[M + H]^+$: calcd 471.0, found 470.4.

HRMS m/z $[M + H]^+$: calcd 470.2066, found 470.2061.

HPLC: t_R = 8.70, purity ≥ 95% (UV: 254/ 280 nm).

Synthesis of *tert*-butyl (5-((5-chloro-4-((3-cyclopropyl-1*H*-pyrazol-5-yl)amino)pyrimidin-2-yl)amino)pentyl)carbamate (58c)

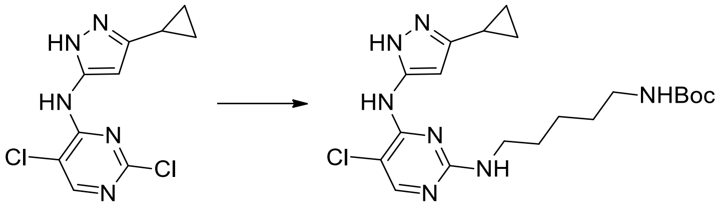

The title compound was prepared according to the procedure of **56c**, using **55** (60 mg, 0.22 mmol) and *tert*-butyl (5-aminopentyl)carbamate (45 mg, 0.22 mmol). The mixture was stirred for 8 h at 80 °C to obtain the product (50 mg, 52%) as a colorless oil.

^{1}H NMR (300 MHz, DMSO-d6) δ 12.11 (s, 1H), 8.42 (s, 1H), 7.91 (s, 1H), 7.02 (s, 1H), 6.74 (t, J = 5.6 Hz, 1H), 6.31 (s, 1H), 3.27 – 3.13 (m, 2H), 2.90 (q, J = 6.5 Hz, 2H), 1.93 – 1.80 (m, 1H), 1.58 – 1.46 (m, 2H), 1.43 – 1.34 (m, 11H), 1.33 – 1.21 (m, 2H), 0.98 – 0.85 (m, 2H), 0.73 – 0.61 (m, 2H).

^{13}C NMR (75 MHz, DMSO) δ 160.41, 158.17, 155.59, 154.56, 101.48, 93.37, 77.29, 40.99, 29.30, 28.77, 28.26, 23.87, 7.69.

MS-ESI m/z $[M + H]^+$: calcd 437.0, found 436.4.

HRMS m/z $[M + H]^+$: calcd 436.2222, found 436.2218.

HPLC: t_R = 7.56, purity ≥ 95% (UV: 254/ 280 nm).

Synthesis of N^2-(6-aminohexyl)-N^4-(3-cyclopropyl-1*H*-pyrazol-5-yl)pyrimidine-2,4-diamine (59)

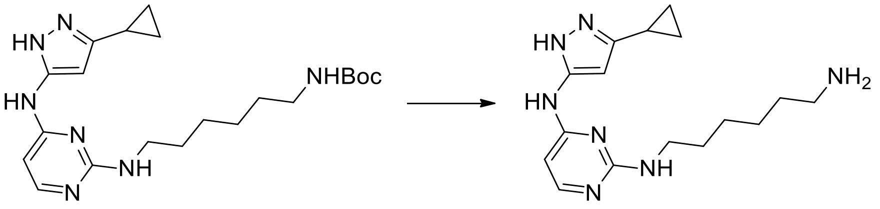

56e (50 mg, 0.12 mmol, 1.0 eq) was dissolved in 4 mL anhydrous DCM. TFA (549 mg, 4.81 mmol, 40.0 eq) was added at 0 °C and the reaction mixture was allowed to warm up to rt overnight. The solvent was evaporated under reduced pressure. The residue was dissolved in methanol and neutralized with saturated K_2CO_3 solution. The solvent was again evaporated under reduced pressure and the crude product was purified by flash chromatography using H_2O/ acetonitrile as an eluent to obtain the desired product with impurities. The product was used without further purification.

MS-ESI m/z [M + H]$^+$: calcd 316.4, found 316.2.

Synthesis of N-(6-((4-((3-cyclopropyl-1*H*-pyrazol-5-yl)amino)pyrimidin-2-yl)amino)hexyl)acetamide (60)

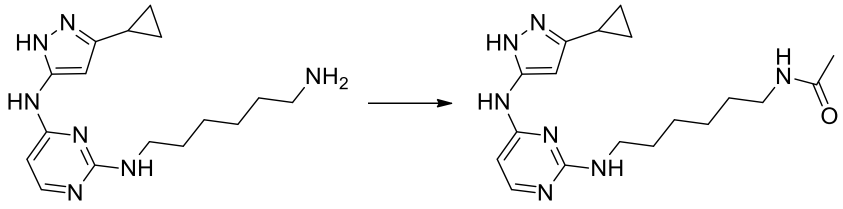

Acetic acid (7 mg, 0.12 mmol, 1.0 eq) and HATU (55 mg, 0.14 mmol, 1.2 eq) were dissolved in 4 mL anhydrous DMF. DIPEA (37 mg 0.39 mmol, 2.4 eq) was added and the resulting mixture was stirred at rt for 1 h. **59** (38 mg, 0.12 mmol, 1.0 eq) was added and the reaction mixture was stirred at rt for further 18 h. The solvent was evaporated under reduced pressure and the crude product was purified by flash chromatography using DCM/ ethanol as an eluent to obtain the desired product (13 mg, 30%) as a colorless oil.

^{1}H NMR (300 MHz, DMSO-d6) δ 12.42 (s, 1H), 11.12 (s, 1H), 8.47 (s, 1H), 7.92 – 7.68 (m, 2H), 6.57 – 6.17 (m, 2H), 3.39 – 3.21 (m, 2H), 3.00 (q, J = 6.4 Hz, 2H), 1.97 – 1.82 (m, 1H), 1.77 (s, 3H), 1.67 – 1.50 (m, 2H), 1.47 – 1.23 (m, 6H), 1.02 – 0.90 (m, 2H), 0.83 – 0.62 (m, 2H).

^{13}C NMR (75 MHz, DMSO) δ 168.91, 153.77, 150.30, 146.28, 142.21, 97.72, 93.29, 40.93, 38.41, 29.14, 28.36, 26.17, 22.60, 7.86, 6.76.

MS-ESI m/z $[M + H]^+$: calcd 358.5, found 358.3.

HRMS m/z $[M + H]^+$: calcd 358.2350, found 358.2352.

HPLC: t_R = 6.51, purity ≥ 95% (UV: 254/ 280 nm).

Synthesis of methyl 5-((2-chloropyrimidin-4-yl)amino)-1*H*-pyrazole-3-carboxylate (73)

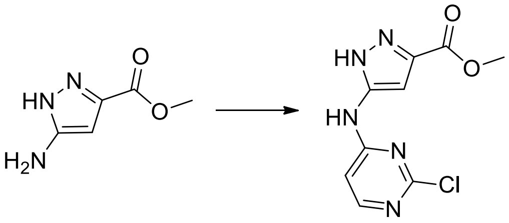

The title compound was prepared according to the procedure of **53**, using methyl 3-amino-1*H*-pyrazole-5-carboxylate (500 mg, 3.54 mmol) and 2,4-dichloropyrimidine (480 mg, 3.22 mmol). The mixture was stirred at 50 °C for 72 h to obtain the product (132 mg, 16%) as a white solid.

^{1}H NMR (250 MHz, DMSO-d6) δ 13.70 (s, 1H), 10.63 (s, 1H), 8.20 (d, J = 5.9 Hz, 1H), 7.19 – 6.81 (m, 2H), 3.86 (s, 3H).

^{13}C NMR (151 MHz, DMSO) δ 160.56, 159.39, 147.77, 133.08, 128.15, 127.41, 99.45, 52.04.

MS-ESI m/z $[M + Na]^+$: calcd 276.7, found 276.1.

Synthesis of methyl 5-((2,5-dichloropyrimidin-4-yl)amino)-1*H*-pyrazole-3-carboxylate (74)

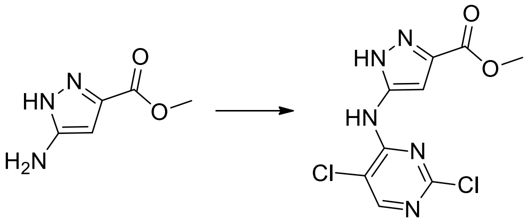

The title compound was prepared according to the procedure of **53**, using methyl 3-amino-1*H*-pyrazole-5-carboxylate (500 mg, 3.54 mmol) and 2,4,5-trichloropyrimidine (591 mg, 3.22 mmol). The mixture was stirred at 60 °C for 72 h to obtain the product (781 mg, 84%) as a beige solid.

^{1}H NMR (250 MHz, DMSO-d6) δ 13.87 (s, 1H), 10.10 (s, 1H), 8.40 (s, 1H), 7.06 (s, 1H), 3.86 (s, 3H).

^{13}C NMR (126 MHz, DMSO) δ 159.22, 156.95, 156.77, 155.60, 146.39, 133.11, 113.43, 102.23, 52.12.

MS-ESI m/z $[M + H]^+$: calcd 287.1, found 286.0.

Synthesis of methyl 5-((2-chloroquinazolin-4-yl)amino)-1*H*-pyrazole-3-carboxylate (75)

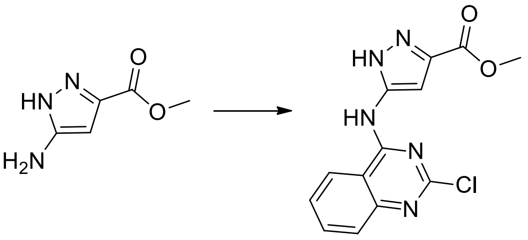

The title compound was prepared according to the procedure **53**, using methyl 3-amino-1H-pyrazole-5-carboxylate (500 mg, 3.54 mmol) and 2,4-dichloroquinazoline (641 mg, 3.22 mmol). The mixture was stirred at 60 °C for 72 h to obtain the product (823 mg, 84%) as a white solid.

^{1}H NMR (300 MHz, DMSO-d6) δ 13.88 (s, 1H), 11.12 (s, 1H), 8.67 (d, J = 8.3 Hz, 1H), 7.88 (t, J = 7.6 Hz, 1H), 7.73 (d, J = 8.3 Hz, 1H), 7.61 (t, J = 7.6 Hz, 1H), 7.35 (s, 1H), 3.89 (s, 3H).

^{13}C NMR (75 MHz, DMSO) δ 159.32, 158.58, 156.07, 150.82, 147.41, 134.16, 132.93, 126.87, 126.77, 123.63, 113.45, 101.83, 52.11.

MS-ESI m/z $[M + H]^+$: calcd 304.7, found 304.1.

Synthesis of methyl 5-((2-((4-(2-((*tert*-butoxycarbonyl)amino)ethyl)phenyl)amino)pyrimidin-4-yl)amino)-1*H*-pyrazole-3-carboxylate (76a)

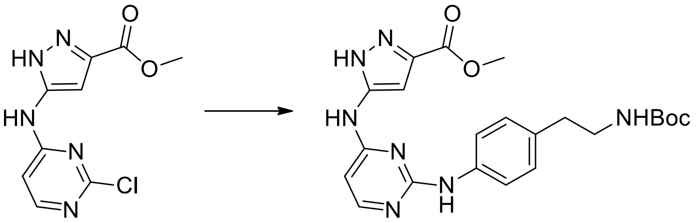

The title compound was prepared according to the procedure of **56b**, using **73** (214 mg, 0.84 mmol) and *tert*-butyl 4-aminophenethylcarbamate (181 mg, 0.77 mmol). The mixture was stirred for 18 h under reflux to obtain the product (219 mg, 63%) as a light yellow solid.

^{1}H NMR (250 MHz, DMSO-d6) δ 13.87 (s, 1H), 11.29 (s, 1H), 10.50 (s, 1H), 8.00 (d, J = 6.9 Hz, 1H), 7.47 (d, J = 8.0 Hz, 2H), 7.23 (d, J = 8.1 Hz, 2H), 7.06 (s, 1H), 6.90 (t, J = 5.3 Hz, 1H), 6.52 (s, 1H), 3.87 (s, 3H), 3.22 – 3.10 (m, 2H), 2.80 – 2.65 (m, 2H), 1.37 (s, 9H).

^{13}C NMR (126 MHz, DMSO) δ 160.11, 155.54, 146.85, 136.35, 133.35, 129.22, 122.79, 100.87, 99.04, 77.52, 52.04, 41.52, 35.06, 28.24.

MS-ESI m/z [M + H]$^+$: calcd 454.5, found 454.1.

HRMS m/z [M + Na]$^+$: calcd 476.2017, found 476.2038.

HPLC: t_R = 6.09, purity ≥ 95% (UV: 254/ 280 nm).

Synthesis of methyl 5-((2-((3-(2-((*tert*-butoxycarbonyl)amino)ethyl)phenyl)amino)pyrimidin-4-yl)amino)-1*H*-pyrazole-3-carboxylate (76b)

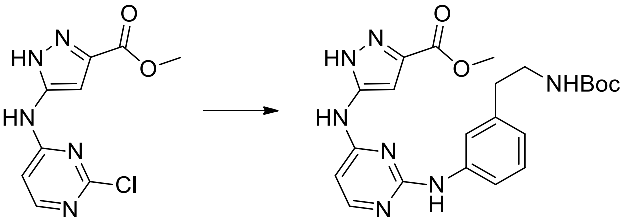

The title compound was prepared according to the procedure of **56b**, using **73** (225 mg, 0.89 mmol) and *tert*-butyl 3-aminophenethylcarbamate (191 mg, 0.81 mmol). The mixture was stirred for 18 h under reflux to obtain the product (178 mg, 49%) as a light yellow solid.

^{1}H NMR (250 MHz, DMSO-d6) δ 13.85 (s, 1H), 11.33 (s, 1H), 10.54 (s, 1H), 8.01 (d, J = 6.7 Hz, 1H), 7.54 – 7.28 (m, 3H), 7.08 (d, J = 7.1 Hz, 1H), 6.98 (s, 1H), 6.85 (t, J = 5.6 Hz, 1H), 6.52 (s, 1H), 3.84 (s, 3H), 3.16 – 3.06 (m, 2H), 2.75 – 2.64 (m, 2H), 1.34 (s, 9H).

^{13}C NMR (126 MHz, DMSO) δ 160.28, 159.49, 155.52, 153.45, 147.09, 140.65, 136.85, 133.51, 129.09, 125.61, 123.38, 121.02, 100.73, 99.19, 77.53, 51.93, 41.30, 35.37, 28.22.

MS-ESI m/z [M + H]$^+$: calcd 454.5, found 454.3.

HRMS m/z [M + H]$^+$: calcd 454.2197, found 454.2182.

HPLC: t_R = 6.07, purity ≥ 95% (UV: 254/ 280 nm).

Synthesis of methyl 5-((2-((5-((*tert*-butoxycarbonyl)amino)pentyl)amino)pyrimidin-4-yl)amino)-1*H*-pyrazole-3-carboxylate (76c)

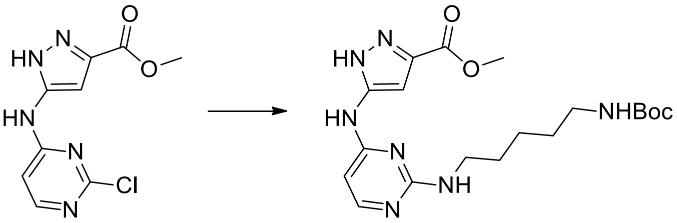

The title compound was prepared according to the procedure of **56c**, using **73** (180 mg, 0.71 mmol) and *tert*-butyl (5-aminopentyl)carbamate (144 mg, 0.71 mmol). The mixture was stirred for 5 h at 120 °C to obtain the product (142 mg, 45%) as a white solid.

^{1}H NMR (400 MHz, DMSO-d6) δ 13.38 (s, 1H), 9.91 (d, J = 185.8 Hz, 1H), 7.83 (s, 1H), 7.21 (s, 1H), 6.75 (s, 2H), 6.04 (d, J = 53.4 Hz, 1H), 3.82 (s, 3H), 3.23 (q, J = 6.3 Hz, 2H), 2.91 (q, J = 6.4 Hz, 2H), 1.61 – 1.46 (m, 2H), 1.36 (s, 13H).

^{13}C NMR (101 MHz, DMSO) δ 162.50, 160.04, 157.02, 156.06, 150.13, 142.02, 100.07, 96.24, 77.78, 52.27, 41.26, 40.66, 29.78, 29.39, 28.74, 24.33.

MS-ESI m/z $[M + H]^+$: calcd 420.5, found 420.9.

HRMS m/z $[M + H]^+$: calcd 420.2354, found 420.2350.

HPLC: t_R = 5.57, purity ≥ 95% (UV: 254/ 280 nm).

Synthesis of methyl 5-((2-((2-(2-((*tert*-butoxycarbonyl)amino)ethoxy)ethyl)amino)pyrimidin-4-yl)amino)-1*H*-pyrazole-3-carboxylate (76d)

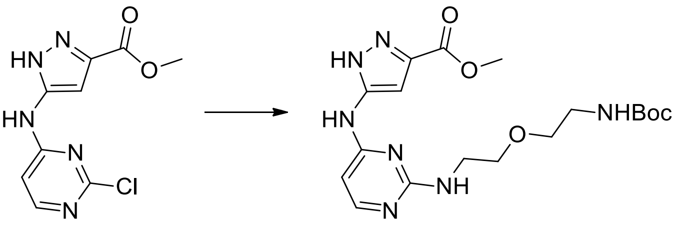

The title compound was prepared according to the procedure of **56c**, using **73** (200 mg, 0.79 mmol) and *tert*-butyl (2-(2-aminoethoxy)ethyl)carbamate (161 mg, 0.79 mmol). The mixture was stirred for 5 h at 120 °C to obtain the product (10 mg, 31%) as a colorless oil.

^{1}H NMR (500 MHz, DMSO-d6) δ 13.39 (s, 1H), 9.91 (d, J = 245.4 Hz, 1H), 7.86 (s, 1H), 7.54 – 5.86 (m, 4H), 3.82 (s, 3H), 3.60 – 3.49 (m, 2H), 3.46 – 3.38 (m, 4H), 3.09 (q, J = 5.9 Hz, 2H), 1.36 (s, 9H).

^{13}C NMR (126 MHz, DMSO) δ 162.14, 159.69, 156.87, 155.63, 149.28, 141.64, 132.78, 99.45, 96.01, 92.69, 77.62, 69.08, 51.72, 40.48, 28.22.

MS-ESI m/z $[M + H]^+$: calcd 422.5, found 422.9.

HRMS m/z $[M + H]^+$: calcd 422.2146, found 422.2135.

HPLC: t_R = 5.18, purity ≥ 95% (UV: 254/ 280 nm).

Synthesis of methyl 5-((2-((6-((*tert*-butoxycarbonyl)amino)hexyl)amino)pyrimidin-4-yl)amino)-1*H*-pyrazole-3-carboxylate (76e)

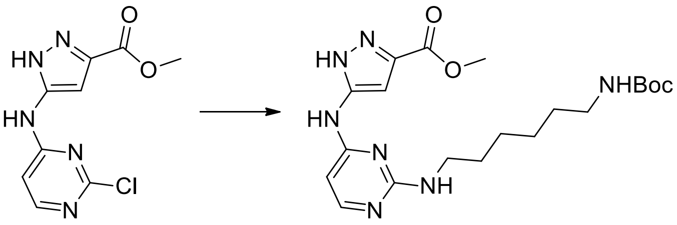

The title compound was prepared according to the procedure of **56c**, using **73** (50 mg, 0.20 mmol) and *tert*-butyl (6-aminohexyl)carbamate (43 mg, 0.20 mmol). The mixture was stirred for 5 h at 120 °C to obtain the product (36 mg, 42%) as a colorless oil.

^{1}H NMR (400 MHz, DMSO-d6) δ 13.37 (s, 1H), 9.90 (d, J = 169.7 Hz, 1H), 7.85 (s, 1H), 7.17 (s, 1H), 6.94 – 6.58 (m, 2H), 6.07 (s, 1H), 3.81 (s, 3H), 3.23 (q, J = 6.7 Hz, 2H), 2.98 – 2.83 (m, 2H), 1.57 – 1.45 (m, 2H), 1.40 – 1.23 (m, 15H).

^{13}C NMR (101 MHz, DMSO) δ 162.04, 159.47, 156.64, 155.60, 149.06, 140.95, 132.46, 99.15, 95.72, 77.29, 51.72, 40.65, 29.53, 29.24, 28.27, 26.31, 26.18.

MS-ESI m/z [M + H]$^+$: calcd 434.5, found 435.0.

HRMS m/z [M + H]$^+$: calcd 434.2510, found 434.2500.

HPLC: t_R = 5.86, purity ≥ 95% (UV: 254/ 280 nm).

Synthesis of methyl 5-((2-((4-(cyanomethyl)phenyl)amino)pyrimidin-4-yl)amino)-1*H*-pyrazole-3-carboxylate (76f)

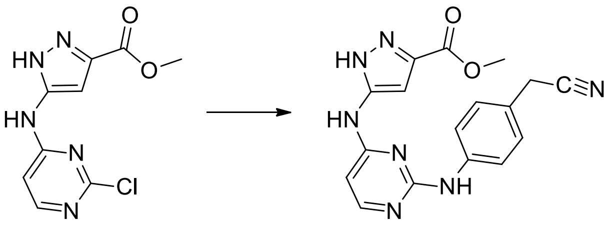

The title compound was prepared according to the procedure of **56a**, using **73** (55 mg, 0.22 mmol) and 2-(4-aminophenyl)acetonitrile (29 mg, 0.22 mmol). The mixture was stirred for 18 h under reflux to obtain the product (46 mg, 61%) as a white solid.

^{1}H NMR (300 MHz, DMSO-d6) δ 11.52 (s, 1H), 10.90 (s, 1H), 8.05 (d, J = 7.1 Hz, 1H), 7.58 (d, J = 8.1 Hz, 2H), 7.40 (d, J = 8.3 Hz, 2H), 7.01 (s, 1H), 6.56 (s, 1H), 4.08 (s, 2H), 3.88 (s, 3H).

^{13}C NMR (75 MHz, DMSO) δ 160.20, 159.36, 152.75, 146.04, 143.59, 135.95, 133.88, 128.85, 127.98, 123.09, 119.23, 100.74, 99.31, 52.14, 21.99.

MS-ESI m/z $[M + H]^+$: calcd 350.4, found 350.2.

HRMS m/z $[M + H]^+$: calcd 350.1360, found 350.1363.

HPLC: t_R = 6.79, purity ≥ 95% (UV: 254/ 280 nm).

Synthesis of methyl 5-((2-((4-(((*tert*-butoxycarbonyl)amino)methyl)benzyl)amino)pyrimidin-4-yl)amino)-1*H*-pyrazole-3-carboxylate (76g)

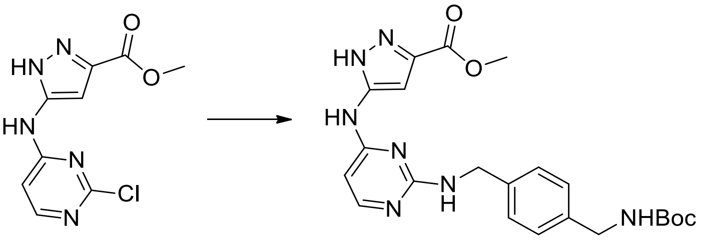

The title compound was prepared according to the procedure of **56c**, using **73** (150 mg, 0.59 mmol) and *tert*-butyl 4-(aminomethyl)benzylcarbamate (140 mg, 0.59 mmol). The mixture was stirred for 5 h at 120 °C to obtain the product (71 mg, 26%) as a white solid.

^{1}H NMR (400 MHz, DMSO-d6) δ 13.39 (s, 1H), 9.95 (d, J = 203.0 Hz, 1H), 7.86 (s, 1H), 7.39 – 7.11 (m, 5H), 6.12 (s, 1H), 4.46 (d, J = 6.1 Hz, 2H), 4.08 (d, J = 6.1 Hz, 2H), 3.83 (s, 3H), 1.38 (s, 9H).

^{13}C NMR (101 MHz, DMSO) δ 161.88, 159.45, 156.66, 155.78, 149.13, 141.49, 139.09, 138.33, 127.28, 126.96, 126.83, 96.28, 77.72, 51.72, 43.83, 43.15, 28.25.

MS-ESI m/z $[M + H]^+$: calcd 454.5, found 455.1

HRMS m/z $[M + H]^+$: calcd 454.2197, found 454.2190.

HPLC: t_R = 5.60, purity ≥ 95% (UV: 254/ 280 nm).

Synthesis of methyl 5-((2-((4-(((*tert*-butoxycarbonyl)amino)methyl)phenyl)amino)pyrimidin-4-yl)amino)-1*H*-pyrazole-3-carboxylate (76h)

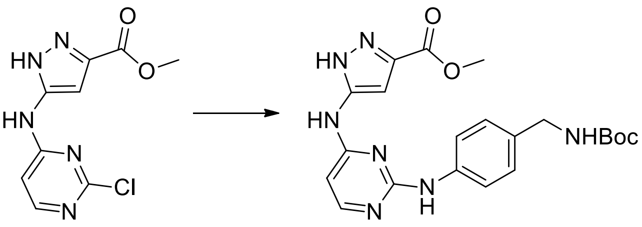

The title compound was prepared according to the procedure of **56b**, using **73** (226 mg, 0.89 mmol) and *tert*-butyl 4-aminobenzylcarbamate (180 mg, 0.81 mmol). The mixture was stirred for 18 h under reflux to obtain the product (228 mg, 64%) as a white solid.

^{1}H NMR (500 MHz, DMSO-d6) δ 13.18 (d, J = 722.0 Hz, 1H), 11.46 (s, 1H), 10.70 (s, 1H), 8.00 (s, 1H), 7.47 (d, J = 8.0 Hz, 2H), 7.41 (t, J = 6.2 Hz, 1H), 7.29 (d, J = 8.1 Hz, 2H), 7.21 – 6.97 (m, 1H), 6.50 (s, 1H), 4.16 (d, J = 6.0 Hz, 2H), 3.88 (s, 3H), 1.40 (s, 9H).

^{13}C NMR (126 MHz, DMSO) δ 160.20, 155.83, 152.89, 143.48, 137.58, 135.01, 133.33, 127.77, 122.86, 100.87, 99.23, 77.86, 52.13, 43.05, 28.26.

MS-ESI m/z [M + H]$^+$: calcd 440.5, found 440.2.

HRMS m/z [M + H]$^+$: calcd 440.2041, found 440.2038.

HPLC: t_R = 5.86, purity ≥ 95% (UV: 254/ 280 nm).

Synthesis of methyl 5-((2-((4-((*tert*-butoxycarbonyl)amino)benzyl)amino)pyrimidin-4-yl)amino)-1*H*-pyrazole-3-carboxylate (76i)

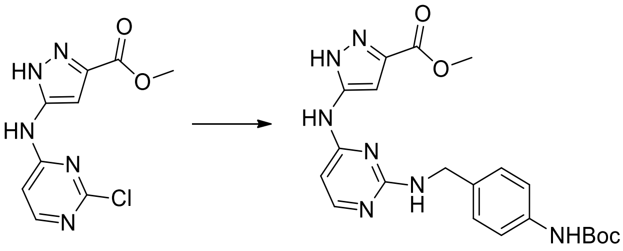

The title compound was prepared according to the procedure of **56c**, using **73** (150 mg, 0.59 mmol) and *tert*-butyl (4-(aminomethyl)phenyl)carbamate (131 mg, 0.59 mmol). The mixture was stirred for 3 h at 120 °C to obtain the product (45 mg, 17%) as a white solid.

^{1}H NMR (400 MHz, DMSO-d6) δ 13.34 (s, 1H), 9.87 (d, J = 138.1 Hz, 1H), 9.24 (s, 1H), 7.87 (s, 1H), 7.59 – 6.81 (m, 6H), 6.09 (s, 1H), 4.41 (d, J = 6.1 Hz, 2H), 3.82 (s, 3H), 1.45 (s, 9H).

^{13}C NMR (101 MHz, DMSO) δ 161.86, 159.46, 156.56, 152.80, 138.03, 134.23, 127.79, 127.51, 118.04, 96.14, 78.86, 51.71, 43.66, 28.14.

MS-ESI m/z [M + H]$^+$: calcd 440.5, found 441.0.

HRMS m/z [M + H]$^+$: calcd 440.2041, found 440.2040.

HPLC: t_R = 5.79, purity ≥ 95% (UV: 254/ 280 nm).

Synthesis of methyl 5-((2-((4-(2-((*tert*-butoxycarbonyl)amino)ethyl)phenyl)amino)-5-chloropyrimidin-4-yl)amino)-1*H*-pyrazole-3-carboxylate (77a)

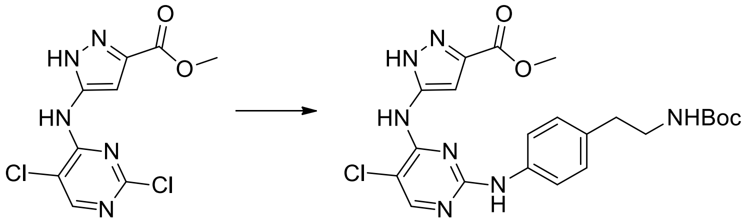

The title compound was prepared according to the procedure of **56b**, using **74** (170 mg, 0.59 mmol) and *tert*-butyl 4-aminophenethylcarbamate (127 mg, 0.54 mmol). The mixture was stirred for 18 h under reflux to obtain the product (14 mg, 5%) as a light yellow solid.

^{1}H NMR (250 MHz, DMSO-d6) δ 9.92 (s, 1H), 9.88 (s, 1H), 8.23 (s, 1H), 7.50 (d, J = 7.4 Hz, 2H), 7.09 (d, J = 7.5 Hz, 2H), 7.00 – 6.77 (m, 2H), 3.85 (s, 3H), 3.18 – 3.01 (m, 2H), 2.72 – 2.58 (m, 2H), 1.36 (s, 9H).

^{13}C NMR (75 MHz, DMSO) δ 160.79, 155.83, 155.40, 155.23, 151.51, 143.10, 137.10, 133.41, 128.67, 119.73, 103.59, 77.37, 51.73, 41.55, 34.90, 28.16.

MS-ESI m/z $[M + H]^+$: calcd 489.0, found 488.2.

HRMS m/z $[M + H]^+$: calcd 488.1808, found 488.1799.

HPLC: t_R = 9.01, purity ≥ 95% (UV: 254/ 280 nm).

Synthesis of methyl 5-((2-((3-(2-((*tert*-butoxycarbonyl)amino)ethyl)phenyl)amino)-5-chloropyrimidin-4-yl)amino)-1*H*-pyrazole-3-carboxylate (77b)

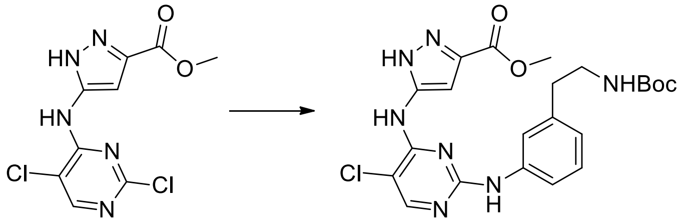

The title compound was prepared according to the procedure of **56b**, using **74** (170 mg, 0.59 mmol) and *tert*-butyl 3-aminophenethylcarbamate (127 mg, 0.54 mmol). The mixture was stirred for 18 h under reflux to obtain the product (23 mg, 9%) as a light yellow solid.

^{1}H NMR (300 MHz, DMSO-d6) δ 13.82 – 13.29 (m, 1H), 9.99 (s, 1H), 9.72 (s, 1H), 8.22 (s, 1H), 7.53 (d, J = 8.2 Hz, 1H), 7.42 (s, 1H), 7.17 (s, 1H), 6.88 – 6.73 (m, 2H), 6.62 (s, 1H), 3.83 (s, 3H), 3.22 – 3.04 (m, 2H), 2.70 – 2.56 (m, 2H), 1.37 (s, 9H).

^{13}C NMR (75 MHz, DMSO) δ 157.65, 155.50, 154.62, 140.16, 139.83, 128.46, 126.57, 121.82, 118.74, 116.55, 103.68, 77.51, 51.59, 41.58, 35.77, 28.26.

MS-ESI m/z $[M + H]^+$: calcd 489.0, found 488.2.

HRMS m/z $[M + H]^+$: calcd 488.1808, found 488.1802.

HPLC: t_R = 9.03, purity ≥ 95% (UV: 254/ 280 nm).

Synthesis of methyl 5-((2-((5-((*tert*-butoxycarbonyl)amino)pentyl)amino)-5-chloropyrimidin-4-yl)amino)-1*H*-pyrazole-3-carboxylate (77c)

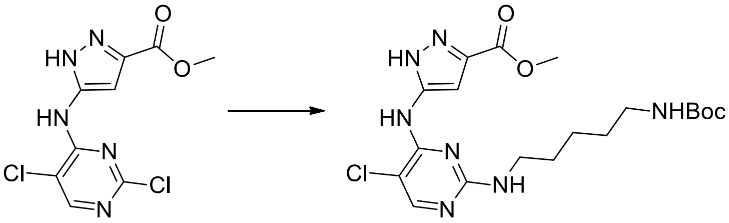

The title compound was prepared according to the procedure of **56c**, using **74** (50 mg, 0.17 mmol) and *tert*-butyl (5-aminopentyl)carbamate (35 mg, 0.17 mmol). The mixture was stirred for 3 h at 80 °C to obtain the product (28 mg, 35%) as a white solid.

^{1}H NMR (300 MHz, DMSO-d6) δ 13.50 (d, J = 68.2 Hz, 1H), 9.36 (d, J = 271.2 Hz, 1H), 7.99 (d, J = 26.2 Hz, 1H), 7.63 – 6.31 (m, 3H), 3.80 (s, 3H), 3.29 – 3.12 (m, 2H), 2.99 – 2.84 (m, 2H), 1.63 – 1.43 (m, 2H), 1.44 – 1.25 (m, 13H).

^{13}C NMR (75 MHz, DMSO) δ 160.48, 160.03, 155.59, 155.20, 141.57, 140.72, 101.18, 95.10, 77.30, 51.49, 40.73, 29.27, 28.71, 28.25, 23.79.

MS-ESI m/z $[M + H]^+$: calcd 454.9, found 454.2.

HRMS m/z $[M + H]^+$: calcd 454.1964, found 454.1954.

HPLC: t_R = 7.59, purity ≥ 95% (UV: 254/ 280 nm).

Synthesis of methyl 5-((2-((2-(2-((*tert*-butoxycarbonyl)amino)ethoxy)ethyl)amino)-5-chloropyrimidin-4-yl)amino)-1*H*-pyrazole-3-carboxylate (77d)

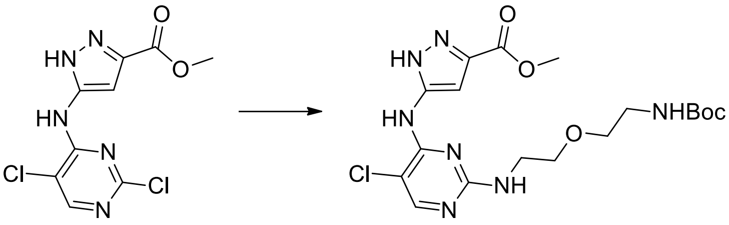

The title compound was prepared according to the procedure of **56c**, using **74** (200 mg, 0.69 mmol) and *tert*-butyl (2-(2-aminoethoxy)ethyl)carbamate (142 mg, 0.69 mmol). The mixture was stirred for 8 h at 80 °C to obtain the product (147 mg, 46%) as a white solid.

^{1}H NMR (300 MHz, DMSO-d6) δ 13.53 (d, J = 61.3 Hz, 1H), 9.38 (d, J = 280.8 Hz, 1H), 8.02 (d, J = 22.6 Hz, 1H), 7.17 (d, J = 40.1 Hz, 1H), 6.77 (t, J = 5.5 Hz , 1H), 6.57 (s, 1H), 3.92 – 3.75 (m, 3H), 3.58 – 3.48 (m, 2H), 3.49 – 3.35 (m, 4H), 3.17 – 3.01 (m, 2H), 1.38 (s, 9H).

^{13}C NMR (75 MHz, DMSO) δ 163.17, 160.84, 156.09, 155.59, 154.53, 142.03, 141.04, 101.91, 95.75, 78.10, 69.55, 69.41, 52.46, 51.95, 41.18, 28.69.

MS-ESI m/z $[M + H]^+$: calcd 456.9, found 456.3.

HRMS m/z $[M + H]^+$: calcd 457.1790, found 457.1785.

HPLC: t_R = 7.35, purity ≥ 95% (UV: 254/ 280 nm).

Synthesis of methyl 5-((2-((6-((*tert*-butoxycarbonyl)amino)hexyl)amino)-5-chloropyrimidin-4-yl)amino)-1*H*-pyrazole-3-carboxylate (77e)

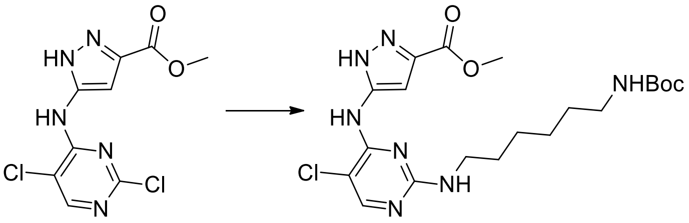

The title compound was prepared according to the procedure of **56c**, using **74** (200 mg, 0.69 mmol) and *tert*-butyl (6-aminohexyl)carbamate (150 mg, 0.69 mmol). The mixture was stirred for 8 h at 80 °C to obtain the product (177 mg, 54%) as a colorless oil.

^{1}H NMR (300 MHz, DMSO-d6) δ 13.49 (d, J = 68.2 Hz, 1H), 9.33 (d, J = 284.3 Hz, 1H), 7.98 (d, J = 28.7 Hz, 1H), 7.17 (d, J = 43.4 Hz, 1H), 6.73 (t, J = 5.7 Hz, 1H), 6.65 – 6.41 (m, 1H), 3.90 – 3.76 (m, 3H), 3.29 – 3.14 (m, 2H), 2.95 – 2.83 (m, 2H), 1.60 – 1.44 (m, 2H), 1.39 – 1.20 (m, 15H).

^{13}C NMR (75 MHz, DMSO) δ 162.58, 159.99, 155.54, 155.04, 153.78, 147.66, 132.63, 101.06, 95.10, 77.26, 51.91, 51.45, 40.72, 29.49, 29.00, 28.25, 26.23, 26.11.

MS-ESI m/z $[M + H]^+$: calcd 469.0, found 468.4.

HRMS m/z $[M + H]^+$: calcd 468.2121, found 468.2116.

HPLC: t_R = 7.82, purity ≥ 95% (UV: 254/ 280 nm).

Synthesis of methyl 5-((2-((4-(2-((*tert*-butoxycarbonyl)amino)ethyl)phenyl)amino)quinazolin-4-yl)amino)-1*H*-pyrazole-3-carboxylate (78a)

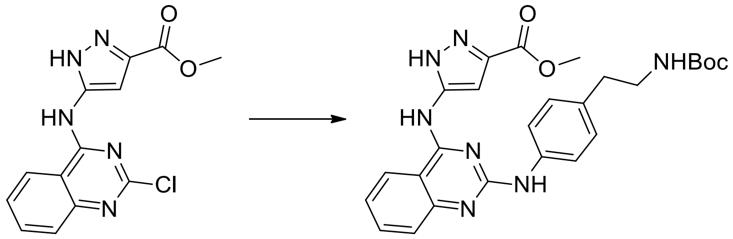

The title compound was prepared according to the procedure of **56b**, using **75** (300 mg, 0.99 mmol) and *tert*-butyl 4-aminophenethylcarbamate (212 mg, 0.90 mmol). The mixture was stirred for 18 h at 70 °C to obtain the product (325 mg, 72%) as a yellow solid.

^{1}H NMR (300 MHz, DMSO-d6) δ 13.32 (s, 1H), 11.84 (s, 1H), 10.76 (s, 1H), 8.73 (d, J = 8.2 Hz, 1H), 7.87 (t, J = 7.7 Hz, 1H), 7.61 (d, J = 8.2 Hz, 1H), 7.55 – 7.41 (m, 3H), 7.23 (d, J = 8.0 Hz, 2H), 7.13 (s, 1H), 6.92 (t, J = 5.4 Hz, 1H), 3.88 (s, 3H), 3.24 – 3.09 (m, 2H), 2.81 – 2.67 (m, 2H), 1.37 (s, 9H).

^{13}C NMR (75 MHz, DMSO) δ 159.64, 158.44, 155.56, 151.92, 145.61, 139.54, 136.79, 135.78, 134.22, 129.28, 124.88, 124.78, 122.92, 117.59, 110.25, 102.96, 77.55, 52.06, 41.49, 35.13, 28.25.

MS-ESI m/z [M + H]$^+$: calcd 505.6, found 505.2.

HRMS m/z [M + H]$^+$: calcd 504.2354, found 504.2348.

HPLC: t_R = 7.77, purity ≥ 95% (UV: 254/ 280 nm).

Synthesis of methyl 5-((2-((3-(2-((*tert*-butoxycarbonyl)amino)ethyl)phenyl)amino)quinazolin-4-yl)amino)-1*H*-pyrazole-3-carboxylate (78b)

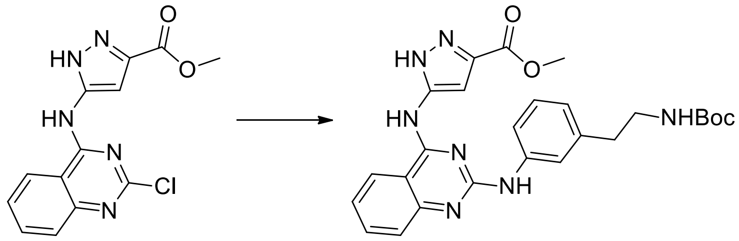

The title compound was prepared according to the procedure of **56b**, using **75** (300 mg, 0.99 mmol) and *tert*-butyl 3-aminophenethylcarbamate (233 mg, 0.99 mmol). The mixture was stirred for 18 h at 70 °C to obtain the product (305 mg, 61%) as a yellow solid.

^{1}H NMR (300 MHz, DMSO-d6) δ 13.65 (d, J = 246.4 Hz, 1H), 11.82 (s, 1H), 10.70 (s, 1H), 8.72 (d, J = 8.3 Hz, 1H), 7.88 (t, J = 7.8 Hz, 1H), 7.65 (d, J = 8.3 Hz, 1H), 7.50 (t, J = 7.7 Hz, 1H), 7.45 – 7.29 (m, 3H), 7.13 (d, J = 7.3 Hz, 1H), 7.06 (s, 1H), 6.85 (t, J = 5.9 Hz, 1H), 3.86 (s, 3H), 3.20 – 3.06 (m, 2H), 2.74 – 2.64 (m, 2H), 1.34 (s, 9H).

^{13}C NMR (75 MHz, DMSO) δ 159.75, 158.31, 155.56, 152.14, 140.75, 139.90, 136.16, 135.74, 129.18, 126.19, 124.95, 124.70, 123.51, 121.24, 117.69, 110.35, 102.58, 77.60, 51.95, 41.28, 35.38, 28.24.

MS-ESI m/z $[M + H]^+$: calcd 505.6, found 505.4.

HRMS m/z $[M + H]^+$: calcd 504.2354, found 504.2347.

HPLC: t_R = 8.11, purity ≥ 95% (UV: 254/ 280 nm).

Synthesis of methyl 5-((2-((5-((*tert*-butoxycarbonyl)amino)pentyl)amino)quinazolin-4-yl)amino)-1*H*-pyrazole-3-carboxylate (78c)

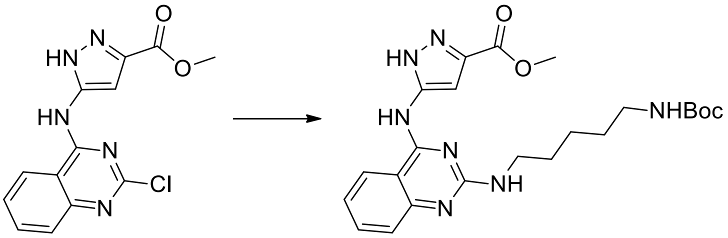

The title compound was prepared according to the procedure **56c**, using **75** (300 mg, 0.99 mmol) and *tert*-butyl (5-aminopentyl)carbamate (200 mg, 0.99 mmol). The mixture was stirred for 8 h at 90 °C to obtain the product (233 mg, 50%) as a yellow solid.

^{1}H NMR (250 MHz, DMSO-d6) δ 14.04 (s, 1H), 11.60 (s, 1H), 8.59 (d, J = 8.1 Hz, 1H), 8.10 – 7.65 (m, 2H), 7.62 – 7.24 (m, 2H), 6.76 (s, 1H), 3.87 (s, 3H), 3.53 – 3.42 (m, 2H), 3.03 – 2.87 (m, 2H), 1.75 – 1.54 (m, 2H), 1.46 – 1.25 (m, 13H).

^{13}C NMR (75 MHz, DMSO) δ 156.10, 136.42, 135.13, 125.12, 124.67, 117.61, 110.68, 102.74, 77.82, 52.56, 41.71, 40.17, 29.66, 29.02, 28.73, 24.05.

MS-ESI m/z $[M + H]^+$: calcd 470.6, found 470.5.

HRMS m/z $[M + H]^+$: calcd 470.2510, found 470.2505.

HPLC: t_R = 7.91, purity ≥ 95% (UV: 254/ 280 nm).

Synthesis of methyl 3-((2-((4-(2-aminoethyl)phenyl)amino)pyrimidin-4-yl)amino)-1*H*-pyrazole-5-carboxylate (79)

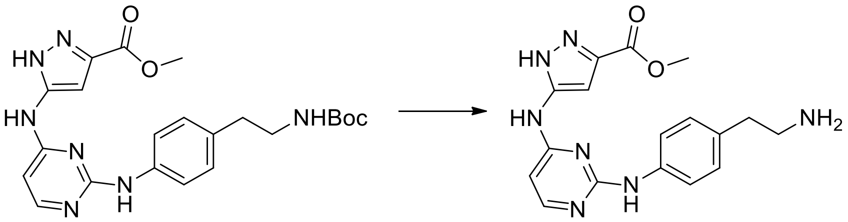

76a (50 mg, 0.1 mmol) was dissolved in 4 mL anhydrous DCM. TFA (503 mg, 4.4 mmol) was added at 0 °C and the reaction mixture was allowed to warm up to rt overnight. The solvent was evaporated under reduced pressure. The residue was dissolved in methanol and neutralized with saturated K_2CO_3 solution. The solvent was again evaporated under reduced pressure and the crude product was purified by flash chromatography using H_2O/ acetonitrile as an eluent to obtain the desired product (21 mg, 54%) as a yellow solid.

^{1}H NMR (250 MHz, DMSO-d6) δ 9.27 (s, 1H), 8.03 (d, J = 5.7 Hz, 1H), 7.69 – 7.53 (m, 2H), 7.19 – 7.06 (m, 2H), 6.81 (s, 1H), 6.30 (d, J = 5.7 Hz, 1H), 3.84 (s, 3H), 2.84 – 2.70 (m, 2H), 2.68 – 2.54 (m, 2H).

^{13}C NMR (126 MHz, DMSO) δ 160.93, 159.55, 159.08, 156.32, 151.48, 145.39, 138.58, 132.90, 128.62, 119.03, 98.07, 96.95, 51.72, 43.72, 39.02.

MS-ESI m/z $[M + H]^+$: calcd 354.4, found 354.7.

HRMS m/z $[M + Na]^+$: calcd 376.1492, found 376.1485.

HPLC: t_R = 10.09, purity ≥ 95% (UV: 254/ 280 nm).

Synthesis of methyl 3-((2-((4-aminobenzyl)amino)pyrimidin-4-yl)amino)-1*H*-pyrazole-5-carboxylate (80)

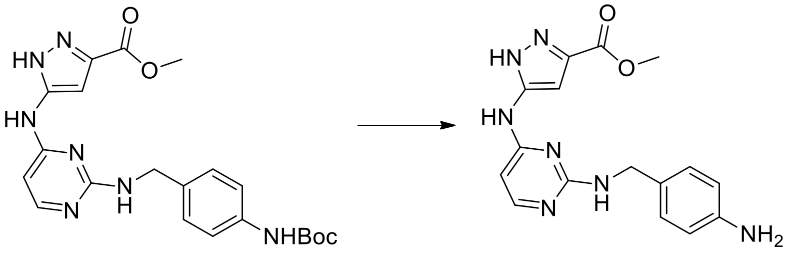

76i (20 mg, 0.05 mmol) was dissolved in 1 mL anhydrous DCM. TFA (208 mg, 1.8 mmol) was added at 0 °C and the reaction mixture was allowed to warm up to rt overnight. The solvent was evaporated under reduced pressure. The residue was dissolved in methanol and neutralized with saturated K_2CO_3 solution. The solvent was again evaporated under reduced pressure and the crude product was purified by flash chromatography using H_2O/ acetonitrile as an eluent to obtain the desired product (5 mg, 36%) as a yellow solid.

^{1}H NMR (250 MHz, DMSO-d6) δ 13.38 (s, 1H), 9.81 (s, 1H), 7.88 (d, J = 5.5 Hz, 1H), 7.26 (s, 1H), 7.01 (d, J = 8.3 Hz, 2H), 6.50 (d, J = 8.3 Hz, 2H), 6.07 (d, J = 4.8 Hz, 1H), 4.89 (s, 2H), 4.30 (d, J = 5.9 Hz, 2H), 3.81 (s, 3H).

MS-ESI m/z $[M + H]^+$: calcd 340.4, found 340.6.

HRMS m/z $[M + H]^+$: calcd 340.1517, found 340.1529.

HPLC: t_R = 10.13, purity ≥ 95% (UV: 254/ 280 nm).

Synthesis of 2-chloro-*N*-(3-methyl-1*H*-pyrazol-5-yl)pyrimidin-4-amine (87)

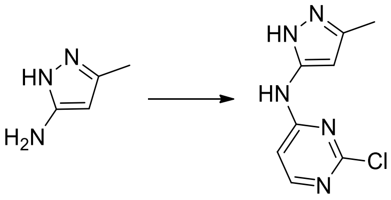

The title compound was prepared according to the procedure of **53**, using 5-methyl-1*H*-pyrazol-3-amine (500 mg, 5.15 mmol) and 2,4-dichloropyrimidine (697 mg, 4.68 mmol). The mixture was stirred at 60 °C for 72 h to obtain the product (466 mg, 48%) as a beige solid.

^{1}H NMR (300 MHz, DMSO-d6) δ 12.13 (s, 1H), 10.28 (s, 1H), 8.15 (d, J = 5.9 Hz, 1H), 7.15 (s, 1H), 6.09 (s, 1H), 2.22 (s, 3H).

^{13}C NMR (75 MHz, DMSO) δ 160.77, 159.37, 147.35, 142.17, 138.83, 104.97, 95.50, 10.61.

MS-ESI m/z $[M + H]^+$: calcd 210.6, found 210.2.

Synthesis of 2-chloro-*N*-(3-isopropyl-1*H*-pyrazol-5-yl)pyrimidin-4-amine (88)

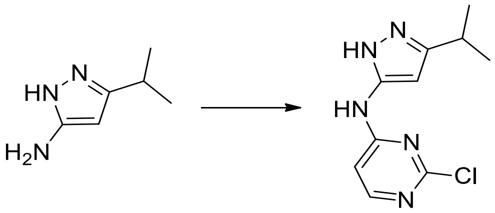

The title compound was prepared according to the procedure **53**, using 5-isopropyl-1*H*-pyrazol-3-amine (500 mg, 3.99 mmol) and 2,4-dichloropyrimidine (541 mg, 3.63 mmol). The mixture was stirred at 60 °C for 120 h to obtain the product (543 mg, 63%) as a beige solid.

^{1}H NMR (300 MHz, DMSO-d6) δ 12.17 (s, 1H), 10.28 (s, 1H), 8.16 (d, J = 6.0 Hz, 1H), 7.20 (s, 1H), 6.07 (s, 1H), 2.93 (p, J = 6.9 Hz, 1H), 1.21 (d, J = 6.9 Hz, 6H).

^{13}C NMR (75 MHz, DMSO) δ 161.09, 160.80, 159.35, 149.85, 147.06, 104.94, 92.75, 25.29, 22.21.

MS-ESI m/z $[M + H]^+$: calcd 238.7, found 238.2.

Synthesis of *N*-(3-(*tert*-butyl)-1*H*-pyrazol-5-yl)-2-chloropyrimidin-4-amine (89)

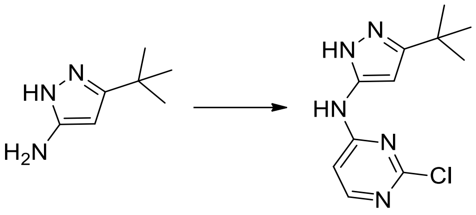

The title compound was prepared according to the procedure of **53**, using 5-(*tert*-butyl)-1*H*-pyrazol-3-amine (500 mg, 3.59 mmol) and 2,4-dichloropyrimidine (486 mg, 3.27 mmol). The mixture was stirred at 60 °C for 72 h to obtain the product (688 mg, 84%) as a beige solid.

^{1}H NMR (300 MHz, DMSO-d6) δ 12.17 (s, 1H), 10.28 (s, 1H), 8.16 (d, J = 5.9 Hz, 1H), 7.24 (s, 1H), 6.04 (s, 1H), 1.26 (s, 9H).

^{13}C NMR (75 MHz, DMSO) δ 160.80, 159.35, 157.60, 152.96, 146.72, 104.86, 92.35, 30.66, 29.89.

MS-ESI m/z $[M + H]^+$: calcd 252.7, found 252.2

Synthesis of 5-((2-chloropyrimidin-4-yl)amino)-*N*-methyl-1*H*-pyrazole-3-carboxamide (90)

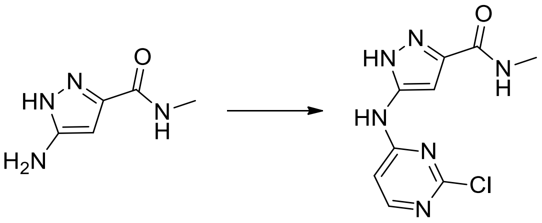

The title compound was prepared according to the procedure of **53**, using 3-amino-N-methyl-1*H*-pyrazole-5-carboxamide (350 mg, 2.50 mmol) and 2,4-dichloropyrimidine (338 mg, 2.27 mmol). The mixture was stirred at 60 °C for 48 h to obtain the product (82 mg, 14%) as a white solid.

^{1}H NMR (300 MHz, DMSO-d6) δ 13.18 (s, 1H), 10.49 (s, 1H), 8.52 (d, J = 5.2 Hz, 1H), 8.20 (d, J = 5.9 Hz, 1H), 7.18 (s, 1H), 6.85 (s, 1H), 2.76 (d, J = 4.5 Hz, 3H).

^{13}C NMR (126 MHz, DMSO) δ 160.84, 160.77, 159.46, 158.95, 147.31, 137.29, 105.11, 95.89, 25.55.

MS-ESI m/z $[M + H]^+$: calcd 253.7, found 253.2.

Synthesis of isopropyl 3-((2-chloropyrimidin-4-yl)amino)-1*H*-pyrazole-5-carboxylate (91)

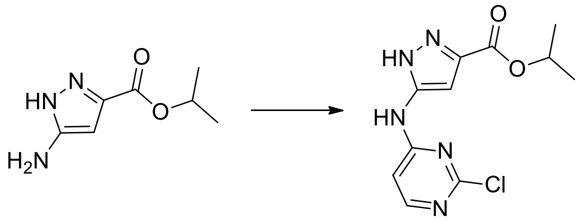

The title compound was prepared according to the procedure of **53**, using isopropyl 3-amino-1*H*-pyrazole-5-carboxylate (509 mg, 3.01 mmol) and 2,4-dichloropyrimidine (448 mg, 3.01 mmol). The mixture was stirred at 60 °C for 48 h to obtain the product (363 mg, 43%) as a beige solid with impurities.

MS-ESI m/z [M + H]+: calcd 282.7, found 282.1.

Synthesis of *tert*-butyl 3-((2-chloropyrimidin-4-yl)amino)-1*H*-pyrazole-5-carboxylate (92)

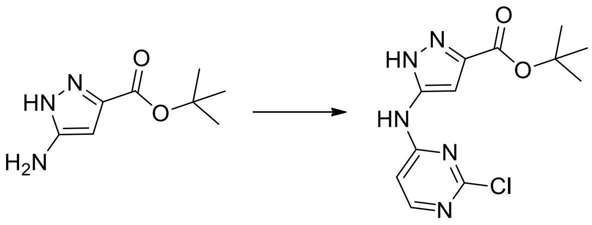

The title compound was prepared according to the procedure of **53**, using *tert*-butyl 3-amino-1*H*-pyrazole-5-carboxylate (500 mg, 2.73 mmol) and 2,4-dichloropyrimidine (407 mg, 2.73 mmol). The mixture was stirred at 60 °C for 48 h to obtain the product (565 mg, 35%) as a white solid.

^{1}H NMR (400 MHz, DMSO-d6) δ 13.49 (s, 1H), 10.61 (s, 1H), 8.20 (d, J = 5.9 Hz, 1H), 7.27 – 6.55 (m, 2H), 1.54 (s, 9H).

^{13}C NMR (101 MHz, DMSO) δ 160.59, 159.40, 158.09, 147.59, 142.19, 134.61, 105.37, 99.20, 81.95, 27.79.

MS-ESI m/z $[M + H]^+$: calcd 296.7, found 296.1.

Synthesis of *tert*-butyl 4-((4-((3-methyl-1*H*-pyrazol-5-yl)amino)pyrimidin-2-yl)amino)phenethyl-carbamate (93a)

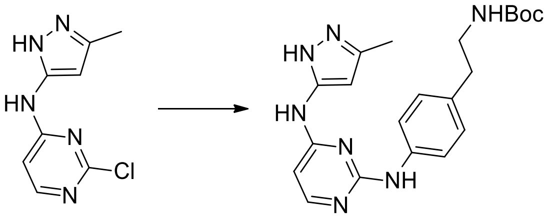

The title compound was prepared according to the procedure of **56a**, using **87** (50 mg, 0.24 mmol) and *tert*-butyl 4-aminophenethylcarbamate (56 mg, 0.24 mmol). The mixture was stirred for 18 h under reflux to obtain the product (66 mg, 67%) as a white solid.

^{1}H NMR (300 MHz, DMSO-d6) δ 12.41 (s, 1H), 11.20 (s, 1H), 10.68 (s, 1H), 7.96 (s, 1H), 7.45 (d, J = 6.5 Hz, 2H), 7.25 (d, J = 8.0 Hz, 2H), 6.91 (t, J = 5.6 Hz, 1H), 6.45 (s, 1H), 6.24 (s, 1H), 3.16 (q, J = 6.9 Hz, 2H), 2.78 – 2.66 (m, 2H), 2.19 (s, 3H), 1.37 (s, 9H).

^{13}C NMR (75 MHz, DMSO) δ 159.67, 155.54, 152.57, 145.99, 142.74, 139.27, 136.66, 134.69, 129.15, 123.31, 98.95, 97.03, 77.53, 41.57, 34.98, 28.25, 10.63.

MS-ESI m/z $[M + H]^+$: calcd 410.5, found 410.4.

HRMS m/z $[M + H]^+$: calcd 410.2299, found 410.2297.

HPLC: t_R = 7.30, purity ≥ 95% (UV: 254/ 280 nm).

Synthesis of *tert*-butyl (5-((4-((3-methyl-1*H*-pyrazol-5-yl)amino)pyrimidin-2-yl)amino)pentyl)-carbamate (93b)

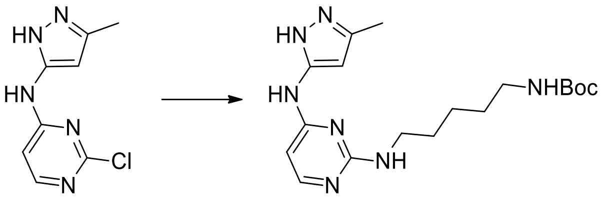

The title compound was prepared according to the procedure **56c**, using **87** (60 mg, 0.29 mmol) and *tert*-butyl (5-aminopentyl)carbamate (58 mg, 0.29 mmol). The mixture was stirred for 8 h at 90 °C to obtain the product (31 mg, 29%) as a colorless oil.

^{1}H NMR (300 MHz, DMSO-d6) δ 11.84 (s, 1H), 9.30 (s, 1H), 7.78 (d, J = 5.7 Hz, 1H), 6.75 (t, J = 5.7 Hz, 1H), 6.62 (s, 1H), 6.33 – 6.07 (m, 2H), 3.21 (q, J = 6.6 Hz, 2H), 2.91 (q, J = 6.5 Hz, 2H), 2.18 (s, 3H), 1.58 – 1.47 (m, 2H), 1.44 – 1.37 (m, 2H), 1.36 (s, 9H), 1.32 – 1.22 (m, 2H).

^{13}C NMR (75 MHz, DMSO) δ 162.09, 159.66, 156.04, 155.60, 148.52, 138.40, 95.58, 95.15, 77.31, 41.30, 39.89, 29.36, 28.97, 28.28, 23.94, 11.07.

MS-ESI m/z $[M + H]^+$: calcd 376.5, found 376.4.

HRMS m/z $[M + H]^+$: calcd 376.2456, found 376.2458.

HPLC: t_R = 7.08, purity ≥ 95% (UV: 254/ 280 nm).

Synthesis of *tert*-butyl 4-((4-((3-isopropyl-1*H*-pyrazol-5-yl)amino)pyrimidin-2-yl)amino)phenethyl-carbamate (94a)

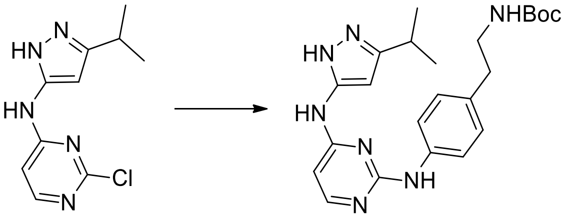

The title compound was prepared according to the procedure **56a**, using **88** (60 mg, 0.25 mmol) and *tert*-butyl 4-aminophenethylcarbamate (60 mg, 0.25 mmol). The mixture was stirred for 18 h at 70 °C to obtain the product (70 mg, 64%) as a white solid.

^{1}H NMR (300 MHz, DMSO-d6) δ 12.41 (s, 1H), 11.22 (s, 1H), 10.62 (s, 1H), 7.96 (d, J = 5.8 Hz, 1H), 7.43 (d, J = 7.9 Hz, 2H), 7.24 (d, J = 8.2 Hz, 2H), 6.90 (t, J = 5.0 Hz, 1H), 6.45 (s, 1H), 6.22 (s, 1H), 3.21 – 3.07 (m, 2H), 2.98 – 2.81 (m, 1H), 2.74 – 2.66 (m, 2H), 1.37 (s, 9H), 1.15 (d, J = 6.9 Hz, 6H).

^{13}C NMR (75 MHz, DMSO) δ 159.67, 155.52, 152.65, 149.96, 145.70, 142.19, 136.62, 134.50, 129.22, 123.45, 99.10, 94.05, 77.52, 41.45, 35.03, 28.25, 25.35, 22.21.

MS-ESI m/z $[M + H]^+$: calcd 438.6, found 438.5.

HRMS m/z $[M + H]^+$: calcd 438.2612, found 438.2609.

HPLC: t_R = 7.92, purity ≥ 95% (UV: 254/ 280 nm).

Synthesis of *tert*-butyl (5-((4-((3-isopropyl-1*H*-pyrazol-5-yl)amino)pyrimidin-2-yl)amino)pentyl)-carbamate (94b)

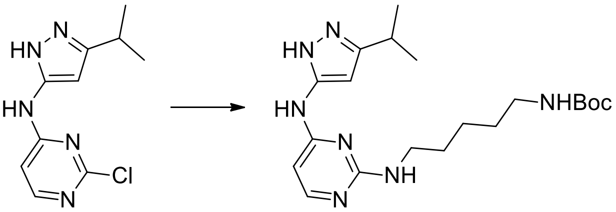

The title compound was prepared according to the procedure of **56c**, using **88** (60 mg, 0.25 mmol) and *tert*-butyl (5-aminopentyl)carbamate (51 mg, 0.25 mmol). The mixture was stirred for 8 h at 90 °C to obtain the product (22 mg, 22%) as a yellow solid.

^{1}H NMR (300 MHz, DMSO-d6) δ 11.97 (s, 1H), 9.71 (s, 1H), 7.78 (d, J = 6.0 Hz, 1H), 6.98 (s, 1H), 6.74 (t, J = 5.7 Hz, 1H), 6.45 – 6.04 (m, 2H), 3.25 (q, J = 6.9 Hz, 2H), 2.96 – 2.82 (m, 3H), 1.62 – 1.47 (m, 2H), 1.45 – 1.26 (m, 13H), 1.21 (d, J = 6.9 Hz, 6H).

^{13}C NMR (75 MHz, DMSO) δ 160.54, 159.70, 155.61, 153.36, 149.65, 147.25, 96.01, 92.67, 77.34, 40.75, 29.32, 28.86, 28.29, 25.61, 23.90, 22.34.

MS-ESI m/z $[M + H]^+$: calcd 404.5, found 404.5.

HRMS m/z $[M + H]^+$: calcd 404.2769, found 404.2767.

HPLC: t_R = 7.81, purity ≥ 95% (UV: 254/ 280 nm).

Synthesis of *tert*-butyl 4-((4-((3-(*tert*-butyl)-1*H*-pyrazol-5-yl)amino)pyrimidin-2-yl)amino)phenethyl-carbamate (95a)

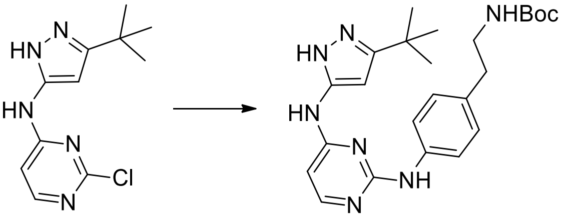

The title compound was prepared according to the procedure of **56b**, using **89** (50 mg, 0.20 mmol) and *tert*-butyl 4-aminophenethylcarbamate (47 mg, 0.20 mmol). The mixture was stirred for 18 h under reflux to obtain the product (70 mg, 79%) as a yellow solid.

^{1}H NMR (300 MHz, DMSO-d6) δ 12.38 (s, 1H), 11.24 (s, 1H), 10.65 (s, 1H), 7.96 (d, J = 4.5 Hz, 1H), 7.42 (d, J = 7.7 Hz, 2H), 7.23 (d, J = 8.0 Hz, 2H), 6.89 (t, J = 5.2 Hz, 1H), 6.45 (s, 1H), 6.21 (s, 1H), 3.22 – 3.08 (m, 2H), 2.76 – 2.62 (m, 2H), 1.37 (s, 9H), 1.20 (s, 9H).

^{13}C NMR (75 MHz, DMSO) δ 159.59, 155.51, 152.98, 152.52, 145.46, 142.22, 136.67, 134.40, 129.26, 123.32, 99.15, 93.71, 77.51, 41.39, 35.02, 30.71, 29.87, 28.24.

MS-ESI m/z [M + H]$^+$: calcd 452.6, found 452.4.

HRMS m/z [M + H]$^+$: calcd 452.2769, found 452.2763.

HPLC: t_R = 7.78, purity ≥ 95% (UV: 254/ 280 nm).

Synthesis of *tert*-butyl (5-((4-((3-(*tert*-butyl)-1*H*-pyrazol-5-yl)amino)pyrimidin-2-yl)amino)pentyl)-carbamate (95b)

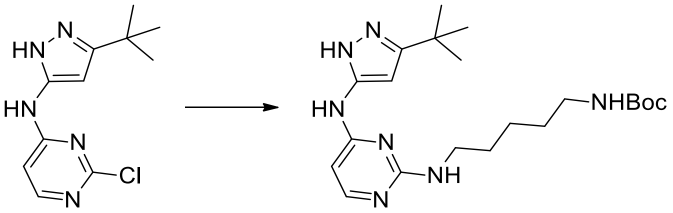

The title compound was prepared according to the procedure of **56c**, using **89** (60 mg, 0.24 mmol) and *tert*-butyl (5-aminopentyl)carbamate (48 mg, 0.24 mmol). The mixture was stirred for 8 h at 90 °C to obtain the product (24 mg, 24%) as a colorless oil.

^{1}H NMR (300 MHz, DMSO-d6) δ 11.86 (s, 1H), 9.27 (s, 1H), 7.77 (d, J = 5.7 Hz, 1H), 6.73 (t, J = 5.3 Hz, 1H), 6.59 (s, 1H), 6.38 (s, 1H), 6.14 (s, 1H), 3.23 (q, J = 6.7 Hz, 2H), 2.90 (q, J = 6.5 Hz, 2H), 1.58 – 1.46 (m, 2H), 1.44 – 1.22 (m, 22H).

^{13}C NMR (75 MHz, DMSO) δ 162.10, 159.74, 156.02, 155.57, 151.97, 148.06, 95.55, 92.47, 77.29, 40.69, 30.73, 30.05, 29.32, 29.03, 28.27, 23.92.

MS-ESI m/z [M + H]$^+$: calcd 418.6, found 418.5.

HRMS m/z [M + H]$^+$: calcd 418.2925, found 418.2924.

HPLC: t_R = 7.65, purity ≥ 95% (UV: 254/ 280 nm).

Synthesis of 2-(4-((4-((3-(*tert*-butyl)-1*H*-pyrazol-5-yl)amino)pyrimidin-2-yl)amino)phenyl)-acetonitrile (95c)

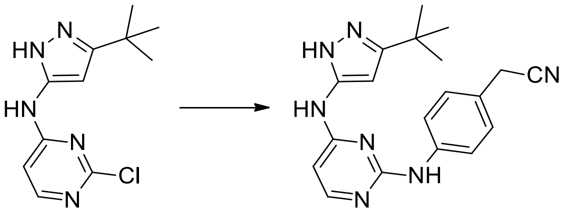

The title compound was prepared according to the procedure of **56b**, using **89** (55 mg, 0.22 mmol) and 2-(4-aminophenyl)acetonitrile (29 mg, 0.22 mmol). The mixture was stirred for 18 h under reflux to obtain the product (31 mg, 41%) as a white solid.

^{1}H NMR (300 MHz, DMSO-d6) δ 12.43 (s, 1H), 11.26 (s, 1H), 10.81 (s, 1H), 7.99 (d, J = 6.9 Hz, 1H), 7.56 (d, J = 8.0 Hz, 2H), 7.39 (d, J = 8.3 Hz, 2H), 6.49 (s, 1H), 6.19 (s, 1H), 4.04 (s, 2H), 1.21 (s, 9H).

^{13}C NMR (75 MHz, DMSO) δ 159.77, 153.14, 152.57, 145.39, 142.44, 136.06, 128.82, 127.96, 123.51, 119.02, 99.32, 93.71, 30.73, 29.90, 21.91.

MS-ESI m/z $[M + H]^+$: calcd 348.4, found 348.3.

HRMS m/z $[M + H]^+$: calcd 348.1931, found 348.1933.

HPLC: t_R = 7.27, purity ≥ 95% (UV: 254/ 280 nm).

Synthesis of *tert*-butyl 4-((4-((3-(methylcarbamoyl)-1*H*-pyrazol-5-yl)amino)pyrimidin-2-yl)amino)-phenethylcarbamate (96a)

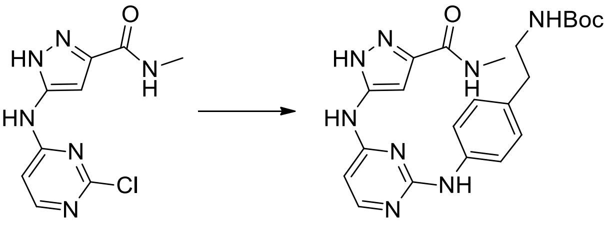

The title compound was prepared according to the procedure of **56b**, using **90** (28 mg, 0.11 mmol) and *tert*-butyl 4-aminophenethylcarbamate (26 mg, 0.11 mmol). The mixture was stirred for 24 h at 70 °C to obtain the product (20 mg, 40%) as a yellow solid.

^{1}H NMR (300 MHz, DMSO-d6) δ 13.08 (s, 1H), 10.12 (d, J = 126.5 Hz, 1H), 9.40 (d, J = 98.9 Hz, 1H), 8.35 (s, 1H), 8.04 (s, 1H), 7.64 (d, J = 8.0 Hz, 2H), 7.10 (d, J = 8.1 Hz, 2H), 6.98 – 6.77 (m, 1H), 6.24 (s, 1H), 3.19 – 3.07 (m, 2H), 2.78 (d, J = 4.6 Hz, 3H), 2.68 – 2.59 (m, 2H), 1.37 (s, 9H).

^{13}C NMR (75 MHz, DMSO) δ 164.36, 159.06, 155.55, 151.53, 142.19, 138.52, 132.28, 129.03, 128.71, 119.31, 114.78, 100.24, 98.02, 77.50, 41.76, 34.97, 28.28, 25.60.

MS-ESI m/z $[M + H]^+$: calcd 453.5, found 454.0.

HRMS m/z $[M + Na]^+$: calcd 475.2177, found 475.2173.

HPLC: t_R = 7.04, purity ≥ 95% (UV: 254/ 280 nm).

Synthesis of *tert*-butyl (5-((4-((3-(methylcarbamoyl)-1*H*-pyrazol-5-yl)amino)pyrimidin-2-yl)amino)-pentyl)carbamate (96b)

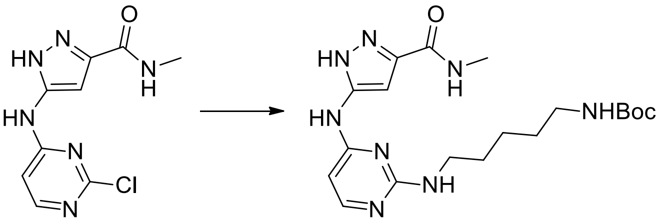

The title compound was prepared according to the procedure of **56c**, using **90** (30 mg, 0.12 mmol) and *tert*-butyl (5-aminopentyl)carbamate (24 mg, 0.12 mmol). The mixture was stirred for 8 h at 90 °C to obtain the product (17 mg, 34%) as a white solid.

^{1}H NMR (300 MHz, DMSO-d6) δ 12.95 (d, J = 48.6 Hz, 1H), 9.74 (d, J = 191.6 Hz, 1H), 8.36 – 7.75 (m, 2H), 7.33 – 6.86 (m, 1H), 6.75 (t, J = 4.9 Hz, 1H), 6.60 – 5.86 (m, 2H), 3.24 (q, J = 6.6 Hz, 2H), 2.90 (q, J = 6.5 Hz, 2H), 2.76 (d, J = 4.6 Hz, 3H), 1.59 – 1.45 (m, 2H), 1.45 – 1.21 (m, 13H).

^{13}C NMR (75 MHz, DMSO) δ 164.36, 162.01, 159.74, 156.72, 155.62, 151.55, 142.21, 100.24, 95.70, 77.33, 40.58, 29.30, 28.93, 28.28, 25.59, 23.89.

MS-ESI m/z $[M + H]^+$: calcd 419.5, found 419.8.

HRMS m/z $[M + H]^+$: calcd 419.2514, found 419.2524.

HPLC: t_R = 6.83, purity ≥ 95% (UV: 254/ 280 nm).

Synthesis of 5-((2-((4-(cyanomethyl)phenyl)amino)pyrimidin-4-yl)amino)-*N*-methyl-1*H*-pyrazole-3-carboxamide (96c)

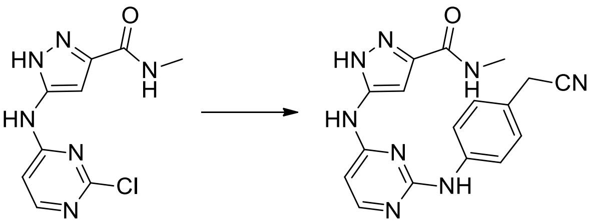

The title compound was prepared according to the procedure **56a**, using **90** (24 mg, 0.10 mmol) and 2-(4-aminophenyl)acetonitrile (13 mg, 0.10 mmol). The mixture was stirred for 18 h under reflux to obtain the product (15 mg, 45%) as a yellow solid.

^{1}H NMR (300 MHz, DMSO-d6) δ 11.28 (s, 1H), 10.90 (s, 1H), 8.56 (s, 1H), 8.14 – 7.92 (m, 1H), 7.61 (d, J = 8.1 Hz, 2H), 7.38 (d, J = 8.1 Hz, 2H), 7.19 (s, 1H), 6.57 (s, 1H), 4.04 (s, 2H), 2.79 (d, J = 4.5 Hz, 3H).

^{13}C NMR (75 MHz, DMSO) δ 160.50, 159.22, 152.53, 145.57, 144.26, 138.51, 136.11, 128.96, 127.72, 122.60, 119.27, 99.11, 98.18, 25.60, 21.97.

MS-ESI m/z $[M + H]^+$: calcd 349.4, found 349.6.

HRMS m/z $[M + H]^+$: calcd 349.1520, found 349.1525.

HPLC: t_R = 6.23, purity ≥ 95% (UV: 254/ 280 nm).

Synthesis of isopropyl 3-((2-((5-((*tert*-butoxycarbonyl)amino)pentyl)amino)pyrimidin-4-yl)amino)-1*H*-pyrazole-5-carboxylate (97b)

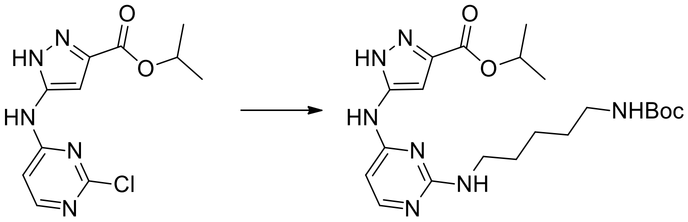

The title compound was prepared according to the procedure of **56c**, using **91** (138 mg, 0.49 mmol) and *tert*-butyl (5-aminopentyl)carbamate (99 mg, 0.49 mmol). The mixture was stirred for 6 h at 100 °C to obtain the product (8 mg, 4%) as a yellow solid.

^{1}H NMR (400 MHz, DMSO-d6) δ 13.32 (s, 1H), 9.89 (d, J = 172.8 Hz, 1H), 7.83 (s, 1H), 7.15 (s, 1H), 6.74 (s, 2H), 6.10 (s, 1H), 5.11 (q, J = 12.9, 6.6 Hz, 1H), 3.24 (q, J = 6.6 Hz, 2H), 2.90 (q, J = 6.6 Hz, 2H), 1.58 – 1.47 (m, 2H), 1.44 – 1.28 (m, 19H).

^{13}C NMR (101 MHz, DMSO) δ 156.59, 155.58, 96.06, 91.63, 77.29, 68.23, 29.29, 28.88, 28.26, 23.86, 21.66, 13.39, 12.99.

MS-ESI m/z $[M + H]^+$: calcd 448.5, found 448.5.

HRMS m/z $[M + H]^+$: calcd 448.2673, found 448.2667.

HPLC: t_R = 6.16, purity ≥ 95% (UV: 254/ 280 nm).

Synthesis of isopropyl 3-((2-((4-((tert-butoxycarbonyl)amino)benzyl)amino)pyrimidin-4-yl)amino)-1*H*-pyrazole-5-carboxylate (97d)

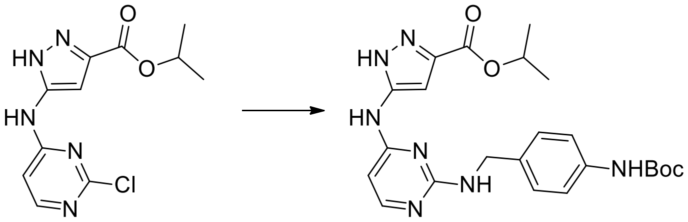

The title compound was prepared according to the procedure of **56c**, using **91** (138 mg, 0.49 mmol) and *tert*-butyl (4-(aminomethyl)phenyl)carbamate (109 mg, 0.49 mmol). The mixture was stirred for 6 h at 100 °C to obtain the product (8 mg, 4%) as a beige solid.

^{1}H NMR (400 MHz, DMSO-d6) δ 13.31 (s, 1H), 9.91 (d, J = 194.0 Hz, 1H), 9.23 (s, 1H), 7.83 (s, 1H), 7.65 – 6.93 (m, 6H), 6.12 (s, 1H), 5.11 (s, 1H), 4.42 (d, J = 6.2 Hz, 2H), 1.45 (s, 9H), 1.30 (d, J = 6.3 Hz, 6H).

^{13}C NMR (101 MHz, DMSO) δ 162.00, 159.59, 158.67, 156.43, 152.78, 148.97, 137.95, 134.39, 127.73, 127.25, 117.99, 99.18, 96.05, 78.84, 68.27, 43.59, 28.13, 21.65.

MS-ESI m/z $[M + H]^+$: calcd 468.5, found 468.5.

HRMS m/z $[M + H]^+$: calcd 468.2351, found 468.2354.

HPLC: t_R = 6.24, purity ≥ 95% (UV: 254/ 280 nm).

Synthesis of *tert*-butyl 3-((2-((5-((*tert*-butoxycarbonyl)amino)pentyl)amino)pyrimidin-4-yl)amino)-1*H*-pyrazole-5-carboxylate (98b)

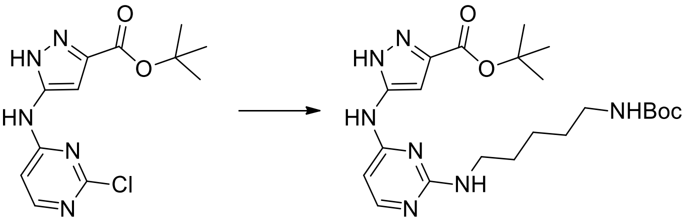

The title compound was prepared according to the procedure of **56c**, using **92** (168 mg, 0.57 mmol) and *tert*-butyl (5-aminopentyl)carbamate (115 mg, 0.57 mmol). The mixture was stirred for 6 h at 100 °C to obtain the product (14 mg, 5%) as a yellow oil.

^{1}H NMR (400 MHz, DMSO-d6) δ 13.25 (d, J = 59.3 Hz, 1H), 9.86 (d, J = 176.8 Hz, 1H), 7.81 (s, 1H), 7.10 (s, 1H), 6.73 (s, 2H), 6.10 (s, 1H), 3.24 (q, J = 6.6 Hz, 2H), 2.90 (q, J = 6.6 Hz, 2H), 1.56 – 1.47 (m, 11H), 1.42 – 1.26 (m, 13H).

^{13}C NMR (101 MHz, DMSO) δ 162.18, 159.53, 158.61, 156.31, 155.57, 149.02, 134.08, 99.07, 95.80, 81.44, 77.29, 40.76, 29.31, 28.88, 28.27, 28.13, 27.85, 23.88.

MS-ESI m/z $[M + H]^+$: calcd 462.6, found 462.5.

HRMS m/z $[M + H]^+$: calcd 462.2819, found 462.2823.

HPLC: t_R = 6.36, purity ≥ 95% (UV: 254/ 280 nm).

Synthesis of *tert*-butyl 3-((2-((4-((*tert*-butoxycarbonyl)amino)benzyl)amino)pyrimidin-4-yl)amino)-1*H*-pyrazole-5-carboxylate (98d)

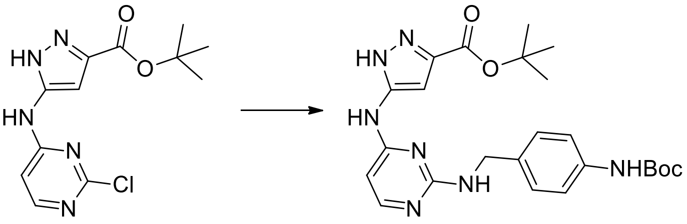

The title compound was prepared according to the procedure of **56c**, using **92** (135 mg, 0.46 mmol) and *tert*-butyl (4-(aminomethyl)phenyl)carbamate (101 mg, 0.46 mmol). The mixture was stirred for 6 h at 100 °C to obtain the product (26 mg, 12%) as a white solid.

^{1}H NMR (400 MHz, DMSO-d6) δ 13.26 (d, J = 60.0 Hz, 1H), 10.26 – 9.51 (m, 1H), 9.39 – 9.05 (m, 1H), 7.83 (s, 1H), 7.65 – 7.02 (m, 6H), 6.13 (s, 1H), 4.42 (d, J = 6.2 Hz, 2H), 1.52 (s, 9H), 1.45 (s, 9H).

^{13}C NMR (101 MHz, DMSO) δ 162.05, 159.57, 158.46, 156.39, 152.79, 148.89, 137.99, 134.44, 127.79, 127.38, 117.99, 99.26, 96.07, 81.51, 78.85, 43.63, 28.14, 27.85.

MS-ESI m/z $[M + H]^+$: calcd 482.6, found 482.5.

HRMS m/z $[M + H]^+$: calcd 482.2507, found 482.2510.

HPLC: t_R = 6.58, purity ≥ 95% (UV: 254/ 280 nm).

7.10.3. Synthesis of 3-aminopyrazole-based macrocycles

Synthesis of methyl 5-((2-chloro-5-methylpyrimidin-4-yl)amino)-1*H*-pyrazole-3-carboxylate (100)

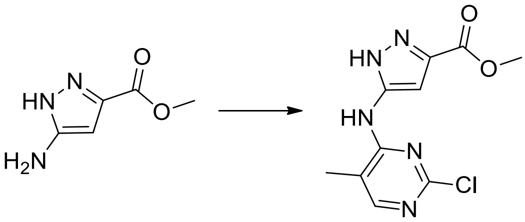

The title compound was prepared according to the procedure of **53**, using methyl 3-amino-1*H*-pyrazole-5-carboxylate (500 mg, 3.54 mmol) and 2,4-dichloro-5-methylpyrimidine (525 mg, 3.22 mmol). The mixture was stirred at 60 °C for 72 h to obtain the product (60 mg, 7%) as a white solid.

^{1}H NMR (250 MHz, DMSO-d6) δ 13.73 (s, 1H, a), 9.68 (s, 1H, b), 8.05 (s, 1H, e), 7.14 (s, 1H, c), 3.86 (s, 3H, f), 2.16 (d, J = 0.9 Hz, 3H, d).

^{13}C NMR (126 MHz, DMSO) δ 159.55, 159.31, 156.84, 156.30, 147.62, 132.81, 114.32, 101.26, 52.05, 13.36.

MS-ESI m/z [M + H]$^+$: calcd 266.7, found 266.0.

Synthesis of methyl 5-((2-((4-(2-((*tert*-butoxycarbonyl)amino)ethyl)phenyl)amino)-5-methylpyrimidin-4-yl)amino)-1*H*-pyrazole-3-carboxylate (101)

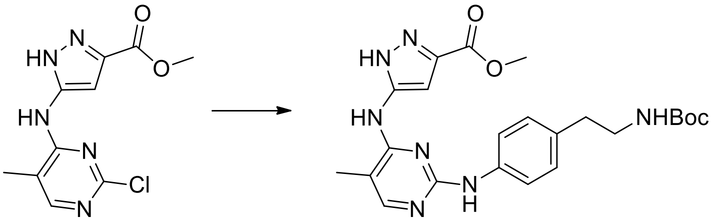

The title compound was prepared according to the procedure of **56b**, using **100** (91 mg, 0.34 mmol) and *tert*-butyl 4-aminophenethylcarbamate (73 mg, 0.31 mmol). The mixture was stirred for 18 h under reflux to obtain the product (178 mg, 49%) as a white solid with impurities. It was used without further purification.

MS-ESI m/z [M + H]$^+$: calcd 468.5, found 468.2.

Synthesis of methyl 5-((2-((2-(2-((*tert*-butoxycarbonyl)amino)ethoxy)ethyl)amino)quinazolin-4-yl)amino)-1*H*-pyrazole-3-carboxylate (78d)

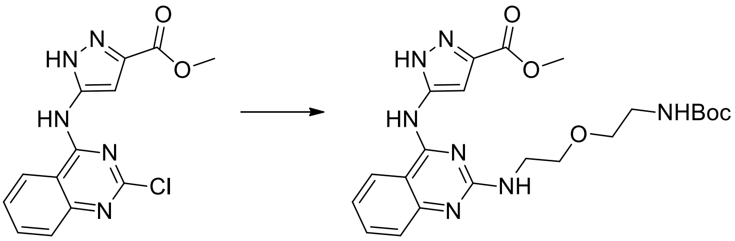

The title compound was prepared according to the procedure of **56c**, using **75** (300 mg, 0.99 mmol) and *tert*-butyl (2-(2-aminoethoxy)ethyl)carbamate (202 mg, 0.99 mmol). The mixture was stirred for 10 h at 90 °C to obtain the product (151 mg, 32%) as a yellow solid with impurities.

MS-ESI m/z [M + H]$^+$: calcd 472.5, found 472.2.

Synthesis of methyl 5-((2-((6-((*tert*-butoxycarbonyl)amino)hexyl)amino)quinazolin-4-yl)amino)-1*H*-pyrazole-3-carboxylate (78e)

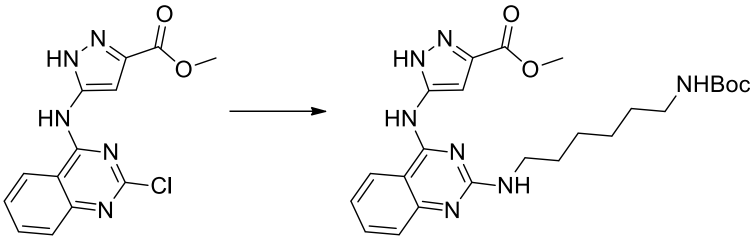

The title compound was prepared according to the procedure of **56c**, using **75** (300 mg, 0.99 mmol) and *tert*-butyl (6-aminohexyl)carbamate (214 mg, 0.99 mmol). The mixture was stirred for 10 h at 90 °C to obtain the product (181 mg, 38%) as a yellow solid with impurities.

MS-ESI m/z $[M + H]^+$: calcd 484.6, found 484.3.

Synthesis of methyl 3-((2-((4-(2-aminoethyl)phenyl)amino)pyrimidin-4-yl)amino)-1*H*-pyrazole-5-carboxylate (102a)

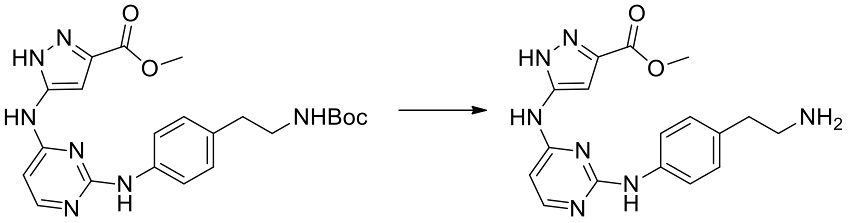

76a (50 mg, 0.1 mmol) was dissolved in 4 mL anhydrous DCM. TFA (503 mg, 4.4 mmol) was added at 0 °C and the reaction mixture was allowed to warm up to rt overnight. The solvent was evaporated under reduced pressure. The residue was dissolved in methanol and neutralized with saturated K_2CO_3 solution. The solvent was again evaporated under reduced pressure and the crude product was used without further purification to obtain the desired product as a white solid together with salts.

MS-ESI m/z $[M + H]^+$: calcd 354.4, found 354.7.

Synthesis of methyl 5-((2-((3-(2-aminoethyl)phenyl)amino)pyrimidin-4-yl)amino)-1*H*-pyrazole-3-carboxylate (102b)

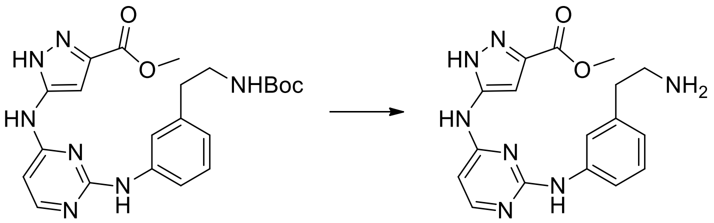

The title compound was prepared according to the procedure of **102a**, using **76b** (178 mg, 0.39 mmol). The desired product was obtained as a white solid with impurities.

MS-ESI m/z $[M + H]^+$: calcd 354.4, found 354.1.

Synthesis of methyl 5-((2-((5-aminopentyl)amino)pyrimidin-4-yl)amino)-1*H*-pyrazole-3-carboxylate (102c)

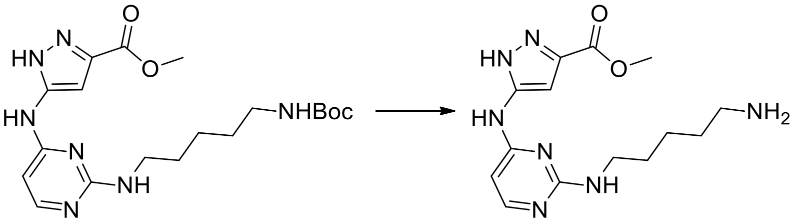

The title compound was prepared according to the procedure of **102a**, using **76c** (142 mg, 0.34 mmol). The desired product was obtained as a white solid with impurities.

Synthesis of methyl 5-((2-((2-(2-aminoethoxy)ethyl)amino)pyrimidin-4-yl)amino)-1*H*-pyrazole-3-carboxylate (102d)

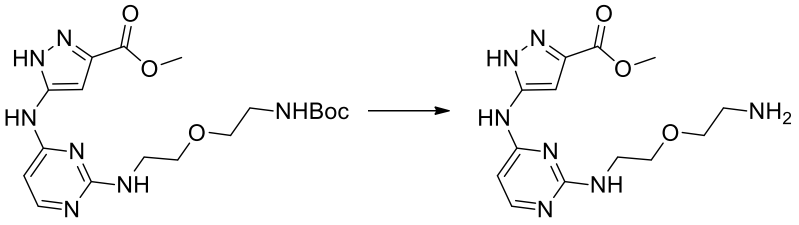

The title compound was prepared according to the procedure of **102a**, using **76d** (100 mg, 0.24 mmol). The desired product was obtained as a white solid with impurities.

MS-ESI m/z $[M + H]^+$: calcd 322.3, found 322.2

Synthesis of methyl 5-((2-((6-aminohexyl)amino)pyrimidin-4-yl)amino)-1*H*-pyrazole-3-carboxylate (102e)

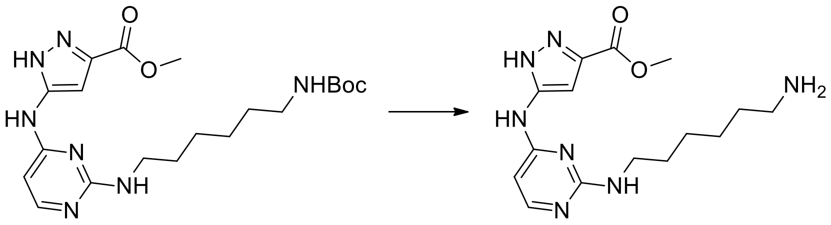

The title compound was prepared according to the procedure of **102a**, using **76e** (95 mg, 0.22 mmol). The desired product was obtained as a white solid with impurities.

Synthesis of methyl 5-((2-((4-(2-aminoethyl)phenyl)amino)-5-chloropyrimidin-4-yl)amino)-1*H*-pyrazole-3-carboxylate (103a)

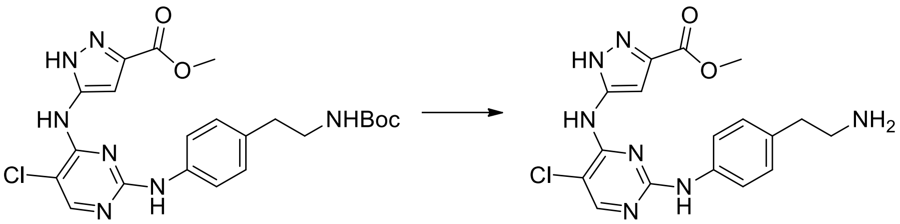

The title compound was prepared according to the procedure of **102a**, using **77a** (308 mg, 0.63 mmol). The desired product was obtained as a white solid with impurities.

Synthesis of methyl 5-((2-((3-(2-aminoethyl)phenyl)amino)-5-chloropyrimidin-4-yl)amino)-1*H*-pyrazole-3-carboxylate (103b)

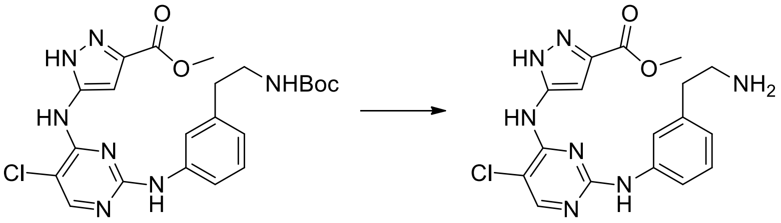

The title compound was prepared according to the procedure of **102a**, using **77b** (293 mg, 0.60 mmol). The desired product was obtained as a white solid with impurities.

Synthesis of methyl 5-((2-((5-aminopentyl)amino)-5-chloropyrimidin-4-yl)amino)-1*H*-pyrazole-3-carboxylate (103c)

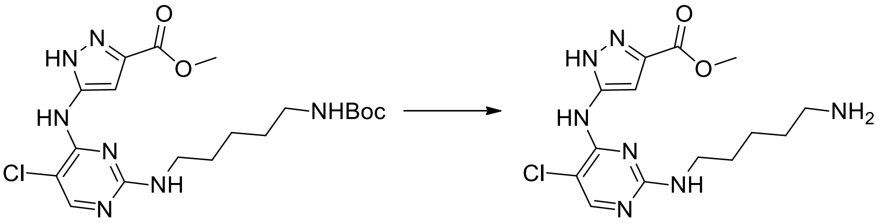

The title compound was prepared according to the procedure of **102a**, using **77c** (162 mg, 0.36 mmol). The desired product was obtained as a white solid with impurities.

MS-ESI m/z $[M + H]^+$: calcd 354.9, found 354.1.

Synthesis of methyl 5-((2-((2-(2-aminoethoxy)ethyl)amino)-5-chloropyrimidin-4-yl)amino)-1*H*-pyrazole-3-carboxylate (103d)

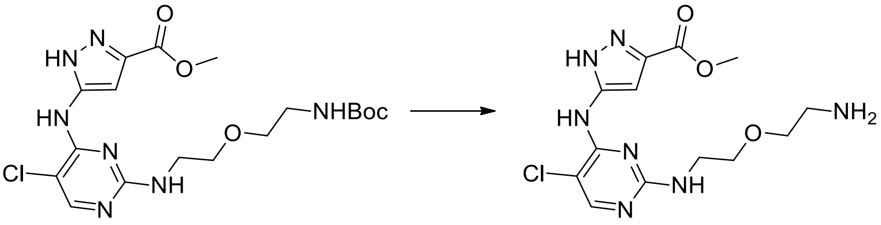

The title compound was prepared according to the procedure of **102a**, using **77d** (110 mg, 0.24 mmol). The desired product was obtained as a white solid with impurities.

Synthesis of methyl 5-((2-((6-aminohexyl)amino)-5-chloropyrimidin-4-yl)amino)-1*H*-pyrazole-3-carboxylate (103e)

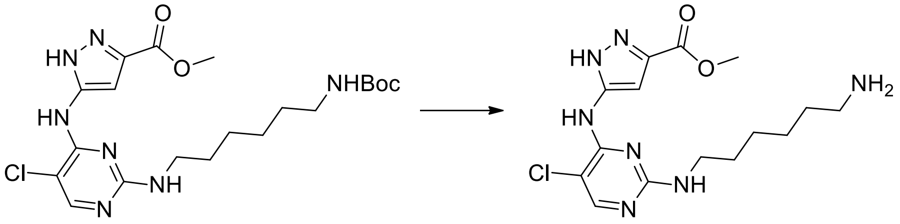

The title compound was prepared according to the procedure of **102a**, using **77e** (141 mg, 0.30 mmol). The desired product was obtained as a white solid with impurities.

MS-ESI m/z $[M + H]^+$: calcd 368.8, found 368.3.

Synthesis of methyl 5-((2-((4-(2-aminoethyl)phenyl)amino)-5-methylpyrimidin-4-yl)amino)-1*H*-pyrazole-3-carboxylate (104a)

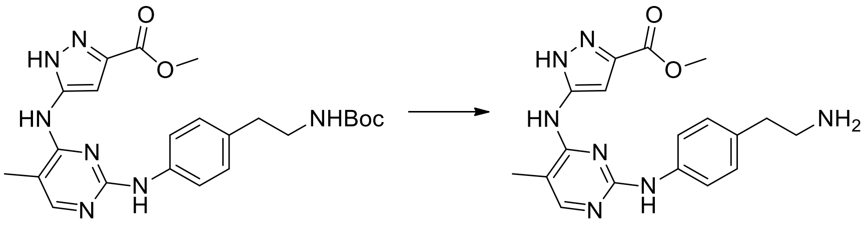

The title compound was prepared according to the procedure of **102a**, using **101a** (112 mg, 0.24 mmol). The desired product was obtained as a white solid with impurities.

Synthesis of methyl 5-((2-((4-(2-aminoethyl)phenyl)amino)quinazolin-4-yl)amino)-1*H*-pyrazole-3-carboxylate (105a)

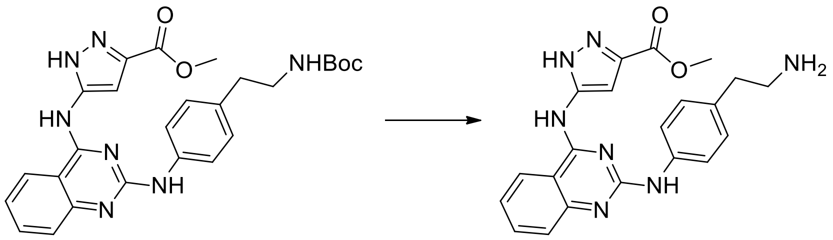

The title compound was prepared according to the procedure of **102a**, using **78a** (282 mg, 0.56 mmol). The desired product was obtained as a white solid with impurities.

Synthesis of methyl 5-((2-((3-(2-aminoethyl)phenyl)amino)quinazolin-4-yl)amino)-1*H*-pyrazole-3-carboxylate (105b)

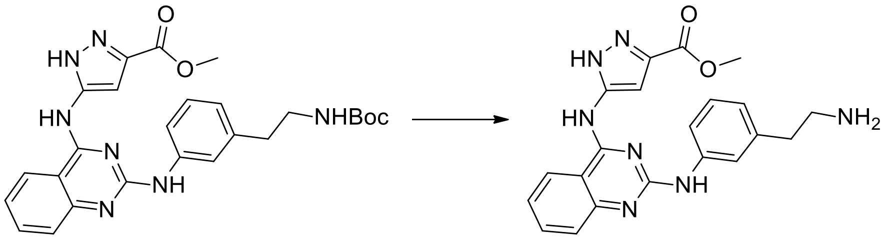

The title compound was prepared according to the procedure of **102a**, using **78b** (316 mg, 0.63 mmol). The desired product was obtained as a white solid with impurities.

Synthesis of methyl 5-((2-((5-aminopentyl)amino)quinazolin-4-yl)amino)-1*H*-pyrazole-3-carboxylate (105c)

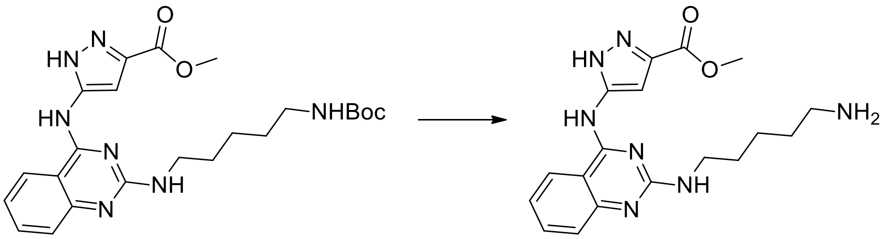

The title compound was prepared according to the procedure of **102a**, using **78c** (266 mg, 0.57 mmol). The desired product was obtained as a white solid with impurities.

Synthesis of methyl 5-((2-((2-(2-aminoethoxy)ethyl)amino)quinazolin-4-yl)amino)-1*H*-pyrazole-3-carboxylate (105d)

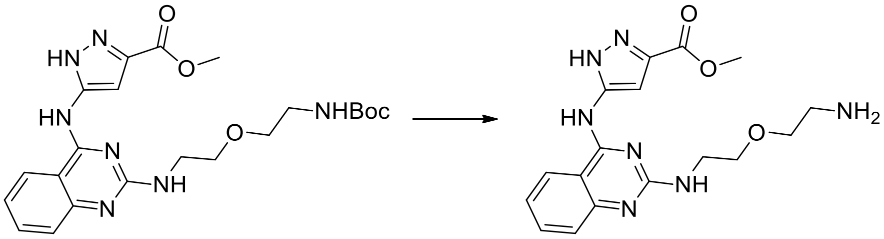

The title compound was prepared according to the procedure of **102a**, using **78d** (147 mg, 0.31 mmol). The desired product was obtained as a white solid with impurities.

Synthesis of methyl 5-((2-((6-aminohexyl)amino)quinazolin-4-yl)amino)-1*H*-pyrazole-3-carboxylate (105e)

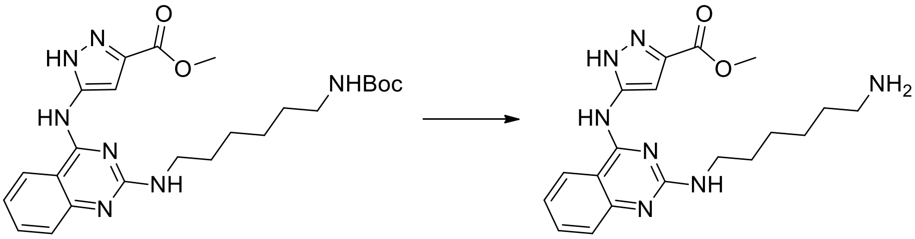

The title compound was prepared according to the procedure of **102a**, using **78e** (181 mg, 0.37 mmol). The desired product was obtained as a white solid with impurities.

Synthesis of 5-((2-((4-(2-aminoethyl)phenyl)amino)pyrimidin-4-yl)amino)-1*H*-pyrazole-3-carboxylic acid (106a)

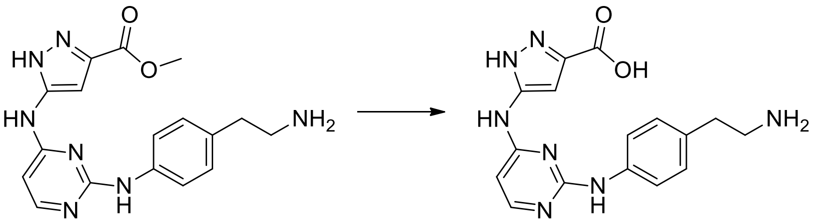

102a (160 mg, 0.45 mmol, 1.0 eq) and lithium hydroxide monohydrate (95 mg, 2.26 mmol, 5.0 eq) were dissolved in 8.9 mL THF and 2.3 mL H_2O. The resulting mixture was stirred at 50 °C for 16 h. The solvent was removed under reduced pressure, the residue was dissolved in H_2O and it was neutralized with a 10% HCl. The solvent was removed under reduced pressure and the crude product was purified by flash chromatography using acetonitrile/ water as an eluent to obtain the desired product (116 mg, 75%) as a white solid.

^{1}H NMR (500 MHz, DMSO-d6) δ 12.22 (d, J = 69.1 Hz, 1H), 9.50 (d, J = 139.2 Hz, 1H), 8.99 (d, J = 38.6 Hz, 1H), 8.17 – 7.87 (m, 1H), 7.69 (d, J = 8.2 Hz, 1H), 7.55 (d, J = 8.0 Hz, 1H), 7.32 – 7.01 (m, 2H), 6.50 (s, 1H), 6.18 (d, J = 74.4 Hz, 1H), 3.27 – 3.22 (m, 2H), 2.60 (t, J = 6.8 Hz, 2H).

^{13}C NMR (126 MHz, DMSO) δ 159.85, 159.80, 155.91, 147.38, 139.06, 138.64, 132.66, 132.12, 128.61, 128.50, 119.03, 97.77, 43.34, 35.56.

MS-ESI m/z $[M + H]^+$: calcd 340.4, found 340.6.

HRMS m/z $[M + H]^+$: calcd 340.1517, found 340.1524.

HPLC: t_R = 9.87, purity ≥ 95% (UV: 254/ 280 nm).

Synthesis of 5-((2-((3-(2-aminoethyl)phenyl)amino)pyrimidin-4-yl)amino)-1*H*-pyrazole-3-carboxylic acid (106b)

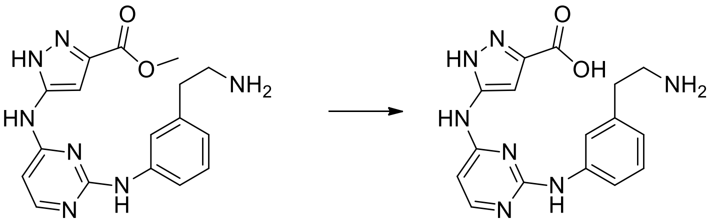

The title compound was prepared according to the procedure of **106a**, using **102b** (139 mg, 0.39 mmol). The desired product was obtained as a white solid with salts.

MS-ESI m/z $[M + H]^+$: calcd 340.4, found 340.2.

HRMS m/z $[M + Na]^+$: calcd 362.1336, found 362.1338.

Synthesis of 5-((2-((5-aminopentyl)amino)pyrimidin-4-yl)amino)-1*H*-pyrazole-3-carboxylic acid (106c)

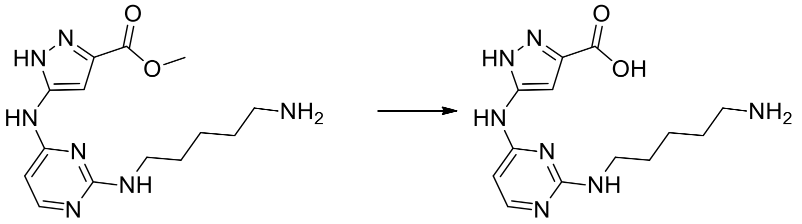

The title compound was prepared according to the procedure of **106a**, using **102c** (108 mg, 0.34 mmol). The desired product was obtained as a white solid with salts.

MS-ESI m/z $[M + H]^+$: calcd 306.3, found 306.2.

HRMS m/z $[M + H]^+$: calcd 306.1673, found 306.1674.

Synthesis of 5-((2-((2-(2-aminoethoxy)ethyl)amino)pyrimidin-4-yl)amino)-1*H*-pyrazole-3-carboxylic acid (106d)

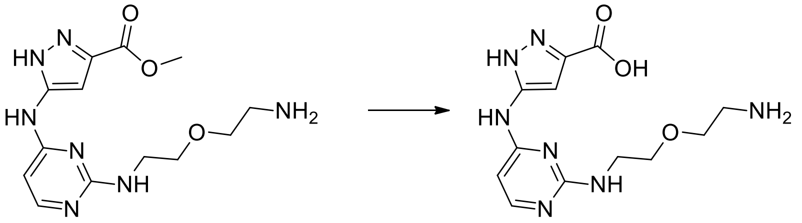

The title compound was prepared according to the procedure of **106a**, using **102d** (84 mg, 0.24 mmol). The desired product was obtained as a white solid with salts.

MS-ESI m/z $[M + H]^+$: calcd 308.3, found 308.2.

Synthesis of 5-((2-((6-aminohexyl)amino)pyrimidin-4-yl)amino)-1*H*-pyrazole-3-carboxylic acid (106e)

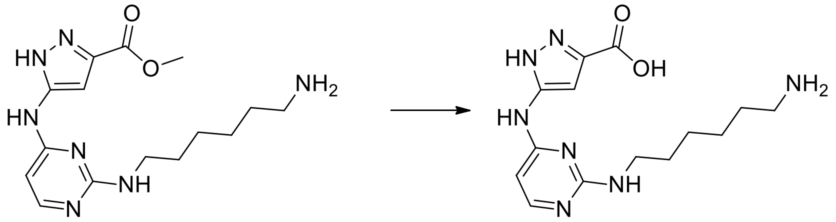

The title compound was prepared according to the procedure of **106a**, using **102e** (73 mg, 0.22 mmol). The desired product (41 mg, 59%) was obtained as a white solid.

^{1}H NMR (500 MHz, DMSO-d6) δ 12.15 (s, 1H, c), 9.40 (s, 1H, d), 8.56 (s, 2H, n), 7.72 (d, J = 5.6 Hz, 1H, f), 6.89 (s, 1H, b), 6.67 (s, 1H, g), 5.97 (s, 1H, e), 3.27 – 3.19 (m, 2H, h), 2.84 – 2.73 (m, 2H, m), 1.65 –1.53 (m, 4H, I, l), 1.51 – 1.41 (m, 2H, j), 1.39 – 1.31 (m, 2H, k).

^{13}C NMR (126 MHz, DMSO) δ 162.30, 159.78, 155.73, 97.70, 95.41, 41.07, 38.19, 29.52, 27.75, 26.60, 25.13.

MS-ESI m/z $[M + H]^+$: calcd 320.4, found 320.6.

HRMS m/z $[M + H]^+$: calcd 320.1830, found 320.1841.

HPLC: t_R = 9.87, purity ≥ 95% (UV: 254/ 280 nm).

Synthesis of 5-((2-((4-(2-aminoethyl)phenyl)amino)-5-chloropyrimidin-4-yl)amino)-1*H*-pyrazole-3-carboxylic acid (107a)

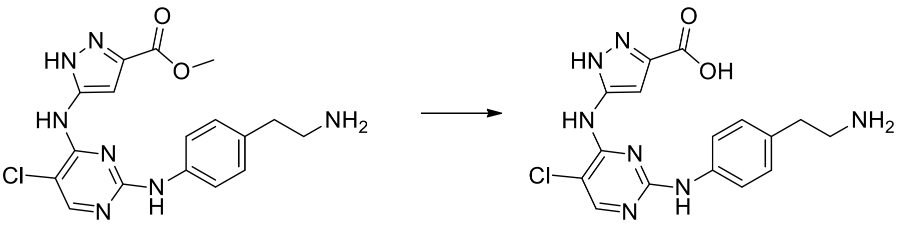

The title compound was prepared according to the procedure of **106a**, using **103a** (244 mg, 0.63 mmol). The desired product was obtained as a white solid with salts.

MS-ESI m/z $[M + H]^+$: calcd 374.8, found 374.1.

Synthesis of 5-((2-((3-(2-aminoethyl)phenyl)amino)-5-chloropyrimidin-4-yl)amino)-1*H*-pyrazole-3-carboxylic acid (107b)

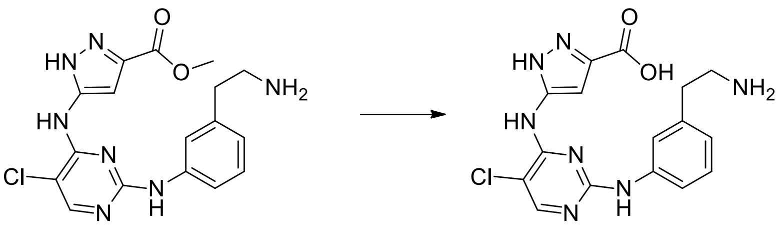

The title compound was prepared according to the procedure of **106a**, using **103b** (233 mg, 0.60 mmol). The desired product was obtained as a white solid with salts.

MS-ESI m/z $[M + H]^+$: calcd 374.8, found 374.1.

Synthesis of 5-((2-((5-aminopentyl)amino)-5-chloropyrimidin-4-yl)amino)-1*H*-pyrazole-3-carboxylic acid (107c)

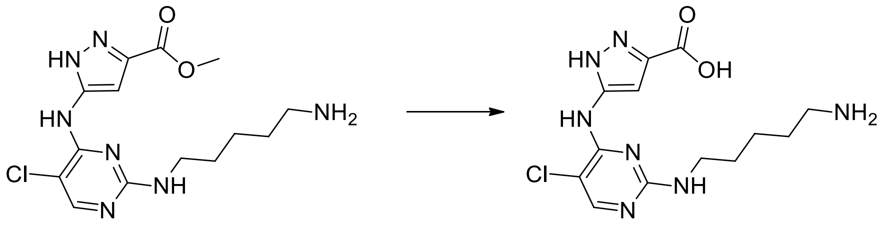

The title compound was prepared according to the procedure of **106a**, using **103c** (162 mg, 0.46 mmol). The desired product was obtained as a white solid with salts.

MS-ESI m/z $[M + H]^+$: calcd 340.8, found 340.1.

HRMS m/z $[M + H]^+$: calcd 340.1283, found 340.1286.

Synthesis of 5-((2-((2-(2-aminoethoxy)ethyl)amino)-5-chloropyrimidin-4-yl)amino)-1*H*-pyrazole-3-carboxylic acid (107d)

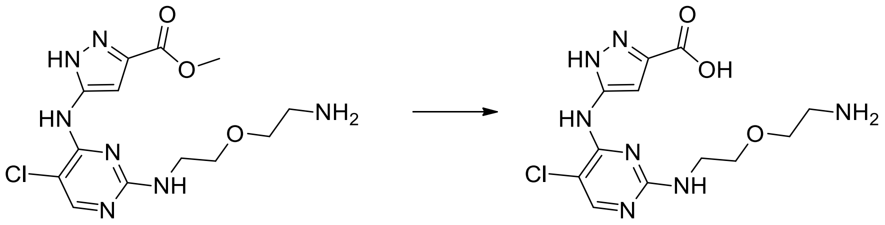

The title compound was prepared according to the procedure of **106a**, using **103d** (86 mg, 0.24 mmol). The desired product was obtained as a white solid with salts.

MS-ESI m/z $[M + H]^+$: calcd 342.8, found 342.3.

HRMS m/z $[M + H]^+$: calcd 342.1076, found 342.1080.

Synthesis of 5-((2-((6-aminohexyl)amino)-5-chloropyrimidin-4-yl)amino)-1*H*-pyrazole-3-carboxylic acid (107e)

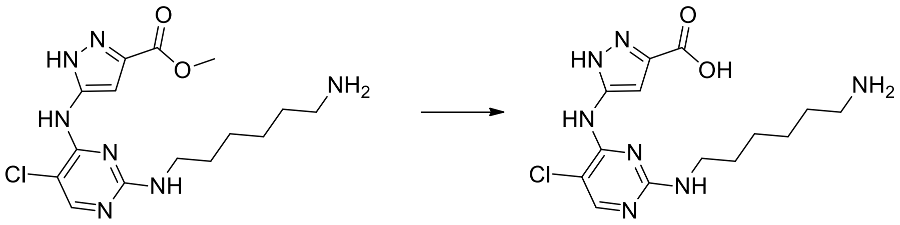

The title compound was prepared according to the procedure of **106a**, using **103e** (110 mg, 0.30 mmol). The desired product was obtained as a white solid with salts.

MS-ESI m/z $[M + H]^+$: calcd 354.8, found 354.3.

HRMS m/z $[M + H]^+$: calcd 354.1440, found 354.1440.

Synthesis of 5-((2-((4-(2-aminoethyl)phenyl)amino)-5-methylpyrimidin-4-yl)amino)-1*H*-pyrazole-3-carboxylic acid (108a)

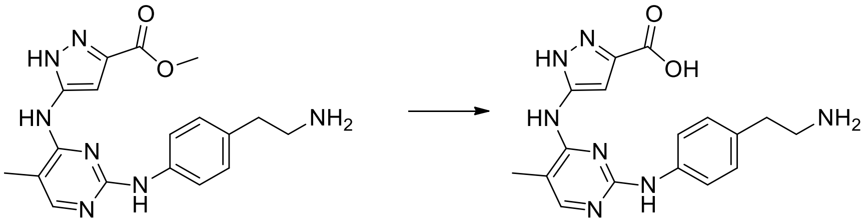

The title compound was prepared according to the procedure of **106a**, using **104a** (88 mg, 0.24 mmol). The desired product was obtained as a white solid with salts.

MS-ESI m/z $[M + H]^+$: calcd 354.4, found 354.2.

Synthesis of 5-((2-((4-(2-aminoethyl)phenyl)amino)quinazolin-4-yl)amino)-1*H*-pyrazole-3-carboxylic acid (109a)

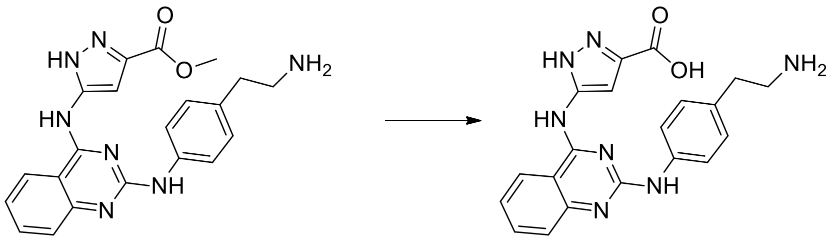

The title compound was prepared according to the procedure of **106a**, using **105a** (225 mg, 0.56 mmol). The desired product was obtained as a white solid with salts.

MS-ESI m/z $[M + H]^+$: calcd 390.4, found 390.3.

Synthesis of 5-((2-((3-(2-aminoethyl)phenyl)amino)quinazolin-4-yl)amino)-1*H*-pyrazole-3-carboxylic acid (109b)

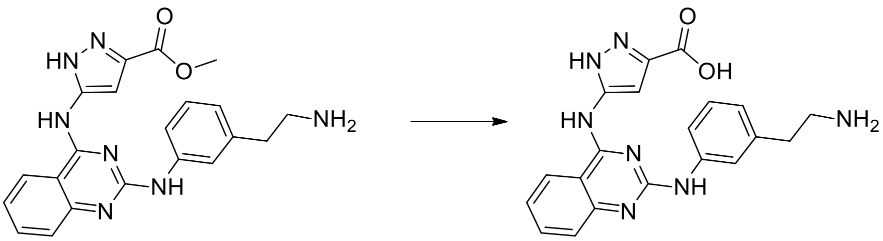

The title compound was prepared according to the procedure of **106a**, using **105b** (250 mg, 0.62 mmol). The desired product was obtained as a white solid with salts.

MS-ESI m/z $[M + H]^+$: calcd 390.4, found 390.2.

Synthesis of 5-((2-((5-aminopentyl)amino)quinazolin-4-yl)amino)-1*H*-pyrazole-3-carboxylic acid (109c)

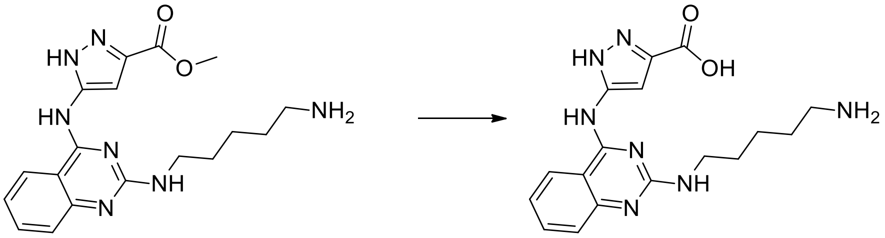

The title compound was prepared according to the procedure of **106a**, using **105c** (209 mg, 0.57 mmol). The desired product was obtained as a white solid with salts.

MS-ESI m/z $[M + H]^+$: calcd 356.4, found 356.3.

Synthesis of 5-((2-((2-(2-aminoethoxy)ethyl)amino)quinazolin-4-yl)amino)-1*H*-pyrazole-3-carboxylic acid (109d)

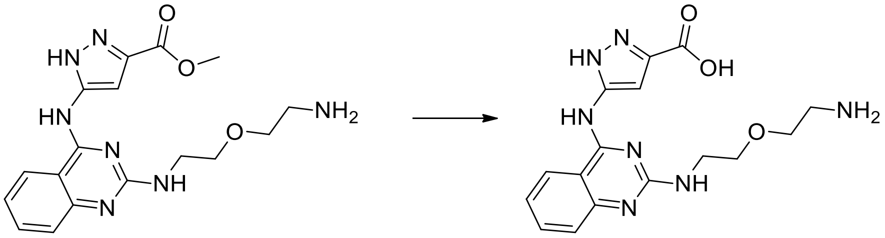

The title compound was prepared according to the procedure of **106a**, using **105d** (115 mg, 0.31 mmol). The desired product was obtained as a white solid with salts.

MS-ESI m/z $[M + H]^+$: calcd 358.4, found 358.2.

Synthesis of 5-((2-((6-aminohexyl)amino)quinazolin-4-yl)amino)-1*H*-pyrazole-3-carboxylic acid (109e)

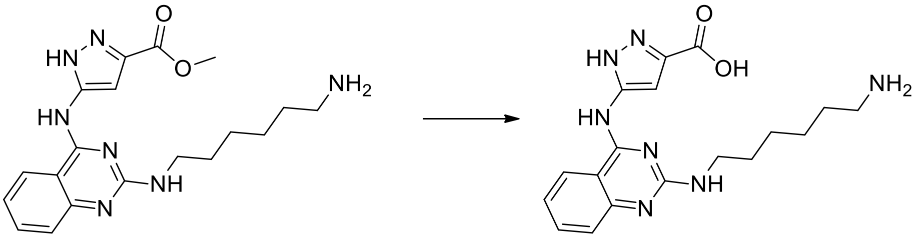

The title compound was prepared according to the procedure of **106a**, using **105e** (143 mg, 0.37 mmol). The desired product was obtained as a white solid with salts.

MS-ESI m/z $[M + H]^+$: calcd 370.4, found 370.2.

Synthesis of (Z)-1¹H-2,4,8-triaza-3(4,2)-pyrimidina-1(3,5)-pyrazola-5(1,4)-benzenacyclononaphan-9-one (110a)

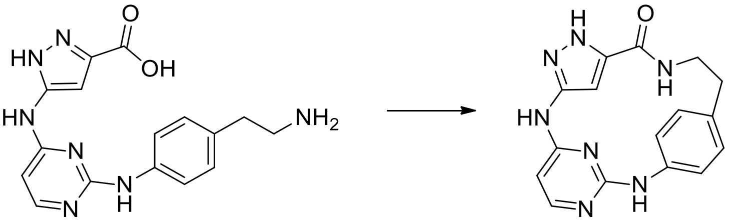

106a (100 mg, 0.29 mmol, 1.0 eq) and HATU (1334 mg, 0.35 mmol, 1.2 eq) were dissolved in 100 mL anhydrous DMF. DIPEA (99 mg, 0.77 mmol, 2.6 eq) was added to the resulting mixture and it was stirred at 70 °C for 16 h. The solvent was removed under reduced pressure and the crude product was purified by flash chromatography using acetonitrile/ water as an eluent and by preparative HPLC to obtain the product (2 mg, 2%) as a white solid.

^{1}H NMR (250 MHz, DMSO-d6) δ 13.12 (s, 1H), 11.06 (s, 1H), 9.99 (s, 1H), 7.92 (d, J = 7.1 Hz, 1H), 7.25 (d, J = 8.3 Hz, 2H), 7.18 (d, J = 8.4 Hz, 2H), 6.97 (t, J = 6.0 Hz, 1H), 6.30 (d, J = 7.0 Hz, 1H), 5.74 (s, 1H), 3.54 (dd, J = 13.0, 6.7 Hz, 2H), 2.98 (t, J = 6.9 Hz, 2H).

^{13}C NMR (126 MHz, DMSO) δ 159.55, 159.46, 157.93, 157.68, 145.58, 137.73, 137.58, 135.42, 130.67, 128.68, 102.65, 98.42, 37.78, 32.52.

MS-ESI m/z $[M + H]^+$: calcd 322.3, found 322.6.

HRMS m/z $[M + H]^+$: calcd 322.1411, found 322.1403.

HPLC: t_R = 10.36, purity ≥ 95% (UV: 254/ 280 nm).

Synthesis of (Z)-1¹H-2,4,8-triaza-3(4,2)-pyrimidina-1(3,5)-pyrazola-5(1,3)-benzenacyclononaphan-9-one (110b)

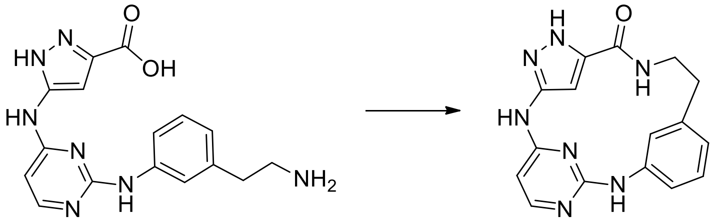

The title compound was prepared according to the procedure **110a**, using **106b** (20 mg, 0.06 mmol). The mixture was stirred for 16 h at 70 °C to obtain the product (8 mg, 42%) as a white solid.

^{1}H NMR (250 MHz, DMSO-d6) δ 13.01 (s, 1H), 9.88 (s, 1H), 9.25 (s, 1H), 8.46 (s, 1H), 8.16 (s, 1H), 7.98 (d, J = 5.7 Hz, 1H), 7.32 (s, 1H), 7.15 (t, J = 7.7 Hz, 1H), 6.97 (d, J = 7.7 Hz, 1H), 6.76 (d, J = 7.3 Hz, 1H), 6.24 (d, J = 5.7 Hz, 1H), 3.53 – 3.42 (m, 4H), 2.86 – 2.70 (m, 4H).

^{13}C NMR (126 MHz, DMSO) δ 161.19, 160.84, 160.18, 159.76, 156.30, 148.09, 140.92, 138.67, 134.70, 128.48, 121.12, 117.42, 98.58, 97.99, 45.20, 44.58.

MS-ESI m/z $[M + H]^+$: calcd 322.3, found 322.2.

HRMS m/z $[M + H]^+$: calcd 322.1411, found 322.1409.

HPLC: t_R = 10.57, purity ≥ 95% (UV: 254/ 280 nm).

Synthesis of (Z)-3^{1}H-2,5,11-triaza-1(4,2)-pyrimidina-3(3,5)-pyrazolacycloundecaphan-4-one (110c)

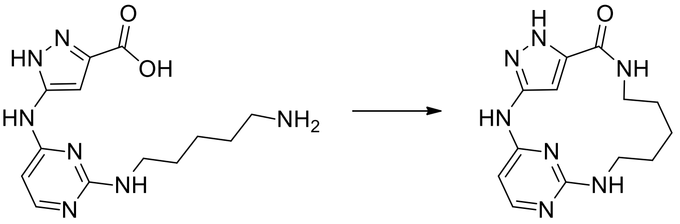

The title compound was prepared according to the procedure **110a**, using **106c** (100 mg, 0.33 mmol). The mixture was stirred for 16 h at rt to obtain the product (10 mg, 10%) as a white solid.

^{1}H NMR (500 MHz, DMSO-d6) δ 13.40 (s, 1H), 11.44 (s, 1H), 8.56 (t, J = 6.0 Hz, 1H), 8.10 (t, J = 7.3 Hz, 1H), 7.86 (d, J = 7.1 Hz, 1H), 7.35 (s, 1H), 6.32 (d, J = 7.1 Hz, 1H), 3.57 – 3.34 (m, 2H), 3.34 – 3.18 (m, 2H), 1.74 – 1.61 (m, 4H), 1.55 – 1.39 (m, 2H).

^{13}C NMR (126 MHz, DMSO) δ 160.34, 159.81, 153.79, 146.73, 143.04, 134.63, 98.11, 97.62, 42.12, 41.20, 27.92, 25.17, 22.35.

MS-ESI m/z $[M + H]^+$: calcd 288.2, found 288.2.

HRMS m/z $[M + H]^+$: calcd 288.1567, found 288.1569.

HPLC: t_R = 9.81, purity ≥ 95% (UV: 254/ 280 nm).

Synthesis of (Z)-3^{1}H-8-oxa-2,5,11-triaza-1(4,2)-pyrimidina-3(5,3)-pyrazolacycloundecaphan-4-one (110d)

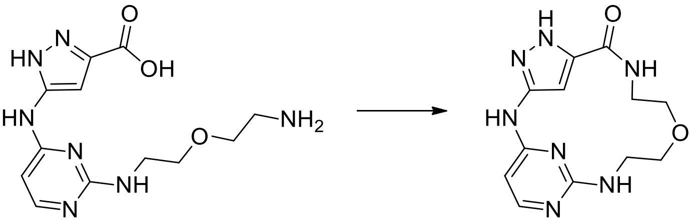

The title compound was prepared according to the procedure **110a**, using **106d** (73 mg, 0.24 mmol). The mixture was stirred for 16 h at 70 °C to obtain the product (2 mg, 3%) as a light yellow solid.

^{1}H NMR (250 MHz, DMSO-d6) δ 13.13 (s, 1H), 10.75 (s, 1H), 7.85 (s, 2H), 7.67 (s, 1H), 7.55 (s, 1H), 6.21 (s, 1H), 3.73 – 3.58 (m, 4H), 3.53 – 3.42 (m, 4H).

MS-ESI m/z $[M + H]^+$: calcd 290.3, found 290.2.

HRMS m/z $[M + Na]^+$: calcd 312.1179, found 312.1177.

HPLC: t_R = 9.86, purity ≥ 95% (UV: 254/ 280 nm).

Synthesis of (Z)-3^{1}H-2,5,12-triaza-1(4,2)-pyrimidina-3(3,5)-pyrazolacyclododecaphan-4-one (110e)

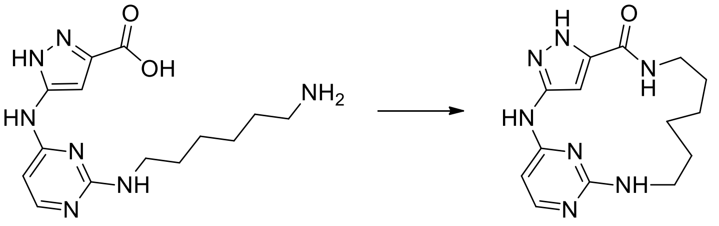

The title compound was prepared according to the procedure **110a**, using **106e** (31 mg, 0.10 mmol). The mixture was stirred for 16 h at 35 °C to obtain the product (5 mg, 17%) as a white solid.

^{1}H NMR (500 MHz, DMSO-d6) δ 13.35 (s, 1H), 11.01 (s, 1H), 8.25 (s, 1H), 8.00 (s, 1H), 7.83 (d, J = 6.9 Hz, 1H), 7.23 (s, 1H), 6.24 (d, J = 6.8 Hz, 1H), 3.28 – 3.25 (m, 4H), 1.60 – 1.53 (m, 2H), 1.52 – 1.46 (m, 2H), 1.42 – 1.34 (m, 3H), 1.31 – 1.21 (m, 2H).

^{13}C NMR (126 MHz, DMSO) δ 161.33, 159.65, 154.90, 146.16, 145.27, 138.29, 102.55, 97.76, 42.01, 38.76, 29.61, 27.88, 27.64, 24.81.

MS-ESI m/z $[M + H]^+$: calcd 302.4, found 302.5.

HRMS m/z $[M + H]^+$: calcd 302.1724, found 302.1730.

HPLC: t_R = 10.46, purity ≥ 95% (UV: 254/ 280 nm).

Synthesis of (Z)-3^5-chloro-1^1H-2,4,8-triaza-3(4,2)-pyrimidina-1(3,5)-pyrazola-5(1,4)-benzenacyclononaphan-9-one (111a)

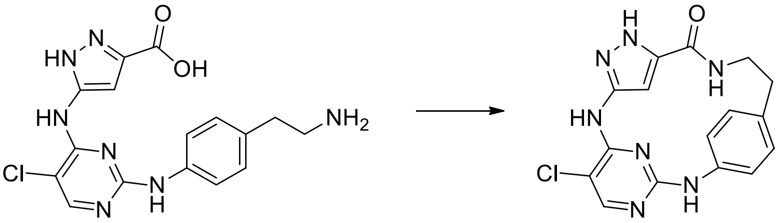

The title compound was prepared according to the procedure **110a**, using **107a** (58 mg, 0.16 mmol). The mixture was stirred for 16 h at 70 °C to obtain the product (5 mg, 9%) as a white solid.

^{1}H NMR (300 MHz, DMSO-d6) δ 12.87 (s, 1H), 9.17 (s, 1H), 8.91 (s, 1H), 8.01 (s, 1H), 7.10 – 6.99 (m, 4H), 6.93 (s, 1H), 5.84 (s, 1H), 3.47 (q, J = 6.5 Hz, 2H), 2.91 (t, J = 6.6 Hz, 2H).

^{13}C NMR (75 MHz, DMSO) δ 160.63, 159.63, 155.14, 154.62, 146.26, 138.10, 137.04, 135.46, 129.92, 128.22, 103.00, 102.67, 38.09, 32.41.

MS-ESI m/z $[M + H]^+$: calcd 356.8, found 356.1.

HRMS m/z $[M + H]^+$: calcd 356.1021, found 356.1023.

HPLC: t_R = 6.23, purity ≥ 95% (UV: 254/ 280 nm).

Synthesis of (Z)-3^5-chloro-1^1H-2,4,8-triaza-3(4,2)-pyrimidina-1(3,5)-pyrazola-5(1,3)-benzenacyclononaphan-9-one (111b)

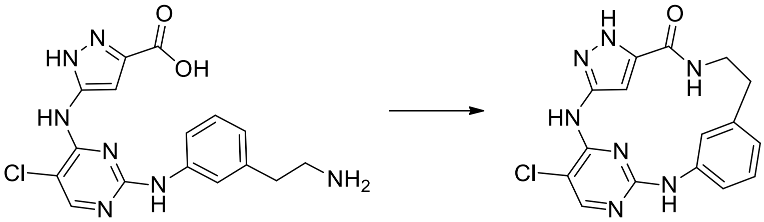

The title compound was prepared according to the procedure **110a**, using **107b** (100 mg, 0.27 mmol). The mixture was stirred for 16 h at 70 °C to obtain the product (5 mg, 5%) as a white solid.

^{1}H NMR (300 MHz, DMSO-d6) δ 9.51 (s, 1H), 9.23 (s, 1H), 8.37 (s, 1H), 8.14 (s, 2H), 7.19 – 7.05 (m, 2H), 7.01 – 6.93 (m, 1H), 6.77 (s, 1H), 3.15 – 3.05 (m, 2H), 2.75 – 2.68 (m, 2H).

MS-ESI m/z $[M + H]^+$: calcd 356.8, found 356.3.

HRMS m/z $[M + H]^+$: calcd 356.1021, found 356.1021.

HPLC: t_R = 6.76, purity ≥ 95% (UV: 254/ 280 nm).

Synthesis of (Z)-1^5-chloro-3^1H-2,5,11-triaza-1(4,2)-pyrimidina-3(3,5)-pyrazolacyclo-undecaphan-4-one (111c)

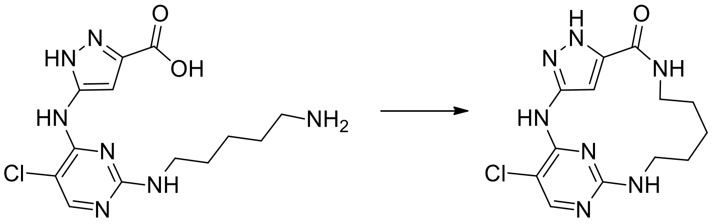

The title compound was prepared according to the procedure **110a**, using **107c** (46 mg, 0.14 mmol). The mixture was stirred for 16 h at 50 °C to obtain the product (3 mg, 7%) as a white solid.

^{1}H NMR (300 MHz, DMSO-d6) δ 13.10 (s, 1H), 9.00 (s, 1H), 7.99 (t, J = 7.2 Hz, 1H), 7.91 (s, 1H), 7.34 (s, 1H), 7.24 (t, J = 5.6 Hz, 1H), 3.28 – 3.26 (m, 2H), 3.25 – 3.16 (m, 2H), 1.71 – 1.54 (m, 4H), 1.48 – 1.36 (m, 2H).

MS-ESI m/z $[M + H]^+$: calcd 322.8, found 322.2.

HRMS m/z $[M + H]^+$: calcd 322.1178, found 322.1179.

HPLC: t_R = 6.01, purity ≥ 95% (UV: 254/ 280 nm).

Synthesis of (Z)-1^5-chloro-3^1H-8-oxa-2,5,11-triaza-1(4,2)-pyrimidina-3(3,5)-pyrazolacyclo-undecaphan-4-one (111d)

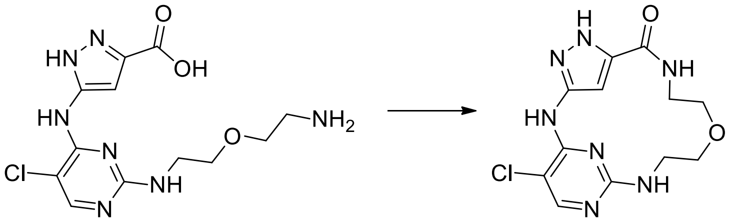

The title compound was prepared according to the procedure **110a**, using **107d** (70 mg, 0.20 mmol). The mixture was stirred for 16 h at 50 °C to obtain the product (3 mg, 5%) as a beige solid.

^{1}H NMR (300 MHz, DMSO-d6) δ 10.14 (s, 1H), 8.13 (s, 1H), 7.90 (t, J = 7.4 Hz, 1H), 7.76 (s, 1H), 7.43 (s, 1H), 3.48 – 3.36 (m, 8H).

MS-ESI m/z $[M + H]^+$: calcd 324.7, found 324.2.

HRMS m/z $[M + H]^+$: calcd 324.0970, found 324.0971.

HPLC: t_R = 5.72, purity ≥ 95% (UV: 254/ 280 nm).

Synthesis of (Z)-1^5-chloro-3^{1}H-2,5,12-triaza-1(4,2)-pyrimidina-3(3,5)-pyrazolacyclododecaphan-4-one (111e)

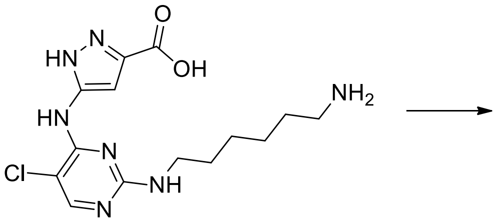

The title compound was prepared according to the procedure **110a**, using **107e** (58 mg, 0.16 mmol). The mixture was stirred for 16 h at 50 °C to obtain the product (22 mg, 40%) as a white solid.

^{1}H NMR (300 MHz, DMSO-d6) δ 13.09 (s, 1H), 9.23 (s, 1H), 8.18 (t, J = 5.7 Hz, 1H), 7.92 (s, 1H), 7.23 – 7.03 (m, 2H), 3.11 – 3.01 (m, 2H), 2.91 – 2.81 (m, 2H), 1.62 – 1.43 (m, 6H), 1.43 – 1.29 (m, 2H).

^{13}C NMR (75 MHz, DMSO) δ 161.41, 160.86, 159.62, 155.97, 154.11, 102.66, 100.92, 44.28, 41.58, 29.61, 27.56, 27.09, 24.45.

MS-ESI m/z [M + H]$^+$: calcd 336.8, found 336.2.

HRMS m/z [M + H]$^+$: calcd 336.1334, found 336.1336.

HPLC: t_R = 6.09, purity ≥ 95% (UV: 254/ 280 nm).

Synthesis of (Z)-3^5-methyl-1^{1}H-2,4,8-triaza-3(4,2)-pyrimidina-1(3,5)-pyrazola-5(1,4)-benzenacyclononaphan-9-one (112a)

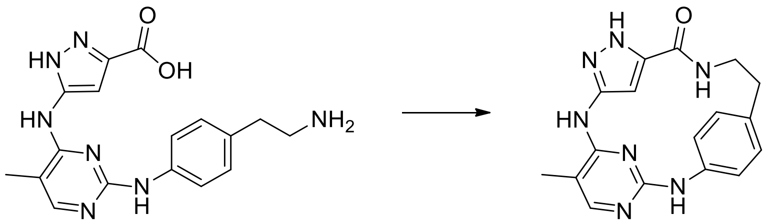

The title compound was prepared according to the procedure **110a**, using **108a** (80 mg, 0.23 mmol). The mixture was stirred for 16 h at 50 °C to obtain the product (9 mg, 12%) as a white solid.

^{1}H NMR (500 MHz, DMSO-d6) δ 12.73 (s, 1H), 8.88 (s, 1H), 8.49 (s, 1H), 7.76 (s, 1H), 7.07 (d, J = 8.4 Hz, 2H), 7.01 (d, J = 8.3 Hz, 2H), 6.76 (s, 1H), 5.92 (s, 1H), 3.46 (q, J = 6.6 Hz, 2H), 2.91 (t, J = 6.7 Hz, 2H), 1.99 (d, J = 0.8 Hz, 3H).

MS-ESI m/z [M + H]$^+$: calcd 336.4, found 336.2.

HRMS m/z $[M + H]^+$: calcd 336.1567, found 336.1572.

HPLC: t_R = 6.04, purity ≥ 95% (UV: 254/ 280 nm).

Synthesis of (Z)-1^{1}H-2,4,8-triaza-3(4,2)-quinazolina-1(3,5)-pyrazola-5(1,4)-benzenacyclononaphan-9-one (113a)

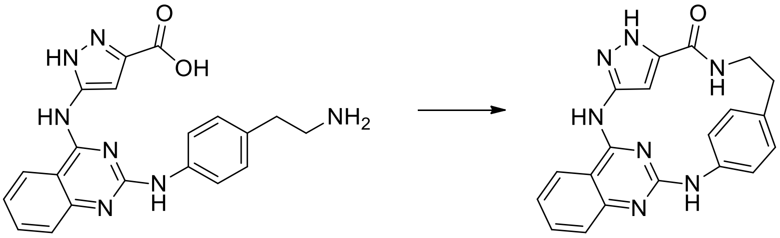

The title compound was prepared according to the procedure **110a**, using **109a** (210 mg, 0.54 mmol). The mixture was stirred for 16 h at 50 °C to obtain the product (7 mg, 4%) as a yellow solid.

^{1}H NMR (500 MHz, DMSO-d6) δ 13.32 (s, 1H), 11.64 (s, 1H), 10.47 (s, 1H), 8.57 (d, J = 8.2 Hz, 1H), 7.88 (t, J = 7.8 Hz, 1H), 7.61 (d, J = 8.4 Hz, 1H), 7.48 (t, J = 7.7 Hz, 1H), 7.30 – 7.18 (m, 5H), 5.85 (s, 1H), 3.55 (q, J = 6.5 Hz, 2H), 2.99 (t, J = 6.7 Hz, 2H).

^{13}C NMR (126 MHz, DMSO) δ 159.49, 157.68, 153.82, 153.77, 145.34, 140.65, 137.88, 135.59, 135.03, 130.59, 128.47, 124.75, 124.47, 117.89, 110.15, 103.84, 37.91, 32.44.

MS-ESI m/z $[M + H]^+$: calcd 372.4, found 372.6.

HRMS m/z $[M + H]^+$: calcd 372.1567, found 372.1569.

HPLC: t_R = 6.36, purity ≥ 95% (UV: 254/ 280 nm).

Synthesis of (Z)-1^{1}H-2,4,8-triaza-3(4,2)-quinazolina-1(3,5)-pyrazola-5(1,3)-benzenacyclononaphan-9-one (113b)

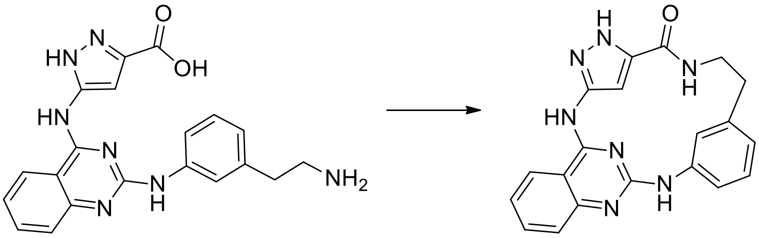

The title compound was prepared according to the procedure **110a**, using **109b** (240 mg, 0.62 mmol). The mixture was stirred for 16 h at 50 °C to obtain the product (10 mg, 4%) as a yellow solid.

^{1}H NMR (400 MHz, DMSO-d6) δ 13.44 (s, 1H), 11.81 (s, 1H), 10.88 (s, 1H), 8.65 (d, J = 8.8 Hz, 1H), 8.10 (s, 1H), 7.97 – 7.86 (m, 2H), 7.61 (d, J = 8.4 Hz, 1H), 7.50 (t, J = 7.7 Hz, 1H), 7.36 (t, J = 7.7 Hz, 1H), 7.09 (d, J = 8.3 Hz, 2H), 6.92 (s, 1H), 3.74 – 3.63 (m, 2H), 2.87 – 2.80 (m, 2H).

^{13}C NMR (101 MHz, DMSO) δ 162.36, 159.20, 158.86, 158.16, 152.60, 139.91, 137.20, 135.87, 129.26, 127.50, 126.28, 124.99, 124.64, 117.99, 117.45, 115.06, 110.19, 100.73, 44.37, 34.34.

MS-ESI m/z $[M + H]^+$: calcd 372.4, found 372.6.

HRMS m/z $[M + H]^+$: calcd 372.1567, found 372.1572.

HPLC: t_R = 6.40, purity ≥ 95% (UV: 254/ 280 nm).

Synthesis of (Z)-3^{1}H-2,5,11-triaza-1(4,2)-quinazolina-3(3,5)-pyrazolacycloundecaphan-4-one (113c)

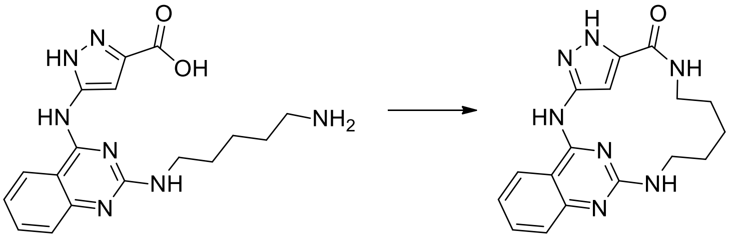

The title compound was prepared according to the procedure **110a**, using **109c** (180 mg, 0.51 mmol). The mixture was stirred for 16 h at 50 °C to obtain the product (5 mg, 3%) as a light yellow solid.

^{1}H NMR (500 MHz, DMSO-d6) δ 13.20 (s, 1H), 10.59 (s, 1H), 8.40 (d, J = 8.2 Hz, 1H), 8.03 (t, J = 7.2 Hz, 1H), 7.59 – 7.48 (m, 2H), 7.26 (dd, J = 8.4, 1.2 Hz, 1H), 7.19 (t, J = 1071.7, 5.4 Hz, 1H), 7.14 – 7.05 (m, 1H), 3.43 – 3.33 (m, 4H), 1.77 – 1.59 (m, 4H), 1.57 – 1.41 (m, 2H).

^{13}C NMR (126 MHz, DMSO) δ 160.68, 158.41, 157.50, 151.31, 148.19, 134.21, 133.02, 123.52, 123.26, 120.56, 110.12, 98.36, 41.90, 41.07, 28.27, 27.26, 22.57.

MS-ESI m/z $[M + H]^+$: calcd 338.4, found 338.3.

HRMS m/z $[M + H]^+$: calcd 338.1724, found 338.1730.

HPLC: t_R = 6.34, purity ≥ 95% (UV: 254/ 280 nm).

Synthesis of (Z)-3^{1}H-8-oxa-2,5,11-triaza-1(4,2)-quinazolina-3(3,5)-pyrazolacycloundecaphan-4-one (113d)

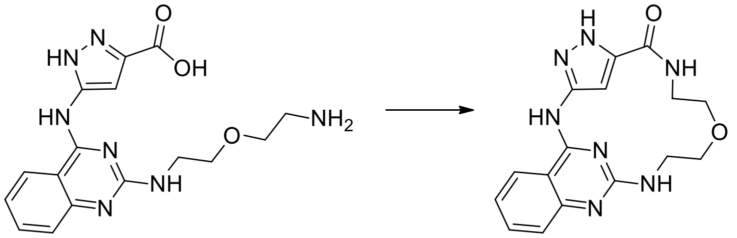

The title compound was prepared according to the procedure **110a**, using **109d** (100 mg, 0.28 mmol). The mixture was stirred for 16 h at 50 °C to obtain the product (21 mg, 22%) as a white solid.

^{1}H NMR (400 MHz, DMSO-d6) δ 13.55 (s, 1H), 11.87 (s, 1H), 8.83 (t, J = 5.7 Hz, 1H), 8.62 (d, J = 8.3 Hz, 1H), 7.99 (t, J = 7.1 Hz, 1H), 7.86 – 7.80 (m, 1H), 7.58 (s, 1H), 7.55 – 7.35 (m, 2H), 3.76 – 3.58 (m, 8H).

^{13}C NMR (101 MHz, DMSO) δ 161.43, 159.33, 158.02, 153.32, 146.39, 139.75, 135.73, 134.84, 124.62, 116.94, 109.76, 100.71, 69.14, 66.96, 41.70, 34.33.

MS-ESI m/z $[M + H]^+$: calcd 340.4, found 340.2.

HRMS m/z $[M + H]^+$: calcd 340.1517, found 340.1513.

HPLC: t_R = 6.05, purity ≥ 95% (UV: 254/ 280 nm).

Synthesis of (Z)-3^{1}H-2,5,12-triaza-1(4,2)-quinazolina-3(3,5)-pyrazolacyclododecaphan-4-one (113e)

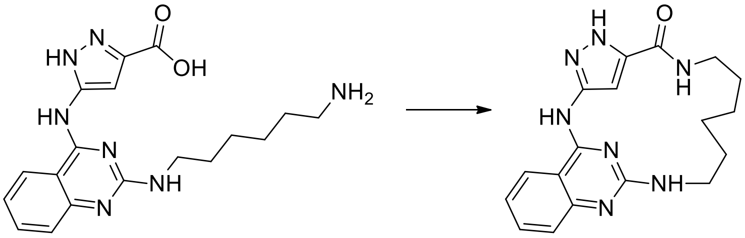

The title compound was prepared according to the procedure **110a**, using **109e** (90 mg, 0.24 mmol). The mixture was stirred for 16 h at 50 °C to obtain the product (17 mg, 20%) as a yellow solid.

^{1}H NMR (400 MHz, DMSO-d6) δ 13.57 (s, 1H), 11.64 (s, 1H), 8.67 (t, J = 5.9 Hz, 1H), 8.54 (d, J = 8.2 Hz, 1H), 8.36 (t, J = 6.1 Hz, 1H), 7.85 (t, J = 7.7 Hz, 1H), 7.53 – 7.42 (m, 2H), 7.27 (s, 1H), 3.34 – 3.23 (m, 4H), 1.68 – 1.53 (m, 2H), 1.56 – 1.47 (m, 2H), 1.46 – 1.34 (m, 2H), 1.31 – 1.19 (m, 2H).

^{13}C NMR (101 MHz, DMSO) δ 159.26, 158.89, 154.01, 152.79, 140.15, 135.77, 124.50, 124.42, 118.66, 117.06, 109.57, 103.48, 41.55, 38.50, 29.29, 27.44, 26.96, 24.27.

MS-ESI m/z $[M + H]^+$: calcd 352.4, found 352.7.

HRMS m/z $[M + H]^+$: calcd 352.1880, found 352.1882.

HPLC: t_R = 6.41, purity ≥ 95% (UV: 254/ 280 nm).

8. Abbreviations

%Ctrl	percent of control
ABL	tyrosine-protein kinase ABL1
ACN	acetonitrile
ADP	adenosine diphosphate
ALL	acute lymphoblastic leukemia
AMPK	5' AMP-activated protein kinase
AMPPNP	adenylyl imidodiphosphate
AREG	amphiregulin
ATP	adenosine triphosphate
BMP	bone morphogenetic protein
BMPR2	bone morphogenetic protein receptor type II
Boc	*tert*-butyloxycarbonyl
BRET	bioluminescent resonance energy transfer
BTC	betacellulin
CDK	cyclin-dependent kinase
CML	chronic myelogenous leukemia
CNS	central nervous system
conc.	concentration
DCM	dichloromethane
DFG	aspartic acid-phenylalanine-glycine
DIPEA	*N,N*-diisopropylethylamine
DMF	*N,N*-dimethylformamide
DMSO	dimethyl sulfoxide
DSF	differential scanning fluorimetry
EC_{50}	half-maximal effective concentration

EE	ethyl acetate
EGF	epidermal growth factor
EGFR	epidermal growth factor receptor
EPGN	epigen
eq	equivalents
EREG	epiregulin
ESI	electron spray ionization
et al.	(lat.) et alii or et aliae
EtOH	ethanol
FDA	U. S. Food and Drug Administration
Gck	germinal center kinase
h	hour(s)
HATU	1-[bis(dimethylamino)methylene]-1H-1,2,3-triazolo[4,5-b]pyridinium 3-oxide hexafluorophosphate
HBEGF	heparin-binding EGF-like growth factor
HPAH	heritable pulmonary arterial hypertension
HPLC	high performance liquid chromatography
HRD	histidine-arginine-aspartic acid
HRMS	high resolution mass spectrometry
IC_{50}	half maximum inhibitory concentration
IPAH	idiopathic pulmonary arterial hypertension
ITC	isothermal titration calorimetry
K_D	dissociation constant
M	molarity (mol/L)
m/z	mass-to-charge ratio
MEK	dual specificity mitogen-activated protein kinase kinase

MeOH	methanol
min	minute(s)
MS	mass spectrometry
MST	mammalian STE20-like protein kinases
mTOR	mechanistic target of rapamycin
MW	microwave
n.d.	not determined
NDR	nuclear Dbf2-related
NMR	nuclear magnetic resonance
oN	over night
PAH	pulmonary arterial hypertension
PAK	P21-activated kinase
PDB	protein data bank
PP2A	protein phosphatase 2A
ppm	parts per million
PTB	phosphotyrosine binding
ROCK	rho-associated protein kinase
RT	room temperature
S_{35}	selectivity-score with a threshold of 35 %Ctrl
SCC	cutaneous squamous cell carcinoma
SGC	Structural Genomics Consortium
SH2	Src homology 2
TEA	triethylamine
TFA	trifluoroacetic acid
TGFα	transforming growth factor-α
THF	tetrahydrofuran

TKI	tyrosine kinase inhibitor
TLC	thin-layer chromatography
T_m	melting temperature
t_R	retention time
WT	wild type
YAP	yes-associated protein 1
ΔG	free binding energy
ΔH	enthalpy
ΔS	entropy
ΔT_m	T_m-shift

Amino acids

Amino acid	Three letter code	One letter code
Alanine	Aln	A
Arginine	Arg	R
Asparagine	Asn	N
Aspartic acid	Asp	D
Cystein	Cys	C
Glutamic acid	Glu	E
Glutamine	Gln	Q
Glycine	Gly	G
Histidine	His	H
Isoleucine	Ile	I
Leucine	Leu	L
Lysine	Lys	K
Methionine	Met	M
Phyenylalanine	Phe	F
Proline	Pro	P
Serine	Ser	S
Threonine	Thr	T
Tryptophan	Trp	W
Tyrosine	Tyr	Y
Valine	Val	V

9. References

(1) Cohen, P. Protein Kinases — the Major Drug Targets of the Twenty-First Century? *Nat. Rev. Drug Discov.* **2002**, *1* (April), 309–315.

(2) Kunick, C.; Egert-Schmidt, A. M. Jung, Kompetitiv, Erfolgreich: Die Kurze Geschichte Der Proteinkinase-Inhibitoren. *Pharm. Unserer Zeit* **2008**, *37* (5), 360–368.

(3) Hidaka, H.; Inagaki, M.; Kawamoto, S.; Sasaki, Y. Isoquinolinesulfonamides, Novel and Potent Inhibitors of Cyclic Nucleotide Dependent Protein Kinase and Protein Kinase C. *Biochemistry* **1984**, *23* (21), 5036–5041.

(4) Sung, H.; Ferlay, J.; Siegel, R. L.; Laversanne, M.; Soerjomataram, I.; Jemal, A.; Bray, F. Global Cancer Statistics 2020: GLOBOCAN Estimates of Incidence and Mortality Worldwide for 36 Cancers in 185 Countries. *CA. Cancer J. Clin.* **2021**, *71* (3), 209–249.

(5) Roskoski, R. Properties of FDA-Approved Small Molecule Protein Kinase Inhibitors: A 2022 Update. *Pharmacol Res.* **2022**, *175*, 106037.

(6) Roskoski, R. Properties of FDA-Approved Small Molecule Protein Kinase Inhibitors: A 2023 Update. *Pharmacol. Res.* **2022**, *175* (November 2022), 106552.

(7) Craig Venter, J.; Adams, M. D.; Myers, E. W.; Li, P. W.; Mural, R. J.; Sutton, G. G.; Smith, H. O.; Yandell, M.; Evans, C. A.; Holt, R. A.; Gocayne, J. D.; Amanatides, P.; Ballew, R. M.; Huson, D. H.; Wortman, J. R.; Zhang, Q.; Kodira, C. D.; Zheng, X. H.; Chen, L.; Skupski, M.; Subramanian, G.; Thomas, P. D.; Zhang, J.; Gabor Miklos, G. L.; Nelson, C.; Broder, S.; Clark, A. G.; Nadeau, J.; McKusick, V. A.; Zinder, N.; Levine, A. J.; Roberts, R. J.; Simon, M.; Slayman, C.; Hunkapiller, M.; Bolanos, R.; Delcher, A.; Dew, I.; Fasulo, D.; Flanigan, M.; Florea, L.; Halpern, A.; Hannenhalli, S.; Kravitz, S.; Levy, S.; Mobarry, C.; Reinert, K.; Remington, K.; Abu-Threideh, J.; Beasley, E.; Biddick, K.; Bonazzi, V.; Brandon, R.; Cargill, M.; Chandramouliswaran, I.; Charlab, R.; Chaturvedi, K.; Deng, Z.; di Francesco, V.; Dunn, P.; Eilbeck, K.; Evangelista, C.; Gabrielian, A. E.; Gan, W.; Ge, W.; Gong, F.; Gu, Z.; Guan, P.; Heiman, T. J.; Higgins, M. E.; Ji, R. R.; Ke, Z.; Ketchum, K. A.; Lai, Z.; Lei, Y.; Li, Z.; Li, J.; Liang, Y.; Lin, X.; Lu, F.; Merkulov, G. V.; Milshina, N.; Moore, H. M.; Naik, A. K.; Narayan, V. A.; Neelam, B.; Nusskern, D.; Rusch, D. B.; Salzberg, S.; Shao, W.; Shue, B.; Sun, J.; Yuan Wang, Z.; Wang, A.; Wang, X.; Wang, J.; Wei, M. H.; Wides, R.; Xiao, C.; Yan, C.; Yao, A.; Ye, J.; Zhan, M.; Zhang, W.; Zhang, H.; Zhao, Q.; Zheng, L.; Zhong, F.; Zhong, W.; Zhu, S. C.; Zhao, S.; Gilbert, D.; Baumhueter, S.; Spier, G.; Carter, C.; Cravchik, A.; Woodage, T.; Ali, F.; An, H.; Awe, A.; Baldwin, D.; Baden, H.; Barnstead, M.; Barrow, I.; Beeson, K.; Busam, D.; Carver, A.; Center, A.; Lai Cheng, M.; Curry, L.; Danaher, S.; Davenport, L.; Desilets, R.; Dietz, S.; Dodson, K.; Doup, L.; Ferriera, S.; Garg, N.; Gluecksmann, A.; Hart, B.; Haynes, J.; Haynes, C.; Heiner, C.; Hladun, S.; Hostin, D.; Houck, J.; Howland, T.; Ibegwam, C.; Johnson, J.; Kalush, F.; Kline, L.; Koduru, S.; Love, A.; Mann, F.; May, D.; McCawley, S.; McIntosh, T.; McMullen, I.; Moy, M.; Moy, L.; Murphy, B.; Nelson, K.; Pfannkoch, C.; Pratts, E.; Puri, V.; Qureshi, H.; Reardon, M.; Rodriguez, R.; Rogers, Y. H.; Romblad, D.; Ruhfel, B.; Scott, R.; Sitter, C.; Smallwood, M.; Stewart, E.; Strong, R.; Suh, E.; Thomas, R.; Ni Tint, N.; Tse, S.; Vech, C.; Wang, G.; Wetter, J.; Williams, S.; Williams, M.; Windsor, S.; Winn-Deen, E.; Wolfe, K.; Zaveri, J.; Zaveri, K.; Abril, J. F.; Guigo, R.; Campbell, M. J.; Sjolander, K. V.; Karlak, B.; Kejariwal, A.; Mi, H.; Lazareva, B.; Hatton, T.; Narechania, A.; Diemer, K.; Muruganujan, A.; Guo, N.; Sato, S.; Bafna, V.; Istrail, S.; Lippert, R.; Schwartz, R.; Walenz, B.; Yooseph, S.; Allen, D.; Basu, A.; Baxendale, J.; Blick, L.; Caminha, M.; Carnes-Stine, J.; Caulk, P.; Chiang, Y. H.; Coyne, M.; Dahlke, C.; Deslattes Mays, A.; Dombroski, M.; Donnelly, M.; Ely, D.; Esparham, S.; Fosler, C.; Gire, H.; Glanowski, S.; Glasser, K.; Glodek, A.; Gorokhov, M.; Graham, K.; Gropman, B.; Harris, M.; Heil, J.; Henderson, S.; Hoover, J.; Jennings, D.; Jordan, C.; Jordan, J.; Kasha, J.; Kagan, L.; Kraft, C.; Levitsky, A.; Lewis, M.; Liu, X.; Lopez, J.; Ma, D.; Majoros, W.; McDaniel, J.; Murphy, S.; Newman, M.; Nguyen, T.; Nguyen, N.; Nodell, M.; Pan, S.; Peck, J.; Peterson, M.; Rowe, W.; Sanders, R.; Scott, J.; Simpson, M.; Smith, T.; Sprague, A.; Stockwell, T.; Turner, R.; Venter, E.; Wang, M.; Wen, M.; Wu, D.; Wu, M.; Xia, A.; Zandieh, A.; Zhu, X. The Sequence of the Human Genome. *Science (80-.).* **2001**, *291* (5507), 1304–1351.

(8) Hanks, S. K.; Hunter, T. The Eukaryotic Protein Kinase Superfamily: Kinase (Catalytic) Domain Structure and Classification. *FASEB* **1995**, *9*, 576–596.

(9) Manning, G.; Whyte, D. B.; Martinez, R.; Hunter, T.; Sudarsanam, S. The Protein Kinase Complement of the Human Genome. *Science (80-.).* **2002**, *298* (5600), 1912–1934.

(10) Byrne, D. P.; Foulkes, D. M.; Eyers, P. A. Pseudokinases: Update on Their Functions and Evaluation as New Drug Targets. *Future Med. Chem.* **2017**, *9* (2), 245–265.

(11) Raju, S.; Shaw, A. S. What Is the Point of Pseudokinases? *Elife* **2015**, *4* (e07771), 1–3.

(12) Ubersax, J. A.; Ferrell, J. E. Mechanisms of Specificity in Protein Phosphorylation. *Nat. Rev. Mol. Cell Biol.* **2007**, *8* (7), 530–541.

(13) Vulpetti, A.; Bosotti, R. Sequence and Structural Analysis of Kinase ATP Pocket Residues. *Farmaco* **2004**, *59*, 759–765.

(14) Druker, B. J.; Lydon, N. B. Lessons Learned from the Development of an Abl Tyrosine Kinase Inhibitor for Chronic Myelogenous Leukemia. *J. Clin. Invest.* **2000**, *105* (1), 3–7.

(15) Hunter, T.; Blume-Jensen, P. Oncogenic Kinase Signalling. *Nature* **2001**, *411* (6835), 355–365.

(16) Cohen, P. The Role of Protein Phosphorylation in Human Health and Disease. *Eur. J. Biochem.* **2001**, *268* (19), 5001–5010.

(17) Fabbro, D.; Cowan-Jacob, S. W.; Moebitz, H. Ten Things You Should Know about Protein Kinases. *Br. J. Pharmacol.* **2015**, *172* (11), 2675–2700.

(18) Knighton, D. R.; Zheng, J.; Eyck, L. F. T. E. N.; Ashford, V. A.; Xuong, N.; Taylor, S. S.; Sowadski, J. M. Crystal Structure of the Catalytic Subunit of Cyclic Adenosine Monophosphate-Dependent Protein Kinase. *Science (80-.).* **1991**, *253*, 407–414.

(19) Schwartz, P. A.; Murray, B. W. Protein Kinase Biochemistry and Drug Discovery. *Bioorg. Chem.* **2011**, *39*, 192–210.

(20) Kornev, A. P.; Taylor, S. S. Defining the Conserved Internal Architecture of a Protein Kinase. *Biochim. Biophys. Acta - Proteins Proteomics* **2010**, *1804* (3), 440–444.

(21) Roskoski, R. Classification of Small Molecule Protein Kinase Inhibitors Based upon the Structures of Their Drug-Enzyme Complexes. *Pharmacol. Res.* **2016**, *103*, 26–48.

(22) Endicott, J. A.; Noble, M. E.; Johnson, L. N. The Structural Basis for Control of Eukaryotic Protein Kinases. *Annu. Rev. Biochem.* **2012**, *81*, 587–613.

(23) Nolen, B.; Taylor, S.; Ghosh, G. Regulation of Protein Kinases: Controlling Activity through Activation Segment Conformation. *Mol. Cell* **2004**, *15* (5), 661–675.

(24) Taylor, S. S.; Kornev, A. P. Protein Kinases: Evolution of Dynamic Regulatory Proteins. *Trends Biochem. Sci.* **2011**, *36* (2), 65–77.

(25) Kornev, A. P.; Taylor, S. S.; Ten Eyck, L. F. A Helix Scaffold for the Assembly of Active Protein Kinases. *PNAS* **2008**, *105* (38), 14377–14382.

(26) Tamaoki, T.; Nomoto, H.; Takahashi, I.; Kato, Y.; Morimoto, M.; Tomita, F. Staurosporine, a Potent Inhibitor of Phospholipid/Ca++ Dependent Protein Kinase. *Biochem. Biophys. Res. Commun.* **1986**, *135* (2), 397–402.

(27) Shibuya, M.; Suzuki, Y.; Sugita, K.; Saito, I.; Sasaki, T.; Takakura, K.; Nagata, I.; Kikuchi, H.; Takemae, T.; Hidaka, H.; Nakashima, M. Effect of AT877 on Cerebral Vasospasm after Aneurysmal Subarachnoid Hemorrhage. *J. Neurosurg.* **1992**, *76* (4), 571–577.

(28) Zhao, J.; Zhou, D.; Guo, J.; Ren, Z.; Zhou, L.; Wang, S.; Xu, B.; Wang, R. Effect of Fasudil Hydrochloride, a Protein Kinase Inhibitor, on Cerebral Vasospasm and Delayed Cerebral Ischemic Symptoms after Aneurysmal Subarachnoid Hemorrhage: Results of a Randomized Trial of Fasudil Hydrochloride versus Nimodipine. *Neurol. Med. Chir. (Tokyo).* **2006**, *46* (9), 421–427.

(29) Heitman, J.; Movva, N. R.; Hall, M. N. Targets for Cell Cycle Arrest by the Immunosuppressant Rapamycin in Yeast. *Science (80-.).* **1991**, *253* (5022), 905–909.

(30) Brown, E. J.; Albers, M. W.; Bum Shin, T.; Ichikawa, K.; Keith, C. T.; Lane, W. S.; Schreiber, S. L. A Mammalian Protein Targeted by G1-Arresting Rapamycin-Receptor Complex. *Nature* **1994**, *369* (6483), 756–758.

(31) Müller, S.; Chaikuad, A.; Gray, N. S.; Knapp, S. The Ins and Outs of Selective Kinase Inhibitor Development. *Nat. Chem. Bio.* **2015**, *11*, 818–821.

(32) Lamba, V.; Ghosh, I. New Directions in Targeting Protein Kinases: Focusing upon True Allosteric and Bivalent Inhibitors. *Curr. Pharm. Des.* **2012**, *18*, 2936–2945.

(33) Liu, Y.; Gray, N. S. Rational Design of Inhibitors That Bind to Inactive Kinase Conformations. *Nat. Chem. Bio.* **2006**, *2*, 358–364.

(34) Davis, M. I.; Hunt, J. P.; Herrgard, S.; Ciceri, P.; Wodicka, L. M.; Pallares, G.; Hocker, M.; Treiber, D. K.; Zarrinkar, P. P. Comprehensive Analysis of Kinase Inhibitor Selectivity. *Nat. Biotechnol.* **2011**, *29* (11), 1046–1051.

(35) Cerchione, C.; Locatelli, F.; Martinelli, G. Dasatinib in the Management of Pediatric Patients With Philadelphia Chromosome-Positive Acute Lymphoblastic Leukemia. *Front. Oncol.* **2021**, *11* (March), 1–7.

(36) McCafferty, E. H.; Dhillon, S.; Deeks, E. D. Dasatinib: A Review in Pediatric Chronic Myeloid Leukemia. *Pediatr. Drugs* **2018**, *20* (6), 593–600.

(37) Wu, P.; Nielsen, T. E.; Clausen, M. H. FDA-Approved Small-Molecule Kinase Inhibitors. *Trends Pharmacol. Sci.* **2015**, *36*, 422–439.

(38) Zuccotto, F.; Ardini, E.; Casale, E.; Angiolini, M. Through the “Gatekeeper Door”: Exploiting the Active Kinase Conformation. *J. Med. Chem.* **2010**, *53*, 2681–2694.

(39) Zhao, Z.; Wu, H.; Wang, L.; Liu, Y.; Knapp, S.; Liu, Q.; Gray, N. S. Exploration of Type II Binding Mode: A Privileged Approach for Kinase Inhibitor Focused Drug Discovery? *ACS Chem. Biol.* **2014**, *9* (6), 1230–1241.

(40) Karaman, M. W.; Herrgard, S.; Treiber, D. K.; Gallant, P.; Atteridge, C. E.; Campbell, B. T.; Chan, K. W.; Ciceri, P.; Davis, M. I.; Edeen, P. T.; Faraoni, R.; Floyd, M.; Hunt, J. P.; Lockhart, D. J.; Milanov, Z. V.; Morrison, M. J.; Pallares, G.; Patel, H. K.; Pritchard, S.; Wodicka, L. M.; Zarrinkar, P. P. A Quantitative Analysis of Kinase Inhibitor Selectivity. *Nat. Biotechnol.* **2008**, *26* (1), 127–132.

(41) O’Hare, T.; Shakespeare, W. C.; Zhu, X.; Eide, C. A.; Rivera, V. M.; Wang, F.; Adrian, L. T.; Zhou, T.; Huang, W. S.; Xu, Q.; Metcalf, C. A.; Tyner, J. W.; Loriaux, M. M.; Corbin, A. S.; Wardwell, S.; Ning, Y.; Keats, J. A.; Wang, Y.; Sundaramoorthi, R.; Thomas, M.; Zhou, D.; Snodgrass, J.; Commodore, L.; Sawyer, T. K.; Dalgarno, D. C.; Deininger, M. W. N.; Druker, B. J.; Clackson, T. AP24534, a Pan-BCR-ABL Inhibitor for Chronic Myeloid Leukemia, Potently Inhibits the T315I Mutant and Overcomes Mutation-Based Resistance. *Cancer Cell* **2009**, *16* (5), 401–412.

(42) Cowan-Jacob, S. W.; Jahnke, W.; Knapp, S. Novel Approaches for Targeting Kinases: Allosteric Inhibition, Allosteric Activation and Pseudokinases. *Futur. Med. Chem.* **2014**, *6*, 541–561.

(43) Tomita, N.; Hayashi, Y.; Suzuki, S.; Oomori, Y.; Aramaki, Y.; Matsushita, Y.; Iwatani, M.; Iwata, H.; Okabe, A.; Awazu, Y.; Isono, O.; Skene, R. J.; Hosfield, D. J.; Miki, H.; Kawamoto, T.; Hori, A.; Baba, A. Structure-Based Discovery of Cellular-Active Allosteric Inhibitors of FAK. *Bioorganic Med. Chem. Lett.* **2013**, *23* (6), 1779–1785.

(44) Attwood, M. M.; Fabbro, D.; Sokolov, A. V.; Knapp, S.; Schiöth, H. B. Trends in Kinase Drug Discovery: Targets, Indications and Inhibitor Design. *Nat. Rev. Drug Discov.* **2021**, *20* (11), 839–861.

(45) Lugowska, I.; Koseła-Paterczyk, H.; Kozak, K.; Rutkowski, P. Trametinib: A MEK Inhibitor for Management of Metastatic Melanoma. *Onco. Targets. Ther.* **2015**, *8*, 2251–2259.

(46) Koelblinger, P.; Dornbierer, J.; Dummer, R. A Review of Binimetinib for the Treatment of Mutant Cutaneous Melanoma. *Futur. Oncol.* **2017**, *13* (20), 1–12.

(47) Gavrin, L. K.; Saiah, E. Approaches to Discover Non-ATP Site Kinase Inhibitors.

Medchemcomm **2013**, *4* (1), 41–51.

(48) Wu, P.; Clausen, M. H.; Nielsen, T. E. Allosteric Small-Molecule Kinase Inhibitors. *Pharmacol. Ther.* **2015**, *156*, 59–68.

(49) Zhang, J.; Adrián, F. J.; Jahnke, W.; Cowan-Jacob, S. W.; Li, A. G.; Iacob, R. E.; Sim, T.; Powers, J.; Dierks, C.; Sun, F.; Guo, G. R.; Ding, Q.; Okram, B.; Choi, Y.; Wojciechowski, A.; Deng, X.; Liu, G.; Fendrich, G.; Strauss, A.; Vajpai, N.; Grzesiek, S.; Tuntland, T.; Liu, Y.; Bursulaya, B.; Azam, M.; Manley, P. W.; Engen, J. R.; Daley, G. Q.; Warmuth, M.; Gray, N. S. Targeting Bcr-Abl by Combining Allosteric with ATP-Binding-Site Inhibitors. *Nature* **2010**, *463* (7280), 501–506.

(50) Liu, Q.; Sabnis, Y.; Zhao, Z.; Zhang, T.; Buhrlage, S. J.; Jones, L. H.; Gray, N. S. Developing Irreversible Inhibitors of the Protein Kinase Cysteinome. *Chem Biol* **2013**, *20* (2), 146–159.

(51) Garuti, L.; Roberti, M.; Bottegoni, G. Irreversible Protein Kinase Inhibitors. *Curr. Med. Chem.* **2011**, *18*, 2981–2994.

(52) Potashman, M. H.; Duggan, M. E. Covalent Modifiers: An Orthogonal Approach to Drug Design. *J. Med. Chem.* **2009**, *52* (5), 1231–1246.

(53) Keating, G. M. Afatinib: A Review in Advanced Non-Small Cell Lung Cancer. *Target. Oncol.* **2016**, *11* (6), 825–835.

(54) Motzer, R. J.; Escudier, B.; Oudard, S.; Hutson, T. E.; Porta, C.; Bracarda, S.; Grünwald, V.; Thompson, J. A.; Figlin, R. A.; Hollaender, N.; Kay, A.; Ravaud, A. Phase 3 Trial of Everolimus for Metastatic Renal Cell Carcinoma: Final Results and Analysis of Prognostic Factors. *Cancer* **2010**, *116* (18), 4256–4265.

(55) MacDonald, A. S. A Worldwide, Phase III, Randomized, Controlled, Safety and Efficacy Study of a Sirolimus/Cyclosporine Regimen for Prevention of Acute Rejection in Recipients of Primary Mismatched Renal Allografts. *Transplantation* **2001**, *71* (2), 271–280.

(56) Woodward, R. B.; Logusch, E.; Nambiar, K. P.; Sakan, K.; Ward, D. E.; Au-Yeung, B. W.; Balaram, P.; Browne, L. J.; Card, P. J.; Chen, C. H.; Chenevert, R. B.; Fliri, A.; Frobel, K.; Gals, H. J.; Garratt, D. G.; Hayakawa, K.; Heggie, W.; Hesson, D. P.; Hoppe, D.; Hoppe, I.; Hyatt, J. A.; Ikeda, D.; Jacobi, P. A.; Kim, K. S.; Kobuke, Y.; Kojima, K.; Krowicki, K.; Lee, V. J.; Leutert, T.; Malchenko, S.; Martens, J.; Matthews, R. S.; Ong, B. S.; Press, J. B.; Rajan Babu, T. V.; Rousseau, G.; Sauter, H. M.; Suzuki, M.; Tatsuta, K.; Tolbert, L. M.; Truesdale, E. A.; Uchida, I.; Ueda, Y.; Uyehara, T.; Vasella, A. T.; Vladuchick, W. C.; Wade, P. A.; Williams, R. M.; Wong, H. N. C. Asymmetric Total Synthesis of Erythromycin. 1. Synthesis of an Erythronolide A Seco Acid Derivative via Asymmetric Induction. *J. Am. Chem. Soc.* **1981**, *103* (11), 3210–3213.

(57) Lipinski, C. A.; Lombardo, F.; Dominy, B. W.; Feeney, P. J. Experimental and Computational Approaches to Estimate Solubility and Permeability in Drug Discovery and Development Settings. *Adv. Drug Deliv Rev.* **2001**, *46*, 3–26.

(58) Marsault, E.; Peterson, M. L. Macrocycles Are Great Cycles: Applications, Opportunities, and Challenges of Synthetic Macrocycles in Drug Discovery. *J. Med. Chem.* **2011**, *54* (7), 1961–2004.

(59) Fang, Z.; Song, Y.; Zhan, P.; Zhang, Q.; Liu, X. Conformational Restriction: An Effective Tactic in 'Follow-on'-Based Drug Discovery. *Futur. Med. Chem.* **2014**, *6* (8), 885–901.

(60) Driggers, E. M.; Hale, S. P.; Lee, J.; Terrett, N. K. The Exploration of Macrocycles for Drug Discovery — an Underexploited Structural Class. *Nat. Rev. Drug Discov.* **2008**, *7*, 608–624.

(61) Mallinson, J.; Collins, I. Macrocycles in New Drug Discovery. *Future Med. Chem.* **2012**, *4* (11), 1409–1438.

(62) Collins, J. C.; James, K. Emac - A Comparative Index for the Assessment of Macrocyclization Efficiency. *Medchemcomm* **2012**, *3* (12), 1489–1495.

(63) Blankenstein, J.; Zhu, J. Conformation-Directed Macrocyclization Reactions. *European J. Org. Chem.* **2005**, *2005* (10), 1939–2139.

(64) Martí-Centelles, V.; Pandey, M. D.; Burguete, M. I.; Luis, S. V. Macrocyclization Reactions:

The Importance of Conformational, Configurational, and Template-Induced Preorganization. *Chem. Rev.* **2015**, *115* (16), 8736–8834.

(65) Amrhein, J. A.; Knapp, S.; Hanke, T. Synthetic Opportunities and Challenges for Macrocyclic Kinase Inhibitors. *J. Med. Chem.* **2021**, *64* (12), 7991–8009.

(66) Gradillas, A.; Pérez-Castells, J. Macrocyclization by Ring-Closing Metathesis in the Total Synthesis of Natural Products: Reaction Conditions and Limitations. *Angew. Chemie - Int. Ed.* **2006**, *45* (37), 6086–6101.

(67) Lücking, U.; Siemeister, G.; Schäfer, M.; Briem, H.; Krüger, M.; Lienau, P.; Jautelat, R. Macrocyclic Aminopyrimidines as Multitarget CDK and VEGF-R Inhibitors with Potent Antiproliferative Activities. *ChemMedChem* **2007**, *2* (1), 63–77.

(68) Biffis, A.; Centomo, P.; Del Zotto, A.; Zecca, M. Pd Metal Catalysts for Cross-Couplings and Related Reactions in the 21st Century: A Critical Review. *Chem. Rev.* **2018**, *118* (4), 2249–2295.

(69) Han, S.-Y.; Kim, Y.-A. Recent Development of Peptide Coupling Reagents in Organic Synthesis. *Tetrahedron* **2004**, *60* (11), 2447–2467.

(70) Mitsunobu, O. The Use of Diethyl Azodicarboxylate and Triphenylphosphine in Synthesis and Transformation of Natural Products. *Synthesis (Stuttg).* **1981**, *1981*, 1–28.

(71) Eduful, B. J.; O'Byrne, S. N.; Temme, L.; Asquith, C. R. M.; Liang, Y.; Picado, A.; Pilotte, J. R.; Hossain, M. A.; Wells, C. I.; Zuercher, W. J.; Catta-Preta, C. M. C.; Zonzini Ramos, P.; Santiago, A. D. S.; Couñago, R. M.; Langendorf, C. G.; Nay, K.; Oakhill, J. S.; Pulliam, T. L.; Lin, C.; Awad, D.; Willson, T. M.; Frigo, D. E.; Scott, J. W.; Drewry, D. H. Hinge Binder Scaffold Hopping Identifies Potent Calcium/Calmodulin-Dependent Protein Kinase Kinase 2 (CAMKK2) Inhibitor Chemotypes. *J. Med. Chem.* **2021**, *64* (15), 10849–10877.

(72) Xing, L.; Klug-Mcleod, J.; Rai, B.; Lunney, E. A. Kinase Hinge Binding Scaffolds and Their Hydrogen Bond Patterns. *Bioorganic Med. Chem.* **2015**, *23* (19), 6520–6527.

(73) Chen, J.; Xu, H.; Pawlak, S.; James, L. P.; Peltz, G.; Lee, K.; Ginman, K.; Bergeron, M.; Pithavala, Y. K. The Effect of Rifampin on the Pharmacokinetics and Safety of Lorlatinib: Results of a Phase One, Open-Label, Crossover Study in Healthy Participants. *Adv. Ther.* **2020**, *37* (2), 745–758.

(74) Johnson, T. W.; Richardson, P. F.; Bailey, S.; Brooun, A.; Burke, B. J.; Collins, M. R.; Cui, J. J.; Deal, J. G.; Deng, Y.; Dinh, D.; Engstrom, L. D.; He, M.; Ho, J.; Ho, R. L.; Huang, Q.; Kania, R. S.; Kath, J. C.; Lam, H.; Lam, J. L.; Le, P. T.; Lingardo, L.; Liu, W.; Mctigue, M.; Palmer, C. L.; Sach, N. W.; Smeal, T.; Smith, G. L.; Stewart, A. E.; Timofeevski, S.; Zhu, H.; Zhu, J.; Zou, H. Y.; Edwards, M. P. Discovery of (10R)-7-Amino-12-Fluoro-2,10,16-Trimethyl-15-Oxo- 10,15,16,17-Tetrahydro-2H-8,4-(Metheno)Pyrazolo[4,3-h][2,5,11]-Benzoxadiazacyclotetradecine-3-Carbonitrile (PF-06463922), a Macrocyclic Inhibitor of Anaplastic Lymphoma Kinase (ALK) and c- Ro. *J. Med. Chem.* **2014**, *57*, 4720–4744.

(75) Basit, S.; Ashraf, Z.; Lee, K.; Latif, M. First Macrocyclic 3rd-Generation ALK Inhibitor for Treatment of ALK/ROS1 Cancer: Clinical and Designing Strategy Update of Lorlatinib. *Eur. J. Med. Chem.* **2017**, *134*, 348–356.

(76) Engelhardt, H.; Böse, D.; Petronczki, M.; Scharn, D.; Bader, G.; Baum, A.; Bergner, A.; Chong, E.; Döbel, S.; Egger, G.; Engelhardt, C.; Ettmayer, P.; Fuchs, J. E.; Gerstberger, T.; Gonnella, N.; Grimm, A.; Grondal, E.; Haddad, N.; Hopfgartner, B.; Kousek, R.; Krawiec, M.; Kriz, M.; Lamarre, L.; Leung, J.; Mayer, M.; Patel, N. D.; Simov, B. P.; Reeves, J. T.; Schnitzer, R.; Schrenk, A.; Sharps, B.; Solca, F.; Stadtmüller, H.; Tan, Z.; Wunberg, T.; Zoephel, A.; McConnell, D. B. Start Selective and Rigidify: The Discovery Path toward a Next Generation of EGFR Tyrosine Kinase Inhibitors. *J. Med. Chem.* **2019**, *62* (22), 10272–10293.

(77) Shen, Y.; Boivin, R.; Yoneda, N.; Du, H.; Schiller, S.; Matsushima, T.; Goto, M.; Shirota, H.; Gusovsky, F.; Lemelin, C.; Jiang, Y.; Zhang, Z.; Pelletier, R.; Ikemori-Kawada, M.; Kawakami, Y.; Inoue, A.; Schnaderbeck, M.; Wang, Y. Discovery of Anti-Inflammatory Clinical Candidate E6201, Inspired from Resorcylic Lactone LL-Z1640-2, III. *Bioorganic Med. Chem. Lett.* **2010**, *20* (10), 3155–3157.

(78) Pallis, M.; Abdul-Aziz, A.; Burrows, F.; Seedhouse, C.; Grundy, M.; Russell, N. The Multi-Kinase Inhibitor TG02 Overcomes Signalling Activation by Survival Factors to Deplete MCL1 and XIAP and Induce Cell Death in Primary Acute Myeloid Leukaemia Cells. *Br. J. Haematol.* **2012**, *159* (2), 191–203.

(79) William, A. D.; Lee, A. C. H.; Blanchard, S.; Poulsen, A.; Teo, E. L.; Nagaraj, H.; Tan, E.; Chen, D.; Williams, M.; Sun, E. T.; Goh, K. C.; Ong, W. C.; Goh, S. K.; Hart, S.; Jayaraman, R.; Pasha, M. K.; Ethirajulu, K.; Wood, J. M.; Dymock, B. W. Discovery of the Macrocycle 11-(2-Pyrrolidin-1-Yl-Ethoxy)-14,19-Dioxa-5,7, 26-Triaza-Tetracyclo[19.3.1.1(2,6).1(8,12)]Heptacosa-1(25),2(26),3,5,8,10,12(27) ,16,21,23-Decaene (SB1518), a Potent Janus Kinase 2/Fms-like Tyrosine Kinase-3 (JAK2/FLT3) Inhibito. *J. Med. Chem.* **2011**, *54* (13), 4638–4658.

(80) William, A. D.; Lee, A. C.; Poulsen, A.; Goh, K. C.; Madan, B.; Hart, S.; Tan, E.; Wang, H.; Nagaraj, H.; Chen, D.; Lee, C. P.; Sun, E. T.; Jayaraman, R.; Pasha, M. K.; Ethirajulu, K.; Wood, J. M.; Dymock, B. W. Discovery of the Macrocycle (9E)-15-(2-(Pyrrolidin-1-Yl)Ethoxy)-7,12,25- Trioxa-19,21,24-Triaza-Tetracyclo[18.3.1.1(2,5).1(14,18)]Hexacosa-1(24),2,- 4,9,14(26),15,17,20,22-Nonaene (SB1578), a Potent Inhibitor of Janus Kinase 2/Fms-LikeTyrosine Kinase-3 (J. *J. Med. Chem.* **2012**, *55*, 2623–2640.

(81) Huber, K. V. M.; Salah, E.; Radic, B.; Gridling, M.; Elkins, J. M.; Stukalov, A.; Jemth, A. S.; Göktürk, C.; Sanjiv, K.; Strömberg, K.; Pham, T.; Berglund, U. W.; Colinge, J.; Bennett, K. L.; Loizou, J. I.; Helleday, T.; Knapp, S.; Superti-Furga, G. Stereospecific Targeting of MTH1 by (S)-Crizotinib as an Anticancer Strategy. *Nature* **2014**, *508* (7495), 222–227.

(82) Carpenter, G.; King, L.; Cohen, S. Epidermal Growth Factor Stimulates Phosphorylation in Membrane Preparations in Vitro. *Nature* **1978**, *276* (5686), 409–410.

(83) Jorissen, R. N.; Walker, F.; Pouliot, N.; Garrett, T. P. J.; Ward, C. W.; Burgess, A. W. Epidermal Growth Factor Receptor: Mechanisms of Activation and Signalling. *Exp. Cell Res.* **2003**, *284* (1), 31–53.

(84) Burgess, A. W.; Cho, H. S.; Eigenbrot, C.; Ferguson, K. M.; Garrett, T. P. J.; Leahy, D. J.; Lemmon, M. A.; Sliwkowski, M. X.; Ward, C. W.; Yokoyama, S. An Open-and-Shut Case? Recent Insights into the Activation of EGF/ErbB Receptors. *Mol. Cell* **2003**, *12* (3), 541–552.

(85) Linggi, B.; Carpenter, G. ErbB Receptors: New Insights on Mechanisms and Biology. *Trends Cell Biol.* **2006**, *16* (12), 649–656.

(86) Zhang, X.; Gureasko, J.; Shen, K.; Cole, P. A.; Kuriyan, J. An Allosteric Mechanism for Activation of the Kinase Domain of Epidermal Growth Factor Receptor. *Cell* **2006**, *125* (6), 1137–1149.

(87) Dawson, J. P.; Berger, M. B.; Lin, C.-C.; Schlessinger, J.; Lemmon, M. A.; Ferguson, K. M. Epidermal Growth Factor Receptor Dimerization and Activation Require Ligand-Induced Conformational Changes in the Dimer Interface. *Mol. Cell. Biol.* **2005**, *25* (17), 7734–7742.

(88) Sigismund, S.; Avanzato, D.; Lanzetti, L. Emerging Functions of the EGFR in Cancer. *Mol. Oncol.* **2018**, *12*, 3–20.

(89) Kovacs, E.; Zorn, J. A.; Huang, Y.; Barros, T.; Kuriyan, J. A Structural Perspective on the Regulation of the Epidermal Growth Factor Receptor. *Annu. Rev. Biochem.* **2015**, *84*, 739–764.

(90) Williams, R.; Sanghera, J.; Wu, F.; Carbonaro-Hall, D.; Campbell, D. L.; Warburton, D.; Pelech, S.; Hall, F. Identification of a Human Epidermal Growth Factor Receptor-Associated Protein Kinase as a New Member of the Mitogen-Activated Protein Kinase/Extracellular Signal-Regulated Protein Kinase Family. *J. Biol. Chem.* **1993**, *268* (24), 18213–18217.

(91) Phillips, R. J.; Mestas, J.; Gharaee-Kermani, M.; Burdick, M. D.; Sica, A.; Belperio, J. A.; Keane, M. P.; Strieter, R. M. Epidermal Growth Factor and Hypoxia-Induced Expression of CXC Chemokine Receptor 4 on Non-Small Cell Lung Cancer Cells Is Regulated by the Phosphatidylinositol 3-Kinase/PTEN/AKT/Mammalian Target of Rapamycin Signaling Pathway and Activation of Hypoxia Ind. *J. Biol. Chem.* **2005**, *280* (23), 22473–22481.

(92) Nakamura, N.; Chin, H.; Miyasaka, N.; Miura, O. An Epidermal Growth Factor Receptor/Jak2 Tyrosine Kinase Domain Chimera Induces Tyrosine Phosphorylation of Stat5 and

Transduces a Growth Signal in Hematopoietic Cells. *J. Biol. Chem.* **1996**, *271* (32), 19483–19488.

(93) Normanno, N.; De Luca, A.; Bianco, C.; Strizzi, L.; Mancino, M.; Maiello, M. R.; Carotenuto, A.; De Feo, G.; Caponigro, F.; Salomon, D. S. Epidermal Growth Factor Receptor (EGFR) Signaling in Cancer. *Gene* **2006**, *366* (1), 2–16.

(94) Mitsudomi, T.; Yatabe, Y. Epidermal Growth Factor Receptor in Relation to Tumor Development: EGFR Gene and Cancer. *FEBS J.* **2010**, *277* (2), 301–308.

(95) Voldborg, B. R.; Damstrup, L.; Spang-Thomsen, M.; Skovgaard Poulsen, H. Epidermal Growth Factor Receptor (EGFR) and EGFR Mutations, Function and Possible Role in Clinical Trials. *Ann. Oncol.* **1997**, *8*, 1197–1206.

(96) Molina, J. R.; Yang, P.; Cassivi, S. D.; Schild, S. E.; Adjei, A. A. Non-Small Cell Lung Cancer: Epidemiology, Risk Factors, Treatment, and Survivorship. *Mayo Clin. Proc.* **2008**, *83* (5), 584–594.

(97) Ahmed, S. M.; Salgia, R. Epidermal Growth Factor Receptor Mutations and Susceptibility to Targeted Therapy in Lung Cancer. *Respirology* **2006**, *11* (6), 687–692.

(98) Kobayashi, Y.; Mitsudomi, T. Not All Epidermal Growth Factor Receptor Mutations in Lung Cancer Are Created Equal: Perspectives for Individualized Treatment Strategy. *Cancer Sci.* **2016**, *107* (9), 1179–1186.

(99) Harrison, P. T.; Vyse, S.; Huang, P. H. Rare Epidermal Growth Factor Receptor (EGFR) Mutations in Non-Small Cell Lung Cancer. *Semin. Cancer Biol.* **2020**, *61*, 167–179.

(100) Gazdar, A. F. Activating and Resistance Mutations of EGFR in Non-Small-Cell Lung Cancer: Role in Clinical Response to EGFR Tyrosine Kinase Inhibitors. *Oncogene* **2009**, *28* (Suppl 1), S24–S31.

(101) Thress, K. S.; Paweletz, C. P.; Felip, E.; Cho, B. C.; Stetson, D.; Dougherty, B.; Lai, Z.; Markovets, A.; Vivancos, A.; Kuang, Y.; Ercan, D.; Matthews, S. E.; Cantarini, M.; Barrett, J. C.; Jänne, P. A.; Oxnard, G. R. Acquired EGFR C797S Mutation Mediates Resistance to AZD9291 in Non-Small Cell Lung Cancer Harboring EGFR T790M. *Nat. Med.* **2015**, *21* (6), 560–562.

(102) Yang, Z.; Yang, N.; Ou, Q.; Xiang, Y.; Jiang, T.; Wu, X.; Bao, H.; Tong, X.; Wang, X.; Shao, Y. W.; Liu, Y.; Wang, Y.; Zhou, C. Investigating Novel Resistance Mechanisms to Third-Generation EGFR Tyrosine Kinase Inhibitor Osimertinib in Non–Small Cell Lung Cancer Patients. *Clin. Cancer Res.* **2018**, *24* (13), 3097–3107.

(103) Amrhein, J. A.; Beyett, T. S.; Feng, W. W.; Krämer, A.; Weckesser, J.; Schaeffner, I. K.; Rana, J. K.; Jänne, P. A.; Eck, M. J.; Knapp, S.; Hanke, T. Macrocyclization of Quinazoline-Based EGFR Inhibitors Leads to Exclusive Mutant Selectivity for EGFR L858R and Del19. *J. Med. Chem.* **2022**, *65* (23), 15679–15697.

(104) Paez, J. G.; Jänne, P. A.; Lee, J. C.; Tracy, S.; Greulich, H.; Gabriel, S.; Herman, P.; Kaye, F. J.; Lindeman, N.; Boggon, T. J.; Naoki, K.; Sasaki, H.; Fujii, Y.; Eck, M. J.; Sellers, W. R.; Johnson, B. E.; Meyerson, M. EGFR Mutations in Lung Cancer: Correlation with Clinical Response to Gefitinib Therapy. *Science (80-.).* **2004**, *304* (5676), 1497–1500.

(105) Carey, K. D.; Garton, A. J.; Romero, M. S.; Kahler, J.; Thomson, S.; Ross, S.; Park, F.; Haley, J. D.; Gibson, N.; Sliwkowski, M. X. Kinetic Analysis of Epidermal Growth Factor Receptor Somatic Mutant Proteins Shows Increased Sensitivity to the Epidermal Growth Factor Receptor Tyrosine Kinase Inhibitor, Erlotinib. *Cancer Res.* **2006**, *66* (16), 8163–8172.

(106) Gridelli, C.; De Marinis, F.; Di Maio, M.; Cortinovis, D.; Cappuzzo, F.; Mok, T. Gefitinib as First-Line Treatment for Patients with Advanced Non-Small-Cell Lung Cancer with Activating Epidermal Growth Factor Receptor Mutation: Review of the Evidence. *Lung Cancer* **2011**, *71* (3), 249–257.

(107) Harvey, R. D.; Adams, V. R.; Beardslee, T.; Medina, P. Afatinib for the Treatment of EGFR Mutation-Positive NSCLC: A Review of Clinical Findings. *J. Oncol. Pharm. Pract.* **2020**, *26* (6), 1461–1474.

(108) Wang, S.; Cang, S.; Liu, D. Third-Generation Inhibitors Targeting EGFR T790M Mutation in

Advanced Non-Small Cell Lung Cancer. *J. Hematol. Oncol.* **2016**, *9* (1), 1–7.

(109) Remon, J.; Steuer, C. E.; Ramalingam, S. S.; Felip, E. Osimertinib and Other Third-Generation EGFR TKI in EGFR-Mutant NSCLC Patients. *Ann. Oncol.* **2018**, *29* (Supplement 1), i20–i27.

(110) Wells, C. I.; Vasta, J. D.; Corona, C. R.; Wilkinson, J.; Zimprich, C. A.; Ingold, M. R.; Pickett, J. E.; Drewry, D. H.; Pugh, K. M.; Schwinn, M. K.; Hwang, B. (Brian); Zegzouti, H.; Huber, K. V. M.; Cong, M.; Meisenheimer, P. L.; Willson, T. M.; Robers, M. B. Quantifying CDK Inhibitor Selectivity in Live Cells. *Nat. Commun.* **2020**, *11* (1), 2743.

(111) Doonan, J. H.; Kitsios, G. Functional Evolution of Cyclin-Dependent Kinases. *Mol. Biotechnol.* **2009**, *42* (1), 14–29.

(112) Malumbres, M.; Barbacid, M. Mammalian Cyclin-Dependent Kinases. *Trends Biochem. Sci.* **2005**, *30* (11), 630–641.

(113) Lim, S.; Kaldis, P. Cdks, Cyclins and CKIs: Roles beyond Cell Cycle Regulation. *Dev.* **2013**, *140* (15), 3079–3093.

(114) Malumbres, M.; Harlow, E.; Hunt, T.; Hunter, T.; Lahti, J. M.; Manning, G.; Morgan, D. O.; Tsai, L. H.; Wolgemuth, D. J. Cyclin-Dependent Kinases: A Family Portrait. *Nat. Cell Biol.* **2009**, *11* (11), 1275–1276.

(115) Axtman, A.; Drwry, D.; Wells, C. CDK16: The Pick of the Understudied PCTAIRE Kinases. *Nat. Rev. Drug Discov.* **2019**, *18* (7), 2019.

(116) Davidson, G.; Niehrs, C. Emerging Links between CDK Cell Cycle Regulators and Wnt Signaling. *Trends Cell Biol.* **2010**, *20* (8), 453–460.

(117) Liu, M.; Xu, Z.; Du, Z.; Wu, B.; Jin, T.; Xu, K.; Xu, L.; Li, E.; Xu, H. The Identification of Key Genes and Pathways in Glioma by Bioinformatics Analysis. *J. Immunol. Res.* **2017**, *2017*, 1278081.

(118) de Oliveira Pepino, R.; Coelho, F.; Janku, T. A. B.; Alencar, D. P.; de Azevedo, W. F.; Canduri, F. Overview of PCTK3/CDK18: A Cyclin-Dependent Kinase Involved in Specific Functions in Post-Mitotic Cells. *Curr. Med. Chem.* **2021**, *28* (33), 6846–6865.

(119) Mokalled, M. H.; Johnson, A.; Kim, Y.; Oh, J.; Olson, E. N. Myocardin-Related Transcription Factors Regulate the Cdk5/Pctaire1 Kinase Cascade to Control Neurite Outgrowth, Neuronal Migration and Brain Development. *Development* **2010**, *137* (14), 2365–2374.

(120) Mikolcevic, P.; Sigl, R.; Rauch, V.; Hess, M. W.; Pfaller, K.; Barisic, M.; Pelliniemi, L. J.; Boesl, M.; Geley, S. Cyclin-Dependent Kinase 16/PCTAIRE Kinase 1 Is Activated by Cyclin Y and Is Essential for Spermatogenesis. *Mol. Cell. Biol.* **2012**, *32* (4), 868–879.

(121) Palmer, K. J.; Konkel, J. E.; Stephens, D. J. PCTAIRE Protein Kinases Interact Directly with the COPII Complex and Modulate Secretory Cargo Transport. *J. Cell Sci.* **2005**, *118* (17), 3839–3847.

(122) Chen, X. Y.; Gu, X. T.; Saiyin, H.; Wan, B.; Zhang, Y. J.; Li, J.; Wang, Y. L.; Gao, R.; Wang, Y. F.; Dong, W. P.; Najjar, S. M.; Zhang, C. Y.; Ding, H. F.; Liu, J. O.; Yu, L. Brain-Selective Kinase 2 (BRSK2) Phosphorylation on PCTAIRE1 Negatively Regulates Glucose-Stimulated Insulin Secretion in Pancreatic β-Cells. *J. Biol. Chem.* **2012**, *287* (36), 30368–30375.

(123) Shimizu, K.; Uematsu, A.; Imai, Y.; Sawasaki, T. Pctaire1/Cdk16 Promotes Skeletal Myogenesis by Inducing Myoblast Migration and Fusion. *FEBS Lett.* **2014**, *588* (17), 3030–3037.

(124) Li, X.; Li, J.; Xu, L.; Wei, W.; Cheng, A.; Zhang, L.; Zhang, M.; Wu, G.; Cai, C. CDK16 Promotes the Progression and Metastasis of Triple-Negative Breast Cancer by Phosphorylating PRC1. *J. Exp. Clin. Cancer Res.* **2022**, *41* (1), 1–18.

(125) Mikolcevic, P.; Rainer, J.; Geley, S. Orphan Kinases Turn Eccentric: A New Class of Cyclin Y-Activated, Membrane-Targeted CDKs. *Cell Cycle* **2012**, *11* (20), 3758–3768.

(126) Whittaker, S. R.; Mallinger, A.; Workman, P.; Clarke, P. A. Inhibitors of Cyclin-Dependent Kinases as Cancer Therapeutics. *Pharmacol. Ther.* **2017**, *173*, 83–105.

(127) Charrasse, S.; Carena, I.; Hagmann, J.; Woods-Cook, K.; Ferrari, S. PCTAIRE-1: Characterization, Subcellular Distribution, and Cell Cycle- Dependent Kinase Activity. *Cell Growth Differ.* **1999**, *10* (9), 611–620.

(128) Chu, I. M.; Hengst, L.; Slingerland, J. M. The Cdk Inhibitor P27 in Human Cancer: Prognostic Potential and Relevance to Anticancer Therapy. *Nat. Rev. Cancer* **2008**, *8* (4), 253–267.

(129) Yanagi, T.; Matsuzawa, S. I. PCTAIRE1/PCTK1/CDK16: A New Oncotarget? *Cell Cycle* **2015**, *14* (4), 463–464.

(130) Gillani, S. Q.; Reshi, I.; Nabi, N.; Nisa, M. U.; Sarwar, Z.; Bhat, S.; Roberts, T. M.; Higgins, J. M. G.; Andrabi, S. PCTAIRE1 Promotes Mitotic Progression and Resistance against Antimitotic and Apoptotic Signals. *J. Cell Sci.* **2022**, *135* (3).

(131) Yanagi, T.; Hata, H.; Mizuno, E.; Kitamura, S.; Imafuku, K.; Nakazato, S.; Wang, L.; Nishihara, H.; Tanaka, S.; Shimizu, H. PCTAIRE1/CDK16/PCTK1 Is Overexpressed in Cutaneous Squamous Cell Carcinoma and Regulates P27 Stability and Cell Cycle. *J. Dermatol. Sci.* **2017**, *86* (2), 149–157.

(132) Wang, H.; Liu, H.; Min, S.; Shen, Y.; Li, W.; Chen, Y.; Wang, X. CDK16 Overexpressed in Non-Small Cell Lung Cancer and Regulates Cancer Cell Growth and Apoptosis via a P27-Dependent Mechanism. *Biomed. Pharmacother.* **2018**, *103*, 399–405.

(133) Xie, J.; Li, Y.; Jiang, K.; Hu, K.; Zhang, S.; Dong, X.; Dai, X.; Liu, L.; Zhang, T.; Yang, K.; Huang, K.; Chen, J.; Shi, S.; Zhang, Y.; Wu, G.; Xu, S. CDK16 Phosphorylates and Degrades P53 to Promote Radioresistance and Predicts Prognosis in Lung Cancer. *Theranostics* **2018**, *8* (3), 650–662.

(134) White, E. The Role for Autophagy in Cancer. *J. Clin. Invest.* **2015**, *125* (1), 42–46.

(135) Vervoorts, J.; Neumann, D.; Lüscher, B. The CCNY (Cyclin Y)-CDK16 Kinase Complex: A New Regulator of Autophagy Downstream of AMPK. *Autophagy* **2020**, *16* (9), 1724–1726.

(136) Dohmen, M.; Krieg, S.; Agalaridis, G.; Zhu, X.; Shehata, S. N.; Pfeiffenberger, E.; Amelang, J.; Bütepage, M.; Buerova, E.; Pfaff, C. M.; Chanda, D.; Geley, S.; Preisinger, C.; Sakamoto, K.; Lüscher, B.; Neumann, D.; Vervoorts, J. AMPK-Dependent Activation of the Cyclin Y/CDK16 Complex Controls Autophagy. *Nat. Commun.* **2020**, *11* (1), 1032.

(137) Dixon-Clarke, S. E.; Shehata, S. N.; Krojer, T.; Sharpe, T. D.; Von Delft, F.; Sakamoto, K.; Bullock, A. N. Structure and Inhibitor Specificity of the PCTAIRE-Family Kinase CDK16. *Biochem. J.* **2017**, *474* (5), 699–713.

(138) Choong, I. C.; Serafimova, I.; Fan, J.; Stockett, D.; Chan, E.; Cheeti, S.; Lu, Y.; Fahr, B.; Pham, P.; Arkin, M. R.; Walker, D. H.; Hoch, U. A Diaminocyclohexyl Analog of SNS-032 with Improved Permeability and Bioavailability Properties. *Bioorganic Med. Chem. Lett.* **2008**, *18* (21), 5763–5765.

(139) Liu, F.; Ventura, F.; Doody, J.; Massagué, J. Human Type II Receptor for Bone Morphogenic Proteins (BMPs): Extension of the Two-Kinase Receptor Model to the BMPs. *Mol. Cell. Biol.* **1995**, *15* (7), 3479–3486.

(140) Mueller, T. D.; Nickel, J. Promiscuity and Specificity in BMP Receptor Activation. *FEBS Lett.* **2012**, *586* (14), 1846–1859.

(141) Agnew, C.; Ayaz, P.; Kashima, R.; Loving, H. S.; Ghatpande, P.; Kung, J. E.; Underbakke, E. S.; Shan, Y.; Shaw, D. E.; Hata, A.; Jura, N. Structural Basis for ALK2/BMPR2 Receptor Complex Signaling through Kinase Domain Oligomerization. *Nat. Commun.* **2021**, *12* (1).

(142) Nickel, J.; Sebald, W.; Groppe, J. C.; Mueller, T. D. Intricacies of BMP Receptor Assembly. *Cytokine Growth Factor Rev.* **2009**, *20* (5–6), 367–377.

(143) Huse, M.; Chen, Y. G.; Massagué, J.; Kuriyan, J. Crystal Structure of the Cytoplasmic Domain of the Type I TGFβ Receptor in Complex with FKBP12. *Cell* **1999**, *96* (3), 425–436.

(144) Fessel, J. P.; Loyd, J. E.; Austin, E. D. The Genetics of Pulmonary Arterial Hypertension in the Post-BMPR2 Era. *Pulm. Circ.* **2011**, *1* (3), 305–319.

(145) Jiramongkolchai, P.; Owens, P.; Hong, C. C. Emerging Roles of the Bone Morphogenetic Protein Pathway in Cancer: Potential Therapeutic Target for Kinase Inhibition. *Biochem.*

Soc. Trans. **2016**, *44* (4), 1117–1134.

(146) Andruska, A.; Spiekerkoetter, E. Consequences of BMPR2 Deficiency in the Pulmonary Vasculature and beyond: Contributions to Pulmonary Arterial Hypertension. *Int. J. Mol. Sci.* **2018**, *19* (9), 1–24.

(147) Rosenzweig, B. L.; Imamura, T.; Okadome, T.; Cox, G. N.; Yamashita, H.; Ten Dijke, P.; Heldin, C. H.; Miyazono, K. Cloning and Characterization of a Human Type II Receptor for Bone Morphogenetic Proteins. *Proc. Natl. Acad. Sci. U. S. A.* **1995**, *92* (17), 7632–7636.

(148) Salazar, V. S.; Gamer, L. W.; Rosen, V. BMP Signalling in Skeletal Development, Disease and Repair. *Nat. Rev. Endocrinol.* **2016**, *12* (4), 203–221. https://doi.org/10.1038/nrendo.2016.12.

(149) Martinez, G.; Loveland, K. L.; Clark, A. T.; Dziadek, M.; Bertram, J. F. Expression of Bone Morphogenetic Protein Receptors in the Developing Mouse Metanephros. *Exp. Nephrol.* **2001**, *9* (6), 372–379. https://doi.org/10.1159/000052635.

(150) Derwall, M.; Malhotra, R.; Lai, C. S.; Beppu, Y.; Aikawa, E.; Seehra, J. S.; Zapol, W. M.; Bloch, K. D.; Yu, P. B. Inhibition of Bone Morphogenetic Protein Signaling Reduces Vascular Calcification and Atherosclerosis. *Arterioscler. Thromb. Vasc. Biol.* **2012**, *32* (3), 613–622. https://doi.org/10.1161/ATVBAHA.111.242594.

(151) Pousada, G.; Lupo, V.; Cástro-Sánchez, S.; Álvarez-Satta, M.; Sánchez-Monteagudo, A.; Baloira, A.; Espinós, C.; Valverde, Di. Molecular and Functional Characterization of the BMPR2 Gene in Pulmonary Arterial Hypertension. *Sci. Rep.* **2017**, *7* (1), 1–19.

(152) Yousef, H.; Morgenthaler, A.; Schlesinger, C.; Bugaj, L.; Conboy, I. M.; Schaffer, D. V. Age-Associated Increase in BMP Signaling Inhibits Hippocampal Neurogenesis. *Stem Cells* **2015**, *33* (5), 1577–1588.

(153) Austin, E. D.; Loyd, J. E. The Genetics of Pulmonary Arterial Hypertension. *Circ. Res.* **2014**, *115* (1), 189–200.

(154) Chaikuad, A.; Thangaratnarajah, C.; von Delft, F.; Bullock, A. N. Structural Consequences of BMPR2 Kinase Domain Mutations Causing Pulmonary Arterial Hypertension. *Sci. Rep.* **2019**, *9* (1), 1–10.

(155) Engers, D. W.; Frist, A. Y.; Lindsley, C. W.; Hong, C. H.; Hopkins, C. R. Synthesis and Structure-Activity Relationships of a Novel and Selective Bone Morphogenetic Protein Receptor (BMP) Inhibitor Derived from the Pyrazolo[1.5-a]Pyrimidine Scaffold of Dorsomorphin: The Discovery of ML347 as an ALK2 versus ALK3 Selective MLPCN . *Bioorganic Med. Chem. Lett.* **2013**, *23* (11), 3248–3252.

(156) Strange, K.; Denton, J.; Nehrke, K. Ste20-Type Kinases: Evolutionarily Conserved Regulators of Ion Transport and Cell Volume. *Physiology* **2006**, *21* (1), 61–68.

(157) Olesen, S. H.; Zhu, J. Y.; Martin, M. P.; Schönbrunn, E. Discovery of Diverse Small-Molecule Inhibitors of Mammalian Sterile20-like Kinase 3 (MST3). *ChemMedChem* **2016**, *3*, 1137–1144.

(158) Ling, P.; Lu, T. J.; Yuan, C. J.; Lai, M. D. Biosignaling of Mammalian Ste20-Related Kinases. *Cell. Signal.* **2008**, *20* (7), 1237–1247.

(159) Yang, J.; Jiang, Q.; Yu, X.; Xu, T.; Wang, Y.; Deng, J.; Liu, Y.; Chen, Y. STK24 Modulates Excitatory Synaptic Transmission in Epileptic Hippocampal Neurons. *CNS Neurosci. Ther.* **2020**, *26* (8), 851–861.

(160) Wan, Y. W.; Sabbagh, E.; Raese, R.; Qian, Y.; Luo, D.; Denvir, J.; Vallyathan, V.; Castranova, V.; Guo, N. L. Hybrid Models Identified a 12-Gene Signature for Lung Cancer Prognosis and Chemoresponse Prediction. *PLoS One* **2010**, *5* (8).

(161) Lee, K.-T.; Chang, C.-L.; Li, C.-Y.; Song, H.; Shan, Y.-S.; Lai, M.-D. The Oncogenic Role of MST3 in Human Gastric Cancer. *Am. J. Cancer Res.* **2018**, *8* (10), 2130–2139.

(162) Cho, C. Y.; Lee, K. T.; Chen, W. C.; Wang, C. Y.; Chang, Y. S.; Huang, H. L.; Hsu, H. P.; Yen, M. C.; Lai, M. Z.; Lai, M. D. MST3 Promotes Proliferation and Tumorigenicity through the VAV2/Rac1 Signal Axis in Breast Cancer. *Oncotarget* **2016**, *7* (12), 14586–14604.

(163) Chen, S.; Fang, Y.; Xu, S.; Reis, C.; Zhang, J. Mammalian Sterile20-like Kinases: Signalings and Roles in Central Nervous System. *Aging Dis.* **2018**, *9* (3), 537–552.

(164) Wu, H. Y.; Lin, C. Y.; Chen, T. C.; Pan, S. T.; Yuan, C. J. Mammalian Ste20-like Protein Kinase 3 Plays a Role in Hypoxia-Induced Apoptosis of Trophoblast Cell Line 3A-Sub-E. *Int. J. Biochem. Cell Biol.* **2011**, *43* (5), 742–750.

(165) Cornils, H.; Kohler, R. S.; Hergovich, A.; Hemmings, B. A. Downstream of Human NDR Kinases: Impacting on c-Myc and P21 Protein Stability to Control Cell Cycle Progression. *Cell Cycle* **2011**, *10* (12), 1897–1904.

(166) Hwang, J.; Pallas, D. C. STRIPAK Complexes: Structure, Biological Function, and Involvement in Human Diseases. *Int. J. Biochem. Cell Biol.* **2014**, *47* (1), 118–148.

(167) Thompson, B. J.; Sahai, E. MST Kinases in Development and Disease. *J. Cell Biol.* **2015**, *210* (6), 871–882.

(168) Madsen, C. D.; Hooper, S.; Tozluoglu, M.; Bruckbauer, A.; Fletcher, G.; Erler, J. T.; Bates, P. A.; Thompson, B.; Sahai, E. STRIPAK Components Determine Mode of Cancer Cell Migration and Metastasis. *Nat. Cell Biol.* **2015**, *17* (1), 68–80. https://doi.org/10.1038/ncb3083.

(169) Wu, X.; Wu, J.; Hu, W.; Wang, Q.; Liu, H.; Chu, Z.; Lv, K.; Xu, Y. MST4 Kinase Inhibitor Hesperadin Attenuates Autophagy and Behavioral Disorder via the MST4/AKT Pathway in Intracerebral Hemorrhage Mice. *Behav. Neurol.* **2020**, *2020*, 1–9.

(170) Lin, J. L.; Chen, H. C.; Fang, H. I.; Robinson, D.; Kung, H. J.; Shih, H. M. MST4, a New Ste20-Related Kinase That Mediates Cell Growth and Transformation via Modulating ERK Pathway. *Oncogene* **2001**, *20* (45), 6559–6569.

(171) Dian, M. J.; Li, J.; Zhang, X. L.; Li, Z. J.; Zhou, Y.; Zhou, W.; Zhong, Q. L.; Pang, W. Q.; Lin, X. L.; Liu, T.; Liu, Y. A.; Li, Y. L.; Han, L. X.; Zhao, W. T.; Jia, J. S.; Xiao, S. J.; Xiao, D.; Xia, J. W.; Hao, W. C. MST4 Negatively Regulates the EMT, Invasion and Metastasis of HCC Cells by Inactivating PI3K/AKT/Snail1 Axis. *J. Cancer* **2021**, *12* (15), 4463–4477.

(172) Yu, H.; Zhang, W.; Han, P.; Yang, B.; Feng, X.; Zhou, P.; Zhu, X.; Zhou, B.; Chen, W.; Qian, J.; Yu, J. MST4 Regulates Epithelial – Mesenchymal Transition of Choriocarcinoma by Mediating TGF- β 1 Expression. *Onco Targets Ther.* **2020**, *13*, 11935–11946.

(173) Hao, W. C.; Zhong, Q. L.; Pang, W. Q.; Dian, M. J.; Li, J.; Han, L. X.; Zhao, W. T.; Zhang, X. L.; Xiao, S. J.; Xiao, D.; Lin, X. L.; Jia, J. S. MST4 Inhibits Human Hepatocellular Carcinoma Cell Proliferation and Induces Cell Cycle Arrest via Suppression of PI3K/AKT Pathway. *J. Cancer* **2020**, *11* (17), 5106–5117.

(174) Huang, T.; Kim, C. K.; Alvarez, A. A.; Pangeni, R. P.; Wan, X.; Song, X.; Shi, T.; Yang, Y.; Sastry, N.; Horbinski, C. M.; Lu, S.; Stupp, R.; Kessler, J. A.; Nishikawa, R.; Nakano, I.; Sulman, E. P.; Lu, X.; James, C. D.; Yin, X. M.; Hu, B.; Cheng, S. Y. MST4 Phosphorylation of ATG4B Regulates Autophagic Activity, Tumorigenicity, and Radioresistance in Glioblastoma. *Cancer Cell* **2017**, *32* (6), 840-855.e8.

(175) An, L.; Nie, P.; Chen, M.; Tang, Y.; Zhang, H.; Guan, J.; Cao, Z.; Hou, C.; Wang, W.; Zhao, Y.; Xu, H.; Jiao, S.; Zhou, Z. MST4 Kinase Suppresses Gastric Tumorigenesis by Limiting YAP Activation via a Non-Canonical Pathway. *J. Exp. Med.* **2020**, *217* (6), 1–20.

(176) Henderson, J. L.; Kormos, B. L.; Hayward, M. M.; Coffman, K. J.; Jasti, J.; Kurumbail, R. G.; Wager, T. T.; Verhoest, P. R.; Noell, G. S.; Chen, Y.; Needle, E.; Berger, Z.; Steyn, S. J.; Houle, C.; Hirst, W. D.; Galatsis, P. Discovery and Preclinical Profiling of 3-[4-(Morpholin-4-Yl)-7H-pyrrolo[2,3-d]Pyrimidin-5-Yl]Benzonitrile (PF-06447475), a Highly Potent, Selective, Brain Penetrant, and in Vivo Active LRRK2 Kinase Inhibitor. *J. Med. Chem.* **2015**, *58*, 419–432.

(177) Ndubaku, C. O.; Crawford, J. J.; Drobnick, J.; Aliagas, I.; Campbell, D.; Dong, P.; Dornan, L. M.; Duron, S.; Epler, J.; Gazzard, L.; Heise, C. E.; Hoeflich, K. P.; Jakubiak, D.; La, H.; Lee, W.; Lin, B.; Lyssikatos, J. P.; Maksimoska, J.; Marmorstein, R.; Murray, L. J.; O’Brien, T.; Oh, A.; Ramaswamy, S.; Wang, W.; Zhao, X.; Zhong, Y.; Blackwood, E.; Rudolph, J. Design of Selective PAK1 Inhibitor G-5555: Improving Properties by Employing an Unorthodox Low-PKa Polar Moiety. *ACS Med. Chem. Lett.* **2015**, *6* (12), 1241–1246.

(178) Xiong, W.; Matheson, C. J.; Xu, M.; Backos, D. S.; Mills, T. S.; Salian-Mehta, S.; Kiseljak-Vassiliades, K.; Reigan, P.; Wierman, M. E. Structure-Based Screen Identification of a Mammalian Ste20-like Kinase 4 (MST4) Inhibitor with Therapeutic Potential for Pituitary Tumors. *Mol. Cancer Ther.* **2016**, *15* (3), 412–420.

(179) Statsuk, A. V.; Maly, D. J.; Seeliger, M. A.; Fabian, M. A.; Biggs, W. H.; Lockhart, D. J.; Zarrinkar, P. P.; Kuriyan, J.; Shokat, K. M. Tuning a Three-Component Reaction for Trapping Kinase Substrate Complexes. *J. Am. Chem. Soc.* **2008**, *130* (51), 17568–17574.

(180) But, T. Y. S.; Toy, P. H. The Mitsunobu Reaction: Origin, Mechanism, Improvements, and Applications. *Chem. - An Asian J.* **2007**, *2* (11), 1340–1355.

(181) Lyssikatos, J. P.; Marmsater, F. P.; Zhao, Q.; Greschuk, J. M. WO 2007/059257 A2, 2007.

(182) Valeur, E.; Bradley, M. Amide Bond Formation: Beyond the Myth of Coupling Reagents. *Chem. Soc. Rev.* **2009**, *38*, 606–631.

(183) Blakely, C. M.; Bivona, T. G. Resiliency of Lung Cancers to EGFR Inhibitor Treatment Unveiled, Offering Opportunities to Divide and Conquer EGFR Inhibitor Resistance. *Cancer Discov.* **2012**, *2* (10), 872–875. https://doi.org/10.1158/2159-8290.CD-12-0387.

(184) Joshi, S. C. Sol-Gel Behavior of Hydroxypropyl Methylcellulose (HPMC) in Ionic Media Including Drug Release. *Materials (Basel).* **2011**, *4* (10), 1861–1905.

(185) Li, F.; MacKenzie, K. R.; Jain, P.; Santini, C.; Young, D. W.; Matzuk, M. M. Metabolism of JQ1, an Inhibitor of Bromodomain and Extra Terminal Bromodomain Proteins, in Human and Mouse Liver Microsomes. *Biol. Reprod.* **2020**, *103* (2), 427–436.

(186) Zhang, S.; Jin, S.; Griffin, C.; Feng, Z.; Lin, J.; Venkatakrishnan, K.; Gupta, N. Effects of Itraconazole and Rifampin on the Pharmacokinetics of Mobocertinib (TAK-788), an Oral Epidermal Growth Factor Receptor Inhibitor, in Healthy Volunteers. *Clin. Pharmacol. Drug Dev.* **2021**, *10* (9), 1044–1053.

(187) Hanke, T.; Dehm, F.; Liening, S.; Popella, S. D.; MacZewsky, J.; Pillong, M.; Kunze, J.; Weinigel, C.; Barz, D.; Kaiser, A.; Wurglics, M.; Lämmerhofer, M.; Schneider, G.; Sautebin, L.; Schubert-Zsilavecz, M.; Werz, O. Aminothiazole-Featured Pirinixic Acid Derivatives as Dual 5-Lipoxygenase and Microsomal Prostaglandin E2 Synthase-1 Inhibitors with Improved Potency and Efficiency in Vivo. *J. Med. Chem.* **2013**, *56* (22), 9031–9044.

(188) Yano, S.; Hoffman, R. M. Real-Time Determination of the Cell-Cycle Position of Individual Cells within Live Tumors Using FUCCI Cell-Cycle Imaging Shuya. *Cells* **2018**, *7* (168), 168.

(189) Zielke, N.; Edgar, B. A. FUCCI Sensors: Powerful New Tools for Analysis of Cell Proliferation. *Wiley Interdiscip. Rev. Dev. Biol.* **2015**, *4* (5), 469–487.

(190) Tjaden, A.; Chaikuad, A.; Kowarz, E.; Marschalek, R.; Knapp, S.; Schröder, M.; Müller, S. Image-Based Annotation of Chemogenomic Libraries for Phenotypic Screening. *Molecules* **2022**, *27* (4), 1439.

(191) Brasca, M. G.; Amboldi, N.; Ballinari, D.; Cameron, A.; Casale, E.; Cervi, G.; Colombo, M.; Colotta, F.; Croci, V.; D’Alessio, R.; Fiorentini, F.; Isacchi, A.; Mercurio, C.; Moretti, W.; Panzeri, A.; Pastori, W.; Pevarello, P.; Quartieri, F.; Roletto, F.; Traquandi, G.; Vianello, P.; Vulpetti, A.; Ciomei, M. Identification of N,1,4,4-Tetramethyl-8-{[4-(4-Methylpiperazin-1-Yl)Phenyl] Amino}-4,5-Dihydro-1H-Pyrazolo[4,3-h]Quinazoline-3-Carboxamide (PHA-848125), a Potent, Orally Available Cyclin Dependent Kinase Inhibitor. *J. Med. Chem.* **2009**, *52* (16), 5152–5163.

(192) Lewis, E. A.; Murphy, K. P. Isothermal Titration Calorimetry. *Methods Mol. Biol.* **2005**, *305*, 1–16.

(193) Adasme, M. F.; Linnemann, K. L.; Bolz, S. N.; Kaiser, F.; Salentin, S.; Haupt, V. J.; Schroeder, M. PLIP 2021: Expanding the Scope of the Protein-Ligand Interaction Profiler to DNA and RNA. *Nucleic Acids Res.* **2021**, *49* (W1), W530–W534.

(194) Dai, L.; Luo, C. Y.; Hu, G. X.; Chen, G.; Wu, C. X.; Yin, J.; Jiang, Z. Y.; Hu, G. F.; Zhao, J.; Fu, W. F. Comparative Analysis of First-Line Treatment Regimens for Advanced EGFR-Mutant Non-Small Cell Lung Cancer Patients with Stable Brain Metastases. *Ann. Cardiothorac. Surg.* **2020**, *9* (4), 2062–2071.

(195) Sielecki, T. M.; Johnson, T. L.; Liu, J.; Muckelbauer, J. K.; Grafstrom, R. H.; Cox, S.; Boylan, J.; Burton, C. R.; Chen, H.; Smallwood, A.; Chang, C. H.; Boisclair, M.; Benfield, P. A.; Trainor, G. L.; Seitz, S. P. Quinazolines as Cyclin Dependent Kinase Inhibitors. *Bioorganic Med. Chem. Lett.* **2001**, *11* (9), 1157–1160.

(196) Sullivan, J. E.; Holdgate, G. A.; Campbell, D.; Timms, D.; Gerhardt, S.; Breed, J.; Breeze, A. L.; Bermingham, A.; Pauptit, R. A.; Norman, R. A.; Embrey, K. J.; Read, J.; VanScyoc, W. S.; Ward, W. H. J. Prevention of MKK6-Dependent Activation by Binding to P38α MAP Kinase. *Biochemistry* **2005**, *44* (50), 16475–16490.

(197) Nitulescu, G. M. Quantitative and Qualitative Analysis of the Anti-Proliferative Potential of the Pyrazole Scaffold in the Design of Anticancer Agents. *Molecules* **2022**, *27* (10), 8854.

(198) El-gamal, M. I.; Zaraei, S. O.; Madkour, M. M.; Anbar, H. S. Evaluation of Substituted Pyrazole-Based Kinase Inhibitors in One Decade (2011–2020): Current Status and Future Prospects. *Molecules* **2022**, *27* (1), 330.

(199) Carter, T. A.; Wodicka, L. M.; Shah, N. P.; Velasco, A. M.; Fabian, M. A.; Treiber, D. K.; Milanov, Z. V.; Atteridge, C. E.; Biggs, W. H.; Edeen, P. T.; Floyd, M.; Ford, J. M.; Grotzfeld, R. M.; Herrgard, S.; Insko, D. E.; Mehta, S. A.; Patel, H. K.; Pao, W.; Sawyers, C. L.; Varmus, H.; Zarrinkar, P. P.; Lockhart, D. J. Inhibition of Drug-Resistant Mutants of ABL, KIT, and EGF Receptor Kinases. *Proc. Natl. Acad. Sci. U. S. A.* **2005**, *102* (31), 11011–11016.

10. List of Figures

Figure 1. Graphic representation of the human kinome in a so-called kinome tree. The six classes of serine/ threonine-specific protein kinases (TKL, STE, CK1, AGC, CAMK, and CMGC) and tyrosine kinases (TK) are assigned by their structural similarity. 5

Figure 2. Graphical representation of the reversible transfer of the ɣ-phosphate from ATP to a substrate, catalyzed by a protein kinase. (Adapted from Ubersax *et. al.*)[12] 6

Figure 3. A. The tertiary structure of protein kinase A in complex with ATP is shown with its surface (PDB: 1ATP). B. Detailed structure of the ATP binding pocket (PDB: 1ATP) with a stick and ball representation. ATP is colored by elements in gold, the coordinated Mg^{2+} ions are shown as spheres in brown, and important sections are highlighted. The hinge region is shown in blue, the P-loop in green, the αC-helix in dark red, the DFG-motif in yellow, the A-loop in light pink, and the catalytic loop in dark grey. C. Simplified illustration of the different regions in the ATP binding pocket. The adenine region is colored in blue, the solvent-exposed region in dark red, the phosphate region in light pink, and the hydrophobic back pocket in green. 8

Figure 4. A. Schematic representation of a canonical type I binding mode. The inhibitor (gold) binds to the active conformation of the kinase (light blue), whereby the DFG-motif (grey) is pointing into the binding pocket. (Adapted from Wu *et. al.*)[37] B. Crystal structure of the type I kinase inhibitor dasatinib (gold) in complex with ABL (PDB: 2GQG). Hydrogen bonds are shown as dashed lines (black) and important sections are highlighted. 9

Figure 5. A. Schematic representation of a canonical type II binding mode. The inhibitor (gold) binds to the inactive conformation of the kinase (light blue), whereby the DFG-motif (grey) is pointing outwards the binding pocket. (Adapted from Wu *et. al.*)[37] B. Crystal structure of the type II kinase inhibitor ponatinib (gold) in complex with ABL (PDB: 3OXZ). Hydrogen bonds are shown as dashed lines (black) and important sections are highlighted. 10

Figure 6. A. Schematic representation of a type III binding mode. The inhibitor (gold) binds to an allosteric pocket beside the ATP binding pocket of the kinase (light blue). (Adapted from Wu *et. al.*)[37] B. Crystal structure of the type III kinase inhibitor binimetinib and AMP-PNP (gold) in complex with MEK1 (PDB: 7M0U). Hydrogen bonds are shown as dashed lines (black), Mg^{2+} ion is shown as a brown sphere and important sections are highlighted. 10

Figure 7. A. Crystal structure of the type IV kinase inhibitor GNF-2 (gold) in complex with ABL (PDB: 3K5V). Imatinib binds to the ATP binding pocket and GNF-2 (gold) to an allosteric binding pocket distant from the ATP binding pocket of the kinase (light blue). B. Crystal structure of the covalent kinase inhibitor afatinib (gold) in complex with EGFR (PDB: 4G5J). Hydrogen bonds are shown as dashed lines (black) and important sections are highlighted. Afatinib interacts with Met793 through a hydrogen bond and with C797 through a covalent bond. C. Schematic representation of the composition of covalent kinase inhibitors. The non-covalent inhibitor (gold) is attached to a linker motif (light blue) with connects it with an electrophilic warhead (green). 11

Figure 8. A. Schematic representation of a macrocyclic scaffold. The linear pharmacophore is connected through a linker motif. (Adapted from Mallinson *et. al.*).[61] B. Common hinge-binding moieties which can be used for macrocyclization: quinazoline, quinoline, 7*H*-pyrrolo[2,3-*d*]pyrimidin-4-amine, pyrazolo[1,5-*a*]pyrimidine, 1*H*-pyrazole-3-amine, 1*H*-pyrrolo[2,3-*b*]pyridine, 1*H*-indazole, 2-aminopyridine, pyrimidin-4,6-diamine (top left to bottom right).[71,72] C. Overview of different reaction types, used for macrocyclization reactions. (Adapted from Amrhein *et. al.*).[65] .. 13

Figure 9. A. Overview of the optimization of the potency and pharmacokinetic properties from the first (1) to the third generation ALK/ ROS inhibitor lorlatinib (2).[75,81] B. Overview of the optimization steps from aminobenzimidazole (3) to the macrocycle BI-4020 (4).[76] 14

Figure 10. A. Schematic representation of EGFR. The extracellular domain (green) includes the domains I, II, III, and IV, followed by the transmembrane domain (light blue). The intracellular domain (dark blue) consists of the juxtamembrane domain, the tyrosine kinase domain, and the C-terminal regulatory domain. B. Schematic representation of the EGFR activation. The binding of a ligand (gold) induces a structural rearrangement, followed by a formation of a dimer (Adapted from Sigismund *et. al.*).[88] C. The activation of EGFR is induced through ligand binding, followed by the autophosphorylation at the C-terminus. This causes the stimulation of different pathways, highlighted in different colors (Adapted from Amrhein *et. al.*).[103] D. Pie chart of the proportions of EGFR mutations in adenocarcinoma, whereby the resistance mutants T790M and C797S were filtered out (Adapted from Amrhein *et. al.*).[103] 16

Figure 11. Chemical structures of approved first, second, and third generation EGFR inhibitors and published inhibitors, targeting EGFR. 17

Figure 12. A. Phylogenetic tree of the CDK family. B. CDK16 phosphorylates p27 at S10, thus initiating the degradation of p27 via ubiquitination. This leads to cell growth and anti-apoptosis (Adapted from Yanagi *et. al.*). [129] C. Schematic representation of the autophagy pathway. AMPK phosphorylates cyclin Y (CCNY) at S326 inducing the formation of the CDK16/ cyclin Y complex. The complex is autophosphorylating itself at S336, promoting autophagy (Adapted from Dohmen *et. al.*).[136] D. Alignment of key residues of the ATP binding pocket of CDK14 – 18 and CDK2. Differences in comparison to CDK16 are highlighted in grey. 19

Figure 13. Chemical structures of published kinase inhibitors which target CDK16 however, no selective CDK16 inhibitor is known. 20

Figure 14. A. Schematic representation of type I and II receptor kinases. Type II receptors (blue) consist of an extracellular domain (light blue), a transmembrane domain (blue), an intracellular juxtamembrane domain, and a kinase domain (dark blue). Type I receptors (green) consist of an extracellular domain (light green), a transmembrane domain (green), an intracellular juxtamembrane domain, a kinase domain (middle green), and an additional GS-box (dark green). The GS-box locks the αC-helix of the kinase domain in the inactive conformation. B. Schematic representation of the canonical BMP pathway. A type I and type II homodimer form a tetrameric complex. The type I receptors are phosphorylated at the GS-box through the type II receptor, inducing the phosphorylation of Smad1, 5, 8. A heterotrimer complex is formed with Smad4, which translocates into the nucleus and activates target responsive genes (Adapted from Agnew *et. al.* and Andruska *et. al.*).[141,146] 22

Figure 15. Chemical structures of kinase inhibitors, targeting BMPR2. 23

Figure 16. A. Alignment of MST1 – 4, YSK1, and PAK1. Differences in comparison to MST3 are highlighted in grey. B. Phylogenetic tree of the STE family, containing the subfamilies PAKI – II and GckI – VIII. C. Schematic representation of MST3 signaling. MST3 can be activated through caspases, thus promoting apoptosis. MST3 can phosphorylate (P) NDR kinases, leading to cell cycle regulation via c-MYC and p21. D. Schematic representation of MST4 signaling. MST4 can phosphorylate ATG4B to promote autophagy. Furthermore, MST4 can autophosphorylate (AP) itself, leading to a complex formation with GM130, enabling the control of cell migration. 25

Figure 17. Chemical structures of kinase inhibitors, targeting MST3 or MST4. 26

Figure 18. Schematic representation of the aim of this thesis. Gefitinib (5) and 23 serve as starting points for the two projects. The modified structural motifs are highlighted in light blue and the desired kinome-wide selectivity is illustrated in a kinome tree, shown below the chemical structure. Through a SAR-based design, several macrocycles ought to be synthesized, optimized, and subsequently characterized for their biological activity. 28

Figure 19. A. Graphical representation of the selectivity data of 25f assessed by DSF. B. Graphical representation of the selectivity data of 26f assessed by DSF. A phylogenetic tree (Cell Signaling Technology) was used to highlight ΔTm data that was depicted as red circles as indicated in the figure capture. C. Selectivity profile of 26f assessed by the KinomeScan® panel at a screening concentration of 1 µM. Mutants and atypical kinases are depicted in the lower panel. D. Waterfall plot of the selectivity data of 26f. The remaining activity (%) was plotted against the number of tested kinases. The selectivity score of 26f was determined with a cut off value of 35% remaining activity. E. Table showing the top hits of the KINOMEscan® profiling of 26f with a remaining activity < 35% at 1 µM. 42

Figure 20. A. Crystal structure of EGFR WT in complex with 39d (PDB: 7U99). B. Superimposition of the structure of 25f (PDB: 7U9A, grey carbon atoms) and gefitinib (PDB: 2ITZ, cyan carbon atoms). C. Superimposition of the structure of the macrocycle 39d (PDB: 7U99, cyan carbon atoms) and 25f (PDB: 7U9A, grey carbon atoms). D. Crystal structure of EGFR T790M/V948R in complex with 39f (PDB: 7U98). E. Superimposition of the catalytic domain structure in complex with 39d (PDB: 7U99, grey carbon atoms) and 26f (cyan carbon atoms) which was docked into EGFR WT (Glide, Schrodinger). F. Comparison of the different binding modes of the two macrocycles 39d (grey) and 26f (blue)... 43

Figure 21. Results of Western blot assays using compounds 39f, 48, 39d, 25f, and 26f against EGFR WT and the most important EGFR mutants. BI-4020, gefitinib, osimertinib, and mobocertinib were used as a reference. EGFR phosphorylation (pEGFR) was used for the detection of pathway activation. Additionally, total protein levels of EGFR and HSP90 were monitored as loading and expression controls. 46

Figure 22. Results of Western blot assays using compounds 39f, 48, 39d, 25f, and 26f against EGFR WT and the most interesting EGFR mutants L858R, L858R/C797S, Del19, and Del19/C797S. BI-4020, gefitinib, and osimertinib were used as a reference. AKT and ERK1/2 phosphorylation (pAKT, pERK1/2) was used for the detection of signaling pathway inactivation. Additionally, total protein levels of AKT, ERK1/2, and HSP90 were monitored as loading and expression controls. 47

Figure 23. A. Chemical stability of 26f under acid conditions using 0.1M HCl and neutral conditions using a PBS buffer. The compound was incubated at rt for 184 minutes and measured by HPLC in triplicates. B. Solubility of 26f using different solvents. The compound was incubated at 37 °C for 24 hours and measured by HPLC in triplicates. 48

Figure 24. A. Graphic representation of the selectivity data of 23 preserved from the DSF assay, illustrated with Cell Signaling Technology. B. Graphic representation of the selectivity data of 76i preserved from the DSF assay, illustrated with Cell Signaling Technology. C. Graphic representation of the selectivity data of 97d preserved from the DSF assay, illustrated with Cell Signaling Technology.. 54

Figure 25. Volcano plots of stabilized (positive amplitude) and destabilized (negative amplitude) proteins of 23, 76b, 76d, 76e, 76h, and 76i. 55

Figure 26. Cellular IC_{50} values of 76i, 97d, and 98d against the CDK family were determined using NanoBRET^{TM} technology in a 11-dose-response curve in duplicates. 58

Figure 27. A. Metabolic stability of 76i [10 µM] and 98d [10 µM] after treatment of activated microsomes. The residual amount of compound was determined after 0, 15, 30, and 60 minutes and was plotted in percent against the time in minutes. The data is given as a mean ± SEM, measured in triplicates. B. Normalized cell count of HCT116-FUCCI cells after 0h, 6h, 12h, 24h, 48h and 72h of compound exposure (76i [1 µM, 5 µM, 10 µM], 98d [1 µM, 5 µM, 10 µM]) in comparison to cells exposed to 0.1% DMSO. Error bars show SEM of two biological replicates. C. Fraction of healthy, fragmented and pyknosed nuclei after 24 h of 1µM and 10 µM compound exposure (98d) in HCT116 cells. Average data of two biological duplicates are shown. D. Fractions of red (G1), green (G2/M) or yellow (S) cells after 24 h of compound exposure (76i [1 µM, 5 µM, 10 µM], 98d [1 µM, 5 µM, 10 µM], 97d [1 µM, 5 µM, 10 µM], 1 [1 µM, 5 µM, 10 µM], Milciclib [1 µM, 10 µM]) in comparison to cells exposed to 0.1% DMSO. Error bars show SEM of two biological replicates. E. Fluorescence Image of HCT116-FUCCI cells after 48h of compounds exposure (76i [10 µM], 98d [10 µM]) in comparison to cells exposed to Milciclib [1 µM] and cells exposed to 0.1% DMSO. 60

Figure 28. A. Isothermal titration calorimetry (ITC) measurement of 110a against BMPR2 revealed a low three-digit nanomolar binding affinity. B. IC_{50} values of 23, 110a, 110b, and 110c against BMPR2. The values were determined by an ADP-Glo™ assay in a duplicate measurement. IC_{50} values against GSK3A and GSK3B were determined using the NanoBRET™ assay platform in a duplicate measurement. The corresponding DSF assay data is shown for each compound. 64

Figure 29. A. Graphical representation of the selectivity data of 110a assessed by DSF. A phylogenetic tree (Cell Signaling Technology) was used to highlight ΔTm data that was depicted as red circles as indicated in the figure capture. B. Selectivity profile of 110a assessed by the KinomeScan® panel at a screening concentration of 1 µM. Mutants and atypical kinases are depicted in the lower panel. C. Waterfall plot of the selectivity data of 110a. The remaining activity (%) was plotted against the number of tested kinases. The selectivity score of 110a was determined with a cut off value of 35% remaining activity. D. Table showing the top hits of the KINOMEscan® profiling of 110a with a remaining activity < 35% at 1 µM. 65

Figure 30. Binding mode of 110a and 23 in complex with the kinase domain of the type II receptor BMPR2. The molecules were docked into the active conformation of BMPR2. The compounds are illustrated in gold, the hinge region of the kinase is shown in pale red, the P-loop in dark blue, the αC-helix in cyan, and the DFG-motif in green. The interactions were predicted, using PLIP.[193] ... 66

Figure 31. Graphical representation of the selectivity data of 113c assessed by DSF. A phylogenetic tree (Cell Signaling Technology) was used to highlight ΔTm data that was depicted as red circles as indicated in the figure capture. 69

Figure 32. ITC measurement of 113c against MST4 revealed a low three-digit nanomolar binding affinity. 69

Figure 33. A. Crystal structure of MST3 in complex with 113c. Macrocycle 113c was identified as an ATP competitive type I inhibitor. Rotated representation of the ATP-binding pocket in complex with 113c is shown beside. The hydrogen bonds are illustrated in dashed lines. The P-loop is tilted towards the C-terminal lobe. The compound is illustrated in gold, the hinge region of the kinase is shown in pale red, the P-loop in dark blue, the αC-helix in cyan, and the DFG-motif in green. B. Superimposition of the crystal structure of 113c (pale blue) with a crystal structure of AMP-PNP in complex with MST3 (PDB: 4QML, pale orange). F47 is shifted 6.2Å towards the C-terminal lobe and packs against the activation loop. 72

Figure 34. Metabolic stability of 113c [10 µM] after treatment of activated microsomes. The residual amount of compound was determined after 0, 15, 30, and 60 minutes and was plotted in percent against the time in minutes. The data is given as a mean ± SEM, measured in triplicates........... 73

Figure 35. A. Graphical representation of the structural modifications of the quinazoline-based macrocycles. B. Optimization of the selectivity profile of gefitinib (5) was achieved through the macrocyclic kinase inhibitor 26f. The conserved quinazoline hinge-binding moiety is highlighted in purple. 79

Figure 36. A. Graphical representation of the structural modifications of the 3-aminopyrazole-based macrocycles. B. Optimization of the selectivity profile of the promiscuous kinase inhibitor 23 was achieved through various SAR studies. The CDK16 inhibitor 98d, the BMPR2 inhibitor 110a, and the MST3/ MST4 inhibitor 113c were achieved. The conserved *N*-(1*H*-pyrazol-3-yl)pyrimidin-4-amine scaffold is highlighted in purple. 81

11. List of Schemes

Scheme 1. Synthesis of the macrocycles 26a–f. Reagents and conditions: (a) 2-aminophenol derivatives and ethanol, 17 h, 70 °C; (b) diethylene glycol, TPP, DIAD, THF, and toluene, 20 h, rt – 40 °C. 29

Scheme 2. General mechanism of a Mitsunobu reaction, using TPP and DIAD as coupling reagents. 30

Scheme 3. Synthesis of the macrocycles 38a–f and 39a–f. Reagents and conditions: (a) 6-chloro-1-hexanol or 2-[2-(2-chloroethoxy)ethoxy]ethanol, TPP, DIAD, and toluene, 2 – 5 h, rt – 80 °C; (b) 2-aminophenols and ethanol, 18 h, 70 °C; (c) NaH and DMF, 24 h, 0 – 60 °C. 31

Scheme 4. Synthesis of the macrocycles 42a–d. Reagents and conditions: (a) 2-(2-chloroethoxy)ethanol, TPP, DIAD, and toluene, 2 h, rt – 80 °C; (b) 3-aminophenols and ethanol, 18 h, 70 °C; (c) NaH and DMF, 24 h, 0 – 60 °C. 31

Scheme 5. Synthesis of the macrocycle 48. Reagents and conditions: (a) acetic anhydride and pyridine, 1 h, 50 °C; (b) thionyl chloride and DMF, 3 h, 70 °C; (c) NH_3 and methanol, 1 h, rt; (d) 2-amino-4-chloro-5-fluorophenol and ethanol, 18 h, 70 °C; (e) diethylene glycol, TPP, DIAD, THF, and toluene, 20 h, rt - 40 °C. 32

Scheme 6. Synthesis of 56a–f, 57a–e, 58a,c and 60. Reagents and conditions: (a) TEA and isopropanol, 48 h, 55 – 80 °C; (b) TEA and ethanol, microwave, 5 – 10 h, 80 – 90 °C; (c) HCl and ethanol, reflux, 4 – 18h; (d) TFA and DCM, 0 °C – rt, oN; (e) Acetic acid, HATU, DIPEA, and DMF, rt, oN. 33

Scheme 7. General mechanism of an amide coupling, using HATU as a coupling reagent. 33

Scheme 8. Synthesis of compounds 76a–i, 77a–e, 78a–c, 79, and 80. Reagents and conditions: (a) TEA and isopropanol, 24 – 72 h, 50 – 60 °C; (b) TEA and ethanol, microwave, 3 – 8 h, 80 – 120 °C; (c) HCl and ethanol, 70 °C – reflux, 18 h; (d) TFA and DCM, 0 °C – rt, oN. 34

Scheme 9. Synthesis of compounds 93a–b, 94a–b, 95a–c, 96a–c, 97b,d, and 98b,d. Reagents and conditions: (a) TEA and isopropanol, 18 – 120 h, 60 °C; (b) TEA and ethanol, microwave, 8 h, 90 °C; (c) HCl and ethanol, 70 °C – reflux, 18h. 35

Scheme 10. Synthesis of the macrocycles 110a–e, 111a–e, 112a, and 113a–e. Reagents and conditions: (a) TEA and isopropanol, 24 – 72 h, 50 – 60 °C; (b) TEA and ethanol, microwave, 3 – 8 h, 80 – 120 °C; (c) HCl and ethanol, 70 °C – reflux, 18 h; (d) TFA and DCM, 0 °C – rt, oN; (e) $LiOH*H_2O$, THF, and H_2O, 18 h, 55 °C; (f) HATU, DIPEA, and DMF, 18 h, rt – 60 °C. 36

12. List of Tables

Table 1. Potency of the quinazoline-based macrocycles 26a–f, 38a–f, 39a–f, 42a–f, and 48 against EGFR WT and its mutants. 38

Table 2. DSF data of 25f, 26a–f, and 38a–f. Staurosporine was used as a positive control. The newly synthesized compounds were screened in an *in-house* panel of 103 kinases. No stabilization of the kinase is indicated in pale green, while a high stabilization is indicated in dark green. 40

Table 3. DSF data of 39a–f, 42a–d, and 48. Staurosporine was used as a positive control. The newly synthesized compounds were screened in an *in-house* panel of 103 kinases. No stabilization of the kinase is indicated in pale green, while a high stabilization is indicated in dark green. 41

Table 4. Cell based activity data (Ba/F3 cell model) of 25f, 26f, 39d, 39f, and 48 tested against cells expressing EGFR WT and its mutants. Gefitinib, BI-4020, osimertinib, and mobocertinib were used as a reference. IC_{50} values for cell proliferation were assessed by a cell titer-glo assay in triplicates ± SD. Dark green indicates a high and pale green a low potency against the desired kinase. 45

Table 5. DSF data of the first series of derivatives 23, 56a–f, 57a–e, 58a,c, and 60. Staurosporine was used as a positive control. The newly synthesized compounds were screened in an *in-house* panel of 104 kinases. No stabilization of the kinase is indicated in pale green and a high stabilization in dark green. 50

Table 6. DSF data of the second series of derivatives 76a–i, 77a–e, 78a–c, 79, and 80. Staurosporine was used as a positive control. The newly synthesized compounds were screened in an *in-house* panel of 104 kinases. No stabilization of the kinase is indicated in pale green and a high stabilization in dark green. 51

Table 7. DSF data of the third series of derivatives 93a–b, 94a–b, 95a–c, 96a–c, 97b,d, and 98b,d. Staurosporine was used as a positive control. The newly synthesized compounds were screened in an *in-house* panel of 104 kinases. No stabilization of the kinase is indicated in pale green and a high stabilization in dark green. 53

Table 8. Table of the binding affinities of the *N*-(1*H*-pyrazole-3-yl)pyrimidine-4-amine-based inhibitors against CDK16.. 57

Table 9. DSF data of the pyrazole-based macrocyclic kinase inhibitors 110a–e. 23 and staurosporine were used as a positive control. The newly synthesized compounds were screened in an *in-house* panel of 104 kinases. No stabilization of the kinase is indicated in pale green, a high stabilization is indicated in dark green. 62

Table 10. DSF data of the pyrazole-based macrocyclic kinase inhibitors 111a–e, 112a, and 113a–e. 23 and staurosporine were used as a positive control. The newly synthesized compounds were screened in an *in-house* panel of 104 kinases. No stabilization of the kinase is indicated in pale green, while a high stabilization is indicated in dark green. 68

Table 11. DSF data and the corresponding NanoBRET^{TM} data for the macrocyclic kinase inhibitors 111a–e, 112a, and 113a–e. Lead structure 23 was used as a reference. IC$_{50}$ values were determined using the NanoBRET^{TM} assay in a 11-point dose−response curve in duplicates. 71

13. Acknowledgements

First of all, I want to thank Prof. Dr. Stefan Knapp for the possibility to work in his group at the Structural Genomics Consortium (SGC) in Frankfurt, the supervision during my thesis, the suggestions and advices to improve my work and the freedom to design my own scientific projects.

Also thanks to Prof. Dr. Eugen Proschak for reviewing my PhD thesis.

Special thanks to Thomas Hanke for the support, the discussions and the constant helpfulness throughout my thesis. Additional thanks for the lecturing skills and the proofreading of my thesis.

I would also like to thank my cooperation partners Tyler Beyett and Will Feng from the Dana-Farber Cancer Institute in Boston for providing the crystal structures, the *in vitro* and cellular data and for the support to advance the EGFR project.

Special thanks to my collaboration partners and colleagues of the SGC Frankfurt team, especially to Lena Marie Berger and Benedict Tilman-Berger for the cellular NanoBRET^{TM} data, Andreas Krämer for providing the proteins for the DSF assay and my ITC data, Dimitrios Ilias Balourdas and Andreas Jörger for providing the crystal structure of MST3, Lewis Elson for doing the DSF assays and Amelie Tjaden for the cell cycle assay. Furthermore I would like to thank Dr. Susanne Müller-Knapp for her continuous support.

Many thanks to my laboratoy colleagues Christian Kurz, Tim Weiser, Theresa Mensing and Nicolai Raig for the great working atmosphere in the best lab, the many conversations and their continuous support by solving problems. Also thanks to the best chemistry subgroup, which enables a great time during my PhD thesis with the small coffee breaks and various discussions.

Of course I would like to thank all non-named current and former members of the whole working group for the always pleasant time.

Further I want to thank Ralf Braden and Haotian Wang for the good time and the continuous help through my laboratory work.

Thanks to the NMR service department at the University of Frankfurt for the chance to record my spectra there and the mass spectrometry department, especially Uwe Hener and Matthias Brandl for the measured mass and high-resolution mass spectrometry.

Also special thanks to my interns Jonathan Hoppen, Christian Piesold, Janik Weckesser, Fabian Sinsel, Simon Mittag and my master student Philipp Lahnstein who supported me within the different projects and gave me the chance to improve my leadership skills.

I would also like to emphasize Thomas Hanke, Christian Kurz, Tim Weiser, Jörg Winkle, and Marcel Amrhein who proofread my thesis.

I would like to thank my husband Marcel Amrhein for the continuous support, his understanding, and the motivation, he gave me during the time of my PhD thesis. The last few years would not have been so easy without his love and encouragement.

Finally, thanks to my family, especially Anja Breitenbach, Thomas Breitenbach, Jörg Winkle, Vivienne Winkle, and my friends for the unconditional support and the emotional backing. Also a big thank you to Andrea Amrhein and Heinz Amrhein for their support during the last years.

Without all of you, I would not have been able to carry out all these years with the necessary freedom.

14. Publications

Amrhein, J. A.; Knapp, S.; Hanke, T. Synthetic Opportunities and Challenges for Macrocyclic Kinase Inhibitors. *J. Med. Chem.* **2021**, *64* (12), 7991–8009.

Kurz, C. G.; Preuss, F.; Tjaden, A.; Cusack, M.; **Amrhein, J. A.**; Chatterjee, D.; Mathea, S.; Berger, L. M.; Berger, B. T.; Krämer, A.; Weller, M.; Weiss, T.; Müller, S.; Knapp, S.; Hanke, T. Illuminating the Dark: Highly Selective Inhibition of Serine/Threonine Kinase 17A with Pyrazolo[1,5-a]Pyrimidine-Based Macrocycles. *J. Med. Chem.* **2022**, *65* (11), 7799–7817.

Amrhein, J. A.; Beyett, T. S.; Feng, W. W.; Krämer, A.; Weckesser, J.; Schaeffner, I. K.; Rana, J. K.; Jänne, P. A.; Eck, M. J.; Knapp, S.; Hanke, T. *J. Med. Chem.* **2022,** *65* (23), 15679-15697

Amrhein, J. A.; Berger, L. M.; Tjaden, A.; Krämer, A.; Elson, L.; Tolvanen, T.; Martinez-Molina, D.; Kaiser, A.; Schubert-Zsilavecz, M.; Müller, S.; Knapp, S.; Hanke, T. Discovery of 3-Amino-1*H*-Pyrazole-Based Kinase Inhibitors to Illuminate the Understudied PCTAIRE Family. *Int. J. Mol. Sci.* **2022**, *23* (23), 14834.

Amrhein, J. A.; Berger, B. T.; Berger, L. M.; Kalampaliki, A.; Wang, G.; Krämer, A.; Knapp, S.; Hanke, T. Design and Synthesis of Pyrazole-based Macrocyclic Kinase Inhibitors targeting BMPR2. Manuscript in preparation.

Amrhein, J. A.; Berger, L. M.; Balourdas, D. I.; Jörger, A.; Tjaden, A.; Krämer, A.; Berger, B. T.; Elson, L.; Kaiser, A.; Schubert-Zsilavecz, M.; Müller, S; Knapp, S.; Hanke, T. Synthesis of Pyrazole-based Macrocycles lead to a highly selective MST3/4 inhibitor. Manuscript in preparation.

15. Curriculum Vitae

16. Appendix

^{1}H, ^{13}C NMR, HPLC, and ESI data of compound **25a**

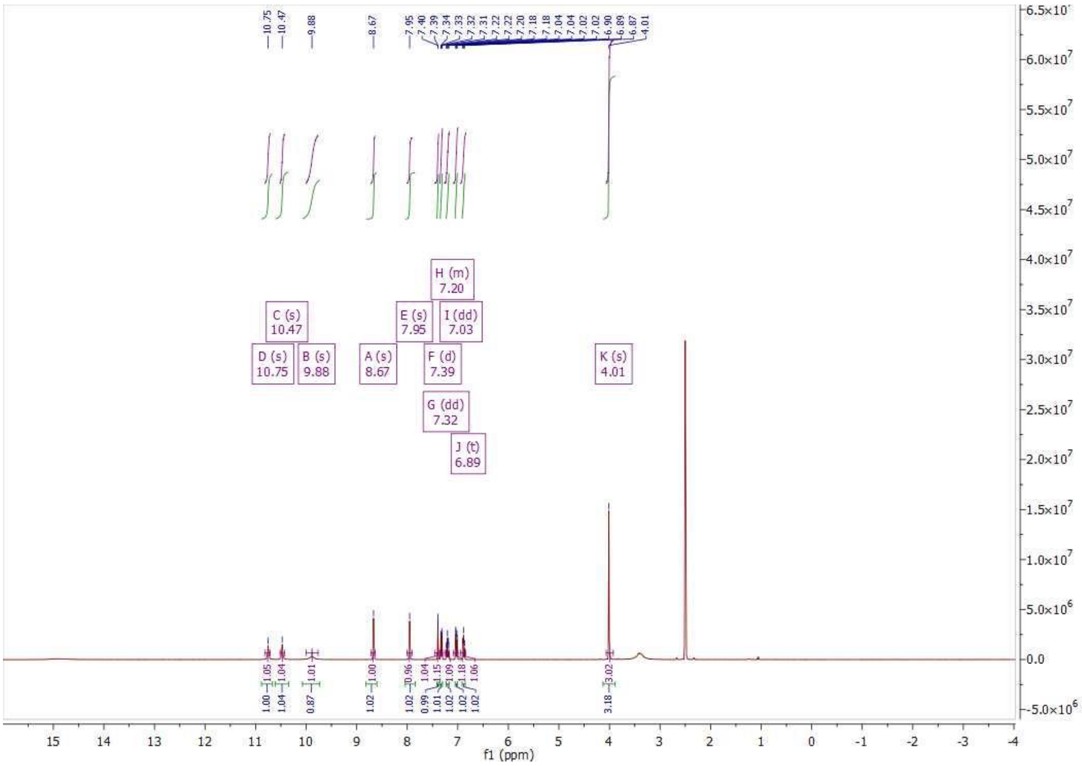

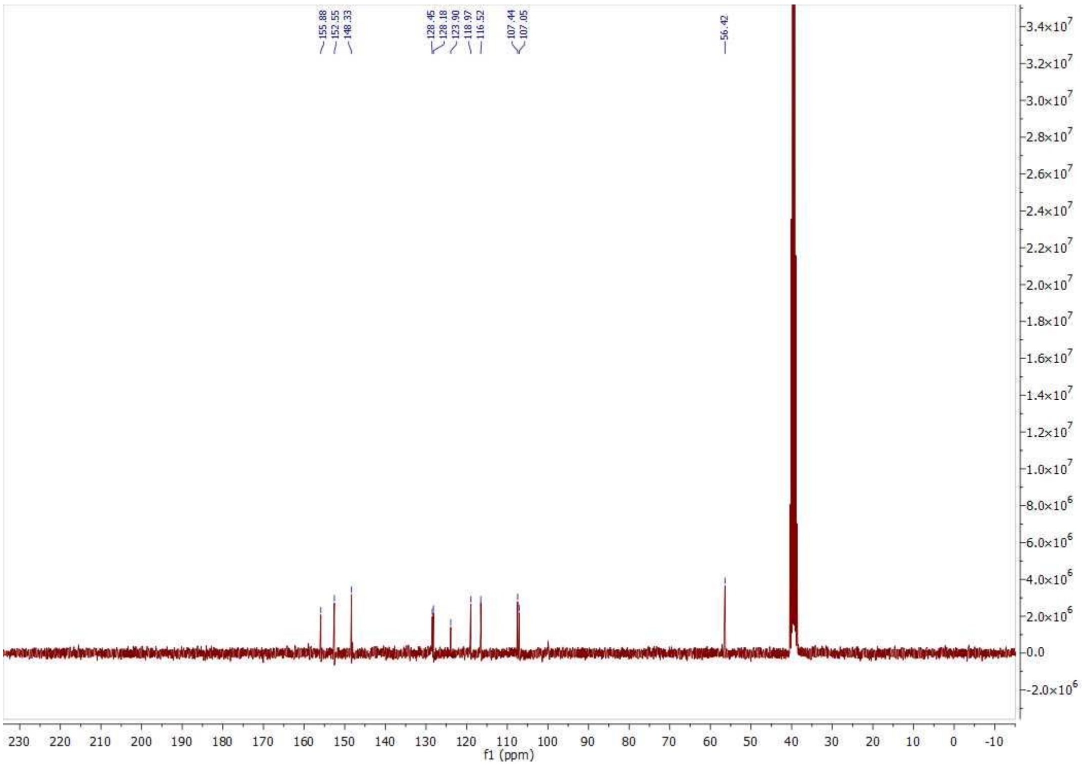

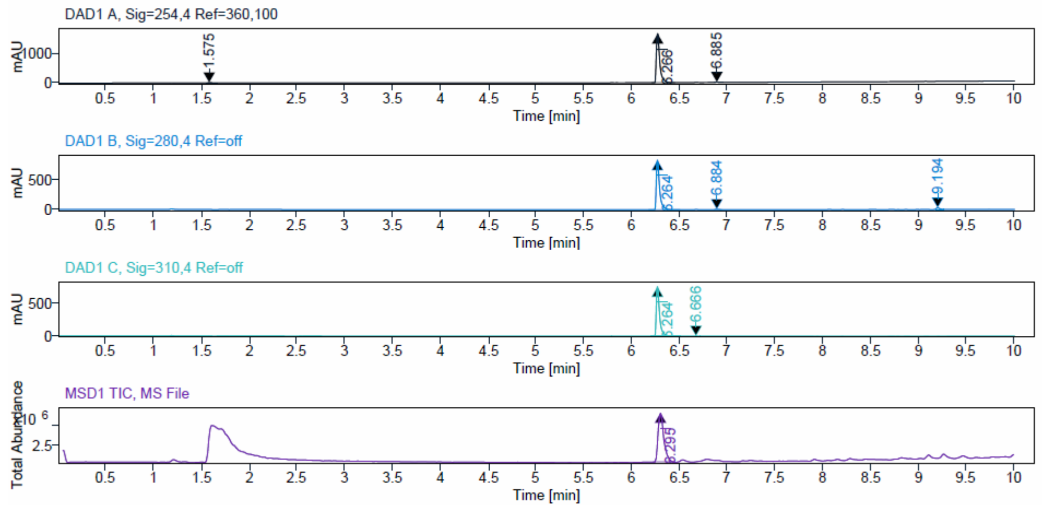

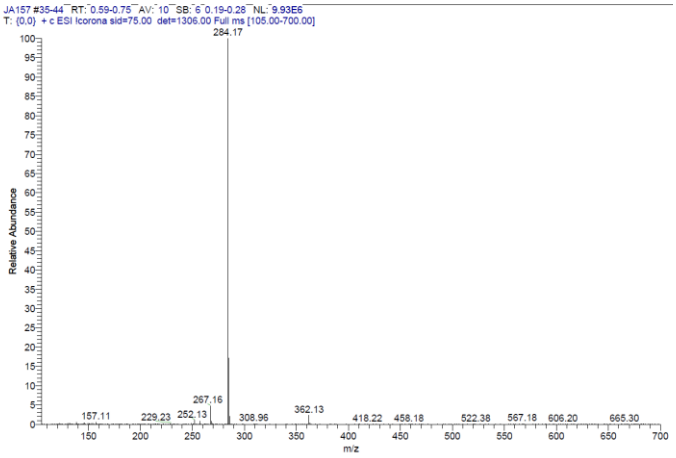

^{1}H, ^{13}C NMR, HPLC, and ESI data of compound **25b**

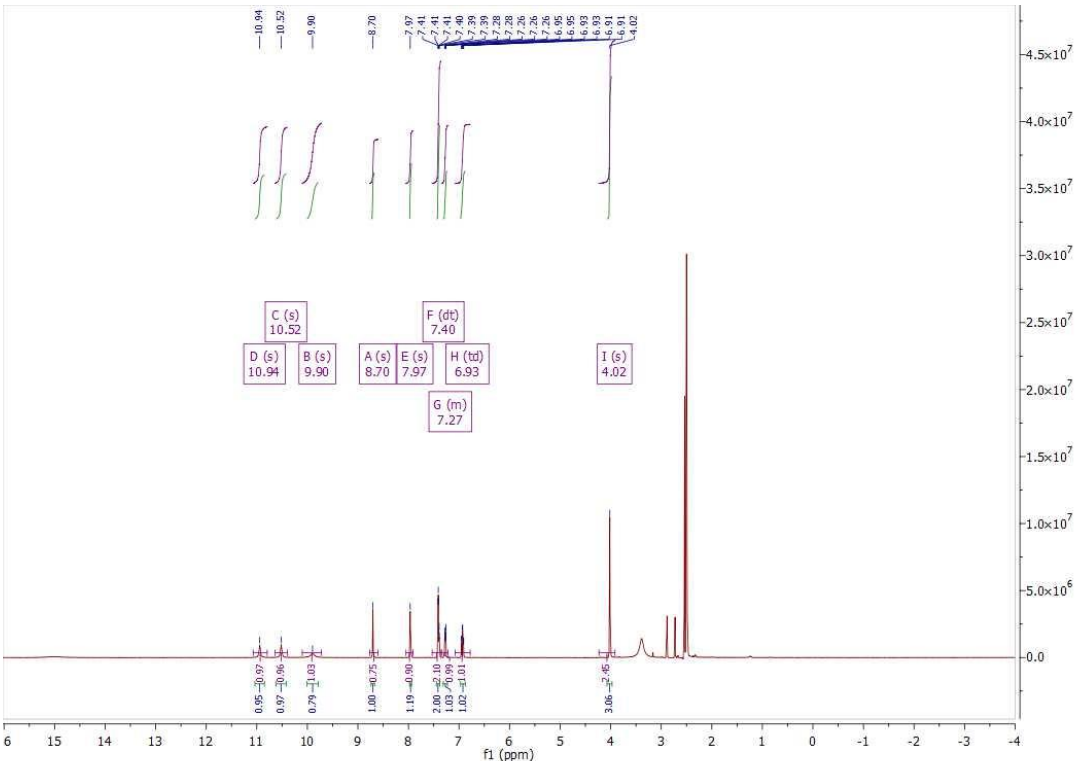

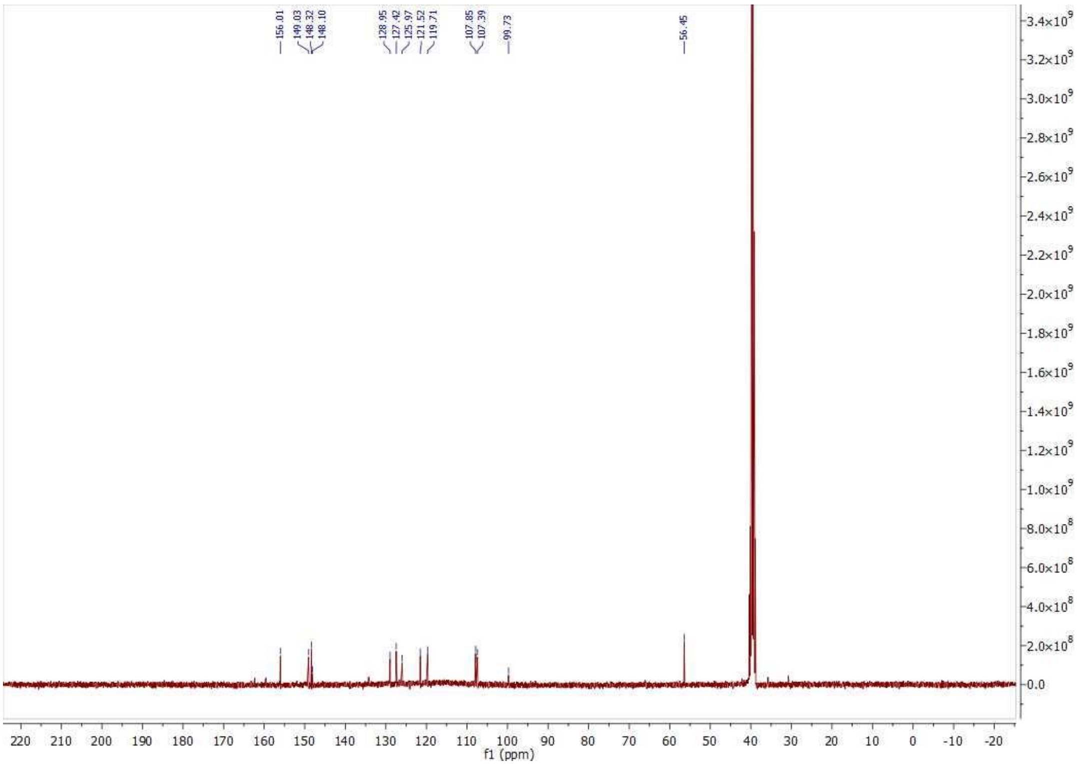
156.01
149.03
148.32
148.10
128.95
127.42
125.97
121.52
119.71
107.85
107.39
99.73
56.45
3.4×10^9
3.2×10^9
3.0×10^9
2.8×10^9
2.6×10^9
2.4×10^9
2.2×10^9
2.0×10^9
1.8×10^9
1.6×10^9
1.4×10^9
1.2×10^9
1.0×10^9
8.0×10^8
6.0×10^8
4.0×10^8
2.0×10^8
0.0
220 210 200 190 180 170 160 150 140 130 120 110 100 90 80 70 60 50 40 30 20 10 0 -10 -20
f1 (ppm)

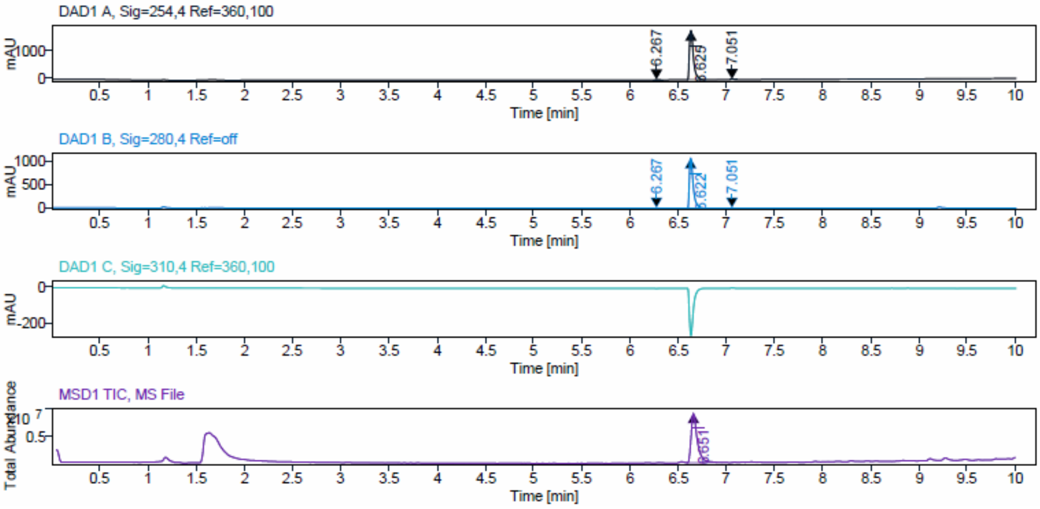
DAD1 A, Sig=254,4 Ref=360,100
mAU
1000
0
6.267
6.629
7.051
0.5 1 1.5 2 2.5 3 3.5 4 4.5 5 5.5 6 6.5 7 7.5 8 8.5 9 9.5 10
Time [min]
DAD1 B, Sig=280,4 Ref=off
mAU
1000
500
0
6.267
6.622
7.051
Time [min]
DAD1 C, Sig=310,4 Ref=360,100
mAU
0
-200
Time [min]
MSD1 TIC, MS File
Total Abundance
x10 7
0.5
6.651
Time [min]

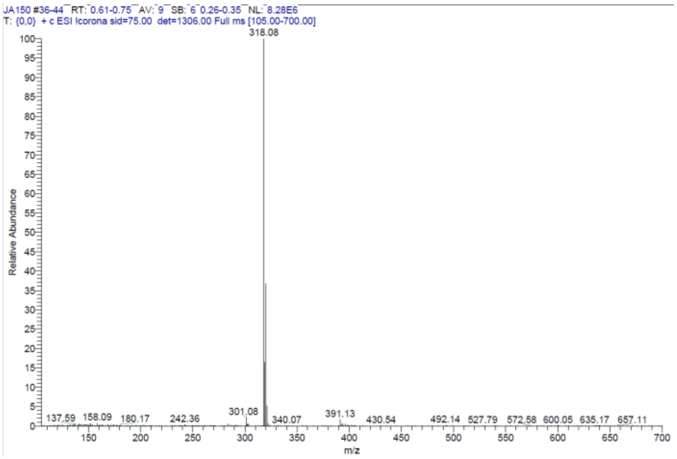
JA150 #36-44 RT: 0.61-0.75 AV: 9 SB: 6 0.26-0.35 NL: 8.28E6
T: {0,0} + c ESI !corona sid=75.00 det=1306.00 Full ms [105.00-700.00]
318.08
Relative Abundance
100 95 90 85 80 75 70 65 60 55 50 45 40 35 30 25 20 15 10 5 0
137.59
158.09
180.17
242.36
301.08
340.07
391.13
430.54
492.14
527.79
572.58
600.05
635.17
657.11
150 200 250 300 350 400 450 500 550 600 650 700
m/z

^{1}H, ^{13}C NMR, HPLC, and ESI data of compound **25c**

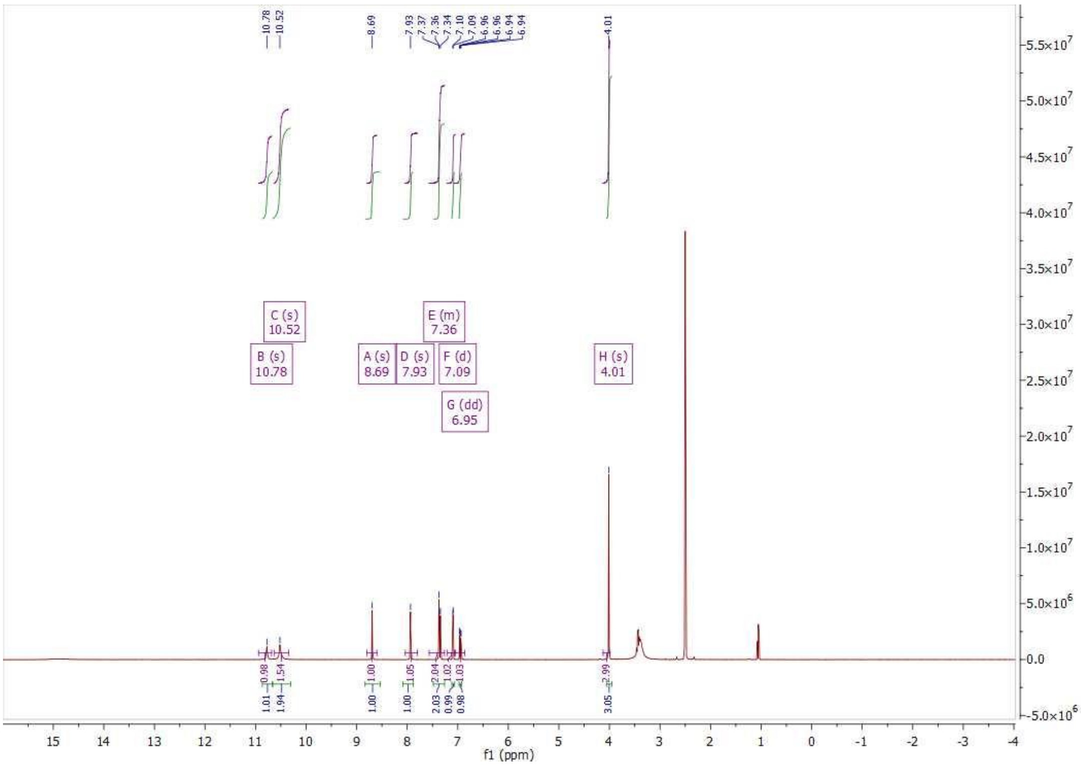

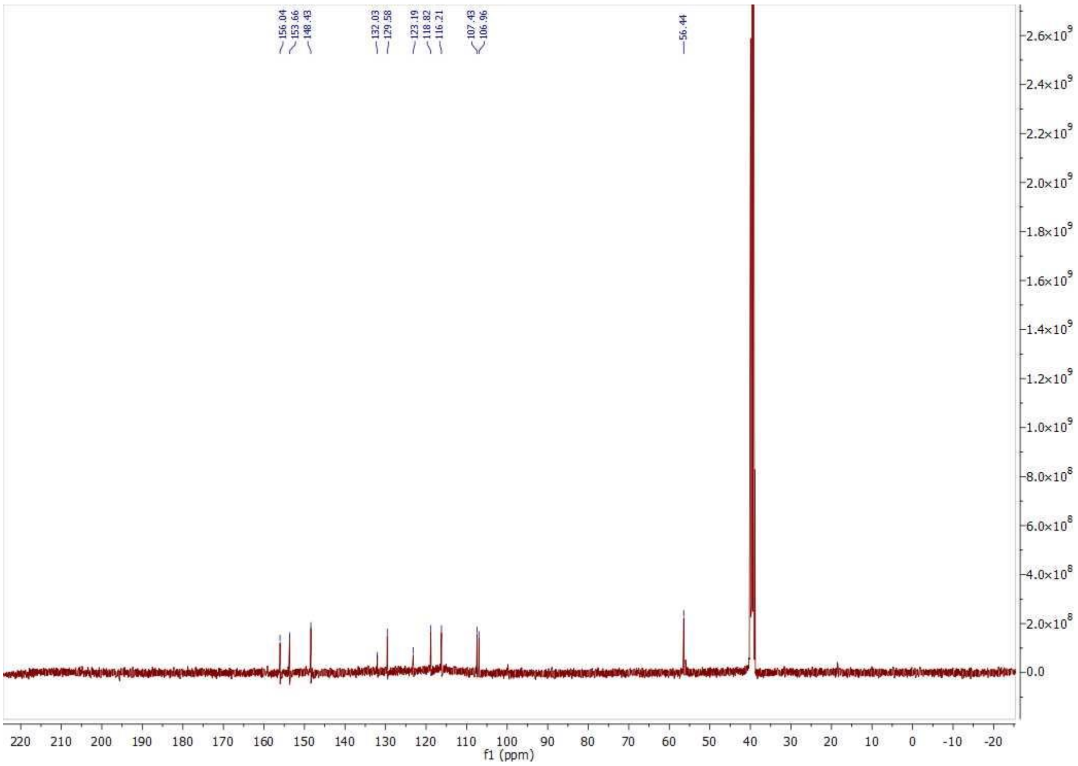

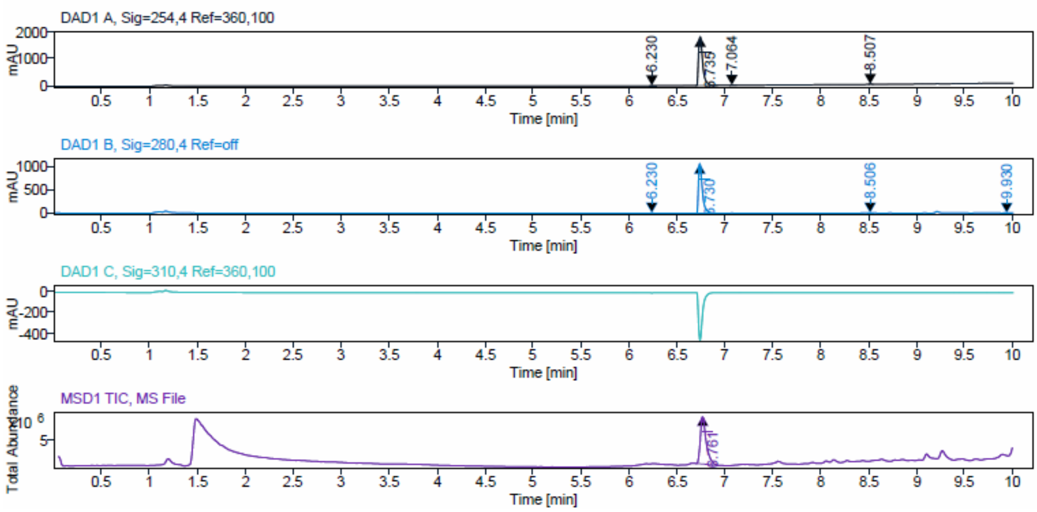

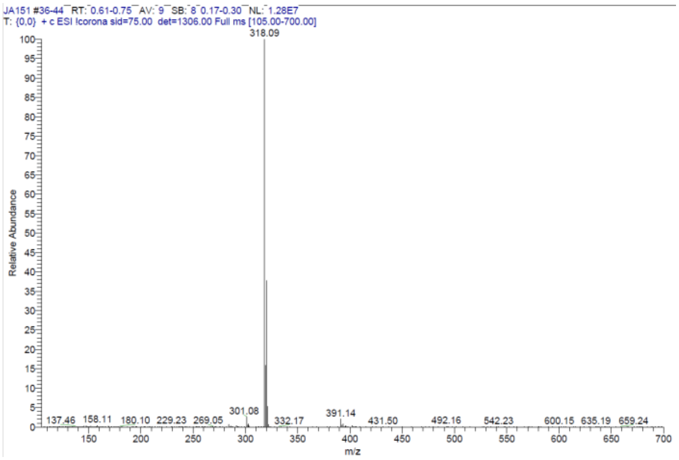

^{1}H, ^{13}C NMR, HPLC, and ESI data of compound **25d**

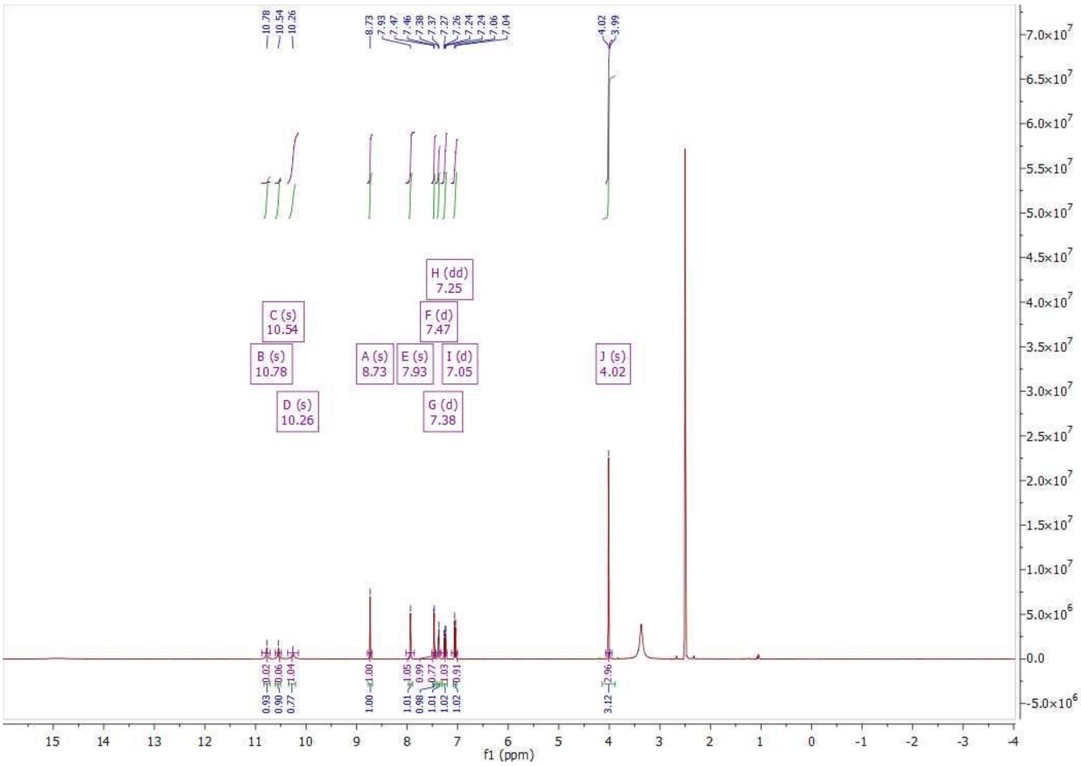

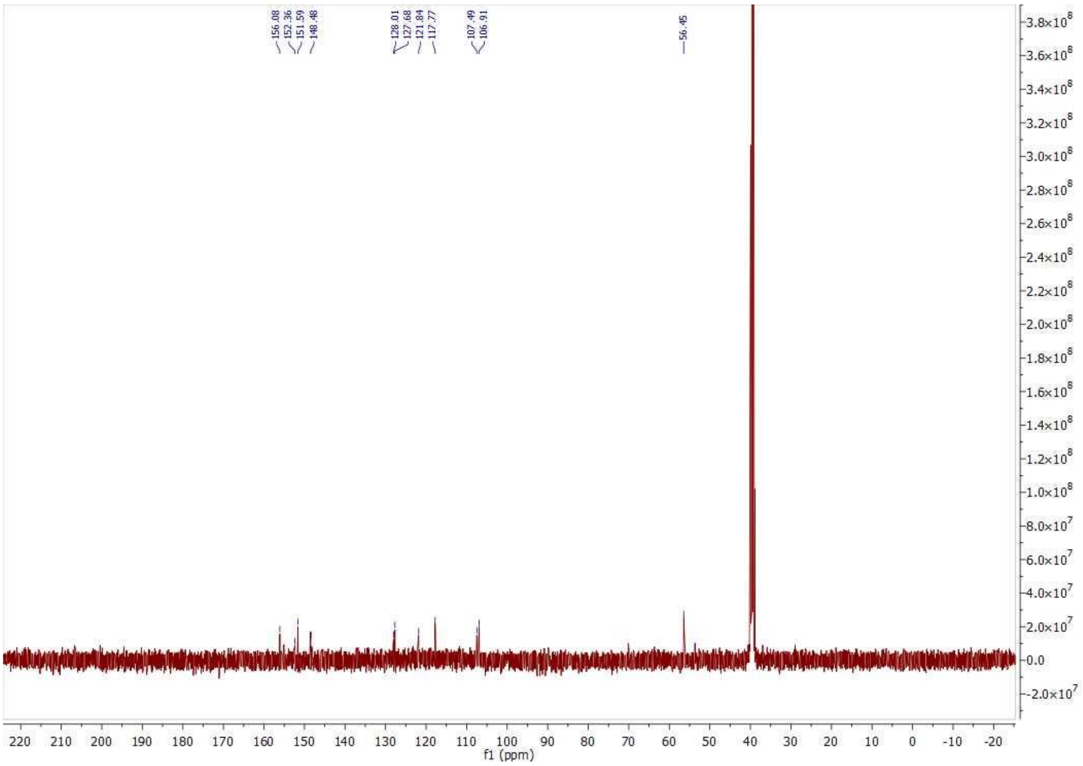
156.08
152.36
151.59
148.48
128.01
127.68
121.84
117.77
107.49
106.91
56.45
3.8×10^8
3.6×10^8
3.4×10^8
3.2×10^8
3.0×10^8
2.8×10^8
2.6×10^8
2.4×10^8
2.2×10^8
2.0×10^8
1.8×10^8
1.6×10^8
1.4×10^8
1.2×10^8
1.0×10^8
8.0×10^7
6.0×10^7
4.0×10^7
2.0×10^7
0.0
-2.0×10^7
220 210 200 190 180 170 160 150 140 130 120 110 100 90 80 70 60 50 40 30 20 10 0 -10 -20
f1 (ppm)

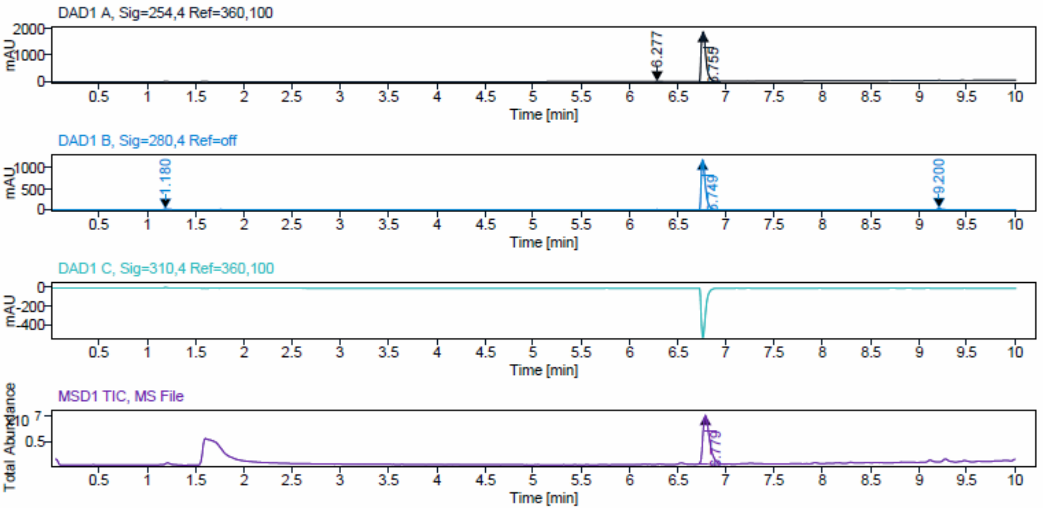
DAD1 A, Sig=254,4 Ref=360,100
mAU
2000
1000
0
6.277
6.758
DAD1 B, Sig=280,4 Ref=off
mAU
1000
500
0
1.180
6.749
9.200
DAD1 C, Sig=310,4 Ref=360,100
mAU
0
-200
-400
MSD1 TIC, MS File
Total Abundance
x10 7
0.5
6.779
0.5 1 1.5 2 2.5 3 3.5 4 4.5 5 5.5 6 6.5 7 7.5 8 8.5 9 9.5 10
Time [min]

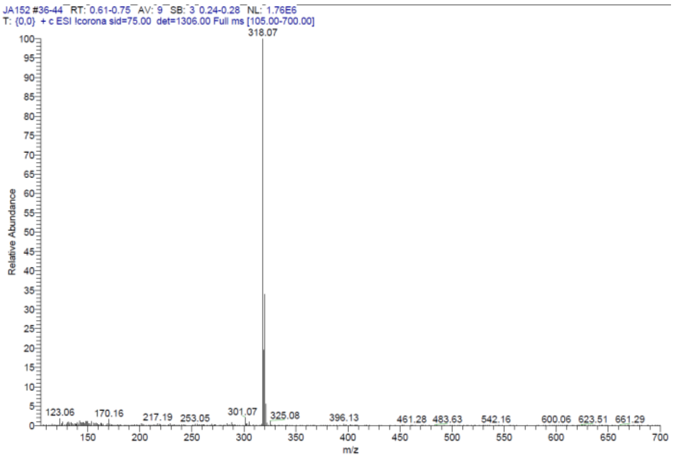
JA152 #36-44 RT: 0.61-0.75 AV: 9 SB: 3 0.24-0.28 NL: 1.76E6
T: {0,0} + c ESI !corona sid=75.00 det=1306.00 Full ms [105.00-700.00]
318.07
Relative Abundance
100 95 90 85 80 75 70 65 60 55 50 45 40 35 30 25 20 15 10 5 0
123.06
170.16
217.19
253.05
301.07
325.08
396.13
461.28
483.63
542.16
600.06
623.51
661.29
150 200 250 300 350 400 450 500 550 600 650 700
m/z

^{1}H, ^{13}C NMR, HPLC, and ESI data of compound **25e**

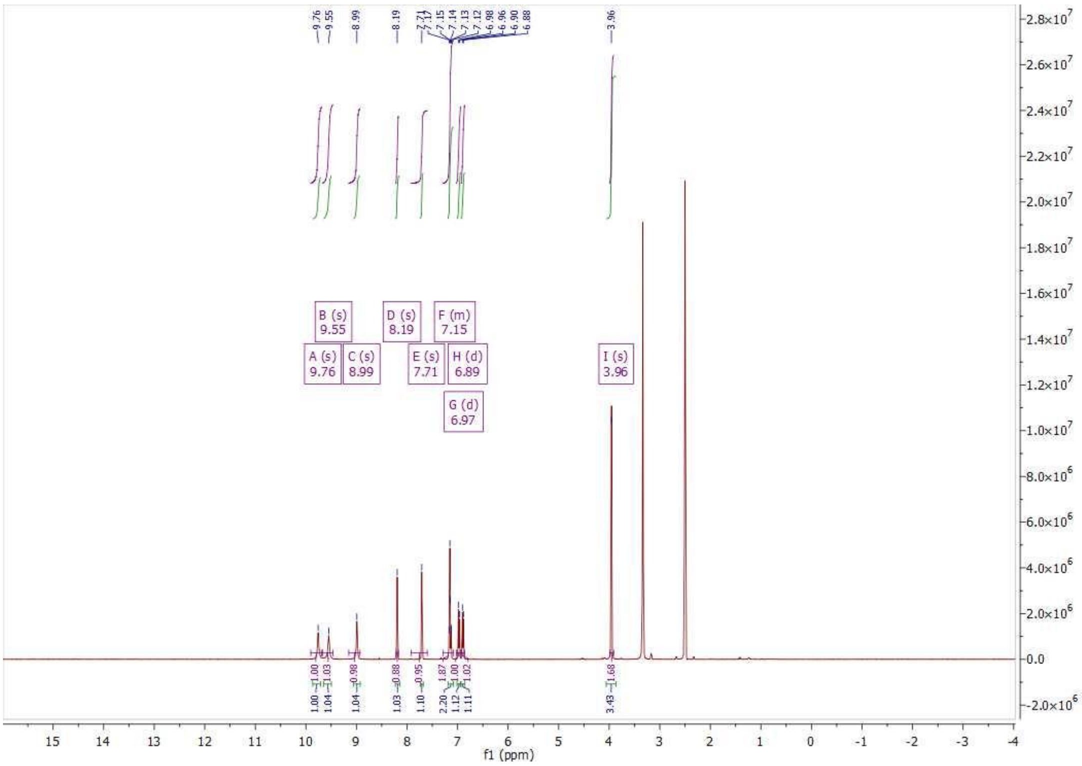

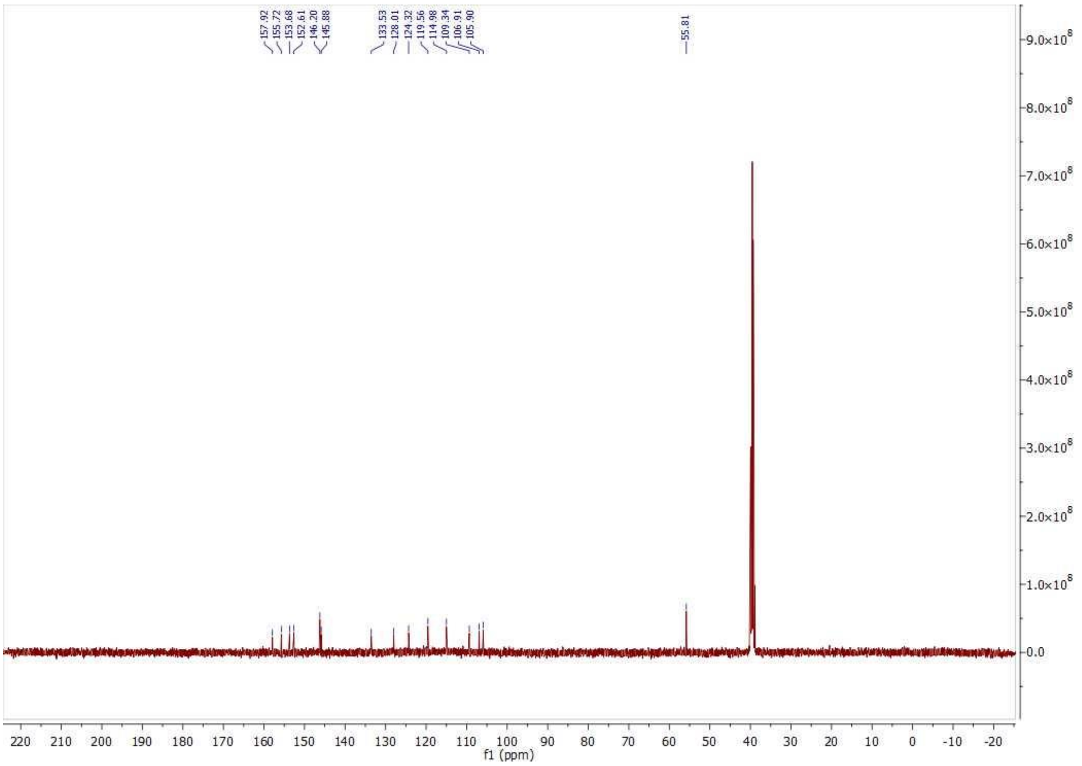

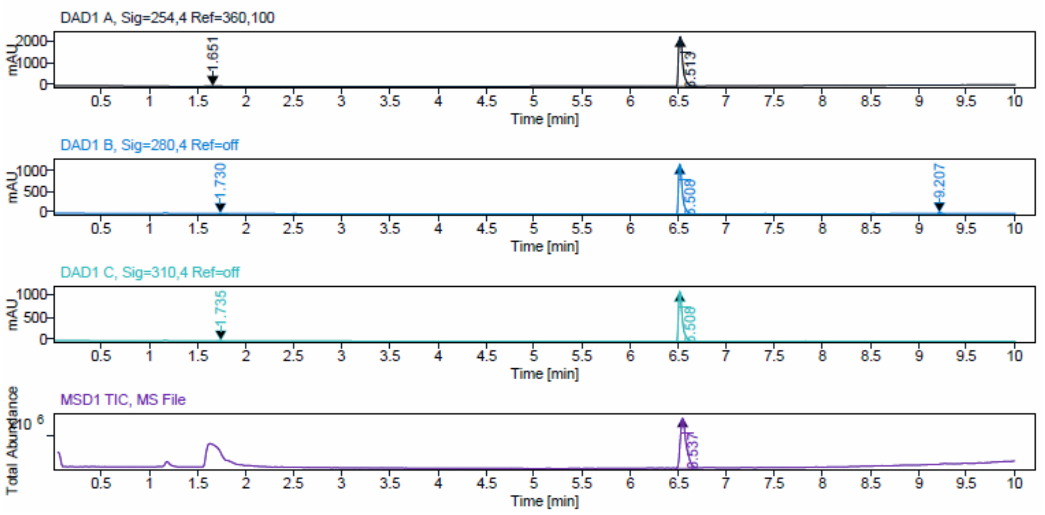

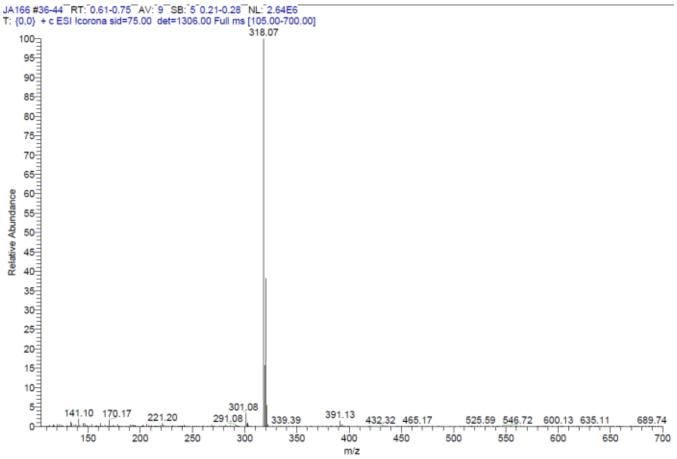

^{1}H, ^{13}C NMR, HPLC, and ESI data of compound **25f**

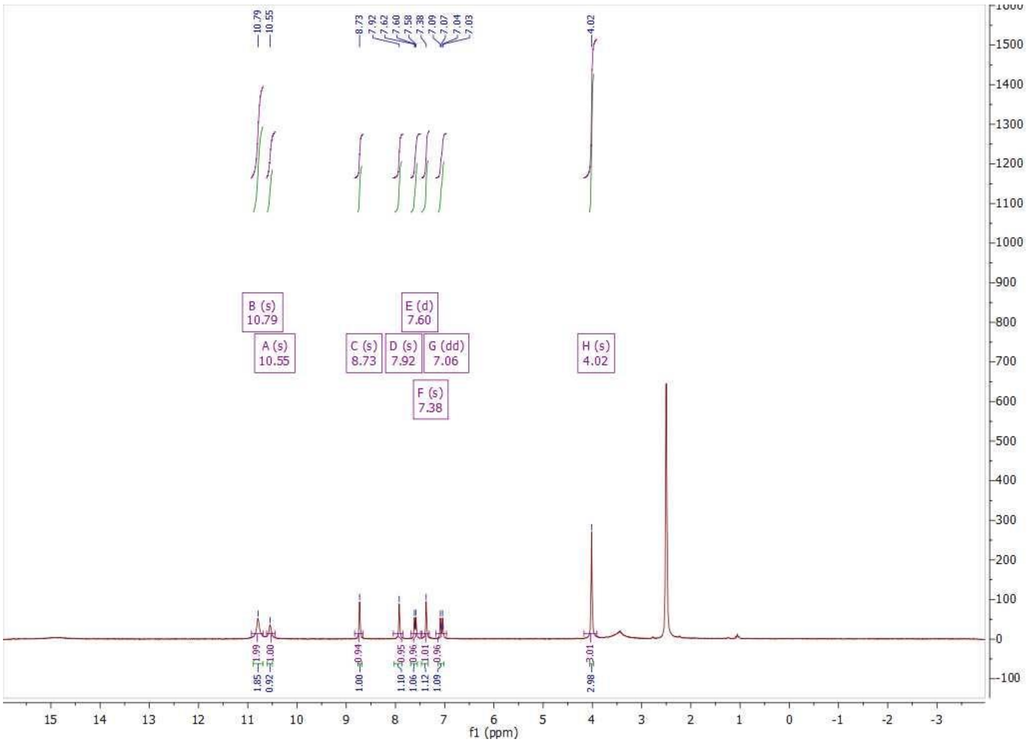

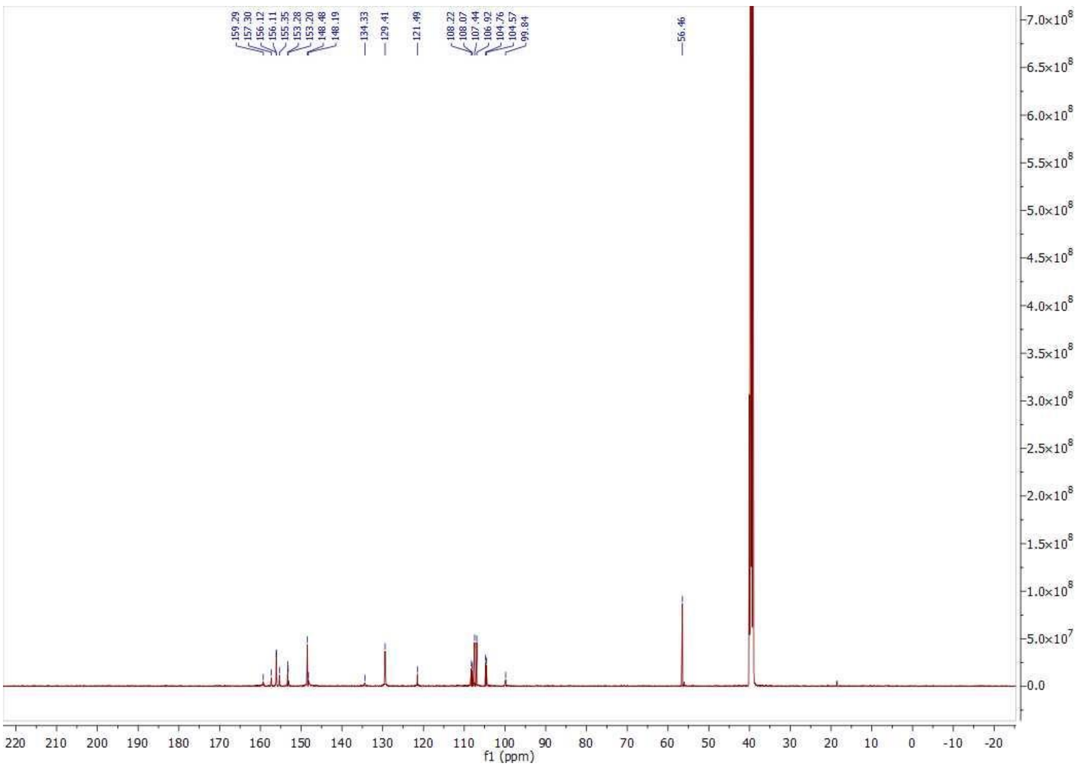
159.29
157.30
156.12
156.11
155.35
153.28
153.20
148.48
148.19
134.33
129.41
121.49
108.22
108.07
107.44
106.92
104.76
104.57
99.84
56.46
7.0×10^8
6.5×10^8
6.0×10^8
5.5×10^8
5.0×10^8
4.5×10^8
4.0×10^8
3.5×10^8
3.0×10^8
2.5×10^8
2.0×10^8
1.5×10^8
1.0×10^8
5.0×10^7
0.0
220 210 200 190 180 170 160 150 140 130 120 110 100 90 80 70 60 50 40 30 20 10 0 -10 -20
f1 (ppm)

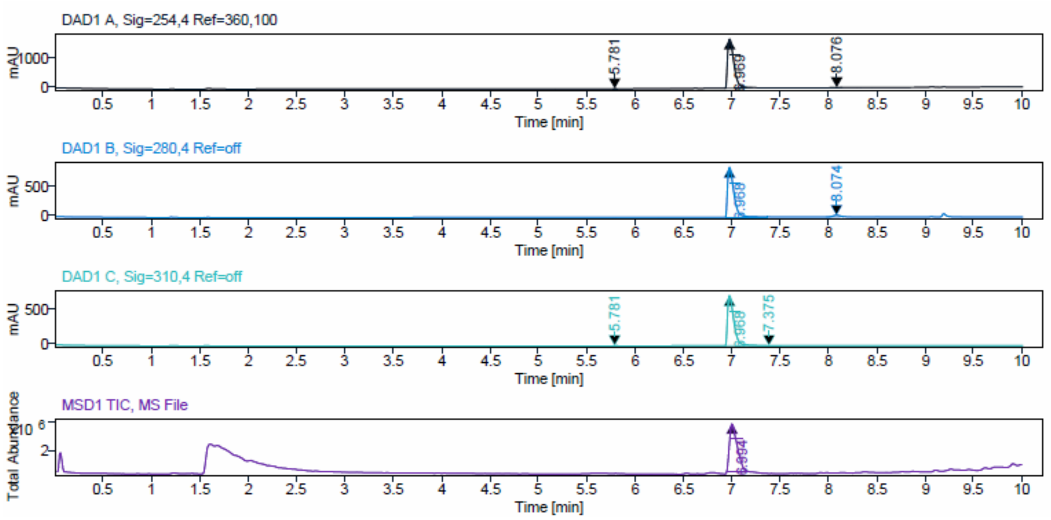
DAD1 A, Sig=254,4 Ref=360,100
mAU
1000
0
5.781
6.969
8.076
Time [min]
DAD1 B, Sig=280,4 Ref=off
mAU
500
0
6.968
8.074
Time [min]
DAD1 C, Sig=310,4 Ref=off
mAU
500
0
5.781
6.969
7.375
Time [min]
MSD1 TIC, MS File
Total Abundance
10^6
2
6.984
0.5 1 1.5 2 2.5 3 3.5 4 4.5 5 5.5 6 6.5 7 7.5 8 8.5 9 9.5 10
Time [min]

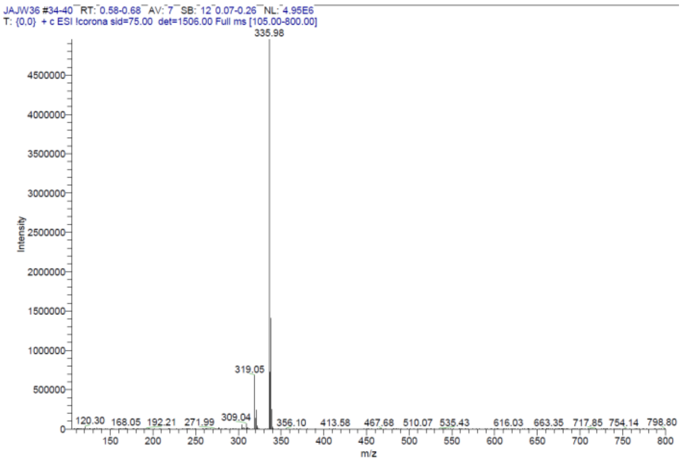
JAJW36 #34-40 RT: 0.58-0.68 AV: 7 SB: 12 0.07-0.26 NL: 4.95E6
T: {0,0} + c ESI !corona sid=75.00 det=1506.00 Full ms [105.00-800.00]
335.98
319.05
120.30
168.05
192.21
271.99
309.04
356.10
413.58
467.68
510.07
535.43
616.03
663.35
717.85
754.14
798.80
Intensity
4500000
4000000
3500000
3000000
2500000
2000000
1500000
1000000
500000
0
150 200 250 300 350 400 450 500 550 600 650 700 750 800
m/z

^{1}H, ^{13}C NMR, HPLC, and ESI data of compound **26a**

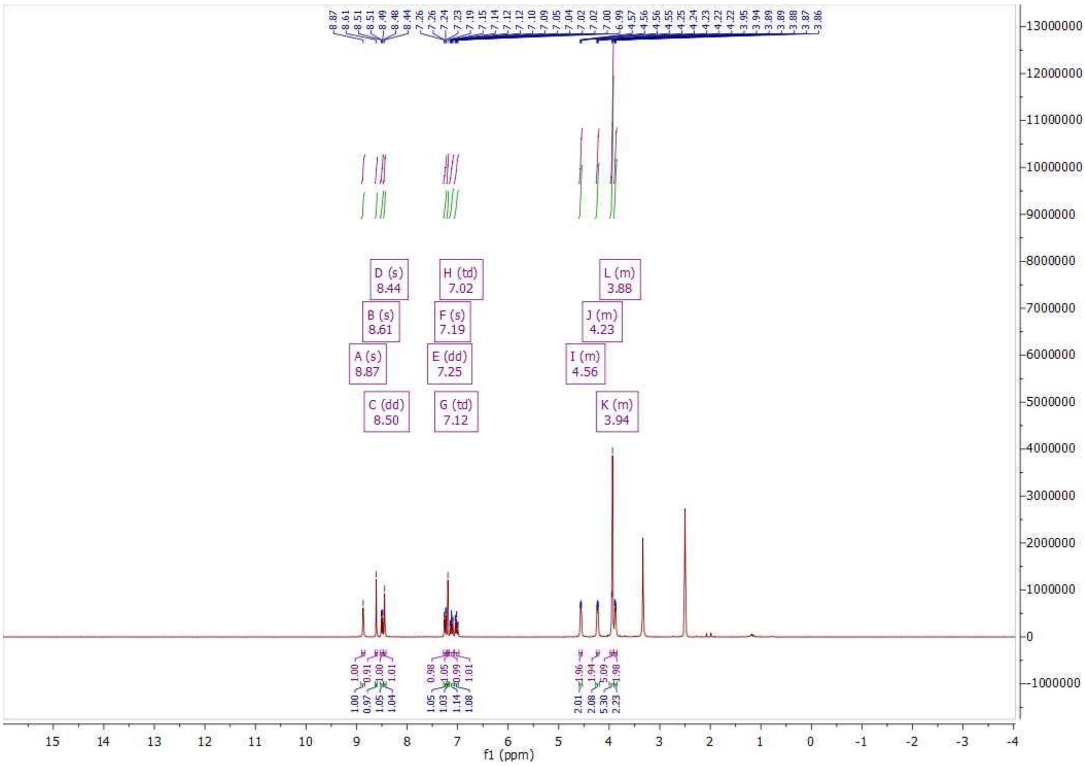

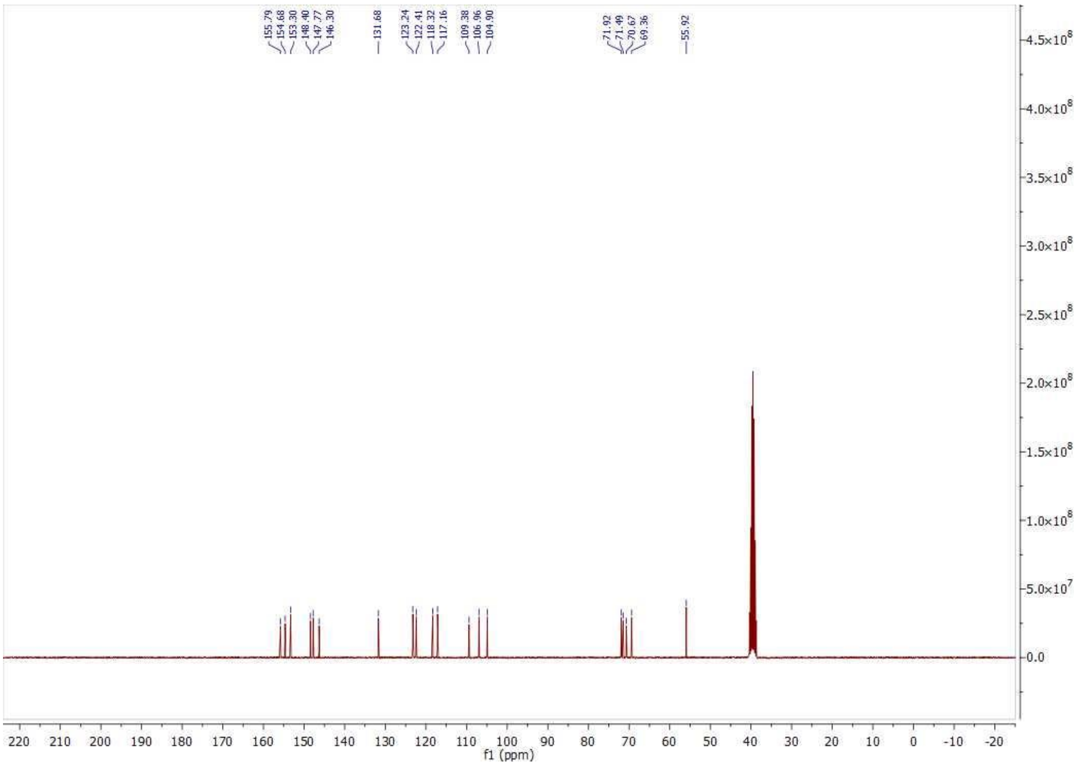

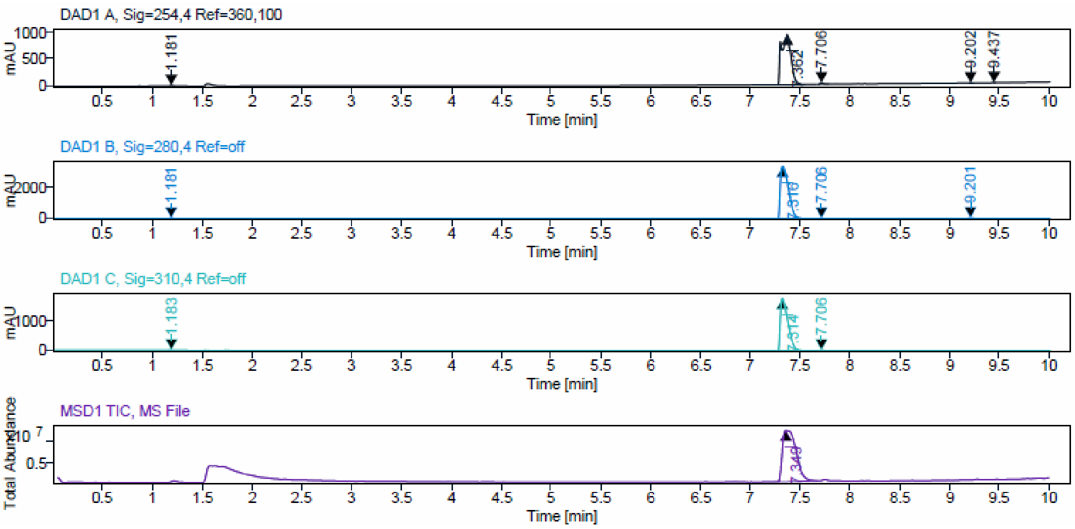

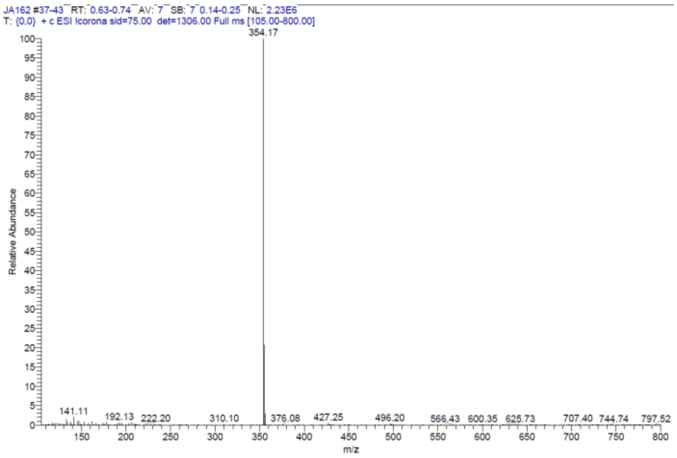

^{1}H, ^{13}C NMR, HPLC, and ESI data of compound **26b**

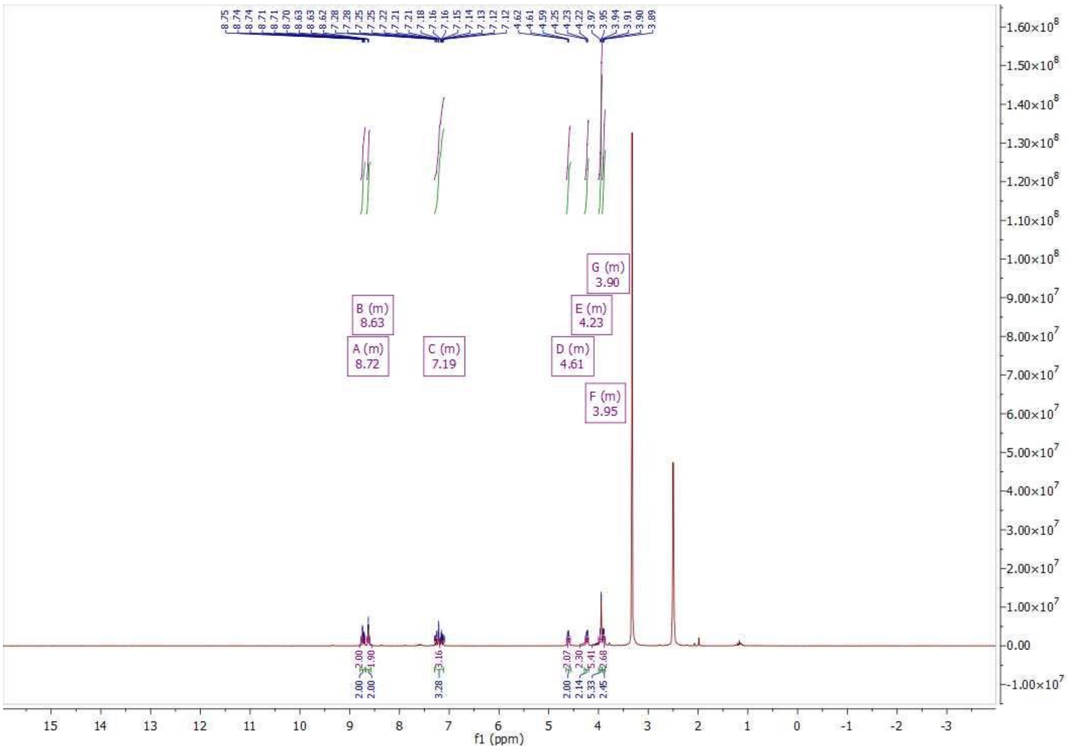

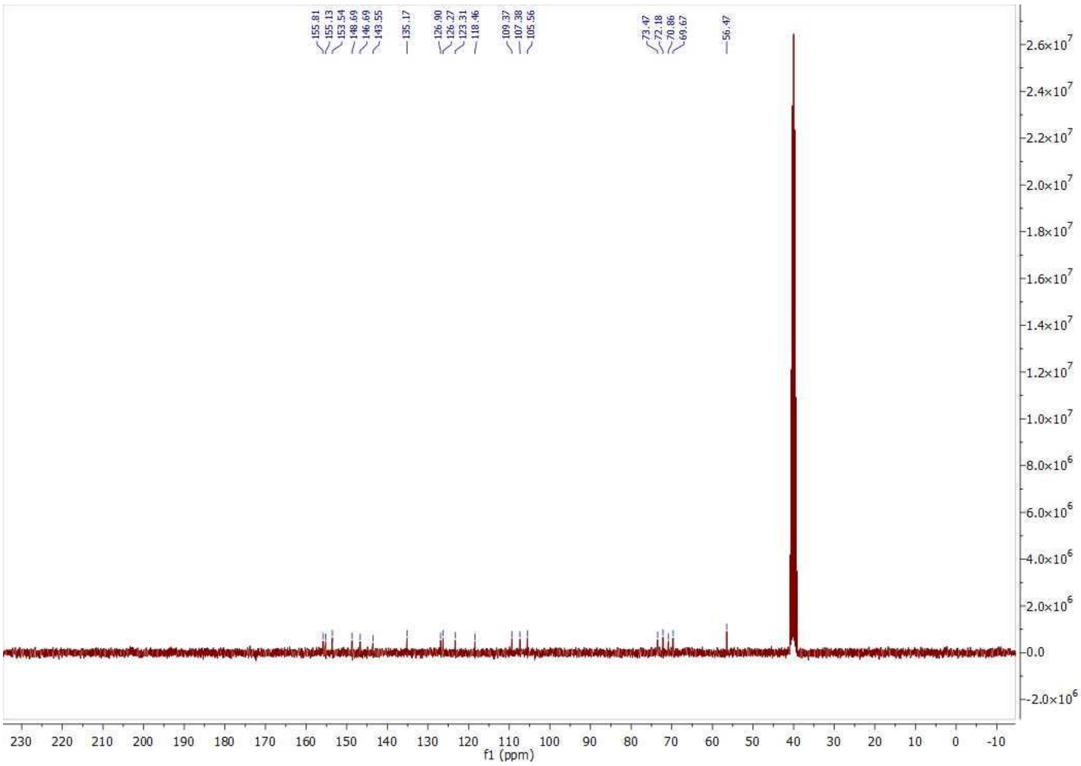
155.81
155.13
153.54
148.69
146.69
143.55
135.17
126.90
126.27
123.31
118.46
109.37
107.38
105.56
73.47
72.18
70.86
69.67
56.47
2.6×10^7
2.4×10^7
2.2×10^7
2.0×10^7
1.8×10^7
1.6×10^7
1.4×10^7
1.2×10^7
1.0×10^7
8.0×10^6
6.0×10^6
4.0×10^6
2.0×10^6
0.0
-2.0×10^6
230 220 210 200 190 180 170 160 150 140 130 120 110 100 90 80 70 60 50 40 30 20 10 0 -10
f1 (ppm)

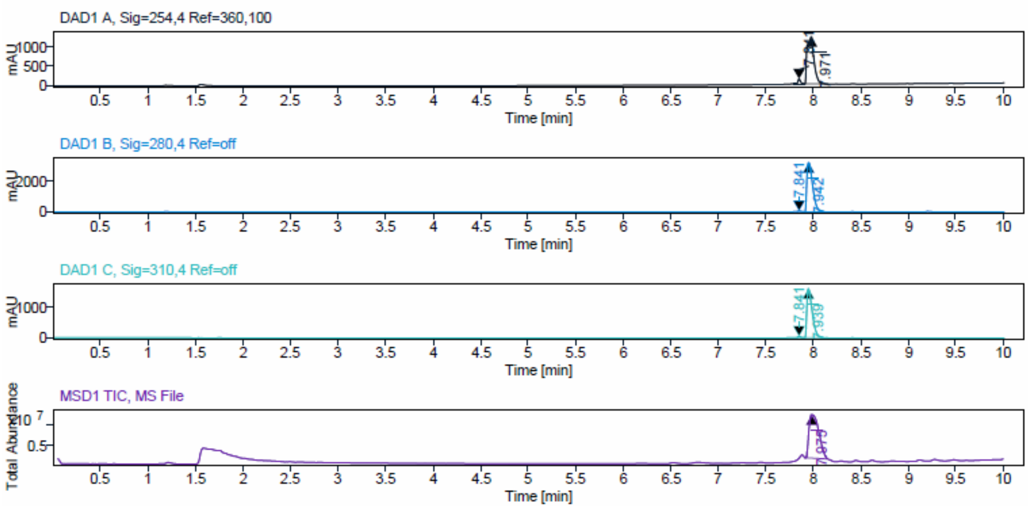
DAD1 A, Sig=254,4 Ref=360,100
mAU
1000
500
0
.971
Time [min]
DAD1 B, Sig=280,4 Ref=off
mAU
2000
0
7.841
.942
Time [min]
DAD1 C, Sig=310,4 Ref=off
mAU
1000
0
7.841
.939
Time [min]
MSD1 TIC, MS File
Total Abundance
x10 7
0.5
Time [min]
0.5 1 1.5 2 2.5 3 3.5 4 4.5 5 5.5 6 6.5 7 7.5 8 8.5 9 9.5 10

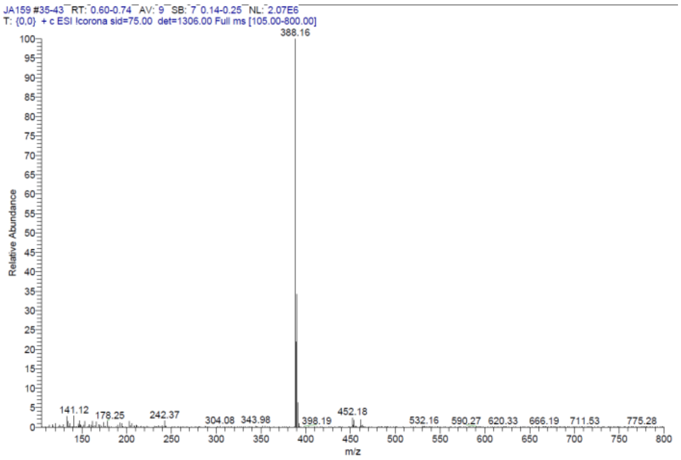
JA159 #35-43 RT: 0.60-0.74 AV: 9 SB: 7 0.14-0.25 NL: 2.07E6
T: {0,0} + c ESI !corona sid=75.00 det=1306.00 Full ms [105.00-800.00]
388.16
Relative Abundance
100 95 90 85 80 75 70 65 60 55 50 45 40 35 30 25 20 15 10 5 0
141.12
178.25
242.37
304.08
343.98
398.19
452.18
532.16
590.27
620.33
666.19
711.53
775.28
150 200 250 300 350 400 450 500 550 600 650 700 750 800
m/z

^1H, ^{13}C NMR, HPLC, and ESI data of compound **26c**

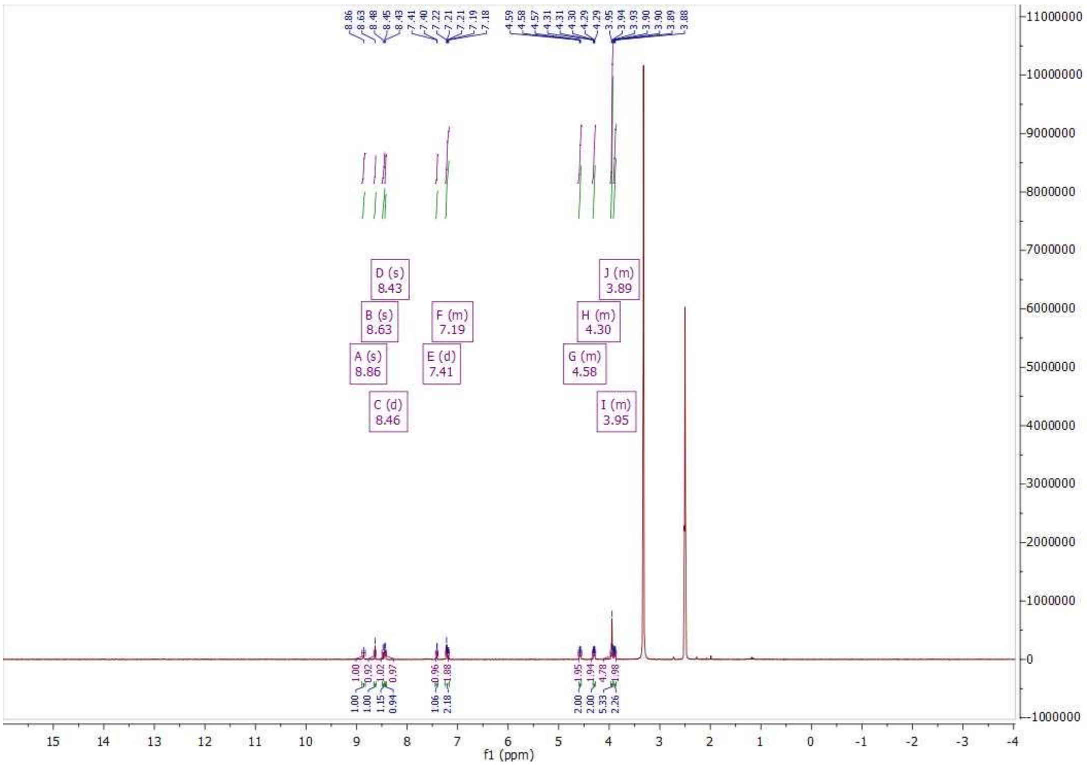

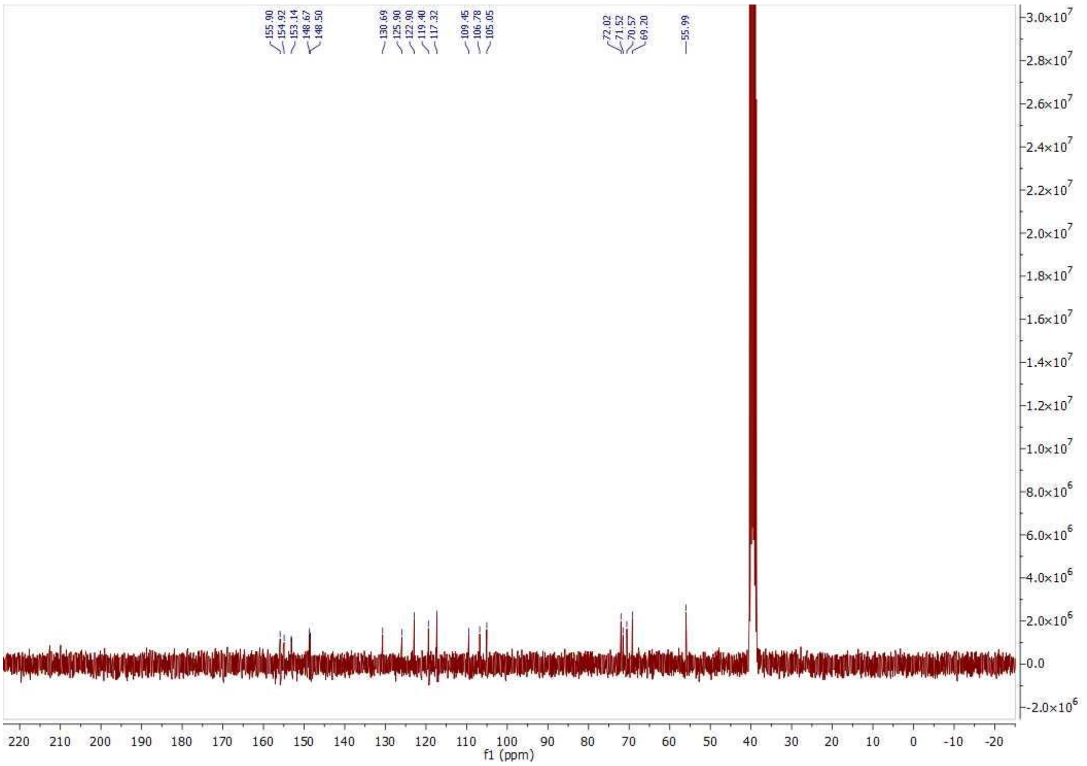

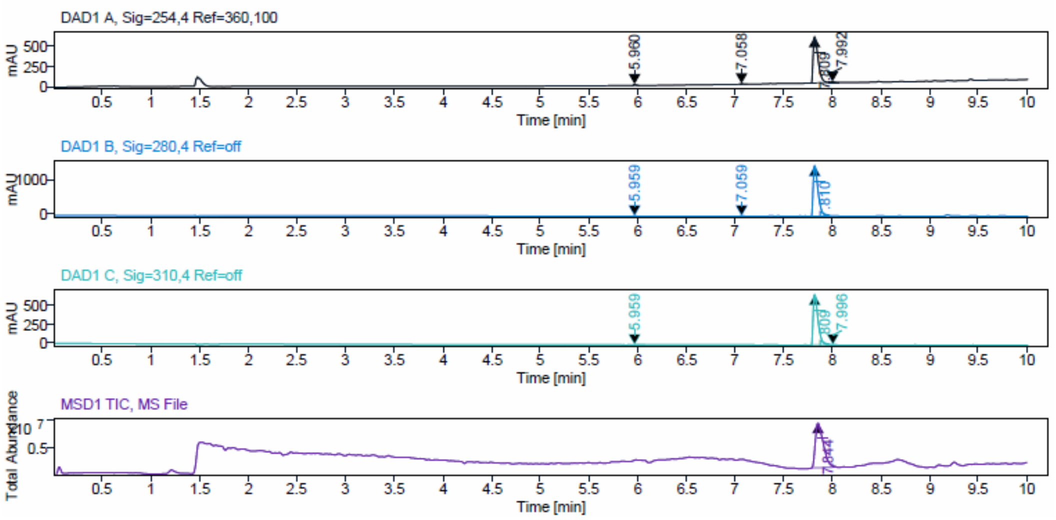

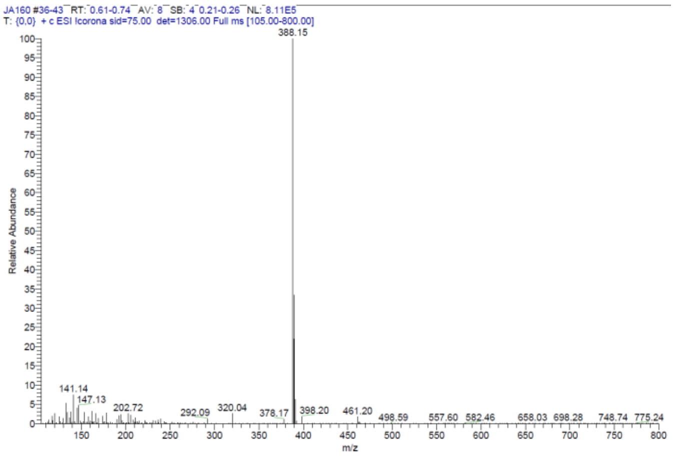

^{1}H, ^{13}C NMR, HPLC, and ESI data of compound **26d**

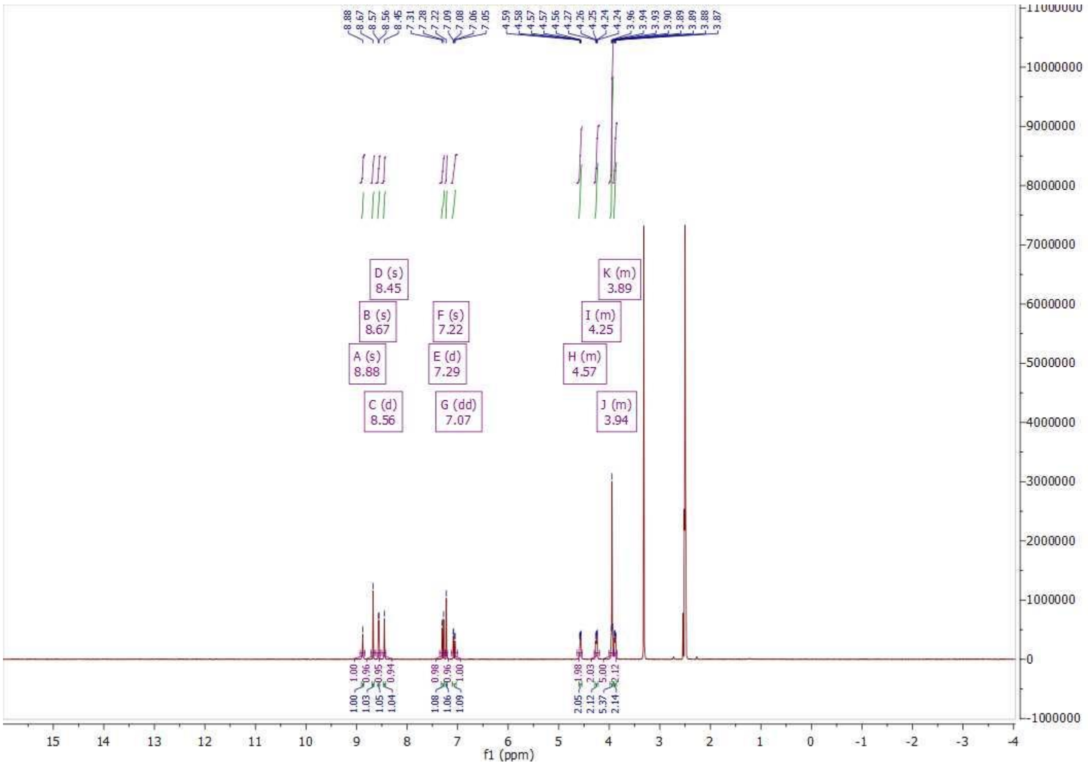

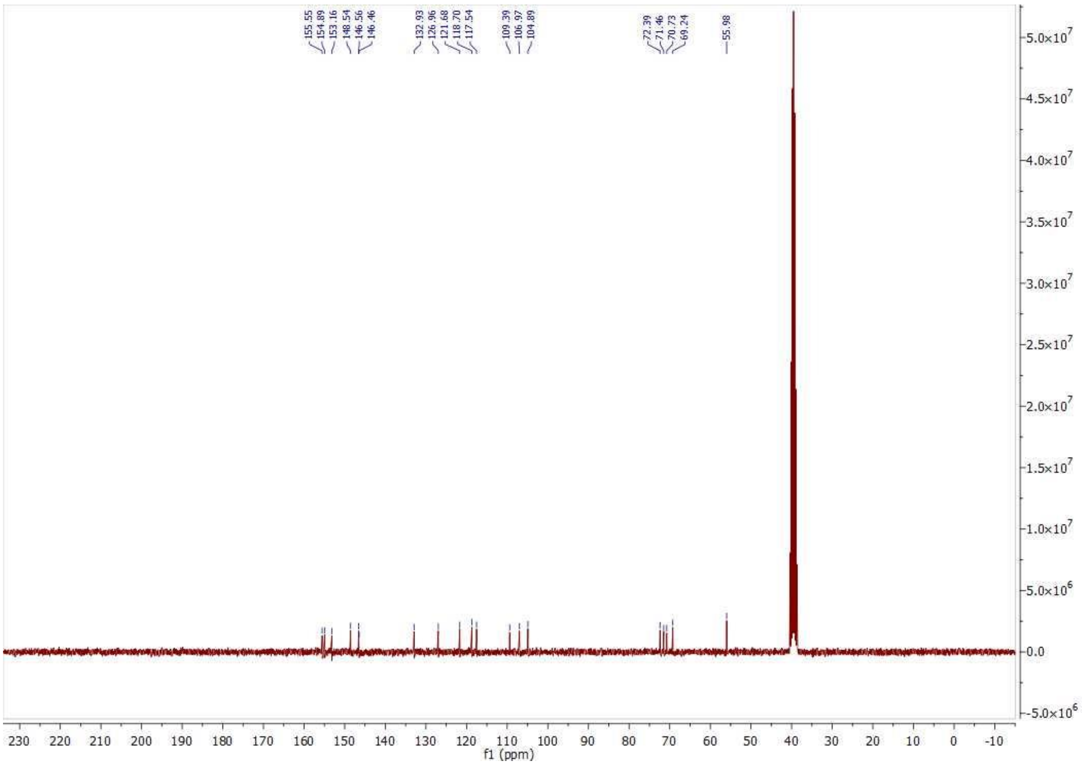
155.55
154.89
153.16
148.54
146.56
146.46
132.93
126.96
121.68
118.70
117.54
109.39
106.97
104.89
72.39
71.46
70.73
69.24
55.98
5.0×10^7
4.5×10^7
4.0×10^7
3.5×10^7
3.0×10^7
2.5×10^7
2.0×10^7
1.5×10^7
1.0×10^7
5.0×10^6
0.0
-5.0×10^6
230 220 210 200 190 180 170 160 150 140 130 120 110 100 90 80 70 60 50 40 30 20 10 0 -10
f1 (ppm)

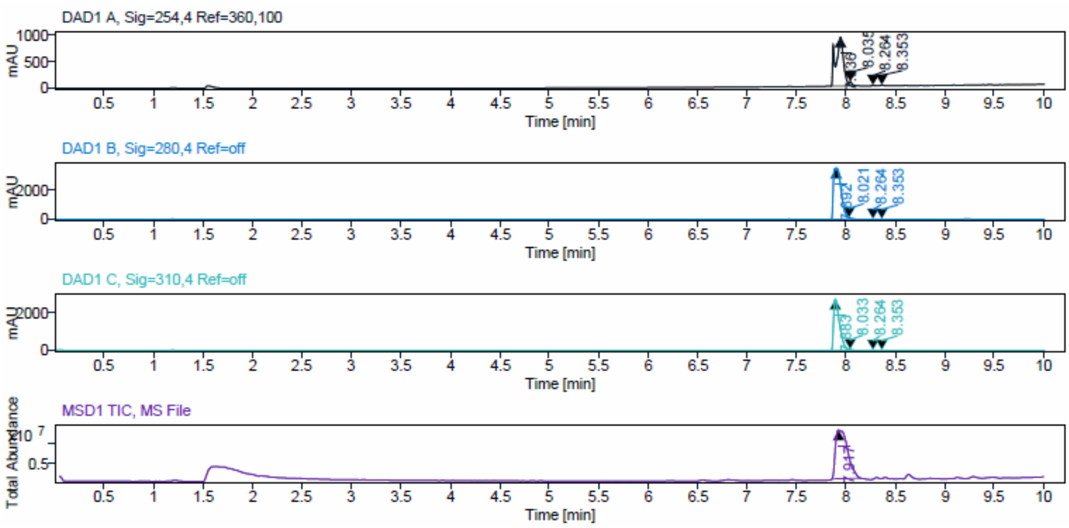
DAD1 A, Sig=254,4 Ref=360,100
mAU
1000
500
0
8.035
8.264
8.353
DAD1 B, Sig=280,4 Ref=off
mAU
2000
0
7.892
8.021
8.264
8.353
DAD1 C, Sig=310,4 Ref=off
mAU
2000
0
7.883
8.033
8.264
8.353
MSD1 TIC, MS File
Total Abundance
x10 7
0.5
0.5 1 1.5 2 2.5 3 3.5 4 4.5 5 5.5 6 6.5 7 7.5 8 8.5 9 9.5 10
Time [min]

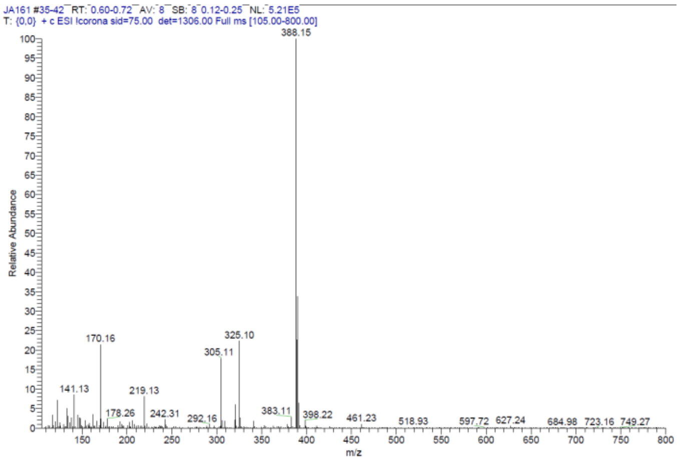
JA161 #35-42 RT: 0.60-0.72 AV: 8 SB: 8 0.12-0.25 NL: 5.21E5
T: {0,0} + c ESI !corona sid=75.00 det=1306.00 Full ms [105.00-800.00]
388.15
170.16
325.10
305.11
141.13
219.13
178.26
242.31
292.16
383.11
398.22
461.23
518.93
597.72
627.24
684.98
723.16
749.27
Relative Abundance
100 95 90 85 80 75 70 65 60 55 50 45 40 35 30 25 20 15 10 5 0
150 200 250 300 350 400 450 500 550 600 650 700 750 800
m/z

^{1}H, ^{13}C NMR, HPLC, and ESI data of compound **26e**

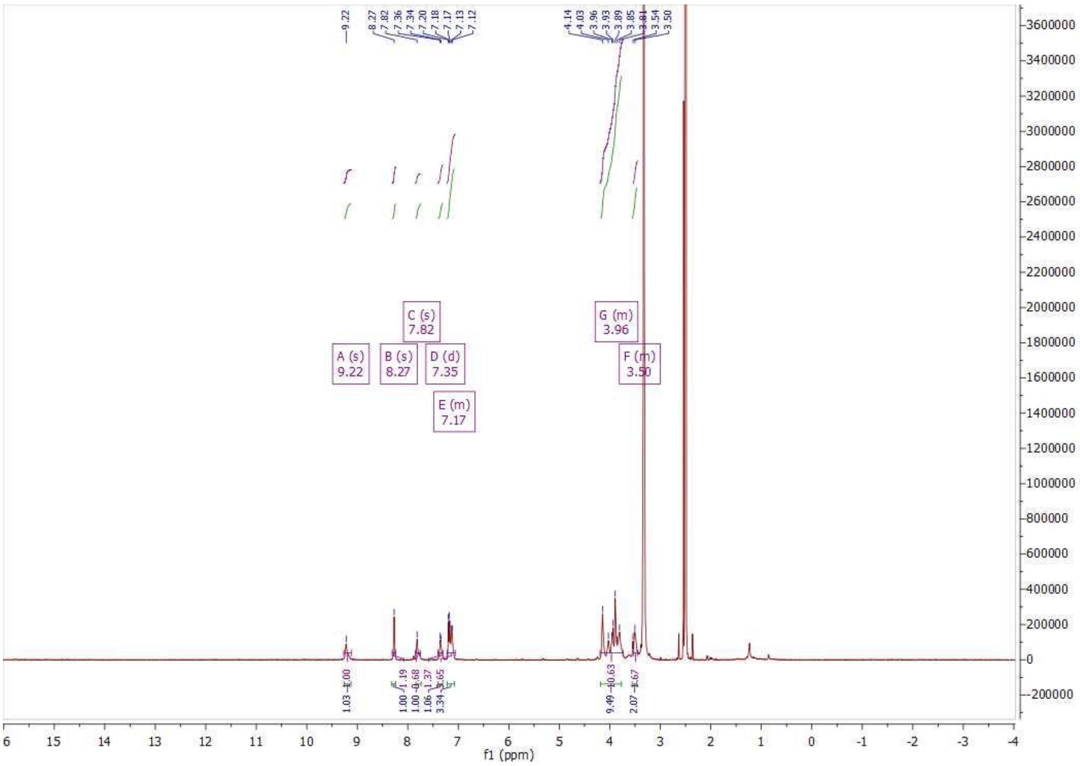

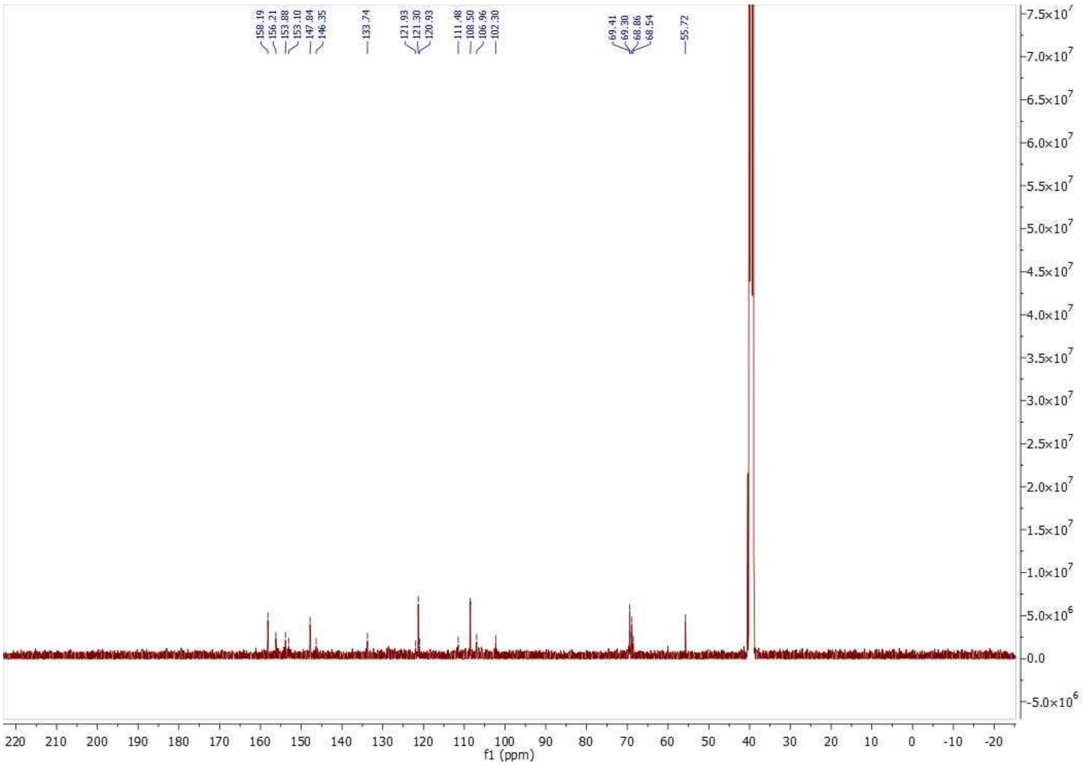

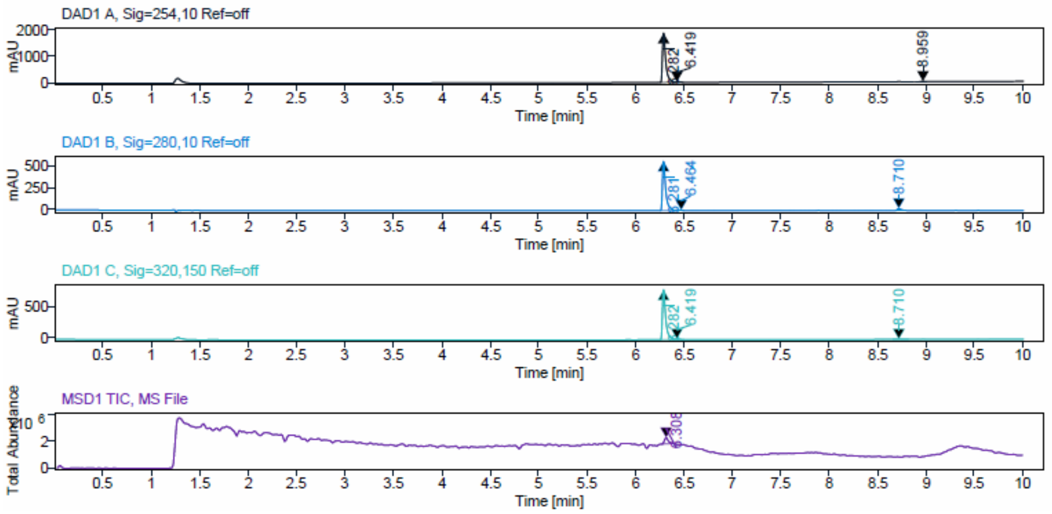

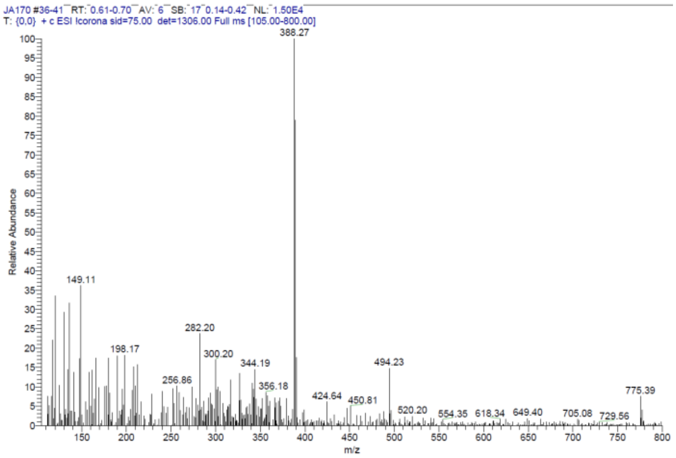

^{1}H, ^{13}C NMR, HPLC, and ESI data of compound **26f**

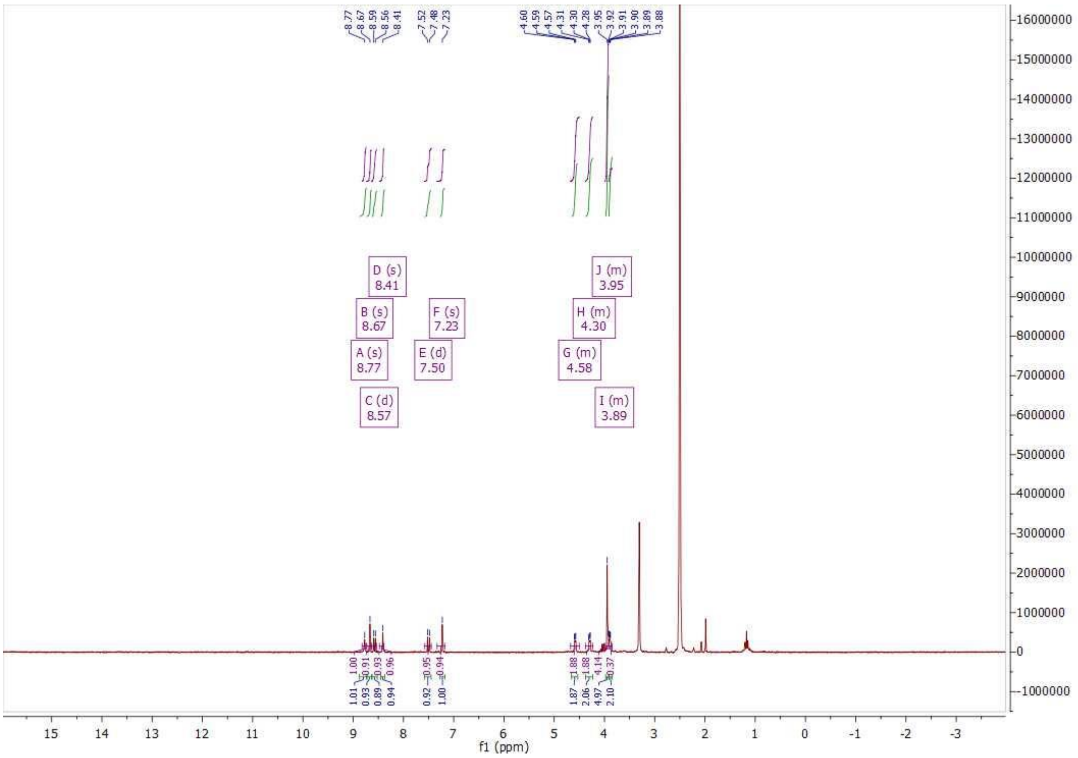

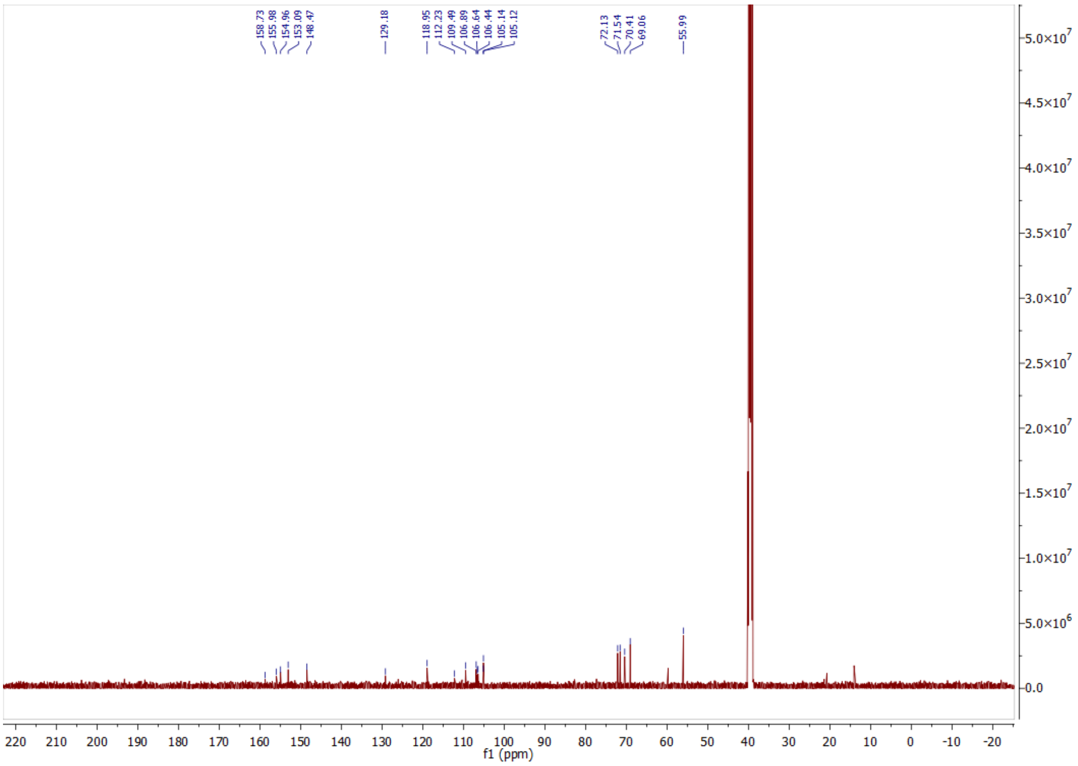
158.73
155.98
154.96
153.09
148.47
129.18
118.95
112.23
109.49
106.89
106.64
106.44
105.14
105.12
72.13
71.54
70.41
69.06
55.99
5.0×10^7
4.5×10^7
4.0×10^7
3.5×10^7
3.0×10^7
2.5×10^7
2.0×10^7
1.5×10^7
1.0×10^7
5.0×10^6
0.0
220 210 200 190 180 170 160 150 140 130 120 110 100 90 80 70 60 50 40 30 20 10 0 -10 -20
f1 (ppm)

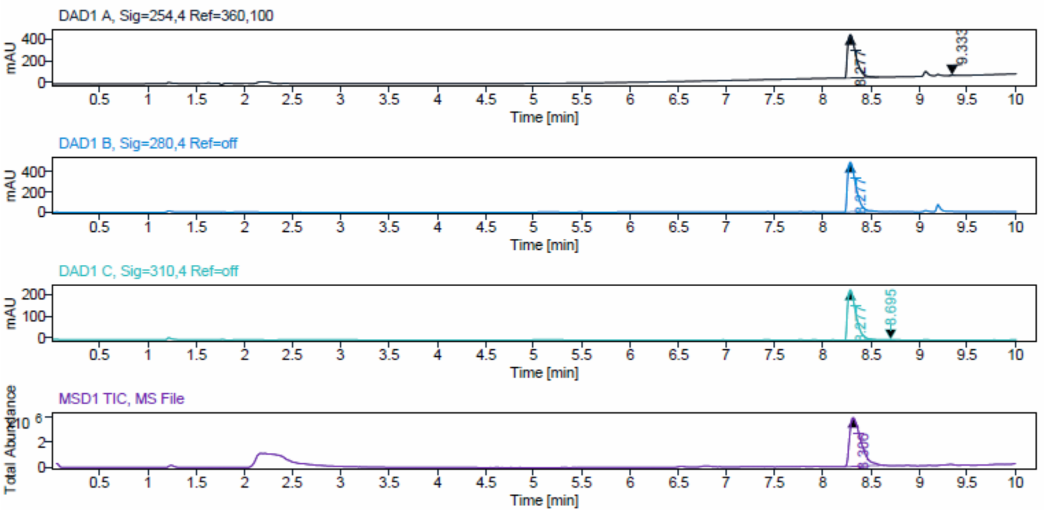
DAD1 A, Sig=254,4 Ref=360,100
mAU
400
200
0
8.277
9.333
Time [min]
DAD1 B, Sig=280,4 Ref=off
mAU
8.277
Time [min]
DAD1 C, Sig=310,4 Ref=off
mAU
200
100
0
8.277
8.695
Time [min]
MSD1 TIC, MS File
Total Abundance
x10^6
2
0
8.300
0.5 1 1.5 2 2.5 3 3.5 4 4.5 5 5.5 6 6.5 7 7.5 8 8.5 9 9.5 10
Time [min]

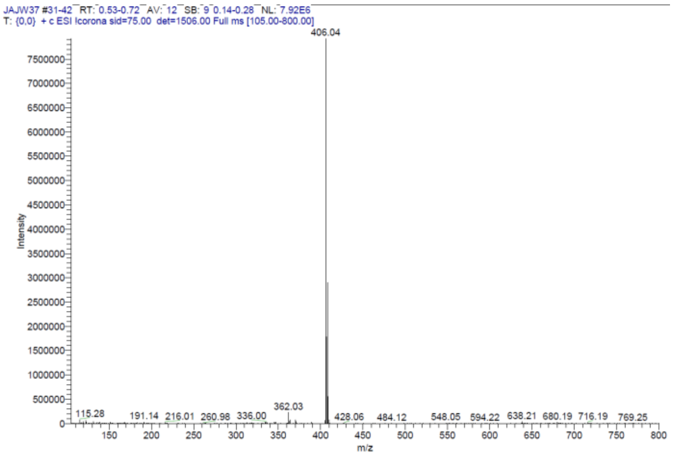
JAJW37 #31-42 RT: 0.53-0.72 AV: 12 SB: 9 0.14-0.28 NL: 7.92E6
T: {0,0} + c ESI Icorona sid=75.00 det=1506.00 Full ms [105.00-800.00]
406.04
362.03
115.28
191.14
216.01
260.98
336.00
428.06
484.12
548.05
594.22
638.21
680.19
716.19
769.25
Intensity
m/z

^{1}H NMR, ESI data of compound **34**

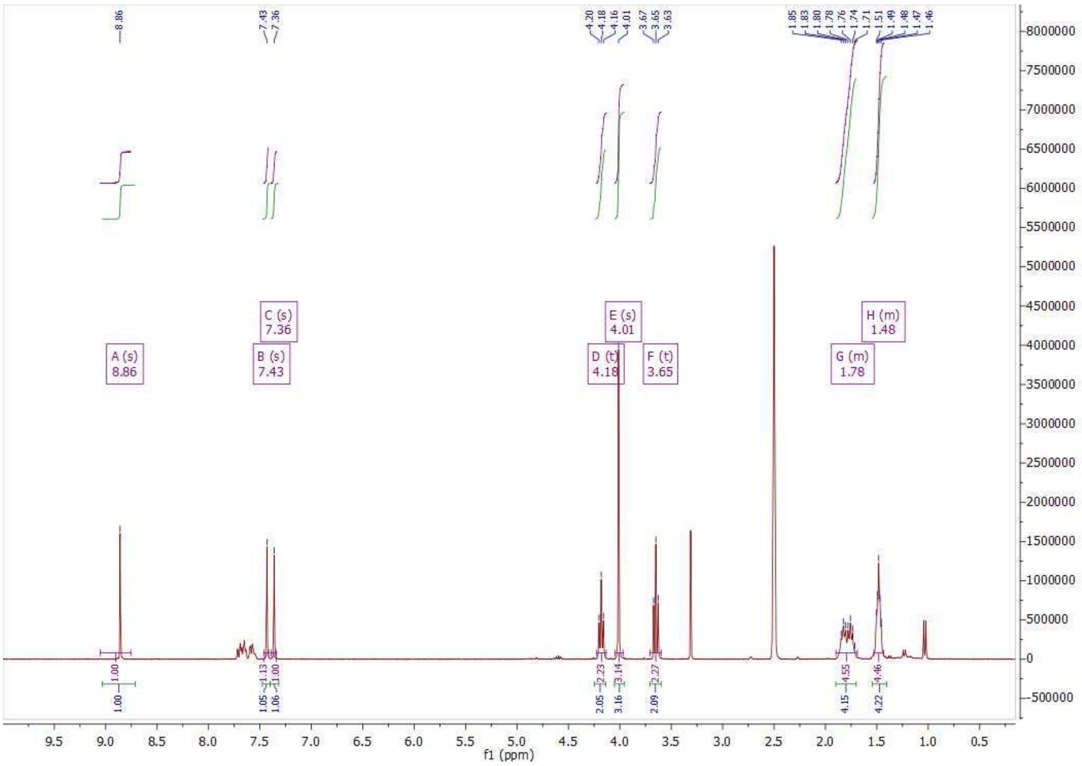

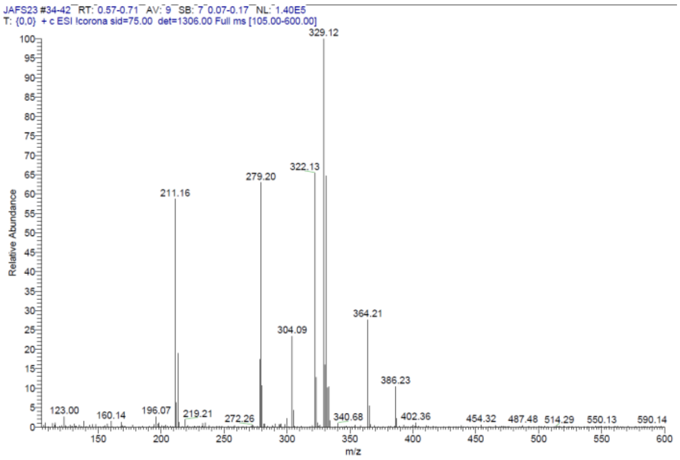

^{1}H, ^{13}C NMR, HPLC, and ESI data of compound **36a**

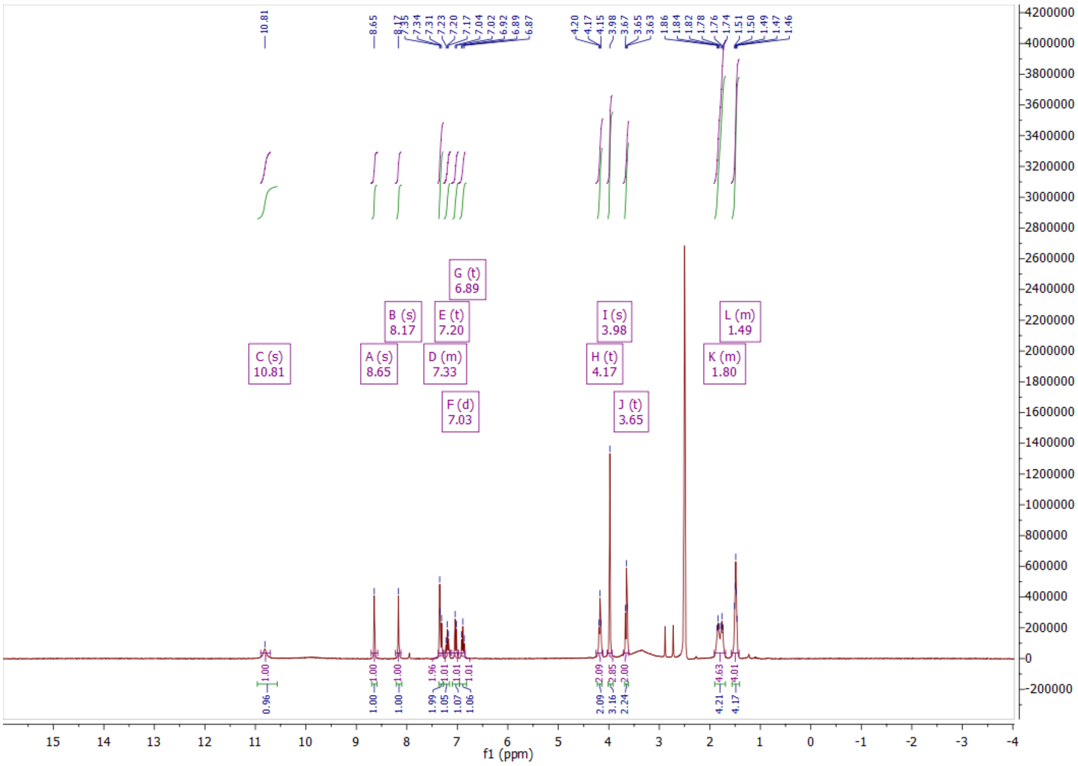

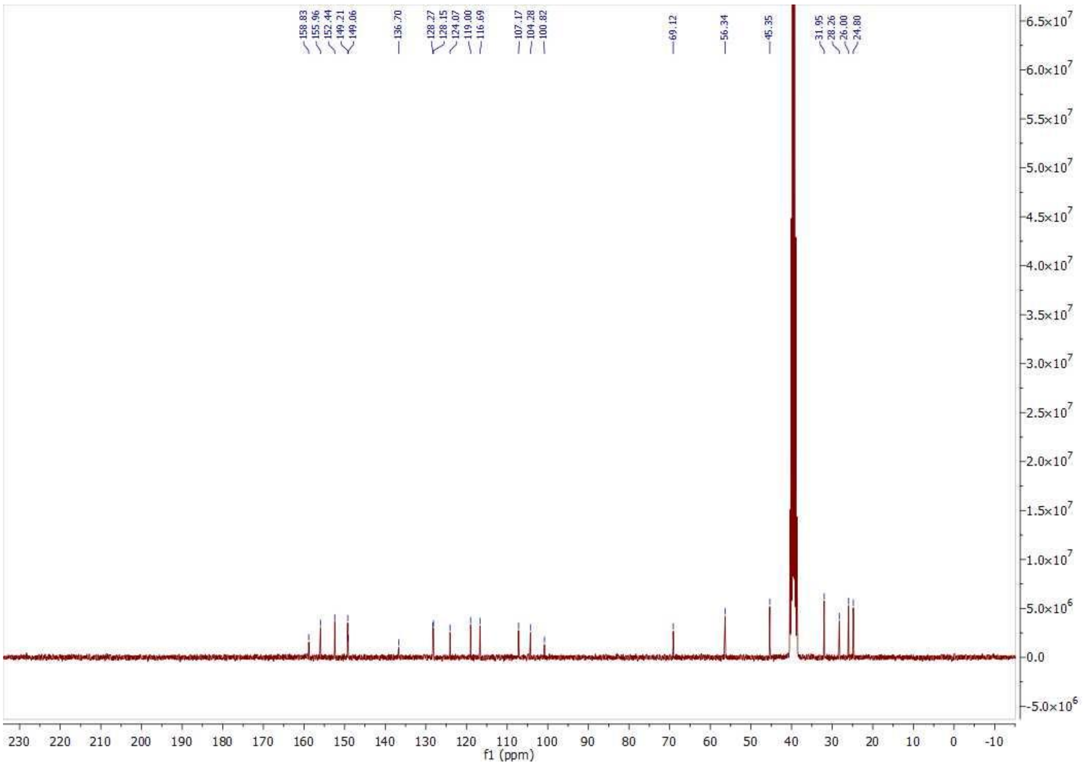

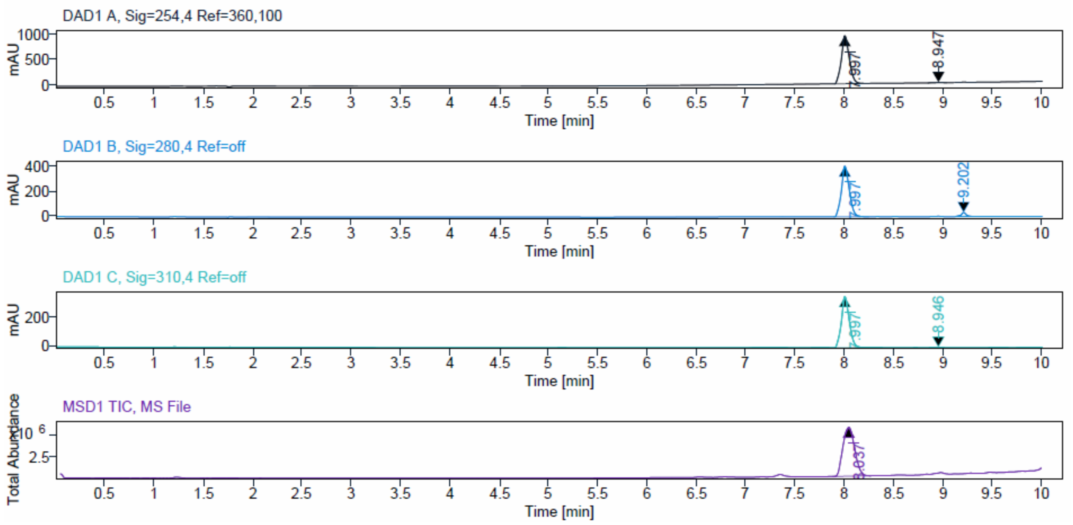

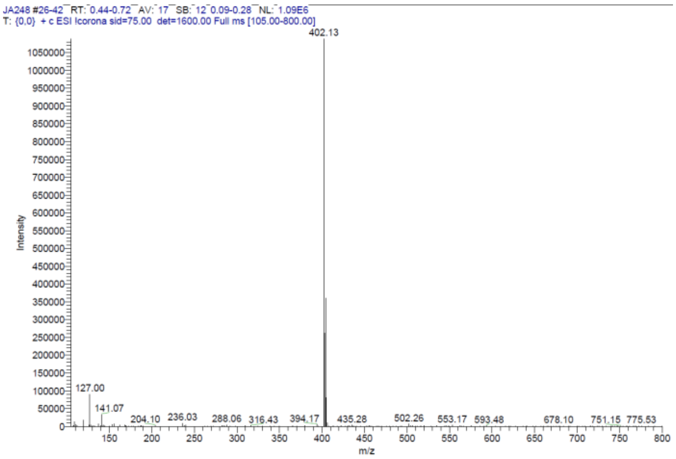

^{1}H, ^{13}C NMR, HPLC, and ESI data of compound **36b**

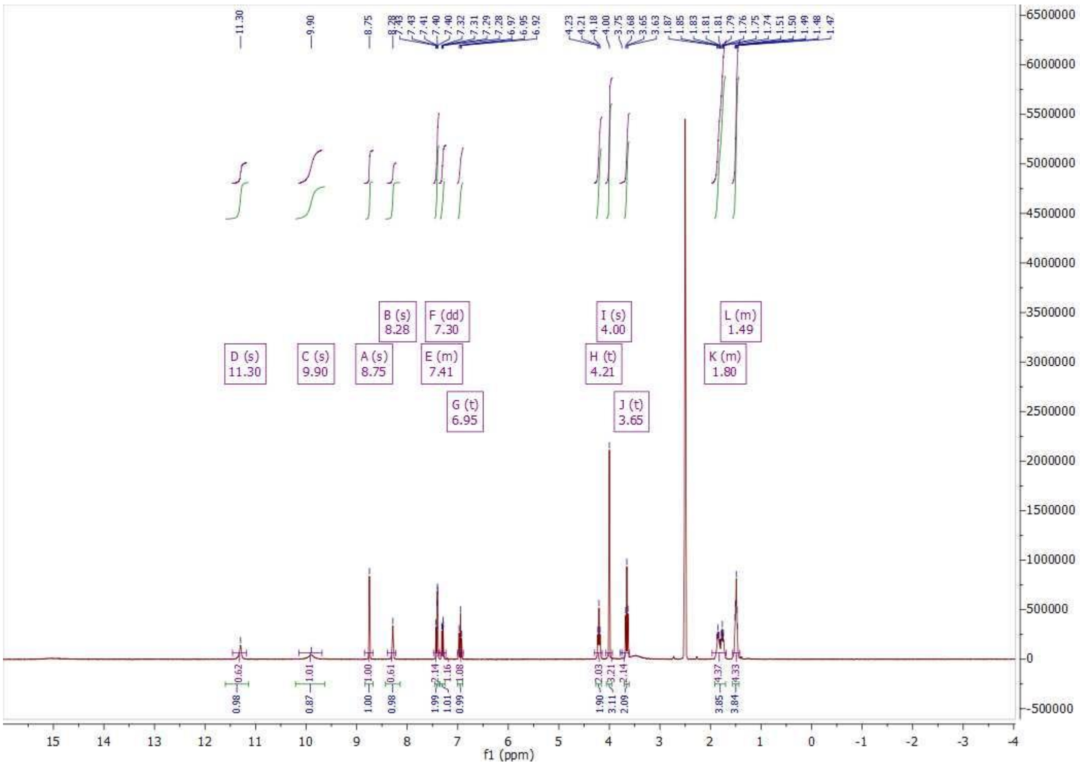

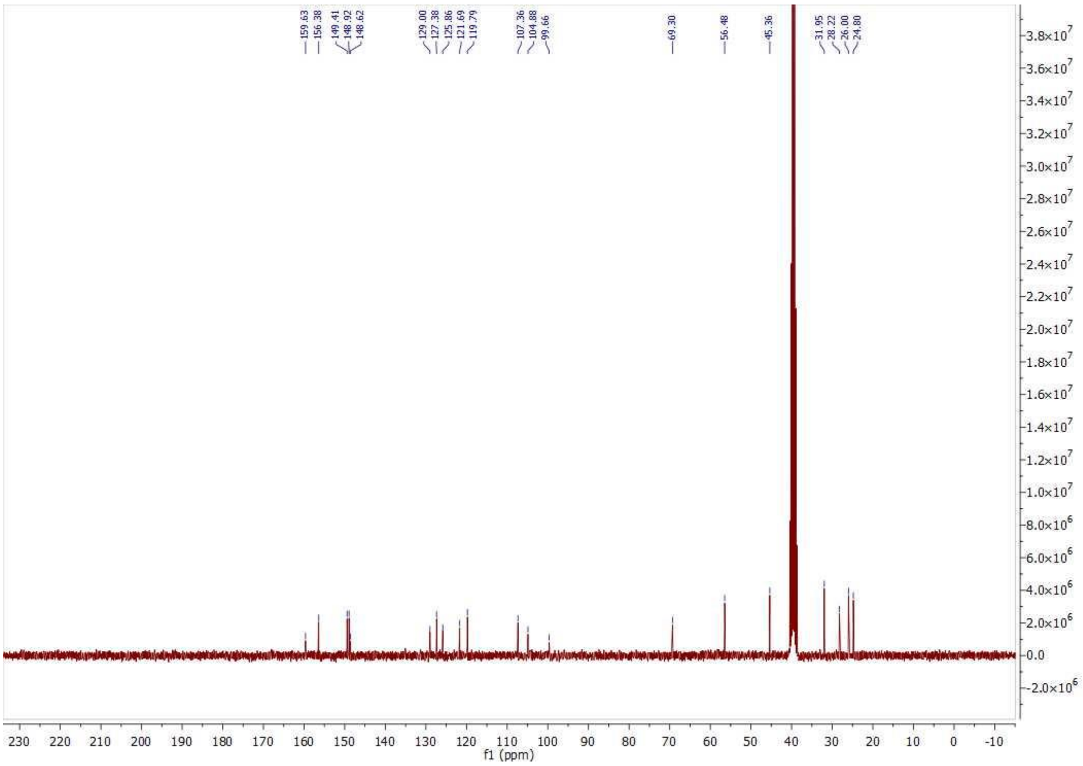
159.63
156.38
149.41
148.92
148.62
129.00
127.38
125.86
121.69
119.79
107.36
104.88
99.66
69.30
56.48
45.36
31.95
28.22
26.00
24.80
3.8×10^7
3.6×10^7
3.4×10^7
3.2×10^7
3.0×10^7
2.8×10^7
2.6×10^7
2.4×10^7
2.2×10^7
2.0×10^7
1.8×10^7
1.6×10^7
1.4×10^7
1.2×10^7
1.0×10^7
8.0×10^6
6.0×10^6
4.0×10^6
2.0×10^6
0.0
-2.0×10^6
230 220 210 200 190 180 170 160 150 140 130 120 110 100 90 80 70 60 50 40 30 20 10 0 -10
f1 (ppm)

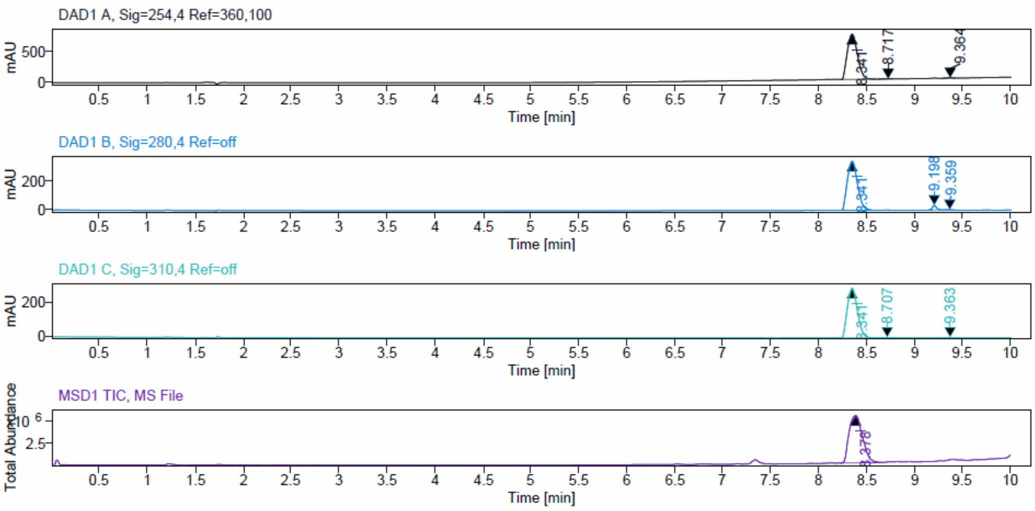
DAD1 A, Sig=254,4 Ref=360,100
mAU
500
0
8.341
8.717
9.364
0.5 1 1.5 2 2.5 3 3.5 4 4.5 5 5.5 6 6.5 7 7.5 8 8.5 9 9.5 10
Time [min]
DAD1 B, Sig=280,4 Ref=off
mAU
200
0
8.341
9.198
9.359
0.5 1 1.5 2 2.5 3 3.5 4 4.5 5 5.5 6 6.5 7 7.5 8 8.5 9 9.5 10
Time [min]
DAD1 C, Sig=310,4 Ref=off
mAU
200
0
8.341
8.707
9.363
0.5 1 1.5 2 2.5 3 3.5 4 4.5 5 5.5 6 6.5 7 7.5 8 8.5 9 9.5 10
Time [min]
MSD1 TIC, MS File
Total Abundance
x10 6
2.5
8.378
0.5 1 1.5 2 2.5 3 3.5 4 4.5 5 5.5 6 6.5 7 7.5 8 8.5 9 9.5 10
Time [min]

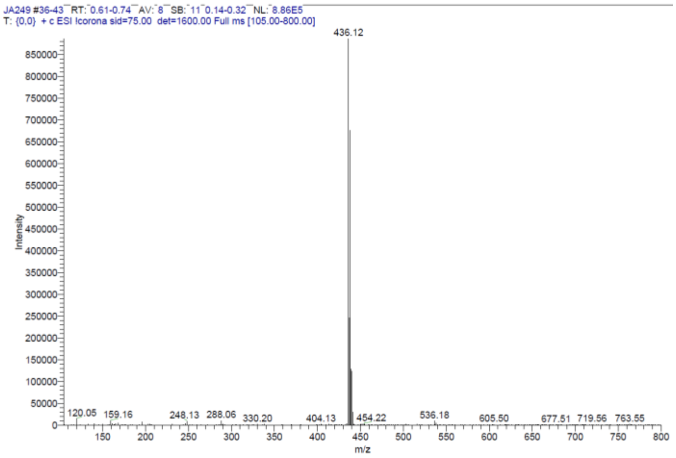
JA249 #36-43 RT: 0.61-0.74 AV: 8 SB: 11 0.14-0.32 NL: 8.86E5
T: {0,0} + c ESI !corona sid=75.00 det=1600.00 Full ms [105.00-800.00]
436.12
850000
800000
750000
700000
650000
600000
550000
500000
450000
400000
350000
300000
250000
200000
150000
100000
50000
0
Intensity
120.05
159.16
248.13
288.06
330.20
404.13
454.22
536.18
605.50
677.51
719.56
763.55
150 200 250 300 350 400 450 500 550 600 650 700 750 800
m/z

^1H, ^{13}C NMR, HPLC, and ESI data of compound **36c**

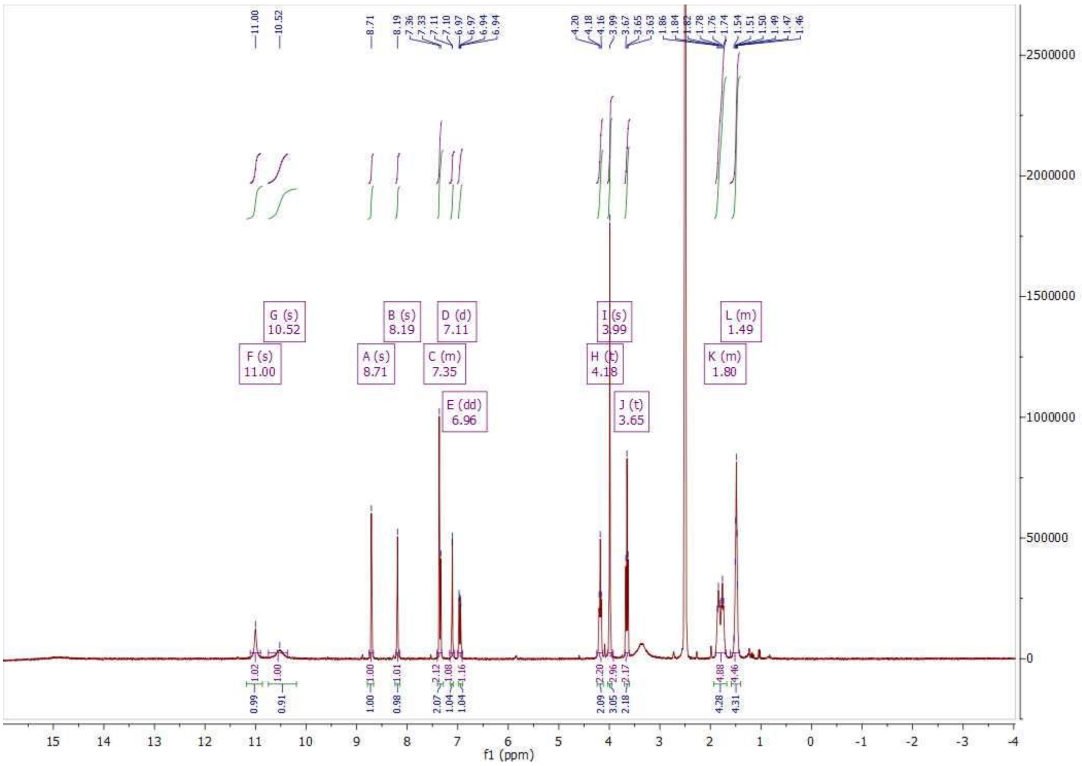

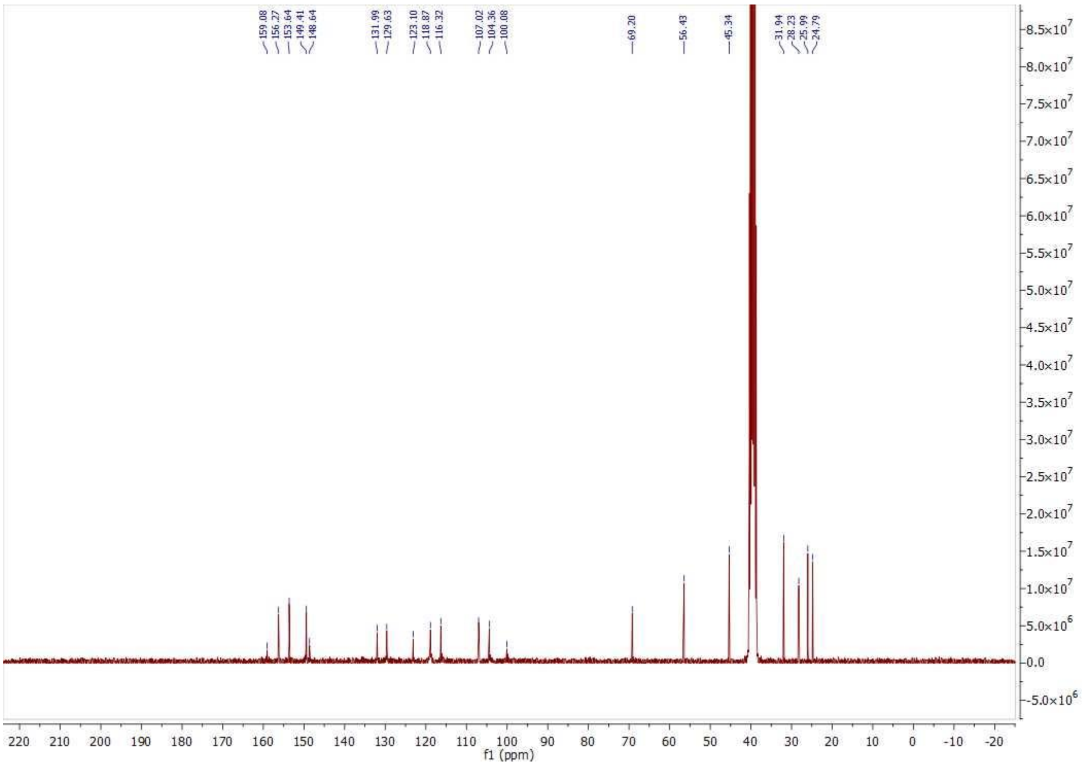

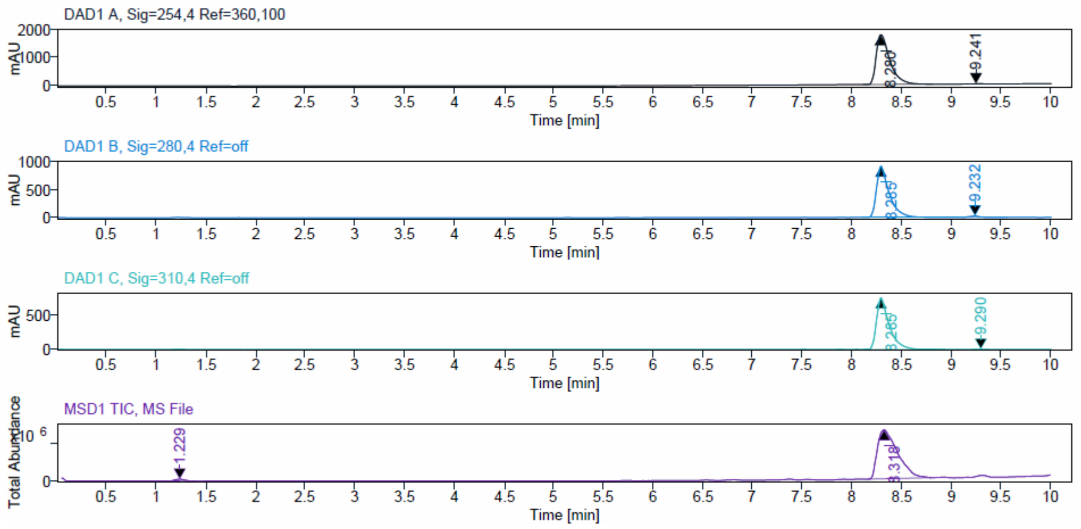

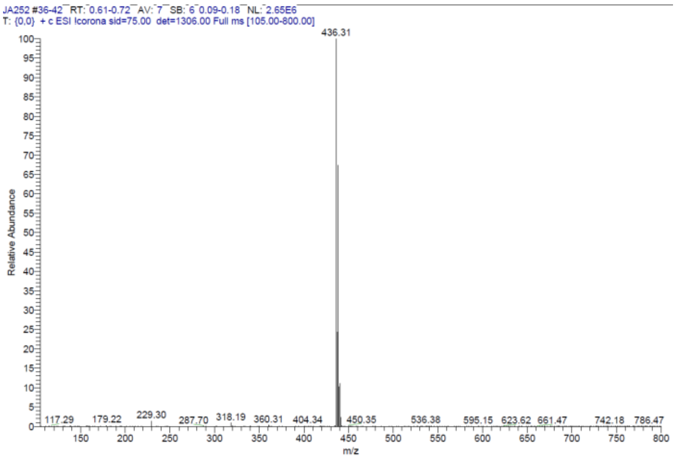

^{1}H, ^{13}C NMR, HPLC, and ESI data of compound **36d**

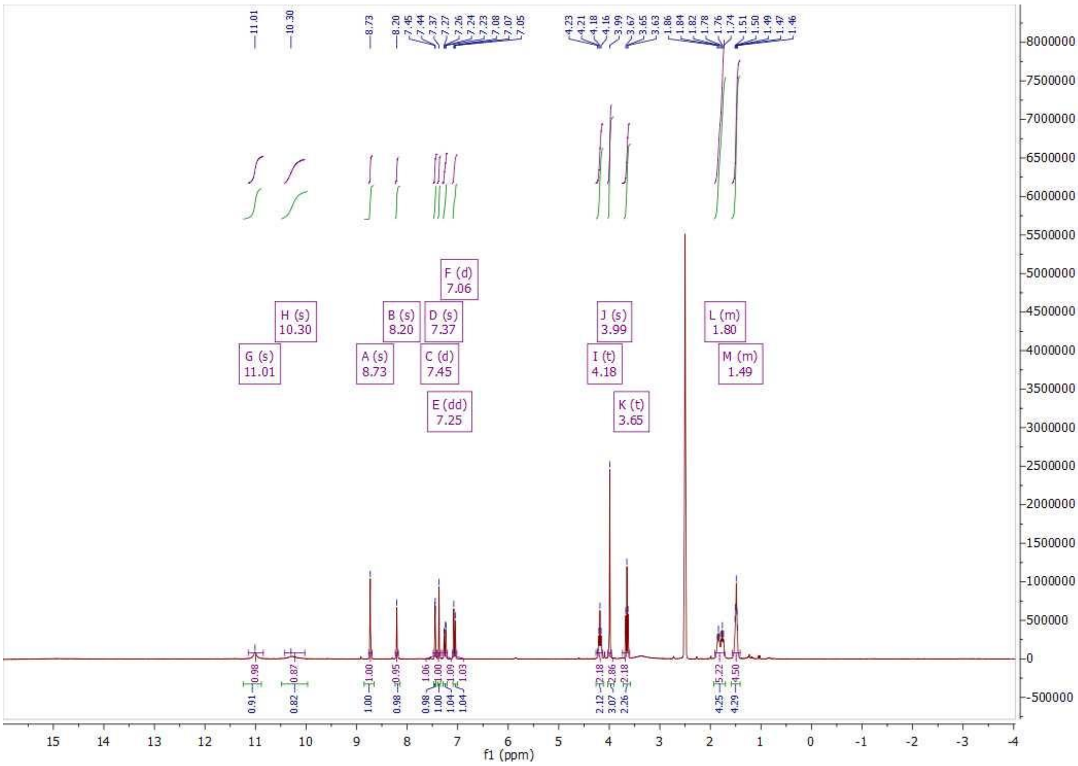

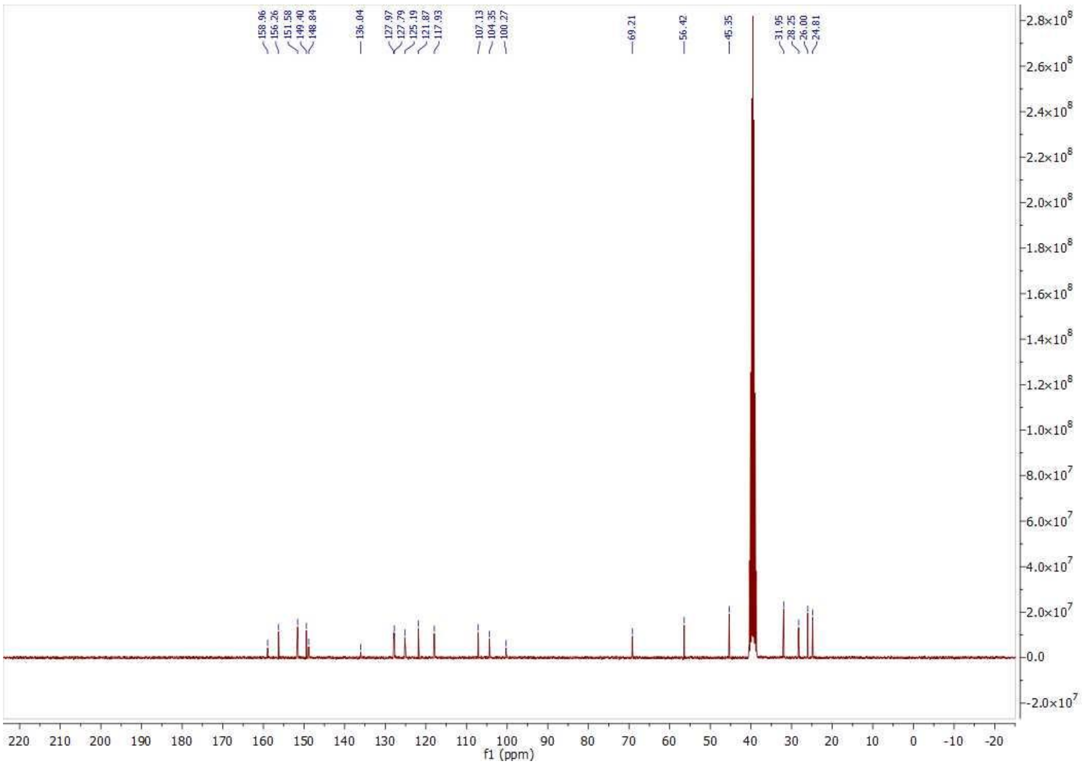
158.96
156.26
151.58
149.40
148.84
136.04
127.97
127.79
125.19
121.87
117.93
107.13
104.35
100.27
69.21
56.42
45.35
31.95
28.25
26.00
24.81
2.8×10^8
2.6×10^8
2.4×10^8
2.2×10^8
2.0×10^8
1.8×10^8
1.6×10^8
1.4×10^8
1.2×10^8
1.0×10^8
8.0×10^7
6.0×10^7
4.0×10^7
2.0×10^7
0.0
-2.0×10^7
220 210 200 190 180 170 160 150 140 130 120 110 100 90 80 70 60 50 40 30 20 10 0 -10 -20
f1 (ppm)

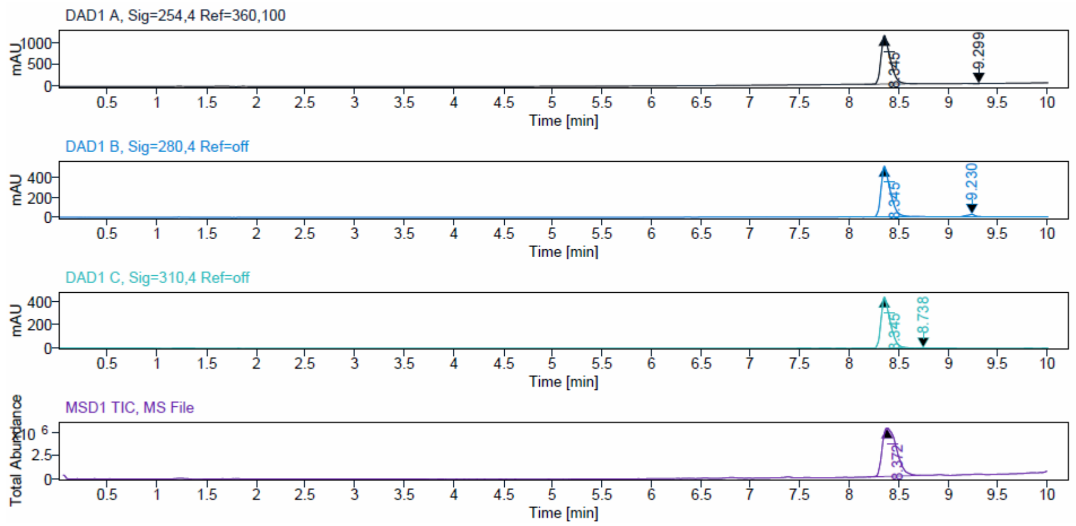
DAD1 A, Sig=254,4 Ref=360,100
mAU
1000
500
0
8.345
9.299
Time [min]
DAD1 B, Sig=280,4 Ref=off
mAU
400
200
0
8.345
9.230
Time [min]
DAD1 C, Sig=310,4 Ref=off
mAU
400
200
0
8.345
8.738
Time [min]
MSD1 TIC, MS File
Total Abundance
x10 6
2.5
0
8.372
0.5 1 1.5 2 2.5 3 3.5 4 4.5 5 5.5 6 6.5 7 7.5 8 8.5 9 9.5 10
Time [min]

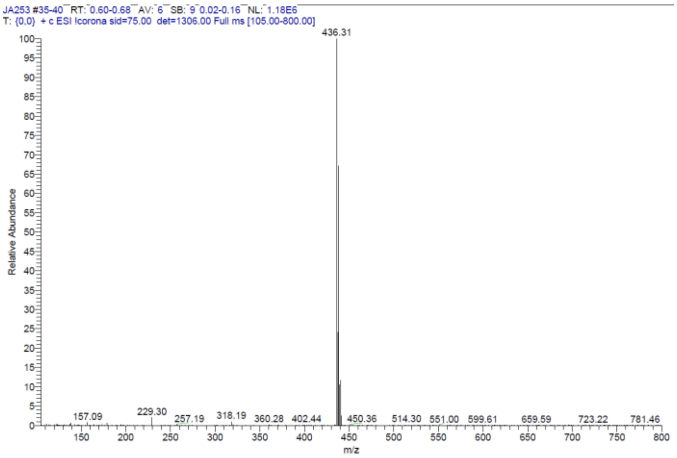
JA253 #35-40 RT: 0.60-0.68 AV: 6 SB: 9 0.02-0.16 NL: 1.18E6
T: {0,0} + c ESI !corona sid=75.00 det=1306.00 Full ms [105.00-800.00]
436.31
157.09
229.30
257.19
318.19
360.28
402.44
450.36
514.30
551.00
599.61
659.59
723.22
781.46
Relative Abundance
100 95 90 85 80 75 70 65 60 55 50 45 40 35 30 25 20 15 10 5 0
150 200 250 300 350 400 450 500 550 600 650 700 750 800
m/z

^{1}H, ^{13}C NMR, HPLC, and ESI data of compound **36e**

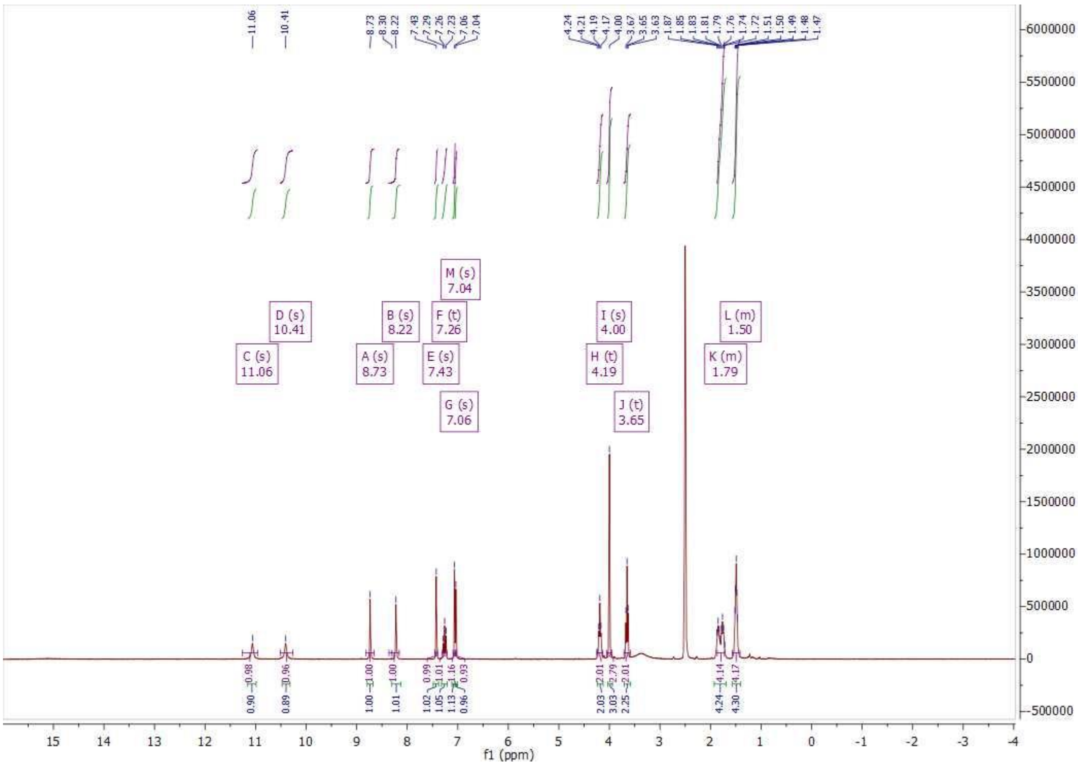

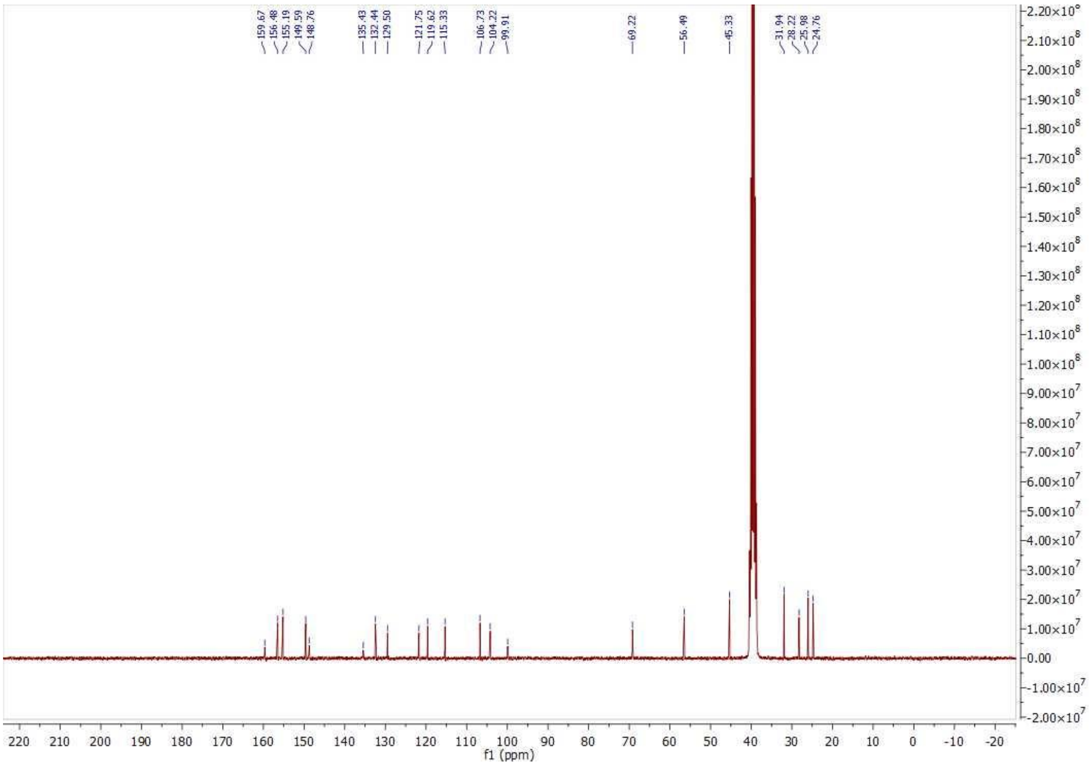

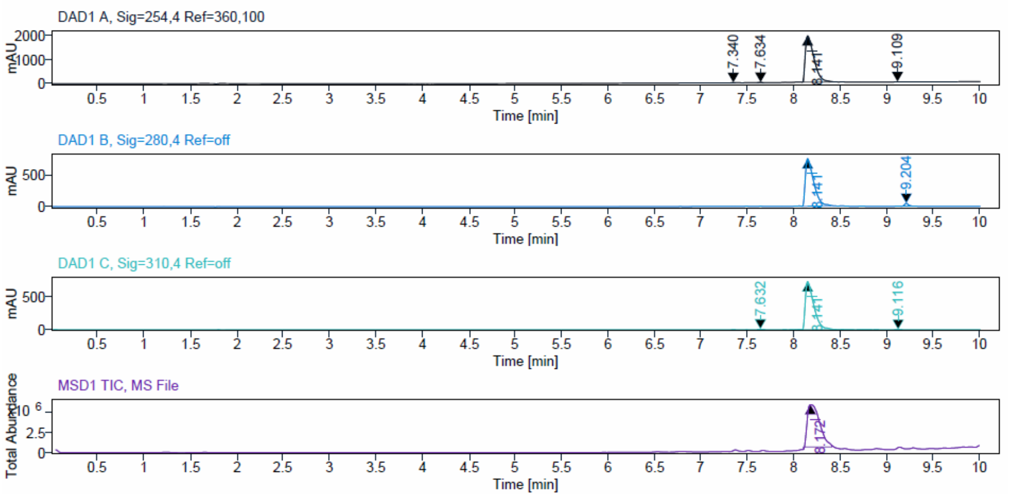

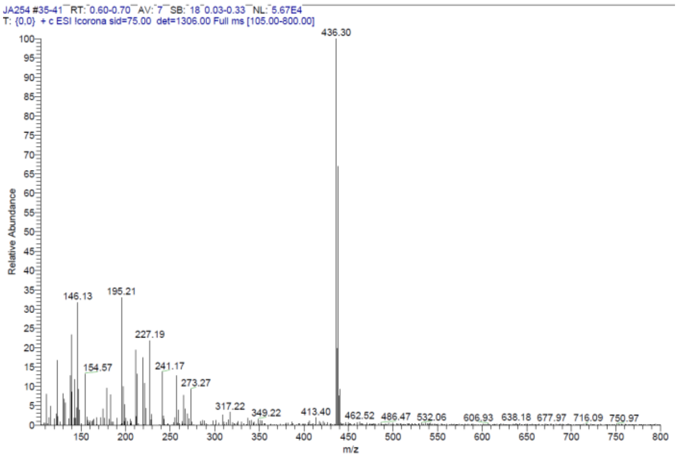

^{1}H, ^{13}C NMR, HPLC, and ESI data of compound **36f**

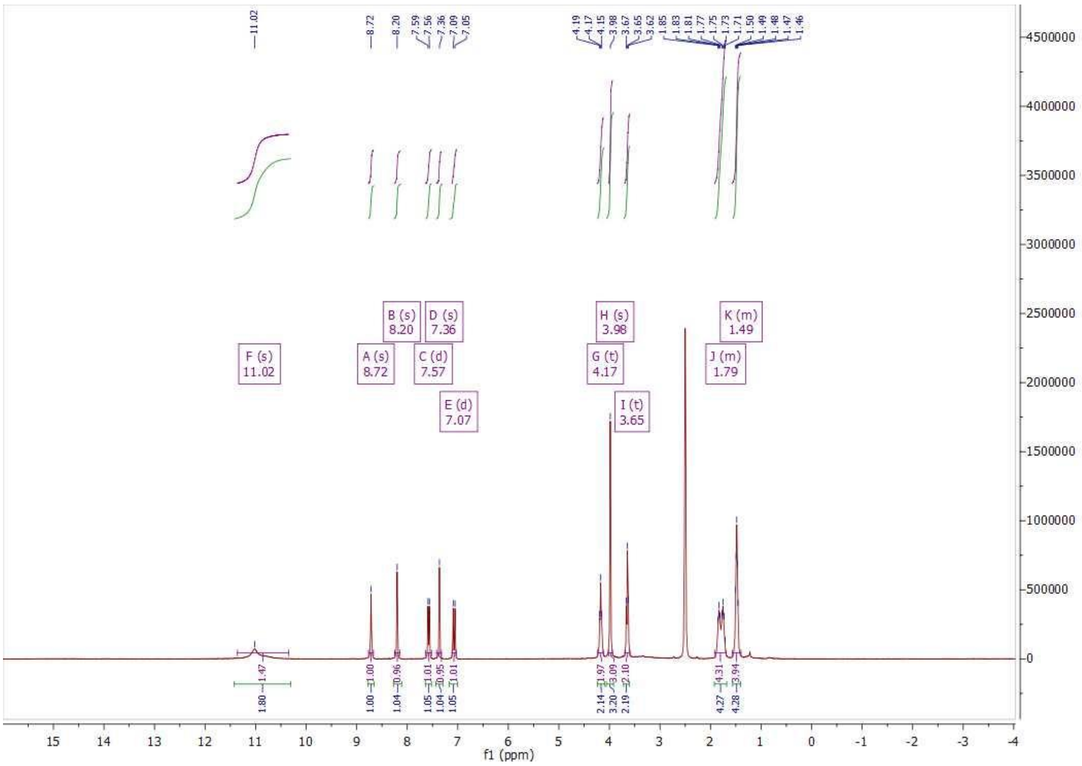

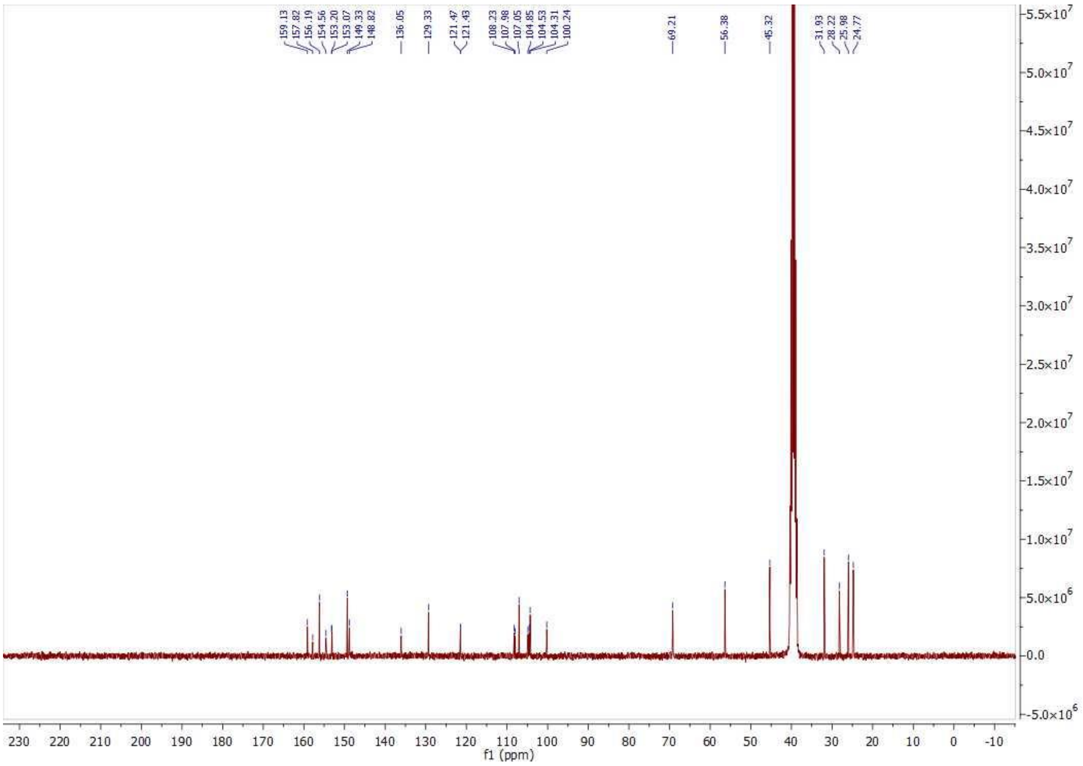

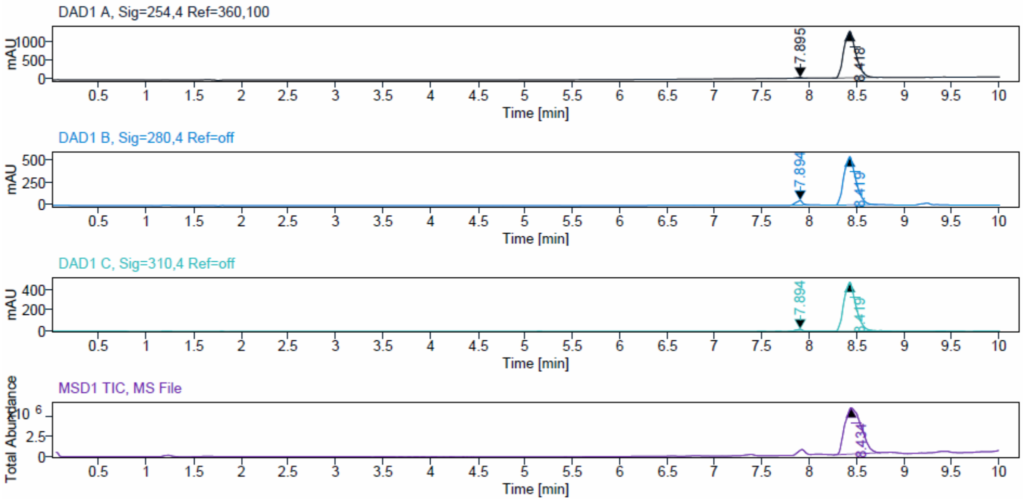

JA255 #34-43 RT: 0.58-0.74 AV: 10 SB: 31 0.07-0.60 NL: 2.35E5
T: {0,0} + c ESI !corona sid=75.00 det=1306.00 Full ms [105.00-800.00]

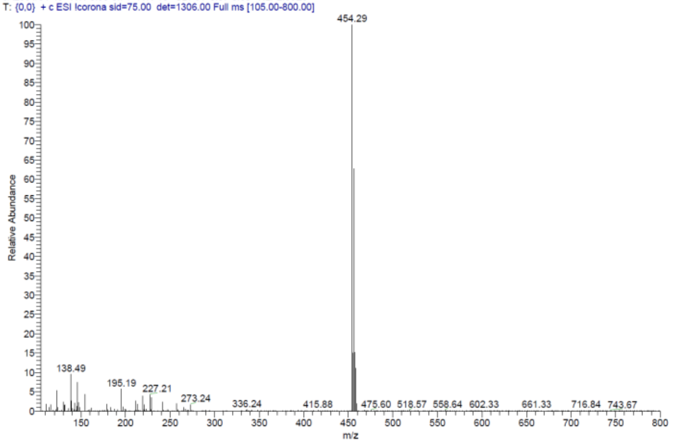

^{1}H, ^{13}C NMR, HPLC, and ESI data of compound **37a**

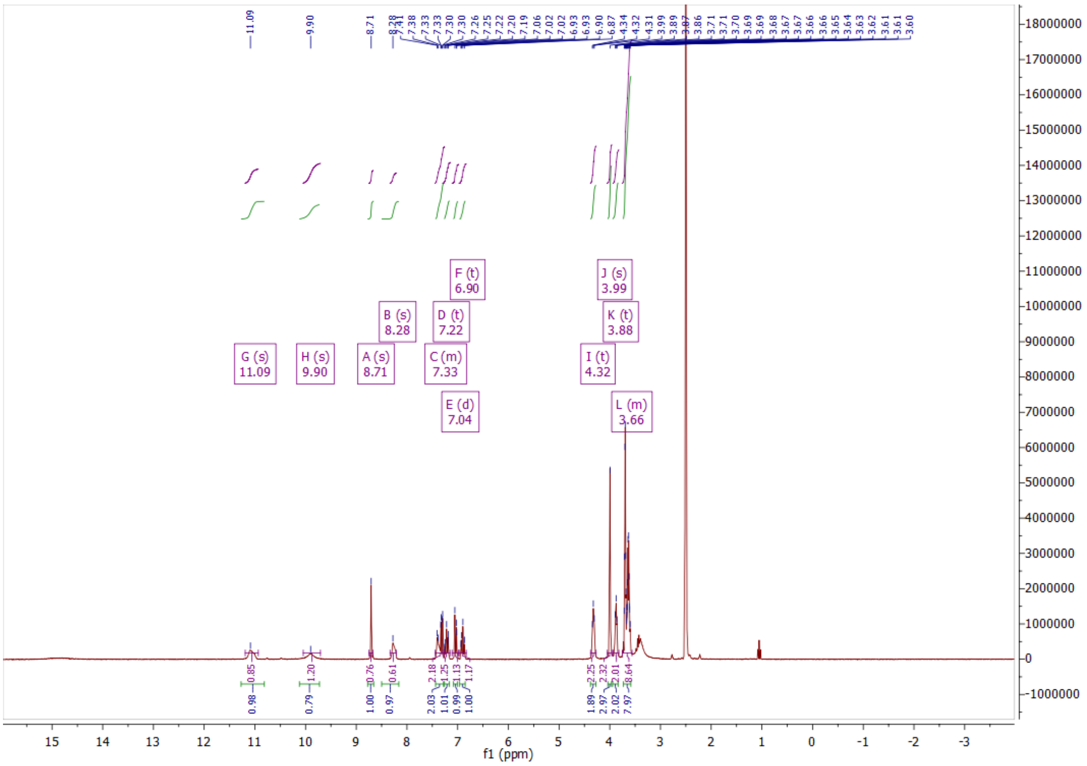

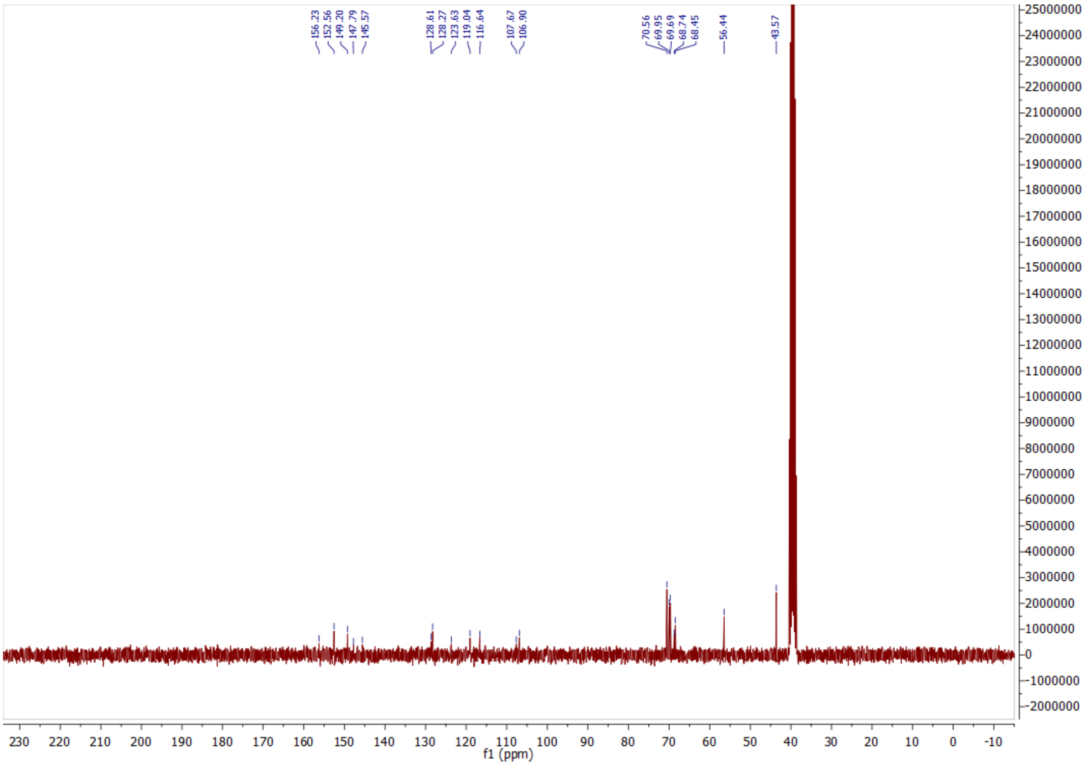

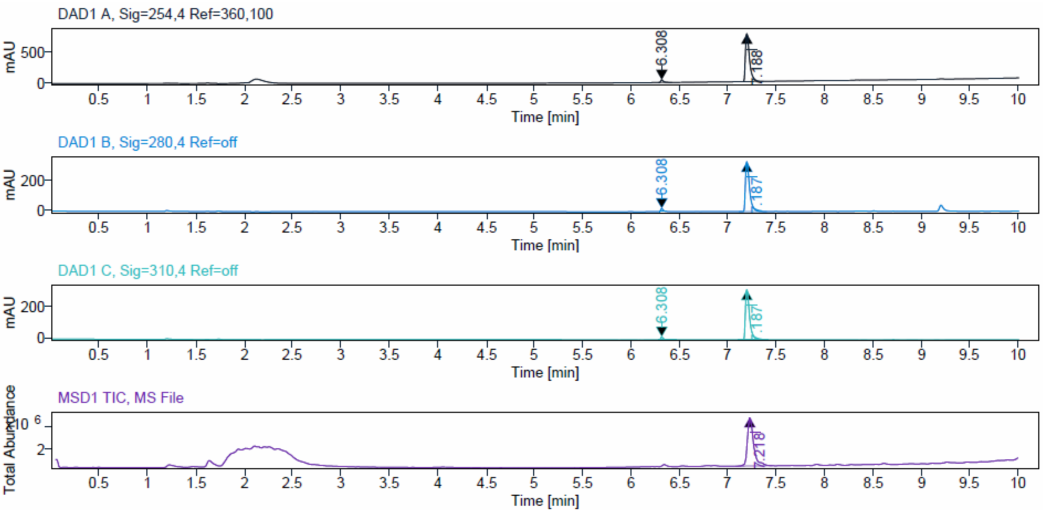

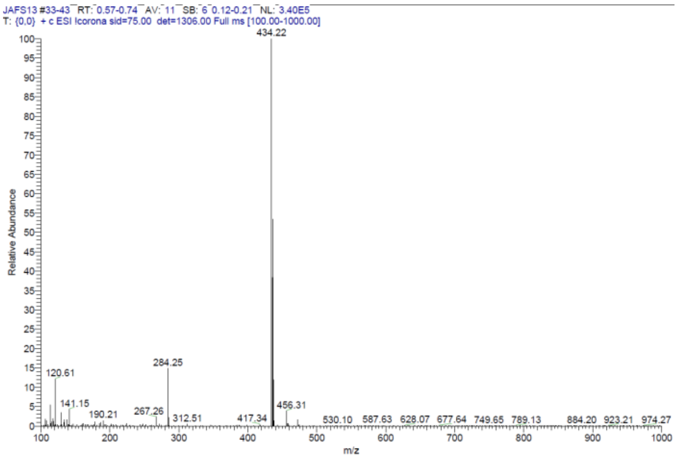

^{1}H, ^{13}C NMR, HPLC, and ESI data of compound **37b**

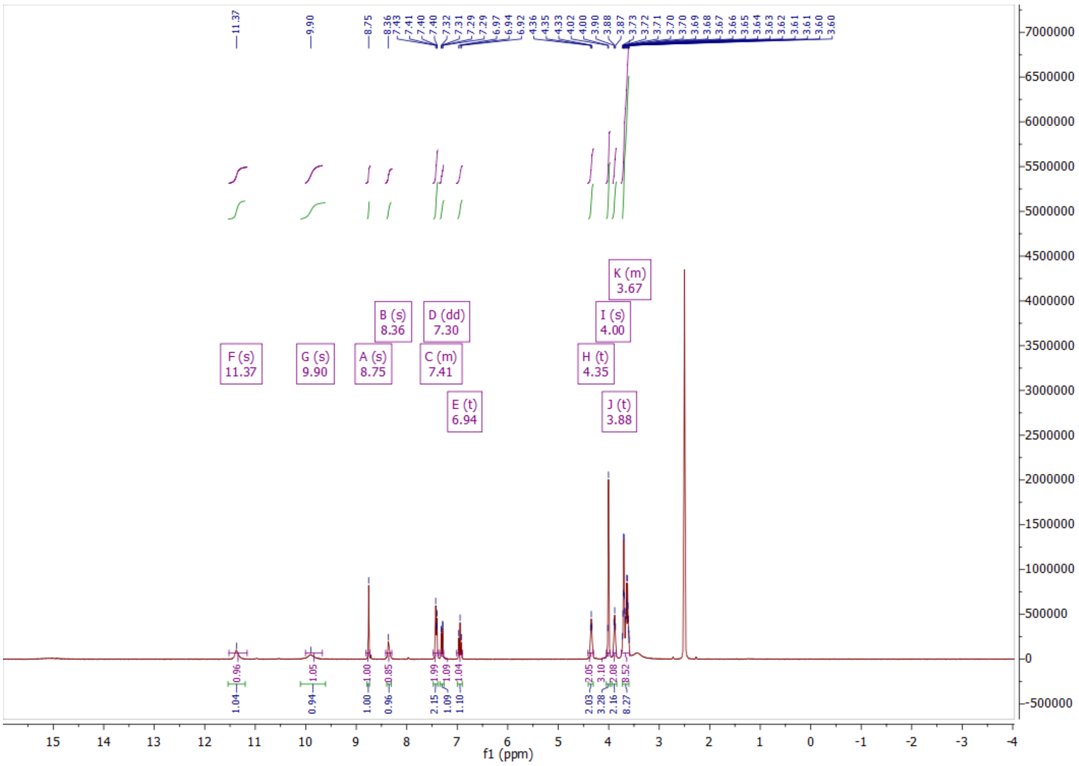

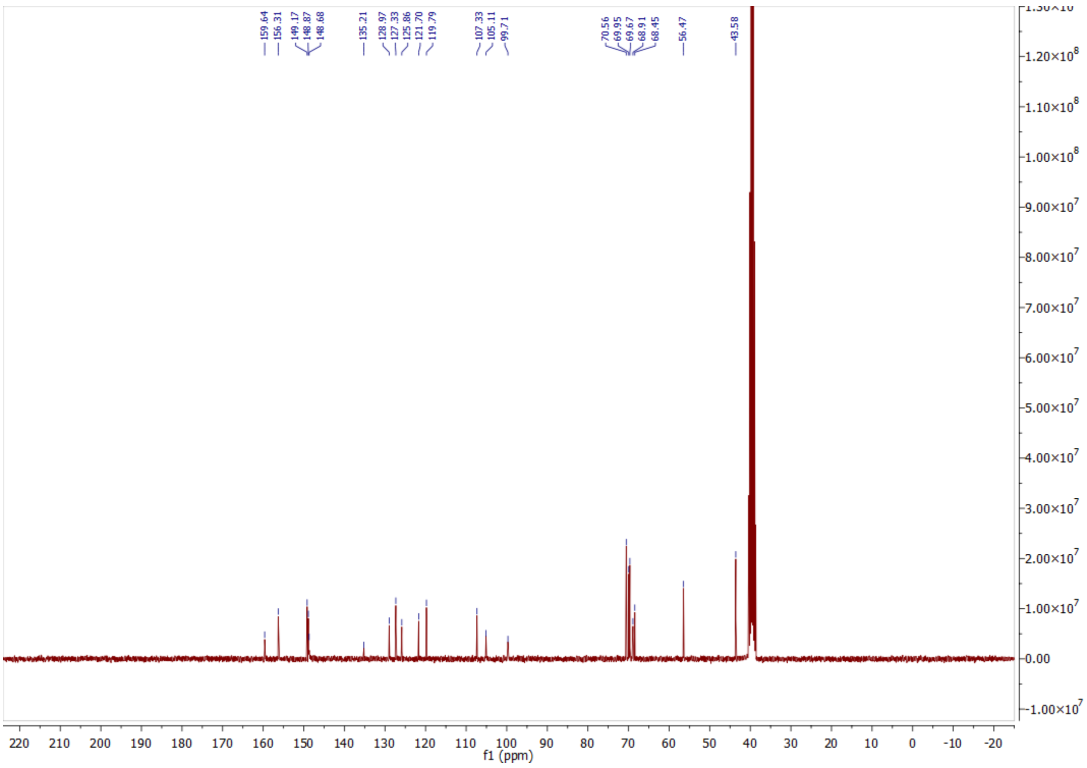
159.64
156.31
149.17
148.87
148.68
135.21
128.97
127.33
125.86
121.70
119.79
107.33
105.11
99.71
70.56
69.95
69.67
68.91
68.45
56.47
43.58
1.20×10⁸
1.10×10⁸
1.00×10⁸
9.00×10⁷
8.00×10⁷
7.00×10⁷
6.00×10⁷
5.00×10⁷
4.00×10⁷
3.00×10⁷
2.00×10⁷
1.00×10⁷
0.00
-1.00×10⁷
220 210 200 190 180 170 160 150 140 130 120 110 100 90 80 70 60 50 40 30 20 10 0 -10 -20
f1 (ppm)

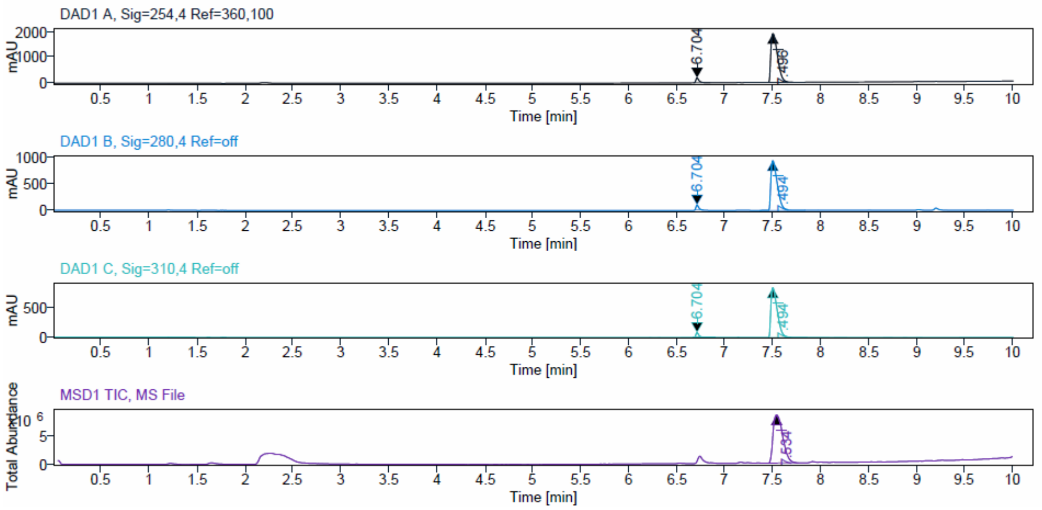
DAD1 A, Sig=254,4 Ref=360,100
mAU
2000
1000
0
6.704
7.496
DAD1 B, Sig=280,4 Ref=off
1000
500
0
6.704
7.494
DAD1 C, Sig=310,4 Ref=off
500
0
6.704
7.494
MSD1 TIC, MS File
Total Abundance
×10⁶
5
0
7.534
0.5 1 1.5 2 2.5 3 3.5 4 4.5 5 5.5 6 6.5 7 7.5 8 8.5 9 9.5 10
Time [min]

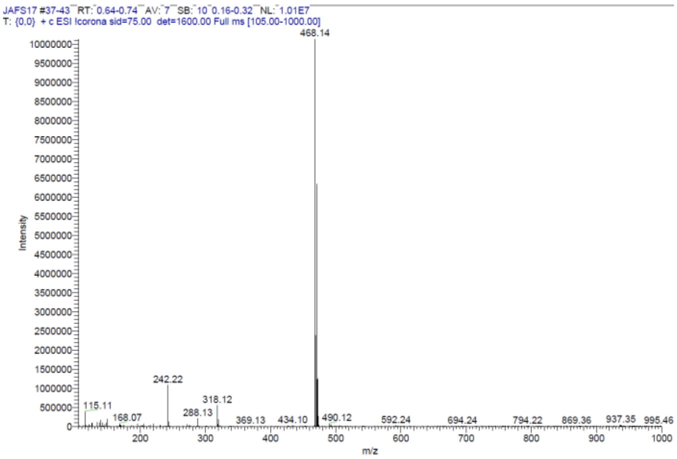
JAFS17 #37-43 RT: 0.64-0.74 AV: 7 SB: 10 0.16-0.32 NL: 1.01E7
T: {0,0} + c ESI !corona sid=75.00 det=1600.00 Full ms [105.00-1000.00]
468.14
242.22
318.12
288.13
115.11
168.07
369.13
434.10
490.12
592.24
694.24
794.22
869.36
937.35
995.46
Intensity
10000000
9500000
9000000
8500000
8000000
7500000
7000000
6500000
6000000
5500000
5000000
4500000
4000000
3500000
3000000
2500000
2000000
1500000
1000000
500000
0
200 300 400 500 600 700 800 900 1000
m/z

^{1}H, ^{13}C NMR, HPLC, and ESI data of compound **37c**

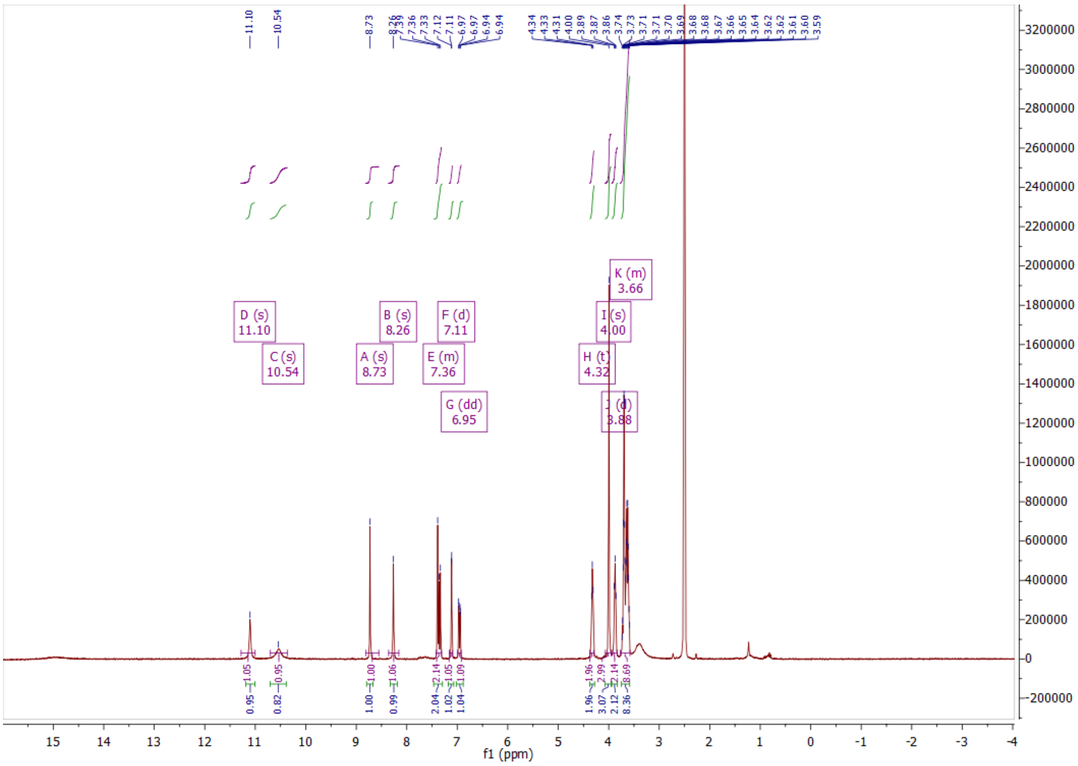

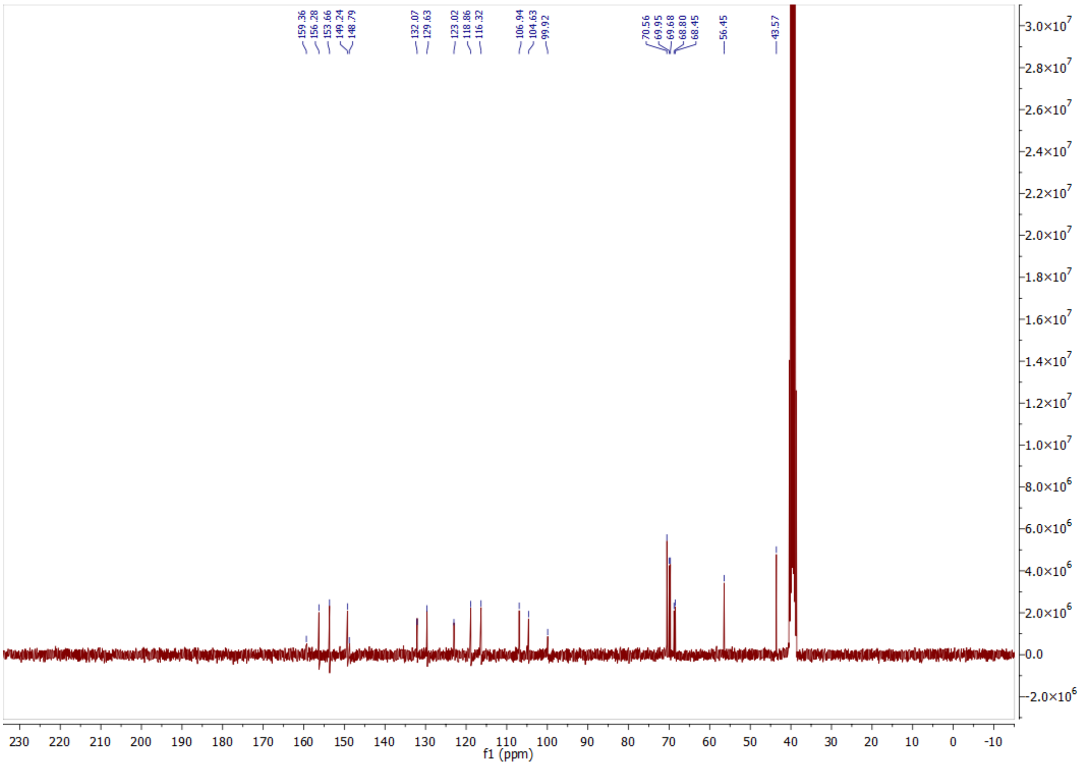

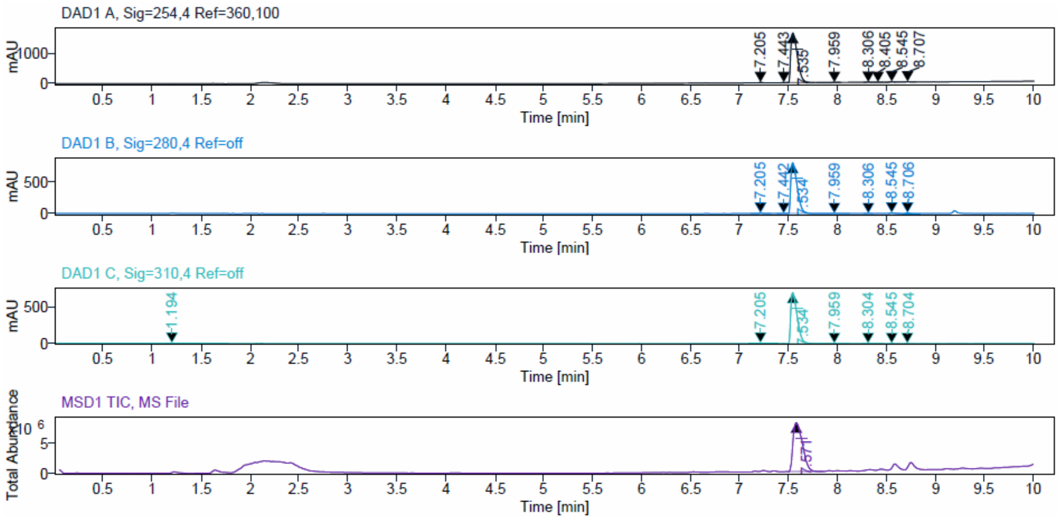

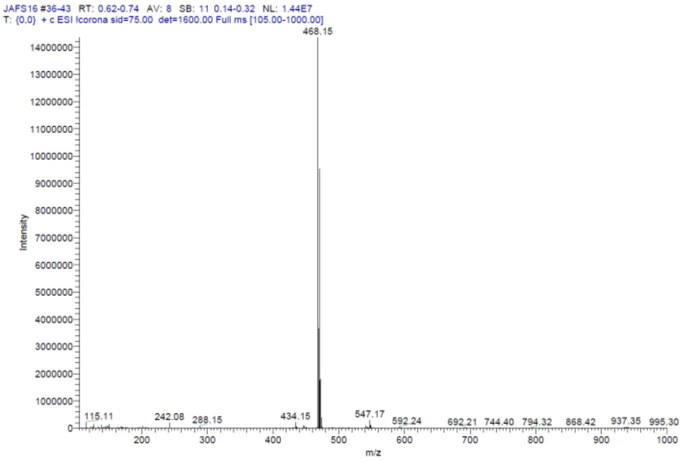

ESI, HRMS, ^{1}H, ^{13}C NMR and HPLC data of compound **37d**

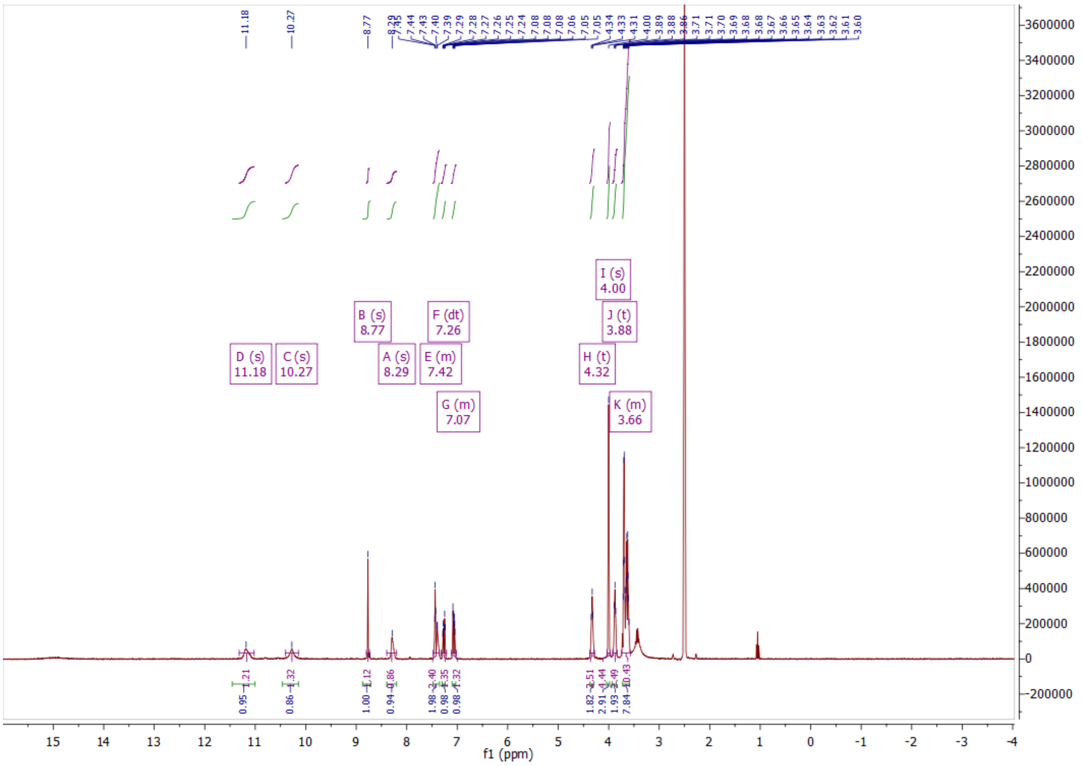

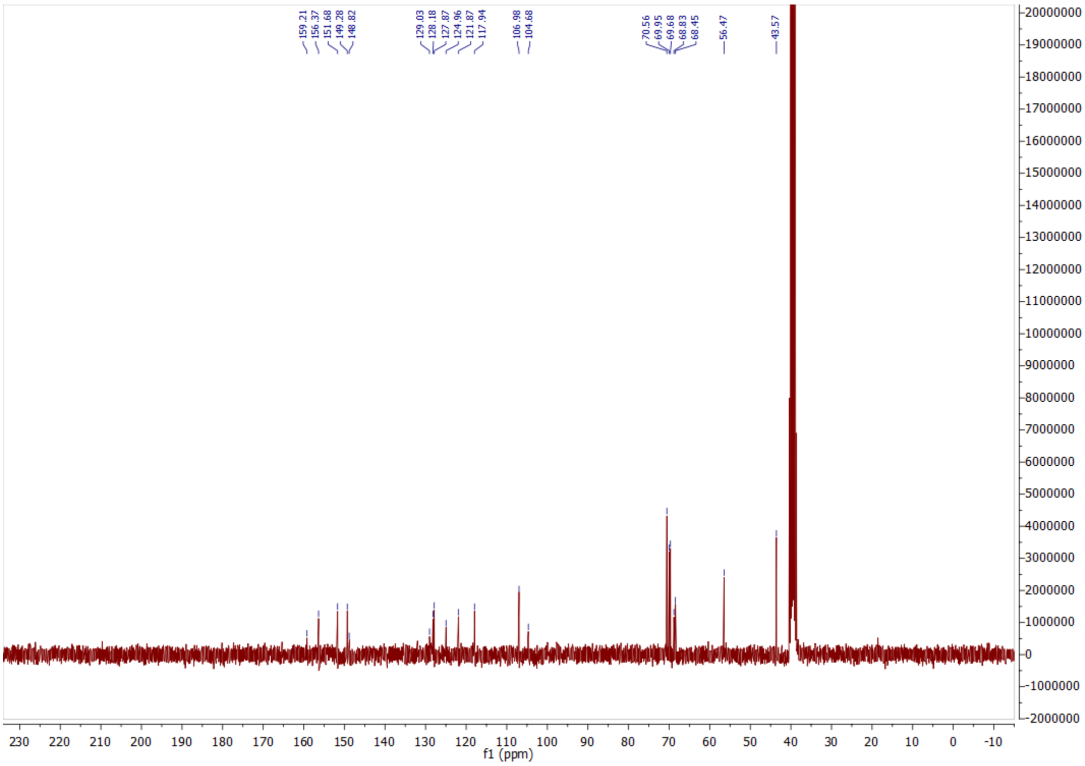
159.21
156.37
151.68
149.28
148.82
129.03
128.18
127.87
124.96
121.87
117.94
106.98
104.68
70.56
69.95
69.68
68.83
68.45
56.47
43.57
20000000
19000000
18000000
17000000
16000000
15000000
14000000
13000000
12000000
11000000
10000000
9000000
8000000
7000000
6000000
5000000
4000000
3000000
2000000
1000000
0
-1000000
-2000000
230 220 210 200 190 180 170 160 150 140 130 120 110 100 90 80 70 60 50 40 30 20 10 0 -10
f1 (ppm)

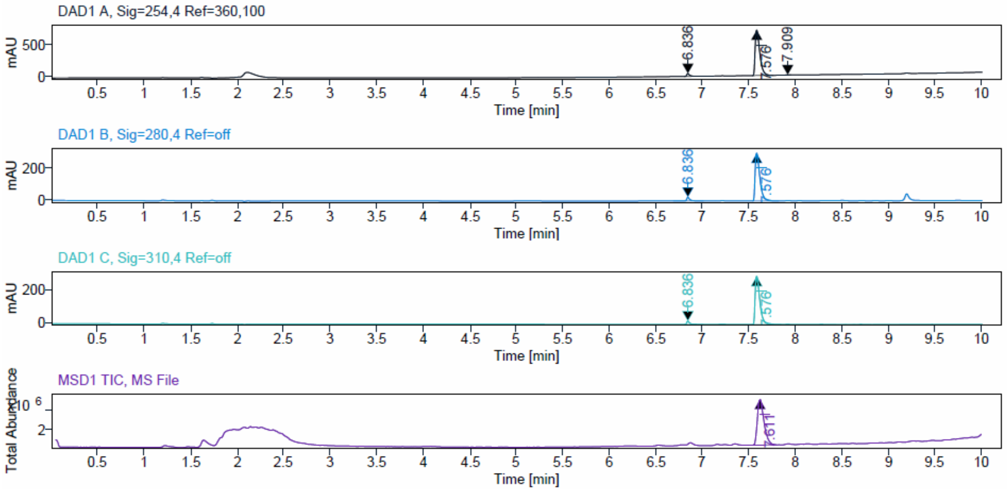
DAD1 A, Sig=254,4 Ref=360,100
mAU
500
0
6.836
576
7.909
0.5 1 1.5 2 2.5 3 3.5 4 4.5 5 5.5 6 6.5 7 7.5 8 8.5 9 9.5 10
Time [min]
DAD1 B, Sig=280,4 Ref=off
mAU
200
0
6.836
576
0.5 1 1.5 2 2.5 3 3.5 4 4.5 5 5.5 6 6.5 7 7.5 8 8.5 9 9.5 10
Time [min]
DAD1 C, Sig=310,4 Ref=off
mAU
200
0
6.836
576
0.5 1 1.5 2 2.5 3 3.5 4 4.5 5 5.5 6 6.5 7 7.5 8 8.5 9 9.5 10
Time [min]
MSD1 TIC, MS File
Total Abundance
10 6
2
611
0.5 1 1.5 2 2.5 3 3.5 4 4.5 5 5.5 6 6.5 7 7.5 8 8.5 9 9.5 10
Time [min]

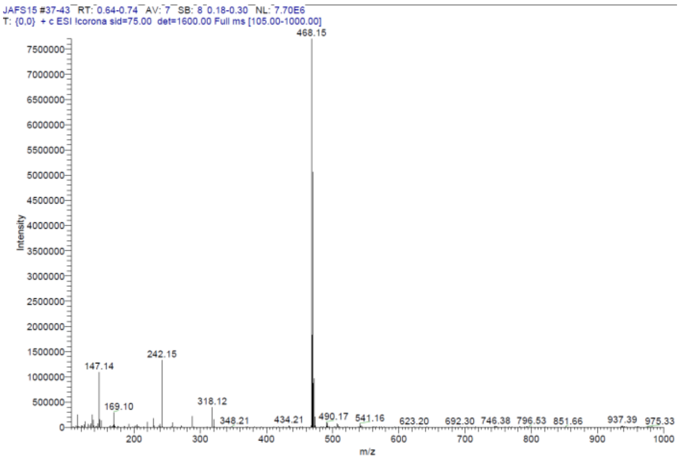
JAFS15 #37-43 RT: 0.64-0.74 AV: 7 SB: 8 0.18-0.30 NL: 7.70E6
T: {0,0} + c ESI !corona sid=75.00 det=1600.00 Full ms [105.00-1000.00]
468.15
7500000
7000000
6500000
6000000
5500000
5000000
4500000
4000000
3500000
3000000
2500000
2000000
1500000
1000000
500000
0
Intensity
147.14
242.15
169.10
318.12
348.21
434.21
490.17
541.16
623.20
692.30
746.38
796.53
851.66
937.39
975.33
200 300 400 500 600 700 800 900 1000
m/z

^{1}H, ^{13}C NMR, HPLC, and ESI data of compound **37e**

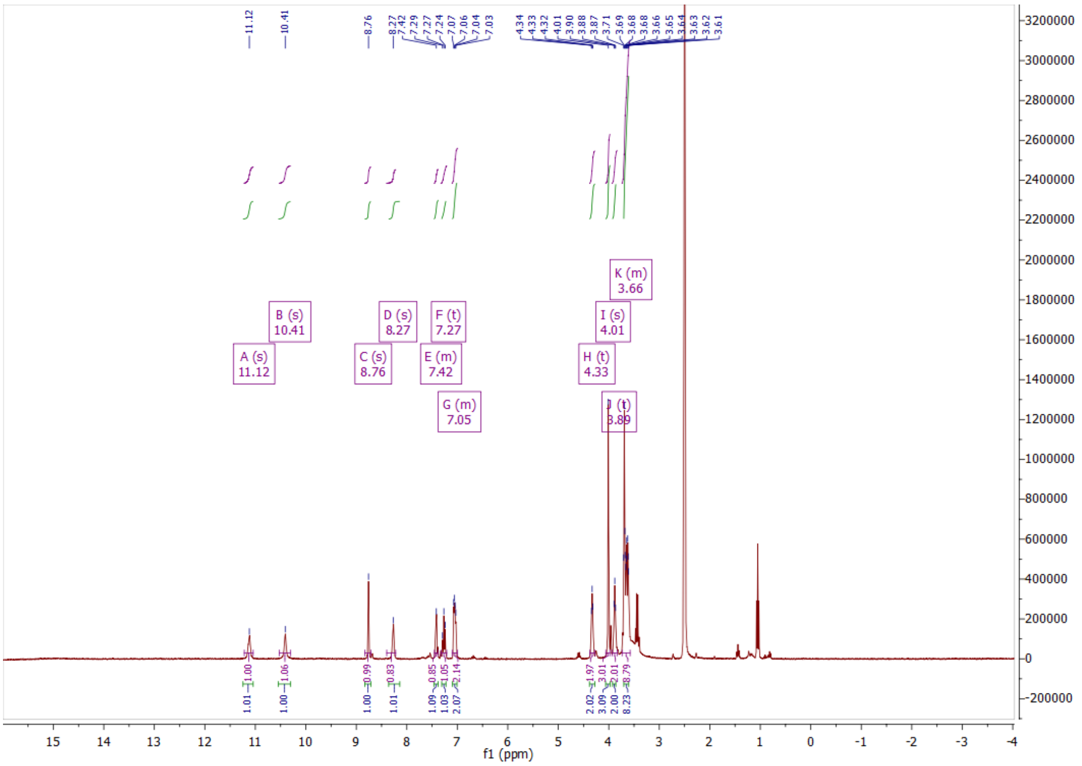

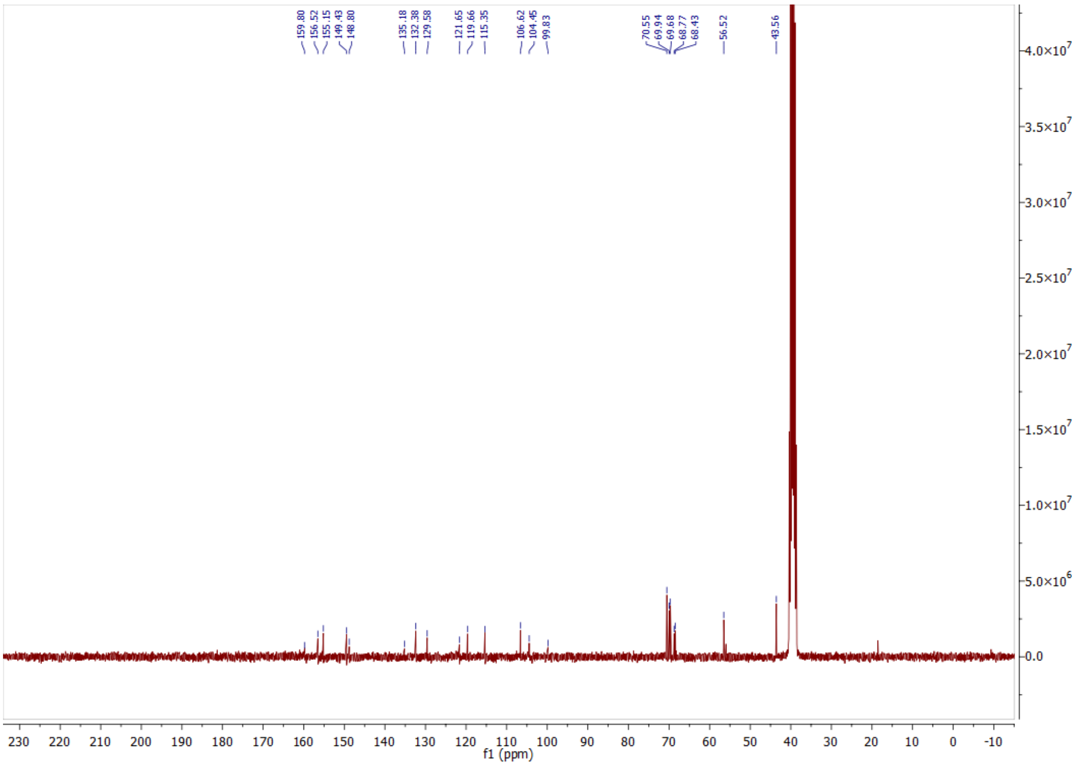

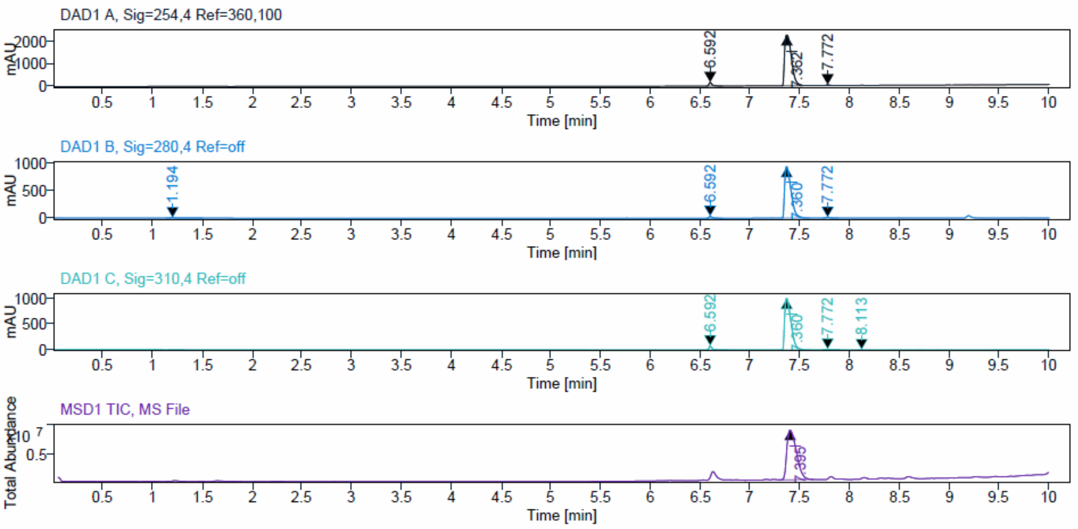

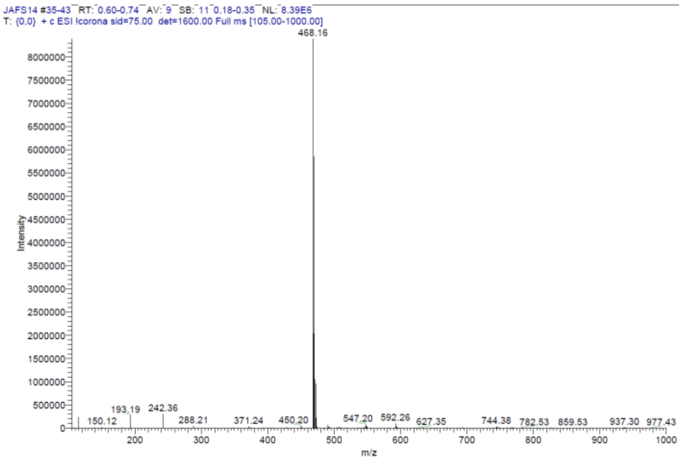

^{1}H, ^{13}C NMR, HPLC, and ESI data of compound **38a**

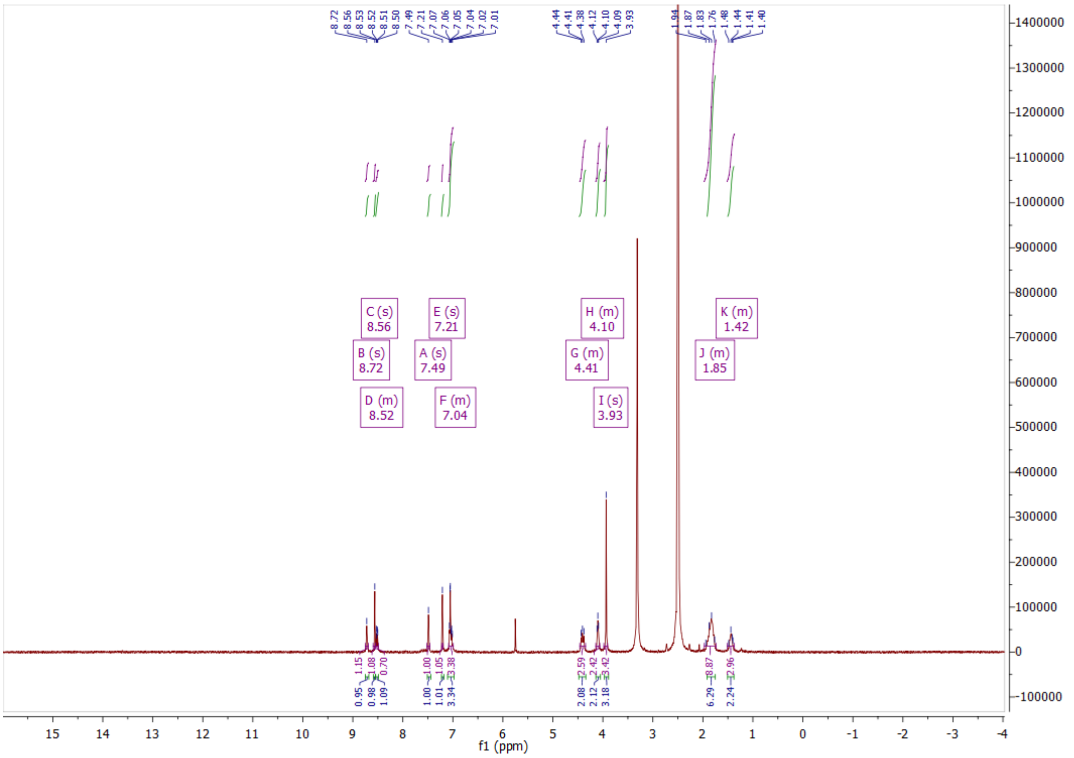

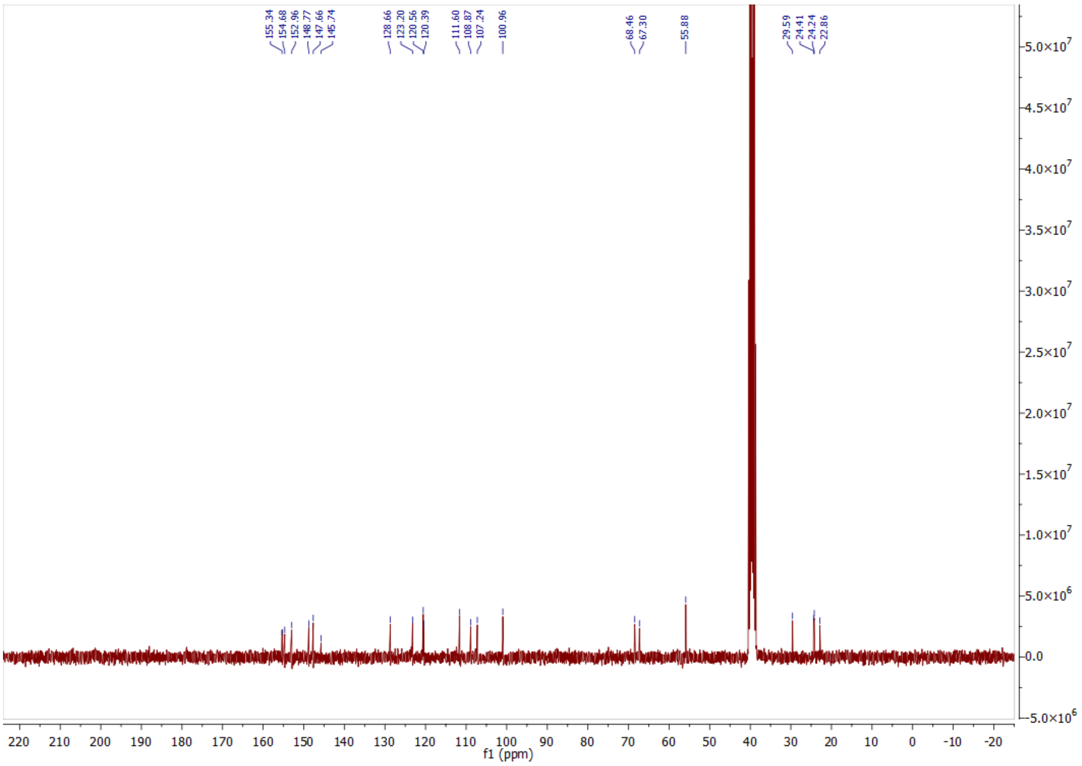
155.34
154.68
152.96
148.77
147.66
145.74
128.66
123.20
120.56
120.39
111.60
108.87
107.24
100.96
68.46
67.30
55.88
29.59
24.41
24.24
22.86
5.0×10^7
4.5×10^7
4.0×10^7
3.5×10^7
3.0×10^7
2.5×10^7
2.0×10^7
1.5×10^7
1.0×10^7
5.0×10^6
0.0
-5.0×10^6
220 210 200 190 180 170 160 150 140 130 120 110 100 90 80 70 60 50 40 30 20 10 0 -10 -20
f1 (ppm)

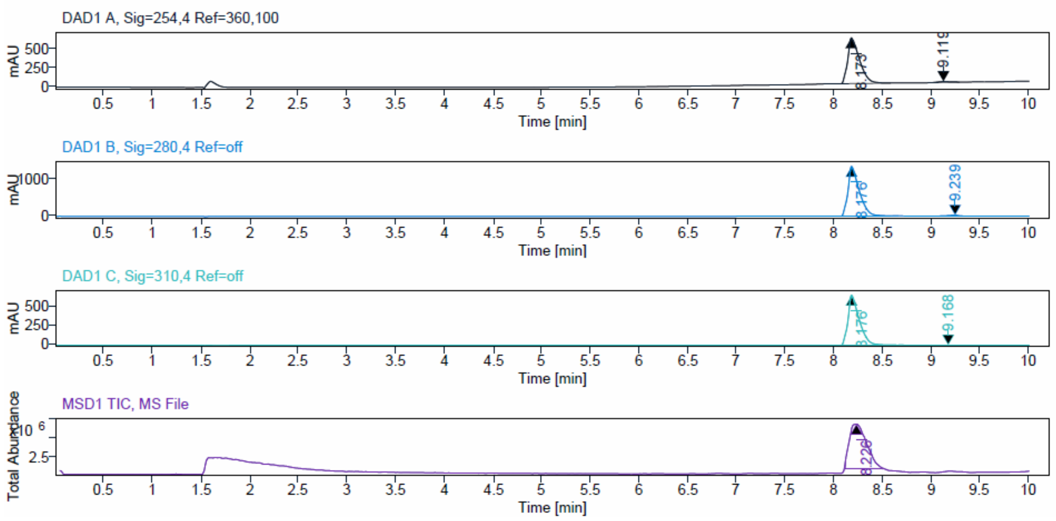
DAD1 A, Sig=254,4 Ref=360,100
mAU
500
250
0
8.173
9.119
Time [min]
DAD1 B, Sig=280,4 Ref=off
mAU
1000
0
8.176
9.239
Time [min]
DAD1 C, Sig=310,4 Ref=off
mAU
500
250
0
8.176
9.168
Time [min]
MSD1 TIC, MS File
Total Abundance
x10 6
2.5
8.226
0.5 1 1.5 2 2.5 3 3.5 4 4.5 5 5.5 6 6.5 7 7.5 8 8.5 9 9.5 10
Time [min]

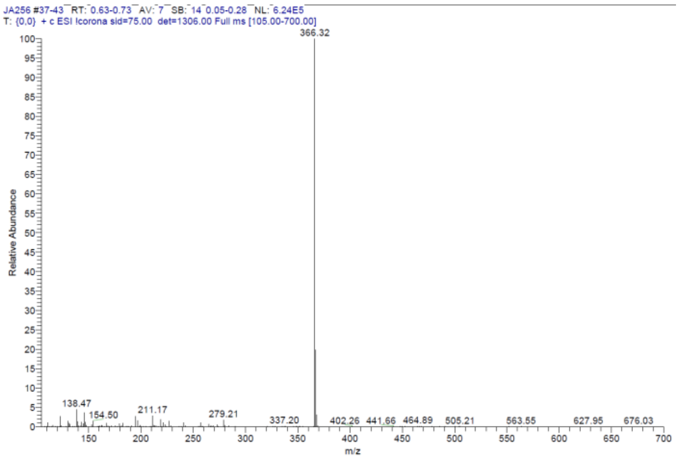
JA256 #37-43 RT: 0.63-0.73 AV: 7 SB: 14 0.05-0.28 NL: 6.24E5
T: {0,0} + c ESI !corona sid=75.00 det=1306.00 Full ms [105.00-700.00]
366.32
138.47
154.50
211.17
279.21
337.20
402.26
441.66
464.89
505.21
563.55
627.95
676.03
Relative Abundance
100 95 90 85 80 75 70 65 60 55 50 45 40 35 30 25 20 15 10 5 0
150 200 250 300 350 400 450 500 550 600 650 700
m/z

^{1}H, ^{13}C NMR, HPLC, and ESI data of compound **38b**

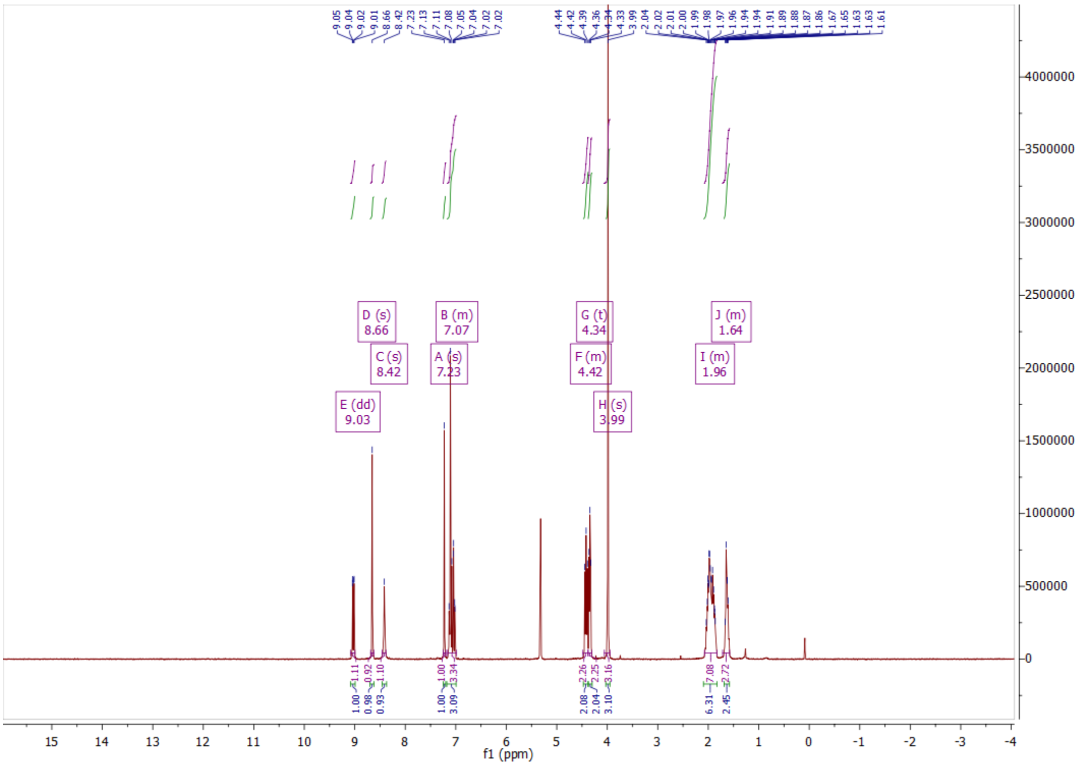

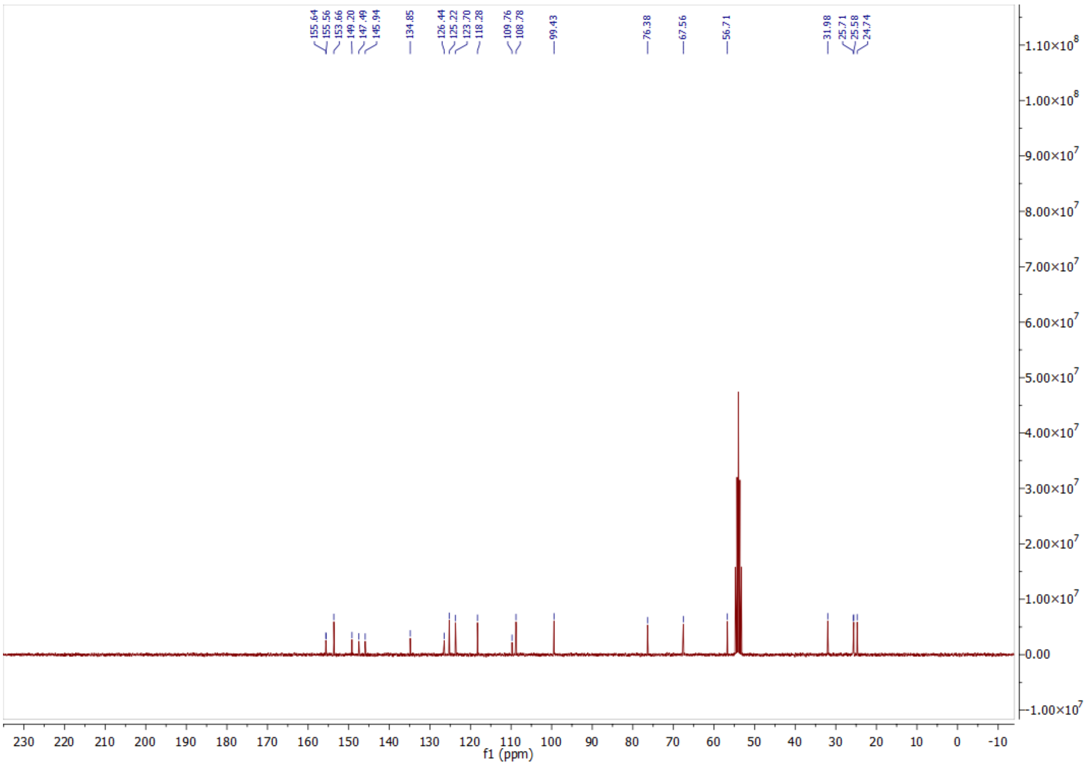

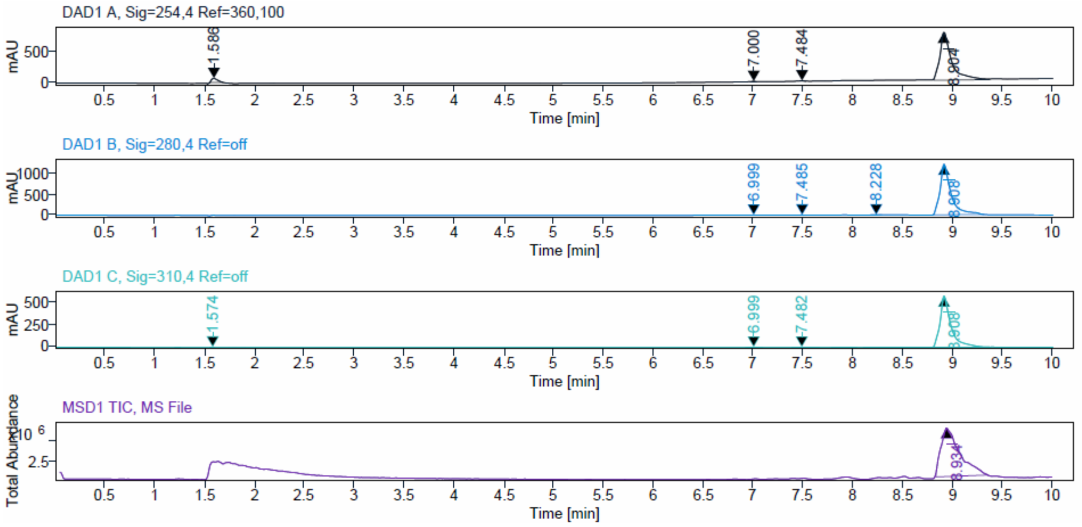

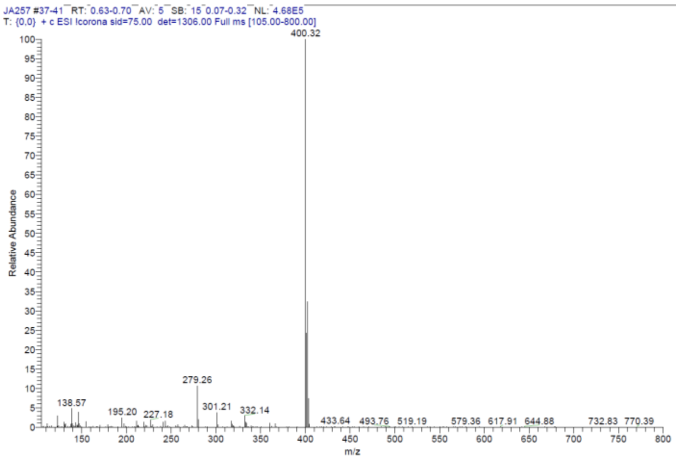

ESI, HRMS, ^{1}H, ^{13}C NMR and HPLC data of compound **38c**

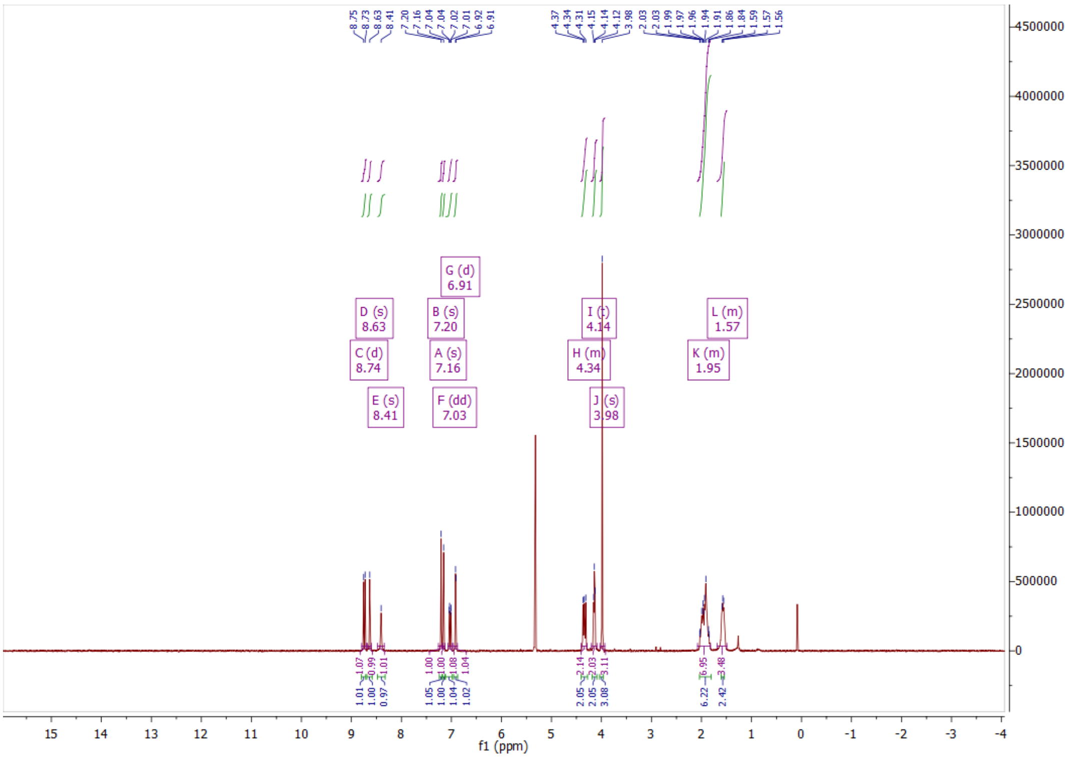

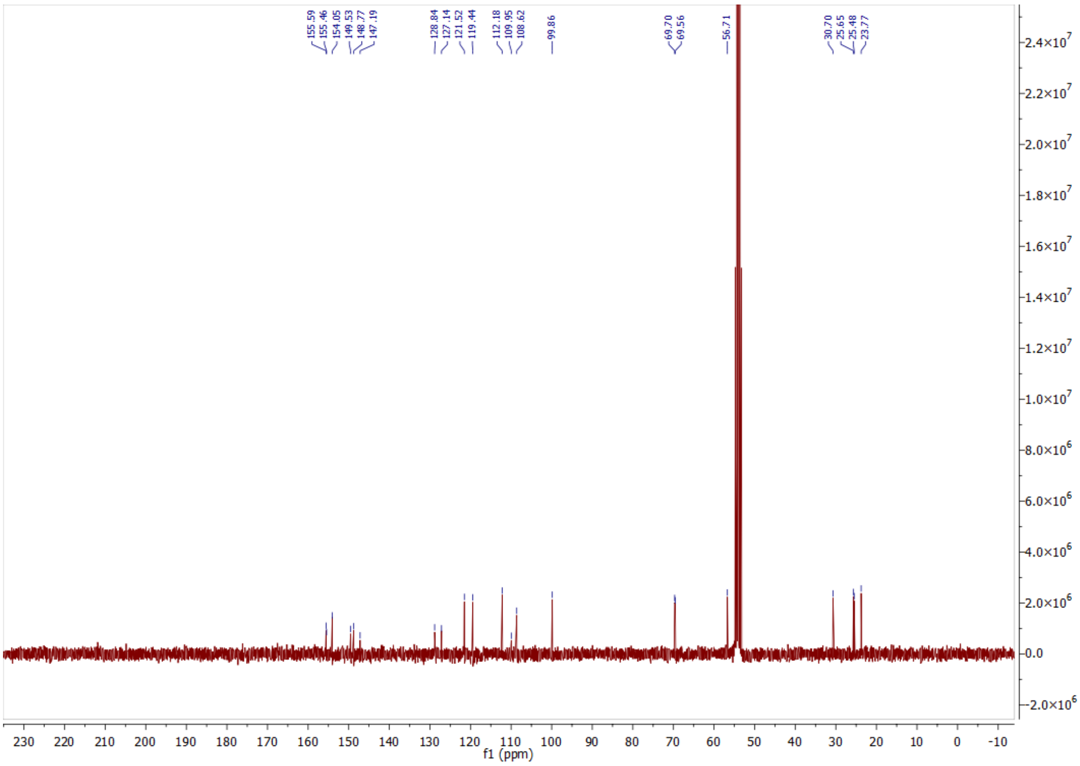
155.59
155.46
154.05
149.53
148.77
147.19
128.84
127.14
121.52
119.44
112.18
109.95
108.62
99.86
69.70
69.56
56.71
30.70
25.65
25.48
23.77
2.4×10^7
2.2×10^7
2.0×10^7
1.8×10^7
1.6×10^7
1.4×10^7
1.2×10^7
1.0×10^7
8.0×10^6
6.0×10^6
4.0×10^6
2.0×10^6
0.0
−2.0×10^6
230 220 210 200 190 180 170 160 150 140 130 120 110 100 90 80 70 60 50 40 30 20 10 0 -10
f1 (ppm)

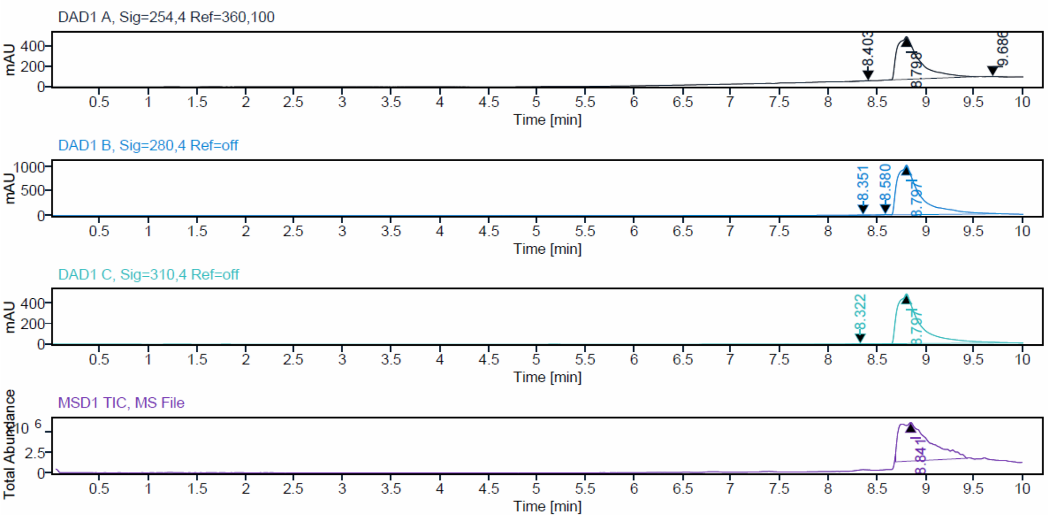
DAD1 A, Sig=254,4 Ref=360,100
mAU
400
200
0
8.403
8.798
9.686
DAD1 B, Sig=280,4 Ref=off
1000
500
8.351
8.580
8.797
DAD1 C, Sig=310,4 Ref=off
8.322
8.797
MSD1 TIC, MS File
Total Abundance
x10 6
2.5
8.841
0.5 1 1.5 2 2.5 3 3.5 4 4.5 5 5.5 6 6.5 7 7.5 8 8.5 9 9.5 10
Time [min]

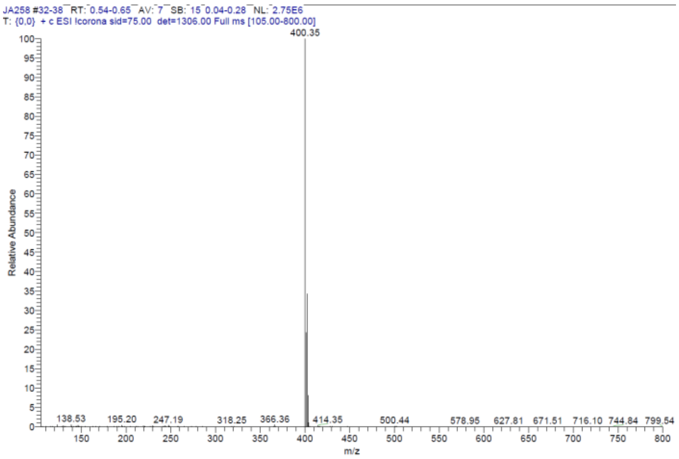
JA258 #32-38 RT: 0.54-0.65 AV: 7 SB: 15 0.04-0.28 NL: 2.75E6
T: {0,0} + c ESI !corona sid=75.00 det=1306.00 Full ms [105.00-800.00]
400.35
138.53
195.20
247.19
318.25
366.36
414.35
500.44
578.95
627.81
671.51
716.10
744.84
799.54
Relative Abundance
0 5 10 15 20 25 30 35 40 45 50 55 60 65 70 75 80 85 90 95 100
150 200 250 300 350 400 450 500 550 600 650 700 750 800
m/z

^{1}H, ^{13}C NMR, HPLC, and ESI data of compound **38d**

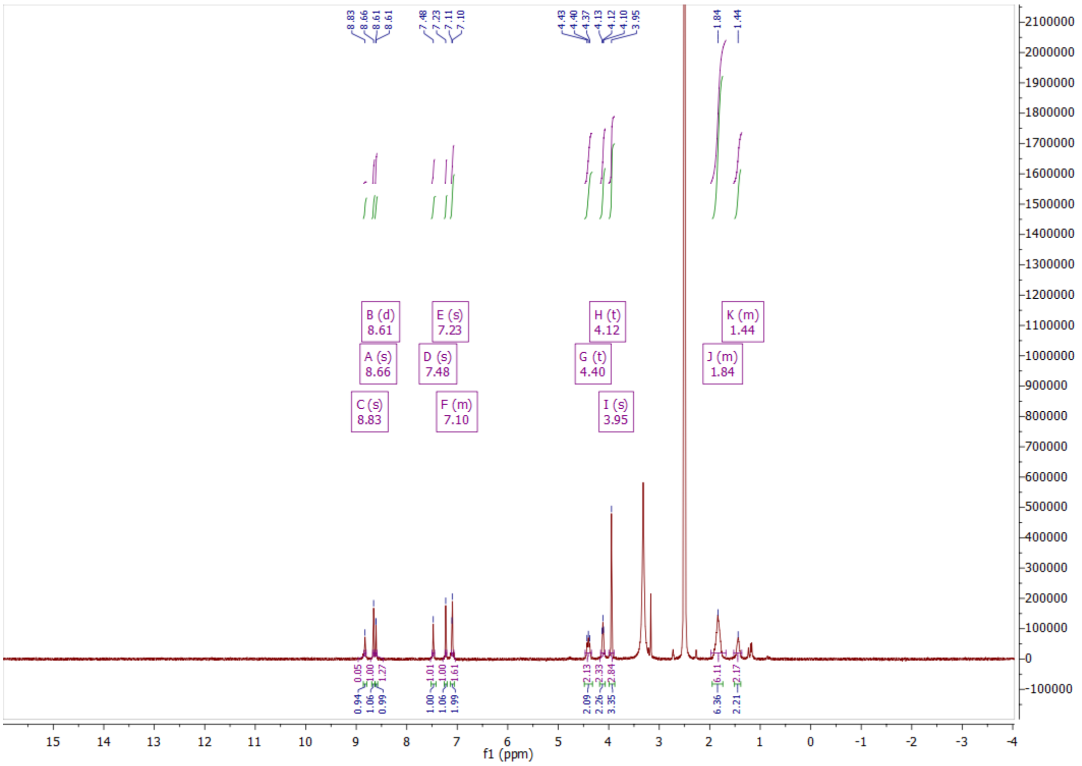

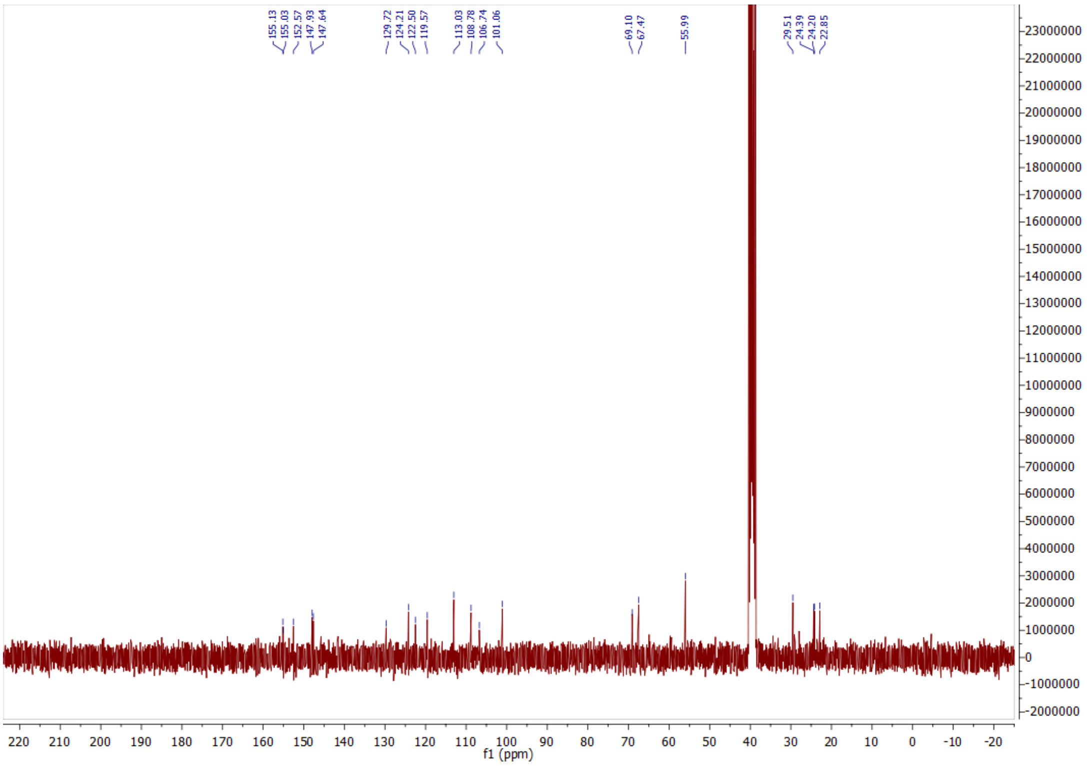

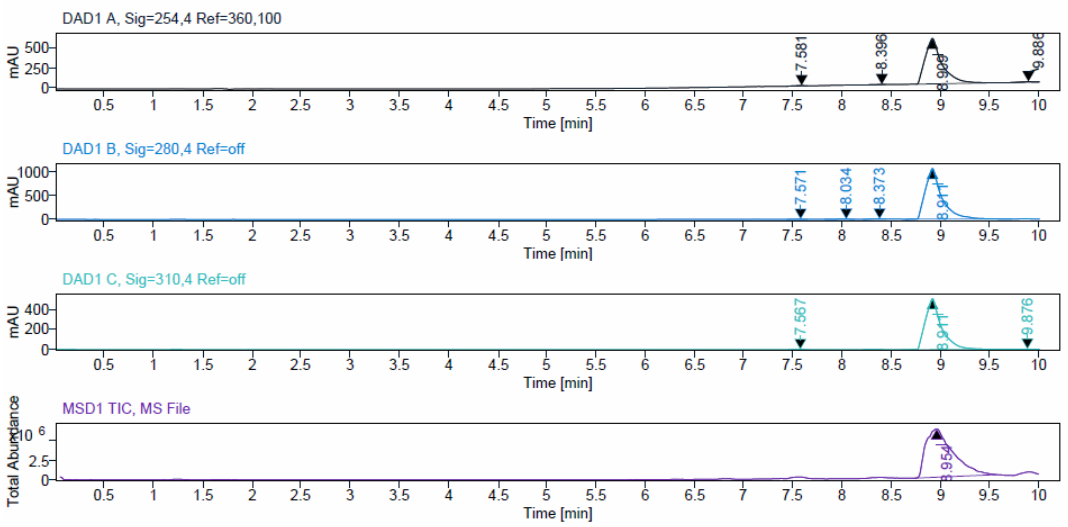

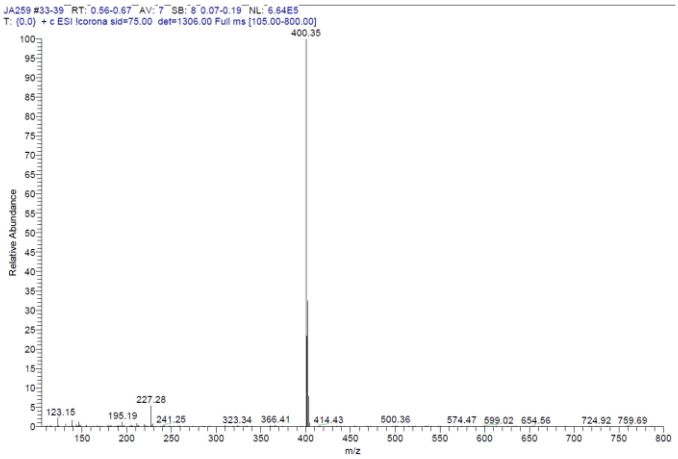

^{1}H, ^{13}C NMR, HPLC, and ESI data of compound **38e**

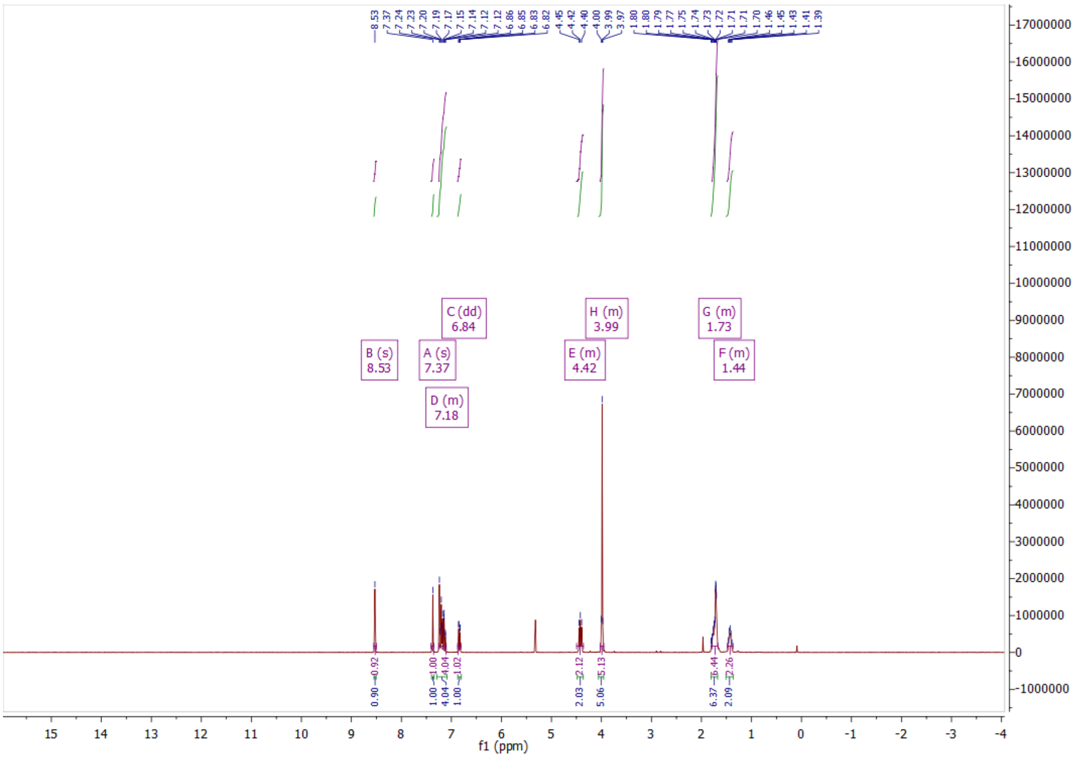

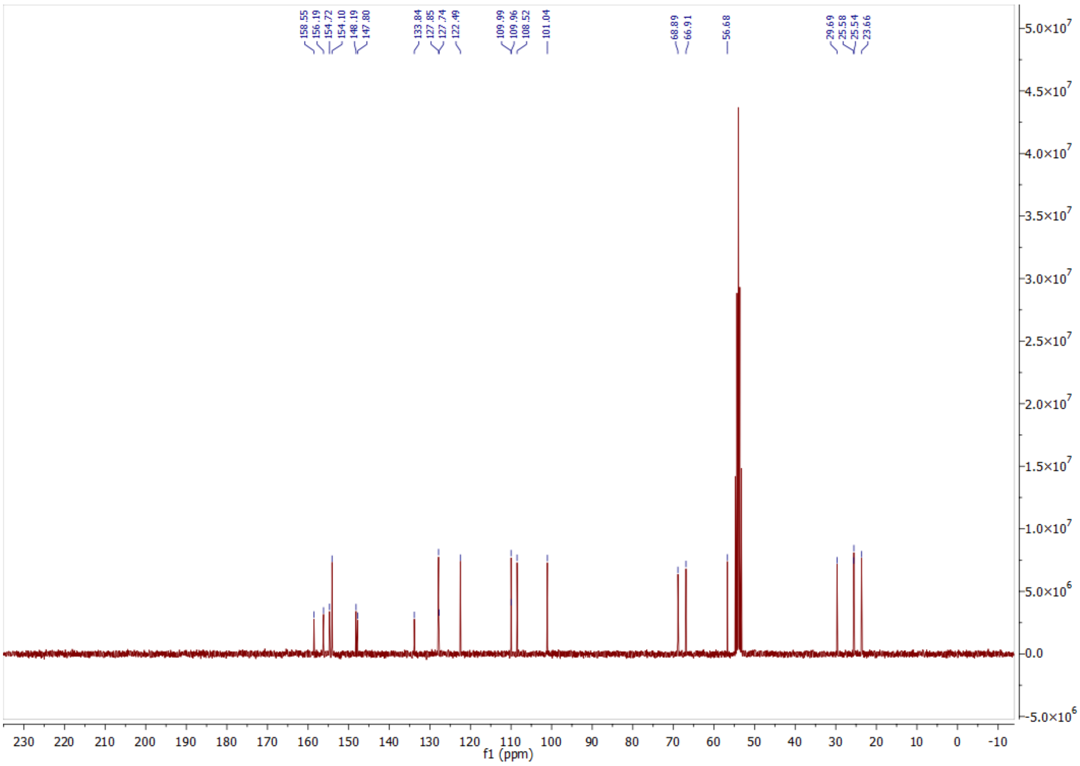
158.55
156.19
154.72
154.10
148.19
147.80
133.84
127.85
127.74
122.49
109.99
109.96
108.52
101.04
68.89
66.91
56.68
29.69
25.58
25.54
23.66
5.0×10^7
4.5×10^7
4.0×10^7
3.5×10^7
3.0×10^7
2.5×10^7
2.0×10^7
1.5×10^7
1.0×10^7
5.0×10^6
0.0
-5.0×10^6
230 220 210 200 190 180 170 160 150 140 130 120 110 100 90 80 70 60 50 40 30 20 10 0 -10
f1 (ppm)

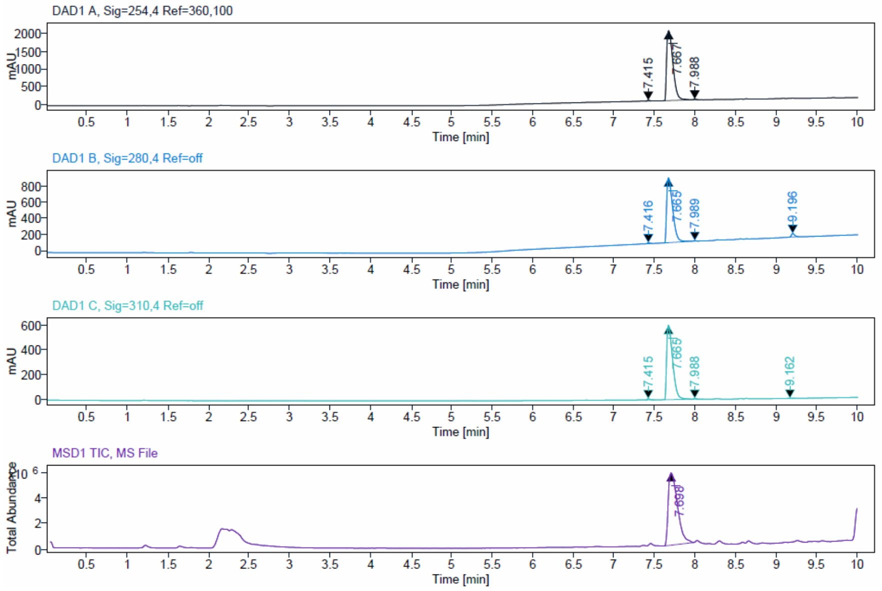
DAD1 A, Sig=254,4 Ref=360,100
mAU
7.415
7.667
7.988
DAD1 B, Sig=280,4 Ref=off
7.416
7.665
7.989
9.196
DAD1 C, Sig=310,4 Ref=off
7.415
7.665
7.988
9.162
MSD1 TIC, MS File
Total Abundance
x10 6
7.698
Time [min]

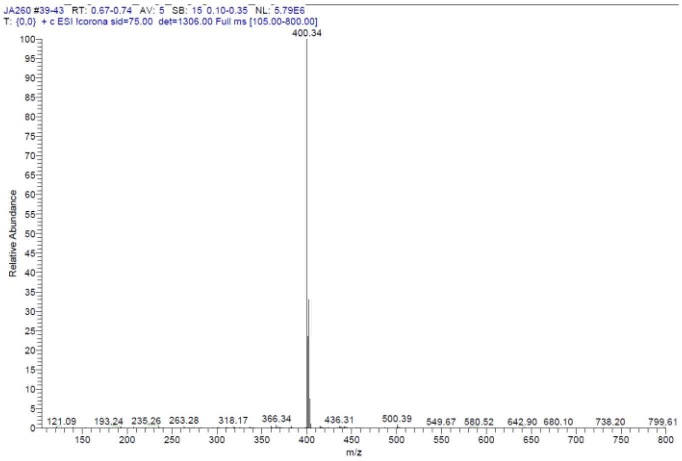
JA260 #39-43 RT: 0.67-0.74 AV: 5 SB: 15 0.10-0.35 NL: 5.79E6
T: {0,0} + c ESI Icorona sid=75.00 det=1306.00 Full ms [105.00-800.00]
400.34
Relative Abundance
121.09
193.24
235.26
263.28
318.17
366.34
436.31
500.39
549.67
580.52
642.90
680.10
738.20
799.61
m/z

^{1}H, ^{13}C NMR, HPLC, and ESI data of compound **38f**

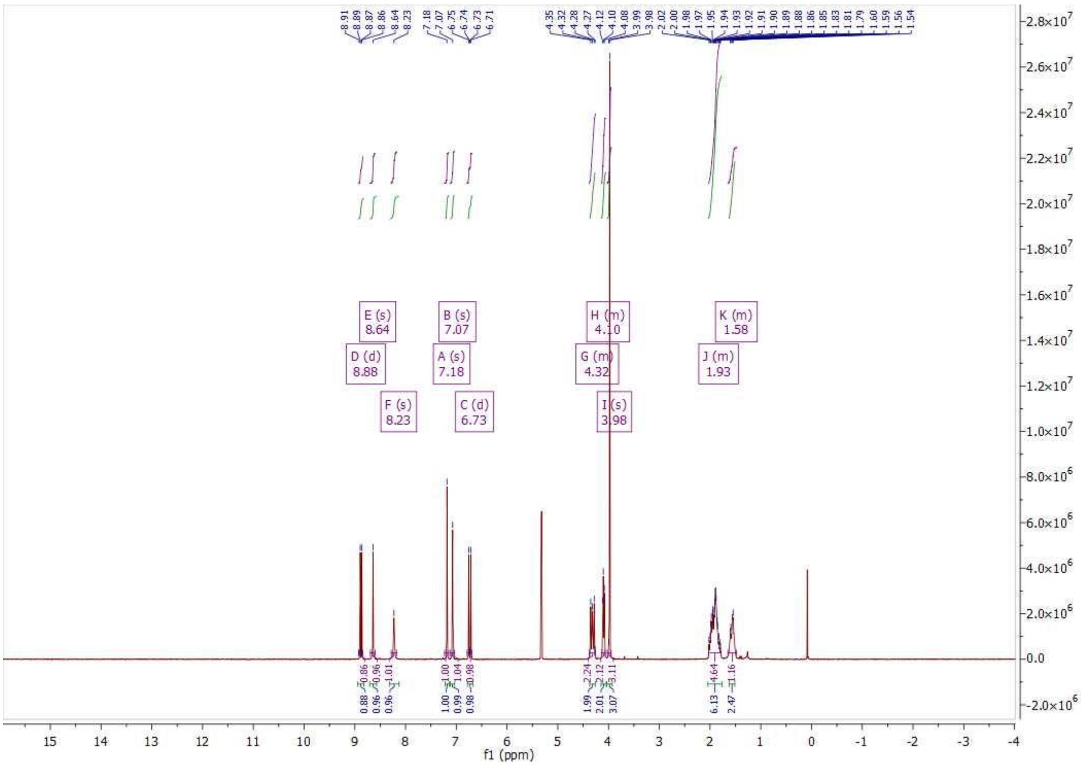

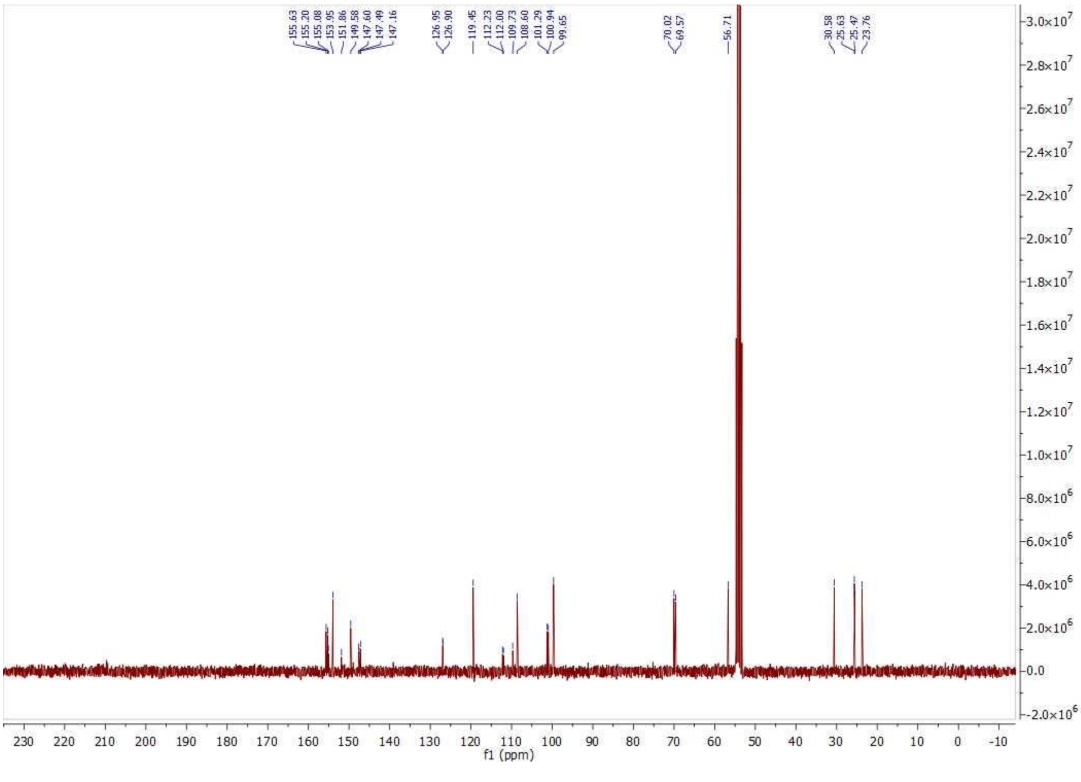

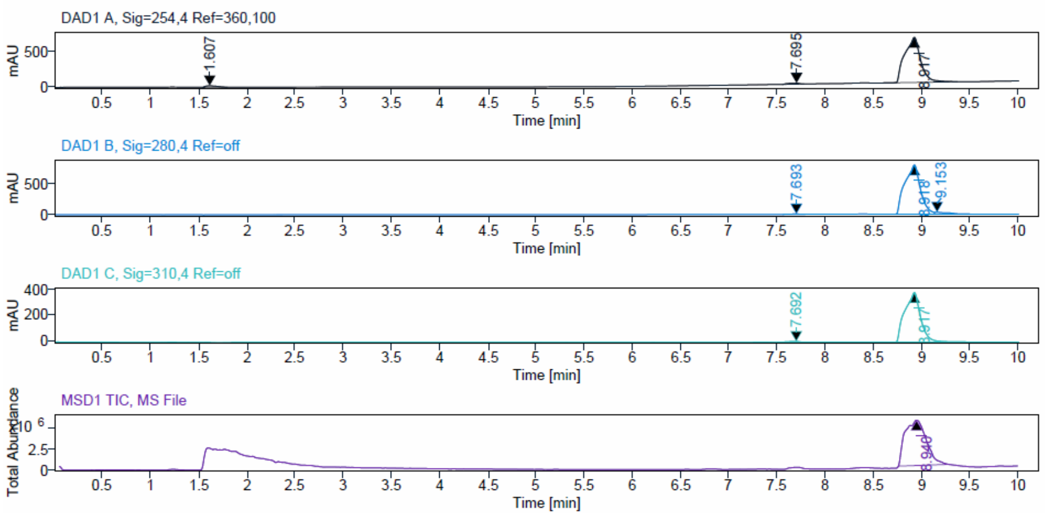

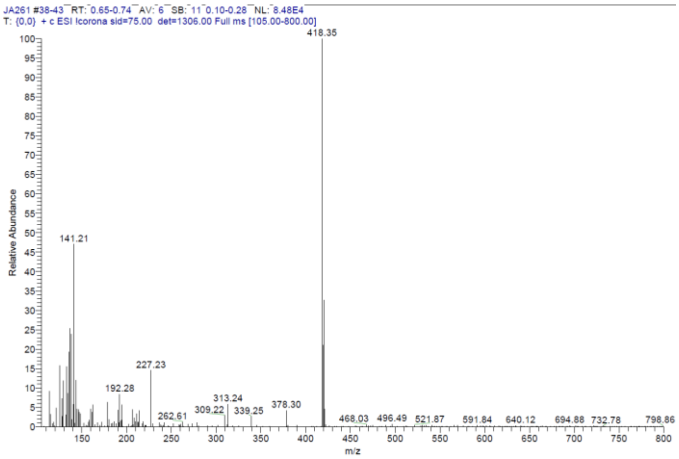

^{1}H, ^{13}C NMR, HPLC, and ESI data of compound **39a**

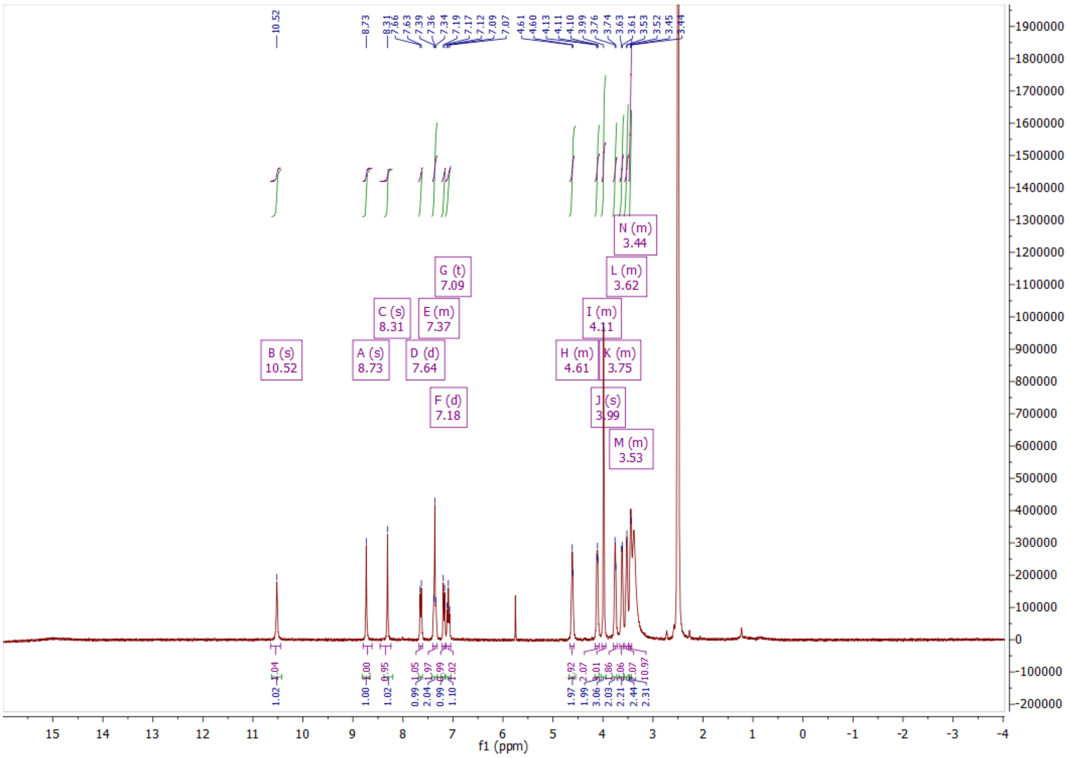

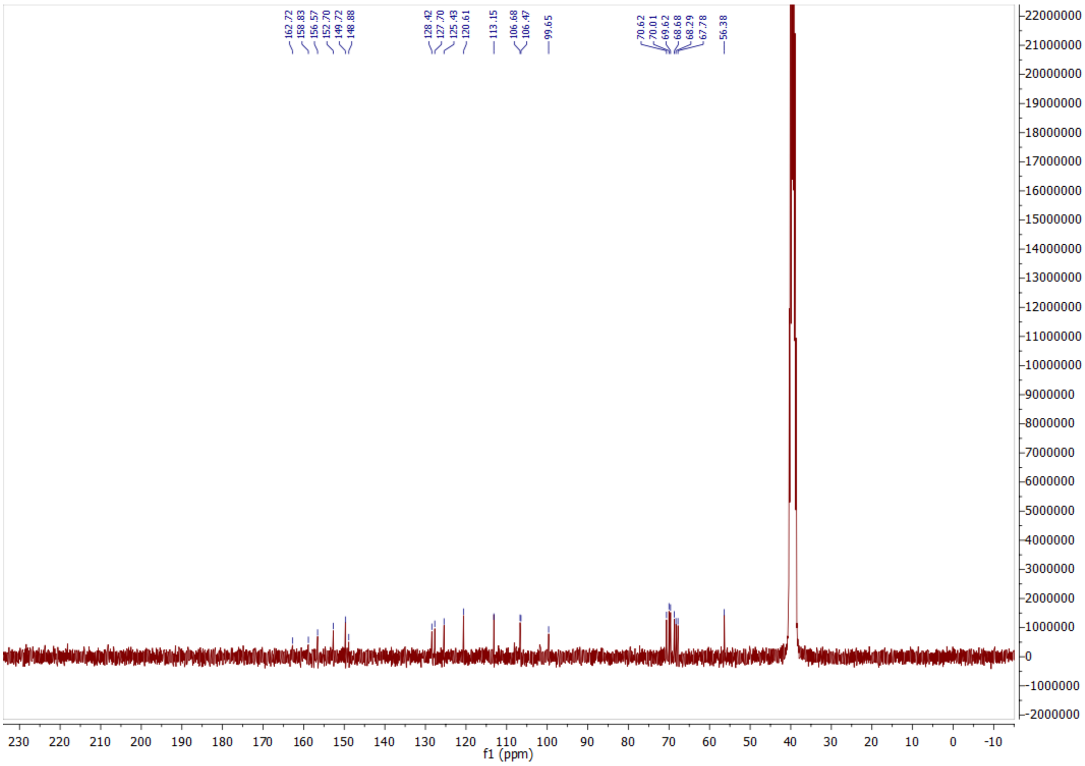
162.72
158.83
156.57
152.70
149.72
148.88
128.42
127.70
125.43
120.61
113.15
106.68
106.47
99.65
70.62
70.01
69.62
68.68
68.29
67.78
56.38
22000000
21000000
20000000
19000000
18000000
17000000
16000000
15000000
14000000
13000000
12000000
11000000
10000000
9000000
8000000
7000000
6000000
5000000
4000000
3000000
2000000
1000000
0
-1000000
-2000000
230 220 210 200 190 180 170 160 150 140 130 120 110 100 90 80 70 60 50 40 30 20 10 0 -10
f1 (ppm)

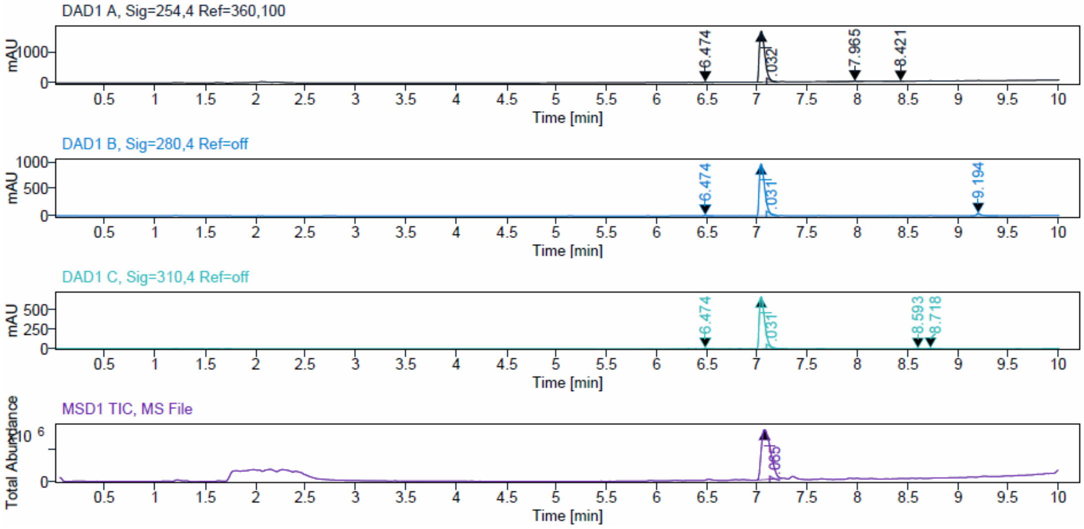
DAD1 A, Sig=254,4 Ref=360,100
mAU
1000
0
6.474
.032
7.965
8.421
0.5 1 1.5 2 2.5 3 3.5 4 4.5 5 5.5 6 6.5 7 7.5 8 8.5 9 9.5 10
Time [min]
DAD1 B, Sig=280,4 Ref=off
mAU
1000
500
0
6.474
.031
9.194
0.5 1 1.5 2 2.5 3 3.5 4 4.5 5 5.5 6 6.5 7 7.5 8 8.5 9 9.5 10
Time [min]
DAD1 C, Sig=310,4 Ref=off
mAU
500
250
0
6.474
.031
8.593
8.718
0.5 1 1.5 2 2.5 3 3.5 4 4.5 5 5.5 6 6.5 7 7.5 8 8.5 9 9.5 10
Time [min]
MSD1 TIC, MS File
Total Abundance
10 6
0
7.065
0.5 1 1.5 2 2.5 3 3.5 4 4.5 5 5.5 6 6.5 7 7.5 8 8.5 9 9.5 10
Time [min]

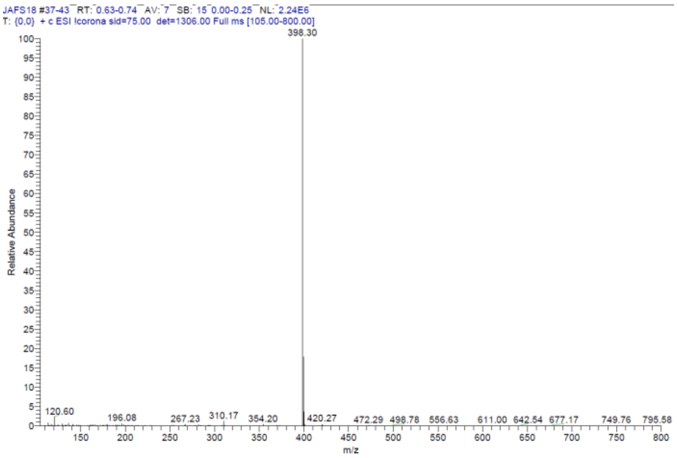
JAFS18 #37-43 RT: 0.63-0.74 AV: 7 SB: 15 0.00-0.25 NL: 2.24E6
T: {0,0} + c ESI !corona sid=75.00 det=1306.00 Full ms [105.00-800.00]
398.30
Relative Abundance
100
95
90
85
80
75
70
65
60
55
50
45
40
35
30
25
20
15
10
5
0
120.60
196.08
267.23
310.17
354.20
420.27
472.29
498.78
556.63
611.00
642.54
677.17
749.76
795.58
150 200 250 300 350 400 450 500 550 600 650 700 750 800
m/z

^{1}H, ^{13}C NMR, HPLC, and ESI data of compound **39b**

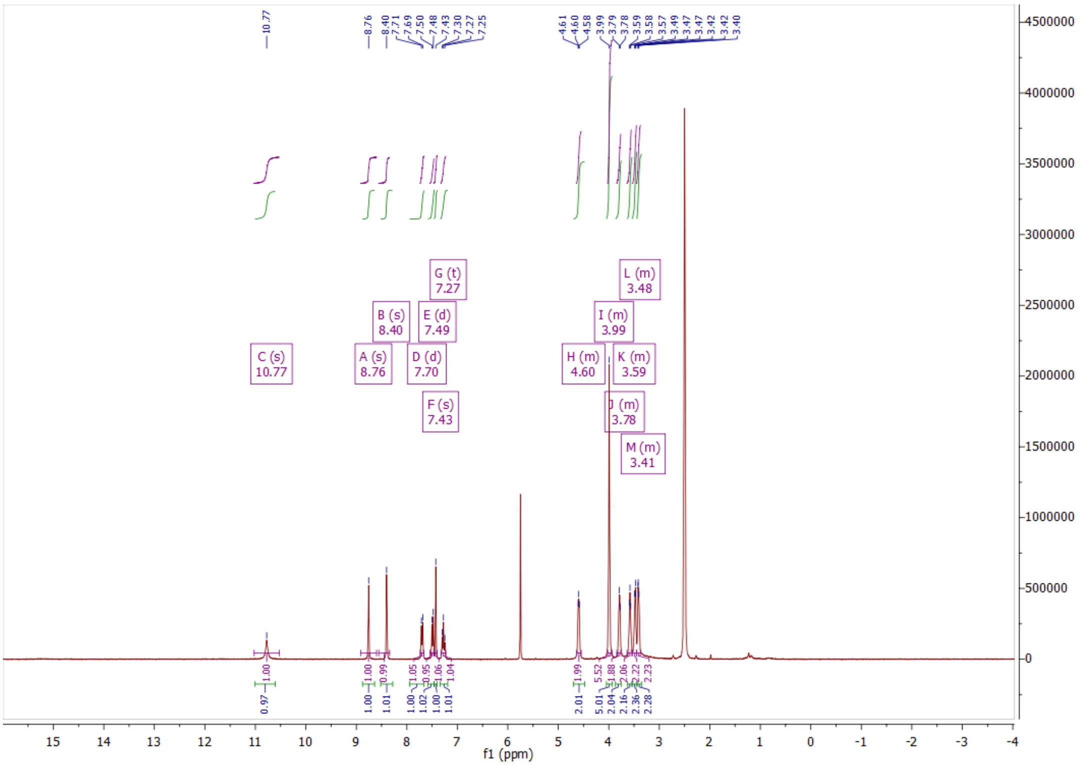

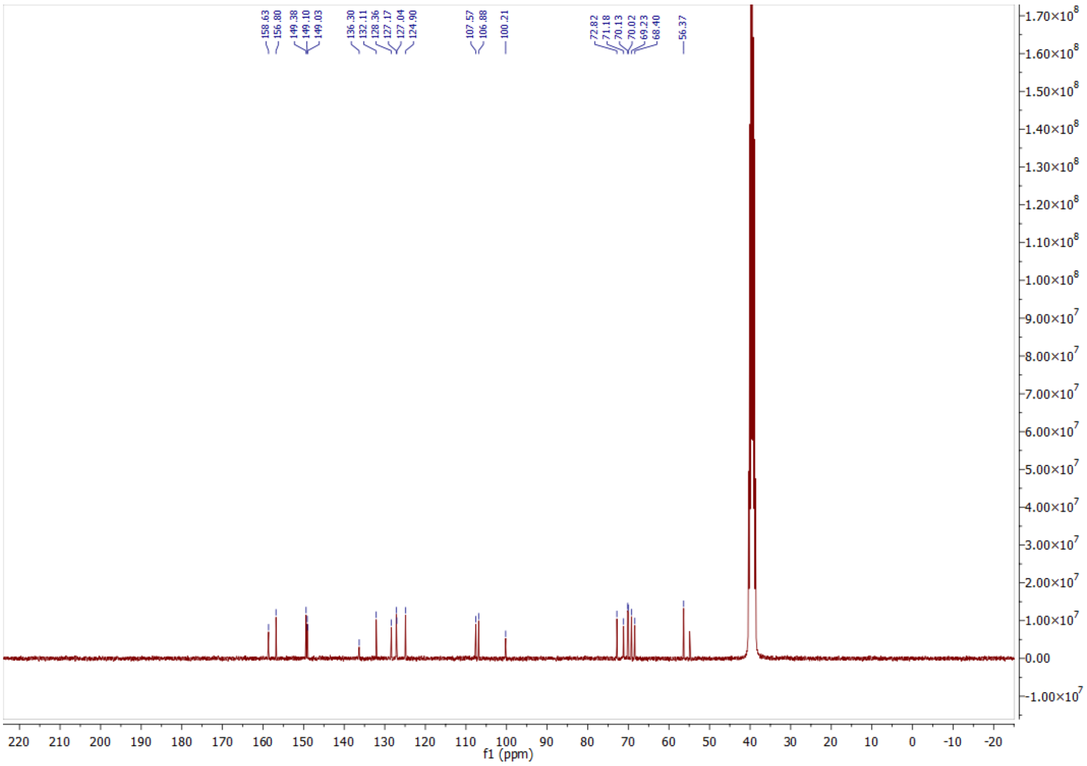

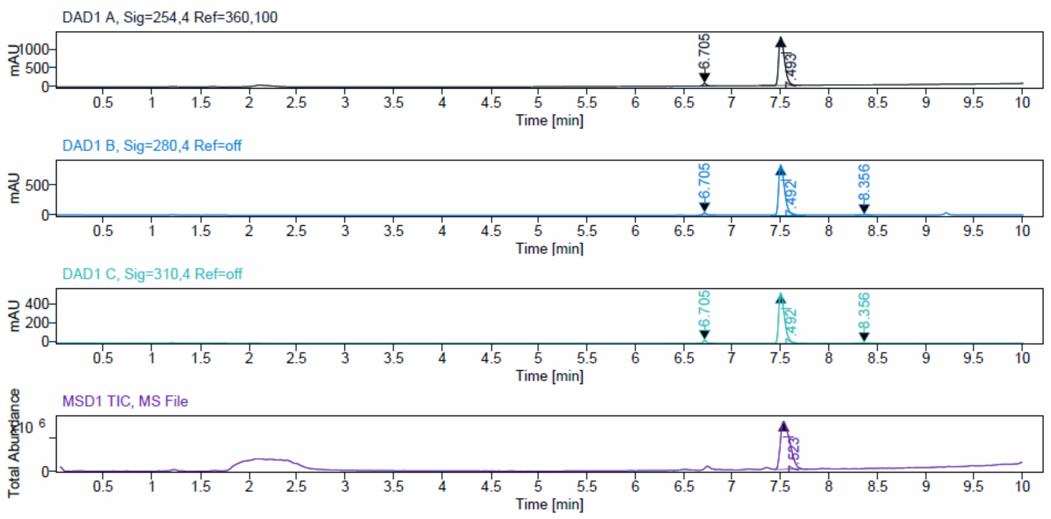

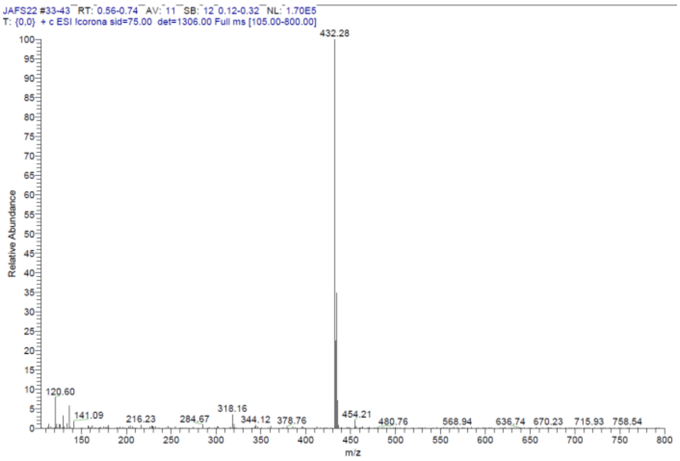

^{1}H, ^{13}C NMR, HPLC, and ESI data of compound **39c**

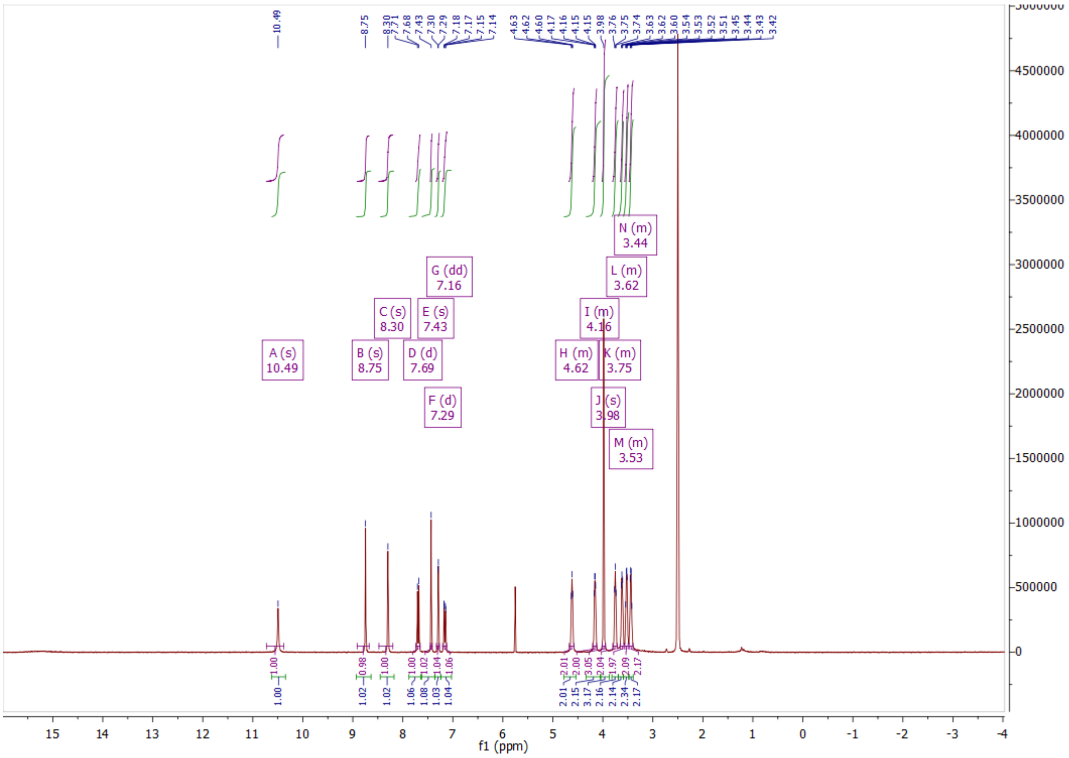

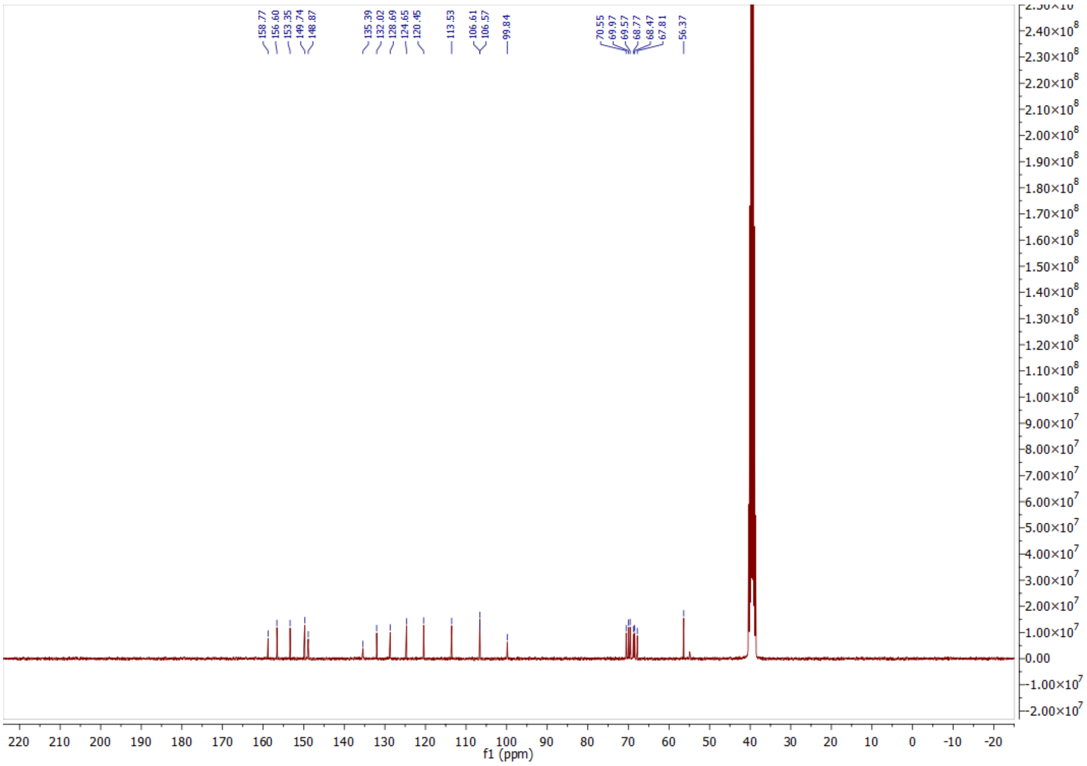
158.77
156.60
153.35
149.74
148.87
135.39
132.02
128.69
124.65
120.45
113.53
106.61
106.57
99.84
70.55
69.97
69.57
68.77
68.47
67.81
56.37
2.40×10⁸
2.30×10⁸
2.20×10⁸
2.10×10⁸
2.00×10⁸
1.90×10⁸
1.80×10⁸
1.70×10⁸
1.60×10⁸
1.50×10⁸
1.40×10⁸
1.30×10⁸
1.20×10⁸
1.10×10⁸
1.00×10⁸
9.00×10⁷
8.00×10⁷
7.00×10⁷
6.00×10⁷
5.00×10⁷
4.00×10⁷
3.00×10⁷
2.00×10⁷
1.00×10⁷
0.00
-1.00×10⁷
-2.00×10⁷
220 210 200 190 180 170 160 150 140 130 120 110 100 90 80 70 60 50 40 30 20 10 0 -10 -20
f1 (ppm)

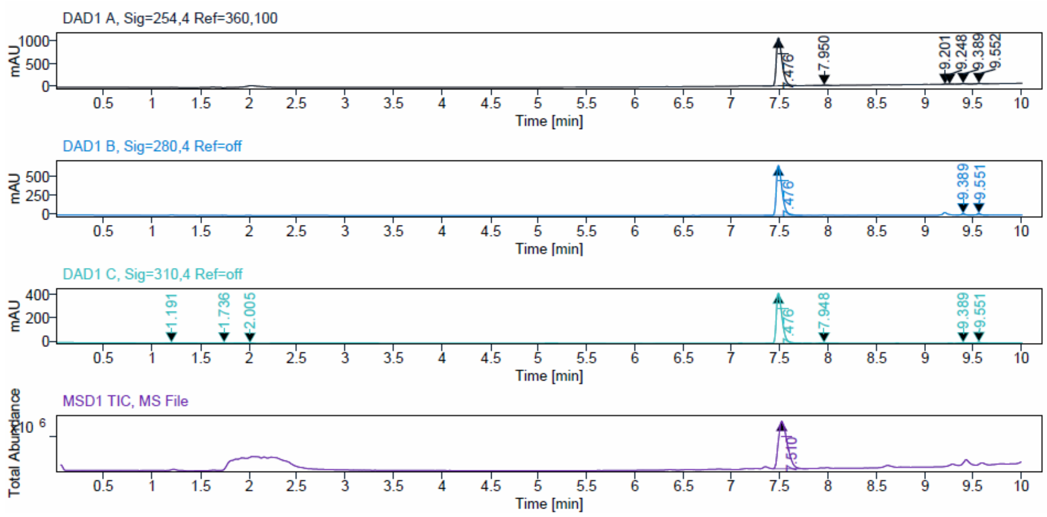
DAD1 A, Sig=254,4 Ref=360,100
mAU
1000
500
0
7.476
7.950
9.201
9.248
9.389
9.552
Time [min]
DAD1 B, Sig=280,4 Ref=off
mAU
500
250
0
7.476
9.389
9.551
Time [min]
DAD1 C, Sig=310,4 Ref=off
mAU
400
200
0
1.191
1.736
2.005
7.476
7.948
9.389
9.551
Time [min]
MSD1 TIC, MS File
Total Abundance
x10 6
7.510
0.5 1 1.5 2 2.5 3 3.5 4 4.5 5 5.5 6 6.5 7 7.5 8 8.5 9 9.5 10
Time [min]

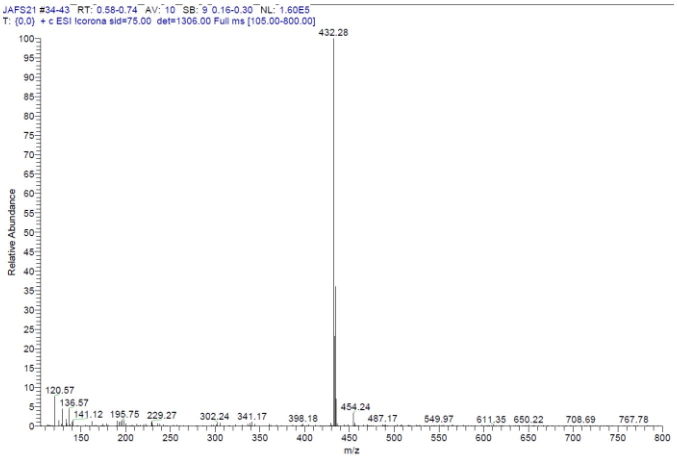
JAFS21 #34-43 RT: 0.58-0.74 AV: 10 SB: 9 0.16-0.30 NL: 1.60E5
T: {0,0} + c ESI !corona sid=75.00 det=1306.00 Full ms [105.00-800.00]
432.28
120.57
136.57
141.12
195.75
229.27
302.24
341.17
398.18
454.24
487.17
549.97
611.35
650.22
708.69
767.78
Relative Abundance
100 95 90 85 80 75 70 65 60 55 50 45 40 35 30 25 20 15 10 5 0
150 200 250 300 350 400 450 500 550 600 650 700 750 800
m/z

^{1}H, ^{13}C NMR, HPLC, and ESI data data of compound **39d**

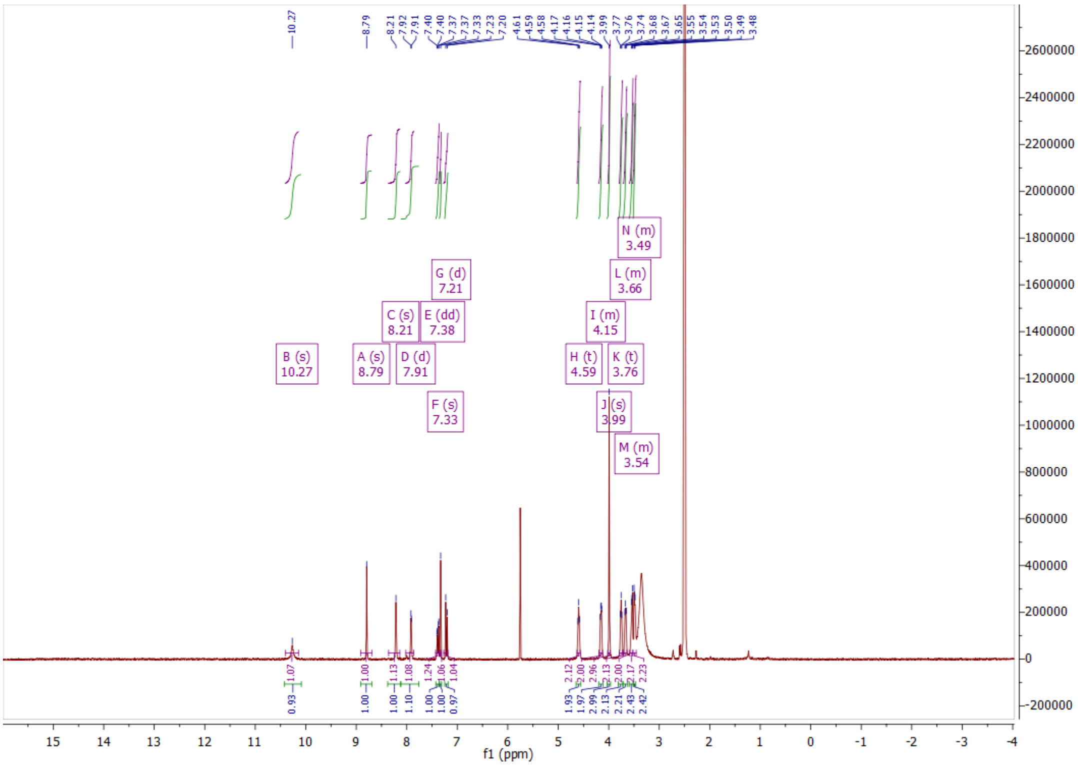

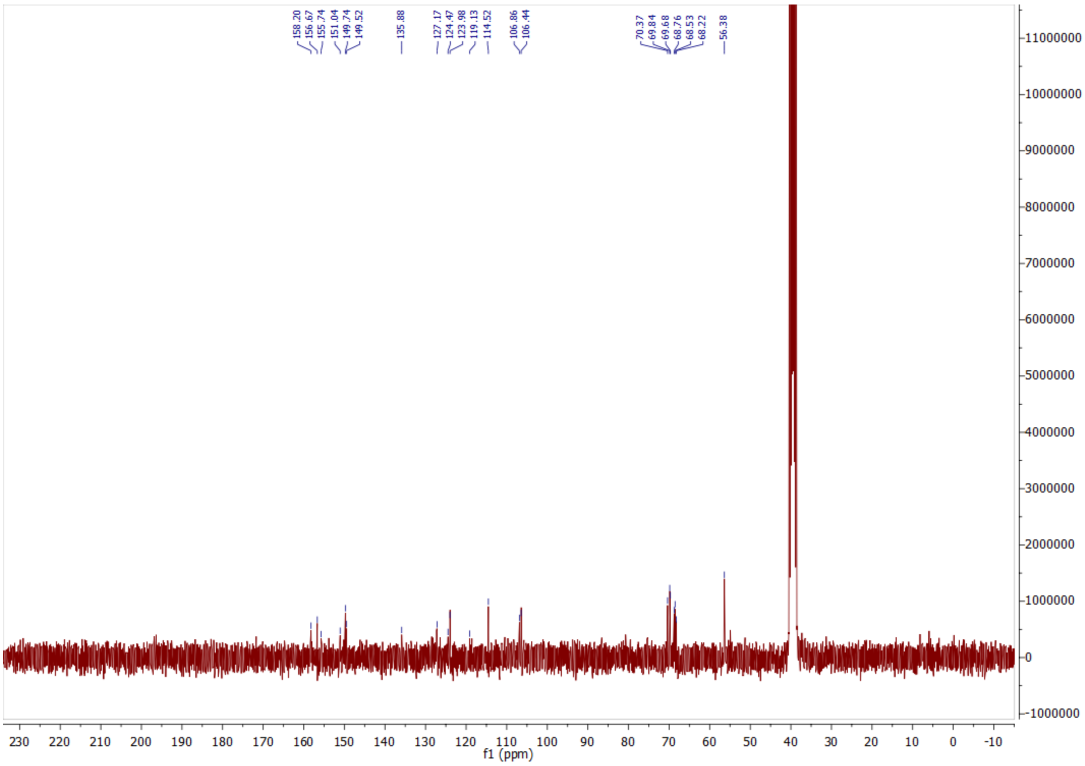

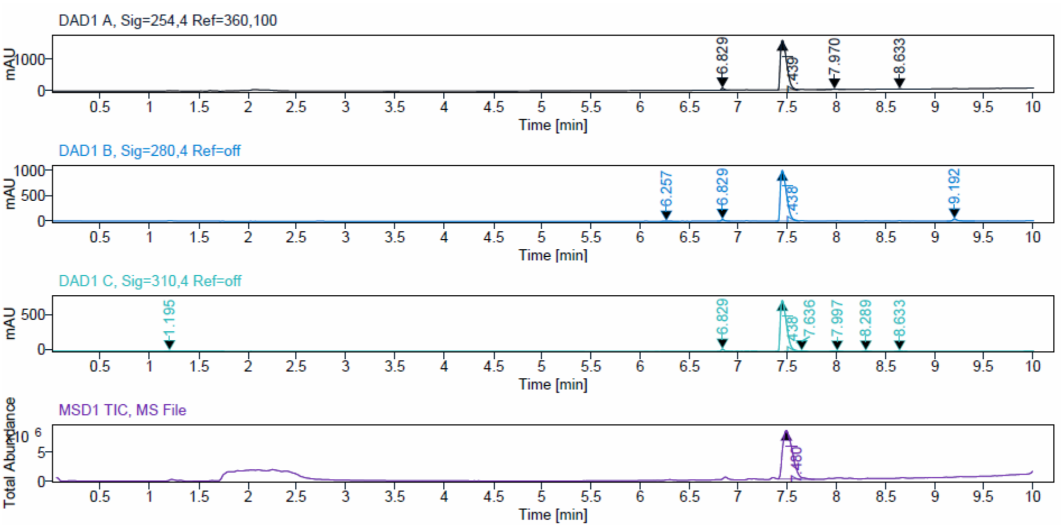

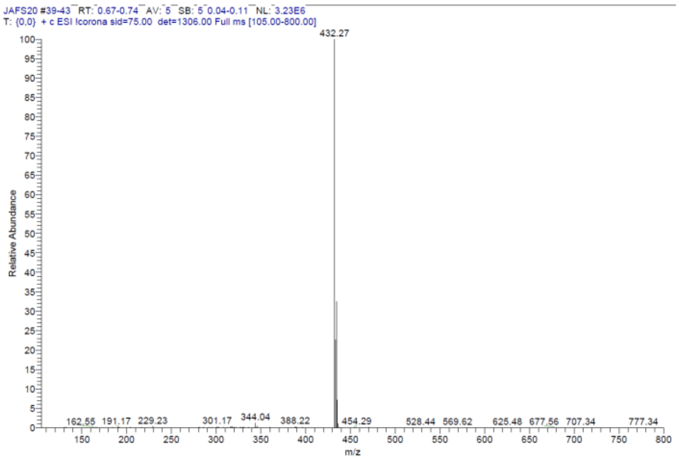

^{1}H, ^{13}C NMR, HPLC, and ESI data of compound **39e**

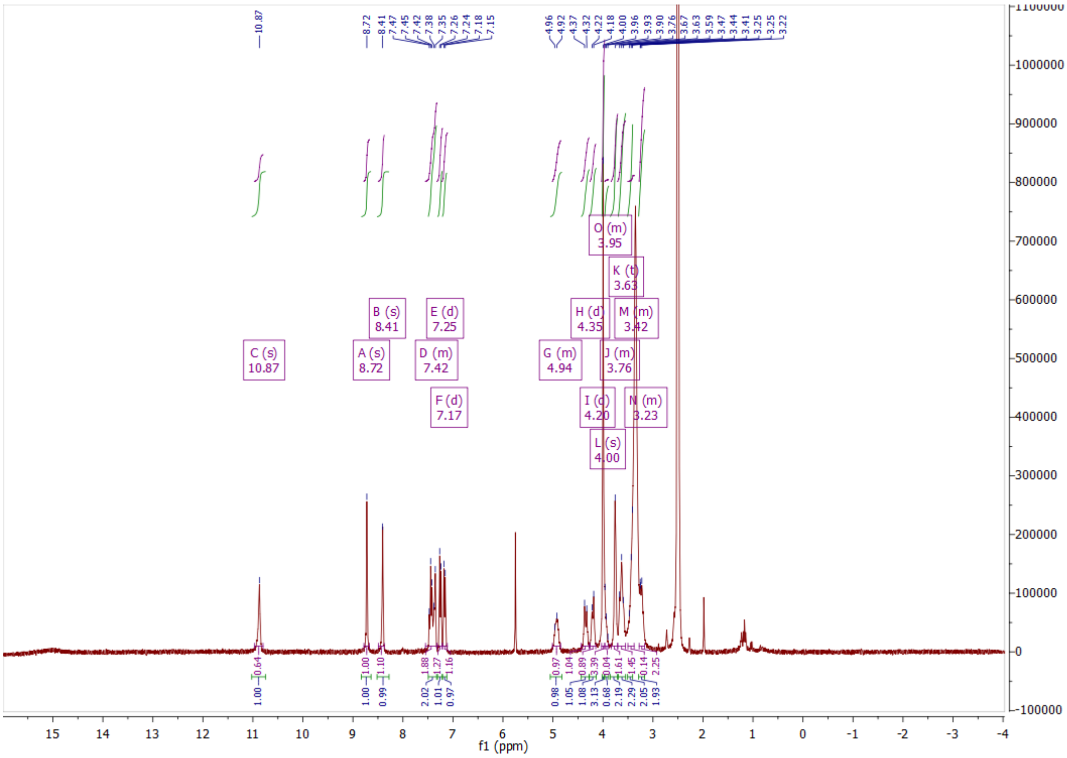

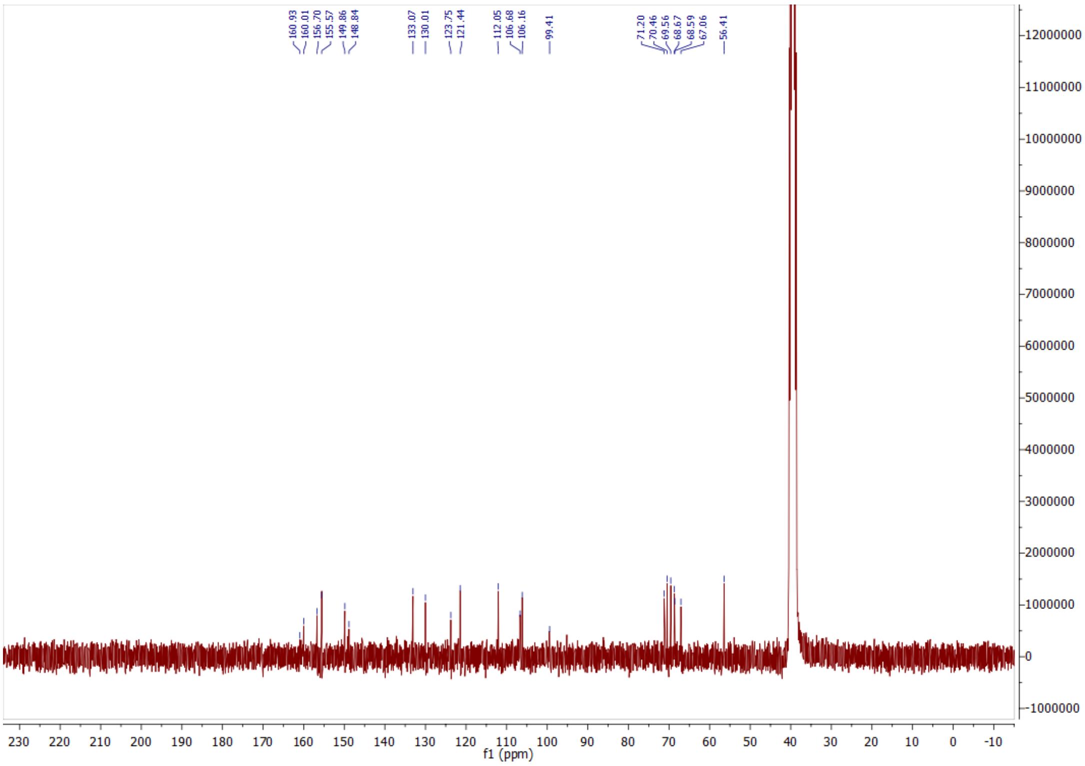
160.93
160.01
156.70
155.57
149.86
148.84
133.07
130.01
123.75
121.44
112.05
106.68
106.16
99.41
71.20
70.46
69.56
68.67
68.59
67.06
56.41
12000000
11000000
10000000
9000000
8000000
7000000
6000000
5000000
4000000
3000000
2000000
1000000
0
-1000000
230 220 210 200 190 180 170 160 150 140 130 120 110 100 90 80 70 60 50 40 30 20 10 0 -10
f1 (ppm)

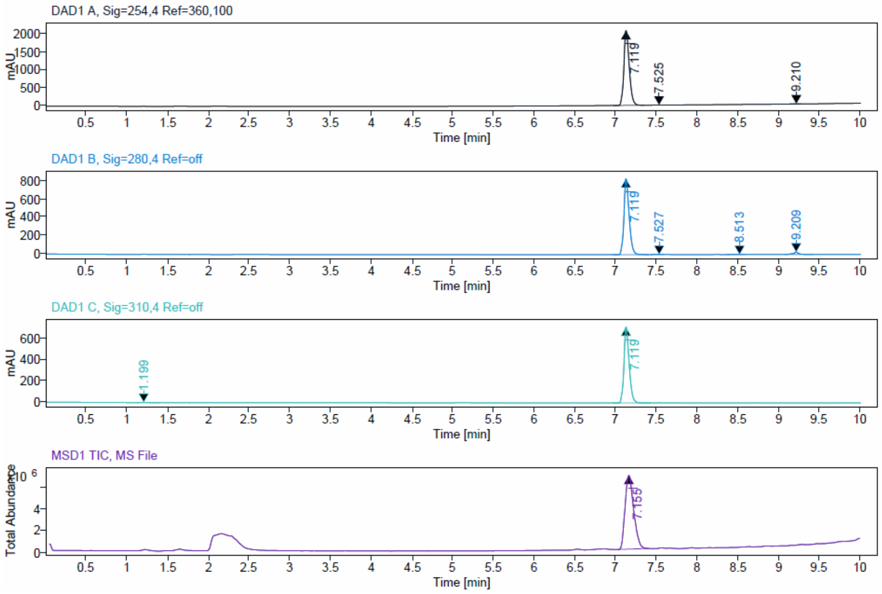
DAD1 A, Sig=254,4 Ref=360,100
mAU
2000
1500
1000
500
0
7.119
7.525
9.210
0.5 1 1.5 2 2.5 3 3.5 4 4.5 5 5.5 6 6.5 7 7.5 8 8.5 9 9.5 10
Time [min]
DAD1 B, Sig=280,4 Ref=off
mAU
800
600
400
200
0
7.119
7.527
8.513
9.209
Time [min]
DAD1 C, Sig=310,4 Ref=off
mAU
600
400
200
0
1.199
7.119
Time [min]
MSD1 TIC, MS File
Total Abundance
x10 6
4
2
0
7.155
Time [min]

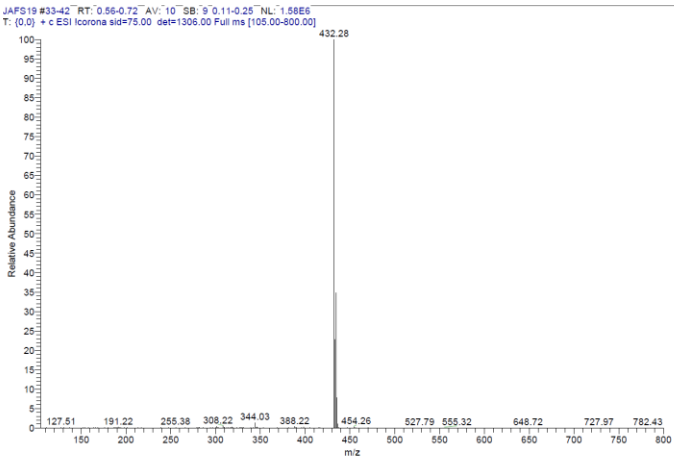
JAFS19 #33-42 RT: 0.56-0.72 AV: 10 SB: 9 0.11-0.25 NL: 1.58E6
T: {0,0} + c ESI !corona sid=75.00 det=1306.00 Full ms [105.00-800.00]
432.28
Relative Abundance
100
95
90
85
80
75
70
65
60
55
50
45
40
35
30
25
20
15
10
5
0
127.51
191.22
255.38
308.22
344.03
388.22
454.26
527.79
555.32
648.72
727.97
782.43
150 200 250 300 350 400 450 500 550 600 650 700 750 800
m/z

^{1}H, ^{13}C NMR, HPLC, and ESI data of compound **39f**

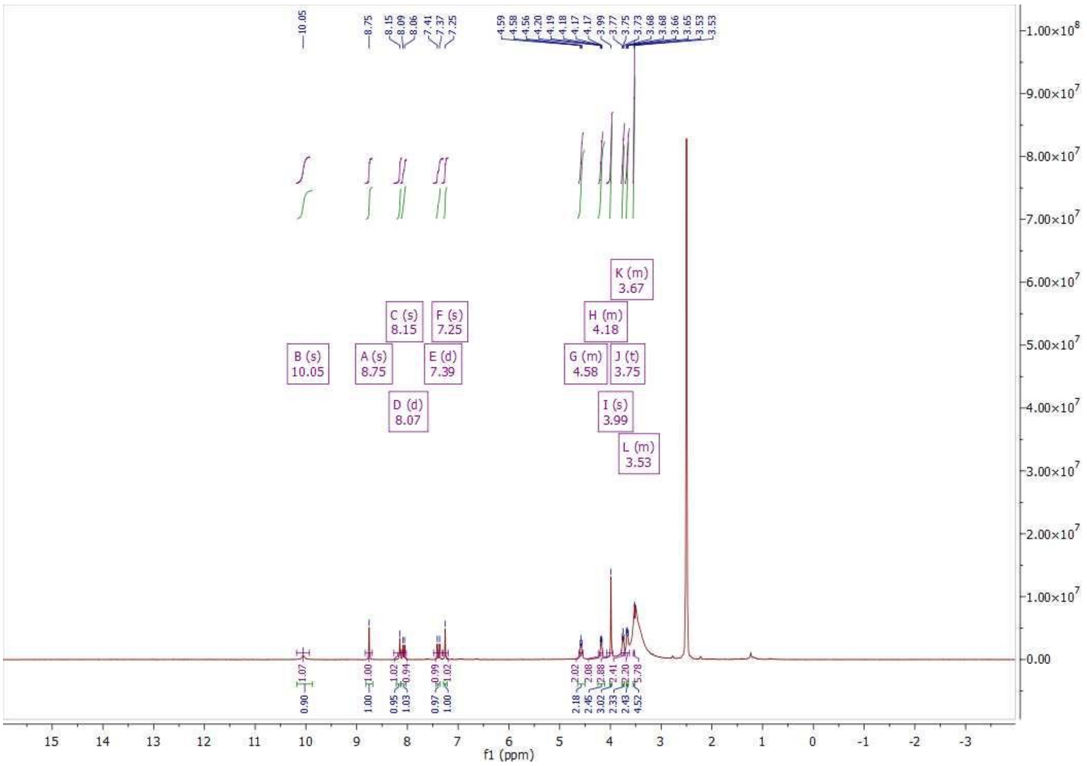

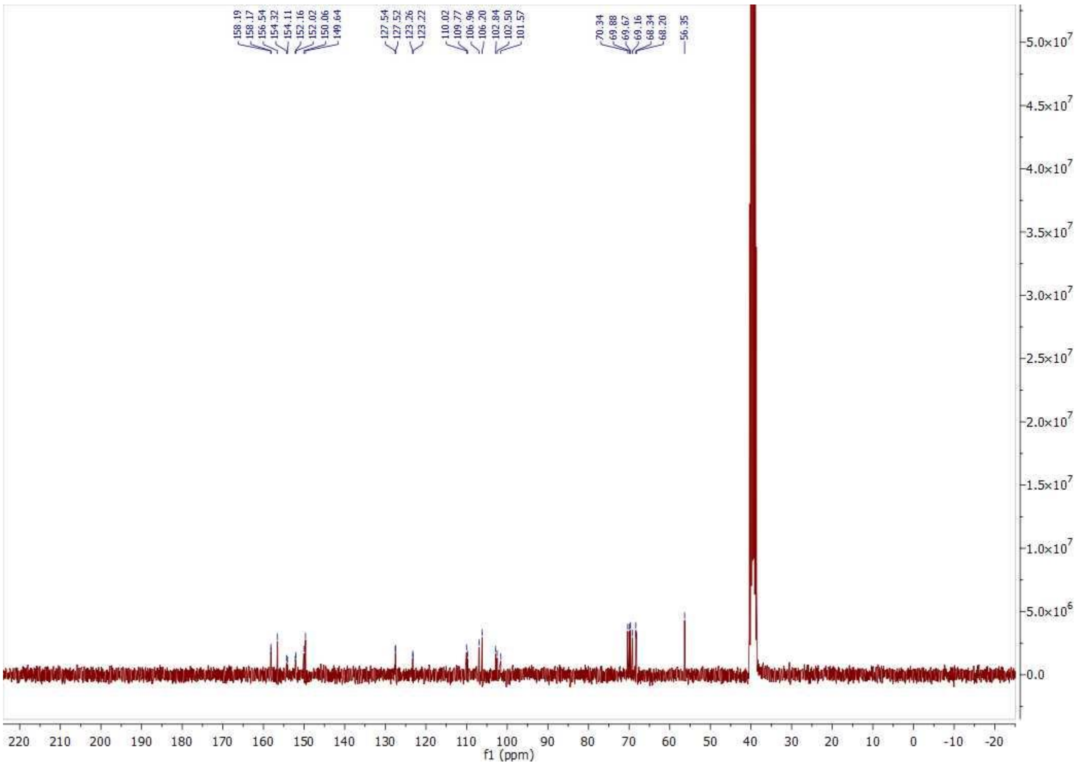

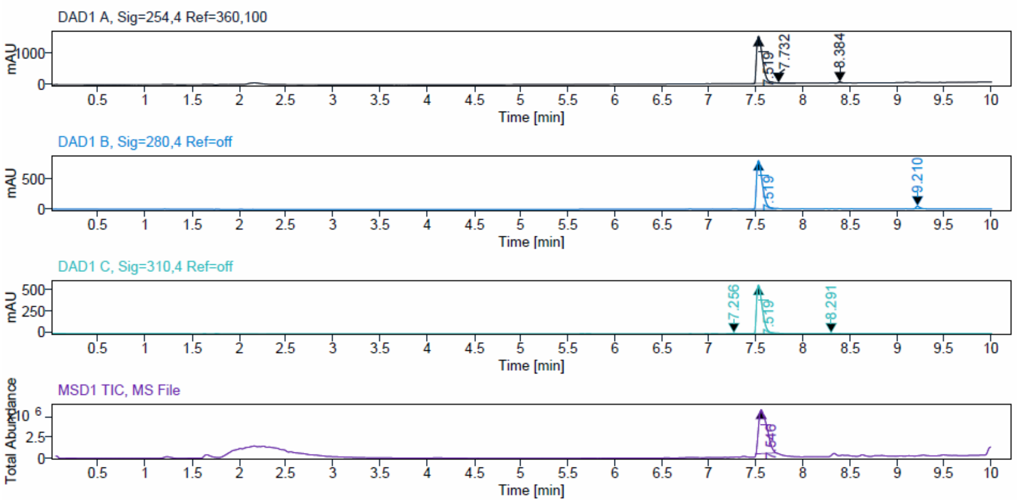

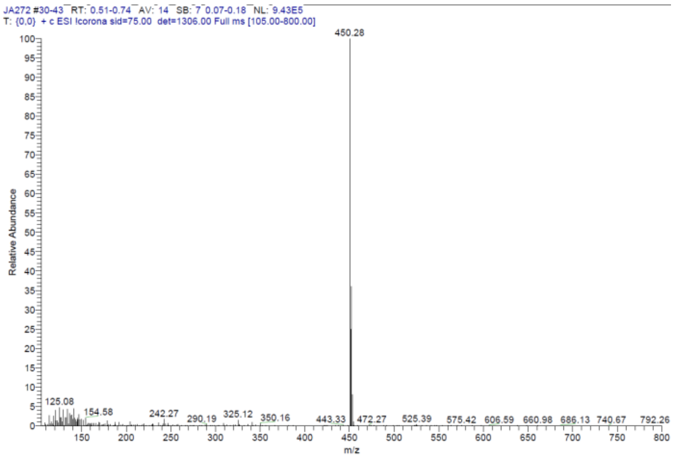

^{1}H and ^{13}C NMR data of compound **40**

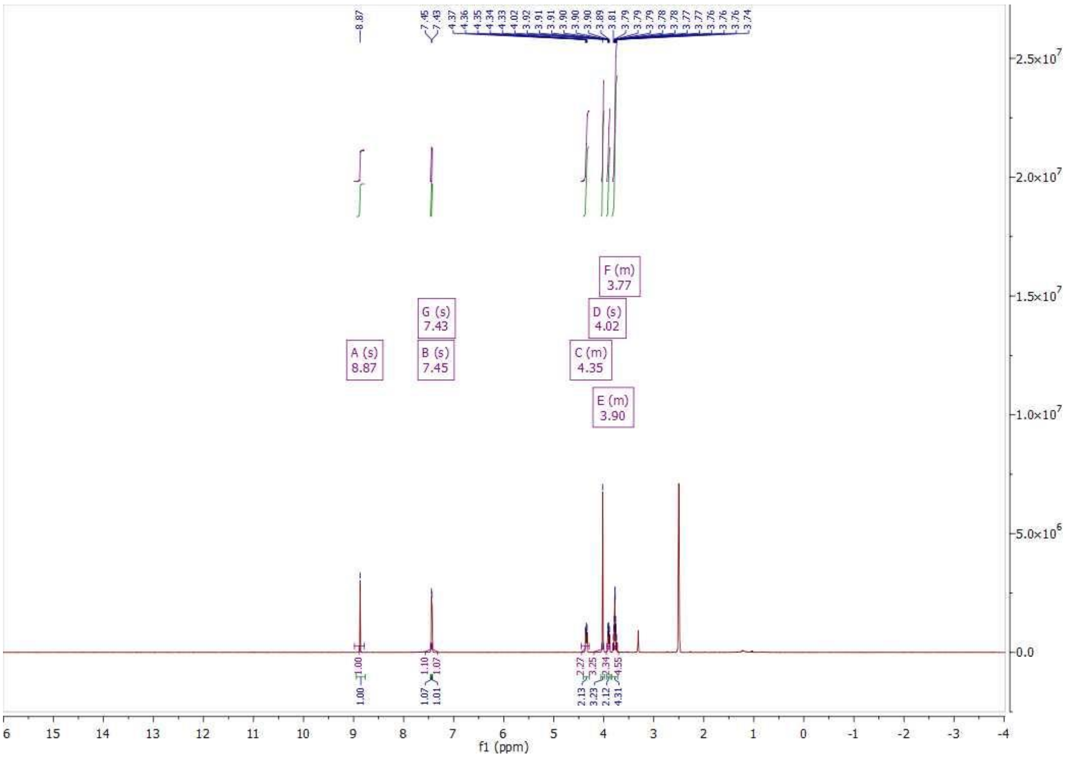

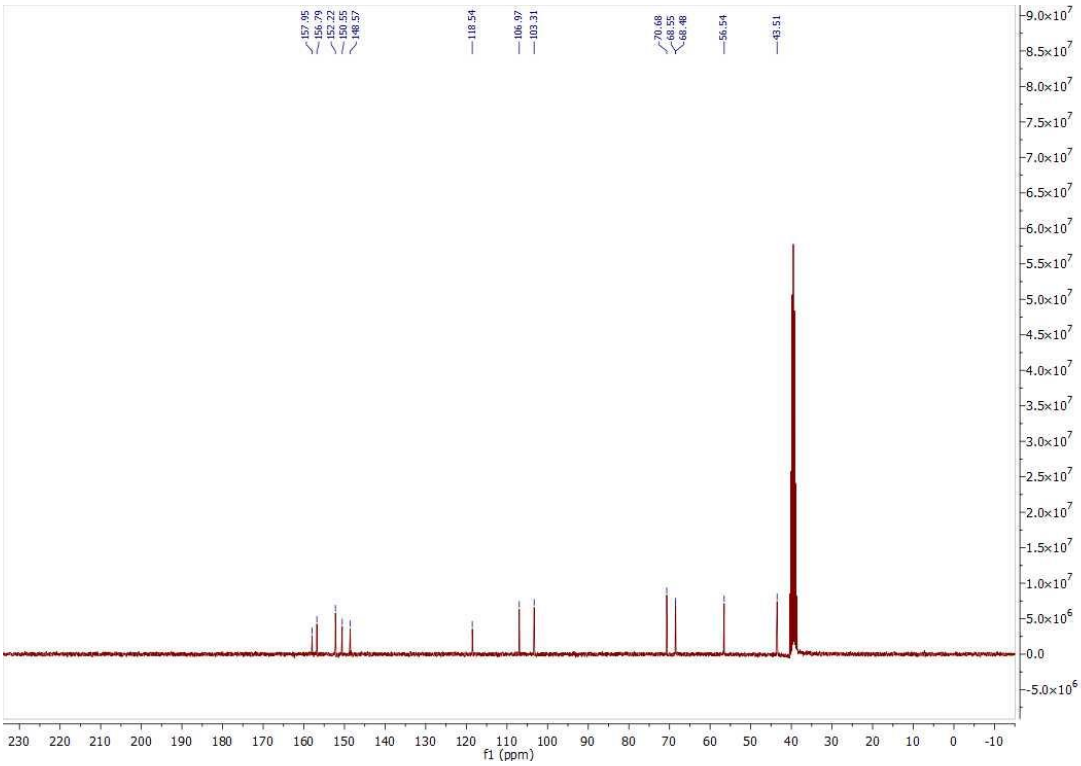

^{1}H, ^{13}C NMR, HPLC, and ESI data of compound **41a**

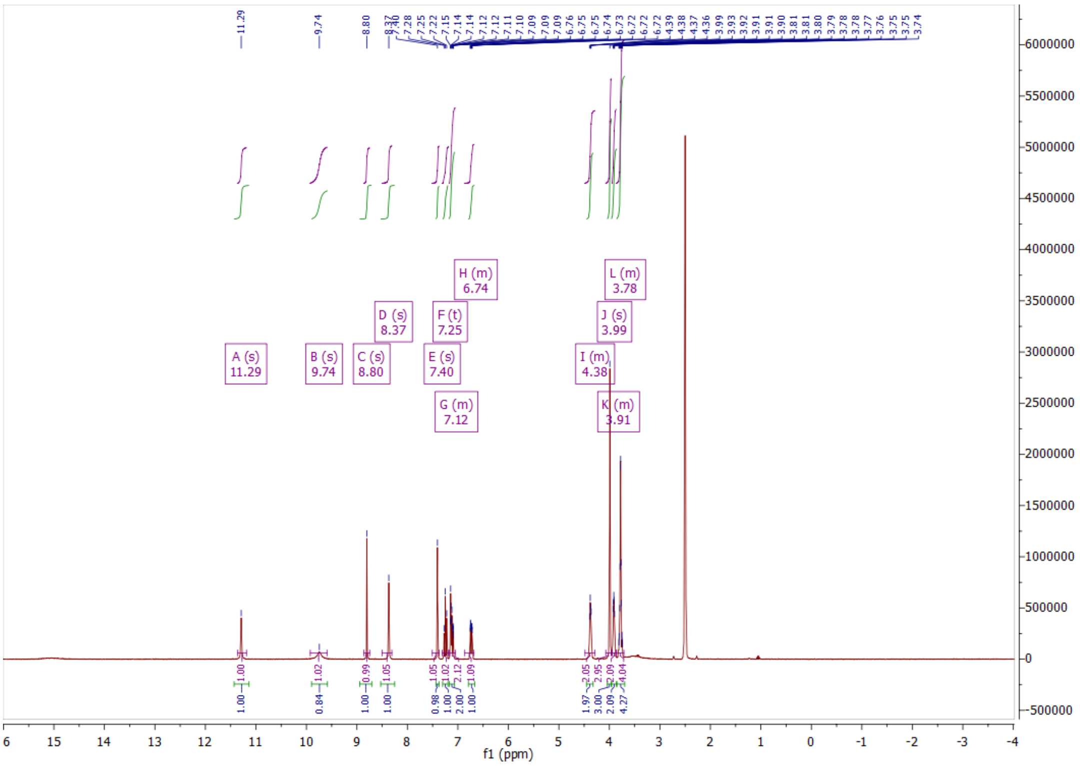

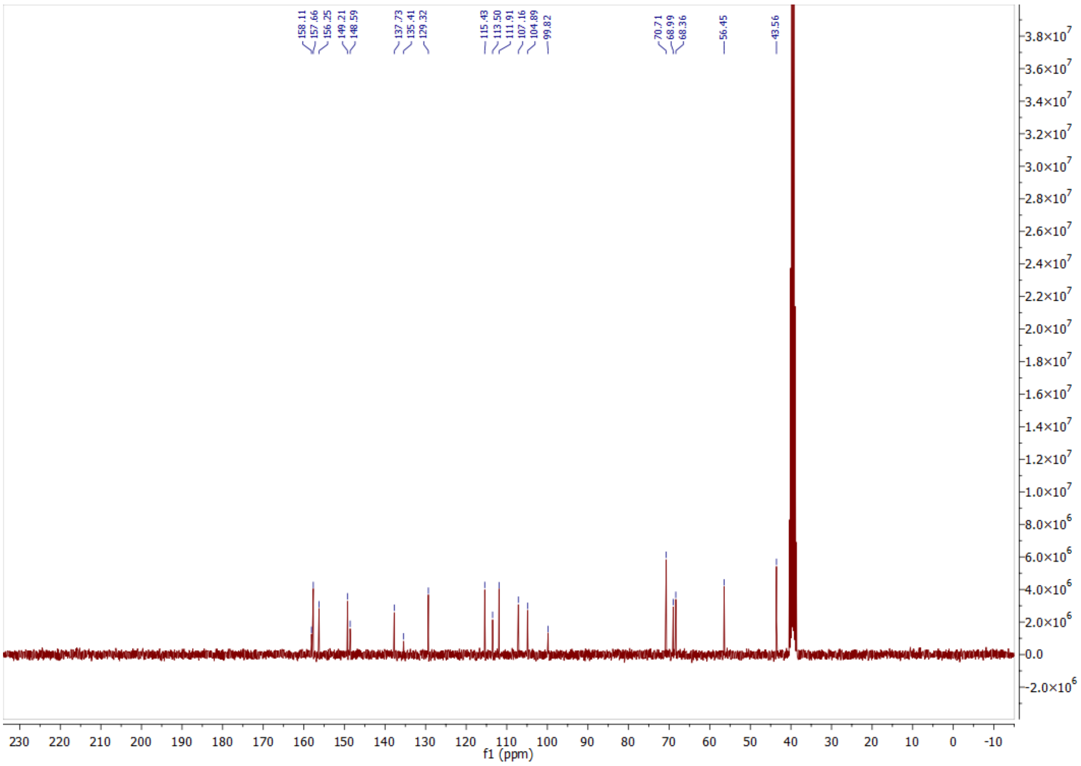
158.11
157.66
156.25
149.21
148.59
137.73
135.41
129.32
115.43
113.50
111.91
107.16
104.89
99.82
70.71
68.99
68.36
56.45
43.56
3.8×10^7
3.6×10^7
3.4×10^7
3.2×10^7
3.0×10^7
2.8×10^7
2.6×10^7
2.4×10^7
2.2×10^7
2.0×10^7
1.8×10^7
1.6×10^7
1.4×10^7
1.2×10^7
1.0×10^7
8.0×10^6
6.0×10^6
4.0×10^6
2.0×10^6
0.0
−2.0×10^6
230 220 210 200 190 180 170 160 150 140 130 120 110 100 90 80 70 60 50 40 30 20 10 0 -10
f1 (ppm)

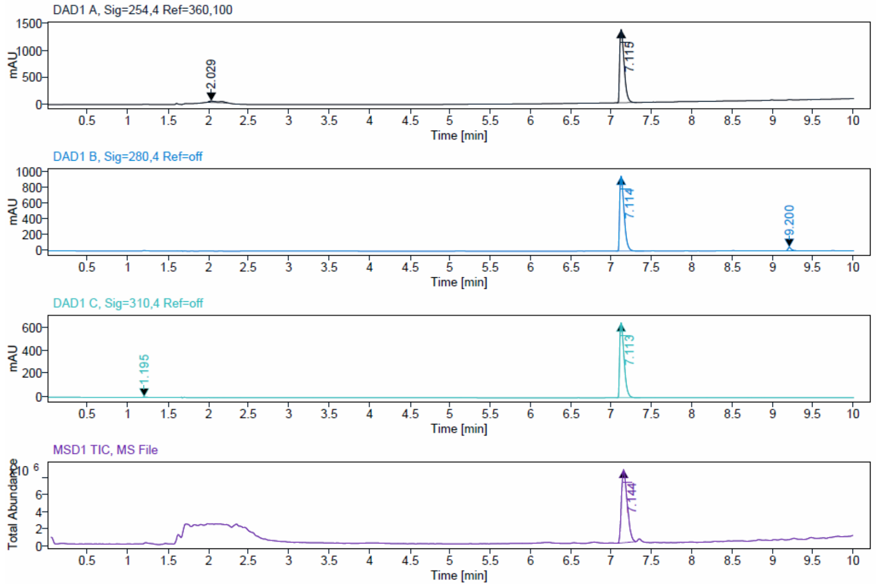
DAD1 A, Sig=254,4 Ref=360,100
mAU
1500
1000
500
0
2.029
7.115
Time [min]
DAD1 B, Sig=280,4 Ref=off
mAU
1000
800
600
400
200
0
7.114
9.200
Time [min]
DAD1 C, Sig=310,4 Ref=off
mAU
600
400
200
0
1.195
7.113
Time [min]
MSD1 TIC, MS File
Total Abundance
10 6
6
4
2
0
7.144
0.5 1 1.5 2 2.5 3 3.5 4 4.5 5 5.5 6 6.5 7 7.5 8 8.5 9 9.5 10
Time [min]

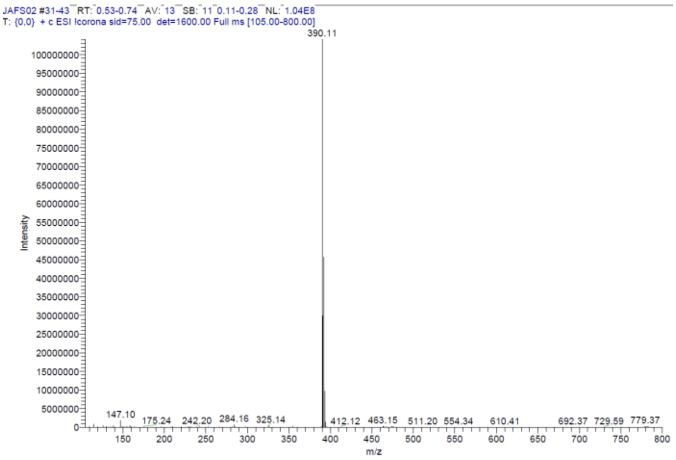
JAFS02 #31-43 RT: 0.53-0.74 AV: 13 SB: 11 0.11-0.28 NL: 1.04E8
T: {0,0} + c ESI Icorona sid=75.00 det=1600.00 Full ms [105.00-800.00]
390.11
Intensity
100000000
95000000
90000000
85000000
80000000
75000000
70000000
65000000
60000000
55000000
50000000
45000000
40000000
35000000
30000000
25000000
20000000
15000000
10000000
5000000
0
147.10
175.24
242.20
284.16
325.14
412.12
463.15
511.20
554.34
610.41
692.37
729.59
779.37
150 200 250 300 350 400 450 500 550 600 650 700 750 800
m/z

^{1}H, ^{13}C NMR, HPLC, and ESI data of compound **41b**

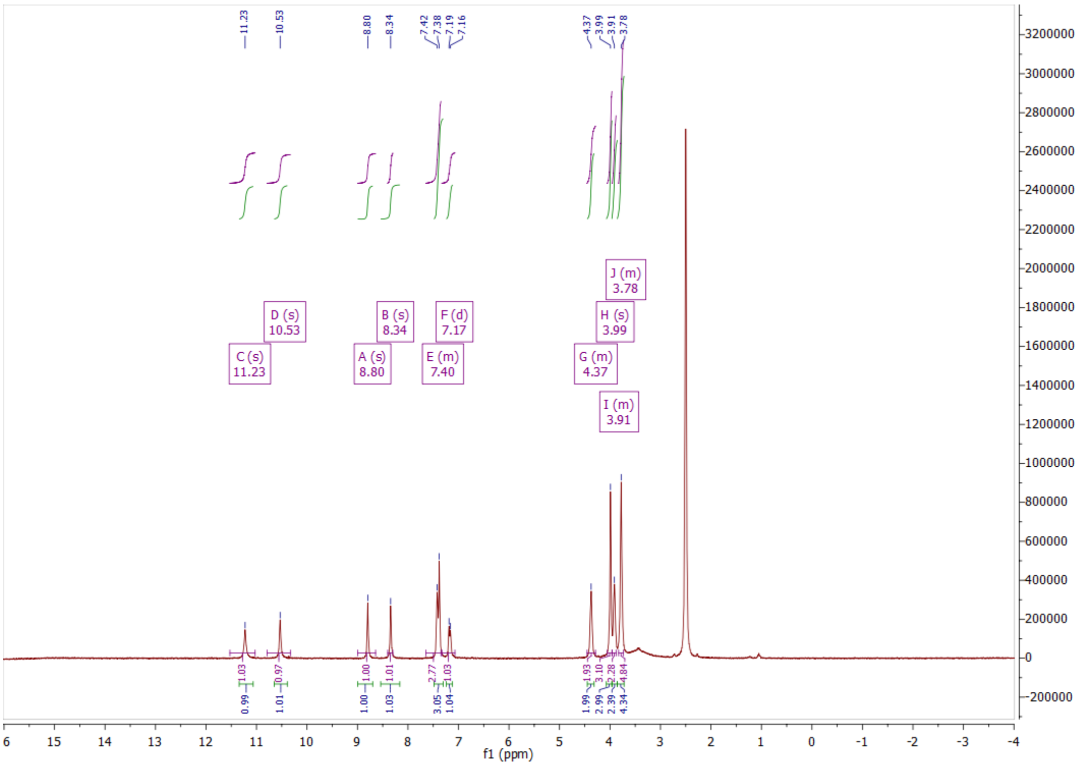

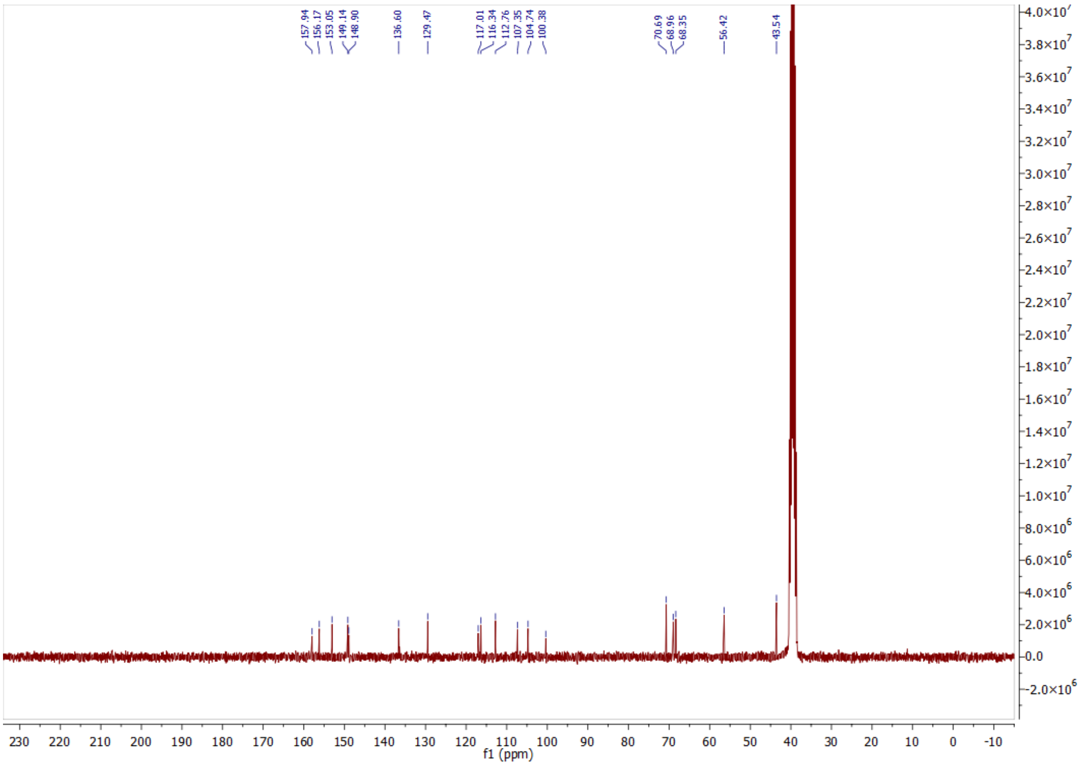

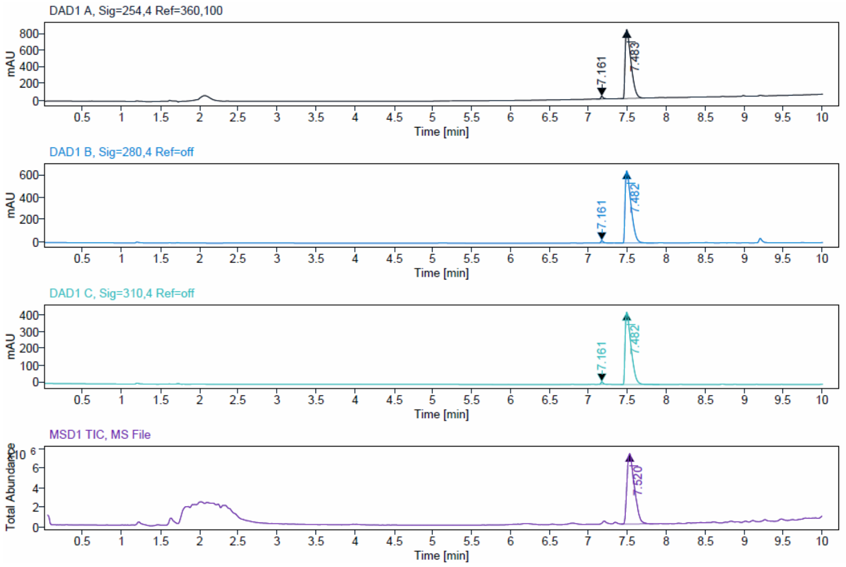

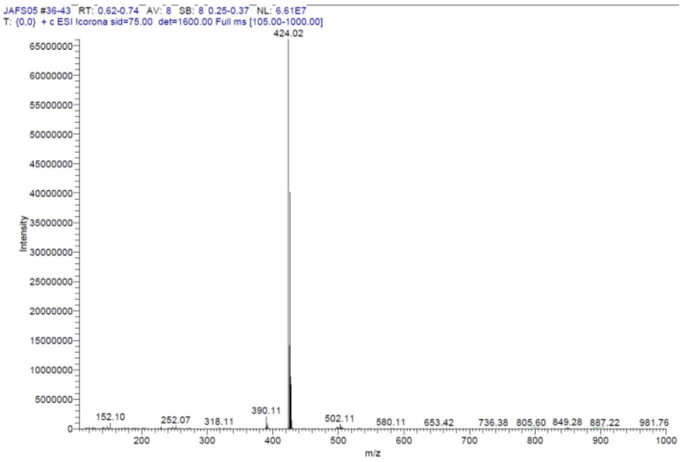

^{1}H, ^{13}C NMR, HPLC, and ESI data of compound **41c**

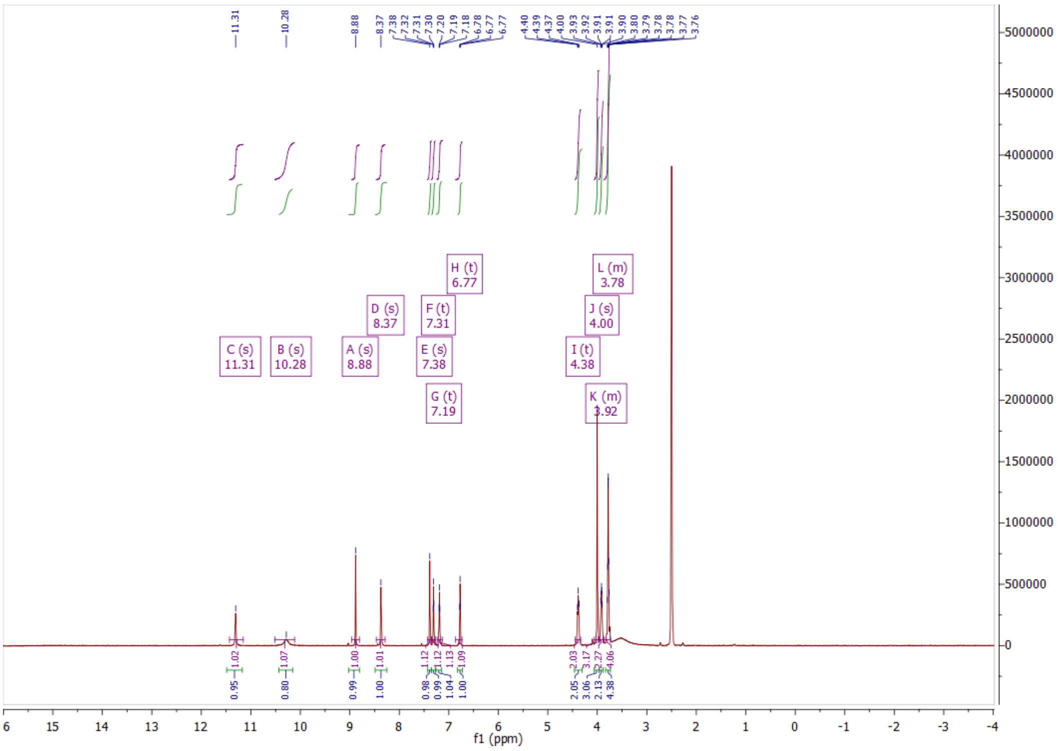

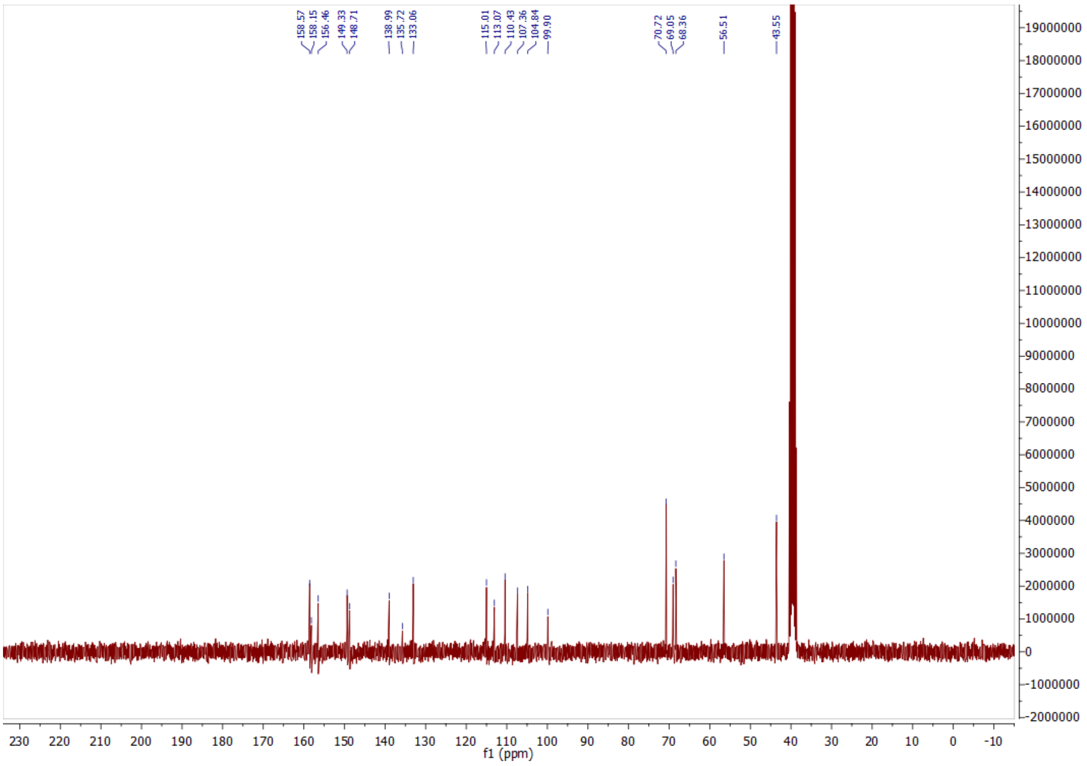
158.57
158.15
156.46
149.33
148.71
138.99
135.72
133.06
115.01
113.07
110.43
107.36
104.84
99.90
70.72
69.05
68.36
56.51
43.55
19000000
18000000
17000000
16000000
15000000
14000000
13000000
12000000
11000000
10000000
9000000
8000000
7000000
6000000
5000000
4000000
3000000
2000000
1000000
0
-1000000
-2000000
230 220 210 200 190 180 170 160 150 140 130 120 110 100 90 80 70 60 50 40 30 20 10 0 -10
f1 (ppm)

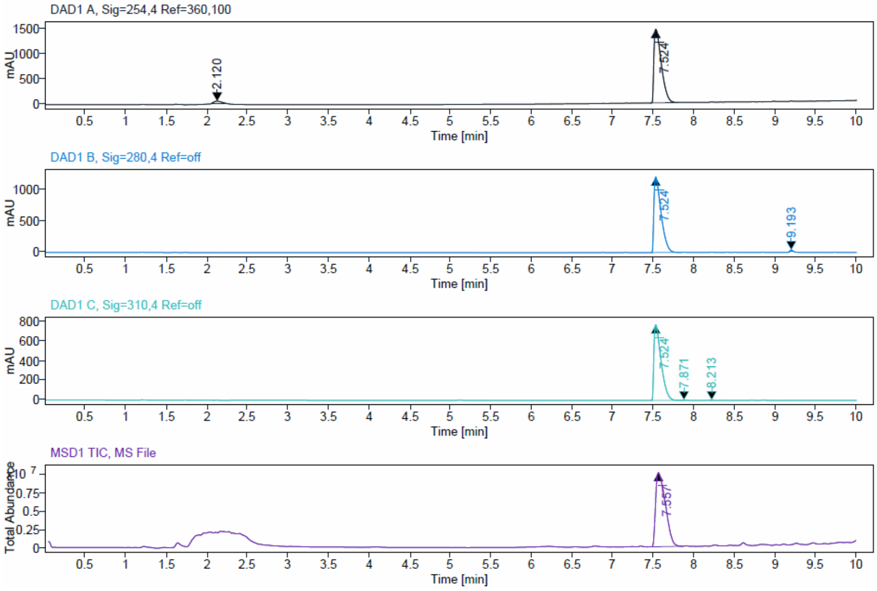
DAD1 A, Sig=254,4 Ref=360,100
mAU
1500
1000
500
0
2.120
7.524
Time [min]
DAD1 B, Sig=280,4 Ref=off
mAU
1000
500
0
7.524
9.193
Time [min]
DAD1 C, Sig=310,4 Ref=off
mAU
800
600
400
200
0
7.524
7.871
8.213
Time [min]
MSD1 TIC, MS File
Total Abundance
x10 7
0.75
0.5
0.25
0
7.557
Time [min]
0.5 1 1.5 2 2.5 3 3.5 4 4.5 5 5.5 6 6.5 7 7.5 8 8.5 9 9.5 10

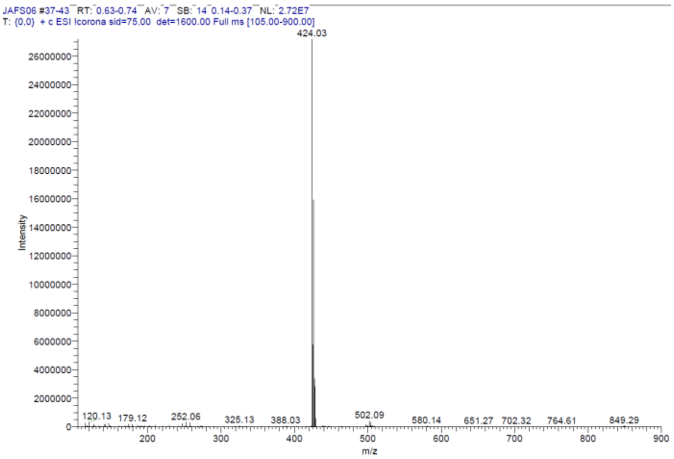
JAFS06 #37-43 RT: 0.63-0.74 AV: 7 SB: 14 0.14-0.37 NL: 2.72E7
T: {0,0} + c ESI Icorona sid=75.00 det=1600.00 Full ms [105.00-900.00]
424.03
Intensity
26000000
24000000
22000000
20000000
18000000
16000000
14000000
12000000
10000000
8000000
6000000
4000000
2000000
0
120.13
179.12
252.06
325.13
388.03
502.09
580.14
651.27
702.32
764.61
849.29
200 300 400 500 600 700 800 900
m/z

^{1}H, ^{13}C NMR, HPLC, and ESI data of compound **41d**

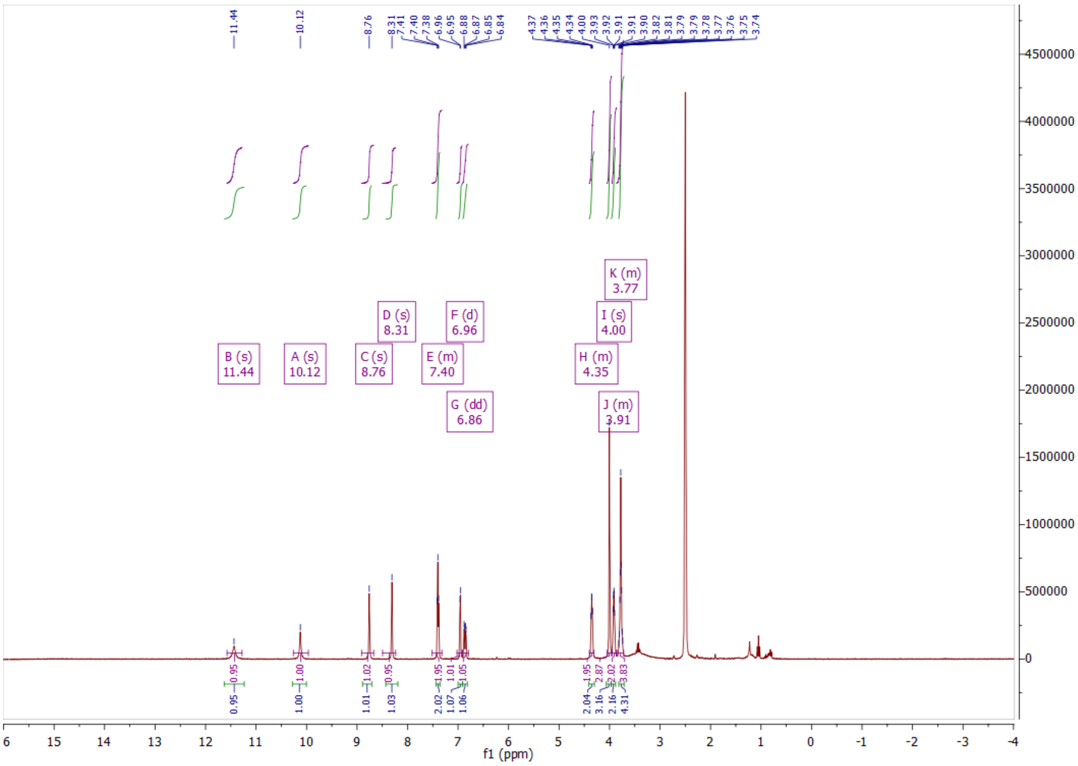

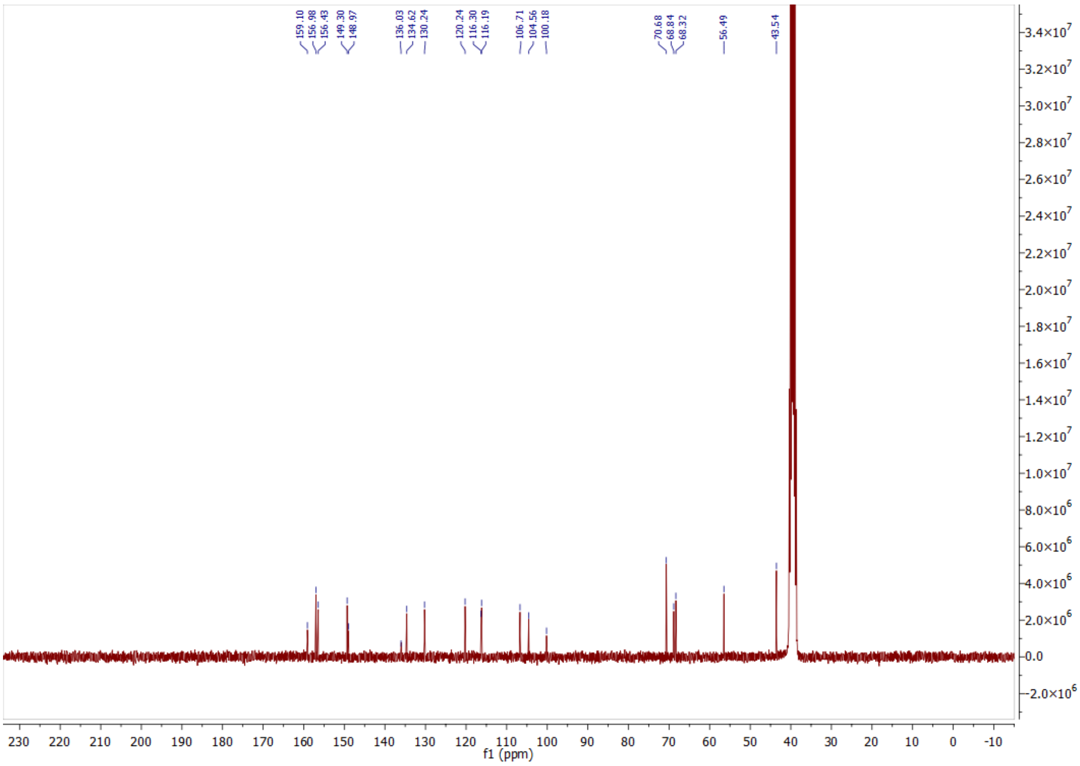

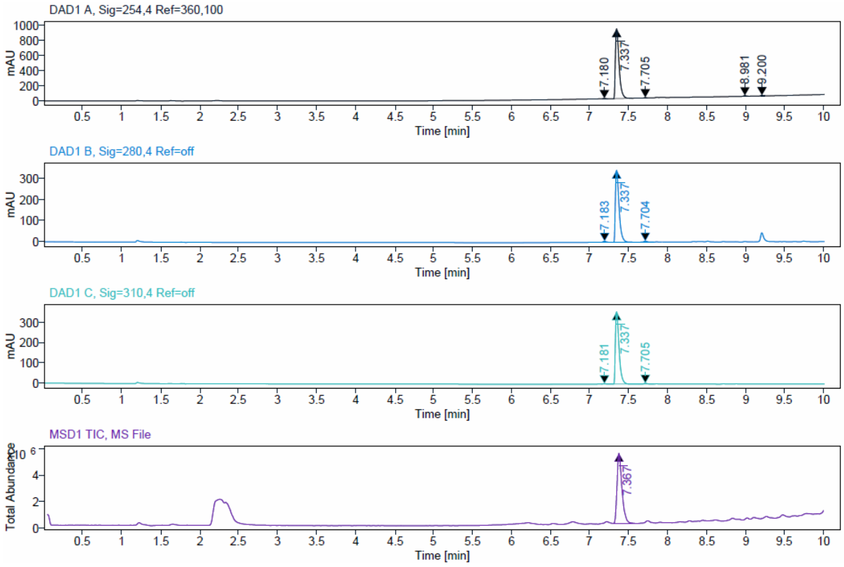

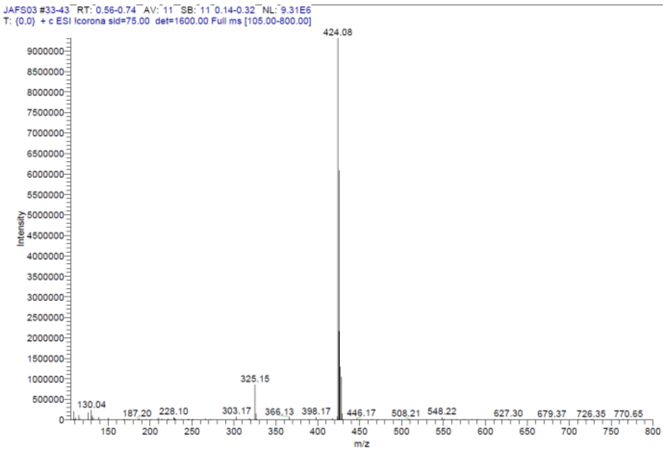

^{1}H, ^{13}C NMR, HPLC, and ESI data of compound **42a**

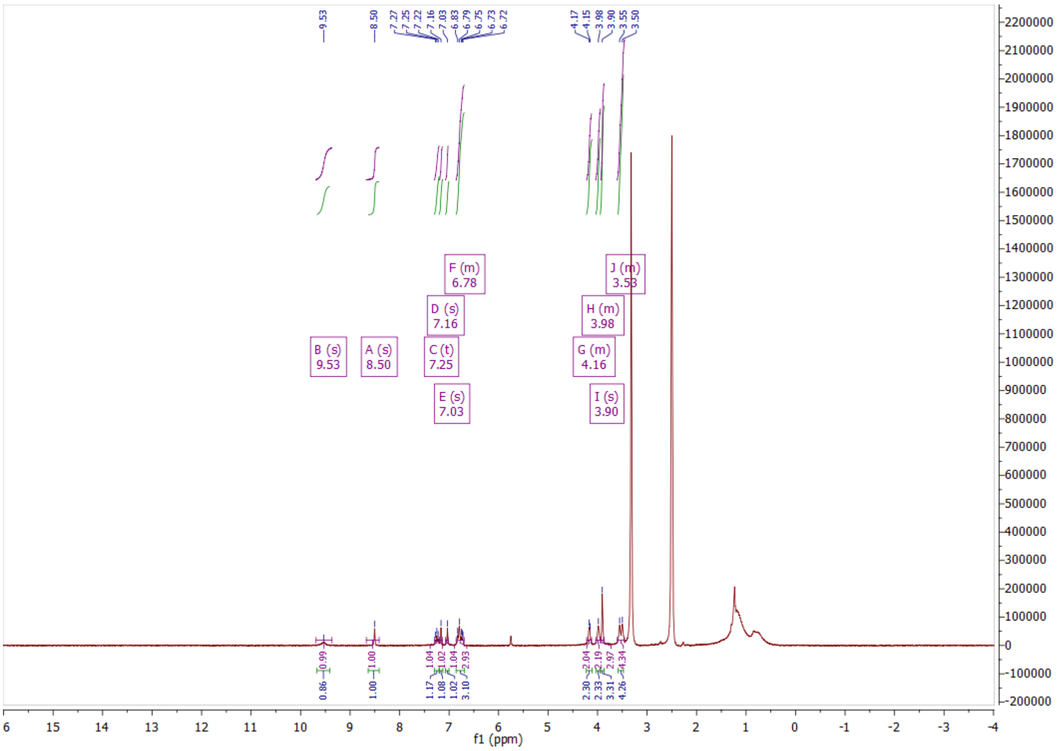

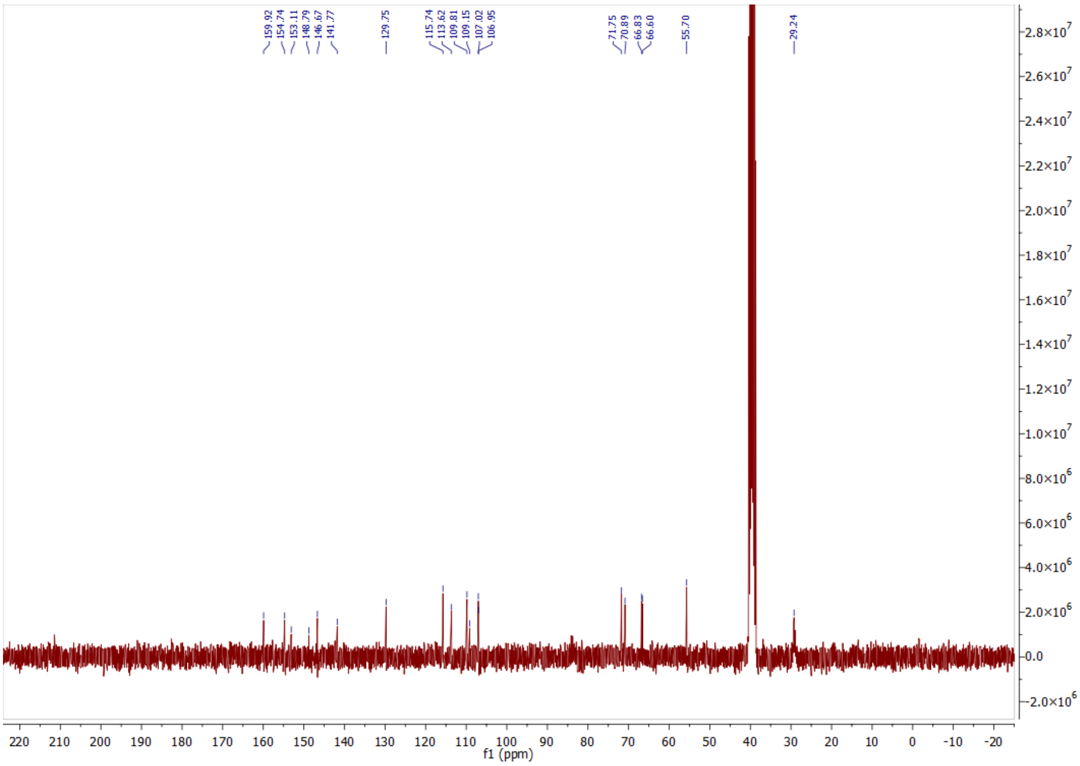
159.92
154.74
153.11
148.79
146.67
141.77
129.75
115.74
113.62
109.81
109.15
107.02
106.95
71.75
70.89
66.83
66.60
55.70
29.24
2.8×10^7
2.6×10^7
2.4×10^7
2.2×10^7
2.0×10^7
1.8×10^7
1.6×10^7
1.4×10^7
1.2×10^7
1.0×10^7
8.0×10^6
6.0×10^6
4.0×10^6
2.0×10^6
0.0
−2.0×10^6
220 210 200 190 180 170 160 150 140 130 120 110 100 90 80 70 60 50 40 30 20 10 0 -10 -20
f1 (ppm)

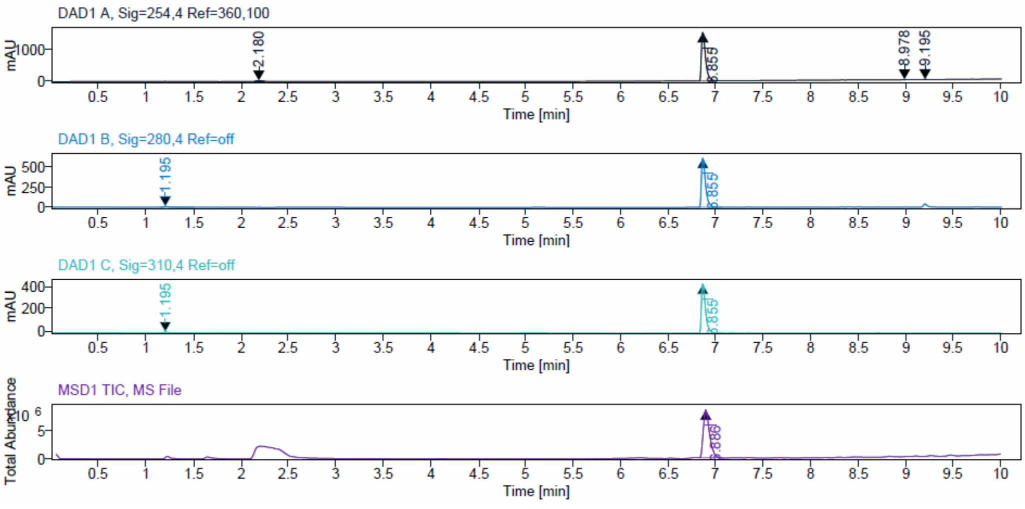
DAD1 A, Sig=254,4 Ref=360,100
mAU
1000
0
2.180
6.855
8.978
9.195
Time [min]
DAD1 B, Sig=280,4 Ref=off
mAU
500
250
0
1.195
6.855
Time [min]
DAD1 C, Sig=310,4 Ref=off
mAU
400
200
0
1.195
6.855
Time [min]
MSD1 TIC, MS File
Total Abundance
x10 6
5
0
6.880
Time [min]
0.5 1 1.5 2 2.5 3 3.5 4 4.5 5 5.5 6 6.5 7 7.5 8 8.5 9 9.5 10

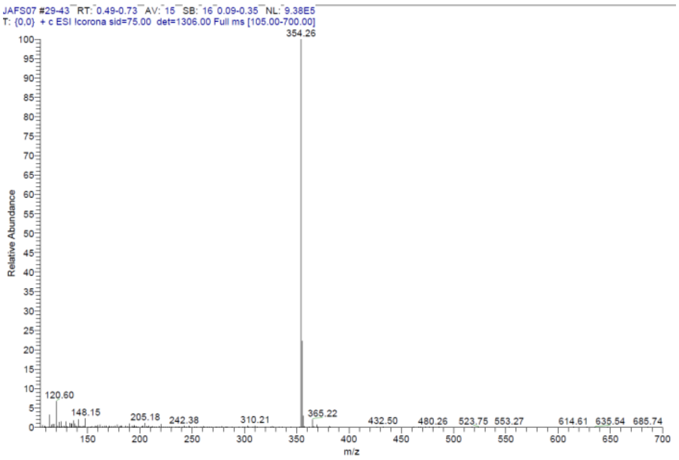
JAFS07 #29-43 RT: 0.49-0.73 AV: 15 SB: 16 0.09-0.35 NL: 9.38E5
T: {0,0} + c ESI Icorona sid=75.00 det=1306.00 Full ms [105.00-700.00]
354.26
120.60
148.15
205.18
242.38
310.21
365.22
432.50
480.26
523.75
553.27
614.61
635.54
685.74
Relative Abundance
0 5 10 15 20 25 30 35 40 45 50 55 60 65 70 75 80 85 90 95 100
150 200 250 300 350 400 450 500 550 600 650 700
m/z

^{1}H, ^{13}C NMR, HPLC, and ESI data of compound **42b**

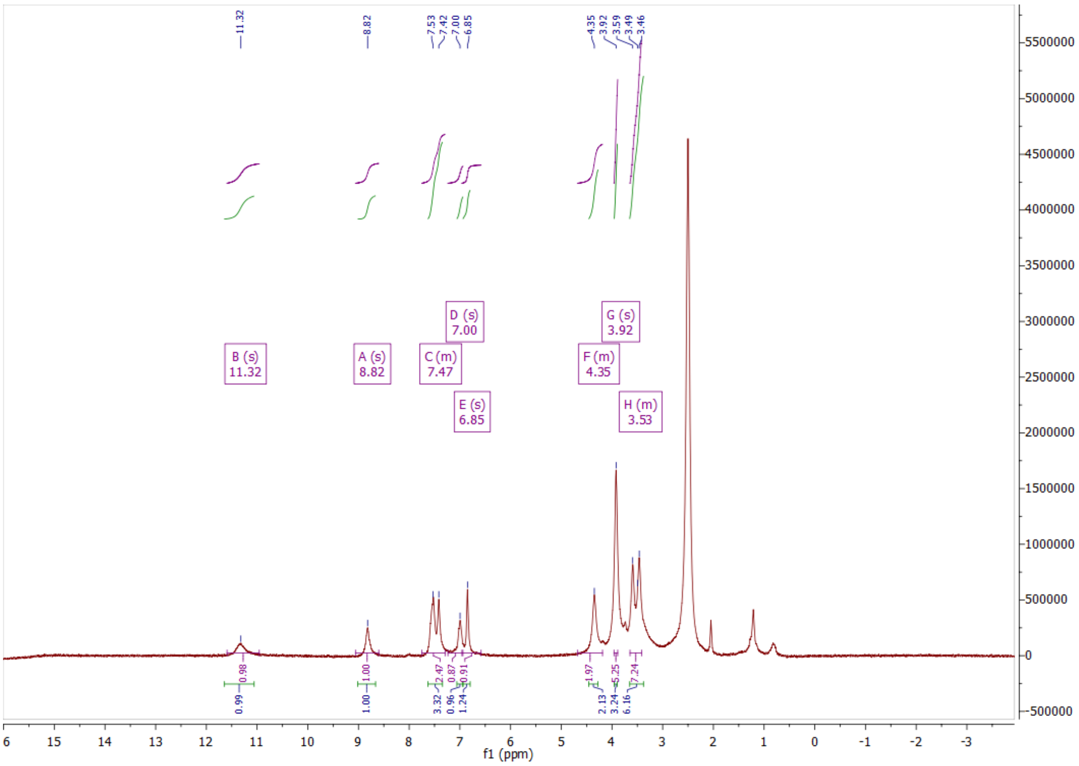

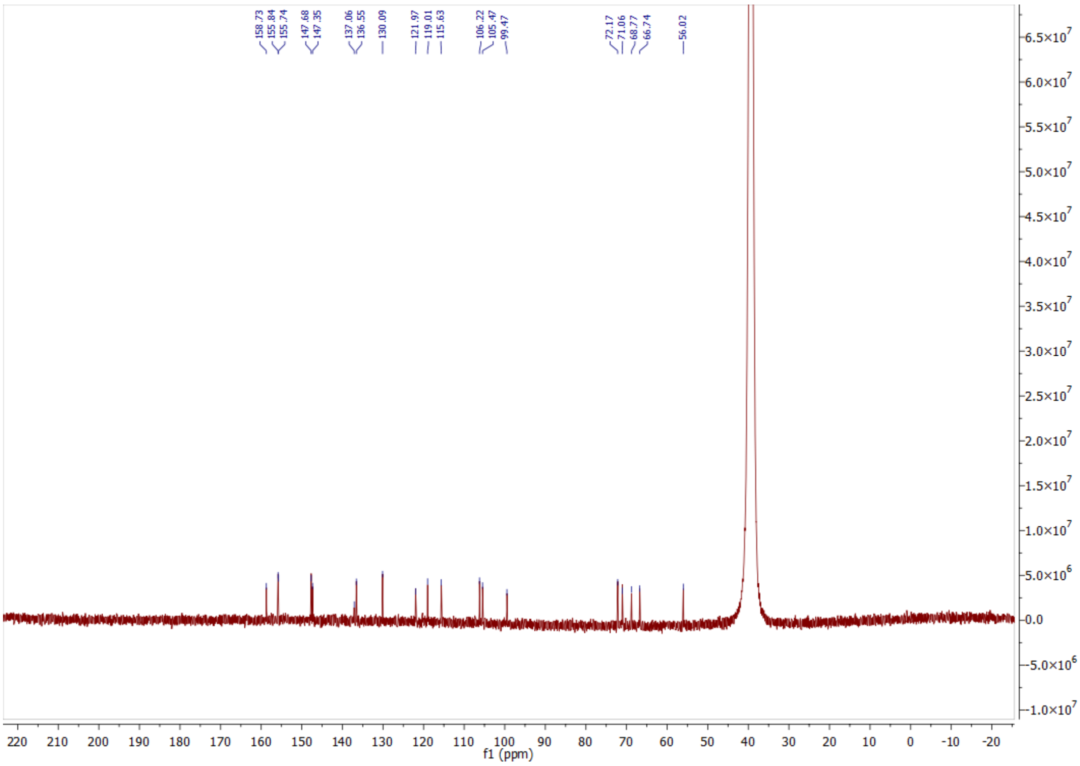

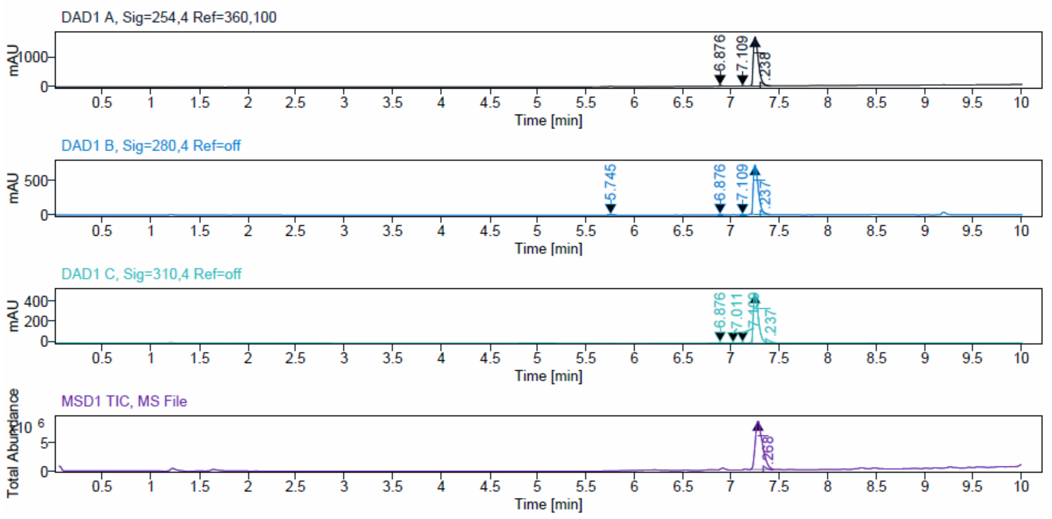

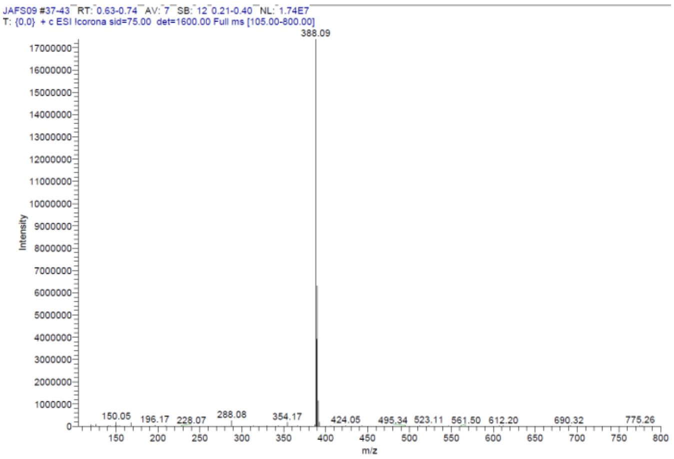

^{1}H, ^{13}C NMR, HPLC, and ESI data of compound **42c**

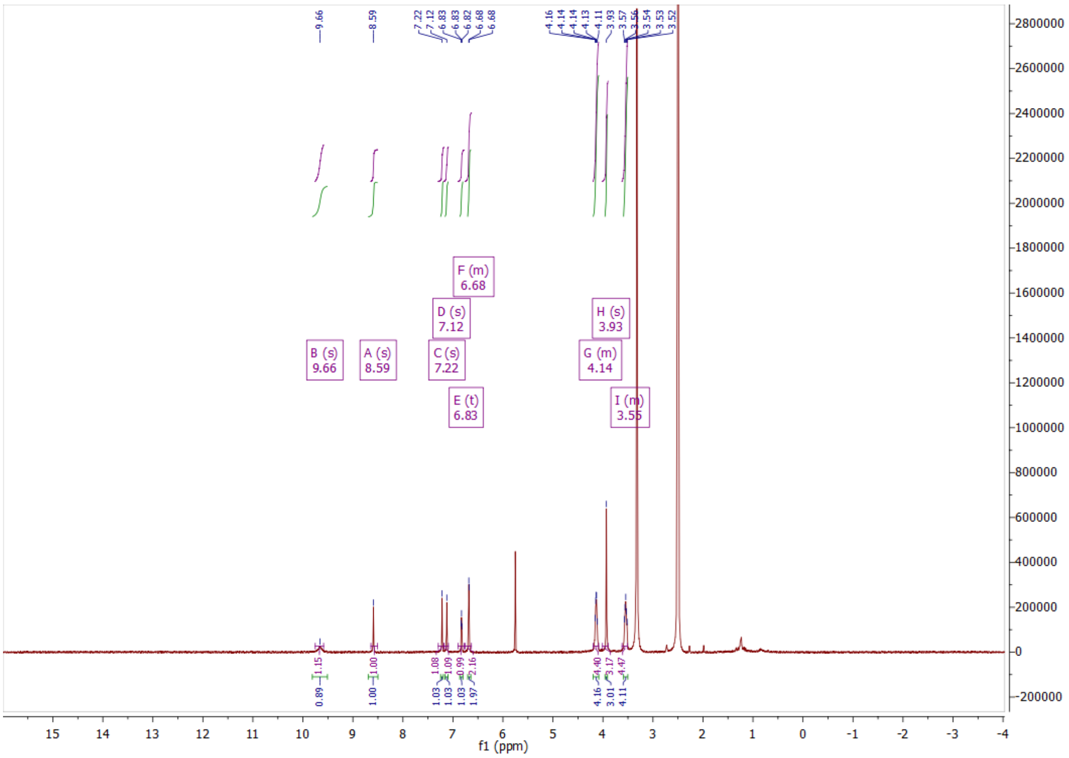

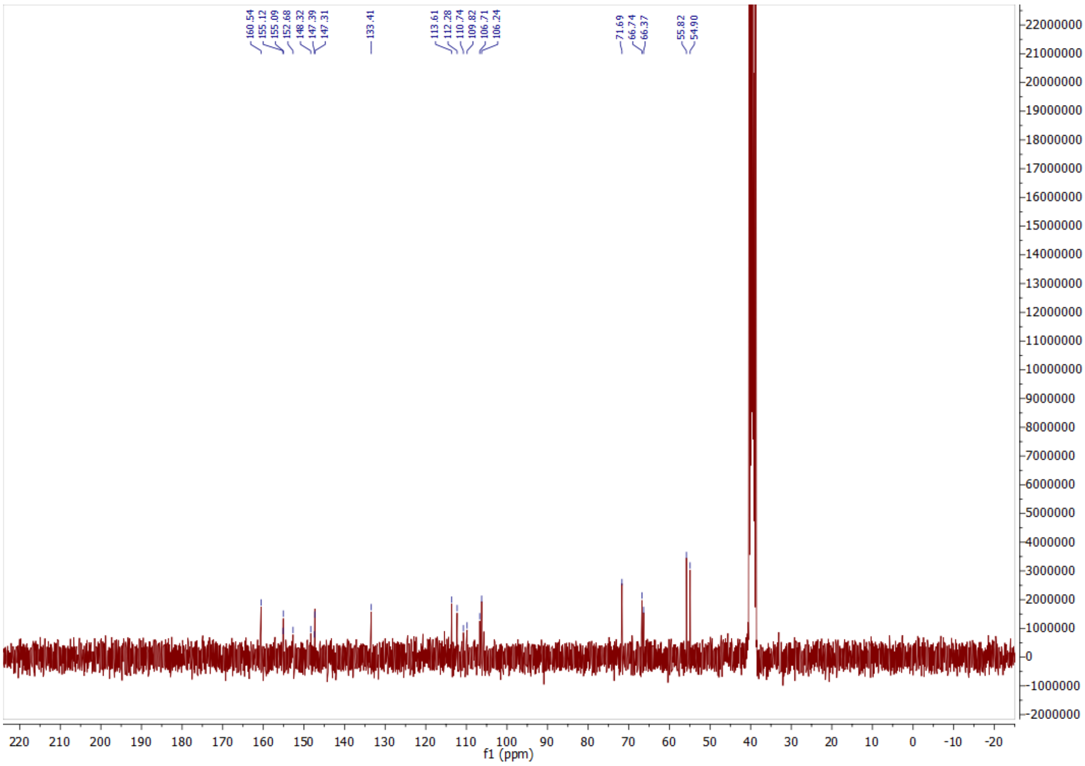
160.54
155.12
155.09
152.68
148.32
147.39
147.31
133.41
113.61
112.28
110.74
109.82
106.71
106.24
71.69
66.74
66.37
55.82
54.90
22000000
21000000
20000000
19000000
18000000
17000000
16000000
15000000
14000000
13000000
12000000
11000000
10000000
9000000
8000000
7000000
6000000
5000000
4000000
3000000
2000000
1000000
0
-1000000
-2000000
220 210 200 190 180 170 160 150 140 130 120 110 100 90 80 70 60 50 40 30 20 10 0 -10 -20
f1 (ppm)

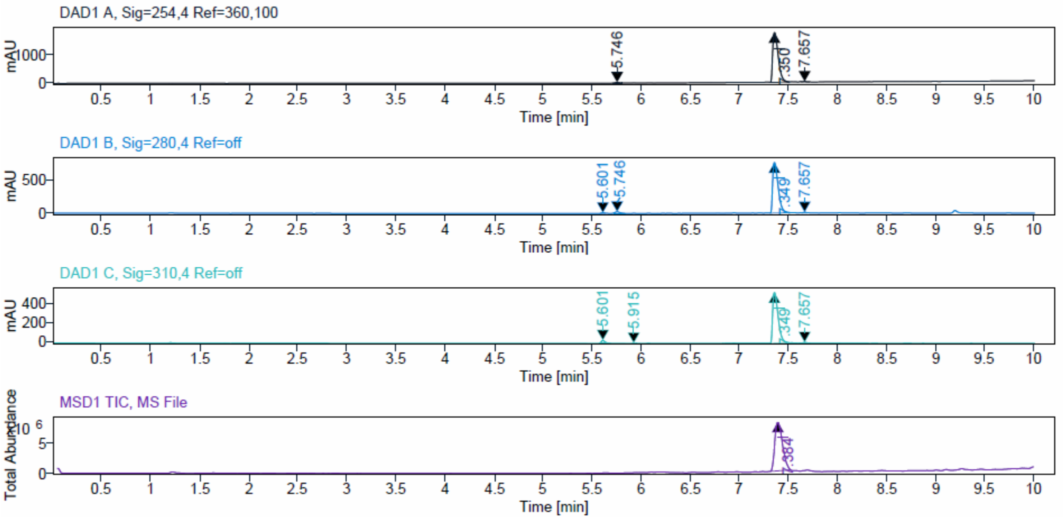
DAD1 A, Sig=254,4 Ref=360,100
mAU
1000
0
5.746
.350
7.657
Time [min]
DAD1 B, Sig=280,4 Ref=off
mAU
500
0
5.601
5.746
.349
7.657
Time [min]
DAD1 C, Sig=310,4 Ref=off
mAU
400
200
0
5.601
5.915
.349
7.657
Time [min]
MSD1 TIC, MS File
Total Abundance
x10 6
5
0
7.384
Time [min]
0.5 1 1.5 2 2.5 3 3.5 4 4.5 5 5.5 6 6.5 7 7.5 8 8.5 9 9.5 10

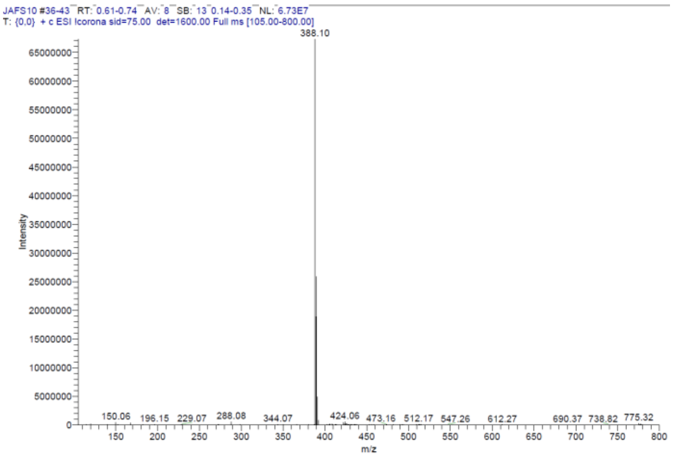
JAFS10 #36-43 RT: 0.61-0.74 AV: 8 SB: 13 0.14-0.35 NL: 6.73E7
T: {0,0} + c ESI !corona sid=75.00 det=1600.00 Full ms [105.00-800.00]
388.10
Intensity
65000000
60000000
55000000
50000000
45000000
40000000
35000000
30000000
25000000
20000000
15000000
10000000
5000000
0
150.06
196.15
229.07
288.08
344.07
424.06
473.16
512.17
547.26
612.27
690.37
738.82
775.32
150 200 250 300 350 400 450 500 550 600 650 700 750 800
m/z

^{1}H, ^{13}C NMR, HPLC, and ESI data of compound **42d**

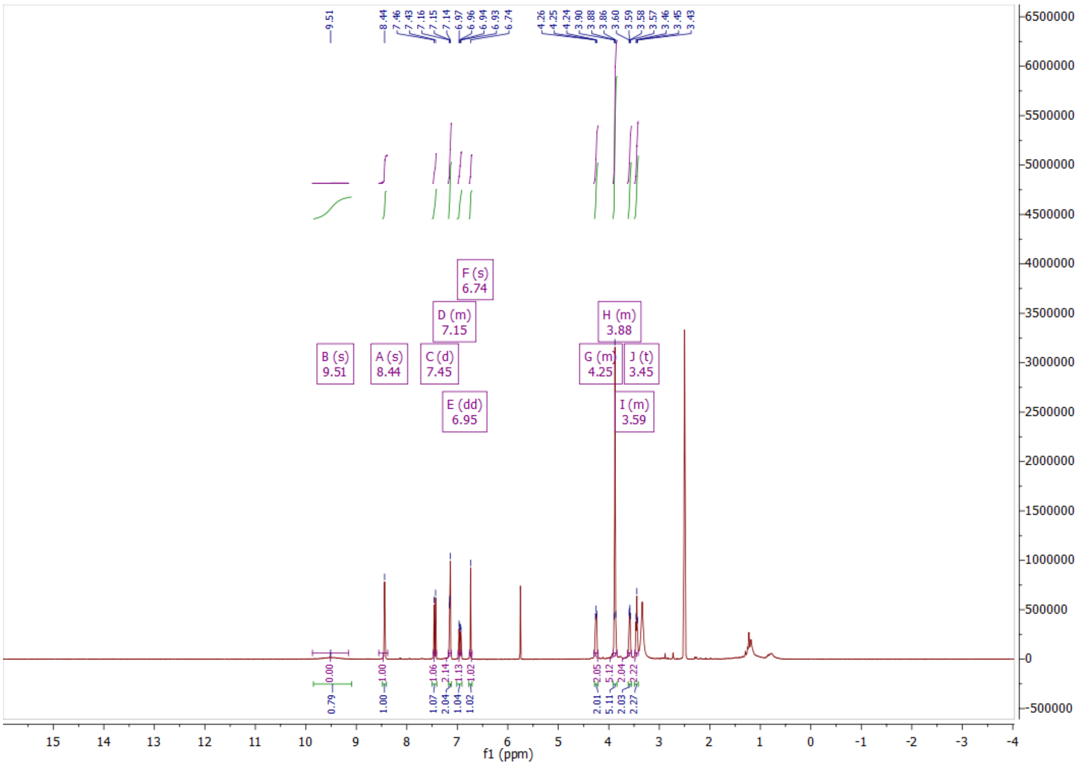

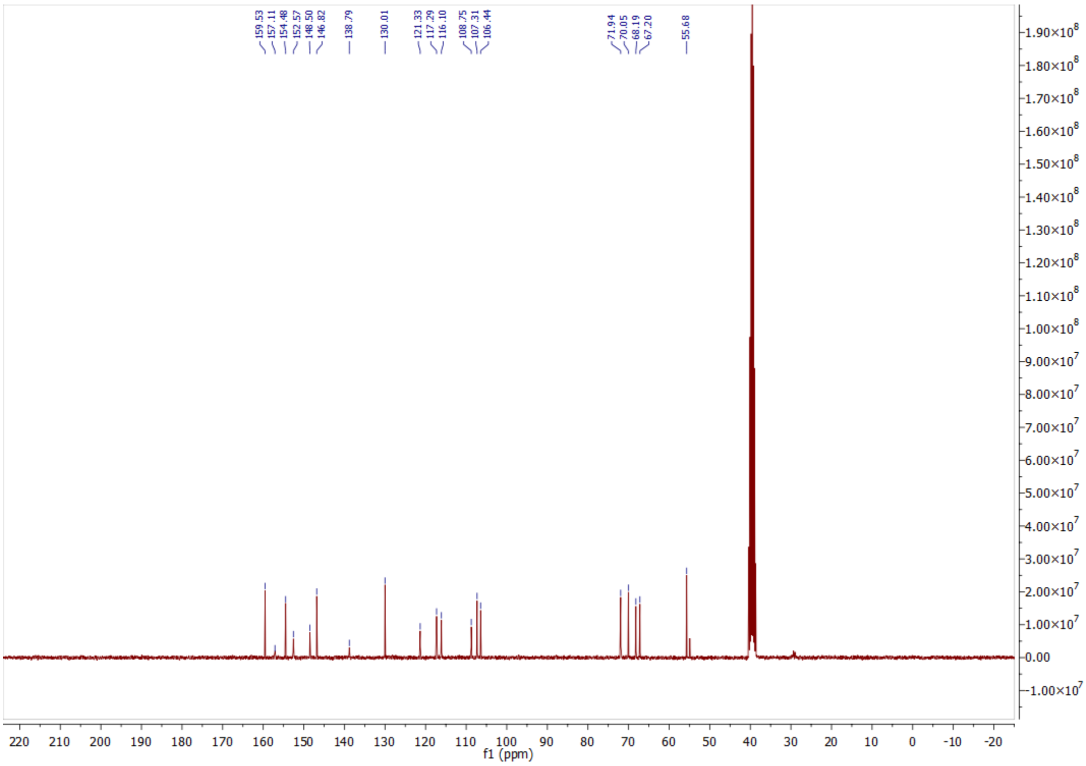

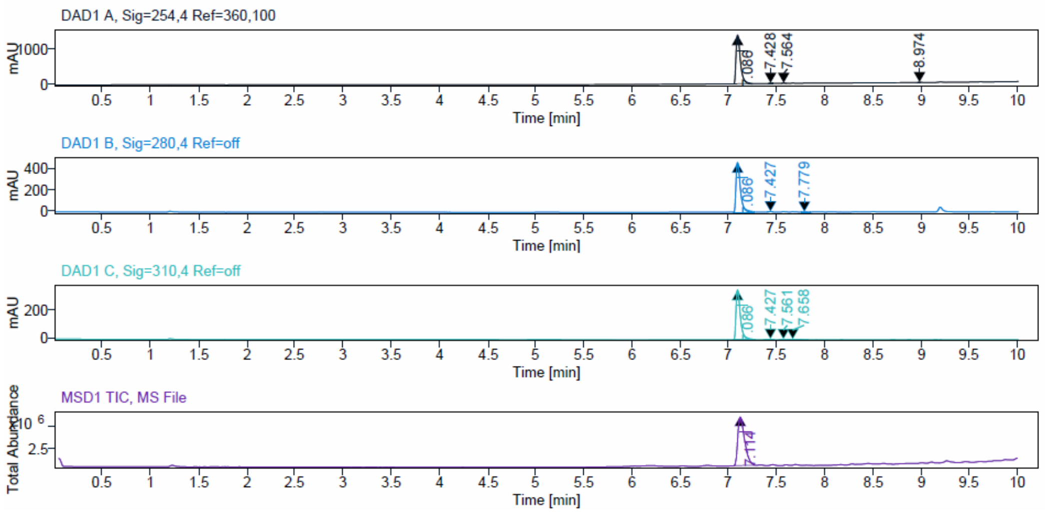

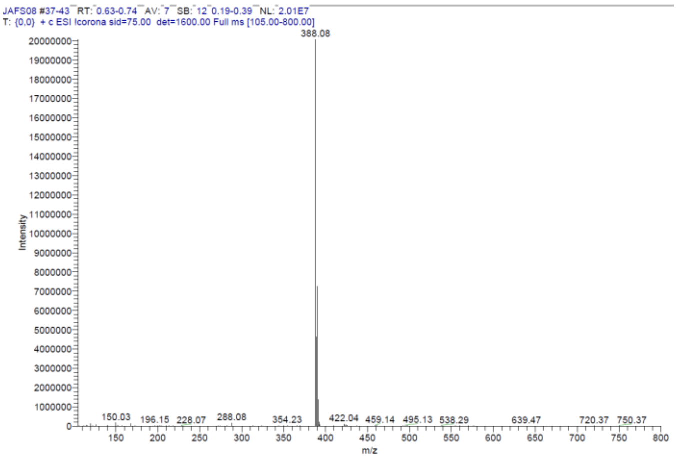

^{1}H NMR and ESI data of compound **44**

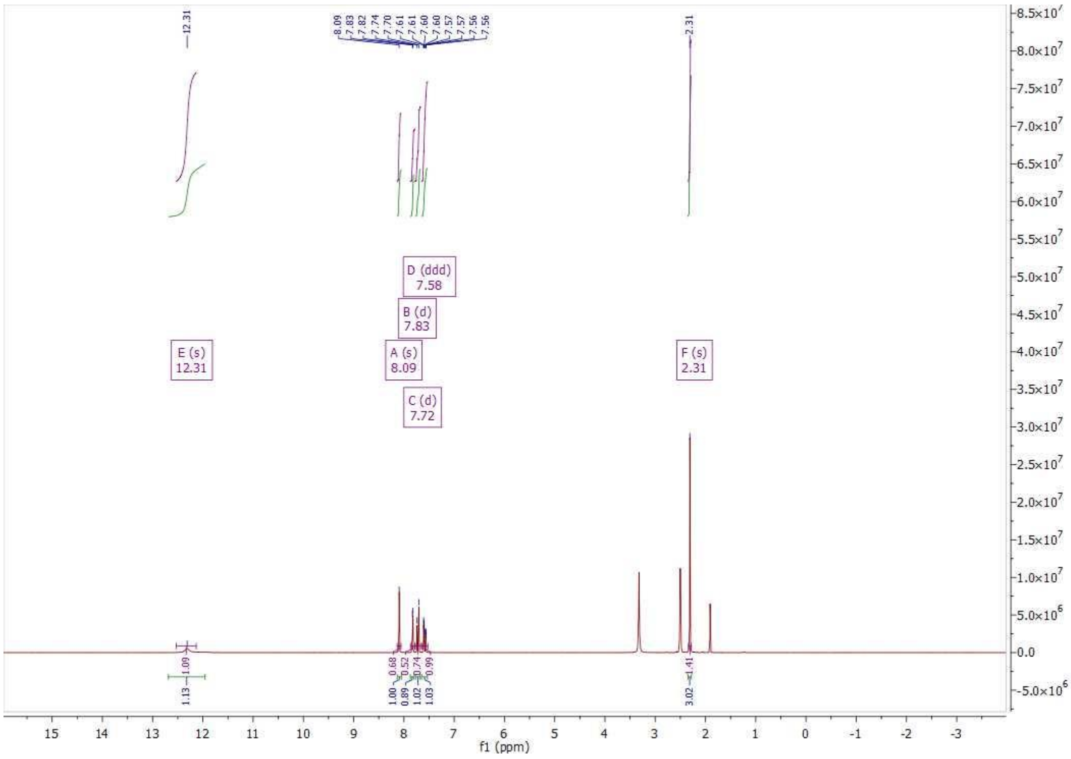

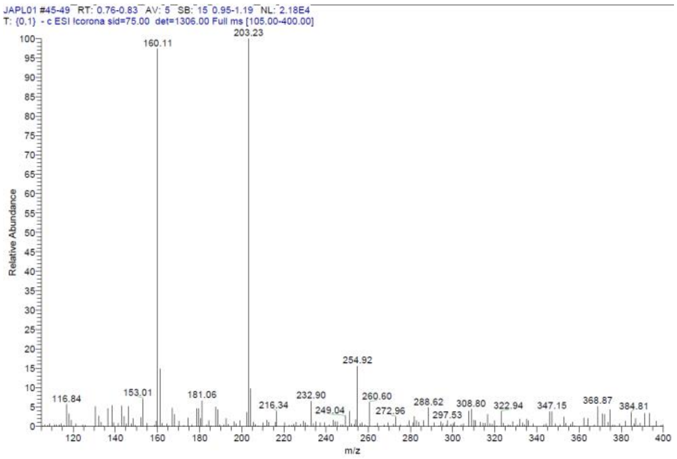

^{1}H NMR and ESI data of compound **45**

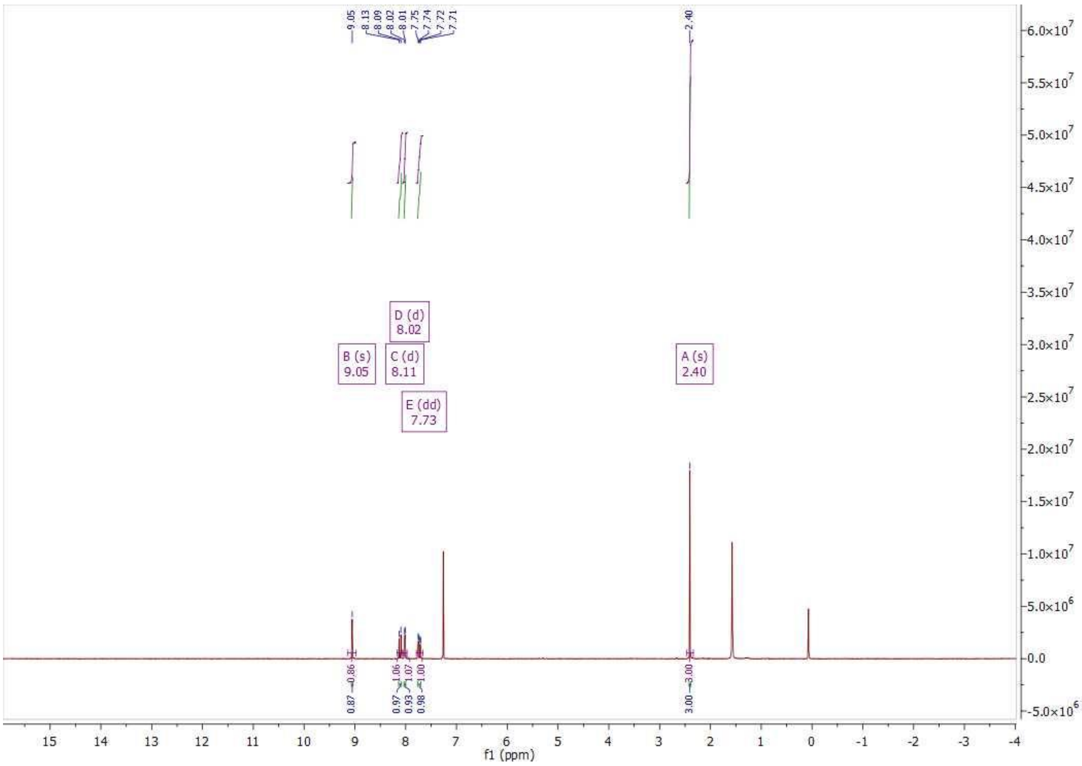

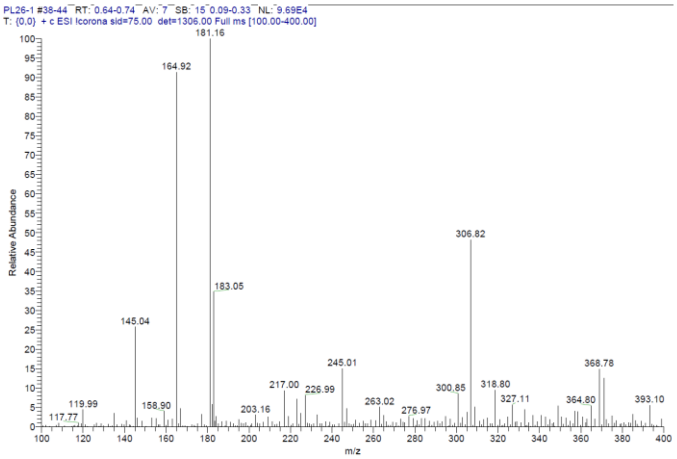

^{1}H NMR and ESI data of compound **46**

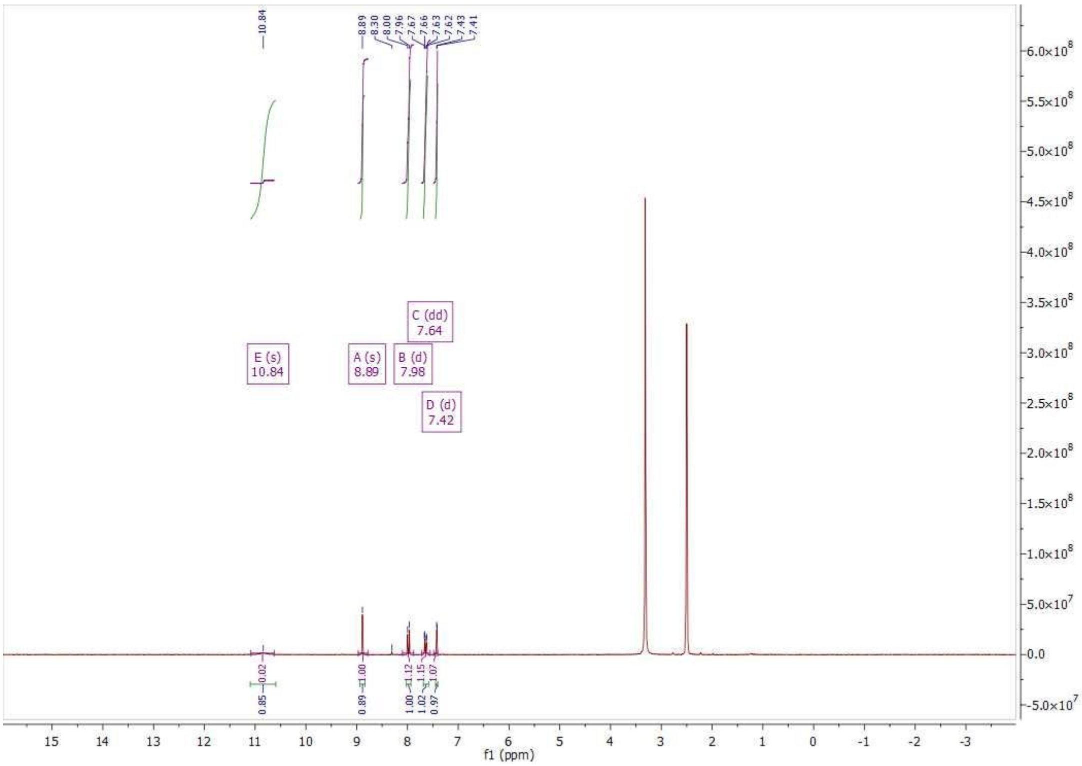

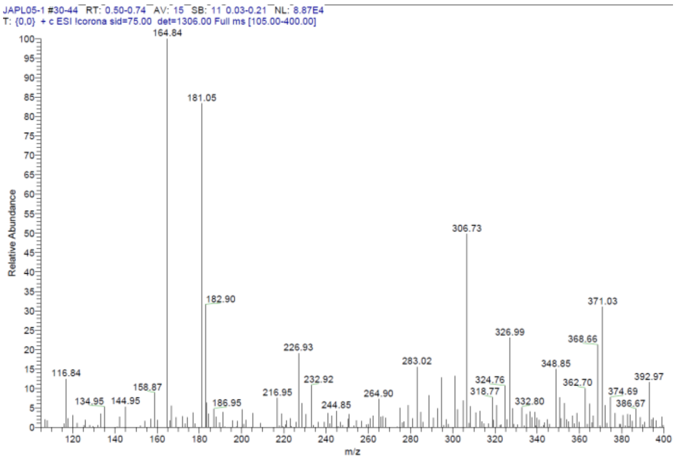

^{1}H, ^{13}C NMR, HPLC, and ESI data of compound **47**

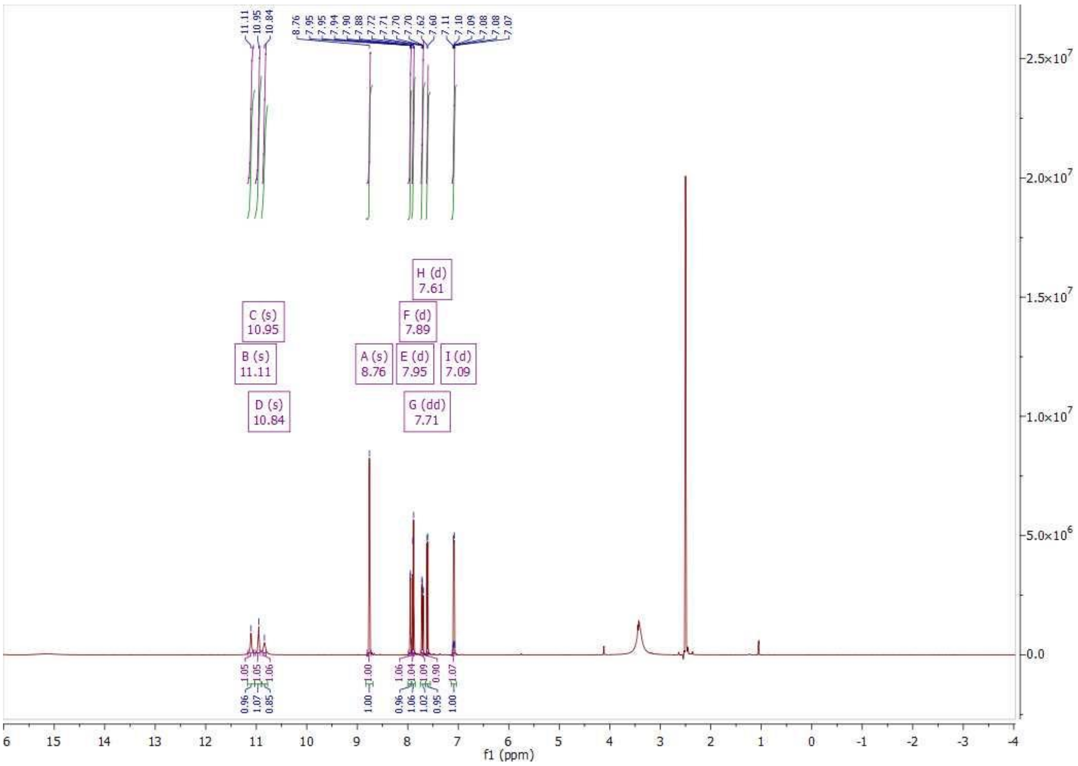

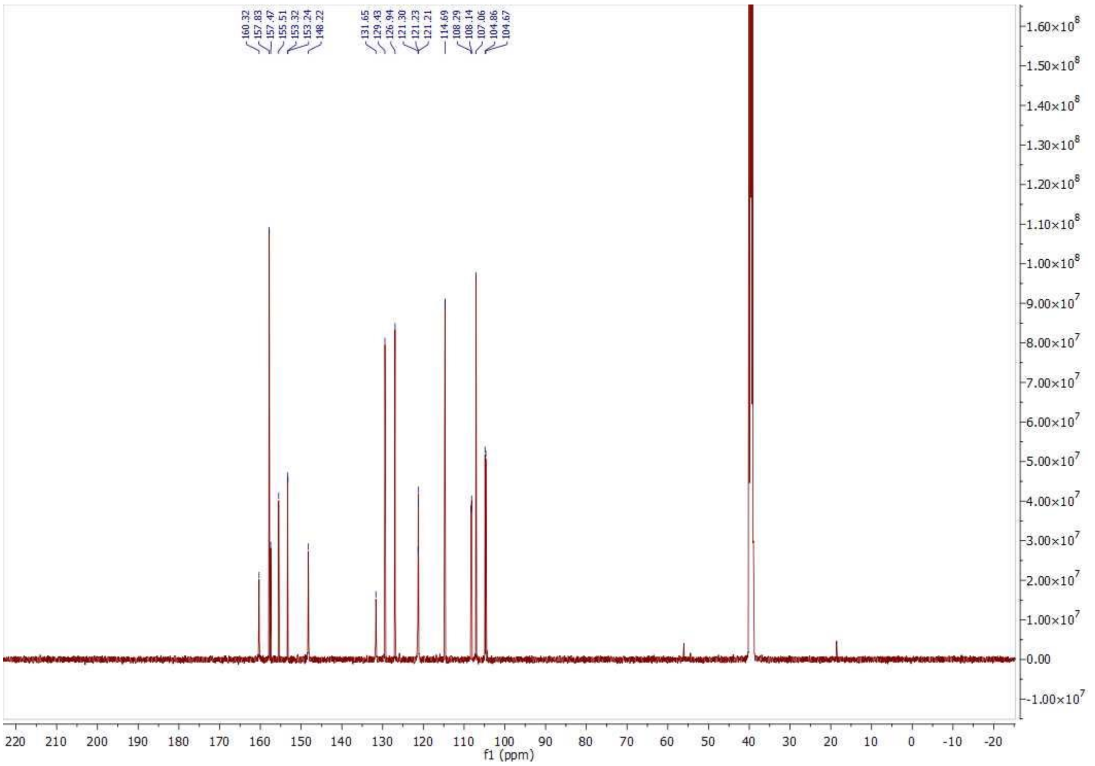

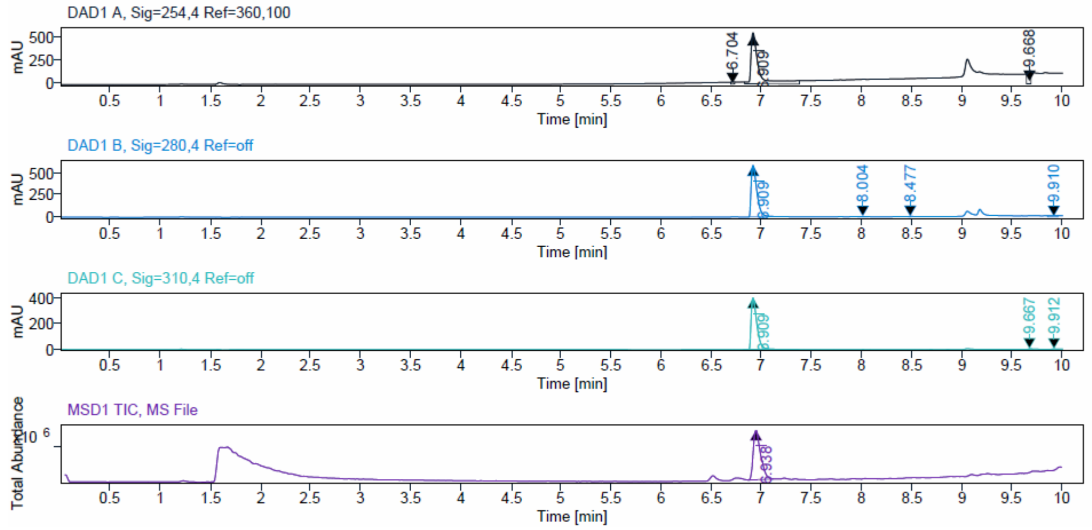

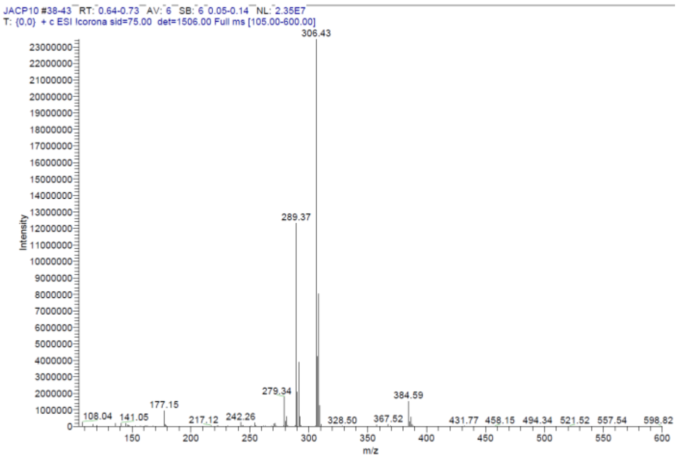

^{1}H, ^{13}C NMR, HPLC, and ESI data of compound **48**

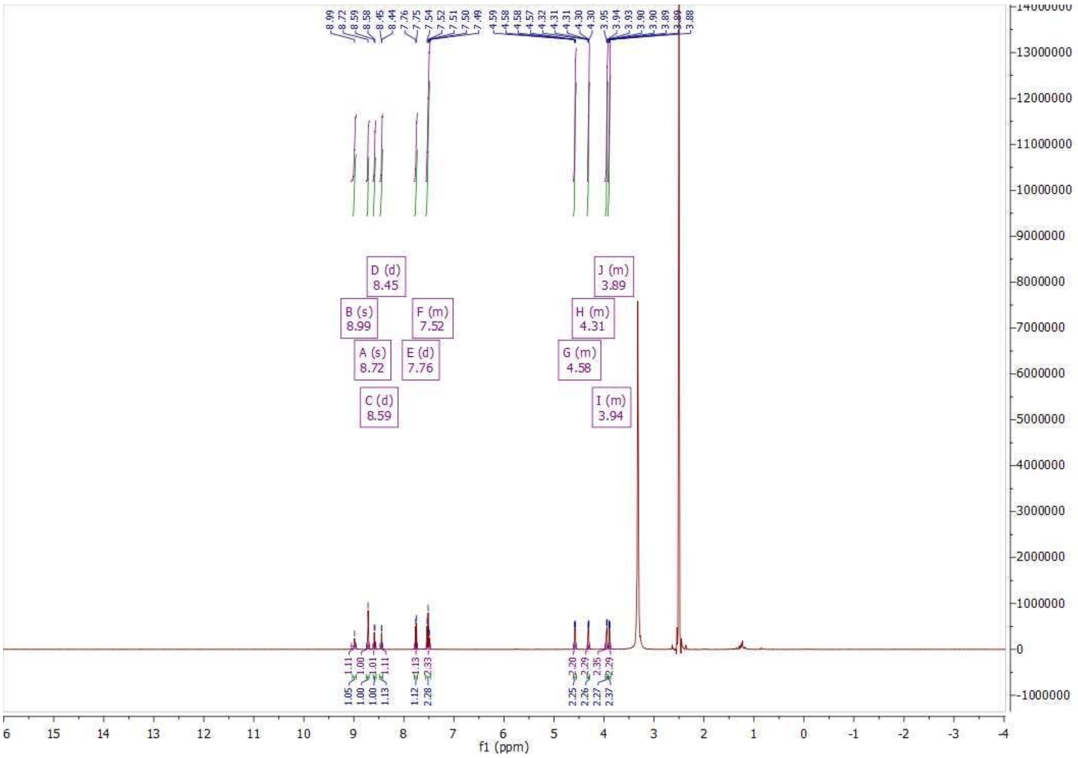

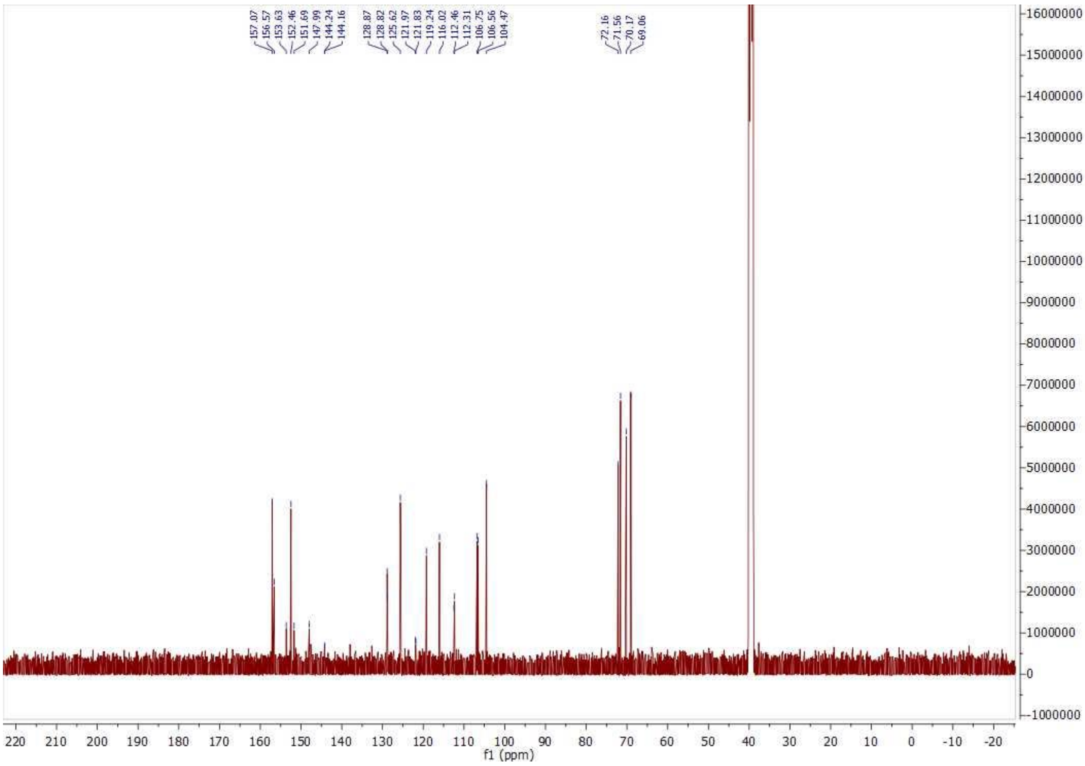
157.07
156.57
153.63
152.46
151.69
147.99
144.24
144.16
128.87
128.82
125.62
121.97
121.83
119.24
116.02
112.46
112.31
106.75
106.56
104.47
72.16
71.56
70.17
69.06
16000000
15000000
14000000
13000000
12000000
11000000
10000000
9000000
8000000
7000000
6000000
5000000
4000000
3000000
2000000
1000000
0
-1000000
220 210 200 190 180 170 160 150 140 130 120 110 100 90 80 70 60 50 40 30 20 10 0 -10 -20
f1 (ppm)

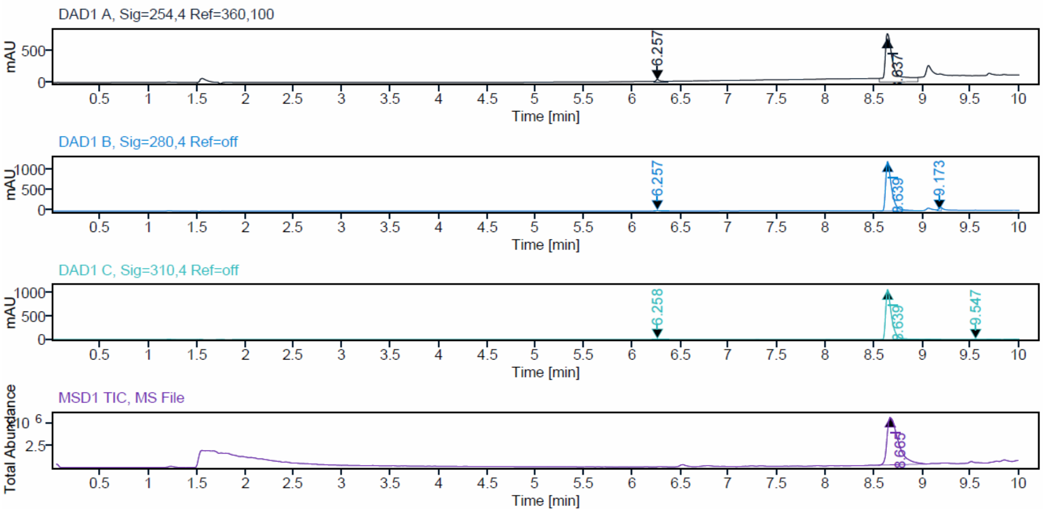
DAD1 A, Sig=254,4 Ref=360,100
mAU
500
0
6.257
637
0.5 1 1.5 2 2.5 3 3.5 4 4.5 5 5.5 6 6.5 7 7.5 8 8.5 9 9.5 10
Time [min]
DAD1 B, Sig=280,4 Ref=off
mAU
1000
500
0
6.257
8.639
9.173
Time [min]
DAD1 C, Sig=310,4 Ref=off
mAU
1000
500
0
6.258
8.639
9.547
Time [min]
MSD1 TIC, MS File
Total Abundance
10 6
2.5
8.665
Time [min]

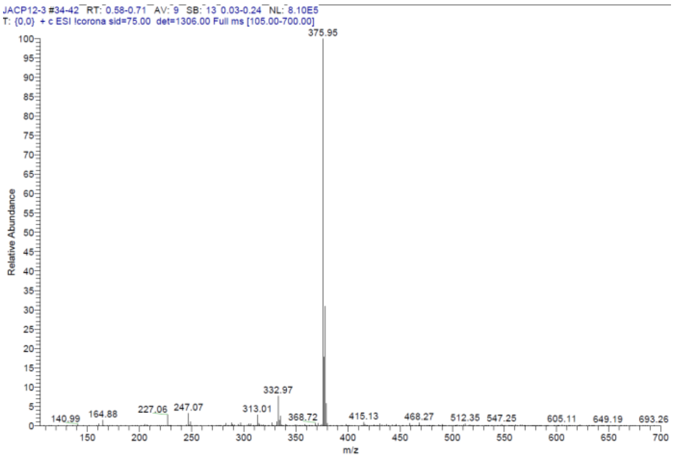
JACP12-3 #34-42 RT: 0.58-0.71 AV: 9 SB: 13 0.03-0.24 NL: 8.10E5
T: {0,0} + c ESI !corona sid=75.00 det=1306.00 Full ms [105.00-700.00]
375.95
Relative Abundance
100 95 90 85 80 75 70 65 60 55 50 45 40 35 30 25 20 15 10 5 0
140.99
164.88
227.06
247.07
313.01
332.97
368.72
415.13
468.27
512.35
547.25
605.11
649.19
693.26
150 200 250 300 350 400 450 500 550 600 650 700
m/z

^{1}H, ^{13}C NMR, and ESI data of compound **53**

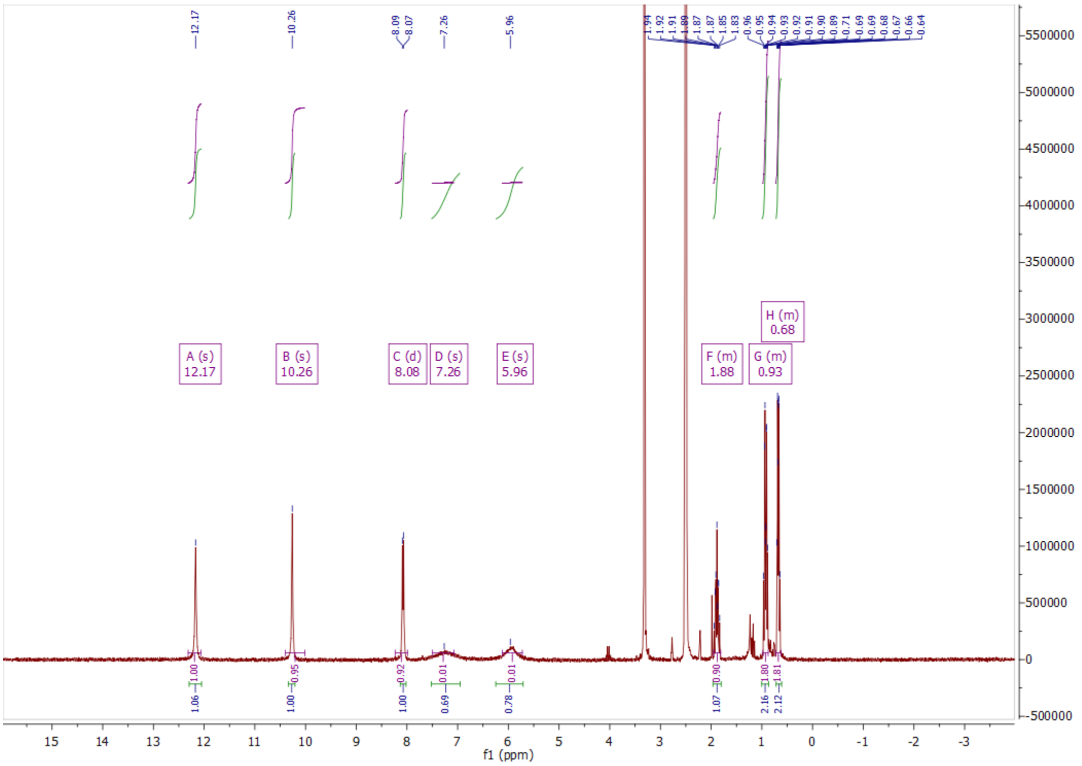

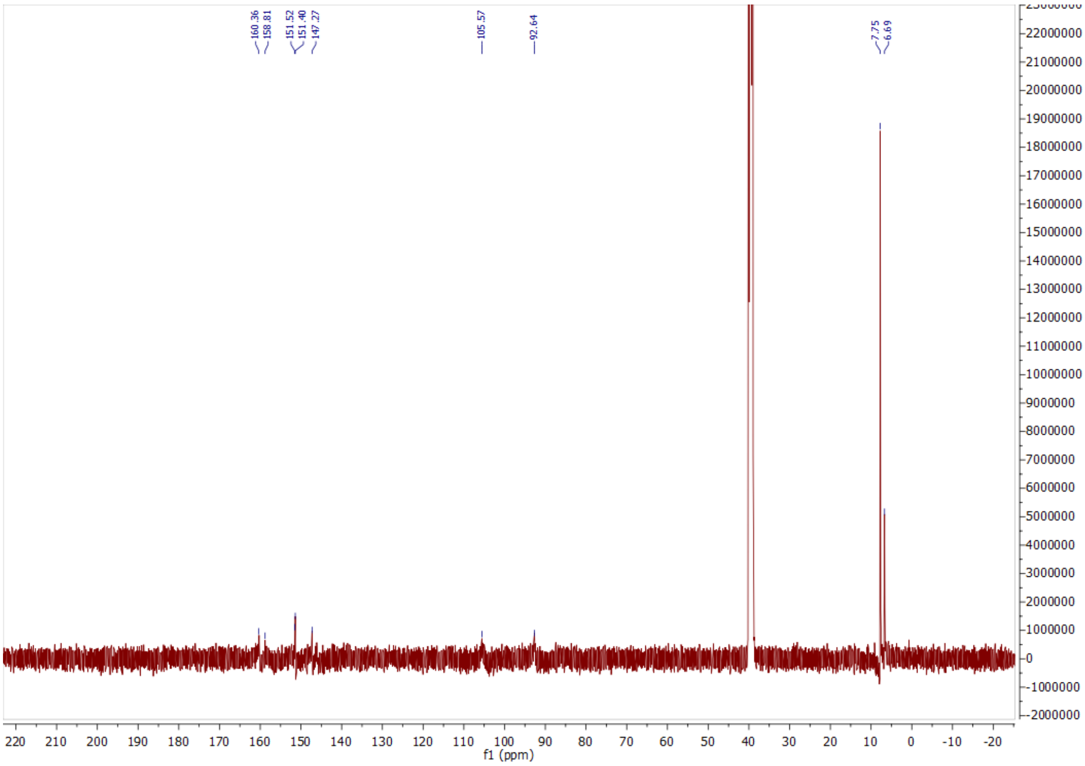

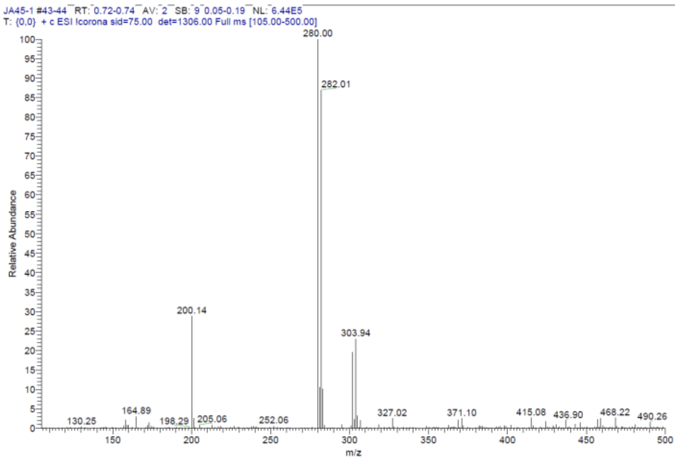

^{1}H, ^{13}C NMR, and ESI data of compound **54**

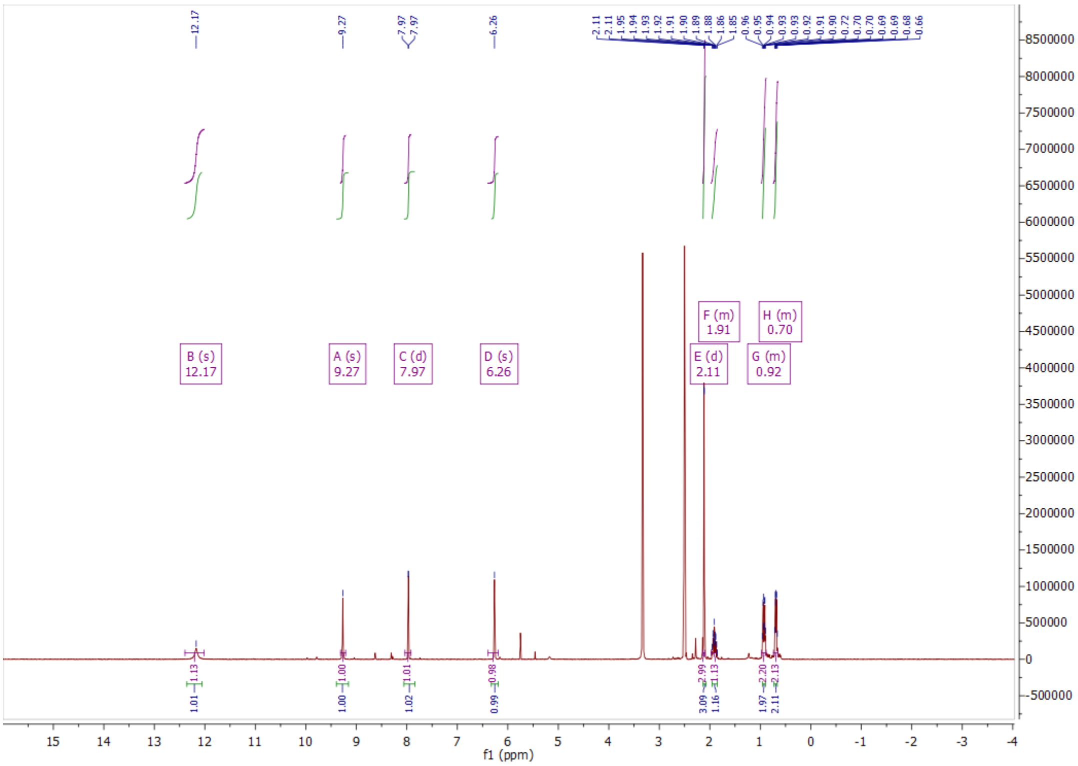

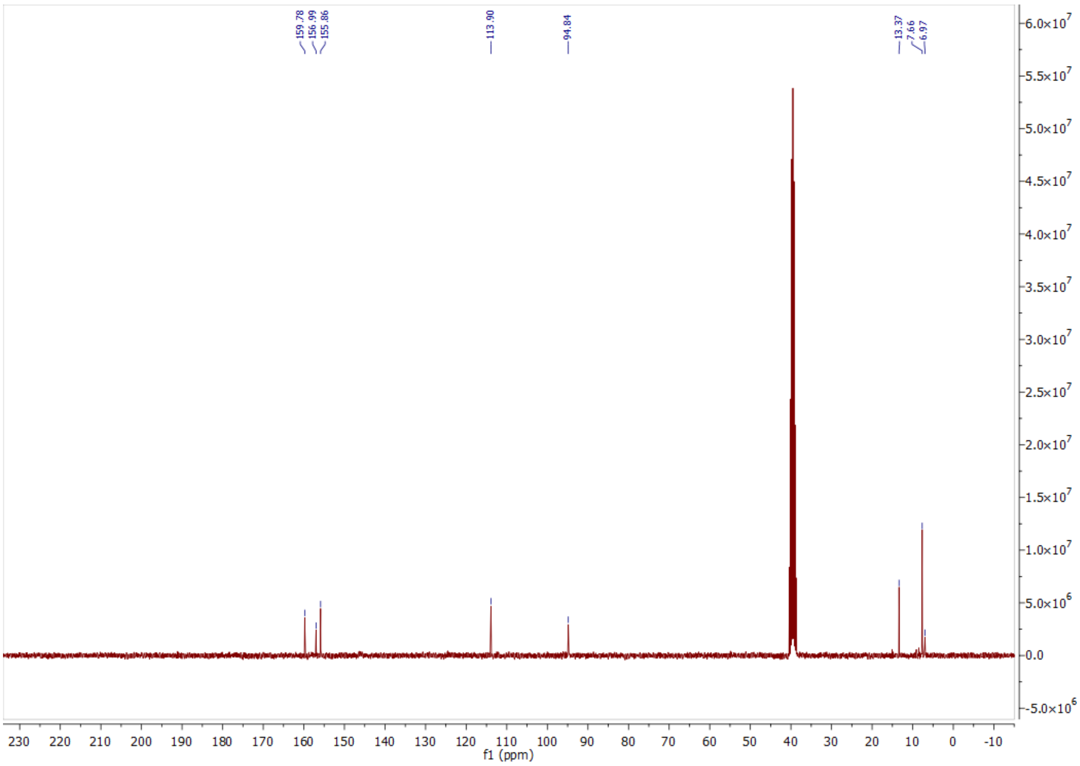
159.78
156.99
155.86
113.90
94.84
13.37
7.66
6.97
6.0×10^7
5.5×10^7
5.0×10^7
4.5×10^7
4.0×10^7
3.5×10^7
3.0×10^7
2.5×10^7
2.0×10^7
1.5×10^7
1.0×10^7
5.0×10^6
0.0
-5.0×10^6
230 220 210 200 190 180 170 160 150 140 130 120 110 100 90 80 70 60 50 40 30 20 10 0 -10
f1 (ppm)

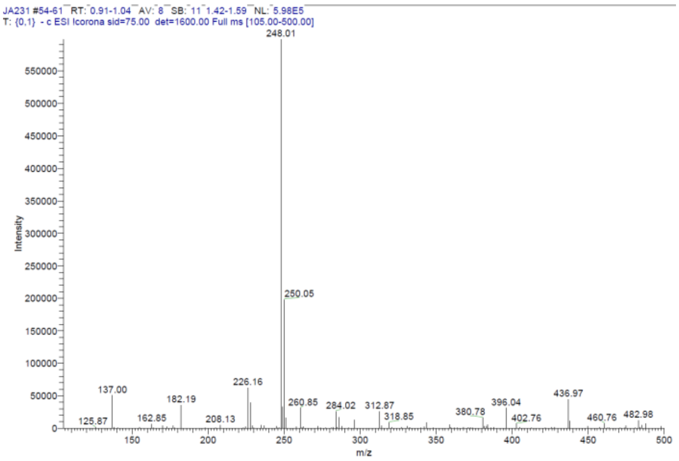
JA231 #54-61 RT: 0.91-1.04 AV: 8 SB: 11 1.42-1.59 NL: 5.98E5
T: {0,1} - c ESI Icorona sid=75.00 det=1600.00 Full ms [105.00-500.00]
248.01
250.05
226.16
137.00
182.19
125.87
162.85
208.13
260.85
284.02
312.87
318.85
380.78
396.04
402.76
436.97
460.76
482.98
Intensity
550000
500000
450000
400000
350000
300000
250000
200000
150000
100000
50000
0
150 200 250 300 350 400 450 500
m/z

^{1}H, ^{13}C NMR, and ESI data of compound **55**

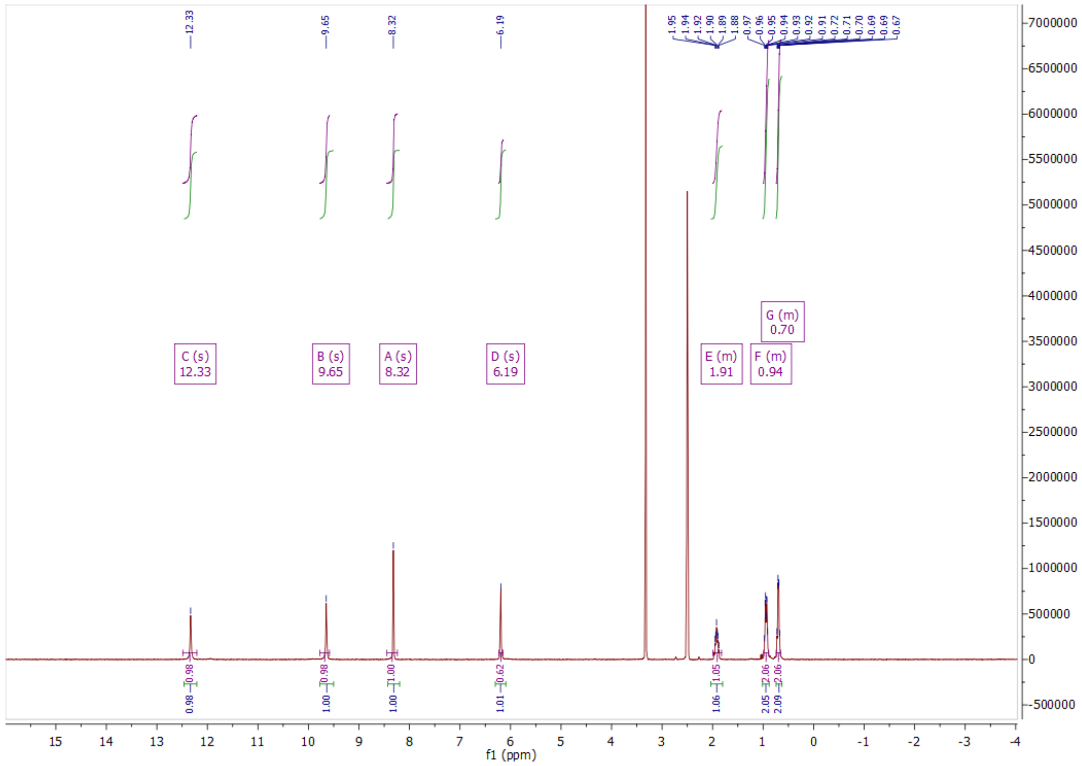

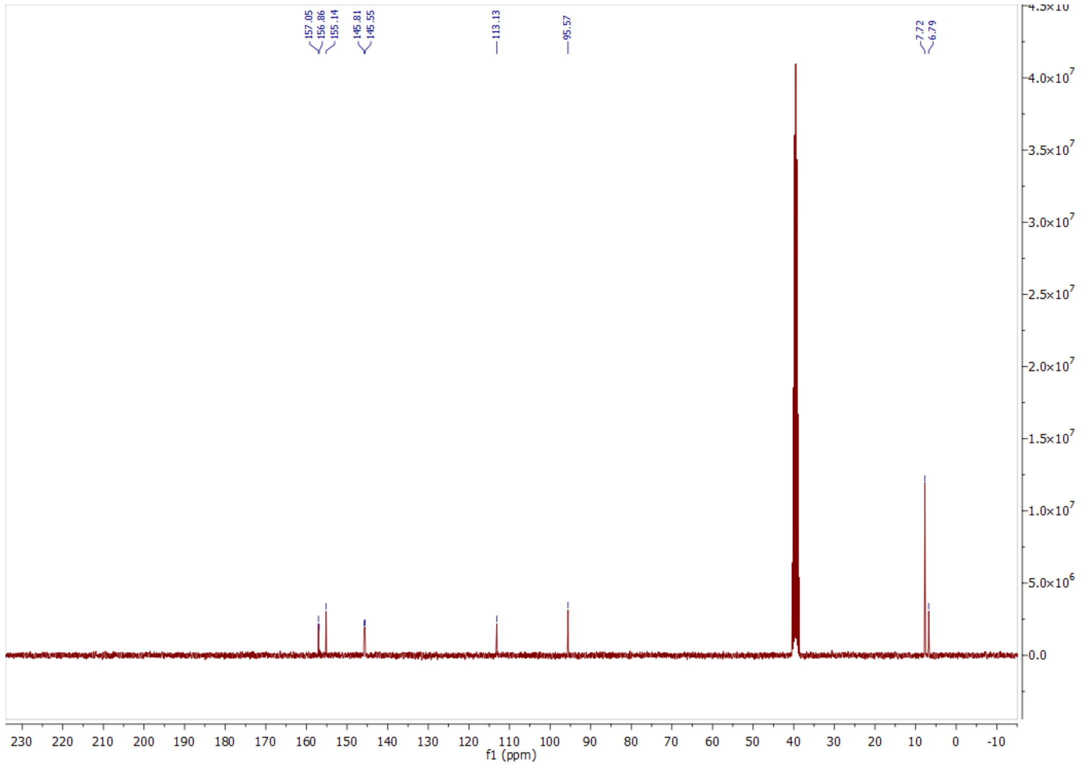

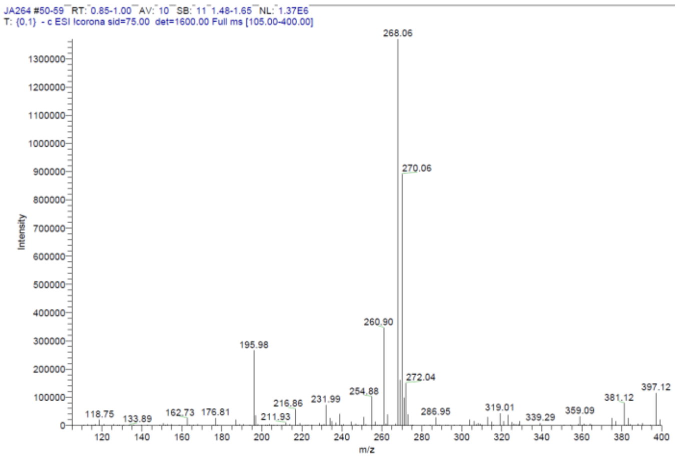

^{1}H, ^{13}C NMR, HPLC, and ESI data of compound **56a**

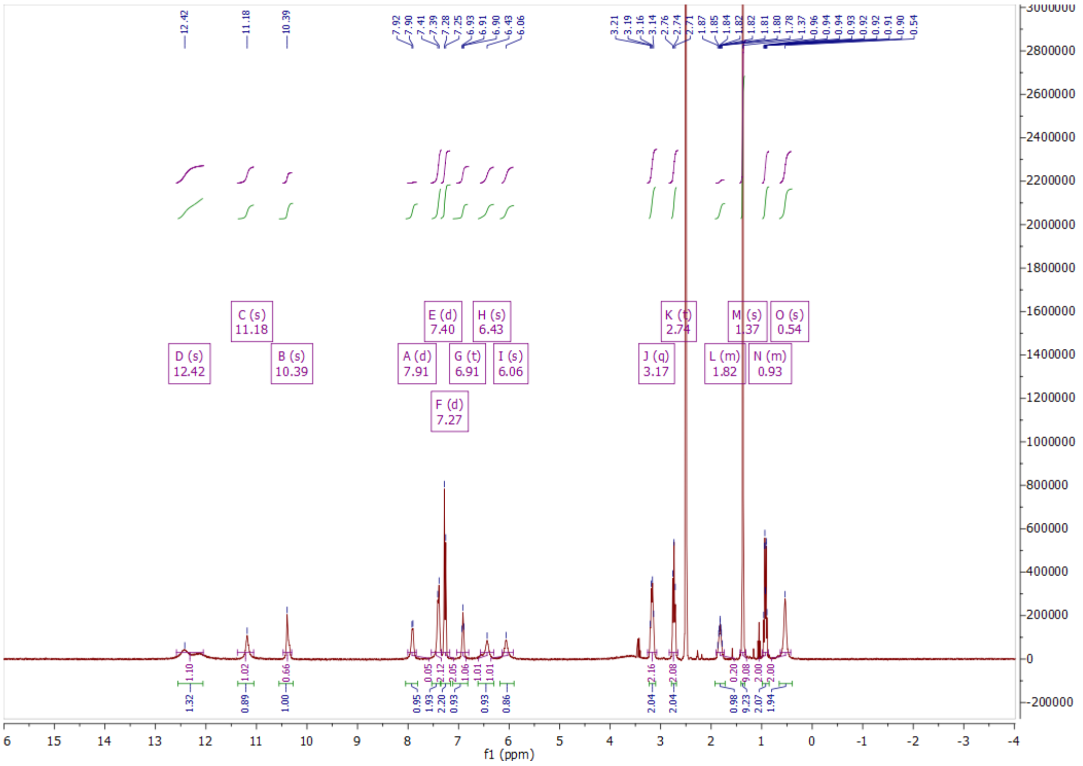

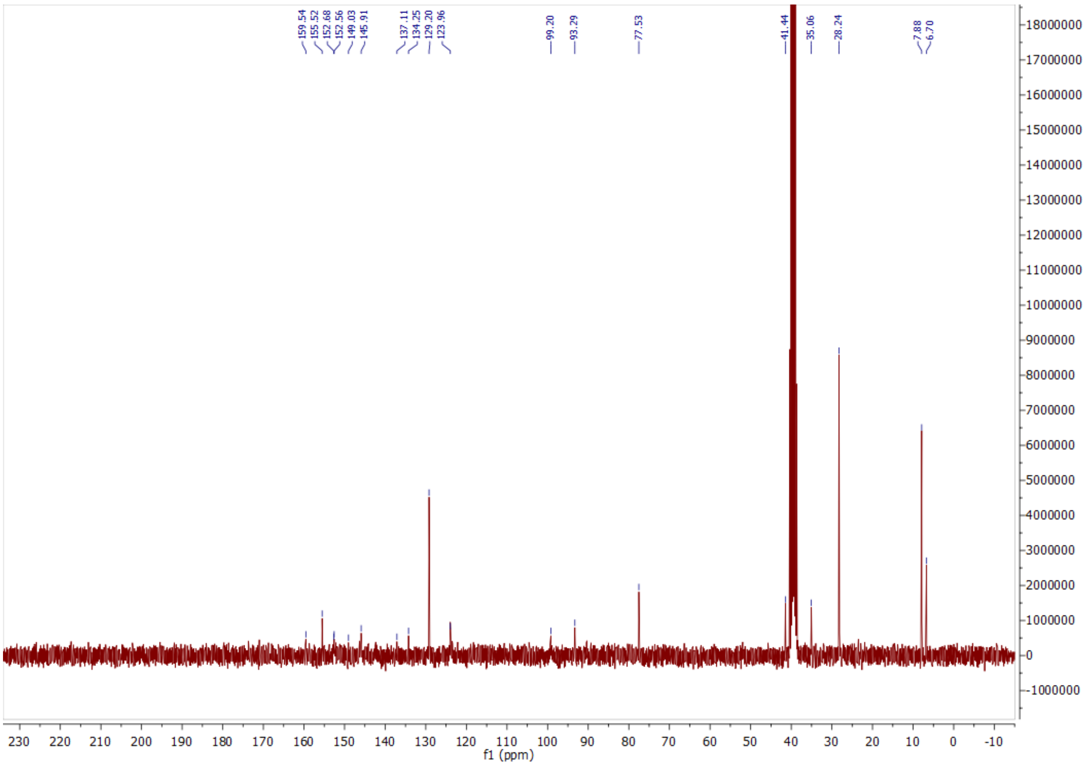
159.54
155.52
152.68
152.56
149.03
145.91
137.11
134.25
129.20
123.96
99.20
93.29
77.53
41.44
35.06
28.24
7.88
6.70
18000000
17000000
16000000
15000000
14000000
13000000
12000000
11000000
10000000
9000000
8000000
7000000
6000000
5000000
4000000
3000000
2000000
1000000
0
-1000000
230 220 210 200 190 180 170 160 150 140 130 120 110 100 90 80 70 60 50 40 30 20 10 0 -10
f1 (ppm)

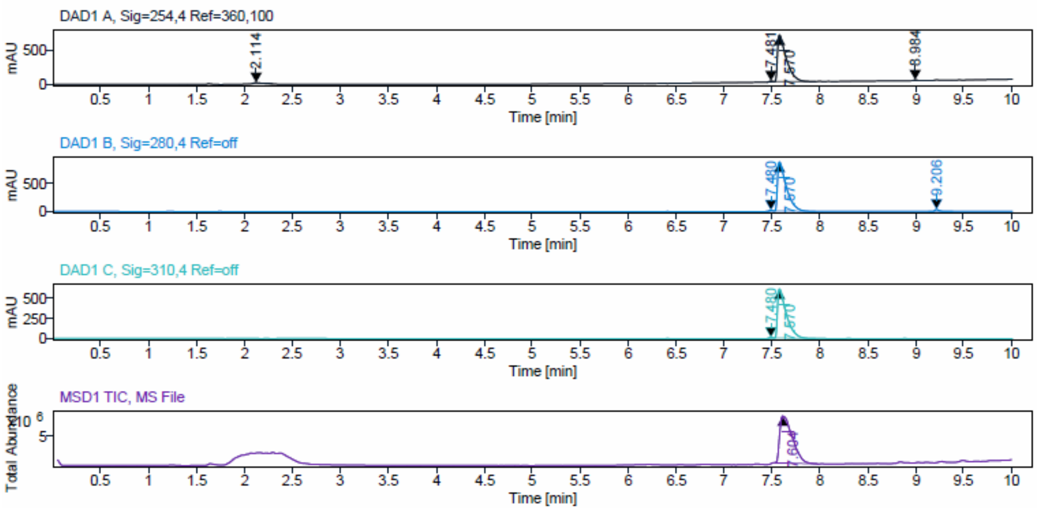
DAD1 A, Sig=254,4 Ref=360,100
mAU
500
0
2.114
7.481
7.670
8.984
DAD1 B, Sig=280,4 Ref=off
7.480
7.670
9.206
DAD1 C, Sig=310,4 Ref=off
250
7.480
7.670
MSD1 TIC, MS File
Total Abundance
x10 6
5
7.604
0.5 1 1.5 2 2.5 3 3.5 4 4.5 5 5.5 6 6.5 7 7.5 8 8.5 9 9.5 10
Time [min]

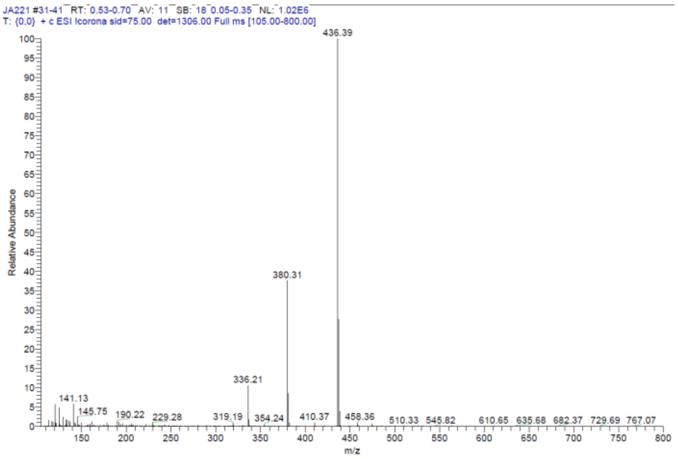
JA221 #31-41 RT: 0.53-0.70 AV: 11 SB: 18 0.05-0.35 NL: 1.02E6
T: {0,0} + c ESI !corona sid=75.00 det=1306.00 Full ms [105.00-800.00]
Relative Abundance
436.39
380.31
336.21
141.13
145.75
190.22
229.28
319.19
354.24
410.37
458.36
510.33
545.82
610.65
635.68
682.37
729.69
767.07
100 95 90 85 80 75 70 65 60 55 50 45 40 35 30 25 20 15 10 5 0
150 200 250 300 350 400 450 500 550 600 650 700 750 800
m/z

^{1}H, ^{13}C NMR, HPLC, and ESI data of compound **56b**

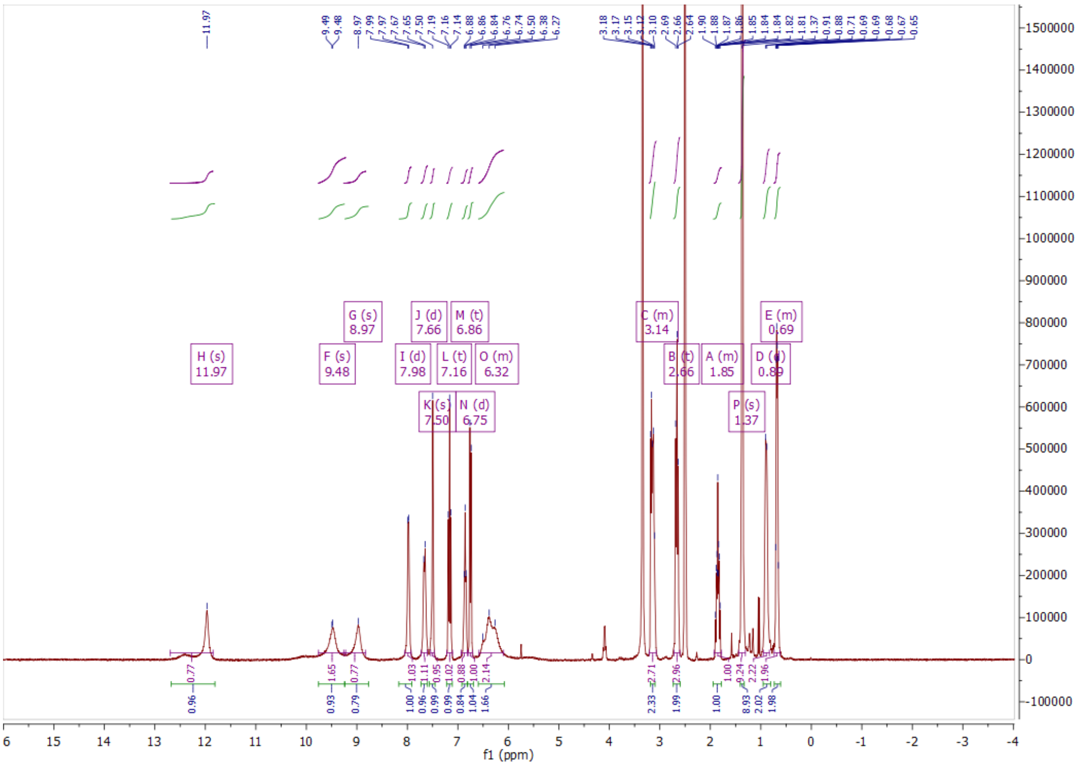

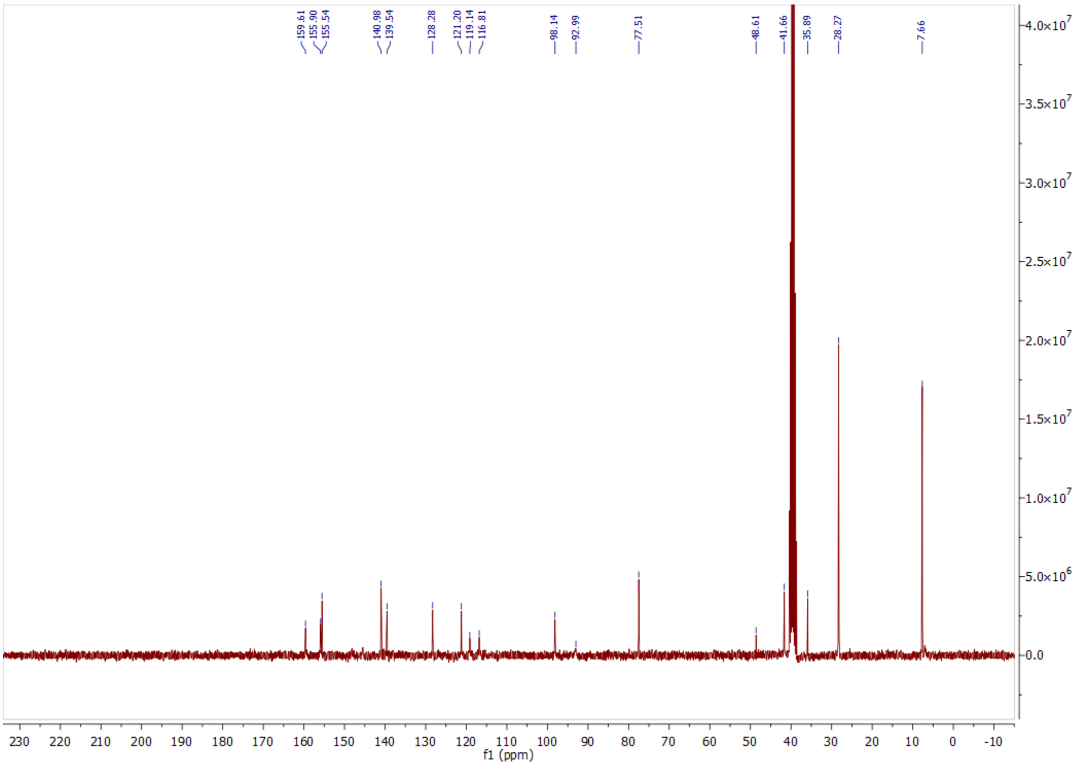

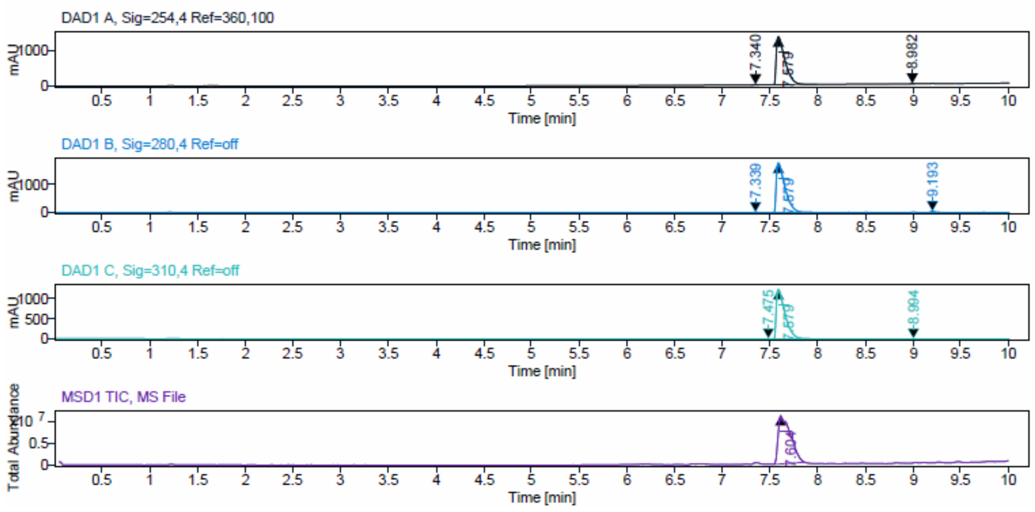

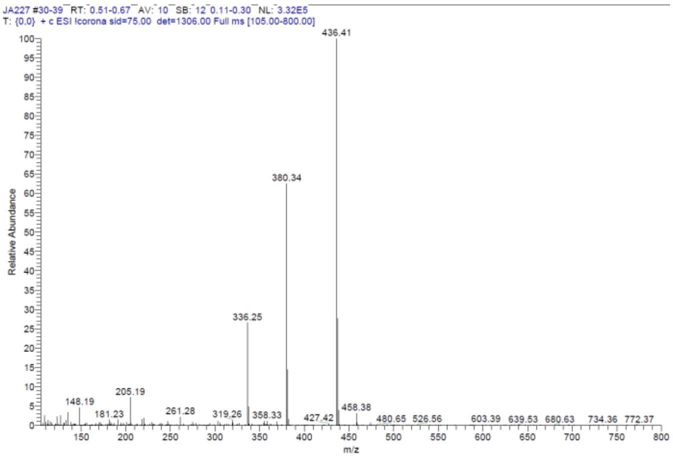

^{1}H, ^{13}C NMR, HPLC, and ESI data of compound **56c**

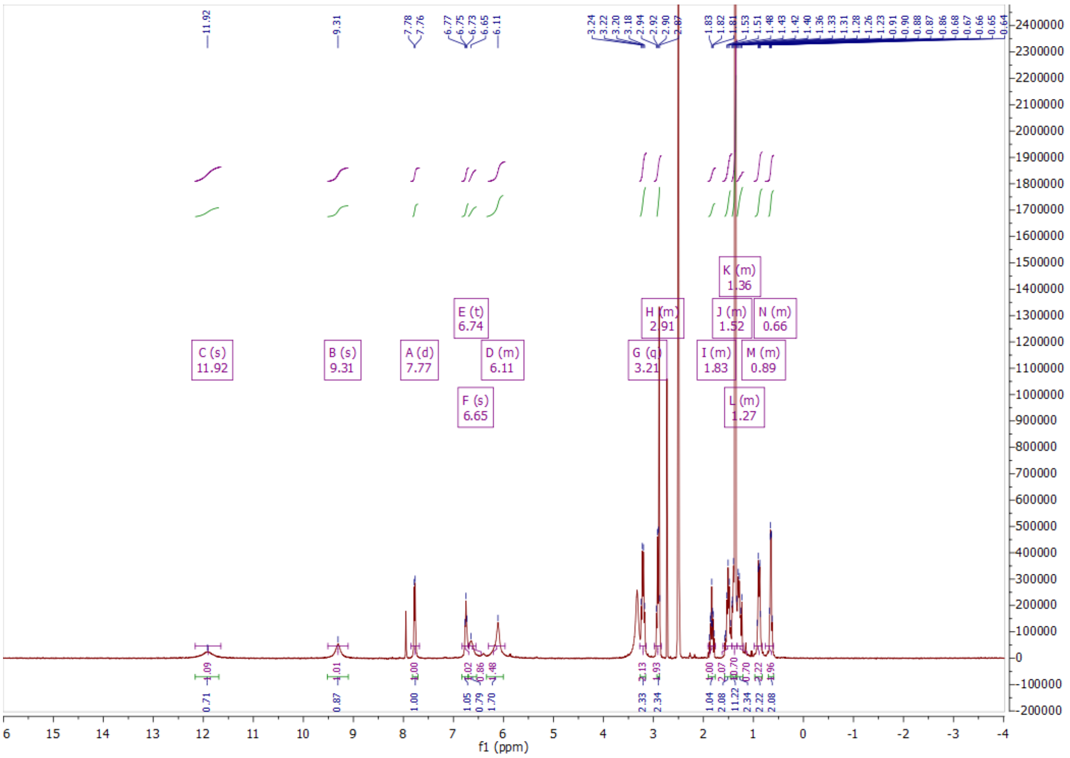

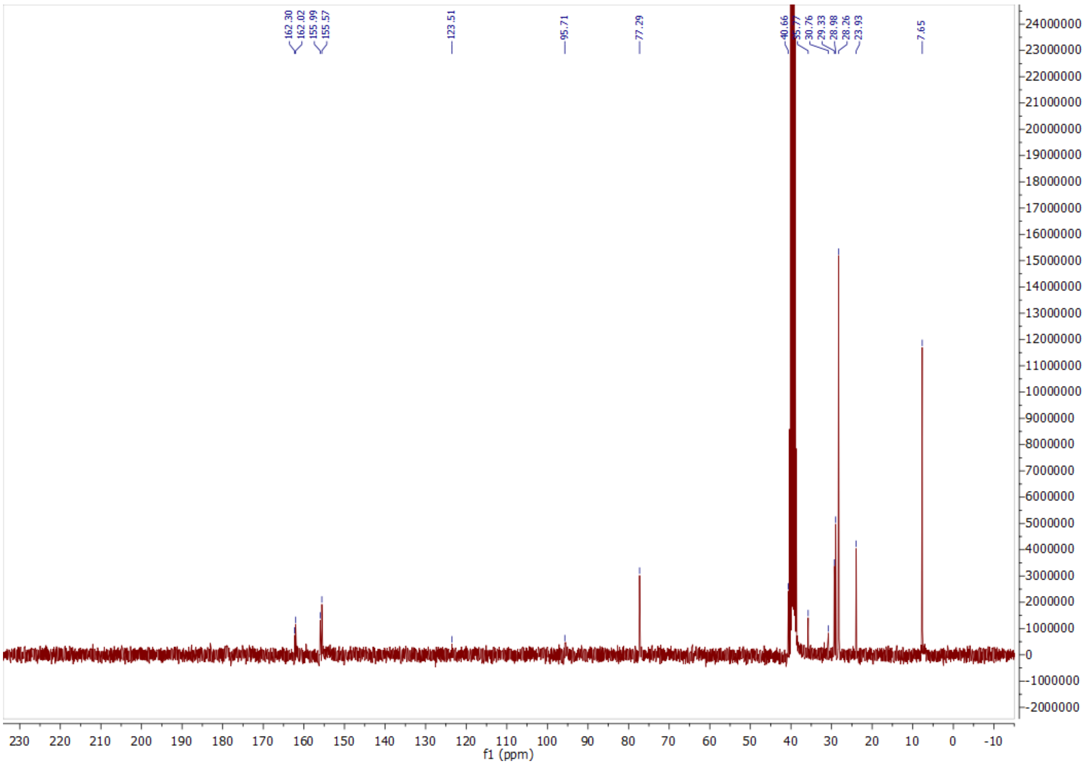
162.30
162.02
155.99
155.57
123.51
95.71
77.29
40.66
35.77
30.76
29.33
28.98
28.26
23.93
7.65
24000000
23000000
22000000
21000000
20000000
19000000
18000000
17000000
16000000
15000000
14000000
13000000
12000000
11000000
10000000
9000000
8000000
7000000
6000000
5000000
4000000
3000000
2000000
1000000
0
-1000000
-2000000
230 220 210 200 190 180 170 160 150 140 130 120 110 100 90 80 70 60 50 40 30 20 10 0 -10
f1 (ppm)

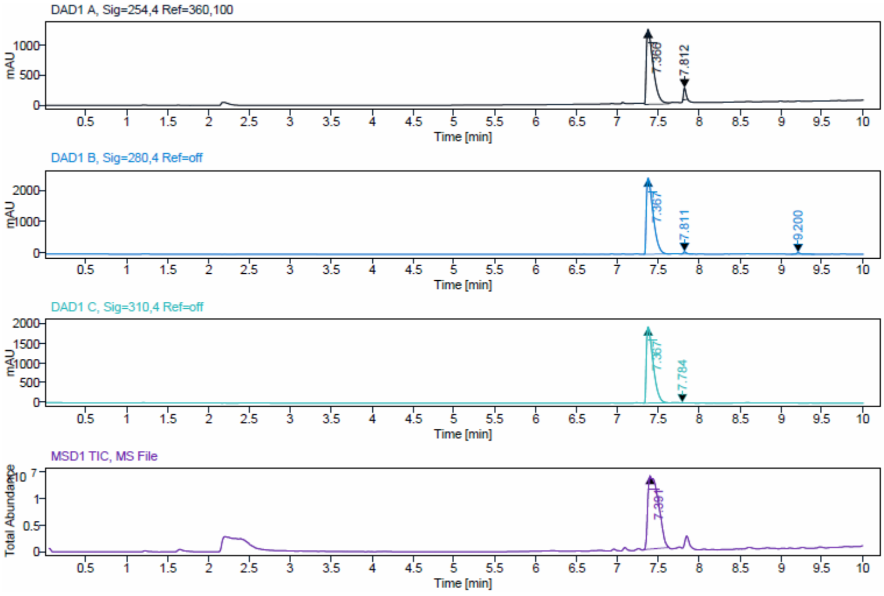
DAD1 A, Sig=254,4 Ref=360,100
mAU
1000
500
0
7.369
7.812
Time [min]
DAD1 B, Sig=280,4 Ref=off
mAU
2000
1000
0
7.367
7.811
9.200
Time [min]
DAD1 C, Sig=310,4 Ref=off
mAU
2000
1500
1000
500
0
7.367
7.784
Time [min]
MSD1 TIC, MS File
Total Abundance
x10 7
1
0.5
0
7.391
Time [min]
0.5 1 1.5 2 2.5 3 3.5 4 4.5 5 5.5 6 6.5 7 7.5 8 8.5 9 9.5 10

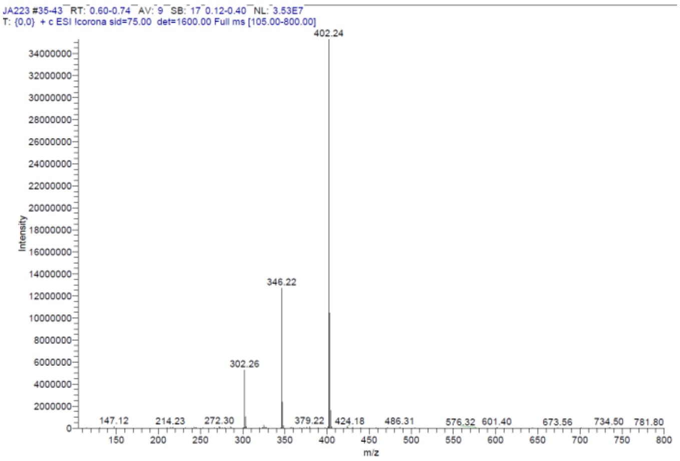
JA223 #35-43 RT: 0.60-0.74 AV: 9 SB: 17 0.12-0.40 NL: 3.53E7
T: {0,0} + c ESI Icorona sid=75.00 det=1600.00 Full ms [105.00-800.00]
402.24
346.22
302.26
147.12
214.23
272.30
379.22
424.18
486.31
576.32
601.40
673.56
734.50
781.80
Intensity
34000000
32000000
30000000
28000000
26000000
24000000
22000000
20000000
18000000
16000000
14000000
12000000
10000000
8000000
6000000
4000000
2000000
0
150 200 250 300 350 400 450 500 550 600 650 700 750 800
m/z

^{1}H, ^{13}C NMR, HPLC, and ESI data of compound **56d**

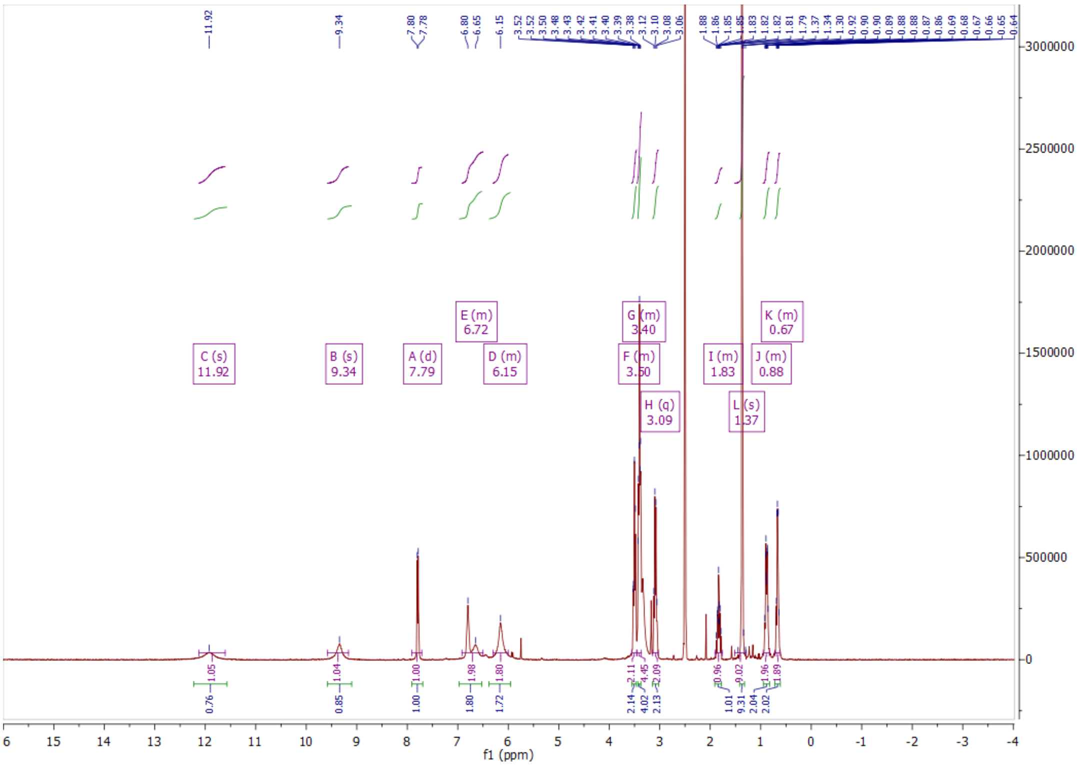

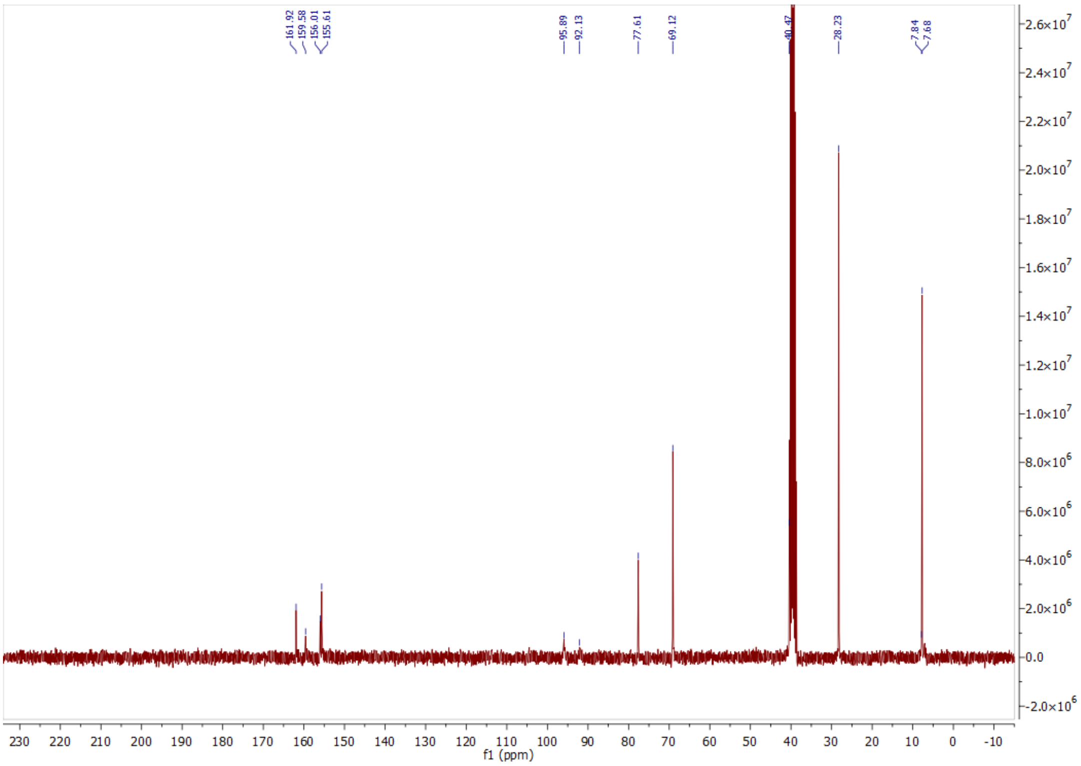

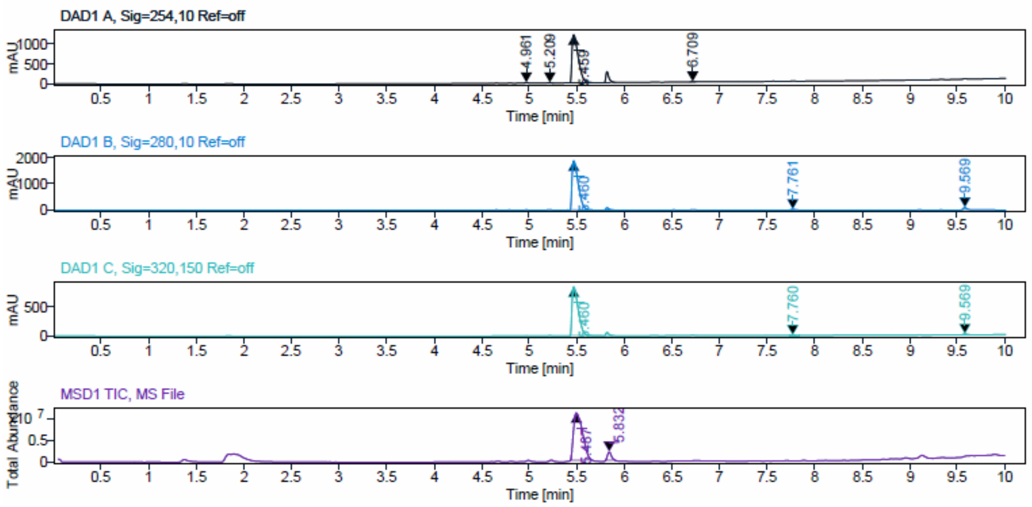

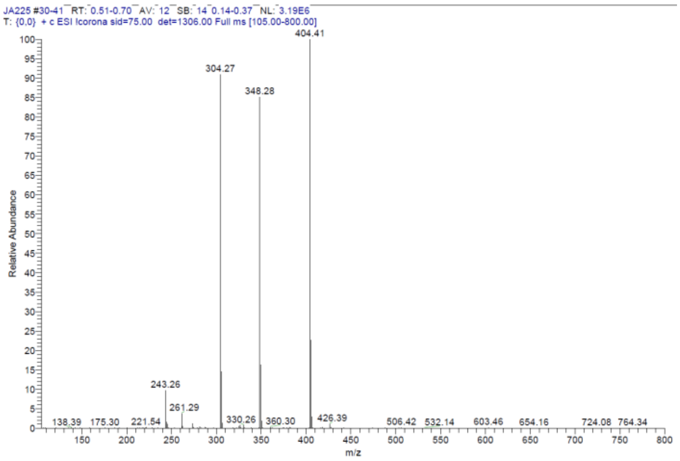

ESI, HRMS, ^{1}H, ^{13}C NMR and HPLC data of compound **56e**

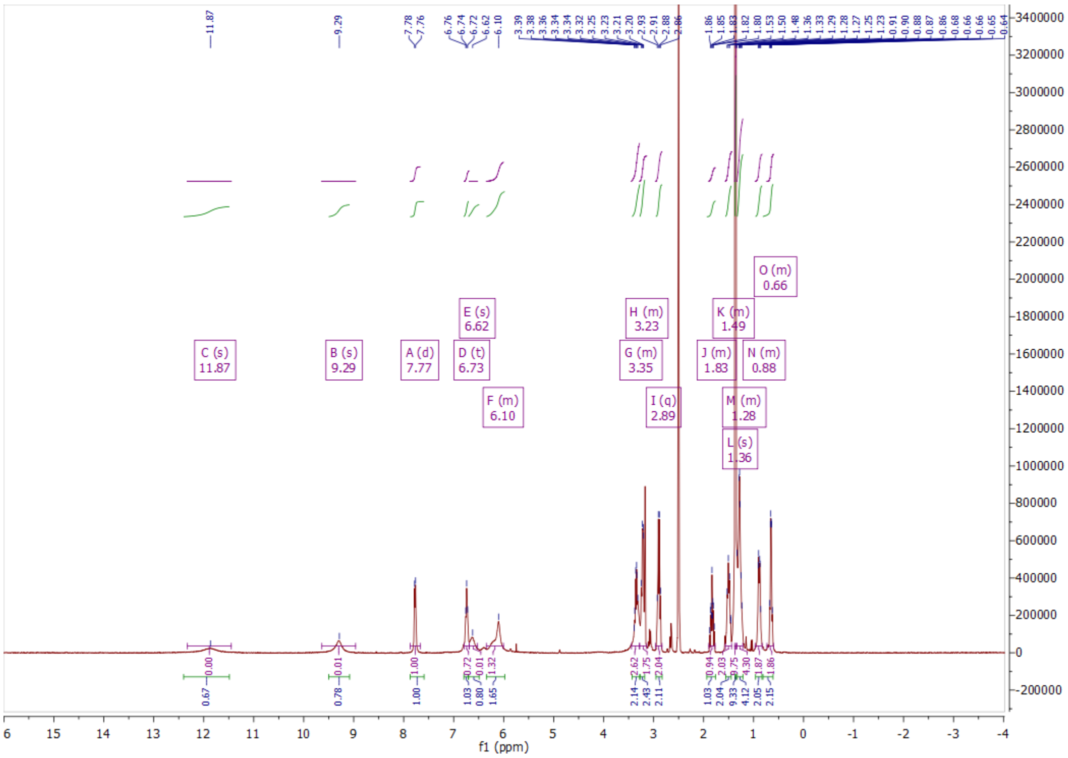

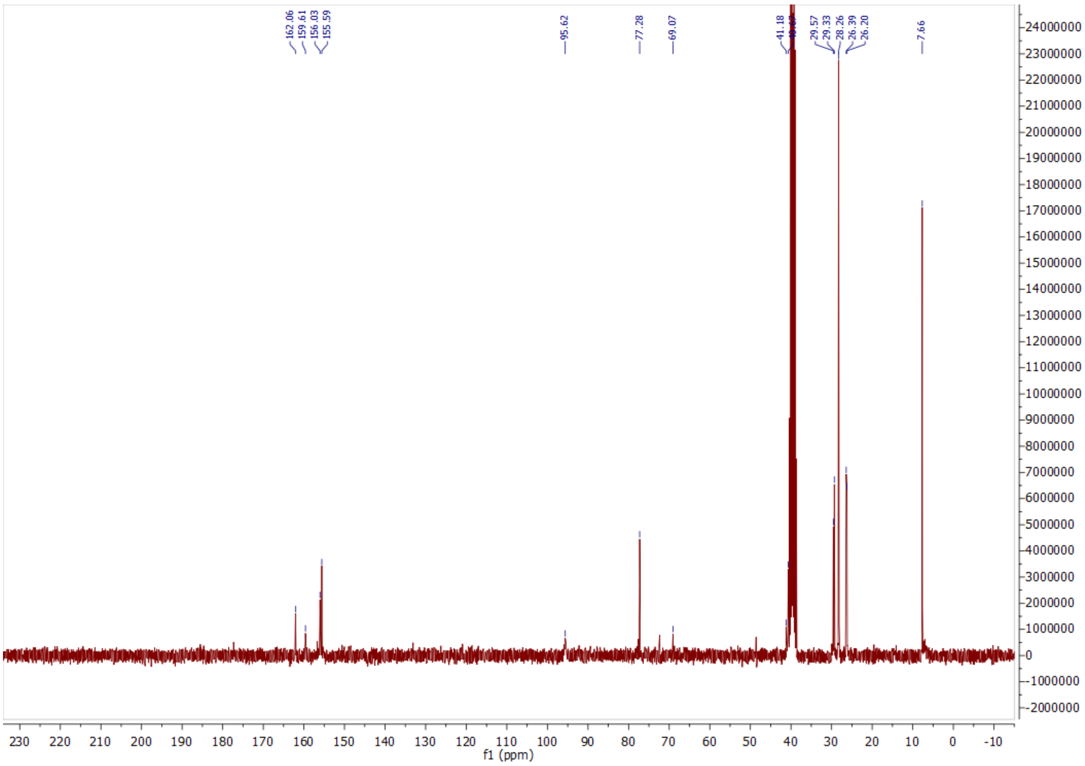
162.06
159.61
156.03
155.59
95.62
77.28
69.07
41.18
40.67
29.57
29.33
28.26
26.39
26.20
7.66
24000000
23000000
22000000
21000000
20000000
19000000
18000000
17000000
16000000
15000000
14000000
13000000
12000000
11000000
10000000
9000000
8000000
7000000
6000000
5000000
4000000
3000000
2000000
1000000
0
-1000000
-2000000
230 220 210 200 190 180 170 160 150 140 130 120 110 100 90 80 70 60 50 40 30 20 10 0 -10
f1 (ppm)

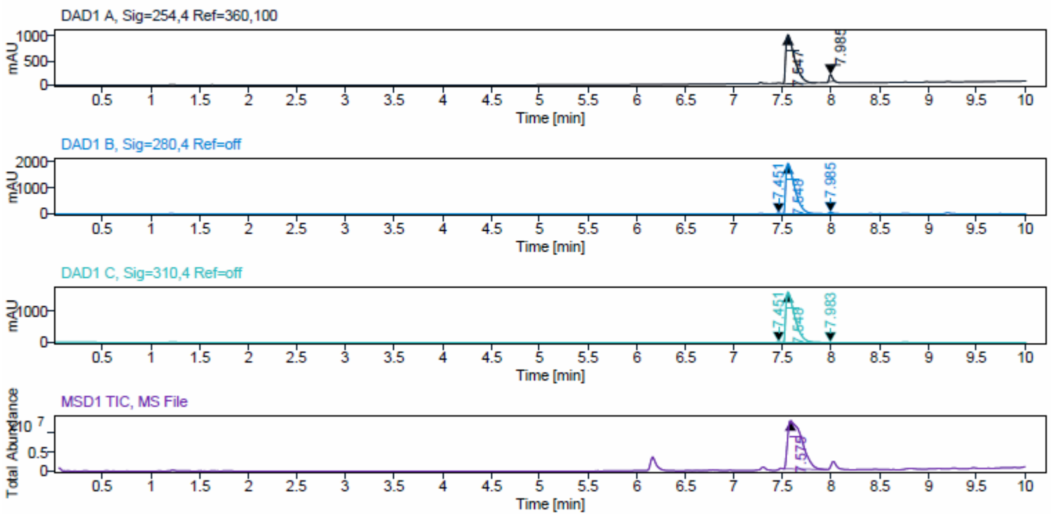
DAD1 A, Sig=254,4 Ref=360,100
mAU
1000
500
0
7.547
7.985
Time [min]
DAD1 B, Sig=280,4 Ref=off
mAU
2000
1000
0
7.451
7.549
7.985
Time [min]
DAD1 C, Sig=310,4 Ref=off
mAU
1000
0
7.451
7.549
7.983
Time [min]
MSD1 TIC, MS File
Total Abundance
x10 7
0.5
0
7.575
Time [min]
0.5 1 1.5 2 2.5 3 3.5 4 4.5 5 5.5 6 6.5 7 7.5 8 8.5 9 9.5 10

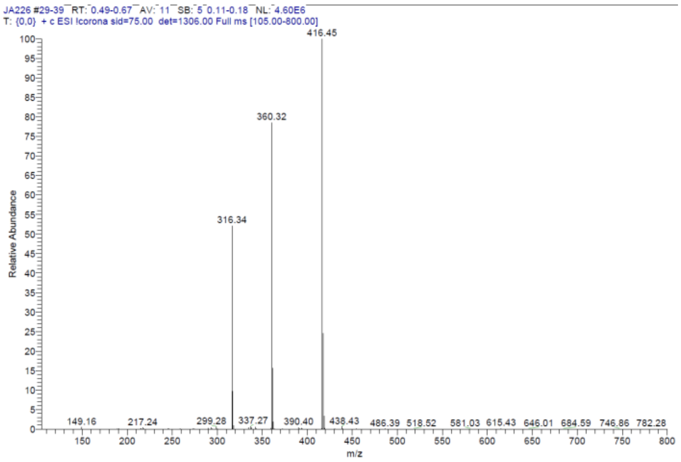
JA226 #29-39 RT: 0.49-0.67 AV: 11 SB: 5 0.11-0.18 NL: 4.60E6
T: {0,0} + c ESI !corona sid=75.00 det=1306.00 Full ms [105.00-800.00]
416.45
360.32
316.34
149.16
217.24
299.28
337.27
390.40
438.43
486.39
518.52
581.03
615.43
646.01
684.59
746.86
782.28
Relative Abundance
100 95 90 85 80 75 70 65 60 55 50 45 40 35 30 25 20 15 10 5 0
150 200 250 300 350 400 450 500 550 600 650 700 750 800
m/z

^{1}H, ^{13}C NMR, HPLC, and ESI data of compound **56f**

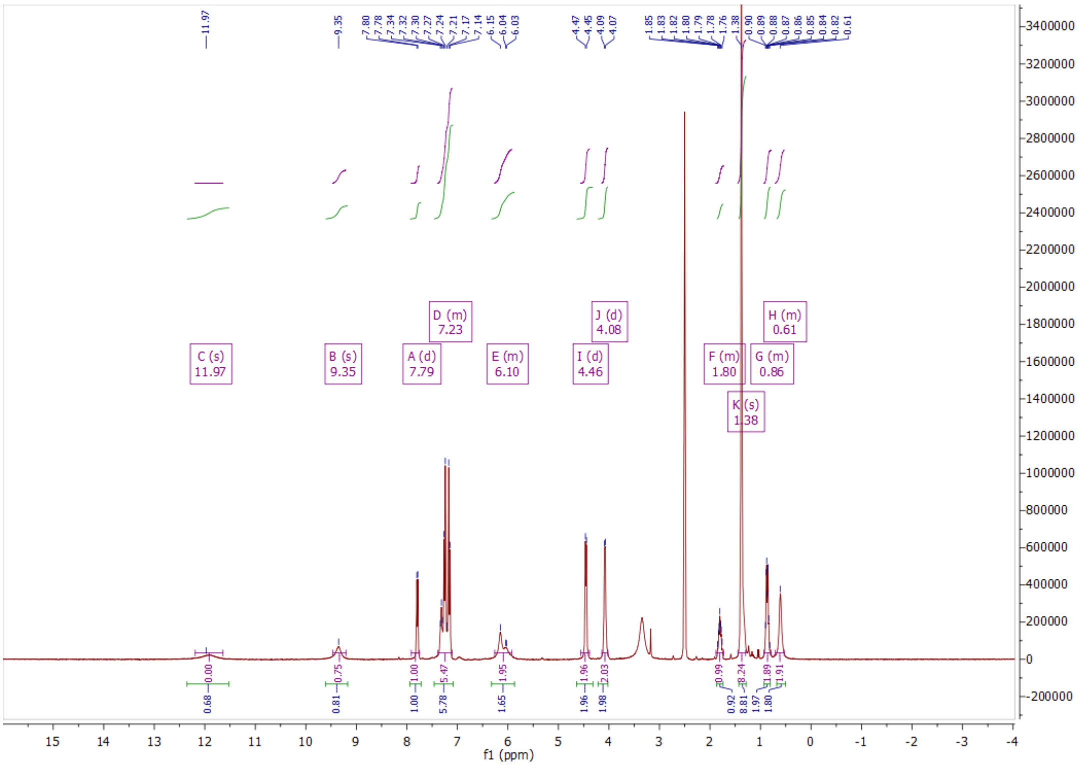

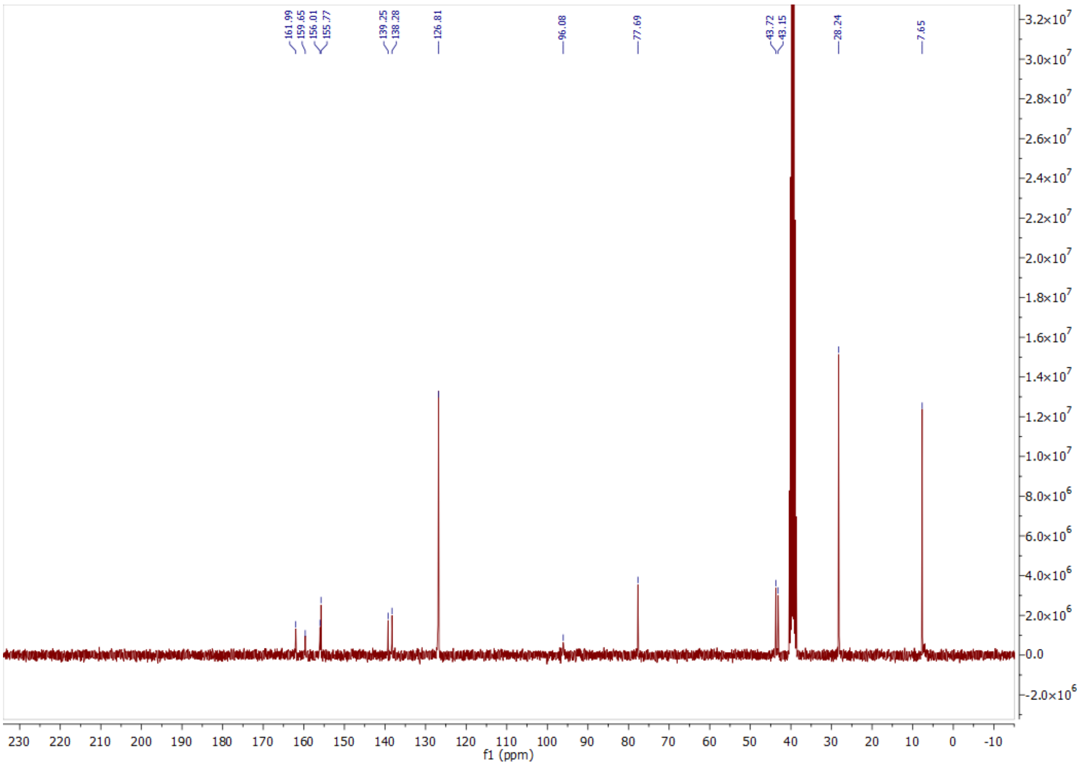

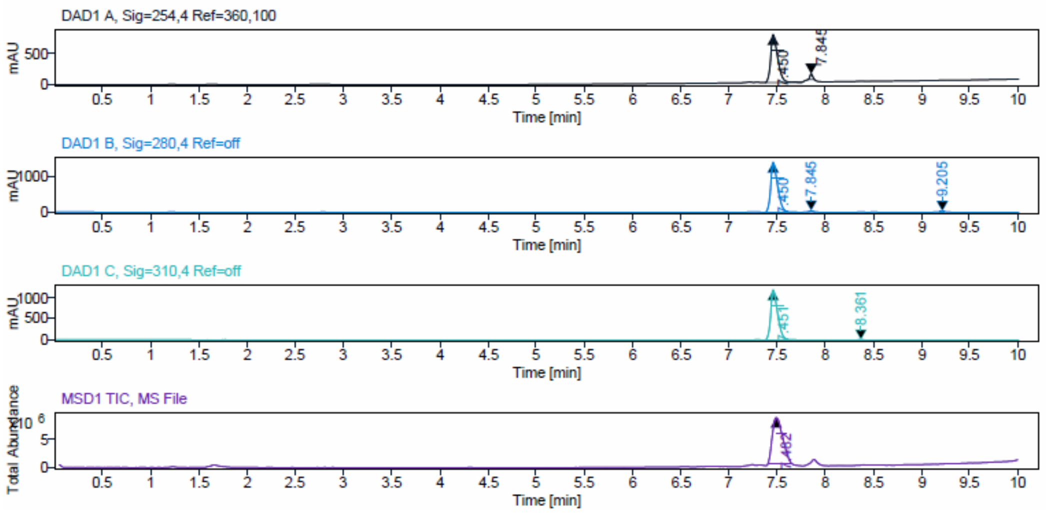

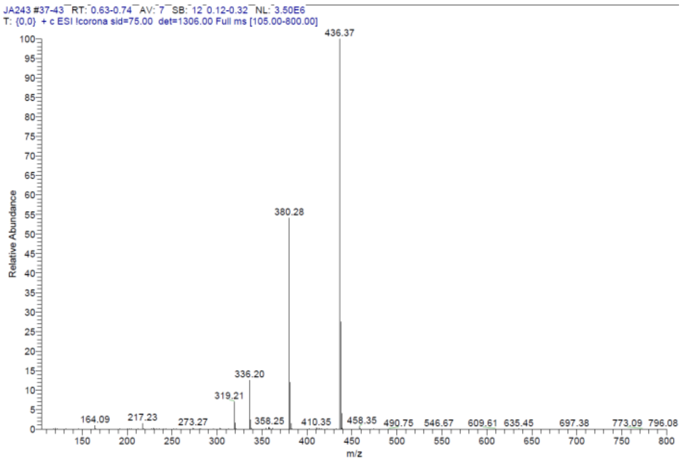

^{1}H, ^{13}C NMR, HPLC, and ESI data of compound **57a**

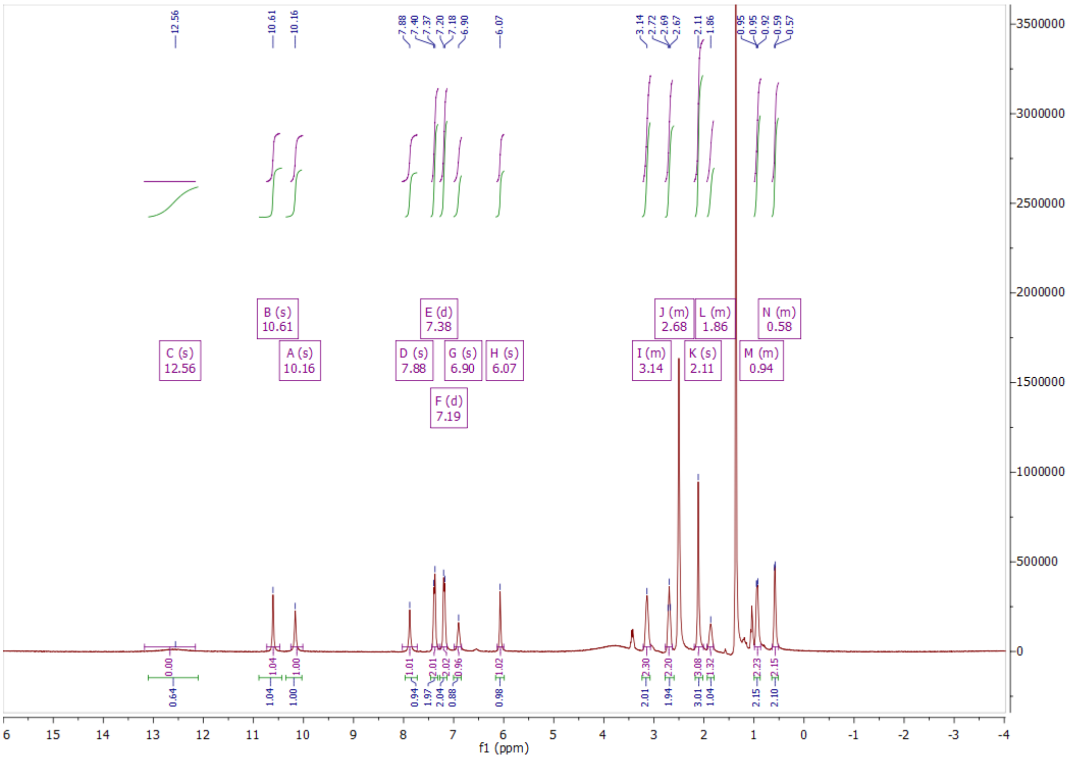

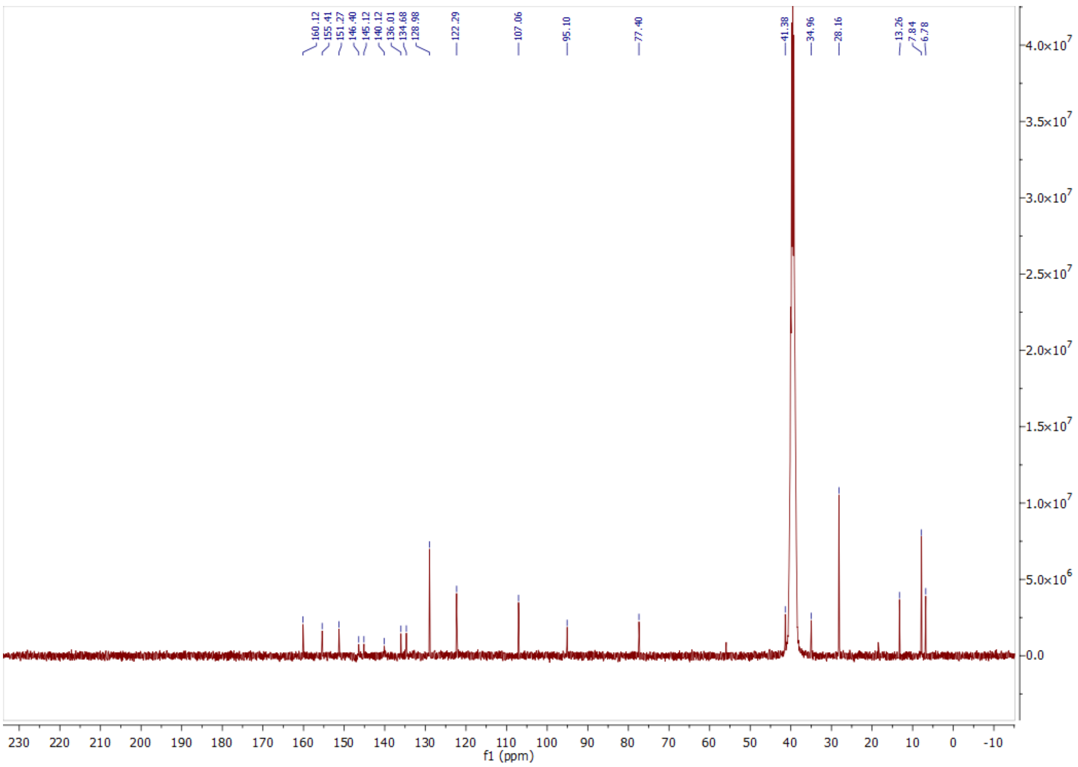
160.12
155.41
151.27
146.40
145.12
140.12
136.01
134.68
128.98
122.29
107.06
95.10
77.40
41.38
34.96
28.16
13.26
7.84
6.78
4.0×10^7
3.5×10^7
3.0×10^7
2.5×10^7
2.0×10^7
1.5×10^7
1.0×10^7
5.0×10^6
0.0
230 220 210 200 190 180 170 160 150 140 130 120 110 100 90 80 70 60 50 40 30 20 10 0 -10
f1 (ppm)

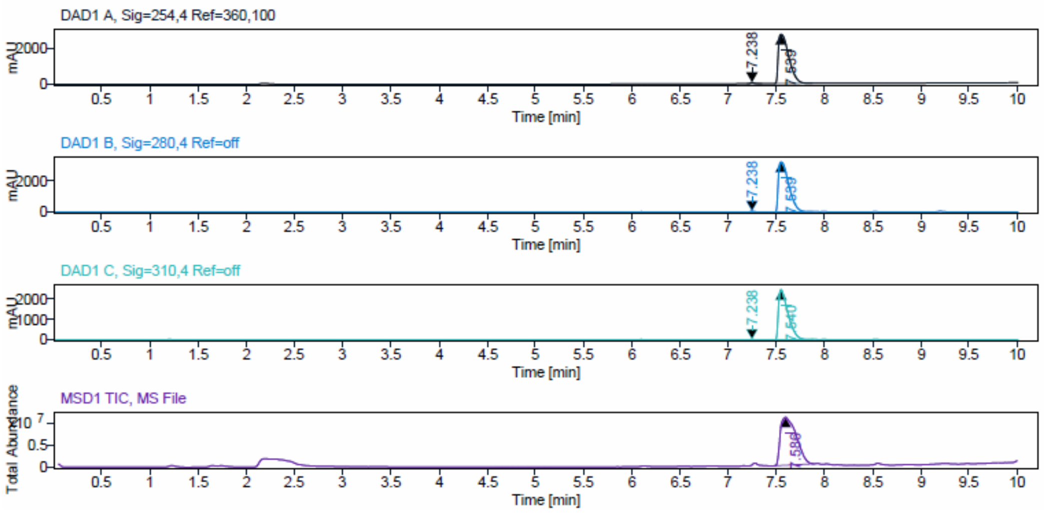
DAD1 A, Sig=254,4 Ref=360,100
mAU
2000
0
7.238
7.538
Time [min]
DAD1 B, Sig=280,4 Ref=off
mAU
2000
0
7.238
7.539
Time [min]
DAD1 C, Sig=310,4 Ref=off
mAU
2000
1000
0
7.238
7.540
Time [min]
MSD1 TIC, MS File
Total Abundance
x10 7
0.5
0
7.580
0.5 1 1.5 2 2.5 3 3.5 4 4.5 5 5.5 6 6.5 7 7.5 8 8.5 9 9.5 10
Time [min]

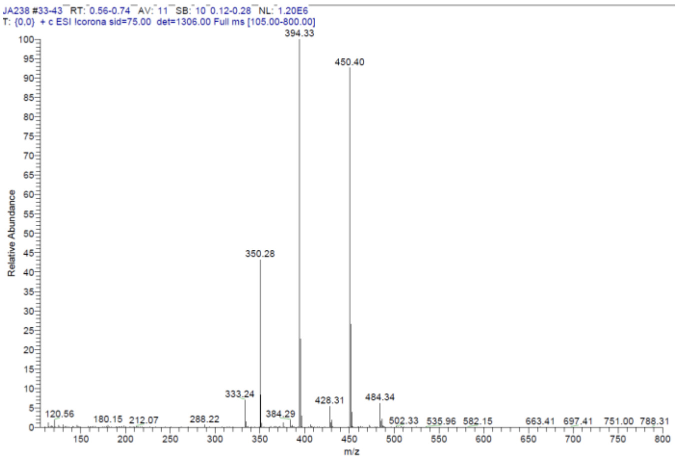
JA238 #33-43 RT: 0.56-0.74 AV: 11 SB: 10 0.12-0.28 NL: 1.20E6
T: {0,0} + c ESI Icorona sid=75.00 det=1306.00 Full ms [105.00-800.00]
394.33
450.40
350.28
333.24
384.29
428.31
484.34
120.56
180.15
212.07
288.22
502.33
535.96
582.15
663.41
697.41
751.00
788.31
Relative Abundance
100 95 90 85 80 75 70 65 60 55 50 45 40 35 30 25 20 15 10 5 0
150 200 250 300 350 400 450 500 550 600 650 700 750 800
m/z

^{1}H, ^{13}C NMR, HPLC, and ESI data of compound **57b**

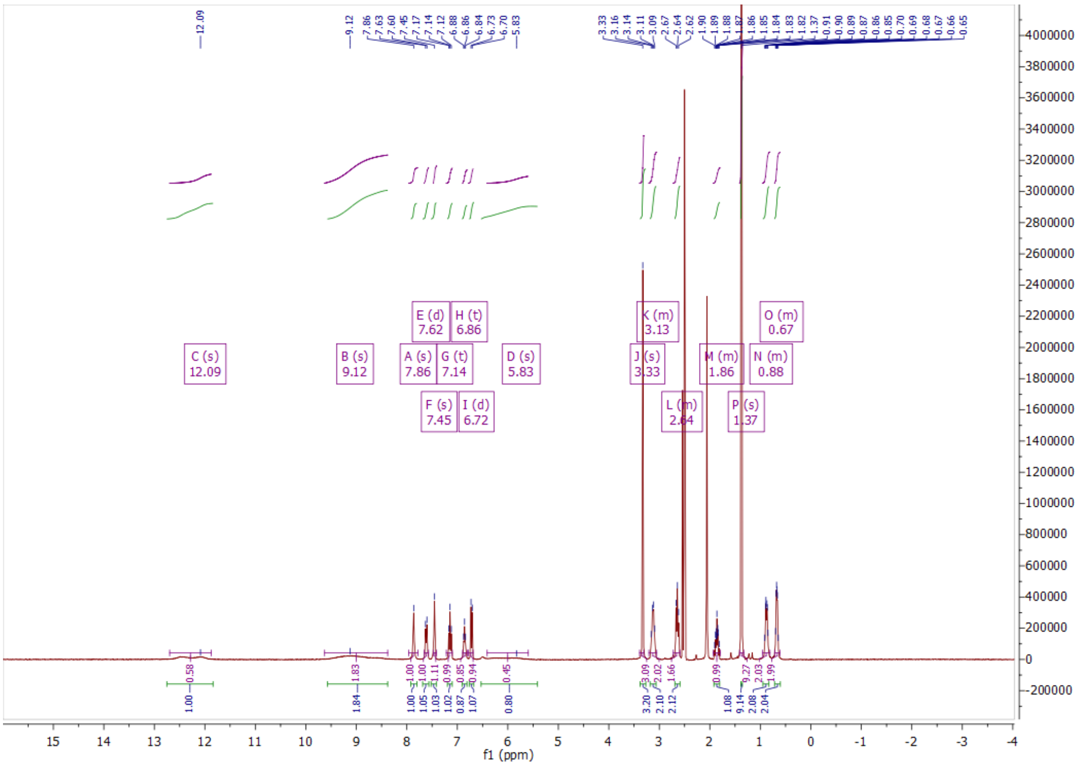

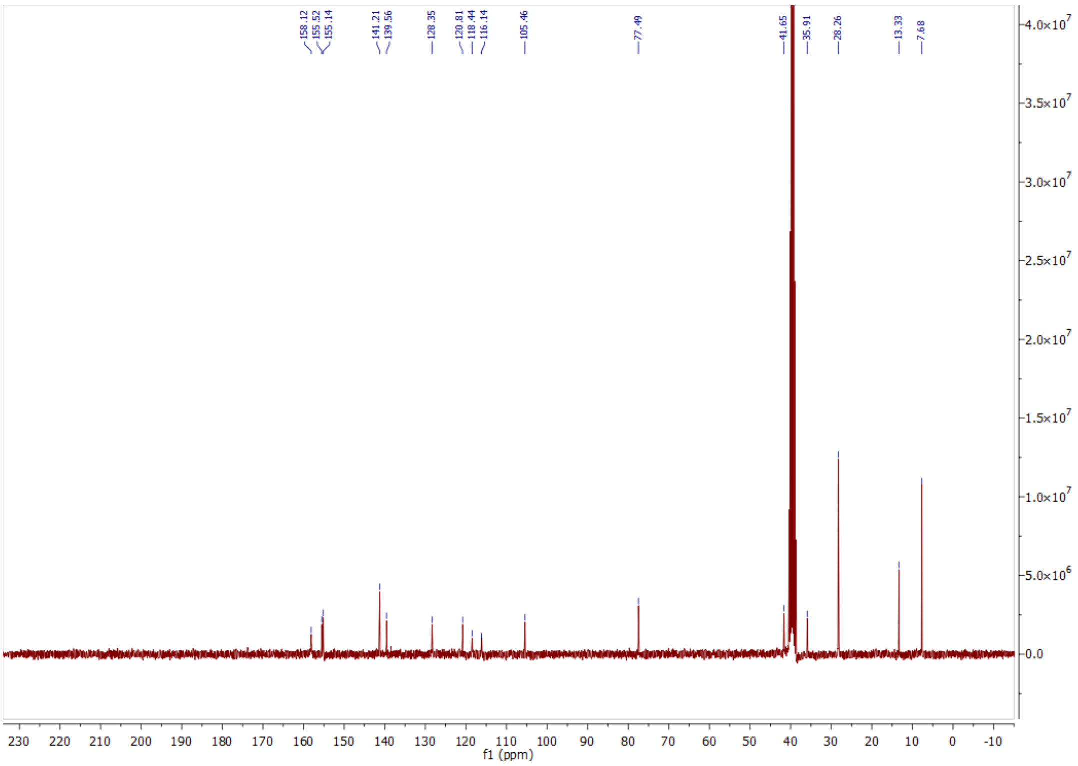

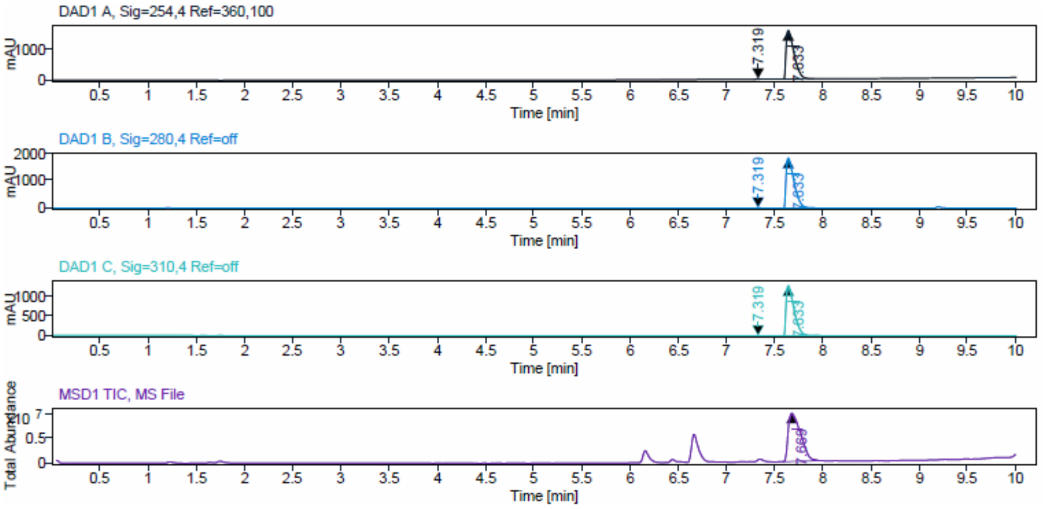

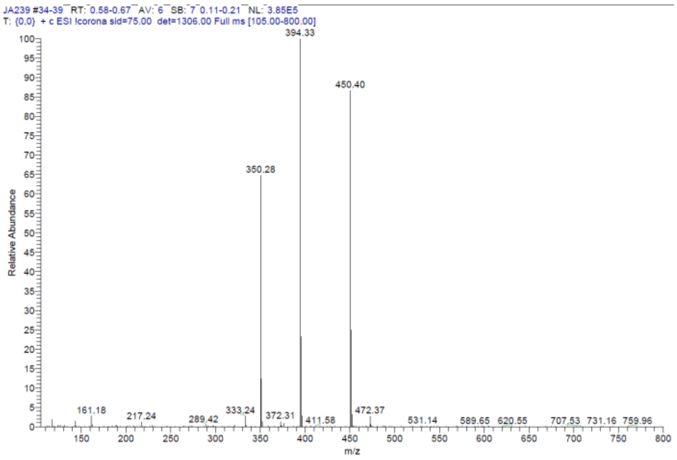

^{1}H NMR, HPLC, and ESI data of compound **57c**

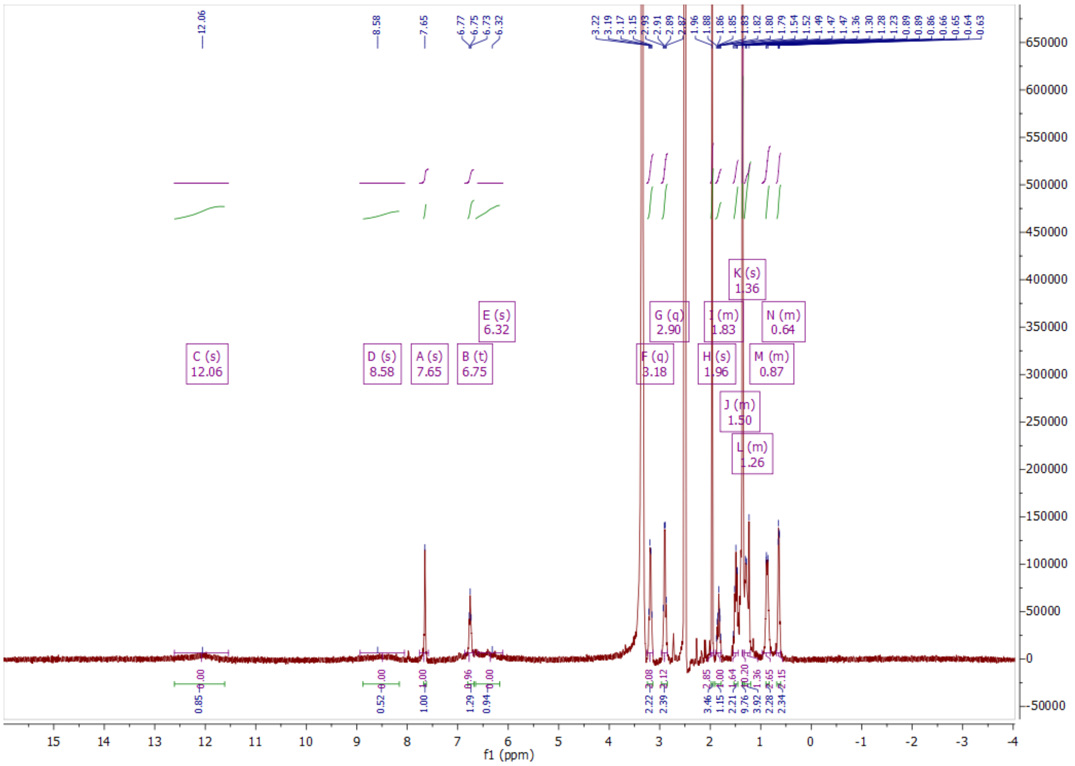

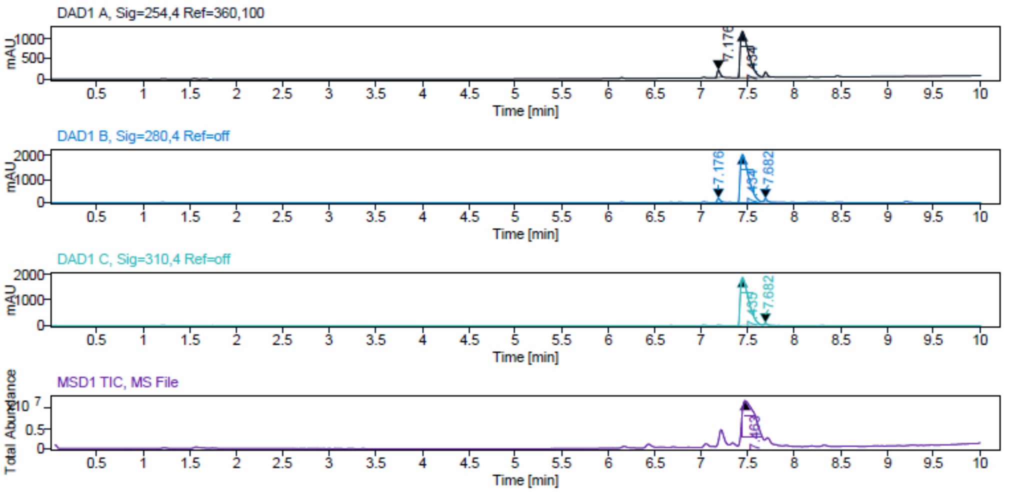

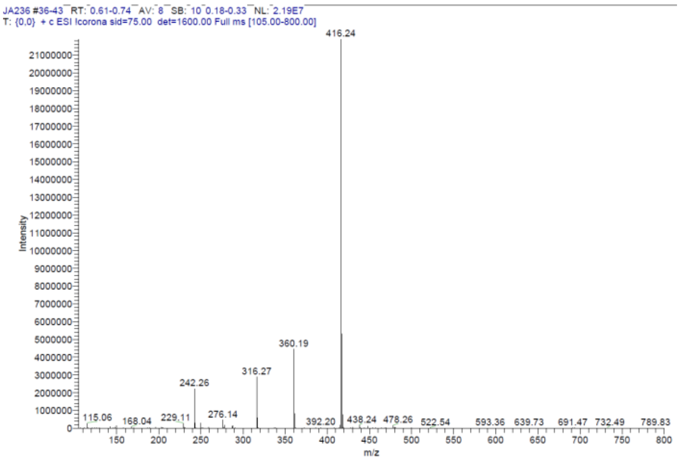

^{1}H, ^{13}C NMR, HPLC, and ESI data of compound **57d**

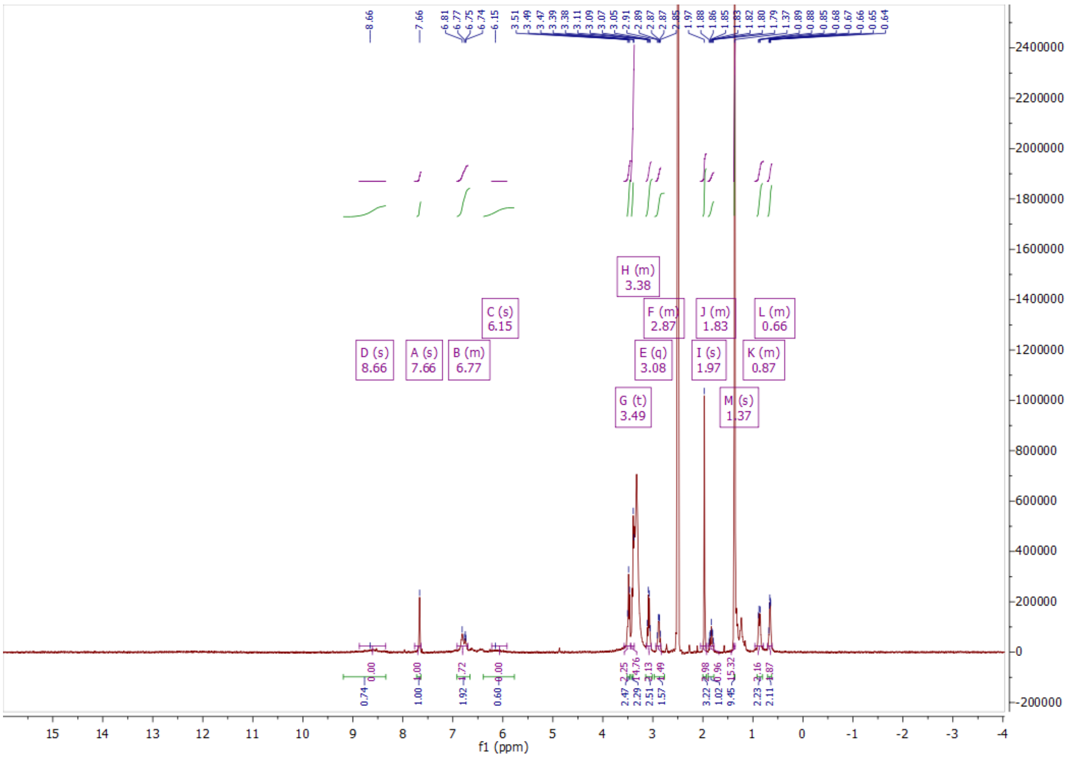

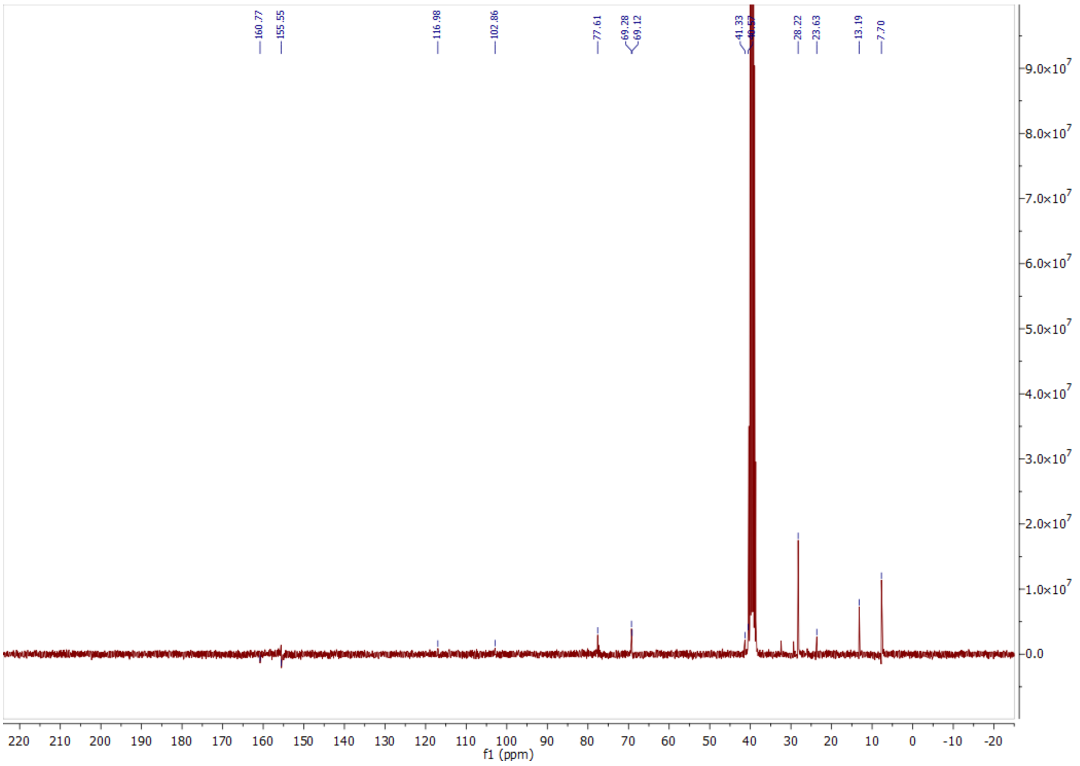
160.77
155.55
116.98
102.86
77.61
69.28
69.12
41.33
40.57
28.22
23.63
13.19
7.70
9.0×10^7
8.0×10^7
7.0×10^7
6.0×10^7
5.0×10^7
4.0×10^7
3.0×10^7
2.0×10^7
1.0×10^7
0.0
220 210 200 190 180 170 160 150 140 130 120 110 100 90 80 70 60 50 40 30 20 10 0 -10 -20
f1 (ppm)

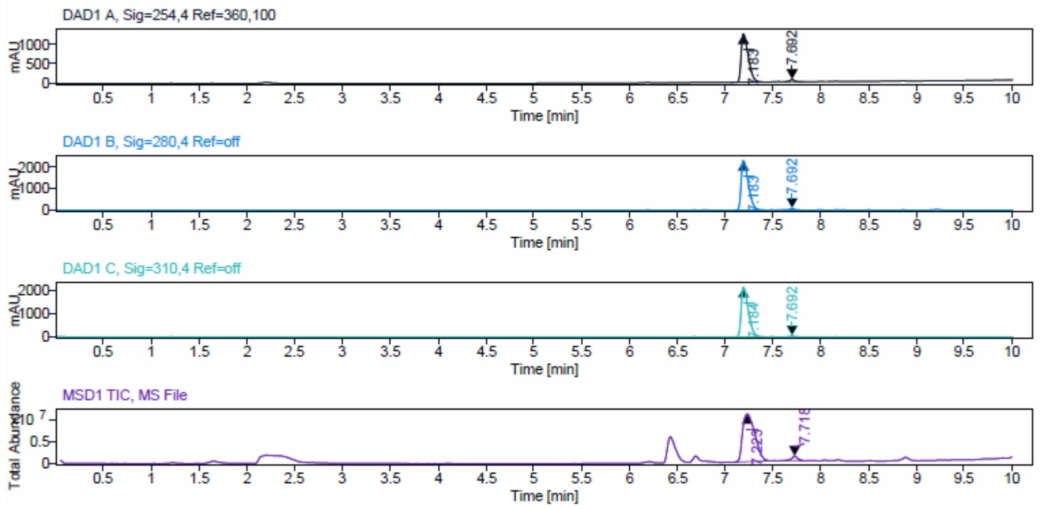
DAD1 A, Sig=254,4 Ref=360,100
mAU
1000
500
0
7.183
7.692
Time [min]
DAD1 B, Sig=280,4 Ref=off
mAU
2000
1000
0
7.183
7.692
Time [min]
DAD1 C, Sig=310,4 Ref=off
mAU
2000
1000
0
7.184
7.692
Time [min]
MSD1 TIC, MS File
Total Abundance
x10 7
0.5
0
7.223
7.718
0.5 1 1.5 2 2.5 3 3.5 4 4.5 5 5.5 6 6.5 7 7.5 8 8.5 9 9.5 10
Time [min]

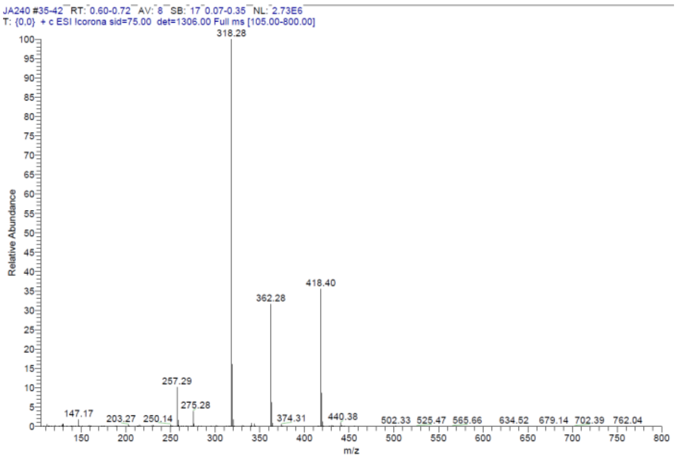
JA240 #35-42 RT: 0.60-0.72 AV: 8 SB: 17 0.07-0.35 NL: 2.73E6
T: {0,0} + c ESI !corona sid=75.00 det=1306.00 Full ms [105.00-800.00]
Relative Abundance
318.28
418.40
362.28
257.29
275.28
147.17
203.27
250.14
374.31
440.38
502.33
525.47
565.66
634.52
679.14
702.39
762.04
m/z

^{1}H NMR, HPLC, and ESI data of compound **57e**

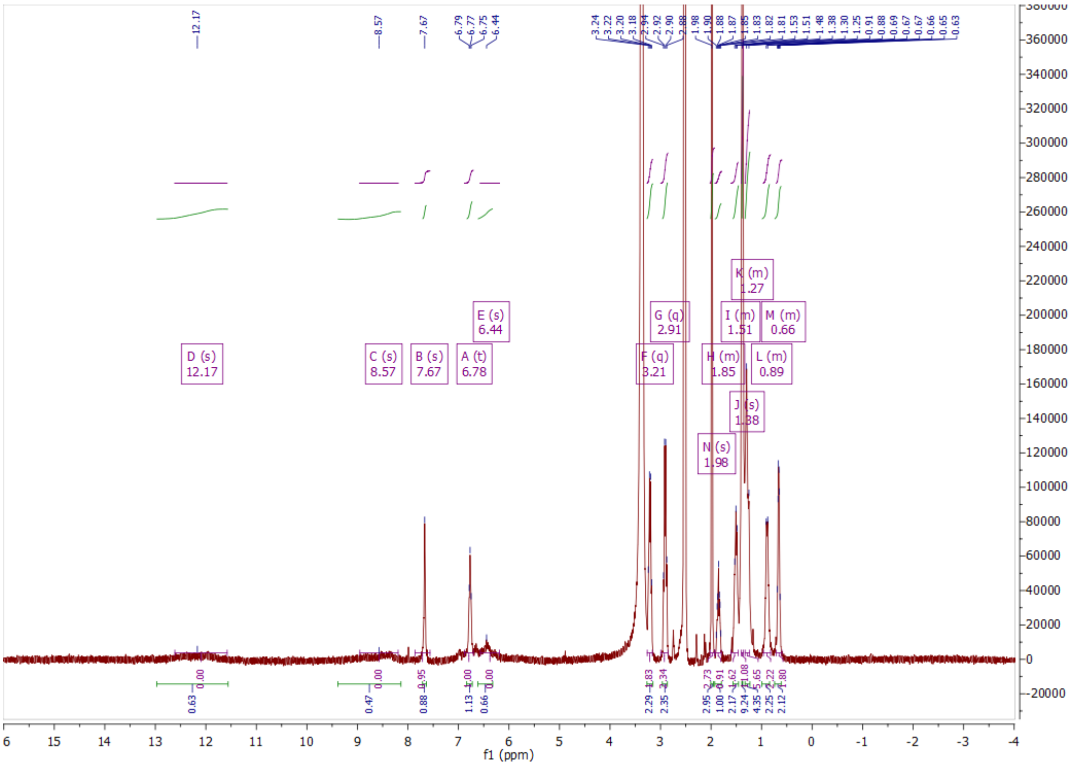

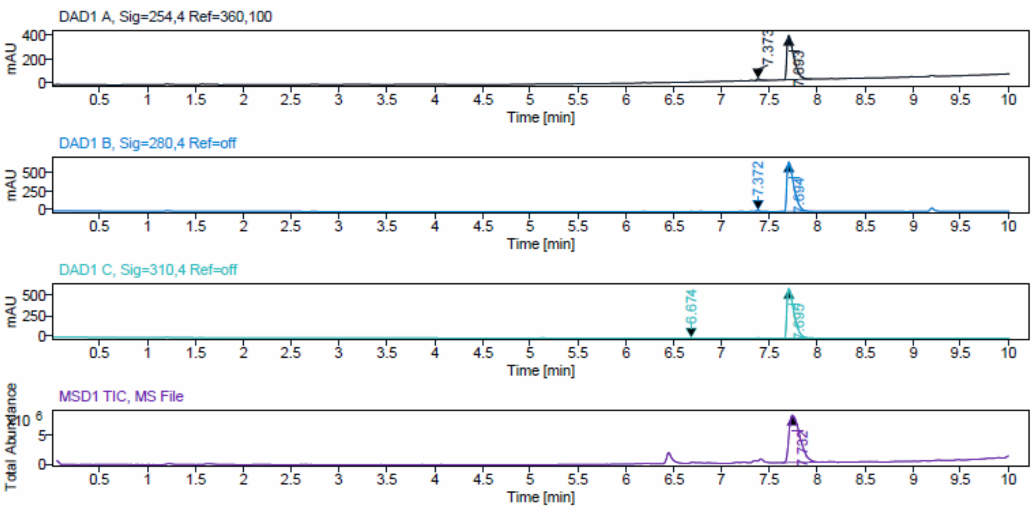

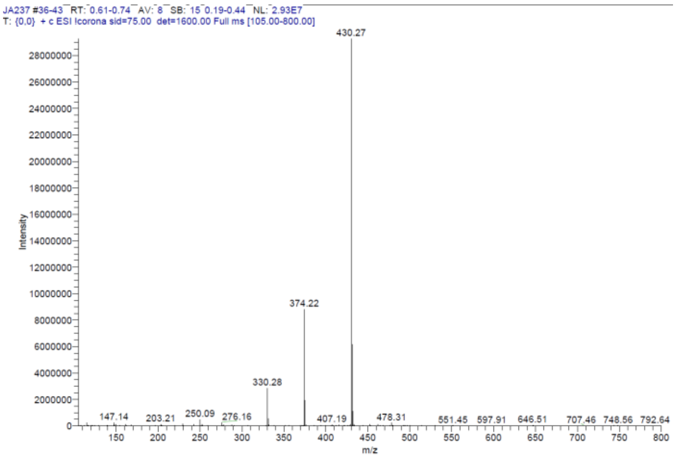

^{1}H, ^{13}C NMR, HPLC, and ESI data of compound **58a**

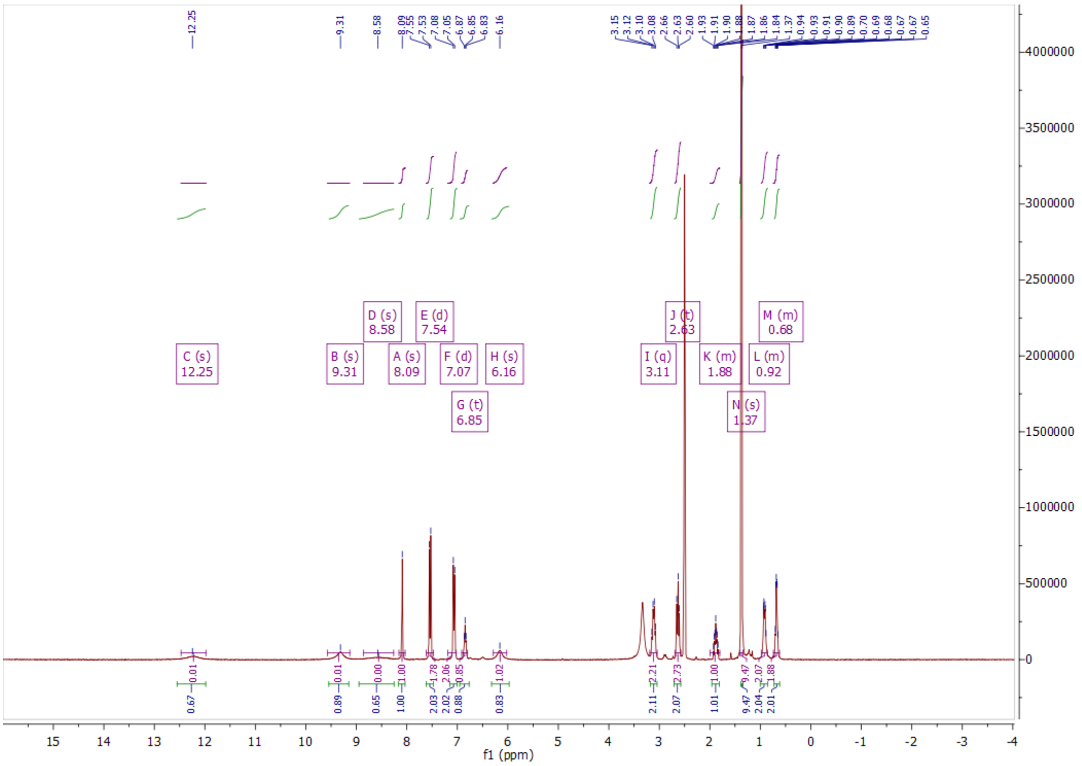

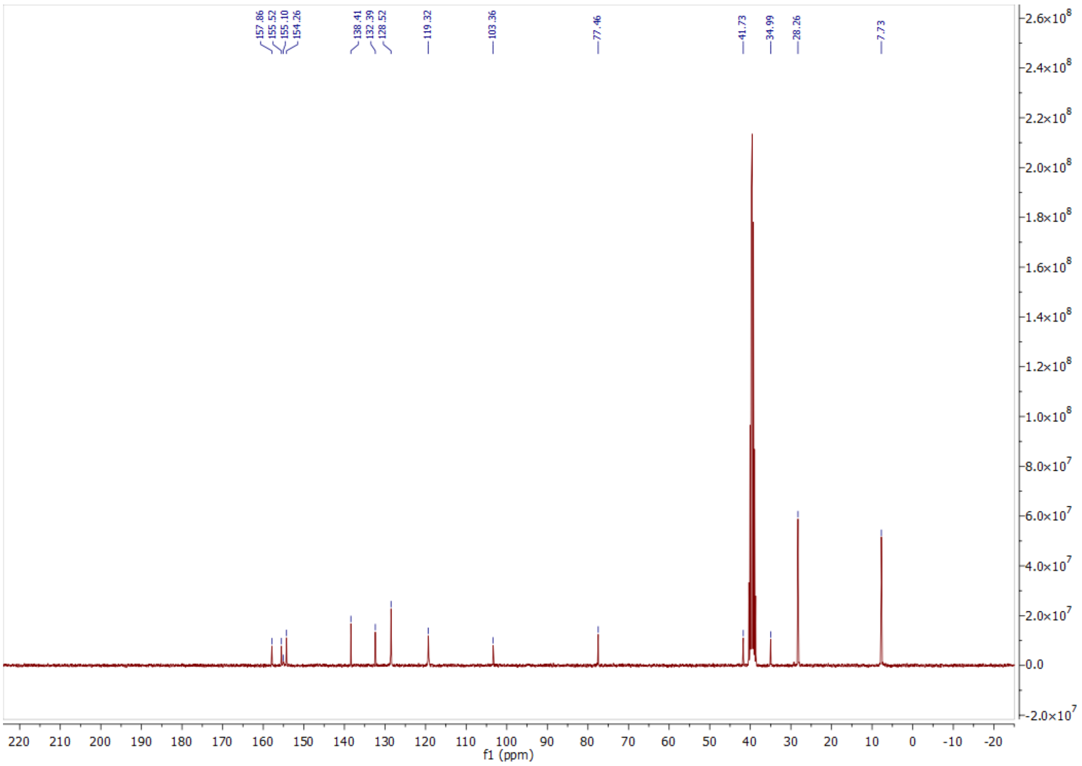

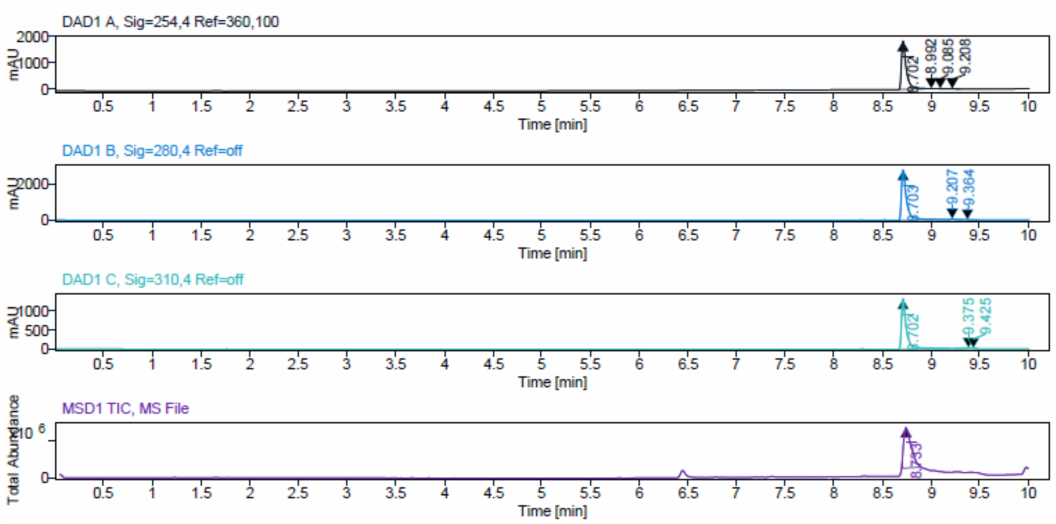

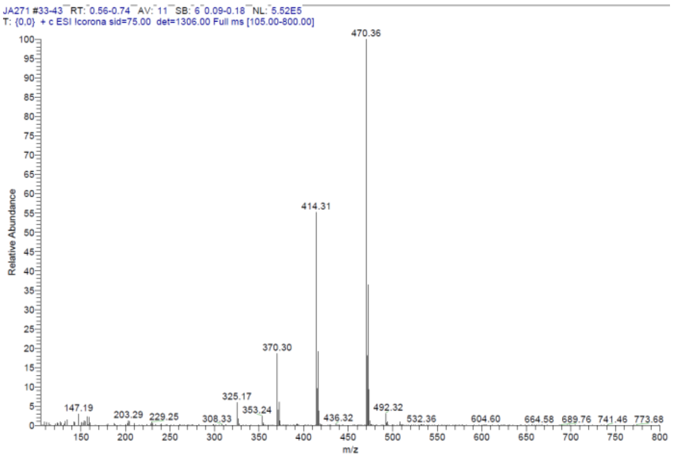

^{1}H, ^{13}C NMR, HPLC, and ESI data of compound **58c**

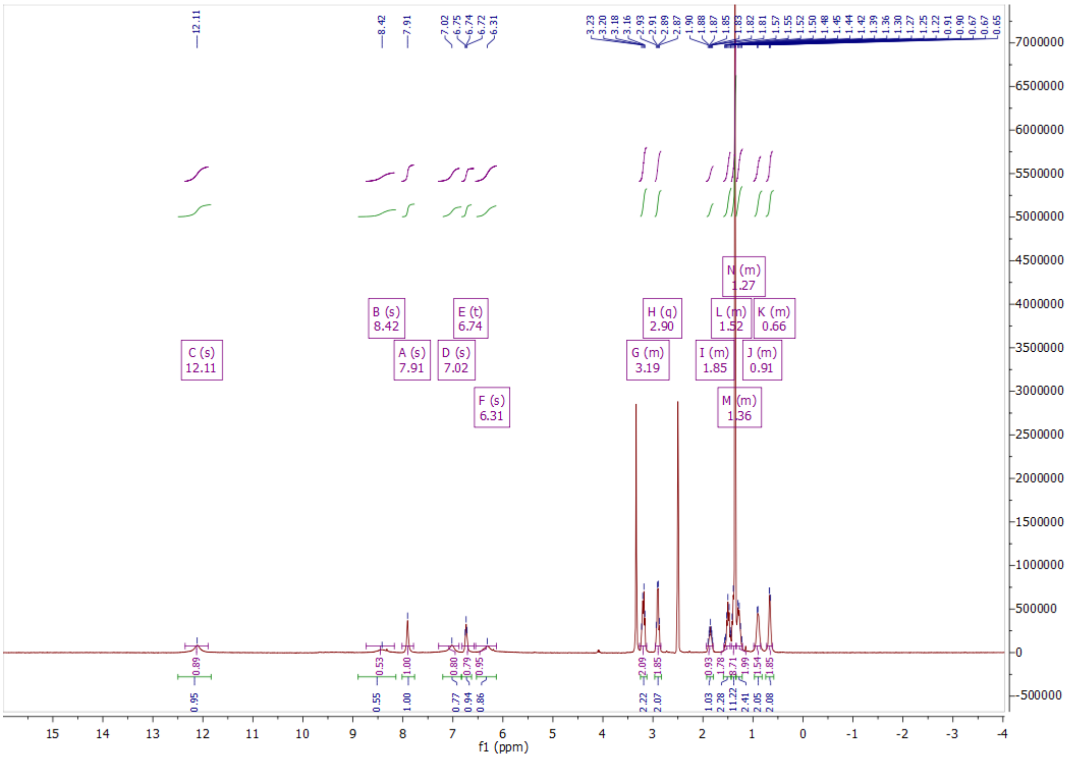

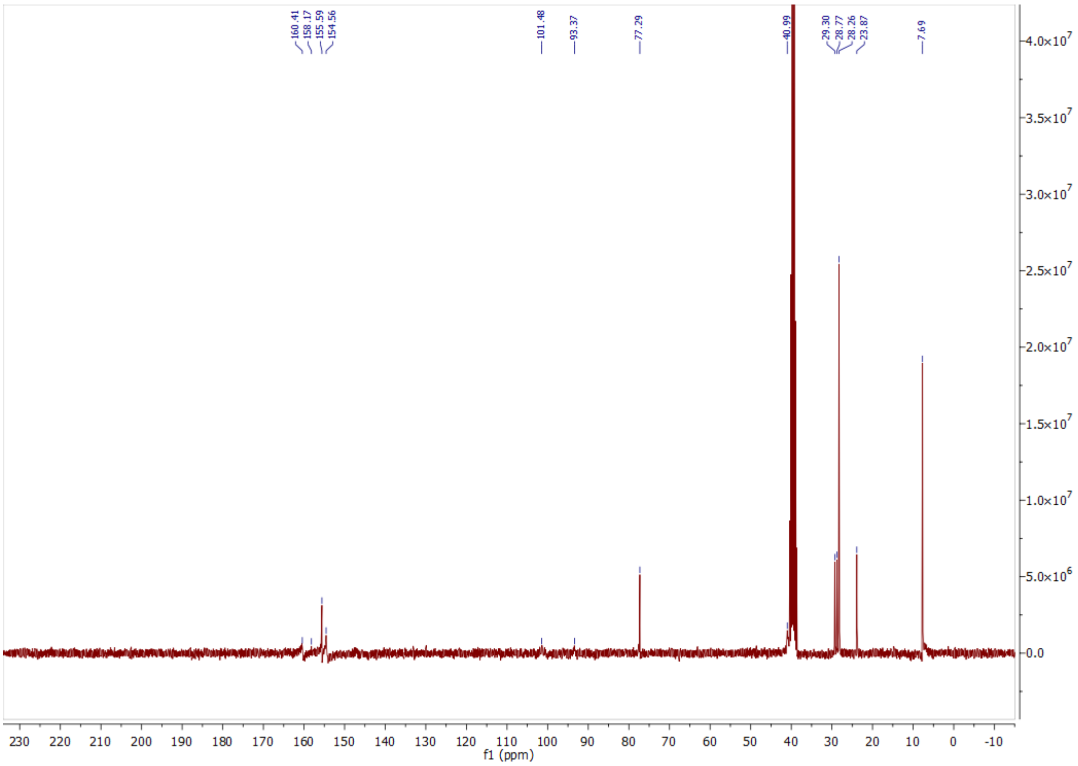
160.41
158.17
155.59
154.56
101.48
93.37
77.29
40.99
29.30
28.77
28.26
23.87
7.69
4.0×10^7
3.5×10^7
3.0×10^7
2.5×10^7
2.0×10^7
1.5×10^7
1.0×10^7
5.0×10^6
0.0
230 220 210 200 190 180 170 160 150 140 130 120 110 100 90 80 70 60 50 40 30 20 10 0 -10
f1 (ppm)

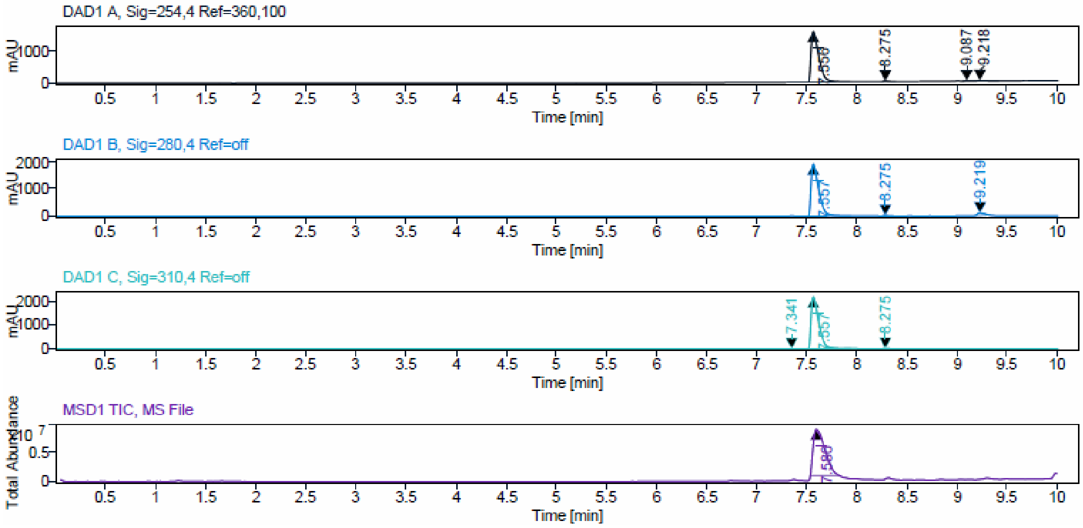
DAD1 A, Sig=254,4 Ref=360,100
mAU
1000
0
7.558
8.275
9.087
9.218
Time [min]
DAD1 B, Sig=280,4 Ref=off
mAU
2000
1000
0
7.557
8.275
9.219
Time [min]
DAD1 C, Sig=310,4 Ref=off
mAU
2000
1000
0
7.341
7.557
8.275
Time [min]
MSD1 TIC, MS File
Total Abundance
x10 7
0.5
0
7.580
0.5 1 1.5 2 2.5 3 3.5 4 4.5 5 5.5 6 6.5 7 7.5 8 8.5 9 9.5 10
Time [min]

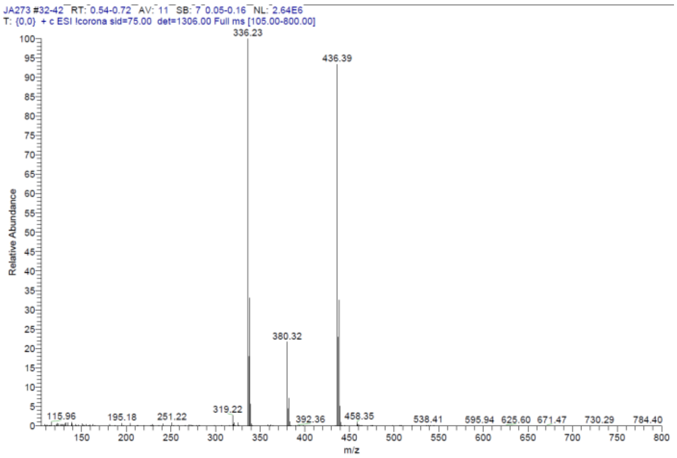
JA273 #32-42 RT: 0.54-0.72 AV: 11 SB: 7 0.05-0.16 NL: 2.64E6
T: {0,0} + c ESI !corona sid=75.00 det=1306.00 Full ms [105.00-800.00]
336.23
436.39
380.32
319.22
115.96
195.18
251.22
392.36
458.35
538.41
595.94
625.60
671.47
730.29
784.40
Relative Abundance
0 5 10 15 20 25 30 35 40 45 50 55 60 65 70 75 80 85 90 95 100
150 200 250 300 350 400 450 500 550 600 650 700 750 800
m/z

^{1}H, ^{13}C NMR, HPLC, and ESI data of compound **60**

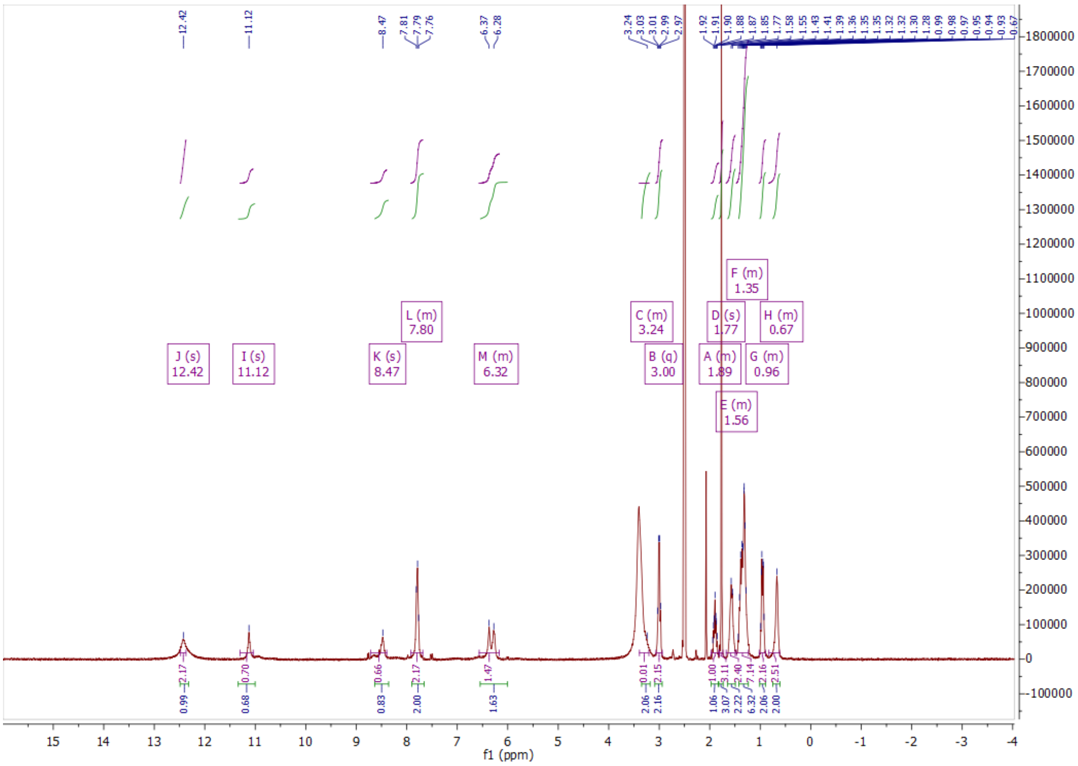

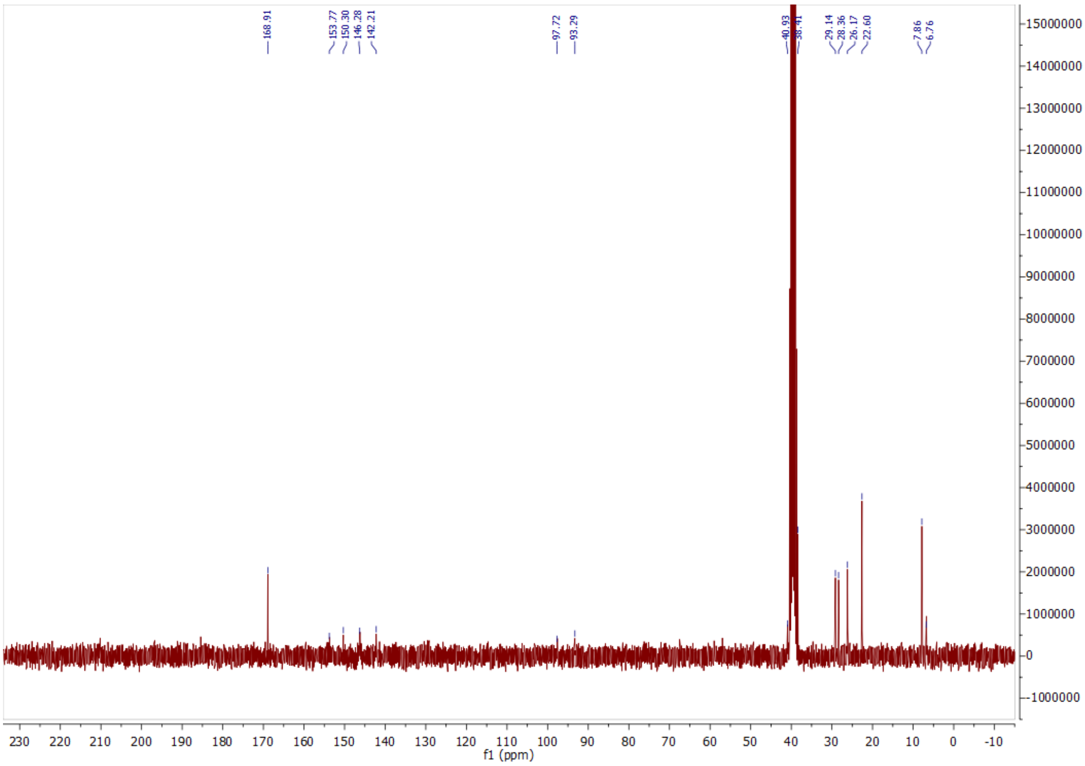

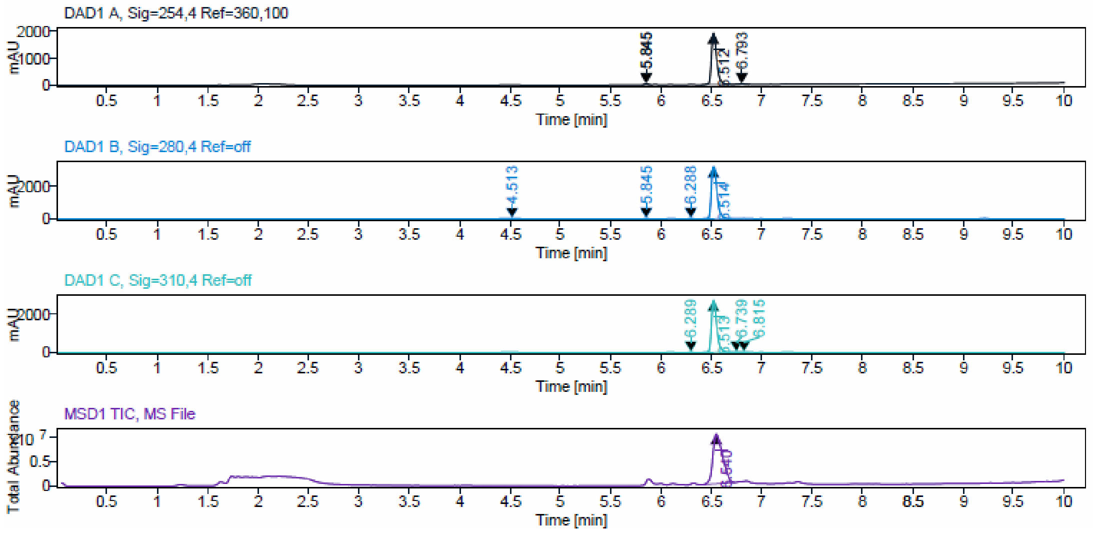

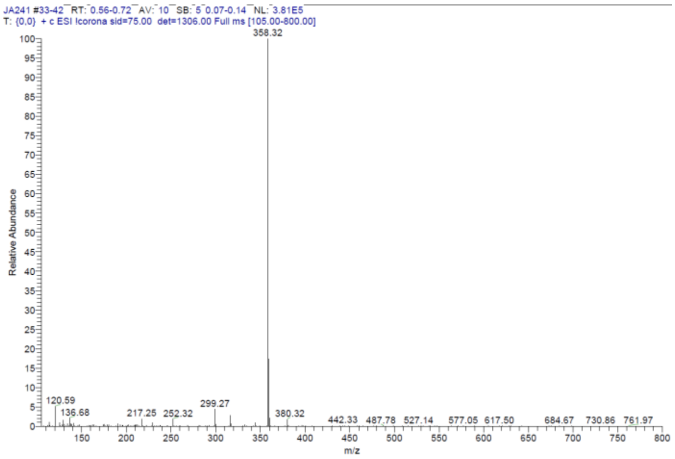

^{1}H, ^{13}C NMR and ESI data of compound **73**

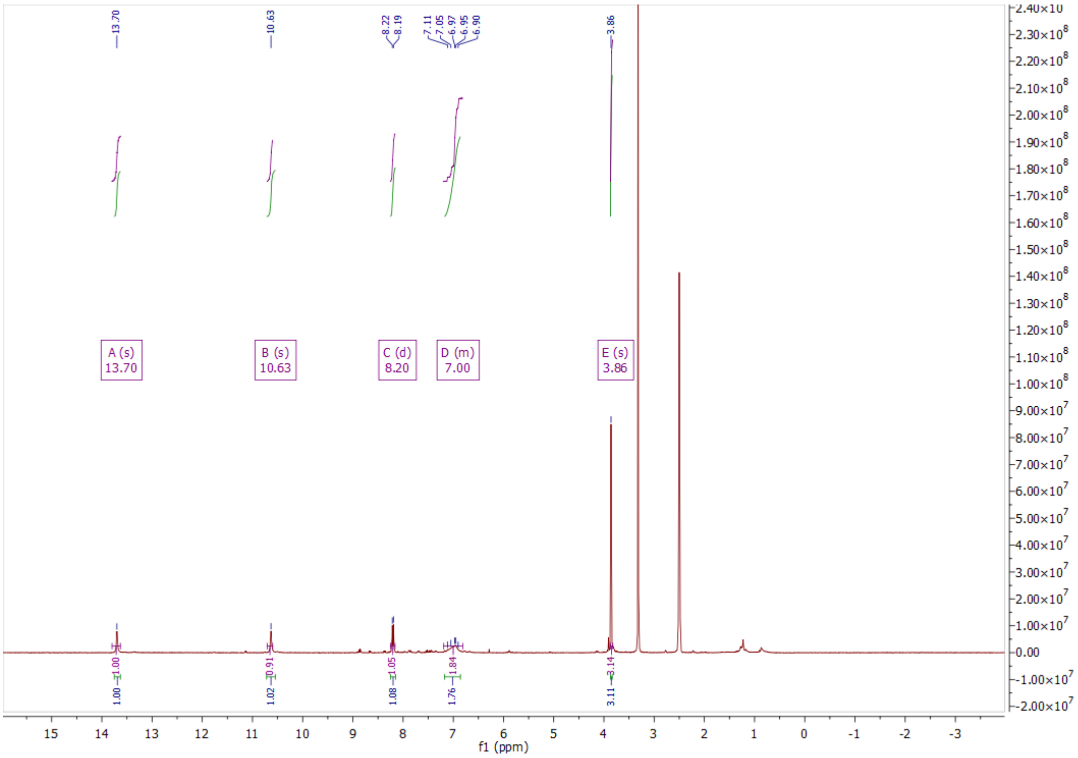

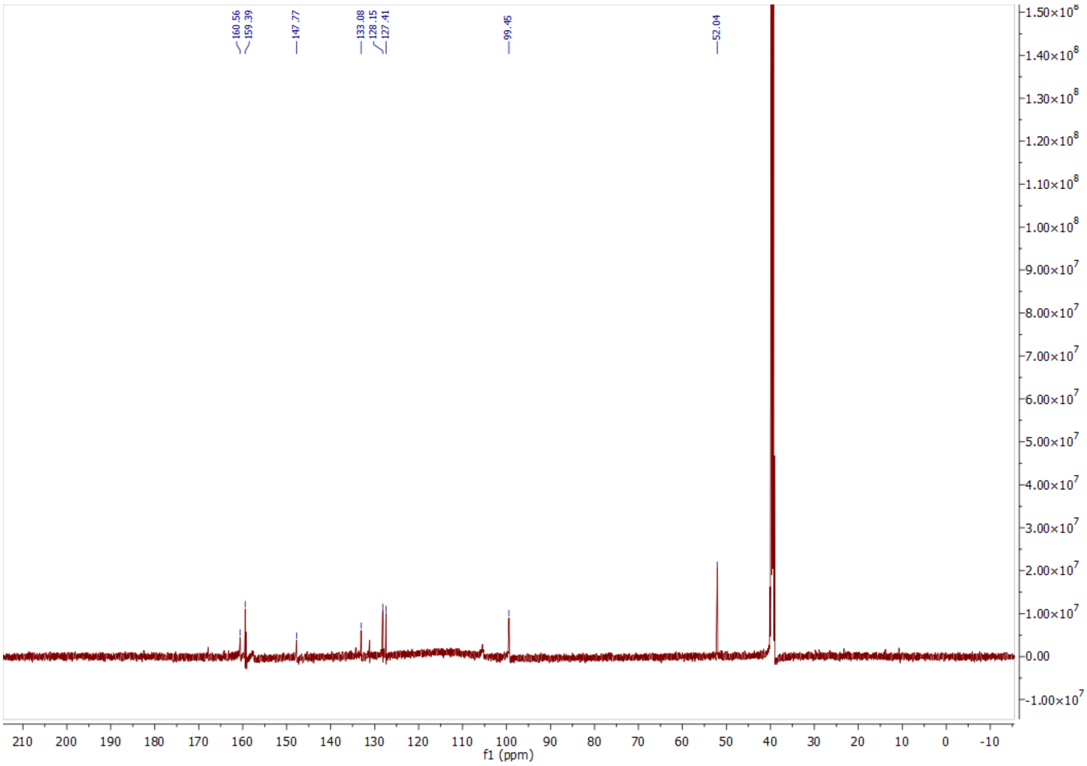
160.56
159.39
147.77
133.08
128.15
127.41
99.45
52.04
1.50×10^8
1.40×10^8
1.30×10^8
1.20×10^8
1.10×10^8
1.00×10^8
9.00×10^7
8.00×10^7
7.00×10^7
6.00×10^7
5.00×10^7
4.00×10^7
3.00×10^7
2.00×10^7
1.00×10^7
0.00
-1.00×10^7
210 200 190 180 170 160 150 140 130 120 110 100 90 80 70 60 50 40 30 20 10 0 -10
f1 (ppm)

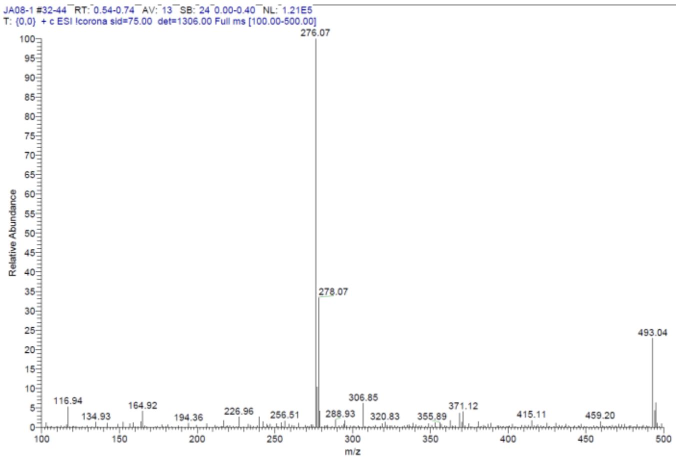
JA08-1 #32-44 RT: 0.54-0.74 AV: 13 SB: 24 0.00-0.40 NL: 1.21E5
T: {0,0} + c ESI !corona sid=75.00 det=1306.00 Full ms [100.00-500.00]
276.07
278.07
493.04
116.94
134.93
164.92
194.36
226.96
256.51
288.93
306.85
320.83
355.89
371.12
415.11
459.20
Relative Abundance
100 95 90 85 80 75 70 65 60 55 50 45 40 35 30 25 20 15 10 5 0
100 150 200 250 300 350 400 450 500
m/z

^{1}H, ^{13}C NMR and ESI data of compound **74**

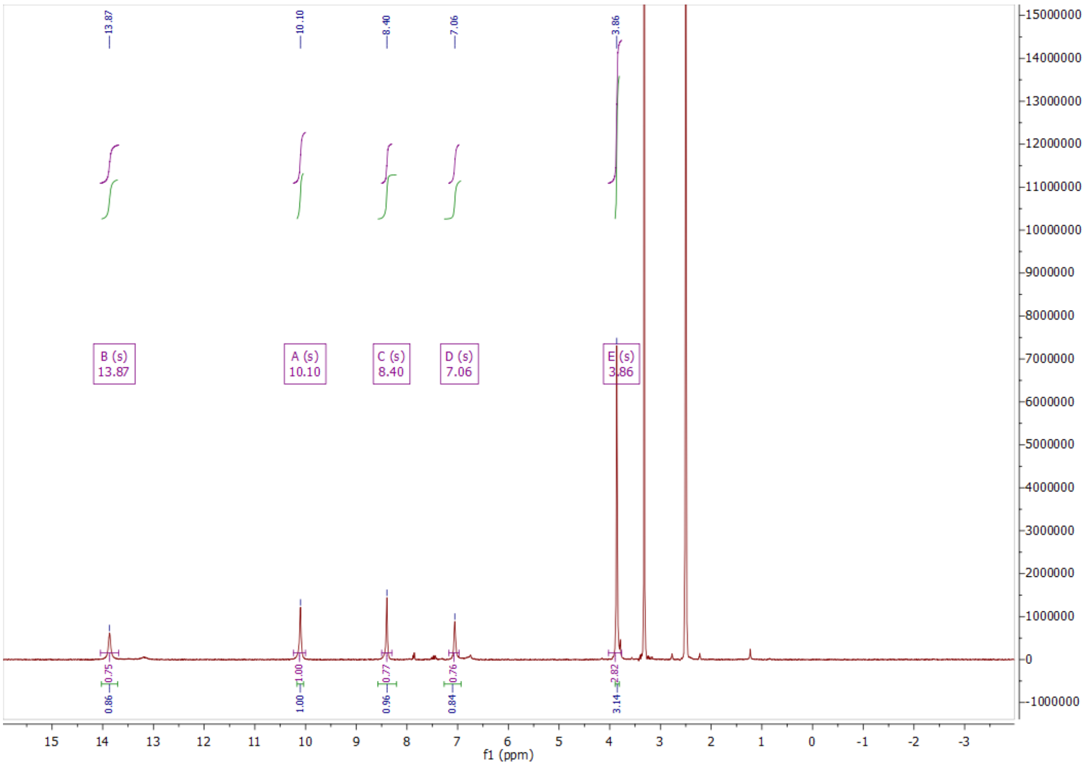

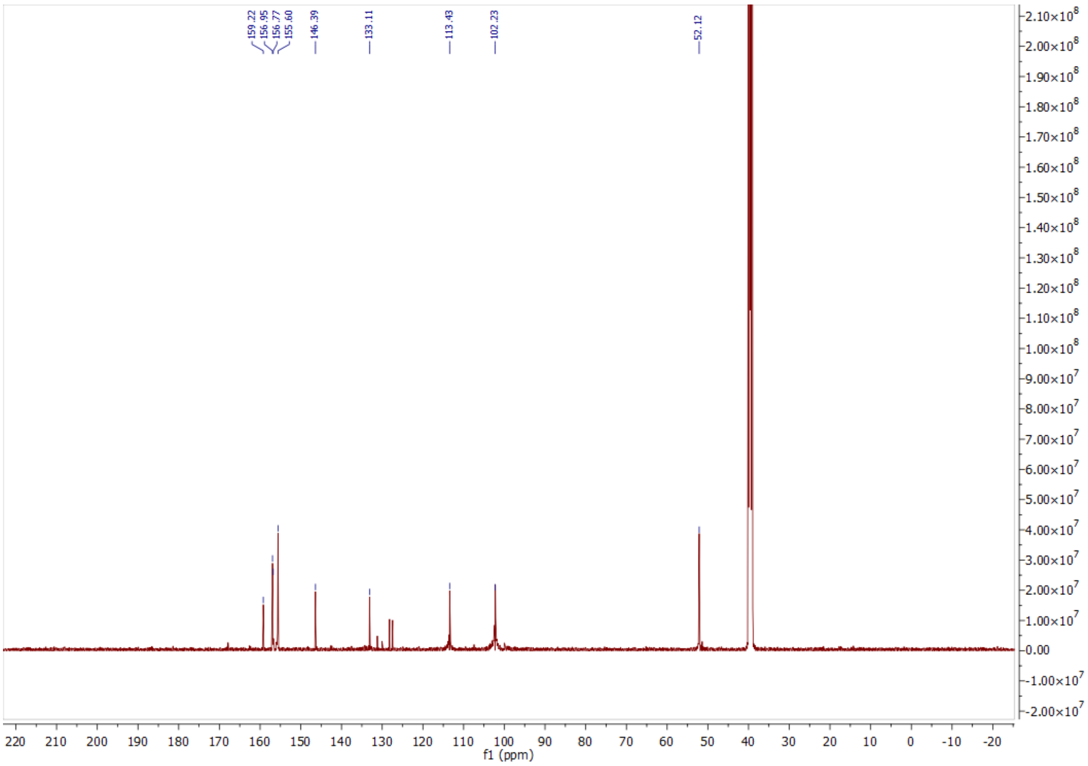

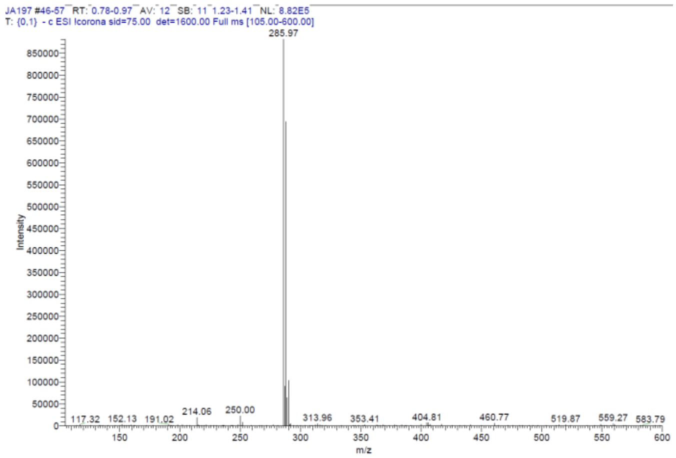

^{1}H, ^{13}C NMR, and ESI data of compound **75**

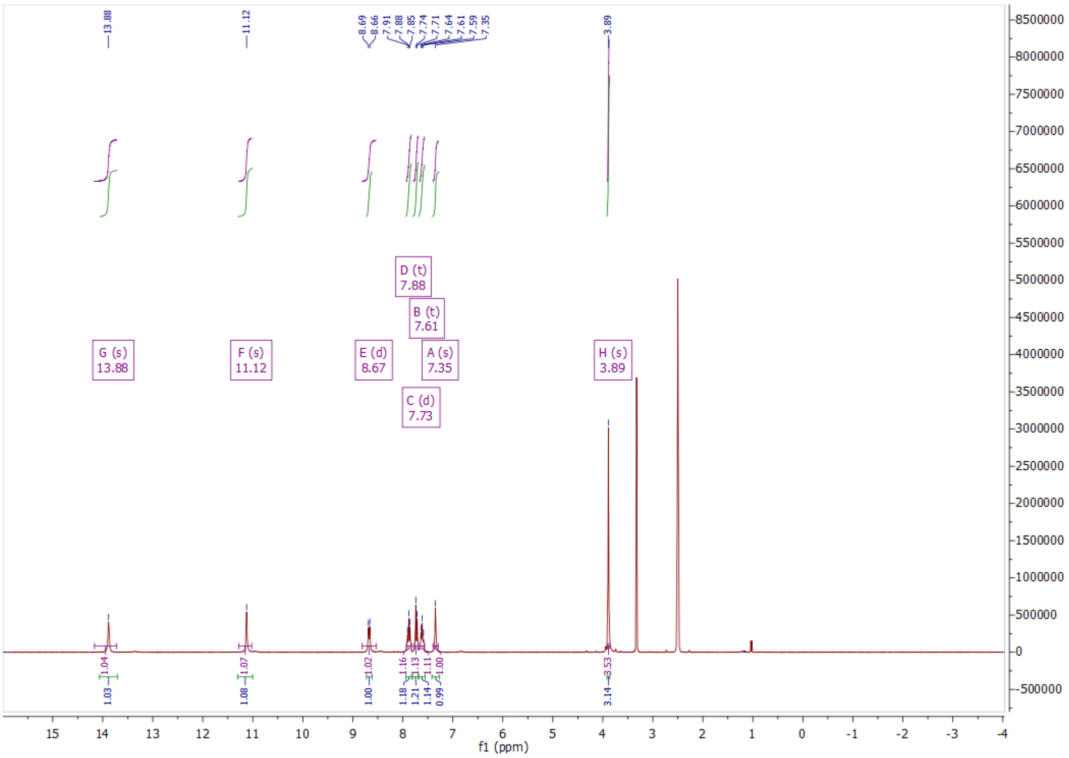

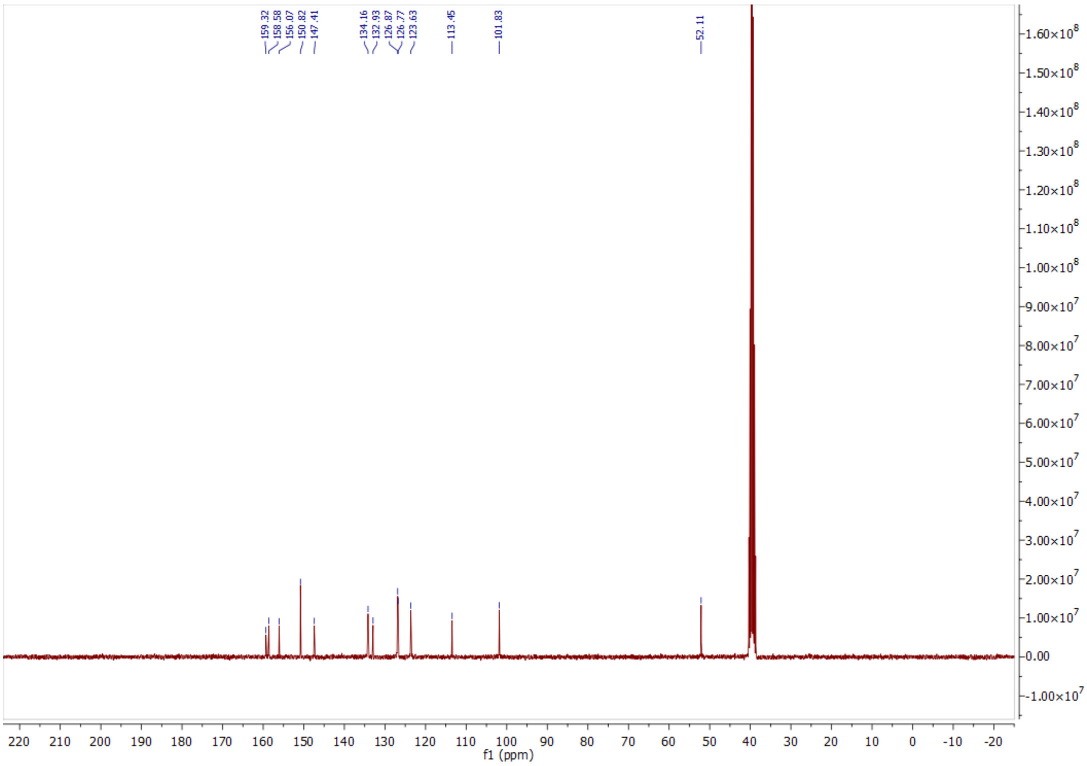
159.32
158.58
156.07
150.82
147.41
134.16
132.93
126.87
126.77
123.63
113.45
101.83
52.11
1.60×10^8
1.50×10^8
1.40×10^8
1.30×10^8
1.20×10^8
1.10×10^8
1.00×10^8
9.00×10^7
8.00×10^7
7.00×10^7
6.00×10^7
5.00×10^7
4.00×10^7
3.00×10^7
2.00×10^7
1.00×10^7
0.00
-1.00×10^7
220 210 200 190 180 170 160 150 140 130 120 110 100 90 80 70 60 50 40 30 20 10 0 -10 -20
f1 (ppm)

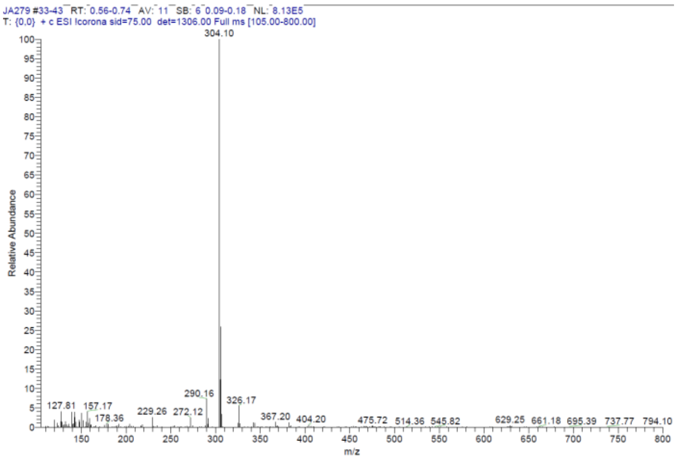
JA279 #33-43 RT: 0.56-0.74 AV: 11 SB: 6 0.09-0.18 NL: 8.13E5
T: {0,0} + c ESI !corona sid=75.00 det=1306.00 Full ms [105.00-800.00]
304.10
290.16
326.17
127.81
157.17
178.36
229.26
272.12
367.20
404.20
475.72
514.36
545.82
629.25
661.18
695.39
737.77
794.10
Relative Abundance
100 95 90 85 80 75 70 65 60 55 50 45 40 35 30 25 20 15 10 5 0
150 200 250 300 350 400 450 500 550 600 650 700 750 800
m/z

^{1}H, ^{13}C NMR, HPLC, and ESI data of compound **76a**

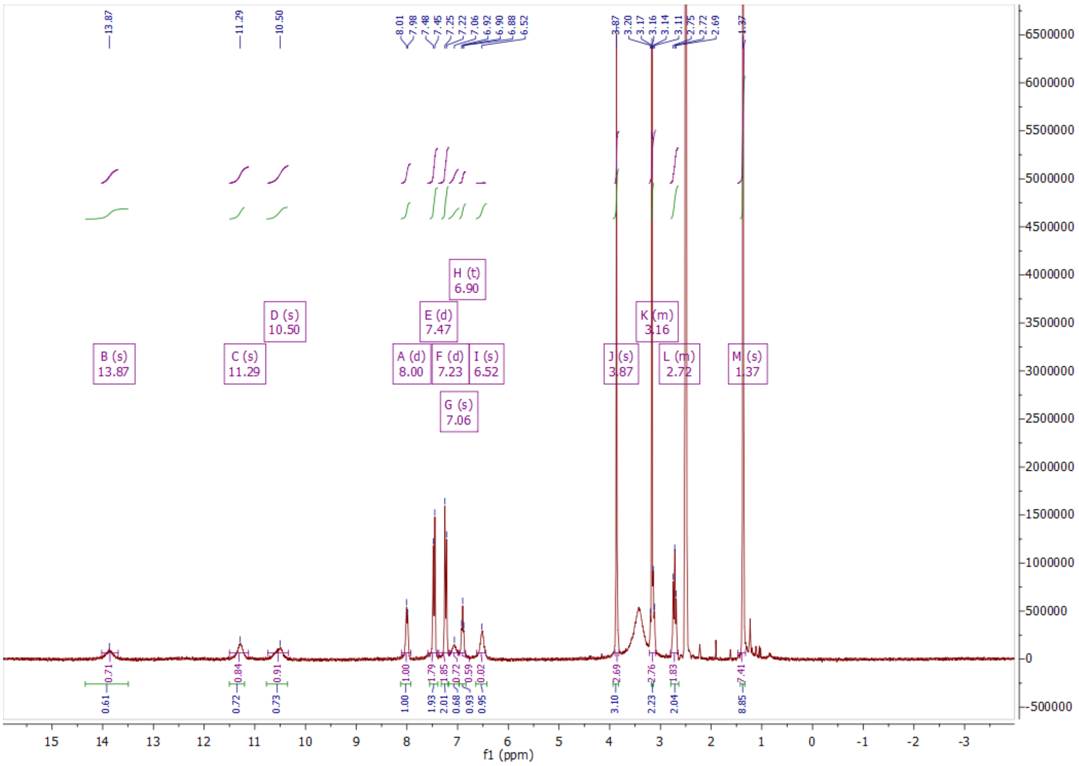

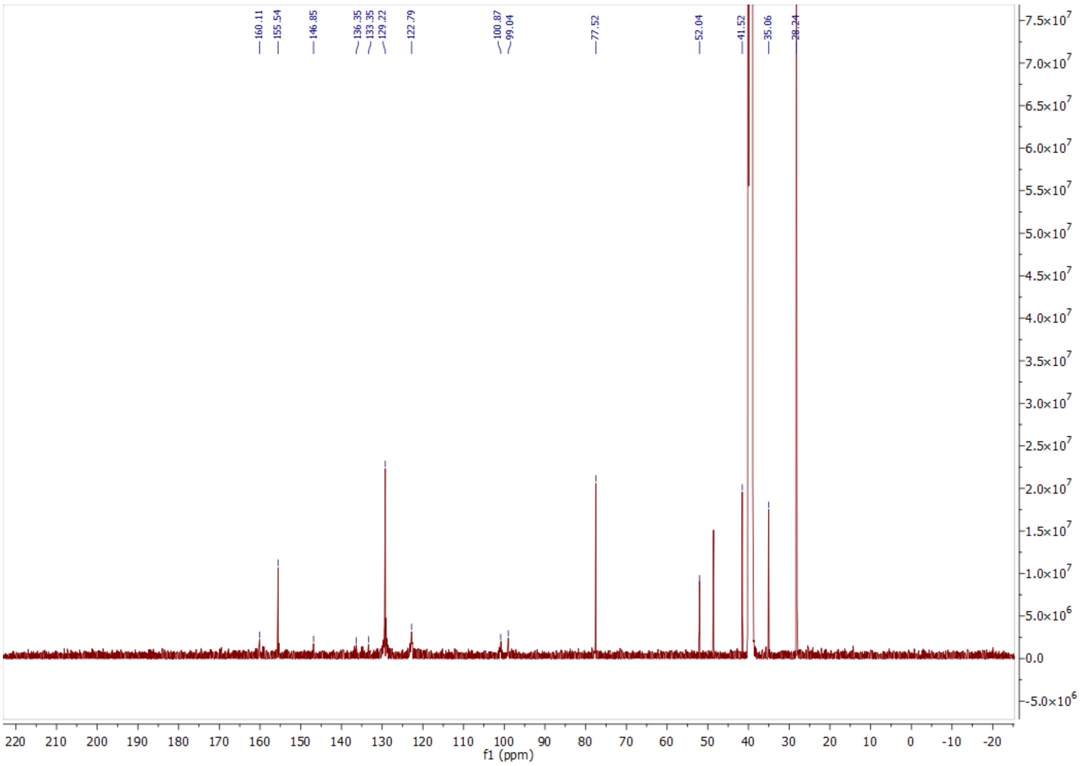

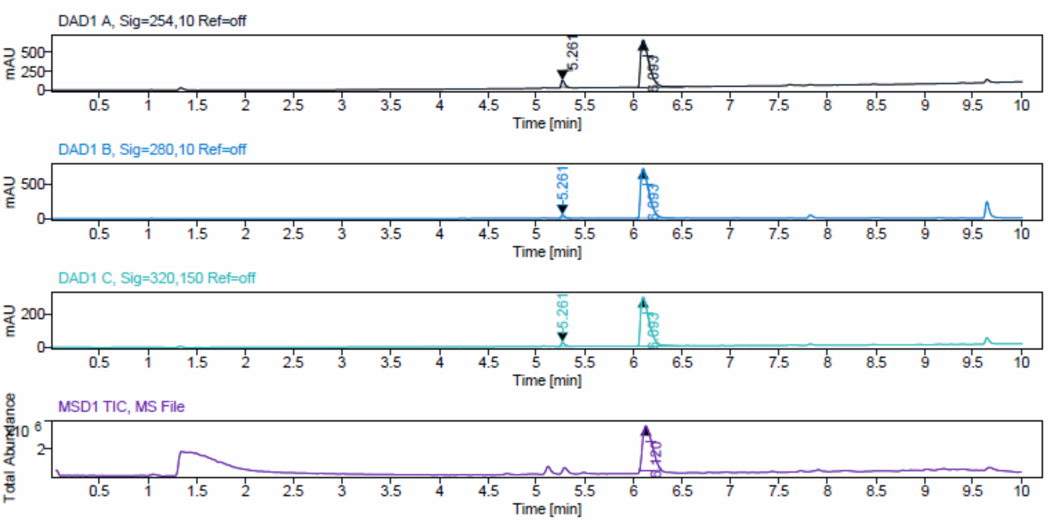

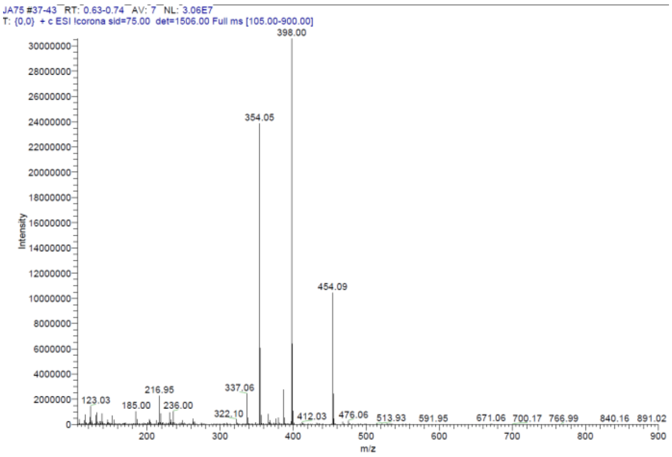

^{1}H, ^{13}C NMR, HPLC, and ESI data of compound **76b**

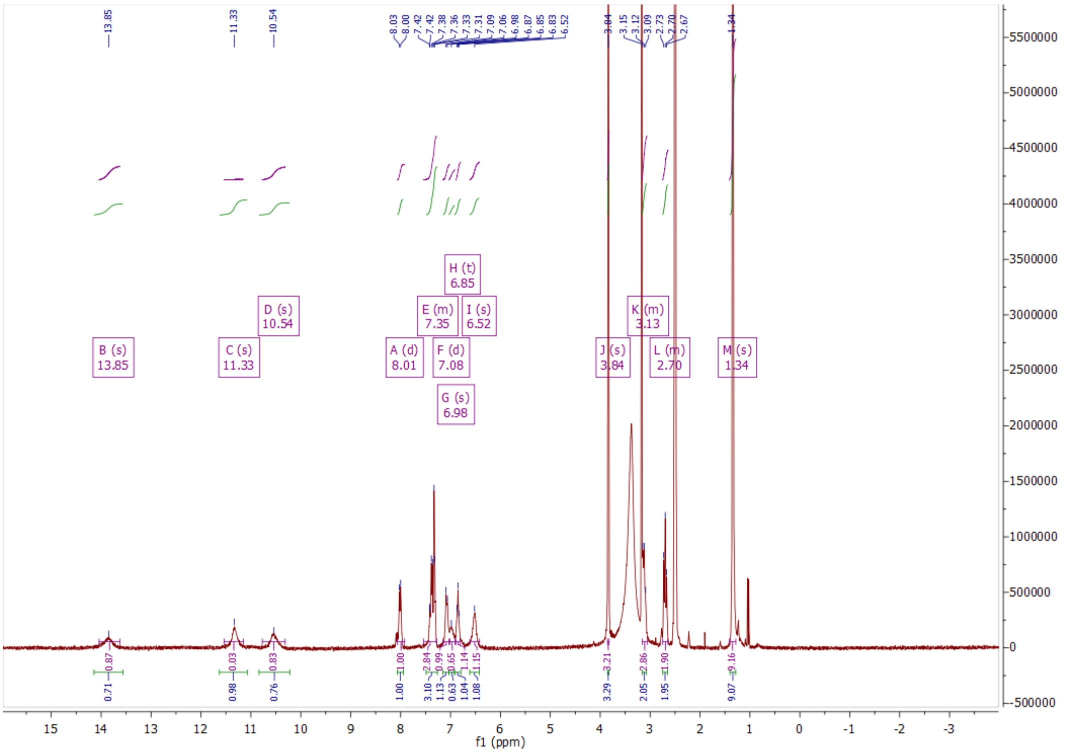

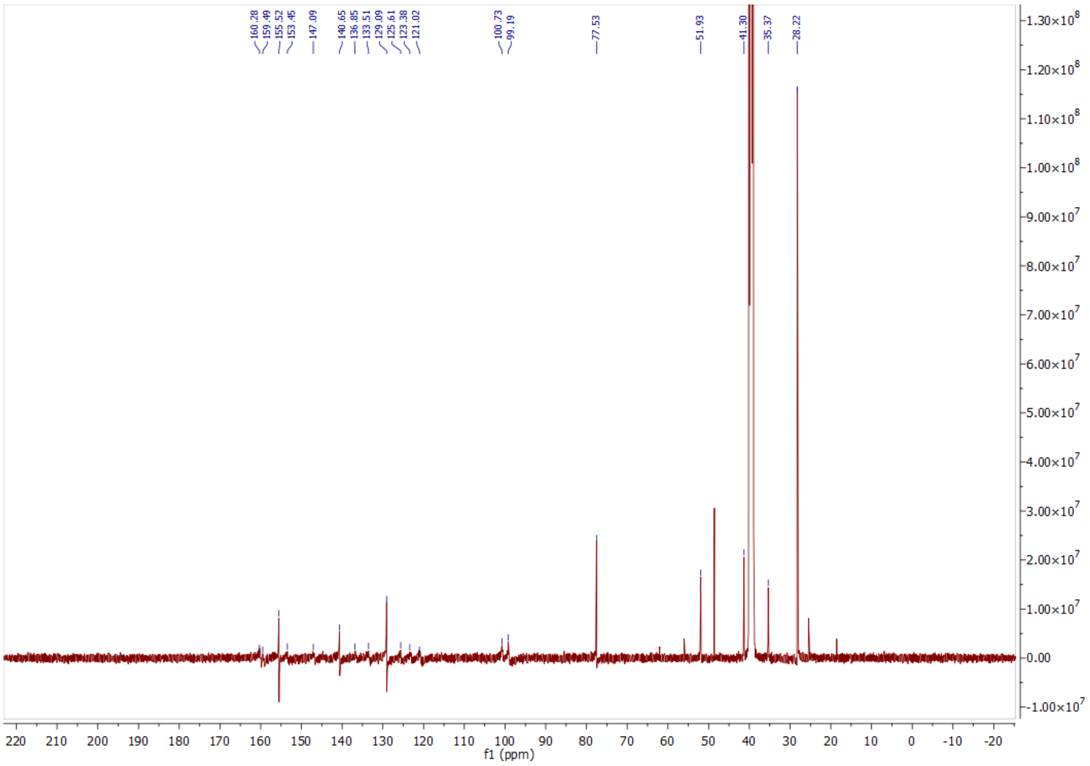
160.28
159.49
155.52
153.45
147.09
140.65
136.85
133.51
129.09
125.61
123.38
121.02
100.73
99.19
77.53
51.93
41.30
35.37
28.22
1.30×10^8
1.20×10^8
1.10×10^8
1.00×10^8
9.00×10^7
8.00×10^7
7.00×10^7
6.00×10^7
5.00×10^7
4.00×10^7
3.00×10^7
2.00×10^7
1.00×10^7
0.00
-1.00×10^7
220 210 200 190 180 170 160 150 140 130 120 110 100 90 80 70 60 50 40 30 20 10 0 -10 -20
f1 (ppm)

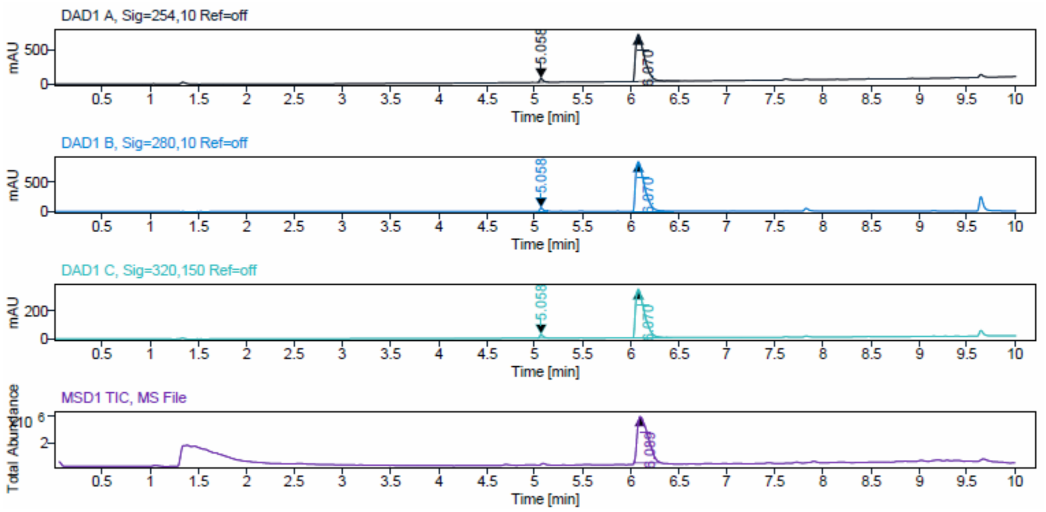
DAD1 A, Sig=254,10 Ref=off
mAU
500
0
5.058
Time [min]
DAD1 B, Sig=280,10 Ref=off
mAU
500
0
5.058
Time [min]
DAD1 C, Sig=320,150 Ref=off
mAU
200
0
5.058
Time [min]
MSD1 TIC, MS File
Total Abundance
x10 6
2
0.5 1 1.5 2 2.5 3 3.5 4 4.5 5 5.5 6 6.5 7 7.5 8 8.5 9 9.5 10
Time [min]

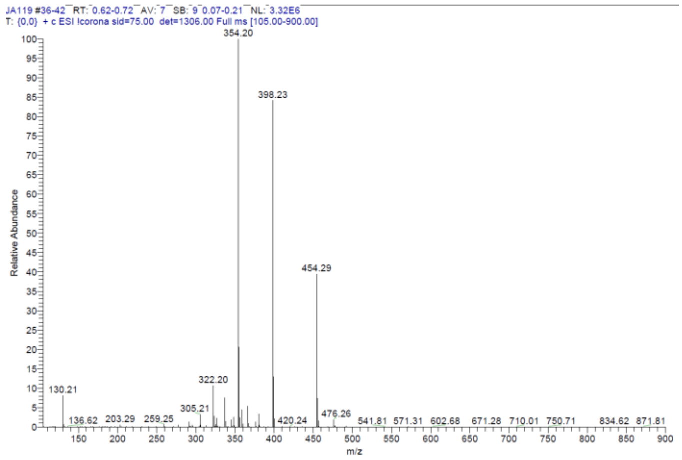
JA119 #36-42 RT: 0.62-0.72 AV: 7 SB: 9 0.07-0.21 NL: 3.32E6
T: {0,0} + c ESI Icorona sid=75.00 det=1306.00 Full ms [105.00-900.00]
354.20
398.23
454.29
322.20
130.21
305.21
136.62
203.29
259.25
420.24
476.26
541.81
571.31
602.68
671.28
710.01
750.71
834.62
871.81
Relative Abundance
m/z

^{1}H, ^{13}C NMR, HPLC, and ESI data of compound **76c**

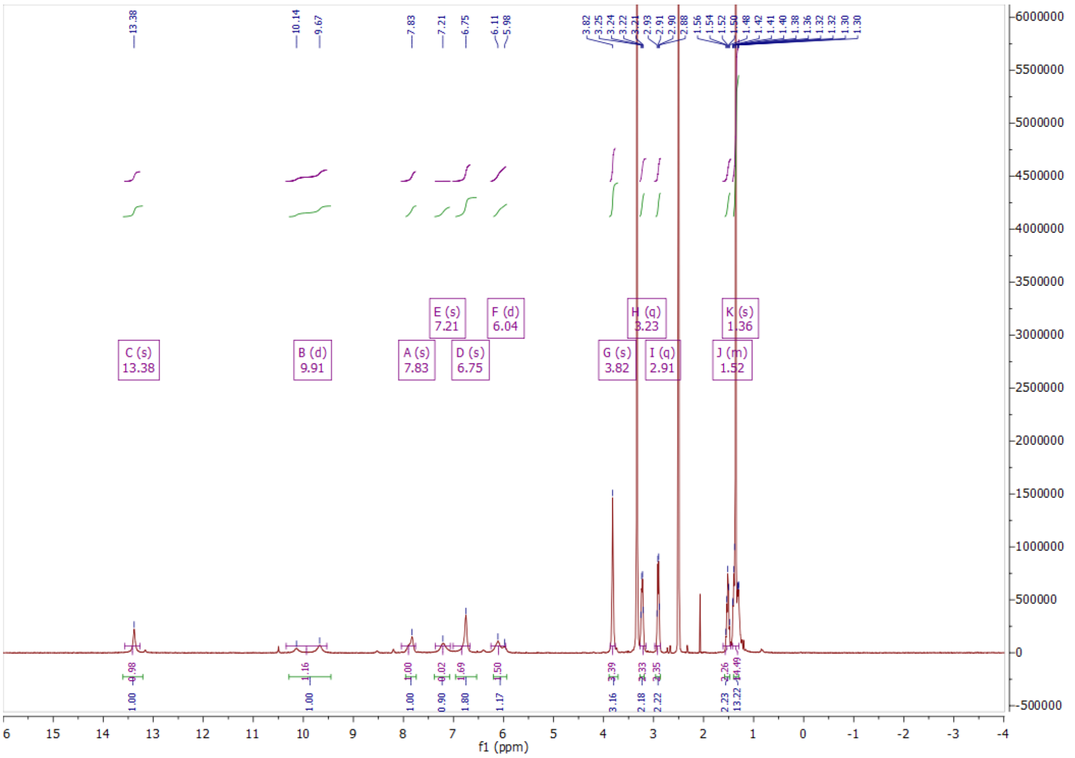

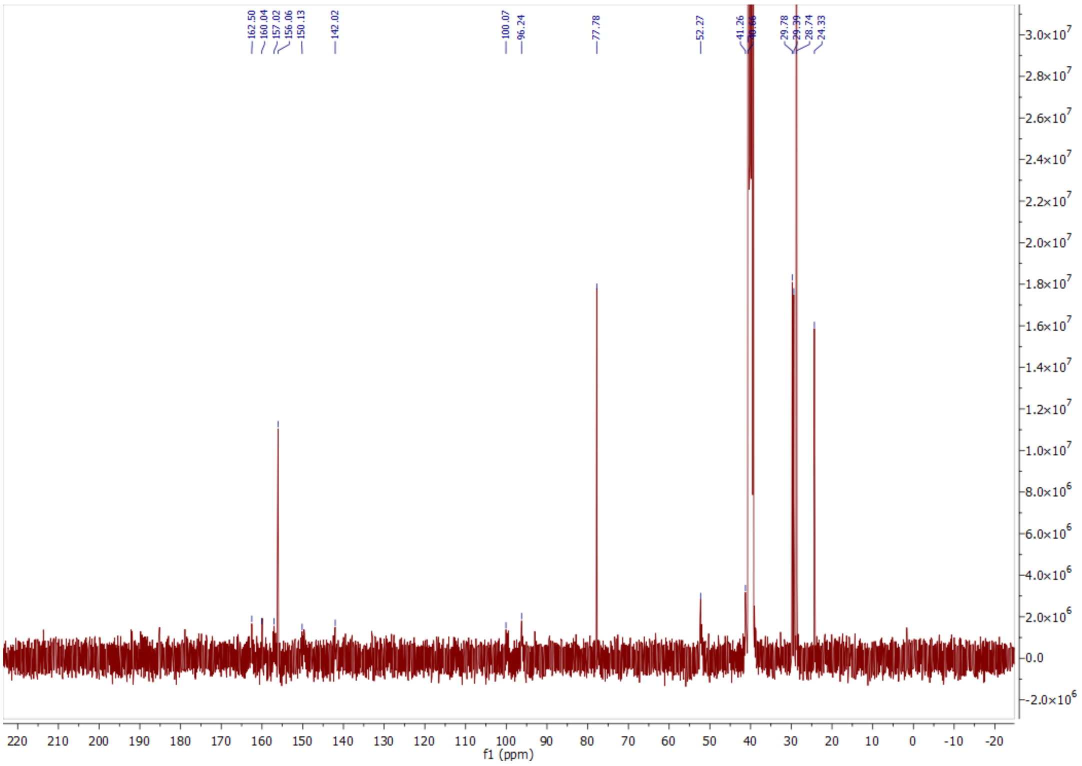

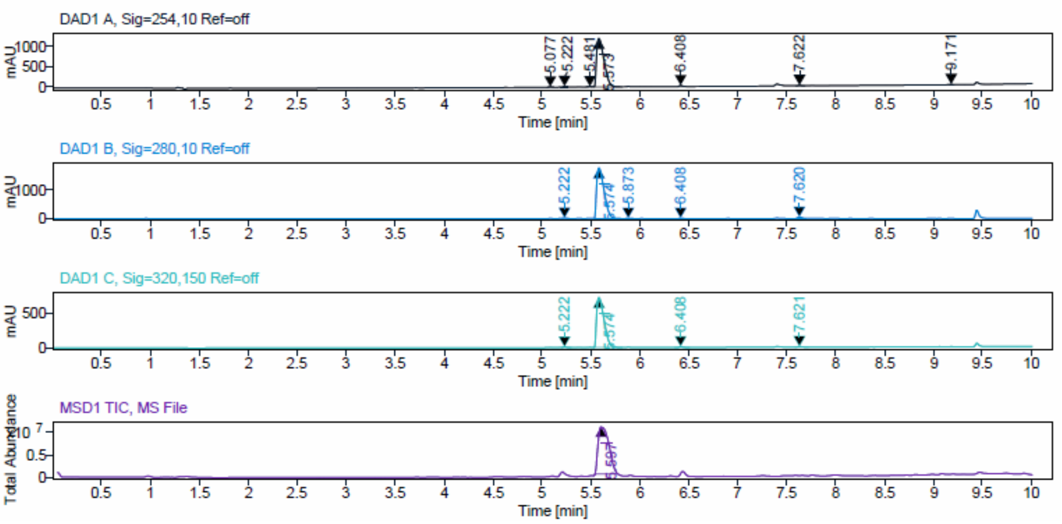

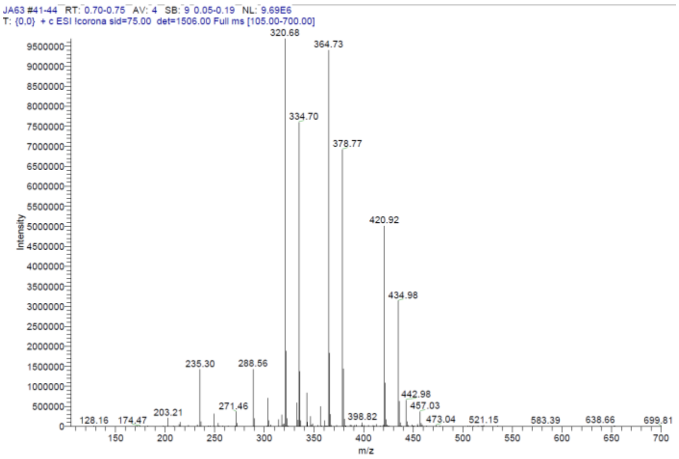

^1H, ^{13}C NMR, HPLC, and ESI data of compound **76d**

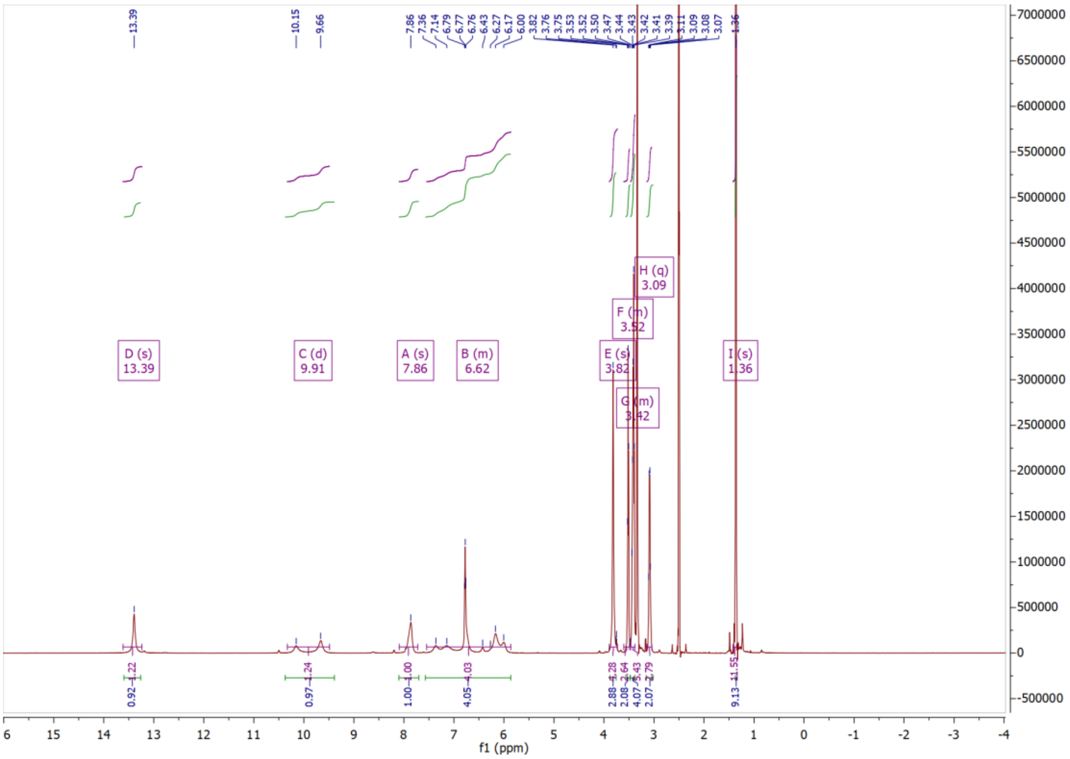

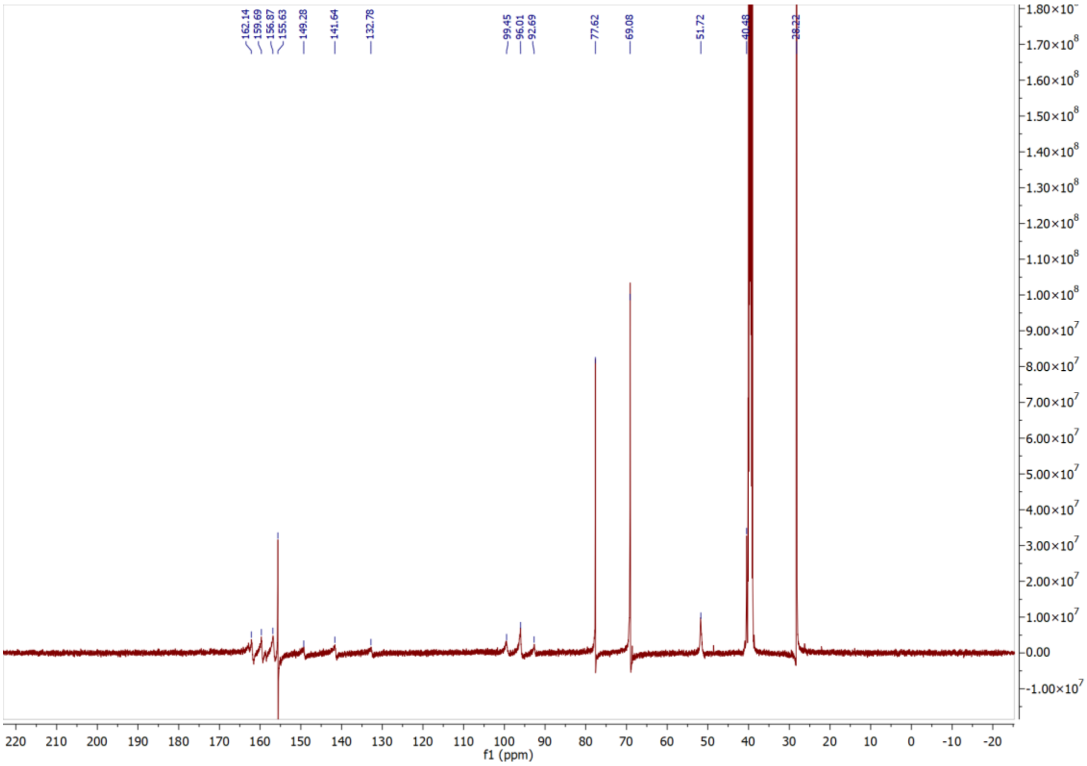
162.14
159.69
156.87
155.63
149.28
141.64
132.78
99.45
96.01
92.69
77.62
69.08
51.72
40.48
28.22
1.80×10
1.70×10^8
1.60×10^8
1.50×10^8
1.40×10^8
1.30×10^8
1.20×10^8
1.10×10^8
1.00×10^8
9.00×10^7
8.00×10^7
7.00×10^7
6.00×10^7
5.00×10^7
4.00×10^7
3.00×10^7
2.00×10^7
1.00×10^7
0.00
-1.00×10^7
220 210 200 190 180 170 160 150 140 130 120 110 100 90 80 70 60 50 40 30 20 10 0 -10 -20
f1 (ppm)

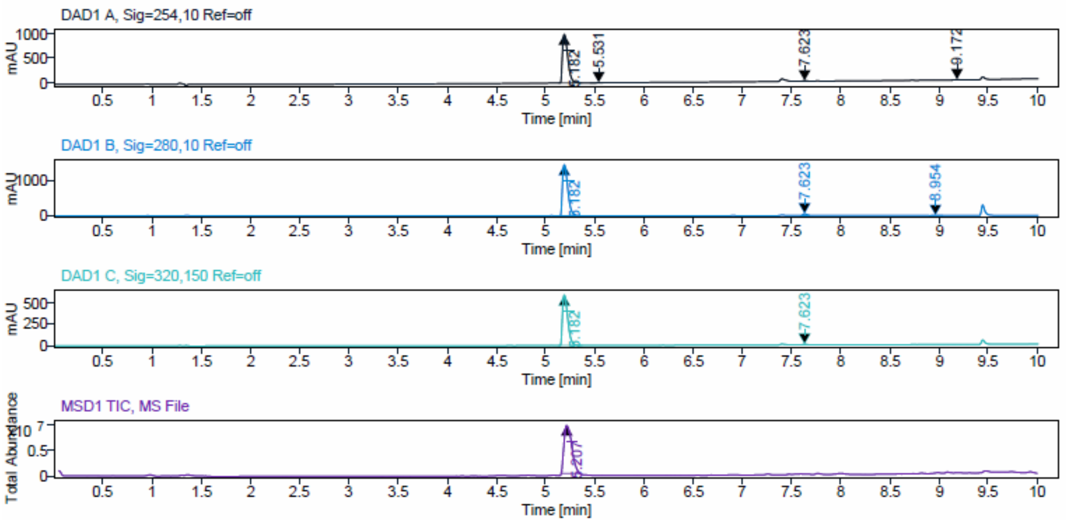
DAD1 A, Sig=254,10 Ref=off
mAU
1000
500
0
5.182
5.531
7.623
9.172
Time [min]
DAD1 B, Sig=280,10 Ref=off
mAU
1000
0
5.182
7.623
8.954
Time [min]
DAD1 C, Sig=320,150 Ref=off
mAU
500
250
0
5.182
7.623
Time [min]
MSD1 TIC, MS File
Total Abundance
10 7
0.5
0
5.207
Time [min]
0.5 1 1.5 2 2.5 3 3.5 4 4.5 5 5.5 6 6.5 7 7.5 8 8.5 9 9.5 10

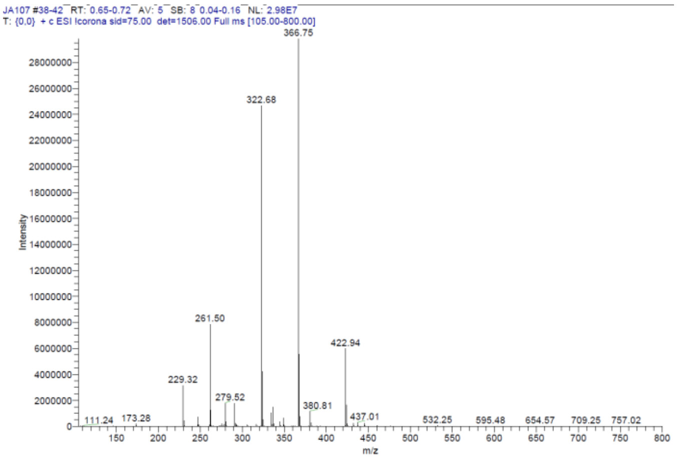
JA107 #38-42 RT: 0.65-0.72 AV: 5 SB: 8 0.04-0.16 NL: 2.98E7
T: {0,0} + c ESI !corona sid=75.00 det=1506.00 Full ms [105.00-800.00]
366.75
322.68
261.50
422.94
229.32
279.52
380.81
437.01
111.24
173.28
532.25
595.48
654.57
709.25
757.02
Intensity
28000000
26000000
24000000
22000000
20000000
18000000
16000000
14000000
12000000
10000000
8000000
6000000
4000000
2000000
0
150 200 250 300 350 400 450 500 550 600 650 700 750 800
m/z

ESI, HRMS, ^{1}H, ^{13}C NMR and HPLC data of compound **76e**

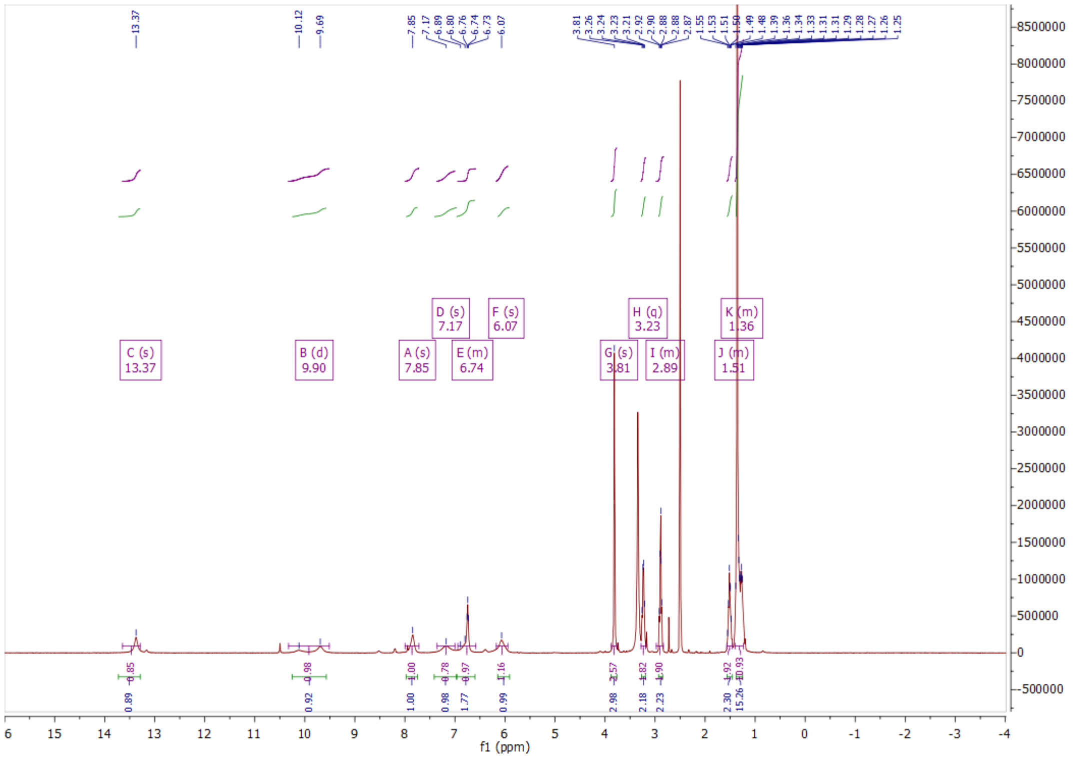

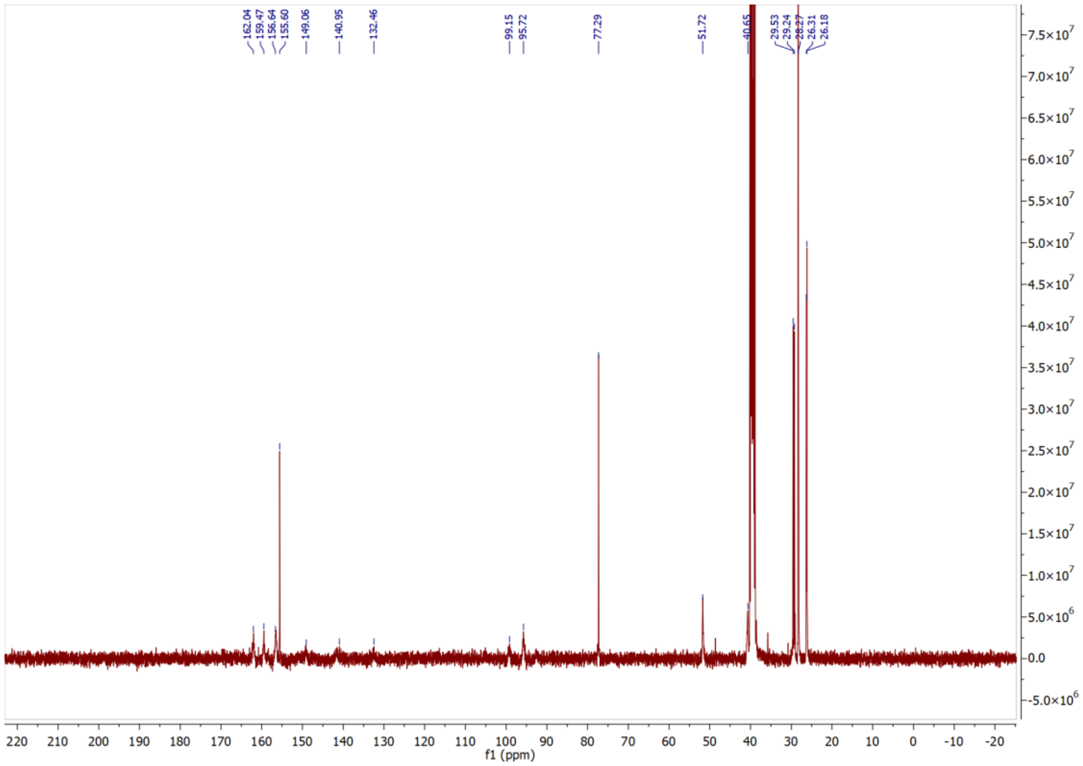

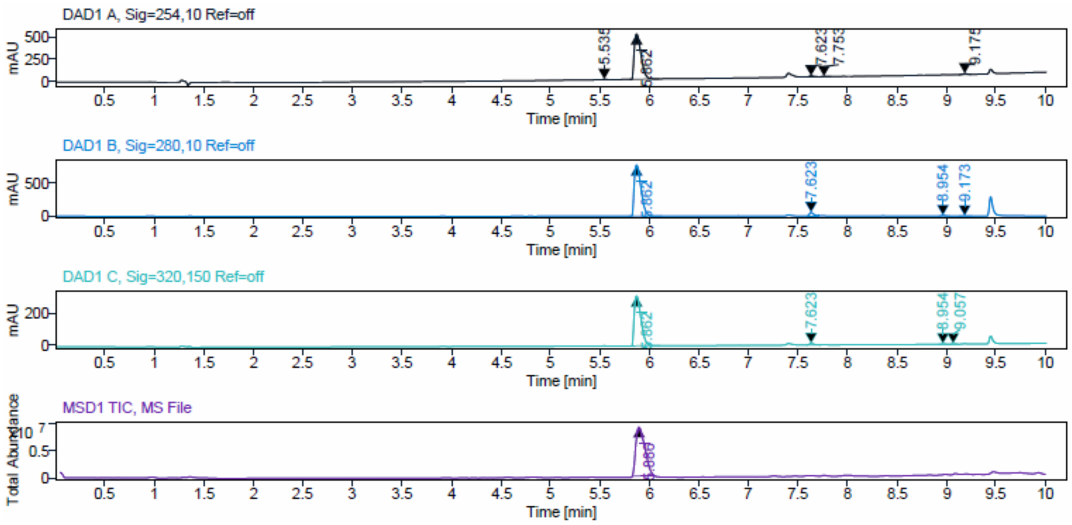

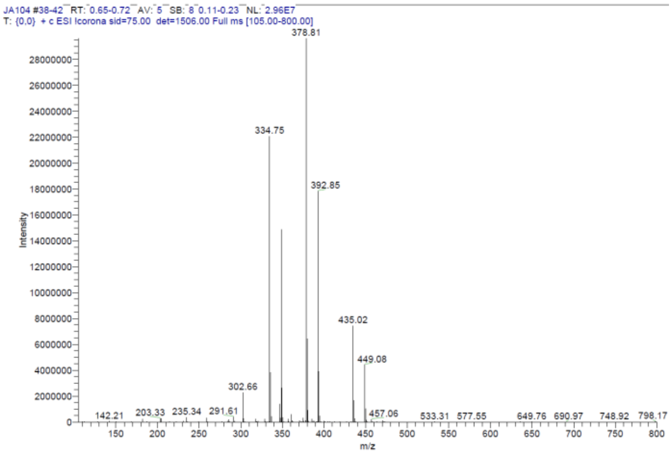

^{1}H, ^{13}C NMR, HPLC, and ESI data of compound **76f**

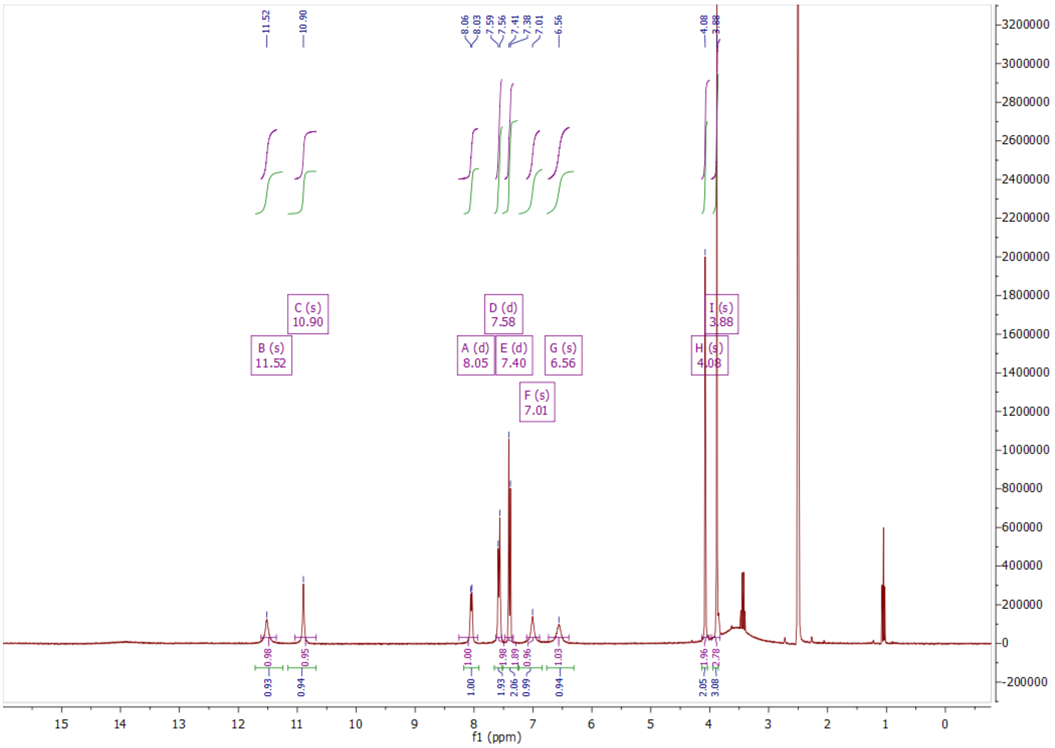

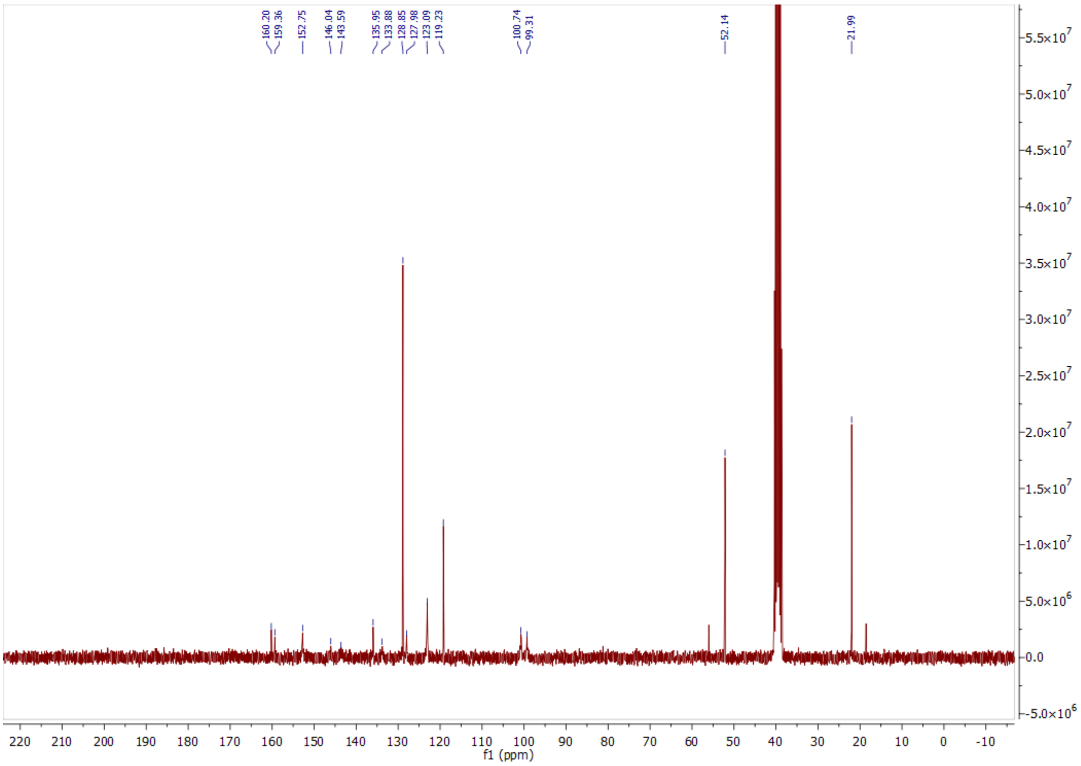
160.20
159.36
152.75
146.04
143.59
135.95
133.88
128.85
127.98
123.09
119.23
100.74
99.31
52.14
21.99
5.5×10⁷
5.0×10⁷
4.5×10⁷
4.0×10⁷
3.5×10⁷
3.0×10⁷
2.5×10⁷
2.0×10⁷
1.5×10⁷
1.0×10⁷
5.0×10⁶
0.0
-5.0×10⁶
220 210 200 190 180 170 160 150 140 130 120 110 100 90 80 70 60 50 40 30 20 10 0 -10
f1 (ppm)

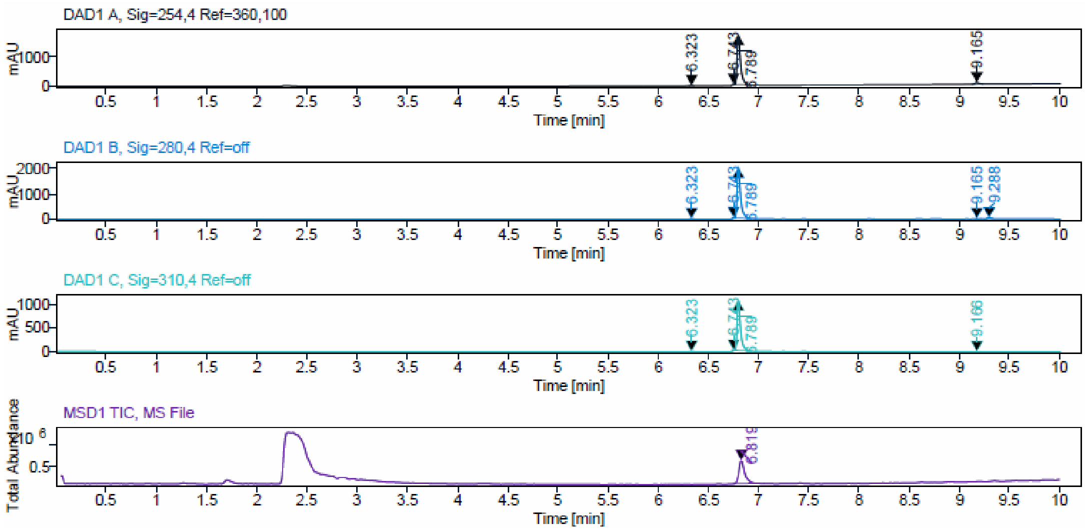
DAD1 A, Sig=254,4 Ref=360,100
mAU
1000
0
6.323
6.743
6.789
9.165
0.5 1 1.5 2 2.5 3 3.5 4 4.5 5 5.5 6 6.5 7 7.5 8 8.5 9 9.5 10
Time [min]
DAD1 B, Sig=280,4 Ref=off
mAU
2000
1000
0
6.323
6.743
6.789
9.165
9.288
0.5 1 1.5 2 2.5 3 3.5 4 4.5 5 5.5 6 6.5 7 7.5 8 8.5 9 9.5 10
Time [min]
DAD1 C, Sig=310,4 Ref=off
mAU
1000
500
0
6.323
6.743
6.789
9.166
0.5 1 1.5 2 2.5 3 3.5 4 4.5 5 5.5 6 6.5 7 7.5 8 8.5 9 9.5 10
Time [min]
MSD1 TIC, MS File
Total Abundance
x10 6
0.5
6.819
0.5 1 1.5 2 2.5 3 3.5 4 4.5 5 5.5 6 6.5 7 7.5 8 8.5 9 9.5 10
Time [min]

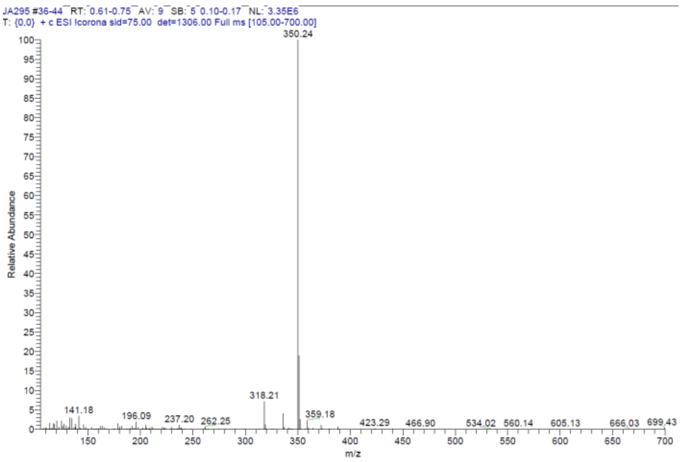
JA295 #36-44 RT: 0.61-0.75 AV: 9 SB: 5 0.10-0.17 NL: 3.35E6
T: {0,0} + c ESI !corona sid=75.00 det=1306.00 Full ms [105.00-700.00]
350.24
318.21
141.18
196.09
237.20
262.25
359.18
423.29
466.90
534.02
560.14
605.13
666.03
699.43
Relative Abundance
100 95 90 85 80 75 70 65 60 55 50 45 40 35 30 25 20 15 10 5 0
150 200 250 300 350 400 450 500 550 600 650 700
m/z

^{1}H, ^{13}C NMR, HPLC, and ESI data of compound **76g**

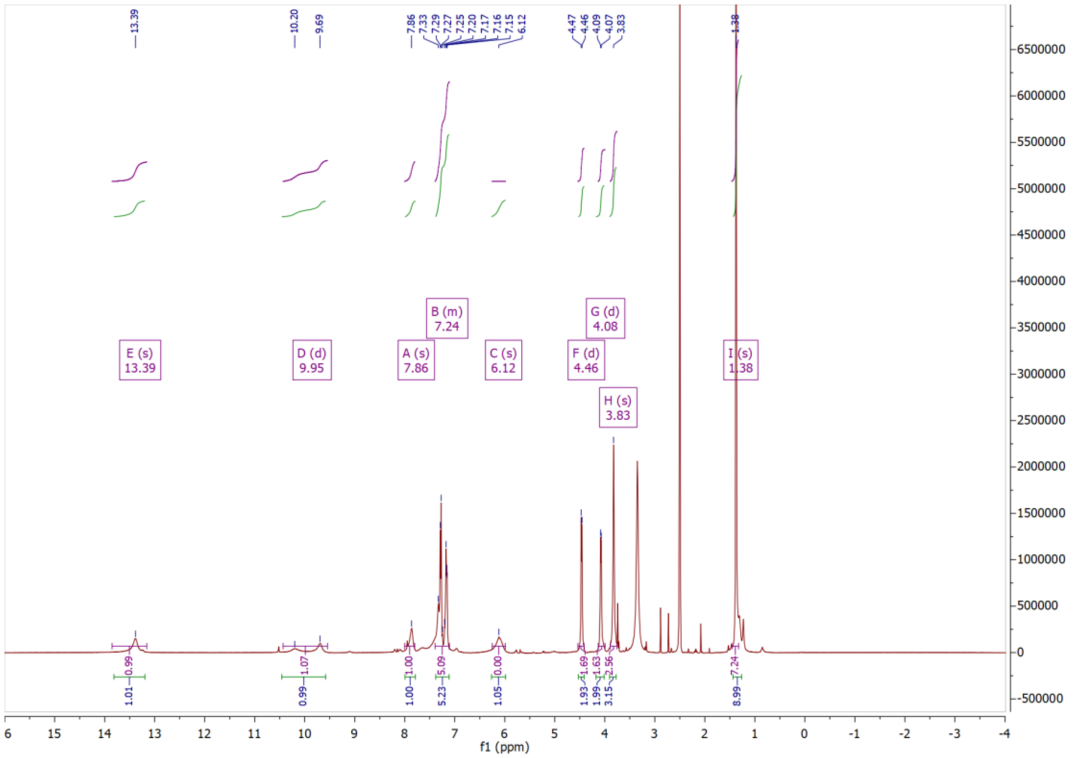

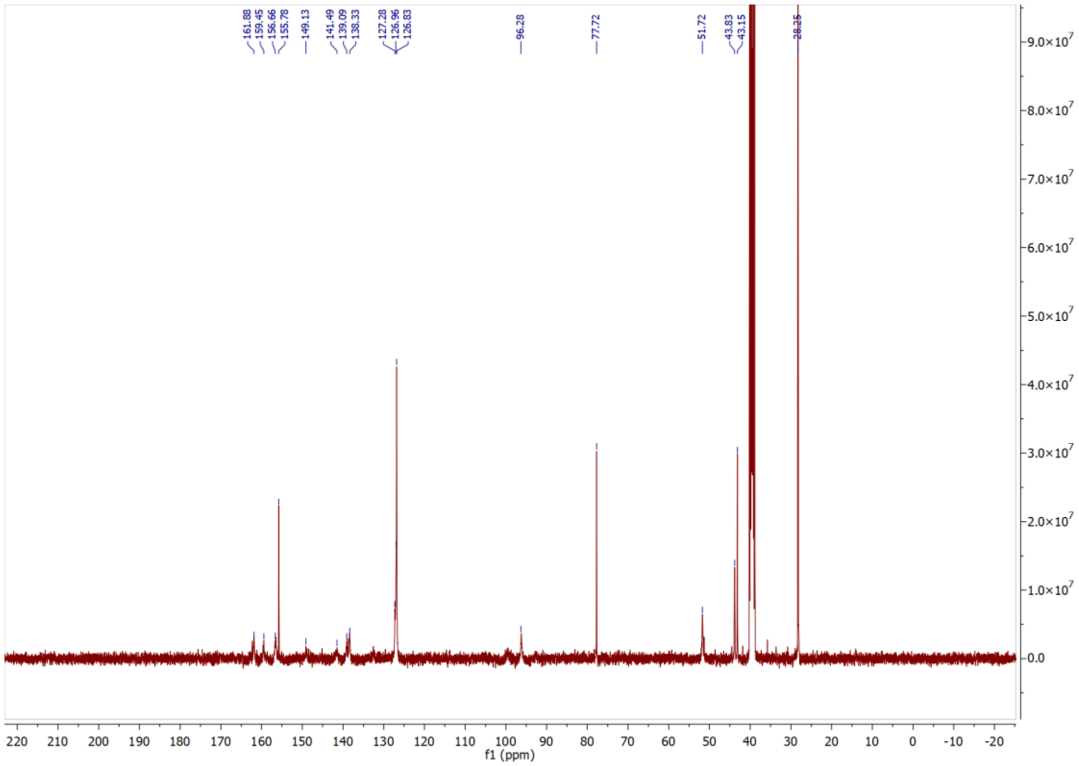

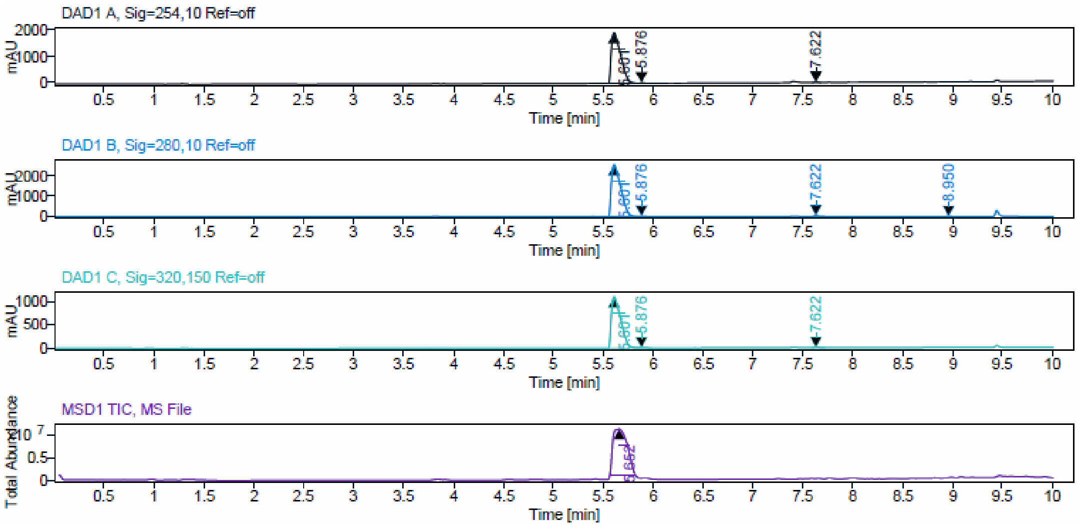

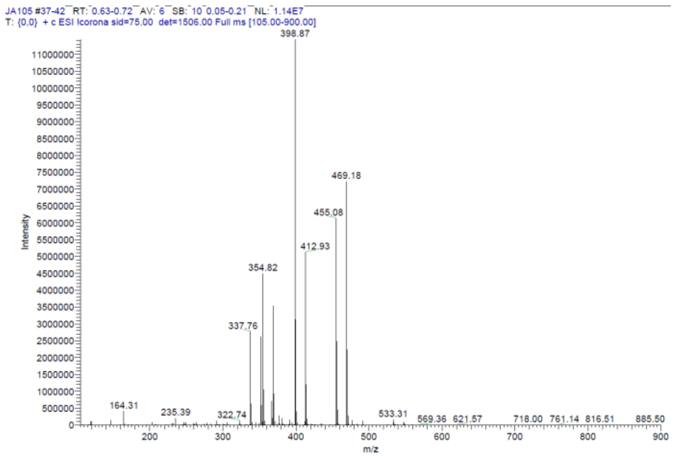

^{1}H, ^{13}C NMR, HPLC, and ESI data of compound **76h**

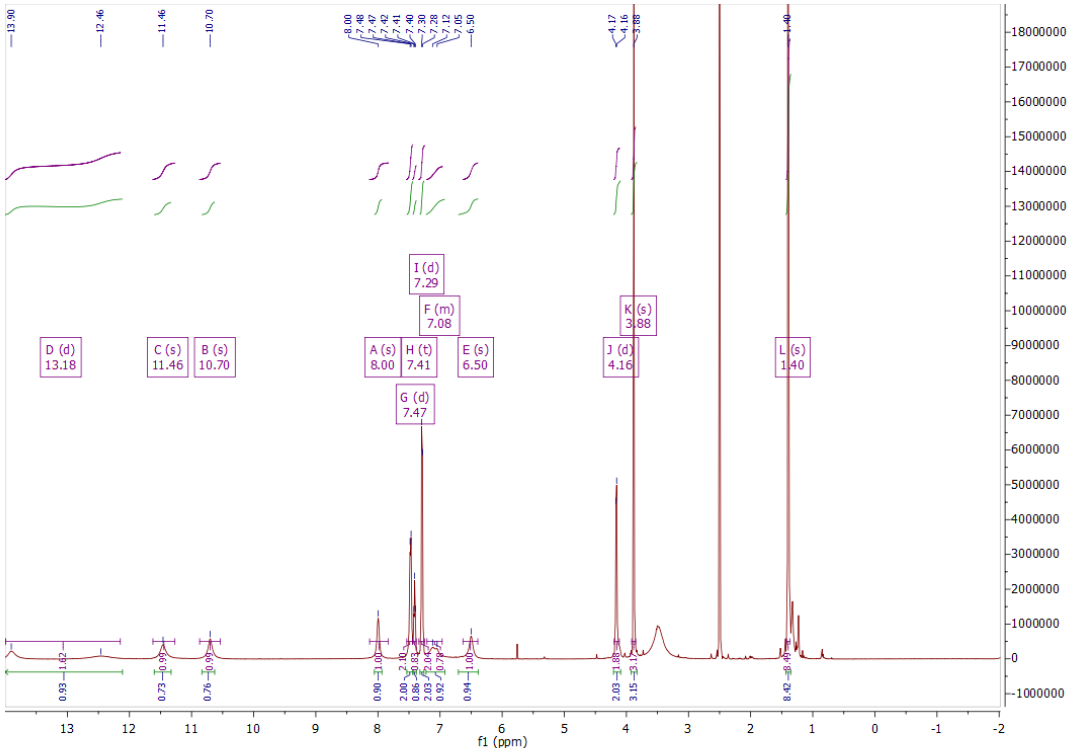

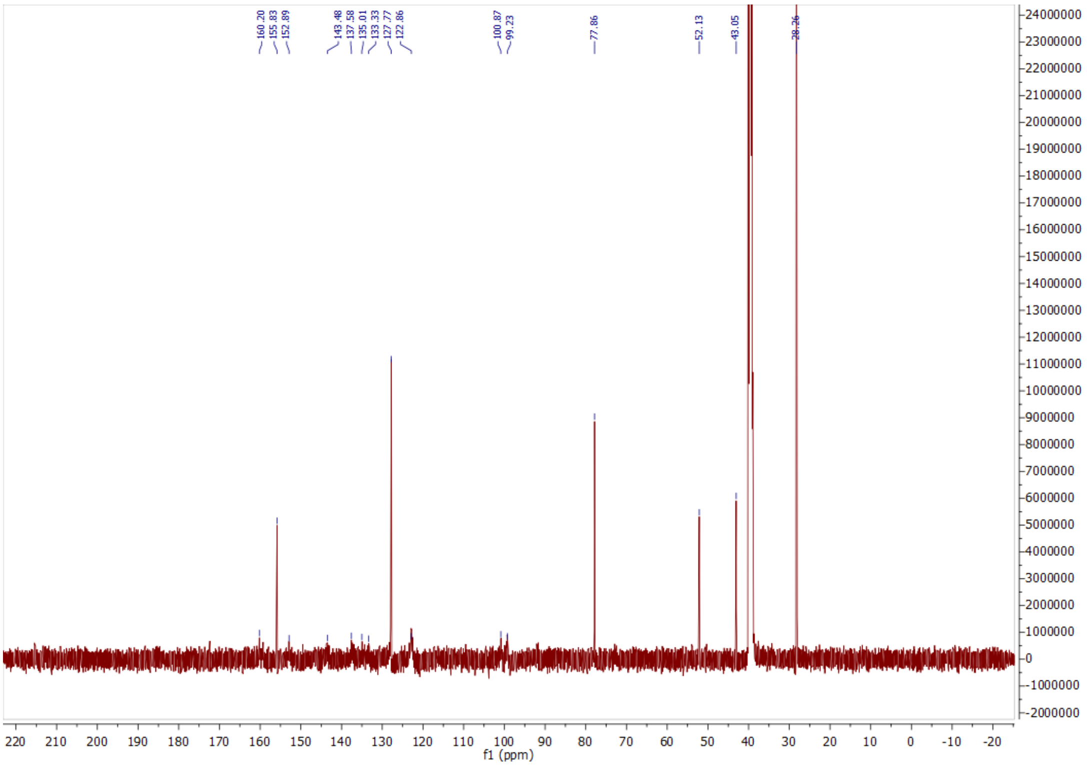
160.20
155.83
152.89
143.48
137.58
135.01
133.33
127.77
122.86
100.87
99.23
77.86
52.13
43.05
28.26
24000000
23000000
22000000
21000000
20000000
19000000
18000000
17000000
16000000
15000000
14000000
13000000
12000000
11000000
10000000
9000000
8000000
7000000
6000000
5000000
4000000
3000000
2000000
1000000
0
-1000000
-2000000
220 210 200 190 180 170 160 150 140 130 120 110 100 90 80 70 60 50 40 30 20 10 0 -10 -20
f1 (ppm)

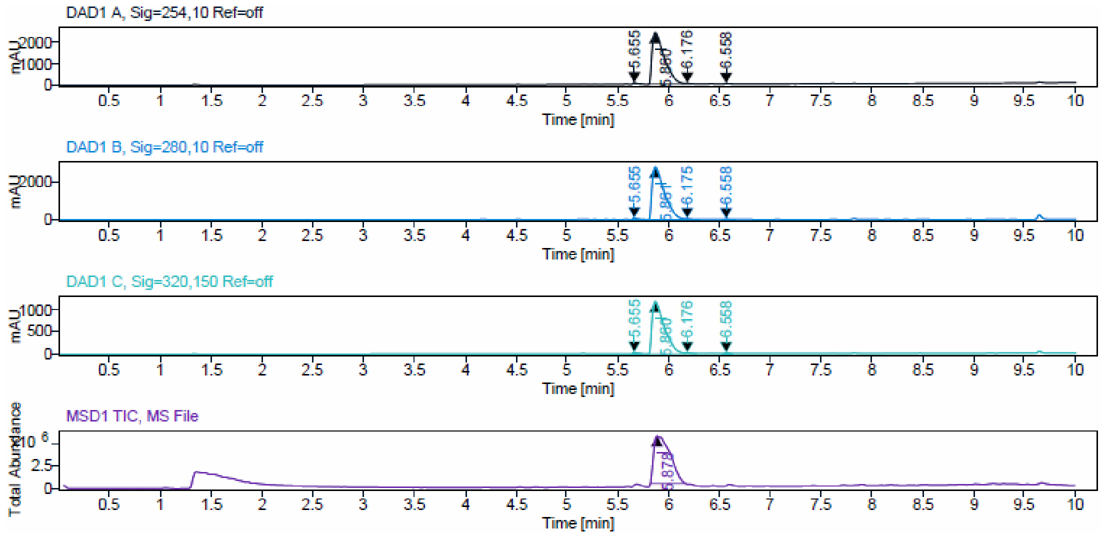
DAD1 A, Sig=254,10 Ref=off
mAU
2000
1000
0
5.655
5.860
6.176
6.558
0.5 1 1.5 2 2.5 3 3.5 4 4.5 5 5.5 6 6.5 7 7.5 8 8.5 9 9.5 10
Time [min]
DAD1 B, Sig=280,10 Ref=off
mAU
2000
0
5.655
5.861
6.175
6.558
Time [min]
DAD1 C, Sig=320,150 Ref=off
mAU
1000
500
0
5.655
5.860
6.176
6.558
Time [min]
MSD1 TIC, MS File
Total Abundance
x10 6
2.5
0
5.878
Time [min]

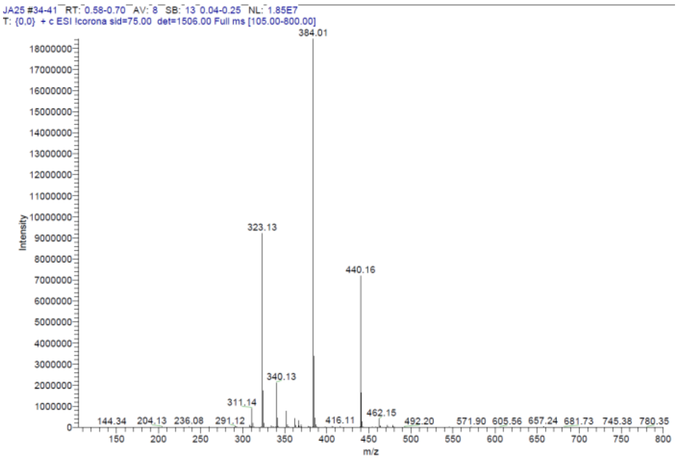
JA25 #34-41 RT: 0.58-0.70 AV: 8 SB: 13 0.04-0.25 NL: 1.85E7
T: {0,0} + c ESI !corona sid=75.00 det=1506.00 Full ms [105.00-800.00]
384.01
323.13
440.16
340.13
311.14
462.15
144.34
204.13
236.08
291.12
416.11
492.20
571.90
605.56
657.24
681.73
745.38
780.35
Intensity
18000000
17000000
16000000
15000000
14000000
13000000
12000000
11000000
10000000
9000000
8000000
7000000
6000000
5000000
4000000
3000000
2000000
1000000
0
150 200 250 300 350 400 450 500 550 600 650 700 750 800
m/z

^{1}H, ^{13}C NMR, HPLC, and ESI data of compound **76i**

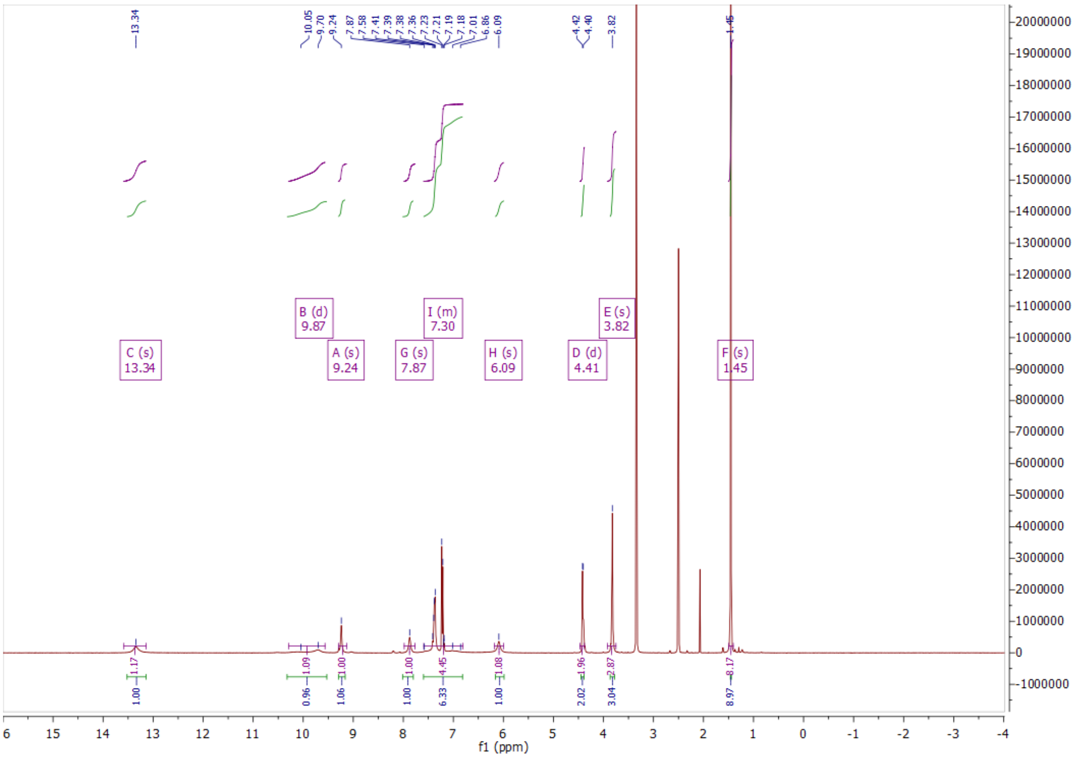

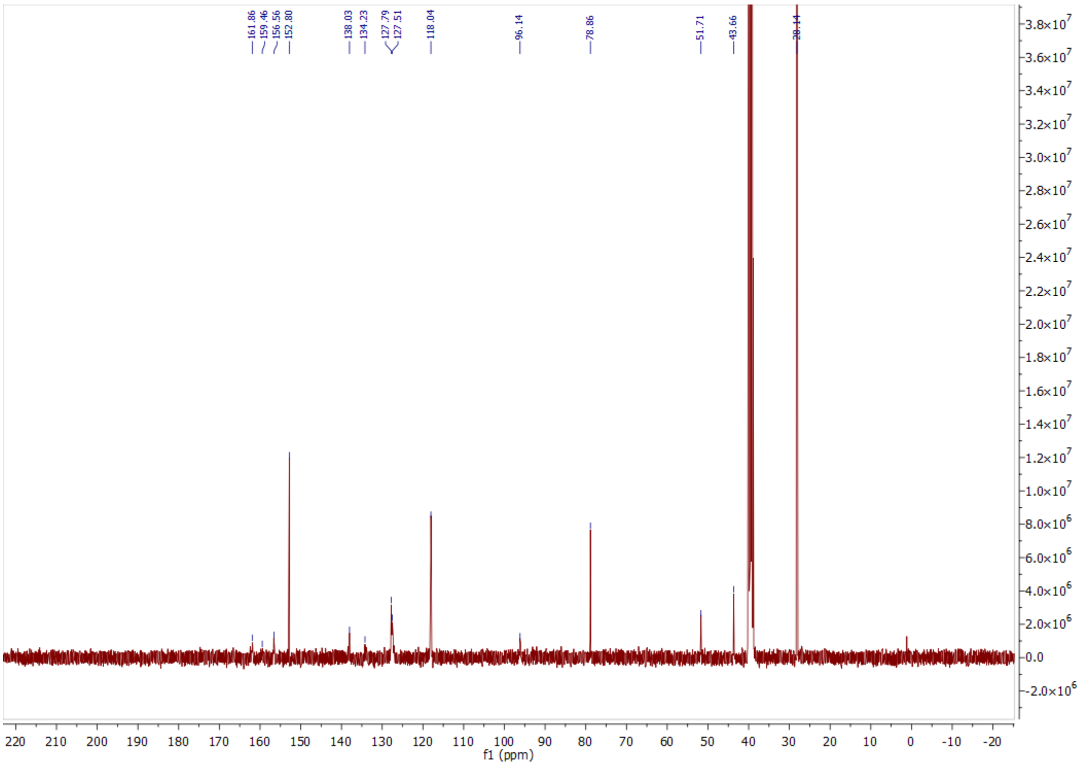

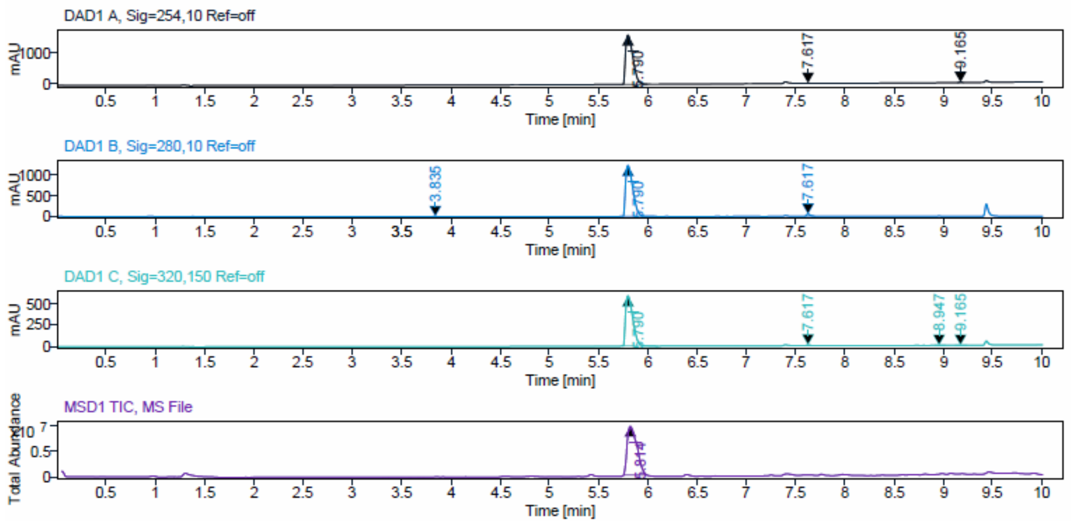

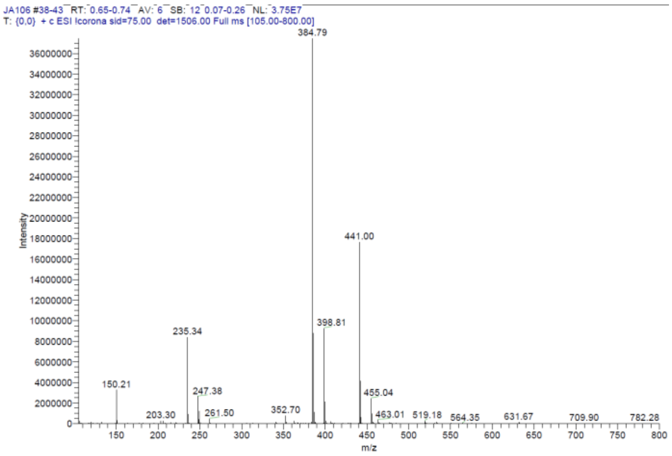

^{1}H, ^{13}C NMR, HPLC, and ESI data of compound **77a**

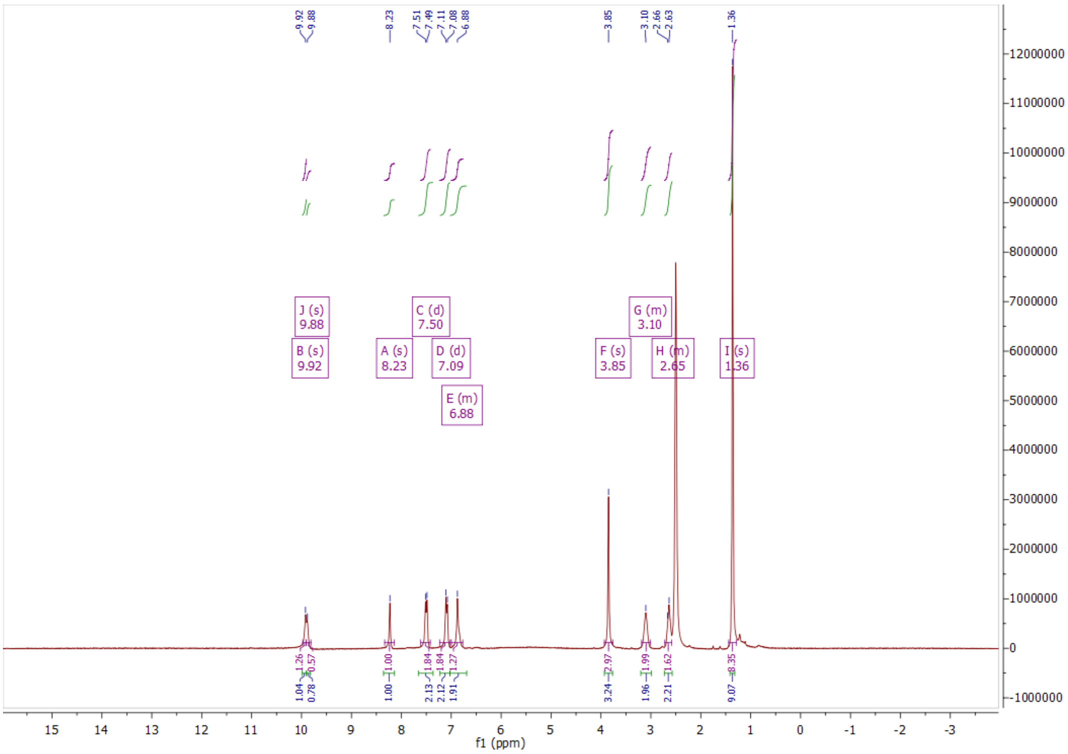

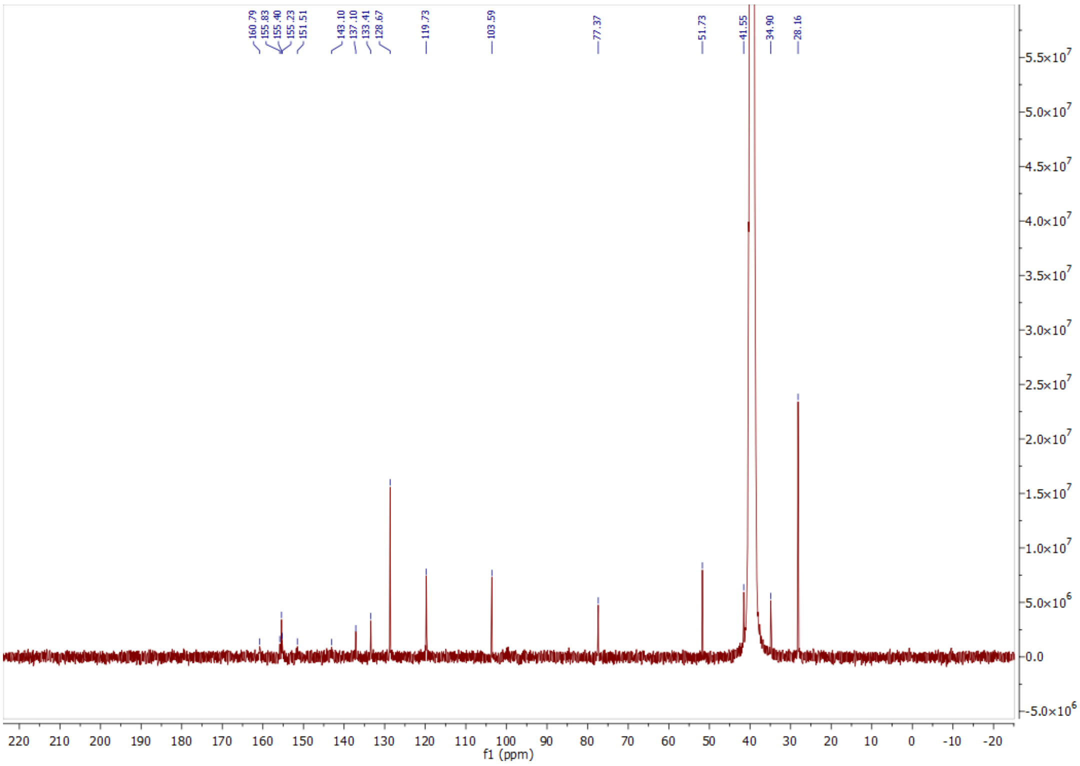
160.79
155.83
155.40
155.23
151.51
143.10
137.10
133.41
128.67
119.73
103.59
77.37
51.73
41.55
34.90
28.16
f1 (ppm)

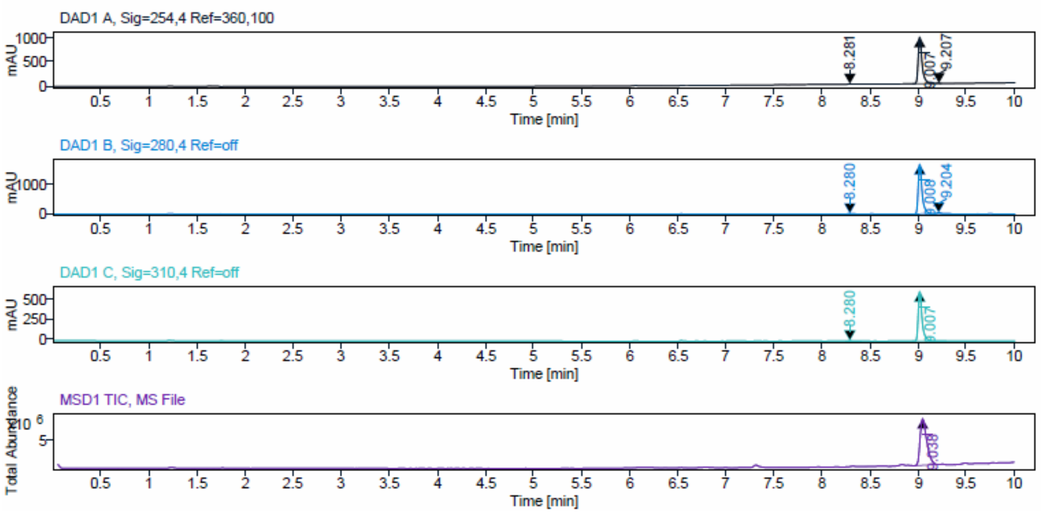
DAD1 A, Sig=254,4 Ref=360,100
DAD1 B, Sig=280,4 Ref=off
DAD1 C, Sig=310,4 Ref=off
MSD1 TIC, MS File
mAU
Total Abundance
Time [min]
8.281
9.007
9.207
8.280
9.008
9.204
9.007
9.038

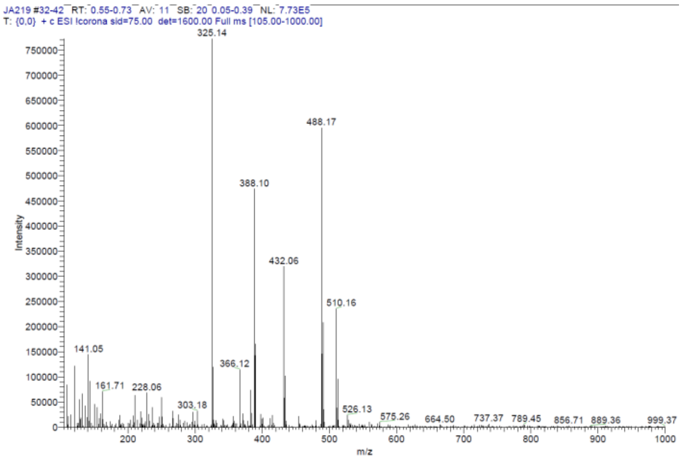
JA219 #32-42 RT: 0.55-0.73 AV: 11 SB: 20 0.05-0.39 NL: 7.73E5
T: {0,0} + c ESI Icorona sid=75.00 det=1600.00 Full ms [105.00-1000.00]
325.14
488.17
388.10
432.06
510.16
141.05
366.12
161.71
228.06
303.18
526.13
575.26
664.50
737.37
789.45
856.71
889.36
999.37
Intensity
m/z

^{1}H, ^{13}C NMR, HPLC, and ESI data of compound **77b**

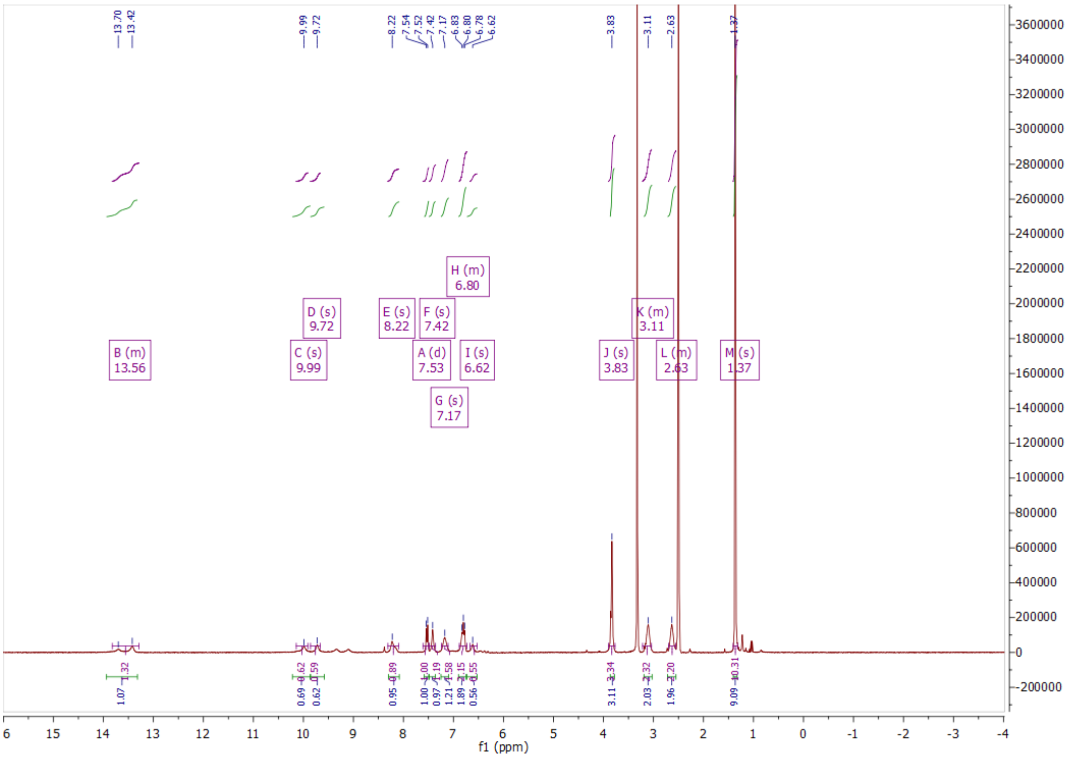

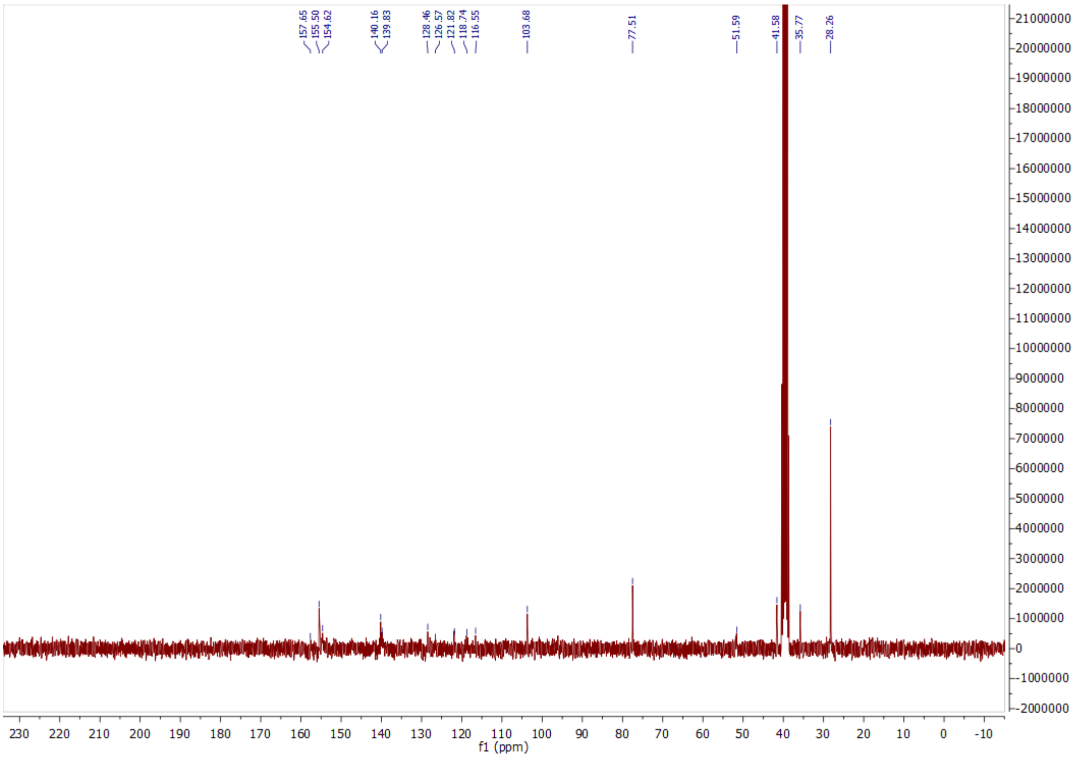

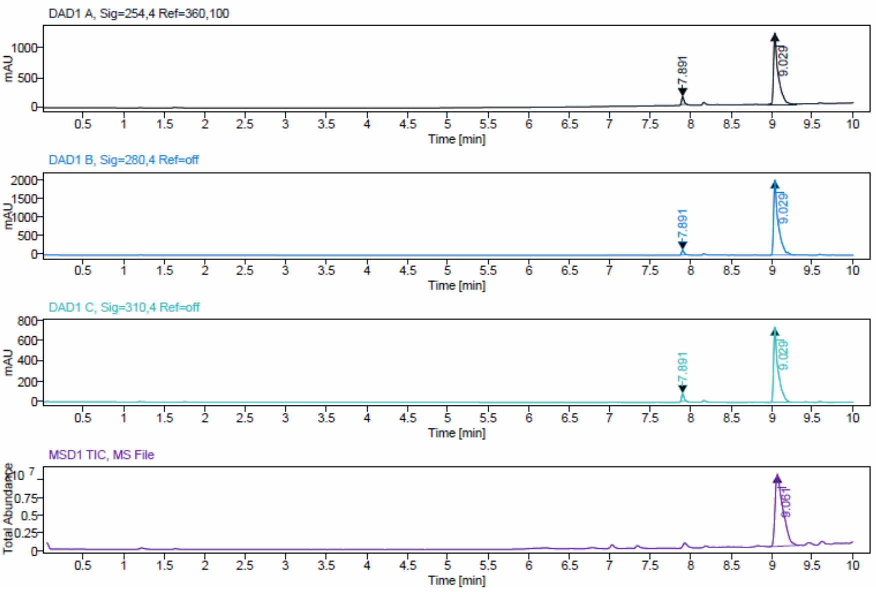
DAD1 A, Sig=254,4 Ref=360,100
mAU
1000
500
0
7.891
9.029
0.5
1
1.5
2
2.5
3
3.5
4
4.5
5
5.5
6
6.5
7
7.5
8
8.5
9
9.5
10
Time [min]
DAD1 B, Sig=280,4 Ref=off
mAU
2000
1500
1000
500
0
7.891
9.029
Time [min]
DAD1 C, Sig=310,4 Ref=off
mAU
800
600
400
200
0
7.891
9.029
Time [min]
MSD1 TIC, MS File
Total Abundance
x10 7
0.75
0.5
0.25
0
9.061
Time [min]

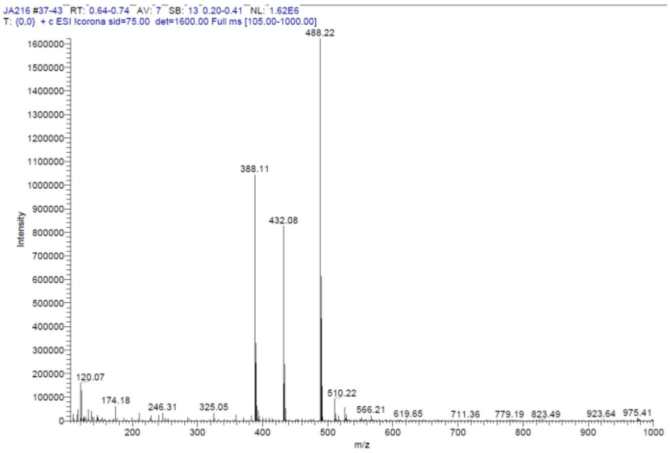
JA216 #37-43 RT: 0.64-0.74 AV: 7 SB: 13 0.20-0.41 NL: 1.62E6
T: {0,0} + c ESI !corona sid=75.00 det=1600.00 Full ms [105.00-1000.00]
Intensity
1600000
1500000
1400000
1300000
1200000
1100000
1000000
900000
800000
700000
600000
500000
400000
300000
200000
100000
0
488.22
388.11
432.08
120.07
174.18
246.31
325.05
510.22
566.21
619.65
711.36
779.19
823.49
923.64
975.41
200
300
400
500
600
700
800
900
1000
m/z

^{1}H, ^{13}C NMR, HPLC, and ESI data of compound **77c**

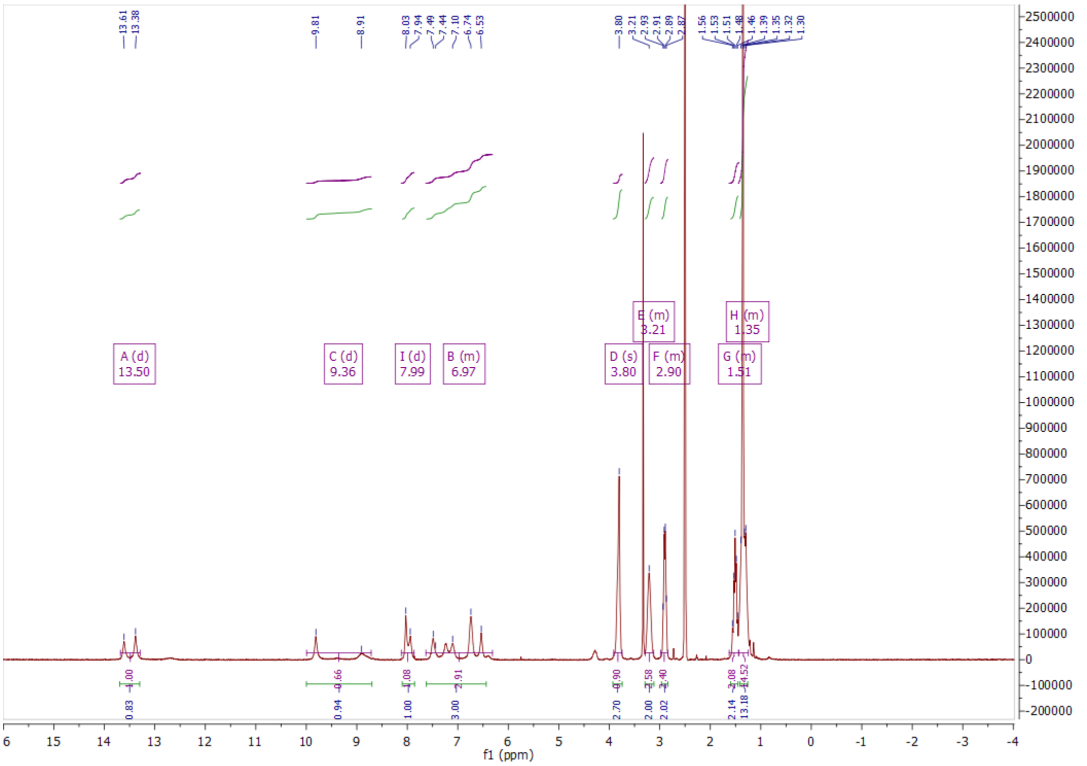

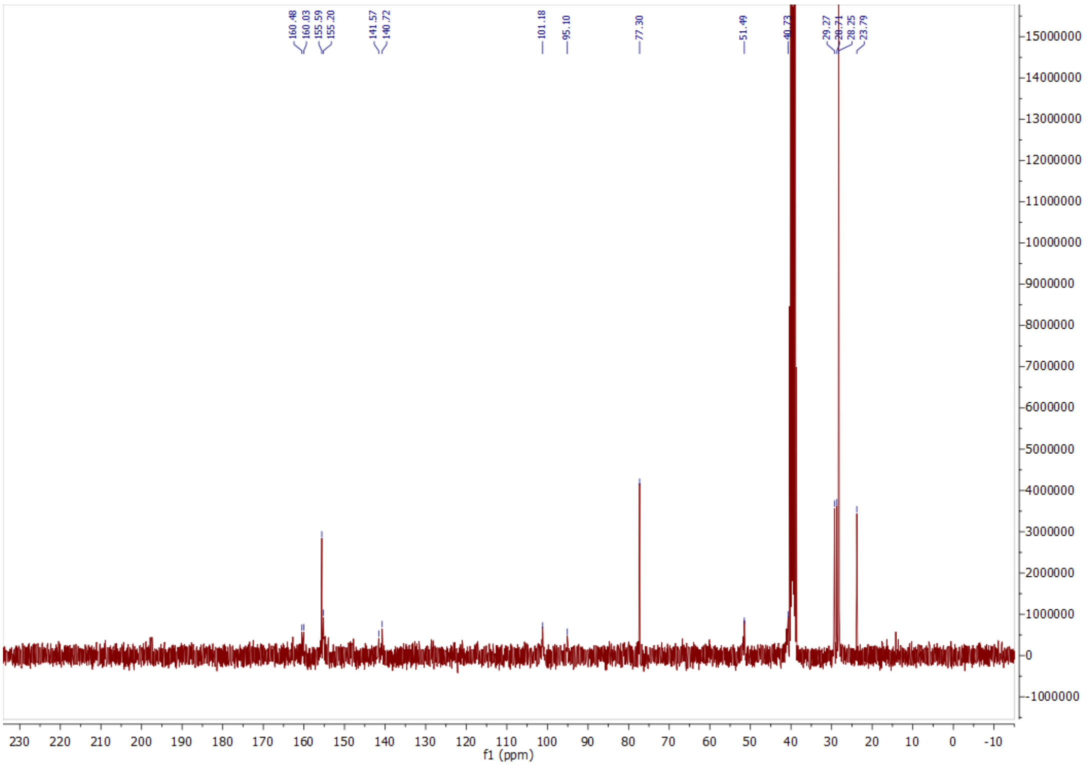

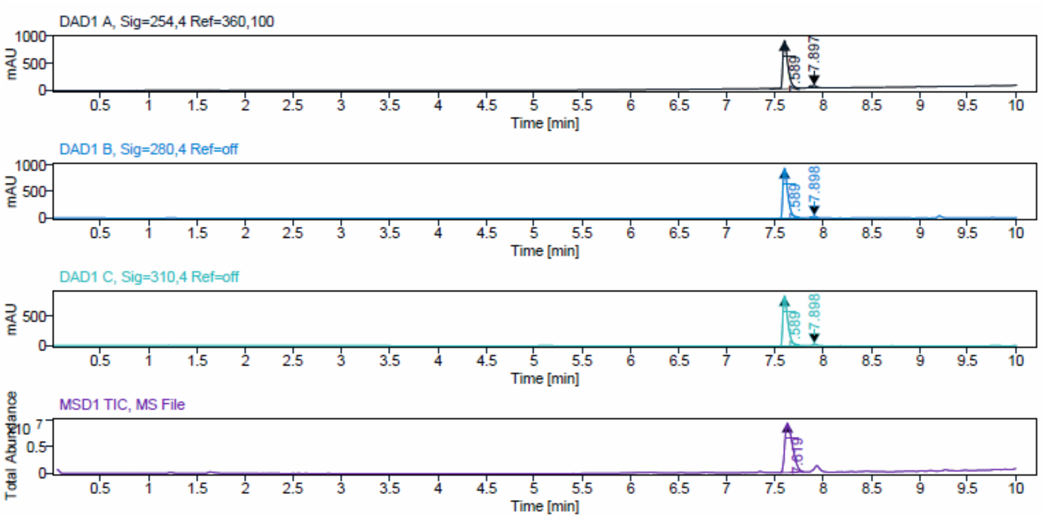

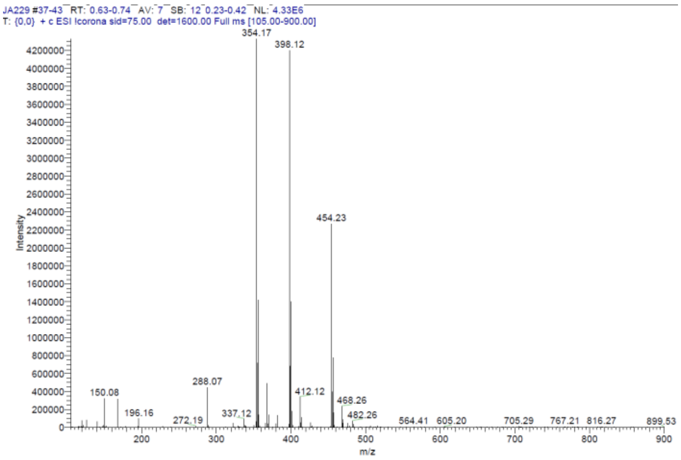

ESI, HRMS, ^{1}H, ^{13}C NMR and HPLC data of compound **77d**

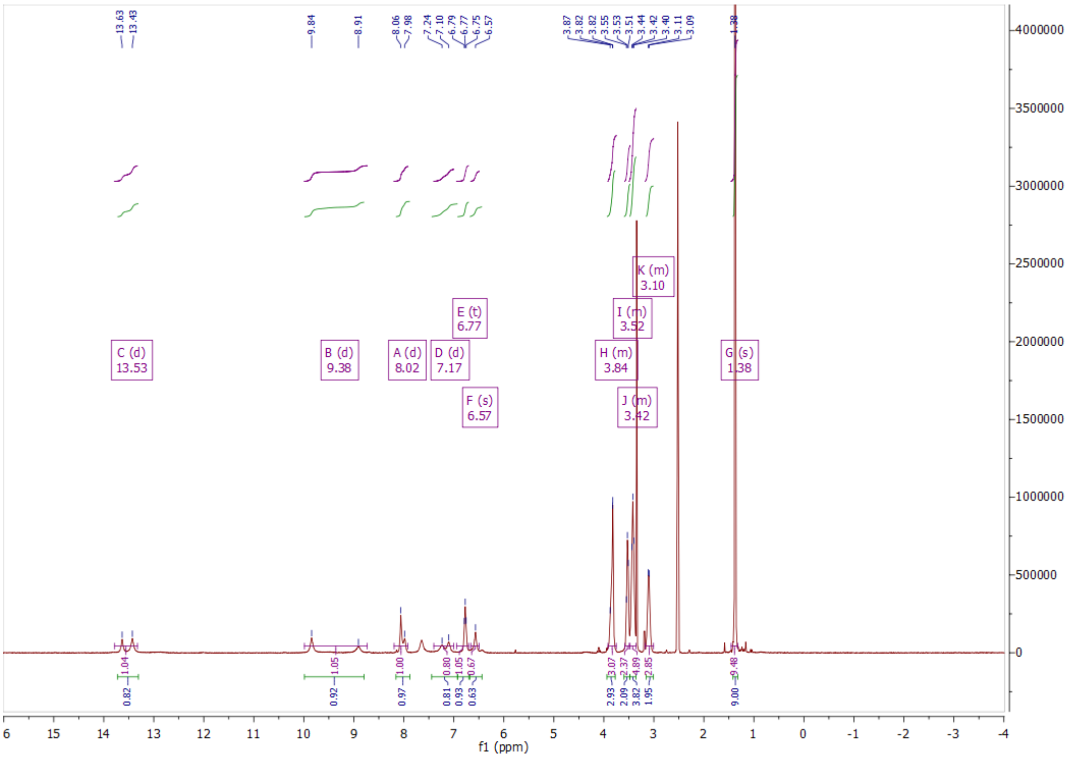

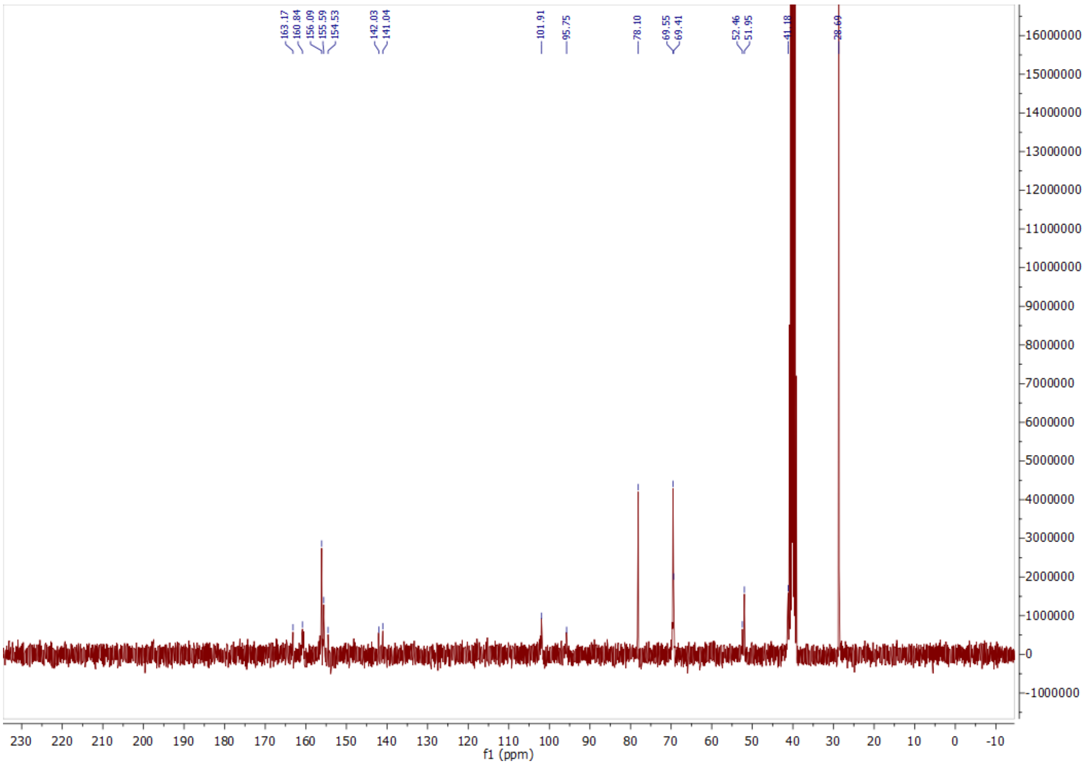
163.17
160.84
156.09
155.59
154.53
142.03
141.04
101.91
95.75
78.10
69.55
69.41
52.46
51.95
41.18
28.69
16000000
15000000
14000000
13000000
12000000
11000000
10000000
9000000
8000000
7000000
6000000
5000000
4000000
3000000
2000000
1000000
0
-1000000
230 220 210 200 190 180 170 160 150 140 130 120 110 100 90 80 70 60 50 40 30 20 10 0 -10
f1 (ppm)

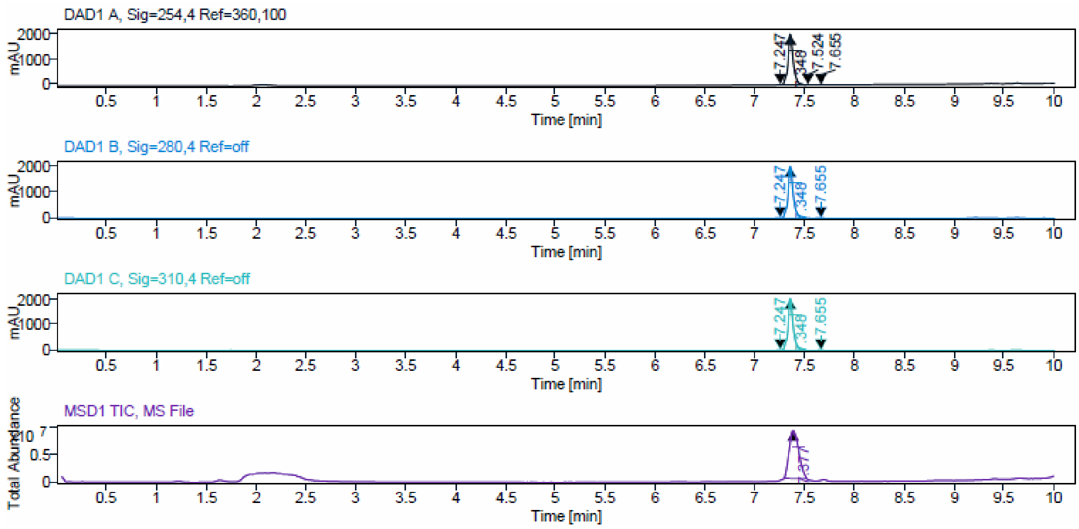
DAD1 A, Sig=254,4 Ref=360,100
mAU
2000
1000
0
7.247
.348
7.524
7.655
Time [min]
DAD1 B, Sig=280,4 Ref=off
mAU
7.247
.348
7.655
Time [min]
DAD1 C, Sig=310,4 Ref=off
mAU
7.247
.348
7.655
Time [min]
MSD1 TIC, MS File
Total Abundance
x10 7
0.5
0
.377
0.5 1 1.5 2 2.5 3 3.5 4 4.5 5 5.5 6 6.5 7 7.5 8 8.5 9 9.5 10
Time [min]

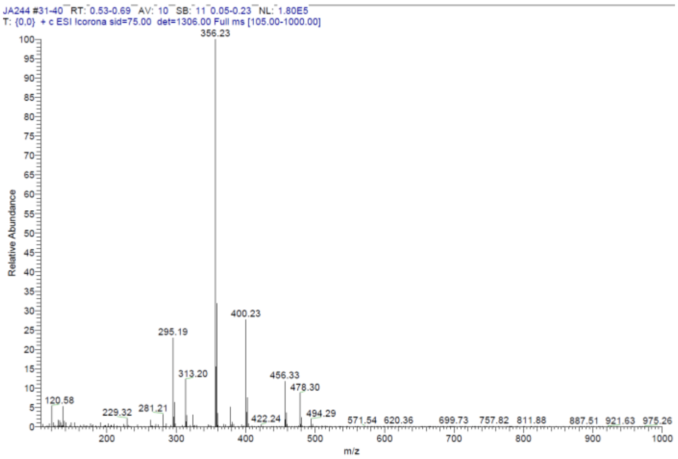
JA244 #31-40 RT: 0.53-0.69 AV: 10 SB: 11 0.05-0.23 NL: 1.80E5
T: {0,0} + c ESI Icorona sid=75.00 det=1306.00 Full ms [105.00-1000.00]
Relative Abundance
100
95
90
85
80
75
70
65
60
55
50
45
40
35
30
25
20
15
10
5
0
356.23
400.23
295.19
313.20
456.33
478.30
120.58
229.32
281.21
422.24
494.29
571.54
620.36
699.73
757.82
811.88
887.51
921.63
975.26
200 300 400 500 600 700 800 900 1000
m/z

^{1}H, ^{13}C NMR, HPLC, and ESI data of compound **77e**

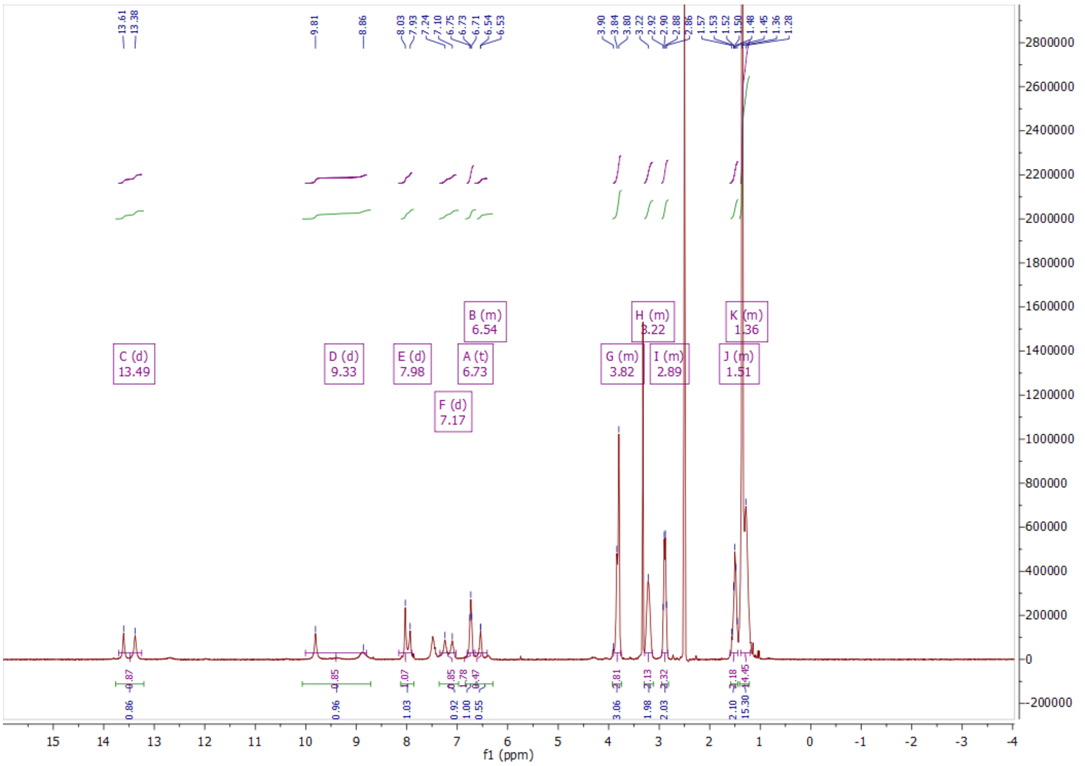

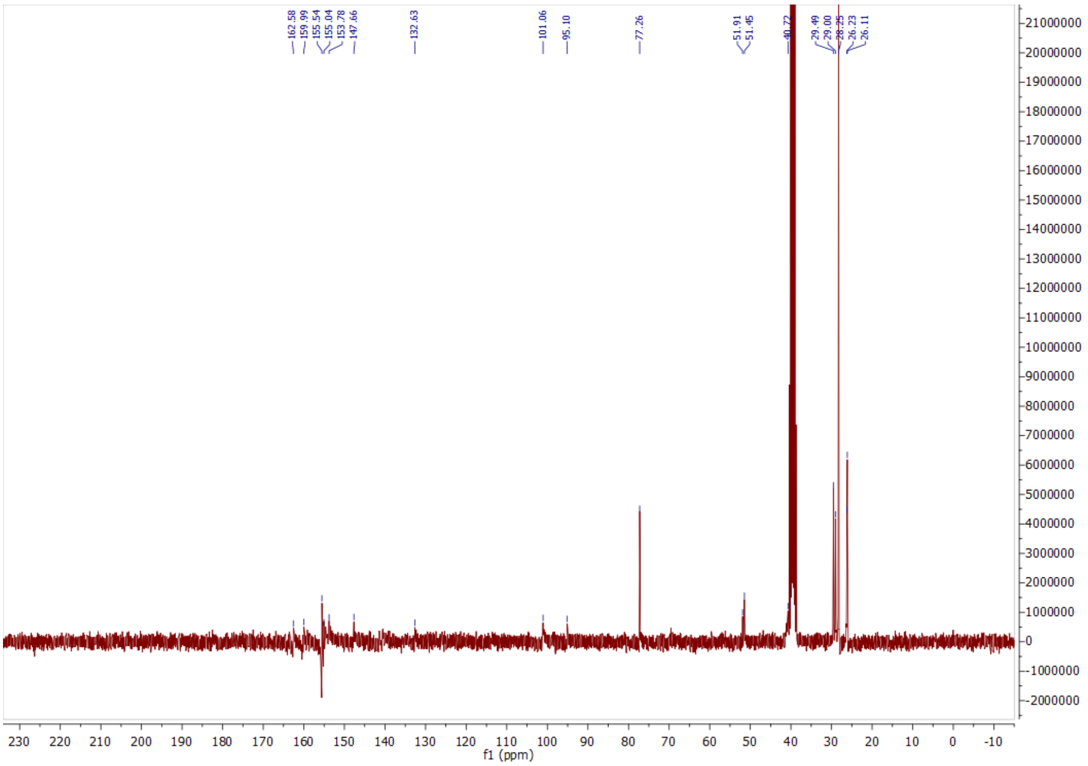

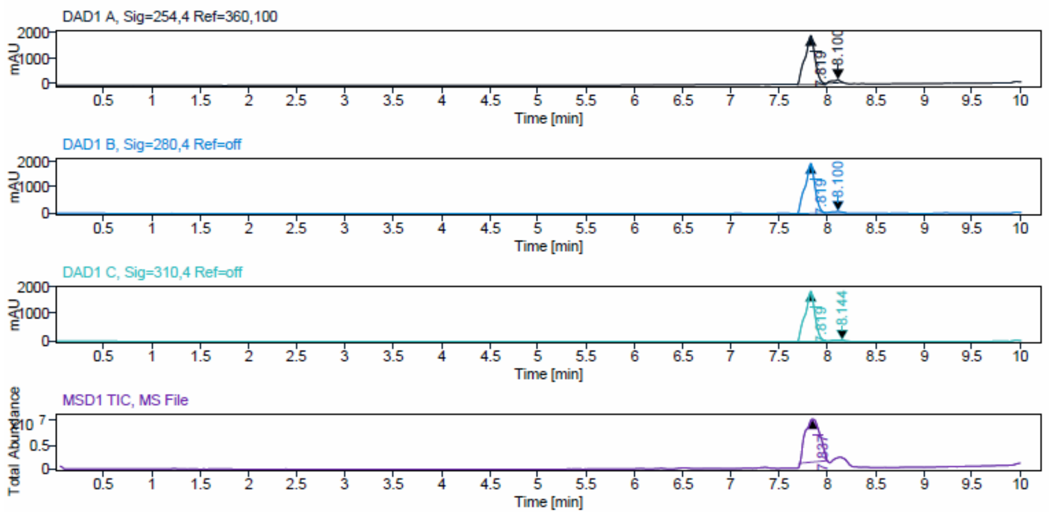

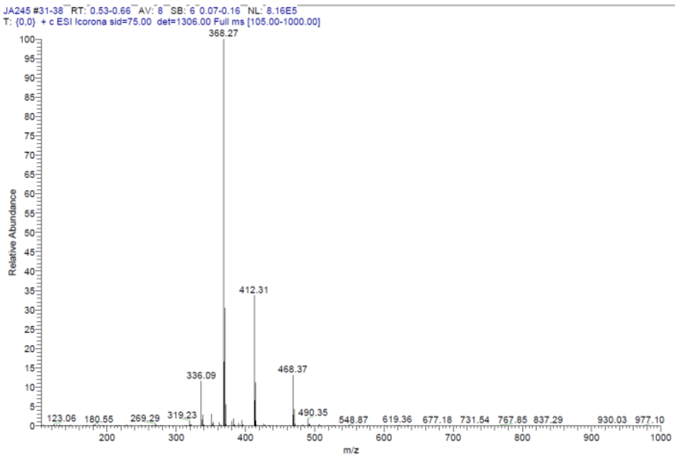

^1H, ^{13}C NMR, HPLC, and ESI data of compound **78a**

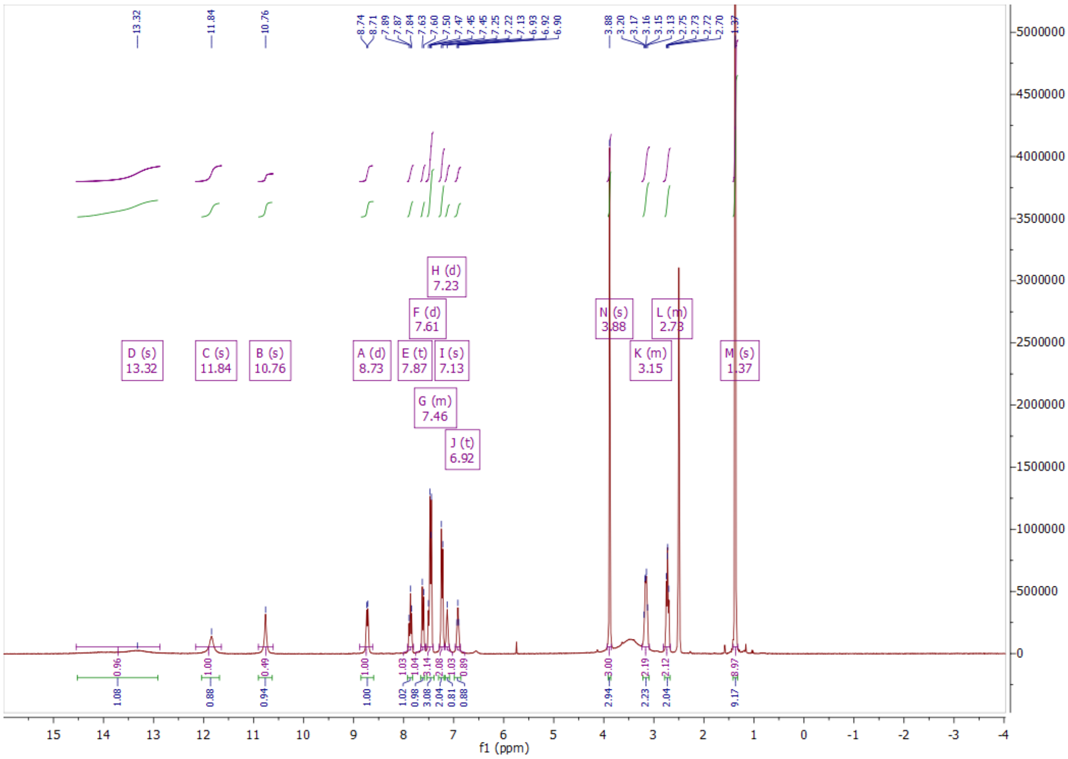

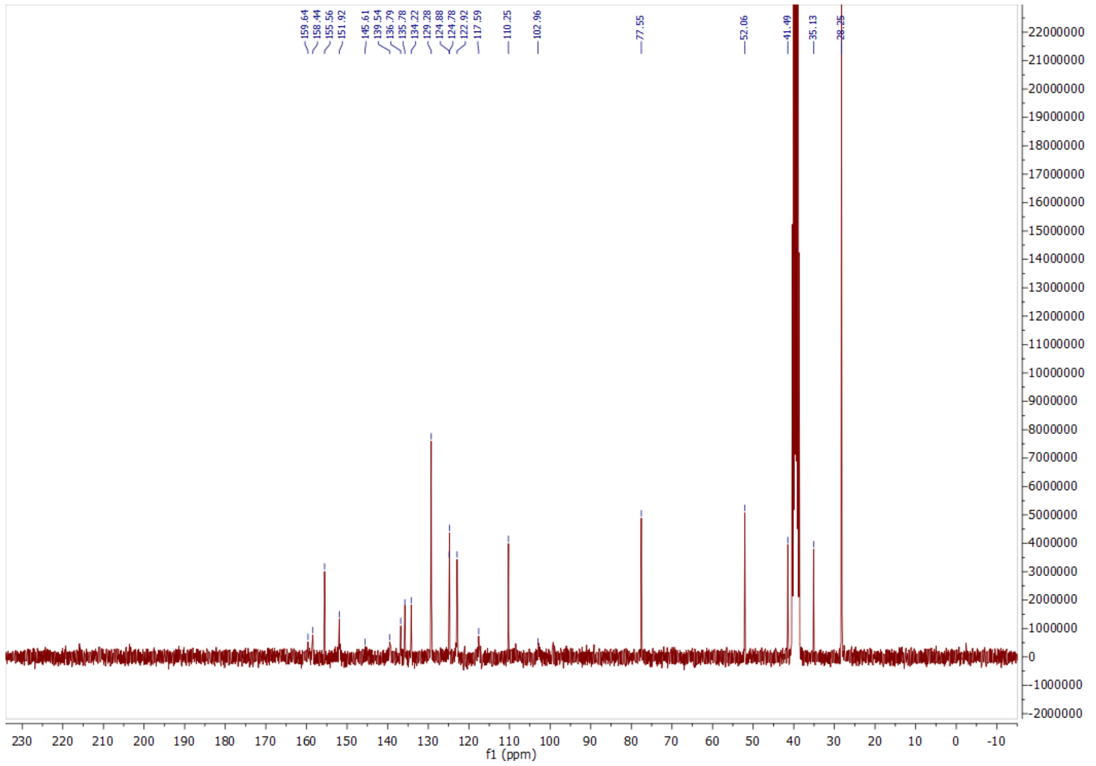
159.64
158.44
155.56
151.92
145.61
139.54
136.79
135.78
134.22
129.28
124.88
124.78
122.92
117.59
110.25
102.96
77.55
52.06
41.49
35.13
28.25
22000000
21000000
20000000
19000000
18000000
17000000
16000000
15000000
14000000
13000000
12000000
11000000
10000000
9000000
8000000
7000000
6000000
5000000
4000000
3000000
2000000
1000000
0
-1000000
-2000000
230 220 210 200 190 180 170 160 150 140 130 120 110 100 90 80 70 60 50 40 30 20 10 0 -10
f1 (ppm)

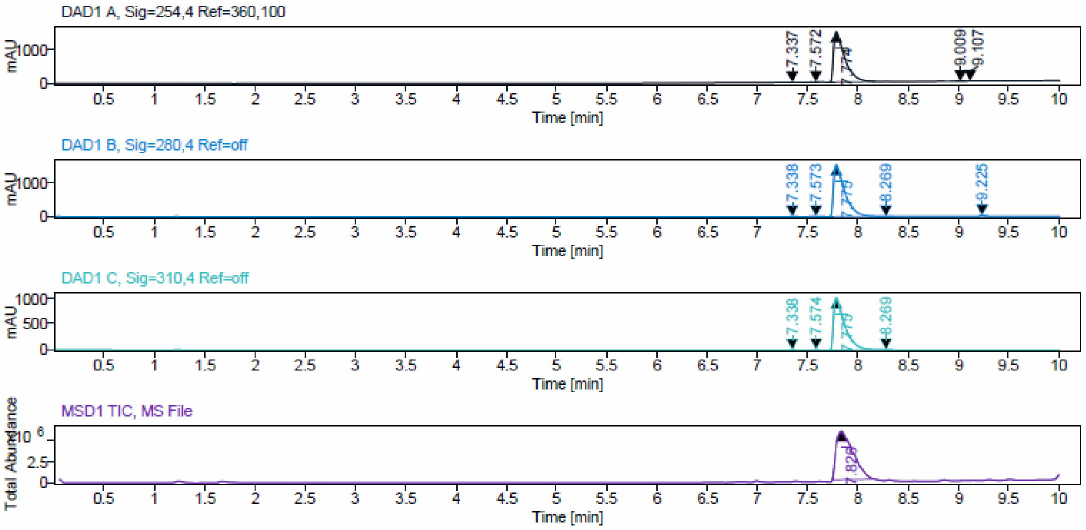
DAD1 A, Sig=254,4 Ref=360,100
mAU
1000
0
7.337
7.572
7.774
9.009
9.107
0.5 1 1.5 2 2.5 3 3.5 4 4.5 5 5.5 6 6.5 7 7.5 8 8.5 9 9.5 10
Time [min]
DAD1 B, Sig=280,4 Ref=off
mAU
1000
0
7.338
7.573
7.775
8.269
9.225
Time [min]
DAD1 C, Sig=310,4 Ref=off
mAU
1000
500
0
7.338
7.574
7.779
8.269
Time [min]
MSD1 TIC, MS File
Total Abundance
x10 6
2.5
0
7.828
Time [min]

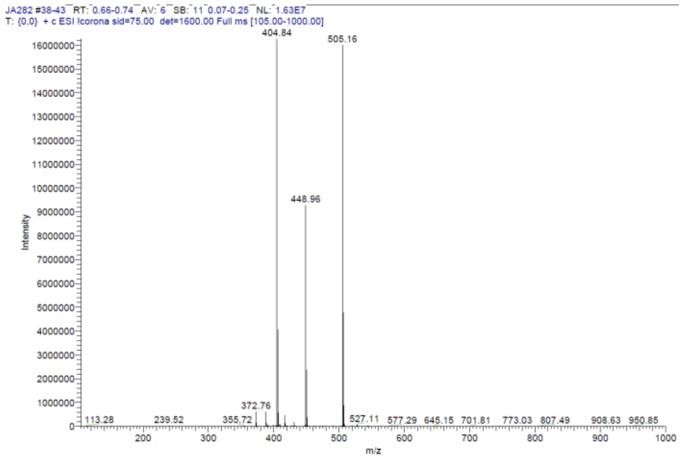
JA282 #38-43 RT: 0.66-0.74 AV: 6 SB: 11 0.07-0.25 NL: 1.63E7
T: {0,0} + c ESI !corona sid=75.00 det=1600.00 Full ms [105.00-1000.00]
404.84
505.16
448.96
372.76
113.28
239.52
355.72
527.11
577.29
645.15
701.81
773.03
807.49
908.63
950.85
Intensity
16000000
15000000
14000000
13000000
12000000
11000000
10000000
9000000
8000000
7000000
6000000
5000000
4000000
3000000
2000000
1000000
0
200 300 400 500 600 700 800 900 1000
m/z

^{1}H, ^{13}C NMR, HPLC, and ESI data of compound **78b**

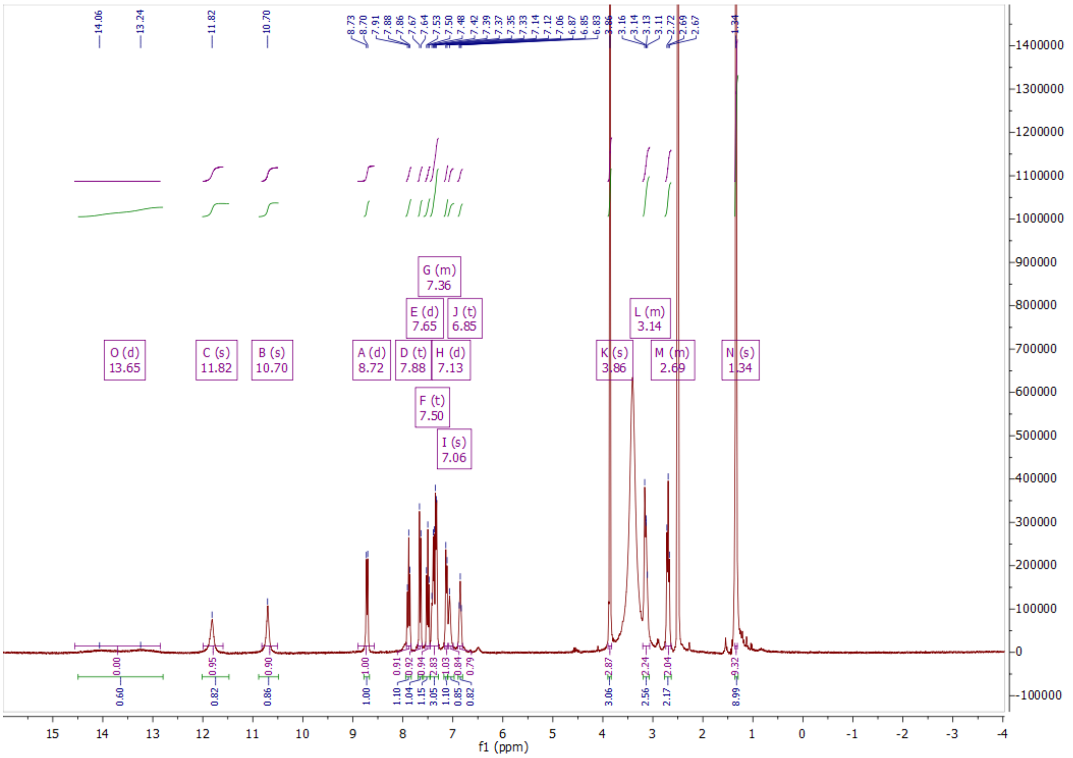

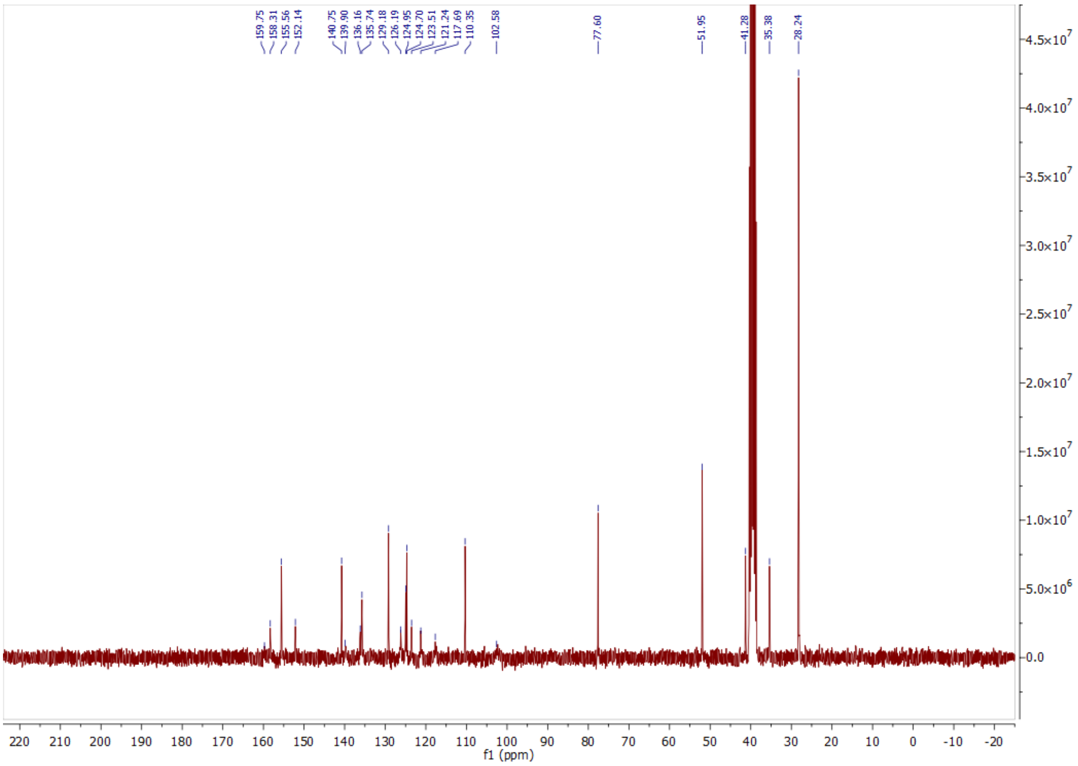

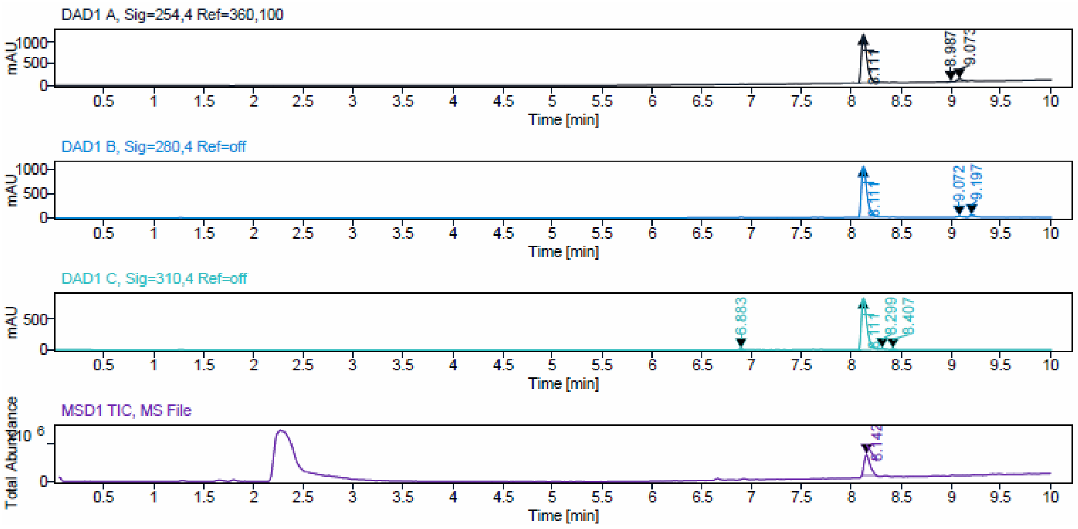

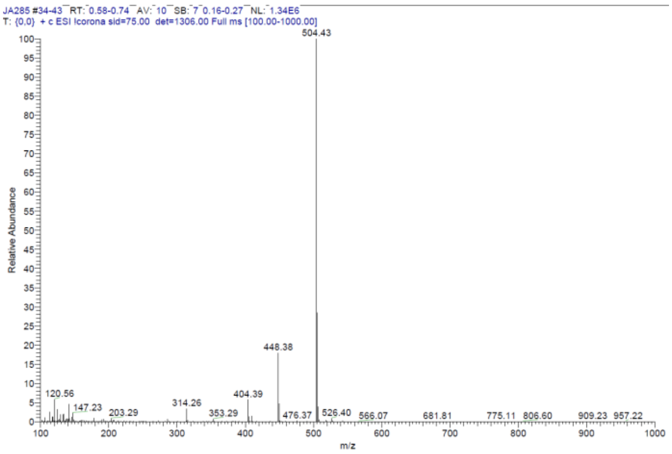

^{1}H, ^{13}C NMR, HPLC, and ESI data of compound **78c**

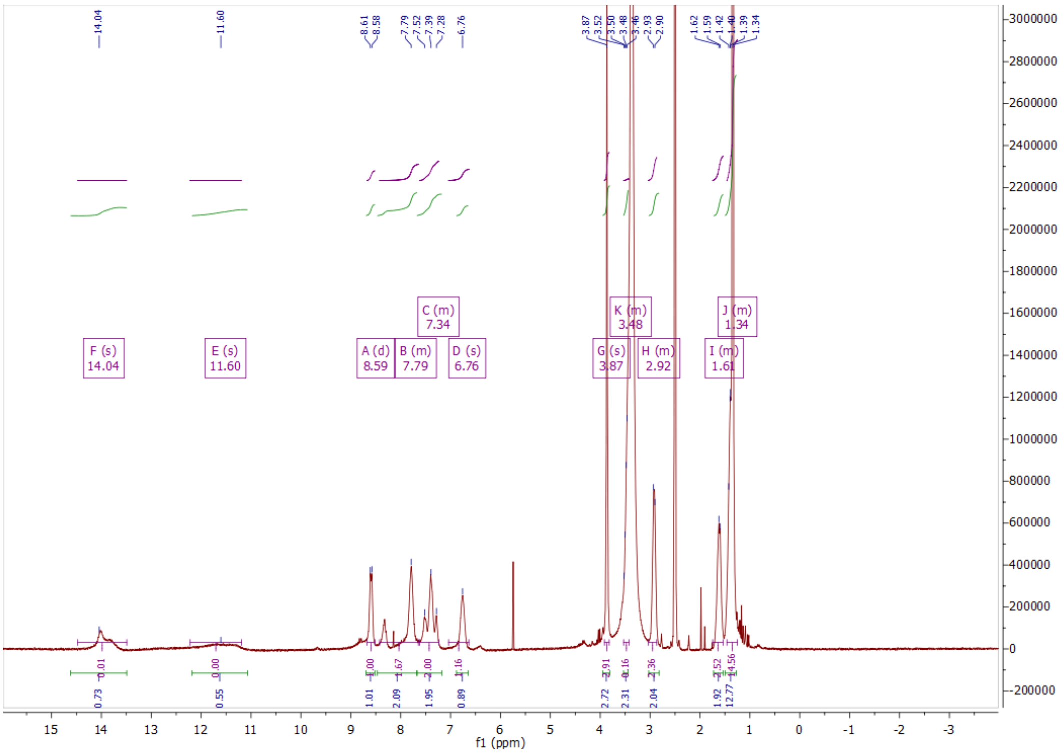

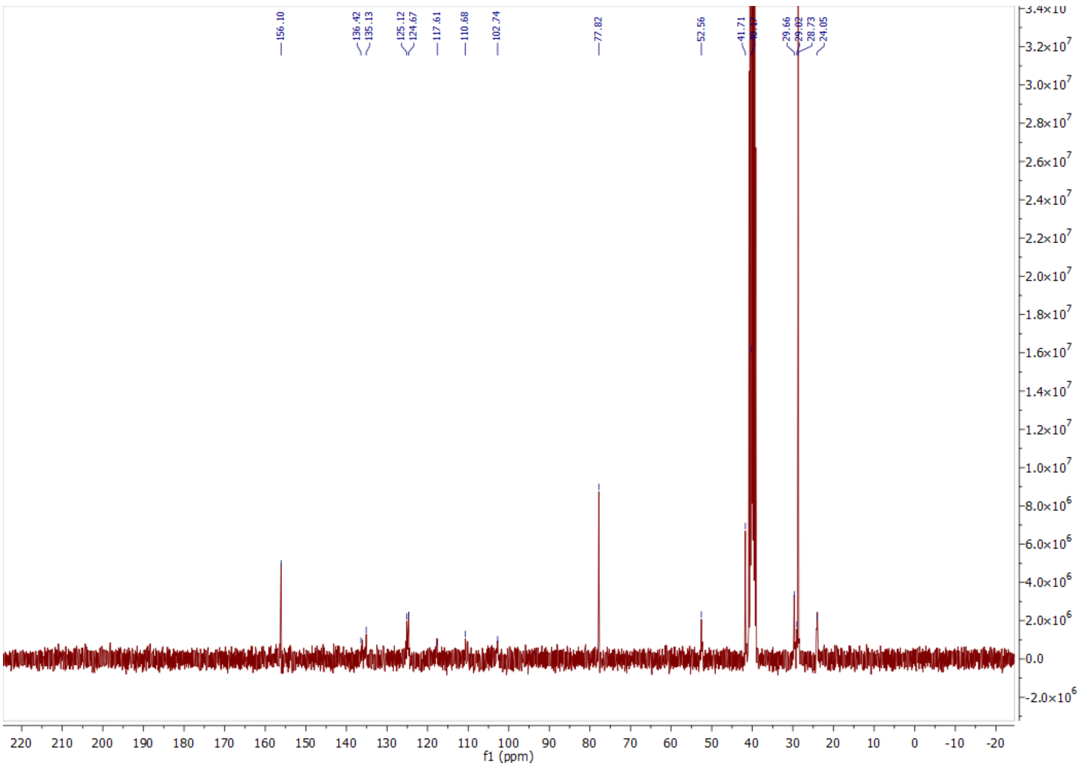
156.10
136.42
135.13
125.12
124.67
117.61
110.68
102.74
77.82
52.56
41.71
40.17
29.66
29.02
28.73
24.05
3.4×10
3.2×10^7
3.0×10^7
2.8×10^7
2.6×10^7
2.4×10^7
2.2×10^7
2.0×10^7
1.8×10^7
1.6×10^7
1.4×10^7
1.2×10^7
1.0×10^7
8.0×10^6
6.0×10^6
4.0×10^6
2.0×10^6
0.0
-2.0×10^6
220 210 200 190 180 170 160 150 140 130 120 110 100 90 80 70 60 50 40 30 20 10 0 -10 -20
f1 (ppm)

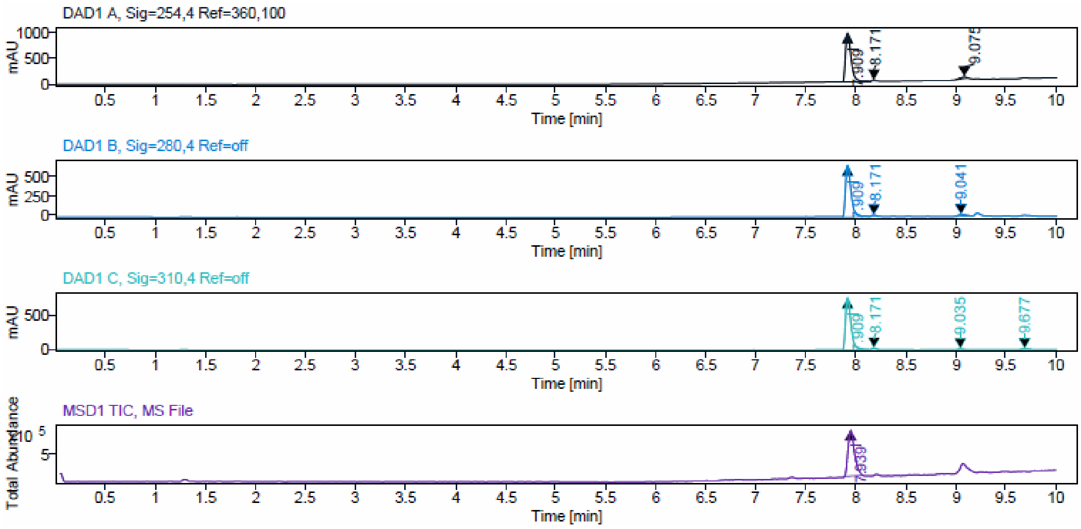
DAD1 A, Sig=254,4 Ref=360,100
mAU
1000
500
0
8.171
9.075
Time [min]
DAD1 B, Sig=280,4 Ref=off
mAU
500
250
0
8.171
9.041
Time [min]
DAD1 C, Sig=310,4 Ref=off
mAU
500
0
8.171
9.035
9.677
Time [min]
MSD1 TIC, MS File
Total Abundance
x10 5
5
0.5 1 1.5 2 2.5 3 3.5 4 4.5 5 5.5 6 6.5 7 7.5 8 8.5 9 9.5 10
Time [min]

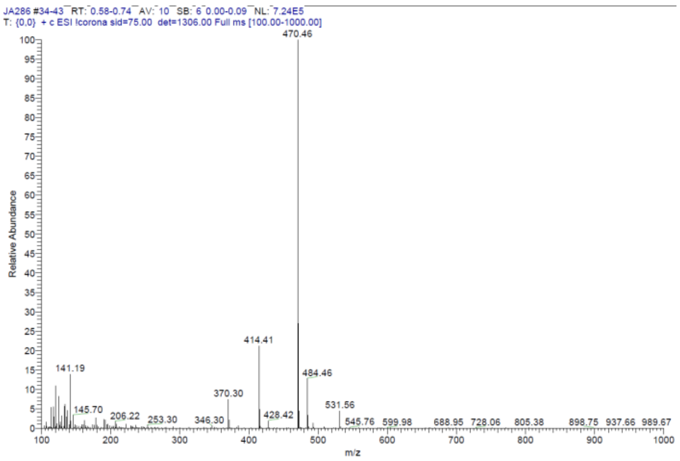
JA286 #34-43 RT: 0.58-0.74 AV: 10 SB: 6 0.00-0.09 NL: 7.24E5
T: {0,0} + c ESI !corona sid=75.00 det=1306.00 Full ms [100.00-1000.00]
470.46
414.41
141.19
484.46
370.30
531.56
145.70
206.22
253.30
346.30
428.42
545.76
599.98
688.95
728.06
805.38
898.75
937.66
989.67
Relative Abundance
100 95 90 85 80 75 70 65 60 55 50 45 40 35 30 25 20 15 10 5 0
100 200 300 400 500 600 700 800 900 1000
m/z

^{1}H, ^{13}C NMR, HPLC, and ESI data of compound **79**

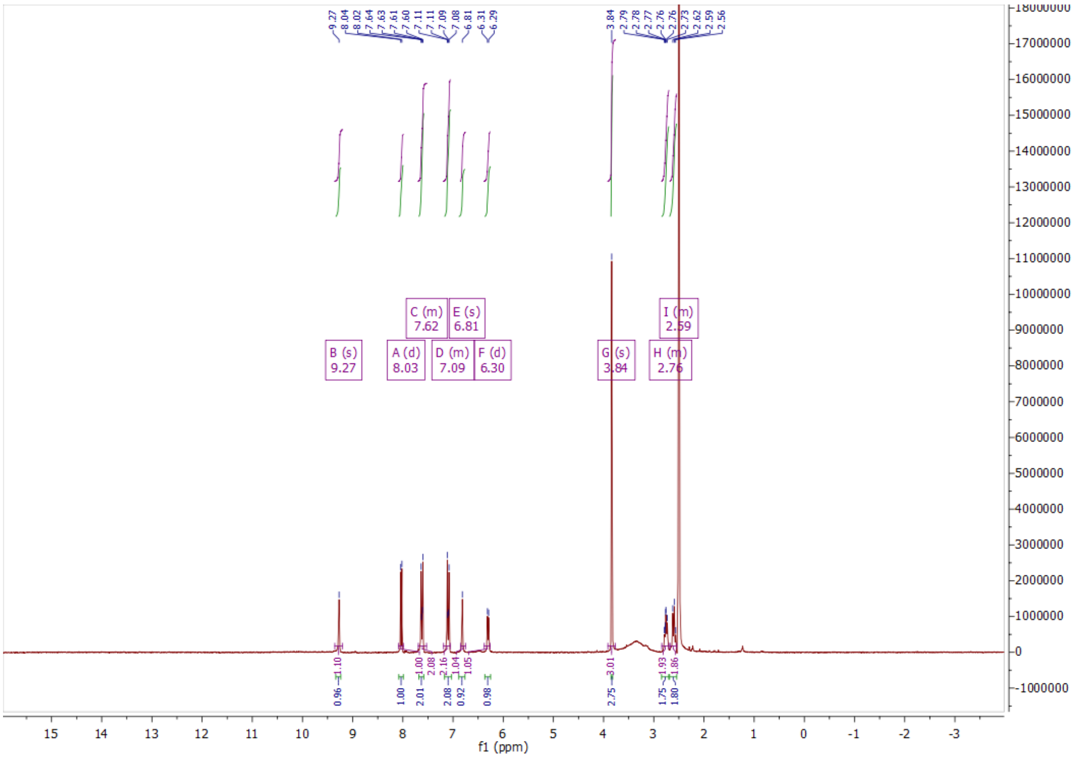

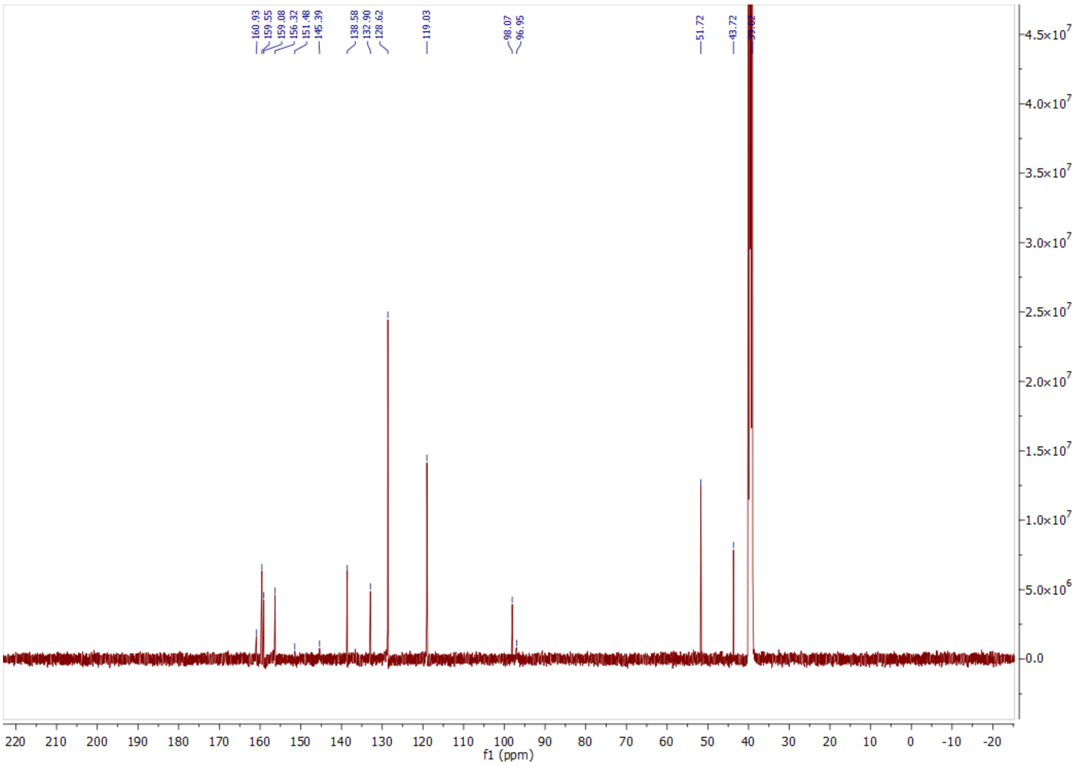

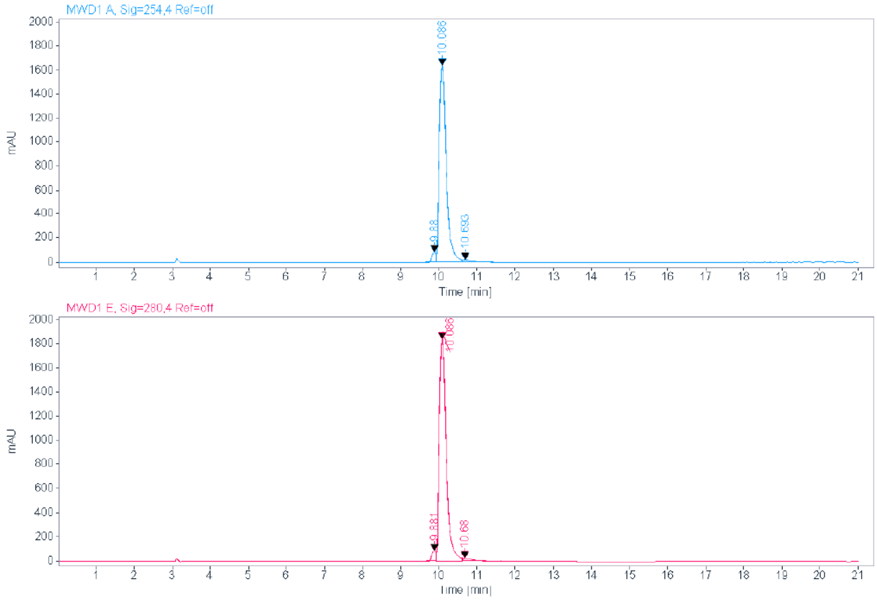
MWD1 A, Sig=254,4 Ref=off
mAU
2000
1800
1600
1400
1200
1000
800
600
400
200
0
10.086
9.88
10.693
Time [min]
1 2 3 4 5 6 7 8 9 10 11 12 13 14 15 16 17 18 19 20 21
MWD1 E, Sig=280,4 Ref=off
mAU
10.086
9.881
10.68
Time [min]

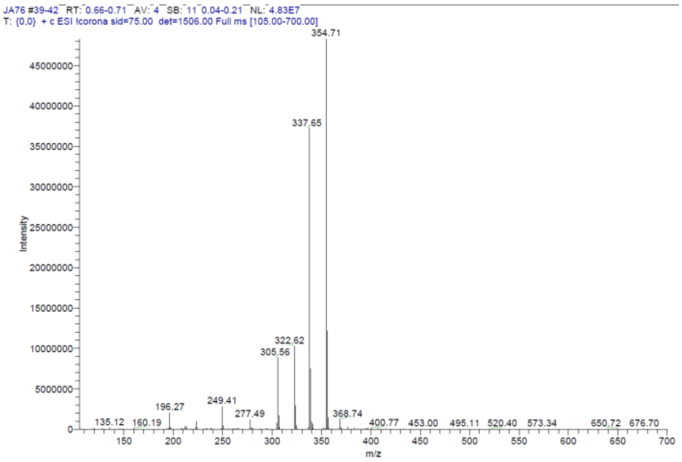
JA76 #39-42 RT: 0.66-0.71 AV: 4 SB: 11 0.04-0.21 NL: 4.83E7
T: {0,0} + c ESI !corona sid=75.00 det=1506.00 Full ms [105.00-700.00]
Intensity
45000000
40000000
35000000
30000000
25000000
20000000
15000000
10000000
5000000
0
354.71
337.65
322.62
305.56
368.74
277.49
249.41
196.27
135.12
160.19
400.77
453.00
495.11
520.40
573.34
650.72
676.70
m/z
150 200 250 300 350 400 450 500 550 600 650 700

^{1}H NMR, HPLC, and ESI data of compound **80**

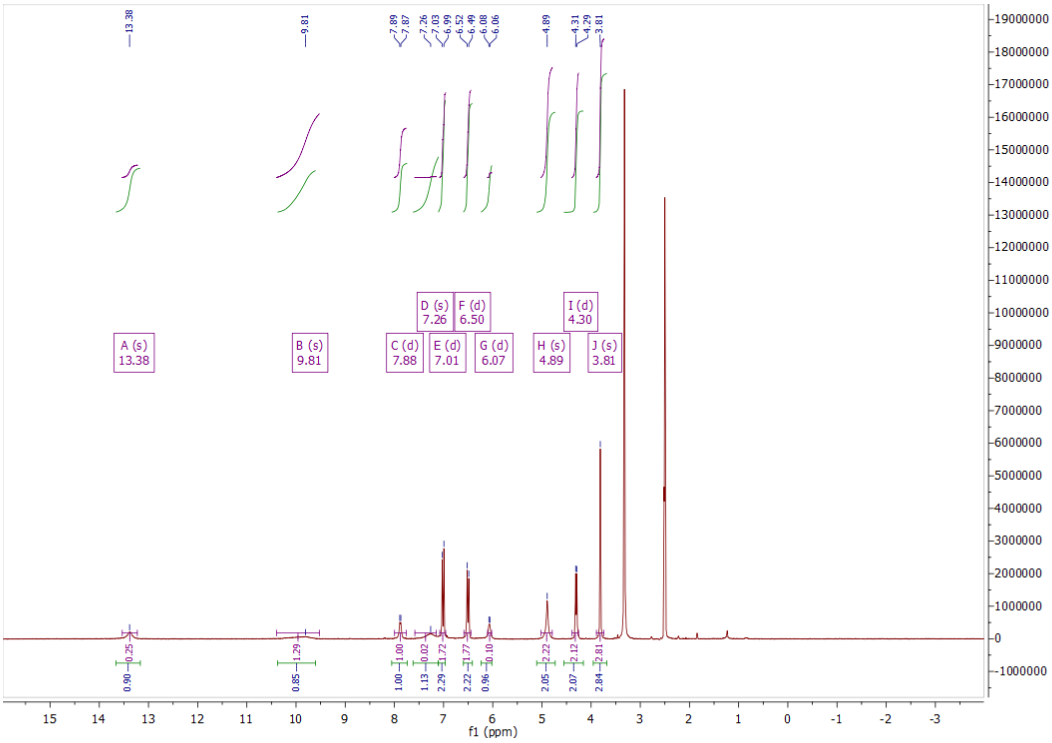

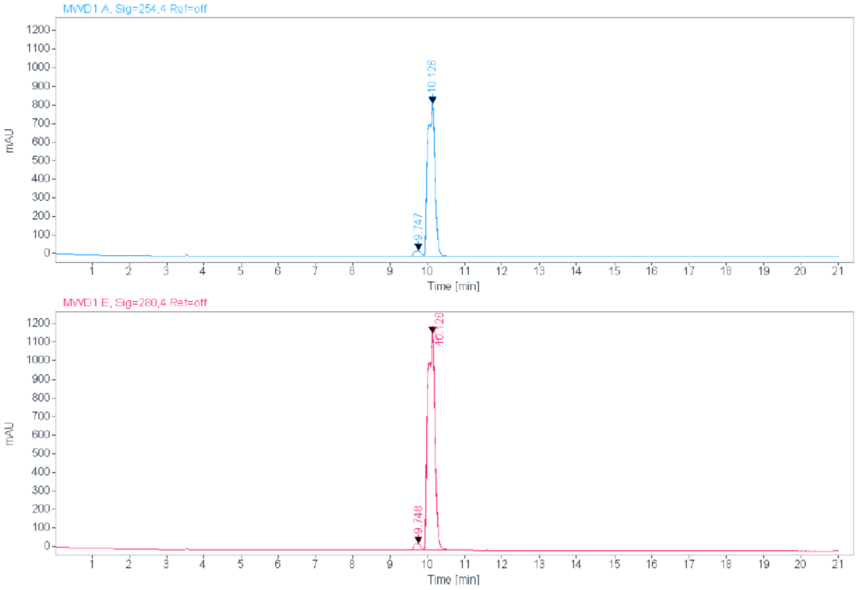

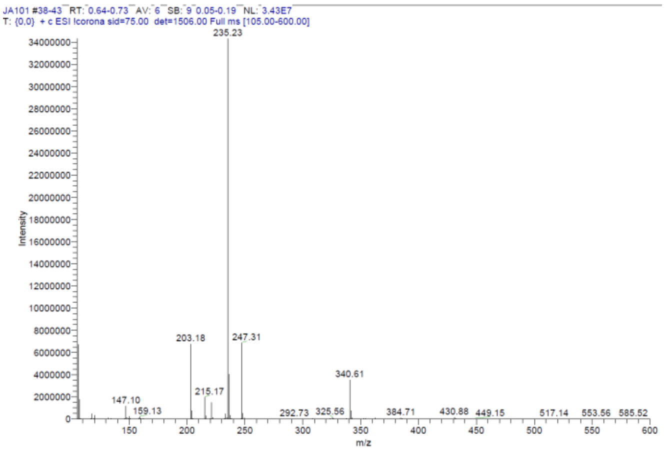

^{1}H and ^{13}C NMR, and ESI data of compound **87**

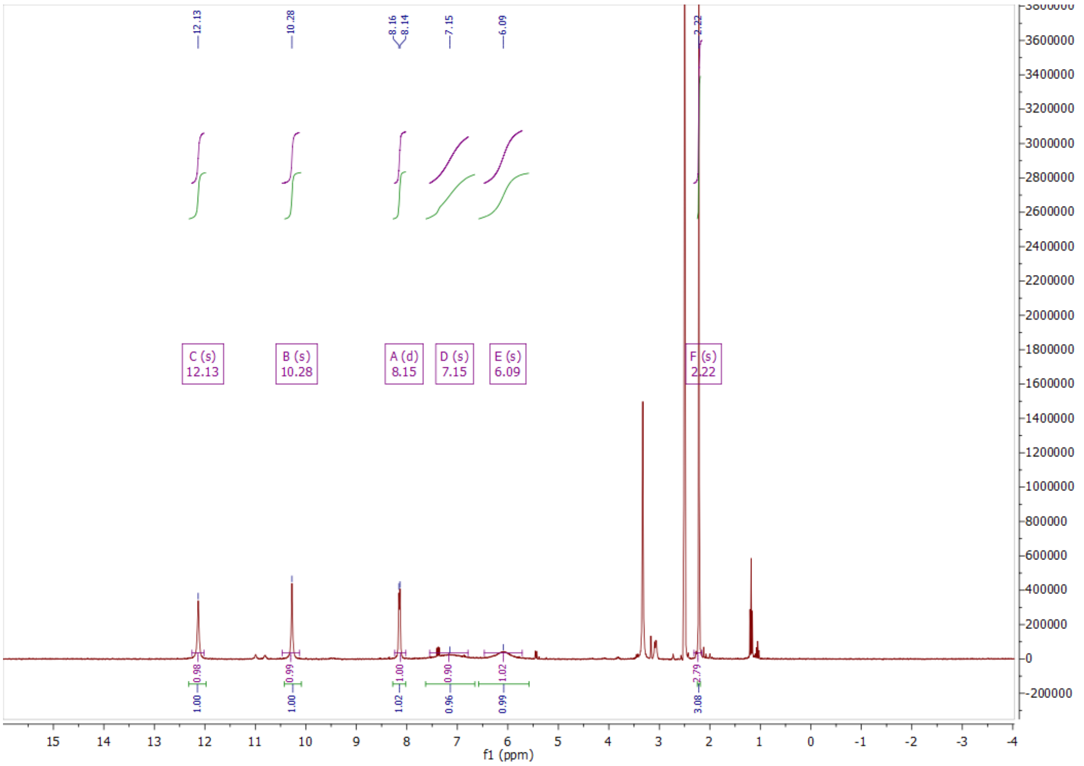

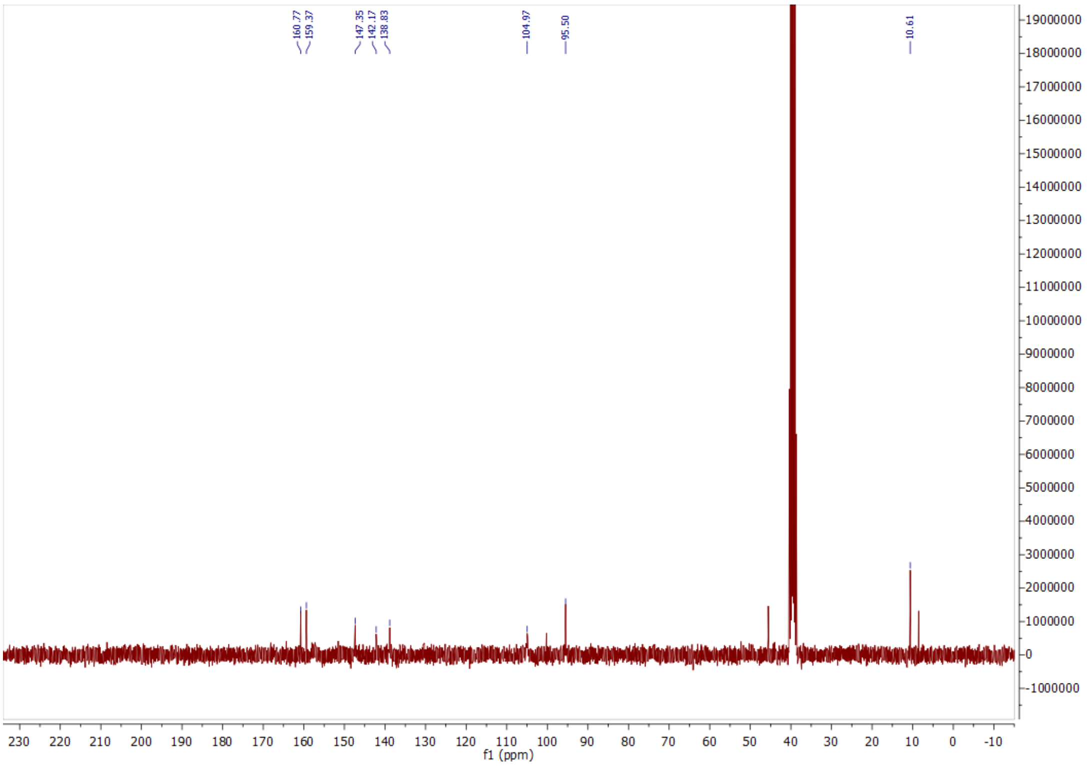

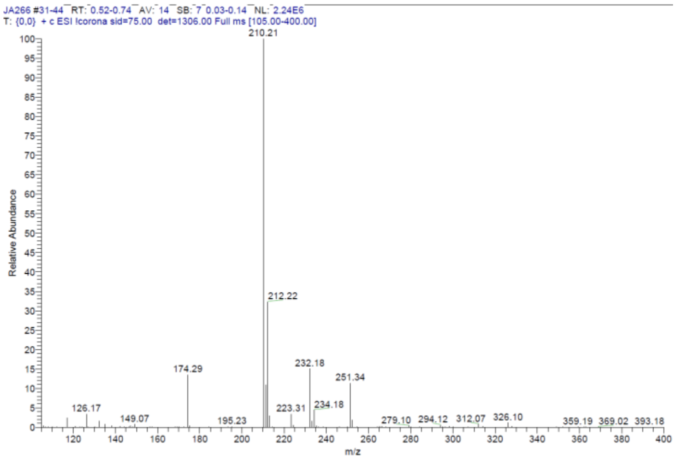

^{1}H, ^{13}C NMR, and ESI data of compound **88**

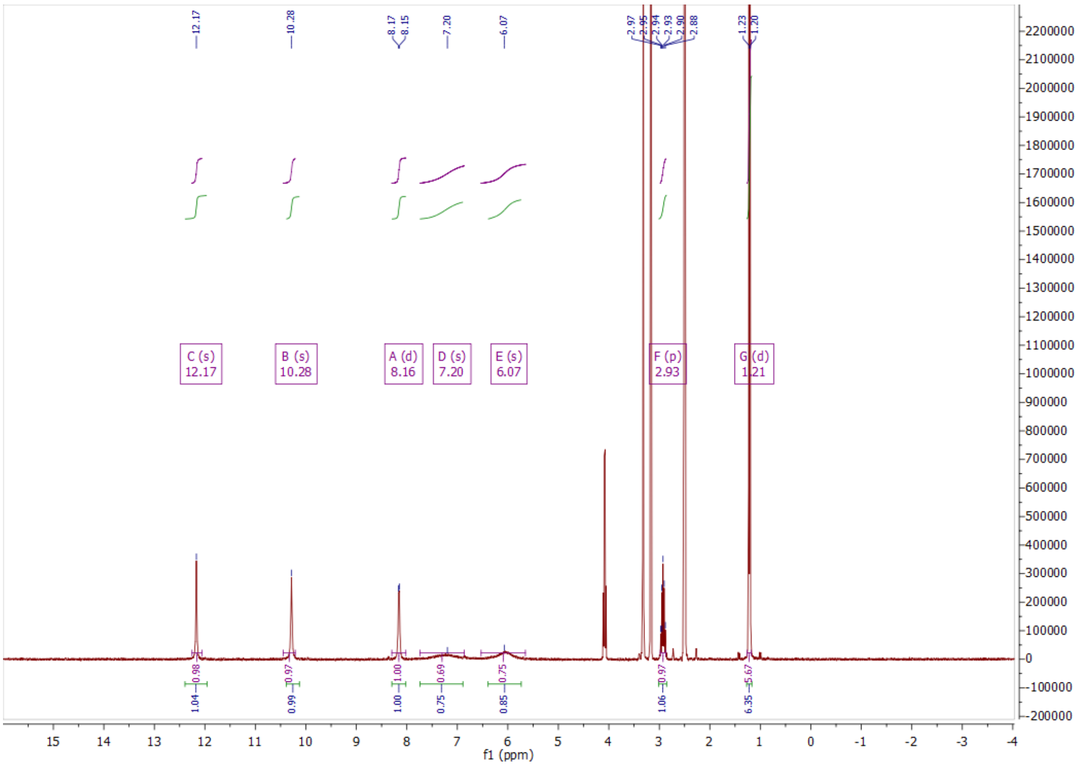

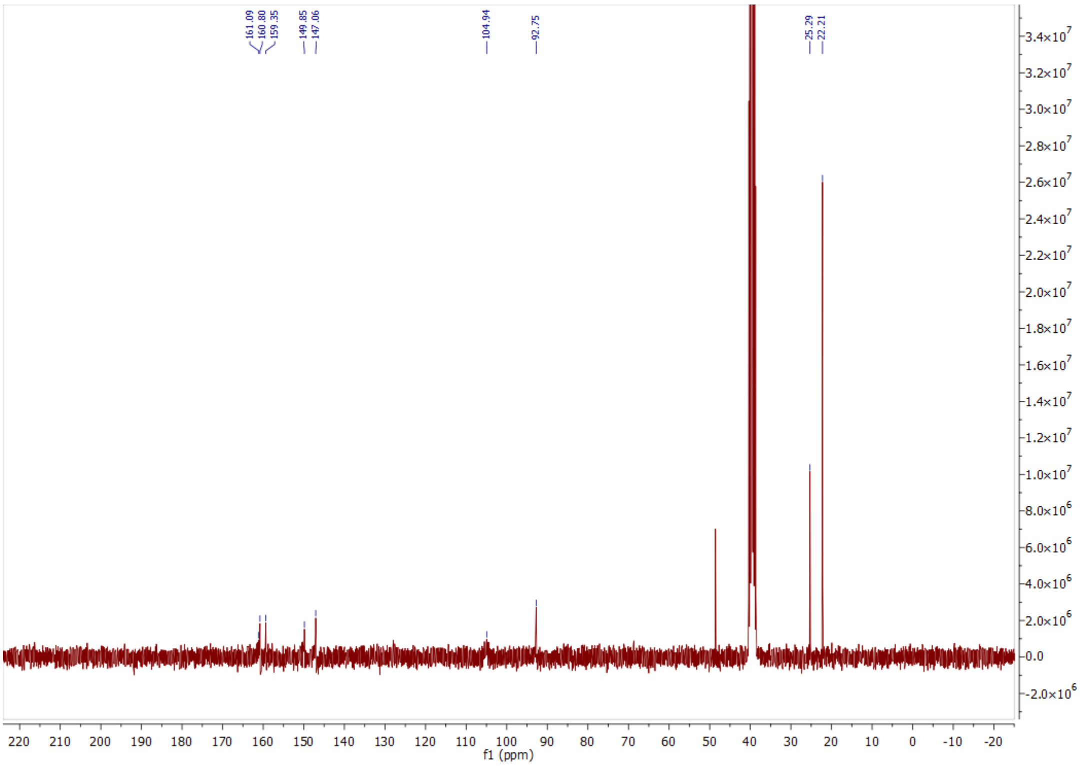
161.09
160.80
159.35
149.85
147.06
104.94
92.75
25.29
22.21
3.4×10^7
3.2×10^7
3.0×10^7
2.8×10^7
2.6×10^7
2.4×10^7
2.2×10^7
2.0×10^7
1.8×10^7
1.6×10^7
1.4×10^7
1.2×10^7
1.0×10^7
8.0×10^6
6.0×10^6
4.0×10^6
2.0×10^6
0.0
-2.0×10^6
220 210 200 190 180 170 160 150 140 130 120 110 100 90 80 70 60 50 40 30 20 10 0 -10 -20
f1 (ppm)

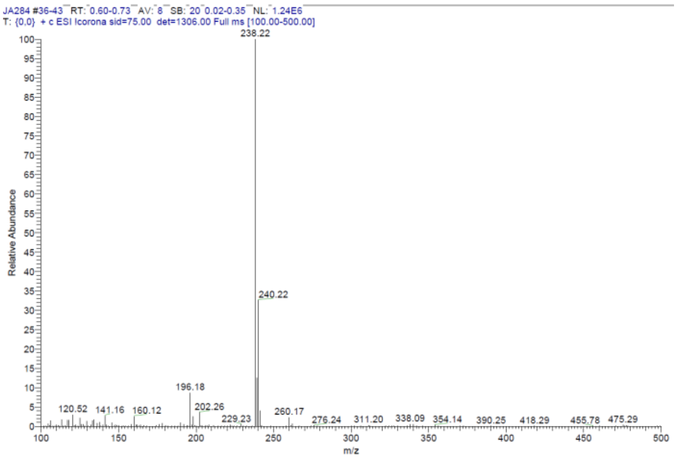
JA284 #36-43 RT: 0.60-0.73 AV: 8 SB: 20 0.02-0.35 NL: 1.24E6
T: {0,0} + c ESI Icorona sid=75.00 det=1306.00 Full ms [100.00-500.00]
238.22
240.22
196.18
202.26
229.23
260.17
120.52
141.16
160.12
276.24
311.20
338.09
354.14
390.25
418.29
455.78
475.29
Relative Abundance
100 95 90 85 80 75 70 65 60 55 50 45 40 35 30 25 20 15 10 5 0
100 150 200 250 300 350 400 450 500
m/z

^{1}H, ^{13}C NMR, and ESI data of compound **89**

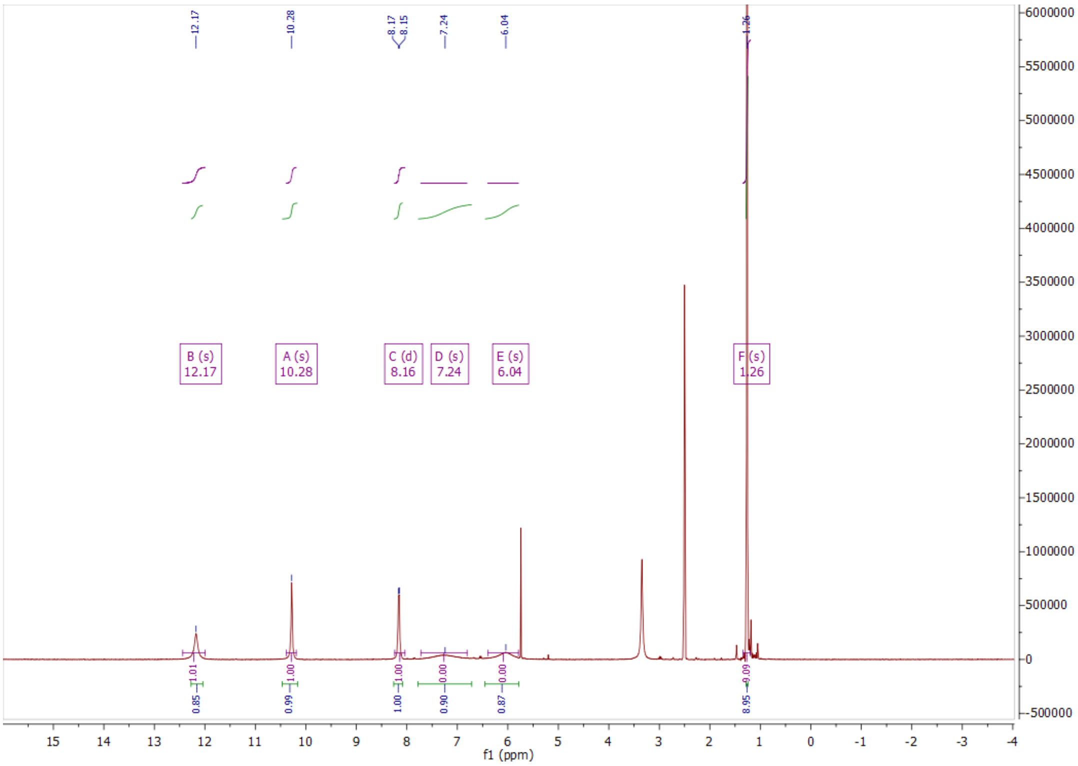

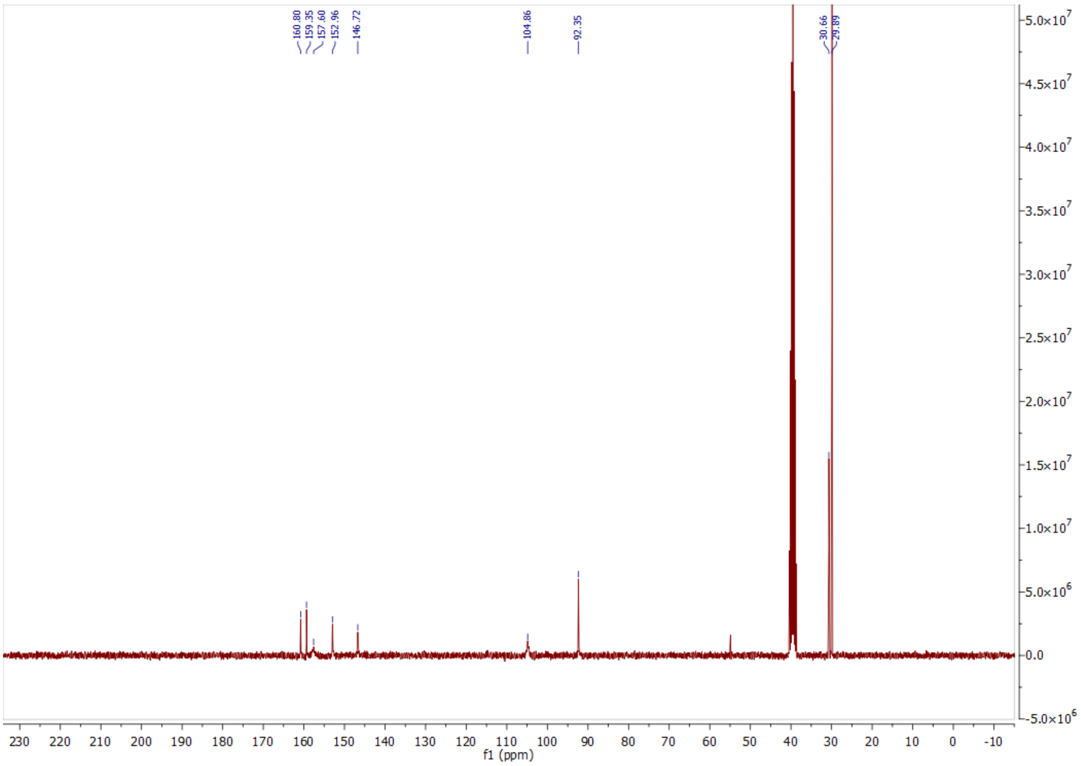

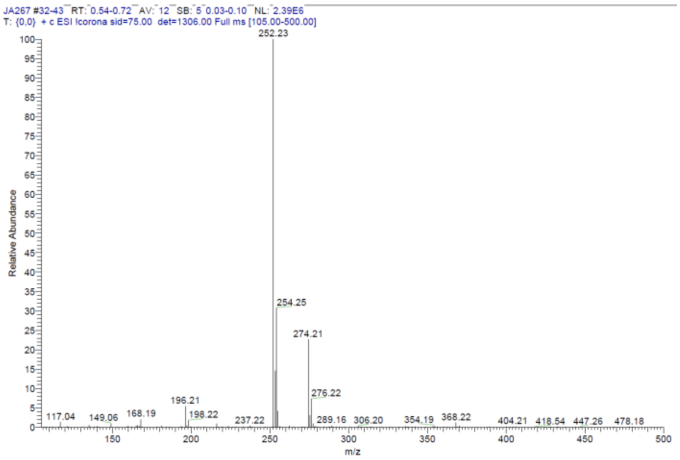

^1H, ^{13}C NMR, and ESI data of compound **90**

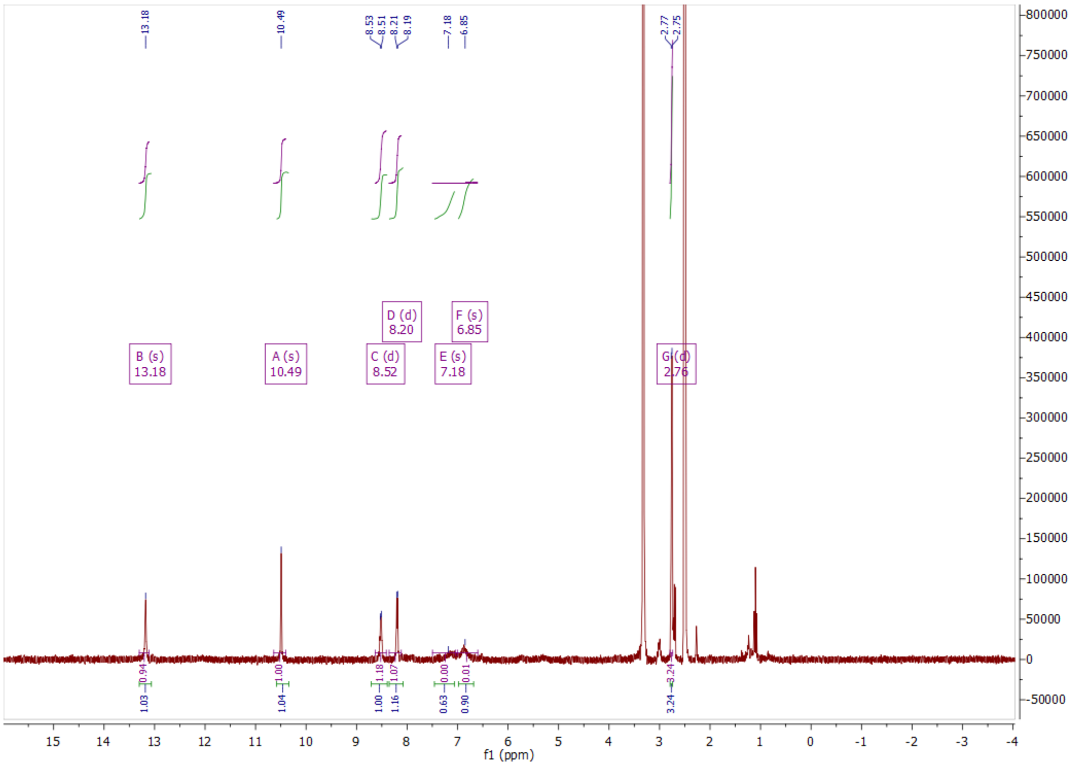

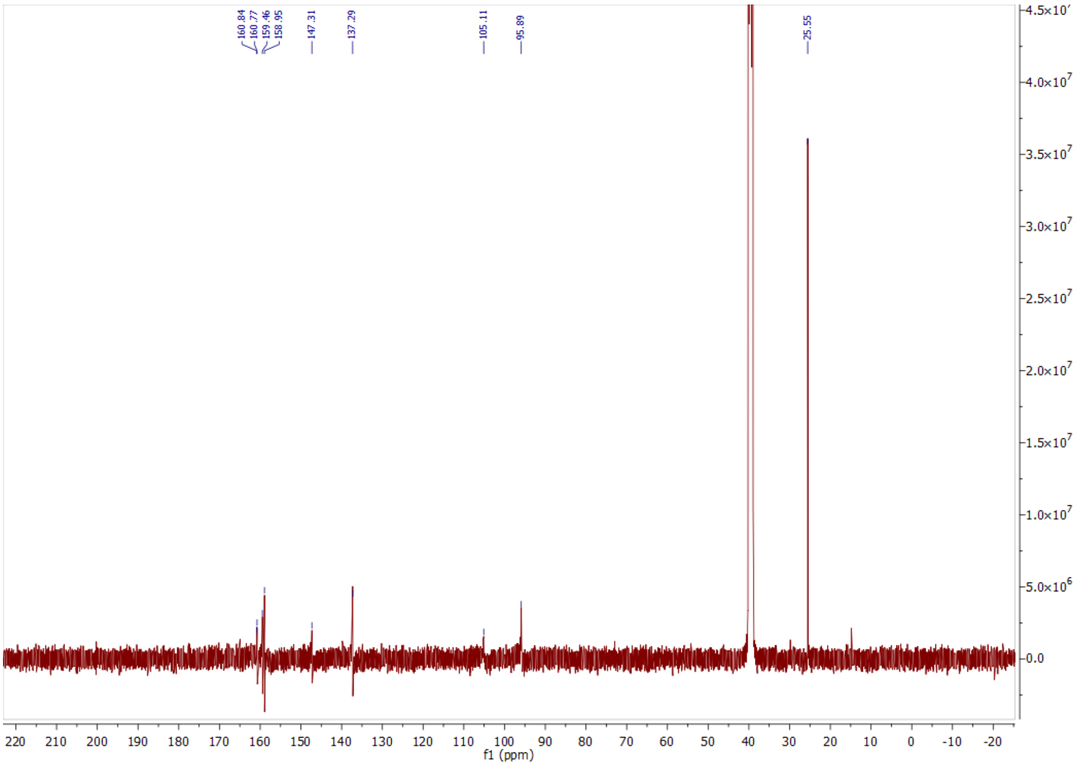

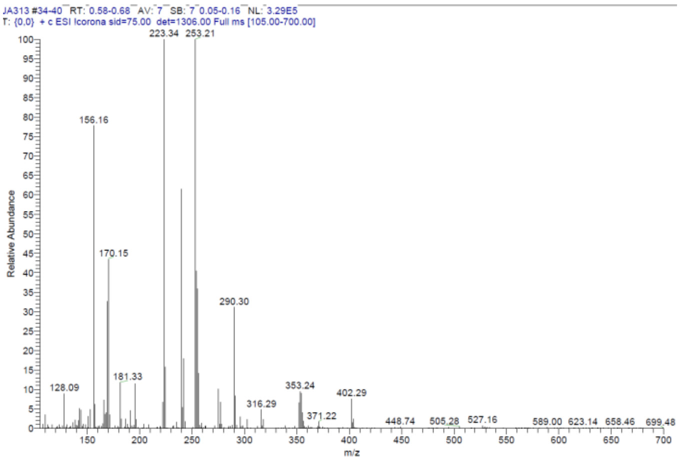

ESI data of compound **91**

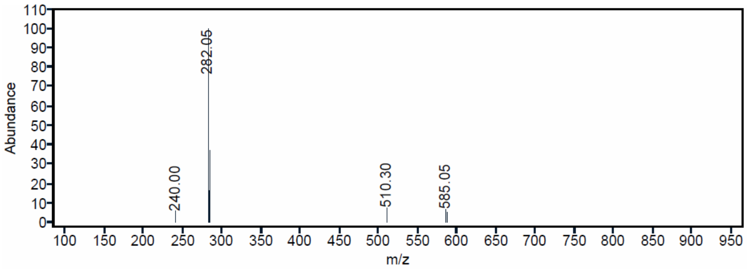

^{1}H, ^{13}C NMR, and ESI data of compound **92**

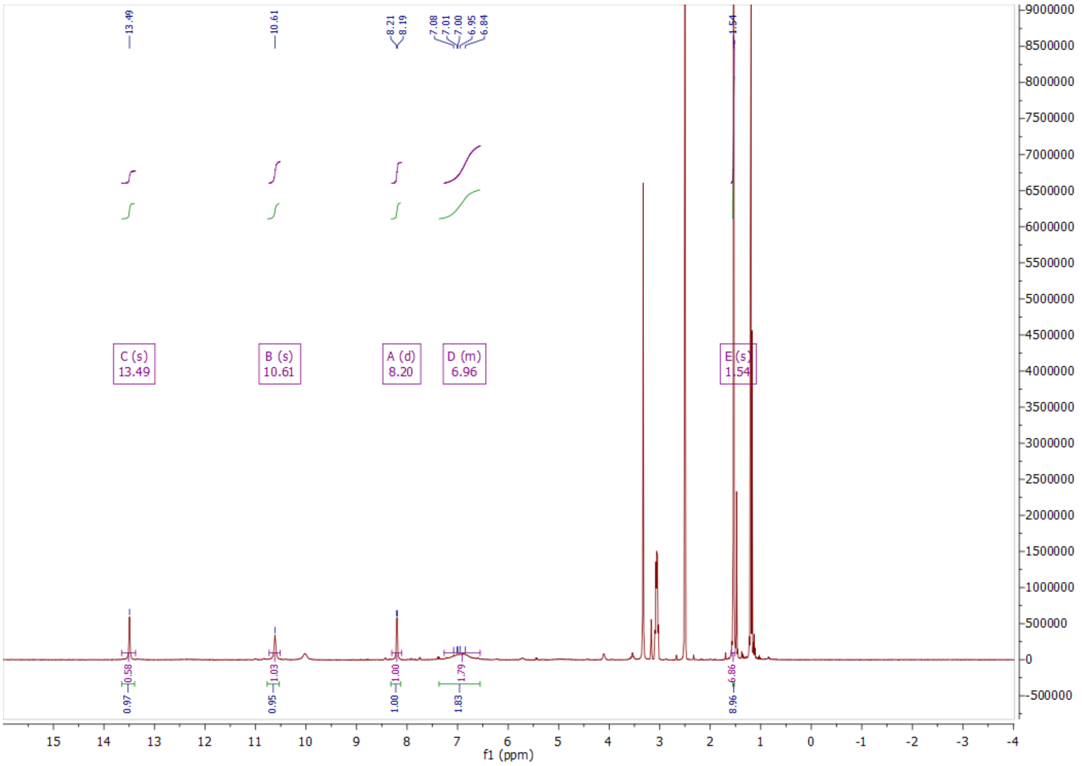

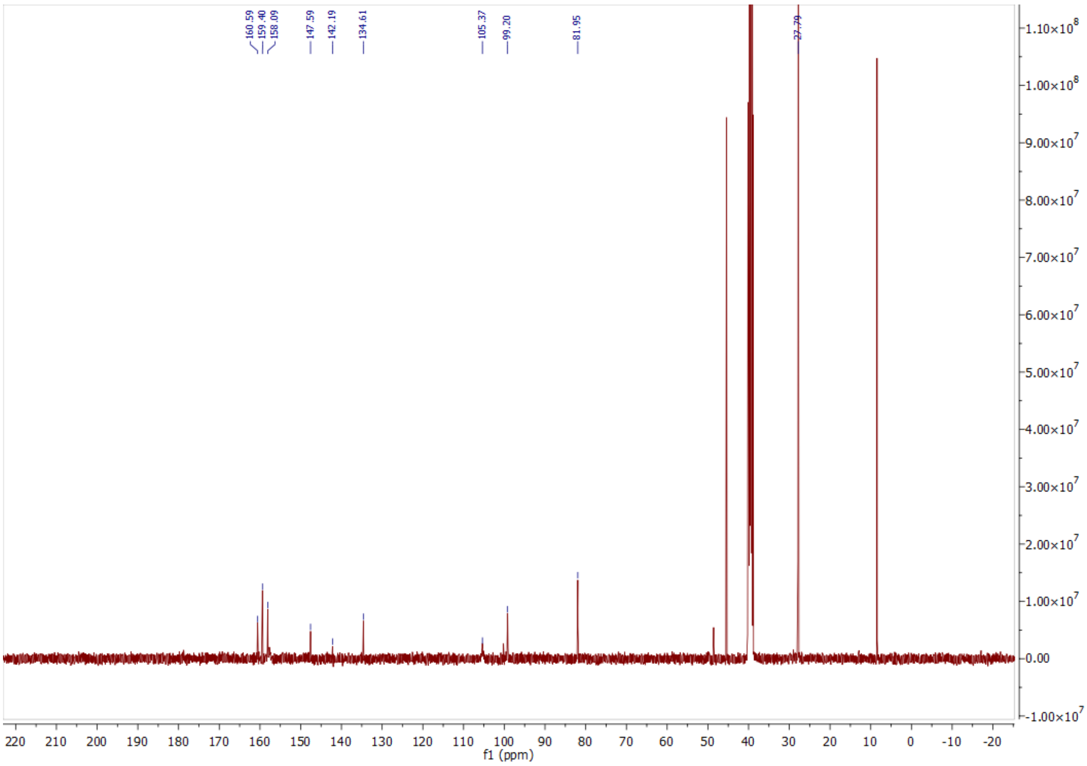

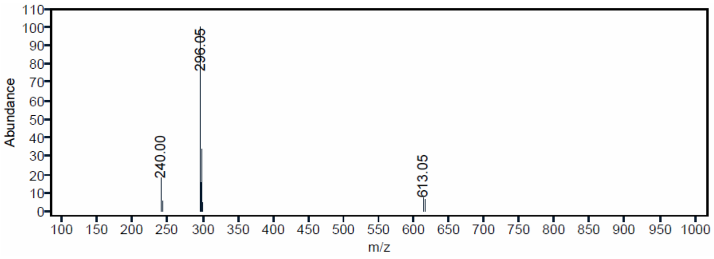

^{1}H, ^{13}C NMR, HPLC, and ESI data of compound **93a**

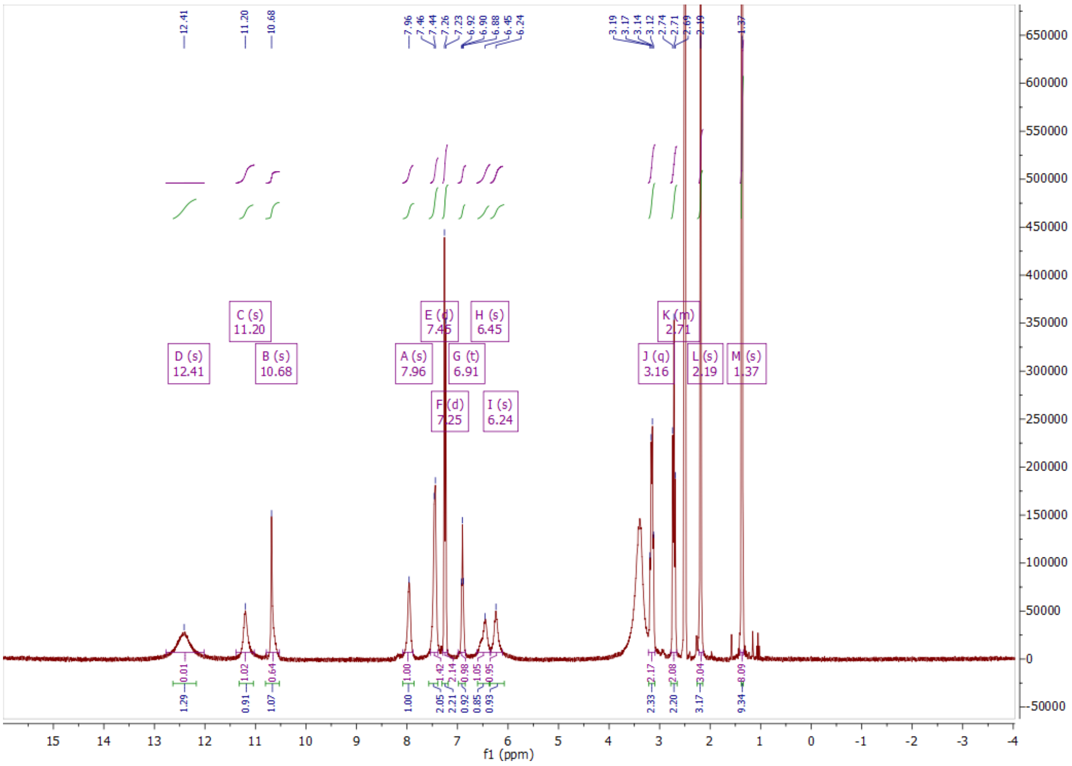

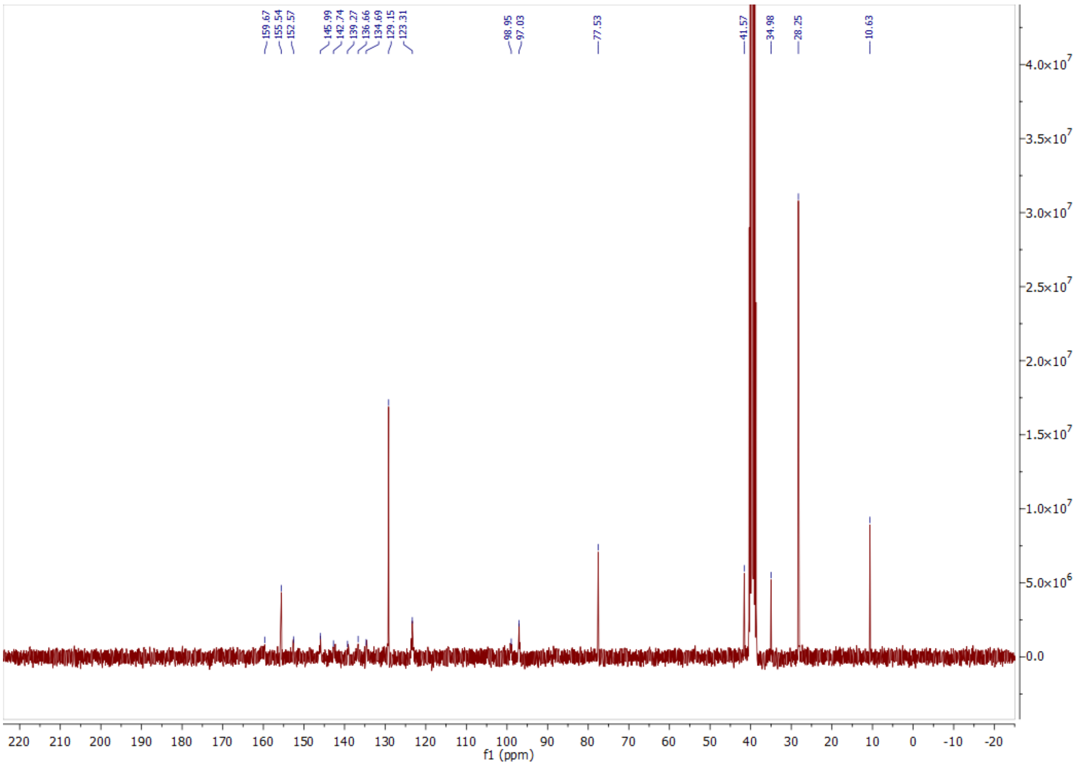
159.67
155.54
152.57
145.99
142.74
139.27
136.66
134.69
129.15
123.31
98.95
97.03
77.53
41.57
34.98
28.25
10.63
4.0×10^7
3.5×10^7
3.0×10^7
2.5×10^7
2.0×10^7
1.5×10^7
1.0×10^7
5.0×10^6
0.0
220 210 200 190 180 170 160 150 140 130 120 110 100 90 80 70 60 50 40 30 20 10 0 -10 -20
f1 (ppm)

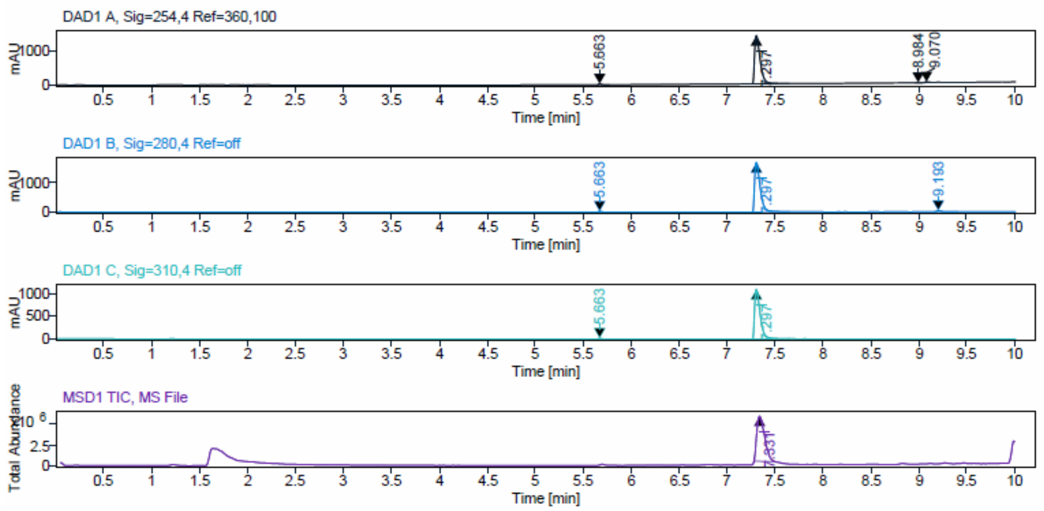
DAD1 A, Sig=254,4 Ref=360,100
mAU
1000
0
5.663
7.297
8.984
9.070
Time [min]
DAD1 B, Sig=280,4 Ref=off
mAU
1000
0
5.663
7.297
9.193
Time [min]
DAD1 C, Sig=310,4 Ref=off
mAU
1000
500
0
5.663
7.297
Time [min]
MSD1 TIC, MS File
Total Abundance
x10 6
2.5
0
7.331
Time [min]
0.5 1 1.5 2 2.5 3 3.5 4 4.5 5 5.5 6 6.5 7 7.5 8 8.5 9 9.5 10

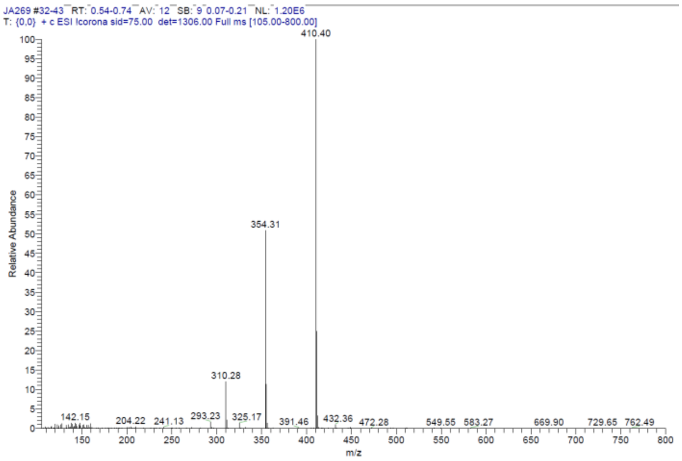
JA269 #32-43 RT: 0.54-0.74 AV: 12 SB: 9 0.07-0.21 NL: 1.20E6
T: {0,0} + c ESI Icorona sid=75.00 det=1306.00 Full ms [105.00-800.00]
410.40
354.31
310.28
142.15
204.22
241.13
293.23
325.17
391.46
432.36
472.28
549.55
583.27
669.90
729.65
762.49
Relative Abundance
m/z
100 95 90 85 80 75 70 65 60 55 50 45 40 35 30 25 20 15 10 5 0
150 200 250 300 350 400 450 500 550 600 650 700 750 800

^{1}H, ^{13}C NMR, HPLC, and ESI data of compound **93b**

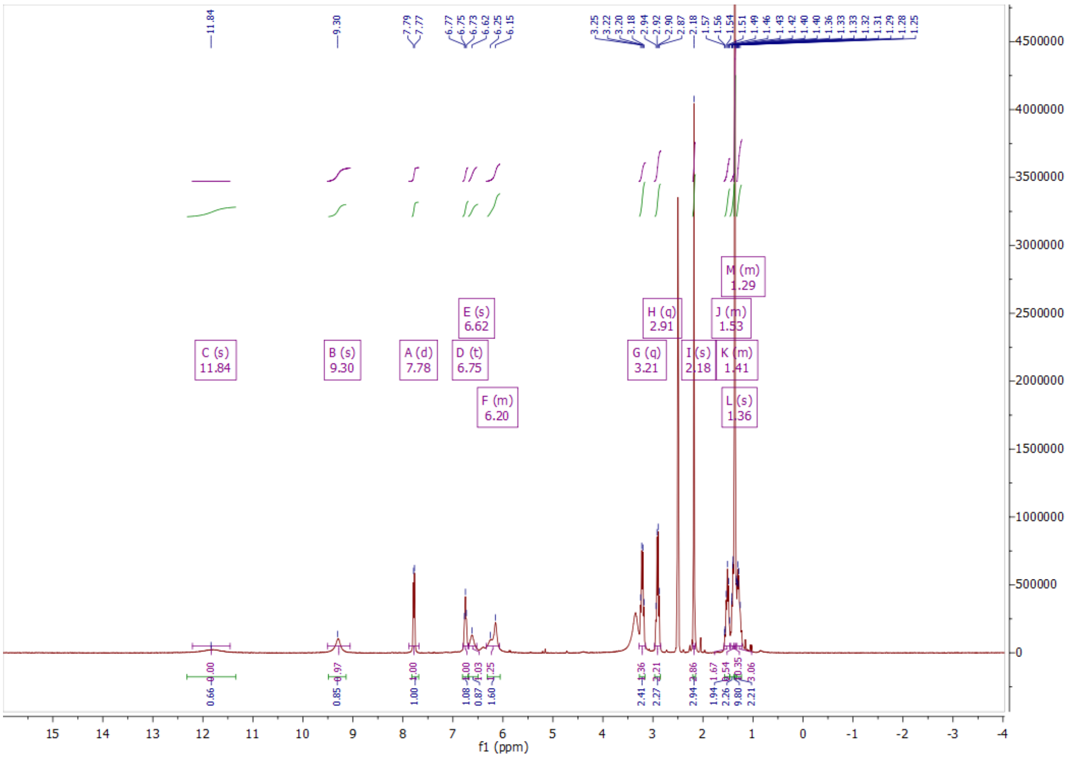

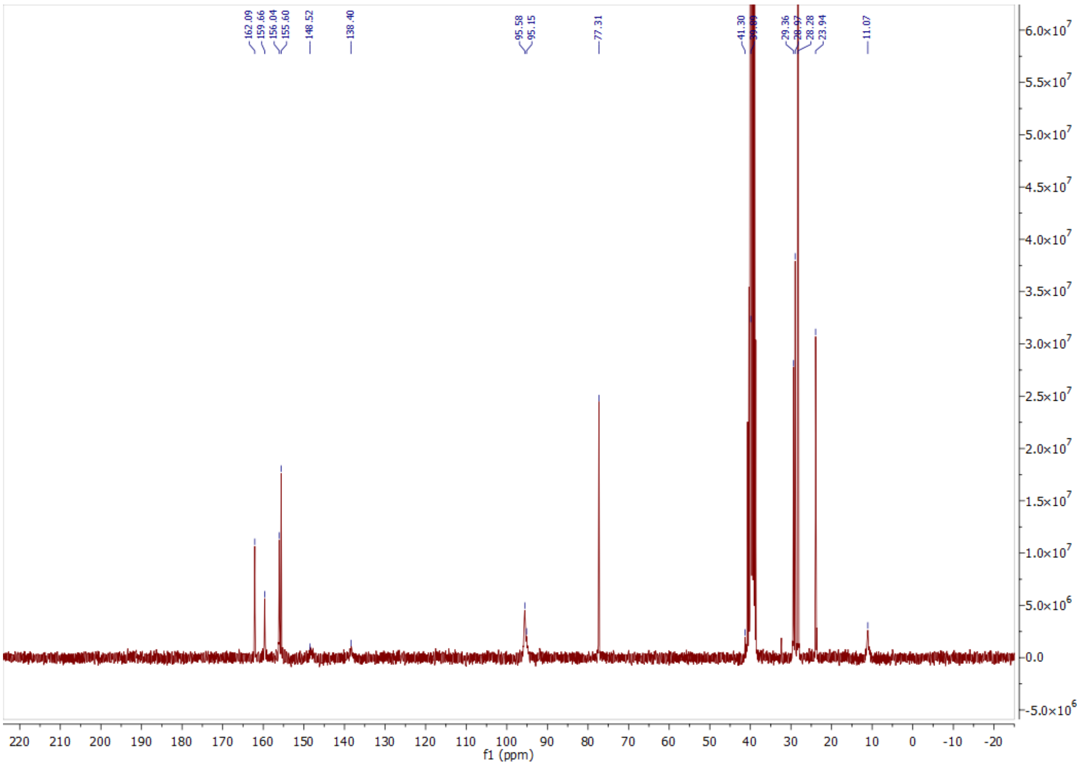

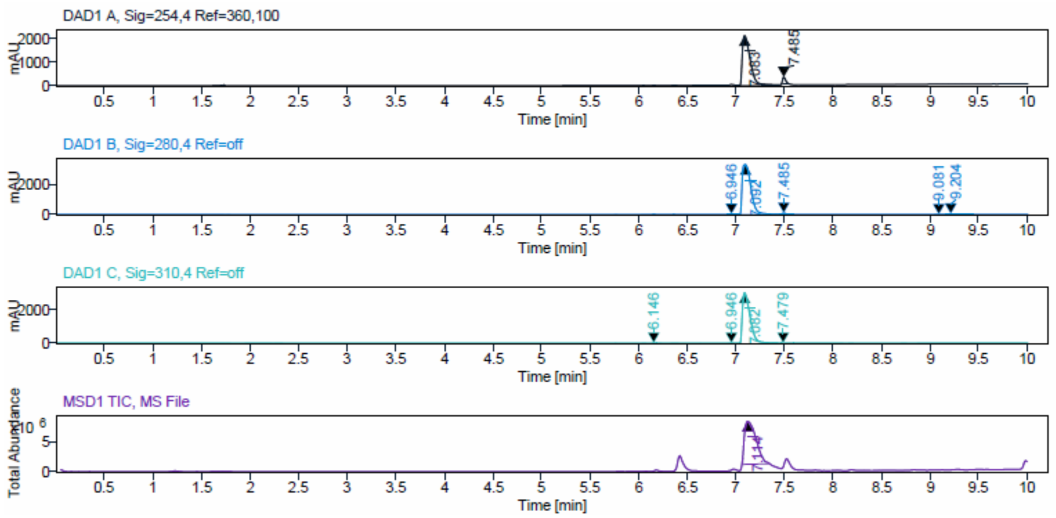

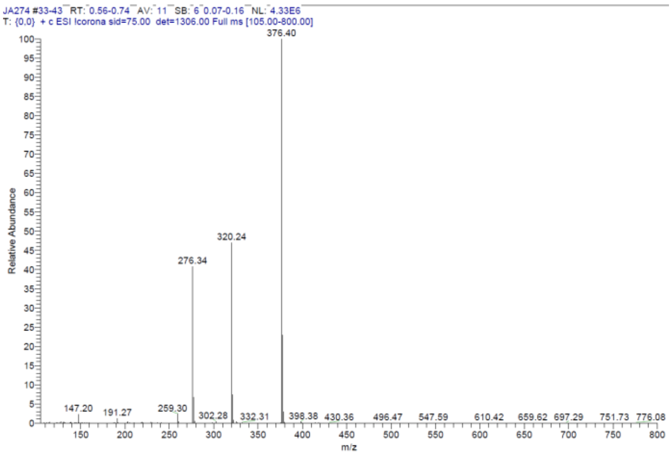

^{1}H, ^{13}C NMR, HPLC, and ESI data of compound **94a**

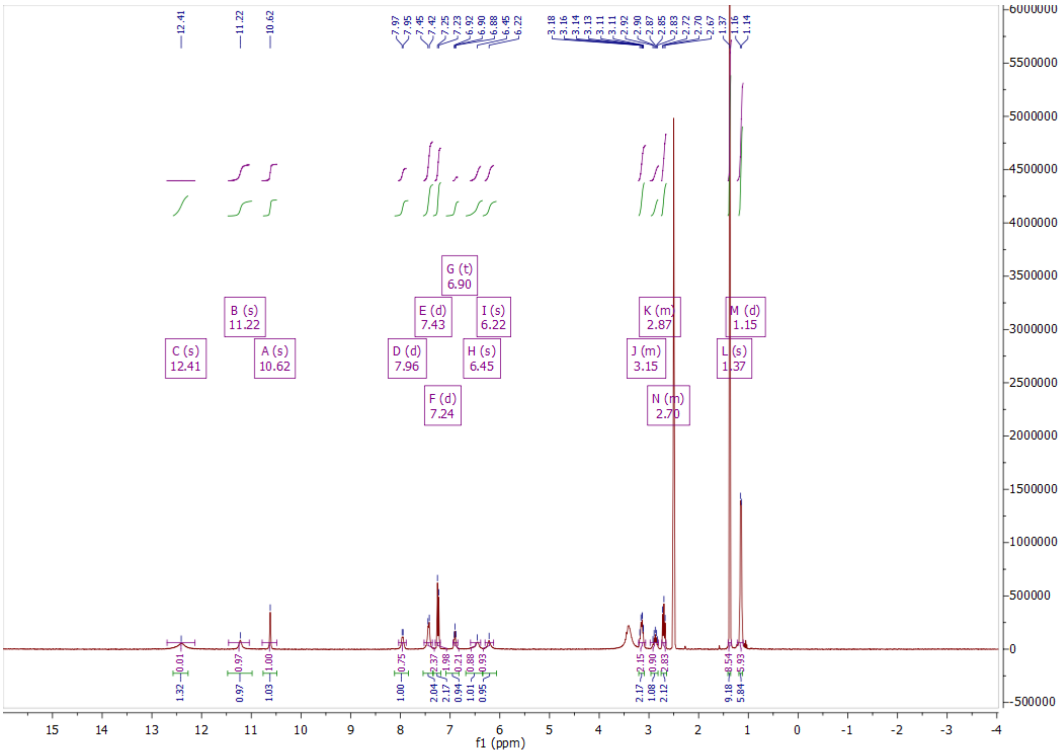

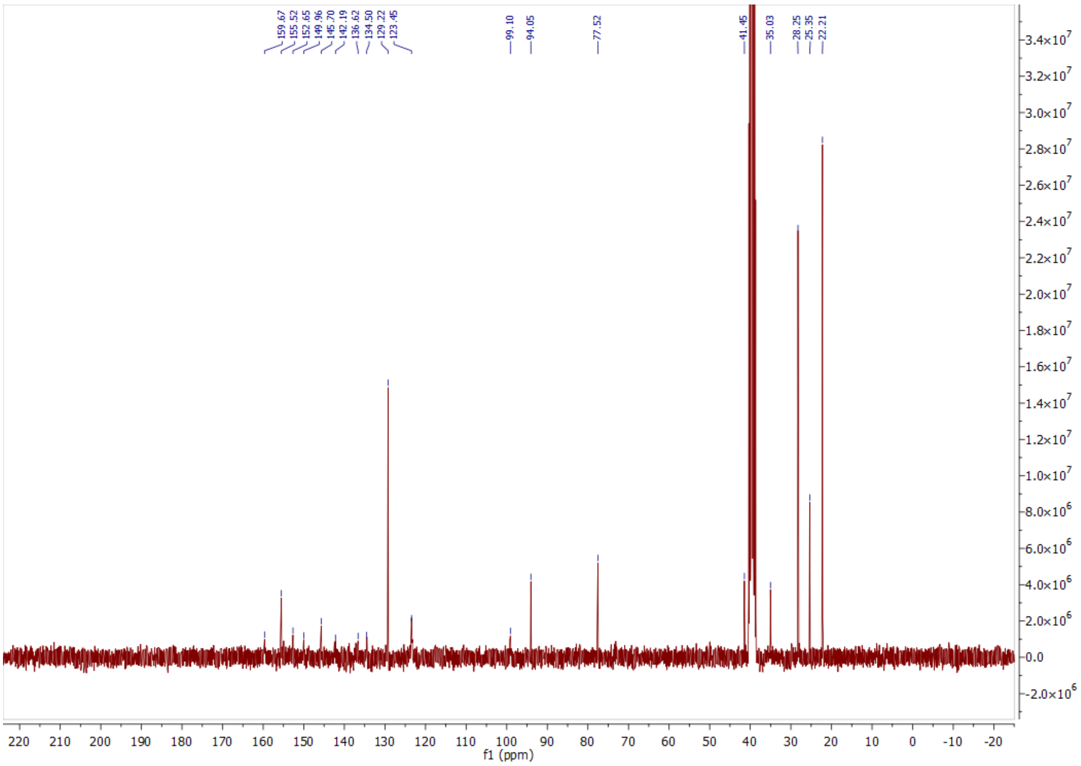

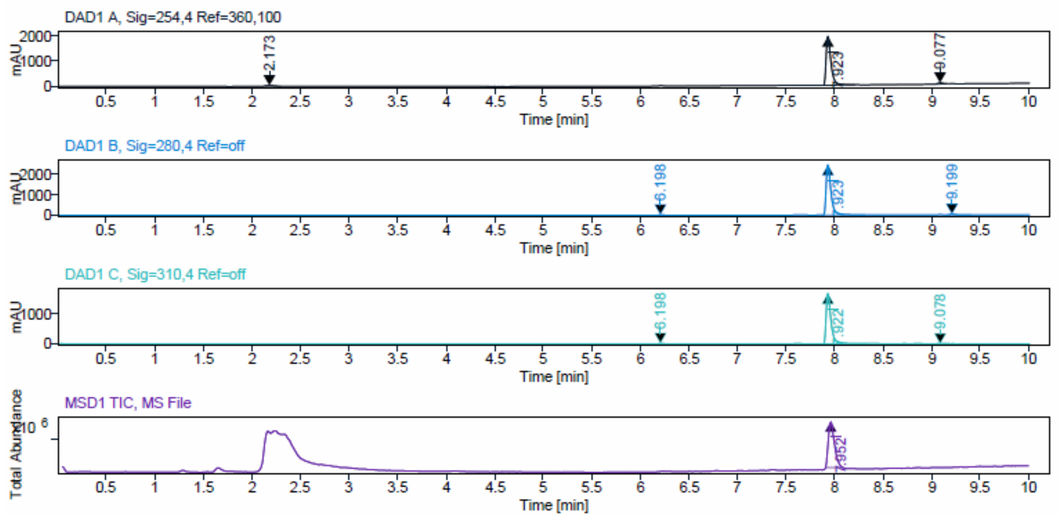

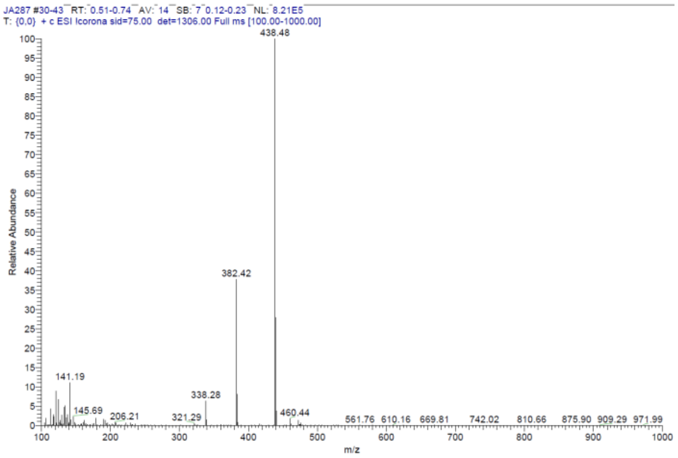
JA287 #30-43 RT: 0.51-0.74 AV: 14 SB: 7 0.12-0.23 NL: 8.21E5
T: {0,0} + c ESI Icorona sid=75.00 det=1306.00 Full ms [100.00-1000.00]

^{1}H, ^{13}C NMR, HPLC, and ESI data of compound **94b**

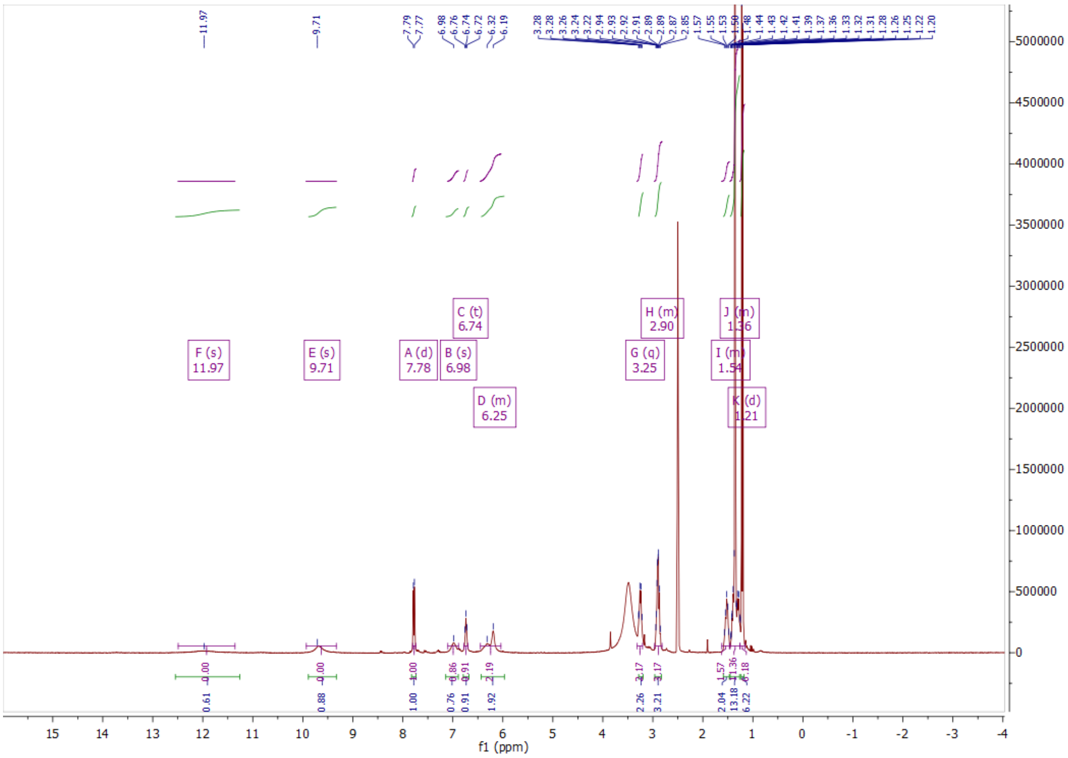

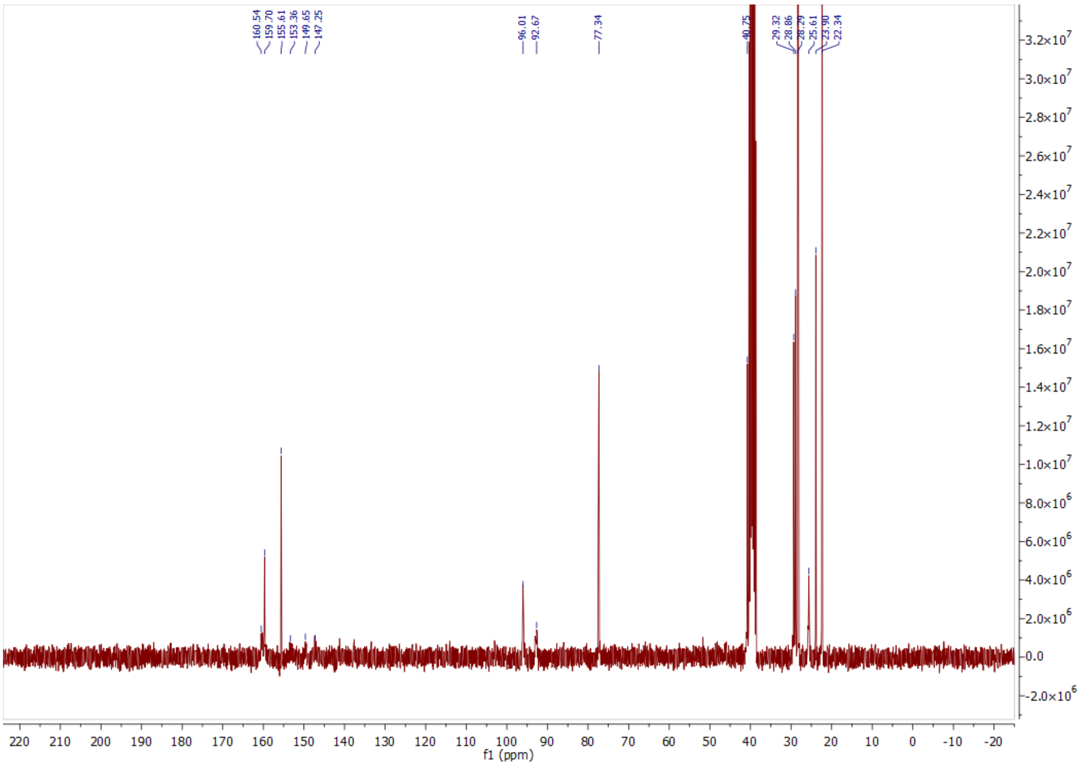

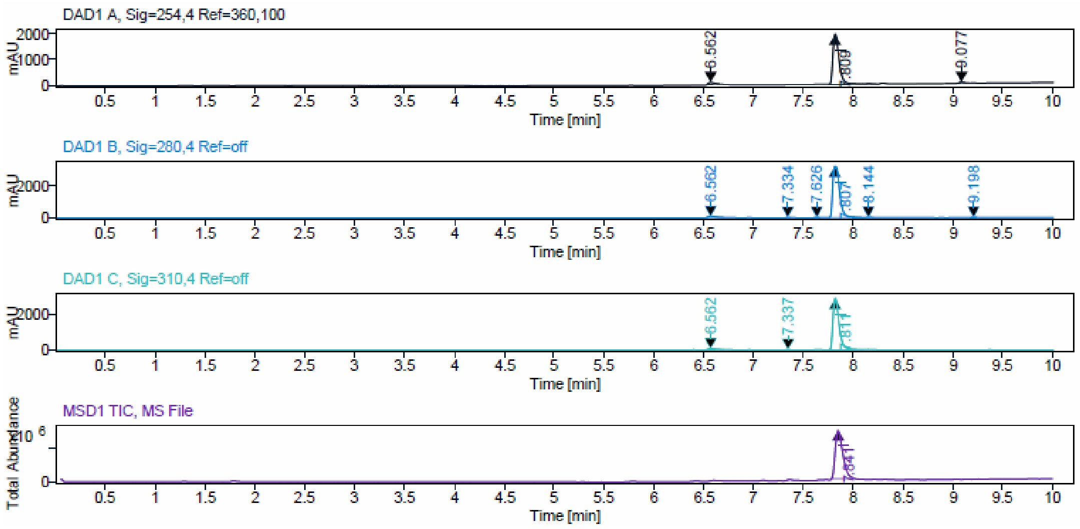

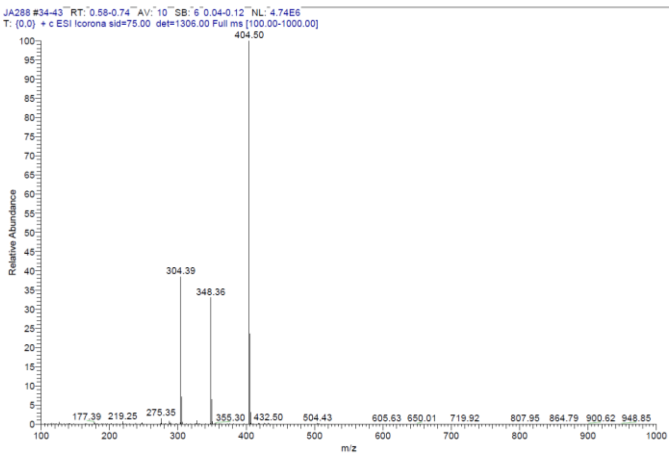

^{1}H, ^{13}C NMR, HPLC, and ESI data of compound **95a**

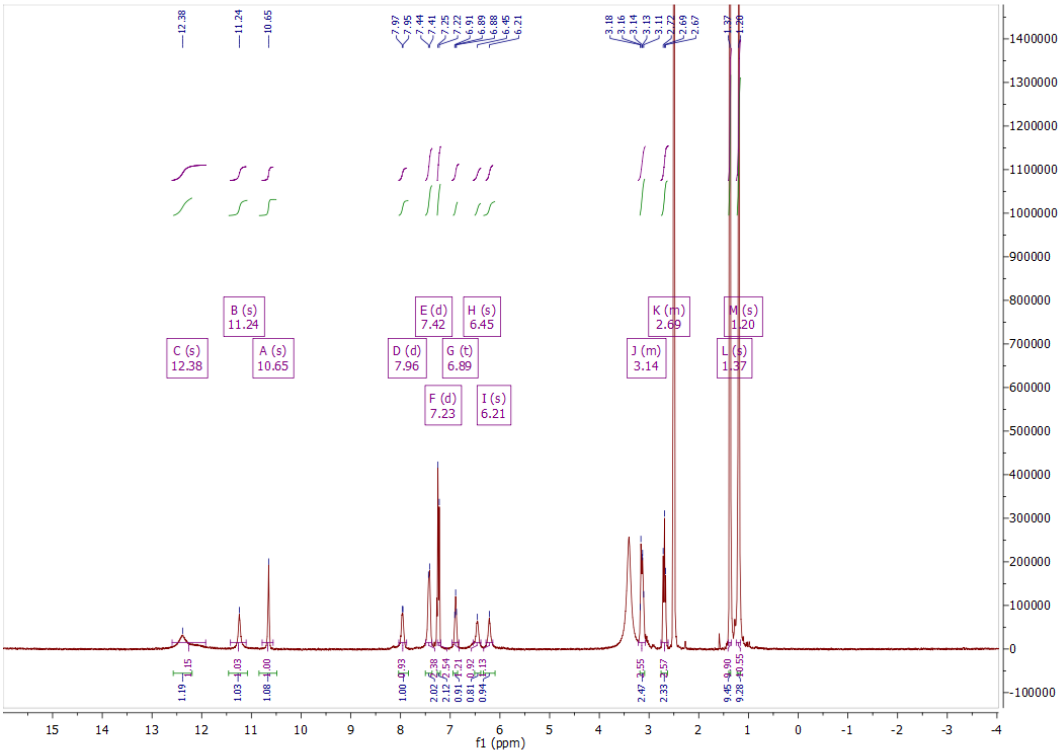

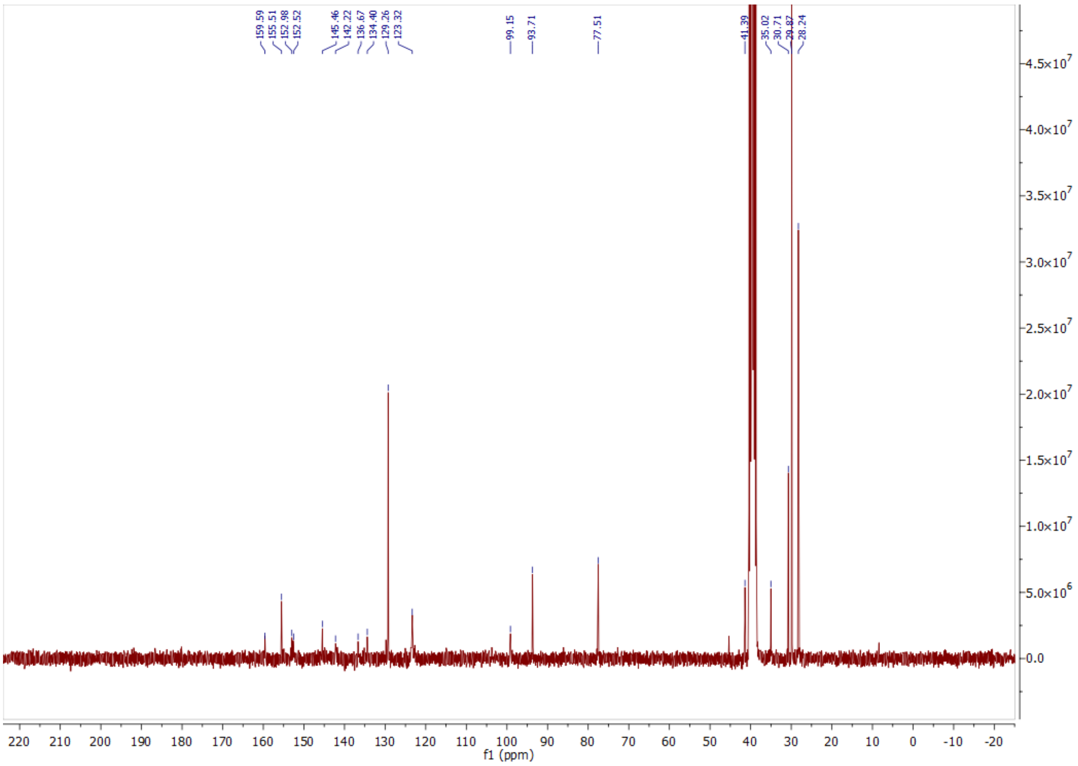
159.59
155.51
152.98
152.52
145.46
142.22
136.67
134.40
129.26
123.32
99.15
93.71
77.51
41.39
35.02
30.71
29.87
28.24
4.5×10^7
4.0×10^7
3.5×10^7
3.0×10^7
2.5×10^7
2.0×10^7
1.5×10^7
1.0×10^7
5.0×10^6
0.0
220 210 200 190 180 170 160 150 140 130 120 110 100 90 80 70 60 50 40 30 20 10 0 -10 -20
f1 (ppm)

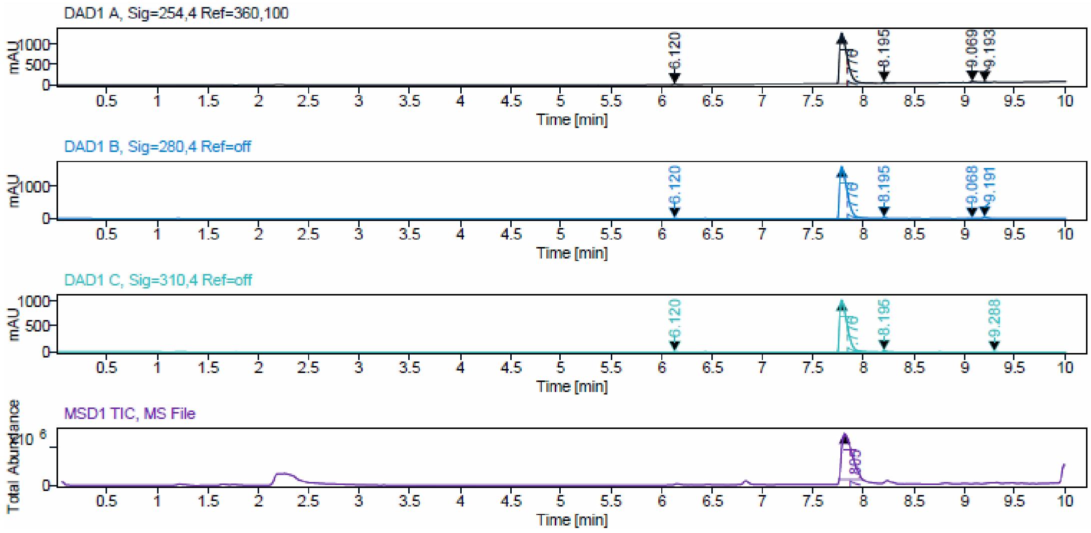
DAD1 A, Sig=254,4 Ref=360,100
mAU
1000
500
0
6.120
7.776
8.195
9.069
9.193
DAD1 B, Sig=280,4 Ref=off
mAU
1000
0
6.120
7.776
8.195
9.068
9.191
DAD1 C, Sig=310,4 Ref=off
mAU
1000
500
0
6.120
7.776
8.195
9.288
MSD1 TIC, MS File
Total Abundance
10^6
0
7.809
0.5 1 1.5 2 2.5 3 3.5 4 4.5 5 5.5 6 6.5 7 7.5 8 8.5 9 9.5 10
Time [min]

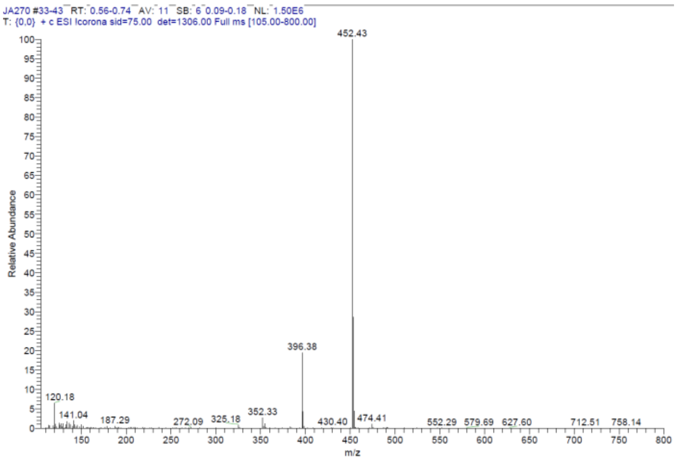
JA270 #33-43 RT: 0.56-0.74 AV: 11 SB: 6 0.09-0.18 NL: 1.50E6
T: {0,0} + c ESI Icorona sid=75.00 det=1306.00 Full ms [105.00-800.00]
Relative Abundance
100 95 90 85 80 75 70 65 60 55 50 45 40 35 30 25 20 15 10 5 0
452.43
396.38
120.18
141.04
187.29
272.09
325.18
352.33
430.40
474.41
552.29
579.69
627.60
712.51
758.14
150 200 250 300 350 400 450 500 550 600 650 700 750 800
m/z

^{1}H, ^{13}C NMR, HPLC, and ESI data of compound **95b**

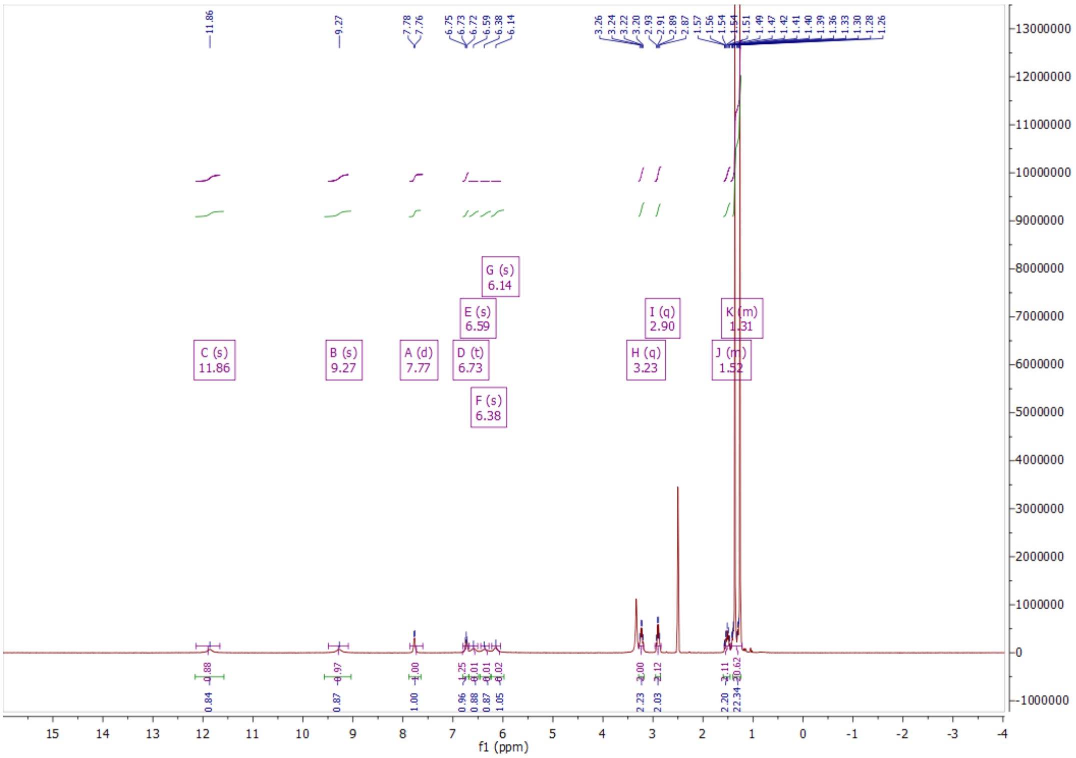

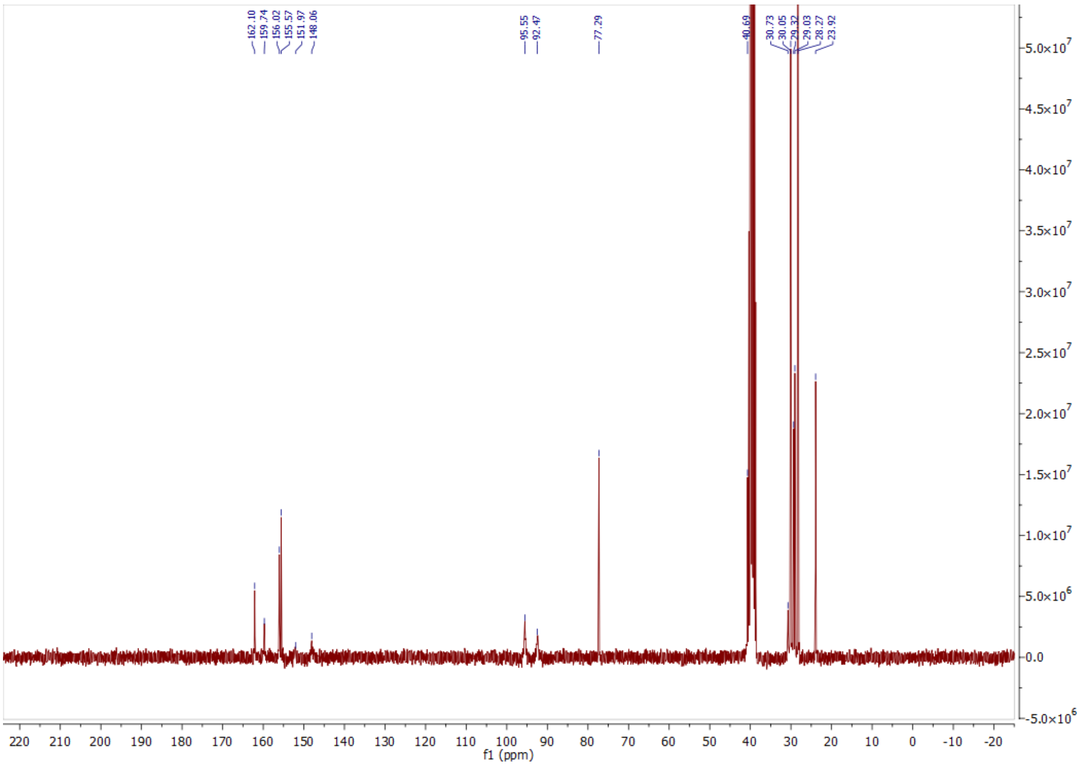

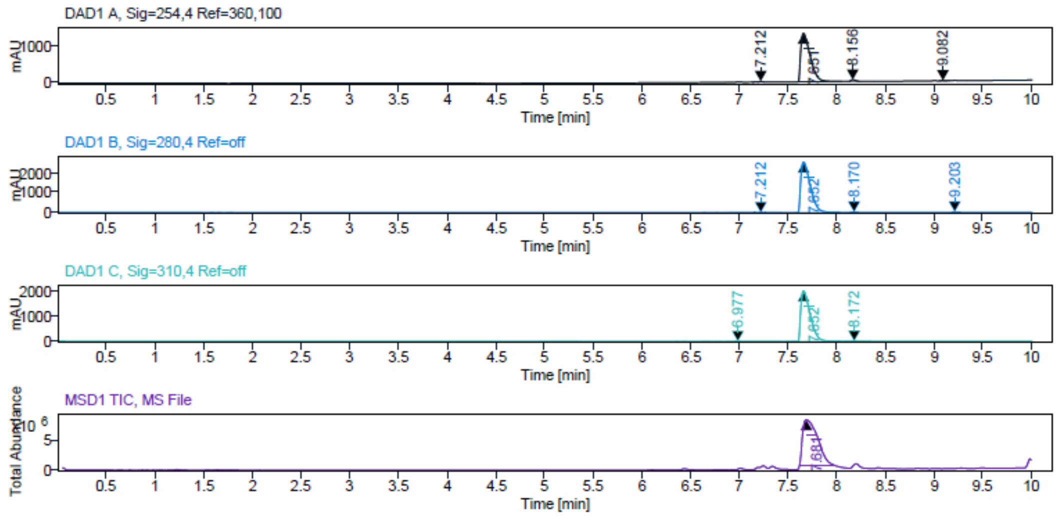

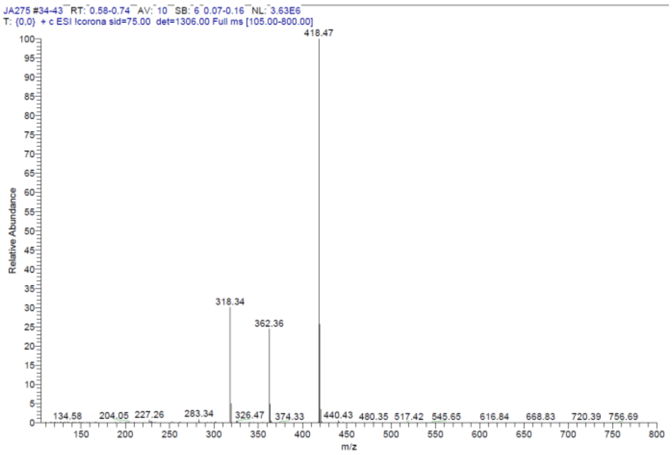

^{1}H, ^{13}C NMR, HPLC, and ESI data of compound **95c**

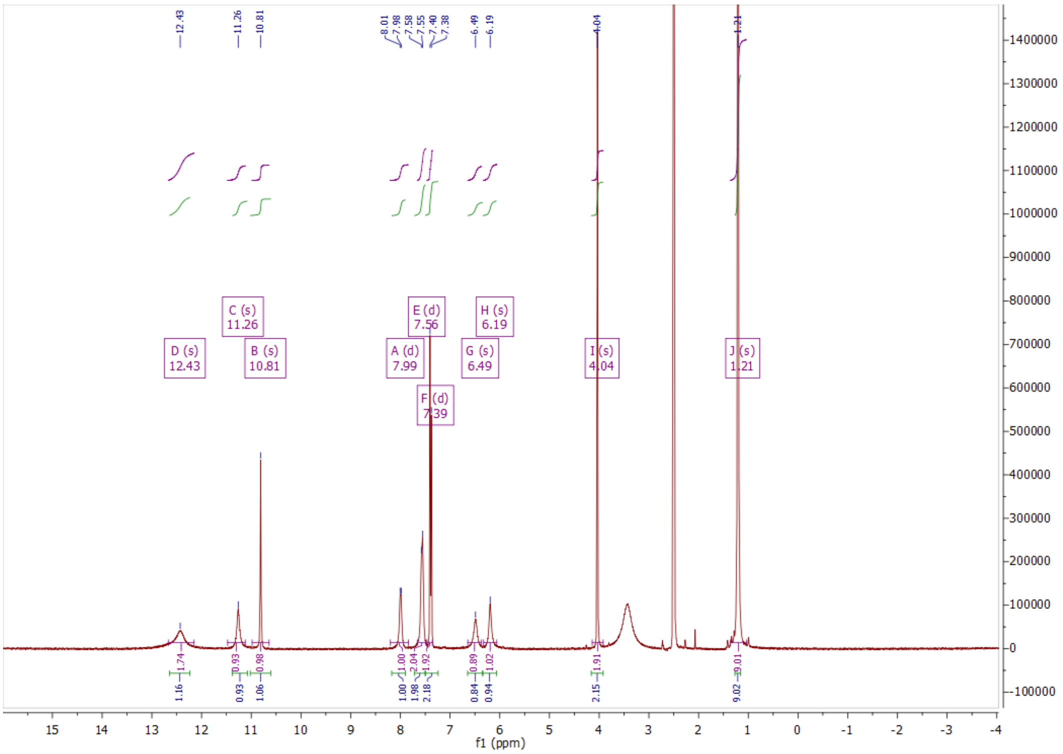

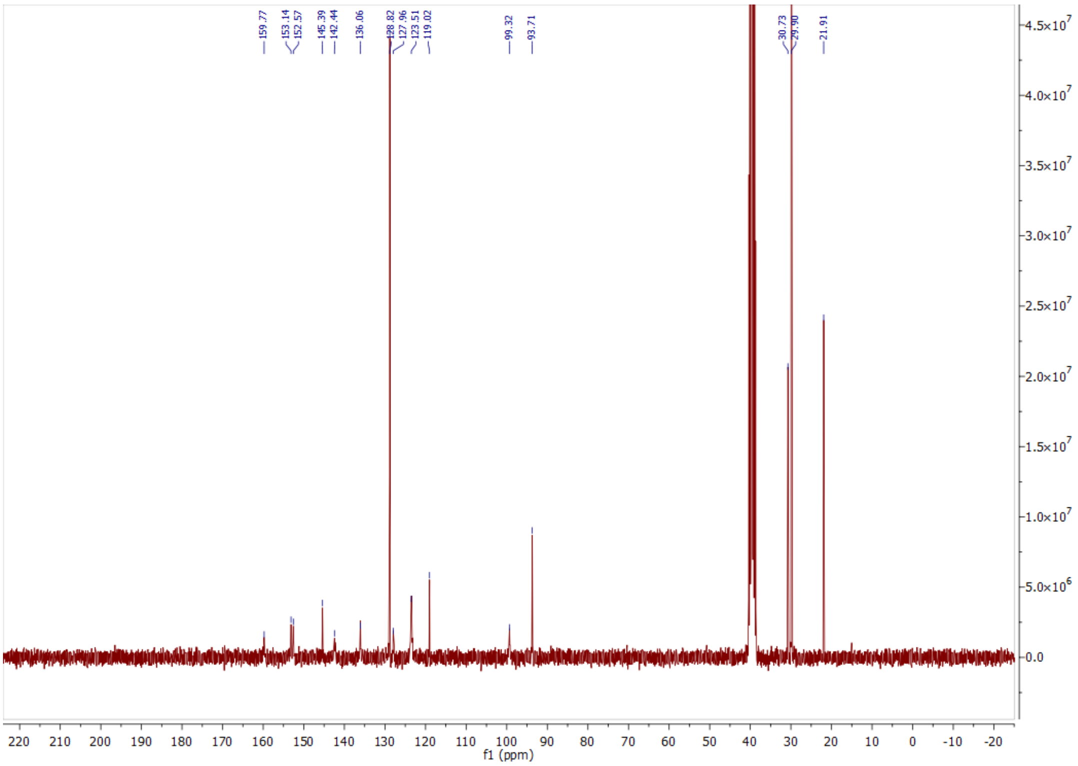
159.77
153.14
152.57
145.39
142.44
136.06
128.82
127.96
123.51
119.02
99.32
93.71
30.73
29.90
21.91
f1 (ppm)

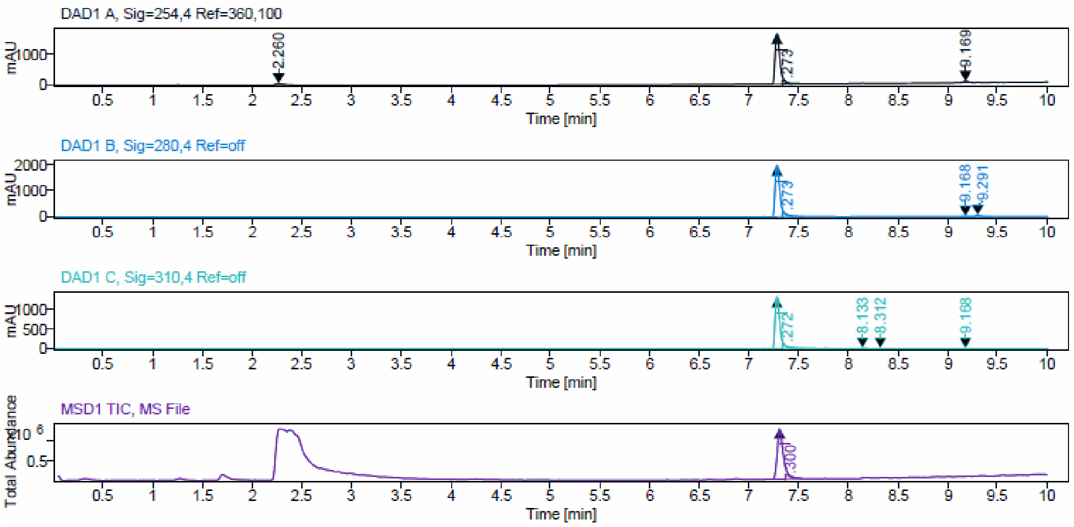
DAD1 A, Sig=254,4 Ref=360,100
DAD1 B, Sig=280,4 Ref=off
DAD1 C, Sig=310,4 Ref=off
MSD1 TIC, MS File
mAU
Total Abundance
Time [min]
2.260
7.273
9.169
9.168
9.291
7.272
8.133
8.312
7.300

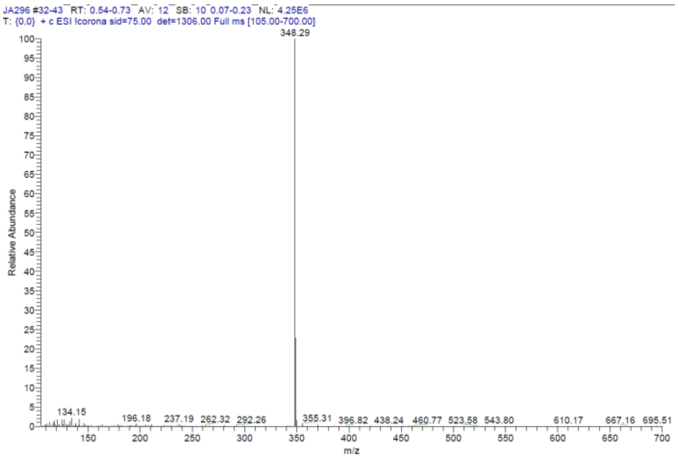
JA296 #32-43 RT: 0.54-0.73 AV: 12 SB: 10 0.07-0.23 NL: 4.25E6
T: {0,0} + c ESI Icorona sid=75.00 det=1306.00 Full ms [105.00-700.00]
Relative Abundance
m/z
348.29
134.15
196.18
237.19
262.32
292.26
355.31
396.82
438.24
460.77
523.58
543.80
610.17
667.16
695.51

^{1}H, ^{13}C NMR, HPLC, and ESI data of compound **96a**

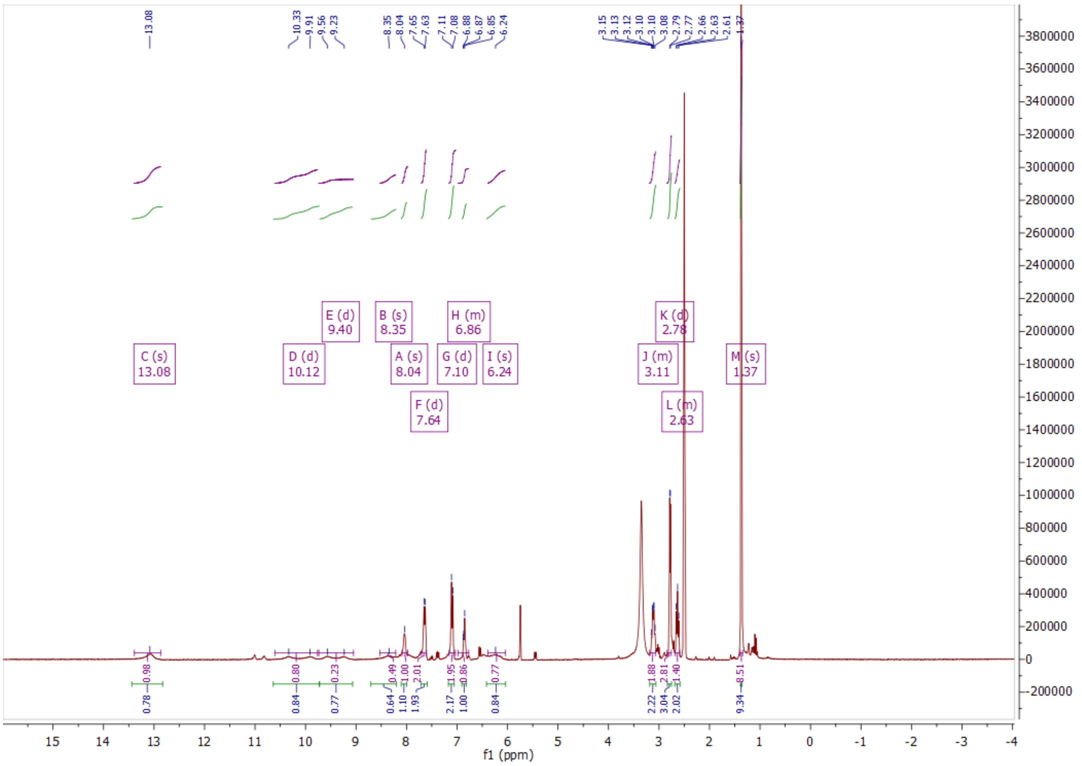

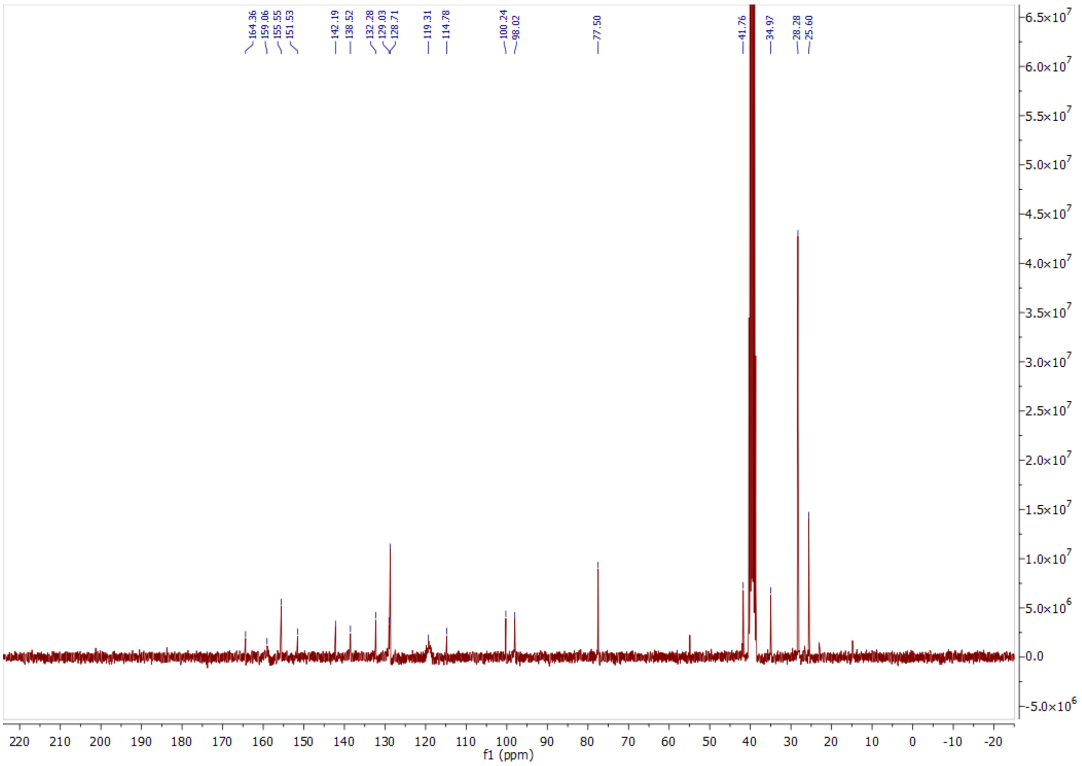

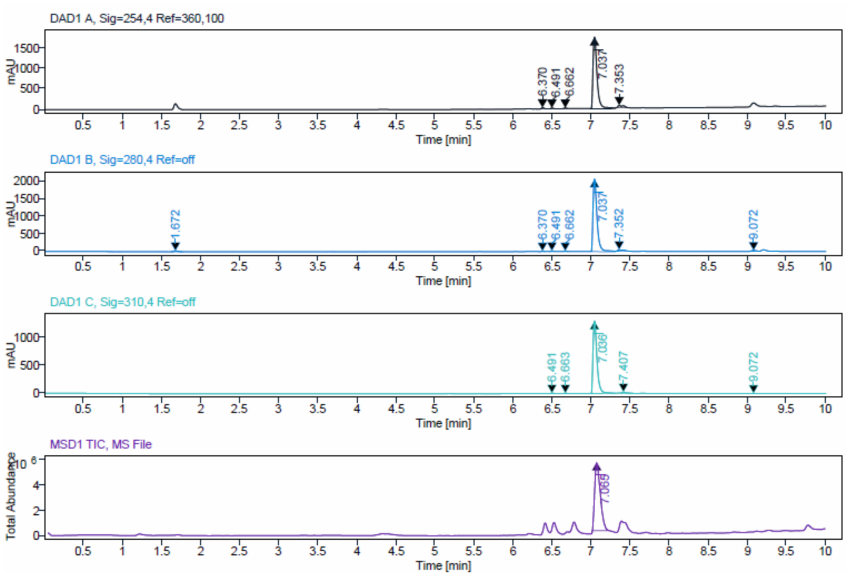

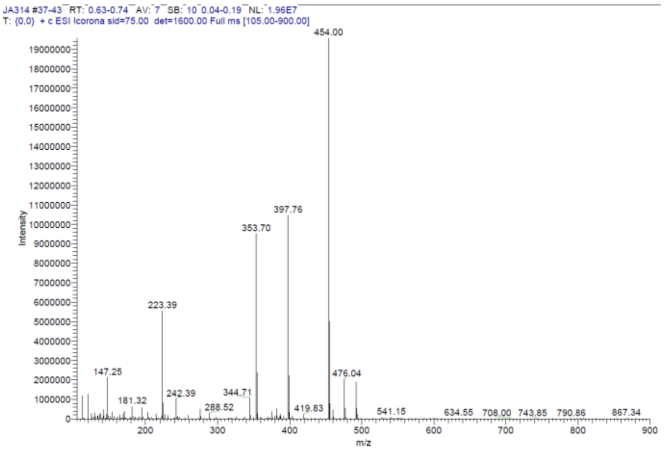

^{1}H, ^{13}C NMR, HPLC, and ESI data of compound **96b**

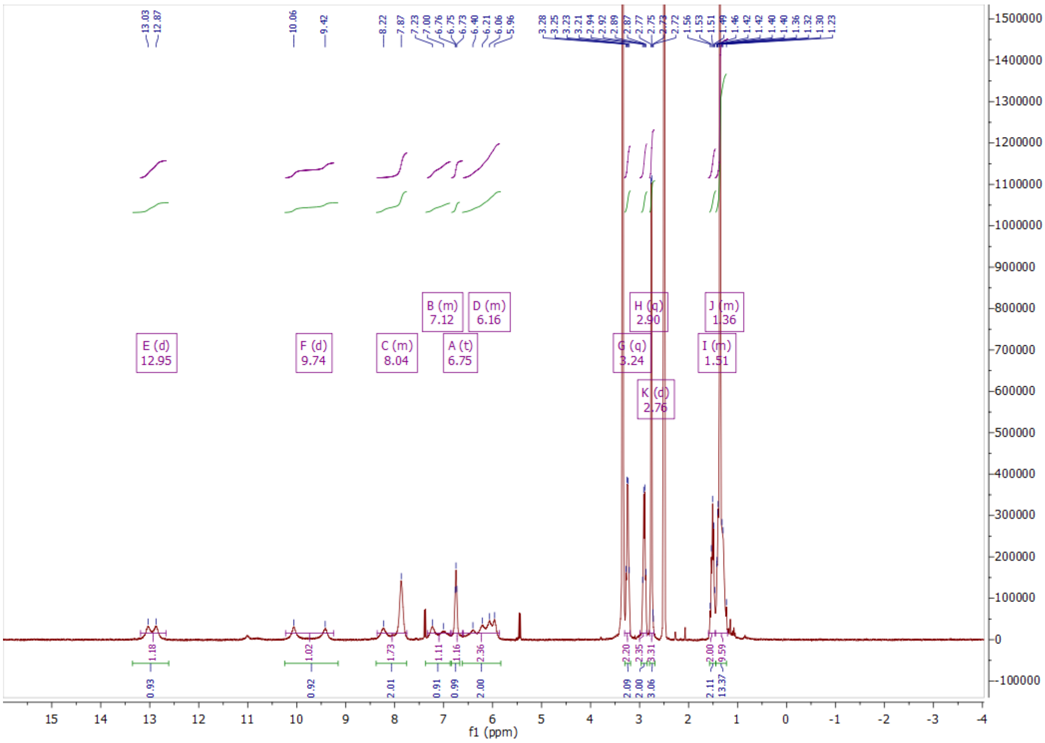

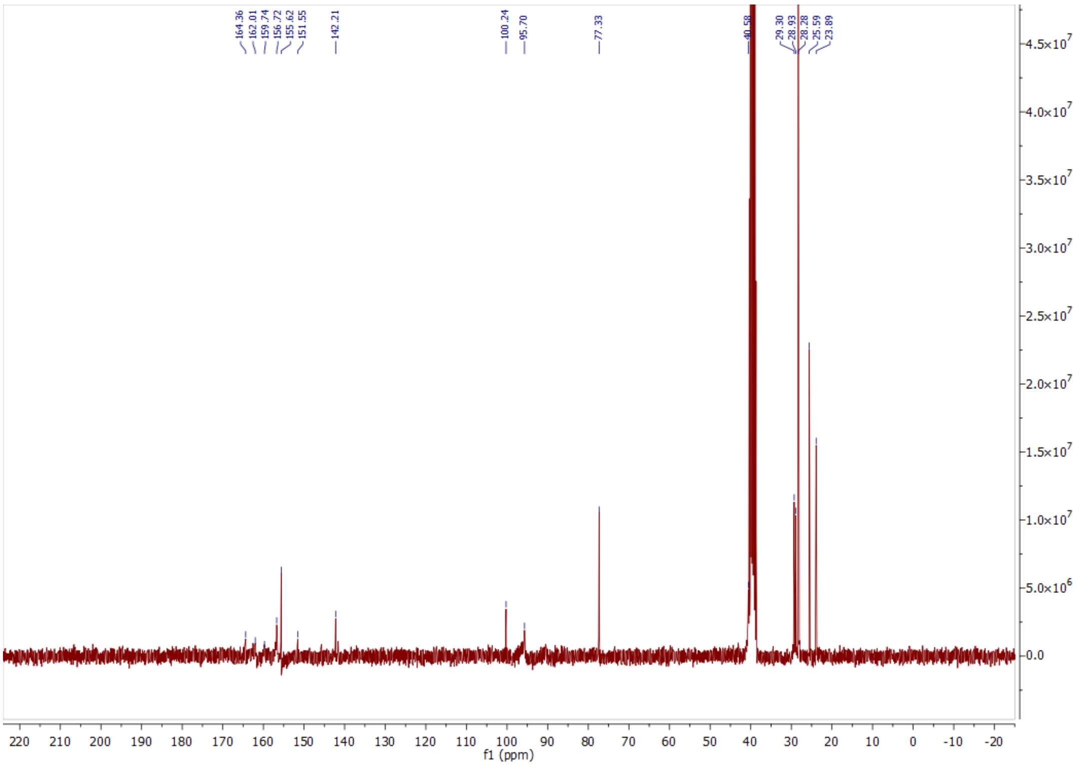
164.36
162.01
159.74
156.72
155.62
151.55
142.21
100.24
95.70
77.33
40.58
29.30
28.93
28.28
25.59
23.89
4.5×10^7
4.0×10^7
3.5×10^7
3.0×10^7
2.5×10^7
2.0×10^7
1.5×10^7
1.0×10^7
5.0×10^6
0.0
220 210 200 190 180 170 160 150 140 130 120 110 100 90 80 70 60 50 40 30 20 10 0 -10 -20
f1 (ppm)

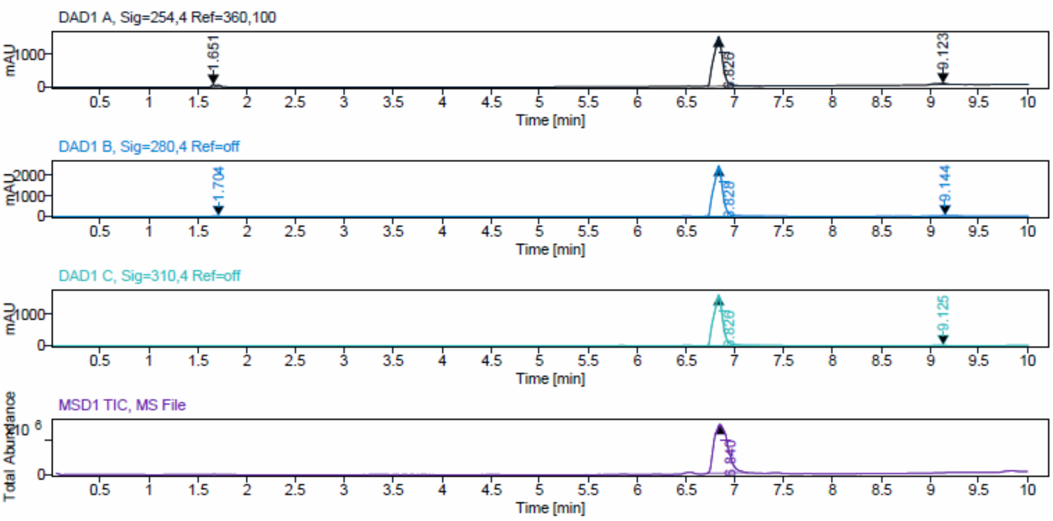
DAD1 A, Sig=254,4 Ref=360,100
mAU
1000
0
1.651
9.123
DAD1 B, Sig=280,4 Ref=off
mAU
2000
1000
0
1.704
9.144
DAD1 C, Sig=310,4 Ref=off
mAU
1000
0
9.125
MSD1 TIC, MS File
Total Abundance
10 6
0
0.5 1 1.5 2 2.5 3 3.5 4 4.5 5 5.5 6 6.5 7 7.5 8 8.5 9 9.5 10
Time [min]

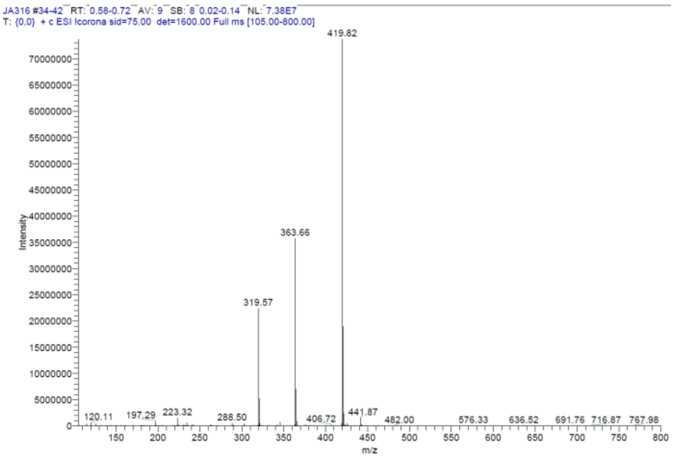
JA316 #34-42 RT: 0.58-0.72 AV: 9 SB: 8 0.02-0.14 NL: 7.38E7
T: {0,0} + c ESI Icorona sid=75.00 det=1600.00 Full ms [105.00-800.00]
419.82
363.66
319.57
120.11
197.29
223.32
288.50
406.72
441.87
482.00
576.33
636.52
691.76
716.87
767.98
Intensity
70000000
65000000
60000000
55000000
50000000
45000000
40000000
35000000
30000000
25000000
20000000
15000000
10000000
5000000
0
150 200 250 300 350 400 450 500 550 600 650 700 750 800
m/z

^{1}H, ^{13}C NMR, HPLC, and ESI data of compound **96c**

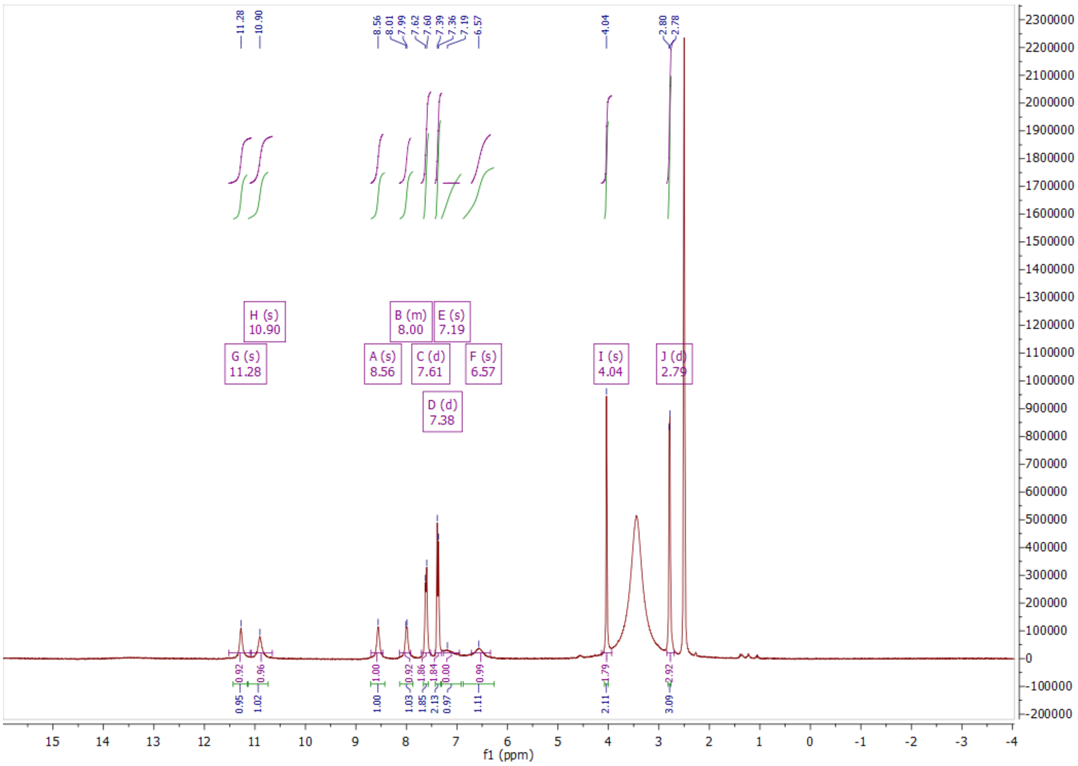

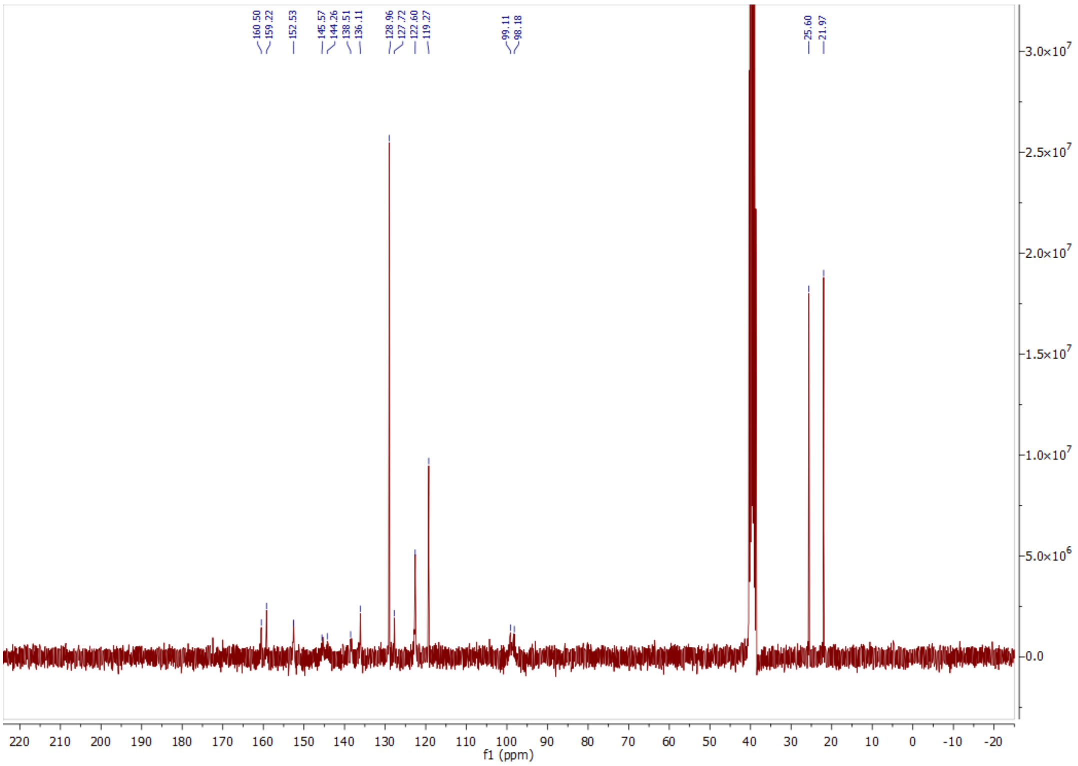

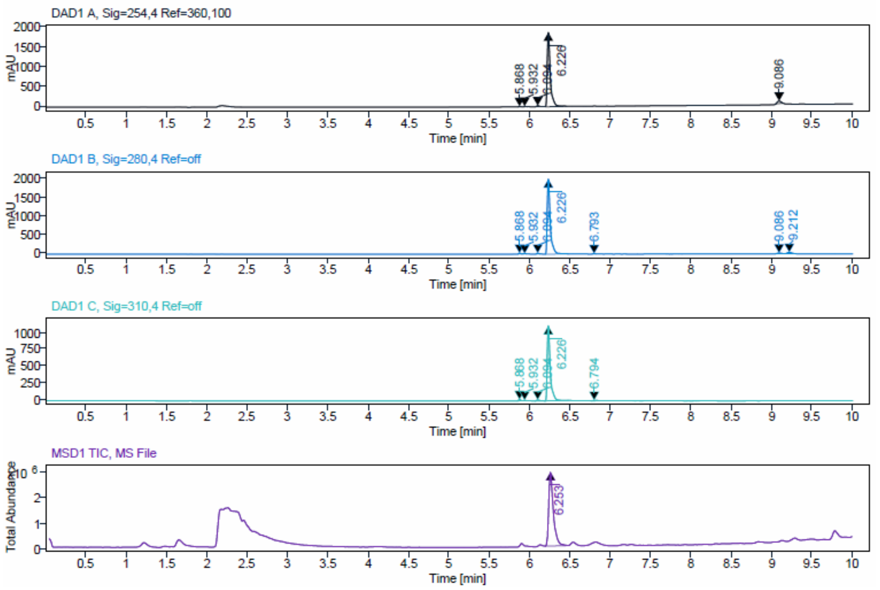
DAD1 A, Sig=254,4 Ref=360,100
mAU
5.868
5.932
6.226
9.086
Time [min]
DAD1 B, Sig=280,4 Ref=off
5.868
5.932
6.226
6.793
9.086
9.212
DAD1 C, Sig=310,4 Ref=off
5.868
5.932
6.226
6.794
MSD1 TIC, MS File
Total Abundance
x10 6
6.253

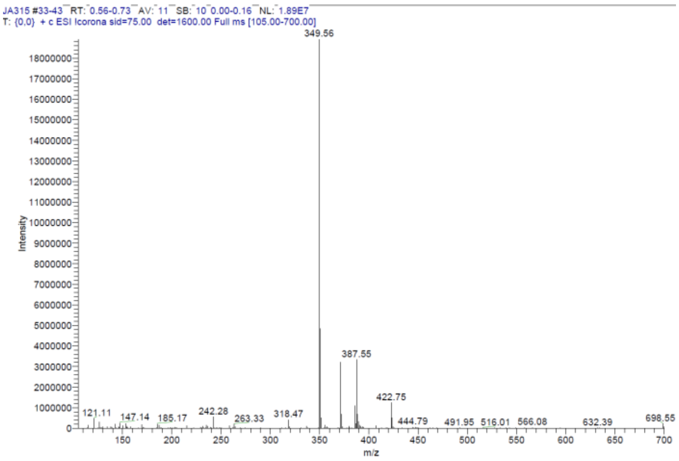
JA315 #33-43 RT: 0.56-0.73 AV: 11 SB: 10 0.00-0.16 NL: 1.89E7
T: {0,0} + c ESI Icorona sid=75.00 det=1600.00 Full ms [105.00-700.00]
Intensity
m/z
349.56
387.55
422.75
121.11
147.14
185.17
242.28
263.33
318.47
444.79
491.95
516.01
566.08
632.39
698.55

^{1}H, ^{13}C NMR, HPLC, and ESI data of compound **97b**

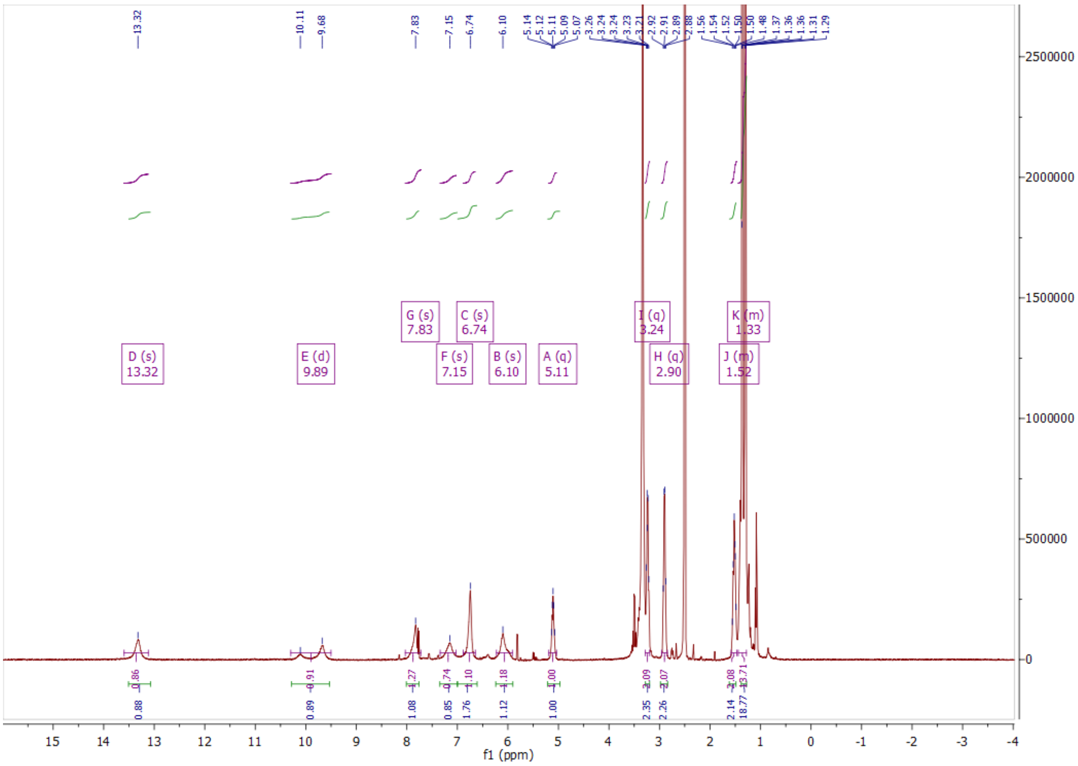

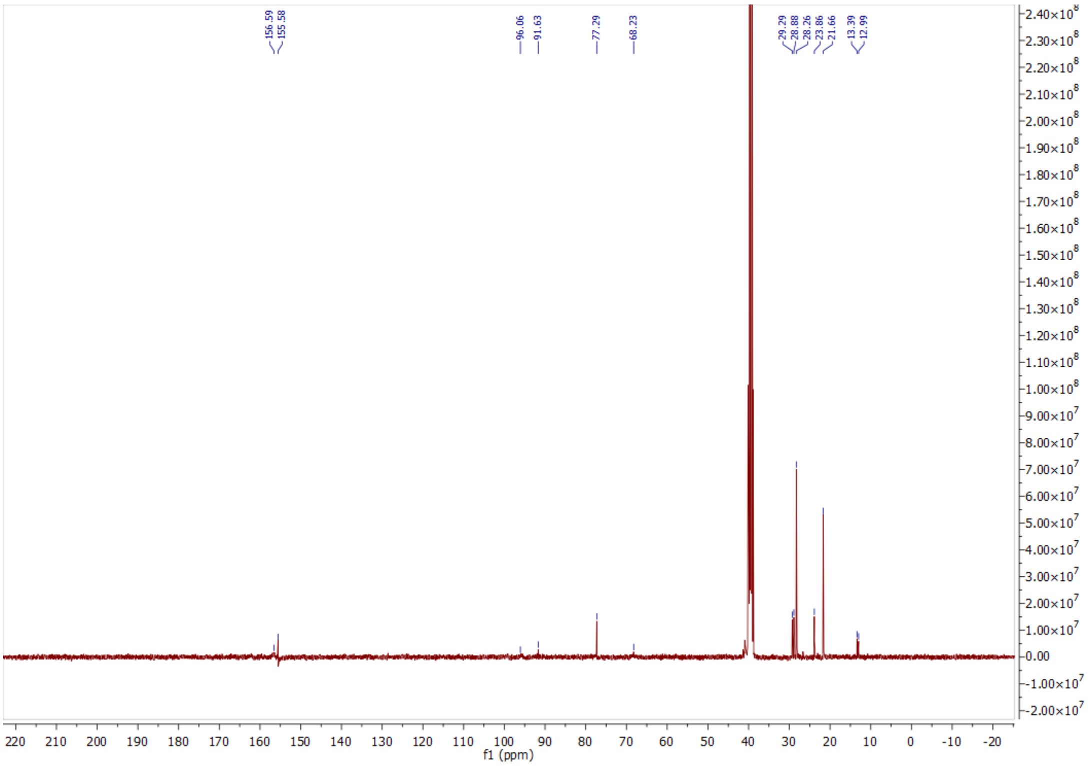

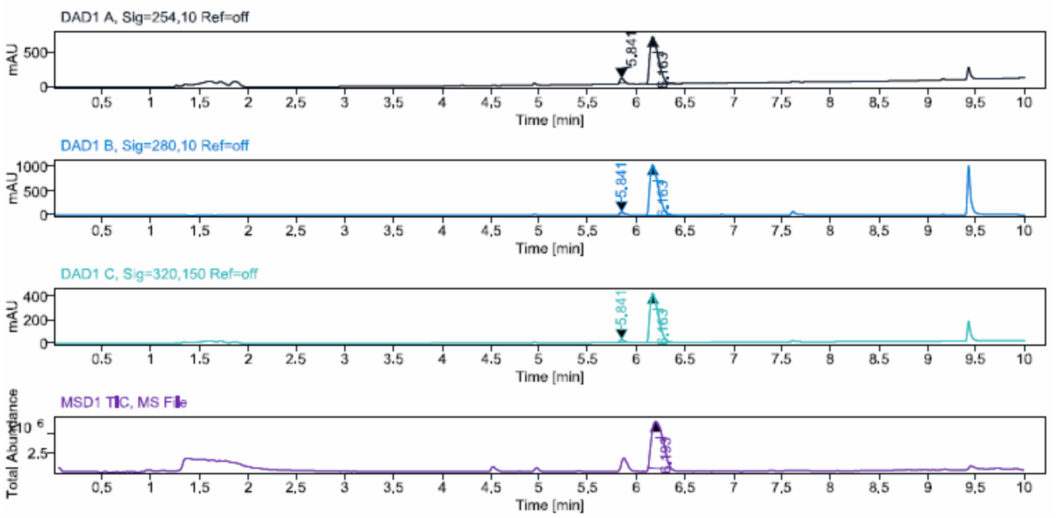

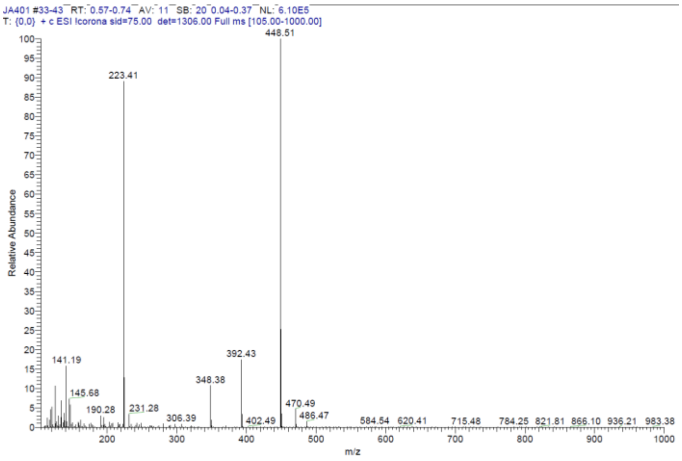

^{1}H, ^{13}C NMR, HPLC, and ESI data of compound **97d**

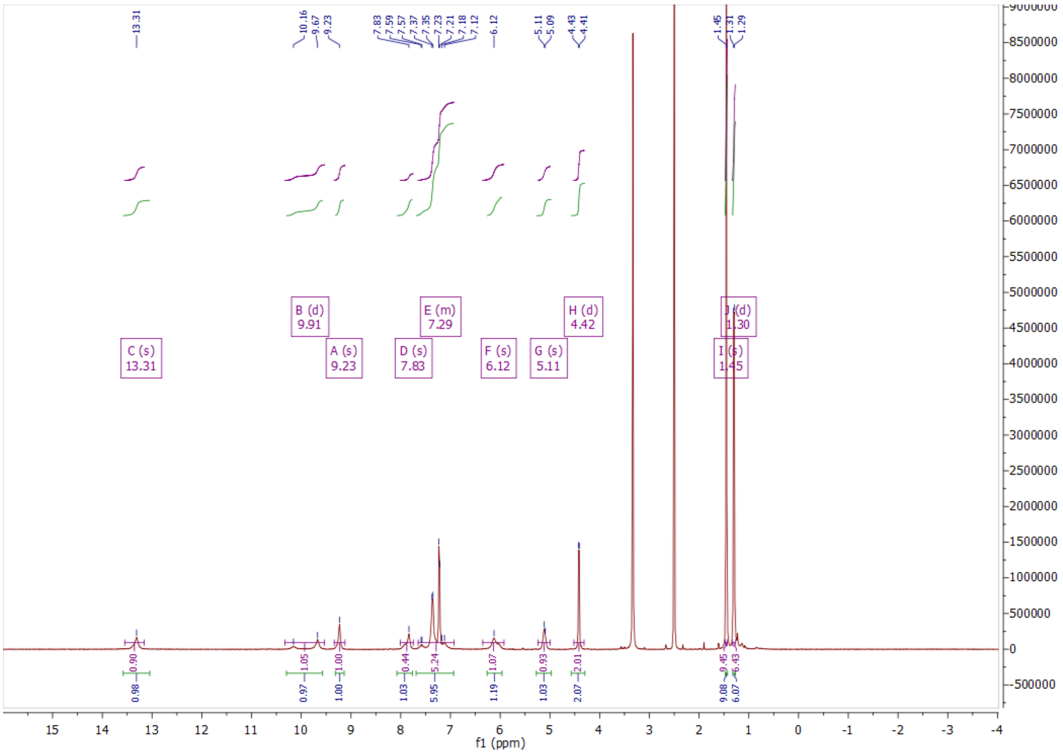

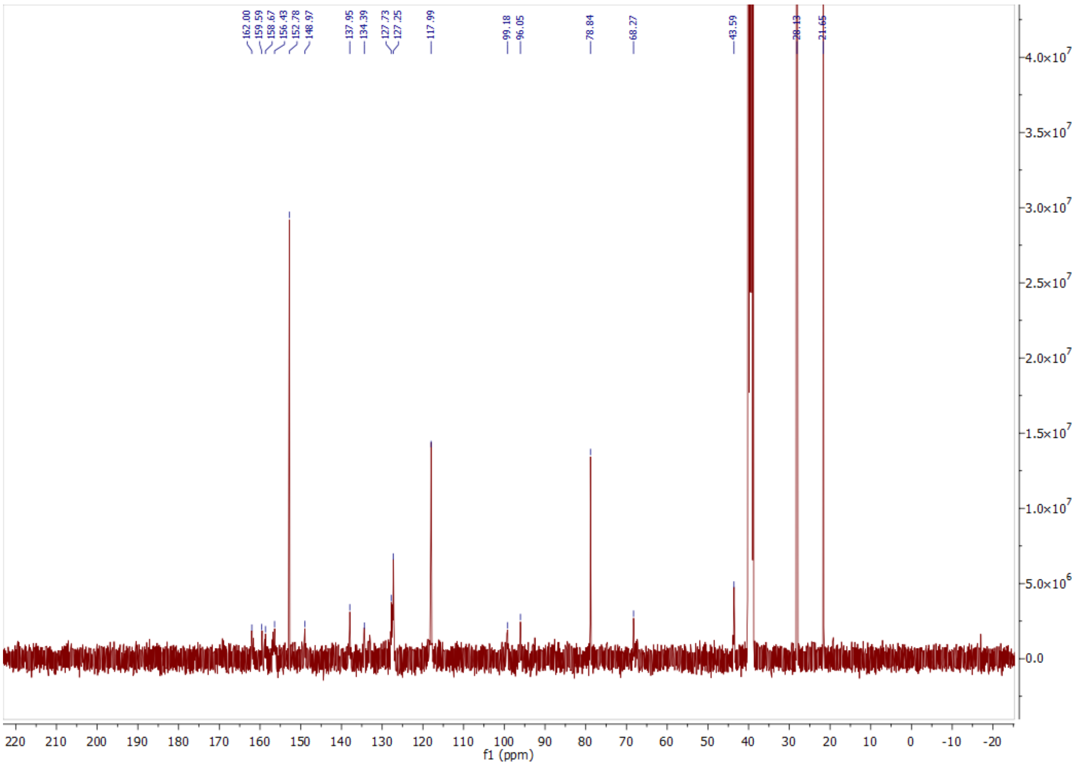
162.00
159.59
158.67
156.43
152.78
148.97
137.95
134.39
127.73
127.25
117.99
99.18
96.05
78.84
68.27
43.59
28.13
21.65
4.0×10^7
3.5×10^7
3.0×10^7
2.5×10^7
2.0×10^7
1.5×10^7
1.0×10^7
5.0×10^6
0.0
220 210 200 190 180 170 160 150 140 130 120 110 100 90 80 70 60 50 40 30 20 10 0 -10 -20
f1 (ppm)

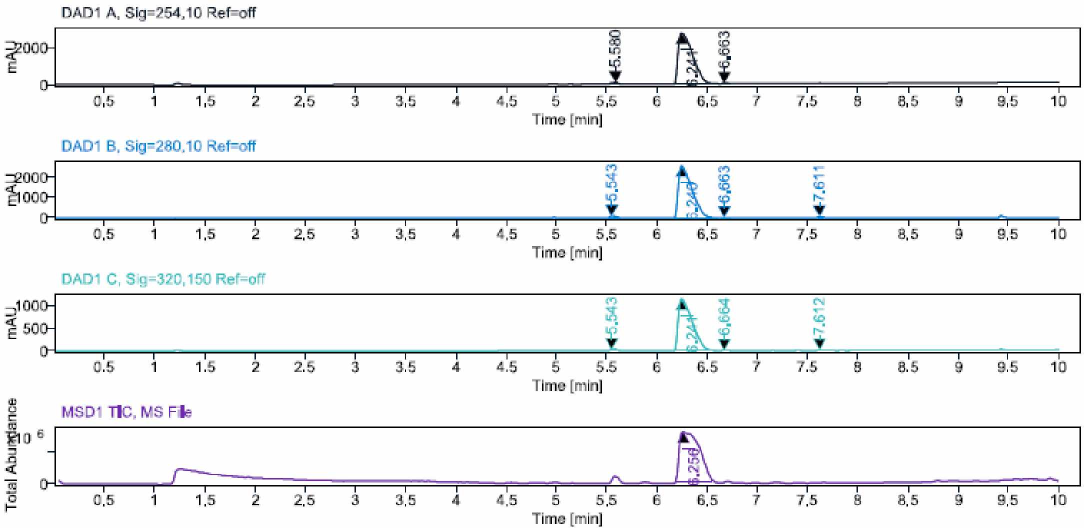
DAD1 A, Sig=254,10 Ref=off
mAU
2000
0
5.580
6.241
6.663
DAD1 B, Sig=280,10 Ref=off
mAU
2000
1000
0
5.543
6.240
6.663
7.611
DAD1 C, Sig=320,150 Ref=off
mAU
1000
500
0
5.543
6.244
6.664
7.612
MSD1 TIC, MS File
Total Abundance
x10 6
0
6.256
0,5 1 1,5 2 2,5 3 3,5 4 4,5 5 5,5 6 6,5 7 7,5 8 8,5 9 9,5 10
Time [min]

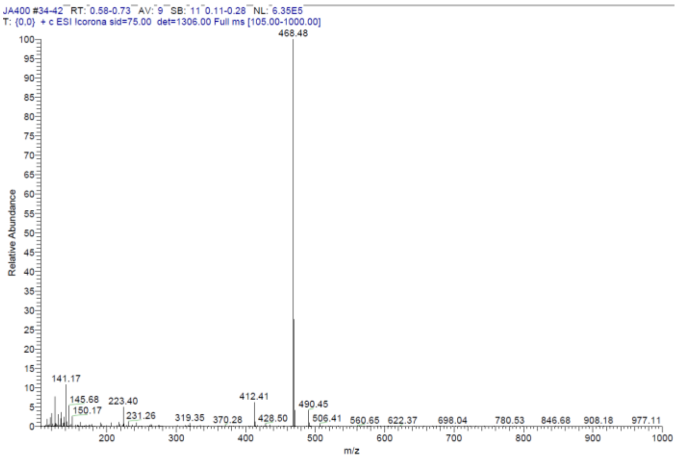
JA400 #34-42 RT: 0.58-0.73 AV: 9 SB: 11 0.11-0.28 NL: 6.35E5
T: {0,0} + c ESI !corona sid=75.00 det=1306.00 Full ms [105.00-1000.00]
468.48
141.17
145.68
150.17
223.40
231.26
319.35
370.28
412.41
428.50
490.45
506.41
560.65
622.37
698.04
780.53
846.68
908.18
977.11
Relative Abundance
100 95 90 85 80 75 70 65 60 55 50 45 40 35 30 25 20 15 10 5 0
200 300 400 500 600 700 800 900 1000
m/z

^{1}H, ^{13}C NMR, HPLC, and ESI data of compound **98b**

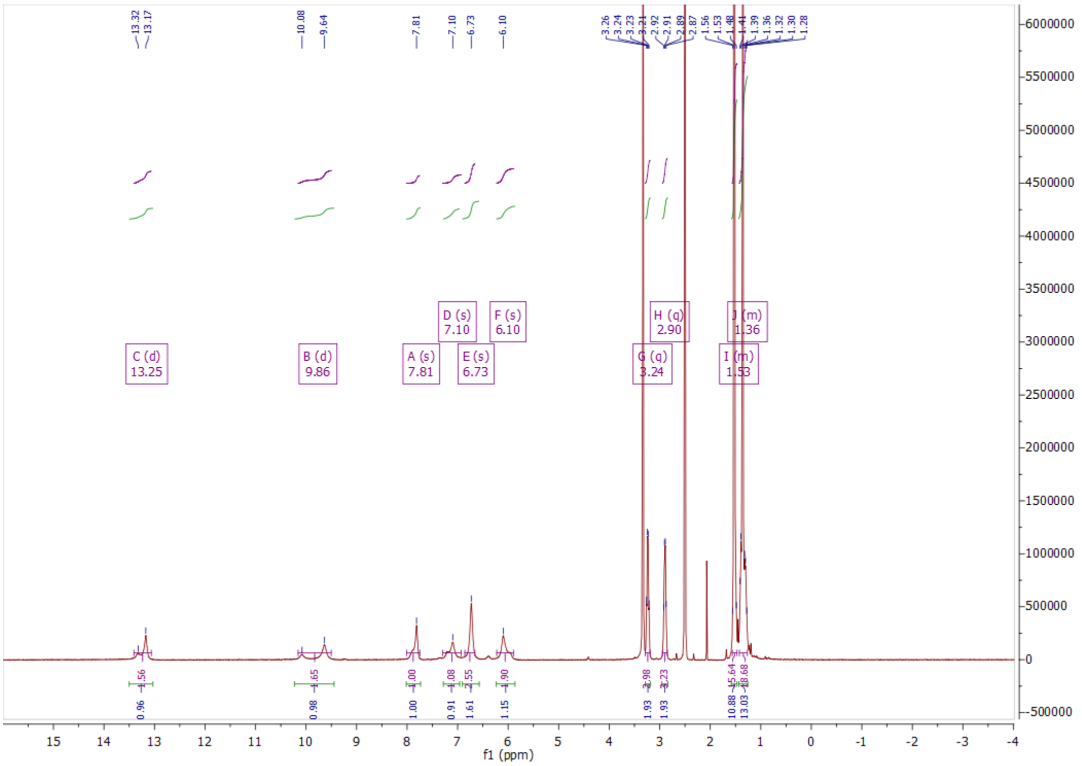

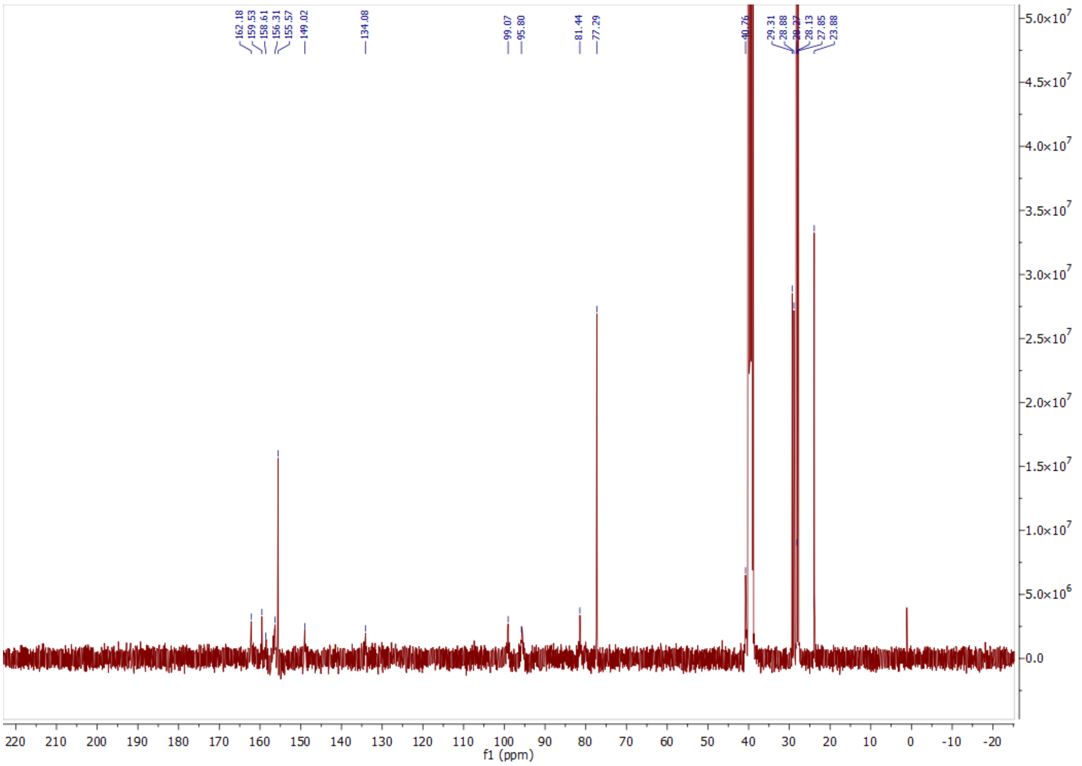

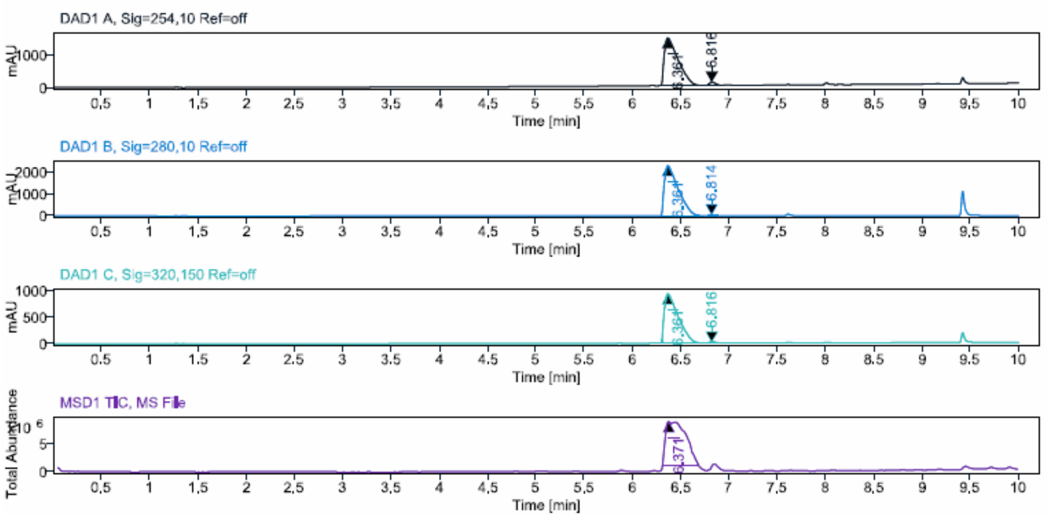

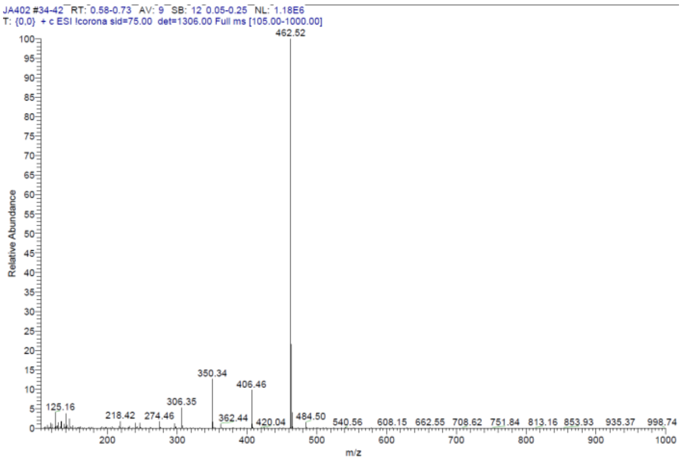

^{1}H, ^{13}C NMR, HPLC, and ESI data of compound **98d**

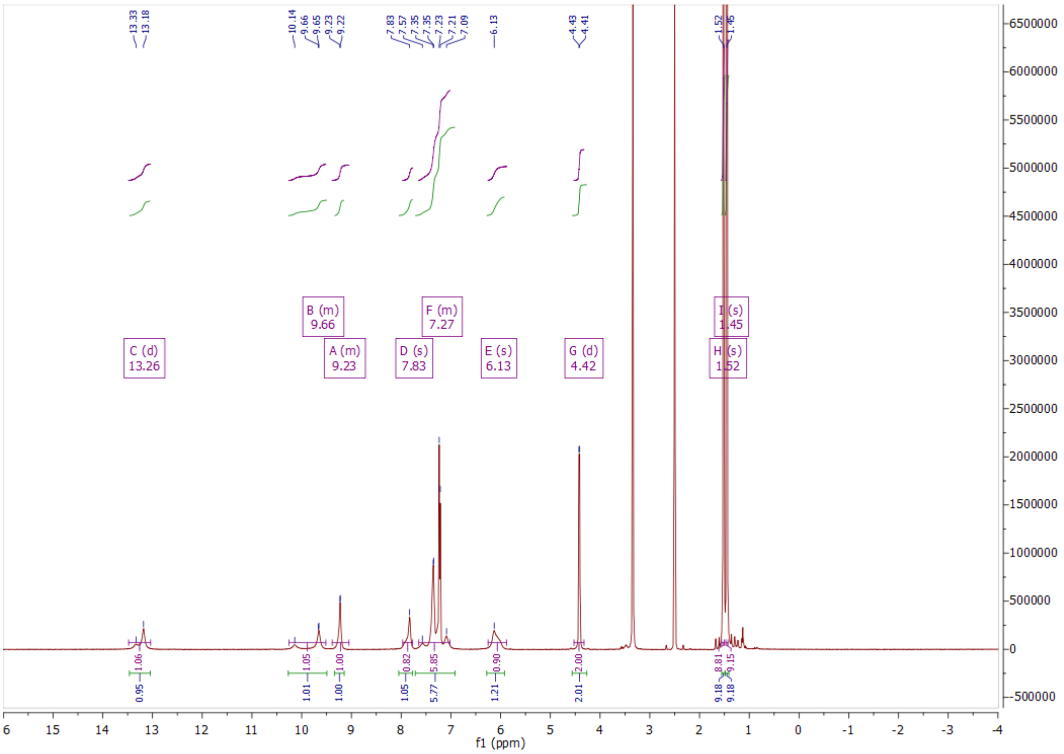

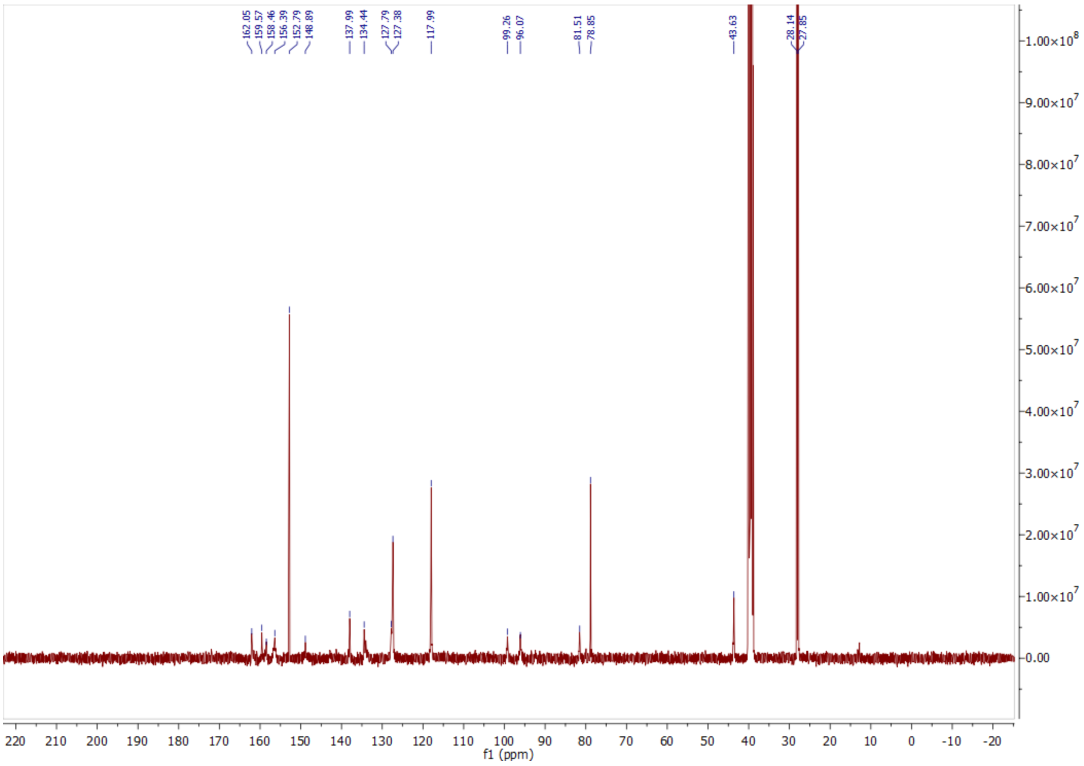
162.05
159.57
158.46
156.39
152.79
148.89
137.99
134.44
127.79
127.38
117.99
99.26
96.07
81.51
78.85
43.63
28.14
27.85
1.00×10^8
9.00×10^7
8.00×10^7
7.00×10^7
6.00×10^7
5.00×10^7
4.00×10^7
3.00×10^7
2.00×10^7
1.00×10^7
0.00
220 210 200 190 180 170 160 150 140 130 120 110 100 90 80 70 60 50 40 30 20 10 0 -10 -20
f1 (ppm)

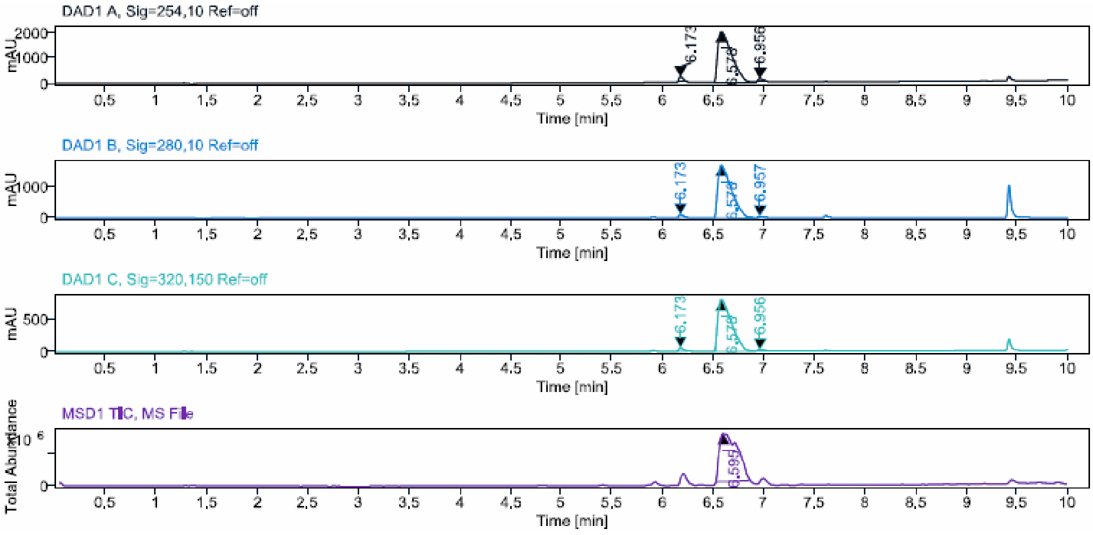
DAD1 A, Sig=254,10 Ref=off
mAU
2000
1000
0
6.173
6.578
6.956
DAD1 B, Sig=280,10 Ref=off
mAU
1000
0
6.173
6.578
6.957
DAD1 C, Sig=320,150 Ref=off
mAU
500
0
6.173
6.578
6.956
MSD1 TIC, MS File
Total Abundance
10^6
0
6.595
0,5 1 1,5 2 2,5 3 3,5 4 4,5 5 5,5 6 6,5 7 7,5 8 8,5 9 9,5 10
Time [min]

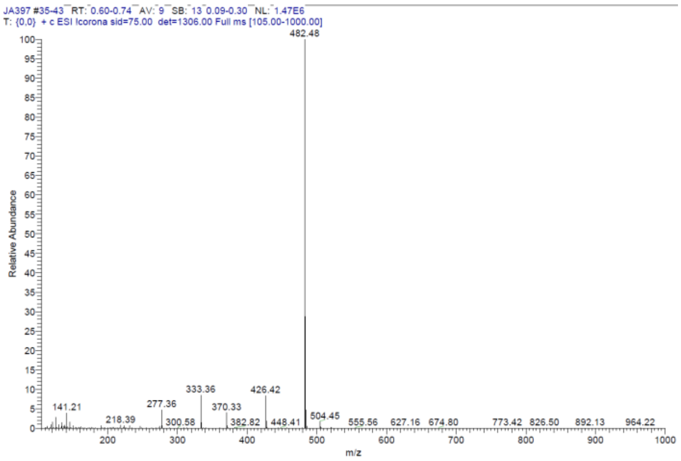
JA397 #35-43 RT: 0.60-0.74 AV: 9 SB: 13 0.09-0.30 NL: 1.47E6
T: {0,0} + c ESI !corona sid=75.00 det=1306.00 Full ms [105.00-1000.00]
482.48
141.21
218.39
277.36
300.58
333.36
370.33
382.82
426.42
448.41
504.45
555.56
627.16
674.80
773.42
826.50
892.13
964.22
Relative Abundance
100 95 90 85 80 75 70 65 60 55 50 45 40 35 30 25 20 15 10 5 0
200 300 400 500 600 700 800 900 1000
m/z

^{1}H, ^{13}C NMR, and ESI data of compound **100**

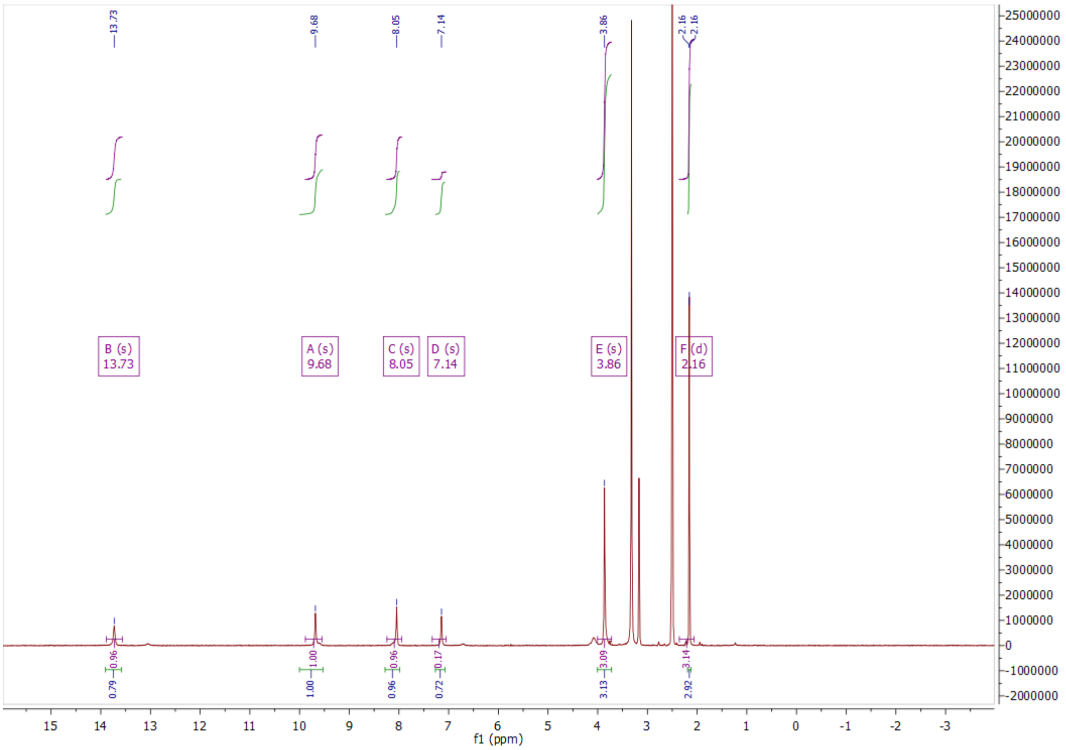

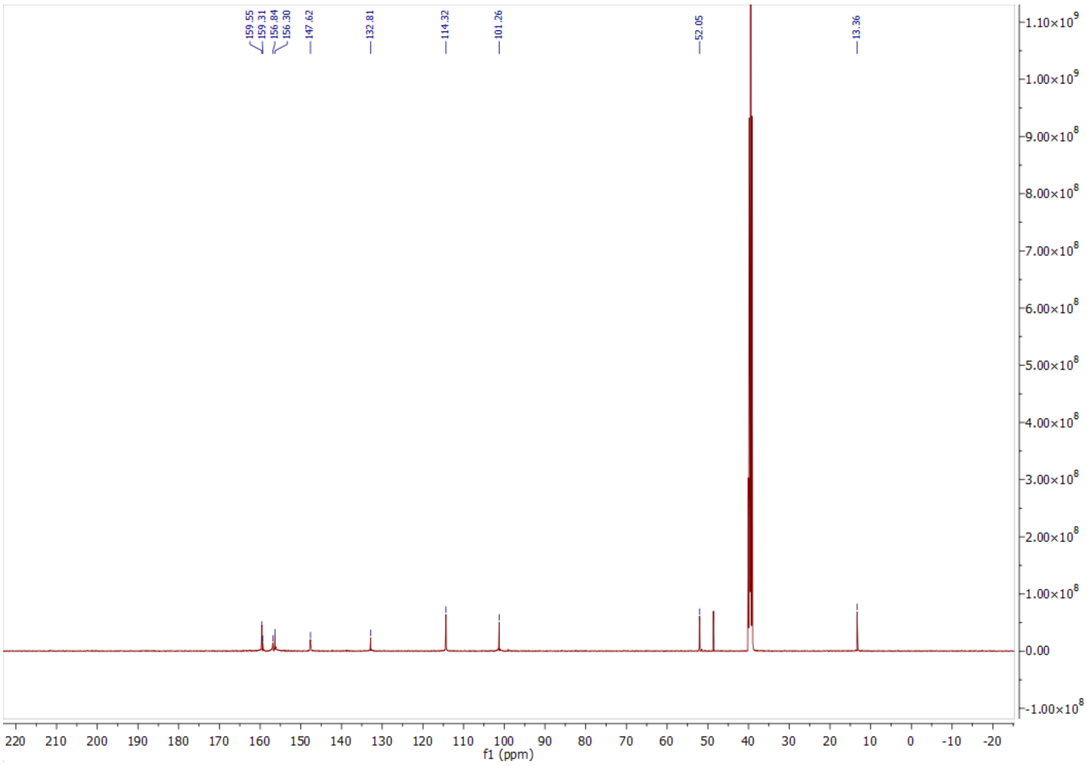

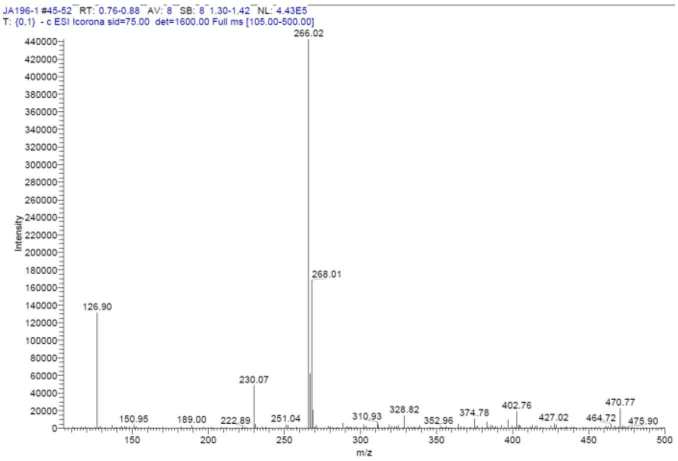

ESI data of compound **101a**

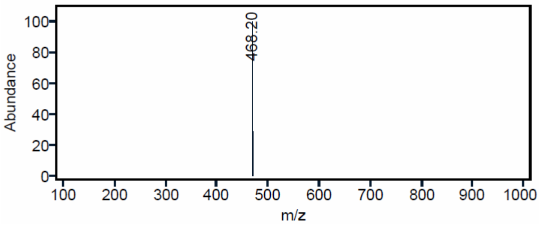

ESI data of compound **78d**

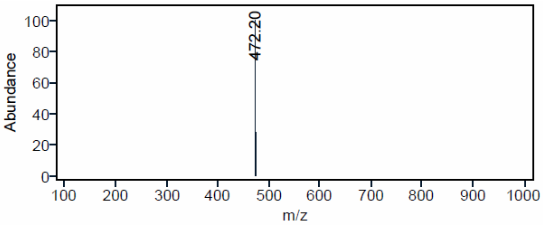

ESI data of compound **78e**

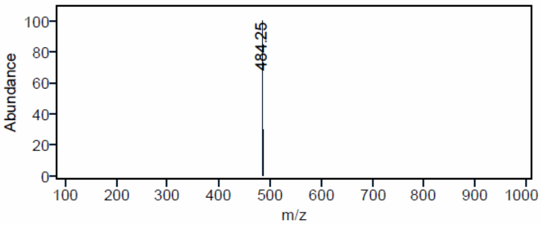

ESI data of compound **102a**

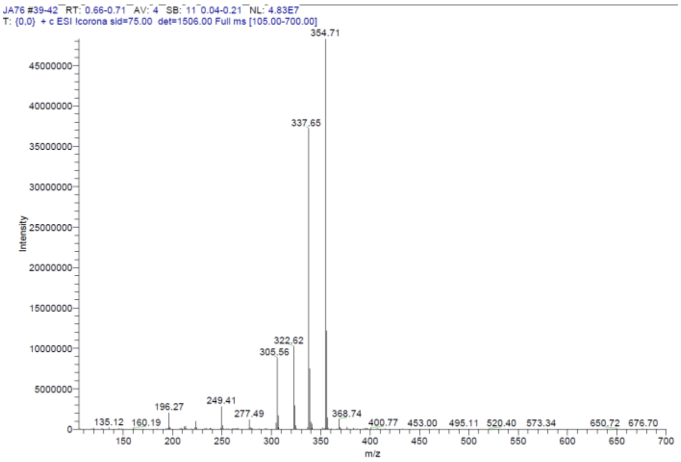

ESI data of compound **102b**

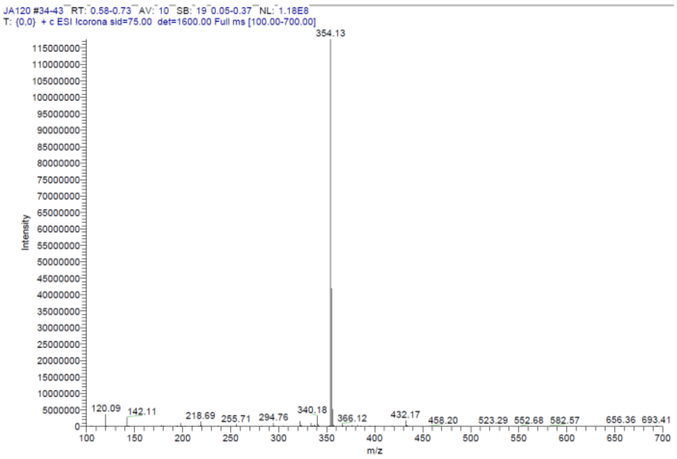

ESI data of compound **102d**

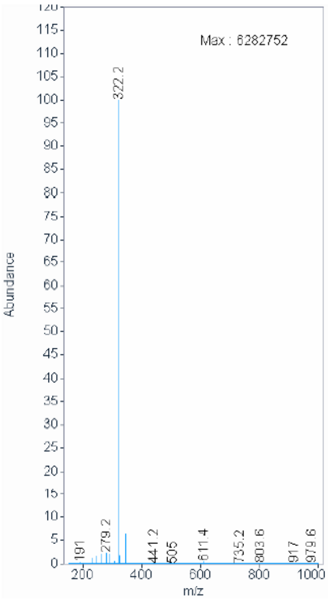

ESI data of compound **103c**

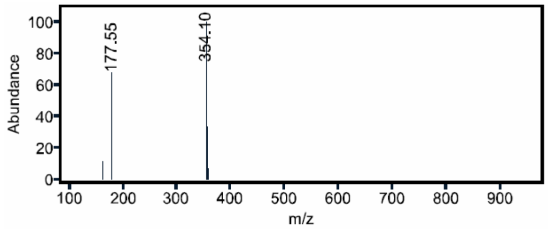

ESI data of compound **103e**

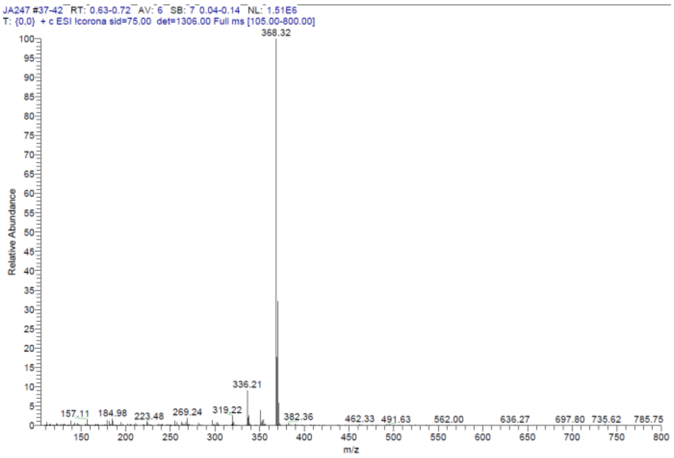

^{1}H, ^{13}C NMR, HPLC, and ESI data of compound **106a**

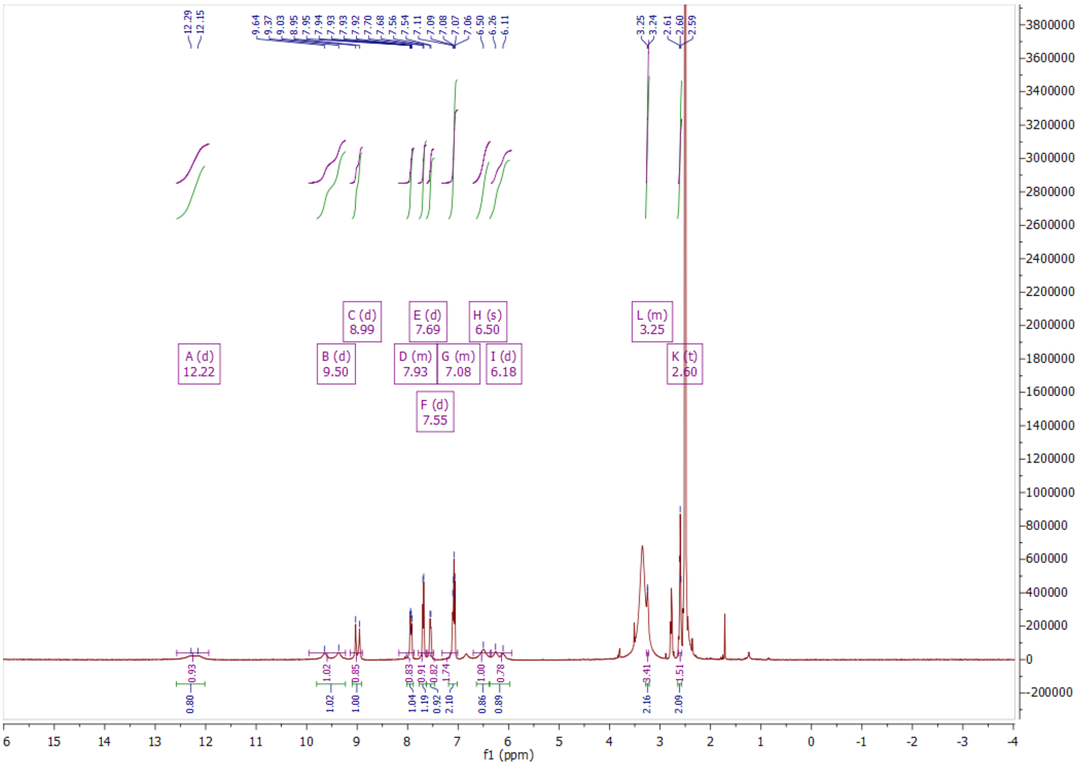

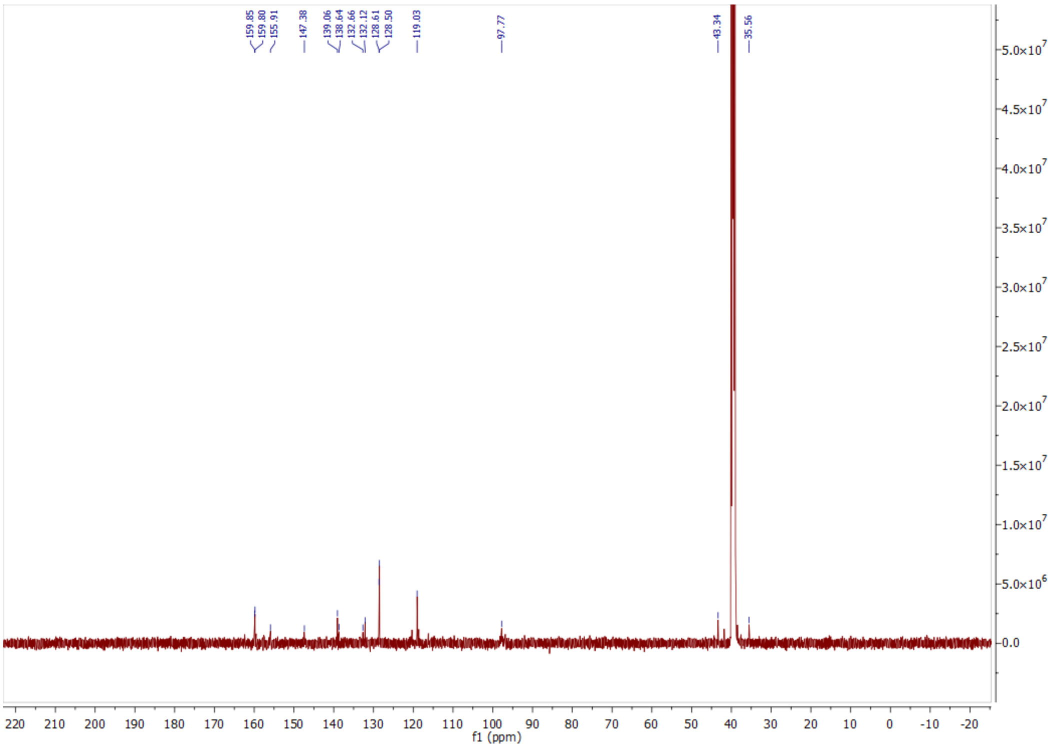
159.85
159.80
155.91
147.38
139.06
138.64
132.66
132.12
128.61
128.50
119.03
97.77
43.34
35.56
5.0×10^7
4.5×10^7
4.0×10^7
3.5×10^7
3.0×10^7
2.5×10^7
2.0×10^7
1.5×10^7
1.0×10^7
5.0×10^6
0.0
220 210 200 190 180 170 160 150 140 130 120 110 100 90 80 70 60 50 40 30 20 10 0 -10 -20
f1 (ppm)

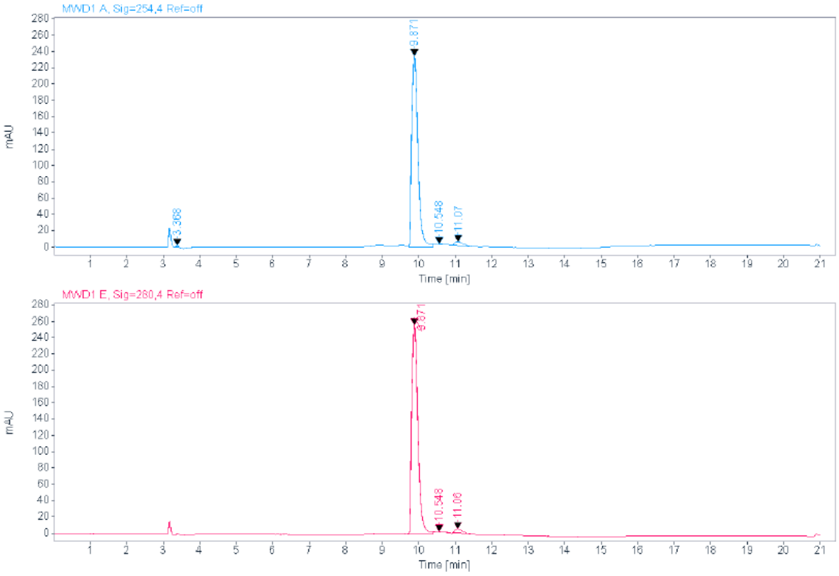
MWD1 A, Sig=254,4 Ref=off
mAU
9.871
3.368
10.548
11.07
Time [min]
MWD1 E, Sig=280,4 Ref=off
mAU
9.871
10.548
11.06
Time [min]
0 20 40 60 80 100 120 140 160 180 200 220 240 260 280
1 2 3 4 5 6 7 8 9 10 11 12 13 14 15 16 17 18 19 20 21

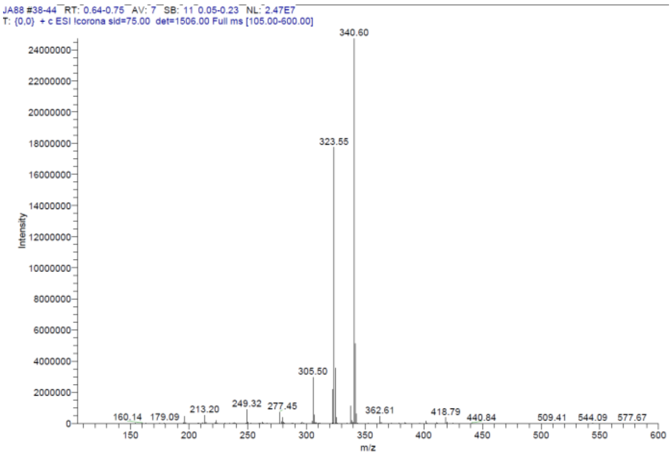
JA88 #38-44 RT: 0.64-0.75 AV: 7 SB: 11 0.05-0.23 NL: 2.47E7
T: {0,0} + c ESI !corona sid=75.00 det=1506.00 Full ms [105.00-600.00]
340.60
323.55
305.50
249.32
277.45
213.20
179.09
160.14
362.61
418.79
440.84
509.41
544.09
577.67
Intensity
0 2000000 4000000 6000000 8000000 10000000 12000000 14000000 16000000 18000000 20000000 22000000 24000000
150 200 250 300 350 400 450 500 550 600
m/z

ESI data of compound **106b**

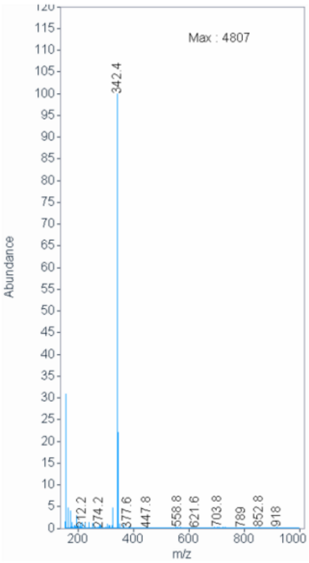

ESI data of compound **106c**

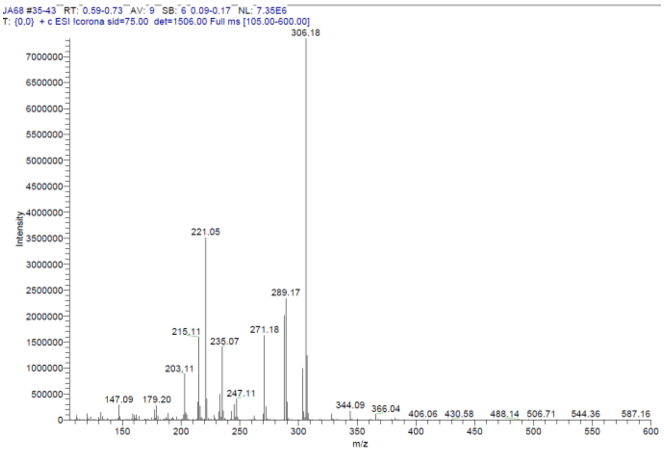

ESI data of compound **106d**

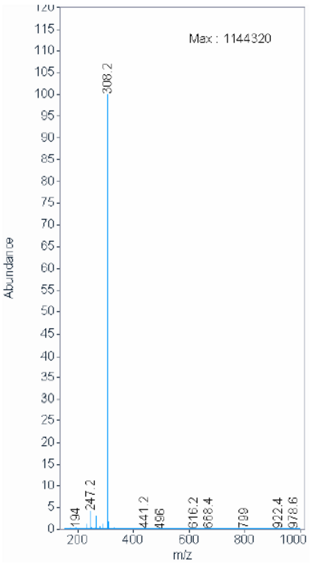

^{1}H, ^{13}C NMR, HPLC, and ESI data of compound **106e**

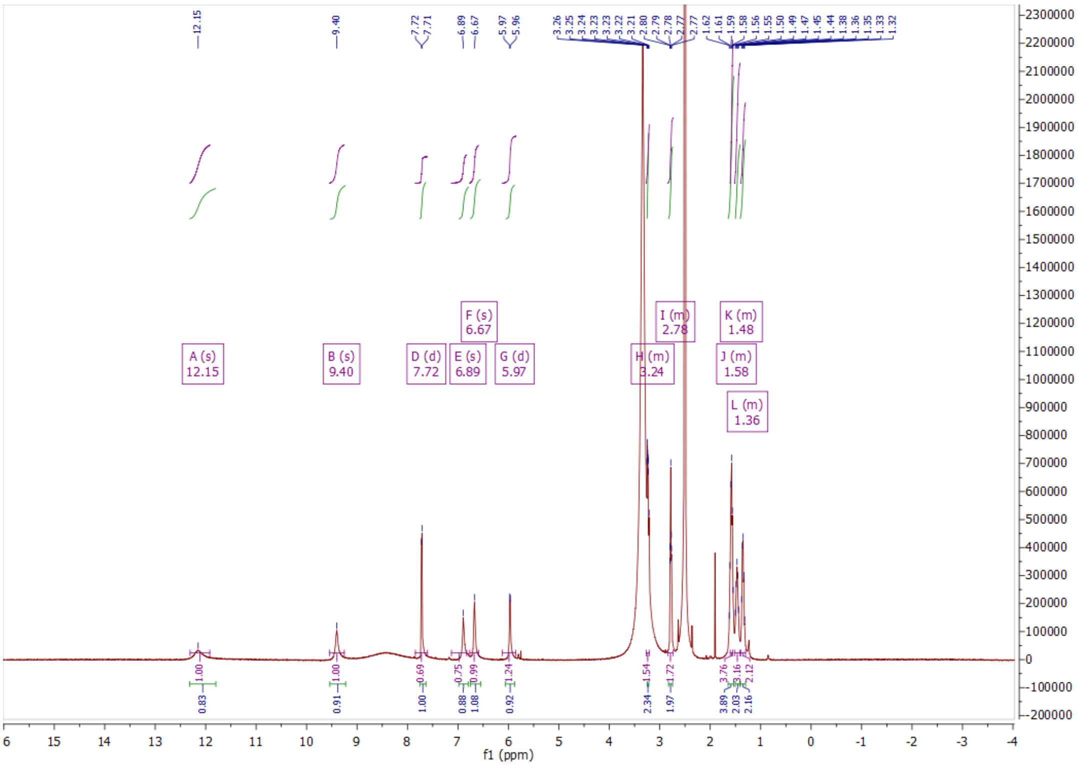

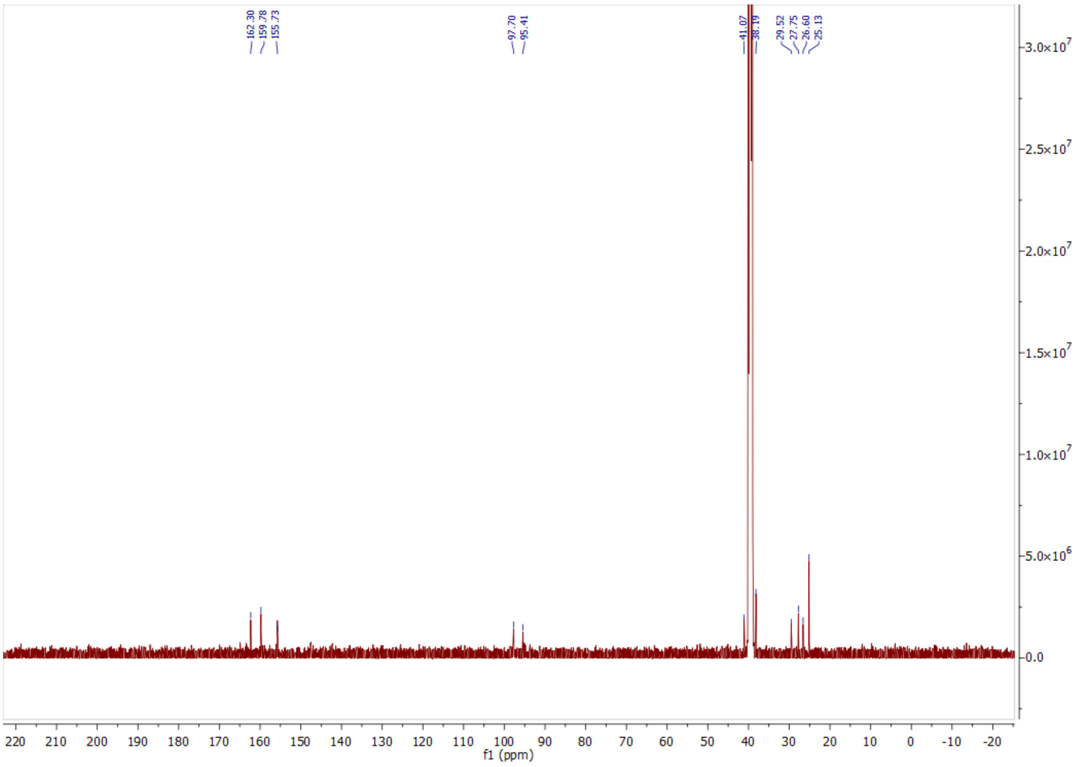

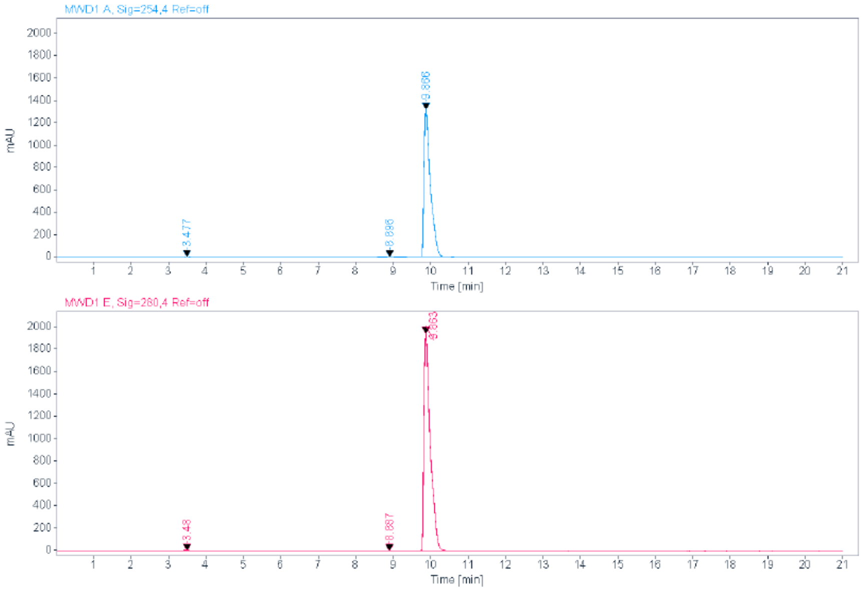

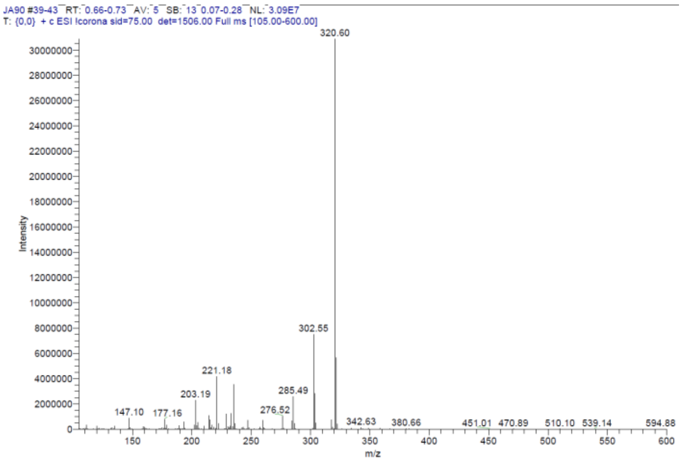

ESI data of compound **107a**

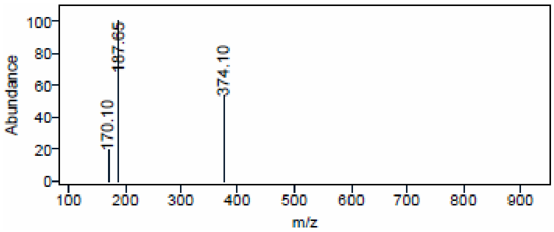

ESI data of compound **107b**

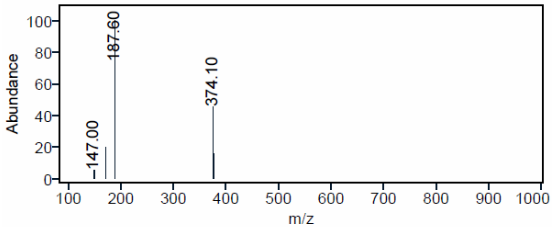

ESI data of compound **107c**

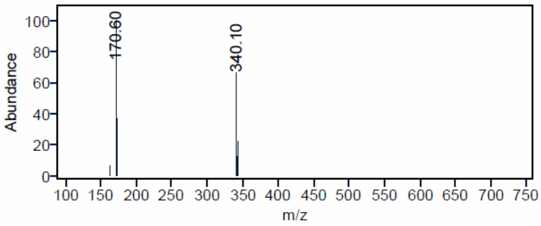

ESI data of compound **107d**

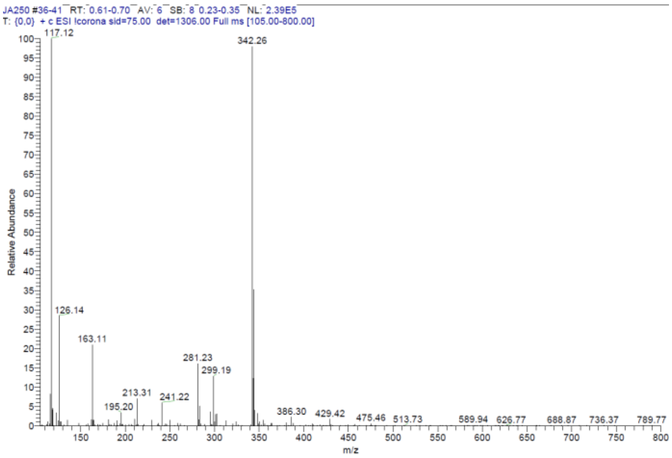

ESI data of compound **107e**

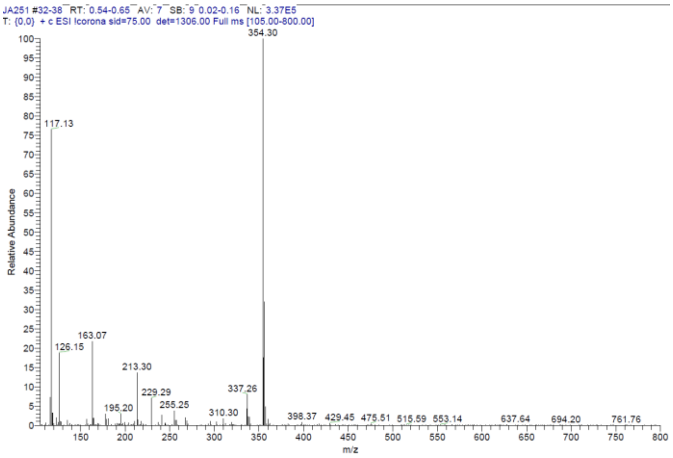

ESI data of compound **108a**

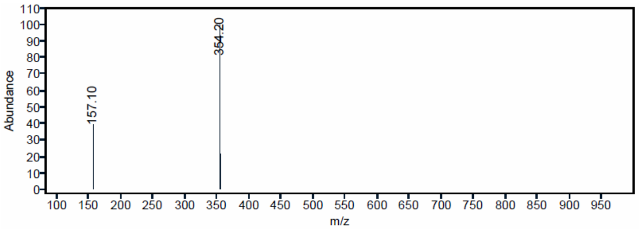

ESI data of compound **109a**

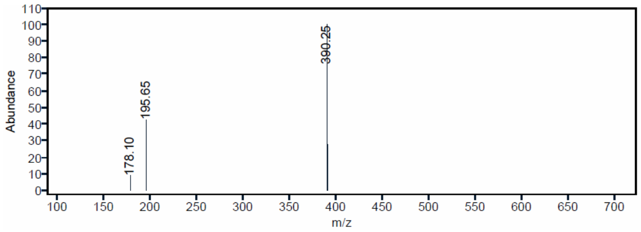

ESI data of compound **109b**

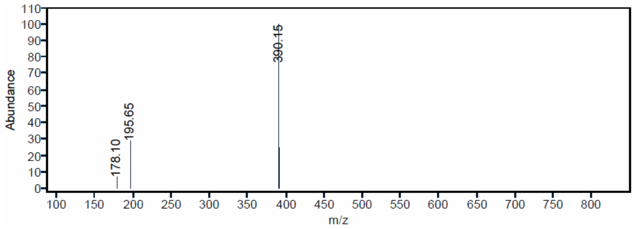

ESI data of compound **109c**

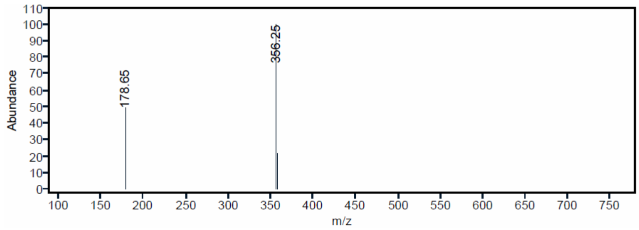

ESI data of compound **109d**

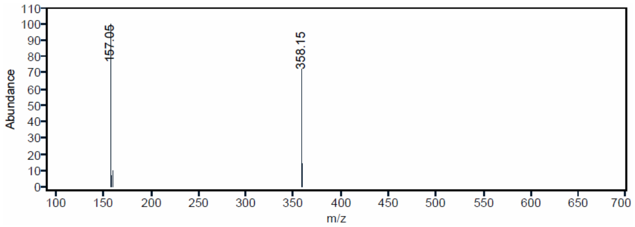

ESI data of compound **109e**

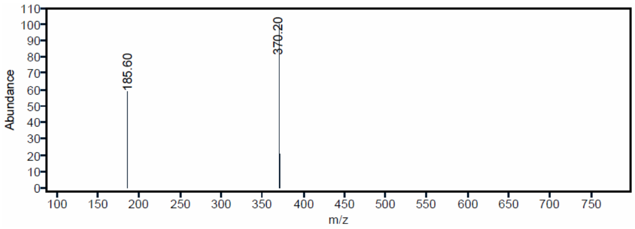

^{1}H, ^{13}C NMR, HPLC, and ESI data of compound **110a**

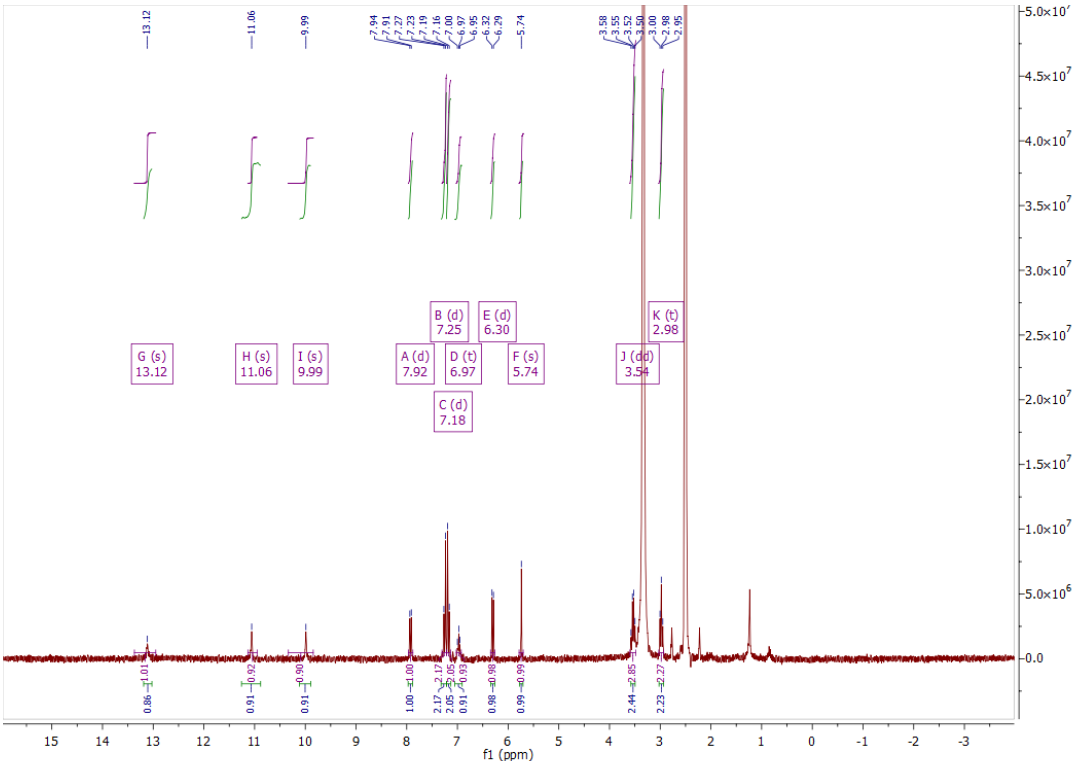

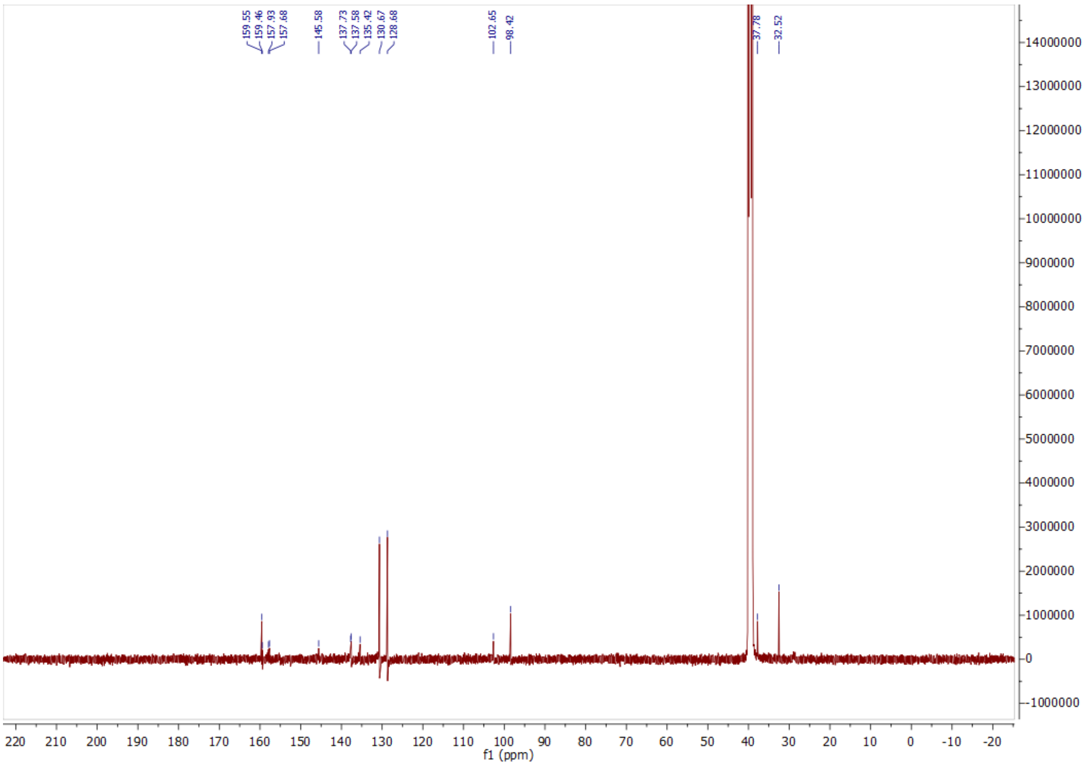

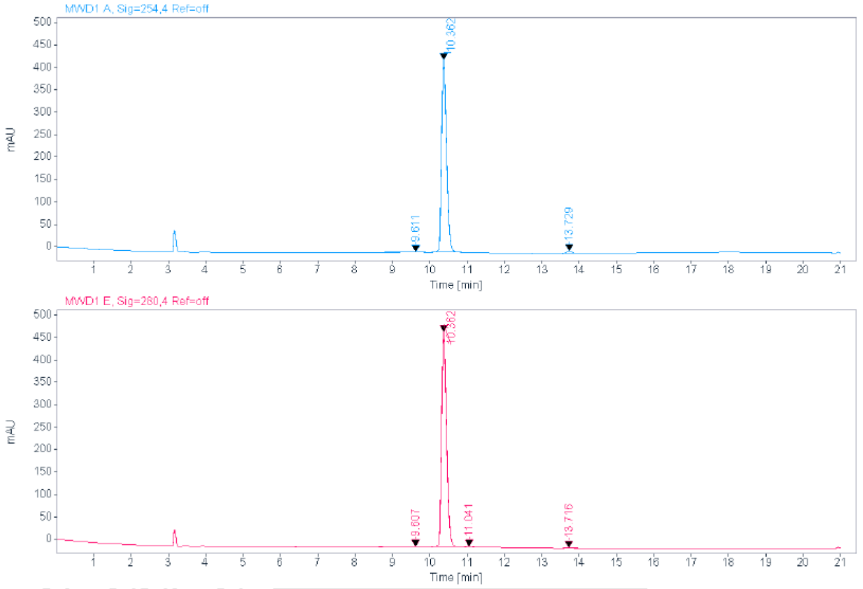

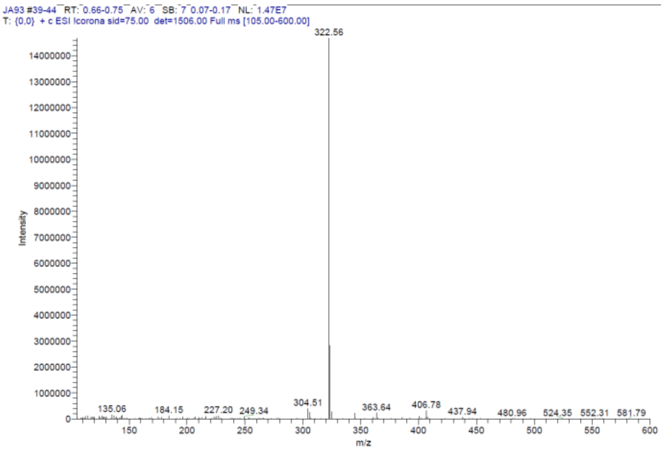

^{1}H, ^{13}C NMR, HPLC, and ESI data of compound **110b**

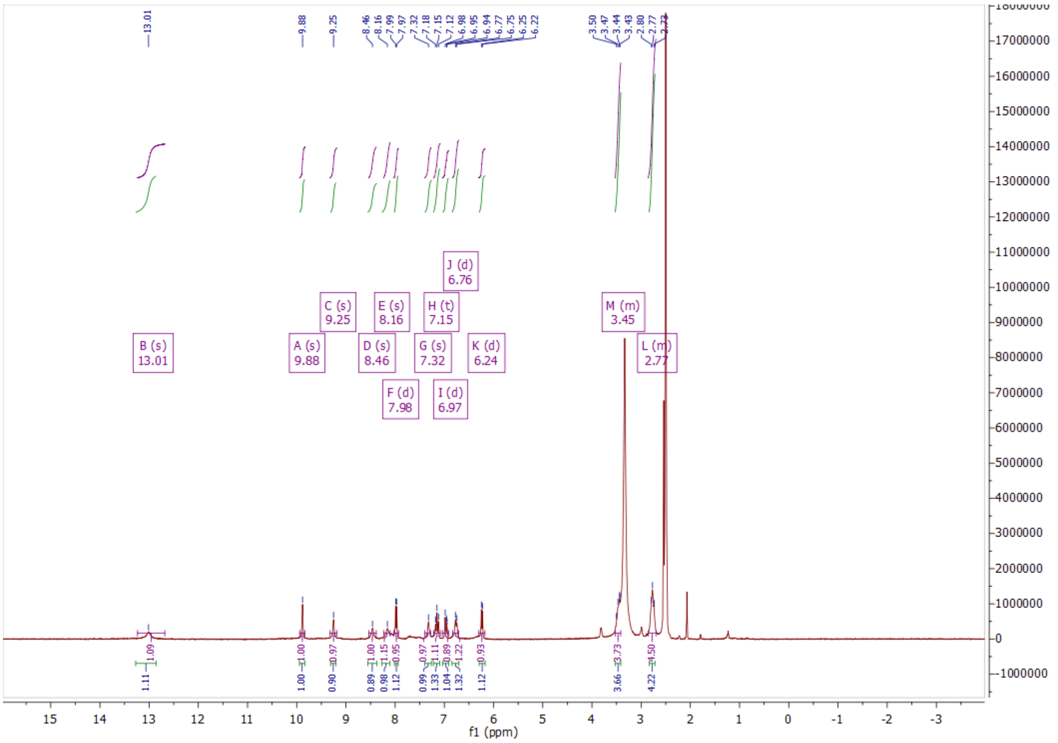

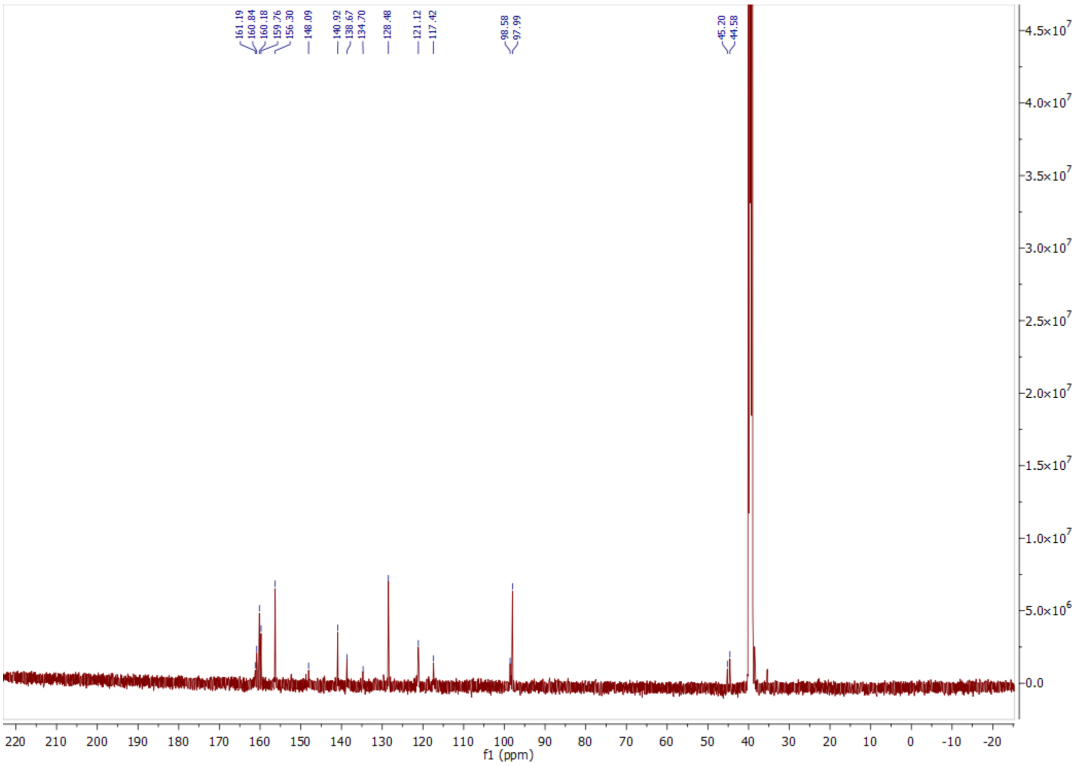
161.19
160.84
160.18
159.76
156.30
148.09
140.92
138.67
134.70
128.48
121.12
117.42
98.58
97.99
45.20
44.58
4.5×10^7
4.0×10^7
3.5×10^7
3.0×10^7
2.5×10^7
2.0×10^7
1.5×10^7
1.0×10^7
5.0×10^6
0.0
220 210 200 190 180 170 160 150 140 130 120 110 100 90 80 70 60 50 40 30 20 10 0 -10 -20
f1 (ppm)

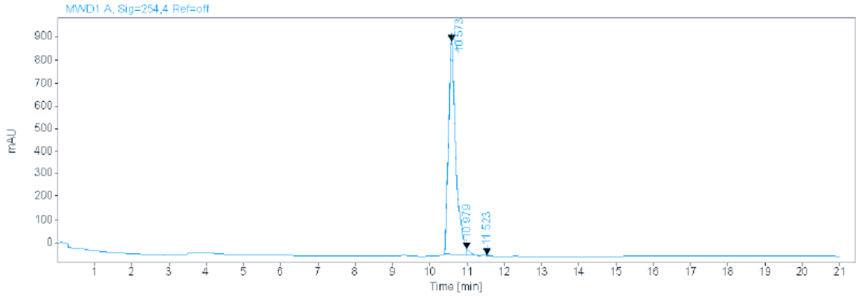
MWD1 A, Sig=254,4 Ref=off
mAU
900
800
700
600
500
400
300
200
100
0
10.573
10.979
11.523
1 2 3 4 5 6 7 8 9 10 11 12 13 14 15 16 17 18 19 20 21
Time [min]

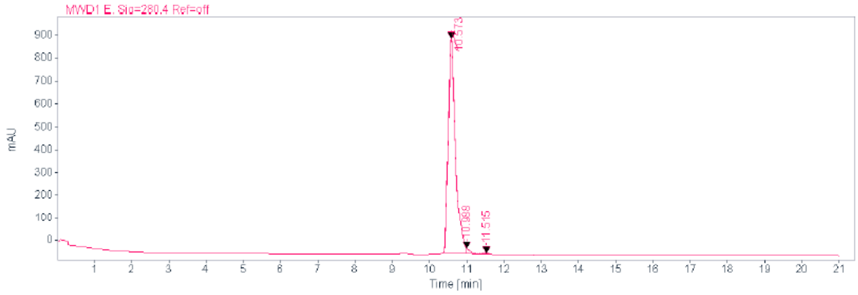
MWD1 E, Sig=280,4 Ref=off
mAU
900
800
700
600
500
400
300
200
100
0
10.573
10.988
11.515
1 2 3 4 5 6 7 8 9 10 11 12 13 14 15 16 17 18 19 20 21
Time [min]

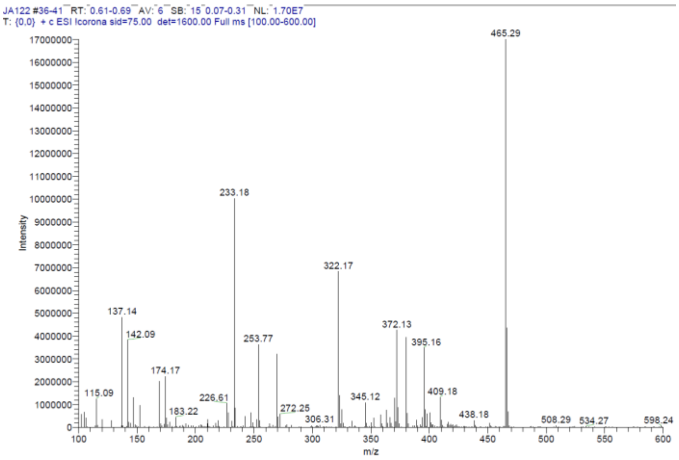
JA122 #36-41 RT: 0.61-0.69 AV: 6 SB: 15 0.07-0.31 NL: 1.70E7
T: {0,0} + c ESI Icorona sid=75.00 det=1600.00 Full ms [100.00-600.00]
Intensity
17000000
16000000
15000000
14000000
13000000
12000000
11000000
10000000
9000000
8000000
7000000
6000000
5000000
4000000
3000000
2000000
1000000
0
465.29
233.18
322.17
137.14
142.09
372.13
395.16
253.77
174.17
409.18
115.09
226.61
345.12
183.22
272.25
438.18
306.31
508.29
534.27
598.24
100 150 200 250 300 350 400 450 500 550 600
m/z

^{1}H, ^{13}C NMR, HPLC, and ESI data of compound **110c**

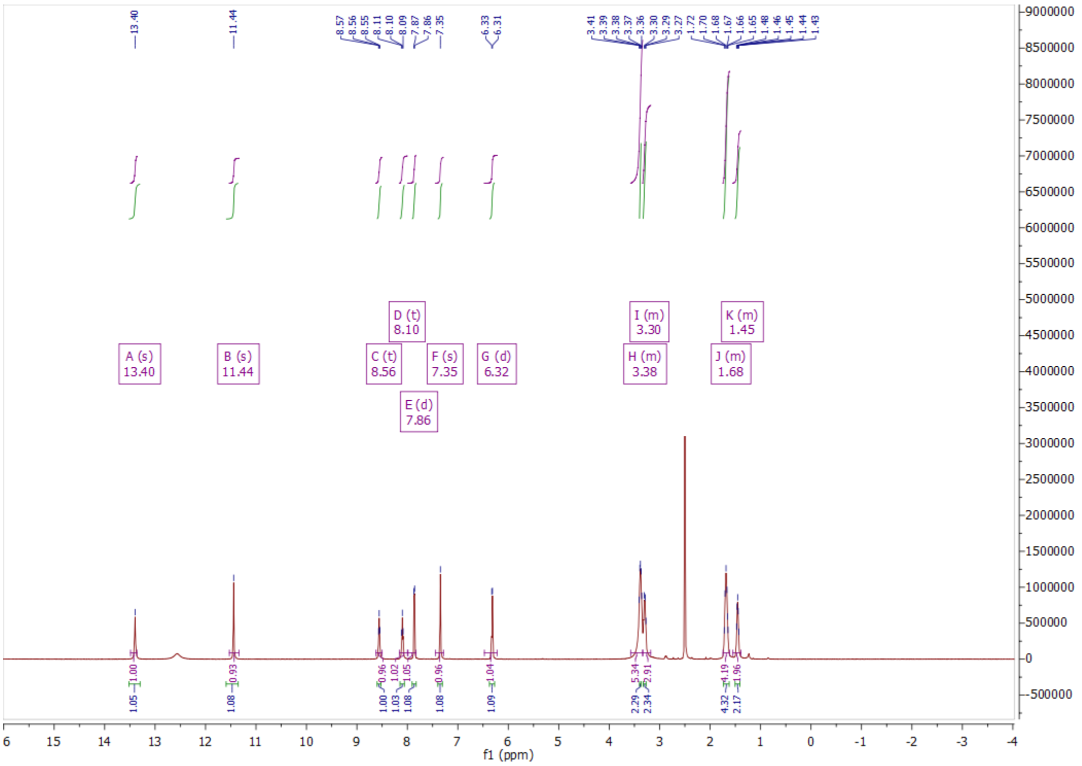

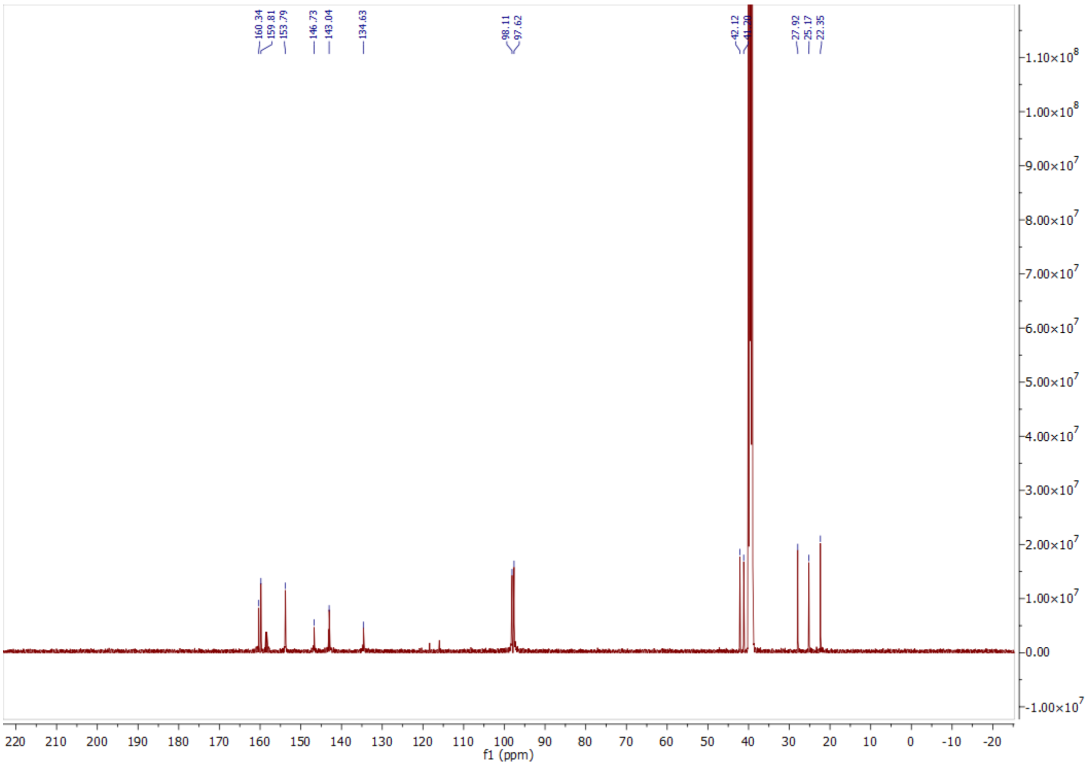

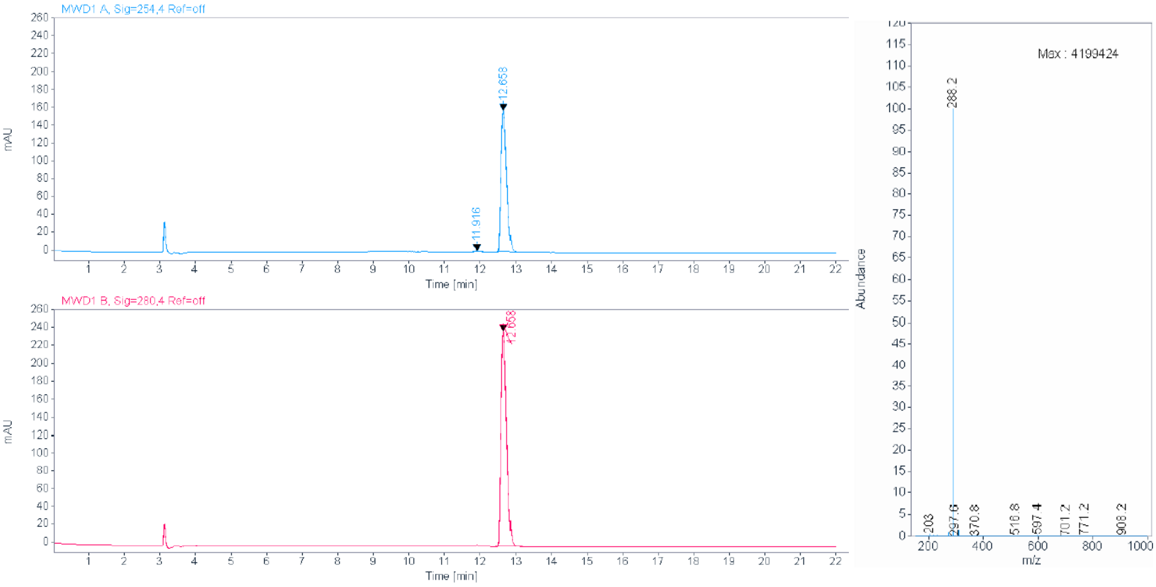

^{1}H NMR, HPLC, and ESI data of compound **110d**

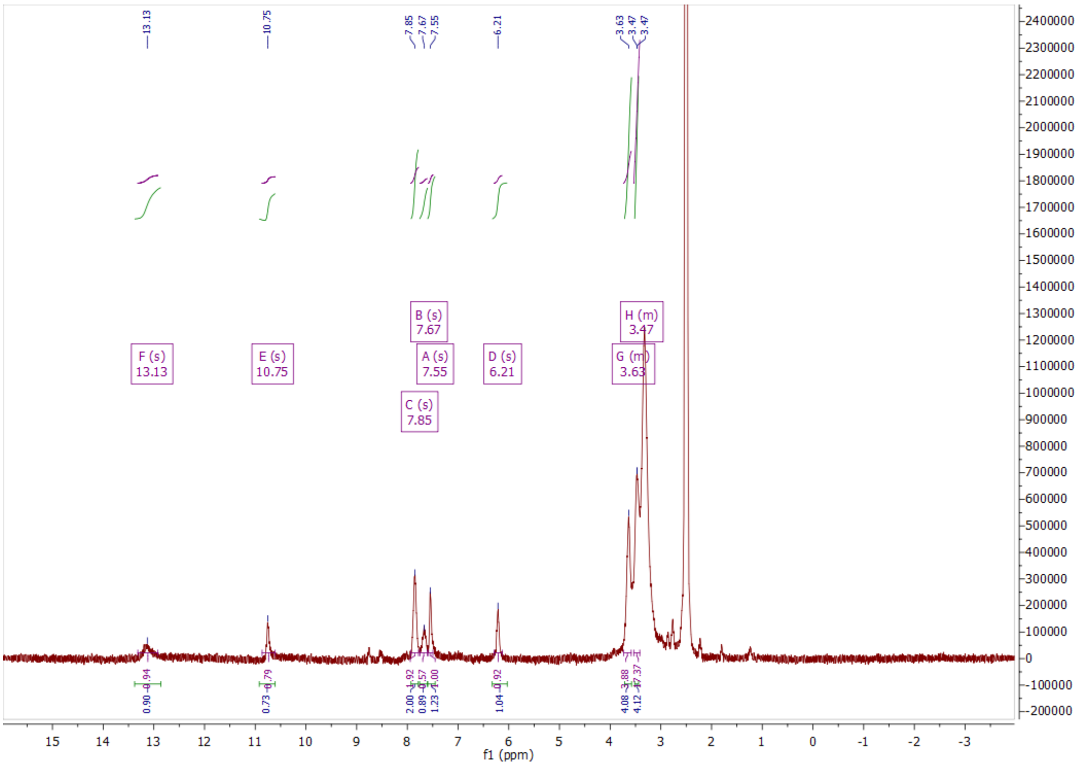

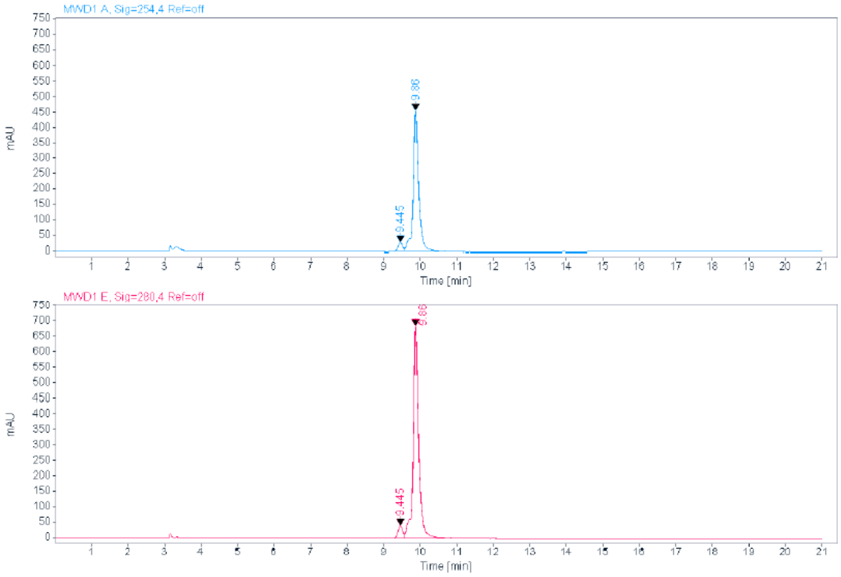

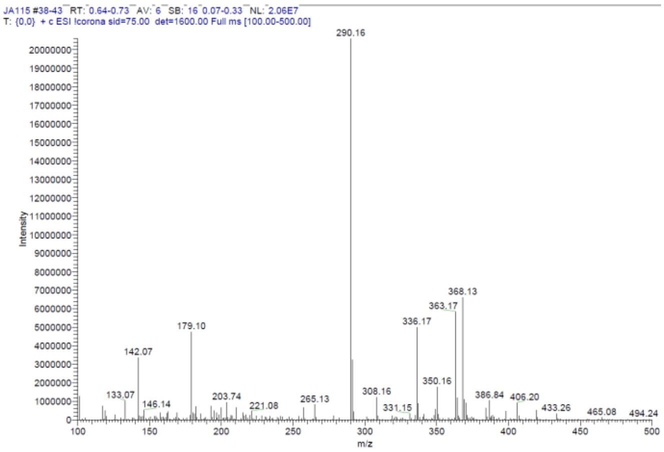

^1H, ^{13}C NMR, HPLC, and ESI data of compound **110e**

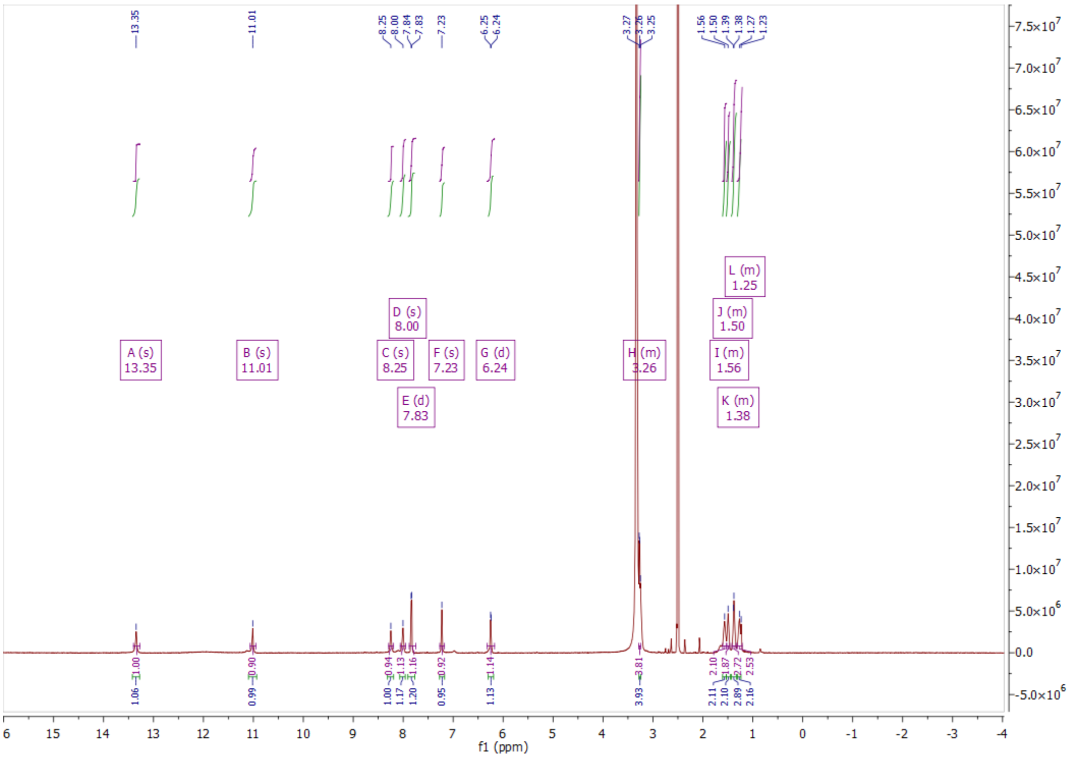

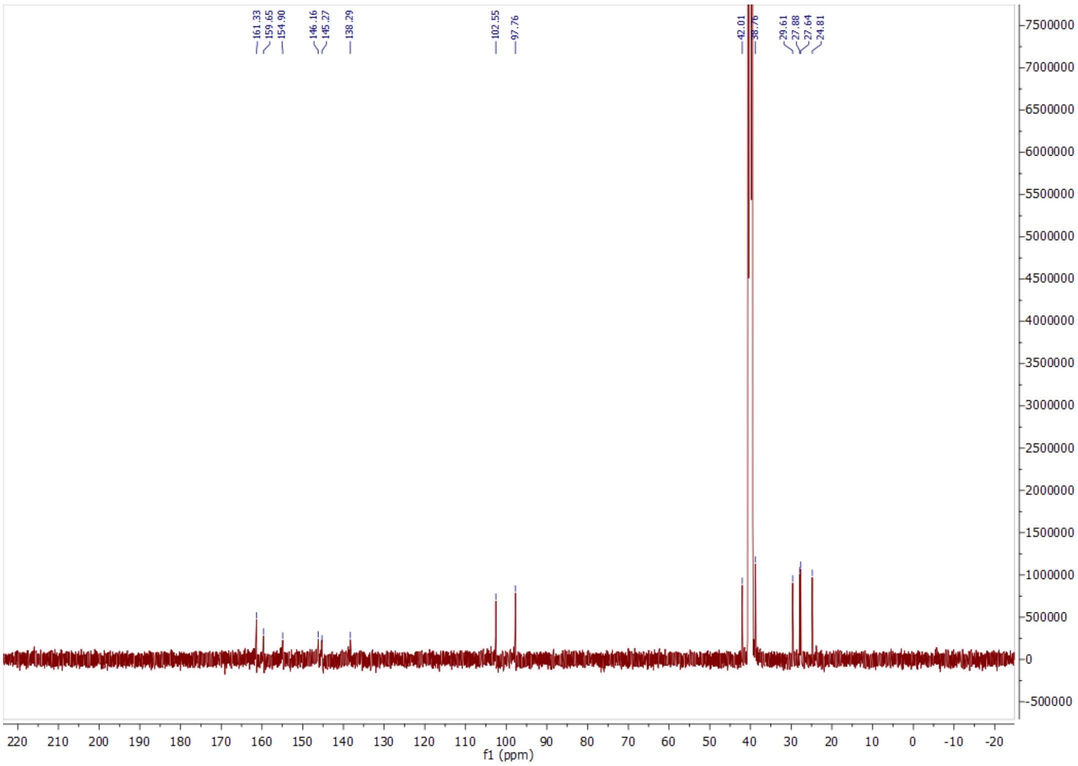
161.33
159.65
154.90
146.16
145.27
138.29
102.55
97.76
42.01
38.76
29.61
27.88
27.64
24.81
7500000
7000000
6500000
6000000
5500000
5000000
4500000
4000000
3500000
3000000
2500000
2000000
1500000
1000000
500000
0
-500000
220 210 200 190 180 170 160 150 140 130 120 110 100 90 80 70 60 50 40 30 20 10 0 -10 -20
f1 (ppm)

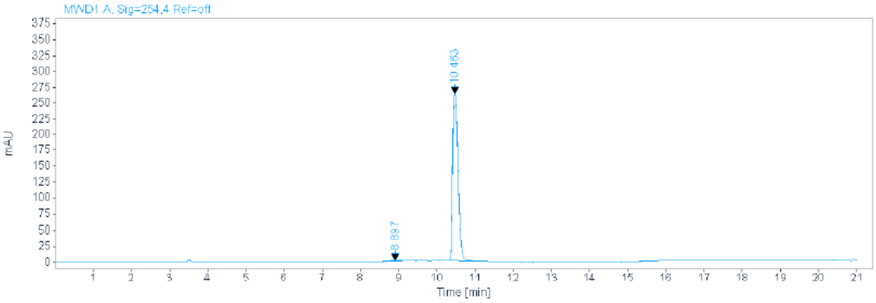
MWD1 A, Sig=254,4 Ref=off
mAU
375 350 325 300 275 250 225 200 175 150 125 100 75 50 25 0
10.463
8.897
1 2 3 4 5 6 7 8 9 10 11 12 13 14 15 16 17 18 19 20 21
Time [min]

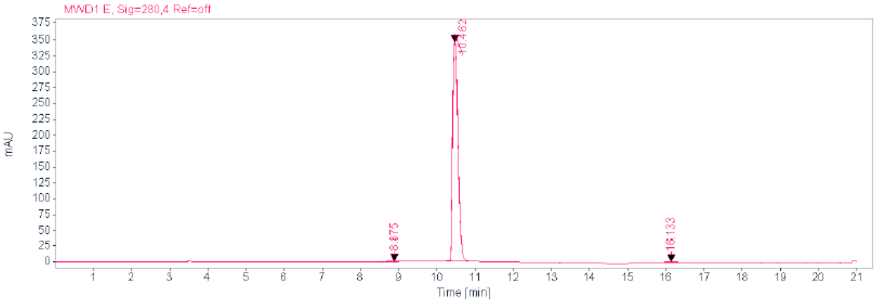
MWD1 E, Sig=280,4 Ref=off
mAU
375 350 325 300 275 250 225 200 175 150 125 100 75 50 25 0
10.462
8.875
16.133
1 2 3 4 5 6 7 8 9 10 11 12 13 14 15 16 17 18 19 20 21
Time [min]

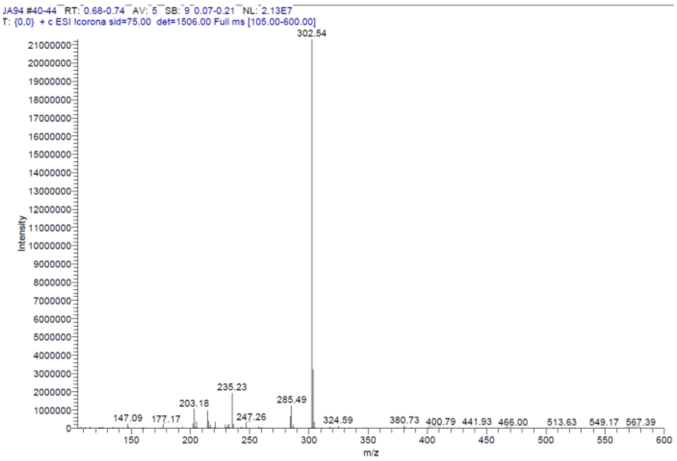
JA94 #40-44 RT: 0.68-0.74 AV: 5 SB: 9 0.07-0.21 NL: 2.13E7
T: {0,0} + c ESI !corona sid=75.00 det=1506.00 Full ms [105.00-600.00]
302.54
Intensity
21000000 20000000 19000000 18000000 17000000 16000000 15000000 14000000 13000000 12000000 11000000 10000000 9000000 8000000 7000000 6000000 5000000 4000000 3000000 2000000 1000000 0
235.23
203.18
285.49
147.09
177.17
247.26
324.59
380.73
400.79
441.93
466.00
513.63
549.17
567.39
150 200 250 300 350 400 450 500 550 600
m/z

^{1}H, ^{13}C NMR, HPLC, and ESI data of compound **111a**

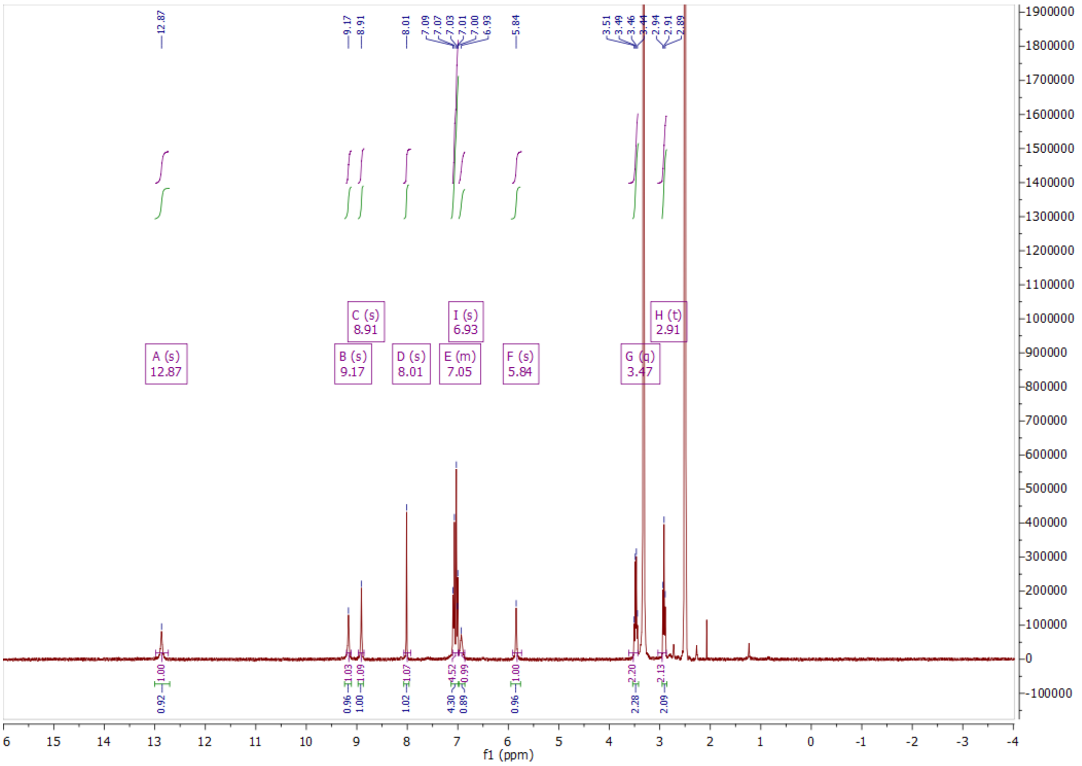

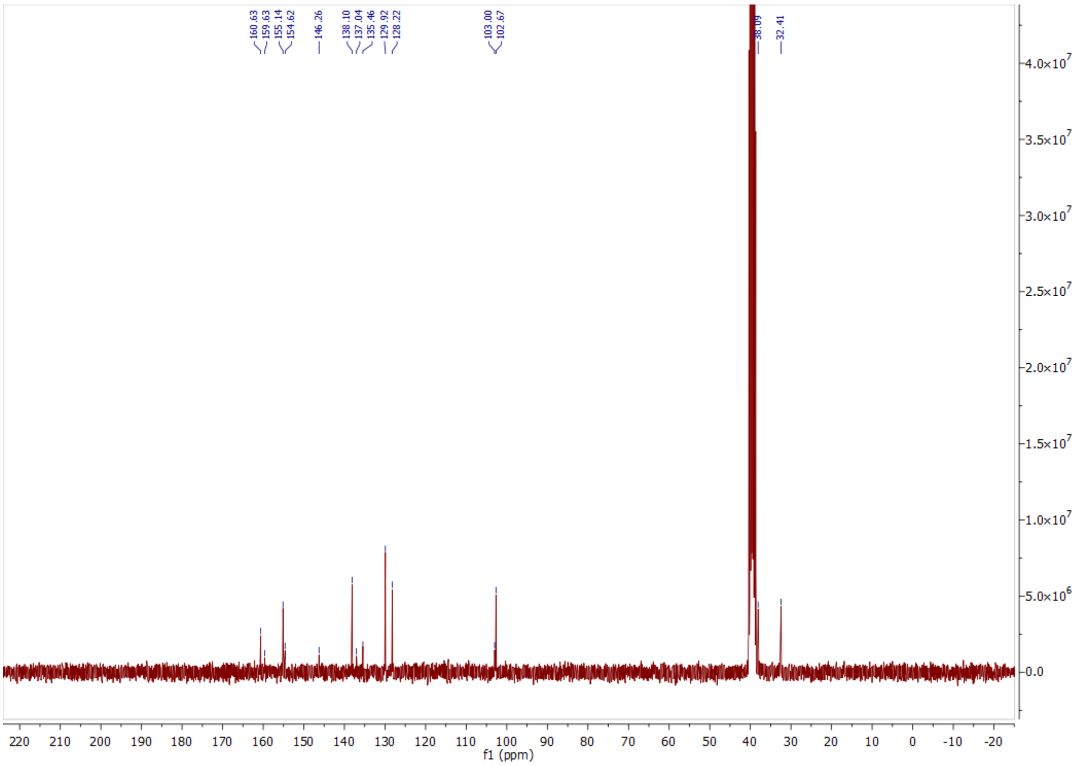

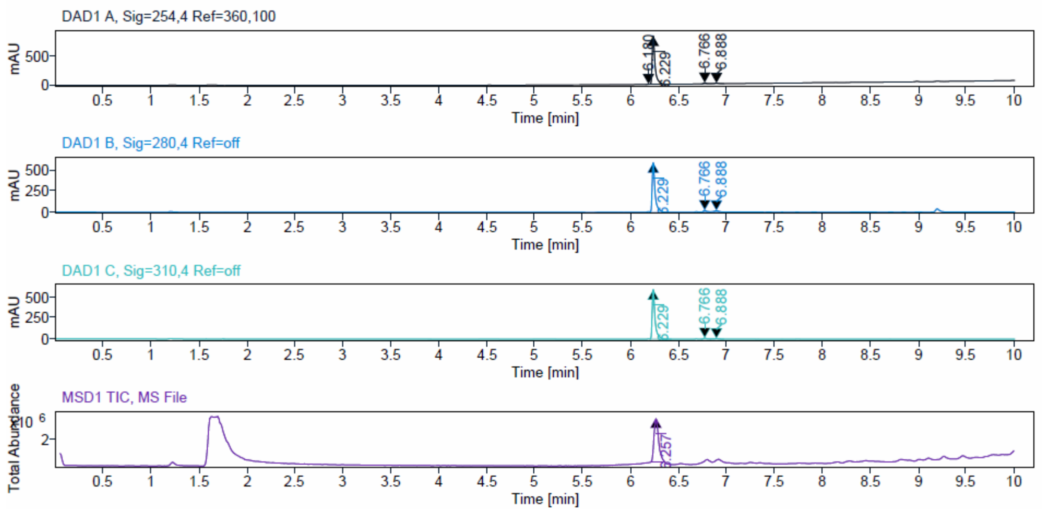

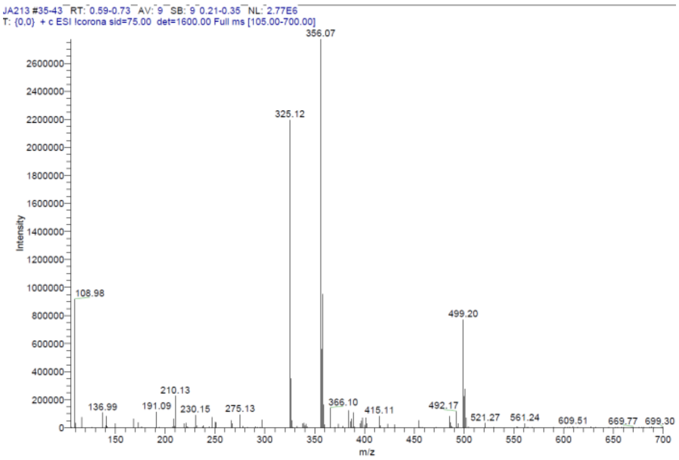

^{1}H NMR, HPLC, and ESI data of compound **111b**

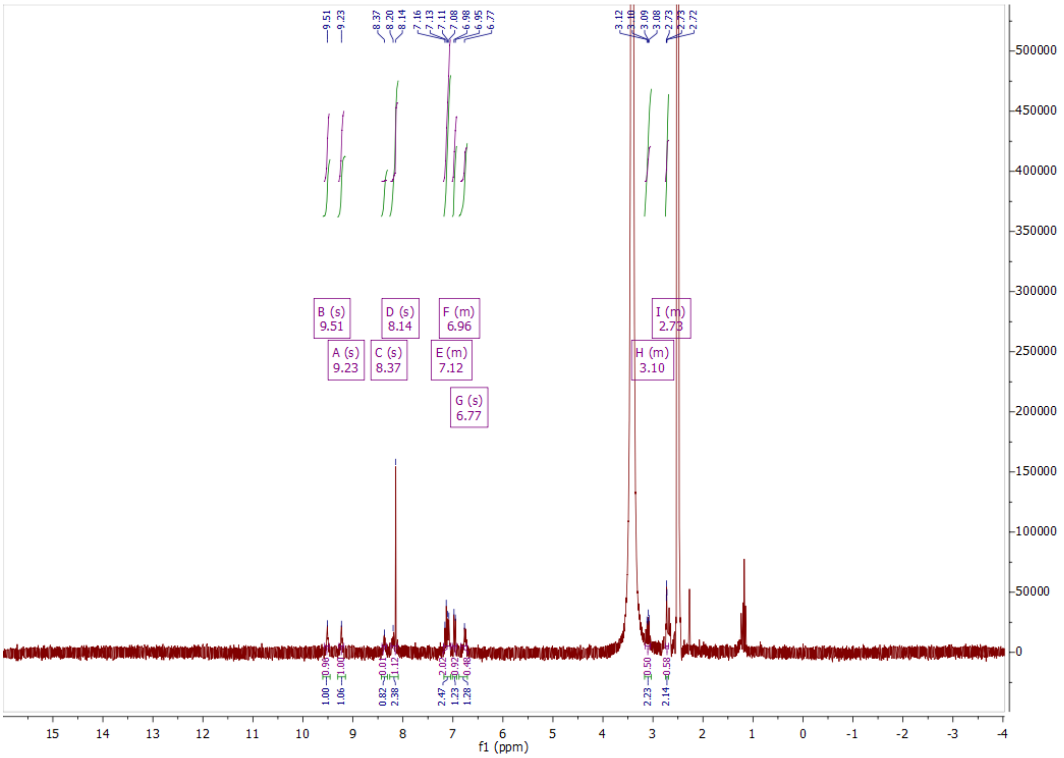

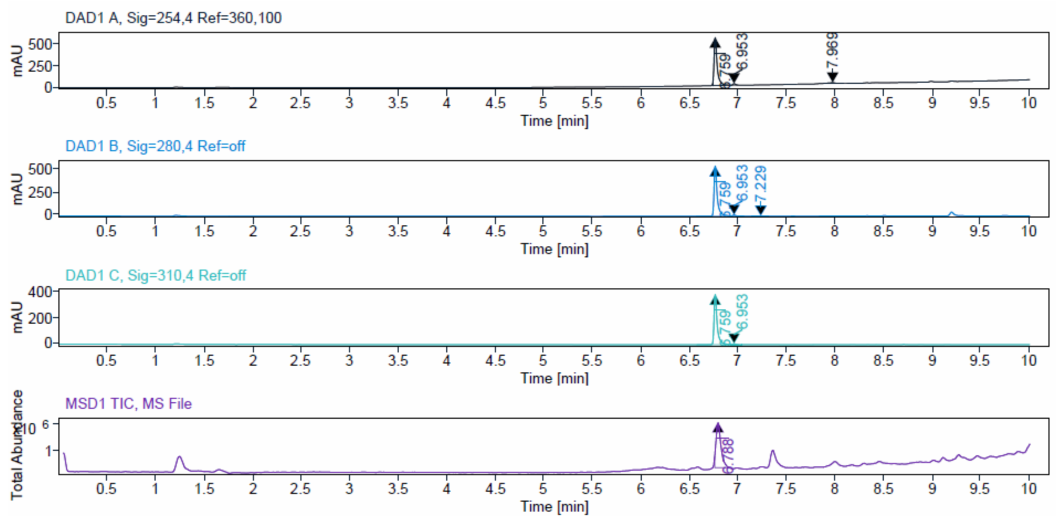

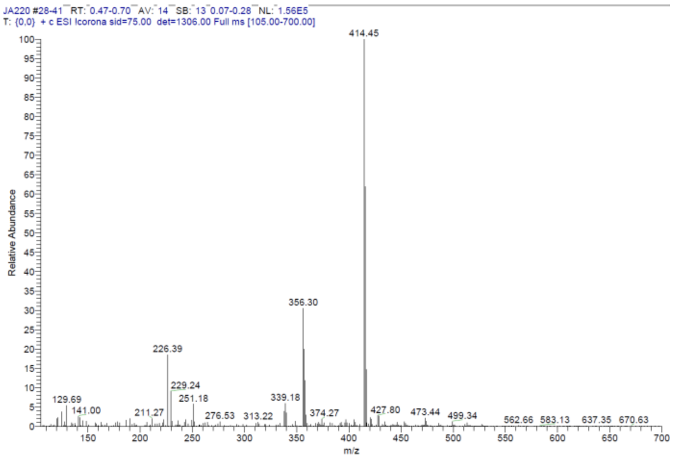

^{1}H NMR, HPLC, and ESI data data of compound **111c**

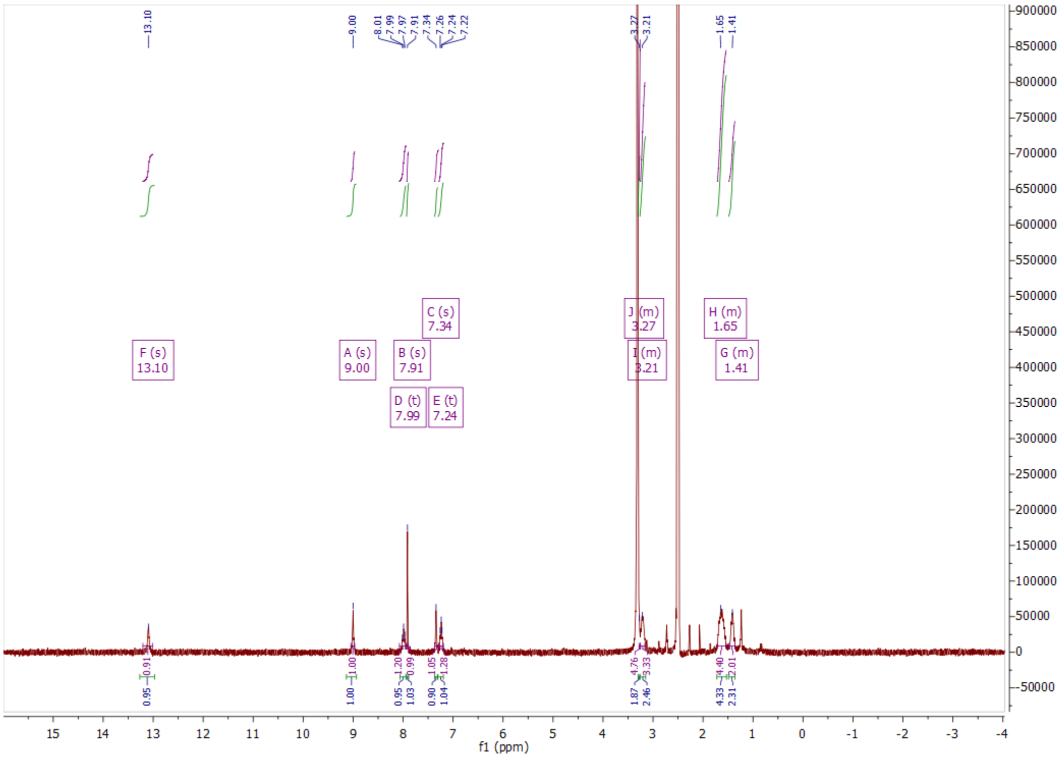

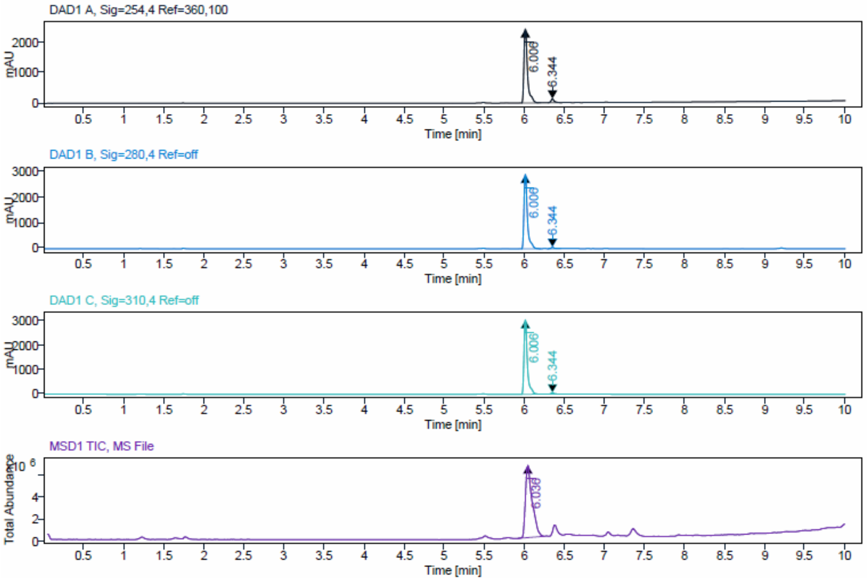
DAD1 A, Sig=254,4 Ref=360,100
mAU
2000
1000
0
6.000
6.344
0.5
1
1.5
2
2.5
3
3.5
4
4.5
5
5.5
6
6.5
7
7.5
8
8.5
9
9.5
10
Time [min]
DAD1 B, Sig=280,4 Ref=off
mAU
3000
2000
1000
0
6.000
6.344
Time [min]
DAD1 C, Sig=310,4 Ref=off
mAU
3000
2000
1000
0
6.000
6.344
Time [min]
MSD1 TIC, MS File
Total Abundance
x10 6
4
2
0
6.036
Time [min]

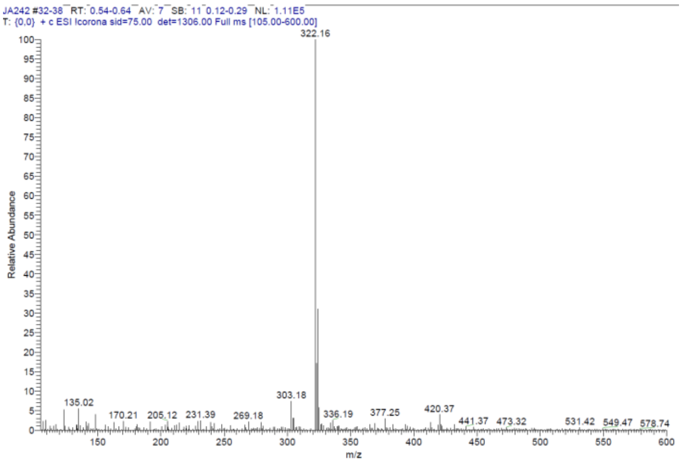
JA242 #32-38 RT: 0.54-0.64 AV: 7 SB: 11 0.12-0.29 NL: 1.11E5
T: {0,0} + c ESI Icorona sid=75.00 det=1306.00 Full ms [105.00-600.00]
Relative Abundance
100
95
90
85
80
75
70
65
60
55
50
45
40
35
30
25
20
15
10
5
0
322.16
303.18
135.02
170.21
205.12
231.39
269.18
336.19
377.25
420.37
441.37
473.32
531.42
549.47
578.74
150
200
250
300
350
400
450
500
550
600
m/z

^{1}H NMR, HPLC, and ESI data of compound **111d**

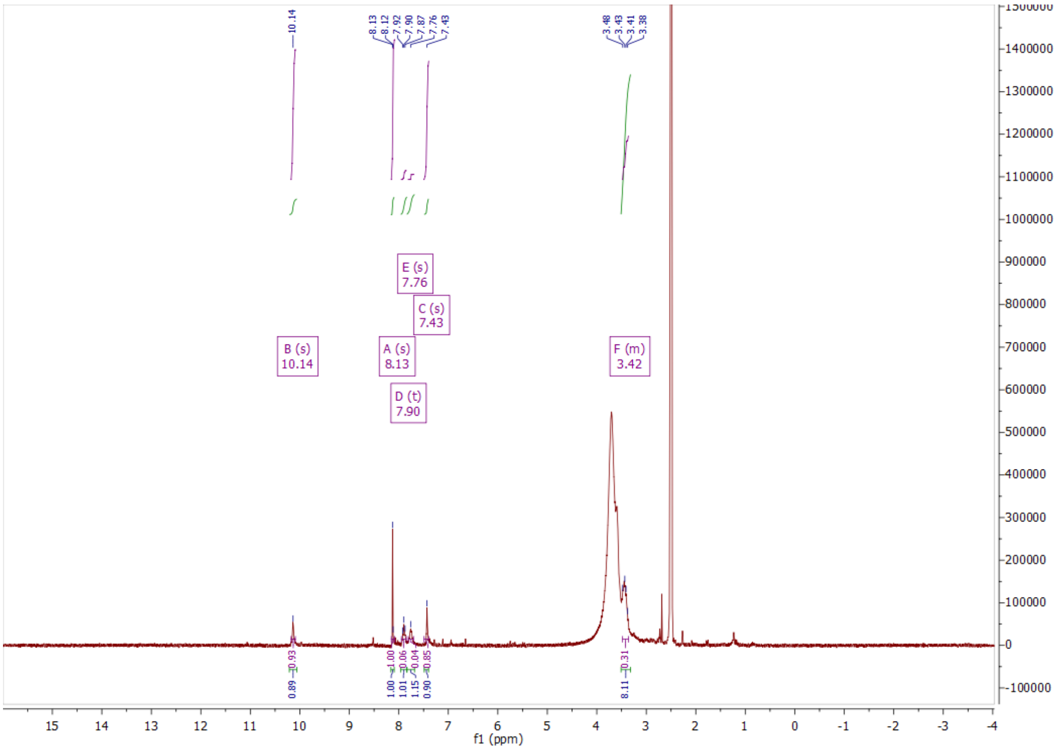

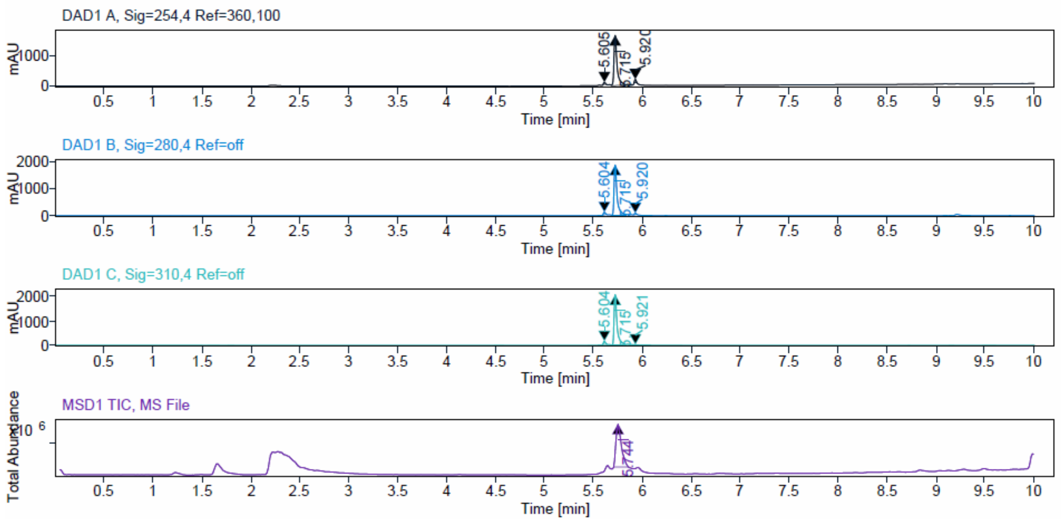

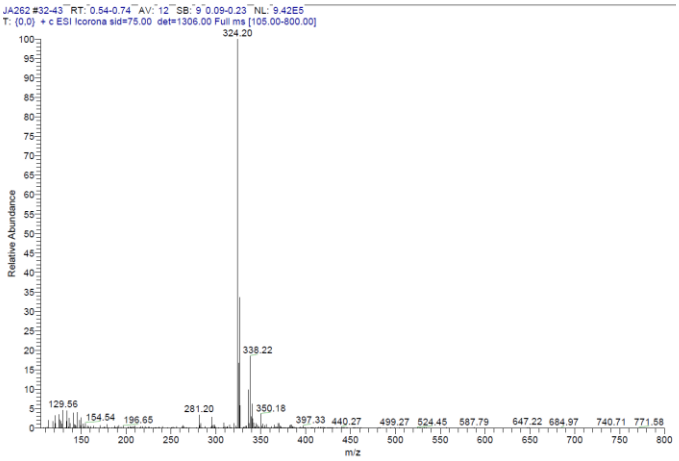

^{1}H, ^{13}C NMR, HPLC, and ESI data of compound **111e**

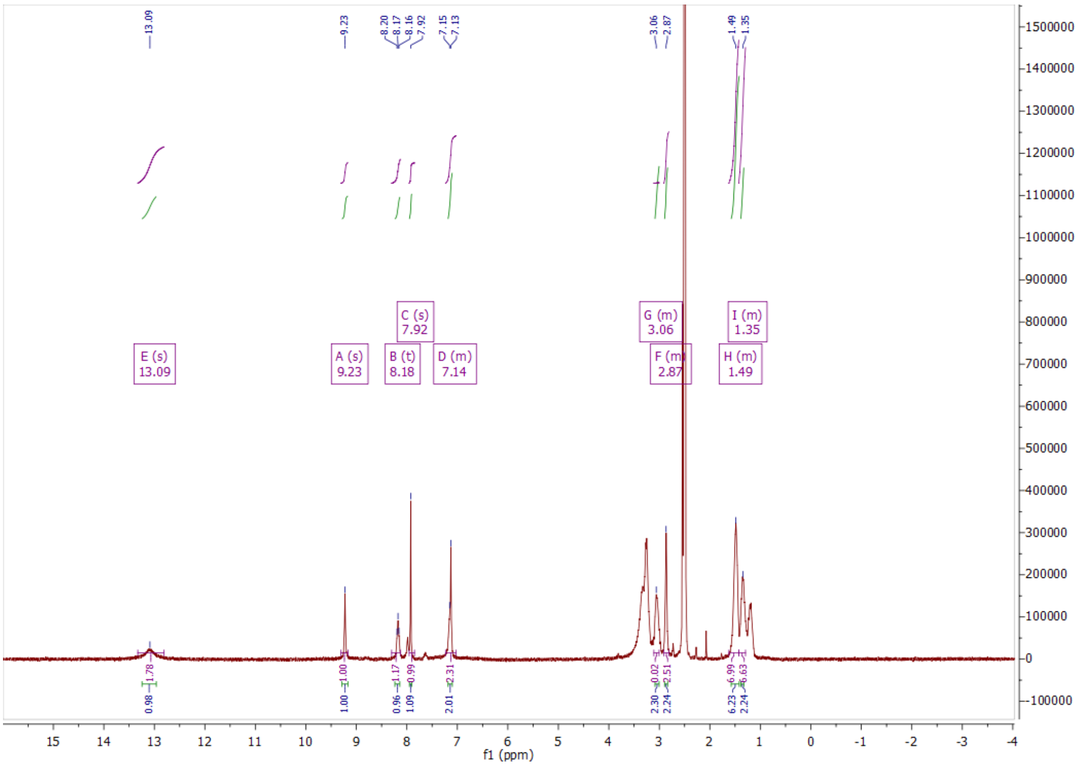

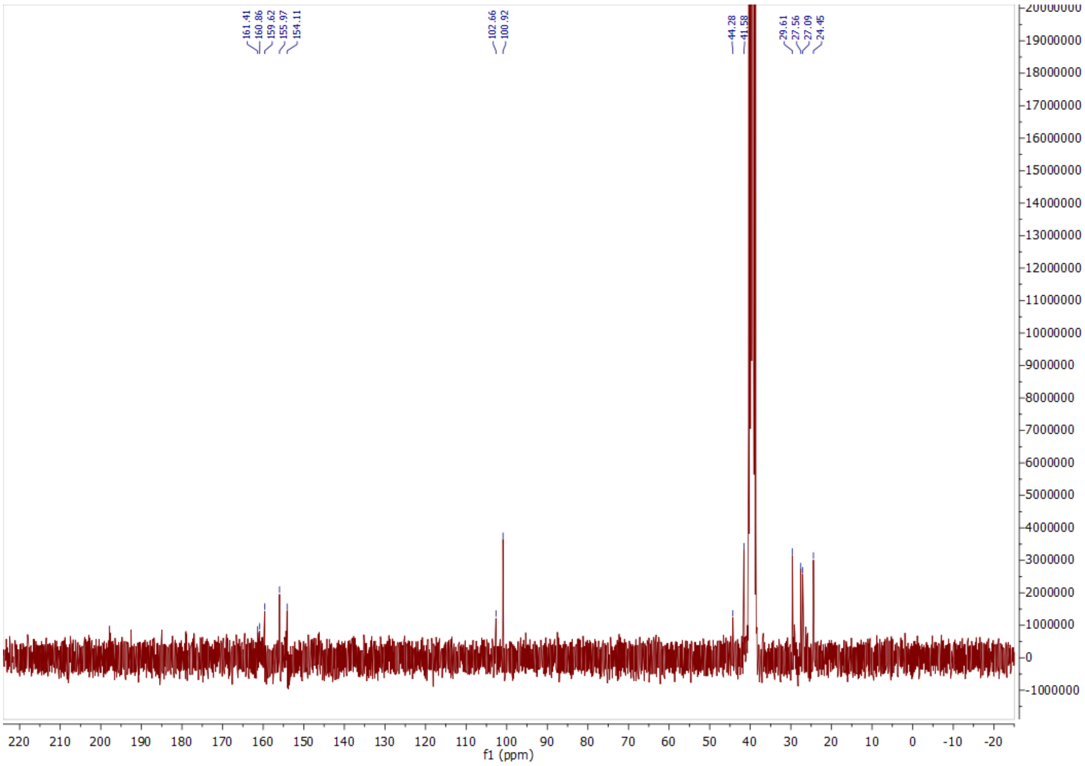

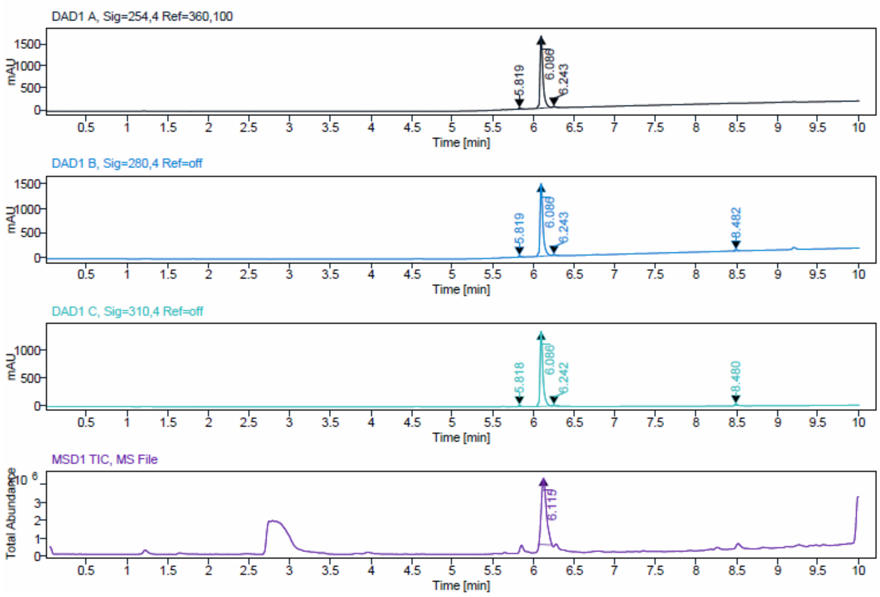
DAD1 A, Sig=254,4 Ref=360,100
mAU
1500
1000
500
0
5.819
6.086
6.243
Time [min]
DAD1 B, Sig=280,4 Ref=off
mAU
1500
1000
500
0
5.819
6.086
6.243
8.482
Time [min]
DAD1 C, Sig=310,4 Ref=off
mAU
1000
500
0
5.818
6.086
6.242
8.480
Time [min]
MSD1 TIC, MS File
Total Abundance
x10 6
3
2
1
0
6.119
0.5
1
1.5
2
2.5
3
3.5
4
4.5
5
5.5
6
6.5
7
7.5
8
8.5
9
9.5
10
Time [min]

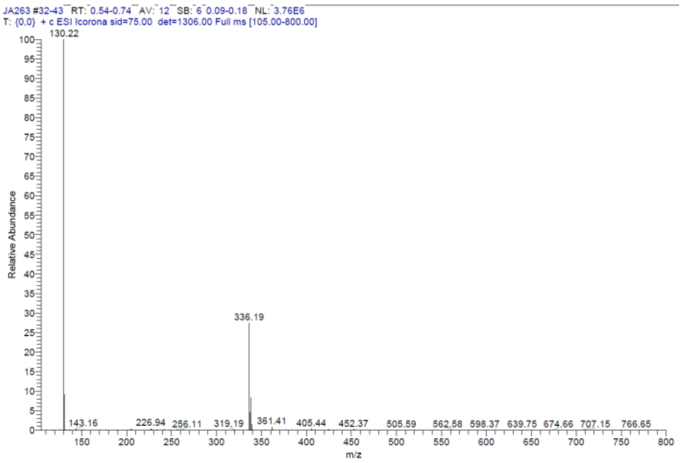
JA263 #32-43 RT: 0.54-0.74 AV: 12 SB: 6 0.09-0.18 NL: 3.76E6
T: {0,0} + c ESI Icorona sid=75.00 det=1306.00 Full ms [105.00-800.00]
Relative Abundance
100
95
90
85
80
75
70
65
60
55
50
45
40
35
30
25
20
15
10
5
0
130.22
336.19
143.16
226.94
256.11
319.19
361.41
405.44
452.37
505.59
562.58
598.37
639.75
674.66
707.15
766.65
150
200
250
300
350
400
450
500
550
600
650
700
750
800
m/z

^{1}H NMR, HPLC, and ESI data of compound **112a**

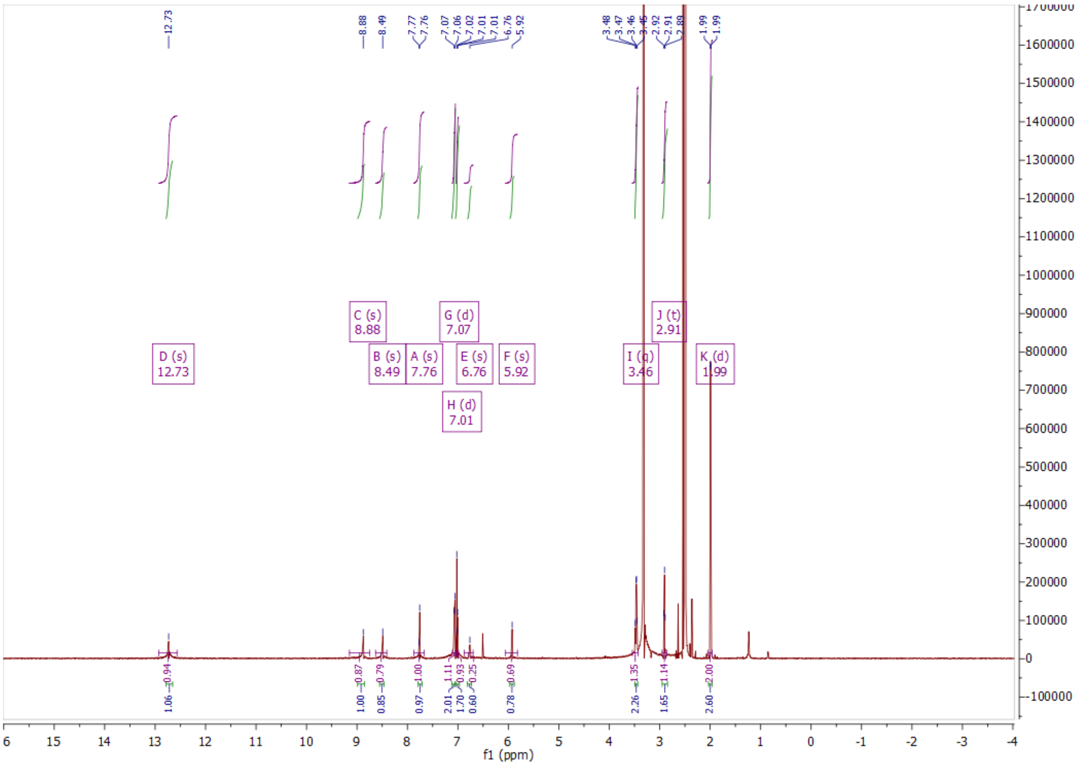

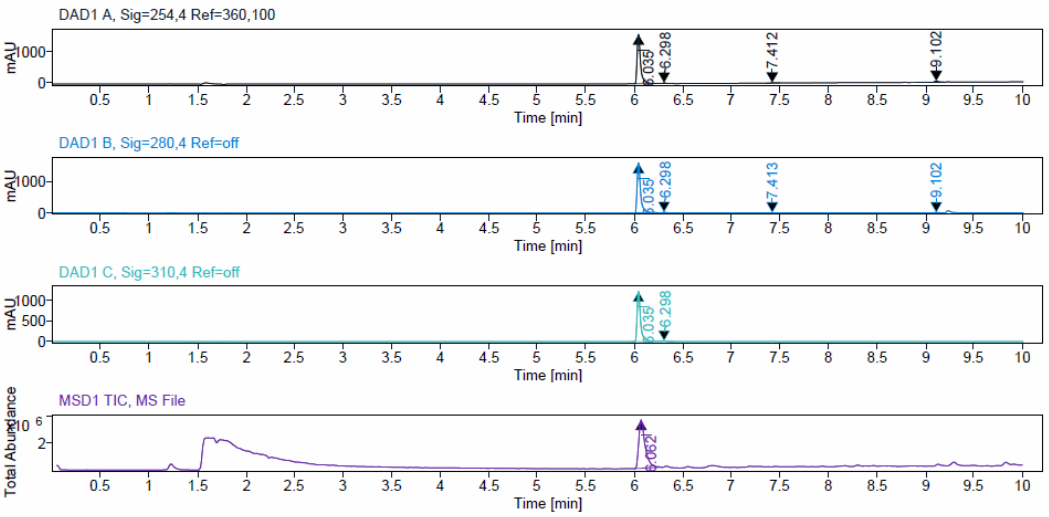

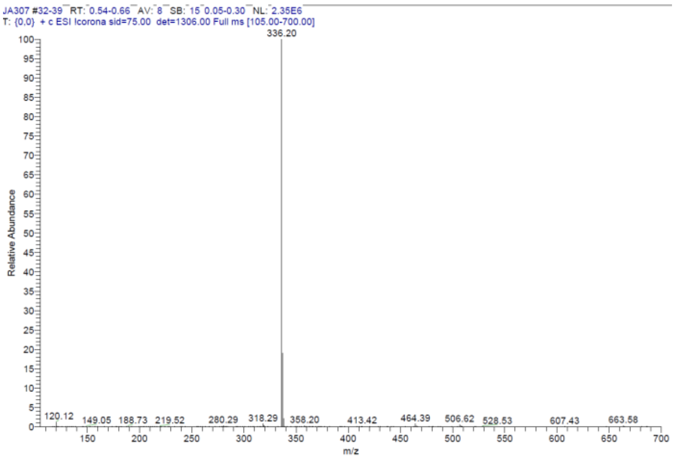

^{1}H, ^{13}C NMR, HPLC, and ESI data of compound **113a**

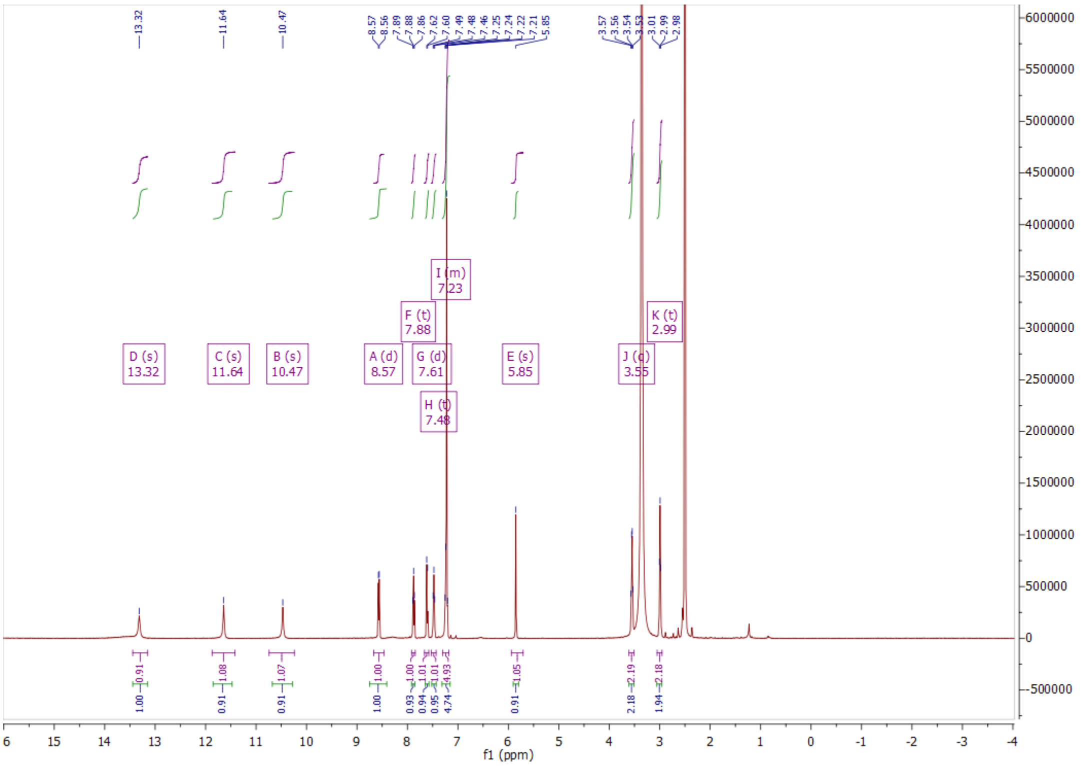

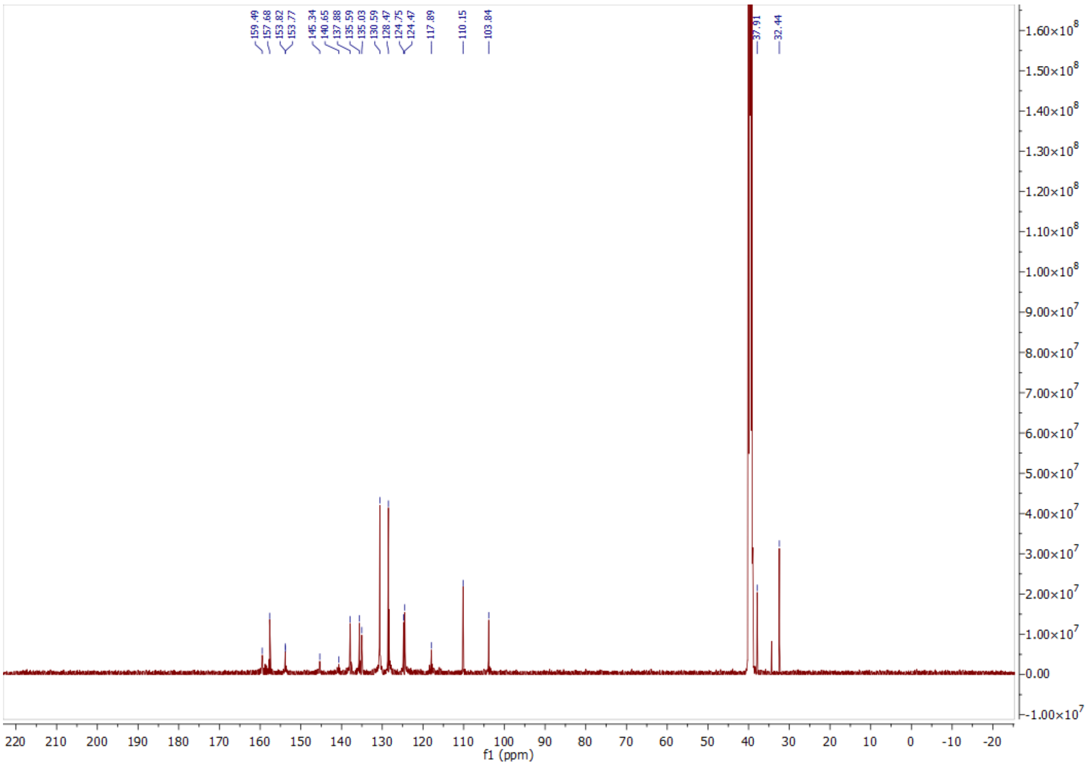

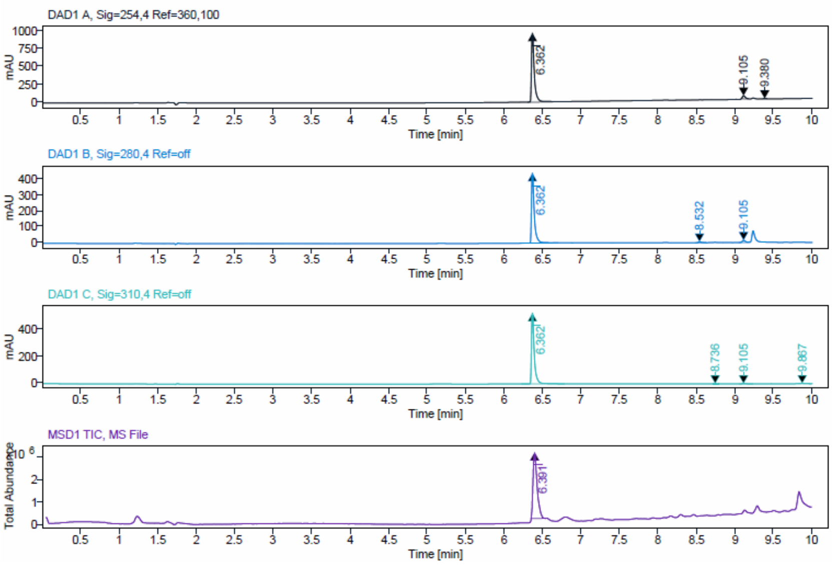

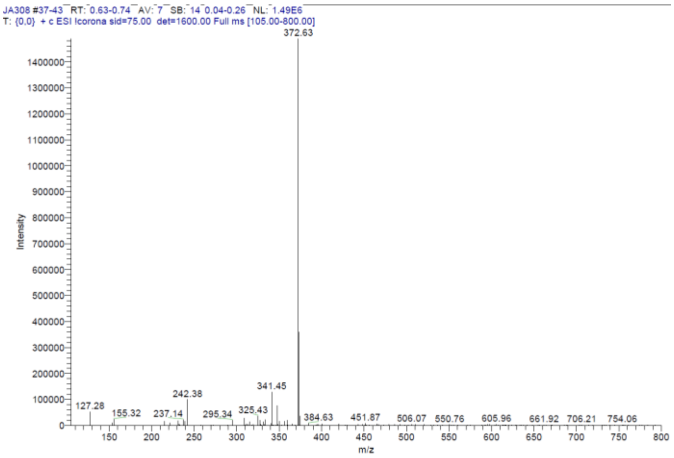

ESI, HRMS, ^{1}H, ^{13}C NMR and HPLC data of compound **113b**

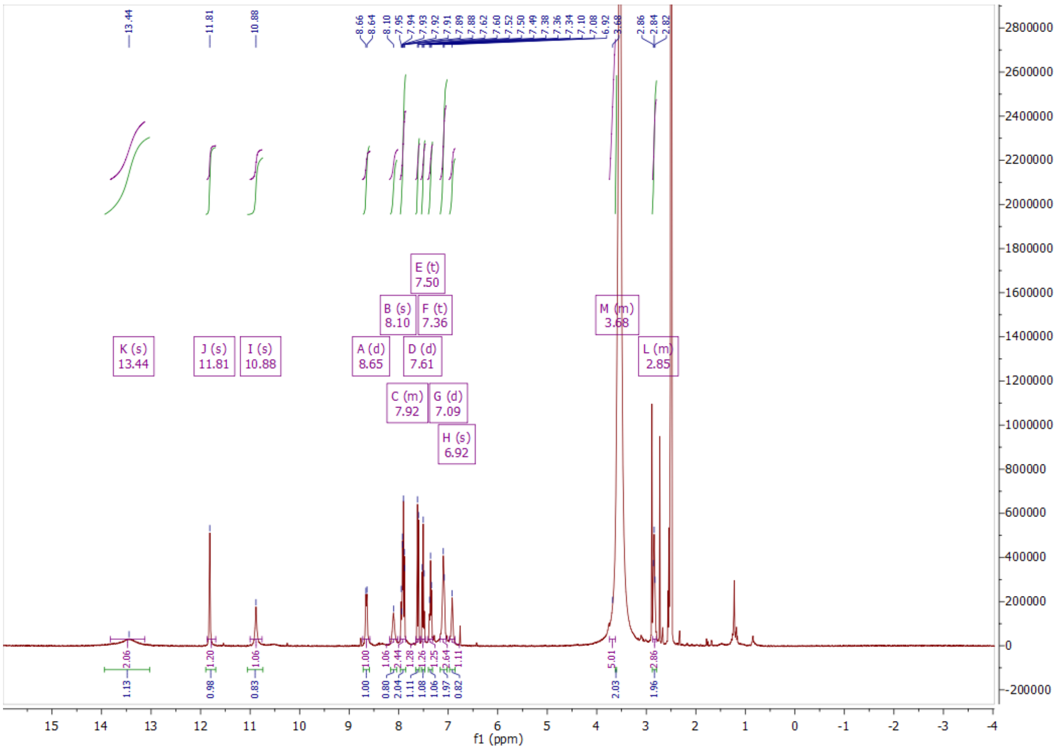

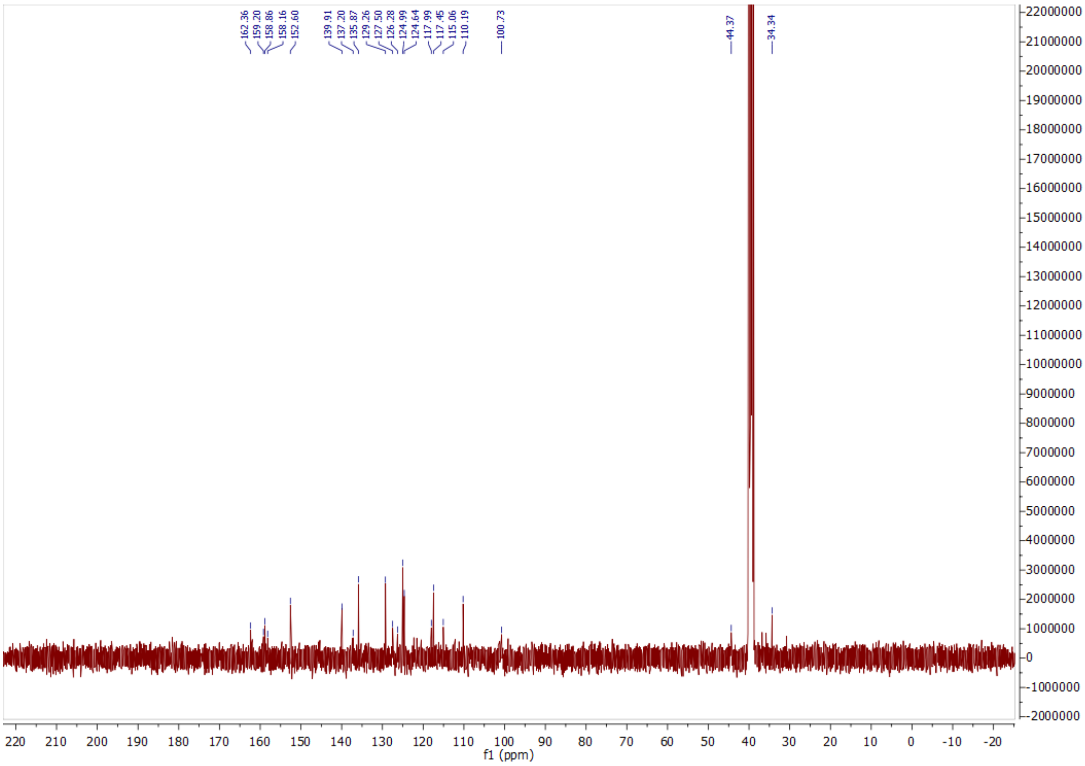
162.36
159.20
158.86
158.16
152.60
139.91
137.20
135.87
129.26
127.50
126.28
124.99
124.64
117.99
117.45
115.06
110.19
100.73
44.37
34.34
22000000
21000000
20000000
19000000
18000000
17000000
16000000
15000000
14000000
13000000
12000000
11000000
10000000
9000000
8000000
7000000
6000000
5000000
4000000
3000000
2000000
1000000
0
-1000000
-2000000
220 210 200 190 180 170 160 150 140 130 120 110 100 90 80 70 60 50 40 30 20 10 0 -10 -20
f1 (ppm)

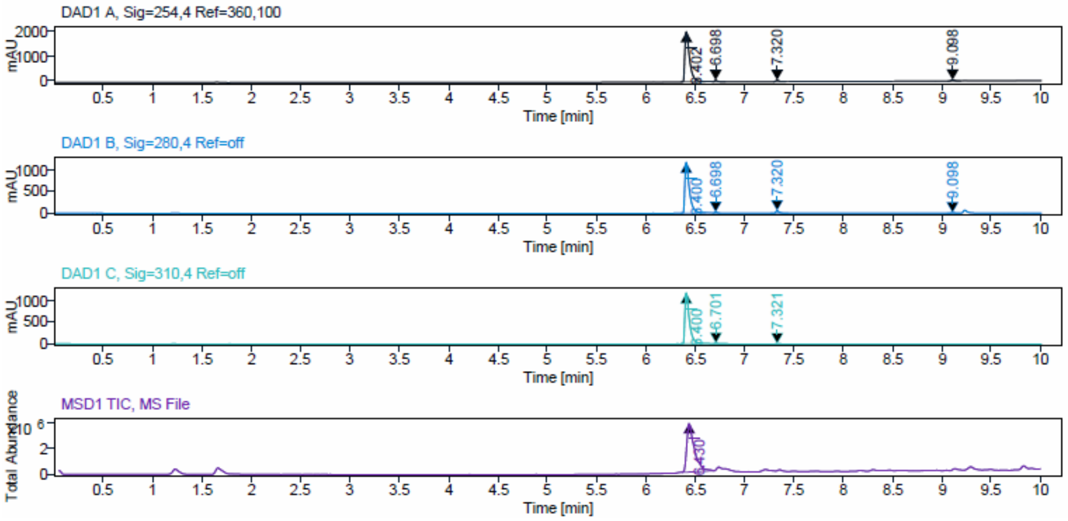
DAD1 A, Sig=254,4 Ref=360,100
mAU
2000
1000
0
6.402
6.698
7.320
9.098
0.5 1 1.5 2 2.5 3 3.5 4 4.5 5 5.5 6 6.5 7 7.5 8 8.5 9 9.5 10
Time [min]
DAD1 B, Sig=280,4 Ref=off
mAU
1000
500
0
6.400
6.698
7.320
9.098
0.5 1 1.5 2 2.5 3 3.5 4 4.5 5 5.5 6 6.5 7 7.5 8 8.5 9 9.5 10
Time [min]
DAD1 C, Sig=310,4 Ref=off
mAU
1000
500
0
6.400
6.701
7.321
0.5 1 1.5 2 2.5 3 3.5 4 4.5 5 5.5 6 6.5 7 7.5 8 8.5 9 9.5 10
Time [min]
MSD1 TIC, MS File
Total Abundance
x10 6
2
0
6.430
0.5 1 1.5 2 2.5 3 3.5 4 4.5 5 5.5 6 6.5 7 7.5 8 8.5 9 9.5 10
Time [min]

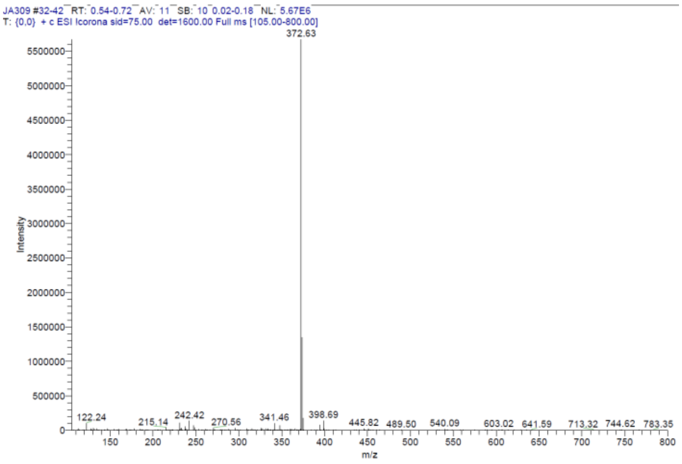
JA309 #32-42 RT: 0.54-0.72 AV: 11 SB: 10 0.02-0.18 NL: 5.67E6
T: {0,0} + c ESI Icorona sid=75.00 det=1600.00 Full ms [105.00-800.00]
372.63
Intensity
5500000
5000000
4500000
4000000
3500000
3000000
2500000
2000000
1500000
1000000
500000
0
122.24
215.14
242.42
270.56
341.46
398.69
445.82
489.50
540.09
603.02
641.59
713.32
744.62
783.35
150 200 250 300 350 400 450 500 550 600 650 700 750 800
m/z

^{1}H, ^{13}C NMR, HPLC, and ESI data of compound **113c**

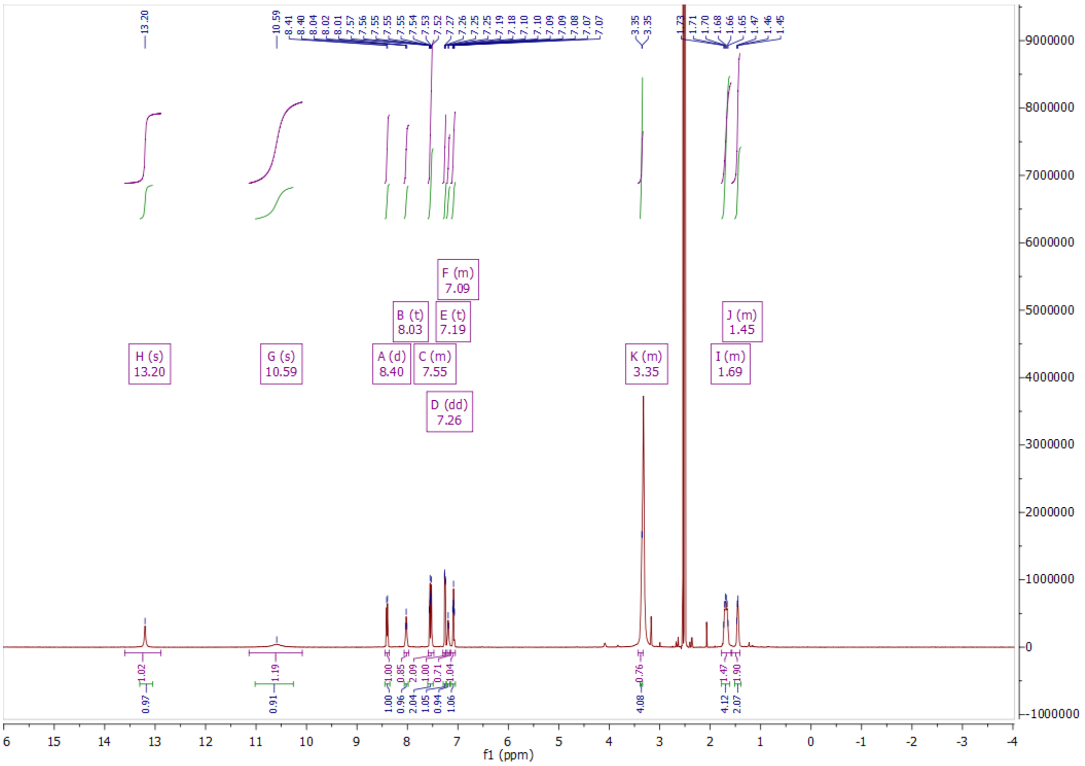

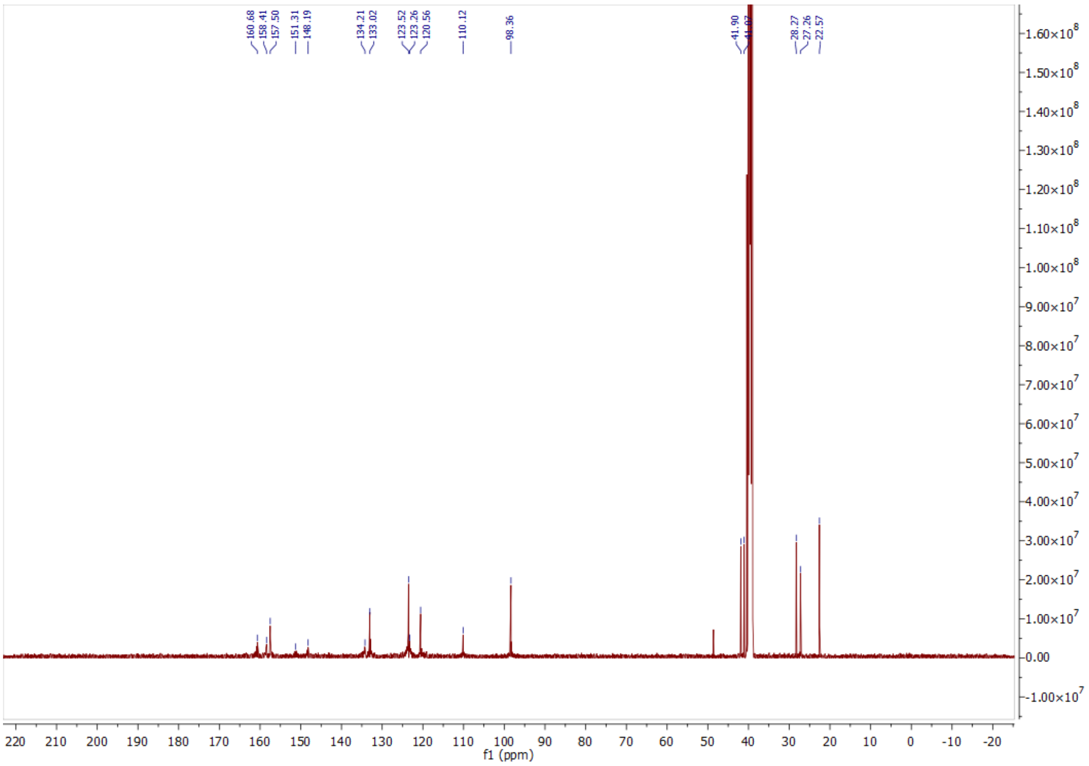

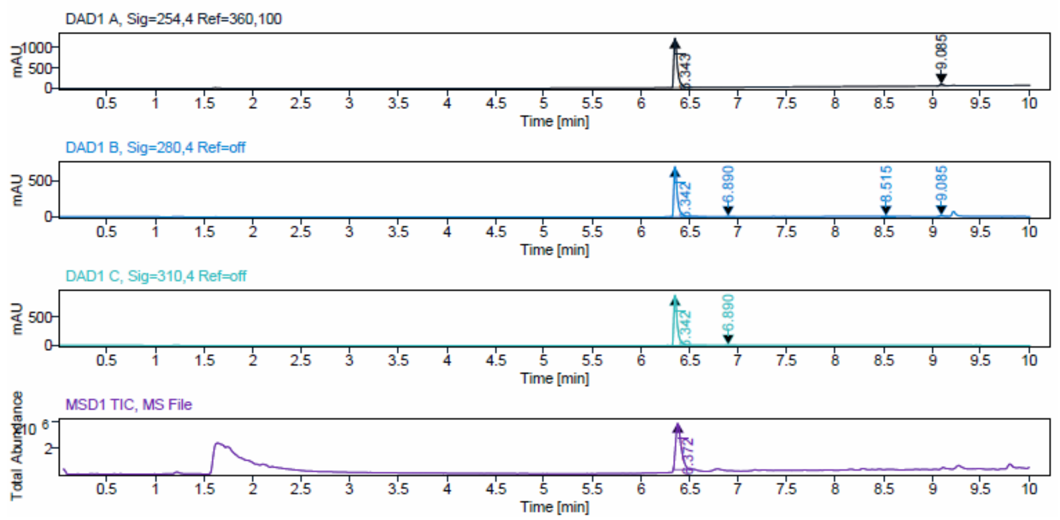

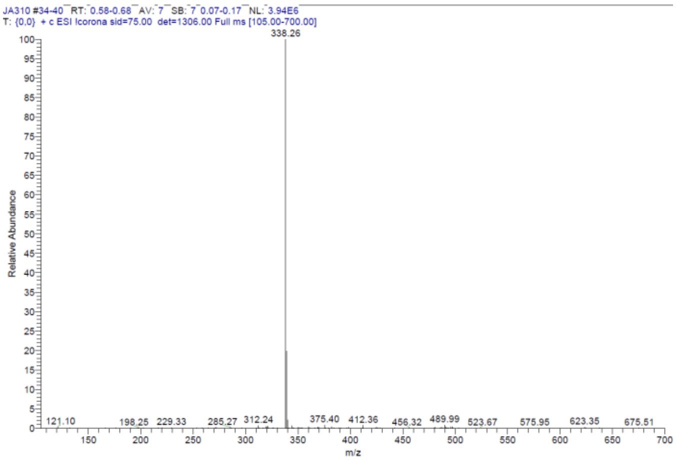

^{1}H, ^{13}C NMR, HPLC, and ESI data of compound **113d**

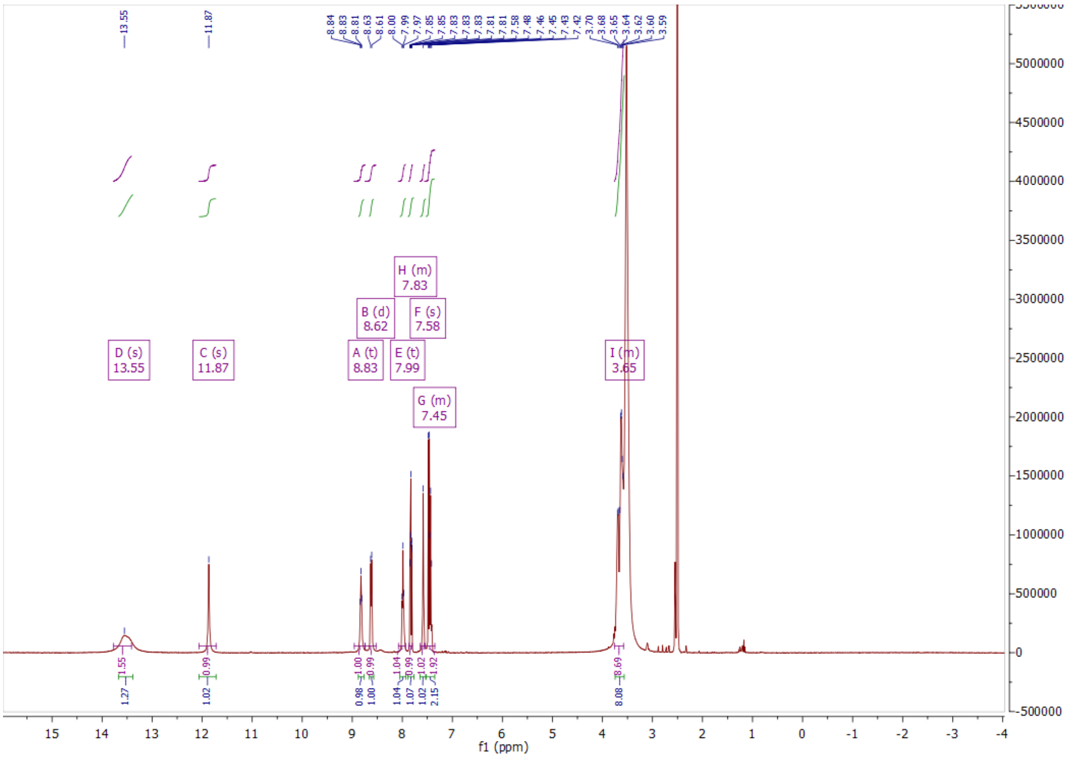

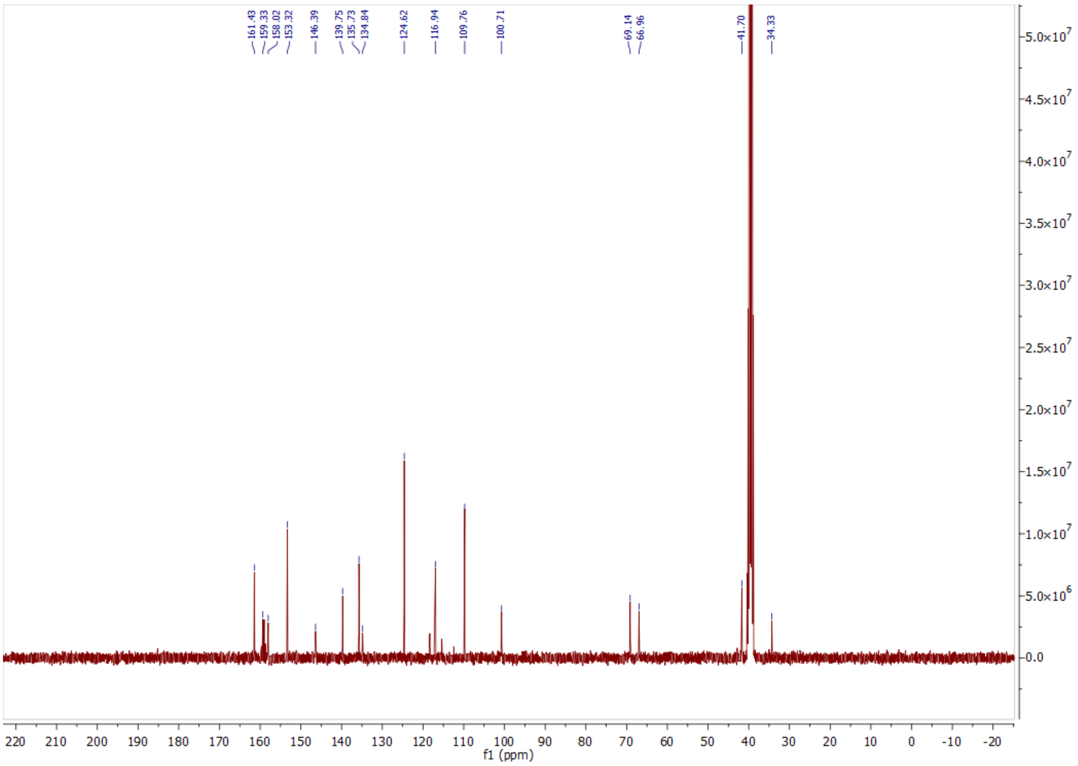
161.43
159.33
158.02
153.32
146.39
139.75
135.73
134.84
124.62
116.94
109.76
100.71
69.14
66.96
41.70
34.33
5.0×10^7
4.5×10^7
4.0×10^7
3.5×10^7
3.0×10^7
2.5×10^7
2.0×10^7
1.5×10^7
1.0×10^7
5.0×10^6
0.0
220 210 200 190 180 170 160 150 140 130 120 110 100 90 80 70 60 50 40 30 20 10 0 -10 -20
f1 (ppm)

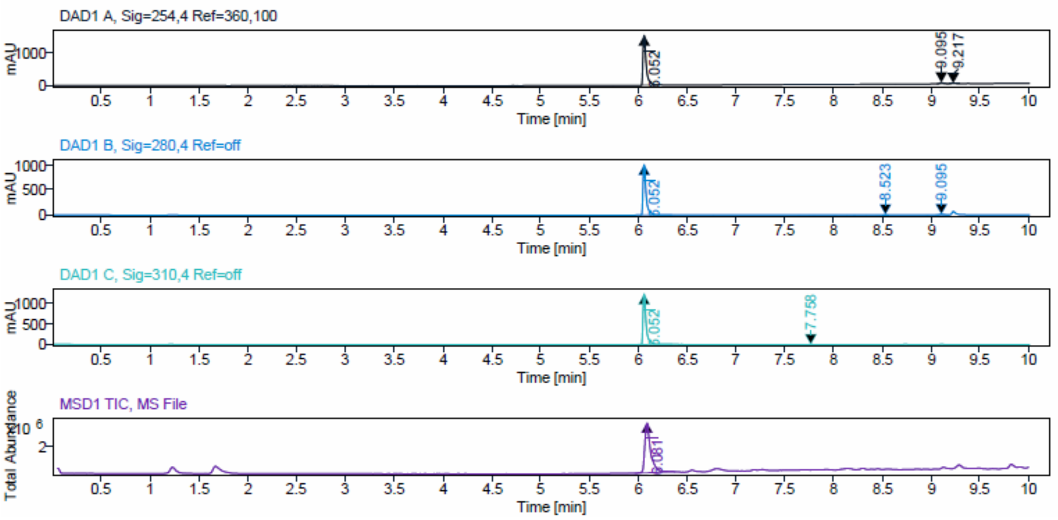
DAD1 A, Sig=254,4 Ref=360,100
mAU
1000
0
6.052
9.095
9.217
Time [min]
DAD1 B, Sig=280,4 Ref=off
mAU
1000
500
0
6.052
8.523
9.095
Time [min]
DAD1 C, Sig=310,4 Ref=off
mAU
1000
500
0
6.052
7.758
Time [min]
MSD1 TIC, MS File
Total Abundance
x10 6
2
6.081
Time [min]
0.5 1 1.5 2 2.5 3 3.5 4 4.5 5 5.5 6 6.5 7 7.5 8 8.5 9 9.5 10

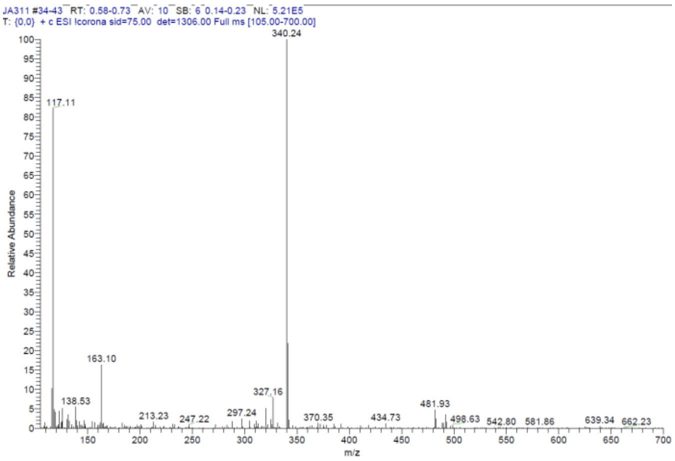
JA311 #34-43 RT: 0.58-0.73 AV: 10 SB: 6 0.14-0.23 NL: 5.21E5
T: {0,0} + c ESI Icorona sid=75.00 det=1306.00 Full ms [105.00-700.00]
Relative Abundance
340.24
117.11
163.10
138.53
327.16
213.23
247.22
297.24
370.35
434.73
481.93
498.63
542.80
581.86
639.34
662.23
m/z

^{1}H, ^{13}C NMR, HPLC, and ESI data of compound **113e**

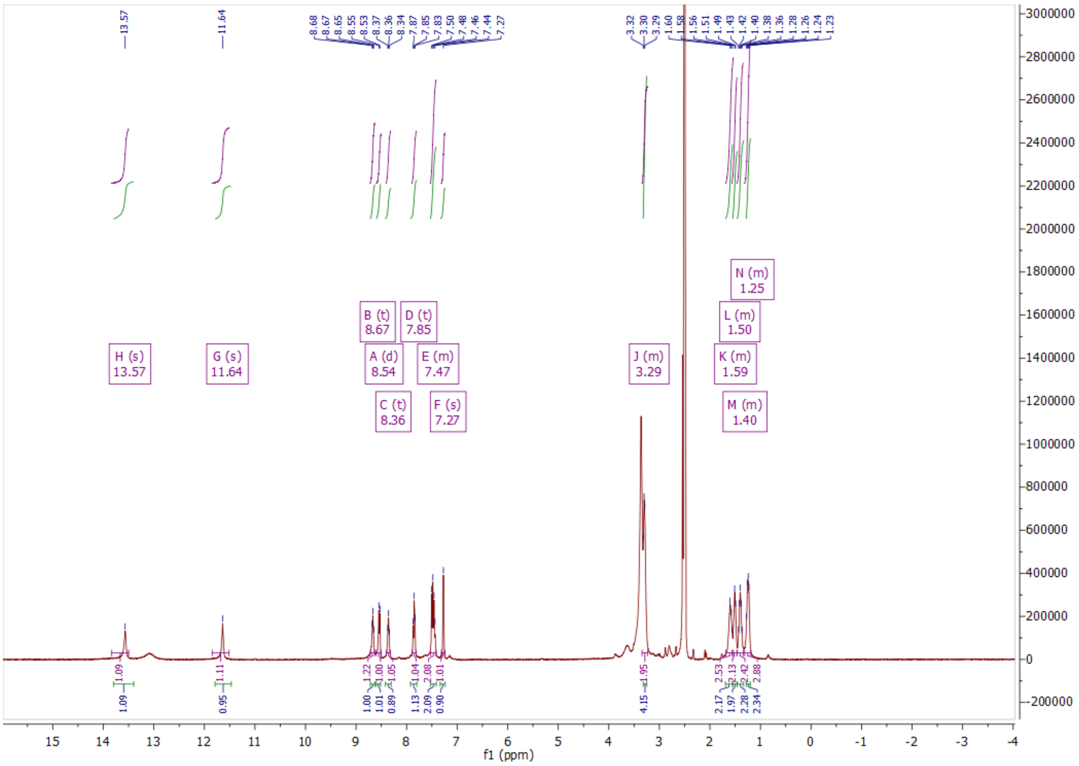

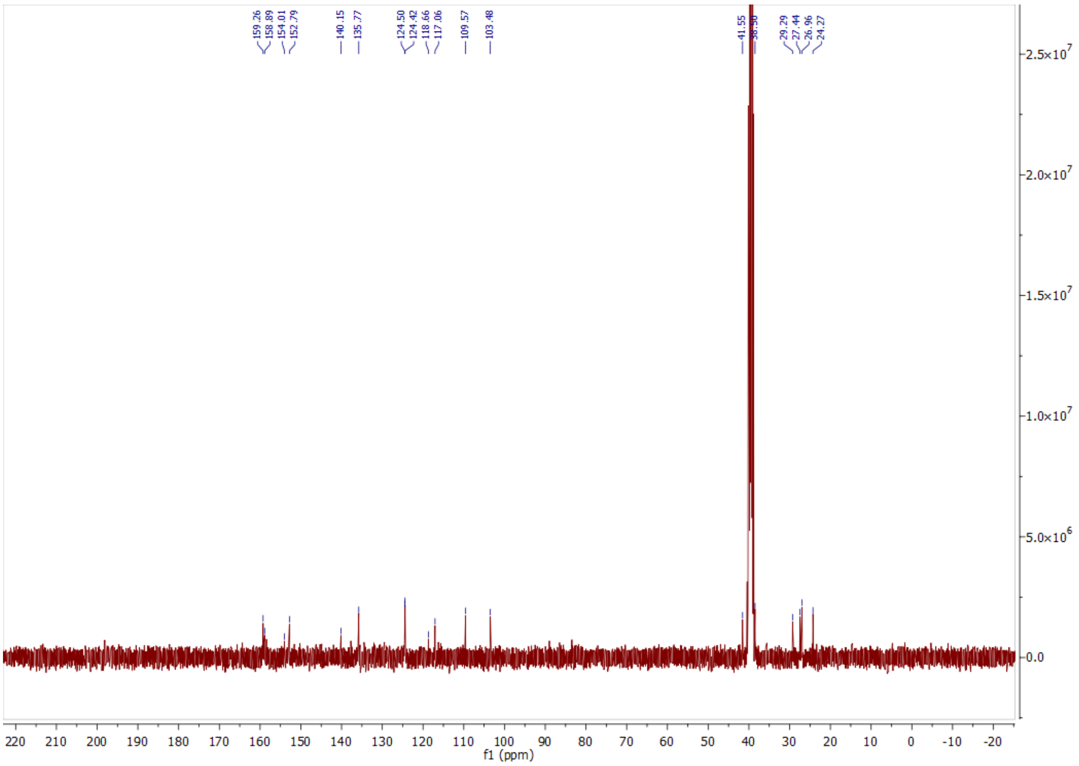

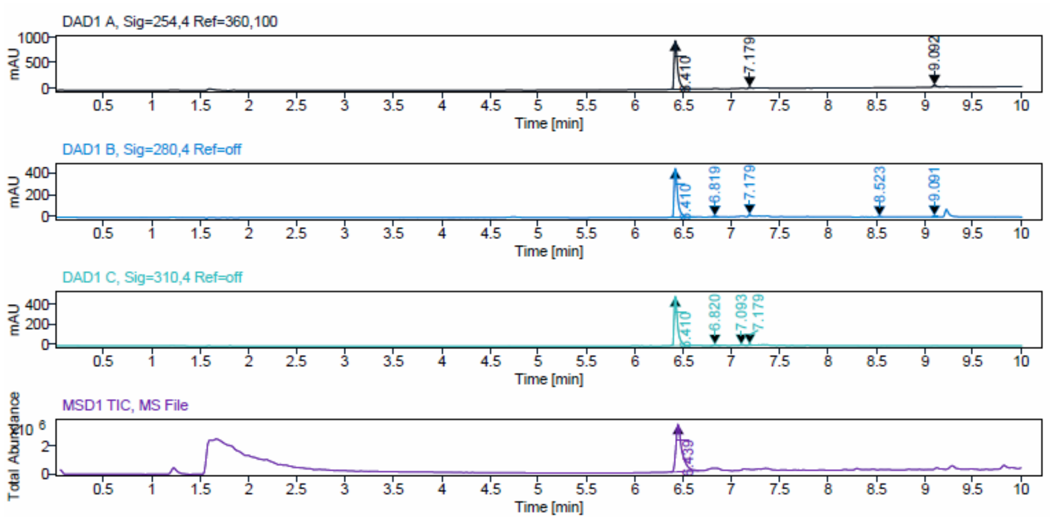
DAD1 A, Sig=254,4 Ref=360,100
mAU
1000
500
0
6.410
7.179
9.092
Time [min]
DAD1 B, Sig=280,4 Ref=off
400
200
6.410
6.819
7.179
8.523
9.091
DAD1 C, Sig=310,4 Ref=off
6.410
6.820
7.093
7.179
MSD1 TIC, MS File
Total Abundance
x10 6
2
6.439
0.5
1
1.5
2
2.5
3
3.5
4
4.5
5
5.5
6
6.5
7
7.5
8
8.5
9
9.5
10

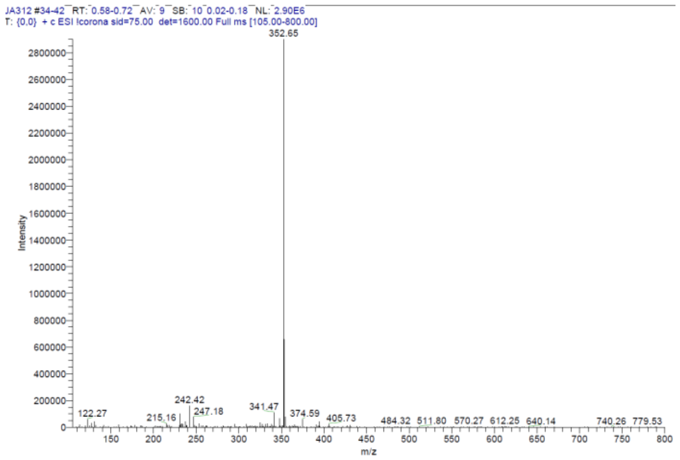
JA312 #34-42 RT: 0.58-0.72 AV: 9 SB: 10 0.02-0.18 NL: 2.90E6
T: {0,0} + c ESI !corona sid=75.00 det=1600.00 Full ms [105.00-800.00]
352.65
Intensity
2800000
2600000
2400000
2200000
2000000
1800000
1600000
1400000
1200000
1000000
800000
600000
400000
200000
0
122.27
215.16
242.42
247.18
341.47
374.59
405.73
484.32
511.80
570.27
612.25
640.14
740.26
779.53
150
200
250
300
350
400
450
500
550
600
650
700
750
800
m/z

17. Eidesstattliche Erklärung

Erklärung

Ich erkläre hiermit, dass ich mich bisher keiner Doktorprüfung im Mathematisch-Naturwissenschaftlichen Bereich unterzogen habe.

Frankfurt am Main, den ………………………………………………………………..

(Unterschrift)

Versicherung

Ich erkläre hiermit, dass ich die vorgelegte Dissertation über

…………………………………………………………………

„Synthesis of macrocyclic kinase inhibitors“…………………

…………………………………………………………………

selbstständig angefertigt und mich anderer Hilfsmittel als der in ihr angegebenen nicht bedient habe, insbesondere, dass alle Entlehnungen aus anderen Schriften mit Angabe der betreffenden Schrift gekennzeichnet sind. Ich versichere, die Grundsätze der guten wissenschaftlichen Praxis beachtet, und nicht die Hilfe einer kommerziellen Promotionsvermittlung in Anspruch genommen zu haben.

Frankfurt am Main, den ………………………………………………………………..

(Unterschrift)